

**proceedings of the
Twelfth International
MACHINE TOOL
DESIGN AND RESEARCH
Conference**

edited by

F. KOENIGSBERGER and S. A. TOBIAS

PROCEEDINGS OF THE
TWELFTH INTERNATIONAL
MACHINE TOOL DESIGN AND RESEARCH
CONFERENCE

PROCEEDINGS OF THE
TWELFTH INTERNATIONAL
MACHINE TOOL DESIGN AND RESEARCH
CONFERENCE

*held in Manchester
15–17 September 1971*

Edited by
F. KOENIGSBERGER
*Professor of Machine Tool Engineering
University of Manchester Institute of Science and Technology*

and

S. A. TOBIAS
*Chance Professor and Head of Department
Department of Mechanical Engineering
University of Birmingham*

MACMILLAN EDUCATION

All rights reserved. No part of this
publication may be reproduced or transmitted,
in any form or by any means, without permission.

*First published 1972 by
THE MACMILLAN PRESS LTD
London and Basingstoke
Associated companies in New York Toronto
Dublin Melbourne Johannesburg and Madras*

SBN 333 13318 8

ISBN 978-1-349-01399-9 ISBN 978-1-349-01397-5 (eBook)
DOI 10.1007/978-1-349-01397-5

© The Macmillan Press Limited 1972
Softcover reprint of the hardcover 1st edition 1972 978-0-333-13318-7

CONTENTS

Introduction. F. KOENIGSBERGER	1
Opening address. H. OPITZ	2
ADAPTIVE CONTROL	
Adaptive control for turning operations. A. LEDERGERBER	7
The on-line control of cutting conditions using direct feedback. N. F. SHILLAM	15
NUMERICALLY CONTROLLED MACHINE TOOL DESIGN	
Developments in automation for NC lathes. R. L. MACDONALD and M. THORNEY-CROFT	25
The modular range of NC machine tools. D. GRINDROD and G. FARNWORTH	31
Machine tools – the total concept. C. A. SPARKES	41
METAL FORMING	
On the isostatic compaction and hydrostatic extrusion of iron powder. J. M. ALEXANDER and D. R. QUAINTON	51
Development of a new precision shearing process opposed dies shearing process. K. KONDO and K. MAEDA	61
Hot forging of grey cast irons. R. FARNWORTH and B. W. ROOKS	69
MACHINE TOOL ELEMENT DESIGN	
Behaviour of the horizontal stiffness and the micro-sliding on the bolted joint under the normal pre-load. M. MASUKO, Y. ITO and C. FUJIMOTO	81
Calculating the elastic and plastic components of deflection of plane joints formed from machined surfaces. R. E. SCHOFIELD and R. H. THORNLEY	89
Experimental study on the optimum interface pressure on a bolted joint considering the damping capacity. Y. ITO and M. MASUKO	97
Some aspects of wear on disc clutches used in machine tools. H. LEVY, E. LENZ and K. LOEWY	107
Cutting forces in machining and their routine measurement with multi-component piezo-electric force transducers. G. H. GAUTSCHI	113
The effect of appearance considerations on the design of a small NC milling machine. E. J. HUNTLEY, R. ROSE and J. S. SHEEN	121
METAL FORMING	
Stress wave fracturing of a bar. S. T. S. AL-HASSANI and W. JOHNSON	129
Expanding sheet forming method for automobile bumpers. K. KOSHINO	141
The design of a press for use in the hydrostatic extrusion process. R. W. THATCHER and J. A. PENNELL	147
Die performance in high-energy rate forging. A. THOMAS and K. DENHAM	153
The production of tensile test specimens by an economical blanking process and its feasibility for practical application. T. NAKAGAWA, Y. FURUKAWA and K. YOSHIDA.	161
Bending of thin-walled tubes by combined external mechanical forces and internal fluid pressure. C. BOYD and F. W. TRAVIS.	169
MACHINE TOOL FEED DRIVES AND GUIDEWAYS	
Special design features of NC contouring machines. G. ENGEL.	179
A method of calculation for two-way flow-control valves depending on imposed dynamic performance. I. MAZILU	187
The choice of ballslideways for machine tools. J. de FRAINE	193
The improvement of the accuracy of electrohydraulic cylinder drives. A. DE PENNINGTON, D. W. MARSLAND and R. BELL.	199
An economic technique for the improvement of the stability of hydraulic cylinder drives. P. GALE and R. BELL	207
The specification and performance of electrohydraulic motor drives for numerically controlled machine tools. S. K. CESSFORD and R. BELL	217

GRINDING AND ELECTRO CHEMICAL MACHINING

Objective method for determining grinding wheel life. F. SZEKERES.	229
On the rounding-up process in high-production internal grinding machines by digital computer simulation. R. S. HAHN and R. P. LINDSAY	235
Geometrical configurations for stability in the centreless grinding process. D. L. RICHARDS, W. B. ROWE and F. KOENIGSBERGER	241
Electron beam, the multi-role tool for modern fabrication. K. H. von GROTE and A. H. MELEKA	247
Hydraulic approach to electrolyte flow in electrochemical machining. S. ITO and K. SEIMIYA	259
Vertical spindle electrochemical surface grinding. M. M. SFANTSIKOPOULOS and C. F. NOBLE	265
Effect of surface finish produced during ECM upon the fatigue life of Nimonic 80A. J. M. EVANS, P. J. BODEN and A. A. BAKER	271

MACHINE TOOL TESTING

A study of identification of dynamic characteristics of machine tools by means of micro tremor. H. SATO and T. AKUTSU.	281
Establishing standard cutting conditions for performance testing of universal metal cutting machine tools. M. BURDEKIN, A. COWLEY and J. TLUSTY	289
The development of a dynamic performance test for lathes. B. J. STONE	299
A new hydraulic vibrator. J. I. ROBERTS, R. LAWThER and G. PENDLEBURY	309
Inspection and acceptance tests for NC machine tools. K. JUSTEL	315
Positioning accuracy of NC machine tools. C. P. HEMINGRAY, A. COWLEY and M. BURDEKIN	319
Machine tool testing – a practical approach. J. W. ANDERSON	325
Techniques for testing accuracy of NC machine tools. J. TLUSTY	333

METAL PROCESSING

Metallurgical and residual stress investigations of explosively welded specimens. R. PRÜMMER	349
Forming force required for tube-forming. Y. TOZAWA and K. KAWADA	355
A study of the strain histories and drawing-in in a pressed steel shell. R. A. ETHERIDGE and F. J. MORBEY	359
The quantitative effect of tool geometry and strain-hardening on the critical punch force in cup drawing. J. A. G. KALS	367
Determination of tool-life equations by step turning test. T. S. KIANG and G. BARROW	379
The effect of component tolerance upon optimum machining conditions. J. R. CROOKALL and R. C. MALTBY	387
Thermoelectric characteristics of carbides. C. BUS, N. A. L. TOUWEN, P. C. VEENSTRA and A. C. H. van der WOLF	397
Carbide size and distribution and their effect on the performance of high-speed-steel tools. IVO KVASNICKA	401

DIGITAL COMPUTER-AIDED DESIGN AND CONTROL

The programmed approach in control systems. R. DOANE and D. HOLLAND	411
A system for direct numerical control of machine tools. G. SPUR and W. WENTZ.	421
Report on a special DNC system. G. STUTE and R. NANN	429
The design and development of a numerical control system using a small digital computer. C. J. CHARNLEY and S. SRINIVASAN	433
Computer approach to dynamically optimum design of machine tool structures. M. YOSHIMURA and T. HOSHI	439
Efficiency and accuracy of the flexibility and stiffness methods for the calculation of beam-like redundant structures. L. van der NOORTGATE	447
The finite-element method applied to the deformation analysis of thin-walled columns. S. HINDUJA and A. COWLEY.	455

METAL CUTTING

Tool-life equations and machining economics. G. BARROW	481
Selection of cutting speeds based on uncertain data. R. L. KEGG	495
Use of the scanning electron microscope to study the function of manganese sulphide inclusions in resulphurised free-machining steels. W. J. WILBER, A. W. J. CHISHOLM and E. J. PATTINSON	499

METAL CUTTING contd.

Assessing machinability from fundamental work material properties. W. F. HASTINGS, P. L. B. OXLEY and M. G. STEVENSON	507
The use of a cutting force spectrum for tool wear compensation during turning. N. AKGERMAN and J. FRISCH.	517

SYSTEM DESIGN AND IDENTIFICATION

Designing in digital space. W. B. HEGINBOTHAM	529
A computer-aided study of the texture of the working surfaces of grinding wheels. C. P. BHATEJA, A. W. J. CHISHOLM and E. J. PATTINSON	535
Digital computation of surface topography. H. KALISZER, D. J. GRIEVE and G. W. ROWE	543
Choosing manufacturing resources. G. A. E. SEWELL	551

METAL FORMING

The analysis of rotary forging investigations as an aid to design. E. APPLETON and R. A. C. SLATER	557
Tool-life test in clamp shearing of steel bar and wire. T. NAKAGAWA and K. MIYAMOTO	567
Elastic stresses at seals in plain and necked open-ended cylinders under internal and external pressures. B. LENGYEL and D. C. HARVEY	573

INDEXES

Authors and contributors	581
Technical	583

INTRODUCTION

I am delighted that Professor Opitz has accepted our invitation to present the opening address to this Conference. As a scientist, researcher, teacher and adviser to universities and industry Professor Opitz needs no introduction. The laboratory which he created after his appointment to the Chair of machine tools and production technology at the Technical University Aachen in 1936, and which today is one of the most, if not the most important laboratory of its kind in the world, can speak louder and with more emphasis than any words of mine could hope to achieve.

There is practically no aspect in the academic and industrial field concerned with production engineering which has not in some way been positively influenced by the work carried out in the Aachen laboratory. His studies of tool wear and machinability have resulted in the development of new methods and materials. His research into high speed grinding has led to considerable progress both inside and outside Europe. His proposals for and contributions to workpiece classification, part family manufacture, group technology, computer-aided design and NC programming languages have enhanced the efficiency of many industrial organisations.

When last June Professor Opitz mentioned that the 1971 Aachen Kolloquium may be the last to take place under his leadership our selfish interests made us suddenly think of the fact that the 1971 International Machine Tool Design and Research Conference in Manchester may be the last which he would attend when still in office at Aachen.

The organisers of our International Machine Tool Design and Research Conferences owe a particular debt of gratitude to Professor Opitz, because from the first and very modest beginning until today he has given us not only his wholehearted support, but also his active participation to every one of the 12 conferences which took place between 1960 and today. His positive contributions have enhanced the value of the conferences and his moral support has given great encouragement to the organisers.

I must mention in this connection that we in Manchester are especially indebted to Professor Opitz for his advice as external examiner in our post-graduate courses which has strengthened the impact on our young engineers who specialise in the field of machine tools. I am also sure that the regular

exchange of staff between Aachen and Manchester has been of benefit to all concerned.

During his long and distinguished career Professor Opitz has been invited to carry out many duties which not only brought honour to him but also great benefit to those for whom they were performed. Mention may be made of his two terms of office as Rector of the Technical University Aachen, his membership of many research committees and working groups at national and international level and in particular his Presidency of the International Institute of Production Engineering Research (CIRP). Universities and public bodies of many countries have honoured him; the Universities of Louvain, Strathclyde and Cincinnati have conferred on him honorary doctorates, and we are particularly proud that he also accepted the honorary fellowship of UMIST. In addition to this he has received many decorations from engineering associations and governments.

Through the success of his work Professor Opitz has proved that the needs of the machine tool manufacturing and user industry can be fully covered only if the approach of a teaching and research unit is geared towards its special problems rather than being dictated by the requirements of a general engineering discipline. We are aware of the fact that Universities must play an ever increasing part in the development of machine tool technology as well as production engineering in this country. We know that this can be done most efficiently only if the role of the university, both in the line of research and teaching, is backed by efforts to anticipate the needs of this specialised field. Professor Opitz has proved that this is possible if a committed and professional interest exists across a diversity of the disciplines involved and if work is planned and carried out in an independent manner completely devoted to the needs of the machine tool manufacturing and using industry.

We at UMIST have every intention of continuing to work along this path on which regrettably we have only been able to proceed at a relatively slow pace. We have no doubt, however, that we shall succeed in achieving the aims which we set ourselves and for the purpose of which we are organising this conference. It gives me great pleasure to ask Professor Opitz to declare the 12th International Machine Tool Design and Research Conference open.

F Koenigsberger

OPENING ADDRESS

Professor Dr-Ing, Dres hc, H. Opitz, *Laboratorium für Werkzeugmaschinen und Betriebslehre der Technischen Hochschule Aachen, West Germany*

Production engineering in industry will soon have to undergo some considerable changes because in the long run it will be impossible to adapt by conventional means existing production plant and equipment to future requirements. Forecasts for the year 2000 predict a nine-fold increase in turnover compared with 1960; at the same time only a small increase in population has been predicted for industrial nations. With decreasing working hours this situation leads to the necessity of increasing considerably the required productivity per worker.

Moreover, it is known that the cycles of innovation become shorter and shorter and only those who will realise future developments in good time and adjust themselves accordingly, will be able to survive. It is also necessary to stress here the fact that we do not aim at technical progress merely for its own sake but that economic and social political requirements demand a higher volume of production at lower costs for the single product and with reduced human effort. It is clear already today that these tasks will only be solved in the near future by a much wider application of electronic data processing equipment in all fields of industrial organisation, as this will no doubt become the foundation for the rationalization of the whole production process. The term 'production process' covers in this connection all activities which are immediately concerned with the manufacture of a new product from design and production planning to complete manufacture.

The development of the necessary basic principles on the one hand for the design of suitable manufacturing systems, on the other, for the provision of the necessary hardware and software, will be a major task of the machine tool industry in years to come. It will, however, no longer be possible to carry out this task within one industrial organisation, due to the actual size of the companies in question.

The development of the last few decades has shown that the path leading to success in research and development has become more and more difficult. The effort for each improvement increases correspondingly to the concept of diminishing returns in such a manner that, different from former times, even a small step forward is only possible at very high financial effort.

Taylor could achieve his pioneering successes, when he developed high speed steel, without great cost by using the production plant in his workshops for his experiments. Today research and development in the field of production engineering requires not only highly qualified staff but also very costly plant and equipment. The necessary means are so considerable that a single company can provide only part of it at the most. The only way to success—this is an unavoidable condition for survival in the markets of tomorrow—is an all embracing co-ordination of all efforts in the fields of research and development, in which industry, universities and government departments work closely together and join in making available the required financial means.

These problems must be solved by *co-operative* research because they are of a fundamental nature and generate new solutions. When planning the necessary work it is, however, important to guard against too narrow a concept of 'fundamental research' purely for ideological reasons. With the increasing complexity of the problems which have to be solved, the boundaries between fundamental and applied research become more fluid, especially in view of the fact that the scientific methods are always the same.

Within the framework of such plans the single company will have enough scope to adapt the jointly found solutions to its specific requirements and to amplify them by further development. For this reason such co-operation need not lead to a reduction in the ability of the various companies to remain competitive with each other.

This concept of University-Industry collaboration has proved very successful in Germany. As an example you may be interested to know that after more than 35 years of such co-operation, today a considerable proportion of my laboratory budget is in fact financed by research contracts from industry. I must stress that in this connection the consultative activity of the laboratory plays a very minor role. The majority of the contracts are research projects based on a systematic and fundamental approach, and they are frequently extended over several years.

Our research activity in Aachen covers the very wide range of work needed by our metalworking industry. The research staff are divided in four groups which are devoted to the problems of production control and management, metal cutting, machine tool design and numerical control. There is also a comprehensive supporting staff. The machine tool design group, for example, is concerned with a range of investigations into the behaviour of machine tools including studies of chatter, kinematic accuracy, the static and dynamic stiffness of structures and the design of machine tool components.

The manner in which the different projects are in fact approached will always be adapted to the specific requirements. For example in the field of gear wheel and gear drive investigations a working group has been established between the laboratory and the majority of well known German manufacturers of gear cutting machines and gear drives. This working group deals with problems which are of interest to all. The current range of studies include the determination of gear drive stiffness, the life testing of gears and the optimum design of bevel gears. Once a year the results are presented at a working meeting and subsequent progress planning adjusted accordingly. This is one example of many.

The co-operation between the laboratory and single firms or whole groups of companies has proved most advantageous to all concerned. The continual and close contact generates a lively exchange of opinions between the partners. This assures on the one hand that the research work is oriented towards the needs and possibilities of practical industry, on

the other if offers the participating companies the very important opportunity of recognising the latest trends and considering them within their own development work. The participation of Government departments in the financing of many projects also ensures that the research results will be available to all those who are interested. There is in fact an obligation to publish, generally immediately, but at the latest within two years of completing a project.

Such research projects can be carried out to the benefit of all concerned only when they are tuned to the needs of all partners. Some specific requirements put forward by companies who provide financial support may, of course, be accommodated within limits. The partnership with the industrial organisation must not result, however, in the freedom of research at universities being restrained. From my many years experience as Director of the Aachen Laboratory. I can state without hesitation that insoluble conflicts between the interested parties can always be avoided when the discussion is maintained at a factual scientific level. To date it has always been possible to come to a general agreement and I have no doubt that this will also be the case in future.

In conclusion may I emphasise the following point. The task which I have sketched requires that the specifications for staff and equipment of a successful research laboratory in the field of machine tools exceed those normally encountered in classical mechanical engineering. On the other hand the rapid technological developments have led to a considerable splintering into many special subjects. However the complexity of the problems which must be solved in connection with the new manufacturing methods and technological processes requires close co-operation between the various specialists because a single person will rarely if ever be able to solve all problems on his own. Interdisciplinary co-operation must, therefore,

be a basic principle in all research laboratories. The combination of scientific fundamental work in different fields is one of the most important foundations for successful research in engineering as a whole. This is why advances in production technology would be impossible without the co-operation of such different disciplines as classical mechanical engineering, materials science, electronics, control engineering, as well as factory organisation, management and economics.

For these reasons I am convinced that the re-organisation of the machine tool division at UMIST as planned by my colleague Koenigsberger represents an important step in the creation of a forward-looking concept for such a research establishment. From my experience over many years I can, therefore, strongly recommend the realisation of these plans.

When work of the kind I described is proceeding at a satisfactory level and an acceptable rate, there remains still the problem of communication between the various interested people. It is over twenty years ago that we started for this purpose the Aachen Machine Tool Colloquia. Over the years we modified the arrangements until we had arrived at what appeared to us the most efficient form of communication. Nevertheless, the undoubted success, which is perhaps best expressed by the number of participants consistently growing until this year we had some 2000 people taking part, seems to indicate the value which industrialists and research workers attribute to such occasions. I have, therefore, watched with particular interest the progress of your International Machine Tool Design and Research Conferences in Birmingham and Manchester, and here again I am convinced that you are proceeding in the right direction. It gives me great pleasure, therefore, to declare the 12th Conference open and to wish it every success.

ADAPTIVE CONTROL

ADAPTIVE CONTROL FOR TURNING OPERATIONS

Dr. Ing. A. LEDERGERBER* **

SUMMARY

This report initially deals with the basic considerations which have led to the development of control systems allowing more automation of the machining cycle than was possible in the past. A description of the system used for a new adaptive control indicates that such adaptive control of machine tools not only caters for optimized automatic production but also considerably reduces the programming effort, in comparison with the conventional programming, when the distribution of cuts is not automated.

The results of a cost comparison for machining two workpieces show that the economical advantages which can be achieved by employing adaptive control for turning operations justify investment in such systems.

Increasing utilization of adaptive control systems in their different versions is to be expected, precisely because such systems contribute towards the automation of small batch production, and therefore consistently expand the development trends originating from the introduction of numerical control.

INTRODUCTION

Efforts towards the development of new production techniques have a common aim, namely, to produce the workpiece defined by the designer in the form of a drawing with the requisite accuracy, while involving the least possible effort and expenditure. Thus, very highly automated methods and machine set-ups were developed some considerable time ago, in particular to deal with medium and large batch production problems. In comparison with machines in small-batch or one-off production, such machine systems operate at lower production costs per workpiece. This is possible because the machines use, as well as their tooling equipment and information, stores such as cams, stops or trip-dog rails, always designed for machining only one specific workpiece as defined by the drawing. As a rule, test runs are carried out to optimize the production cycle before starting up the machine system, and final corrections are made during the setting of each machine, these corrections being necessary to fulfil the intentions shown in Fig. 1. As regards adaptive control, the following points are of particular significance:

Feed and speed corrections in order to:

- shorten cutting times;
- cater for tensile strength differences in workpieces originating from different charge batches or to cover definite workpiece zones;

- adapt machining data to output capacity and dynamic behaviour of the machine;
 - adapt to the 'state of wear' of tools; achieve the required surface finish and profile accuracy.
- Accordingly, corrections of tool traverses and tool

<p>I FEEDS AND SPEEDS</p> <ol style="list-style-type: none"> 1. Shortening of cutting times 2. Adaption of tool life periods for various tools in a tool set 3. Tensile strength differences of workpieces originating from different charges or differences over certain workpiece zones 4. Adaption of machine output rating and its dynamic behaviour 5. Adaption of state of wear of tooling 6. Achievement of prescribed surface finish and profile accuracy 7. Improved chip disposal 	<p>II TOOL TRAVERSES AND POSITIONS</p> <ol style="list-style-type: none"> 1. Shortening of idle times 2. Catering for modified blank dimensions 3. Dimensional corrections caused through <ul style="list-style-type: none"> (a) deflections (b) tool wear <p style="text-align: center;">III WORKPIECE HANDLING</p> <ol style="list-style-type: none"> 1. Catering for modified blank dimensions 2. Shortening of idle times
---	---

Fig. 1 Correction of production systems.

*Werkzeugmaschinenfabrik Gildemeister & Comp. AG., Bielefeld

**Translated from the German by: J. H. Hayes, CEng. FIMechE, FIProdE, FIL, Hayes Engineering Services, 7 Hawtrees, Radlett, Hertfordshire.

positions are effected to avoid idle traverses and thus idle times. This is of particular importance when blank dimensions change or when these differ within a batch.

For one-off and small-batch production, these considerations are essential in view of production costs, because in these cases the causes for any corrections required are the same. However, the salient difference is in assessing the economy of a change in machining data.

In terms of economics, correction is not justifiable if effort and expenditure for establishing the need and for carrying out the correction are greater than the result ultimately achieved. Consequently—and especially in one-off and small-batch production—subsequent adaption of production data is the more justifiable in economic terms, the more rapidly and accurately the need can be established and correction effected.

THE OBJECTS OF ADAPTIVE CONTROL

In conventional programming—quite independently of program storage method—all data such as speeds, feeds and traverses must always take into consideration the extreme values occurring within a work-piece batch. To give an example, Fig. 2 shows the

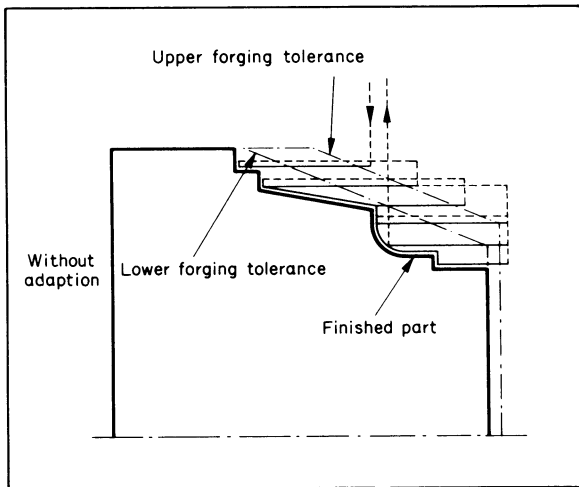


Fig. 2 Conventional distribution of cuts on forged blanks.

conditions when setting the traverses for turning forged blanks. To make sure that the tool does not traverse on any of the workpieces within a batch 'into' the blank at rapid traverse rate, the changeover from rapid traverse to working feed has to occur at a coordinate point outside the maximum blank tolerance. As a result, the tool has to cover a greater or lesser idle traverse after changing over to working feed and therefore 'cuts air' on most of the workpieces. The time required for this is irretrievably lost. Similar conditions apply with regard to cutting speed and feed-rates on workpieces with varying hardnesses or in the case of tool wear.

It is the object of any adaptive control to improve these conditions, and to influence the machining cycle in such a way that the cycle is optimized, considering fully all those factors which affect it.

Making such an ACO (Adaptive Control, Optimiz-

ation) system a reality would demand expenditure which at this stage cannot yet be fully appreciated, and which is only likely to be justifiable in extremely rare cases. In practice, it will suffice to optimize the machining process within pre-established limits and with regard to certain machining parameters. Whether in this case only one or several variable factors are included in the control depends on the machining operations involved and on the result of economic calculations.

A control system of this type would be defined by ACC (Adaptive Control, Constraint).

Regardless of whether attempts are made to provide an ACO or ACC system, it is initially essential to clarify how the machining process is to run off and what influence the individual machining parameters are to have. Answering these questions represents the actual problem and at the same time the key to its solution. The result of this initial, and simultaneously most important partial solution, is the definition of an adaption programme which determines the criteria controlling the adaption process.

ACC for turning operations

The following details are intended to describe a method employed for adaptive control in turning. In comparison with known adaption methods, the salient difference lies in the adaption programme used, this obviating extensive computer operations.

In this case, the adaption programme starts out from a constant pre-selected cutting speed. The speed of rotation is then adapted in relation to the work-piece diameter handled and this through a variation facility and d.c. drive. The significance of a pre-selected cutting speed is indicated by Fig. 3. The 3-D

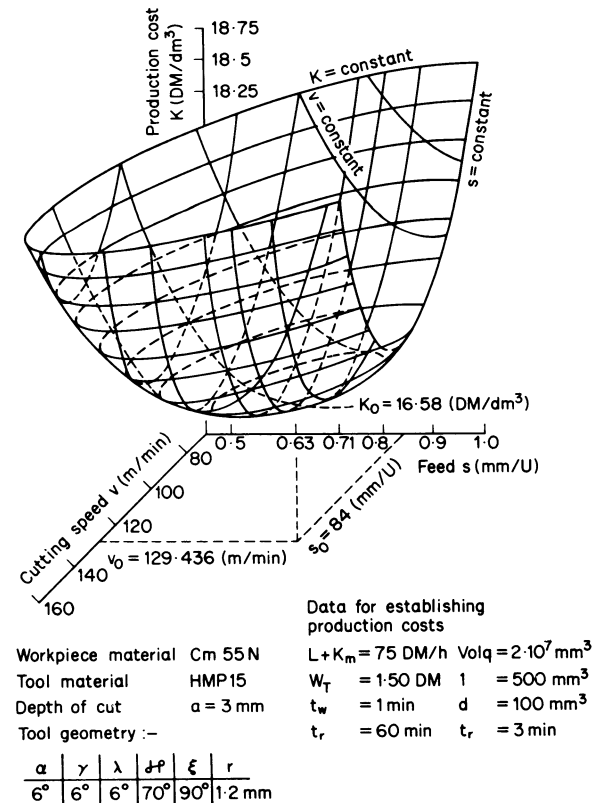


Fig. 3 Machining conditions and production costs (after Koenig-Depierreux).

graph clearly indicates that as far as production costs in machining a certain material are concerned, there is only one optimum cutting speed. Moreover, the illustration also indicates the influence of the feed-rate which represents an optimum value in terms of minimum production costs¹.

In establishing the adaption programme, recognition of the above facts is reflected in that the variable adaptive feed-rate must suit the pre-selected cutting speed—it must also:

(a) allow pre-selection;
and (b) be so arranged that feed-rate variation during adaption can only occur over a limited and pre-selected range.

These restrictions would make the utmost permissible machine loading demanded by the utilization of an adaptive control system doubtful if monitoring of depth of cut is not also included in the adaption programme.

Insofar as the finished part contour permits, depth of cut is controlled in relation to the permissible work spindle torque in such a way that the feed simultaneously cannot exceed or fail to reach the acceptable range.

The control diagram is shown in Fig. 4. It can be seen that machining is monitored by picking a measuring signal (torque) off the spindle, while simultaneously keeping speed under observation. For certain machining operations, such as drilling small holes or tapping, very small torque changes may have to permit evaluation for tool monitoring purposes. Because the torque picked off the work spindle cannot be utilized for this purpose, it may in such cases be desirable to cater for appropriate tool load monitoring with the aid of measurement data transmitters incorporated in the tool mount. This is indicated in the illustration by a dashed line representing the measuring signal of the cutting force. When running a workpiece programme involving several different tools, it would then be necessary—depending on the tool called up—to bring the appro-

prate measurement data transmitter into the monitoring process.

Fig. 5 shows a turning machine with ACC system which was introduced for the first time to the engineering public on the occasion of the 1969 Paris exhibition. In view of the economy of this machine, the many different blanks, widely varying in shape as is shown by the illustration, are noteworthy.

The adaption programme used with this technique permits the preparation of a punched tape independently of the blank shape. This decisive advantage is achieved through automatic distribution of cuts as shown in Fig. 6, orientating itself in relation to maximum acceptable stock removal rate. Contrary to conventional production in which the programmer has to take into consideration in the programme the most unfavourable upper forging tolerance expected, the new adaptive control with distribution of cuts automatically caters for fluctuating forging allowances in such a way that the tool either covers idle traverses at full rapid traverse rate, thereby avoiding the 'cutting of air', or machines the workpiece at the pre-established stock removal rate.

To provide some idea of the processes involved in this new ACC system it is of help to highlight and briefly explain two machining aspects.

One of the most important processes is starting the cut in the blank contour. Here, to achieve the desired reduction in machining time—the turning tool is moved at rapid traverse rate, beginning at a starting point remote from the blank, right up to first contact with the workpiece, quite independently of blank contour.

Fig. 7 shows the relationships which are of interest here. The left-hand illustration indicates three important phases in starting the cut.

1. The programmed starting point remote from the workpiece contour.
2. The point at which the cut begins; that is, the point where the tool first touches the workpiece.
3. The changeover point.

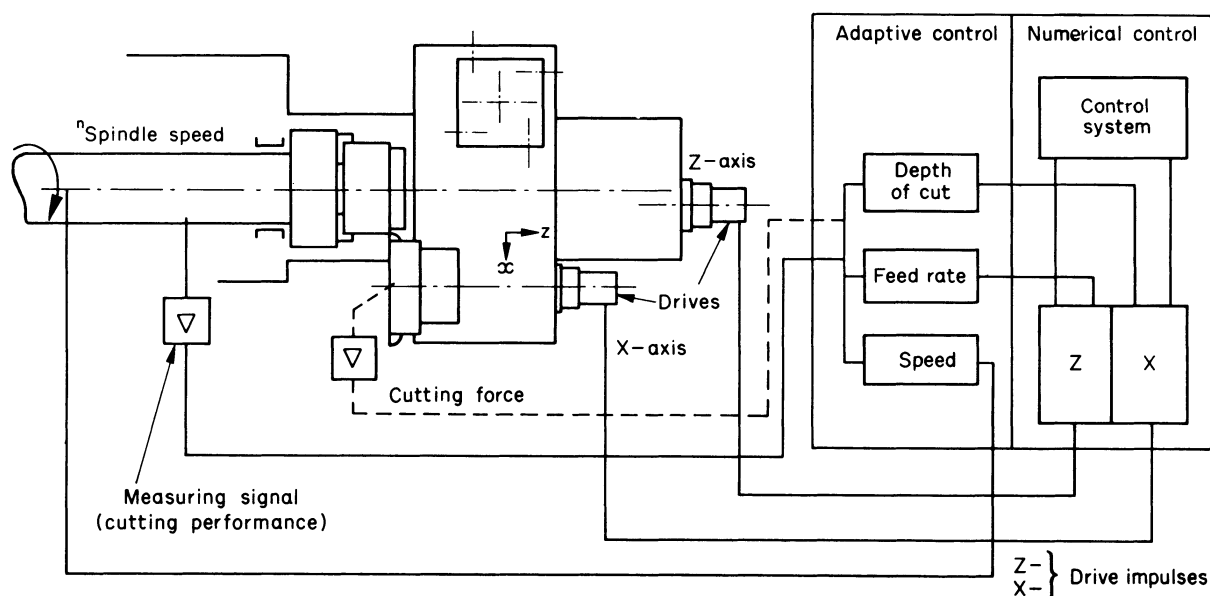


Fig. 4 Adaptive control for turning machine.

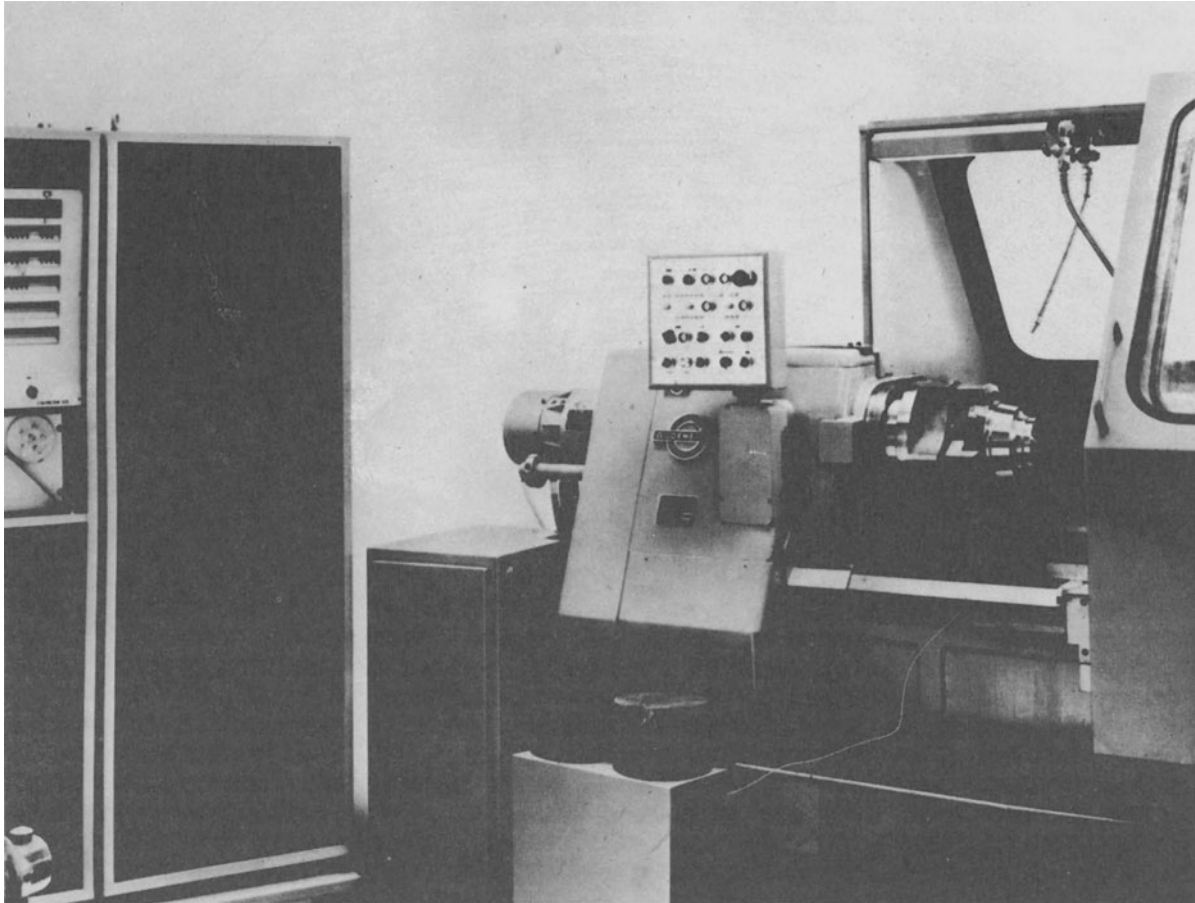


Fig. 5 Turret turning machine with adaptive control.

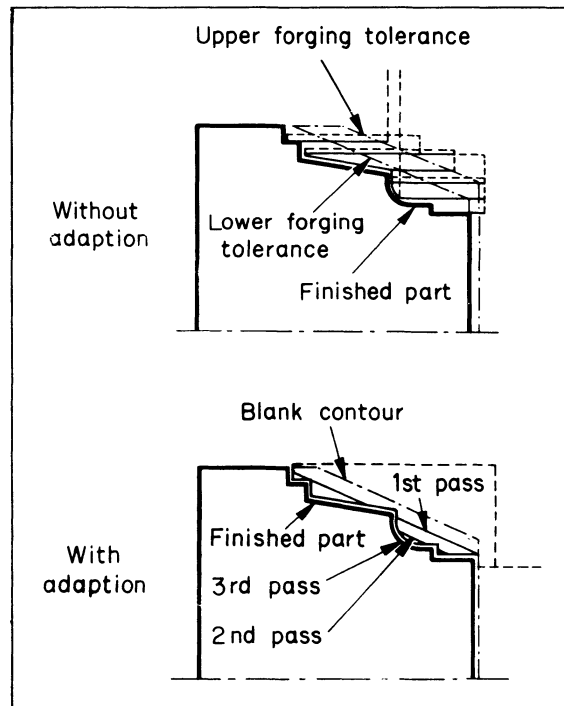


Fig. 6 Distribution of cuts on forged blanks.

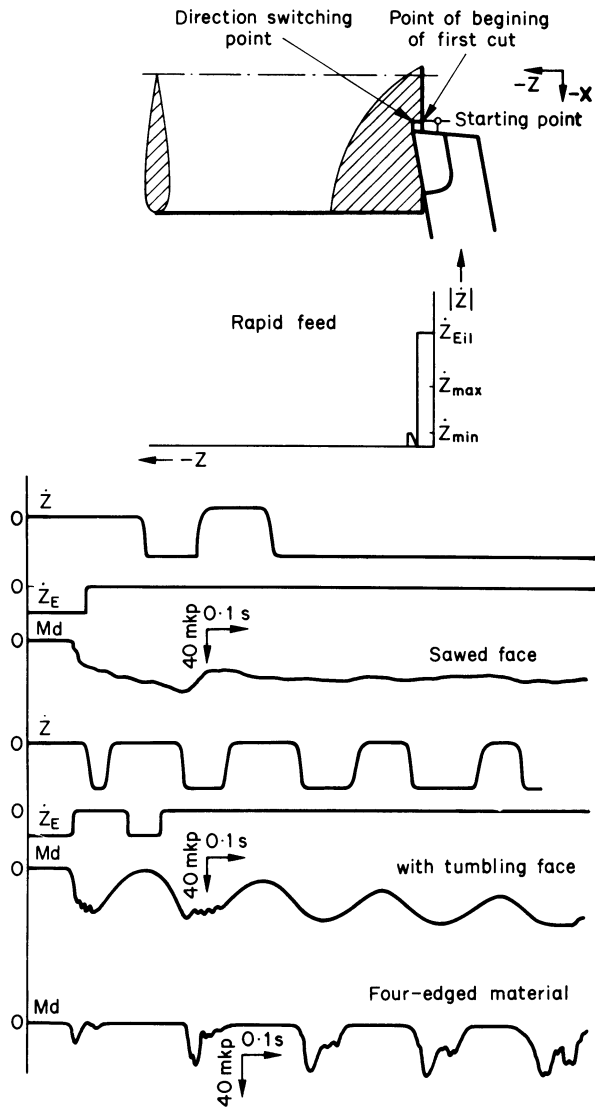


Fig. 7 Start of cut on workpiece when turning with adaptive control.

As mentioned already, the tool moves from the starting point towards the workpiece at rapid traverse rate. As soon as the tool point touches the workpiece, a torque build-up occurs, which is measured by a highly sensitive measuring device in the turning spindle. The increase in torque is used to stop the rapid traverse instantaneously. A timer element in the control system maintains this 'stop'—to allow the tool to cut itself free—until the workpiece has completed at least one revolution at the lowest programmable speed. Subsequently, the tool is moved in the minus z -direction, with the smallest programmable feed so that the torque can increase.

This torque build-up now continues up to the programmed maximum permissible torque. When this value is reached, the feed is stopped in the minus z -direction and changed to the plus x -direction. For longitudinal machining, the values for \dot{z}_{max} and \dot{z}_{min} are freely programmable on the basis of the relationships indicated in the 3-D graph (Fig. 3), but dependent on workpiece and especially on workpiece material. These two limits indicate the variation range over which the feed-rate is automatically controlled in relation to the measured torque. When the adaption

system reaches one of these limits, there is either a reduction in the depth of cut in the case of reaching \dot{z}_{min} or a depth of cut increase in the case of reaching \dot{z}_{max} .

In describing the 'start of cut' process it is pointed out that the feed is initially stopped. This is important on account of the widely varying workpiece faces which might—without the 'stop'—lead to destruction of the tool.

The right-hand half of the illustration shows the diagrams of torques measured and variations in feed-rate. The different torque characteristics applicable to a sawn workpiece face and to a workpiece with face run-out are evident.

For research purposes into the 'start of cut' conditions, an extreme situation producing maximum possible inaccuracy was produced by eccentrically welding a square block to a plate, then machining this assembly with the adaption system described. The lowermost diagram illustrates the torque characteristics. (The diagrams for rapid traverse and feed are not included in this illustration.)

Although it is impossible to go into more detail within the framework of this paper, Fig. 8 shows diagrammatically the adaptive machining of a workpiece with varying machining allowance.

Through the advantages outlined earlier, that is the fact that the workpiece programme need only cover the shape of the finished part contour and the fact that there is automatic distribution of cuts, the control system can recognize the point at which the turning tool starts to cut within the zone of the finishing pass machining allowance.

Fig. 8 shows that when the remaining workpiece contour requires no further machining, the tool is

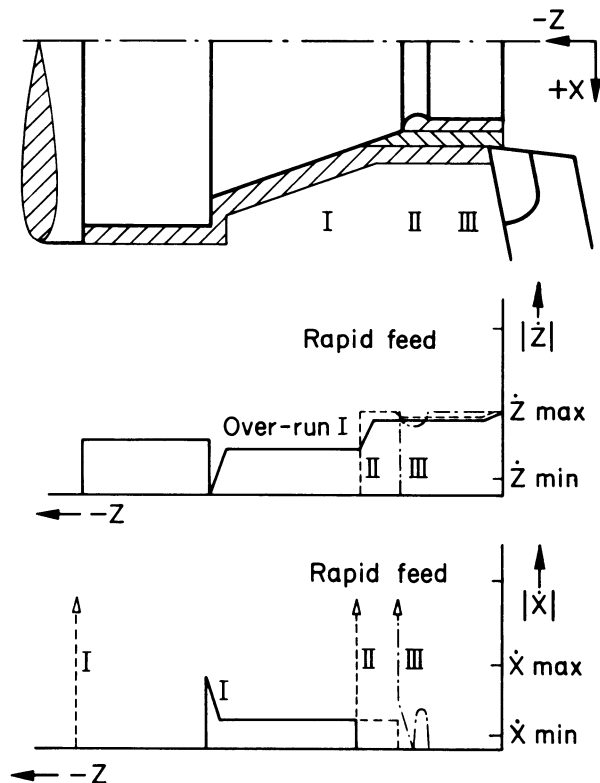


Fig. 8 Distribution of cuts on workpieces with varying machining allowance.

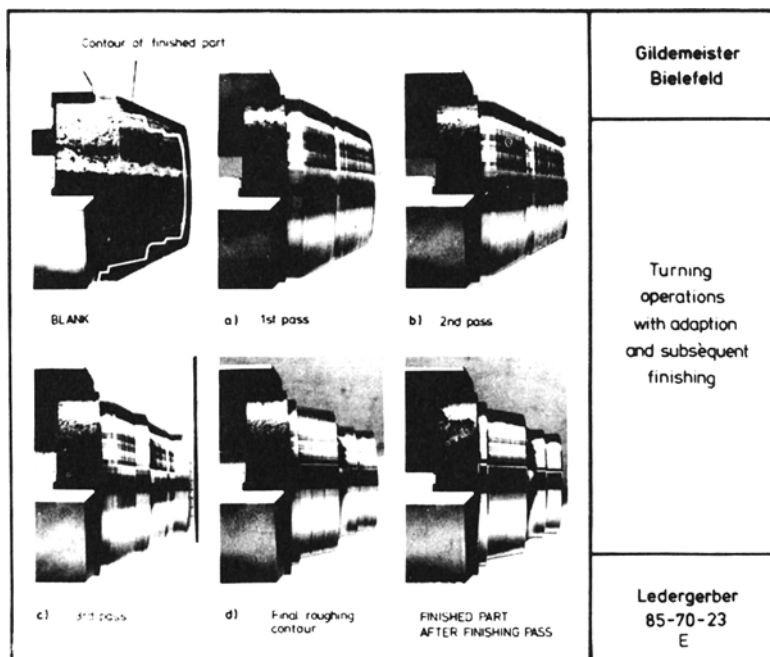


Fig. 9 Adaptive turning with subsequent finishing.

automatically and instantaneously traversed back into its starting position where a further in-feed occurs.

The conditions are similar when the workpiece should be finish-machined at the start and further operations are then to be carried out at its centre or end.

Fig. 9 shows a workpiece which has been photographed after each pass. The actual adaption phases appear in photos *a-d*. The first photo shows the tapered blank and the last the finished workpiece.

The illustration indicates that adaption is only effective during roughing of the workpiece and that the tool will follow the appropriate contour on reaching the finishing machining allowance. In those zones where full depth of cut cannot be attained, the adaption programme tends towards maximum permissible torque by increasing the feed where necessary to the maximum permissible rate.

The reason why the ACC system is only used within the roughing phase lies in exploiting the technique within its economical range and primarily in the fact that workpiece tolerances call for a different tool for the finishing operation to that used for roughing. The finishing operation which follows roughing is programmed conventionally. No time losses are incurred in finishing because this operation starts with an accurately defined machining allowance and the cutting speed is kept constant. Moreover, the feed-rate cannot be adapted to torque during finishing but must be laid down in line with the expected surface finish and cutting tool geometry.

The description of the method so far submitted was intended to highlight the potential advantages of simplified programming and the saving of idle time. This is now followed by an economy calculation indicating the savings possible in numerical terms.

COMPARING THE ECONOMICS OF TURNING WITH AND WITHOUT ADAPTIVE CONTROL

The economy comparison presented here deals with machining the forged stub axle blank—as discussed earlier—but also, as a supplement, the roughing operations carried out on a lathe spindle. The calculation is thus based in each case on a forged blank having a number of preformed shoulders. The profile and dimension tolerances achieved in forging are assumed to comply with the DIN 7527 tolerances laid down for open die forgings. Two batch sizes of $n = 10$ and $n = 20$ off are taken into consideration.

Pure machining costs per workpiece are particularly affected in the case of both workpiece types by the blank tolerances to be expected within a batch and the calculation is based on normal tolerance distribution. Although in the conventional distribution of cuts it is always the maximum deviation in the tolerance pattern which is decisive, machining with the ACC system described here can take the centre of the tolerance pattern into consideration when calculating running times.

Fig. 10 shows, in tabular form and for comparison purposes, the time constituents for the various activities involved in manual programming of both workpieces in this economy comparison. The table shows the savings mentioned earlier, which are the result of largely automatic distribution of cuts in programming the roughing operation with adaption. Accordingly, the time required for the items in lines 4 and 6 is shorter. Moreover, line 9 shows that less time is likely to be required for writing the print-out. The simplified programme also reduces the possibility of errors and leads to a more rapid check of programme, tape

and print-out. Any programme changes which may become necessary can also be made with less effort and more cheaply.

A comparison of the total times shows that savings in manual programming represent 25% in the case of the stub axle and 33% in the case of the spindle.

Activity (manual)		Stub axle		Spindle	
		S3	S3/AC	S3	S3/AC
1 Order clarification	(mins)	15	15	15	15
2 Considerations prior to processing	(mins)	10	10	10	10
3 Establishing the production media	(mins)	5	5	5	5
4 Cut distribution and co-ordinates for roughing	(mins)	20	11	45	18
5 Cut distribution for finishing	(mins)	28	28	31	31
6 Feeds and speeds for roughing	(mins)	13	3	31	5
7 Feeds and speeds for finishing	(mins)	15	15	32	32
8 Program check	(mins)	20	14	30	20
9 Produce tape and write print-out	(mins)	15	9	26	16
10 Checking tape and print-out	(mins)	10	6	18	11
11 Program modification	(mins)	30	20	30	20
Total time (mins)		181	136	273	183

Fig. 10 Comparison of programming times.

When calculating the hourly machine rate, extra expenditure caused by the auxiliary control—including the necessary measurement data transmitters—must be considered. The finishing operation must also not be ignored in this calculation, because higher finishing costs will apply in spite of the identical running times; this is because of higher hourly machine rates.

When taking these provisos into consideration, the calculation—depending on the number of repeat orders—showed notable savings in machining both workpieces.

Fig. 11 shows the potential annual savings in double-shift production for two batch sizes in relation to the number of repeat orders when machining the stub axle or workpieces of similar shape in the ACC system. Although there is not much practical experience to go on so far, the illustration clearly

indicates, even at this stage, the economical advantages of this innovation which can be achieved through simplified programming, particularly when low numbers of repeat orders are involved.

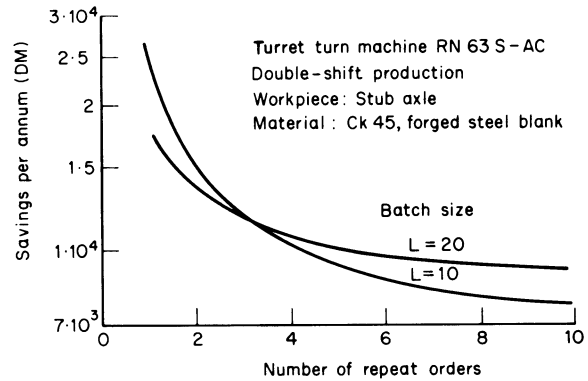


Fig. 11 Savings in production costs through adaption.

REFERENCES

1. KOENIG, W., and DEPIEREREUX, W. R., 'How can feeds and cutting speeds be optimized?', *Industrie-Anzeiger*, 91, 61 (1969).

DISCUSSION

Query from W. S. Blaschke, N.E.L.

The paper refers to only one feedback measurement. Therefore, only one control function can be influenced at a time. What is the strategy for controlling depth of cut, feed and speed?

Reply

The adaptive programme (strategy) of the described ACC System is based on a preselectable speed. The spindle speed is automatically controlled, depending on the position of the cross-slide.

In the same way as the speed, the limits of the feed range for the feed control are preselectable. These limits are of particular impedance for AC, as depth of cut control is initiated as soon as one of these limits is reached. When, for instance, the limit for the minimum permissible feedrate is reached, a reduction of cutting depth takes place. Simultaneously, the feed is increased in order to maintain the programmed chip removal rate. The reversed procedure takes place when the limit for the maximum permissible feedrate is reached.

THE ON-LINE CONTROL OF CUTTING CONDITIONS USING DIRECT FEEDBACK

by

N. F. SHILLAM

SUMMARY

This form of adaptive control could provide a practical method of varying machining speeds and feeds, by the changing cutting conditions giving a direct feedback of cutting performance. Practical tests have been carried out on a lathe and a milling machine.

On the lathe, the control of thrust force gives improved metal removal rate and tool protection in conditions of varying work hardness and geometry.

On the milling machine, using table vibration as the sensed signal, a similarly improved performance has been achieved. A method using tool temperature control by monitoring the tool/workpiece e.m.f. is described from practical results. There are indications that tool life can be controlled, and for turning, improved metal removal rates and surface finish have been achieved.

These systems have been designed to give smoothly controlled machining speeds and feed rates even when the monitored information has large fluctuations caused by variations in workpiece characteristics.

INTRODUCTION

Direct feedback systems are not self optimising, but they do possess a measure of adaptive control in that they vary the rates of the cutting process when changes in that process occur. The systems described here have been fitted to a centre lathe and a vertical mill, both machines having previously been in regular use. Improvements in metal removal rates as a result of using these systems have been observed, with indications of the possibility of defining cutting edge life and also providing a measure of tool protection in the presence of varying workpiece machinability.

An interesting development in control technique resulted from the problems of fitting tool temperature control to the mill. When also applied to the mill table vibration control system, a new concept of metal removal rate is observed. This modified form of control will be considered for future direct feedback systems, because it is sensitive to the peak measured values and may help to remove some of the uncertainties of past observations, particularly with regard to temperature measurement.

An empirical approach has been used throughout this work and the demanded values of temperature, force, and vibration, have been fixed at an arbitrary level for a given run. In practice, the onus would be on the user to decide on the level of input to suit his particular set of conditions and objectives, which would require him to do a number of tests to find an

optimum value of input setting.

The control loops are basically zero-order type, having variable open-loop gains caused by the non-linearity of the measured quantities. So far, only proportional control has been used, but future systems would benefit from the addition of an integral term and an accompanying derivative term may be necessary for adequate stabilisation.

Tungsten carbide tools of the insert type have been used throughout.

DIRECT FEEDBACK APPLIED TO A CENTRE LATHE

Control of average cutting edge temperature using the tool/work thermoelectric e.m.f.

After an examination of other methods of temperature measurement, in particular infra-red, it was decided that because of the obscuration problem inherent in the cutting process, the most effective method was to use the well known tool/work thermoelectric e.m.f. This term describes the voltage produced by the Seebeck e.m.f. and relies on heating of the junction of two dissimilar metals. In order to obtain a practical level of thermoelectric power over a range of work materials it was necessary to confine this work to tungsten carbide tools.

It would be more meaningful to measure the

temperature distribution along the tool rake face, as this provides the maximum tool temperature, but the author has not found a practical method for doing this which would be amenable for use as the feedback quantity in a closed-loop system, although much work has been done by others in this area of temperature investigation¹.

The tool/work e.m.f. suffers from a number of disadvantages because of the variability produced both by tools and workpieces of nominally the same type². Some of this variability may be attributable to noisy signals produced by intermittent chip shorting and there are indications that better accuracy might be obtained if only the peak values of measured e.m.f. are used. A control system technique which enables this feature to be realized will be described later in this report.

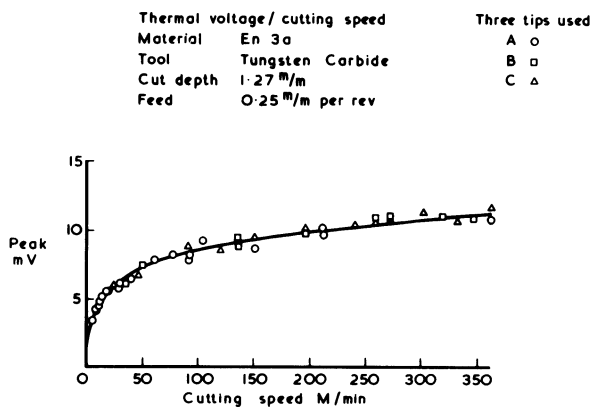


Fig. 1 Variation of thermal e.m.f. with cutting speed.

Fig. 1 shows how the peak e.m.f. varies with cutting speed and also the variability obtained between three insert tools. With regard to the latter, it should be realized that these are multi-edged tools and the total cutting life per insert can ameliorate the variability consideration. The reduction of slope with cutting speed indicates the reduction of tool forces and attainment of plastic chip deformation. At some higher value of cutting speed, rapid burn-out of the cutting edge occurs. Curves show that tungsten carbide tools allow more parts per machine hour to be produced by using higher than usual cutting speeds, thus giving comparatively short cutting edge life. It is the principal object of tool temperature control to provide some indication of tool life, which will enable a repeatable cutting process cycle to be

maintained in these conditions so that a definite number of parts can be produced before a cutting edge change is necessary.

Cutting temperature is chiefly influenced by cutting speed and this becomes the dependent variable in the control system shown in Fig. 2. This is currently fitted to a 6 in, 3 h.p. lathe. Because the ohmic resistance between the spindle and frame is much greater than that of the tool/work interface, it has been possible to measure the e.m.f. at slip rings situated on the spindle, thus allowing an uninsulated toolholder to be used.

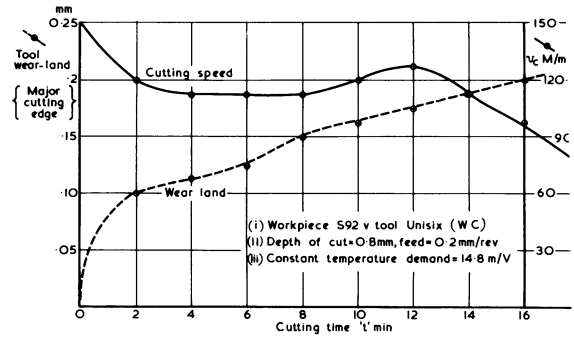


Fig. 3 Turning results using cutting temperature control.

Fig. 3 shows how, for turning, the resultant cutting speed falls after a certain value of wear land has occurred, but further experiments are required to assess how this is affected over a range of demanded input values.

The use of this system when facing, increases the metal removal rate by about 30% as a result of the fact that control of temperature results in an approximate control of cutting speed. Thus the spindle speed automatically increases as the tool approaches centre, and there is the additional benefit of improved surface finish which would make its useful on profiling work.

It should also be mentioned that the tool/work e.m.f. provides a reliable indication of work sensing for mode control and process monitoring purposes.

Control of thrust force

Because it was intended to operate both tool temperature and force control systems together, it was decided that deriving cutting force from a measurement of spindle torque would not be suitable. Acceleration torques caused by the spindle, chuck,

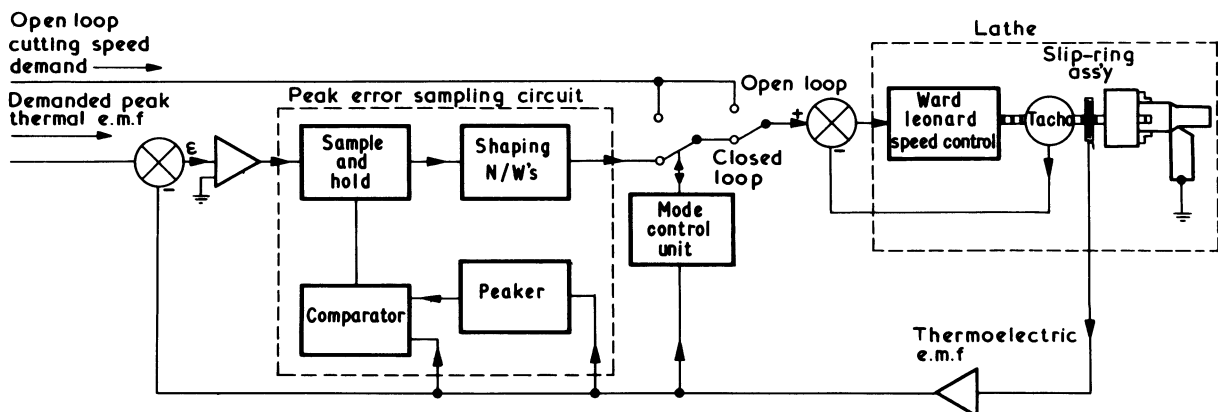


Fig. 2 Lathe cutting temperature control system.

and work inertias would produce cross-coupling between the two systems. Conventional dynamometers were not considered because of the difficulty of using them for production work. Attention was given to the possibility of instrumenting the conventional insert toolholder, and to obtain the thrust force by measuring the deflection of the nose of the toolholder. Initially semiconductor strain gauges were used with a fair amount of success but their temperature dependence necessitated the use of coolant. A more successful approach has been to use a piezo-resistive beam transducer situated at the rear of the toolholder, away from the heat producing area. Nose deflection is communicated to the transducer beam by an arm fastened only at the nose end. This arrangement is quite successful in practice and its drift properties are good enough to allow dry cutting. A thrust force of 200 N produces micro-strain of 100 resulting in an output of 20 mV from a toolholder having a shank with a cross-section of 16 X 16 mm.

This transducer arrangement forms the feedback element in a closed-loop system similar to that shown in Fig. 2, but in this system the dependent variable is feed rate and not cutting speed. Thus by demanding a particular value of thrust force the resultant feed rate will decrease with increasing depth of cut and work hardness. Fig. 4 shows the results obtained from

Material	Description	Measured U.T.S	Cutting speed	Depth of cut	Thrust force	Feed rate	Thermoelectric e.m.f
S 15	3% Ni case hardening	571 MN/m ²	120 M/min	0.9 mm	133 N	100 mm/min	13 mV
EN 32M	Semi-free cutting	680 MN/m ²	120 M/min	0.9 mm	133 N	50 mm/min	10 mV
S 28	Air hardening	1035 MN/m ²	120 M/min	0.9 mm	133 N	25 mm/min	12 mV

Tool force control

Fig. 4 Turning a composite steel bar using force control.

turning a composite bar. For interest, the value of thermoelectric e.m.f. is included.

Above a certain value, cutting speed seems to have little effect on thrust force. Also, it seems to be difficult to correlate the effect of tool wear on thrust force²; however as already mentioned for the tool/work e.m.f., a system which is sensitive to the peak values of the measured quantity may provide more hopeful indications in this respect. Such a system has already been designed and is in construction. It will enable smooth feed rates to be obtained even when turning interrupted cuts.

The object of force control is to set the demanded force to within the limits imposed by the machine power and rigidity so that the highest metal removal rates can be maintained in the presence of varying work geometry and hardness, while providing automatic protection of the cutting edge. The principal disadvantage in instrumenting the tool holder is the problem of taking the wiring from a multi-station toolpost, which will require a three pole switch ganged to the turret spigot. Thought has been given to instrumenting the compound slide to measure thrust force, and this may be developed further in the future.

Both systems together

There is no sign of instability caused by cross-coupling, provided the limits of available power are not approached and the input setting value must take this consideration into account. Fig. 5 shows the

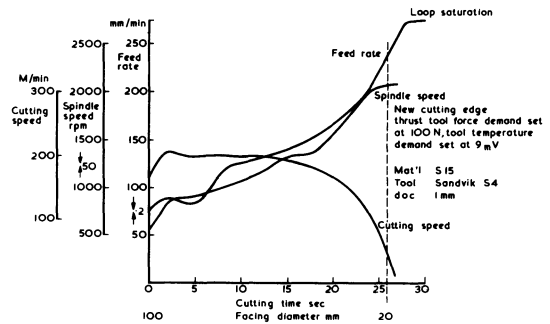


Fig. 5 Facing with temperature and force control.

results obtained from a facing cut. The main criterion here is to increase the metal removal rate while controlling the cutting edge temperature to give a predictable tool life. It is considered that this is best accomplished if both systems are used together. If surface finish is the criterion, then this is fixed by the feed value and tool force control is not needed. The relatively fine feed will give an initial decrease in tool temperature which will increase the cutting speed to achieve the required tool life.

DIRECT FEEDBACK APPLIED TO A VERTICAL MILLING MACHINE

Control of average cutting edge temperature using the tool/work thermoelectric e.m.f.

The milling machine used in these experiments was originally powered by a 5 h.p. motor through gears and belting. In order to fit the closed-loop control system, the conventional drive was removed and the spindle driven directly from a hydraulic motor developing a maximum of 3 h.p. A similar arrangement is fitted for the table drive, which is arranged to operate in one of two modes, either at a selected feed rate or at a constant feed per tooth irrespective of spindle speed. All the work described in this section has been conducted in the latter mode of feed control.

A four tooth, 2 in diameter, end mill was used and the tool/work e.m.f. obtained from a simple slip-ring assembly situated on the spindle at the top of the machine, just before the coupling to the hydraulic motor. As with the lathe, this arrangement is possible because the spindle to frame ohmic resistance is much larger than the tool/work interface resistance when the spindle is rotating. Fig. 6 shows a block diagram of the overall system.

The e.m.f. obtained from commencement of cut is shown in Fig. 7. Irregularities in the cutting behaviour of each tooth are easy to see. As mentioned previously, the interrupted nature of the cut, especially when using only one tooth as in fly-cutting, makes it necessary to have a system capable of working to the

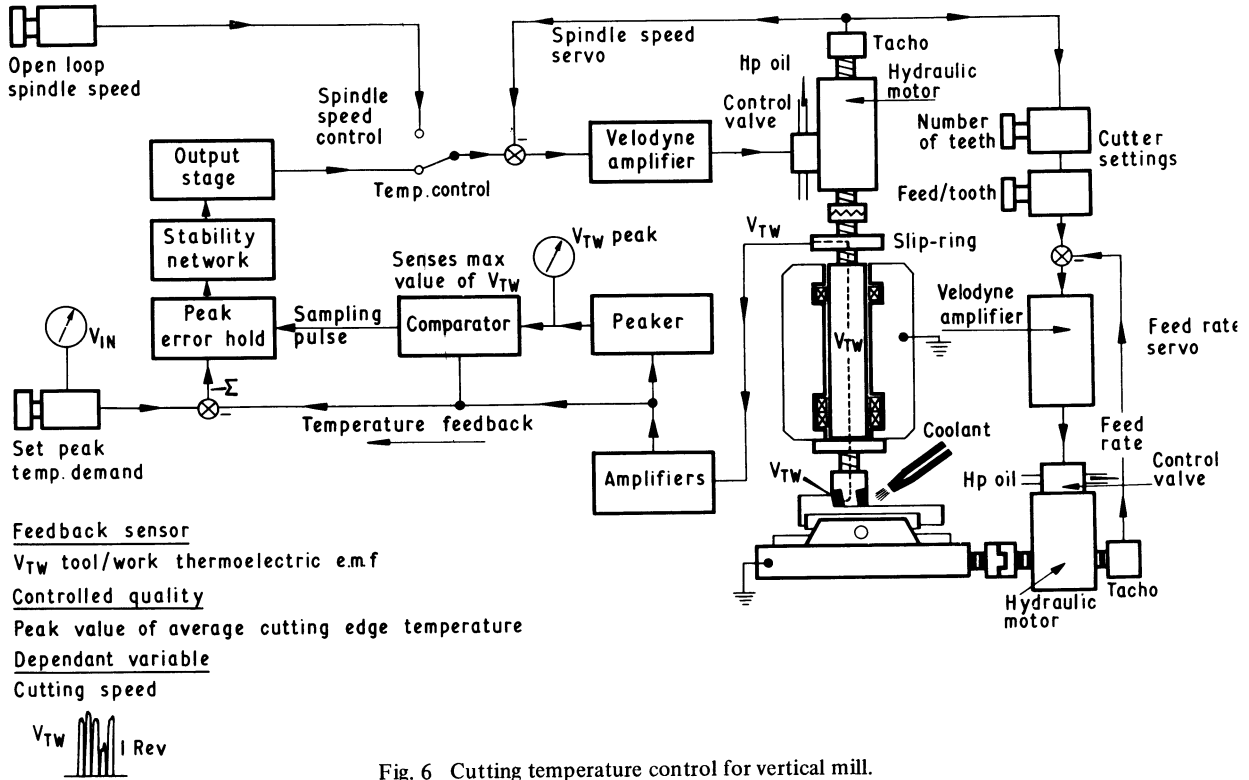


Fig. 6 Cutting temperature control for vertical mill.

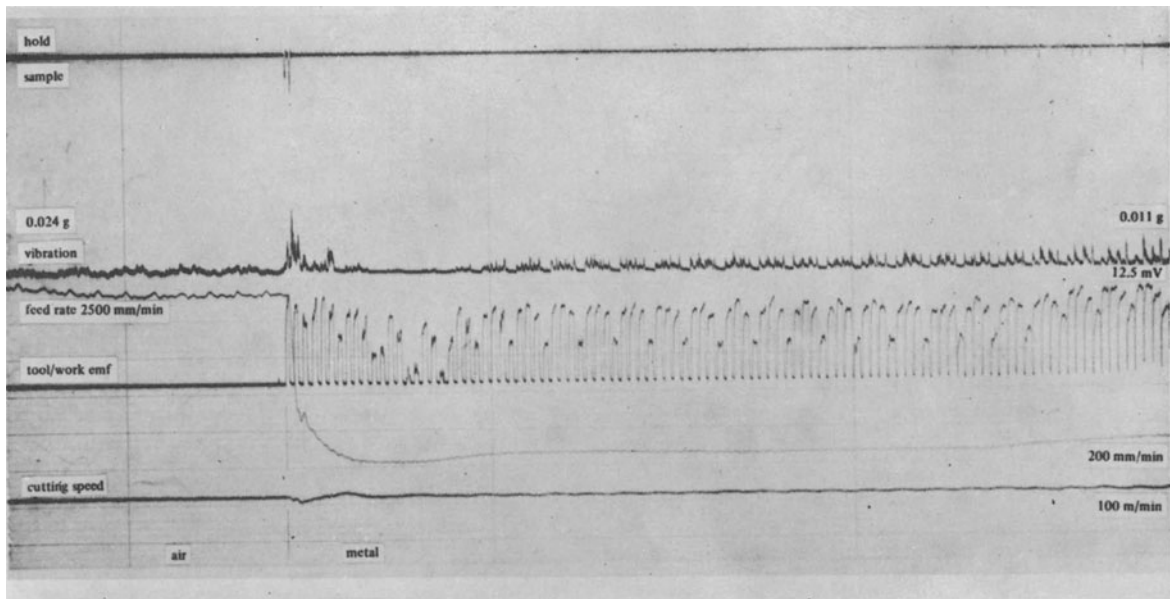


Fig. 7 Mill performance using table vibration control.

peak value of this e.m.f. rather than to some arbitrary variable mean value. The peak sample and hold of the error system shown in Fig. 6 allows the closed-loop error to be sampled only when the value of the output quantity, tool temperature, exceeds the previously held value operated on by an exponential decay term which has a time constant suitable for the process concerned. In this case, the time constant is 2s. In this way the loop error is only sampled as the output quantity approaches its peak value, so that in the extreme case of fly cutting, the system's minor loop spindle velocity servo runs on a steady speed demand during the period when the tooth is cutting air—this demand being remembered from the resultant demand for the cutting speed obtained when the

major loop was closed during the previous cutting metal period. Smooth cutting speeds are obtained both in the fly-cutting and multi-tooth operations.

Unlike the lathe, the milling application does not offer gains in metal removal rates attributable to changes in work geometry because with the constant cutting radius this factor cannot influence cutting speed. The e.m.f. output could be a useful method of monitoring the individual performance of each cutter tooth and would show up tooth damage. However, the justification for closed-loop control must be the possibility of being able to define cutter edge life with reasonable accuracy. This has been prevented so far by the existence of a spurious thermoelectric e.m.f. generated between the insert and the hardened

steel toolholder. Heat from the cutting process flowing through the interface produces a 'cold junction' e.m.f. which increases with cutting time and wear land. In the case of the lathe, this e.m.f. can be reduced to negligible proportions either by the flow of a small amount of coolant on the interface area, or by electrical compensation. For the mill, the former expedient is not so effective as coolant is thrown off the teeth by centrifugal action and electrical compensation is not practical. Work is continuing on this problem.

The effect of this unwanted e.m.f. is shown in Fig. 8, in which it can be seen that new cutting edges produce the highest resultant cutting speed and the

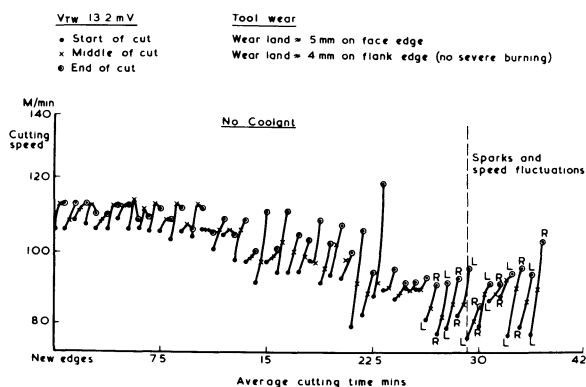


Fig. 8 Mill performance using cutting temperature control.

least increase in speed during a cut. All these cuts were taken immediately one after the other, and at a constant width and depth of cut and feed. There is a general decrease in cutting speed as wear increases and this is further characterized by an increasing speed difference between the commencement and finish of a cut. A similar test was conducted with coolant flowing. The resultant cutting speed was generally 10% lower and decreased more rapidly with time for smaller excursions of cutting speed from start to finish of the cut. This indicated that the coolant was having some effect on the spurious cold junction e.m.f. but it was noticeable that its use resulted in increased wear lands on the cutting edges and severe burning of the nose area. It was concluded from these tests that the cutting edges had a longer life when cutting dry.

After the depth of cut has exceeded twice the nose radius of the tool, further increases have little effect on the thermoelectric e.m.f.; that is, for the milling case, the variation of work geometry has little effect on the resultant e.m.f. and therefore the resultant cutting speed when in closed-loop control. One way of assessing tool life might therefore be to measure the increase in cutting speed during a cut for a given value of demanded temperature. This factor could be taken into account together with the progressively lower values of cutting speed at the start of each cut. In a more sophisticated system using an adaptive controller, these two factors could become further useful items of information describing the cutting process and could be obtained from either open or closed-loop measurements.

Control of table vibration

The original intention was to control the table feed rate, in the x direction, from a single component measurement of cutting force. Initially, an ohmic measurement of the wear land was attempted using an a.c. supply. However, the results were disappointing and a single component cutting force dynamometer using semi-conductor strain gauges was constructed. This had inaccuracies caused by table sag as well as the fact that its use was restricted by the range of workpieces it could handle. It was decided to measure the table vibration caused by the cutting forces and to see whether these could be used to control the table feed rate. It was realised at the time that these measurements are only applicable to this particular machine, but the availability of cheap and reliable accelerometers made the idea attractive as it was not necessary to alter the machine set-up in any way.

Bendix³ use an accelerometer measuring spindle vibration as an input to their adaptively controlled milling machine system but the author has not been able to find any evidence of a system using the table vibration measurement in a direct feedback control mode. It was decided to use table vibration rather than spindle vibration because this is more local to the drive member and takes into account the performance of the table structure and drive mechanism.

The accelerometer is of the piezo-electric type and consists of a suspended mass operating on a barium titanate disc. Although capable of measuring up to 100 g its use in this application is down in the tens of milli 'g' region. The accelerometer is placed to one side of the middle of the table with its sensitive axis in the x direction. In any future design, accelerometers placed at either end, possibly under the table, would be a better arrangement.

It was found that the accelerometer output increased with feed rate, depth of cut, and work hardness, in a manner which appeared hopeful for its use as a feedback element. Increases in cutting speed gave a slight increase in vibration and some of this was thought to be caused by end-play in the spindle which is known to exist. This made it impossible to judge the effect of any machine resonances which may have been present. With regard to this latter feature of a machine tool, it should be noted that the natural frequency of this accelerometer is 5 kHz which is cutoff at 500 Hz using an external filter. This cutoff figure was chosen so that the tooth ripple frequency at maximum cutting speed would not be attenuated by the transducer.

This type of measurement measures the peak level of noise or vibration imparted by the cutting process to the machine. Less transducer output is obtained if the machine is cutting quietly and this is the condition which is approached as the width of cut is increased on a cut along the centre line of a bar or when up-cutting as opposed to down-cutting. Thus, the quietest conditions are obtained when the teeth enter the cut tangentially, and the resultant feed rate obtained when up-cutting is significantly greater than that obtained from down-cutting. In cutting along the centre line with the width of cut increasing, the increasing feed rate demands more power from the

spindle drive and to avoid the possibility of stalling the drive, a constraint limit facility based on spindle power should be fitted.

Because of the spiky nature of the acceleration signal (see Fig. 7) it is necessary to fit peak sample and hold of error in the control loop which is similar to that of the tool temperature control loop, Fig. 6. Thus, the system works to the peak value of table acceleration and so differs from other systems of table control which use substantial smoothing of the transducer signal, reducing the capability of the system to operate satisfactorily at low speeds or when fly-cutting. However, such operation has proved to be possible using this system and a smooth feed rate has been produced in severely fluctuating low-frequency signal conditions.

The use of this form of control opens up a new concept of machining which may be suitable to some cutting conditions but not others. For example, its peak operating sensitivity makes it sensitive to the rigidity of the workpiece, and a lower feed rate will result from machining thin sections compared with more rigid and thicker sections of the workpiece; therefore, some control over surface finish can be expected. It is, of course, very sensitive to chatter which causes a marked reduction in feed rate and so conflicts with existing opinions on this subject.

Fig. 7 shows how, as with temperature control, a quick approach in air is possible. The presence of the workpiece is communicated instantly to the mode control unit by the production of a tool/work e.m.f. This unit then reduces the feed rate to a low value and the control loop is closed when the second sample pulse occurs, allowing the feed rate to increase smoothly under closed-loop control.

Depending on the extent of changes in work geometry, increases in metal removal rates of up to nearly 40% have been recorded. Fig. 8 shows the results from machining a wedge shape test piece.

Both systems together

Unlike the lathe, satisfactory operation using both systems together has not been obtained. This is not caused by any noticeable instability in steady-state conditions but by the fact that the table vibration increases with cutting speed and, as previously mentioned, this may be particular to this type of machine which was not designed for speeds greater than 500 rev/min, and also to spindle end-play. More modern machines are judged to reduce their vibration level with cutting speed⁴, and in this case successful simultaneous operation should be possible.

CONCLUSIONS

The author has attempted to show both the advantages and limitations of closed-loop control. There is much to be learnt from this approach and experience shows that the concept is worthy of further attention, particularly when considering the alternative of putting uncertain cutting information into a computer program or building a mathematical model of the cutting process⁵. The most likely advantages are in increased metal removal rates, some control over tool life and a measure of tool protection. There is the

further possibility of using these measurement techniques as part of an overall process plant monitoring system.

The role of these methods may be more significant in the numerical control field, where their use could lighten the programmer's load and increase productivity. In the author's opinion both systems should be used together in order to obtain maximum production benefits and protection.

ACKNOWLEDGMENTS

I thank Mr H. E. Sefton, UKAEA, for permission to publish Fig. 1, and the Ministry of Aviation Supply for permission to publish this article.

REFERENCES

1. LENZ, E., 'Temperatures in metal cutting', ASM 1968, 1, No. 4, 410. Metal abstracts on International Conference on Manufacturing Technology, 553-567 (1967).
2. SEFTON, H. E., 'A preliminary examination of measurement of the metal cutting process,' MTIRA Conference Paper 5 (April 1970).
3. Bendix Corporation Michigan, USA 'Adaptive control of milling machines,' The Tool and Manufacturing Engineer, ASTME Paper MS 68-638 (May 1969).
4. ARNT, G., 'The development of higher machining speeds,' part 2, *The Production Engineer* (December 1970).
5. ANON 'What's happening to NC computer programming,' *Metalworking Production* (September 1970).

DISCUSSION

Query from Dr. G. Barrow (UMIST)

Cutting tool temperature will of course rise with increasing tool wear. In view of this, when a constant temperature demand is made, the cutting speed will generally decrease with time as indicated by Fig. 3. This means that in many cases a reduction in metal removal rate, and hence an increase in machining costs, will arise. This is obviously not so when facing, but in this case the same result could be obtained more cheaply by employing a constant cutting speed attachment on the cross-slide.

In view of this, I should like to know whether the author has undertaken any economic evaluation studies.

Reply

My work in this field came to an end earlier this year and really was only concerned with the practicality of this form of control whilst pointing the way to economic studies. Constant cutting speed control does not take into account tool wear and could result in rapid tool burn-out, if high cutting speeds are used in an attempt to obtain a plastic chip, with the benefit of consequent reduction of cutting forces. This appears to be the desired aim of many workers in the field, of better utilisation of tungsten-carbide insert tools. The object being to cut in the temperature-sensitive region of the cutting edge, that is, where temperature is the

chief cause of tool wear. I submit that this would be a 'chancy' thing to do if only cutting speed control were used. It is true that in turning the cutting speed reduces with cutting time when using closed-loop temperature control, but studies on this have indicated that a longer tool life will result, rather than in the case of maintaining a given cutting speed.

My view of the main benefit of this form of control is the possibility of defining tool life, so that perhaps an integer number of parts can be produced, and/or certain shift tool life figures for changing cutting edges can be obtained.

Queries from Dr. Ing. M.A. El Hakim, Cairo, Egypt.

- (1) Controlling the feed through the measurement of the thrust force. It is the main cutting force which must be measured owing to its direct effect on the spindle torque as well as on the power consumption, both of which should be kept well below permissible levels. Through the measurement of the thrust force instead, as it is represented in this paper, an overloading of the machine tool under the action of the main cutting force (torque on spindle and power consumption) cannot be avoided. These criteria cannot be judged when measuring the thrust force, as it has no definite relationship to the main cutting force. On the other hand, if the cross-coupling between the main cutting force measured at the spindle and the cutting temperature control systems is liable to occur, it may as well be transmitted to the thrust force through the cutting process.
- (2) Using the cutting temperature feedback loop in turning (cause of the digressive use of cutting temperature while using cutting speed). The digressive rise of the temperature with the cutting speed is not only caused by the plastic flow of chips, as mentioned by Mr. Shillam, as it takes place in a lower range of cutting speeds as well. The main cause of such behaviour is the decreasing time of contact between the chips and tool-face.
- (3) The application of the table vibrations of a milling machine in the control loop to control the table feed.

The amplitude of forced vibration of a machine tool structure depends on the nearness of the exciting frequency (cutting table frequency) from the various natural frequencies of the system. At certain rotational speeds of the milling cutter this can be a source of disturbance. On the other side the table movement results in changing the dynamic stiffness of the structure system which may also lead to a variation in the amplitude for the same cutting conditions.

Reply

- (1) In a control loop the dependent variable, feed-rate, should be controlled from a measurement of the controlling parameter, namely feed-force,

otherwise the integrity of the system is violated. After all, the feed servomotor exerts torque to overcome the moment imposed on it by feed force, not the tangential force which is at right-angles to it. This latter force, as you infer, controls the spindle power and should therefore control cutting speed but *not feed rate*, otherwise a sensible closed-loop operation could not be obtained. Measuring the spindle torque does not produce an accurate measure of the main cutting force, since it includes the acceleration forces due to the masses of the spindle and chuck, plus the workpiece. Any dynamic out-of-balance of the system would add a further error and, as expressed in my paper, a static and dynamic measurement of tool force, be it thrust or main cutting force, must be of sufficient accuracy so that peak measurement of what is essentially a fluctuating phenomena can be a reliable mode. I agree that my system can result in overloading and here a simple measurement of main spindle motor power should be sufficient to obtain power threshold control to limit the cutting rates to a safe value.

- (2) The temperature versus cutting speed is not a linear run. The initial and final slopes vary by as much as 10:1 so it is difficult to see how decreasing time of contact of the chip can be the *main* cause. Friction effects are nonlinear in the "stick-slip" regions that are occurring here, due to the partial welding of the chip to the tool-face for a very short space of time under some low-speed conditions. The plastic flow theory relies on the fact that this condition suddenly happens and results in a decrease in the cutting forces, thus reducing the slope of the temperature (thermoelectric e.m.f.) versus cutting-speed curve.
- (3) I agree with everything said regarding the variability of the mill machine vibration; this was precisely the reason I instrumented and fitted a control-loop to govern the feed-rate from the *peak* value of the table vibration. I assume that when you say the "same cutting conditions", you mean "the same feed and cutting speed". In my system, however, this implies the "same peak vibration", measured on the table which, although not checked in theory or practice, I feel is a measure of the "transient shock load" on the cutting-edge of the tooth. Since both tungsten-carbide and ceramic teeth are prone to damage through excessive shock loads, I thought my control system of interest to users.

Query from J. Peters

The system of on-line control based on tool temperature measurements has been built and shown at the CIRP Manufacturing Seminar in Pisa.

The problem, however, is how to proceed when coolant is used on the tool tip. The Gotwein temperature measurement method is very sensitive to possible electrolytic effects of the tool-to-workpiece contact.

Reply

I am sorry that I am not familiar with the Gotwein method, and so cannot comment on this matter. However, coolant does not appear to be present at the very intimate interface of the cutting edge and the chip, and does not affect the value of the measured thermoelectric e.m.f. (see below) effect, obtained from the tool-work combination. This has been established by supplying pulses of coolant and measuring the thermo e.m.f. during wet and dry cutting. Because the action of the coolant is in the "stick-slip" effect of the chip passing over the flank tool surfaces, rather than in any noticeable voltaic action, this may be due to very low source impedance of the tool-work e.m.f. shorting-out any possible electrolytic effects. Also, if a cold-junction spurious e.m.f. exists due to the temperature rise of the cutting tool (any tungsten carbide) in a steel toolholder, the application of coolant would cause an apparent increase in thermoelectric voltage during cutting, this being due to the reduction in the cold-junction thermoelectric e.m.f. This could be mistaken for an electrolytic effect.

I think it important to realise that the electrolytic effect may be apparent when coolant simultaneously touches work and tool, without a cut being taken and the machine spindle is rotating, but this is hardly a condition to cause worry. As previously mentioned, the virtue of the thermoelectric e.m.f. method is its very low source resistance, if properly utilised, so that it effectively attenuates unwanted electrical signals once a realistic cut is being taken.

Query from R. H. Thornley

Will the author please explain how he calibrated the lathe tool force transducer. I agree that in the initial setting conditions the clamping force provided by the tool-post screws may be offset on the DC level, but surely the variation in clamping force must give a variation in tool stiffness. How is this variation in stiffness accounted for in practice?

Reply

Static calibration was obtained by clamping the tool-holder in a vice and using a dummy insert capable of taking a wire to which weights were attached, the nose of the tool being unclamped and the bending moment being defined by a shallow slot in the front edge of the tool-holder about $1\frac{1}{8}$ in. down from the nose. The two planar resistances of the piezo-resistive transducer connected in a Wheatstone bridge circuit produced a static curve with good linearity and little hysteresis (see graph). Variation in clamping forces had little effect on this curve since, in the first place, the clamping force was, of course, sufficient to prevent movement of the tool-holder in the vice, and secondly the stiffness is decided by the unclamped portion which bends about the reference slot *which must also be unclamped*. If this were not so, variations in clamping force would doubtless affect the calibration curve.

As mentioned in the lecture, if closer investigation shows that this arrangement gives unacceptable errors (although these have not manifested themselves in my work), a torque spanner approach may overcome this problem.

NUMERICALLY CONTROLLED MACHINE
TOOL DESIGN

DEVELOPMENTS IN AUTOMATION FOR NC LATHES

by

R. L. MacDONALD* and M. THORNEYCROFT†

SUMMARY

A customer's desire to purchase a numerically controlled lathe which dramatically reduced production times and had a high degree of built-in automation led to the developments described in this report being embodied in a new machine.

The most significant developments were a new twin-tool concept, a completely on-machine tool setting system which removed the need to use pre-set tooling and tool-offsets, automatic fixture location, computer-aided programming for constant cutting speeds, and rapid automatic tool changing with tool location detection.

This report describes the reasoning behind each development and gives some detailed descriptions. A general description of the machine is given. As the delivery requirements for the machine were such that a number of machines were delivered over a short period, the management methods used are described.

An indication of future developments is also given.

INTRODUCTION

Until 1969–70, numerically controlled lathes were equipped with the means of automating component geometry, changing feed-rate and spindle speed, switching on coolant supply and so on. However, if it is accepted that one of the principal aims of automation is to reduce the influence of the operator in producing a part, then the most significant parts of the production process, that is component location, accuracy of part, cutting-cycle time and surface finish, could still be altered by an operator using the auxiliary controls usually supplied (for example, tool offsets and feed-rate override).

Certain NC users wish to purchase machines automated further than normal and one asked Charles Churchill Ltd, a company within the Machine Tool Division of Tube Investments Ltd, to produce a machine specification which would fulfill their requirements. The job was handled by the Applied Research and Development Division of Charles Churchill Ltd (A.R.D.D.).

The eventual outcome was a machine having a specification which contained features designed to automate the control of the parameters already stated, and the customer placed an order for a number of these machines to be supplied on an extremely tight delivery schedule.

The fact that the initial specification included a high degree of automation meant that the design was not constrained as when normal NC lathes are first designed, and discussions with the customer led to

the concept of using twin tool-turrets on the machine, both tools cutting a mirror-image path in one axis, thus doubling the metal removal rate.

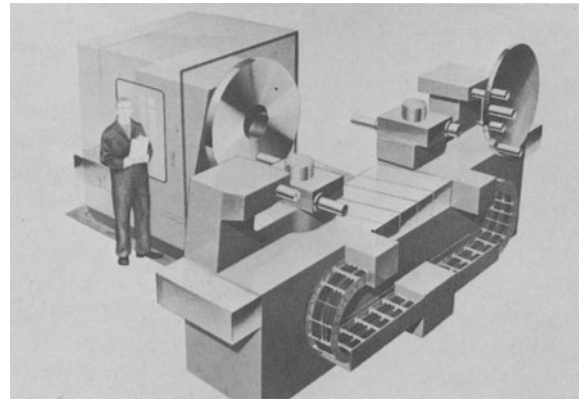


Fig. 1

Fig. 1 shows the first artist's impression of the machine and it can be seen that a T-bed configuration was chosen. We describe here the development of a method of automatically setting both cutting tools when on the machine, thus obviating the need for tool pre-setting or tool-offsets, a method for automatic and rapid tool-changing, the method of programming the machine for efficiency and surface-finish, and we will describe some more advanced features that may be added later.

The machine was called—the Red Century 1250 NC tee-bed lathe.

*Systems Products Manager, Charles Churchill Ltd.

†Research and Development Manager, Charles Churchill Ltd.

General machine description

Fig. 2 shows a line drawing of the machine.

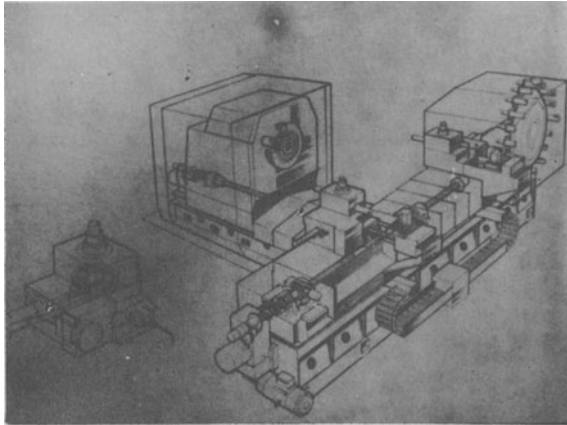


Fig. 2

The Red Century 1250 NC lathe is a numerically controlled turning machine for large disc and ring shaped components. It is of 'T-bed' configuration, with a sliding headstock moving on the 'leg' of the tee (z-axis) and two tool carriages moving on the cross-piece of the tee (x-axis).

Opposite handed recirculating ball leadscrews used on the x-axis carriages ensure that the tools are always moving in precise mirror-image paths, thus a two-start scroll is cut on the component, and linear feed-rates of twice those normally used can be employed, doubling metal removal rate. The machine is designed to accommodate the increased cutting forces that this entails.

Slideways are all hydrostatic, and carriages driven through two-speed gearboxes by Inland Motor d.c. torque-motors with feed-rates from 0.02 mm min^{-1} to 3800 mm min^{-1} .

The spindle frame houses a sixteen-speed gearbox driven by a 40 h.p., d.c. motor. The spindle nose has an ASA taper location and accepts components mounted on accurately machined fixtures. The spindle speed range overall is 1–200 r.p.m.

Tool magazines are provided for each tool-turret which can accommodate twenty tools each. Tool changing is done from the magazines into the non-cutting station of the turrets by means of tool-transfer mechanisms which move only in one plane. The tool-turrets index through one-half turns and are precisely located by face-toothed couplings.

The principal capacities of the machine are as follows:

Maximum swing diameter	1370 mm
Maximum turning diameter	1220 mm
z-axis stroke	865 mm
x-axis stroke (each carriage)	840 mm

To overcome the need for tool-offsets, and operator influence on component geometry, an automatic tool-setting device was mounted on the machine. The tool-setting units can be seen, retracted, at each side of the spindle frame. As will be explained later, the tool-setting system demanded the use of an auxiliary slide on the left-hand carriage on the x-axis. This slide is controlled by rotating the carriage ball-nut for x-

axis motion and by an independent leadscrew for z-axis motion.

Tool setting

The use of preset tooling on NC lathes has become common, but even then it is usually necessary to use tool-offsets during machining cycles to ensure component accuracy. To be able to preset tooling to high degrees of accuracy, expensive presetting fixtures are required and therefore the overall result is that efficiency is reduced. The customer for the new machines desired presetting to be eliminated to the extent that the use of qualified tool-holders and tools was sufficient.

It was soon clear that the use of twin-tool cutting on a workpiece required each tool to have an equal share of the cutting load. This was because any unbalance would tend to overload one tool, and also produce poor surface finish. The materials to be cut by the machine were high tensile nickel/chromium alloys, titanium and so on, and therefore it was decided that it was necessary to produce a method of setting tools on the machine, just before cutting, to the accuracy required, defined as $\pm 0.0003 \text{ in.}$

As the tool-setting operation would now take place during the machine cycle, time was at a premium, the time for a complete tool-setting cycle being specified as 60 s.

After examining the alternative methods that looked feasible, it was decided that a non-contacting, optical method was the most attractive, because wear would not be a problem and reliability high. It would also be possible to set the tools in any quadrant from any direction—something very difficult with the other methods.

Fig. 3 shows the operating principles of the unit eventually developed at the Hinxton Hall research

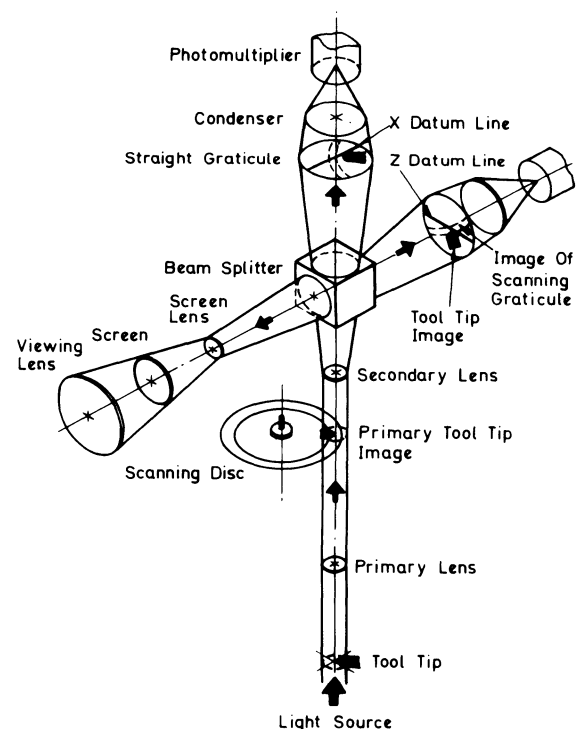


Fig. 3

laboratory of Tube Investments Ltd, in cooperation with A.R.D.D. The tools to be set are positioned under an optical unit which has an optical crosswire, on which the tool should be just touching if it were completely accurate.

A primary image of the tool tip is obtained on a scanning disc through a primary lens. The purpose of scanning the image is dealt with later and at this stage the disc will be ignored and it will be assumed that the image is collected by a secondary lens and projected into a beam-splitter. The beam-splitter simply delivers the image to three separate optical assemblies, the viewing screen, where the tool tip can be seen as with normal optical tool-setting devices, and two straight graticule lines followed by a condenser and photomultiplier. The gratitudes are arranged so that one is oriented in the z-axis of the machine, the other in the x-axis. The width of the graticule slit is 0.002 in., but as the lens system magnifies the tool tip by a factor of ten, the slit width is equivalent to 0.0002 in. With this magnification, the unit by itself can detect a tool tip within ± 0.00005 in, but when combined with the whole machine tool and control system, the performance becomes less good. However, the design specification of ± 0.0003 in, is easily met. When the tool tip is not encroaching the graticule or datum line, the whole graticule is illuminated. When a tool tip crosses the line, part of the graticule is obscured. The photomultiplier can thus detect a change in light-level and, with suitable electronics, give an appropriate signal to the machine's control systems. As it is required to detect the tool just on the point of crossing the line, that is setting on the datum-line, the change in light-level would be small. However, the effect of scanning the image is to deliver an image equivalent to a section of the graticule much smaller than before and the photomultiplier signal changes substantially when the tool is just on the line, thus good discrimination is obtained, hence the use of the scanning disc.

Obviously, with the tool-presetting tolerance of ± 0.020 in., it is necessary to use the photomultiplier signals to drive the tool to the datum line from a position either 0.020 in. from the line or 0.020 in. over the line. Solid state logic is used to achieve the desired results.

Fig. 4 shows how the unit is applied to the machine. Consider first only one x-axis tool slide. The

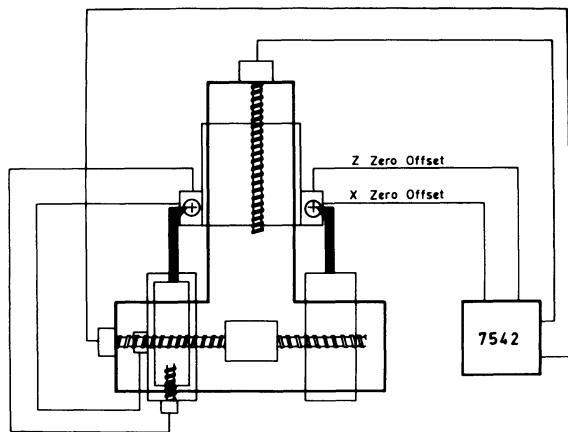


Fig. 4

Automatic Tool Setting Unit (A.T.S.U.) signals are processed and signals fed to standard zero-offset differential resolvers on the GE 7542 control. This has the effect of moving the main or 'master' axes of the machine until the zero position of the machine is set to allow for any inaccuracies in the tool dimensions. For convenience, this is referred to as 'setting the master-tool'.

Because there is a twin-tool fitted, on a mirror-image in the x-axis, after the master tool is set, the other tool, referred to as the 'slave' tool, also requires adjustments. Because there is an ± 0.020 in. tolerance on all tools, the slave tool will seldom be correct after setting the master. Some means therefore had to be found to obtain motion of the x-axis slave turret independent of the x-axis master.

Rotating the slave ball-nut by a wormwheel and screw arrangement enables independent motion in the direction of the x-axis, but to achieve independent z-motion, the slave turret had to be mounted on an auxiliary slide driven in the z-axis by a further recirculating-ball leadscrew and motor. Those details can be seen in cut-away in Fig. 2.

A second A.T.S.U. is used on the slave tools to obtain setting signals for the slave tool-setting motions.

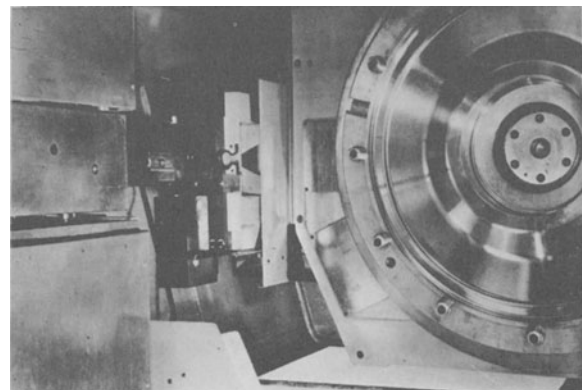


Fig. 5

Fig. 5 shows a unit being used to set a tool. To protect the unit while not in use, it is withdrawn into a sealed cover. An air-blast is used to blow away any stray swarf or coolant from the tip before setting takes place.

Fig. 6 shows a typical tool-setting cycle. The machine is presumed to be cutting and the next tools

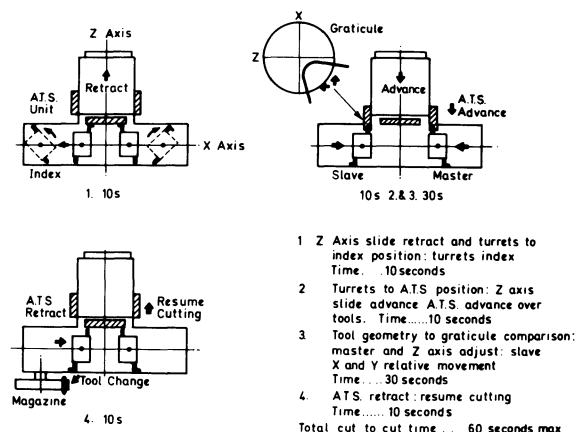


Fig. 6

to be used are already behind the indexing tool-turrets. The sequence and timing of events is given for the absolutely worst case, and, as can be seen, the specified 60 s maximum is achieved.

Where tool-setting is being used it is therefore unnecessary for the machine operator to interrupt the machining cycle to check tool-setting and component geometry, once the tape has been proven. This feature in itself results in considerable savings in floor-to-floor time and as the unit can be applied to many lathes, this development in automation must be considered significant.

Fixture/component location

Turning disc-type components frequently requires the use of fixtures on which the discs are mounted. The fixtures are then offered up to the lathe, clamped, and component location checked and adjusted. This is a time consuming operation, and it means that the lathe is occupied during the setting process. Thus a method of automating the obtaining of an accurate component set-up was found.

By providing a special fixture/component clocking rig, the component and fixture can be clocked separately from the machine. The fixture can then be offered up to the spindle nose and if accurate means are designed for holding and detecting the fixture, there is no need to check by hand.

On the R.C.1250 machine, the fixture is automatically pulled onto the spindle-nose taper by hydraulic means. The taper location used is an accurate non-stick taper which in itself ensures accuracy. However, there are air-gauging transducers attached to the machine spindle frame which detect the fixture and are set to check that it is correctly located. Machine cycle-starts are inhibited if this check is not affirmative, and an indicator lamp informs the machine operator. The automation thus achieved reduces operator influence on component location and reduces floor-to-floor time. Furthermore, as it has been designed in from the start, it provides for the eventual automation of workpiece handling in a way that would not otherwise be possible.

Tool changing

The choice before the machine designers was not whether to specify automatic tool changing, but rather which type of automatic tool changing was desirable. It was established by the customer that a load of twenty tools would be required, and they preferred to identify each toolholder rather than tool-magazine position.

The basic design requirements were defined as follows:

A foolproof identification of toolholder to be used; an absolute minimum time required to obtain a new set of tools in the cutting area; and a means of ensuring and providing that toolholders are located in the tool-turrets with a high degree of accuracy.

The toolholders (and thus the tools) are identified by means of coding screws situated along the ISO 50 taper used to locate the holders in the turrets. The tool number is a six digit binary number, thus allowing $(2^6 - 1)$ unique tool numbers, that is 63 numbers (1 to 63). A seventh coding screw is used to generate an

odd parity. In operation, the tool number is checked twice for number and parity before being inserted in the turret. This is virtually foolproof.

The requirement for twenty tools in each load was not compatible with the need to reduce tool change times. Therefore it was decided that a pair of indexing tool-turrets had to be used. It was then possible to search for a given tool in the magazine and insert it in the rear turret station while a cut was in progress. By this means, only the turret indexing time influenced the complete 'cut-to-cut' time. The turrets index through 180 degrees in 4 s.

Accurate tool-holder location was necessary both as an obvious safeguard, but also to enable the tool-setting operation to achieve a specified performance. One of the most important reasons for checking tool-location was seen to be that the cutting performance of the ISO taper interface on the tools can be seriously reduced if an excess of dirt or swarf is allowed to contaminate the taper. As such contamination would result in a mis-location of the tool, checking the location provides an assurance of the cutting performance.

When the toolholders are inserted in the turret station, the location of the toolholder is detected by a position transducer. If a toolholder is not located accurately enough, the machine is halted when the programme attempts to index the turrets. This process is again completely automatic and it is not possible for the operator to overcome the machine interlock.

Programming

The components to be cut on the machine were of fairly complex geometry, and the customer was already using Exapt 2 as a programming method.

Moreover, the customer desired to be able to produce constant cutting speed conditions over a three to one range of diameters. This in itself resulted in the specification of an S.C.R. controlled, infinitely variable spindle drive with a three to one constant h.p. speed range, but the use of an Exapt 2 post-processor enabled programmers to automatically produce commands on the control tapes to maintain a constant cutting speed. Sixteen gear-changes in the spindle gearbox result in a total speed range of 1–200 r.p.m., the gear change being called automatically by the post-processor if necessary.

One aspect of originally specifying that the machine be programmed only by computer is of interest. By automating the programming it is possible to build into the software the type of interlocks and logical sequences that would normally require extensive hardware solutions. Although for safety reasons some interlocks cannot be software based, it is possible to obtain an overall cost benefit.

Control systems

Fig. 7 shows a block diagram of the control systems used on the machine. The GE7542 two-axis continuous-path control system reads command data either from tape or manual inputs. A.R.D.D. designed and manufactured solid-state (integrated circuit) controls to accept the control signals from the GE control and deliver the appropriate power output signals to the

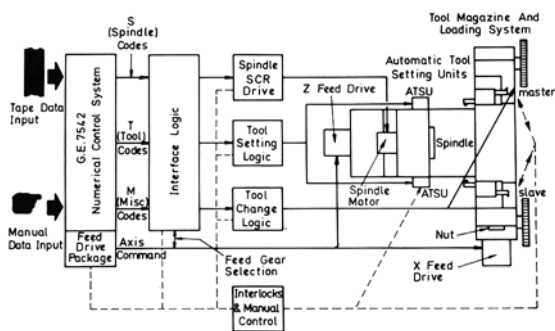


Fig. 7

machine hardware. The accent in design was on reliability and ease of servicing.

The machine slides are driven by electric servo drives, which consist of high performance Ward-Leonard d.c. motor drives, and use Inland Motor equipment. The type of materials being cut demand feed-rates as low as 0.0008 in min⁻¹ and the smooth low speed performance of this type of drive is highly desirable. The low feed-rates required also dictated the use of a gearchange to achieve the desired rapid traverse.

As well as those interlocks and checks described in previous sections of this report, it was decided that wherever possible operator safety, component security and machine protection should be automated. The resulting interlocks are too numerous to mention here, but for example, if the main guards are opened in AUTO cycle, the rapid traverse mode is inhibited, thus protecting the operator when inspecting the cutting process with the guards open.

ECONOMICS

The R.C.1250 machine justifies its extra cost over conventional NC lathes by obtaining higher production rates per unit of capital invested in the machine. The twin-tool cutting is an obvious reason, but not quite so obvious is the fact that floor-to-floor time is reduced by an overall factor which is sometimes as high as three or four. This performance is a result of the high degree of built-in automation additional to the conventional machine's NC controller. Considering floor space saved reduces costs further.

As the component complexity increases and tool changing and setting have more and more significance, then the advantages of automation increase.

PROJECT CONTROL

The management of a single contract of significant value for a number of fairly sophisticated machine tools is perhaps not in itself a problem. However, if the first machine has to be conceived, designed, detailed, manufactured and delivered in 12 months from the receipt of the order, and the complete order delivered within 16 months, then the plain management of such a contract is problematic.

In the case of the R.C.1250, Fig. 8 shows the schedule of events found necessary to achieve the targets set, and it has since become apparent that

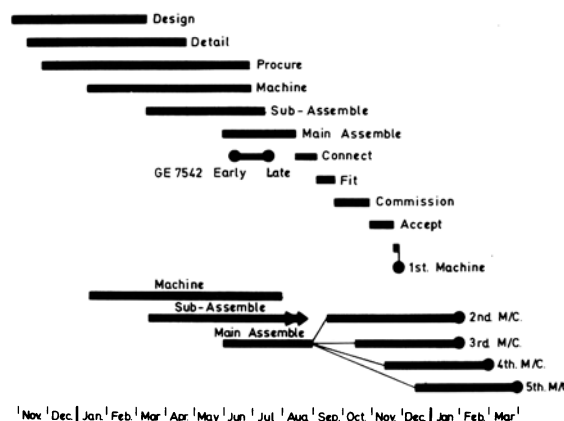


Fig. 8

without careful planning and control the delivery promises that were given and met would have gone by the board.

A computerised critical path analysis method was used to record and report progress, and the customer was continuously informed of the progress being made against the schedule. The principal plan was used to ensure that the correct resources, both in materials and manpower, were made available as and when necessary. Sub-contract detail design and skilled labour was used extensively and Churchill designers and engineers concentrated on the conceptual design work and control of the project.

It was realized that much time can be lost in getting a new machine commissioned and accepted because of inevitable errors that occur in machine and control systems design. To overcome this, all controls were tested on a special machine simulator, which ensured that not only were the machine's sequences and design checked-out, but made certain that when the controls were connected to the actual machine tool hardware, only minimal problems remained.

Furthermore, the fact that the machine tool and its controls were designed and manufactured on the same site assisted greatly in solving the problems of implementing design changes.

The result of this work, and the fact that a fairly young and enthusiastic team worked together well, was that targets were met and deliveries made on time.

There is little doubt that customers for NC machines are demanding shorter delivery times. It is probable that the methods found absolutely essential to achieve the R.C.1250 project will become commonplace in the machine tool builders technique. Further developments in methods for reducing lead-times will occur and we can look forward to being able to quote to customers deliveries that will surely ensure success over competition.

FUTURE DEVELOPMENTS

One future development planned is a tool-wear measurement facility.

Using the control commands given to the automatic tool setting equipment it is possible to measure the tool wear that has occurred between successive

tool-settings. It will be possible to specify for a number of tools the allowable wear, and the tool-wear detection controls will indicate to the operator when each limit is reached. This development further automates the machine.

A further development, using the control servos already existing for the automatic tool-setting equipment, could be the introduction of an adaptive-control system which could automatically compensate for tool-wear, thermal drift and machine tool tip deflections. Obviously simple adaptive control of spindle horsepower is feasible.

Automation of workpiece handling is also feasible. As already described, the fixture clamping controls provide a sound basis for the automatic handling of fixtures. Similarly, a line of R.C.1250 NC lathes would be able to share completely a central tool store, which would enable reductions in cost on the machine tool change hardware to be made.

If current trends towards the use of computers for machine tool control continue, machine control by computer both for motion and sequence logic could be envisaged.

DISCUSSION

Query from Professor Dr. -Ing. G. Spur, Technische Universität, Berlin.

In your paper you mention the possibility of measuring the tool wear. This is important for new developments in optimising adaptive control systems. Could you report something about your measuring device? Is it only an idea or do you have any experience? What kind of tool wear are you measuring?

Reply

The device in question is really a technique for using the existing automatic tool-setting unit. The lathe axes are moved by rotating differential resolvers by means of stepping-motors geared so that one step represents 0.0001 in. Control logic ensures that axes are moved until the tool-tip is set on the ATSU cross-hairs. After cutting for some time, if the axes are again positioned at the "tool-setting position", the ATSU will register that due to tool-wear, the tool tip is no longer at the true datum. The number of pulses required to move the tool to the datum is the analogue of tool wear.

The above facts can be seen to form the basis for a system whereby toolwear can be measured, but at present no practical details are available. Only radial wear is measured.

THE MODULA RANGE OF NC MACHINE TOOLS

by

D. GRINDROD and G. FARNWORTH*

INTRODUCTION

Before the introduction of its Modula range, Marwin Machine Tools Ltd. marketed standard and custom built, numerically controlled machine tools and machining centres for the machining of ferrous and non-ferrous alloys.

The price of these machines typically ranged from thirty thousand pounds (£30,000) to one hundred and fifty thousand pounds (£150,000).

Whilst Marwin had made an increasing impact on the general engineering industries, particularly at the heavier end of the market, the majority of its customers had come from the aircraft industries, both at home and abroad.

Feedback from the sales force had made the Company acutely aware that it could not satisfy the requirements of many small-to-medium sized general engineering companies, on a cost basis alone.

Such companies typically explained that whilst they fully appreciated the benefits of using numerically controlled machine tools, they simply could not afford the relatively high capital cost of such equipment.

In 1969, Marwin decided that in order to continue the growth of the Company, it would be necessary to seek new markets to supplement its existing ones. It is not surprising, therefore, that general engineering was chosen since it was believed that this market would both support the Company's expansion and act as a 'buffer' in the event of recession in the volatile aircraft industries.

Thus, they decided to design a numerically controlled machine tool which could be sold at a price which would suit the pockets of even the smaller users. It was thought that the wide introduction and application of this machine would be compelled on economic grounds alone.

From the original concept of a single numerically controlled (NC) machine tool, emerged a comprehensive range of NC machine tools and machining centres called Marwin Modula.

SPECIFICATION

Once the decision to market a new machine tool had been made, it was necessary to establish a suitable machine specification, within which the Company's designers could work. This specification was jointly conceived by a team representing the design engineering, production and sales functions, working to the following criteria laid down by the Board of Directors.

1. The machine must be specifically aimed at the general engineering industry, both in the United Kingdom and Overseas.
2. The machine must be a basic milling machine, fully capable of boring, drilling and tapping.
3. In accordance with the Company's existing marketing policies
 - (a) As many variations as possible must be offered on the basic machine to cater for the individual requirements of each customer.
 - (b) The machine must 'out specify' competitive products in the same price range.
4. The machine must have numerical control on all axes.
5. The unit cost of the basic machine must be sufficiently low for it to be marketed in the United Kingdom at a selling price of ten thousand pounds (£10,000).

Eight years ago, in his classic paper on 'The Machine Tool of the Future', Dr. Moll¹ presented firm guide lines which aided the satisfaction of criteria 1 and 5.

In his paper, he put forward the answer to the increasing problem of keeping production costs low as being 'automation involving the lowest possible capital expenditure'.

The automation of small batch production which is typical in the general engineering industry is technically feasible with NC, and the capital cost of NC machine tools can be minimised if manufacturers

*Marwin Machine Tools Ltd., Leicester.

offer simplified machines with limited working ranges and reduced cutting capacities, which satisfy the customer's needs only and do not give him excessive technical capabilities and physical capacities that often incur overproportionate capital costs when related to their appropriate usefulness.

Dr. Moll suggested that 'Component Statistics' offer one way of determining the exact requirements of the machine tool user. Component statistics are not an end in themselves, for in order to achieve a competitive product in a free market, the designer should consider many other factors including development in metal cutting, the technical features of machine design, competitors, products, future requirements of manufacturing systems, the plant manufacturing expertise and experience, and cost, before he reaches the final compromise. Such statistics will, however, help in deciding a minimum specification upon which the designer can exercise his judgement. For this reason, therefore, use was made of research surveys carried out at Aachen, and by PERA and VUOSO. This increasing volume of information on machined components relating to their shape, size, weight, material, type of machining operation, desired output and required accuracy, provided an insight into the milling, drilling and boring practice of the general engineering industry.

It was found, for instance, that a machine capable of drilling 2 in. diameter holes will accommodate 95% of work requiring drilling and that 75% of this work can be accommodated with eight cutting tools and a third of drilled workpieces also require milling operations. A strong case must, therefore, exist for an eight-station turret, not merely capable of drilling but fully capable of milling.

Eighty per cent of work requires a combination of machining operations drawn from milling, boring and drilling, and, therefore, a strong case exists for the development of the machining centre philosophy of designing machines capable of milling, boring and drilling a component in one set-up.

Machining is often required on two or three orthogonal axes indicating a need for angular indexing facilities. In fact, 55% of all milled components are well suited to production on a machine equipped with angular indexing. These facilities become even more urgent when it is noted that for drilling, milling and boring operations, the time spent in setting and handling often exceeds the time spent cutting metal.

A machine with a physical capacity to accommodate an 18 in. cube will be suitable for about 80% of all general engineering components that are milled or drilled and about 40% of components that are bored. If this capacity is increased to 18 in. × 18 in. × 32 in., then the machine will accommodate over 50% of all bored work.

Most components weigh less than 60 lb and over 95% of components weigh less than 1 ton and have a maximum envelope dimension less than 60 in.

Over 95% of all components which are milled, bored or drilled are made of cast iron or of a ferrous alloy. Therefore, any machine with a high range of spindle speeds suitable for light alloy metal working will have an extremely limited application in general engineering.

Similarly, an NC milling machine with Continuous Path Control will have a limited application in general engineering since only 9% of milling components have machined surfaces with a curved profile. However, a contouring facility will allow certain components with surfaces which normally would have to be machined by turning, to be milled, e.g. flat plates with a spigot. Hence the usefulness of a milling machine with a contouring facility would be greater than that suggested.

From factors such as these drawn from component statistics and from other factors obtained from technical and marketing surveys, a suitable specification was derived for the basic machine and the machine variations necessary to satisfy the peculiar requirements of the individual customer.

From the start it had been decided that the only economical way of satisfying the marketing criteria for the specification, would be to design the machine on a modular basis, especially as this concept of design and manufacture has been used successfully by the Company on its existing ranges of machine tools.

The term 'modular' or 'unit', is employed to describe a concept in which each of a group of similar or related products, comprises a permutation of modules (units) selected from a specified range of modules. In most cases, a module will consist of an assembly, but could be a sub-assembly or, in an extreme case, it could be a discrete component.

Modularisation constitutes a means of satisfying a relatively wide range of market needs without having to resort to the manufacture of individual custom-designed products with their resultant high design, development, engineering and production costs.

The object of modularisation is to make each module in reasonable size batches. (In Marwin's case, these batch sizes can be extremely low as the Company has its own comprehensive NC machining facilities.) This is generally feasible because a module may appear in numerous different machine variations, and even when only one variation is needed it is the modules peculiar to that variant and not the whole machine that have to be made in correspondingly small quantities.

The economy of production in quantity is achieved not only at the machining stage, but also at the assembly stage, where special facilities can be provided for building its different modules in batches. These batches of modules can be built simultaneously rather than sequentially, and hence the complete machine build time can be minimised since completed modules can be assembled to the main structure (Fig. 1). Each module can be inspected and tested off the machine and any rectification necessary will not disrupt the final build.

The reduction in lead time of machines built by the simultaneous assembly of modules, reduces not only the delivery time to the customer, but also considerably reduces the work in progress and improves profitability.

The satisfaction of Criteria 5, in determining a suitable machine specification proved to have an unexpected and profound influence on the final specification of the machine.

Although the estimated unit production cost of

TABLE I

	Modular			Modulamatic	
	Horiz. Ram	Vert. Ram	Turret Ram	Horiz. Ram	Vert. Ram
Axis Traverse					
X 40" or 60" (1016 mm or 1824 mm)	*	*	*	*	*
Y 20" (508 mm)	*	*	*	*	*
Z 20" (508 mm)	*	*	*	*	*
Extra Vert. Stroke to 30" 716 mm)	*	*	*	*	*
Worktable					
20" x 40" (508 x 1016 mm)	*	*	*	*	*
20" x 60" (508 x 1524 mm)	*	*	*	*	*
40" x 40" (1016 x 1016 mm)	*	*	*	*	*
40" x 60" (1016 x 1524 mm)	*	*	*	*	*
40 International Taper Spindle Nose	*	*	*	*	*
50 International Taper Spindle Nose	*	*			
32 Spindle Speeds					
30 - 3028 revs/min	*	*	*	*	*
10 - 1009 revs/min					
16 Spindle Speeds					
30 - 3028 revs/min	*	*	*		
10 H.P. Spindle Drive	*	*	*	*	*
Feedrate 0.1 - 98"/min	*	*	*	*	*
300"/min rapid	*	*	*	*	*
Tool Retention:					
Power drawbar	*	*		*	*
Quick release chucks			*		
Right Angled Head Attachment	*			*	
Index Table 24" 72 Position Tape Controlled	*	*	*	*	*
Index Table 36" 72 Position Tape Controlled (40" wide worktables only)	1 only			1 only	
Rotary Trunnion Table 18" NC		*	*		
Rotary Table 24" NC	*	*	*	*	*
Rotary Table 36" NC (40" wide worktables only)	1 only			1 only	
Tool Magazine 30 Position				*	*
Tool Magazine 40 Position				*	*
Random Tool Selection				*	*
Sequence Number Display 3 Digit	*	*	*	*	*
Manual Data Input for Continuous Path Control (Standard on point-to-point system)	*	*	*	*	*
Tape controlled Spindle Speeds	*	*	*	Stan- dard	Stan- dard
Tool Length Compensation	*	*	*	*	*
Tape Controlled Spindle Reverse for Tapping	*	*	*	*	*

the machine initially conceived had been minimised by 'modularisation', it became apparent that if a single machine type only were to be marketed, there would be insufficient demand to allow the design and development costs to be amortised over an acceptable period of time.

Therefore, in order to increase this demand, the Company resolved to widen its specification and market a range of basic machine types with associated variations. This could only be feasible economically if these basic machine types incorporated a high percentage of common modules, thus minimising the increase in the total design effort.

The Company also found it necessary to change its basic thinking on the NC of the machine. Originally it was hoped to 'buy out' the complete control package, i.e. the cabinet, power supplies, machine tool logic and the NC logic. However, negotiations with the major NC system manufacturers proved that it would be too costly to purchase the complete package. Consequently, it was decided to buy out a 'standard' NC system logic only, and to design and manufacture the cabinet, power supplied and machine tool logic 'in house'. In this way, the cost of the complete package for a basic 3-axis point to point control with standard options was reduced from about five thousand pounds (£5,000) to three thousand pounds (£3,000).

The final machine specification given to the design team included the following main parameters:-

1. Provision for both horizontal and vertical, single spindle work heads and for an eight spindle vertical turret head.
2. Basic machine to accommodate workpiece envelope size 20 in. X 20 in. X 40 in., with provision for optional 20 in. X 60 in., 40 in. X 40 in. and 40 in. X 60 in. worktables.
3. All worktables to be supported over their full length of traverse.
4. Capable of supporting a workpiece in excess of 1 ton.
5. 10 hp power spindle drive for machining of cast iron and ferrous alloys.
6. Basic machine to have manual tool change facility with provision for optional automatic tool change facilities.
7. A range of optional angular indexing and rotary tables.
8. Basic manual spindle speed selection with provision for automatic speed selection from tape.
9. Basic machine to have full point to point NC on three axes with provision for NC on indexing tables etc., and provision for contouring option.
10. Basic machines and options including the NC system to be built on a 'modular' basis, with the maximum number of modules common to each machine type.
11. The cost of the basic machine must be below £10,000.

The satisfaction of these parameters caused two major headaches in machine design.

The traditional approach to milling machine design of supporting the worktable on 'compound slide-

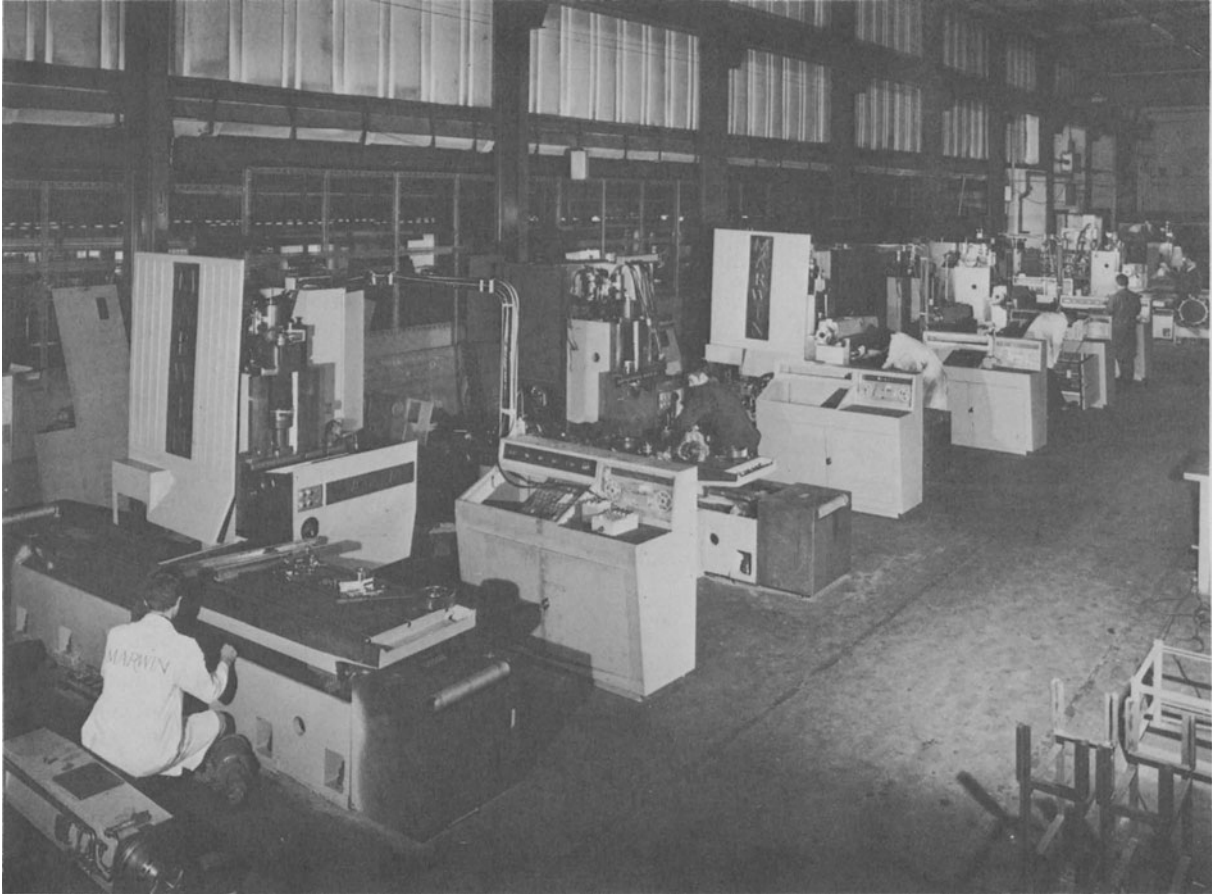


Fig. 1 Part of the Modula main assembly line

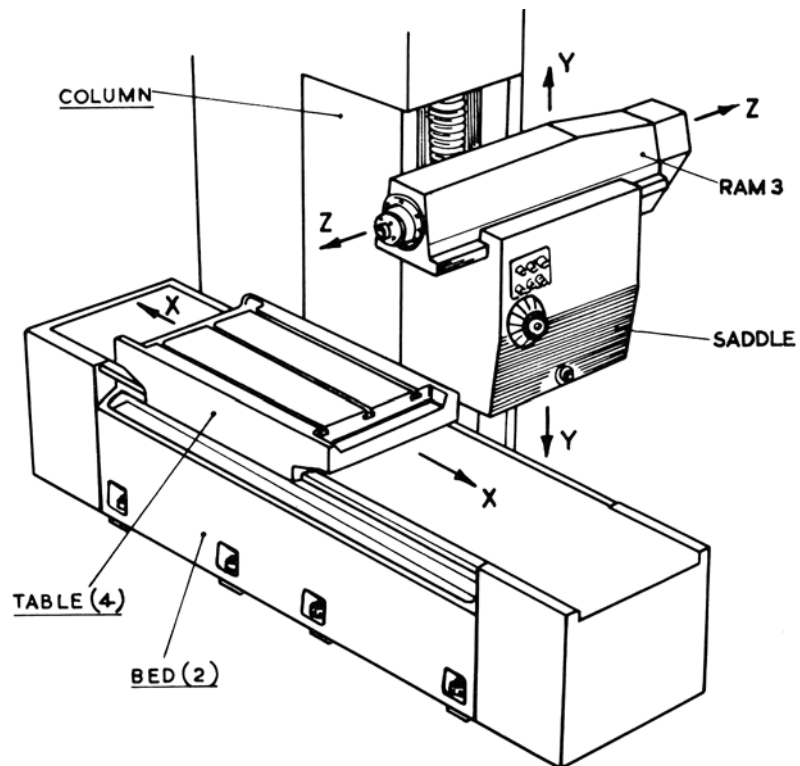


Fig. 2 The main machine modules

ways', severely limits the range of worktable sizes that can be provided without altering the basic machine. The Marwin approach to solving this problem was to support the worktable directly on the machine bed which is mounted on the floor (Fig. 2). This means that the worktable traverses along one axis only (the X axis), and both the worktable size and traverse can be extended very economically by merely increasing the length of the bed.

The other difficult design problem was the provision of the different work head configurations without altering the basic design of the machine. The breakthrough came with the concept of mounting each work head on a ram (Fig. 2), which carries the final drive to the work spindle. Although each ram and headstock is an individual module, all rams are supported by an identical carriage (saddle) which provides the spindle drive.

Thus, there emerged a range or family of machine tools, which the Company named the Marwin Modula and Modulamatic range NC Machining Centres.

The term Modula is used to denote the range of machines with a manual tool selection and change facility. Modulamatic machines are similar but have an automatic tool selection and change facility. The diversity of end product is illustrated by the machine specification offered to the customer (see Table I and Fig. 3).

THE MACHINE STRUCTURE

A basic Modula machine tool consists of the following main structural modules, as shown in Fig. 2.

Bed	: (choice of 2 sizes).
Table	: (choice of 4 sizes).
Column	: (common on all machines)
Saddle	: (common on all machines).
Ram &	: (choice of horizontal, vertical
Headstock	or turret).
3 off Axis	: (common on all machines).
Drive Motor & Gearbox	

A Modulamatic machine consists of the Modula units with an additional tool change unit.

Bed and column

For quantity production, fabricated structures tend to be more costly than castings and since Marwin have their own foundry, full use has been made of cast iron in the development of the main modules in this range of machine tools.

The machine Bed is designed for rigidity and is manufactured from close-grained, stress relieved cast iron. The slideways are of a square form with narrow guideways which are peripheral ground. A central valley between the guideways allows clearance for the X axis leadscrew. The leadscrew and guideways are positioned to prevent crabbing of the worktable.

Large capacity longitudinal coolant troughs are provided on each side of the bed. Provision is made in the base of the bed for eight combined foundation bolts and levelling screws.

The high rigidity required for NC machine tools can be increased by using the foundation to supplement the stiffness of the bed.

The column is made of a similar material to the bed and has substantial internal ribbing for maximum rigidity. A shallow well accommodates the axis drive leadscrew and is located between narrow guideways of a square form. The narrow guideways are peripheral ground and designed to prevent crabbing of the saddle.

The column is accurately located by spigot and dowel and is bolted to the machine bed and is provided with four combined levelling and foundation bolts similar to those on the bed casting.

Worktable

The four sizes of worktable are made of ribbed cast iron and will support workpieces weighing up to 6,000 lb., together with the associated cutting loads. Taper gib adjustment on the narrow guideway is provided.

Slideways

One of the problems confronting the machine tool designer is movement of slides, tables, columns, etc., on guiding surfaces. The basic requirements are:—

- Straightness of motion, which must be maintained within close limits over long periods of service under workshop conditions.
- Uniformity of motion, which must be maintained even for heavy masses and very low speeds.

Providing that the initial form, accuracy and finish of the mating surfaces are suitable, the satisfaction of both these requirements demands a reduction of the coefficient of friction to the lowest practical value.

In NC machine applications, it is particularly important that the stick-slip phenomena should be eliminated as far as possible to enable movement to be imparted reliably in very small increments.

The problem has been tackled in various ways by machine designers and solutions have been sought by using roller bearings and hydrostatic lubrication. Another and more economical approach to the problem is the use of a dry bearing material to remove the negative slope of the friction-velocity characteristic.

One such material, Glacier D.U. has been used by Marwin for several years with considerable success. It has been found even under the most adverse conditions of dirt and coolant, such bearings give trouble-free use, and they have proved particularly useful in coping with vibrations associated with heavy milling. Under such conditions, the higher coefficient of static friction aids the stability of the stationary slides and with the high torques available from hydraulic servo-drives it presents no problems on the moving slides.

Glacier D.U. is made up of three bonded layers; a backing strip of steel; a middle layer of porous bronze impregnated with a mixture of polytetrafluoroethylene (ptfe) and lead; and a surface layer, about 0.001 in. thick of the same ptfе and lead mixture.

In use, a film of the ptfе mixture is transferred to the opposing rubbing surface and this film as well as a thin surface layer on the D.U. is maintained through-

out the working life of the bearing. This material combines the unique dry-friction properties of ptfе with high compressive strength, good heat conductivity and excellent resistance to wear. Strips of the material are attached to the table, saddle, keep plates and gibs. The mating surfaces of the bed, the column and the ram are ground for maximum life and efficiency of operation.

The positioning of the ptfе pads is illustrated in Figs. 4 and 5.

FEED DRIVES

Marwin considered both electric and hydraulic drive systems for the linear axis movements.

In general, electric motors have a low torque-to-inertia ratio when compared with hydraulic motors and, therefore, give a slower 'response'.

Low inertia DC electric drive motors are being developed and their price is falling. However, at the time of consideration, electric drive systems cost approximately 30% more per axis than hydraulic systems. Therefore, a hydraulic feed drive system was chosen for the machine.

Each linear axis movement on the machine is obtained by means of a precision ground recirculating ballscrew driven by a hydraulic motor via a reduction gearbox. The gearbox includes a matched pair of gears which allow adjustment to take up backlash.

The hydraulic motors are rated at nearly 7 hp and can exert an axial thrust on the leadscrew of nearly 3 tons.

Feedback of each axis displacement is obtained by measuring the leadscrew rotation with an optical digitizer which is driven off the leadscrew by a toothed belt. The motors are controlled by servo valves and a tachogenerator provides feedback for the velocity loop.

The feed rate can be varied from 0.1 to 98 in./min, and the rapid traverse rate is 300 in./min.

The deadweight of the saddle gearbox and ram is counterbalanced by a hydraulic cylinder.

A hydraulic power pack supplies oil at a pressure of 1,500 lb/in² to the axis servo drive motors and automatic drawbar (if fitted) and oil at a lower pressure for the operation of the hydraulic counterbalance cylinder, gear change selectors and agitation, and other ancillary services.

The power pack is housed in a steel frame which can be bolted directly to the column, thus enabling the machine to be lifted as one unit. The heavy duty contactors and switchgear panel are also incorporated in the power pack framework.

SPINDLE DRIVE

The work spindle(s) is driven by a 10 hp constant speed motor, through a 16-speed gearbox mounted in the saddle. A two-speed motor can be fitted to provide a selection of 32 spindle speeds.

Seven shafts, supported by ball and roller bearings, carry hardened and ground gearwheels. Four hydraulic rams activate the gear selection and a further hydraulic ram activates the gear agitation.

All work spindle drives are taken from the gearbox via 1:1 helical gearing to an involute splined shaft mounted uppermost in the saddle. Only the final workspindle gearing, mounted in the ram, changes with the workspindle configuration. Motion is transmitted from the saddle splined shaft to the spindle final drive via a further pair of 1:1 helical gears. The input gear is so arranged that it remains fixed relative to the ram, and it slides along the splined shaft to accommodate the movement of the ram.

The bearings and gears in the saddle are lubricated with an oil feed. The final drive to the workspindle is lubricated by a 'micro fog' unit which provides an air and oil vapour. A machine interlock prevents spindle rotation in the event of malfunction of this unit.

The spindle speeds are manually selected by actuating a rotary distribution valve which supplies high pressure oil to the hydraulic gear selector rams. Automatic 'jogging' aligns the gears during selection to ensure smooth and rapid changes. Spindle speeds may be preselected during machining.

The horizontal workspindle is mounted in a matched pair of preloaded, angular contact ball bearings at the front of the ram and a matched pair of roller bearings inside the ram. This bearing configuration has been used successfully by the Company on other machines with spindle speed applications in excess of 4,000 rpm. The spindle is driven directly from the splined shaft by 1:1 helical gears.

The vertical spindle is mounted in a similar manner to the horizontal spindle and is driven through a pair of hardened and lapped spiral bevel gears, one being mounted on the spindle itself and the other on the final drive layshaft, which is driven by the saddle splined shaft via the helical gears.

The cast iron turret carries eight alloy steel spindles mounted in taper roller bearings. Each spindle is provided with its own pair of spiral bevel gears (in constant mesh), one of which is attached to the spindle, the other carrying a coupling half. The matching coupling half is incorporated in the end of a final drive layshaft which is driven by the saddle splined shaft via a 1:1 helical gear.

A precision toothed coupling locates the turret. Half of this coupling is fastened to the turret head and half to the ram. The coupling is separated by a hydraulic cylinder and is rotated by a rack and index gear. The rack is driven by a hydraulic ram.

TOOL CHANGING

The horizontal and vertical workspindle incorporates positive tool retention, and rapid tool changing is assured by the power drawbar fitted as standard. The drawbar is a hydraulically operated type which clamps onto a drawbolt fitted into the threaded end of a standard arbor. When the 'tool release' button is pressed the hydraulic ram moves forward and moves the drawbar forward against the pressure of disc spring washers. The tool retaining cams move forward into a bored out section of the spindle, the cams spring open and the tool is released. The machine is normally supplied with sets of tool holders having either 40 or 50 International taper shank, to facilitate heavy milling and boring.

The 8-position turret incorporates 40 International spindle noses using quick release chucks.

The Modulamatic machines are fitted with an automatic 30-position sequential tool change magazine, a tool change arm, and spindle speed control from tape as standard. A 40-position tool magazine, random tool selection using coded shanks are available as optional extras.

On both horizontal and vertical Modulamatic machines, the tool changing facilities have been designed to avoid the use of complicated mechanisms. The two-position transfer arm simultaneously extracts the tools from the magazine and rotates 180° to return the tools to their new positions. Machining is automatically resumed on completion of the tool change cycle and the next tool required is positioned whilst machining takes place. To ensure correct alignment of single point tools the workspindle always stops in the same rotational position, and so that the tool shanks of all tools are clean, compressed air is blown through the spindle nose during the tool change.

Cutting tools up to 6 in. (152 mm) diameter can be accommodated.

CONTROL SYSTEM

The Modula and Modulamatic machines are provided with both point to point and continuous path (with linear and circular interpolation) control facilities.

Both types of system have been designed by Marwin to reduce the proportion of the total machine tool price accounted for by the NC system. The company manufactures the complete control equipment but incorporate the Plessey NC22 logic system as a 'bought out' item. The use of existing proprietary circuit logic boards gives a reliability, proved in service, with a comprehensive international back-up service and give the automatic, acceleration and deceleration of axis movements without special coding.

The NC system is designed with Transistor-Transistor Logic (TTL) incorporating integrated circuits, on a modular basis. Most machine functions have a separate logic board and most of the optional functions are back wired in.

The basic control system, which is a 3 axis point-to-point type, can be supplied with linear and circular interpolation to provide contouring facilities for the more complex components.

The NC system specification includes the following:—

	Point-to-Point	Contouring
Feedrates :	0.1 – 98.9 in/min 1 – 1999 mm/min	0.1 – 98.9 in/min 1 – 1999 mm/min
Rapid traverse :	300 in/min 7.6 m/min	300 in/min 7.6 m/min
Resolution :	0.0001 in 0.002 mm	0.001 in 0.002 mm
Code :	ISO or EIA Format	ISO or EIA Format
Programming :	Absolute ±	Incremental (slope & arc mode only)
Tape reader speed :	250 ch/s	250 ch/s
Standard features :	3-axis mirror image; full floating zero shift all axes; manual data input; machine zero locate; rapid, incremental and feed jog modes.	
Optional extras :	3-digit sequence number display; tape search; incremental programming; cutter length and diameter compensation; switchable position readout; switchable ISO/EIA Format; plane switching (contouring system only). Imperial/metric switching.	

CONCLUSIONS

This range of machine tools is leading Marwin's attack on the general engineering markets of the world during the early 1970's.

Buyers in general engineering will have the opportunity of getting into three axis numerical control at a modest figure with a machine having serious milling ability with 10 hp at the spindle.

Looking into the future the Modulas must surely play an important role in the development of manufacturing systems with Direct Computer Control becoming a practical reality before 1980.

REFERENCES

1. MOLL, H. H., 'A Users Viewpoint of the Machine Tool of the Future', 4th International MTR Conference, UMIST, Manchester, September, 1963.

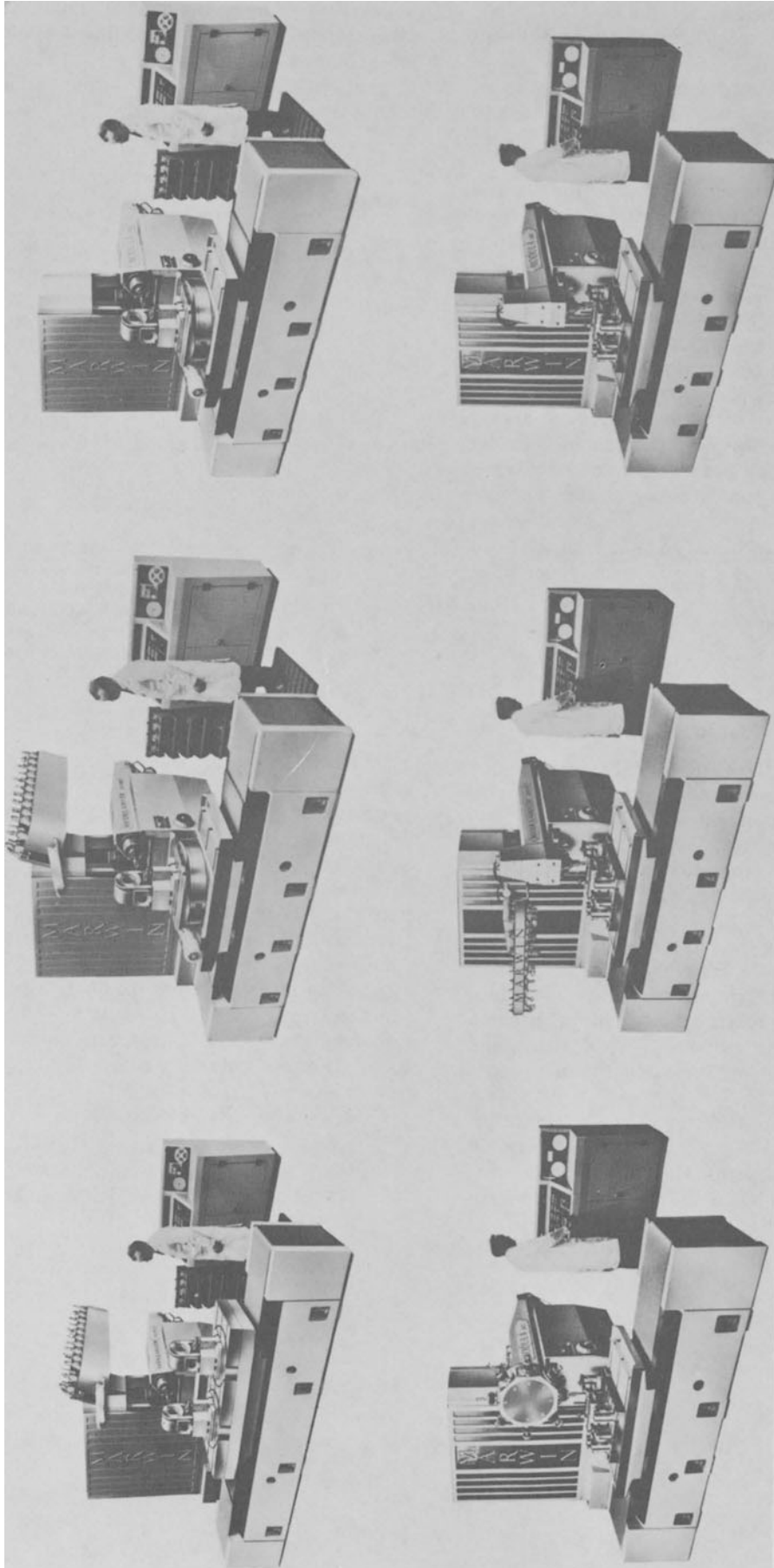


Fig. 3 Some of the Machine Variations in the Modula Range

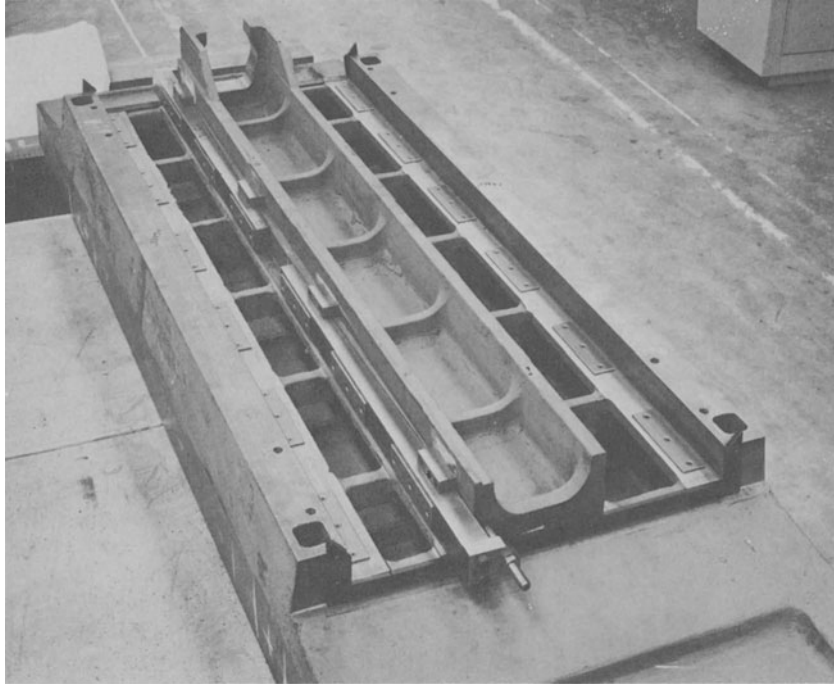


Fig. 4 A worktable on the gibs fitted with PTFE bearing pads

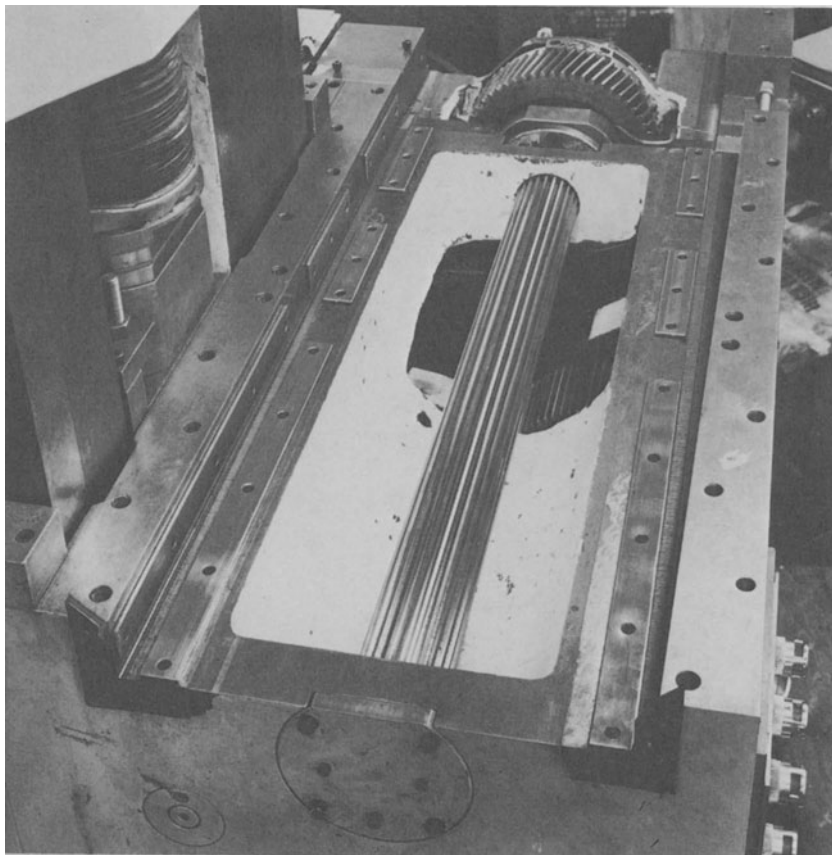


Fig. 5 View of the saddle drive shaft and the PTFE bearing pads of a Modula machine

DISCUSSION*Query from I. S. Morton*

Fig. 4 appears to show that the PTFE-impregnated parts occupy only a small proportion of the total slideway area. Could the authors indicate the unit loading values involved (in, say, lb/in²)?

It is stated (under *slideways*) that contamination by coolant presents no problems. Presumably, however, its presence must reduce the general friction land to some extent. Can it be concluded that the ratio of static to kinetic friction (μ_s/k) nevertheless remains sufficiently constant to leave stick-slip characteristics unchanged?

Reply

For the PTFE bearings used on the Modula worktable, the unit load limit is 2000 lb/in² for more than 10⁷ load cycles. The twelve pads shown in Fig. 4 carry such a small unit load that the area of material used is not controlled by this factor.

The small quantity of cutting fluid reaching the slideway bearings has not materially affected the

stick-slip characteristics of the slideways on a wide range of Marwin NC machines fitted with this type of bearing over the last 6 years.

Query from H. E. Hefford, A. A. Jones and Shipman Ltd.

Please comment on your use of hydraulic drive elements for slide propulsion as offered, to DC electric drive units (as on the RC1250 machine mentioned in another paper).

Reply

Hydraulic drive elements have been used by Marwin on all their NC machine tools. This experience, together with a distinct cost advantage at the development stage of the Modula range, led to their specification for these machines. The drive system may be reconsidered when DC motors offer acceptable technical and economic advantages.

MACHINE TOOLS—THE TOTAL CONCEPT

by

C. A. SPARKES

INTRODUCTION

According to the most reliable statistics at present available, there are approximately one million metal cutting machine tools installed in this country. Based on a sample of several engineering companies, their written down value averages approximately £1000 per machine. It is, thus, reasonable to suggest that the total investment in machine tools in this country is in the region of £1 000 000 000. As there is evidence to indicate that the most efficient of these may be operating only in the region of 70% utilisation, while at the lower end this figure is nearer 15%, it would seem that the majority of machine tools are being used in the lower bracket and a figure of 25–30% would appear to represent the national average. On this basis some 600–700 million pounds' worth of machine tools are not removing metal even if they are being fully manned for the present 40 hour week. Clearly this low level of efficiency is undesirable not only from the point of our capital invested but also the work in progress, stocks, stores and, in fact, every aspect of the national economy.

The argument offered by most managements is that they do not have large numbers of components to deal with and, in most cases, only single ones are required. However, as this situation applies to the majority of companies, it only serves to strengthen the case for a full investigation into methods of improving the present position. There appears, in fact, every reason for a greater proportion of the existing expenditure being devoted to research into non-cutting in preference to the cutting areas of machine tools. Obviously even the slightest improvement in this region would bring immense benefits to all manufacturing industries.

Although the author does not claim to have any positive solutions to the many problems involved, he hopes that by examining and discussing the present floor-to-floor times for machining components in relation to the actual metal removing times, some action may be taken to find a new approach to this subject. A selection of estimated cutting time studies are given in the appendix attached to this paper.

Time studies

From the available data it would appear that the

problem is equally important when considering a simple centre lathe, a drilling machine or the most sophisticated type of machine tool. For example, a modern machining centre, complete with automatic tool changing, is producing lathe headstocks in approximately 270 minutes compared with the previous time of 600 minutes. Nevertheless there are roughly 2000 items of information required to complete this operation so that a saving of only one second per item means a reduction in floor-to-floor time of over 30 minutes. This does not include the possible saving that could be achieved by improved loading and unloading, clamping, cleaning, setting and component design. In actual fact, the metal removal time in this case is only 160 minutes. It might be useful for all time studies to give not only the floor-to-floor period but also the actual time the cutting tool is specifically removing metal. This at least would highlight the aspect of the subject should this be necessary.

Machine tool design

Whilst appreciating the difficulties of designing machine tools to meet all types of operating conditions, it is essential that the designer considers his machine as part of the total manufacturing concept. This must include the general layout of the machine so that it occupies a minimum amount of floor space and allows a factory layout suitable for the best possible work flow, both to and from the final position of the workpiece on the machine. If the machine requires electrical control cabinets, hydraulic units, air filters, coolant systems and measuring arrangements, these should be carefully sited to give the best conditions and preferably occupy a minimum of floor space. Although many modern machine tools already meet these requirements, there are nevertheless a number of examples of units which are scattered around, utilizing valuable floor space and, more important, limiting the possibilities of arranging optimum work flow to and from the machine. In cases where automatic loading is not a feature of the operation, there is an excellent opportunity for improving loading times by the use of built-in lifting facilities rather than compelling the operator to rely on the normal workshop cranes. Even in cases where indivi-

dual components weigh only as little as 10–15 pounds, with a 10 minute time cycle the operator is lifting or loading over 3 tons of work per 40 hour week. A great deal of thought has been given to the problem of worktable or centre heights being designed to the most suitable level at which manual loading of the components is regarded as the only satisfactory method. Here, unfortunately, the designer has to try to satisfy the requirements of tall operators and, at the same time, provide a convenient height for shorter operators. There is no doubt that many existing machines would benefit from a re-examination of their present position.

On certain machines, placing the component in the correct position on the worktable can be an extremely lengthy process. Perhaps some further thought ought to be given to the use of more built-in sensing devices for this purpose. For many years most drilling, milling and boring machines have been designed with conventional tee-slotted tables onto which the components or fixtures are clamped. Present surveys indicate that in certain cases this may not be the best arrangement and alternatives should be sought. There are, of course, other ways of holding the component, for example, by the use of platen loading, but these are not always the complete answer.

There is no doubt that the machine tool designer should also consider the serious problem of how to provide an always clean worktable surface, and one which does not contain raised surface irregularities which make for an inaccurate location of the component. Clearly these are problems which should generally be dealt with at the design stage; the question is how?

Considering the air and hydraulic, or even electrical services which are now generally part of the modern machine tool, it is proposed that far greater use of one or more of these could be made for clamping and unclamping the component. Further, as is already provided in some of the most modern designs, why should these devices not give the correct pressure so as to avoid distortion of the workpiece, not only during roughing but also automatically, at reduced pressure, for the final machining operation. Possibly more built-in gauging and checking of the component before it leaves the machine could be incorporated. Even better, why not arrange for more gauging to take place during the actual machining operations, an idea which, on a number of machines, is the accepted method today.

A careful study of most operators using their machine tools suggests that they are constantly trying to see the point of contact between the cutting edge and the workpiece material. This is often difficult but important in most machining operations. It would help, therefore, if in certain cases greater use would be made of miniature closed-circuit T.V. with a small screen built into the pendant or control panel, similar to the devices now fitted to some large machines.

While this paper is deliberately not concerned with actual metal removing operation of the machine, it is not intended to suggest that this aspect be completely dismissed when the total machining concept is considered. Any possible improvements in this area

should be incorporated by the designer whilst attempting to include some of the suggestions to reduce non-cutting times. At this stage it might be important to mention that the time studies referred to earlier were generally only estimated and not actually obtained on the factory floor. It was considered advisable therefore to carry out a number of tests on components being machined.

The first example was a normal centre lathe. A simple workpiece of sufficient complexity to be representative of a typical engineering item provided the first example. The floor-to-floor time was 15 minutes and the metal removing time 3 minutes, representing a cutting percentage of 20%. In the case of an operation on a conventional 4 ft radial arm drilling machine, a floor-to-floor time of 16 minutes included a total drilling time of 3 minutes, giving a percentage of cutting time to non-cutting time of 19%. As an NC-type control turret drilling machine was available in the same factory, it provided a useful example of a modern type of machine tool. Here the floor-to-floor time of a relatively simple component was 60 minutes and the actual cutting time 20 minutes, giving a percentage of 33%. In this case no account is taken of the time to prepare the tape which, of course, is normally done independently. However, experience in the use of NC machines indicates that, even for the simplest of components, a dry run of the tape on the machine is essential if errors are to be discovered before the workpiece is scrapped. A proportion of this time must, of course, be added to the non-cutting time as this may be a major item on ones off or even on small batch quantities.

The next machine to be checked on the factory floor was a normal Universal Horizontal Boring Machine fitted with punch-card control for the vertical and cross movements. During this test a cast iron unit was machined, which required a crane to lift it on and off the machine table. In addition to the NC of the two traverses, the machine had automatic clamping and unclamping for the slides and the headstock, as well as a special hydraulic tool releasing mechanism in the spindle nose. However, with all these modern facilities the floor-to-floor time was 30 hours and the actual cutting time 9 hours, giving a percentage of 30%. Two further machines were checked, namely a screw-type broaching machine capable of operating a 3 in diameter spline broach, on which the cutting time showed a percentage of 18%, and a conventional cylindrical grinding machine for grinding machine tool spindles from 3–6 in diameter and 10 ft 10 in long, for which the percentage was found to be 20%.

The trend towards Machining Centres, where different operations can be carried out on a single unit, has provided a new approach to the idea of the total machining concept. This trend is also encouraging the designer to look at the problem with a view to developing a type of machine tool which is capable of being integrated into a factory layout so as to provide for the most economical receipt and despatch of the component. While this new and important trend should be continued, it would be a most valuable contribution to the national economy if some fresh thought could be given to existing plant and machinery.

Components

Few will question the idea that the design of many components leaves much to be desired from the point of view of handling them in production. This, of course, is again a question of long-term policy. At present there are many existing cases where the provision of a simple face or flange would help to reduce the assortment of nuts, bolts, washers and various items of packing which only too often adorn the normal machine shop. Locating surfaces could also in many instances be of valuable assistance to the operator when setting his machine. When providing these clamping and locating faces it is, of course, essential to place them in such a position that the component sustains a minimum of distortion during the clamping and machining operations. It is well known to be most difficult if not almost impossible to bore a round hole with a clamping screw placed directly over the centre of the bore.

Factory layout

Maximum benefit is always achieved if the machining process is fully integrated into the work flow pattern. However, until such time as all machines are designed to meet the ideal conditions it is worth while reviewing this area of the non-cutting times.

Many present-day machines with filters, coolant and other units placed around them in positions that make work flow difficult, can sometimes be rearranged to allow for easier access to and from the machining area. The storage of unmachined and machined parts, and the loading and unloading facilities can be sited to give the best work flow path to the cutting position, with the cutting tools and accessories conveniently placed to suit the operator. When factories are specially designed for the use of transfer lines and similar layouts for mass production, these conditions are taken into account in the early planning stages. The present difficulty lies in the need for deciding what can be done with the existing equipment in the many thousands of workshops which are engaged on batch or single component production and which at present form the backbone of this country's engineering industries. In some factories there is even a need for improved swarf removal systems in relation to the general layout of the operating area.

Loading and lifting

Either at the design stage, or as a first operation, most components benefit by being arranged with built-in lifting holes, flanges or devices which greatly assist their handling and machine loading. Often, many components are slung or handled differently at each operation or machining station with a consequent loss of time. The importance of this is clearly illustrated by a study of workshop practices, which shows that the loading and lifting of many components is the major factor during the non-cutting period. The work flow pattern is, in fact, considerably improved when certain machines have their own lifting or transport arrangements. Future machine tools will no doubt have these lifting and loading arrangements designed into the general configuration. Ideally they should be automatically operated, using perhaps some form of

mechanical man which could be programmed to suit a comprehensive range of workshop conditions.

Tools and tool clamping

The area around many machine tools which is not occupied by workpieces is all too often littered with tools and spanners, together with an assorted array of nuts, bolts, washers and other items of packing which the management hope may one day be used for clamping or supporting components on the machine. Although much thought has been given to this matter, it should be possible to find an improved method of storing these tools and tool equipment, accessories and sundry items. There is also the serious problem of lifting and loading the heavier tools from the machine spindle or tool location area. A recent investigation of a large twin-table machining centre, complete with automatic tool changing, showed that at its present production rate, the weight of tools being loaded into and out of the machine per 40 hours is approximately 4 tons. This obviously would have been a most fatiguing task if these tools had to be manually loaded by the operator. While it may be difficult to fit every existing machine with automatic storage and tool clamping mechanisms, this matter is certainly of sufficient importance to rank high on the list of priorities for further original thinking and research while, at the same time, continuing with the development of a number of excellent arrangements which are already available. After the tool or tool holder has been fitted into the spindle or on the supporting face, time is often lost in clamping these into position with sufficient effort to resist movement during cutting and without distorting the accuracy of the tool setting.

Datum setting

Too often, rapid traverse rates, positioning times and approach speeds are accepted as being those which have always been considered as satisfactory for a particular type of machine. However, as these can, and in most cases actually do, represent an important factor in the non-cutting time, there is an urgent need for maximum traverse rates to be considerably increased. Before this can be done, however, the limiting factors must be investigated in each case. Many new designs are, of course, already provided with better facilities, but at the same time many existing machines could no doubt be improved at a reasonable cost.

With regard to devices which are being developed in the field of datum setting, the following is an interesting example. A simple proximity mechanism which allows a display to be presented to the operator, indicates the exact location of a face or bore in relation to the machine tool spindle. A radio or inductive link between this spindle device and a remote meter is placed conveniently on the machine tool. This type of device offers the possibility of connecting the signal with a control mechanism on an NC machine, thus providing an automatic setting arrangement. Many new designs are of course already provided with such or similar facilities. However, it is believed that large numbers of existing machine tools could be improved by the fitting of some simple and reasonably priced datum setting devices.

Feeds and speeds

The use of drives with infinitely variable, mechanical and hydraulic gear boxes has considerably reduced the time for changing the feeds and speeds on most modern machine tools. However, a recent time lapse film suggests that there is a need for more reliable information on the most suitable arrangement of machine tool controls. Whether this should be in the form of a pendant, console or some new method, must be carefully studied before a decision can be taken.

Speed and feed changes in machines with full NC control and automatic tool changing are at present determined by the Planning Office. Nevertheless the timing and calculations in the programme can have a marked effect upon the non-cutting period. A recent experience on one of these machines illustrated the difficulty of programming for maximum approach traverses, combined with the minimum distance between the workpiece and cutting tool, before the actual cutting feed rate was engaged. This is often complicated by the speed of the table rotation when presenting a new face for machining and particularly by the shape of the component itself. Here there is a need to develop some form of simple simulator which could be used by the Planning Office when preparing new programmes for machining centres.

Clamping

As mentioned previously, the question of clamping a component is largely determined by its shape. There are many excellent examples of machining fixtures with first-class locking and clamping devices already built in, in which the whole arrangement is automatically controlled and designed into the machining cycle. Unfortunately, at present, this can only be justified in factories engaged on mass production or large batch quantities. What is needed for the general engineering workshop is perhaps some inexpensive form of encapsulating components so as to provide a simple and accurate locking and clamping face to the work-holding area. Maybe this approach could be similar to the idea recently introduced in the broaching field for the production of aircraft components. Here workshop transport was facilitated and accurate workpiece position ensured during machining operations which consisted of broaching and deburring in an 8-station automated line. The cycle time in this case was reduced from 500 to 30 seconds per workpiece, mainly due to the higher broaching speeds that were made possible by the improved holding facility. A further feature of this particular machine was the use of an instantaneous histogram type of display for in-process gauging. Measured values of the blade dimensions are punched on paper tape and then displayed, thus monitoring the dimensions of the last 100 components to give an accurate indication of broach wear.

The metal used for encapsulation is a tin bismuth eutectic with a dimensional stability of about 0.02% during a period of 1000 hours after casting. This type of metal is also being used successfully for reinforcing a thin-walled tube during a milling operation. Whether or not this method can be extended for more general use is, of course, a matter for further

investigation, but in view of the improvements achieved, further thought in this approach would appear to be fully justified. There are, of course, many examples of independent air or oil clamping and locking units which can be fitted on to angle plates or box fixtures and are thus capable of catering for a variety of component types. However, if these are connected by flexible pipes to improve their versatility, it has been found that under the action of the cutting forces these connections tend to distort, with a subsequent loss of clamping pressure. Apart from a long-term policy of redesigning components which allow for easy accurate location and satisfactory clamping, there is a dire need for some new approach to the problem of workholding systems which are simple, reliable and not too expensive.

CONCLUSIONS

When attempting to be very critical on any subject, there is always the danger that the uninformed may draw the wrong conclusions and imagine that little or no progress has been made with the problem under examination. There is no doubt that some excellent examples exist, some of which were mentioned at the International Congress for Metalworking at Hanover last September. Furthermore, recent machine tool exhibitions bear witness to the industry's progressive approach and adaption of new ideas, not only in the basic models, but also in machines and control systems which are to be used in a totally integrated factory. The modern trend towards the partially or fully integrated workshop naturally covers many of the points referred to in this paper. In the meantime there still remains the national and international problem of improving the very low efficiency of many existing manufacturing plants.

A general review of the many new approaches to design and production illustrates the impact of the comprehensive range of research and development projects which have been undertaken by the machine tool industry and the various Universities and Research Establishments. Studies in group technology, designing for production, value engineering, swarf removal and the use of computer systems for stock and production control, are just a few of the new techniques that, suitably adapted, might be of value to existing general engineering workshops.

The advent of the simple readout system has been invaluable in reducing slide and worktable setting times. Equally important is the housing of a display unit to be located in the most convenient position to suit the operator. Useful progress has been made on loading and clamping devices for many machines, but from the evidence available there is still far too much time lost during the non-cutting cycle because suitable devices for all conditions do not yet appear to be available.

Following the machining of a component there is often, in the case of medium or large size workpieces, the question of inspection and handling. If, however, suitable care is exercised, a readout device has the advantage of allowing the component to be checked on the machine with a considerable saving in the total machining cycle time. Without a doubt a great deal of

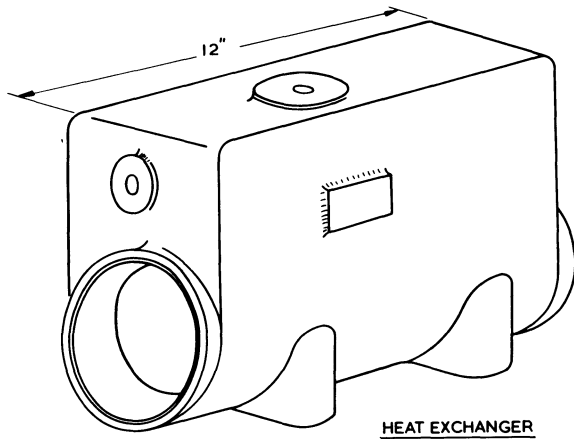
information is available, and many modifications are possible that could be of assistance in improving the efficiency of factories engaged on the production of single components or small batch quantities. Although there are many interesting and valuable methods of holding components onto worktables, they do not yet appear to cover the needs of single or small batch production in the general engineering workshop. Here some new approach is urgently needed; an approach which is simple, inexpensive and, if possible, incorporates suitable lifting points. A solution to this problem would be of considerable assistance in reducing the non-cutting period of manufacture. Furthermore, it should bring a substantial reward to its inventors whilst at the same time improving the national economy by making possible a better utilization of the nation's one million machine tools.

Finally, the author would again emphasise that the principal objective in preparing this paper was not so much to criticise existing practices but to encourage discussion by calling attention to the magnitude and seriousness of the problem of non-cutting times in some machine shops.

APPENDIX

TYPICAL PRODUCTION TIME ANALYSIS FOR BORING MACHINE

KEARNS-RICHARDS 'S' TYPE WITH VERNIER SCALES.

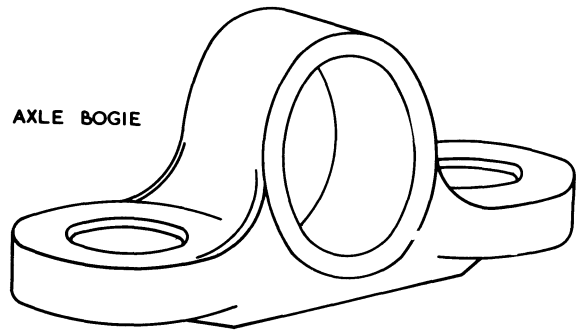


	TIME [SECONDS]
LOAD & UNLOAD	30
CUTTING	72
TOOL CHANGING	—
POSITIONING	30
GAUGING	60
TABLE INDEXING	80
TOTAL	<u>272</u>
CUTTING/ TOTAL TIME	26.5%

Fig. 1

TYPICAL PRODUCTION TIME ANALYSIS FOR BORING MACHINE

KEARNS-RICHARDS MODEL 'YU' WITH READ OUT.

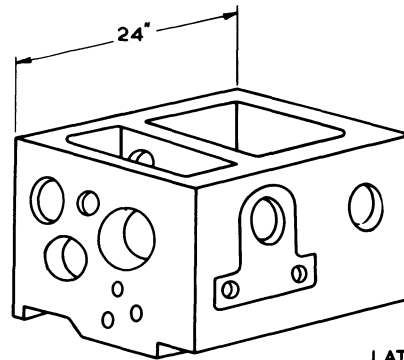


	TIME [MINUTES]
LOAD & UNLOAD	80
CUTTING	59
TOOL CHANGING	13
POSITIONING	3
GAUGING	4
TABLE INDEXING	—
TOTAL	<u>159</u>
CUTTING/ TOTAL TIME	37.2%

Fig. 2

TYPICAL PRODUCTION TIME ANALYSIS FOR BORING MACHINE

KEARNS-RICHARDS 450 MODEL WITH NUMERICAL CONTROL, TWIN TABLES AND AUTOMATIC TOOL CHANGER



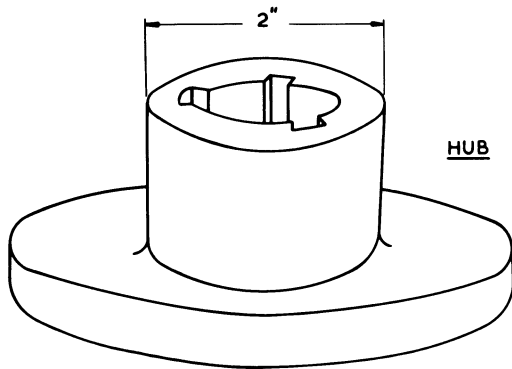
	TIME [MINUTES]
LOAD & UNLOAD	—
CUTTING	166
TOOL CHANGING	65
POSITIONING	35
GAUGING	—
TABLE INDEXING	6
TOTAL	<u>272</u>
CUTTING/ TOTAL TIME	61.0%

Fig. 3

TYPICAL PRODUCTION TIME ANALYSIS FOR BROACHING MACHINE

STAVELEY LAPOINTE

SRV. 20/66



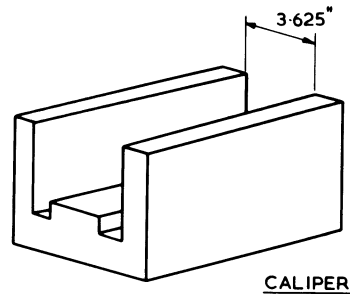
	TIME [SECONDS]
LOAD, PLUNGERS IN.	6
PRESS BUTTONS	2
EXPANDING MANDREL ON.	2
CUTTING	20
EXPANDING MANDREL OFF.	2
REMOVE PARTS	2
BROACH RETURN	6
TOTAL	42
CUTTING/TOTAL TIME	47.5%

Fig. 4

TYPICAL PRODUCTION TIME ANALYSIS FOR BROACHING MACHINE

STAVELEY LAPOINTE.

50/90 D.R.V.



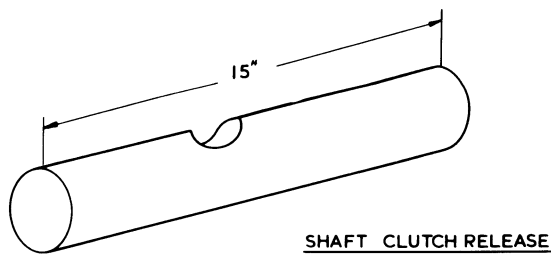
	TIME [SECONDS]
R.H. SLIDE CUTTING	(56)
UNLOAD/RELOAD 2 STATIONS	86
RH. TABLE OUT/L.H. TABLE IN.	4
L.H. SLIDE CUTTING	(56)
UNLOAD/RELOAD 2 STATIONS	86
L.H. TABLE OUT/R.H. TABLE IN	4
TOTAL	180
CUTTING / TOTAL TIME	62.5%

Fig. 6

TYPICAL PRODUCTION TIME ANALYSIS FOR BROACHING MACHINE

STAVELEY LAPOINTE

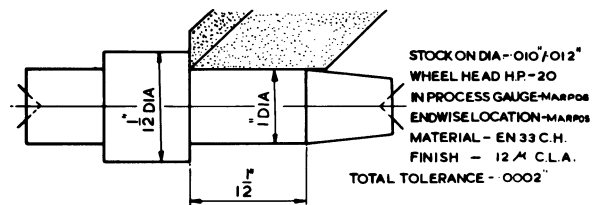
10 x 42 SRV.



	TIME [SECONDS]
LOAD	5
PUSH START BUTTONS	1
CLAMP FIXTURE, TABLE IN	3
CUTTING	17.5
TABLE OUT, UNCLAMP FIXTURE.	3
RETURN STROKE, UNLOAD	6.5
TOTAL	36
CUTTING/TOTAL TIME	49%

Fig. 5

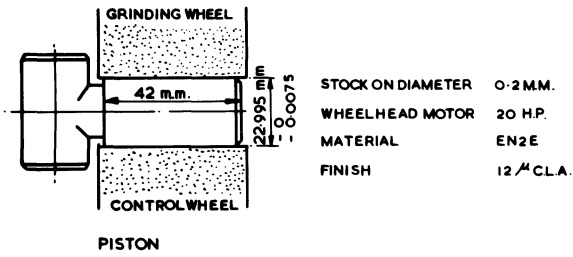
TYPICAL PRODUCTION TIME ANALYSIS FOR AUTOMATIC EXTERNAL GRINDING OPERATION (CHURCHILL 'CA' MODEL)



	TIME [SECONDS]
HAND LOAD ONTO VEE CRADLES	5
TAILSTOCK AND ENDWISE LOCATION	6
WHEEL AND GAUGE ENGAGEMENT	2
GRIND (INCLUDING 5 SEC. DWELL)	20
WHEEL AND GAUGE RETRACTION	2
TAILSTOCK RETRACTION AND UNLOAD	5
AVERAGE WHEEL DRESS PER COMPONENT	3
TOTAL	43
∴ GRINDING / TOTAL TIME	46.5%

Fig. 7

TYPICAL PRODUCTION TIME ANALYSIS FOR AUTOMATIC INFEEED GRINDING OPERATION OF A HEADED COMPONENT CHURCHILL CENTRELESS GRINDER .



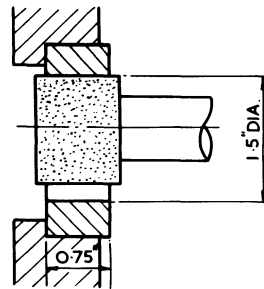
STOCK ON DIAMETER 0.2 M.M.
 WHEEL HEAD MOTOR 20 H.P.
 MATERIAL EN2E
 FINISH 12 μ C.L.A.

	TIME CYCLE [SECONDS]
AUTO EJECTION OF GROUND COMPONENT	1/2
AUTO LOAD UNGROUND COMPONENT	2
RAPID ADVANCE OF HEAD(B) TO GRINDING POSITION	1
GRIND AND SPARK OUT	5
RAPID RETRACTION OF HEAD TO WORK EJECTION POSITION	1/2
	<u>9</u>

THE GRINDING WHEEL IS REDRESSED APPROXIMATELY EVERY 250 COMPONENTS TAKING 2 MINUTES, SAY 1 SECOND PER COMPONENT.
 ∴ GRINDING TIME IS 50% OF TOTAL TIME

Fig. 8

TYPICAL PRODUCTION TIME ANALYSIS FOR AUTOMATIC INTERNAL GRINDING OPERATION CHURCHILL 'HAA' MODEL

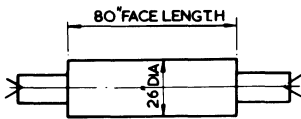


STOCK ON DIA. - 0.08"/0.10"
 WHEEL HEAD HP. - 5 HP.
 DIAMOND SIZING - NOGAUGE
 MATERIAL - EN43 B
 FINISH - 12 μ C.L.A.
 TOTAL TOLERANCE - 0.005

	TIME [SECONDS]
HAND LOAD & CHUCK GRIP	4
WHEEL ENGAGEMENT	1.5
GRIND (INCLUDING 7 SEC DWELL)	27
WHEEL DRESS	5
WHEEL DISENGAGEMENT	1.5
UNLOAD	3
TOTAL	<u>42</u>
GRINDING/ TOTAL TIME	64.5 %

Fig. 10

TYPICAL PRODUCTION TIME ANALYSIS FOR AUTOMATIC EXTERNAL GRINDING OPERATION CHURCHILL 'TWB' MODEL

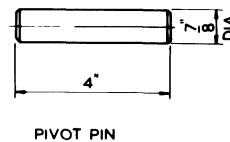


STOCK ON DIA 0.03/0.04"
 WHEEL HEAD HP 40
 NOGAUGE
 MATERIAL CHILLED IRON (SCHC)
 FINISH 15 μ C.L.A.

	TIME [MINUTES]
CRANE LOAD	9
MACHINE PREPARATION	5.0
GRIND - WORKHEAD END RE-SHAPE	7.5
GRIND - TAILSTOCK END RE-SHAPE	7.5
GRIND - ROUGH	1.0
GRIND - SEMI ROUGH	3.0
GRIND - SEMI FINISH	3.5
GRIND - FINISH	13
BREAKDOWN FOR UNLOAD	4
UNLOAD	8.5
TOTAL	<u>62.0</u>
∴ GRINDING/ TOTAL TIME	57%

Fig. 9

TYPICAL PRODUCTION TIME ANALYSIS FOR AUTO. THRO' FEED GRINDING OPERATION OF A CASE HARDENED PARALLEL PIVOT PIN ON A CHURCHILL CENTRELESS GRINDER



STOCK ON DIAMETER 0.08"
 WHEEL HEAD MOTOR 25 H.P.
 MATERIAL EN33CH.
 FINISH 10 μ C.L.A.
 ROUND & PARALLEL TO SIZE WITHIN 0.003"

AUTO FEEDING WITH VIBRATORY BOWL FEEDER & A SHORT CHAIN CONVEYOR
 PASS RATE 7' 0" PER MINUTE
 2 PASSES

WHEEL DRESSING AVERAGED 5 MINUTES PER HOUR
 GRINDING TIME IS 92% OF TOTAL TIME

Fig. 11

DISCUSSION*Query from Prof. Dr.-Ing. G. Spur*

What do you think about automatic planning and programming of NC and conventional machines? I think this must be included in a total concept of machine tools.

Reply

I fully agree with the suggestion that automatic planning and programming of NC and conventional

machines should be included in the total concept of machine tools. Clearly, this approach would eliminate many of the problems I have mentioned in the paper. Nevertheless there are many large and small companies, who already have a considerable proportion of their plant and machines relatively old in design. On these, the proportion of time the cutting tool is in contact with the work is extremely small, and I believe it is in this field that we might improve the general efficiency of these factories.

METAL FORMING

ON THE ISOSTATIC COMPACTION AND HYDROSTATIC EXTRUSION OF IRON POWDER

by

J. M. ALEXANDER* and D. R. QUAINTON†

SUMMARY

This work is a continuation of research at Imperial College into the feasibility of producing viable products from iron powder, without sintering. Further experiments have been carried out to establish the relationship between pressure and density in isostatic compaction and the effect of the back pressure in fluid-to-fluid extrusion of the compacts. The possibility was also investigated of using the design of double reduction die, proposed by Fiorentino and his colleagues at Battelle Memorial Institute, to eliminate the need for fluid-to-fluid extrusion of these brittle compacts.

INTRODUCTION

It appears that little experimental work has been carried out on the hydrostatic extrusion of green metal compacts, whereas cold isostatic compaction of metal powders is becoming a well established procedure. It seems natural to try to link these processes, which require similar equipment, particularly if it would thereby be possible to eliminate the sintering process in some cases.

Isostatic compaction has several advantages over mechanical die or ram compaction, mainly owing to the pressure being applied uniformly and simultaneously to all external surfaces, which thereby produces a reasonably uniform density throughout the volume of the compact. A prerequisite for high density would appear to be the use of a powder composed of a wide range of particle sizes, to ensure the maximum filling of the voids between the larger particles. Irregular shaped particles would also ensure high strength due to mechanical interlocking between particles and large areas over which cold welding can occur. A comprehensive review of the isostatic compaction of powders is given by Morgan and Sands¹, in which reference is made to the work of Balshin, Konopicky and Heckel². Heckel developed an analysis based on a relationship proposed by Konopicky, namely that

$$\ln \frac{1}{1-D} = KP + A \quad (1)$$

where D = relative density of the powder compact (i.e., the ratio of the specific density of the

compact to that of the *material without voids*), P = applied pressure, K and A are constants.

The data obtained from several powders (e.g., iron, copper, nickel and tungsten) reveal that the proportionality proposed by Konopicky between $\ln 1/(1-D)$ and P exists above about 25 000 lbf/in².

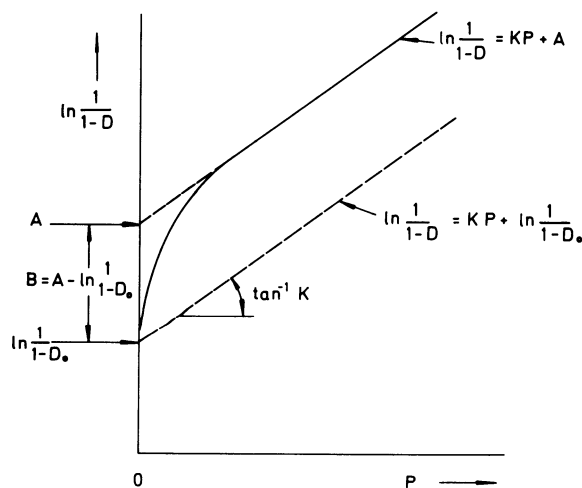


Fig. 1

Below that pressure there is an initial curved portion as indicated in Fig. 1. Thus the constant A is given by

$$A = \ln \frac{1}{1-D_0} + B \quad (2)$$

*Professor of Applied Mechanics, Imperial College, London

†Postgraduate Student, Imperial College, London

where D_0 is the relative apparent density of the powder with no pressure applied and B is a measure of the densification which takes place at low pressures before appreciable interparticle bonding takes place and the relationship becomes linear (assumed to be associated with the plastic deformation and cold welding of the powder particles).

The process of simple hydrostatic extrusion is now well known and will not be described. The equipment used in the present series of experiments for fluid-to-fluid extrusion has been described previously by Alexander and Thiruvarudchelvan³, and is shown diagrammatically in Fig. 2. This equipment incorporates a constant-pressure relief valve to maintain constant back pressure. As alternatives, the fluid into which the billet is extruded can itself be made to extrude a soft billet, so as to maintain its pressure constant, or the billet can be extruded directly into a soft metal billet which is allowed to extrude at a known pressure through a die. Both methods have been used by Oyane et al⁴.

In the simple hydrostatic extrusion of iron powder, isostatically compacted to 103 000 lbf/in² (46 tonf/in²) Alexander and Dove⁵ were able to produce sound products at an extrusion ratio of 6.75. Based on the results of Pugh and Low⁶ for molybdenum metal, and Nilsson⁷ for aluminium powder, they identified four zones as follows:

- Zone A—transverse cracking,
- Zone B—both transverse and longitudinal cracking,
- Zone C—longitudinal cracking,
- Zone D—sound products.

These preliminary results showed that transition occurred through Zone A to Zone D as extrusion ratio is increased. Nilsson's results indicated that the superposition of a back pressure reduced the extrusion ratio at which these transitions occur, although Pugh and Low's results had earlier indicated that sound products could be produced at low values of back pressure and extrusion ratio, and that a maximum back pressure was required to prevent cracking at an extrusion ratio of about 2.0. The density of the green isostatically compacted iron powder was found to rise from 7.23 to 7.45 g/cm³ after hydrostatic extrusion through a ratio of 6.75.

Oyane et al.⁴ hydrostatically extruded sintered copper powder without cracking at ratios greater than 2.7 (without back-pressure), and at ratios of 2.0 with a back pressure of about 20 000 lbf/in². (8.9 tonf/in²) all at *high speed*. At low speed, at extrusion ratio 2.0, cracking was not suppressed even with a back pressure of 22.9 tonf/in². Hydrostatic extrusion of magnesium metal and an aluminium-copper-silicon casting alloy (both brittle materials), using the solid back pressure equipment already mentioned, confirmed Pugh and Low's finding of a maximum critical back pressure to prevent cracking, occurring between extrusion ratios of 2.0 and 3.0.

In all this type of research, the effect of sheathing the billets is of some importance. Bridgman⁸ found that fracture of brittle materials stretched under high pressure was prevented by sheathing, which can help prevent penetration of the fluid into

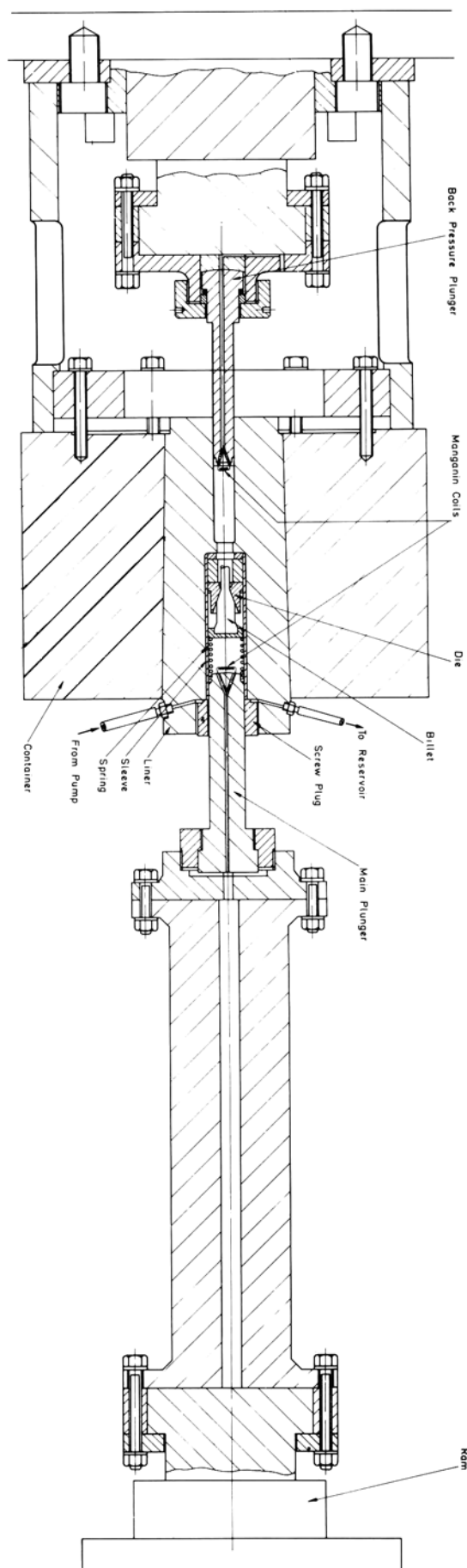


Fig. 2 Hydrostatic extrusion apparatus—back pressure set-up.

the surface pores of the specimen. This behaviour is dependent on the mechanical properties of the sheathing material, of course, and Chandler⁹ found that many of the more obvious sheathing materials such as vulcanized natural rubber, neoprene and silicone change their mechanical properties abruptly over a narrow range of pressure; for example, Young's modulus changes by a factor of about 1000 as shown in Fig. 3. Chandler found that PTFE coating tended to be washed off by the pressurizing fluid, lacquer cracked, copper plating was apparently not thick enough, whilst rubber and a mixture of 'Evostick' and methyl-ethyl-ketone gave the greatest increases in ductility of his specimens. Pugh¹⁰ also found that latex rubber could be used for sheathing cast-iron specimens successfully.

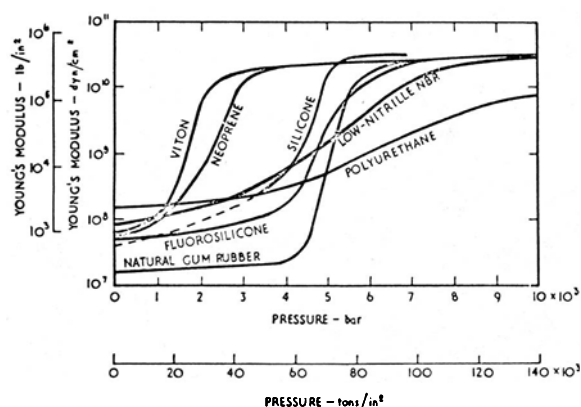


Fig. 3 Pressure dependence of Young's modulus of several rubbers at room temperature.

Alexander and Dove⁵ found that the fluid permeated throughout the whole structure of an iron powder compact which had been compacted at a pressure of 74 000 lbf/in² (33 tonf/in²) to give a relative density of 86.6%, whereas no permeation was apparent in specimens compacted at 103 000 lbf/in² (46 tonf/in²) to 92% relative density. They concluded that no interconnecting pore system was present in the denser specimens and that sheathing would therefore not be required from that point of view, although it might be beneficial from the point of view of preventing the penetration of fluid into surface fissures.

An alternative solution to the problem of overcoming the development of cracking in the hydrostatic extrusion of brittle materials has been proposed by Fiorentino et al.¹¹ Their idea was to impose a second small reduction on the product immediately after its egress from the main hydrostatic extrusion die. This small reduction (2% was found to be optimum) is believed to introduce compressive residual stresses in the surface layers of the material, thereby reducing and even eliminating the tensile residual stresses which are postulated as being usually present and responsible for cracking. These authors used a double reduction die to produce sound products of beryllium and molybdenum at an extrusion ratio of 4.0 which would normally have exhibited severe transverse cracking of the worst type. This work on

the role of die design is of considerable importance; the elimination of the necessity to apply fluid back pressure would considerably simplify the equipment and its operation. In addition, the superposition of a back pressure necessitates raising the pressure on the billet by a similar amount, which often precludes successful operation of the process due to pressure limitation on the equipment.

EXPERIMENTAL WORK

The deformable bag for manufacturing compacts was made from Devcon 'Flexane 95'—a room-temperature curing urethane. It was moulded to the same specification as used and reported previously⁵. The bags shown in detail in Figure 4 were filled with 300 g of iron powder (325 g when longer billets could be accommodated in the extrusion apparatus). The bags were vibrated gently for 2 min to consolidate the powder without the segregation of large and small particles. Sealing was achieved by means of a parallel rubber bung $\frac{3}{4}$ in long and a sliding fit in the bag. A thin washer of Flexane 95 was interposed between bung and powder to avoid forcing the soft bung into the compact. A final seal was made round the top periphery of the bung with a thin film of 'Evostick'.

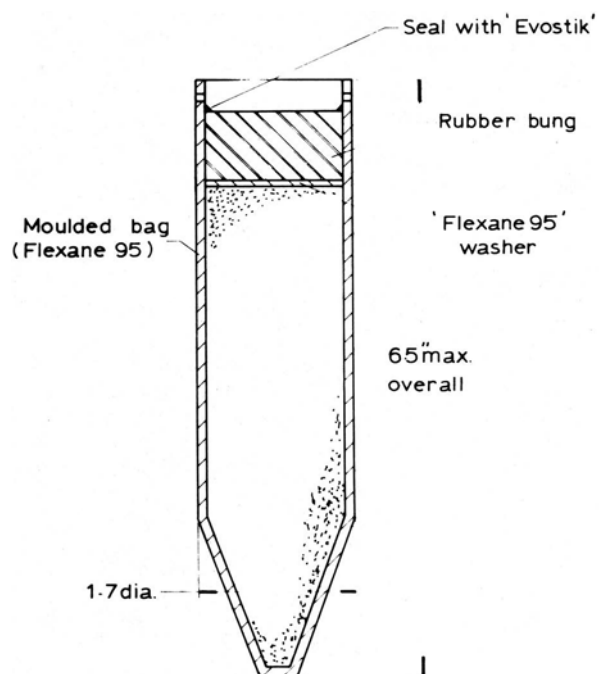


Fig. 4 Bag assembly for isostatic compaction.

The bag assembly was placed in the $1\frac{3}{4}$ in diameter bore of a high-pressure container capable of accepting 110 tonf/in² pressure, which was then filled with the pressure medium—castor oil with 10% methyl alcohol. Pressurization was by means of a punch introduced vertically into the bore of the container,

the whole apparatus being placed between the compression platens of a 250 tonf Avery universal testing machine. The punch seal comprised an O-ring and phosphor-bronze mitre ring, and provision was made for pressure measurement utilizing a manganin coil mounted across two tapered terminals lapped into conical ceramic brushes, which were in turn lapped into the nose of the punch. Details of the nose of the punch are shown in Fig. 5. The manganin coil, of 100 Ω resistance, was connected into a Wheatstone bridge circuit with stabilized d.c. supply and the output was monitored by a U.V. recorder. The pressure thus measured was compared with the pressure determined by the axial load on the punch, as measured on the testing machine. Agreement was within 3%, the difference presumably being due largely to the effect of friction on the seal of the punch, over the pressure range 46–104 tonf/in².

Isostatic compaction tests

The powder used was Hognas NC 100 iron powder, as used in the previous investigation⁵. (MH 100 powder is now designated NC 100.) An analysis of the powder is given in Table 1. Two separate consignments were purchased during the period of the investigation and compacts were made at various pressures between 29.2 and 104 tonf/in². The most suitable method of finding the density was by machining a cylinder from each compact and measuring its dimensions and weight accurately. Machining was carried out using a tungsten-carbide tipped turning tool with a surface speed of 250 ft/min, 0.005 in/rev feed and 0.03 in depth of cut (maximum). The billet nose was turned to an included angle of 38° to facilitate commencement of extrusion in the 40° die. Two diameters were machined onto each billet, the first to provide the required extrusion ratio, the second to prevent total extrusion of the billet. A taper of 40° was machined leading to the second (larger) diameter.

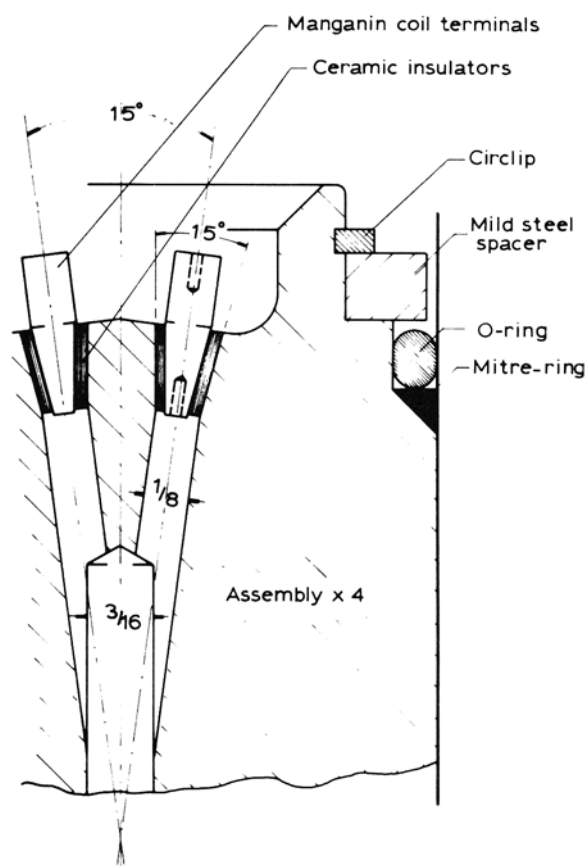


Fig. 5 Plunger nose details (1 $\frac{3}{4}$ dia).

Table 1. Details of Hognas iron powder NC 100 24

Note: This powder is prepared from pure natural magnetite ore by carbon reduction and has an irregular spongy structure.
Suppliers: Hognas (Great Britain) Ltd.

Typical Chemical Analysis (Average Values)

Iron	98+	approx. %
Carbon	0.1	"
Oxygen (loss in weight in hydrogen)	0.6	"
Silica	0.3	"
Sulphur	0.015	"
Phosphorous	0.015	"

Typical Mesh Size Distribution (B.S.S. Mesh Sizes)

+100	1%	maximum
-100 +150	15–25%	maximum
-150 +200	20–30%	"
-200 +240	5–15%	"
-240 +350	15–30%	"
-350	15–30%	"

Theoretical density 7.87 g/cm³
Apparent density (Hall) 2.4 g/cm³

Extrusion equipment

Two sets of equipment were utilized for the hydrostatic extrusion equipment. The horizontal hydraulic press already mentioned³ was used for the initial simple hydrostatic extrusion tests and all the fluid-to-fluid extrusions. The design imposed a restriction on the billet length which could be accommodated within the main pressure chamber, so the tests with the double reduction die and sheathed billets were all conducted in the vertical 250 tonf Avery testing machine already mentioned by adopting an existing vertical backward extrusion set-up which allowed the use of longer billets and easier removal of product and die, as shown in Fig. 6.

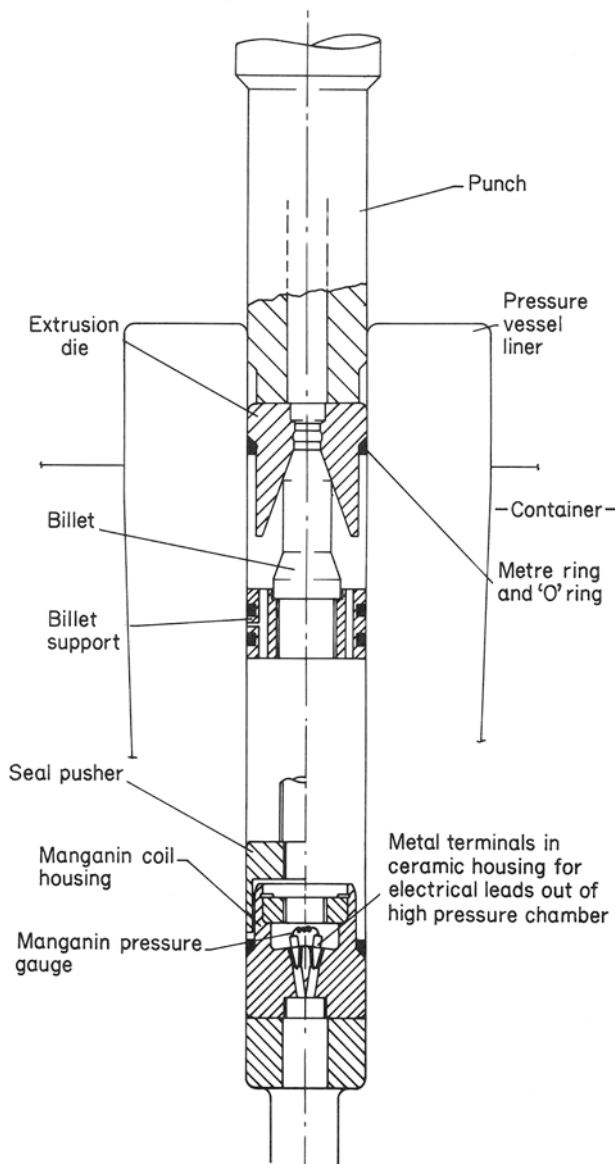


Fig. 6 Backward extrusion arrangement for double reduction dies.

Details of the horizontal equipment are shown in Fig. 2. The main chamber is $1\frac{1}{2}$ in diameter and can accept 110 tonf/in^2 pressure, with the rather limited working stroke of 6 in on each ram. An interesting feature is the thin EN30B sleeve (0.094 in thick) incorporated in the main chamber, which can be replaced if scored.

The experimental procedure for simple hydrostatic extrusion was as follows, with the horizontal arrangement—the die and seal assembly was entered into the main chamber and pushed 'home' against the step in the bore of the liner. The rear end of the billet (1.0 in diameter) was inserted into a machined rubber support and the assembly inserted in the pressurizing chamber until the billet nose located in the die. The rubber support was made so that the counterbore diameter was a close fit around the billet end, whilst the outer periphery, with longitudinal cutouts for oil passage, was a sliding fit in the chamber bore. The plunger was entered approximately one inch into the liner support plug and the chamber filled with fluid by an electrically driven pump.

The procedure for fluid-to-fluid extrusion was similar to that just outlined except that a back pressure plunger was incorporated and the billet had to be held away from the die orifice to facilitate filling of the back pressure chamber. This was achieved by positioning the billet in its support away from the die and inserting a wire-coil compression spring between the rubber support and punch. This spring was of such a length that it was lightly in contact with the billet support and main plunger in the 'fill' position. As the plunger advanced to pressurize the fluid, so the spring transported the billet and support until the billet nose entered the die orifice, thus separating the two pressure chambers. To ensure the removal of all air from the back pressure chamber, it was found necessary (with the main plunger in the 'fill' position and the pump running) to withdraw the plunger momentarily from the container and 'bleed' the chamber.

The lubricant used for all extrusions (with the exception of the sheathed billets) was Acheson 'dag' 1870 warm forming lubricant. This contains finely divided graphite blended with dispersing, stabilizing and binding agents which provide adequate suspension properties in the lubricant bath. This particular lubricant reacts chemically with ferrous metals and produces an extremely thin, adherent dry film on the billet. For the sheathed billet experiments the machined billets were dipped into Evostick thinned with methyl-ethyl ketone, producing a coating of from 0.002 to 0.003 in thickness. No lubricant was applied.

Standard seal-carrying dies were used initially but difficulty was experienced in die and product removal after extrusion. Accordingly an annular groove 0.1 in \times 0.05 in deep was ground on the periphery of the die and an extractor and thin-walled extractor ring were made as shown in Fig. 7. Product removal still necessitated extraction of the seal, however, so a seal-less die assembly was designed based on that used by Thompson and Daniels¹², as shown in Fig. 8. An internally threaded spacer carried the 'O' ring and mitre ring seals and was placed against the step at the end of the main pressure chamber. The die butted against the spacer with a seal ring moulded from Flexane 95 covering the joint. This ring provided an initial seal as well as supporting the die in position prior to pressurization. It was important to ensure that fluid could fill the cavity behind the die and around the sealing ring. This was achieved by providing

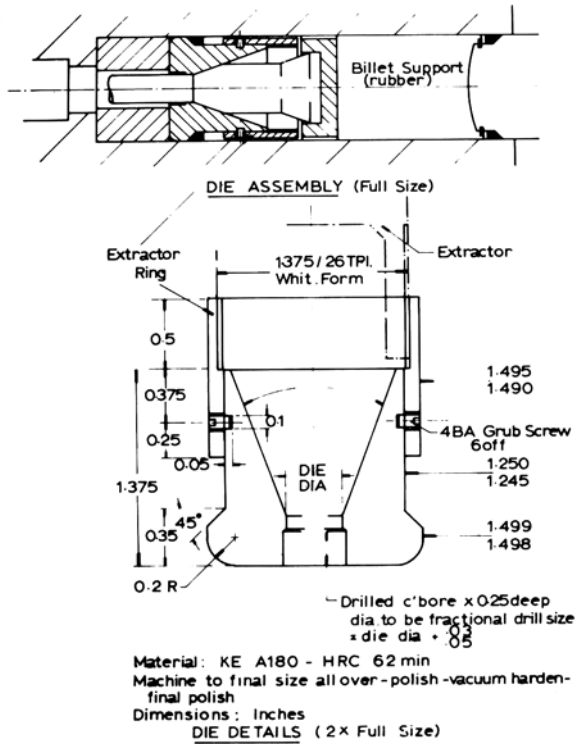


Fig. 7 Hydrostatic extrusion dies.

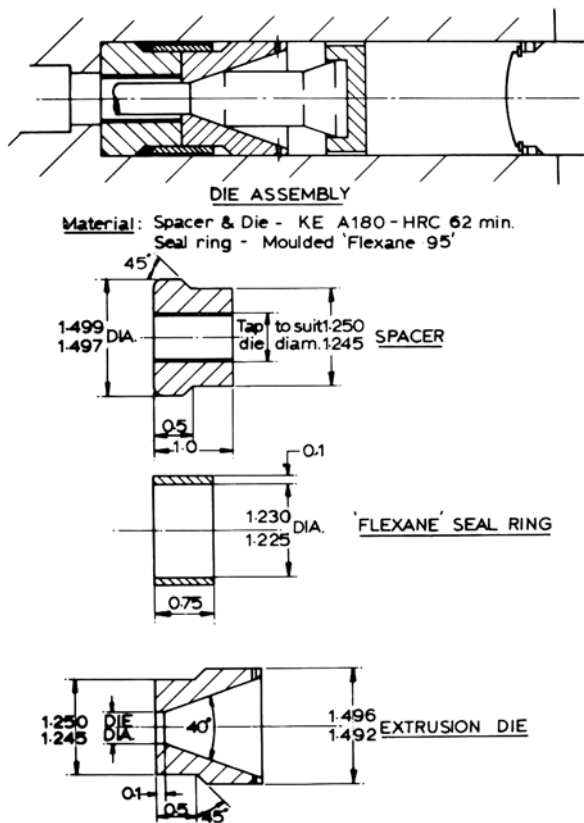
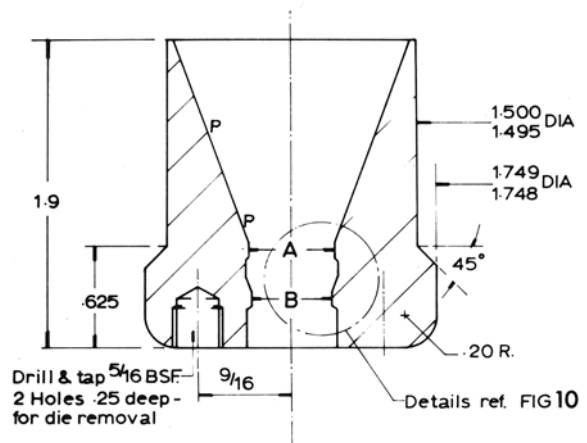


Fig. 8 'Seal-less' die.

a radial clearance of 0.0025 in between the die and the chamber bore. After extrusion, the product and die could easily be removed by hooking a simple extractor into the two holes shown near the mouth of the die.

As mentioned previously, the press used for the double reduction dies was the 250 tonf Avery, as was also used for compacting the powders. A backward extrusion arrangement was adopted as shown in Fig. 6 so that long billets could be extruded and the product and die removed easily. Shown in the figure is the billet support arrangement and the manganin coil housing. The design of the double reduction dies was based on Fiorentino's, details being shown in Figs. 9 and 10.

To enable comparison to be made with the results of the previous investigation⁵, all green compacts produced for subsequent hydrostatic extrusion were compacted at the same pressure as previously, namely, 103 000 lbf/in² (46 tonf/in²).



Material: KE A180 - HRC 62 min.

Die Sizes:

DIA.	A	0.5051	0.4041	0.3031	0.2830
	B	0.500	0.400	0.300	0.280

Machine to final size all over - polish - vacuum harden - final polish

Scale: 2 x Full Size

Fig. 9 Double reduction dies.

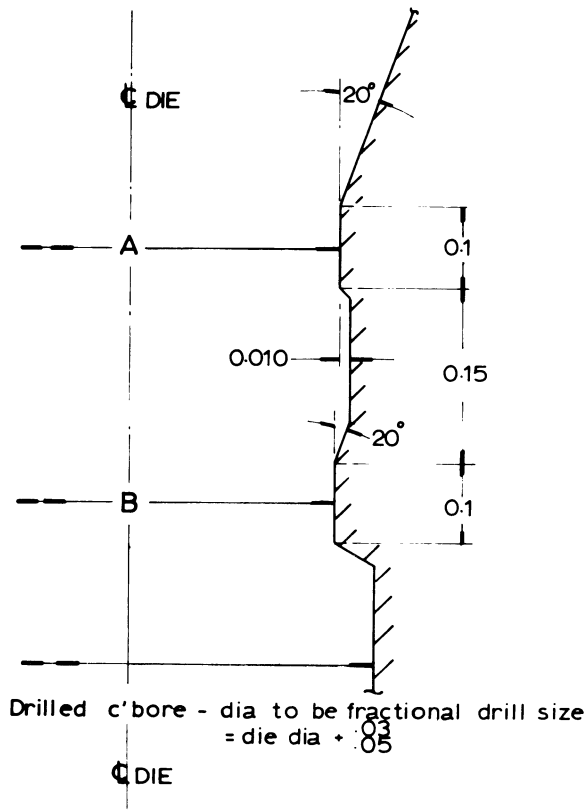


Fig. 10 Double reduction die-die profile details.

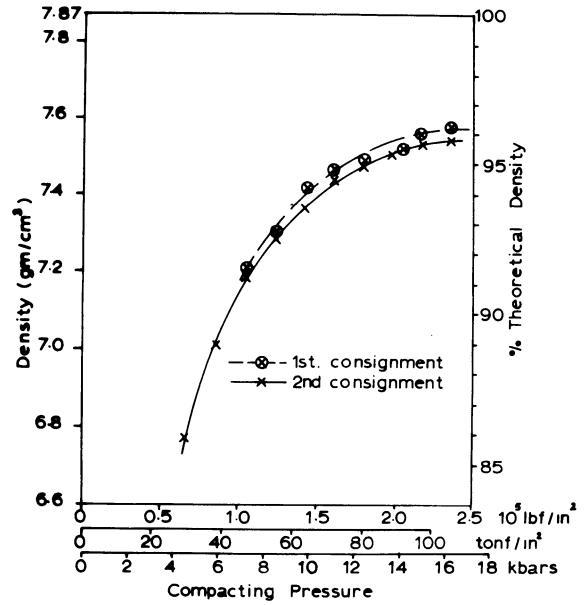


Fig. 11 Effect of compacting pressure on the density of Höganäs NC 100 sponge-iron powder after isostatic compaction.

RESULTS AND DISCUSSION

Isostatic compaction

A total of seventy compacts were made with only one failure (due to a leaking bag). Bags could easily be repaired by local application of additional Flexane 95; in fact, it was often necessary to reinforce areas of the mould which had entrapped air. There was a slight variation between the two consignments of powder used, as shown in Fig. 11, probably due to a difference in particle size distribution which could easily happen within the tolerance stated by the manufacturers (Table 1). It can be seen From Fig. 11 that there would be little point in pressurizing the powder used in this research above about 100 tonf/in², since the relative density achieved seems to be asymptotic to a maximum value of 95.8% (for the second consignment), and that value is very nearly reached at 100 tonf/in² compacting pressure.

Plotting the results in terms of Konopicky's relationship as shown in Fig. 12 reveals that they confirm a higher density achievable by isostatic compaction as compared to die compaction (as shown by Morgan and Sands). The present results also lie very close to the few points published by Morgan and Sands and their greater number reveals that there is no consistent proportionality between $\ln \frac{1}{1-D}$ and pressure, and there is no marked change in slope.

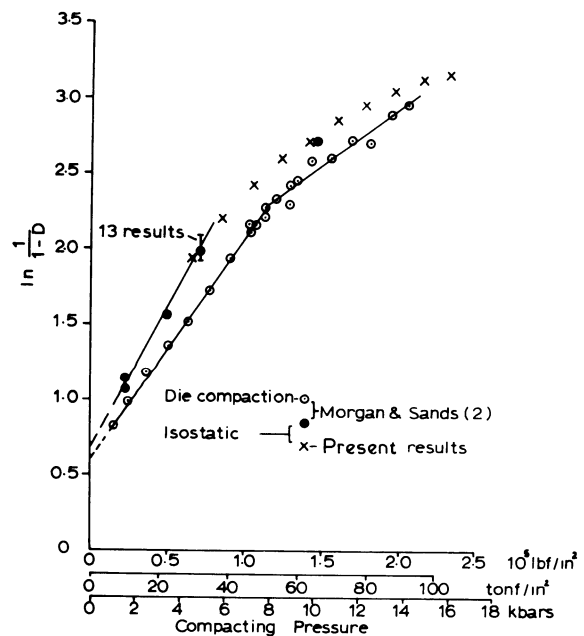


Fig. 12 A comparison of the green density (D) of Höganäs MH100 sponge-iron powder after die or isostatic compaction.

Hydrostatic extrusion

Attention was initially concentrated on determining the effect of back pressure and extrusion ratio, and identifying Zones A, B, C and D on the diagram of back pressure versus extrusion ratio. The results are shown in Fig. 13, from which a general similarity with Nilsson's results can be identified. The effect of the 38° conical nose of the billet (being less than the 40° die) was to produce an extrusion, the front part of which had been subjected to zero extrusion ratio, increasing to a maximum at the full diameter. In the region of sound products it was found that the effect of the low initial extrusion ratio at the front end of the nose was to produce longitudinal cracks which propagated along the product. For short extrusions this gave erroneous results, in that a longitudinal crack formed initially in a situation which would have eventually given a sound product. For this reason some results on the Zone C/Zone D boundary were checked using longer billets.

The results obtained with simple hydrostatic extrusion differed considerably from the previous results obtained⁵, in that an extrusion ratio of only about 5.0 gave a sound product, whereas previously about 6.5 was necessary. The boundaries between all zones were similarly considerably reduced. The only significant difference between the two investigations was in the lubricant; previously P.T.F.E. spray was used, whereas in this series, a graphite-based chemically active lubricant was used. In all extrusions with the graphite lubricant the products were found still to be completely coated with a film of lubricant. Also none of the cracked products exhibited such severe cracking as had been observed in the previous investigation using P.T.F.E. lubricant. Severe rupturing was noticed only for sheathed billets, in which case no lubricant was used.

Several of the products exhibited a marked tendency for their ends to splay out giving rise to a 'tulip' type of defect. This effect was most marked under Zone C conditions and appeared to be due to the immediate tip of the conical end of the specimen breaking away, leaving a blunt rough virgin surface into which the back pressure fluid forced itself.

Experiments with the hydrostatic extrusion of sheathed billets were inconclusive. None of them was successful. Very high pressures were required and very high loading rates to achieve extrusion through high ratios, under which conditions extrusion was rapid and uncontrollable. It is thought that lubrication was ineffective between the sheathed product and the die, as evidenced by severe rupturing in all specimens, but time did not permit a proper investigation to be made.

Five billets were extruded through the double reduction dies, at extrusion ratios of 2.25, 3.1, 4.0, 4.7 and 5.1. In spite of the fact that the dies had unfortunately been made incorrectly, with a 90° taper to the second die instead of a 20° taper, sound products were produced with no evidence of longitudinal cracking as had been found in all the simple hydrostatic extrusion experiments above an extrusion ratio of 2.25. The surface conditions of all the products was poor, because of the scraping rather than deforming action of the second land, but the

results were very encouraging.

As a matter of interest the relationship between extrusion pressure P and extrusion ratio R is shown in Fig. 14, the straight line being the equation

$$P = 51.1 \ln R + 4 \quad (\text{tonf/in}^2) \quad (3)$$

which may be compared with the previous result

$$P = 54.2 \ln R - 3.5 \quad (\text{tonf/in}^2)$$

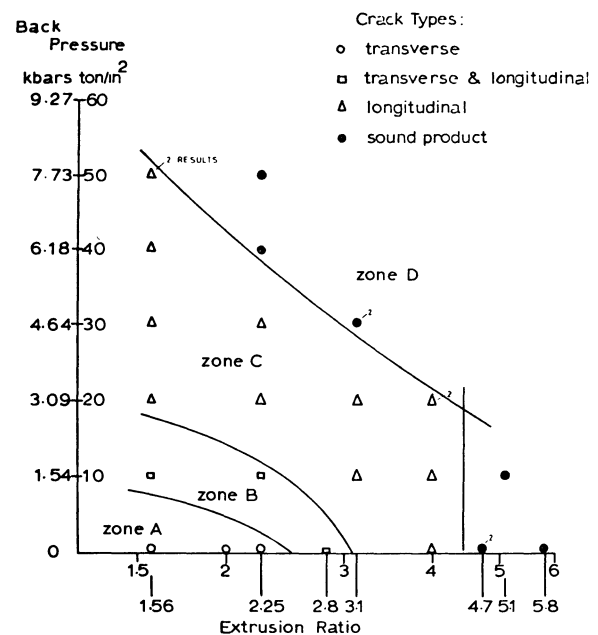


Fig. 13 Back pressure-extrusion ratio diagram for unsintered iron powder compacts.

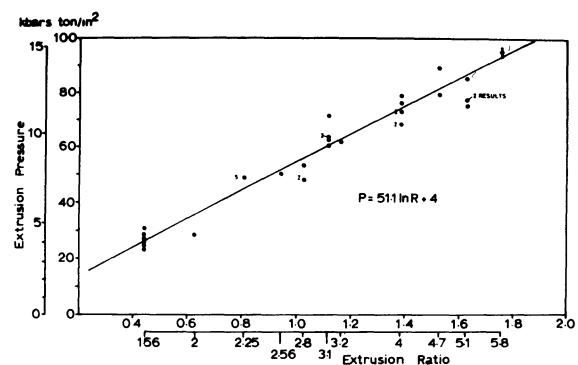


Fig. 14 Variation in extrusion pressure with extrusion ratio.

CONCLUSIONS

1. Sound products of green iron powder compacts, isostatically compacted at 46 tonf/in² pressure, can be produced by simple hydrostatic extrusion at ratios greater than 4·7.
2. Fluid-to-fluid extrusion enables smaller extrusion ratios to be used to produce sound products.
3. Graphite-based lubricant gave better results than P.T.F.E. spray.
4. Long billets must be used to achieve steady-state conditions.
5. Pressure — extrusion ratio relationship for green compacts of iron powder isostatically compacted at 46 tonf/in² pressure is

$$P = 51\cdot1 \ln R + 4 \text{ (tonf/in}^2\text{)}$$
6. Double reduction dies prevent longitudinal cracking between extrusion ratios of 2·25 and 5·1.
7. Proportionality does not exist between $\ln 1/(1-D)$ and compacting pressure.

SUGGESTIONS FOR FURTHER WORK

1. Compaction at 46 tonf/in² gave 91·2% theoretical density, whereas 100 tonf/in² gave 96% theoretical density. It would be of great interest to extrude hydrostatically compacts isostatically compacted to 100 tonf/in², to see if their propensity for cracking were diminished. In other words, to determine the back pressure versus extrusion ratio graph for such compacts.
2. Redesign the double reduction dies to:
 - (i) reduce the scraping action of the second land and promote smooth plastic flow through the die,
 - (ii) reduce the tendency for severe wear of the second land,
 - (iii) split the die so that the second die profile can be formed separately (to achieve (i) and (ii)).
3. Determine the mechanical properties of the products formed by this process. This would necessitate products of a size large enough to enable tensile, impact and fatigue specimens to be made, as well as hardness distributions to be determined.

4. Investigate the effects of particle size distribution of the powder on resultant compact density and the effect on subsequent hydrostatic extrusion.

5. Experiment with other powders, for example, non-ferrous, to establish the parameters required to give sound products.

REFERENCES

1. MORGAN, W. R., and SANDS, R. L., 'Isostatic compaction of metal powders', 1969, *Metals and Materials*, 3 (5), p. 85.
2. HECKEL, R. W., 1961 Trans. Met. Soc. A.I.M.E., 221, p. 1001.
3. ALEXANDER, J. M., and THIRUVARUDCHELVAN, S., 'The billet augmented hydrostatic extrusion of copper', *Annals of the C.I.R.P.*, 1970 (in press).
4. OYANE et al., 'Back pressure extrusion of brittle metals and metallic powder', 1969, *Bulletin J.S.M.E.*, 12, (50), p. 376.
5. ALEXANDER, J. M., and DOVE, L. B., 'A preliminary investigation of the isostatic compaction and hydrostatic extrusion of iron powder', *Annals of the C.I.R.P.*, 1970 (in press).
6. PUGH, H. L.D., and LOW, A. H., 'The hydrostatic extrusion of difficult metals,' 1964/5, *J. Inst. Metals*, 93, p. 201.
7. NILSSON, J., 'Experimental results from ASEA hydrostatic extrusion equipment', 1969 post-experience course in hydrostatic extrusion, Imperial College, London, Unpublished.
8. BRIDGMAN, P. W., 'Studies in large plastic flow and fracture', 1964, Harvard University Press.
9. CHANDLER, E. F., 'Effect of sheathing on the mechanical properties of a material under hydrostatic pressure', 1966, N.E.L. Report No. 255.
10. PUGH, H. L.D., 'Applications of static high pressure to the forming of metals—hydrostatic extrusion', 1966, *Metals Deformation Processing*, II, DMIC Report 226.
11. FIORENTINO, R. J., RICHARDSON, B. D., and SABROFF, A. M., 'Hydrostatic extrusion of brittle materials—role of die design and residual stress formation', 1969, *Metal Forming* (September), p. 243.
12. THOMPSON, P. J., and DANIELS, P. R., 'A nomogram for the prediction of extrusion pressures in the simple hydrostatic extrusion of round bar through conical dies', 1968 U.K.A.E.A. Report.

DEVELOPMENT OF A NEW PRECISION SHEARING PROCESS: OPPOSED DIES SHEARING PROCESS

by

K. KONDO and K. MAEDA*

SUMMARY

Based on the fundamental investigation into the formation mechanism of the smooth sheared surface, a new precision shearing process has been developed. In this process the stock of the material is removed outwards during working; that is, a quasi cutting mechanism is utilized. This process is characterized by the use of an opposing die with a protrusion instead of an ordinary punch in blanking. So, it is named 'opposed dies shearing process'. This research deals with the course of the development, the fundamental characteristics and the conditions of application of this process, and makes the features of this process clear by comparing with those of fine blanking. Among these features, suppression of the burr, applicability to brittle materials and sharply pointed contours, and the prolongation of the tool life may be the most dominant. Further, this paper shows a practical design of the precision shearing press suitable for this process, the features of the tool construction and the practical data concerning several kinds of materials and the blanking shapes.

INTRODUCTION

Development of a precision shearing process had earnestly been desired for a long time because of its high success as a precision working process. Now, fine blanking has satisfied the demand fairly well. But, the positive attempts to extend the application range of this process to many kinds of materials have often met with difficulties.

The authors have found in the fundamental investigations into the formation mechanisms of the sheared surface that there are two kinds of mechanisms for forming the smooth sheared surface; that is, the mechanism by plastic deformation and that by cutting.¹ This research deals with the development of a new precision shearing process which utilizes the cutting mechanism. Owing to the alteration of the working principle itself, this process has many features which are essentially different from those of fine blanking. This paper shows comprehensively the characteristics of this process ranging from the basic mechanism of forming the smooth surface to the practical design of the precision shearing press suitable for this process.

FEATURES OF THE CUTTING MECHANISMS AS A WORKING PRINCIPLE OF THE PRECISION SHEARING PROCESS

Figures 1a and 1b show schematically two kinds of mechanisms for forming the smooth sheared surface.

In the conventional shearing process the smooth portion of the sheared surface is formed by the mechanism of plastic deformation. That is, a shear plane is severely deformed by the penetration of the tools in the material in the direction AB which connects the

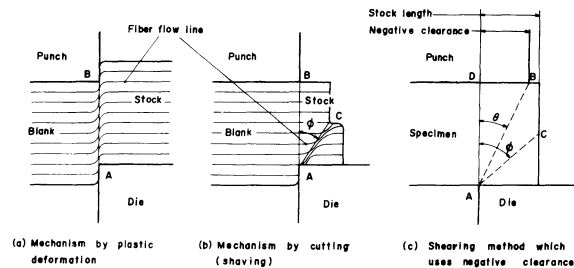


Fig. 1 Mechanisms for the formation of the smooth sheared surface.

two cutting edges, as shown in Fig. 1a. This shear plane coincides with the contour section of the blank, so the shear deformation must be succeeded on the same plane throughout a process. Consequently, the amount of the shear deformation which is necessary to cause separation becomes extremely large and most materials used in the shearing cannot sustain this amount and fracture during working.

In order to utilize the mechanism of plastic deformation as a principle of precision shearing, it is necessary to increase the ductility or plastic deformability of the material so as to sustain this large deformation. Fine blanking realizes this by increasing the hydrostatic pressure in the material near the

*Faculty of Engineering, Shizuoka University

cutting edges through strengthening the restriction of the material by means of the pressure plate with a V-ridge.

On the other hand, in the shaving process in which the conventional cutting mechanism takes place, a severe shear deformation caused by the penetration of the tool occurs along the shear plane AC in Fig. 1b. This shear plane moves upwards to a new position in the stock according to the punch travel. So, the amount of the shear deformation required for each material part becomes relatively small and most materials worked by the shearing can sustain this amount of deformation. In addition, since the shear plane AC has inclination ϕ to the contour section of the blank AB, there remains hardly any chance of the fractured surface becoming formed directly on the blank, even in cases where the crack initiates on the shear plane. These facts show that the cutting mechanism has essentially more desirable features with regard to the application range of the materials than the mechanism of plastic deformation.

However, the cutting mechanism also has a serious defect. That is, to promote this mechanism it is necessary to remove the stock successively during working. So, if the removal is restrained or the stock becomes large, the severe shear deformation plane shifts to AB in Fig. 1b and a fracture soon occurs.

Between these two mechanisms of forming the smooth surface, the mechanism by plastic deformation has been utilized mainly for the principle of several precision shearing processes. Fine blanking is representative of these and its usefulness is beyond doubt. But if we demand much of it, the following problems should be considered.

1. Tool life is much shorter than that for conventional shearing, because a high hydrostatic pressure must be superposed and a critical clearance of 0.01–0.02 mm between the punch and die must be preserved to suppress the fracture^{2,3}

2. In the following cases, the application becomes difficult^{2,4}: (i) less ductile or brittle materials, (ii) thick plates, (iii) products which have sharply pointed contour lines.

3. Because of the necessity to penetrate the V-ridge of the pressure plate into the material, the stock length cannot take short, so the percentage of the stock to the blank becomes fairly large.

4. It has no positive means to suppress the burr.

5. Roll-over of the sheared edge becomes large owing to the rounding of the die edge which is conventionally used to suppress the fracture. This becomes a problem, especially when the product has a sharply pointed contour.

We cannot but think that these problems are mainly responsible for the limit of the working mechanism itself and the only way to solve them is to alter the working mechanism. These are the main reasons for the cutting mechanism being adopted in a new precision shearing process.

Now, in order to utilize the cutting mechanism in a precision shearing process, the application range concerning the stock length must be extended. In this situation, a shearing method which uses negative clearance is taken into consideration. In this method the shear deformation plane caused by the die penetration is formed along plane AC or plane AB in Fig. 1c. These planes are inclined towards the stock side and can move in the material as the die penetration proceeds, so the features of a cutting mechanism are always preserved. The foregoing research by the authors has shown that if the absolute value of the negative clearance is larger than 20% of the material thickness, the smooth sheared surface is always formed regardless of the stock length in the case of the strip shearing by linear cutting tools.¹

By the adoption of the negative clearance method, the extension of the application range of the cutting mechanism concerning the stock length can be achieved. But, the problem of the separation of the blank and stock at the final stage remains.

OPPOSED DIES SHEARING PROCESS

Opposed dies shearing process is conceived by improving the negative clearance method to make it possible to separate the blank completely. By this improvement the suppression of the burr, which is one of the most troublesome problems in the shearing processes, is attained simultaneously. Tools used in blanking by this process are a conventional die, a protruding die which opposes the former, a knockout and an ejector. This process is characterized by the use of such an opposing tool with a protrusion. Arrangement of the tools and the sequence of the tool action are schematically shown in Fig. 2. In the

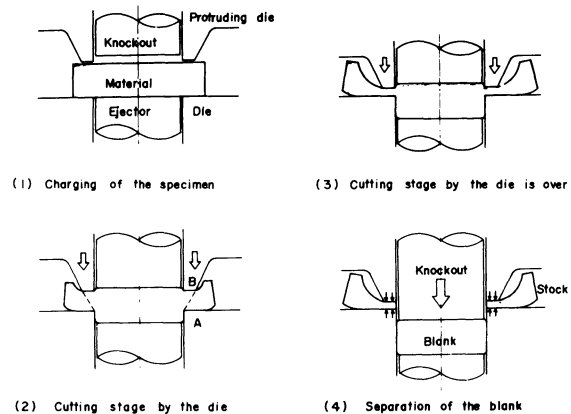


Fig. 2 Illustration of opposed dies shearing process.

earlier stage, a shear deformation plane is formed in the plane of the material that connects the die edge A and the outer edge of the protruding die B, and the tool penetration into the material proceeds from the die edge side solely by means of the cutting mechanism [Fig. 2(2)]. In this case the penetration of the protruding die scarcely occurs if the width of a plane portion at the top of the protruding die is selected to be larger than a certain value. So a smooth surface is formed by the same mechanism as the negative clearance method. In the later stage, deformation shifts to

a state like flat plate compression and the penetration of the protruding die begins. The amount of penetration of the protruding die may also be controlled by setting the knockout to a desired height. After this stage the working load increases rapidly. Therefore, the cutting by the die must stop before this [Fig. 2(3)], the knockout then proceeds and separates the blank [Fig. 2(4)]. At this separating stage, the stock is pinched between the two dies and is subjected to a hydrostatic pressure high enough to preclude any possibility of initiating a fracture. So this last stage resembles fine blanking in its working mechanism. Further, in this case, burring is suppressed by the penetration of the protruding die.

This process can be applied not only to the blanking, but also to the punching when a set of the punch and opposed protruding punch is used, as is shown in Fig. 3. In the punching, it is necessary to provide room for the stock to be removed. Figure 3 shows the case where a pre-punched hole is prepared to provide the room. But, if the diameter of the blank hole to be produced is large enough compared with the material thickness, it is possible to remove the stock only by the promotion of the dishing without preparing the pre-punched hole, because the stock volume to be removed by the protrusion is not so large.

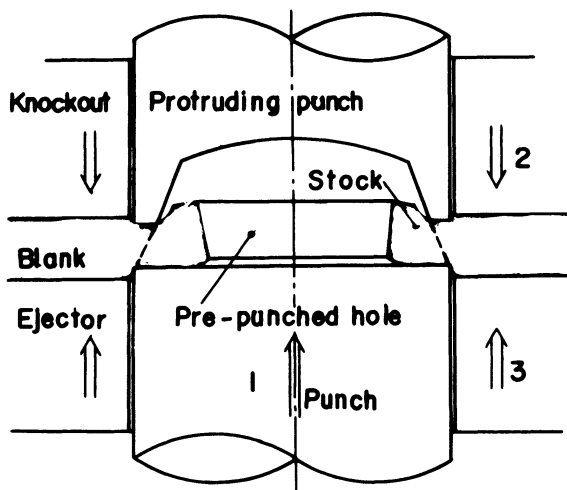


Fig. 3 Opposed dies shearing tools for punching.

DETERMINATION OF THE BASIC WORKING CONDITIONS

In this section, basic working conditions such as the geometry of the protruding tool, the shape of the specimen and the operation timing of the knockout are examined using the blanking of an 18 mm diameter disc from a hard-tempered aluminium strip (A1P1-H, see Table 1) of 1 mm thickness.

The geometry of the protruding die is determined as follows. First, the flank of the protruding die has the same contour as the blank to be produced. The relief side of the protrusion is shaped normally so as not to prevent the removal of the stock. For instance, it may be shaped to have an inclination of 25° from the die flank. The height of the protrusion is usually selected to be 1.0–1.2 times the material thickness.

Next, the plane portion at the top of the protrusion

is provided to reduce the chance of fracture caused from the die edge and to permit the die to penetrate into the material using the cutting mechanism. For this reason, the plane portion must have a width greater than 20% of the material thickness, as in the case of the strip shearing mentioned above. However, if the width becomes too large, the stock will be subjected earlier to the plane compressive deformation. This will raise the working load as is shown in Fig. 4a and an undesirable bulge of the blank edge will occur because a part of the material on the stock side may be forced into the blank. For a variety of materials the range of width which is recommendable is about 30–40% of the material thickness.

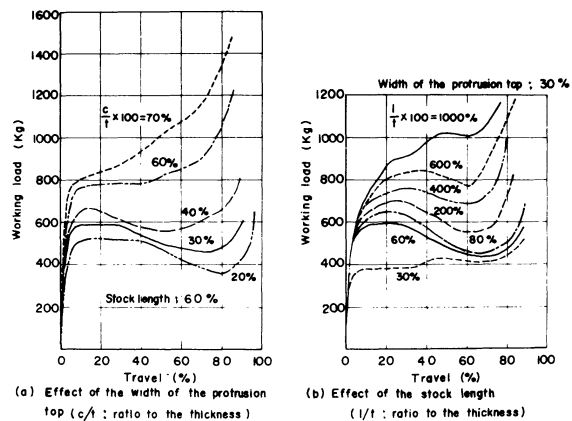


Fig. 4 Effect of the width of the protrusion top and the stock length on the working load.

For application of the present process, it is essential to facilitate the removal of the stock. In shearing along a simple opened contour, stock removal presents no problem, but offers difficulties in shearing along a closed contour. An important method conceived for this purpose, in the case of the blanking, is to prepare an extremely narrow strip and to make the feed of the strip as short as possible so that the stock can be deformed or divided at the section of minimum width of the scrap ribbon during shearing, thereby facilitating the removal of the stock. Figure 4b shows the effect of the minimum width of the scrap ribbon (minimum stock length) on the working load. Owing to the superposition of the expansion resistance of the stock, the working load increases rapidly with increasing minimum stock length. This increase of the load also creates the risk of bulging. So the stock length selected must be rather shorter. This effect of the stock length is discussed in detail later in connection with the quality of the material. Means of stock removal in the case of punching have been explained in the earlier section.

The operation timing of the knockout is desirably delayed whenever possible in order to avoid the initiation of the crack during the separation stage by the knockout. However, it must not be later than the steep increasing stage of the working load, shown in Fig. 4, to avoid the above-mentioned bulge at the blank edge. In this connection, if trouble is taken in making the tool, it is possible to delay the steep increasing stage by modifying the die or protruding die face to be outwardly inclined.

The products blanked by the present process have the following features compared with those of fine blanking:

1. burring is prevented,
2. roll-over of the sheared edge becomes extremely small,
3. internal workhardened region of the sheared surface is scarcely observed, except the small portion which is sheared finally by the operation of the knockout.

The magnitude of the working load necessary for this process is much influenced by the stock length, as shown in Fig. 4b, and becomes nearly equal to that of fine blanking when the stock length is 50% of the thickness. So, if the stock length becomes less than 50%, the working load for the present process becomes accordingly less. In fine blanking, a large holding pressure to penetrate the V-ridge is necessary in addition to this load. Consequently, the total working load necessary for this process becomes smaller than that for fine blanking and this, therefore, is also one of its features.

EXTENSION OF THE APPLICATION RANGE

As the working principle of the present process is essentially different from that of fine blanking, the application limits which have been set to fine blanking may be overcome easily on some occasions. Based on the considerations in the previous section, the applicability of this process concerning the material thickness, the quality of the material, and the contour shape of the blank are examined in this section.

At first, the extension of the application range to thick materials is tried. With thicknesses of only about 1 mm, there are no difficulties in applying the process to every kind of material used in conventional shearing. However, the fractured surface is apt to be formed as the thickness increases. If we extend the fundamental considerations in the previous section, the increase in thickness does not seem as unfavourable for fracturing in the case of the present process, because the severe shear plane shifts continuously during working. But this consideration is inconsistent with the experimental results. To explain this contradiction, the state of the fracturing has been carefully observed. From this observation it has become clear that the fracture in this process is very shallow and groovy, and appears only at the earlier stage of the operation. This is quite different from the fracture of fine blanking or conventional shearing. This type of the fracture will occur with the digging into the blank at the die edge, as is the case in the tear-type cutting in machining.

In the present process, the shear angle θ and the rate of increase of θ to the die stroke are equal for every material thicknesses because the width of the flat top of the protrusion is selected as a percentage of the thickness. However, the absolute speed of increase of θ varies with thickness; the thicker the material, the later the increase in θ . This may be why the shallow fracture occurs easily in the present process with thicker materials. Also, the facility of

formation of the smooth surface portion at the later stage may be explained as resulting from the increase of the shear angle θ in Fig. 1c.

Based on the above understanding, a means of providing a radius to the die edge, which has customarily been practised in fine blanking, is conceived to prevent the shallow fracture caused by the digging in at the earlier stage. Figure 5 shows the application range taking the radius of the die edge and the stock length as the variables in the case of a high-carbon steel in spheroidizing annealing condition (S45C), and a high-strength aluminium alloy (A3P4) about 6 mm thick. It must be noted that the remarkable difference in the application range of these materials appears only for thick materials. That is, in the cases of S45C specimens of 1 mm thickness and A3P4 specimens thinner than 3 mm, the successful ranges extend to the whole region of the diagrams, and in the case of a 3 mm thick specimen of S45C, the limiting line of the successful range becomes the two-dotted chain line in Fig. 5a.

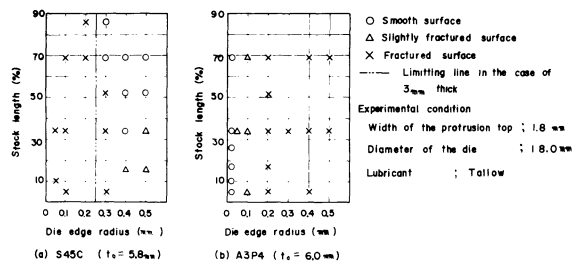


Fig. 5 Application range of the die edge radius and the stock length.

These systematic examinations are carried out with materials which do not exceed 6 mm thickness. However, it has also been confirmed that the present process can be applied to high-carbon steels of 10 mm thickness fairly easily. In these cases the counter pressure by the ejector serves mainly to prevent the dishing of the blank, but may also serve to suppress the fracture by digging, if the pressure is fairly high.

The reason for the remarkable difference in the application range, according to the material properties in Fig. 5, must be discussed. The mechanical properties of these materials are shown in Table 1. In the case of S45C, the release of the stress concentration by means of the rounding of the die edge is well served to prevent the fracture. From the figure, it appears that the increase in stock length also serves to prevent the fracture. This is because the stock must be removed outwards to proceed with the die penetration, and the resistance to this removal causes the superposition of the hydrostatic pressure on the shear plane AB in Fig. 2(2). The longer the stock, the higher the hydrostatic pressure and this is favourable for the prevention of fracture.

In these cases it may seem that although the shear plane is inclined and movable, the shearing mechanism quite resembles that of fine blanking because the increase in the deformability of the material is expected by the superposition of the hydrostatic pressure. However, it must be emphasized that there is an important difference between these. In fine blanking the hydrostatic pressure which is applied by

the pressure plate with a V-ridge in the first stage must be preserved during working. In the present process, the hydrostatic pressure is increased gradually during working, because the stock must always be removed and no fracture is observed in the later stage of the die penetration. It is thus possible to understand that the length of the stock becomes one of the control factors of the hydrostatic pressure which is applied on the inclined shear plane. This feature only results when the principle of the negative clearance method is adopted, and this principle has been utilized in a much simpler form in another paper by the authors.⁵

On the other hand, in the case of A3P4 in Fig. 5(b), the application condition is severely restricted to the sharp edged die. A3P4 is a very brittle material, as is shown in Table 1, so it fractures suddenly during the earlier working stage. However, this fracture occurs along the AB plane in Fig. 1c and gives no fracture on the blank. By this fracturing most of the stock material is removed. After this stage the operation proceeds as one of the shaving process of the remaining triangular stock which is included in the angle θ in Fig. 1c, and the smooth surface is formed with small working load. This is desirable for the tools. When the radial die is used, the workhardening of the material also occurs in the blank along the die radius and the material cannot sustain this hardening, so the sudden fracture results, accompanying the digging of this portion.

In the above, two kinds of working phenomena in the cases of Fig. 5 are made clear. Of these, the latter becomes especially important, because brittle materials which have never been able to shear in fine blanking can be sheared rather easily by this mechanism. As to the applicability to brittle materials, it has been confirmed that the present process can be applied successfully even to non-metallic materials such as phenolic resin laminates, epoxy resin laminates and SMC (fiberglass reinforced plastics) (cf. Fig. 7).

The next problem we are interested in is the parameter which distinguishes the different behaviours of materials as described above. The mechanical properties of the materials which are mainly used in this experiment are summarized in Table 1. Of these materials, only A3P4 behaves in a brittle manner. So, it is possible to conclude that a parameter such as ductility, uniform elongation, workhardening index n , and total elongation cannot be a conclusive parameter of the brittle behaviour in this process. The percentage reduction of the area seems to be the only useful parameter.

It has been confirmed in this experiment that besides the materials shown in Table 1, or mentioned above, stainless-steel (SUS24, SUS27) and tool steel (SK5) can be sheared by this process. The above extensive applicability to a wide range of materials may be the most dominant feature of the present process.

The present process exhibits a further feature in the application range concerning the contour shape of the blank, because the roll-over at the sheared edge can be reduced remarkably. In this research a systematic experiment on the applicability to the sharply pointed contour has been carried out with hard-tempered aluminium specimens (A1P1-H), shown in Table 1. The blanking contour has eight pointed corners, half of which are 60° and the remaining half are 90° (cf. Fig. 7). The corner radius of each point is altered from 0.3 mm to 2.0 mm for the specimens of 3 mm thickness, and from 0.2 mm to 1.0 mm for the specimens of 1 mm thickness. The results show that the sheared surface of each corner has no fracture or roll-over for the specimen of 1 mm thickness. In the cases of the 3 mm thick specimen, the fracture appears only at the corner of 0.3 mm radius, and the smooth surface with a slight roll-over is formed at the other corners above 0.8 mm radius. These data indicate that the present process can be well applied to the severer pointed contours in comparison with fine blanking. However, as to the range of application

Table 1. Mechanical properties of the materials used for experiments

Materials	0.2% proof stress (kg/mm ²)	Ultimate tensile strength, (kg/mm ²)	Work hardening index, n	Total elongation (%)	Reduction of the area (%)
SPHC	27.9	33.8	0.21	44.2	75
S45C	36.1	56.3	0.18	30.9	58
PBP2-H	48.4	60.9	0.03	16.8	65
BsP3-1/4H	—	45.9	0.23	35.6	62
A1P1-1/2H	10.8	12.6	0.03	16.2	80
A1P1-H	13.4	17.4	0.03	7.7	61
A3P4	30.9	47.2	0.16	20.0	23

concerning the contour shape, we must note that this process cannot be applied to the punching of narrow slits or small holes which have no room for removal of the stock.

Finally, we must refer to the tool life of this process. At present, we have little data about the tool life, but these have shown that the tool life is not limited by the increase of the burr as is the case in fine blanking, because there is no chance of burring in this process even if the wear of the cutting edge is increased. So, the tool life becomes much longer than that for fine blanking.

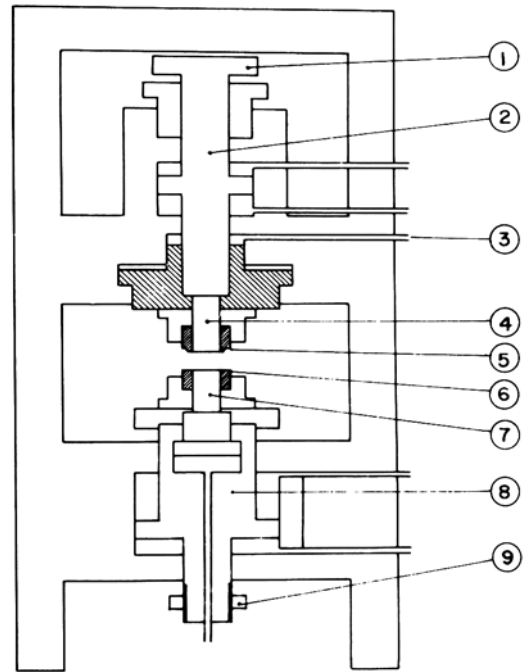
**DEVELOPMENT OF AN OPPOSED
DIES SHEARING PRESS
AND EXAMPLES OF THE
PRODUCTS**

Based on the preceding fundamental experiments, a triple action hydraulic press suitable for this process has been developed. The construction of this press is schematically shown in Fig. 6. This press has a floating device to maintain the pinching pressure of the stock during the final separating stage and mechanical stoppers to guarantee the accuracy of 0.01–0.02 mm for the stopping positions of the ram stroke and knockout stroke.

In addition to the features of the press, the tool construction for this process has the following features: (i) number of tool parts decreases, (ii) rigidity of the tool construction increases,³ (iii) severe fitting of the male and female tools is avoided. These features may also contribute to the prolongation of the tool life.

Examples of the products are shown in Fig. 7. Of these, the largest one is a crank web made of S55C and of 10 mm thickness. The smallest one is a key

made of SPHC, with the width smaller than the thickness. In this product the prevention of roll-over is well served.



- ① Mechanical stopper
- ② Knockout piston
- ③ Floating device
- ④ Knockout
- ⑤ Protruding die
- ⑥ Die
- ⑦ Ejector
- ⑧ Main ram
- ⑨ Mechanical stopper

Fig. 6 Hydraulic press designed for opposed dies shearing process.

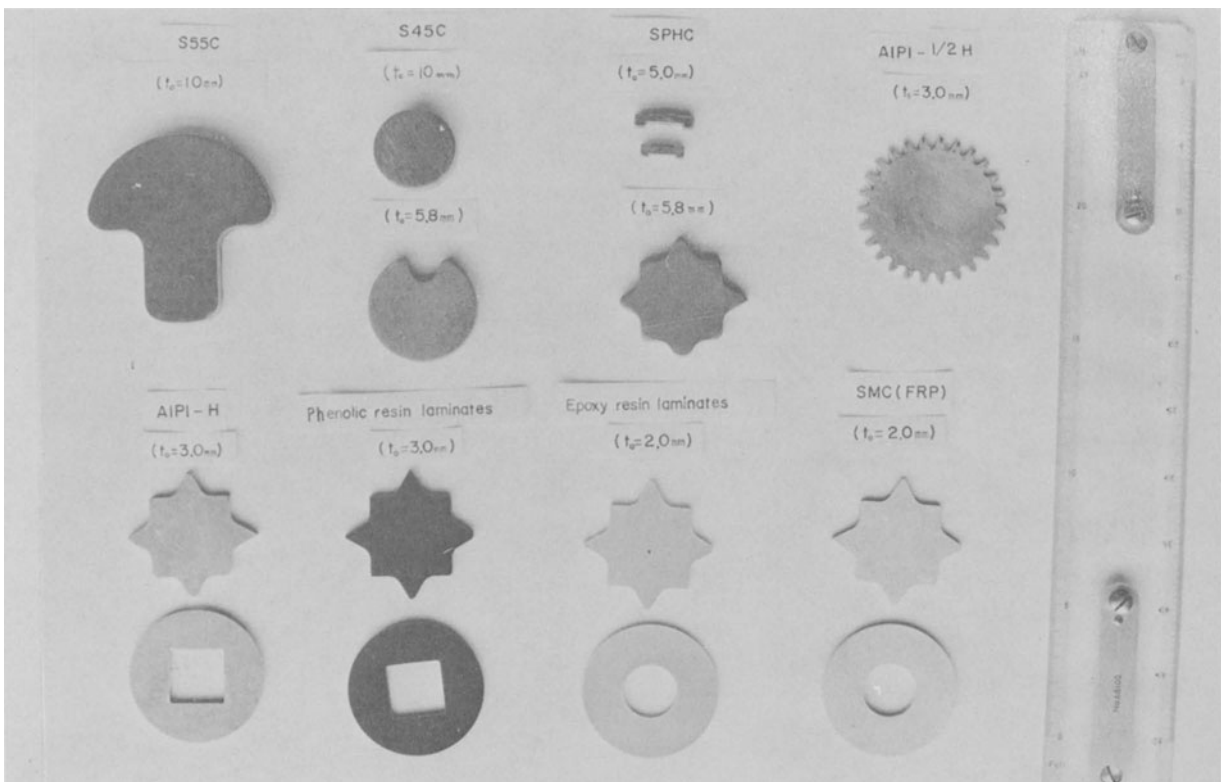


Fig. 7 Examples of the products.

CONCLUSIONS

Based on the fundamental investigation into the formation mechanism of the smooth sheared surface, a new precision shearing process has been developed. In this process, the stock of the material is removed outwards during working, that is, a quasi cutting mechanism is utilized. So, this process has many features which are quite different from those of fine blanking. Among these features, suppression of the burr, applicability to brittle materials and sharply pointed contours, and the prolongation of tool life may be the most dominant.

Acknowledgement

The authors wish to thank Professor Y. Kasuga for drawing our attention to this problem, and Suzuki Motor Co. Ltd. for their support.

REFERENCES

1. KONDO, K., 'Mechanism of Forming the Smooth Sheared Surface in the Shearing Processes', *Bull. of JSME*, 13-59 (1970), pp. 737-753.
2. MAEDA, T., and NAKAGAWA, T., 'Experimental Investigations on Fine Blanking', *J. Japan Soc. Tech. Plasticity*, 9-92 (1968), pp. 618-636.
3. GUIDI, A., 'Some Current Developments in the Fine Blanking Process', *Sheet Metal Indust.*, 46-1 (1969), pp. 41-52.
4. KRAMER, W., 'Untersuchungen beim Genau-schneiden von Stahl und Nichteisenmetallen', *Indust.-Anzeiger*, 90-27 (1968), s. 515-522.
5. KONDO, K., and MAEDA, K., 'Smooth Shearing by Stepped Profile Tool', 21st CIRP Annals, 20/1 (1971), p. 57.

DISCUSSION

Query from M. Maj, McPhersons Ltd., Australia

From Fig. 3 it would seem rather a problem to remove shaved material from the protruding punch (sticking). This would cause problems in any production application of this process.

- (1) Did the authors experience this problem in their tests?
- (2) If so, what measures could be taken to prevent this possibility.
- (3) Could the authors comment on the speed effect (if any), mainly in hydraulic presses (slow) and mechanical presses.

Reply

- (1) No, we did not.

- (2) In cases of less ductile material, the shaved portion can easily be blown off. In cases of ductile material and complicated shape, the shaved portion can be removed by using a simple spring-type ejector: the necessary spring force is fairly small.
- (3) In many precision shearing processes, working speed cannot be increased, mainly because tool life cannot be preserved. But in the present process, preservation of the tool life may be easy. So, the increase of working speed may not be limited from the viewpoint of tool life and it is possible to use a mechanical press. But in this case, adjustment of the knockout timing will become rather difficult.

Consequently, an hydraulic press is much more favourable for this process.

Query from S. Waite, GKN Floform Ltd.

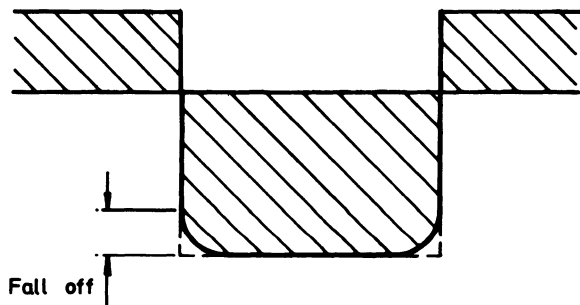
- (1) Can blanks be made direct from strip and does distortion around outer punch give trouble in feeding?

Reply

Blanking can be made directly from strip if a sufficiently narrow strip is used.

Distortion around outer punch does not become troublesome in feeding, because we can successfully suppress the bending by the tool face, cut-off the scrap ribbon at the outlet side, and feed the strip at the inlet side.

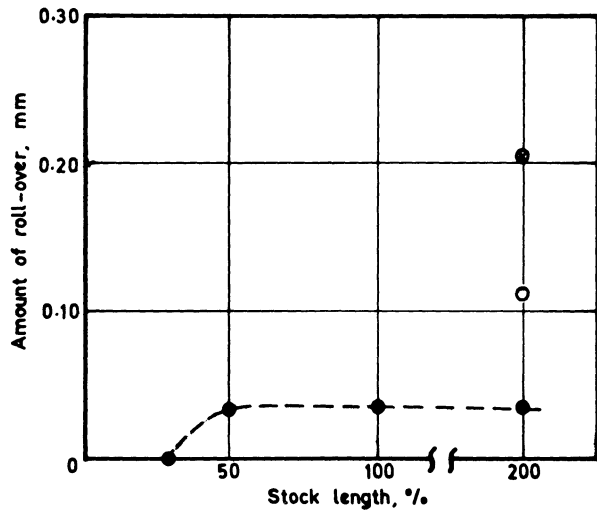
- (2) Could a comparison be made between edge fall off in conventional blanking, fine blanking and the authors' process?



Reply

Yes, we could. We will show the comparison in the following figure. The term 'edge fall off' in your question is written as 'roll-over of the sheared edge' in this paper.

Roll-over in this process is much smaller and can be diminished to almost zero, if the stock length is very short.



Experimental conditions

Material: AIFI-H
 Thickness: 3 mm
 Workpiece: Disc shape
 Blank diameter: 18 mm

● *Conventional method*

Clearance: 0.13 mm
 Counter force: 0.4 ton

○ *Fine blanking*

Clearance: 0.01 mm
 Holding force: 2 ton
 Counter force: 0.4 ton
 Radius of die edge: 0.1 mm

● *Opposed dies shearing process*

Counter force: zero
 Radius of die edge: zero

HOT FORGING OF GREY CAST IRONS

by

R. FARNWORTH and B. W. ROOKS*

SUMMARY

Generally, the paper deals with the high-speed hot forging of grey-iron preforms. The introduction reviews past work in the field of hot working of grey cast irons and indicates the properties that are likely to be upgraded.

Initially, an account is given in which the development of preform shapes for two components is described and the relevant aspects of forging die design discussed. Some general conclusions on preform design are presented. Secondly, the method of producing a grey-iron component from a cast preform is considered. The method of manufacture of a component is described in which the preforms are cast by the gravity die casting technique and then hot forged on a Petro-Forge high-speed hammer.

Two ways of carrying out this process are described. (a) Cast preforms are produced in batches, necessitating heating from room to forging temperature before being placed in the Petro-Forge. (b) The cast preforms are removed from the casting die and placed in a furnace to boost their temperature from 800°C minimum to the forging temperature. Dimensional and tensile properties are then compared, the latter by cutting tensile test specimens from the as-cast, annealed and forged components. An alternative tensile test method is also outlined, in which special test pieces are cast and themselves hot forged in the manner of a preform.

Finally, the overall possibilities of forging cast-iron preforms is discussed and some general conclusion drawn.

INTRODUCTION

Grey-iron castings represent one of the largest single sources of engineering components. Their wide use can be traced to the attraction of a wide range of properties, such as, high compressive strength, good wear resistance, good corrosion resistance etc., coupled with a low overall production cost. However, they do suffer from having rather poor tensile properties, and whilst the yield of grey-iron castings is high from the casting point of view, quite large quantities of material still have to be removed by machining before a finished component is produced.

The main cause of the low strength of grey cast iron is the shape, size and random distribution of the free graphite flakes in the structure¹. Common casting defects such as chilling, porosity, blow holes and misruns tend to reduce their strength even further. By close control of the process many of these faults can be minimized or, by the addition of special elements and close control of the cooling rate, tensile properties can be improved due to the formation of graphite nodules in the structure. Such precautions and techniques put up the costs by factors of two or three but still do little to improve the accuracy and finish of the castings, this being a function of a casting process in which gravity feeding (into sand or permanent dies) is used.

The tensile properties of grey cast iron could be improved by hot working, which would refine the structure and cause such structural changes as the compacting of the branched graphite clusters, the elongation and reorientation of the graphite flakes. In addition hot working could lead to more accurate components resulting in a reduction or even elimination of machining operations. Many of these claims were made by Schlegel² who hot forged high-carbon irons in closed dies on slow-speed double-acting presses. In further work³ he found that castings produced in metal dies gave even better properties if their temperature was not allowed to fall below the recrystallization temperature during transfer from casting to forging. These claims were subjects of patent applications. In contrast, Klyuchnikov⁴ found grey irons to be unsuitable for pressing and forging by methods such as open die forging, whereas in extrusion operations tensile strengths could be doubled. The former claim is in some agreement with work of El-Kalay and others⁵ who were able to upset grey cast iron to only 5% reduction before the onset of cracking, and the latter claim is supported by the work of Barton on the extrusion of grey cast iron⁶. The apparent explanation of these differences is that during extrusion the material is under compression, whereas, in open die forging, the material must at

*Department of Mechanical Engineering, University of Birmingham.

some point be stressed in tension. Thus, in hot forging, if the preform shape can be so designed to minimise or even eliminate tension during forging, the operation can be successful. This is the approach used by Schlegel, and in one publication⁷ he discusses the design of iron castings for use as preforms in hot forging operations capable of quantity production in an integrated cast and forge process.

In the work described in this paper the designs of preforms are considered for two components. In the first part of the work the development of preforms which can be forged on a Petro-Forge into a crack-free component is traced. In the second part, the preforms developed for one of the components is gravity die cast in permanent dies and then forged on a Petro-Forge. Dimensional tolerances and tensile properties of this component are then examined, the results of the latter being augmented by tests on a specially designed tensile test piece which is gravity die cast and then itself forged. The choice of the Petro-Forge (a Mk IIA nominally rated at 10 000 ft lbf) as the forging machine was one of availability rather than of any technological advantage of the high forming speed. However, the machine itself, has a built-in guidance system, infinitely variable energy output, short forming time and low capital and installation costs which would be important considerations in any production applications.

PREFORM DEVELOPMENT

General

Many factors have to be considered in designing the shape of a preform for hot forging purposes, for example, die loads, die wear, energy requirements, etc. Whilst these are also important as far as a brittle material like grey cast iron is concerned, the main problem is to ensure that a crack-free component is produced. Thus, the preform design is a compromise between ensuring that tensile stresses do not arise during forging, whilst promoting maximum metal flow in order to upgrade the material properties.

Owing to the complex nature of metal flow in even simply shaped preforms, it was only possible to develop preforms on a trial and error basis. Thus, preform shapes were produced by machining for this part of the work and the technique was applied to two components, an axisymmetric multi-diameter flange shape and a spur gear.

Multi-diameter flange component

The die sub-set and the shape of this component are shown in Fig. 1. It was considered that this component could be forged in three distinct ways, as illustrated in Fig. 2.

Type 1 preform (Fig. 2a) requires extrusion to fill the central boss region and upsetting to fill the flange. With these conditions it would appear that the preform will be subjected to entirely compressive stresses during forging. Typical forgings sections are shown in Fig. 3a, in which the only variable of note is the diameter A (see Table 1) and it can be seen that the flange has failed by internal shearing. This is due to the fact that metal is being extruded forward into

the central boss whilst the flange is being upset outwards. Increasing the preform flange diameter minimises the failure until with a preform diameter of $3\frac{7}{8}$ in it has been eliminated. However, the other problem is that die filling is very poor and would require energies many times larger than the 10 000 ft lbf available with the MkIIA Petro-Forge, for which die loads may well be excessive. Therefore, this preform shape was abandoned.

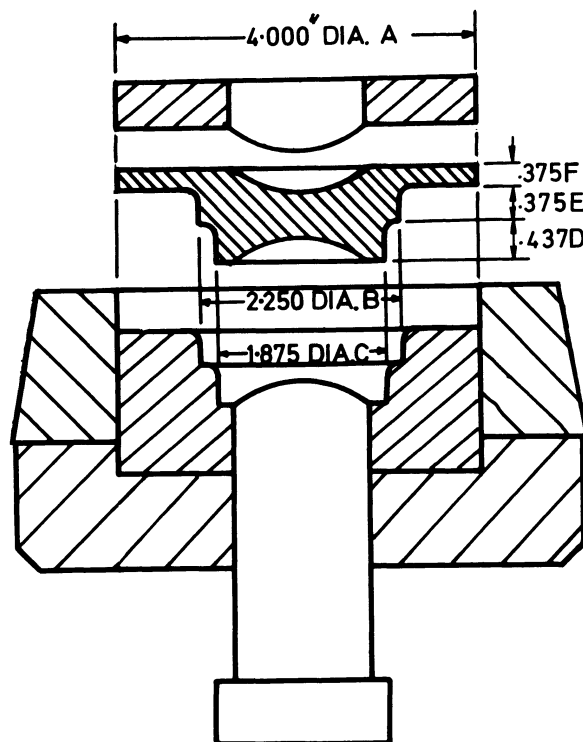


Fig. 1 Flange component and die sub-set.

Type 2 preform (Fig. 2a) requires a combination of upsetting and piercing by the top and bottom punches. It was intended that once the piercing punches had been forced into the preform the chamfered portion would be formed into the small diameter flanges, with displaced metal being forced into the shoulders, as illustrated in Fig. 2a. Forming would then continue by upsetting of the flange. However, as seen from typical forgings in Fig. 3b, gross radial cracking occurred, presumably due to tensile stresses being produced in the flange before any compressive upsetting could take place. By increasing the preform diameter (see Table 2) to $3\frac{7}{8}$ in cracking was prevented but the amount of flange deformation was negligible. Therefore, this design was not pursued.

The last preform, type 3 (Fig. 2c) is entirely formed by upsetting the flange, the central boss being preformed to near its final form. In these conditions the component is forged under laterally compressive loads and with little or no extrusion there is little fear of internal shearing. A range of typical forgings from this preform type is shown in Fig. 3c. In this case, in addition to the diameter A (Fig. 2c), others diameters were varied as indicated in Table 3. Table 4 gives the forging dimensions achieved with preforms of type 3. Reductions in the flange of up to 25% were achieved without signs of cracking and

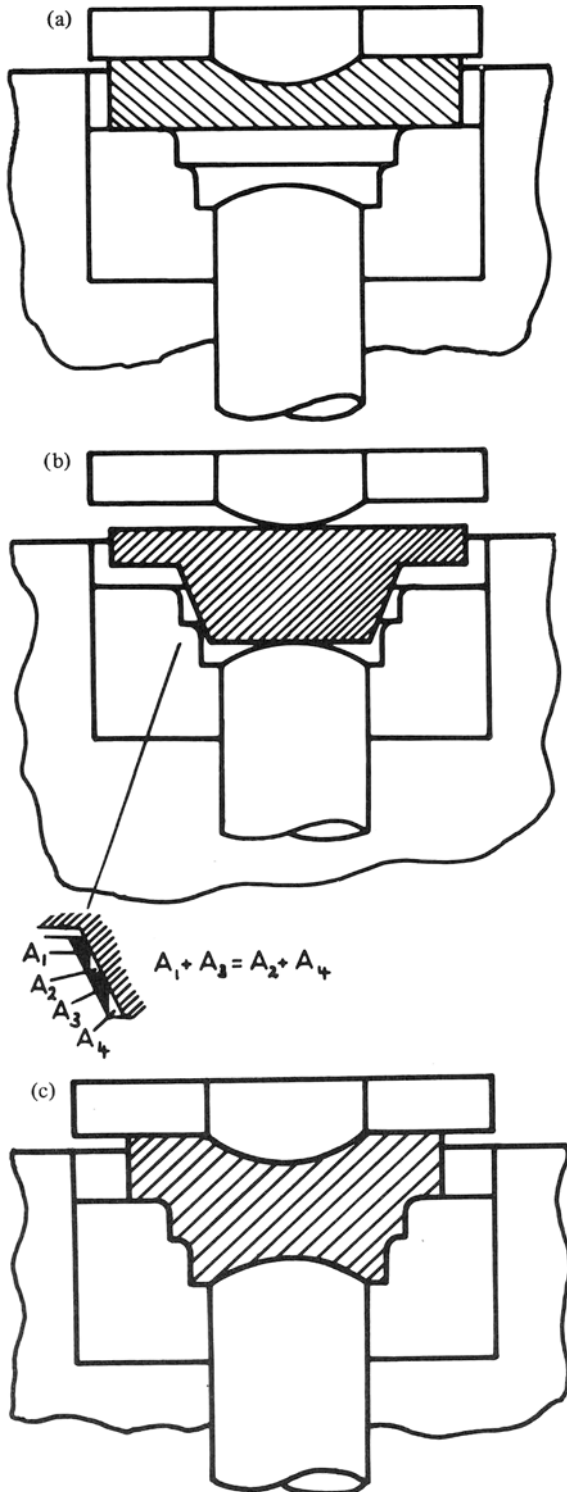


Fig. 2 Preform types for producing the flange component: (a) Preform 1, (b) Preform 2, (c) Preform 3.

surface finish and definitions were always good. Where the dimensions of the central boss region allowed upsetting to take place, die filling was poor and marred by barrelling, the formation of which can be seen on the preform forgings 3.3 and 3.4 in Fig. 3c.

These results showed that with the preforms of type 3 the flange was capable of relatively high plastic deformation, but that barrelling of the central boss region could lead to radial cracking of its periphery and male radii. This problem did not occur where diameters B and C (see Table 3) were very close to the

final size. Therefore, preforms of types 3.1 and 3.2 were selected for further work involving cast preforms and the effects of forging on some of their properties.

It can be concluded from this work that whilst the forgeability of grey cast iron is relatively poor, forging can be accomplished by maintaining a hydrostatic-type of stress system throughout the operation. By such means the flange of the above component was reduced by up to 25%, compared

Table 1. Preform 1 dimensions

Preform	1.1	1.2	1.3
Diameter A	3.875	3.625	3.500

Table 2. Preform 2 dimensions

Preform	2.1	2.2	2.3
Diameter A	3.875	3.750	3.590

Table 3. Preform 3 dimensions (see Fig. 1)

Preform	A	B	C	D	E	F
3 1	3.875	2.200	1.800	0.440	0.370	0.445
3 2	3.750	2.200	1.800	0.405	0.360	0.410
3 3	3.625	2.160	1.620	0.430	0.320	0.510
3 4	3.500	2.140	1.600	0.430	0.280	0.570

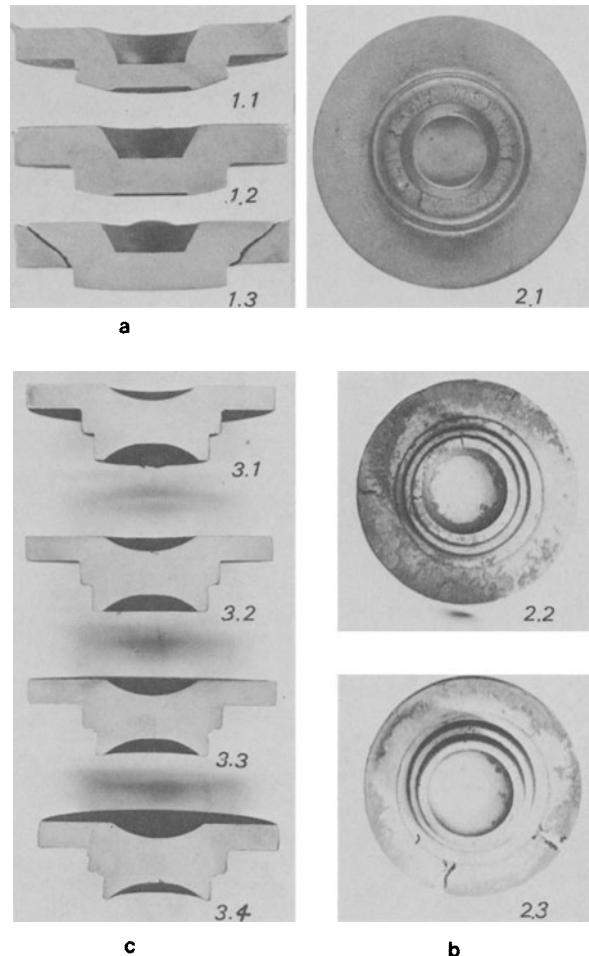
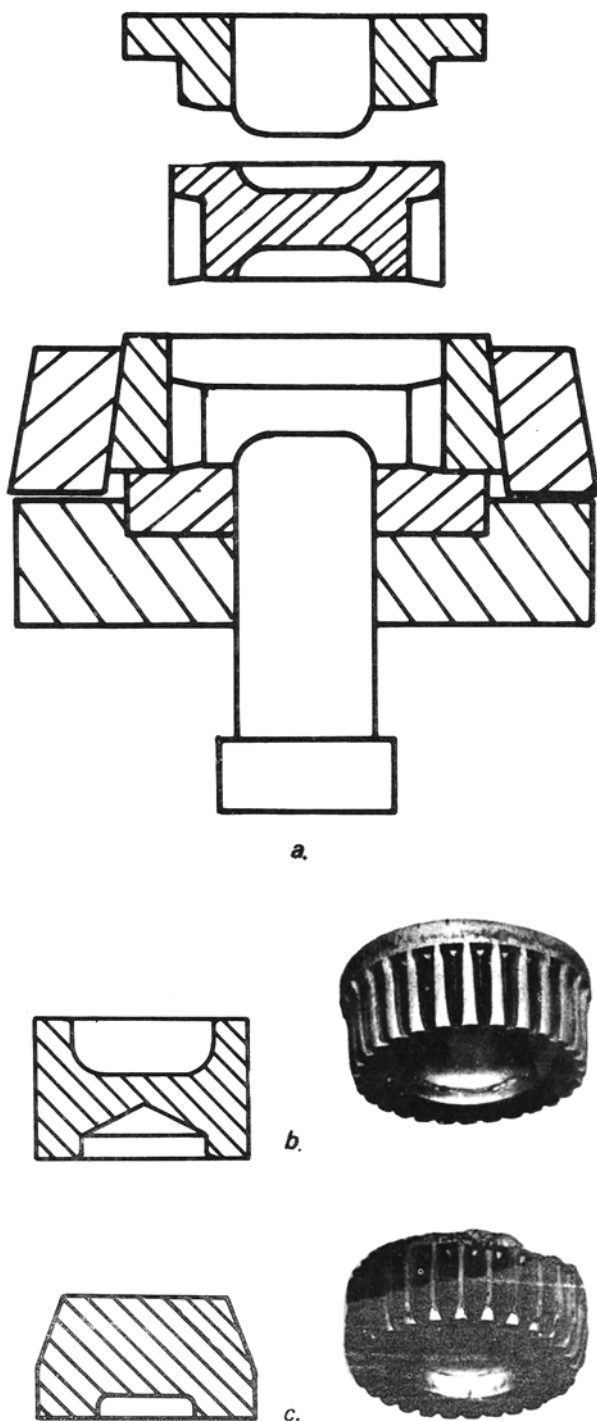


Fig. 3 Typical flange component forgings produced: (a) from preform 1, (b) from preform 2, (c) from preform 3.

Table 4. Results of forging preform 3

Preform	A	B	C	D	E	F	Increase in flange diameter (%)	Reduction in flange thickness (%)
3.1	3.970	2.240	1.870	0.423	0.383	0.375	2.6	6.0
	3.970	2.240	1.860	0.415	0.382	0.393	2.6	4.0
3.2	3.970	2.240	1.870	0.415	0.383	0.397	6.0	13.0
	3.960	2.240	1.870	0.419	0.379	0.402	5.6	12.0
3.3	3.970	2.240	1.780	0.419	0.380	0.395	9.7	23.0
	3.960	2.230	1.790	0.419	0.383	0.398	9.4	22.0
3.4	3.900	2.240	1.730	0.421	0.378	0.427	11.4	25.0
	3.850	2.240	1.750	0.422	0.376	0.442	10.0	22.0



with 5% obtained in earlier investigations⁵. To achieve such conditions it may be necessary to restrict metal flow to those areas where upgrading of material properties is required, leaving other areas only to be coined, which may be sufficient for improving dimensional tolerances. The experience with piercing punches leads to the conclusion that indentation should not be attempted except where the remainder of the component can be laterally compressed for example, as a final operation on a double-acting press.

Spur gear

Apart from its tensile properties, grey cast iron has good gear material properties, such as, wear, corrosion and internal damping. If hot working can improve the tensile properties and at the same time produce a gear that only requires a finish machining operation, the use of grey cast iron gears could widen. That spur gears can be forged in grey iron would seem likely in view of the fact that they would be upset and during upsetting would be radially restrained by the presence of the gear teeth on the periphery. The situation therefore approaches that of the desirable hydrostatic stress system.

Initially work was carried out with an existing die set for producing 3 in diameter D.P. gears, and is shown in Fig. 4a., together with a section of the required component. The major problem in forging this component was that a plain cylindrical portion at the top of the component formed before the teeth were fully filled, and metal had to be forced into the teeth in a vertical direction as the height of the preform decreased during forging. Two examples of preforms and the resulting forging, one at the early stage of preform development and the other the final one, are shown in Fig. 4b and 4c, respectively. With the early preform, die filling into the crests of the work was poor. The final preform (Fig. 4c) was chamfered at the top of its periphery and, together with the action of the bottom piercing punch, was intended to discourage radial flow at the top and encourage it at the bottom in order to produce a component with parallel fully formed gear teeth. As can be seen in Fig. 4c these efforts were partially successful in that full-

Fig. 4 Spur gears produced from the first die set: (a) die set and required gear shape; (b) an early preform and forging; (c) final preform and forging.

form teeth were produced for $\frac{3}{4}$ the length of the gear. However, severe cracking had occurred on the top face due to the severe extrusion taking place both forward into the teeth and backward past the top punch. Further, cracking had occurred on the crests of the gear teeth which was attributed to the excessive straining of the outer fibres of the preform. This leads to the conclusion that this depth of gear tooth was greater than could successfully be forged in grey iron.

It was apparent that if successful grey-iron gear forgings were to be produced, a major redesign of the die set would be necessary. Many of the problems encountered would be minimised if the formation of the plain cylindrical portion at one end of the component could be eliminated. Consequently, the die set

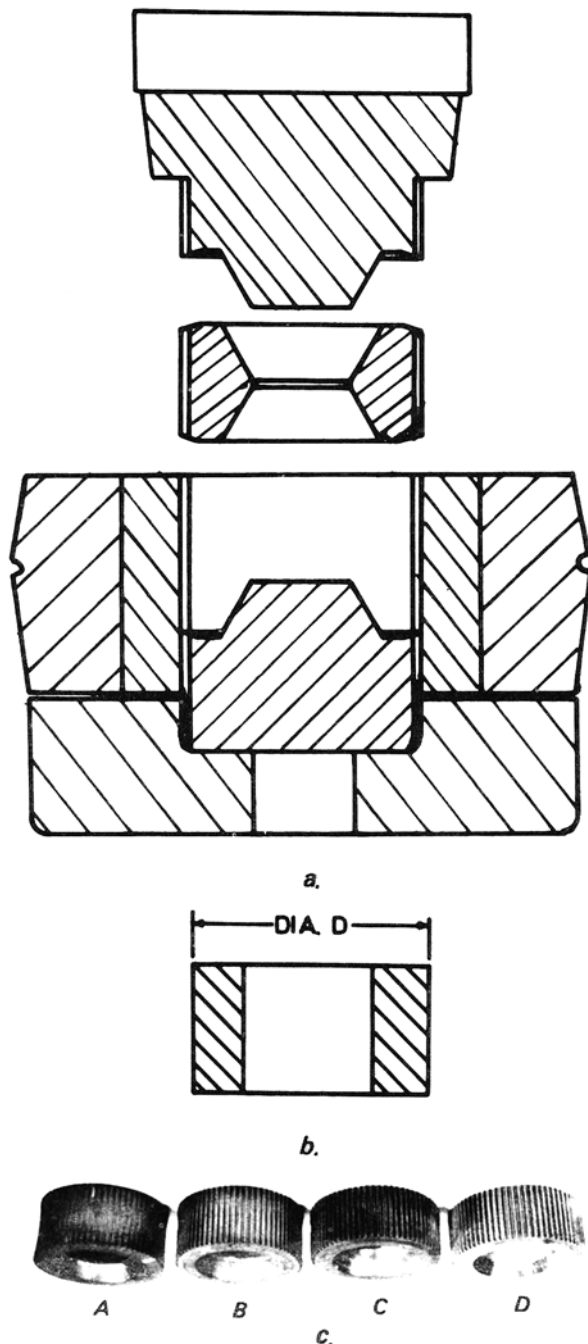


Fig. 5 Spur gears produced in the redesigned die set: (a) die set and required gear shape; (b) preform; (c) typical forgings.

shown in Fig. 5a was designed, in which the punch is provided with the full gear form to mate with the die and thus forge a vertically symmetric component. This die set will produce a 3 in diameter 24 D.P. spur gear. The component can now be forged by a combination of upsetting and piercing by the top and bottom punches. The design of the piercing punches was optimized prior to the design of the die set by carrying out some experiments in which cylindrical rings were forged in a plain cylindrical die set⁸. The angle was chosen so as to produce a parallel-sided component.

The preform used and typical forgings produced with this die set are shown in Figs. 5b and 5c, respectively. Some variation in the outside diameter was necessary so that the preform would enter the die when hot, whilst minimising the amount of radial flow to achieve die filling. These variations are indicated in Table 5 together with the blow energies used. The success of the piercing punches in encouraging radial flow at the top and bottom faces, and so counteracting barrelling, can be judged from the appearance of the low energy blow forgings. The high-energy blow forgings showed good tooth definition and good surface finish.

The main conclusions to be drawn from the work on forging spur gears was that the design of the die was of prime importance. It was necessary to remove the restrictive effect of a plain punch by a mating full-form punch. Whilst this design presents problems in costs and alignment it does produce a good parallel-sided spur gear. In respect of the alignment problem the use of the Petro-Forge with its inherent guidance system was particularly valuable. Preform design for the redesigned die set proved to be straightforward, it being only necessary to have an outside diameter sufficient to enter the die and an internal diameter sufficient to produce the wedge action effect at the top and bottom faces of the component.

FORGING OF CAST PREFORMS

Casting and melting method

The ultimate aim of the investigation was to establish the basis of a production process utilising casting and forging. Forging, of the type envisaged in this process, would be of high volume to minimise die costs and therefore the casting process chosen would have to match the forging process in terms of this volume. The most suitable technique available which satisfies

Table 5. Spur gear preform sizes from redesigned die set

Preform	Diameter D* (in)	Blow energy (ft./lbf.)
A	2.750	850
B	2.740	1240
C	2.720	10 250
D	2.700	12 100

*See Fig. 5b

this requirement was the gravity die casting process. In addition, the employment of the gravity die casting method would:

- (a) enable close control of casting accuracy,
- (b) allow easy application of mechanised handling methods,
- (c) eliminate problems of sand casting such as sand inclusions which would be detrimental to the hot working process and could lead to excessive die wear.

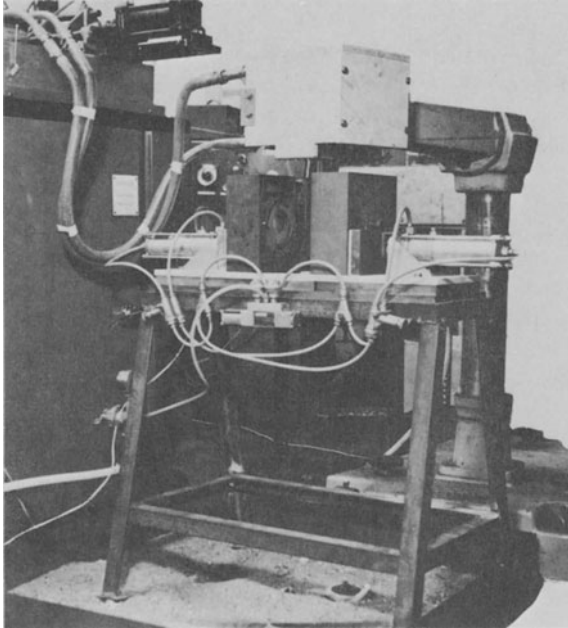


Fig. 6 Die casting arrangement.

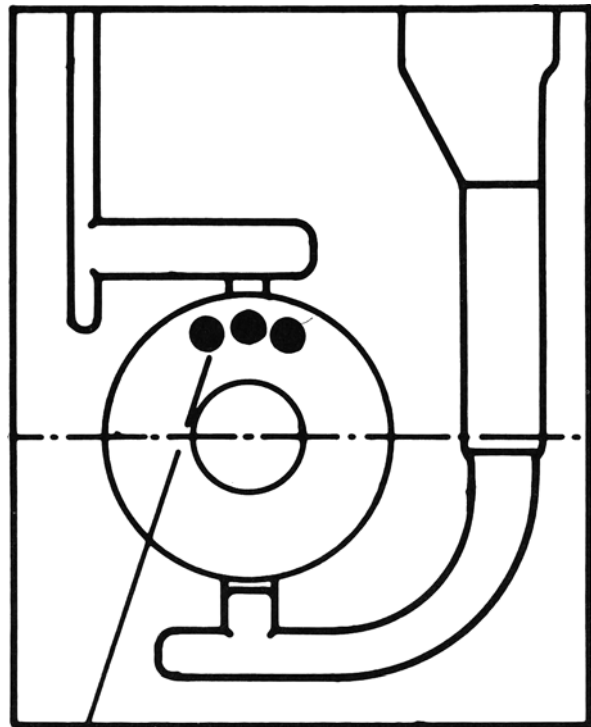
The casting die machine used for producing preforms in the laboratory is shown in Fig. 6. The dies are parted and closed by means of two solenoid valve-controlled air cylinders. Means of preheating the dies was provided by electrical cartridge heaters inserted into both die halves.

Although in a production process the most economical method of melting cast iron is by a cupola, this is not very convenient for laboratory use where small quantities at intermittent intervals are required. The induction heating method used for this investigation is very rapid and convenient. A 75 kW Radyne billet heater was modified to supply power to a heating coil specially designed for the operation. The coil box containing this coil and the crucible can be seen above the casting die in Fig. 6. The bottom pouring technique, which was originally developed for the investment casting technique⁹, was used with this arrangement. Basically, this method employs a crucible (sodium silicate bonded sand in this investigation) which has a hole in the bottom through which the molten metal pours, when the base of the charge, the last part to melt, finally becomes molten. The metal charge can be weighed to give the required amount of metal and thus the method also affords a convenient means of charge mass regulation. In practice a thin plug of metal is inserted into a recess in the bottom of the crucible to act as a temporary seal, and the thickness of this plug together with the heat input to the charge controls the melt pouring temperature.

Cast preform of the flange component. (Fig. 1)

The preform shape to be used for this component was type 3.2 (Fig. 3c) as determined from the preform development work described earlier. The casting die for producing this preform is shown in Fig. 7. The two halves were made from blocks of close-grained grey cast iron with the parting line chosen to be parallel to the flange of the preform and positioned midway in the flange thickness. The surface of each die was prepared by coating with a fine permanent refractory coating which prior to each cast was augmented by a coating of lamp black from an acetylene torch.

The requirements of a good cast preform were complete die filling, with no surface porosity or misruns. Considerable development was required before these requirements were met. From this work



VENT HOLES

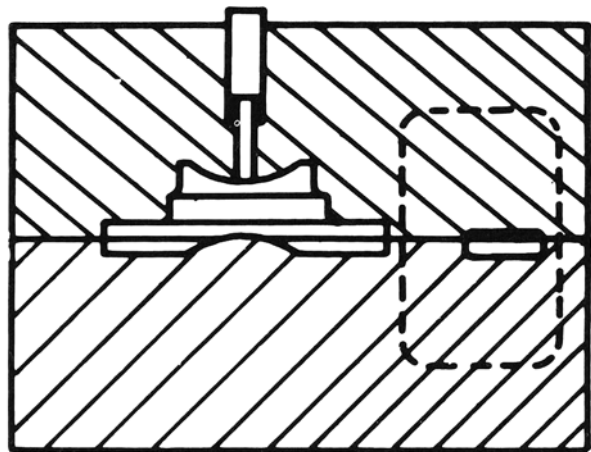


Fig. 7 Casting die design for the flange component.

Table 6. Casting conditions

Charge material	3.57% C, 2.25% Si, 0.014% P, 0.119% S, 0.67% Mn
Charge size	2½ in. diameter × 3½ in. long (mass 3 lb)
Innoculation	0.4% ferro-silicon (75% silicon)
Crucible plug	1 in diameter × ⅛ in thick grey cast iron
Pouring hole	½ in diameter
Average power drawn	30 kW
Overall melting time	3 min
Melting-pouring time	2 min
Melting temperature	1100°C
Pouring temperature	1320°C

Table 7. Cast-reheat-forge test results

Preform Dimension No.	A	Forging dimensions (see Fig. 1)						Blow energy (ft lbf)	Reduction in flange thickness (%)	Ultimate tensile strength (tonf/in ²)	
		A	B	C	D	E	F			Radial	Circum.
1	3.825	3.971	2.225	1.857	0.440	0.375	0.375	4340	7.4	16.9 17.7	16.9 16.9
2	3.825	3.972	2.225	1.855	0.440	0.373	0.377	5200	7.0	15.5 14.5 10.0	12.2 9.2
3	3.825	3.973	2.226	1.860	0.440	0.378	0.373	6500	8.0	—	—
4	3.825	3.972	2.223	1.855	0.440	0.376	0.376	8000	7.7	14.5 13.3	16.9 16.1
5	3.825	3.973	2.225	1.856	0.440	0.377	0.377	12 200	7.9	14.5 16.1	20.5 20.5
6	3.752	3.955	2.222	1.855	0.440	0.378	0.360	7 600	11.0	17.0 15.3 12.5	18.2
7	3.690	3.970	2.225	1.858	0.440	0.375	0.335	11 500	17.0	21.2 20.5 22.9	19.2 18.2

the plug thickness, die preheat temperature, power input and pouring temperature were optimized and the dies modified to improve the runner and riser system and provide adequate venting. The resulting conditions used are exemplified by those given in Table 6.

Preforms produced under the conditions given in Table 6 were forged in two distinct ways:

(a) separation of casting and forging—a batch of preforms were produced consecutively, allowed to cool and then heated up to a temperature of 1000°C before being placed into the Petro-Forge and forged;

(b) integration of casting and forging—each preform was produced separately, removed from the casting die at a temperature of 800°C minimum and immediately placed in a muffle furnace until their temperature was 1000°C, when they were placed in the Petro Forge and forged.

In both tests preforms were forged at varying blow energy and the results for (a) and (b) are given in Tables 7 and 8, respectively. In test (a) two of the

preforms had their large diameter reduced by machining as indicated in Table 7, leading to greater flange reductions after forging.

All the preforms forged, from both tests, showed no signs of radial cracking and with the exception of one low-energy blow, die filling was excellent. These comments equally applied to the two cases where the flange had been reduced in size prior to forging and a reduction of up to 17% was achieved. Surface finish and definition were better in the case of the cast-immediate forge specimens, but otherwise little difference could be detected.

To determine the effect of forging on one of the mechanical properties of grey cast iron, test specimens were cut from the flange of each component and a number from some unforged preforms. Specimens of 1/8 in. diameter (see Fig. 8a) were cut with their axes parallel to the radial directions and perpendicular to this direction; that is, approximately circumferential. These specimens were 'pulled' in a Hounsfield Tensometer and the resulting U.T.S.

Table 8. Cast—immediate forge

Preform No.	Forging dimensions (see Fig. 1)						Blow energy (ft lbf)	Reheat time (min)	Reduction in flange thickness (%)	Ultimate tensile strength (tonf/in ²)	
	A	B	C	D	E	F				Radial	Circum.
8	3.940	2.235	1.840	0.425	0.380	0.385	3660	6	4.9	13.3 13.3	14.1 14.9
9	3.967	2.240	1.845	0.423	0.380	0.375	5300	5	7.6	13.7 16.1	16.9 19.3
10	3.970	2.240	1.860	0.425	0.390	0.375	6290	60	7.6	10.5 —	14.9 18.1
11	3.970	2.240	1.860	0.425	0.385	0.375	7400	6	7.6	13.7 16.1	16.9 19.3
12	3.970	2.240	1.855	0.426	0.385	0.370	8250	4	7.6	15.3 16.1	17.3 14.9
13	3.968	2.240	1.860	0.424	0.385	0.375	10 000	5	7.6	26.9 —	22.1 22.1
14	3.970	2.240	1.860	0.425	0.380	0.375	10 700	5	7.6	21.7 17.3	24.9 18.5

Table 9. As-cast and annealed tensile test results

Ultimate tensile strength (tonf/in ²)					
As-cast			Annealed		
11.7	14.9	16.9	7.2	9.6	10.0
20.4	21.2		12.8	13.7	14.5

values are included in Tables 7 and 8. For comparison, the U.T.S. values obtained from unforged preforms, both in the as-cast and annealed conditions (850°C for 1 hour followed by a slow cool), are given in Table 9.

The spread in U.T.S. values, particularly from the unforged preforms, makes it difficult to draw any categorical conclusion as to the merits of hot working on grey cast iron, but a general trend toward increasing strength with blow energy can be detected. The wide spread, which includes low U.T.S. values of the specimens from the as-cast and annealed preforms compared with the consistently high U.T.S. values obtained at high blow energies (e.g. preforms 5, 7, 13 and 14), suggests that forging is having an effect in minimising non-uniformity effects, for example, closing up blow holes and porosity. Where larger amounts of metal flow were possible in preform 6 and 7, they were reflected in higher U.T.S. values, particularly in the radial direction. It is notable that the circumferential values are generally higher than the radial values. This is probably due to the fact that in the radial direction specimens will extend into the central part of the component where little if any metal flow takes place, whereas in the circumferential direction the specimen is extracted wholly from the worked area.

The overall conclusion drawn is that forging with energy blows of 10 000 ft lbf or over results in increased strength over both the as-cast and annealed

values. This is if the maximum values in each case are compared, or even if the average values are compared, which may be misleading. In a similar comparison, the cast and immediate-forge method shows marginal improvement over the cast—reheat—forge method.

Cast preforms a tensile test-piece

The disadvantage of carrying out tensile tests with specimens cut from a forging, as described above, is that flow lines or aligned grain boundaries may be cut. Also, material properties will change with depth. It is possible, therefore, that the gauge length of the specimen may not be typical of the specimen. To overcome this problem it would be desirable to detect changes in properties by subjecting the whole specimen to a suitable test. This could be attempted in two ways:

(a) a component could be subjected, before and after forging, to simulated service conditions in a machine specially designed for the purpose;

(b) a tensile test-piece could be cast and then forged in a manner similar to that of the component under consideration.

The former course was not pursued due to the fact that its service conditions were unknown, and therefore the latter course was used.

A test-piece was designed, shown in Fig. 8b, which did not conform to any standard but corresponded very closely to the flange of the flange component, Fig. 1. For example the test-piece thickness was

similar to that of the component flange thickness, and the width of the gauge length was similar to the effective width of the flange from the component periphery to its hemispherical cavity. Test-pieces to the above design were cast into appropriately designed grey cast iron dies in a similar manner to that used for the flange component. Owing to the fact that some fettling had to be done to the castings before being placed in the forging die, forging could not follow immediately and therefore only the reheating method could be employed. During forging, the whole of the preform, not just the gauge length, was subjected to a vertical load and upset to fill the

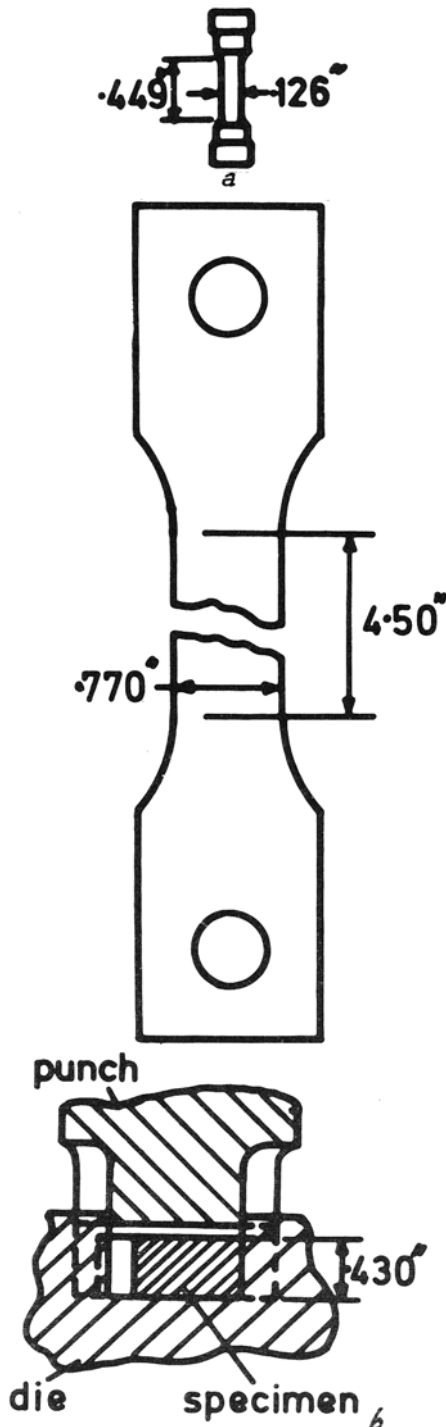


Fig. 8 Tensile test specimens: (a) machined from the flange component; (b) diecast.

die space as shown in Fig. 5b. Forging was carried out on test specimens, of two compositions (see Table 10) at different blow energies. These forged pieces were tensile tested in a 50 ton Denison testing machine together with some as-cast and annealed specimens. These results are listed in Table 10.

No real trend of blow energy can be detected with the results from composition A, which is further confused by a very high value from the annealed specimen, contrary to what is expected and what was obtained for all other tests. Results from composition B show the same trend as the results of the specimens cut from the flange component; that is, increasing strength with increasing blow energy and metal deformation. The higher blow energy specimens exhibit significant improvements over the as-cast and annealed specimens.

SUMMARY OF CONCLUSIONS

Grey cast iron can be forged successfully in closed dies provided the preform design is such that it is subjected to compressive loads only during the entire operation. This may require the deformation to be restricted to certain areas of the component. Two components were forged in this manner: a 4 in diameter multi-diameter flange component, of which the largest flange was upset by up to 25% without cracking, the central boss region only being coined, and a 3 in diameter 24 D.P. spur gear in which the only movement of metal was into the gear teeth.

It was possible to forge accurately repeatable grey-iron components with a good surface finish which could be sufficiently acceptable to either eliminate or minimise machining. The forged faces would provide reliable locations for jiggling purposes.

The tensile strength of grey cast iron was improved by hot working, the improvements being related to blow energy. Cast and immediately forged components, whose temperature was not allowed to fall below the recrystallisation temperature, were marginally stronger than components that had been cast, reheated and then forged.

In a process where a forging preform is cast, the displacement of the metal during forging can be accurately controlled. Thus, areas that require maximum strength can be predesignated. Where the metal is grey cast iron there is no strict limitation on the shape of the preform that can be cast. If the casting process chosen is gravity die casting, mechanization can easily be introduced and preforms can be presented to the forging at a rate sufficient to maintain it in full production. Thus, it is possible, as Schlegel suggested⁶, to arrange for the integration of the preform casting and forging processes. Such a system would include means of removing the runners and risers, manipulation of the hot preforms from the casting machine to the intermediate soaking furnace and to the forging machine, with full or partially automated control of the sequence of events. The forging machine used in this investigation was a Petro-Forge and this would appear to be particularly adaptable to such a system. The inclusion of such a machine at the end of a foundry production line would seem to present no unsurmountable problems.

Table 10. Diecast and forged tensile test pieces

Composition A ¹ 3·57% C, 2·25% Si, 0·014% P, 0·119% S, 0·67% Mn			Composition B ² 3·4% C, 1·65% Si, 0·6% P, 0·12% S, 0·9% Mn		
Blow energy (ft lbf)	Thickness reduction (%)	Ultimate tensile strength (tonf/in ²)	Blow energy (ft lbf)	Thickness reduction (%)	Ultimate tensile strength (tonf/in ²)
2800	0·7	7·8	2500	1·5	4·1
3360	4·6	16·8	5060	5·8	6·2
5840	8·0	20·3	5850	6·0	9·6
7300	11·0	11·3	7000	7·8	15·8
8000	11·8	14·5	7850	8·3	19·8
			8430	10·2	22·0
As cast		12·6	As cast		14·7
As cast		13·9	As cast		7·3
As cast		14·7	Annealed		3·7
Annealed		19·3			

1. Supplied by B.C.I.R.A.

2. B.S.S. 1452 Grade 14

Acknowledgements

This investigation formed part of the Petro-Forge Development Contract sponsored by the Ministry of Technology. The project embraces the design and development of a series of combustion actuated high-energy rate forming machines, as well as basic and applied research into associated processes. The work is carried out under the direction of Professor S. A. Tobias.

The authors are also grateful to Mr J. J. Carroll, of Qualcast Ltd., Derby for his help and suggestions on the design of die casting dies and for the supply of materials. Thanks are also due to the British Cast Iron Research Association, particularly Mr Pinfield, for their helpful advice and supply of materials.

REFERENCES

- GILBERT, G. N. J., *Iron and Steel*, 37, April, May, June 1964, 130-135, 190-194, 315-319.
- SCHLEGEL, F. J. W., 'Process for the Hot Working of Cast Iron Utilising Dies', Patent No. 761, 654, Nov. 21st 1956.
- SCHLEGEL, F. J. W., 'Hot working of Metal Castings', Patent No. 1,078, 781, Aug. 9th 1967.
- KLYUCHNIKOV, S. I., 'The Forging and Pressing of Cast Iron' *Kyznechno-Shtampovschoe*, 1961, 3(3), 19.23.
- EL-KALAY, A. K. A., BRAMLEY, A. N., and ENSOR, T., 'Forgeability of Various Cast Irons using High and Low Forging Speeds', B.C.I.R.A. Report No. W. 138, 1967.
- BARTON, R., 'Hot Extrusion of Cast Iron' *B.C.I.R.A. Journal* 1965, 13(5) Sept., 653-668.
- SCHLEGEL, F. J. W., 'Spanlos Umformen Auf Neuen Wegen' V.D.I., Verlag GmbH, Dusseldorf, 1965.
- FARNWORTH, R., 'The Forging of Cast Irons by High Energy Rate Forming Methods', Ph.D. Thesis, University of Birmingham, September 1970.
- INGALL, J. B., 'An Automatic Bottom Pouring Method for Invested Moulds, Eliminating the Melting Furnace', 10th European Investment Casters Conf., Madrid Oct. 1964.

MACHINE TOOL ELEMENT DESIGN

BEHAVIOUR OF THE HORIZONTAL STIFFNESS AND THE MICRO-SLIDING ON THE BOLTED JOINT UNDER THE NORMAL PRE-LOAD

by

M. MASUKO, Y. ITO and C. FUJIMOTO*

SUMMARY

The damping capacity of a bolted joint is an important parameter for the calculation of the dynamic behaviour of machine tools. According to previous studies, it can be presumed that the damping capacity of the bolted joint is closely related to the horizontal stiffness and the micro-sliding of the bolted joint.

To clarify the behaviour of the horizontal stiffness and the micro-sliding under the normal pre-load, basic experiments were carried out with the simple bolted joint. The horizontal displacements were measured by using the strain gauges when a tangential load was applied to the joint surfaces. Experiments were carried out in the air-conditioning room ($20 \pm 0.2^\circ\text{C}$), as the maximum value of the horizontal displacement is only less than $1\ \mu\text{m}$. During experiments the mean interface pressure, which was given by the normal pre-load, was changed from $0.2\ \text{kg mm}^{-2}$ to $2.5\ \text{kg mm}^{-2}$ and the effects of the methods of machining (which were here ground, lapped and scraped), the machined lay orientation, the surface roughness and of the materials (here mild steel, cast iron, brass and aluminium alloy) of joint surfaces on the horizontal stiffness and on the micro-sliding have been investigated.

From the experimental results, it is clear that the horizontal displacement is the direct sum of the elastic displacement and the micro-sliding on the bolted joint, and furthermore, that the horizontal stiffness and the micro-sliding are changed by the conditions of the joint surfaces.

The conditions of joint surfaces have relatively small effects on the elastic displacement, but have significant effects on the micro-sliding between the joint surfaces.

The experimental results also suggest that the elastic displacement is derived from the concentration of shearing stress on the real contact area between the joint surfaces and micro-sliding is derived from the seizure and the micro-contact between the surface asperities.

INTRODUCTION

On a machine tool there are many bolted joints and it is widely known that these bolted joints can influence the overall static and dynamic behaviour of the tool. The horizontal bending stiffness and the damping capacity are especially important factors, as they determine the dynamic behaviour of the machine tool.

According to previous studies^{1,2}, the horizontal stiffness and the horizontal displacement on the bolted joint are closely related to the horizontal bending stiffness and the damping capacity on the bolted joint; therefore, the behaviour of the horizontal stiffness and the horizontal displacement have been investigated here experimentally and theoretically.

The measurement of these two characteristics is very difficult, because the friction between the joint

surfaces limits the horizontal displacement and the maximum value of this displacement is less than $1\ \mu\text{m}$.

To eliminate the many unknown influences, the basic experiments were carried out with the simple bolted joint having only one connecting bolt, and the horizontal displacements were measured by means of a micro-displacement detector when a tangential load was applied to the joint surfaces.

Apparatus for experiment and experimental procedure

The principal of the apparatus which was used to measure the horizontal displacement on the bolted joints is illustrated in Fig. 1. The lower test specimen 1 was connected tightly by means of the threads on

*Department of Mechanical Engineering for Production, Tokyo Institute of Technology, Tokyo, Japan

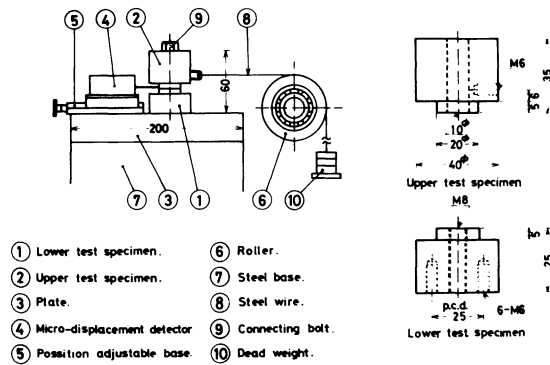


Fig. 1 Apparatus for experiment.

the plate 3, mounted on the horizontal steel base 7 and the upper test specimen 2 was jointed to the lower test specimen by using the M8 connecting bolt 9.

When the horizontal static load was applied parallel to the joint surfaces by means of the dead weights 10 through the roller 6 and the steel wire 8, the horizontal displacements of the joint surfaces were measured with the micro-displacement detector 4 which utilizes the strain gauges. For convenience, the micro-displacement detector was settled on the position-adjustable base 5 and this base also connected tightly to the plate 3.

Experiments were carried out with different pre-loads of the connecting bolt. In all experiments the pre-loads were constrained to suitable values by measuring the elongation of the connecting bolt with the strain gauges attached to the stem of the connecting bolt.

We presumed that the maximum value of the measured displacement was only $1 \mu\text{m}$; therefore, to ensure accuracy of the measured values, the micro-displacement detector was calibrated by using the universal micro measuring machine (Type M.L.D. Mitsuseiki & Co., Ltd) in the air-conditioning room at a temperature of $20 \pm 0.2^\circ\text{C}$ and 70% humidity.

The solid test specimens with shapes and dimensions equivalent to the upper and lower test specimens were used in all experiments in order to eliminate the unknown influences of the apparatus for the experiments; for example, a gap between the lower test specimen and the plate.

After the joint surfaces were degreased with trichlorethylene to obtain the real metal contact conditions, the horizontal displacement was measured after pre-loading for 5 min, because the normal displacement between the joint surfaces is considered to have large response time. The horizontal displacement was measure corresponding to the each step of the horizontal loading and after a time interval of 30 s from the application of the horizontal load.

In considering the actual bolted joints on machine tools, the pre-loads on the joint surfaces were changed from 50 kg to 600 kg. On the test specimen examined, these pre-loads were converted into mean interface pressures between $0.2\text{--}2.5 \text{ kg mm}^{-2}$ by assuming that the pre-load was uniformly distributed on the joint surfaces.

It is very difficult to apply the horizontal load and measure the horizontal displacement at the joint surfaces; therefore, as shown in Fig. 1, the horizontal

loads were applied through the upper test specimen and the horizontal displacements measured just above the joint surfaces.

Test specimens

The shapes and dimensions of the test specimens are shown in Fig. 1. For a uniform contact on the joint surfaces, the upper specimens were made as hollow cylinders with a 10 mm bore and 20 mm outer diameter, and the lower specimens were made as the cylinders having an M8 threaded hole. The overall contact area was about 236 mm^2 .

The experiments were carried out with the specimens which were made of the following; mild steel (J.I.S., SS41B); cast iron (J.I.S., FC25); brass (J.I.S., Bs BM2) and aluminium alloy (J.I.S., A3B2-T4). For the mild steel specimens investigated, the ground surfaces had surface roughness $H_{\text{max}} = 1.0 \mu\text{m}$ and $1.8 \mu\text{m}$ and machine lapped surfaces had surface roughness H_{max} between $0.04\text{--}1.6 \mu\text{m}$ (7 steps). For the cast iron specimens, the ground surfaces which had surface roughness $H_{\text{max}} = 1.0 \mu\text{m}$ and the scraped surfaces which had contact point numbers 10, 20, and 30 per in^2 , were investigated. Specimens made of brass and aluminium alloy were only investigated with ground surfaces having $H_{\text{max}} = 2.0 \mu\text{m}$ and $H_{\text{max}} = 2.5 \mu\text{m}$.

According to previous experimental results³, machine lay orientation has little effect on the normal stiffness of joint surfaces; however, in this study the effects of the machined lay orientation were investigated further for the ground surfaces.

In this kind of study it is very important to eliminate the influences of the waviness on the joint surfaces and the changes of surface topography during the experiments. Changes in the surface topography could not be detected by measuring the surface roughness before and after the experiments; however, the waviness on the joint surfaces could not be eliminated from the examined specimens, especially for the ground and the lapped surfaces. For example, the values of waviness for the ground surfaces were found to be from $0.2 \mu\text{m}$ to $1.0 \mu\text{m}$.

GENERAL CHARACTERISTICS OF THE HORIZONTAL STIFFNESS AND THE MICRO-SLIDING ON THE BOLTED JOINT

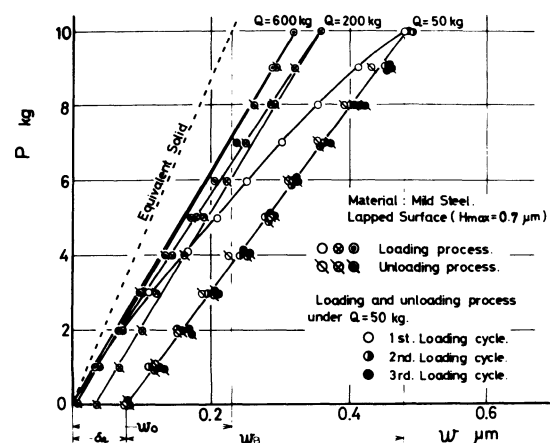


Fig. 2

One of the measured results for the relationships between the tangential load P , and the horizontal displacement w is shown in Fig. 2 under the various normal pre-load, Q . The load-displacement curve for the equivalent solid specimen is also shown by the broken line. The horizontal displacements of the equivalent solid specimen, w_0 , show the fully elastic behaviour of the joint materials independently which is in inverse proportion to Young's modulus; however, these horizontal displacements of the equivalent solid are not related to the normal pre-load.

Although the horizontal displacements for the bolted specimens are larger than for the equivalent solid specimen, the horizontal displacement of the joint surfaces is almost linear with the tangential load during the loading and unloading processes under high normal pre-load. However, under the low normal pre-load the hysteresis of the displacement can be seen after unloading to the initial tangential load, 0.2 kg in this experiment, and a clear residual displacement was found.

This residual displacement can be considered to be caused by the micro-slip between the joint surfaces or the micro-plastic deformation on the joint surface asperities; therefore, in this study the residual displacement is expressed by the characteristic δ_r as shown in Fig. 2 and termed the micro-sliding. From the figure this micro-sliding δ_r is given by

$$\delta_r = w - w_B$$

where w_B is the horizontal displacement at the unloading.

It is shown further from Fig. 2 that the horizontal displacement has some form of stick-slip motion during the loading process under such a high pre-load. However, in these conditions this particular behaviour cannot be explained exactly and further investigations are necessary.

To clarify the characteristics of the horizontal displacement at the unloading w_B , the horizontal displacements of the bolted joint subjected to the repeated tangential load were further investigated. The experimental results shown together in Fig. 2, indicate that the measured values of w_B are similar in each loading and unloading process after the first loading cycle. The displacement w_B may be considered to be caused by the fully elastic deformation between the joint surfaces.

This behaviour of the horizontal displacement on the bolted joint was found in all experiments, although there was a slight difference depending on the joint materials, the surface roughness, the machining method of joint surfaces, and so on.

The results show that the horizontal displacement is the sum of the elastic displacement and the micro-sliding between the joint surfaces. For convenience, the horizontal stiffness, K , and the micro-sliding δ_r for the bolted specimens were used and compared with the horizontal stiffness for the equivalent solid specimens. The horizontal stiffness is written as

$$K = P/w$$

where P is the tangential load.

Furthermore, to ensure accuracy of measurement, the horizontal displacements w were measured under

$P = 10$ kg, as the measured values of w are very small for tangential loads less than 10 kg.

In Fig. 3 the general behaviour of the horizontal

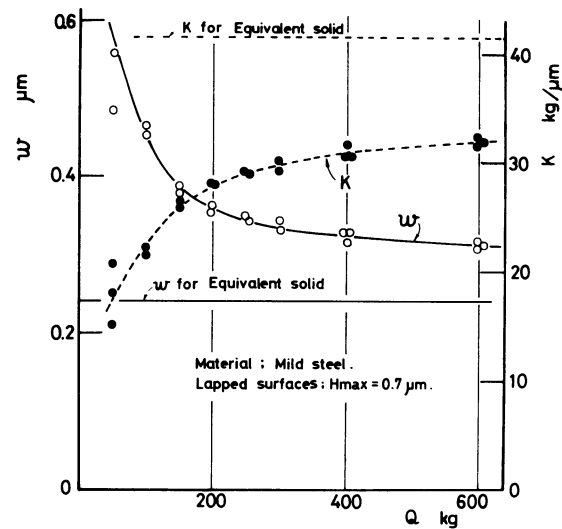


Fig. 3

displacement and the horizontal stiffness for the joint surfaces is shown related to the normal pre-load. It is clear from the results presented that the horizontal stiffness increases with increasing normal pre-load and finally reaches a certain constant value, which is nearly equal to the horizontal stiffness of the equivalent solid test specimens. However, the horizontal stiffness of the bolted specimens is less than the horizontal stiffness of the equivalent solid and has values of about 70–90% of the horizontal stiffness of the equivalent solid in spite of the very high pre-load. Therefore, the additional elastic deformation between the joints which may be caused by the existence of joint surfaces, has significant effects on the decrease in the horizontal stiffness.

EFFECTS OF THE MACHINED LAY ORIENTATIONS AND THE MATERIALS

In Fig. 4 the effects of the machined lay orientations and the materials between the joint surfaces are shown for the ground surfaces by using the mean value of the measured results in order to simplify the presentation of the experimental results. The experimental results show that the machined lay orientations have no effects on the horizontal stiffness and the micro-sliding for the joint surfaces made of mild steel, but have a small effect on these two for the joint surfaces made of cast iron, brass and aluminium alloy.

The horizontal stiffness for the specimens in which the machined lays are at right-angles to each other, are larger than the values for the specimens with the machined lays in parallel, notwithstanding the difference in the joint materials. These effects of the machined lay orientation are found clearly for the joint surfaces made of cast iron and the aluminium alloy; therefore, further experiments for these effects were carried out with the specimens made of cast iron, which had both perpendicular and the parallel machined lays. However, in these cases, the

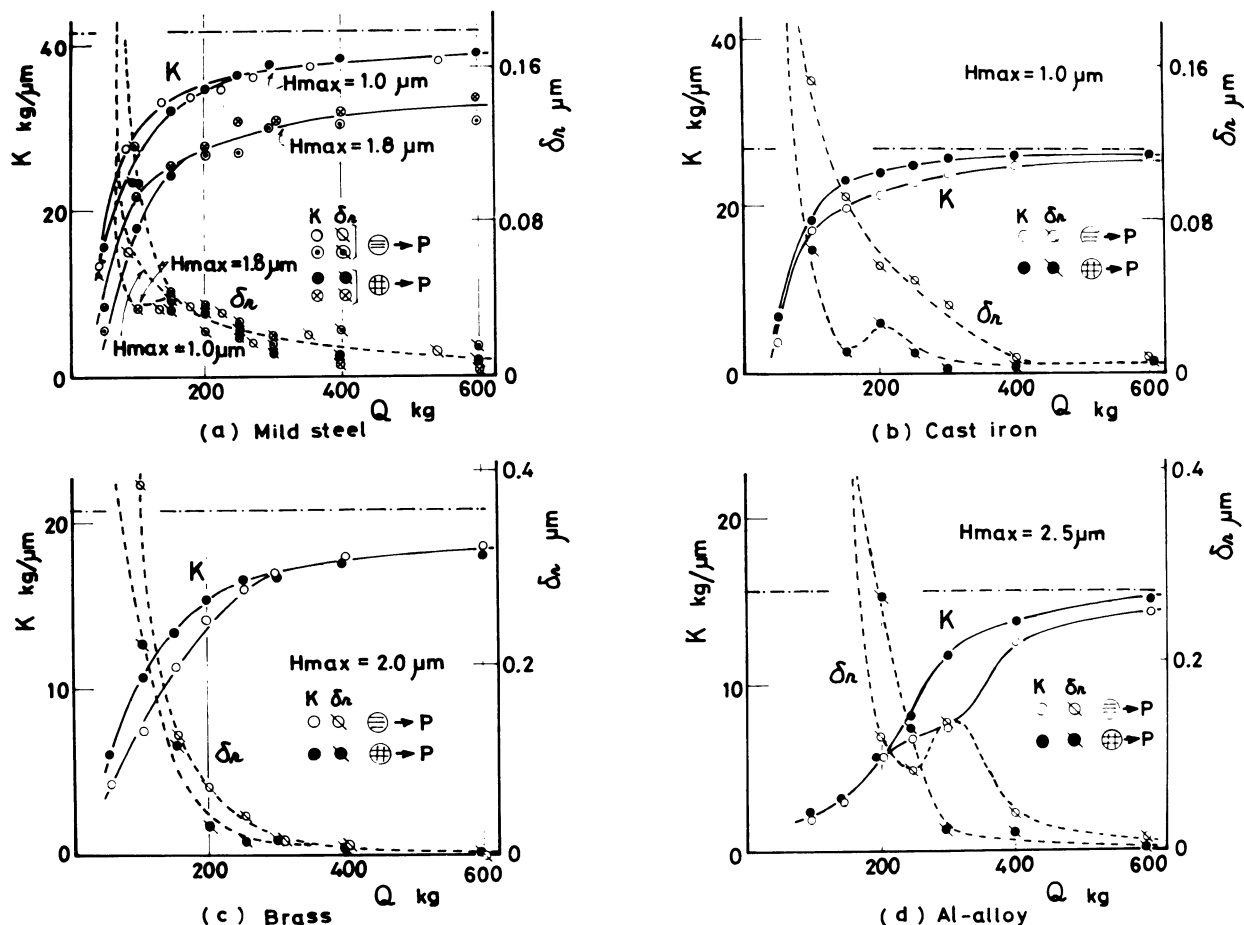


Fig. 4

former specimen was loaded in a direction at 45° and the latter perpendicular to the machined lay orientation. The results are not shown here, but the horizontal stiffness values for the specimens having these machined lay orientations are quite similar to those for the specimens with the right-angled machined lays.

The horizontal stiffness on the bolted joint is influenced by the micro-contact between the joint surfaces, as the effects of the machined lay orientation already mentioned correlate well with the flow pressure of the joint materials.

The micro-slidings between the joint surfaces, the machined lay orientations have quite contrary effects to those of horizontal stiffness. Namely, for the specimens having the right-angled machined lays, the micro-sliding is less than for the specimens having the parallel machined lays; however, for the joint surfaces made of mild steel the effects of the machined lay orientation were not significant.

To clarify the effects of the joint materials, the displacement of the equivalent solid specimen must be eliminated from the overall horizontal displacement of the specimen with the bolted joint, because the horizontal stiffness shown in Fig. 4 was calculated from the measured overall horizontal displacement. From the compensated results, it is clear that the behaviour of the horizontal stiffness is changed by the joint materials. The horizontal stiffness values for the joint surfaces made of mild steel and cast iron are increased steeply with the increasing pre-load and

approach the values for the equivalent solid under the relatively low pre-load. For the joint surfaces made of brass, the horizontal stiffness approaches the stiffness of the equivalent solid for increased pre-load, but the pre-load at which the stiffness becomes constant, occurs at a higher value than for joint surfaces made of mild steel. For the joint surfaces made of aluminium alloy, the horizontal stiffness approaches the stiffness of the equivalent solid under a very high pre-load.

It is also known that the micro-sliding is also saturated with increasing pre-load. The relative pre-loads at which the micro-sliding reaches a constant value, can be stated as follows in order of ascending value; mild steel, cast iron, brass and aluminium alloy.

EFFECT OF SURFACE ROUGHNESS

Results presented in Fig. 4 show that the surface roughness of the joint has significant effects on the horizontal stiffness, which has a high value for the smooth joint surface; however, the surface roughness has no effects on the micro-sliding.

Therefore, for reasons of easy control of surface roughness, the experiments on the effects of the surface roughness on the horizontal stiffness and on the micro-sliding of the joint surfaces were carried out with the lapped surfaces made of mild steel. The experimental results are shown in Fig. 5, and from the results we can confirm that surface roughness affects the horizontal stiffness and the micro-sliding

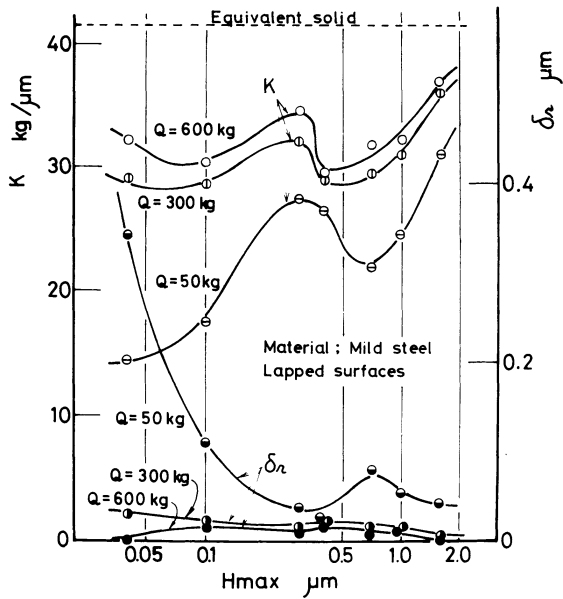


Fig. 5

significantly. The micro-sliding gradually decreases with the roughening of the surface, but the horizontal stiffness has a peak at which the surface roughness, H_{max} is about 0.3 μm .

The reasons why the horizontal stiffness has such particular behaviour can be explained as follows.

The overall horizontal displacement w on the bolted joint is given by

$$w = \delta_B + \delta_r$$

In both these characteristics, the micro-sliding δ_r may be influenced chiefly by the action of prevention between the joint surfaces which is caused by the micro-toothing between the surface asperities. However, the elastic displacement at unloading may be chiefly influenced by the micro-seizure between the joint surfaces, which is closely related to the numbers and mean radius of the contact point⁴. According to the improvement of the surface roughness on the joint, the number of the contact points between the joint surfaces generally increases and supported pressure on the contact points decreases. Therefore, the contact points in the micro-seizure conditions obviously do not uniformly increase with the improvement in the joint surfaces roughness (Fig. 5).

EFFECT OF MACHINING METHOD

The effects of the machining method were investigated with the test specimens with scraped surfaces and also ground surfaces.

The experimental results shown in Fig. 6 compare the horizontal stiffness of the ground and scraped surfaces. They show that the horizontal stiffness of the scraped joint surfaces is less than that of the ground joint surfaces, and the number of contact points per in^2 have significant effects on the horizontal stiffness.

The horizontal stiffness of the scraped joint surfaces is generally increased with increased numbers of contact points, but decreased again with a further

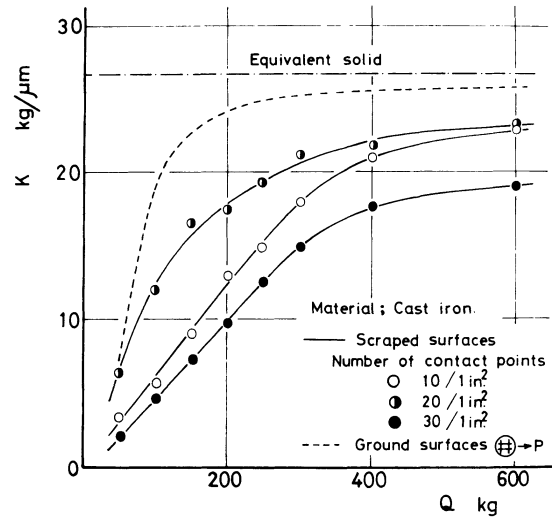


Fig. 6

increase in the numbers of contact points. In this case, the pre-load at which the horizontal stiffness reaches a certain constant value, is decreased with the increasing numbers of contact points and finally remains at a constant value. It can be seen from these results that the horizontal stiffness of the scraped joint surfaces has a peak value for the numbers of contact points.

The micro-sliding for scraped joint surfaces is larger than for the ground surfaces; also with the scraped joint surfaces, the specimens with 20 contact points per in^2 gave the smallest value for the micro-sliding. This result confirms further that the behaviour of the horizontal stiffness is quite the opposite to the relationships between the micro-sliding and the normal pre-load.

The horizontal stiffness of the scraped specimens which are joined together with the different surfaces which have numbers of contact points 10 per in^2 and 20 in^2 , also indicates similar behaviour. However, the horizontal stiffness of this specimen is almost equal to the mean value, which is calculated from the horizontal stiffness of each of the scraped specimens having similar numbers of the contact points.

By taking into consideration the results presented, it is clear that the methods of machining the joint surfaces have significant effects on the horizontal stiffness and also on the micro-sliding.

CONSIDERATION FOR THE ELASTIC DISPLACEMENT ON THE BOLTED JOINT

From the results already presented, it is clear that the elastic displacement, δ_B , on the bolted joint during unloading, is about half the value of the overall horizontal stiffness under the large normal pre-load, and moreover, this elastic displacement is larger than the horizontal displacement of the equivalent solid. Therefore, the elastic displacement is thought to determine the horizontal stiffness of the bolted joint.

When the two rough surfaces are mating with each other, the real contact area between these surfaces, is very small, compared with the apparent contact area

of the joint surfaces, and is given by the value of Q/p_m where Q is the normal pre-load and p_m is the flow pressure of joint materials.⁶ In this condition, the shearing stress between the real contact area subjected to the tangential load P is given by $(P/Q) \cdot p_m$.

If the value of $(P/Q) p_m$ is calculated for the specimens made of mild steel, subjected to $P = 10$ kg and $Q = 50-600$ kg, it is clear that this shearing stress is very large. Therefore, the surface asperities and the layers near the joint surfaces may be deformed by the shearing stress when the tangential load is applied to the bolted joint. The shear deformation of the surface asperities, however, is negligible, as the surface asperities can be thought of as circular-cones having 140-170 degree conical angles for the ground surfaces, and furthermore, the surface asperities were restrained.

From the results, it can be seen that the elastic displacement δ_B is determined by the elastic shearing deformation δ_e between the joint surfaces. By assuming that the real contact area has n junctions and each junction is an identical circle having a radius a , the elastic shear deformation can be calculated by regarding this problem as a problem of elasticity for a semi-infinite elastic solid with a tangential force on its surface.

Here, if the tangential load is considered to be supported uniformly on each junction and each junction is loaded by P/n , from the solution of the elasticity⁵ the elastic tangential deformation of the joint surfaces is given by

$$\delta_e = \frac{P/n}{G \pi a} (2 - \nu) \quad (1)$$

where G is the modulus of elasticity in shear and ν is Poisson's ratio.

Therefore, if the values of n and a are known, the elastic deformation between the joint surfaces can be calculated. Both these values, however, have not yet been fully investigated for the various joint materials and it is very difficult to determine their exact values for the ground joint surfaces made of mild steel. According to the experimental results of Bowden and Tabor⁶, the values of n and a are as follows:

$n = 22$, $a = 0.12$ mm at $Q = 100$ kg; and $n = 35$, $a = 0.12$ mm at $Q = 500$ kg.

In Fig. 7 the theoretical values of δ_e which were calculated from the equation (1) by using these values for n and a , are shown by the full line. The results indicate that the theoretical values of δ_e are qualitatively in good agreement with the experimental values of δ_B ; therefore, it can be said that the elastic displacement δ_B is caused by the elastic shearing deformation between the joint surfaces.

According to equation (1), the apparent contact area has little effect on the elastic deformation; that is, the elastic displacement. The experimental results for the effects of the apparent contact area are shown together in Fig. 7, but the differences in the elastic displacement between the various apparent contact areas cannot be seen.

Therefore, we have further confirmed from these results that equation (1) is a reasonable explanation of the elastic displacement.

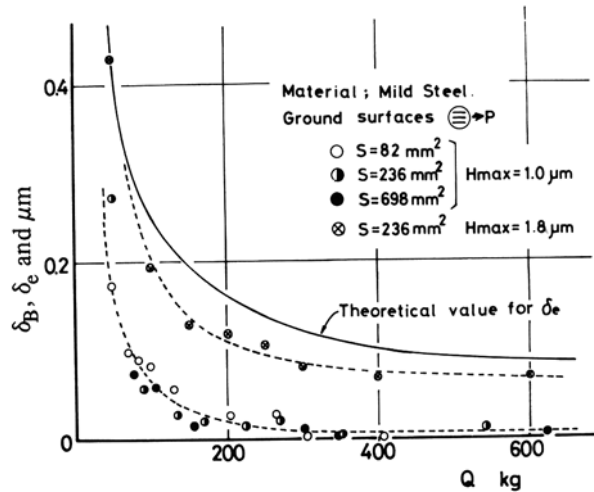


Fig. 7

CONCLUSIONS

In this study the horizontal stiffness and the micro-sliding on the bolted joint under the normal pre-load have been investigated experimentally.

For convenience, the real horizontal stiffnesses per unit area for the bolted joints with various joint surface conditions are presented in Table 1, in which the

Table 1 The values for real horizontal stiffness of bolted joint.

Test Specimens.		k	$\text{kg}/\mu\text{m} \cdot 1/\text{mm}^2$	
		1.0	2.0	
Mild steel	Ground (Hmax=1.0μm) ⊕→P	2.4		
	Ground (Hmax=1.8μm) ⊕→P	2.4		
	Lapped	Hmax=1.6μm	2.4	
		1.0μm	2.4	
		0.7μm	2.4	
	0.3μm	2.4		
		0.1μm	2.4	
0.04μm	2.4			
Cast iron	Ground (Hmax=1.0μm) ⊕→P	4.5		
	Scraped	4.5		
	Numbers of contact point:	4.5		
	10/lin ²	4.5		
20/lin ²	4.5			
30/lin ²	4.5			
Brass	Ground (Hmax=2.0μm) ⊕→P	4.5		
Al-alloy	Ground (Hmax=2.5μm) ⊕→P	4.5		

horizontal stiffness, k , and the mean interface pressure, p , are given by

$$k = \frac{P}{w - w_0} \frac{1}{S} \quad \text{and} \quad p = \frac{Q}{S}$$

where S is the apparent contact area between the joint surfaces.

The experimental results show that the horizontal stiffness and the micro-sliding on the bolted joint are largely influenced by the connecting and the surface conditions, such as the normal pre-load, the surface roughness and the material of joint surfaces, the

machined lay orientation and so on, and show very complicated behaviour for these factors. Furthermore, the horizontal stiffness generally has quite the contrary behaviour to that of the micro-sliding on the bolted joint.

The horizontal stiffness values for the specimens with the bolted joints are lower than for the equivalent solid specimens, and indicate 50–90% of the values of the horizontal stiffness of the equivalent solid under the normal pre-load of 0.5 to 2.0 kg mm⁻².

To clarify this complicated behaviour, the theory of elasticity was used and the expression for the elastic displacement was presented in equation (1) by which we can suggest a reasonable explanation for the experimental results.

However, much interesting behaviour is not satisfactorily explained so far, such as a kind of micro-stick-slip motion during the loading process, the cause of the micro-sliding, the quantitative calculation of the horizontal stiffness with good accuracy, and so on. This necessitates further investigation to solve these problems.

ACKNOWLEDGEMENTS

This study was supported in part by the scientific research fund from the Ministry of Education.

REFERENCES

1. SCHLOSSER, E., 'Der Einfluß ebener verschraubter Fugen auf das statische Verhalten von Werkzeugmaschinenstellen,' *Werkstattstechnik u. Masch.-bau* 47-1 (1957), S. 35.
2. ITO, Y., and MASUKO, M., 'Experimental Study on the Optimum Interface Pressure on a Bolted Joint Considering the Damping Capacity' to be presented in this conference.
3. THORNLEY, R. H., *et al.*, 'The Effect of Surface Topography upon the static Stiffness of Machine Tool Joints,' *Intern. J. Mach. Tool Des. Res.*, 57 5-1/2 (1965).
4. TSUKIZOE, T., *J. Japan Soc. Mech. Engrs.*, 1753, 62-491 (1959-12).
5. MUKI, R., *Progress in Solid Mechanics*, Vol. 1, North Holland, 1960.
6. BOWDEN, F. P., and TABOR, D., 'The Friction and Lubrication of Solids', Oxford, 1954.

DISCUSSION

Query from A. G. Hague, Trent Polytechnic, Nottingham.

Since you have used such a small area of contact, namely 236 mm² (about 0.4 in X 0.4 in. square), how can your results be related to actual surfaces met in machine tool structures, which are of course much larger, with an extra factor to consider – surface waviness or errors in flatness.

Reply

As you point out, the actual bolted joint has a much larger area and has also large surface waviness or errors in flatness compared with our examined specimens.

In this experiment, we have investigated the basic behaviour of the horizontal stiffness and the micro-

sliding, because it is very important to clarify the general behaviour of the bolted joint subjected to the tangential force.

Test specimens with a small area are very convenient for this kind of experiment. With these test specimens it is easy to obtain the required accuracy of the measured value of displacement, and also to hold the joint surfaces together under a constant condition.

Although we have investigated the effects of a surface area on the horizontal stiffness, we cannot, at present, apply these results to an actual machine tool design.

We think that if the results presented in this paper are to be applied to actual surfaces, difficulties may be encountered in choosing the appropriate scale factors.

Although some results that take into consideration the effects of the surface waviness have been presented, a more detailed investigation is required for a better understanding.

Furthermore, according to our preceding results⁸, the model theory was not satisfied for a bolted cantilever subjected to a tangential force. We hope that it may be possible to use the results presented herein for actual joint surfaces at some later date, if more detailed and accurate information regarding the scale factors to be used in a model analysis become available.

(7) Conolly, R. and Thornley, R. H. *Trans. A.S.M.E., Ser. B.*, Vol. 90. No. 1 (1968-2), p. 97.

(8) Ito, Y. and Masuko, M. *Trans. Japan Soc. Mech. Engrs.* Vol. 36, No. 284, (1970-4), p. 649.

Query from R. E. Schofield

I must first congratulate Professor Masuko and his colleagues on their extremely relevant and important paper in this field.

However, I am not at all convinced that the energy loss due to the presence of bolted joints is due entirely to friction or micro-sliding. We have carried out tests where mechanical interlocking of asperities is established and have found no less energy loss than with conventional surfaces. From this we assume that the energy loss is due to a cyclic plastic deformation of the asperities in contact.

When the two surfaces are preloaded, the real contact spots are at the yield boundary of the materials. Since the interfaces are not necessarily parallel to the direction of motion, any horizontal force must cause an increase in pressure and hence a plastic deformation at these joints. There need be no micro-sliding whatsoever between the surfaces. This suggestion would appear to be born out by Fig. 2 in the paper, where subsequent loadings after the first show no evidence of deflection other than elastic. This is consistent with the expectation, since the plastic deformation has taken place at the first loading.

It is also born out by Fig. 4 where surface roughness is shown to have little effect on micro-sliding. I am in absolute agreement with the analysis of the elastic displacement. This is a practically

parallel analysis to the one proposed for normal deflection in our own paper in this session and also to the one proposed in Ref. (1) below.

Ref. (1) Schofield, R. E. Schraubenverhindungen in Werkzeugmaschinen konstruktion. Proceedings 6th Machine Tool Congress, Budapest, 1968.

Reply

As described in the explanation of Fig. 2, we used the term 'micro-sliding' only to express the residual displacement after unloading.

We should like to point out, however, that the micro-sliding defined by us in this paper was also found on the bolted joint in which the friction force determined by the preload of connecting bolt is larger than the applied tangential force.

We have not investigated the detailed cause of this micro-sliding, but we think that it may be derived

from the micro-slip between the joint surfaces or the micro-plastic deformation on the joint surface asperities.

The measured horizontal displacement indicates a sort of infinitesimal stick-slip motion during the loading, though the friction force is larger than the applied tangential force.

We could not measure this stick-slip clearly, because the micro-slip in this condition is very small and less than $0.1 \mu\text{m}$.

However, we further confirmed the existence of the micro-sliding by measuring the change of electrical contact resistance between the joint surfaces.

We consider, therefore, the micro-slip can be naturally found on the bolted joint in which $P > \mu Q$ and a sort of micro-slip can also be found on the bolted joint in which $P < \mu Q$.

These micro-slips are very important to clarify the energy loss due to the presence of a bolted joint.

CALCULATING THE ELASTIC AND PLASTIC COMPONENTS OF DEFLECTION OF PLANE JOINTS FORMED FROM MACHINED SURFACES

by

R. E. SCHOFIELD* and R. H. THORNLEY†

SUMMARY

One of the biggest impediments to the complete computer simulation of Machine Tool Structures is the inability to calculate values of stiffness and damping for the joints. This paper sets out a method whereby the elastic and plastic components of the deflection of joints formed from machined surfaces may be calculated. This knowledge is necessary before the more complicated aspects of quantitative joint analysis, for example, the distribution of pressure from a bolt, may be carried out.

The method involves a mathematical expression of the surface-finish characteristics and develops a mathematical model for the mutual approach of the surfaces. Both the elastic and plastic components are considered and it is shown how these may be used to obtain values of initial deflection and elastic recovery. Experimental results show that the method is valid within the limits of accuracy of the mathematical expression of the surface finish.

NOTATION

θ	Half-angle of lay orientation
λ_p	Plastic component of deflection
λ_e	Elastic component of deflection
λ_t	Total deflection
s	See equation 7 and Fig. 5
β	As defined in Fig. 5
ψ	As defined in Fig. 5
ϕ	As defined in Fig. 5
μ	Poisson's ratio
ξ	Deflection at a point due to uniform pressure over a given area on the surface of a semi-infinite body of elastic material
q	Intensity of pressure over an area on the surface of a semi-infinite body
f	Feed or distance between cusps
r	Half-length of diagonals of contact spots see figure 5
P	Mean interface pressure
Y_c	Yield pressure
E	Young's modulus of elasticity
l_1	Longer side of contact rectangle
l_2	Shorter side of contact rectangle
K_1	Stiffness due to surface characteristics
K_2	Stiffness due to body of material
K_3	Stiffness due to bolts

INTRODUCTION

The complete and accurate computer analysis of a machine tool structure depends on the accurate derivation of the mass, stiffness and damping values of the various elements and joints in the structure.

At present it is impossible to calculate values for the stiffness and damping of joints, and estimates and assumptions have to be made in the light of previous experience. This paper proposes a basis upon which a method of calculating joint stiffness could be developed.

The total compliance of a bolted joint consists of a number of components (Fig. 1) due to

- flange deformation,
- elastic deflection of the body material,
- the compliance due to the surface asperities.

Flange deformation

The parameters governing the flange deformations are

- the rigidity of the flange (effective EI),
- the distribution and design of ribbing,
- the bolt configuration,
- the distributing of pressure from each bolt.

Data concerning (a), (b) and (c) are readily available and their possession would allow complex but soluble analyses of flange deflection providing that

*Department of Production Engineering, Brunel University

†Machine Tool Division, UMIST

(d), the pressure distribution resulting from bolts, were known. This, however, may only be calculated if it is assumed that the flange is a beam on an elastic foundation, the foundation being the surface asperities. Calculation of the distribution of pressure in this case depends on a knowledge of the foundation stiffness. Therefore, the distribution of pressure from the bolts, and hence the flange deformation, can only be calculated if the stiffness or compliance due to the surface asperities is known.

Elastic deflection of the body material

This depends on the pressures exerted on the body, and has the same distribution as the pressure from the bolts. Thus the elastic deflection of the body material also depends on the compliance due to the surface asperities.

Compliance due to surface asperities

This parameter is consequently the basis upon which any calculation of joint stiffness must be developed. The following, therefore, establishes a mechanism for the initial approach of the surface and for the elastic recovery. The parameters affecting these properties are analysed and quantified and a method for their calculation is developed.

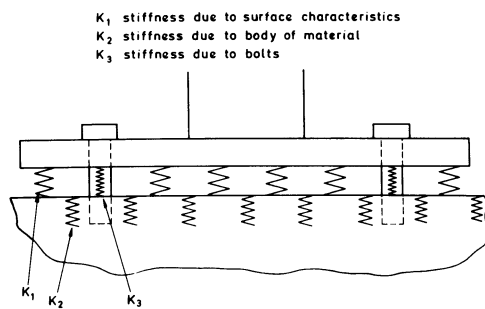


Fig. 1 Surface, body and bolt stiffness of a bolted joint.

MECHANISM OF THE APPROACH OF SURFACES

When two surfaces are placed in contact with negligible normal Mean Interface Pressure, actual contact is made between very few points. As the mean interface pressure is increased, plastic deformation of these points takes place. There is a mutual approach of the surfaces and actual contact is made at additional points. Plastic deformation will continue until the actual area of contact is sufficient to support the load. Therefore, any given value of mean interface pressure will produce an equivalent degree of plastic deformation. There will also be present a degree of elastic deflection which results from the elastic stresses set up in the bodies behind the contacting faces by the localised pressures existing at the points of contact. The total deflection being the sum of the plastic and elastic components is that which is experienced during the initial loading of the joint.

If the mean interface pressure is reduced the surfaces will move apart due to the elastic recovery. This recovery will, of course, be much less than the initial

deflection because the plastic deflection will have resulted in a permanent 'set' in the joint. Any subsequent reimposition of the mean interface pressure will result in a deflection equal to the elastic recovery of the joint until the previous maximum value of mean interface pressure is reached¹. Any increase over this maximum value will result in an additional plastic deformation and deflection. Fig. 2 illustrates these effects.

In a machine tool structure, the ratio between the cross-sectional area of the bolts and the contact area between the faces is rarely higher than 1:8. Using mild steel bolts, a stress higher than 16 tons per in² of bolt area is difficult to achieve. Therefore, a Mean Interface Pressure of 2 tons per in² is the highest reasonably obtainable in practice. Normally, actual mean interface pressures are well below this value. These pressures are therefore very small compared with the yield pressure of the material. Consequently, the real areas of contact and the individual contact spots are comparatively small.

Under the initial loading condition, the approach of the surfaces depends on their bearing area properties. With a knowledge of these properties, the initial deflection can be calculated from the point when the bearing area becomes large enough to support the load. This also depends on the yield pressure or hardness of the material, since this is the maximum pressure which an area of contact can withstand. Since the deformation which gives the contact spots their shape and area is almost entirely plastic (the elastic deflection in the plane of the joint is negligible), a knowledge of the surface topography enables a calculation of this shape and area to be made. The elastic deflection can, therefore, be calculated if it is taken to be that at each contact spot and assumed to be caused by an area of uniformly distributed pressure on the surface of a semi-infinite body.

As illustrated above, for joints occurring in machine tool structures, the mean interface pressures are very small. This results in contact spots which are small and comparatively remote from each other. The elastic deflection can, therefore, be considered as being that of one spot due to the pressure at that spot, which is assumed equal to the yield pressure of the material. The deflection at one spot due to the pressure at another may be neglected because of the above considerations of area and distance. The validity of this assumption was confirmed by a test in which surfaces with 1, 4, 9, 16 and 25 identical contact spots were compressed together. The deflections of the joints so formed were plotted against pressure per contact point and, as can be seen from Figs. 3 and 4, negligible interaction was detected.

It has been shown empirically¹ (Fig. 2) that the unloading curve is identical, regardless of the point on the loading curve from which it commences. This validates the assumption that the unloading curve can be calculated from the elastic components of deflection at any value of mean interface pressure. In the case of conventional machined surfaces, the asperities are, of course, not perfectly similar. Compression, therefore, results in contact spots of different sizes. The maximum elastic recovery of one contact spot will be at its centre and will increase in magnitude

according to its area. Thus, the elastic recovery of a conventional surface will be that of the centre point of its largest contact spot. The foregoing indicates that the parameters governing the stiffness of the surface region are the material properties of the machined surfaces and the surface finish characteristics.

Material properties

The material properties which govern joint deflection are the modulus of elasticity, Poisson's ratio and the flow or yield pressure of the material under the contact conditions. The last is the only one of these which presents any problem, because of the variation of yield pressure with the angle of the contacting asperities. It has been shown¹, however, that the Vickers Hardness test is a suitable simulation of asperity contact and that the value of yield pressure calculated from this test is sufficiently accurate for the calculation of the plastic component of joint deflection.

Surface finish characteristics

Surface error may be considered to fall into two categories:

(a) flatness, due to errors in machining ways or, for example, in the profile of a slab milling cutter;

(b) roughness due to tool geometry and errors due to the following random effects:

1. the machining process throws up random asperities above the geometric tool shape,
2. pieces of the surface are torn out by the tool thus reducing the bearing area,
3. the built-up edge effect leaves particles of material on the surface.

All of these effects are by nature so random that an accurate assessment of the surface properties becomes very difficult. It is well known that the accepted methods for surface assessment do not allow the bearing qualities of the surface to be calculated. It has been proposed,² however, that the bearing area curves and the frequency of high spots is a far more useful method of surface assessment. The authors have developed this hypothesis into a mathematical assessment of surface finish characteristics³ and this assessment is utilized below to calculate values of joint deflection.

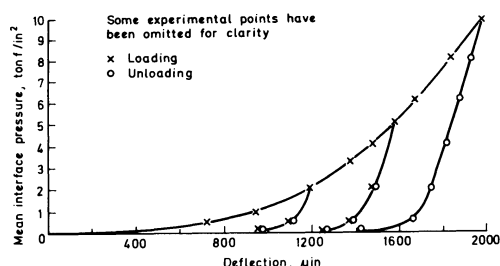


Fig. 2 General Joint Characteristics (after Connolly).

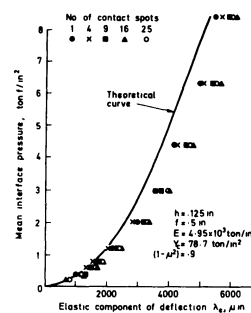


Fig. 3 Relationship between mean interface pressure and elastic components of deflection for varying numbers of contact spots using aluminium specimens.

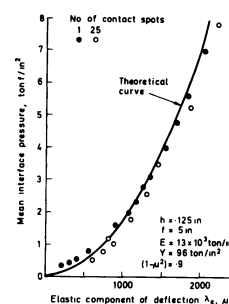


Fig. 4 Relationship between mean interface pressure and elastic component of deflection for varying numbers of contact spots using mild steel specimens.

ANALYSIS OF JOINT DEFLECTION

The following will deal with joints formed from surfaces machined by single-point tools. The analysis may then readily be extended to other surfaces.

Plastic component of deflection

In expressions developed for the approach of surfaces¹, the assumption was made that this calculation of the total approach took into account the elastic component of deflection. It can be seen from the following section that this assumption is incorrect and the approach¹ calculated is, in fact, the plastic component of deflection. Since the elastic component is small compared with the plastic component in joints of the type considered¹, the difference in the experimental result is quite small. The relationships established¹ for total deflection may, therefore, be directly applied to the plastic component; that is

$$\frac{2P}{Y_c} = \left[1 - \left(1 - \frac{\lambda P}{h_1} \right)^{1/2} \right] \left[1 - \left(1 - \frac{\lambda P}{h_2} \right)^{1/2} \right] \quad (1)$$

or if the surfaces are similar

$$\lambda P = h \left[1 - \left(1 - \sqrt{\frac{2P}{Y_c}} \right)^2 \right] \quad (2)$$

Elastic component of deflection

Surfaces machined by single-point tools, and more particularly shaped surfaces, may be expressed in the form of parabolic cusps^{1,2,3}. When two such surfaces are pressed together the contact spots will be of parallelogram shape¹. This analysis depends on the assumption that the elastic deflection due to asperity contact can be expressed as that due to an area on a semi-infinite elastic body subjected to a constant pressure. The area in this case will be that of the individual contact spots and the pressure, the yield pressure of the material under the contact conditions. These assumptions are consistent with the known recovery shape. The parallelogram¹ was defined by the length of its diagonals $2r_1$ and $2r_2$ and the angle of lay orientation 2θ .

Parallelogram area is related to the plastic component of deflection by the equations

$$\frac{2r_1 \sin 2\theta}{f_1} = 1 - \left(1 - \frac{\lambda P}{h_1}\right)^{1/2} \quad (3)$$

and

$$\frac{2r_2 \sin 2\theta}{f_1} = 1 - \left(1 - \frac{\lambda P}{h_2}\right)^{1/2} \quad (4)$$

Values of r_1 and r_2 may therefore be calculated, for a given value of λP , from equations 1 and 2 by substitution in equations 3 and 4 and the parallelogram of constant pressure is thus defined.

The total deflection at a point due to a uniformly distributed load over an area is given by Timoshenko and Goodier⁵ as

$$\xi = \frac{(1 - \mu^2)}{\pi E} q \iint ds \, d\psi \quad (5)$$

where $q = Y_c$ in this case

The maximum deflection will occur at the centre of the area. Consider, therefore, the centre point O of the parallelogram, Fig. 5a. By the theory of superposition, the deflection at this point can be calculated as the sum of the deflections due to the load on each of the four component triangles.

Consider the triangle in Fig. 5b.

$$\int ds = S \quad (6)$$

$$\frac{S}{\sin \beta} = \frac{r_1}{\sin (180 - \beta - \phi)} \quad (7)$$

$$\therefore S = \frac{r_1 \sin \beta}{\sin (\beta + \phi)}$$

substituting equations (6) and (7) in (5)

$$\xi = \frac{(1 - \mu^2) Y_c}{\pi E} \int_0^\psi \frac{r_1 \sin \beta}{\sin (\beta + \phi)} d\phi \quad (8)$$

$$\therefore \xi = \frac{r_1 \sin \beta (1 - \mu^2) Y_c}{\pi E} \int_0^\psi \frac{1}{\sin (\beta + \phi)} d\phi \quad (9)$$

Integrating

$$\xi = \frac{(1 - \mu^2) Y_c r_1 \sin \beta}{2\pi E} \times \log \left[\frac{1 - \cos (\beta + \psi)}{1 + \cos (\beta + \psi)} \frac{(1 + \cos \beta)}{(1 - \cos \beta)} \right] \quad (10)$$

The total deflection ξ_o can therefore be calculated by repeating this procedure for the remaining three triangles and summing the results.

This gives the elastic recovery of one cusp. Thus, the total elastic recovery of the joint will be

$$\lambda_e = 2 \xi_o \quad (11)$$

In the case of cusps of different materials, the individual values of E and μ will have to be inserted, and the total elastic deflection will be

$$\lambda_e = \xi_{o1} + \xi_{o2} \quad (12)$$

Fig. 6 shows how $K_1 r_1$ varies for various ratios of l_1/l_2 and constant contact area, where l_1/l_2 = the ratio of the sides of the contact rectangle

$$\begin{aligned} \text{and } K_1 = & \sin \beta_1 \log \left[\frac{1 - \cos (\beta_1 + \psi_1)}{1 + \cos (\beta_1 + \psi_1)} \frac{(1 + \cos \beta_1)}{(1 - \cos \beta_1)} \right] \\ & + \sin \beta_2 \log \left[\frac{1 - \cos (\beta_2 + \psi_2)}{1 + \cos (\beta_2 + \psi_2)} \frac{(1 + \cos \beta_2)}{(1 - \cos \beta_2)} \right] \end{aligned} \quad (13)$$

It can be seen that the maximum recovery for a given rectangular area occurs for a square and decreases as the length of the contact area increases. Thus, if the lay orientation 2θ is varied and the applied force kept constant, cusps orientated at 90° will recover elastically by a greater amount and the degree of recovery will reduce with the angle of lay orientation.

A square area of contact will result from similar surfaces crossed at an angle of 90° so $h_1 = h_2 = h$; $f_1 = f_2 = f$. In this case $\beta = 45^\circ$ and $\psi = 90^\circ$. Substituting these values in equation 10 yields

$$\xi = \frac{(1 - \mu^2) Y_c r_1}{2\sqrt{2} \pi E} \log \left[\frac{1 + 1/\sqrt{2}}{1 - 1/\sqrt{2}} \frac{1 + 1/\sqrt{2}}{1 - 1/\sqrt{2}} \right] \quad (14)$$

$$\therefore \xi = \frac{3.526 (1 - \mu^2) Y_c r_1}{2\sqrt{2} \pi E} \quad (15)$$

from equation 1

$$\frac{P}{Y_c} = \sqrt{\frac{2r_1^2}{f^2}}$$

$$\therefore r_1 = \sqrt{\frac{Pf^2}{2Y_c}} \quad (16)$$

Substituting in equation 15 yields

$$\xi = \frac{3 \cdot 526 (1 - \mu^2)}{2\sqrt{2} \pi E} \sqrt{\frac{P f^2}{2 Y_c}}$$

$$\therefore \xi = \frac{0 \cdot 28 (1 - \mu^2) \sqrt{(P \cdot Y_c) f}}{E} \quad (17)$$

Since all four triangles are congruent,

$$\xi_o = \frac{1 \cdot 12 (1 - \mu^2) \sqrt{(P \cdot Y_c) f}}{E} \quad (18)$$

$$\text{and } \lambda_e = \frac{2 \cdot 24 (1 - \mu^2) \sqrt{(P \cdot Y_c) f}}{E} \quad (19)$$

The relationships in equations 10, 11 and 19 have been compared with experimental values. The congruency of the unloading curves indicated that the initial assumption that the unloading curve is the elastic recovery of the joint is valid.

Total deflection

As stated above, the relationships in equations 1 and 2 involve the permanent plastic deflection. A value of the total elastic plus plastic deflection of the joint can therefore be obtained by adding the elastic deflection λ_e , equations 10, 11 and 19, to the plastic deflection λ_p equations 1 and 2. That is, the total deflection is

$$\lambda_t = \lambda_p + \lambda_e \quad (20)$$

EXPERIMENTAL PROCEDURE

The experimental procedure was identical to that followed elsewhere^{1,5}, the mean interface pressure was varied, all other parameters being kept constant, and the deflection measured. Tests were carried out on conventionally machined shaped surfaces. The results of these tests are shown in Figs 7a, b and c, and Figs 7d, e and f, respectively.

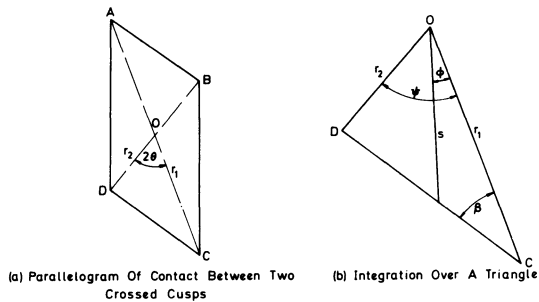


Fig. 5a Parallelogram of contact between two crossed cusps, b Integration over a triangle of contact.

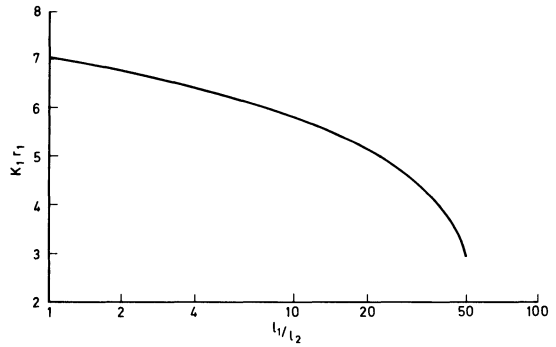


Fig. 6 Relationship between $K_1 r_1$ and l_1/l_2 (equation 13)

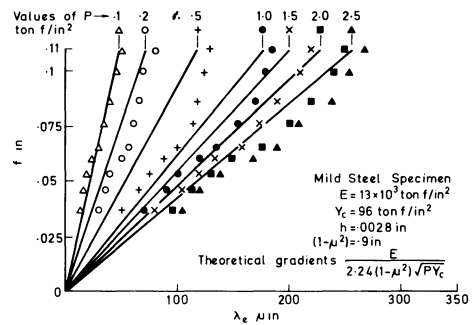


Fig. 7a Relationship between λ_e and f for a variation in values of P for idealised surfaces.

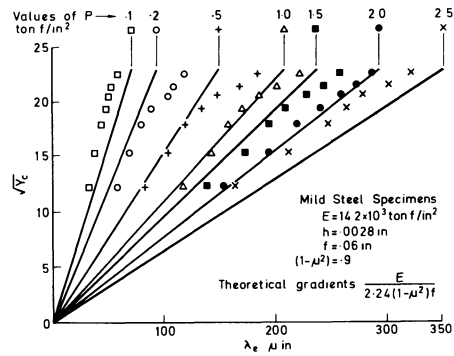


Fig. 7b Relationship between λ_e and $\sqrt{Y_c}$ for idealised surfaces.

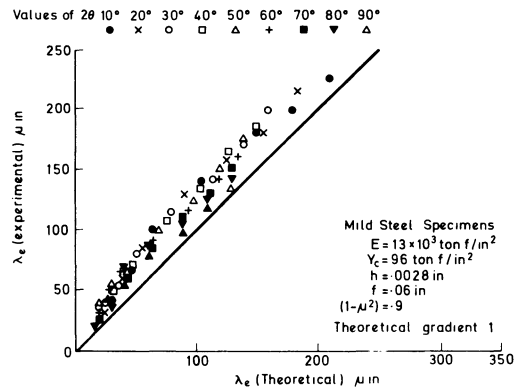


Fig. 7c Comparison of theoretical and experimental values of plastic deflection for a variation in lay orientation for idealised surfaces.

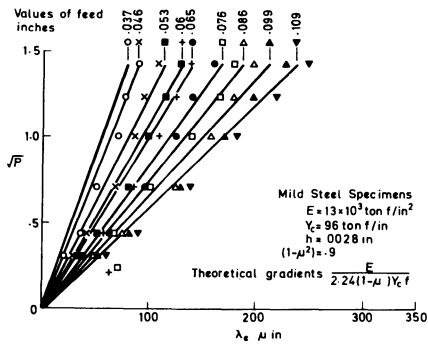


Fig. 7d Relationship between λ_e and \sqrt{P} for a variation in feed values for conventionally shaped surfaces.

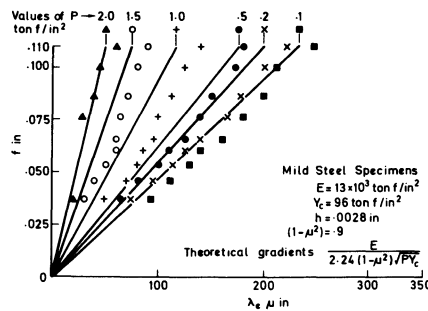


Fig. 7e Relationship between λ_e and f for a variation in values of P for conventionally shaped surfaces.

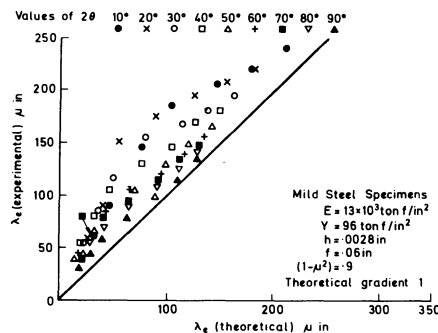


Fig. 7f Comparison between experimental and theoretical values of elastic deflection for a variation in lay orientation for conventionally shaped surfaces.

DISCUSSION OF RESULTS

The close proximity of the experimental results to those predicted theoretically indicates the validity of the theory. In all cases the experimental elastic deflection is greater than that predicted, this tendency being exaggerated with the conventionally shaped surfaces. The incidence of increased deflection in the tests with idealised surfaces is probably due to the effect of superposition of deflection at one contact spot from the load at another. This effect was neglected in the theoretical prediction.

The greater error consistently associated with the conventionally machined surfaces must be due to the inability to measure the surface topography accurately. This impediment is unlikely to be overcome in the foreseeable future. It follows from the theory of elastic deflection that the smaller the real contact spots, the smaller will be the elastic compo-

ponents. It also follows that in general, the larger the number of real contact spots, the smaller will be their area.

The best possible scraped surfaces have 25 contact spots per square inch whereas a theoretical 81 contact spots per square inch exist on a joint formed from surfaces shaped with an 0.109 in feed. Although the real number will be well below 81, it must equally be much higher than 25. A joint with a surface shaped in this way should therefore be considerably stiffer than a scraped joint. This was verified experimentally and the results are shown in Fig. 8. This confirms the conclusion drawn to this effect¹.

(a)	(b)
Idealised shaped surfaces $f = .109$ in	Scraped surfaces 25 spots/in ²
Mild Steel Specimens	Mild Steel Specimens
$E = 13 \times 10^3$ ton f/in ²	$E = 13 \times 10^3$ ton f/in ²
$Y_c = 96$ ton f/in ²	$Y_c = 96$ ton f/in ²
$h = .0028$ in	$h = .00175$ in
$(1 - \mu^2) = .9$	$(1 - \mu^2) = .9$
	$h_c = .00045$ in
	$f_c = .03$ in

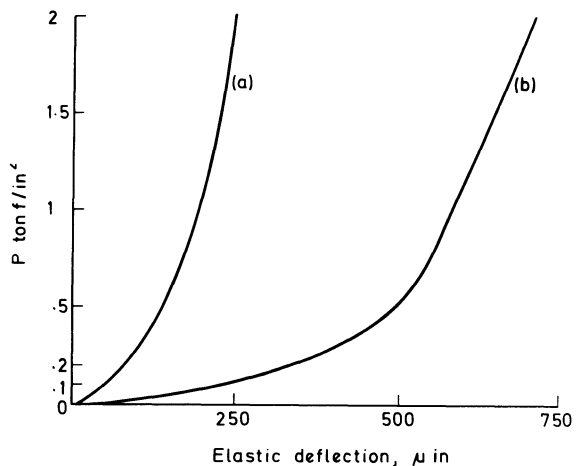


Fig. 8 Comparison between elastic recovery of scraped and shaped surfaces.

CONCLUSIONS

1. The analysis and the assumptions made above for calculating the elastic component of joint deflection are valid.
2. The analysis for total initial deflection¹ is incorrect, but correct for the plastic component only.
3. The elastic component of deflection increases with the ratio of material properties $(1 - \mu^2) (Y_c) / E$, the square root of the mean interface pressure and the frequency of contact spots.
4. The stiffest joint under elastic conditions is formed from a material of low $(1 - \mu^2) (Y_c) / E$ ratio and machined to incorporate asperities of regular geometry with an amplitude sufficiently large to eliminate any surface flatness errors and with the maximum possible number of contact spots. This confirms conclusions (5)¹.
5. A joint manufactured to the conditions of 4. above may be considerably stiffer elastically than the best possible scraped surface.

REFERENCES

1. CONNOLLY, R., SCHOFIELD, R. E., and THORNLEY, R. H., 'The Approach of Machined Surfaces with Particular Reference to their Hardness', 8th International M.T.D.R. Conference, Manchester, September 1967.
2. REASON, R. E., 'The Bearing Parameters of Surface Topography' Rank Taylor Hobson, September 1964.
3. SCHOFIELD, R. E., and THORNLEY, R. H., 'The Mathematical Expression of Surface Finish Characteristics', I.Mech.E. Conference, The Technology and Metrology Surfaces, Oxford, 1968.
4. TIMOSHENKO and GOODIER, 'Theory of Elasticity', McGraw-Hill.
5. THORNLEY, R. H., CONNOLLY, R., BARASH, M. M., and KOENIGSBERGER, F., 'The Effect of Surface Topography on the Static Stiffness of Machine Tool Joints', Proc. 5th International M.T.D.R., 1964.

DISCUSSION*Query from C. Andrew, University of Bristol*

The authors state that the unloading curves from any initial clamping pressure are congruent. This is contrary to my own findings, and contrary to what I would expect, since the greater the plastic flow at any asperity, the higher would be the effective undeformed radii of curvature of the squashed asperities and hence the higher their subsequent elastic stiffness. Perhaps the different results arise from the difficulty in measuring the gradient in the authors' experimental presentation. My own measurements were taken by the comparison of small alternating loads and displacements, a more accurate method.

Reply

We have found that the unloading curves are congruent over a very wide range of tests, from the contact spots of asperities $\frac{1}{4}$ in. high and with a $\frac{1}{2}$ in. base through idealised surfaces to conventionally-machined surfaces of all types. Contrary to Professor Andrew's assertion that congruency is unconnected, the theory advanced in the paper, which shows excellent correlation with experimental results, indicates an expectation of congruency.

The elastic recovery of a surface does not result from elastic deflection of the asperities, which is completely negligible, but from the body of the material behind the asperities. Thus, consideration of their radius of curvature, in all cases a crude assessment, is, in the case of elastic recovery, irrelevant.

Elastic theory states that the recovery of a contact spot will be the greatest at its centre. Subsequent loading will take up this recovery and reform a contact spot of finite area, which on further unload-

ing will allow a corresponding degree of elastic recovery. From this, the unloading curves will be congruent. With respect to the method of measurement, although Professor Andrew's method permits a form of statistical accuracy which our individual tests do not, we feel that the same end is achieved by the large number of tests carried out.

It is difficult to imagine a more accurate measuring system than that used by us, consisting as it did in the application of direct weights with deflective measurement accurate to 10^{-6} in.

Query from R. Noppen

You have mentioned the importance of stress distribution on the stiffness of the bolted joint.

A paper from Aachen University has recently been published in the *Industrie-Anzeiger*. This paper describes a method of determining the stress distribution around the bolt by placing a pressure-sensitive paper between the two surfaces. The results obtained from this method have been generalised and empirical formulae developed.

It has been found that there is good correlation between the stresses predicted by these formulae and the experimental results. Would you, from your experience, say that this approach, which is in fact very easy to use, could prove successful in a wide range of joints used in machine tool structures?

Reply

Empirical procedures, particularly in this field, have one great advantage, their simplicity, and one great disadvantage, the difficulty of applying them universally. I have no doubt that a pressure distribution obtained in the way you suggest would lead to an accurate prediction of the stiffness characteristics of that particular joint. The doubt remains that for each joint configuration or design a separate empirical list of pressure distribution would have to be made. Even if this were the case, it would still make a great simplifying contribution to the study.

Query from N. K. Tewari I. I. T., Delhi, India (at present at Nottingham University)

Referring to Fig. 3, what methods were used to determine the number of contact spots.

Reply

The number of contact spots was not so much determined as designed. Calculation of the number of contact spots, and indeed the real contact area, is always very difficult. Therefore, the surfaces used in this series of tests were specially machined, to give pairs of surfaces with 1, 2, 3, 4 and 5 very pronounced prismatic asperities. Thus, when these surfaces were orientated at 90° , 1, 4, 9, 16 and 25 contact spots respectively were ensured.

EXPERIMENTAL STUDY ON THE OPTIMUM INTERFACE PRESSURE ON A BOLTED JOINT CONSIDERING THE DAMPING CAPACITY

by

Y. ITO and DR. PROF. M. MASUKO*

SUMMARY

The optimum interface pressure on a bolted joint has been investigated experimentally in order to obtain basic information concerning machine tool design and manufacture. The bolted cantilever, which is the model for a bolted joint between a column and a base on a planer, was used to clarify the relationship between the interface pressure and the logarithmic damping decrement on the bolted joint in the different connecting conditions, such as varying diameters of the connecting bolts, distances between both the connecting bolts, thickness of beams and bases and so on.

The bending shock loads were applied to the bolted cantilever to give free damping vibrations in all experiments.

It is clear from the experimental results that the optimum value of the mean interface pressure can be found on the bolted joint where the logarithmic damping decrement is maximum, and furthermore, this optimum value is closely related to the ratio between the thickness of beam and base. The logarithmic damping decrement is also influenced by the connecting conditions of the bolted joint as much as by the optimum mean interface pressure. The distance between the connecting bolts and the conditions of the joint surfaces have further effects on the damping capacity. For example, when the distance between the connecting bolts is changed only at the bolted joint, the logarithmic damping decrement indicates the maximum value at a certain distance where the overlap of Röttscher's pressure cones is about half volume.

The experimental results suggest that the damping capacity on the bolted joint is caused chiefly by the very small slip displacement between the joint surfaces; therefore, this small slip displacement was also considered in this report.

INTRODUCTION

The significance of the bolted joint is widely recognized among machine tool designers and manufacturers, because the overall static and dynamic behaviour of a machine tool is largely influenced by the bolted joints. The static and dynamic behaviour of the bolted joint, especially the dynamic behaviour, has not yet been fully clarified and we can find few studies¹ on this problem.

It is necessary to obtain information on the dynamic behaviour of the bolted joint when a machine tool is designed and manufactured. The dynamic behaviour of the bolted joint is generally expressed by using the following four characteristics: a dynamic stiffness; a damping capacity; a frequency response or a transfer function, and an isolation capacity of vibration on the bolted joint. Of these characteristics, the damping capacity on the bolted joint

is especially important in clarifying the dynamic behaviour of a machine tool; therefore, experiments were carried out with simple bolted cantilevers having two connecting bolts and simulating the bolted joint between a column and a base on a planer.

In all experiments, the overall damping capacity and the natural frequency of the bolted cantilever were measured by using a damped free bending vibration during the decay process, and the measured values were also compared with the damping capacity of the equivalent solid cantilever. To express the damping capacity, the mean logarithmic damping decrement in five cycles was used, and by investigating the correlation between the logarithmic damping decrement and the mean interface pressure on the bolted joint, the optimum interface pressure for maximum damping capacity can be studied.

*Department of Mechanical Engineering for Production, Tokyo Institute of Technology, Tokyo, Japan

This problem is of practical significance as it can explain why the bolted joint has large effects on the damping capacity. Therefore, by considering the experimental results, the causes of damping on the bolted joint have been investigated, and some interesting new behaviour of the small slip displacement between the joint surfaces, which can be assumed to be the principal cause of the large damping capacity on the bolted joint, found.

NOTATION

B	Width of the beam
d	Diameter of the connecting bolt
d_1	Diameter of the bolt-hole
E_{loss}	Friction loss energy
f_n	Natural frequency of the bolted cantilever
	$= \frac{\omega_n}{2\pi}$
H	Thickness of the base
h	Thickness of the beam
k	Foundation modulus of the base
l	Contact length of the bolted joint
P_i	Initial interface pressure by the preload of bolt
P_m	Mean interface pressure by the preload of bolt
P_{opt}	Optimum mean interface pressure
s_a	Distance between the both connecting bolts
u	Relative displacement between the joint surfaces
w	Vibration amplitude
$y(x, t)$	Vibration mode of the beam
α	Coefficient determined by the joint surface conditions
δ	Mean logarithmic damping decrement during five cycles
Δu	αu
μ	Friction coefficient

EXPERIMENTS

The experimental set-up for the measurement of the logarithmic damping decrement and the natural frequency of the bolted cantilever is shown in Fig. 1, in which the examined bolted joint was considered to be the joint between the beam 3 and the base 2. This experimental set-up has already been used in a previous study² which investigated the static bending stiffness of the bolted joint. But in order to measure precisely the logarithmic damping decrement some rebuilding was performed. The logarithmic damping decrement on the bolted joint may be largely influenced by the conditions of the joint surfaces; therefore, it is necessary to maintain the joint surfaces in constant conditions in all experiments. Furthermore, it is necessary that the joint surfaces must be cleaned with trichlorethylene to remove all dirt, oil and grease. Therefore the bases were grooved on the underside and the bolt-holes were drilled throughout, as shown in Fig. 1.

We must consider here another problem namely that the measured logarithmic damping decrement includes unknown damping capacities caused by the experimental set-up. It is impossible to eliminate

completely these unknown damping capacities during their experimental measurement, and it is also very difficult to separate theoretically the damping capacity of the bolted joint only from the overall damping capacity. Therefore, to measure a reliable logarithmic damping decrement on the bolted joint, the vibration amplitude of the base was measured, together with the vibration amplitude of the beam at the loaded point, and by comparing both these values the real logarithmic damping decrement on the bolted joint was determined. Whence, as shown in Fig. 1, both displacement detectors were mounted on the support beam 7 which was connected firmly to the surface plate 1.

All experiments were carried out with the various dimensioned simple bolted cantilevers with two connecting bolts and the various conditions of the joint surfaces, shown together in Fig. 1. The vibration amplitudes of the bolted cantilever and the base were measured simultaneously by using the damped free vibration, after the pre-load of the connecting bolts 4 were controlled and changed by measuring the strain at the stem of connecting bolts with the strain gauges.

To eliminate the additional influences of the mass and the damping capacity which exist in an exciter and a displacement detector, the vibration amplitudes were measured by means of the variable-capacitance pickups 6, which are non-contact detectors. Therefore, before the measurement of the vibration amplitudes, correlations between the change of capacitance and the displacement were examined and recorded on the oscillograph 10. In this case, the displacements were calibrated with the microcator.

The normal bending shock loads were applied to the opposite position of the pickup for the vibration of beam, instead of the usual exciter. To eliminate the influences of the shock loads, the vibration amplitudes were measured after the initial transient had reduced.

The relationships between the logarithmic damping decrement and the mean interface pressure were investigated from the damped free vibration. The total vibration amplitude was 100 μm except when the effects of the vibration amplitude on the logarithmic damping decrement were examined. The latter were calculated as the mean value during the five cycles of vibration; the mean interface pressures were calculated by using Röttscher's pressure cone, assuming that the interface pressure is uniformly distributed over Röttscher's pressure cone.

As already mentioned, the surface conditions may affect the damping capacity of the bolted joint; therefore, in all experiments the joint surfaces were degreased with the trichlorethylene in order to ensure a clean metal contact.

One of the measured results for the logarithmic damping decrements of the bolted cantilever is shown in Fig. 2, which shows that the overall logarithmic damping decrements of the bolted cantilever, δ_{total} , are closely related to the mean interface pressure; but the logarithmic damping decrements, δ_{base} , between the base and the surface plate are almost constant. The values of δ_{base} can be seen to be about 0.08, although there is a slight scatter of the measured values. Compared with the experimental results,

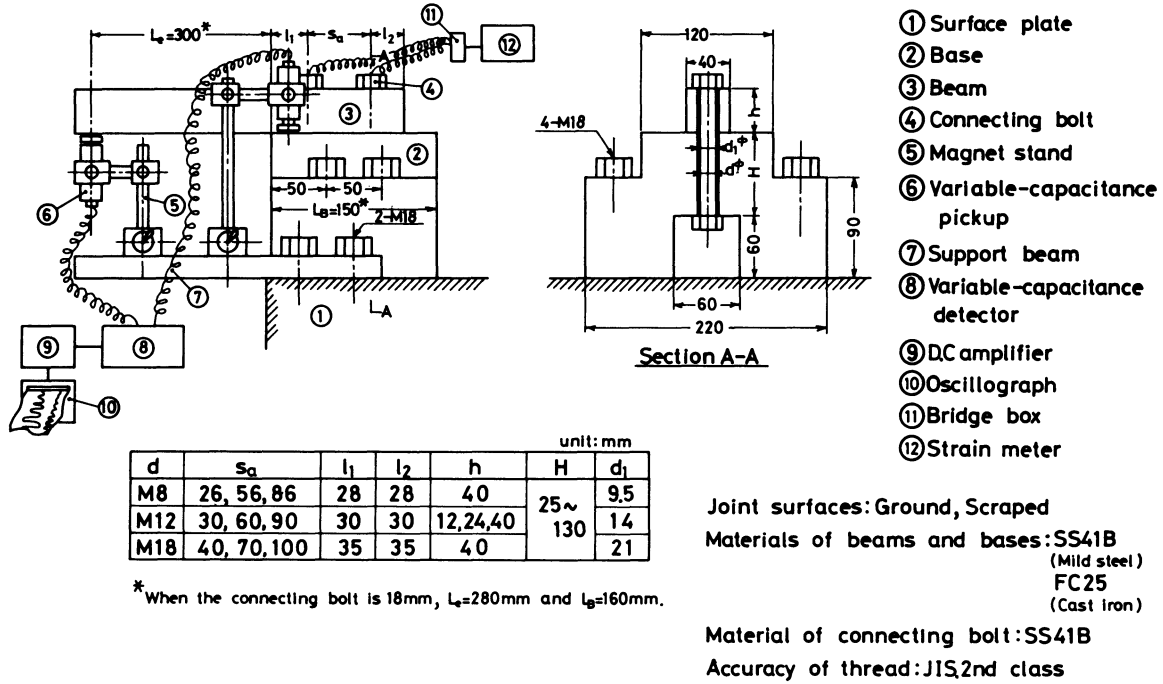


Fig. 1 Experimental set-up

which measured the overall logarithmic damping decrement of the equivalent solid cantilever δ_{solid} , the values of δ_{base} are equal to those of δ_{solid} .

It is known that the difference between the values δ_{total} and δ_{base} is the real damping capacity of the bolted joint, as the equivalent solid cantilever has no bolted joint between the beam 3 and the base 2.

In the following data, the real damping capacities are given by removing the measured values of δ_{base} from the overall logarithmic damping decrement δ_{total} .

In Fig. 2, the relationships between the mean interface pressure and the natural frequency are shown. The mean interface pressure influences chiefly the overall logarithmic damping decrement, but it has only a slight effect on the natural frequency of the bolted cantilever.

In the measurements of the damping capacities, the accuracy of measurement and the reproducibility of the measured value are very important, especially when the damping capacity is caused by friction between the matching surfaces, such as at the bolted joint: As shown in Fig. 2, the reproducibility of the measured values is less than 15%. This value of reproducibility can be maintained in all experiments.

To simplify the further experiments, the effects of the direction of the shock load were investigated by using the same experimental set-up. Although the experimental results are not shown here, the differences between the measured logarithmic damping decrement on the bolted joints subjected to the upward shock load and the downward shock load were found to be 10 to 15%; however, the optimum mean interface pressure explained already is in good agreement in both cases. If reproducibility of 15%, is taken into account, then the effects of the direction of the shock loads may be negligible. In all experiments, therefore, downward shock loads were applied to the bolted cantilever.

In order to apply the experimental results to a machine tool design, it is of interest to know what are the influences on the damping capacity of a bolted joint having a threaded hole. Therefore an experiment was carried out with the bolted cantilever having threaded holes on the bolted joint instead of the through bolt holes.

According to the experimental results, the differences in the logarithmic damping decrement and the optimum mean interface pressure between the above mentioned types of bolted joints cannot be found. However, in the case of the bolted joint with the threaded holes, the measured values were subject to scatter compared with the bolted joint with through bolt-holes, and in this case it was difficult to determine the optimum mean interface pressure from the measured relationships between the logarithmic damping decrement and the mean interface pressure.

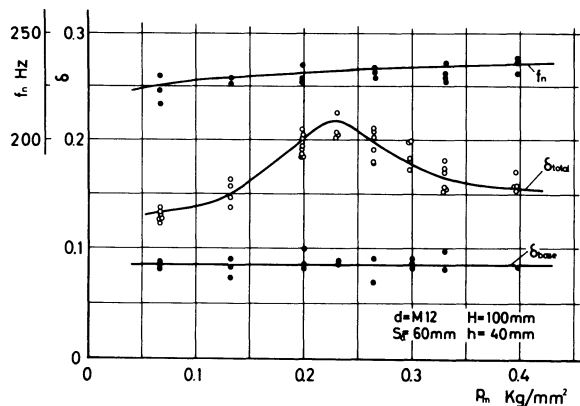


Fig. 2 One of measured results of logarithmic damping decrement. Joint surfaces: Ground, H_{max}=2.0μm; Materials of beam and base: SS41B (Mild steel)

SOME MEASURED RESULTS OF THE LOGARITHMIC DAMPING DECREMENT ON THE BOLTED JOINT

Experiments were also carried out to investigate the effects of the thicknesses of beam and base; the distance between the connecting bolts and the diameter of the connecting bolts on the logarithmic damping decrement of the bolted joint. These effects are shown in Fig. 3. In these figures, however, to simplify the presentation of data, the experimental results are shown by using the mean values of the measured damping capacities.

It is clear from experimental results that the logarithmic damping decrement is closely related to the mean interface pressure and at a certain mean interface pressure the logarithmic damping decrement has a maximum value. This behaviour of the logarithmic damping decrement is found in all experimental results, but as shown in the figures, the relationships between the logarithmic damping decrement and the mean interface pressure on the bolted joint depend on the connecting conditions.

The optimum mean interface pressure at which the logarithmic damping decrement is maximum, is also largely influenced by the connecting conditions.

The effects of the thickness of beam are shown in Fig. 3a, which shows that the logarithmic damping decrement increases and the existence of an optimum mean interface pressure becomes evident with the increased thickness of beam. However, for the thin beam, such as $h = 12$ mm, the mean interface pressure has little effect on the logarithmic damping decrement, and there is no particular behaviour visible in the logarithmic damping decrement. The optimum mean interface pressure indicates further very different values between the beam with $h = 40$ mm and that with $h = 24$ mm.

Fig. 3b shows that the thickness of base also largely affects the damping capacity, and the logarithmic damping decrement is changed widely from 0.08 to 0.2. The optimum mean interface pressure is also changed with the various thicknesses of base, but the thickness of base indicates very complicated effects on the damping capacity, as shown in the figure. The reasons why the thickness of base has these effects on the damping capacity can be explained as follows.

The effects of the base can be classified into two cases as shown by curves *A* and *B* in the Figure. For the curve *A*, in which the base is thick, the logarithmic damping decrement is closely related to the thickness of base and the differences in the logarithmic damping decrements between each bolted joint are large; however, for curve *B*, in which the base is thin, the logarithmic damping decrement indicates roughly the opposite behaviour to the bolted joint with the thick base.

These results are also shown in Fig. 6 in which the logarithmic damping decrement and the natural frequency indicate an almost constant value for the bolted joint with the thin base; however, both these values are changed by the thickness of the base when the base is thick.

Generally, the bolted joint can be regarded as the three coupling vibration systems which include the

vibration system of bolt, of beam and of base; therefore, the behaviour of the logarithmic damping decrement already mentioned can be considered to be caused by the mass effects of the base. From the results it can be seen that the thickness of base and beam are very important characteristics of the damping capacity, and the diameter of the connecting bolts and the distance between both connecting bolts are also very important.

In Figs. 3c and *d* the experimental results on the effects of the distances between both connecting bolts and the diameter of the connecting bolts are shown.

It is clear from Fig. 3c that the distance between the connecting bolts has an effect on the logarithmic damping decrement, but has no effects on the optimum mean interface pressure. The logarithmic damping decrement indicates a high value for the bolted joint, with $s_a = 60$ mm as compared with the bolted joint with $s_a = 30$ mm and $s_a = 90$ mm. By using Rötischer's pressure cone, these results can be handled as the problem of correlation between the logarithmic damping decrement and the overlap of pressure cones.

The bolted joint having $s_a = 60$ mm corresponds to the condition in which the overlap of pressure cones is about half volume. These results are also found on the bolted joint with $d = M18$, though there is a slight difference in behaviour between both the bolted joints. For the bolted joint with $d = M8$, however, the effect of the distance between both connecting bolts cannot be seen clearly, because the actual interface pressure distributions is not expressed exactly by Rötischer's pressure cone³ but is distributed steeply near the bolt-hole in this case.

Furthermore, if the diameter of the connecting bolt is small the pre-load of the connecting bolt can be considered to be a concentric load, and then the localized deflection of the beam occurs easily. Therefore, the overlap of pressure cones is clearly a very important problem for the bolted joint.

In Fig. 3d, the effects of the diameter of the connecting bolt on the damping capacity are shown in the same overlap conditions of the pressure cones details of which are shown in this figure. The value of R_{kx} which indicates the overlap condition of the pressure cones, is nearly 0.5 in this experiment.

From the data presented here it is clear that the diameter of the connecting bolt also has significant effects on the logarithmic damping decrement and the optimum mean interface pressure, which are both increased with the increased diameter of connecting bolts; however, the natural frequency of the bolted cantilever is not so affected. These results also confirm that the damping capacity is strongly related to the interface pressure distribution on the bolted joint.

It has been mentioned by several authors⁴ that the damping capacity on the bolted joint is caused by the friction between the joint surfaces, and therefore they concluded that the surface topography has large effects. To confirm the effects of the surface conditions such as surface roughness, machining method and machined lay orientation of surfaces, experiments were carried out with the bolted cantilever. These indicate maximum damping capacity

according to the previous experimental results. Typical results are shown in Fig. 4. In the experiments, the surface conditions on the actual bolted joint were considered, that is scraped surfaces and the ground surfaces made of cast iron were examined.

From these results, it is seen that the optimum mean interface pressure and the logarithmic damping decrement are slightly changed by the machining method and the machined lay orientation of joint surfaces.

However the surface conditions, for example the machined lay orientation of joint surfaces made of mild steel, have significant effects on the damping

capacity, as shown in Fig. 5. If the difference in Young's modulus between the cast iron and the mild steel is considered, the bending rigidity of the beam made of cast iron corresponds to a steel beam having the equivalent thickness $h \doteq 20$ mm. Therefore, one would not expect a large difference between bolted joints having $h \doteq 24$ mm. However we found differences in the damping capacity between these bolted joints as shown in Fig. 5. It is known that the thickness of the beam and the material of joint surfaces have marked effects, in addition to the effects of the surface topography.

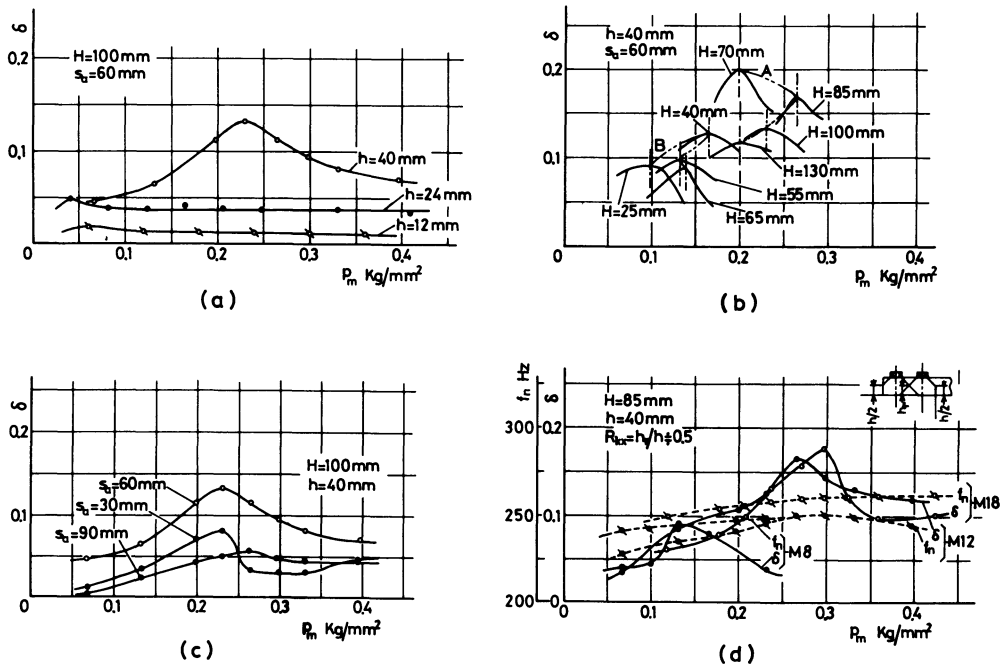


Fig. 3 Effects of the connecting conditions on the logarithmic damping decrement of the bolted joint. $d=M12$, Joint surfaces: Ground, $H_{max}=2.0\mu m$. Materials of the beam and base: SS41B (Mild steel)

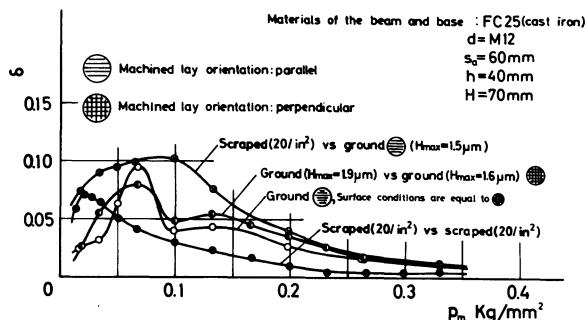


Fig. 4 Effects of the joint surface conditions on the logarithmic damping decrement of the bolted joint

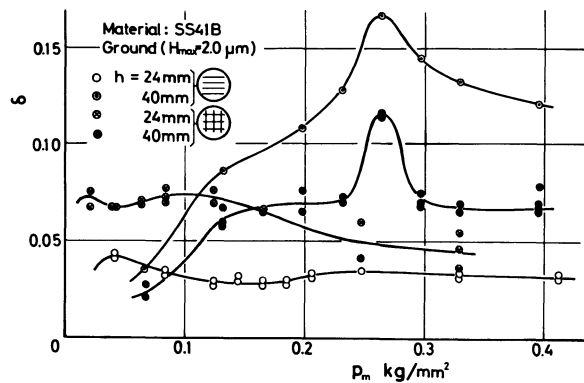


Fig. 5

BEHAVIOUR OF THE MAXIMUM LOGARITHMIC DAMPING DECREMENT AND THE OPTIMUM MEAN INTERFACE PRESSURE

In Fig. 6, the behaviour of the maximum logarithmic damping decrement and the optimum mean interface pressure are shown by considering the ratio between the thickness of base and beam, as the relationships between the maximum logarithmic damping decrement and the value of h/H are very important for the design of the machine tool structure.

When the value of h/H is less than 0.6, the maximum logarithmic damping decrement is changed largely by the increased value of h/H , but when the value is more than 0.6, the maximum logarithmic damping decrement is not so changed. It is interesting to note that there is a steep decrease in the maximum logarithmic damping decrement at the boundary between both the ranges notwithstanding the different values of the mean interface pressure. This singular behaviour of the maximum logarithmic damping decrement was also found in the experimental results for the bolted joint with $h = 24$ mm.

It is shown also in Fig. 6b that the natural frequency of the bolted cantilever indicates quite similar behaviour to the logarithmic damping decrement for the value of h/H . The value of h/H at which the natural frequency of the bolted cantilever is beginning to fall, corresponds exactly to the value of h/H at which the logarithmic damping decrement indicates a steep decrease.

In these conditions, the reasons why this singular behaviour appears on the damping capacity of the bolted joint, cannot be explained; however, we presume that the effects of the normal dynamic contact stiffness between the joint surfaces and the mass of base are changed by the value of h/H as mentioned before. Further investigation into these problems is necessary.

In Fig. 6a, the relationships between the optimum mean interface pressure and the value of h/H are shown. It is known from these results that the optimum mean interface pressure is changed by the value of h/H and indicates the peak value where the value of h/H is about 0.5. This value of h/H is the same for the bolted cantilever with $h = 40$ mm and $h = 24$ mm.

To clarify the more detailed behaviour of the damping capacity on the bolted joint, the effects of the vibration amplitude on the damping capacity were investigated further. By increasing the vibration amplitude, the logarithmic damping decrement is increased and gradually reaches a certain constant value, but the optimum mean interface pressure is not so changed, as is shown in Fig. 7. If the beam is thin, however, the logarithmic damping decrement is related linearly to the vibration amplitude.

CONSIDERATIONS OF THE CAUSE OF DAMPING CAPACITY ON THE BOLTED JOINT

According to the experimental results already mentioned, the damping on the bolted joint may be considered to be a friction damping between the joint

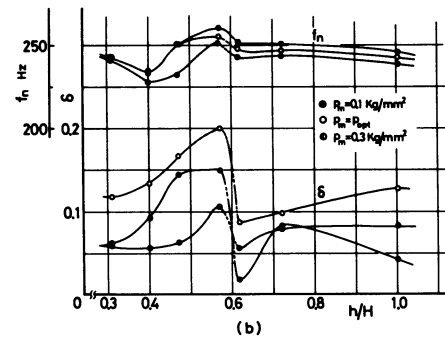
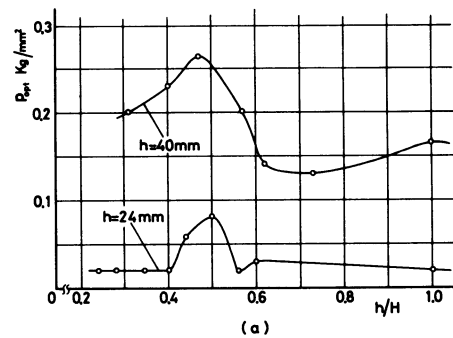


Fig. 6 Effects of the ratio h/H on the logarithmic damping decrement and the optimum mean interface pressure. $d = M12$, $s_a = 60$ mm, Joint surfaces: Ground, $H_{max} = 2.0 \mu\text{m}$, Materials of the beam and base: SS41B

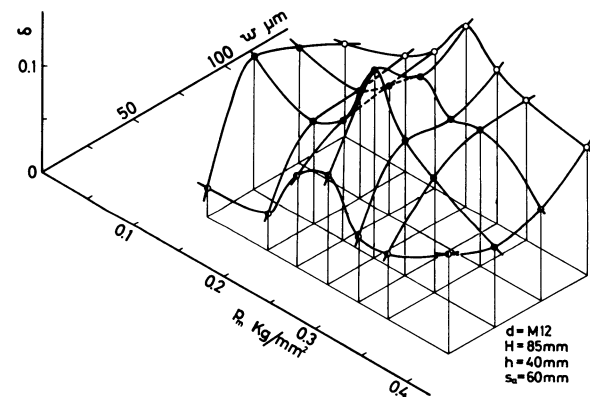


Fig. 7 Relationships between the vibration amplitude and the logarithmic damping decrement of the bolted joint. Joint surfaces: Ground, $H_{max} = 2.0 \mu\text{m}$. Materials of the beam and base: SS41B

surfaces, because the logarithmic damping decrement is related to the vibration amplitude. Therefore, the friction loss energy is determined by a friction force and a relative slip motion.

On the bolted joint, the friction force is given by the pre-load of the connecting bolts, but the cause of the relative slip parallel to the joint surfaces is not so

clear. However, we can give reasonable explanations for most of the experimental results assuming the following mechanism for the slip displacement on the bolted joint.

As shown in Fig. 8, in vibrating conditions the initial contact points *A* on the base and *B* on the beam move into the points *A'* and *B'*; therefore, the relative displacement occurs between the joint surfaces. The results of another study⁵ show that this type of relative displacement is the sum of an elastic displacement and a relative slip. The relative slip has significant effects on the energy loss caused by friction.

By expressing the relative slip between joint surfaces as $\Delta u \doteq \alpha A'B'$, and by assuming that the vibration mode of the beam is given by $y(x, t)$, the slip velocity is written

$$\frac{\partial \Delta u}{\partial t} \doteq \frac{\alpha h}{2} \frac{d}{dt} \left(\frac{\partial y(x, t)}{\partial x} \right)$$

where α is the coefficient determined by the conditions of the joint surfaces and h is the thickness of beam.

The expression for the friction loss energy during one cycle is thus written as

$$E_{\text{loss}} = 2 \int_0^{\frac{\pi}{2\omega}} \int_0^1 \mu \{ p_i + ky(x, t) \} B \alpha h \frac{d}{dt} \left(\frac{\partial y(x, t)}{\partial x} \right) dx dt$$

where p_i is the initial interface pressure and $ky(x, t)$ is the reaction pressure from the base.

From the above expression, the damping capacity on the bolted joint can be related qualitatively to the mean interface pressure, as shown together in Fig. 8, because the friction force is beginning to increase from zero and the micro slip is decreasing almost to zero with the increased mean interface pressure.

By using the recorded curve of the damped free vibration, it is also confirmed that the relative slip is the main cause of the damping on the bolted joint. Careful investigation of the recorded curve shows that the damped free vibration consists of several parts, namely the violently changed vibration amplitude and the constant vibration amplitude during few cycles, and more-over that the overall curve of the damped free vibration can be regarded as the series connexion of the several damped free vibrations with the exponential curve. This particular behaviour of the damped free vibration was found in all experiments, notwithstanding the different connecting conditions of the bolted joints.

The results also suggest that the relative slip between joint surfaces is derived from some sort of infinitesimal stick-slip motion having a displacement within $0.1 \mu\text{m}$; therefore, in the stick conditions, the vibration amplitude remains constant and in the slip conditions it falls steeply. The existence of this infinitesimal stick-slip on the bolted joint has already been pointed out by the experiments on the horizontal bending stiffness of bolted joint⁶, but these are not sufficient. The mechanism of the damping capacity of bolted joints necessitates further investigation

CONCLUSIONS

The behaviour of the damping capacity on bolted joints has been investigated experimentally here, in order to find out the optimum mean interface pressure on the bolted joint while considering the damping capacity.

The experimental results show that the logarithmic damping decrement is closely related to the mean interface pressure, and has a maximum value at a certain value of the mean interface pressure. This logarithmic damping decrement generally increases with an increased thickness of beam and the diameter of the connecting bolt, and furthermore is influenced by the surface topography of joint surfaces. However, the topography of joint surfaces has a little effect compared with the connecting conditions of the bolted joint which have been mentioned.

The experimental results also show that the logarithmic damping decrement indicates a maximum value for the special value of h/H and a special distance between both connecting bolts where the overlap of Röttscher's pressure cones is about half volume.

The optimum mean interface pressure at which the logarithmic damping decrement has its maximum value, is also changed by the connecting and the surface conditions of the bolted joint.

The behaviour of the damping capacities on the bolted joint are very complicated as mentioned already, but the natural frequency of the bolted cantilever is related only to the thickness of beam.

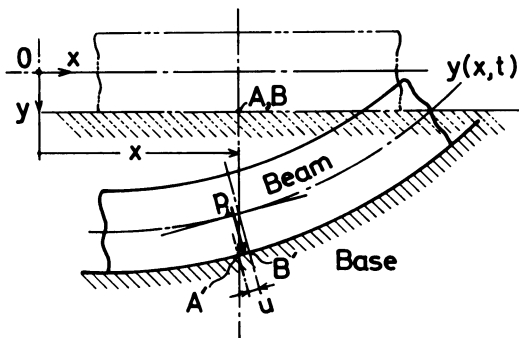
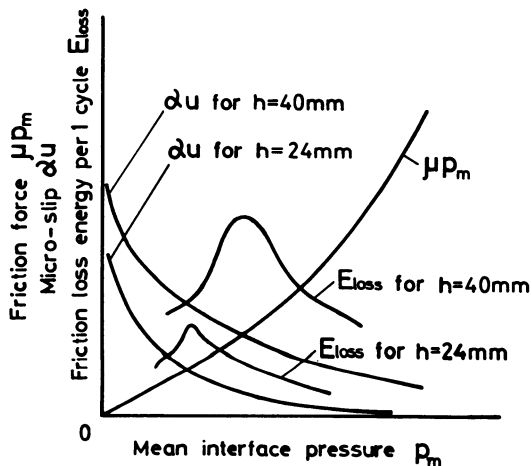


Fig. 8.

In order to explain the behaviour presented here more exactly, the causes of the damping on the bolted joint have been further investigated by considering the experimental results, according to which, it can be considered that the damping capacity on the bolted joint is given by the friction loss between the joint surfaces. The relative slip, which is a principal factor in determining the friction loss energy, can be derived from the bending deflection of the beam on the bolted joint and interesting behaviours on this point can be found.

To clarify the detailed causes of the damping on the bolted joint necessitates further studies on the relative slip between joint surfaces. We are now investigating this problem and will present the results in the near future.

REFERENCES

1. HANKS, B. R., and STEPHENS, D. G., 'The mechanisms and scaling of damping in a practical structural joint,' 36th Shock and Vibration Symposium.
2. MASUKO, M., et al., 'Experimentelle Untersuchung der Statischen Biegesteifigkeit von Verschraubten Fugen an Werkzeugmaschinen,' *Bulletin of JSME*, 122, 12, No 49, (1969-2).
3. MITSUNAGA, K., 'Trans. Japan Soc. Mech. Engrs.,' 1750, 31, No. 231.
4. GOODMAN, L. E., and KLUMPP, J. H., 'Analysis of slip damping with reference to turbine-blade vibration,' *J. Applied Mechanics*, 421 (1956-9).
5. MASUKO, M., et al., 'Behaviour of the horizontal stiffness and the micro-sliding on the bolted joint under the normal pre-load,' to be presented at 12th. Intern. M.T.D.R. conf.
6. ITO, Y., and MASUKO, M., 'Study on the horizontal bending stiffness of bolted joint,' *Bulletin of the JSME.*, 14, No. 74, (1971-8) (to be published).

DISCUSSION

Query from C. Andrew, Bristol University

The cyclic loss of energy due to micro-shear between the two surfaces of a joint is a wear process and gives rise to fretting. Such wear results in a change in the interfacial contact conditions so that, after a long period of vibration, no further wear takes place and the damping stops unless the joint is unbolted and remade. Have the authors investigated such long-term variations in damping?

Reply

As indicated in our reply to Dr. R. E. Schofield in another study⁷, the micro-slip can be found on the bolted joint in which the applied tangential load is less than the friction force defined in the field of wear. Although there is some difference between the fretting and the cyclic loss of energy due to micro-slip between joint surfaces, we agree with a part of your opinion.

For the latter point of your question, however, we would say that the damping may not be stopped. It only decreases and may be held at a certain value after being subjected to a long period of vibration,

because we presume that our investigated micro-slip does not disappear in that case.

This problem is at present being investigated and it is hoped that the results will be published in the near future.

7. Masuko, M. et al. Presented at this Conf.

Query from R. E. Schofield

Again this is a very interesting and important paper in the field. However, I can envisage no physical reason for an optimum energy loss other than a change of mechanism. That is to say, for example in Fig. 2, slip is occurring up to the optimum mean interface pressure, and energy loss increases with increased frictional force. After the optimum, the mechanism of plastic deformation applies and energy loss reduced with increase in contact area. It is noteworthy that this optimum occurs at 0.2 kg/mm^2 , whereas p_m in a practical case could be as much as 3 kg/mm^2 , i.e. 15 times the optimum pressure, certainly indicating that slip is likely below the optimum.

This explanation is born out by Fig. 3a where no optimum occurs for the thinner beams. This is because the thinner beam could allow for a greater concentration of pressure under the bolts than the thicker beams. Fig. 5 also shows similar effects.

Reply

As we have already indicated in our reply to C. Andrew, the term micro-slip is used to indicate the small tangential movement which occurs before the onset of sliding. In practice, micro-slip is applicable to connections where the limiting friction force is greater than the applied tangential force. Furthermore, in Fig. 9 the measured results of δ for $h = 24 \text{ mm}$ is shown and it is easy to find the optimum mean interface pressure. We think that your suggestion for the mechanism of the optimum energy loss is reasonable, but it is possible to explain the mechanism of an optimum energy loss by using the micro-slip mentioned above. For example, in Fig. 2 the micro-slip is occurring up to the optimum mean interface pressure and after this optimum pressure a sort of micro-slip may be seen on the bolted joint.

According to our investigation and calculation using Rotscher's pressure cone, the actual bolted joint found on a planer or a plano-miller has also such a high mean interface pressure as shown in Table 1.

It seems as if the optimum mean interface pressure examined here is lower compared with the actual bolted joint, but as shown in Fig. 10 the static bending stiffness k_b is almost constant at this optimum. We think, therefore, that the value of p_m on the ordinary bolted joint may be higher than necessary.

When bolted joints are used in a machine tool it is necessary to determine an optimum mean interface pressure, by taking into consideration all the different factors, such as the static and dynamic bending and torsional stiffness and frequency response. It is our final objective to solve this problem.

Table 1

Example of machine	Mean initial interface pressure P_i kg/mm ²		
	Materials of connecting bolt		
	J.I.S. SS41B	J.I.S. S45C (Temper)	DIN.10K
Double column plano-miller (Köllmann GmbH)	0.58	1.25	2.24
Double column planer (Billeter GmbH)	0.30	0.65	1.17
Double column planer (Kinoshita Co. Ltd.)	0.46	1.04	1.81

The pre-stress of connecting bolt is equal to $(0.4 \sim 0.6) \sigma_B$, where σ_B is the tensile strength of the material.

SOME ASPECTS OF WEAR ON DISC CLUTCHES USED IN MACHINE TOOLS

by

H. LEVY, E. LENZ and K. LOEWY*

SUMMARY

The aim of this work was the prediction of disc service life in electromagnetic clutches of the types frequently used in machine tools. Wear in these discs occurs as a result of a high engagement rates over short time intervals.

The experimental series included measurements of temperature (by means of an infra red optical pyrometer), hardness, and surface finish, and yielded a nomogram permitting prediction of the time required for the critical temperature-hardness level to be reached.

A metallurgical and theoretical analysis is given.

INTRODUCTION

The problem we considered was the prediction of the disc service life in electromagnetic clutches of the types frequently used in machine tools. Wear in these discs occurs as a result of a high engagement rate over short time intervals. Where the rate is exceptionally high, most manufacturers recommend a clutch with a higher torque capacity, that is, reduced specific pressure.

In this study (a sequel to an earlier paper, see ref. 9), an assortment of discs of different origins was examined. The wear mechanism was analysed, with particular reference to mechanical parameters varying under pre-critical conditions. The relationships between parameters of this type are expected to yield an exact quantitative picture of the wear, permitting prediction of the service life.

LITERATURE SURVEY

The survey covered three categories of publications dealing, respectively, with the metallurgical and mechanical aspects and with the clutches proper. No comprehensive material is available.

Rabinowicz¹ and Archard² presented hypotheses relating surface energy and hardness (see Fig. 1a and 1b) as well as surface energy and temperature. Even though theoretical, the relationship is fairly realistic, with due allowance for various factors appearing in the form of coefficients. Archard derived an expres-

sion relating the flash point (the instantaneous maximum temperature) to the important parameters. This takes the form

$$\theta_m = \frac{f w v}{4J_1 (K_1 + K_2)}$$

where: θ_m , flash point ($^{\circ}\text{F}$ or $^{\circ}\text{C}$); f , coefficient of friction; w , load on junction (lbs or dynes); v , sliding velocity (in. s^{-1} or cm s^{-1}); J , mechanical equivalent of heat; a , junction radius (in. or cm); and K_1 , K_2 , thermal conductivities of materials in contact.

Khrushchev⁸ proposed, for the first time, a relationship between a wear factor ϵ and the hardness of the sliding metals (see Fig. 2) as

$$\epsilon = \frac{\Delta l_s}{\Delta l_m}$$

where ϵ is relative wear resistance.

This relates the linear wear of the test specimen Δl_m for a definite distance moved by it and the linear wear of the standard material Δl_s for the same distance.

As regards disc clutches and brakes, Rosenberg⁵ presented theoretical conclusions (including the service-life aspect) on the basis of tests at a given engagement rate. Schach⁶ also proposed various torque-pressure relationships, and Zhitnitskii⁷, dealt with the radial pressure distribution over the wear surfaces (see Fig. 3).

*Department of Mechanical Engineering, Technion—Israel Institute of Technology, Haifa, Israel

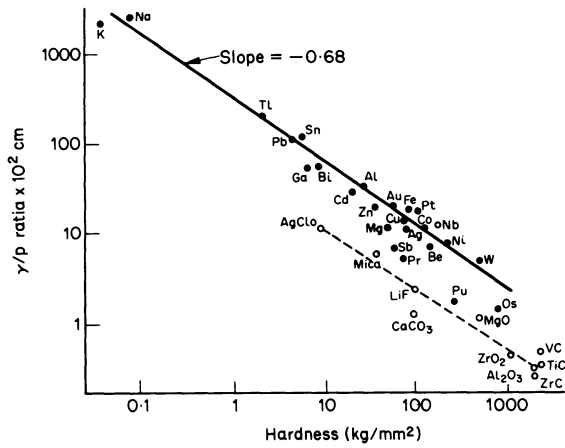


Fig. 1a: Plot of surface energy at the melting point against hardness at room temperature, for some metals and non metals (according to Rabinowicz).

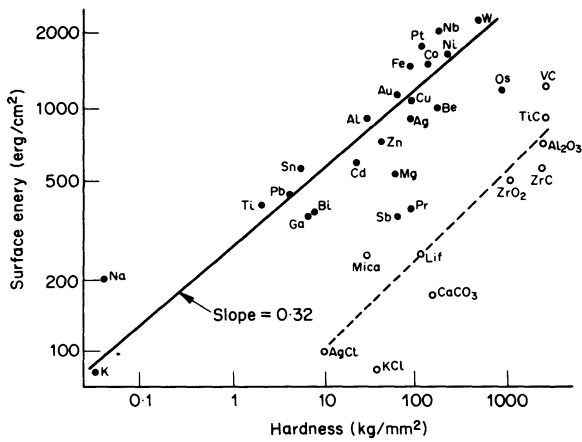


Fig. 1b: Plot of the t/p ratio against hardness for the materials shown in 1a (according to Rabinowicz).

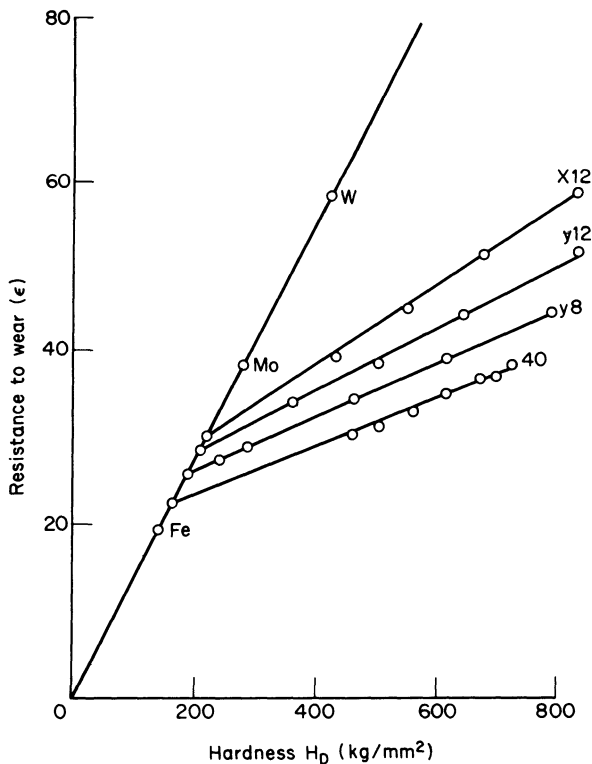


Fig. 2: ϵ - H graph for heat treated steels (according to Kruschev).

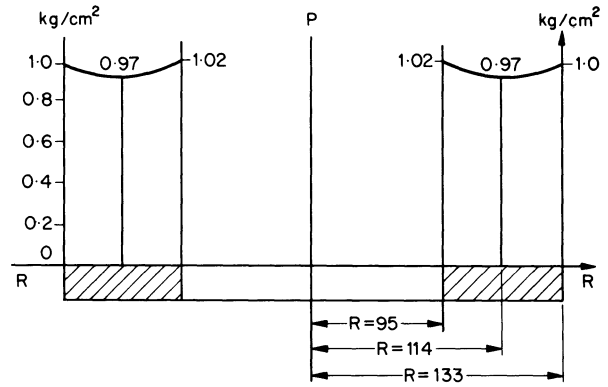


Fig. 3 Pressure distribution on a disc (according to Zhitnitskii).

EXPERIMENTAL SET-UP

All disc specimens tested (taken from five-pair clutches of the same torque capacity—10 kp. m) (see Fig. 4), were made of low-carbon steel, slightly surface-hardened (300 HV, final hardness 500–600 HV.)

Previous work¹⁻³ has indicated the relationship between wear rate and hardness, and surface energy and hardness. Consequently, it is to be expected that wear will be related to temperature. Indeed this has been found by Male³, who related the wear to the mean temperature. In this work, where short duration loading conditions exist, we anticipate that the wear will be more a function of the flash temperature than of the mean temperature over the duration of the loading cycle. For this reason the following measurements have been made.

Temperature measurement

The main measuring apparatus, already described in our earlier paper⁹, is shown in Fig. 5. It comprises two vertical shafts [(1) and (3)], one (mounted on closed roller bearings) rotated by a d.c. motor-driven belt and the other (mounted on a journal bearing) capable of partial rotation and equipped with an arresting device (7). Discs (2) and (4), mounted in two alternative modes, undergo pressure from shaft (3) supplemented by weights (6), as shaft (1) is rotated. The driving motor is equipped with a variable resistance, thereby permitting variation of the load and speed.

The friction temperature can be measured by means of a chromel-alumel thermocouple and an IR optical pyrometer, with maximum sensitivity at approximately 2.5 μ m. The sensitive area is 1mm². The two lenses in the optical system are arranged so that the spot diameter in which the temperature is measured is twice that of the aperture ($f_1 = 25$ mm, $f_2 = 50$ mm, $d_{ap} = 0.2$ mm). (Fig. 6). Measurements were taken radially at different points, but no variation in temperature could be found.

In order to ensure rapid wear, the most extreme torque conditions compatible with machine tool practice were used. The speed limit of the experimental installation being 1,500 r.p.m., the pressure was increased proportionally to give the correct p-n level. (For example, a test at $n = 1,500$ r.p.m. and $p =$

15 kp mm⁻² is equivalent to one at $n = 4,000$ r.p.m. and $p = 5-6$ kp mm⁻² [see line 7, Fig. 7)].

The specific pressure was determined from the total force, (measured with a strain-gauge device) divided by the effective area of the disc, and the speed was measured with an electronic tachometer.

The interval of temperature readings simulated that of clutch engaged (and immediately disengaged) at intervals of 4 and 8 s, respectively, as shown schematically in Fig. 8. The operation was manual and observations were discontinued after permanent changes in disc surface conditions were observed. When this stage was reached, the coefficient of friction (hitherto practically constant) began to change significantly, ruling out comparative conclusions. (Optical temperature measurement becomes inaccurate beyond this point because, with the change in surface condition, the emissivity of the surface changes). Similar results were observed for all the discs tested. The maximum temperature (that is, the temperature obtained at the end of the engagement period) increased with the number of loading cycles. For the 4 s cycle, the maximum temperature was found to increase (approximately) parabolically—and for the 8 s cycle the increase was approximately linear, as shown in Fig. 7.

Surface-hardness-measurement

After completing the temperature measurements, surface hardness was measured on a Vickers apparatus (50p load) and was found to vary with the temperature reached at the end of the load cycle tests. The hardness reached a maximum (1080HV) at 1100 K and decreased thereafter (850 HV at 1,150 K) (see Fig. 9, where each point represents the mean of 5-10 tests). The same pattern was observed in unused discs subjected to a heating and cooling treatment similar to that in the load cycle tests. This indicates a direct correlation between temperature and hardness. (By contrast on correlation between temperature hardness was found for unhardened discs, in which wear was very rapid even at relatively low pressures.)

Comparative examination of disc surfaces before and after wear led to the conclusion that they undergo some sort of abrasive 'grinding', with the abraded particles remaining on the surface and increasing its hardness; parallel grinding tests failed to show the same increase in hardness.

Service-life nomogram

The results are summarized in a nomogram (Fig. 10), giving hardness as a function of temperature (K) and temperature change as a function of $p.n$ and of the clutch-engagement interval.

The wear criterion adopted here was the onset of surface grooving and the change in the coefficient of friction (which, in turn, impairs the reliability of the clutch). These changes occur mostly above the 'critical level' at which permanent change in the surface occurs.

The nomogram permits the prediction of the time required for the critical temperature level to be reached at different $p.n$ values and engagement rates. It also yields the maximum allowable pressure for different speeds in serviceable clutches—any applied pressure in excess of this will cause the coefficients of friction to decrease.

Repeatability

As accuracy was the principal consideration here, special steps were taken to reduce measurement errors and verify the results. The optimal device was calibrated in a helium atmosphere in an exact duplication of the measuring conditions; furthermore, the influence on emissivity of oil filming, surface oxidation, and changes in surface finish were taken into consideration and compensated for. Repeat runs in the same conditions showed an accuracy of $\pm 5\%$. (As the spot diameter (0.2 mm) is relatively large, the average temperature is lower than that which would be obtained with a smaller spot.) As regards hardness, repeat runs showed deviations, but the averages were practically identical.

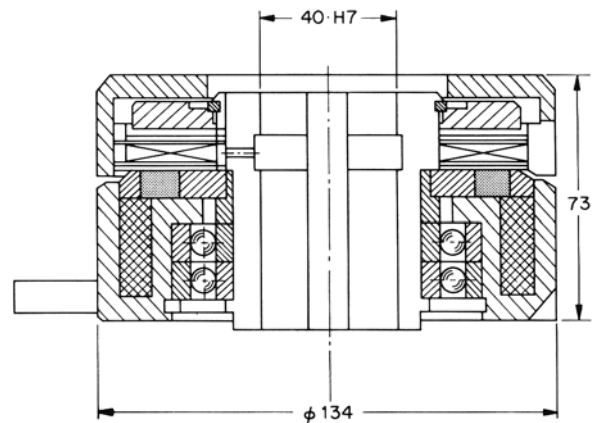


Fig. 4 Electromagnetic disc clutch for 10 kp. m torque.

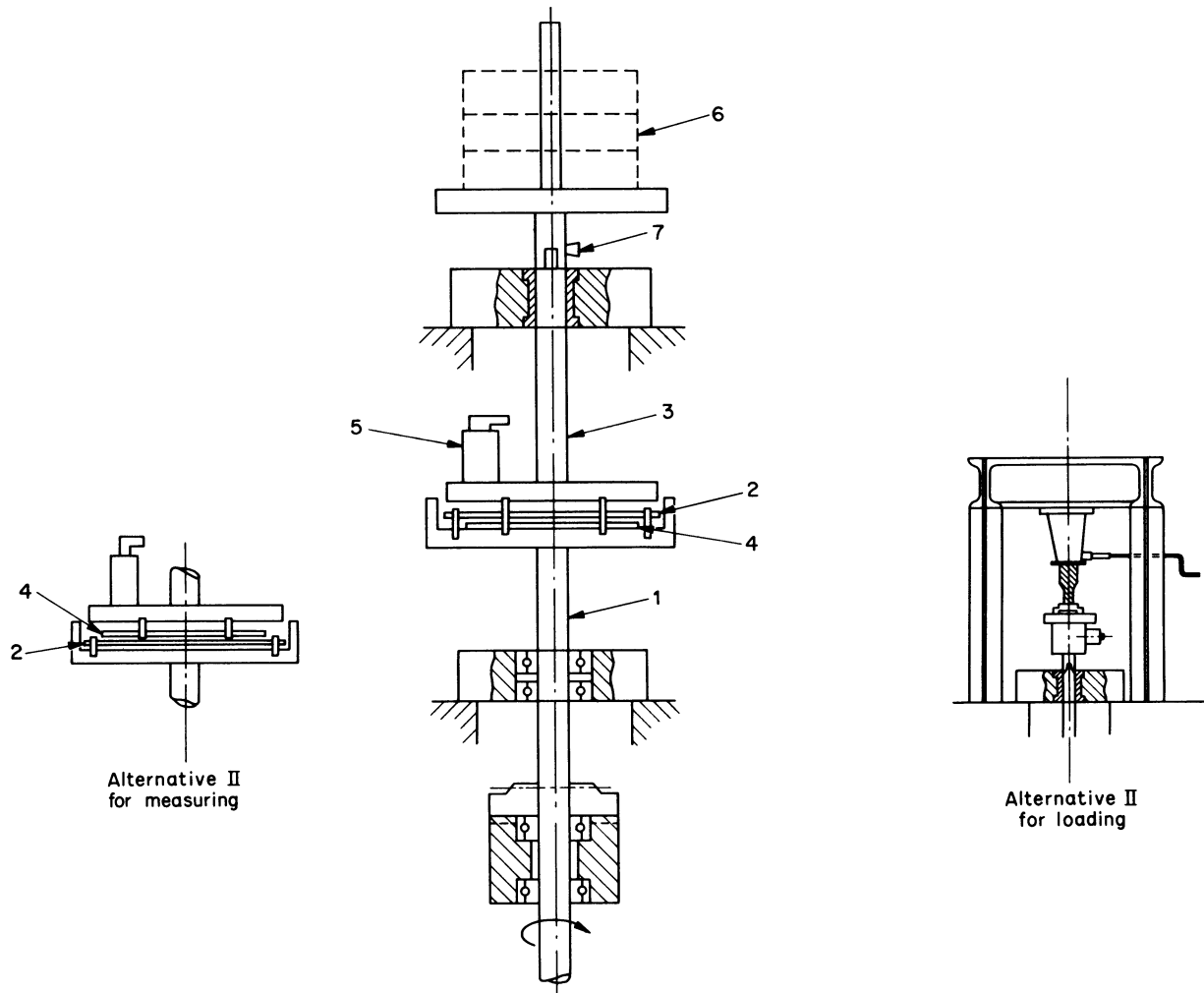


Fig. 5 The main measuring device (schematic view).

- 1, 3 shafts
- 2, 4 discs
- 5 temperature measuring instrument
- 6 weights
- 7 stopping arrangement.

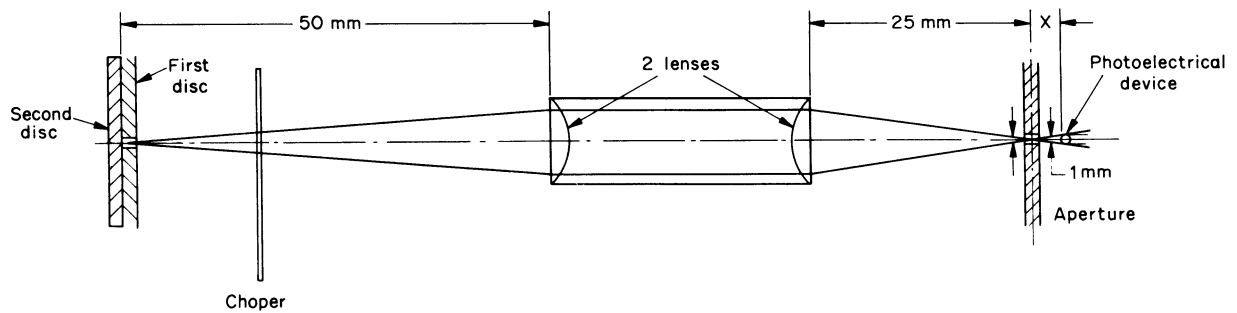


Fig. 6 Schematic arrangement of the optical devices used to measure temperature.

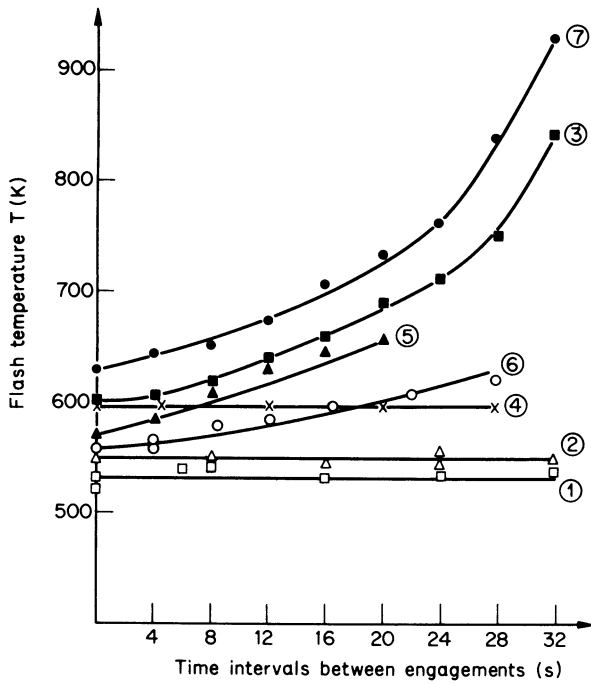


Fig. 7 Temperature measurements related to number of engagements and $p.n$

1. $n = 900$ r.p.m., $p = 10 \text{ kg cm}^{-2}$, $f_1 = 450$ eng.p.h.
2. $n = 900$ r.p.m., $p = 13 \text{ kg cm}^{-2}$, $f_1 = 450$ eng.p.h.
3. $n = 1290$ r.p.m., $p = 19 \text{ kg cm}^{-2}$, $f_2 = 900$ eng.p.h.
4. $n = 1150$ r.p.m., $p = 19 \text{ kg cm}^{-2}$, $f_1 = 450$ eng.p.h.
5. $n = 1150$ r.p.m., $p = 20.5 \text{ kg cm}^{-2}$, $f_2 = 900$ eng.p.h.
6. $n = 1290$ r.p.m., $p = 13 \text{ kg cm}^{-2}$, $f_2 = 900$ eng.p.h.
7. $n = 1500$ r.p.m., $p = 15 \text{ kg cm}^{-2}$, $f_2 = 900$ eng.p.h.

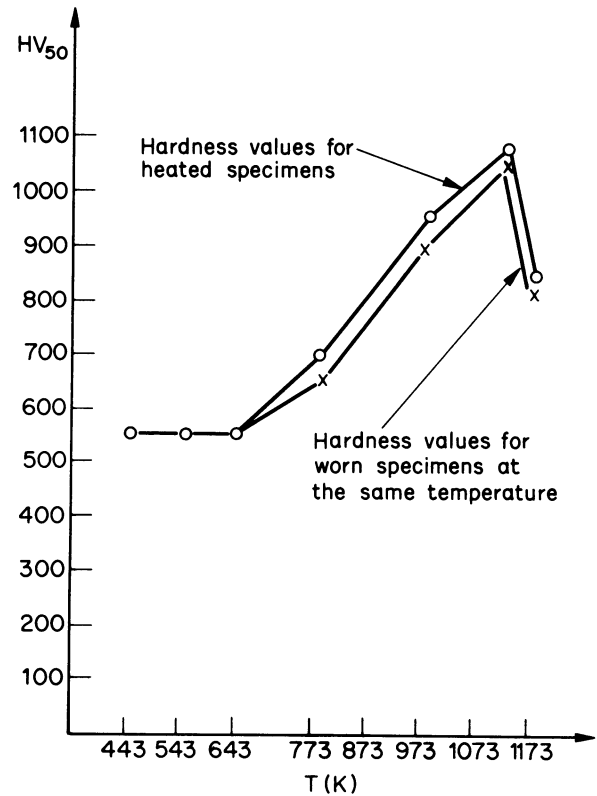


Fig. 9 Hardness against temperature in heated and worn specimen, respectively.

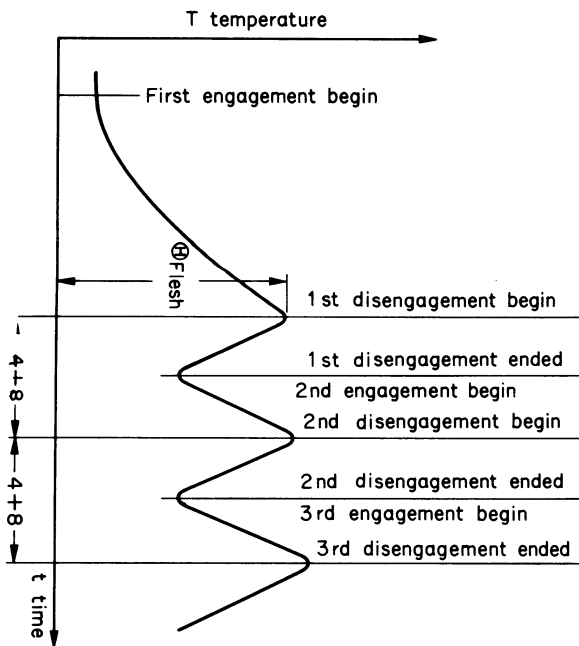


Fig. 8 Schematic representation of temperature variation during cyclic loading tests.

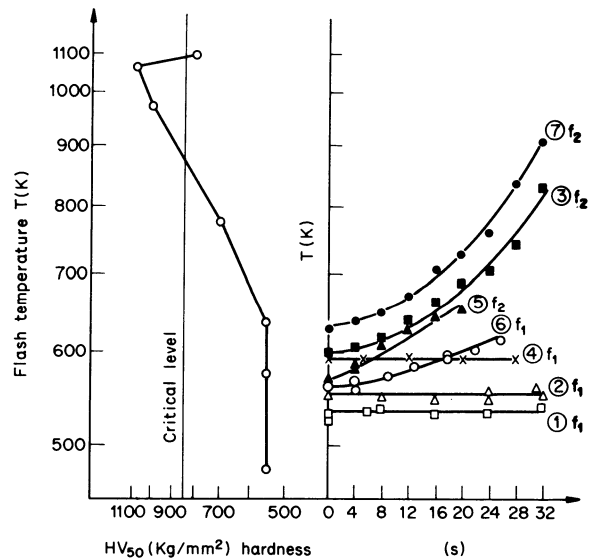


Fig. 10 Service-life nomogram.

1. $n = 900$ r.p.m., $p = 10 \text{ kg cm}^{-2}$, $f_1 = 450$ eng.p.h.
2. $n = 900$ r.p.m., $p = 13 \text{ kg cm}^{-2}$, $f_1 = 450$ eng.p.h.
3. $n = 1290$ r.p.m., $p = 19 \text{ kg cm}^{-2}$, $f_2 = 900$ eng.p.h.
4. $n = 1150$ r.p.m., $p = 19 \text{ kg cm}^{-2}$, $f_2 = 450$ eng.p.h.
5. $n = 1150$ r.p.m., $p = 20.5 \text{ kg cm}^{-2}$, $f_2 = 900$ eng.p.h.
6. $n = 1290$ r.p.m., $p = 13 \text{ kg cm}^{-2}$, $f_2 = 900$ eng.p.h.
7. $n = 1500$ r.p.m., $p = 15 \text{ kg cm}^{-2}$, $f_2 = 900$ eng.p.h.

METALLURGICAL ASPECT OF DISC WEAR

The technique adopted for X-ray examination of the discs was that described by K. Nakajima and J. Kawamoto⁴.

X-ray negatives were taken of a pair of disc specimens, one unused and the other worn, and developed in identical conditions. Results of repeated tests (Fig. 11) show a definite difference in surface carbon density (reflected in the blackness of the lines) between the two specimens (For quantitative analysis, photometric readings were taken with the aid of a photocell and a computer). Apparently, the heat generated by the wear process causes the surface steel to rise above the GSK phase boundary in the iron-carbon diagram (Fig. 12) into a zone representing a mixture of alpha and gamma crystals. After cooling, the carbon content of the steel decreases thus creating a state of 'congestion' reflected by the extra blackness. Where no suitable medium is available for penetration, however, the surface remains unhardened and the small amounts of liberated carbon burn off;

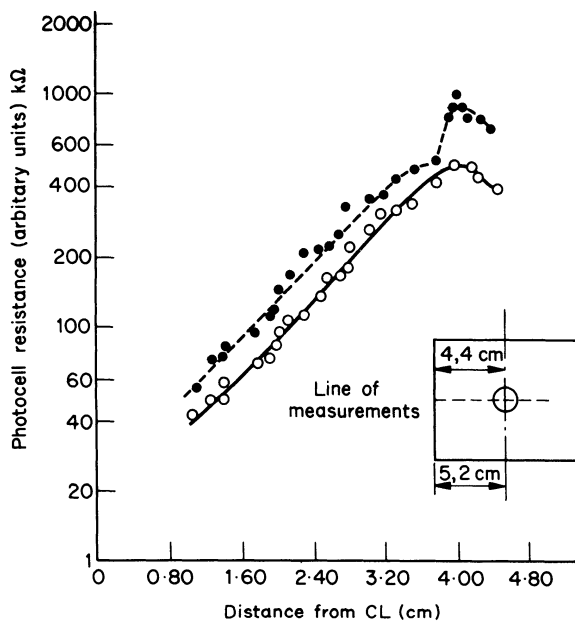


Fig. 11 Photometric readings on X-ray negatives.

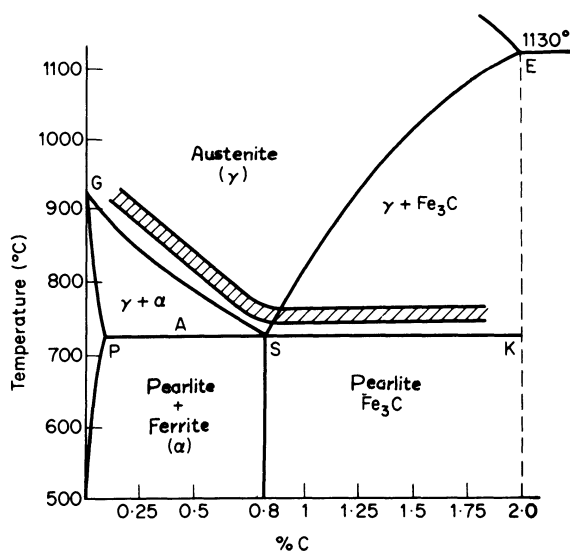


Fig. 12 Fe-C diagram for low-carbon steels.

this can be seen in the unhardened discs (which showed no signs of hardening in the wear tests) and also when a state of saturation has been reached and the carbon can no longer penetrate the crystals. As it burns off, more carbon is liberated from the martensite and an immediate drop in hardness is observed.

CONCLUSIONS

1. For a given hardened disc there exists a maximum temperature, which must not be exceeded if the clutch is to function satisfactorily.

2. At this temperature (and at higher temperatures) carbon diffusion occurs resulting in degradation of the surface composition, loss of hardness, a lower friction coefficient and excessive wear.

3. Below this temperature, however, the surface hardness is an increasing function of temperature, and this represents the useful range of application.

4. If a disc is insufficiently hardened initially, the wear rate is excessive throughout its life and the duration of serviceability is greatly limited.

5. A simple but reliable method has been found for predicting the service life of clutch discs. Our results provide a basis for finding service life with considerable accuracy, and for interpreting surface changes.

6. The results suggest that, provided the plates are initially heat hardened sufficiently (that is, greater than 400 HV), minimal advantage in serviceable life-time is obtained by heat hardening to higher levels.

REFERENCES

1. RABINOWICZ, E., 'Friction and wear of materials,' Wiley (1964).
2. ARCHARD, J. F., and HIRT, W., 'The wear of metals under unlubricated conditions,' *Proc. Roy. Soc., A* 236, 397-410 (1956).
3. MALE, A. T., 'The effect of temperature on the frictional behavior of various metals during mechanical working,' *J. Inst. Metals*, 93, 489-494 (1964-1965).
4. NAKAJIMA, K., KAWAMOTO, J., 'X-ray study of frictional wear in metals,' *Wear*, 11, 21 (1968).
5. ROSENBERG, J. A., 'Issledovanie mnogodiskovykh friktsionnykh muft' (study on multiple friction clutches), *Vestnik vashinostroeniya*, No. 12.
6. SCHACH, W., 'Berechnung einer Lamellenkupplung, Werkstatt- und Betriebstechnik,' 531 (1951).
7. ZHITNITSKII, S. P., 'Raspredelenie udelnogo davleniya po radiusu trushchikhsiya proverkhnostei u mnogodiskovykh (plastinchatyky) tormozov' (radial distribution of specific pressure on wear surfaces in multiple disc brakes). *Trudy Zaporozhskogo mashinostroitel'nogo instituta seria mashinostroeniya*, 3, 3-12 (1959).
8. KHRUSCHEV, M. M., 'Resistance of metals to wear by abrasion as related to hardness,' *Proc. Conf. on Lubrication and Wear (1957)*, *Inst. of Mech. Eng.*, 655-659 (1957).
9. LEVY, H., LOEWY, K., and LENZ, E., 'Temperature distribution on disc clutches in machine tools,' *Annals of the CIRP*, 239-250 (1969).

CUTTING FORCES IN MACHINING AND THEIR ROUTINE MEASUREMENT WITH MULTI-COMPONENT PIEZO-ELECTRIC FORCE TRANSDUCERS

by

G. H. GAUTSCHI*

SUMMARY

Knowledge of actual cutting forces in machining is becoming of paramount importance to both designers and users of machine tools, because optimum machine performance, tool selection, tool life, cutting-edge geometry, combination of tool and material to be machined, accuracy and so on are closely related to the resulting cutting forces. Transducers and platforms for measuring forces in 1, 2 or 3 components and/or torques have been developed and are described here. Quartz is used as the piezo-electric transducer material because it provides extremely high rigidity and excellent dynamic response as well as minimal cross-talk between components. In contrast to other measuring systems, such platforms equal or exceed usual tool holders in terms of rigidity, thus permitting realistic, precise measurements. Practical aspects such as cross-talk between components, frequency response, measuring and recording techniques are discussed and the possibilities of adaptive control by directly mounting transducers into machine tools outlined.

INTRODUCTION

Definition of problem and system requirements

The measurement of cutting forces in machining corresponds to the analytical problem of determining the components of a general force vector in a chosen orthogonal coordinate system and, similarly, the components of a general moment vector in the same coordinate system. Because it is impossible to measure the cutting forces at their actual origin, the reactions have to be measured in a defined plane distant from the cutting edge. Therefore, a measuring system is required which measures correctly, independent of the point of application of the force and/or moments.

In order to obtain true measurements, the measuring system should satisfy the following requirements:

- original rigidities should be maintained, if not exceeded
- dynamic characteristics should be as similar as possible to those of the original set-up
- the mounting of the tool or the workpiece should remain as close as possible as before

- frequency response should be as wide as possible
- cross-talk between components of forces and moments should be minimal
- sensitivities of transducers should be unaffected by time, temperature and mounting of tool and workpiece
- high resolution, that is the capability of measuring small variations in an important force or moment
- non-critical adjustment of zero points, sensitivities, measuring ranges and so on.

A number of cutting force measuring systems have been built mainly by University research laboratories and are described in the literature. Most of these require well-trained personnel and special equipment, which often requires delicate adjustment. The aim of the development of the systems described here is to provide the applied researcher in industry with a simple, efficient tool, permitting him to investigate and compare different tools and materials, to optimize particular machining problems and, in general, to solve the routine problems encountered in machine tool and tool design and use.

*dipl. Ing. ETH/SIA, Kistler Instruments AG, Winterthur, Switzerland

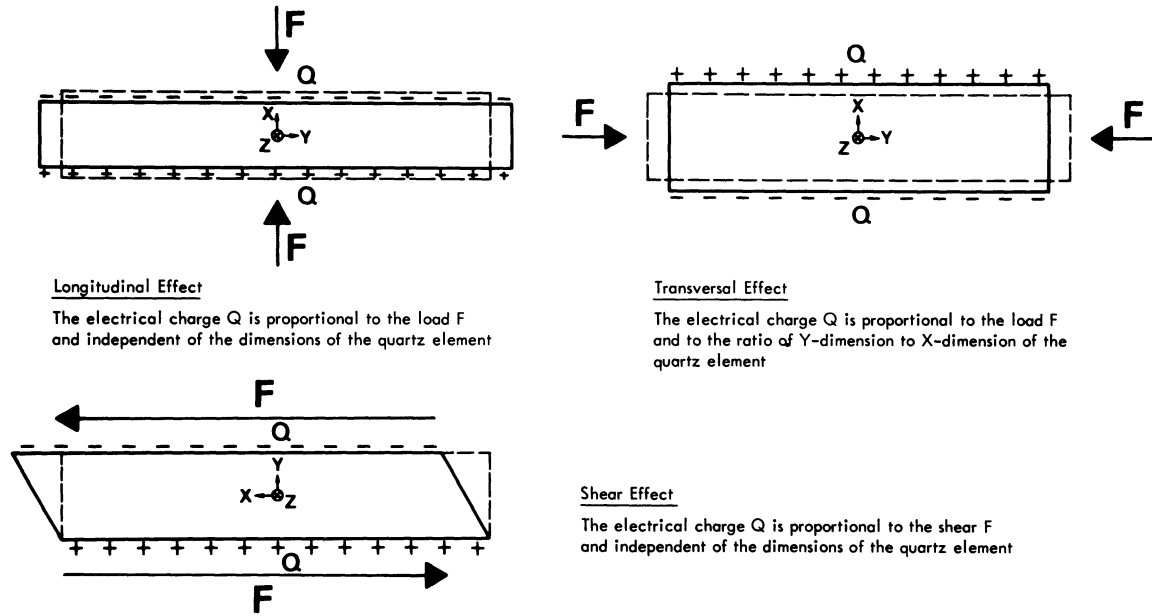


Fig. 1 Piezo-electric effects in quartz. (The coordinate systems shown refer to the crystallographic axes).

THE PIEZO-ELECTRIC PRINCIPLE

Certain crystals have the property that electrical charges appear on their surfaces under mechanical stress. This is caused by the 'piezo-electric effect', discovered by the brothers Curie in 1880.

For force transducers, quartz is one of the most suitable piezo-electrical materials. The following three piezo-electric effects are observed in quartz:

- the longitudinal effect
- the transversal effect
- the shear effect.

Fig. 1 shows, schematically, these three effects.

The electrical charges appearing on the quartz surfaces are collected with electrodes and transformed by a charge amplifier into an analogue vol-

tage. Often, quartz elements are used in pairs as this has the advantage that the sum of the charges can be collected on one central electrode, thus eliminating the need for insulating foils.

The transversal effect is mainly used in cases in which a higher sensitivity ($\text{pC}\cdot\text{N}^{-1}$) is desired, for example in pressure transducers, as it is the only piezo-electric effect in quartz which depends also on the proportions of the element.

TRANSDUCERS

Individual transducers

Suitably cut quartz elements can be mounted in a steel housing, thus forming a force transducer. It is important to note that the steel housing serves only to distribute stresses evenly over the quartz elements and to keep the assembly dry and clean, that is to maintain the necessary high insulation values of over $10^{13}\Omega$.

For uni-axial forces, the longitudinal piezo-effect is most convenient, as the electrical charge appears on the same surfaces as those on which the force acts. Furthermore, the electrical charge is solely proportional to the acting force, thus independent of the dimensions of the quartz element. Fig. 2 shows typical examples of such 'load washers'. Through pre-stressing, a load washer can also be used to measure tension.

Multi-component transducers use several quartz elements arranged mechanically in series, that is the force acting on the transducer acts also on each and every quartz element. Because each element is sensitive to stress in only one direction, because of its selected cut from the crystal, the components of force can be measured individually. In order to use the shear effect, it is either necessary to 'glue' the force-transmitting steel parts to the quartz or to pre-stress the transducer in order to achieve enough fric-

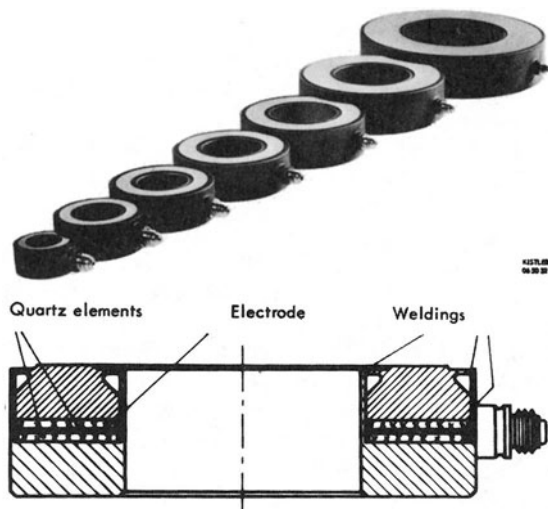


Fig. 2 Load washers. Measuring ranges go from 15 kN (14 mm diameter) to 1 MN(120 mm diameter). Resolution with a standard charge amplifier is about 20 mN on all of them. Compression under full load is typically 15 μm .

tion forces to transmit shear. Fig. 3 shows an example of a 3-component force transducer with a central pair of quartz elements reacting through the longitudinal effect to the axial load while the other two pairs react through the shear effects to the shear forces.

Transducers for moments

A transducer responding to a moment can be designed by arranging a number of small quartz discs—cut for the shear effect—in a circle and orienting their shear-sensitive axes tangentially. With all discs mechanically and electrically in parallel, an electrical charge proportional to the acting moment is generated. Again, it is necessary to pre-stress such a transducer in order to have friction forces available for transmitting the moment. Such a transducer is the heart of the platform for an axial force and a moment transducer shown in Fig. 4.

Measuring platforms

One or several transducers can be used to build a so-called 'measuring platform', which have the advantage that the individual transducers are loaded in a defined way and that the application of the load is much less critical than it would be using a transducer only. Furthermore, platforms permit a larger freedom of the point of load application than a single transducer. Any number of transducers can be connected in parallel to a charge amplifier, and the total signal obtained will be exactly the sum of all forces acting on the transducers. A force of constant magnitude and direction but with a varying point of application will, therefore, always be measured correctly.

I now describe a selection of such measuring platforms. It is, however, possible to build platforms in almost any shape and for any purpose within a wide range of load capacities.

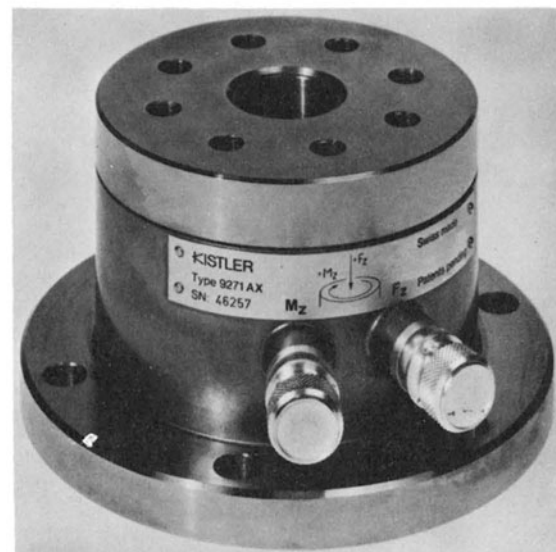
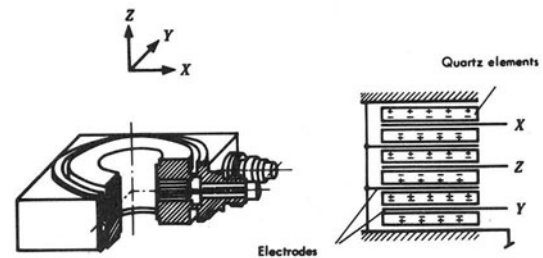
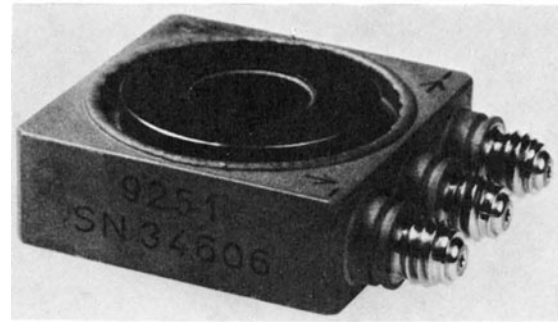


Fig. 3 (top right) Three-component force transducer.

Maximum load in z-direction is 30 kN.

Shear (with 25 kN prestressing in z-direction) ± 2.5 kN

Cross-talk is typically $<1\%$.

Fig. 4 (bottom right) Two-component measuring platform (F_z and M_z).

F_z -range + 20 kN to -5 kN, M_z -range: ± 100 Nm.

Resolutions of F_z about 20 mN and of M_z about 0,2 mN.

Overload capacity: 50%, resonance frequency > 3 kHz.

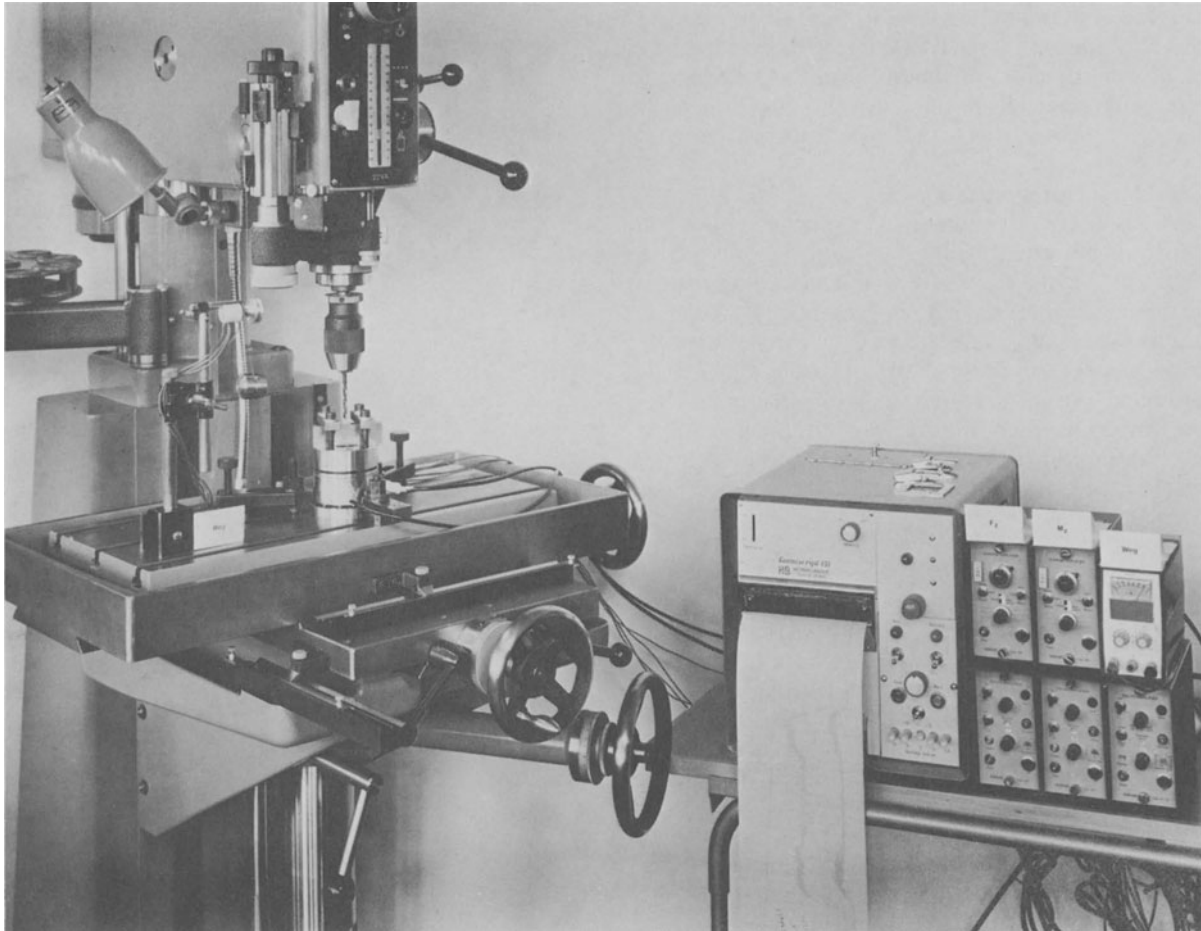


Fig. 5 Multi-component measuring and recording system for feeding force, moment, and drill travel.

CUTTING FORCE MEASUREMENTS

Drilling

Feeding force and torque are two obvious cutting forces acting on a workpiece being drilled. Furthermore, a drifting force may occur in the form of a vector, normal to the drill axis and rotating synchronously with the latter.

It is more convenient to mount the stationary workpiece on a measuring platform rather than to attempt to measure the reactions on the rotating drill. Fig. 5 shows a 2-component measuring platform installed on a drilling machine.

This platform is based on a 2-component transducer (F_z and M_z) which is mounted under high pre-load between the base and top plate of the platform. Should the lateral drift force be of special interest, the platform may be modified by adding another 2-component cell which reacts to shear in the x - and y -directions. The rotating drift force vector would thus be measured in 2 components and be recorded as two sine-like oscillations with a 90° phase difference.

For investigations such as comparing drills with different cutting-edge geometries, or comparing the machinability of supposedly identical materials from different sources, it is imperative that the drill is machine-fed. Only in this way do variations in machinability become clearly evident. Fig. 6 shows the example of a 5 mm bore through cold-drawn flat-bar steel, illustrating the well-known fact that the

surfaces are cold worked and therefore 'tougher' than the relatively undisturbed central zone. With hand-feeding, the operator would automatically tend to 'equalize' the varying resistance.

Turning

Turning produces a cutting force, the orthogonal components of which (main cutting force, feed force and reaction force) are of interest.

In this case it is advantageous to mount the tool on a 3-component measuring platform and measure the reactions on it.

Fig. 7 shows such a platform, which is directly designed as a tool holder and can accommodate tool shafts up to $32 \times 32 \text{ mm}^2$.

Milling

In milling, two approaches may be considered:

- mounting the workpiece on a 3-component measuring platform
- installing transducers directly into the milling cutter.

For relatively small work, the first method is quite satisfactory. The limitations are chiefly the maximum travel, which is given by the admissible eccentricity of the acting force relative to the platform.

Fig. 8 depicts a 3-component platform suitable for smaller milling work. Larger platforms can be built by using bigger transducers or by bridging two platforms with a steel plate.

For investigations of larger milling work, a platform large enough to hold the necessary workpiece becomes a problem, and the second approach of installing transducers directly in the cutter should be

Internal forces, the sum of which is zero, will produce a pseudo cross-talk if the different transducers do not yield equal electrical charges under equal loads.

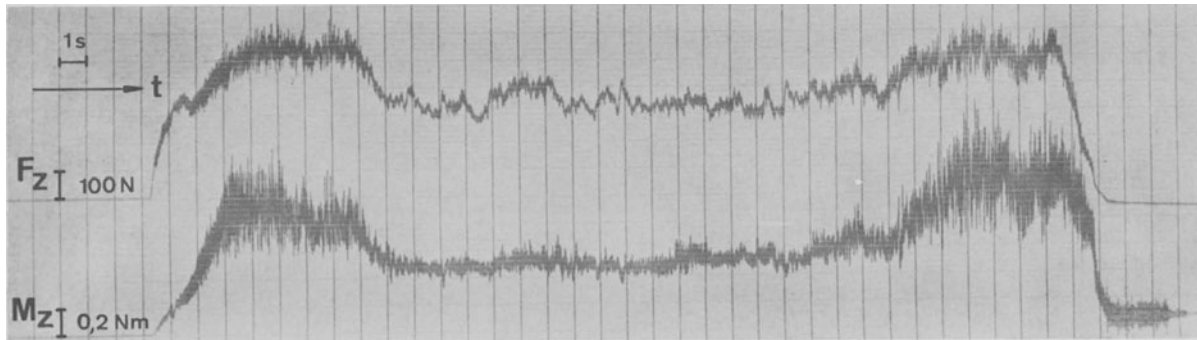
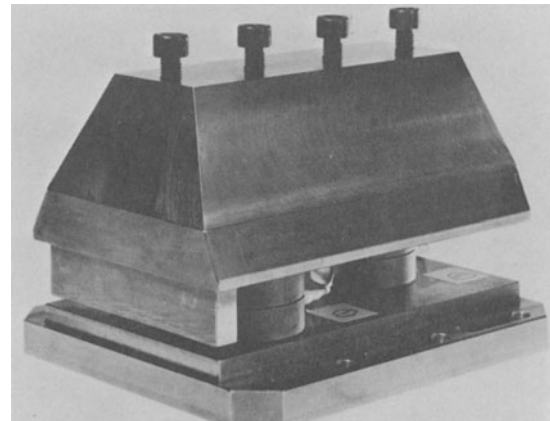


Fig. 6 Recording of feeding force F_z and moment M_z during a 5 mm-bore through cold-drawn flat-bar steel with $n = 1215$ r.p.m. and 0.04 mm rev^{-1} feed.

considered, in spite of the problems of the measuring system, including charge amplifiers which are no longer stationary but which rotate with the cutter.

Fig. 7 Three-component measuring platform for turning. Tool shafts up to 32×32 mm². The protective covers have been removed to expose the three 3-component transducers.

Measuring ranges:	
main cutting force	20 kN
feed force	± 10 kN
reaction force	± 10 kN
Resolution	about 20 mN
Overload capacity	50%
Cross-talk, typically	< 1%
Resonance frequency, typically	2.5 kHz



MEASURING TECHNIQUES

Cross-talk

Theoretically, a transducer or a platform should only respond to loading in the desired axis of sensitivity; that is, the cross-talk between component forces and moments should be zero. In practice, with careful manufacturing and advanced transducer design, it is possible to keep cross-sensitivity below 1%, which is sufficient in most cases. This requires that the quartz elements are cut, ground and polished to within a few minutes of the required crystallographic orientation.

Also, transducers have to be mounted between flat, ground and rigid surfaces in such a way that stresses are distributed as evenly as possible over the contact surface. Pre-stressing bolts have to be well centred and their axes exactly normal to the contact surface.

When several transducers are mounted together in a measuring platform, their respective sensitivities must be as identical as possible.

For special cases, and only with a fixed point of force application, the residual cross-talk can be further reduced with electronic compensation, if the cross-talk is linear. In most practical cases, however, this is not to be recommended, as the procedure is cumbersome and may make things worse if not done very carefully.

Rigidity

Force measurement always involves deformations, because force as such cannot be measured; only its effect on a material can be observed. Piezo-electric transducers use quartz as the material on which the action of force is sensed, that is the quartz is acting as the spring element.

Quartz has a stiffness about 40% that of steel, and because the thickness of the quartz elements is small compared with the total transducer thickness, the rigidity of the transducer is almost identical to a similar piece of solid steel.

The rigidity of platforms depends on their dimensions and proportions. Platforms such as those shown

in Figs 4 and 7 have rigidities which are only slightly less than those of the transducers. But the platform in Fig. 8 is already somewhat 'softer' in the vertical direction if the force is acting midway between the four transducers. Such platforms are inevitably a compromise because, for rigidity, the top plate should be made thicker but, for high resonance, the mass should be kept to a minimum.

Frequency response

The frequency response of a measuring system is rather complex, because it is not always possible to consider a platform (for example) as a simple oscillating system. Such a system would have the normal resonance rise associated with a phase shift. Without special precautions, the measuring range used should not exceed about one-third of the resonant frequency in order to avoid significant errors in amplitude and phase. If the measuring system had a well-defined, unique and reproducible mode of oscillation, it would be possible to build a filter compensating the resonance curve and thus to extend the usable range considerably. Transducers and, even more so, platforms are very complex systems in terms of oscillations and in most cases, such a compensation by a filter would be illusionary.

When considering frequency response, two aspects must be considered:

- the lowest resonant frequency
- the range of frequency occurring in the values to be measured.

Generally two ranges of frequencies can be distinguished in machining:

- low frequencies, from zero to about 2 kHz
- high frequencies, from about 1 kHz to 100 kHz.

The high frequencies are associated with phenomena which belong to the domain of research on the formation of cuttings and so on and are not of interest for the type of cutting force measurements discussed here.

The lower range, up to about 2 kHz, however, comprises the frequencies transmitted through the foundations, the natural frequencies occurring in the different parts of the machine tool, the frequencies induced by the interaction of tool and workpiece (especially those induced by the process of built-up edge) and so on. This range can easily be investigated with multi-component measuring platforms which usually have lowest resonant frequencies above 2–3 kHz.

Suitable instruments for such dynamic investigations are either cathode-ray oscilloscopes or ultraviolet-oscillographs.

Typical lay-out of a multi-component measuring and recording system

Fig. 5 illustrates the installation for measuring the feed force and torque in drilling. Each channel comprises a charge amplifier and a galvo-amplifier, driving a recording galvanometer in the UV-oscillograph. As a third channel, the travel of the drill is recorded by transmitting the vertical movement of the spindle by a wire (kept taut by a counter weight) to a pulley on the shaft of a multi-turn potentiometer. The latter is across a constant d.c. voltage source and an analogue

voltage therefore appears on the slider and is fed to another galvo-amplifier and galvanometer.

TECHNIQUES PARTICULAR TO PIEZO-ELECTRIC SYSTEM

The piezo-electric system has some peculiarities not found in other systems.

Sensitivity:

The sensitivity of a quartz transducer is, barring destruction by mechanical overload or extreme temperatures, constant for an indefinite time.

Linearity and hysteresis:

Quartz is perfectly linear and free of hysteresis. The quality of design, manufacture and assembly solely determine how close the transducer or platform will come to the potential perfection.

Set-up of a measuring chain:

This is reduced by connecting the transducer with a special cable to the charge amplifier, dialling the transducer sensitivity, choosing the desired measuring range and, in the case of a quasi-static measurement, re-setting the amplifier before the actual measurement.

Threshold:

In a piezo-electric system, the threshold is given by the charge amplifier and is, for a given number of quartz elements, almost constant regardless of the upper limit of the measuring range designed into the transducer. A modern, commercially available charge amplifier has a noise level corresponding to under 0.01 pC on the input. If the load washers of Fig. 2 are taken as an example, this means that, with a sensitivity of approx. 2 pC.N^{-1} , the threshold is about 10 to 20 mN. This threshold is independent of the size and thus available on all transducers including those up to 1 MN. The practical significance of this is that the resolution of a measuring chain can attain values of 10^{-8} of the maximum measurable value and it becomes possible to measure minute variations of large forces.

Static and dynamic measurements:

In principle, only dynamic measurements are possible with piezo-electric transducers. In fact, this is the prime domain of this system. But, it is possible to reliably measure quasi-statically, that is depending on the measuring range of the charge amplifier, for periods of minutes to hours, limiting factors being: drift of the amplifier and the quality of insulation of the transducer cable and the input of the charge amplifier. In most cases of cutting force measurement, this limitation poses no problem because the duration of a cut rarely exceeds minutes.

Absolute and relative measurements:

A piezo-electric measuring system has no zero point as such. In quasi-static measurements any given state can be chosen as zero reference by simply re-setting the charge amplifier and thus eliminating the electrical charge that was present. For quasi-static cutting force measurements, this would usually be done just before the tool is to engage. Absolute accuracies with standard measuring platforms and standard

charge amplifiers are typically within $\pm 2\%$ to $\pm 4\%$ without further special calibrations. Precision in repeatability may be better by a factor of about ten.

In quasi-static measurements, the variations of the forces are often small compared with the basic force; that is, the cutting force may show a dynamic part which is only a tiny fraction of the whole, and it seems desirable to 'magnify' this dynamic part. With the piezo-electric system this is most easily done by simply switching to a higher sensitivity during the actual cut and thus obtaining any desired resolution up to the absolute limit already mentioned, irrespective of the simultaneously acting basic force. As an example, the main cutting force in turning may be of about 10 kN on which are superimposed fluctuations of a magnitude of 1 N. Expanding these small fluctuations to full scale reading is achieved simply by increasing the sensitivity on the charge amplifier.

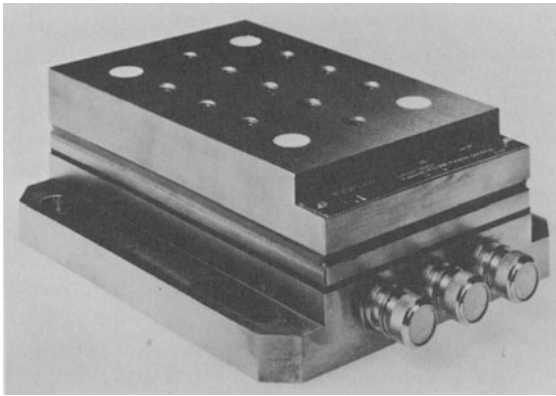


Fig. 8 Three-component measuring platform for milling, grinding and turning. Measuring ranges:

Normal to surface	± 5 kN
Force vector in surface	4 kN
Resolution	about 20 mN
Overload capacity	50%
Cross-talk typically	< 1%
Resonance frequency, typically	4 kHz

ASPECTS OF MOUNTING TRANSDUCERS DIRECTLY INTO MACHINE TOOLS

Requirements

Quartz transducers have to be installed according to certain clearly defined rules in order to show their advantages and to obtain precise and true measurements. In most cases, several transducers are required to take up properly the eccentrically acting forces and the resultant moments. Therefore, the transducers have to be mounted in a plane as close as possible to the point of force application and preferably parallel to two axes of the coordinate system into which the cutting force is to be reduced.

The high rigidity of quartz transducers requires precise and rigid contact surfaces in order to avoid local overloading of the quartz elements by stress peaks and to keep cross-talk to a minimum.

Transducers should preferably be mounted in such a way that the largest force component is acting axially and the smaller ones normal to the axis as shear. Pre-loading is almost always necessary, either to create friction for shear measurement and/or to permit axial tension as well.

POSSIBILITIES FOR ADAPTIVE CONTROL

In adaptive control, the transducers serve to monitor forces in order to

- sense tool-wear
- detect variations of surface quality
- protect against mechanical overloading
- keep cutting forces constant, for example in contour turning.

Sensing for example tool-wear represents a static measurement which, as such, cannot be done piezo-electrically. But a tool is practically never engaged for more than a few minutes at a time and therefore zero level, that is the tool being free and unloaded, can be re-established before each new cycle. This requires an electronic control system which re-sets the charge amplifier at the appropriate instants. Dynamic, relative measurements such as fluctuations of the cutting force (related to surface quality for example) are even easier to achieve as no absolute reference level has to be established periodically.

Signals thus obtained can be fed to discriminators (indicating whether a pre-set value has been exceeded), to peak indicators (recording the maximum value within a given time interval) or be processed in any other way necessary to obtain the signals required to give the desired control of the machine.

Obviously, other types of transducers may also be necessary, such as accelerometers, pressure transducers (for measurements in hydraulic control systems), as well as automatic sensing of workpiece dimensions and so on.

OUTLOOK

The piezo-electric measuring technique has been perfected to the point of becoming a practical tool for routine measurements in applied research and investigations in industry. Modern charge amplifiers and recording equipment are easy to operate without the need to make critical adjustments and no longer require electronic specialists as operators. Installation of transducers and platforms is clearly defined and can be adapted to a wide range of applications.

This report describes the present state of multi-component piezo-electric force and moment measurement and indicates some potential possibilities for its application in machine tool design and use.

Increased mutual feedback between instrument developers and machine designers and users is desirable to create optimum systems, taking full advantage of the inherent and unique characteristics of the piezo-electric system.

REFERENCES

1. SPESCHA, G. A., 'Piezoelektrische Mehrkomponenten-Kraft- und Momentmessung', (Piezoelectric Multi-Component Force and Moment Measurement), Archiv für technisches Messen, No 7, 8 and 9 (1970).
2. BLANKENSTEIN, B., 'Der Zerspanungsprozess als Ursache für Schnittkraftschwankungen beim

Drehen mit Hartmetallwerkzeugen' (The Machining Process as Source of Cutting Force Fluctuations in Turning with Carbide Cutting Tools), Dissertation, Technische Hochschule, Aachen, West Germany, (1968).

Technical data as well as all photographs are from technical documentations of Kistler Instrumente AG, Winterthur, Switzerland

DISCUSSION*Query from B. J. Davies, Staveley Engineering*

What are the indirect and direct effects of temperature on the output of the transducer?

Reply

The direct effect of temperature on a quartz type piezo-electric transducer is a variation of the sensitivity of $0.02\% (^{\circ}\text{C})^{-1}$, i.e. measuring at a temperature 50°C higher will be with the sensitivity reduced by 1%.

The indirect effects are extremely complex. Quartz, like all piezo-electric materials, is anisotropic with respect to elastic constants, thermal expansion and so on. Because the quartz discs have to be sandwiched between metal parts (force introducing parts, electrodes, etc.) with different characteristics, temperature has an indirect effect which results in a signal varying with temperature. In a force transducer this means for example that, if the temperature varies during the measurement, a signal of $\times \text{N } (^{\circ}\text{C})^{-1}$ will be superimposed on the desired signal and a zero offset at the end will be observed. Usually, the temperature varies nearly linearly with time and an approximation can be made by connecting the starting zero with the offset zero at the end by a straight line and using this line as a reference line for intermediate points. An extensive research programme is underway to understand fully these indirect temperature effects and to find practical ways to compensate them fully.

Query from Professor Peters

In the past we have been promised that we would be given a reliable dynamometer which uses the piezo-electric elements. I wish very sincerely that the proposed solution fulfils the need. However, I doubt whether this has been achieved because of the temperature sensitivity problem and the problems associated with light damping, as well as the influence of the mounting of the tool and the dynamometer on the machine.

Reply

Piezo-electric dynamometers have come out of their infancy and most of the early problems (ceramic top plates, failure of electric insulation etc.) have been eliminated. Properly installed (flat and rigid mating surfaces), these dynamometers are now as reliable as any other system. This is substantiated by more than 30 installations already in use.

I did not claim complete absence of temperature sensitivity: nevertheless, considerable improvements have been made and further R-D efforts are underway to eliminate these temperature effects. It should

be born in mind, however, that in a system where measuring deflections are only a few μm , this is a difficult task indeed.

Damping such a dynamometer would be very problematic, to say the least. First of all, a dynamometer installed on a machine tool will hardly ever show a single reproducible mode of oscillation, but an interference of a number of oscillatory modes.

For routine measurements, this means that the lowest resonant frequency f_0 (min) of the installed dynamometer should be determined experimentally (possibly running the machine with the tool disengaged and using the dynamometer as an accelerometer). The usable frequency range in the measurement may then be taken up to about $0.3 \times f_0$ (min). Otherwise, additional accelerometers in appropriate locations and frequency spectrum analysis would have to be brought in.

As pointed out in the paper, dynamometers are only useful for the lower frequency ranges (up to about 2 kHz). High frequency investigations (such as chip formation) in the 10–100 kHz range cannot be done with such dynamometers, however perfect they may be, because the mass between the sensing elements and the tool tip is simply too large. The answer would be, as an example, a subminiature multi-component force transducer that fits directly under the tungsten-carbide tool tip, and that is still far in the future.

Query from A. Russell, N.E.L.

When the device is used in conjunction with charge amplifiers in order to measure high forces down to almost DC frequency, can the higher frequencies still be measured or are they integrated into the long time constant of the charge amplifier?

Reply

The charge amplifier does not integrate the higher frequencies when operating on long time constant.

Long time constant corresponds to the DC-mode on an oscilloscope, while operation on 'short time constant' corresponds to the 'AC-mode' on a scope. Therefore, high frequencies can always be measured. The only limit when working on 'Long time constant' is the fact that the amplitude of the high frequency signals may be very small compared with the DC-compound and the accuracy of the amplitude measurement will be reduced. The frequency, however, can always be determined as long as the oscillations can be recognised as 'ripple' on the basic signal. Frequency response of a modern charge amplifier in the 'Long time constant' mode goes from DC to over 200 kHz.

THE EFFECT OF APPEARANCE CONSIDERATIONS ON THE DESIGN OF A SMALL NC MILLING MACHINE

by

E. J. HUNTLEY, R. ROSE, J. S. SHEEN*

SUMMARY

Problems of appearance in the design of a complex machine tool are discussed here. The design of a small NC milling machine is described, in which considerable attention was given to appearance without adversely influencing its cutting performance or increasing the cost. Although appearance considerations led to the design concept, the approach was found to be justified from design and production advantages alone.

INTRODUCTION

Appearance is a characteristic with no technical definition. There are no formulae on which to base its design, and there is no test equipment to measure the success of the finished product. It is extremely difficult to express clearly what is meant by good appearance, yet at every compromise in the design, appearance has to compete with the other items in the specification, many of which are defined to have numerical values. The only clear fact that is likely to emerge concerning appearance is that it should not increase the cost of the machine. Few, if any, customers would knowingly pay more for a better looking machine. Some customers associated reliability with the more old fashioned designs, and others associated good technical design with good appearance.

In fact, the only consolation for a good looking machine is that it may have the 'edge' on a competitor's machine of equivalent specifications. This is the situation all designers face when deciding what attention should be given to appearance.

We describe here how this apparently unrewarding challenge of appearance was tackled in the design of a continuous path tape-controlled replacement for a manual No. 2 size, knee type vertical milling machine. The description of the design will be confined to those parts most affected in the compromise between appearance, cost and technical requirements.

As well as the technical specifications to which numerical values could be given, there were the following design objectives. (a), To improve the structure. (b), To include feed drives, the performances of

which were suitable for continuous path control. (c), To be of unit construction, with each unit being capable of being tested before final assembly. (d), To be less dependent on skilled fitting, that is, easily assembled. (e), To be produced in small batches, but of sufficiently low cost to encourage the use of continuous path control for general machining. (f), To have ease of access for maintenance and built-in facilities for fault finding. (g), To have clean lines and pleasing appearance, with low finishing costs. (h), To use, where suitable, existing components or sub-assemblies. In this short list, appearance seems insignificant alongside the technical and economic importance of the other items.

Previous experience had shown that, on small machines in particular, it was fatal to try and improve the appearance when the design was nearly completed. Often there is not the space, because small machines usually have the same spindle and feed drive requirements as much larger machines; they use the same cutters and are expected to take the same cuts.

One way of cleaning up the lines is to arrange the sub-assemblies inside the main structure so that just a cover plate shows. Even when this does not ruin the structure, the cost becomes excessive and access for build and maintenance is difficult, especially where piping and wiring are involved.

The effort required to tidy up a design can be surprisingly great and the results far from rewarding. This is because appearance is relative. The fact that the appearance is better than it was, does not help unless it is good enough. As each monstrosity is removed, the others stand out more clearly. The skill comes in knowing when to stop, because a point is

*Staveley Engineering and Research Centre, Worcester.

reached after which the designer's good intentions make matters worse and the machine can become even more hideous than the first attempt which had little pretensions to good looks.

It is not easy even for an experienced designer to judge the appearance of a machine from two-dimensional views showing merely the outline of the main parts. High-lights, shadows and colouring can have a tremendous effect. Small prominent parts can have an effect out of all proportion to their sizes.

The problems are not only confined to the designer. Each of his team has his own idea of good taste and it is difficult to impose a uniformity of concept and to stop personal influences coming through. Further problems arise from last minute modifications when the part that no-one thought would give trouble has to be re-designed and its new shape no longer blends with the machine.

An examination of any machine will show that money has been spent on its appearances, whether it has been deliberate or unconscious. Some examples are easy to recognise, such as letting in cover plates flush with the surface; others infiltrate the whole design and are difficult to separate.

In this example, if the appearance of the new design was to be taken seriously it was obvious that a different approach would be needed. This led to the proposal of designing the machine to be purely functional from the technical and production point of view and then to cover the whole with fibreglass or metal covers as appropriate. An appearance design consultant would be engaged to advise on appearance, so relieving the machine designer of the part that he was least qualified to perform.

The idea of completely covering an object is not new, the human body was made this way as was the motor car, but this approach had not been generally adopted in machine tools, in fact quite the reverse. The reasons were not obvious. The most likely was unfavourable cost, but on the basis of a rough estimate there seemed little or no risk. Some protective covers would be needed whichever design concept was chosen, and therefore the cost of appearance for the completely covered machine would be, in effect, the cost of the extra covers; this would be largely off-set by the amount normally spent on appearances and savings arising from simplifications of parts underneath the covers. From the technical point of view there only seemed to be advantages.

As soon as the first ideas had been committed to paper, the Appearance Design Consultants, F. C. Ashford & Associates, were able to start work and tentative schemes were drawn up for covering the machine; layouts for the various control panels were also considered from the start. Throughout the design there was close liaison with the Appearance Design Consultant and although compromises were inevitable at times, the association was remarkably smooth and rewarding.

The factor that stood out immediately after the tentative outline of the envelope had been agreed was that design beneath the envelope could go ahead concentrating exclusively on technical and cost aspects, and completely ignoring appearance. This turned out to be a considerable psychological advantage to the

design team. In fact, the freedom took a little getting used to and highlighted many ingrained habits that had been costly.

A one-eighth scale model was made out of wood so that it could be easily updated as the design progressed. It was painted in the standard two tone colour scheme with scaled coloured nameplates provided by the Consultants; the control panels were scaled photographs fixed in position. In this way the three-dimensional effect of modifications to the covers was immediately apparent. The model was also found to be an ideal way of keeping design, production and sales teams informed as to the final appearance of the machine, and provided a continual source of encouragement. Photographs of the model looked so realistic, that they were used for advance publicity.

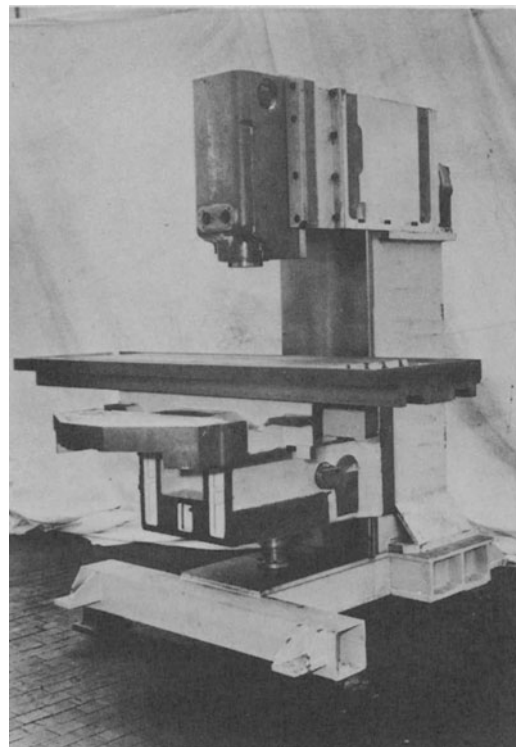


Fig. 1 Basic structure.

The machine was designed with a box section structure of constant width from the knee through to the head ways. As well as its good structural properties it also provided flat surfaces on which to bolt sub-assemblies, often without machining the surface. Every effort was made to confine sub-assemblies to the outside of the structure, to minimise the apertures in the structure and maintain its good torsional characteristics.

By arranging the covers parallel to the constant width structure, a space of constant depth was made available under the covers. Thus, throughout the design, the position of parts mounted on any of the side faces, could be re-arranged quite freely to arrive at the best compromise. In fact, there was no need to fix the positions of the less important parts until the end, with the assurance that these would not affect the design of the covers. Last minuted modifications presented no problems, because parts could be re-arranged to provide space.

By bolting sub-assemblies to the outside of the structure all the faces of the sub-assembly are accessible for build and maintenance except the one by which it is fixed; also a larger surface area is presented, from which to choose when arranging pipe and cable connections. As a result, the large structural elements become relatively simple, which is an added advantage. This arises out of the generalisation that all parts within certain size limits should be designed to the same level of complication, because both the cost and the probability of machining errors increases more steeply with the complication; in particular, large parts should be of less than average complication because they can only be produced on large machines which cost more to run.

The base, column and spindle gearbox were fabricated of mild steel, except for the front face of the column which forms the ways for the cast iron knee, and this was made of E.N.8. This is an interesting application of E.N.8, suggested by Professor Koenigsberger, in that it welds relatively easily and when induction hardened to 45° Rockwell, has adequate wear properties for an intermittently used axis. The remainder of the structure was made of cast iron. A rough comparison with the structure of the manual machine showed that although their bending stiffnesses were similar, the new design had a torsional stiffness almost an order higher.

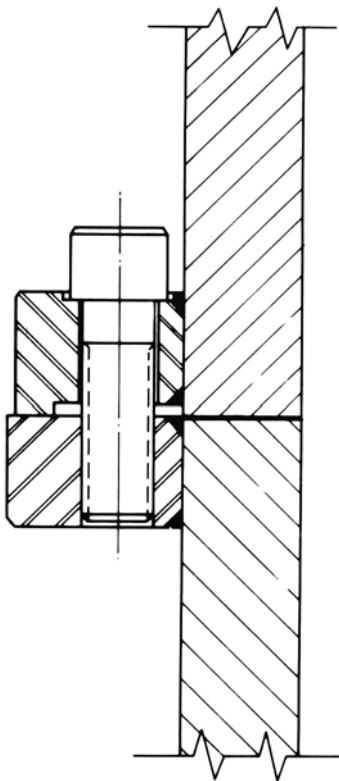


Fig. 2 Flange joint.

An improved flange joint was provided (Fig. 2) by cutting a groove in one of the flanges parallel to the wall, thus the outer edge of the flange acted as a heel point for the bolts to pre-load the walls of the structure together.

The hydraulic power-pack and contactor panel, shared the same chassis and were loosely attached to the side of the machine. This was found to take up

less floor area than separate cabinets having the same accessibility, as well as facilitating piping and wiring, and reducing the covers needed. The N.C. control equipment was fixed, as was the machine control panel, so that the operator would always know where to find them and be able to take the quickest possible action in an emergency.

Wiring and piping are usually very much underrated problems, both in design and production. This is because it falls into a 'no-mans land' in the field of engineering bordered by mechanics, hydraulics and electrics. It is often simply assumed that there will be room for it, and sometimes left to the wireman and pipe fitter to choose the best route.

This machine concept was well suited to pre-formed wiring and piping. A complete conduited wiring system could be assembled onto the outside of the structure; there would be no problems of threading wires or pipes through castings for the sake of appearance, and routing could be direct. On the other hand, if it was to fit, it had to be designed in detail like any other part of the machine.

The economic argument for pre-formed wiring and piping is very sound. Piping and wiring always come towards the end of building when the capital tied up in the machine and its control equipment is virtually a maximum. It is therefore at this stage that the greatest savings can be made by reducing throughput time. One way of doing this is to increase the work force, but on a machine of this size only a limited number can work efficiently at the same time. The best way of reducing throughput time is therefore by using pre-formed assemblies of wiring, conduiting and piping, which can be put together at slack times and thereby improve the work loading of the electrical and hydraulic departments. Furthermore, efficiency is increased by producing the assemblies in batches and by testing and correcting them before they are assembled onto the machine.

The tapped holes for piping, and conduit clips, manifolds, and junction boxes were made by an NC machine during the general machining of the structural components, in order to speed assembly. Two wiring sub-assemblies were designed, one for the NC equipment wiring and the other for the general electrics, and they were routed separately to prevent interference. Flexible conduit was used throughout, with junction boxes as distribution points. Swivel ends to the conduit eased the final assembly onto the machine as did push-on connectors. Because appearance under the covers was unimportant and there was adequate space, routing was made as direct as possible. To obtain accurate lengths for the conduiting and wiring harnesses, the first machine was wired in the normal piecemeal manner and then stripped and measured. The conduited harnesses turned out to be surprisingly heavy and difficult to handle until one or more of the key points had been fixed in place on the machine and this is where the already tapped fixing holes were invaluable.

It is impossible to keep dirt out of the hydraulic system by piping a machine in the conventional way, especially if other work is in progress at the same time; consequently the whole system, including manifolds and fittings have to be finally stripped, cleaned

and the re-assembled. On the other hand, with pre-formed piping, dirt is confined to a piping jig, and pipe fitting is at bench level where there is greater accessibility; also specially hardened pipe fittings can be included in the rig to ensure correct formation of the compression rings. The rapid assembly time of pre-formed pipes, hoses and manifolds, cleaned just before assembly, justifies clearing the machine of all other activities.

The use of jigs does create the problem that the jig cannot take into account the accumulation of tolerances between the two parts of the machine being connected. This is catered for, however, by designing each pipe to contain at least one right-angle bend so that it can flex to take up small tolerances. Shortage of space was most acute around the knee and cross slide (Fig. 3). Pipe, and in particular hose routing, was

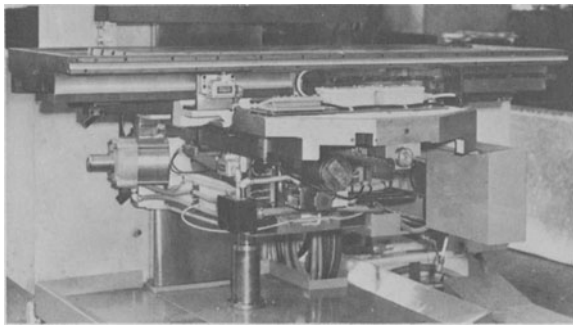


Fig. 3 View under knee and cross slide covers.

made even more difficult by the need to consider the covers of parts moving relative to one another, in a region where swarf and coolant had to be taken into account. By keeping hose lengths to a minimum, hose bores, and therefore their bend diameters were minimised; we took advantage of the characteristics of the feed drive here, in that high flows are only required at fast traverse when loads are light and there is pressure to spare to cover pipe losses. Complication was confined to manifolds, one for each of the feed drive motors and two for distribution; one was fixed to the column and the other to the knee. By aligning the outlets of the manifolds which were to be connected, in either a horizontal or vertical plane, the complexity was greatly reduced, and the number of pipes and hoses reduced to the theoretical minimum.

There now remained the problem of designing the actual covers, and this proved to be more difficult than was thought at first. The envelope had to be divided into sections which could be handled easily but not be prone to damage. Ventilation had to be confined to those places where coolant and dirt would not present problems and where the operators of this and nearby machines would not be subjected to strong draughts. The sections had to be hung on the structure so that the joints were not ugly, although the structural fabrications and castings were to open limits; the covers on the moving parts had to slide past other covers and not leave obvious holes. Certain covers that would have been ideal in fibreglass from a production point of view had to be made

of steel because they provided excellent footholds for climbing onto the machine during building or maintenance.

The problems of mounting the column covers were solved quite simply by providing a frame from which they all hung. Both the covers and the frame were drilled from jigs, thus controlling the horizontal dimensions of the gaps. The bottoms of the covers were attached to the column. Simple resilient mounts provided the means of adjustment at the fixing points and the covers were held in place with knurled nuts, so that they could be removed quickly without tools. The spindle speed change panel was located on the pointer and handle shafts and spring loaded outwards to fit against the inside of the large side cover.

The most difficult covers were those around the knee and cross slide where there was a severe space limitation, coupled with the need to seal against swarf and coolant. The key to this problem was the introduction of an open sided structural box attached to one side of the cross slide, to hold hoses and cables. This box divided the covers conveniently, and allowed the use of a single cover for the front and side of the knee and similarly one for the front and side of the cross slide (Fig. 3).

Towards the end of the project the techniques of cover designing were becoming more apparent. Two basic rules emerged from the experience on this machine. The first is to keep the number of covers to a minimum; do not use two covers where one will do. The second is to keep the number of mounting points for each cover to a minimum; three is ideal.

A measure of the success of the cover design is the comparative absence of hoses and conduits (Fig. 4); this is rare for NC machines with hydraulic feed drives. Even so, one large hose was later introduced on the left of the knee to conduct coolant directly to the tank; it was found that the original open return caused splashing of the operators legs. Machining lights were easily built in under the head cover, which provided better than normal lighting of the machining area without blinding the operator or affecting accessibility. The coolant pipes were designed so that they could be folded and then retracted and out of sight under the covers, where they would not be a nuisance during dry cutting.

A feature of the machine was that datum setting gauges were provided for speeding up the setting of the tool to workpiece datum face spacing. The *X* and *Y* axes gauge is attached to a No. 50 taper arbor for mounting in the spindle nose and is used for setting the spindle centre over the *X*-*Y* datum. A separate gauge is provided for the *Z* axis (Fig. 5) and because this is used every time a tool is changed, it was mounted on the side of the head to be readily available. The gauge is stored under the head cover when not in use and is pulled down and swung under the tool when required.

In the final finishing stage advantages accrue through having separate covers. During building the covers are fitted and then removed for painting; this provides the paint shop with work to fill slack periods. Masking of the machine is no longer required and the covers are of a size that are easily handled in the spray booth. Two tone colour schemes can be

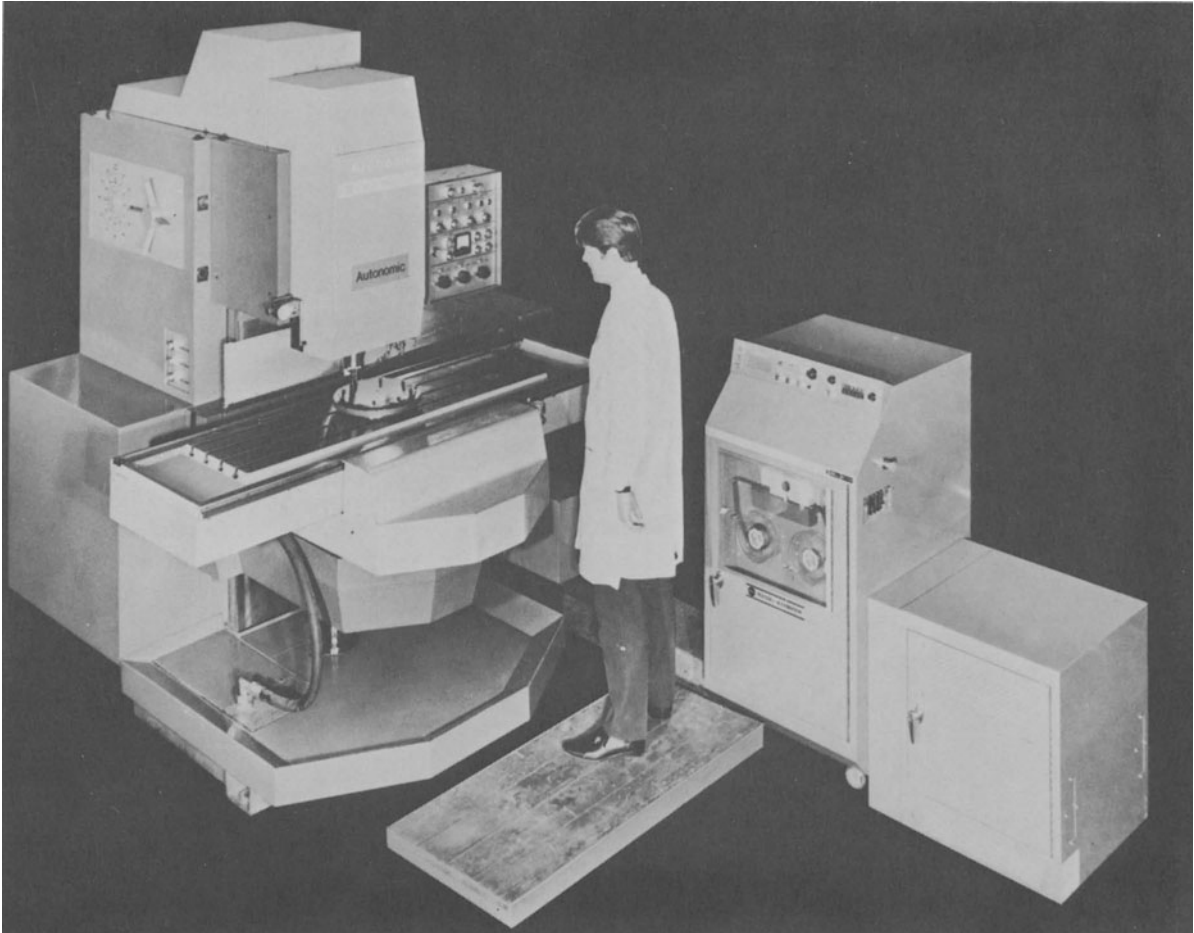


Fig. 4 Completed machine.

provided by spraying each cover the required colour. Special colour schemes for customers can be catered for without interfering with the build, and at relatively short notice. Paint can be allowed to harden thoroughly, and nameplates fitted. In this way, another of those activities that cannot be hurried and which takes place when the capital tied up in the product is greatest, is moved from a series activity with strict timing requirements for the labour, into a parallel activity in which there is more than ample latitude. Furthermore, by using a spare set of covers during cutting tests, it is possible to deliver a gleaming new machine to the customer untouched by swarf and coolant.

In the event of a breakdown the covers can be removed easily and quickly. Virtually the whole of the machine is then readily accessible for examination and repair, and it can be operated in its entirety, without covers, during fault finding.

The consideration of appearance, leading to the decision to completely cover the machine has had far reaching effects on the design. Although only those parts of the machine directly affected by this con-

cept have been described, there is hardly a part that has not benefited technically or cost-wise. The freedom gained by not having to consider appearance took much of the hesitancy out of design and was genuine relief to the design team. There was more room to manoeuvre in the technical, as well as the space, sense. Because of the simple configuration of the machine, parts were less dependant on each other and designs could proceed in parallel rather than in series. Then there were the intangibles such as the enthusiasm and pride given to both the design and production teams in producing a machine that is neat and pleasant to look at which does raise standards. The work of the Appearance Design Consultants was clearly outstanding.

The performance of the machine met the specifications fully; in fact, the machine could not be made to chatter even when the spindle drive was overloaded by 30%.

Final estimates indicated that the simplification of parts and production methods more than matched the cost of the extra covers. It could even be said that the cost of a good appearance was negative here.

DISCUSSION

Query from T. J. Vickersstaff

Could you say from your experience whether or not this machine would require significantly more floor space than one designed by more conventional techniques?

Reply

There is little or no difference in floor space requirements, but better accessibility. In fact various outline sketches were made to justify the final arrangement. On a general basis, the ratio of workpiece capacity to floor area of this machine compares quite favourably with most competitive machines. So often, accessibility for maintenance and, for that matter, stacking of components and the provision of tool cabinets, is neglected and just the minimum area for installing the machine is taken into account.

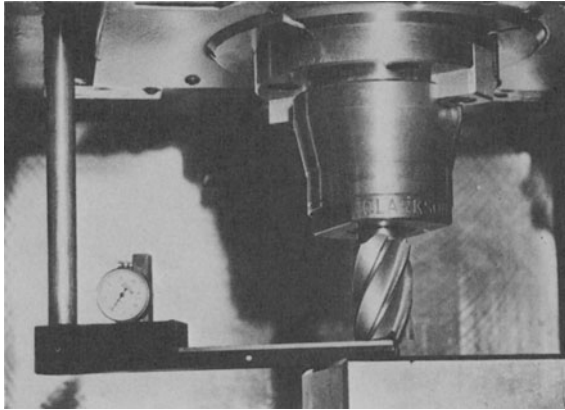


Fig. 5 Z axis datum setting device.

METAL FORMING

STRESS WAVE FRACTURING OF A BAR

by

S. T. S. AL-HASSANI and W. JOHNSON*

SUMMARY

A method is described whereby a bar subjected to a blow at one end induces tensile fracture at a controlled distance from the other end. The piece cut-off, or spall, moves off with a velocity which largely depends on the applied pressure pulse characteristics. Multiple fractures at specific points along the bar are produced, which suggests that this method has potential in the field of fracturing from one long bar, a number of smaller bars of different lengths by the application of a single blow. The particular advantage of this method, namely, that no tool is required in the fracture region, thus commends itself as a valuable method of cutting super alloys, concrete slabs, rocks and ceramics in situations where contamination due to tool contact is not desirable. A simple one-dimensional wave theory is presented to assist in the understanding of the mechanics of the process.

NOTATION

A	cross-sectional area of the specimen
C_0	wave speed in a long bar = $\sqrt{(E/\rho_0)}$
C	dilatational wave speed in a bar with restricted lateral expansion
E	Young's modulus
L	length of bar
M	mass of striker
N	an integer
S	fracture tensile stress
T	period of a sinusoidal pressure pulse
e_x, e_y, e_z	strains in x, y and z directions
l	length of discontinuity
m	mass per unit length of bar
t	time
u	particle displacement at a section distant x from the point of loading
V	particle velocity
x	distance along the bar
δ	length of spall
λ	stress pulse time constant and Lamè constant
μ	coefficient of rigidity
ν	Poisson's ratio
ρ	density
σ	stress
Suffixes	
I	incident
R	reflected
T	transmitted

INTRODUCTION

This work is aimed at constructively utilizing the long known, but inadequately understood phenomenon of fracture due to stress waves. The characteristic features that typify the phenomenon are (i) that the high speed loading is accomplished in a few micro-seconds, (ii) the transient nature of the applied stress pulse, (iii) the reflection and destructive interaction of stress waves and (iv) that the damage is generally located remote from the point of application of the load.

Some of the chief sources of impulsive loading are high-velocity impact of projectiles, water hammer and explosions. The effects are commonly discerned in the form of partial cracks, or total fractures, depending on the relative strength of the impulse, its duration, properties of the material and its geometry. The various pieces that fracture from the parent body are called scabs. The term spalling applies specifically to bars.

Fig. 1 shows a bar of freely supported brittle material whose compressive strength is much greater than its tensile strength, subjected to explosive attack at one end resulting in multiple spalling at the free end. Spallation is the result of tensile reflection from the free end of the bar of the transient compressive pulse induced by the explosion. The number of spalls depends on the ratio of the compressive to tensile strength. The lengths and escape velocities of the spalls depend on the pulse shape.

*Department of Mechanical Engineering, UMIST

Origins of the problem and related investigations

The first observation on fracture due to stress waves seems to have been made by John Hopkinson¹ about a century ago, in his experiments 'On the rupture of iron-wire by a blow'. His work was followed up by his son, Bertram², and a number of other workers³ at the turn of the century. The impetus for further work in this field came during the Second World War when aerial bombardment as well as field artillery was sometimes turned on to both military and civilian targets.

The military engineers^{4,5} are primarily concerned with the destruction caused to buildings, underground shelters, bunkers and other structures, and this has led to the study of penetration, scabbing, perforation and cavity formation. It was observed for instance that a missile which could penetrate x feet into a semi-infinite block of concrete could also perforate a wall of the same material of thickness $2x$ feet. On examination this was attributed to scabbing from a near free surface, which assisted perforation.

Another vitally important phenomenon that was found was the scabbing of the inner face of walls of tanks and armoured vehicles when subjected to attack by shells, bombs and mines in contact with the outer surface. A more recent development is the study of seismic effects and the cracking of subterranean rock due to underground nuclear explosions⁶. Industrial interest in the phenomenon mainly centres around comminution of rock⁷ and fracture during explosive and shock hardening of metals⁸.

An interesting investigation reported by Miklowitz⁹ concerns the tensile testing of brittle materials in which it was noted that fractures were produced at two different cross-sections of the specimen when the rupture load was reached. Experiments were conducted on plexi-glass at a loading rate of 300 lb/min and on high-strength steel at 2000 lb/min. The situation was analysed by considering that two

types of waves emanate from the initial rupturing section. One is a longitudinal compression wave which is, in fact, an unloading wave associated with the decrease in load in the fracture process. The other is a group of flexural strain waves produced by the moment that develops as the crack propagates across the bar from its origin at a surface of discontinuity. It was found that the second fracture usually occurred at a gauge cross-section adjacent to the specimen head farthest from the initial fracture surface. It was shown in the analysis that this second failure is due to the superposition of the longitudinal strain from the unloading wave which, through reflections, becomes tension and the resulting flexural strain, which together exceed the original tensile fracture strain.

Many other related investigations are reported in the literature on stress waves, e.g. that of Davies¹⁰, Rinehart¹¹⁻¹³, Kolsky^{14,15}, and more recently Johnson¹⁶.

Present work

The present work is an exploratory attempt to make use of spalling in bars due to impact loads as a method of cutting brittle materials. The particular advantage of this method lies in the absence of any cutting tool. Preliminary tests were made on rectangular and round bars which were subjected to contact explosives and the impact of bullets at one end. The possibility of cutting from one bar a number of smaller bars of different length in one single blow is investigated.

Fracture at several sections along the bar is promoted by the introduction of grooves or localized external radial compression at the section to be cut. This paper also aims at presenting a rudimentary analysis which assists in the understanding of the process and investigates the influence of the important parameters.

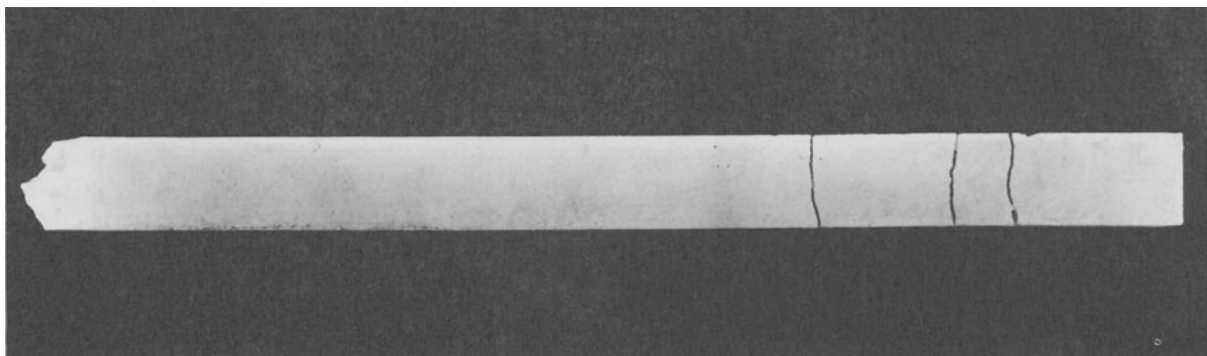


Fig. 1 Multiple spalling in a 1.0×1.0 in section, 15 in long plaster-of-paris bar.

APPARATUS AND MATERIALS

The procedure in all tests was rather simple and efforts were made to keep it to a minimum. Two types of loading methods were employed. The first was contact explosive loading which mainly involved the firing of an I.C.I. No. 6 detonator at one end of the specimen. The second was impact loading by a striker which involved the firing of a mild steel bullet from a 0.25 calibre gun at one end of the bar.

In every test the specimen was supported on a stretched fine wire mesh and positioned accurately so that impact takes place collinearly.

Owing to its sensitivity to impact loading, Perspex was chosen as the material for such preliminary investigation. One-foot long bars of $\frac{3}{8} \times \frac{3}{8}$ in cross-section and $\frac{3}{8}$ in diameter section were tested. The rectangular bars were cut from Perspex sheet whilst the circular rods were cut from rods of as-bought longer length bars. Grooves of rectangular and V-shapes of various sizes and angles were milled at various sections along the bars so that a variety of specimens were made available. Experimental results were obtained for straight uniform bars with localized ring load; the latter was applied through circular rings made from piano wire which was pressed into the surface of the bar by means of a clamp loaded at three symmetrical points around the ring.

EXPERIMENTAL RESULTS

Numerous tests were carried out on various bars having various discontinuities along their length and under various conditions of loading and supports. Some of the results are summarized below.

Explosive cutting of rectangular bars

A uniform $\frac{3}{8} \times \frac{3}{8}$ in cross-section, 12 in long Perspex bar was subjected to explosive pressure from a single I.C.I. No. 6 detonator in contact with one end. A spall 17/16 in long was flung free as shown in Fig. 2, specimen 1. The fracture took place at a section perpendicular to the axis of the bar. Another bar, specimen 2, of the same dimensions as the previous one but containing an all-round rectangular groove 1/32 in deep and $\frac{1}{4}$ in wide cut at a section 1.0 in away from the free end was subjected to the same explosive; the fracture in this case occurred at the sections of discontinuity forming two cut-off pieces as shown in Fig. 2. When the position of the neck was made $\frac{1}{2}$ in and 1.5 in away from the free end, fracture always took place at all the sections of discontinuity. When two more similar bars with wider necks of 1/32 in deep but $\frac{3}{8}$ in wide situated at 1.0 in away from the free end were used, similar behaviour was observed.

Bars with more than one neck were also subjected to an explosive pulse. The aim was to obtain several cuts at specified positions along the bar in one shot. A bar, specimen 3, with two necks $\frac{1}{2}$ in apart, each 1/32 in deep and $\frac{1}{4}$ in wide situated $\frac{1}{2}$ in away from the free end, when subjected to explosive pressure, produced fractures at the two necks. However, fracture did not take place at the farthest section of discontinuity as shown in Fig. 2. Several more bars with

narrower necks gave similar results, although the single unfractured section of discontinuity within the farthest neck alternated from one discontinuity to the other. When bars having three necks each, 1/32 in deep and 3/32 in wide, situated at $\frac{1}{2}$ in distance from the free end were tested, complete fracture consistently took place in all the necks. However, two sections of discontinuity were found always to remain uncut.

In almost all the above necked specimens the fracture seems to have consisted of male and female parts as shown in Fig. 3a. In occasional instances the fracture was a cross as shown in Fig. 3b. Another common feature was the shatter of about $\frac{1}{2}$ in at the loaded end of the specimen due to the high compressive applied pressure.

Explosive tests were also made on rectangular bars with rectangular grooves only on two parallel sides of the bar. Similar results were observed. Fractures occurred at the grooves but not necessarily at every section of discontinuity. It was found, however, that as the grooves became narrower and shallower the cut sections tended to be better defined and of flatter surface. In Fig. 4, specimen 4 is a typical fractured bar with grooves of 1/128 in depth and 1/128 in width made at two parallel sides of the bar.

Bars with more than three grooves gave encouraging results. Fig. 4 shows fractured specimens 5, 6, 7 and 8 originally having 4, 5, 6 and 7 rectangular grooves, respectively. Each groove was 1/32 in deep and 1/32 in wide. Another set of bars with V-shaped grooves of various angles and depth on two sides of the bars were tested. Much the same result was obtained as with bars having rectangular grooves. However, the cut-off surfaces in most of these cases seemed to be more even.

Stress wave cutting of circular bars

Round Perspex rods of $\frac{3}{8}$ in diameter and 12 in long with single all-round rectangular grooves were subjected to explosive pressure at one end. Fracture took place at sections of discontinuity along the bar in a way almost identical with that of rectangular bars. Bars with more than three necks placed at half inch increments from the free end seem to be cut at at least three discontinuities producing at least three smaller bars. However, as with rectangular bars, it was found that the narrower the groove the cleaner the cut. The shape of fracture is in most cases a shallow cup and cone as shown in Fig. 3c.

Attempts were made to cut uniform Perspex rods at several sections along the length without having to initially introduce grooves at these sections. Mild-steel wire 0.03 in diameter was wrapped once around each section to form a ring and was then compressed at three points equally positioned on the periphery to secure localized cutting of the Perspex at the chosen sections. On explosively loading at the far end of the rod, fracture took place at the compressed sections. When more than three stations of localized pressure were applied at $\frac{1}{2}$ in intervals from the free end, fracture did not always occur at the other furthest stations. It seemed, however, that a compressed region along the bar caused similar behaviour as with a groove. The fractured surfaces in all these experi-

ments were found to be rough and a typical section is shown in Fig. 3d.

Impact loading by bullets

Preliminary tests were made into the fracture of Perspex rods due to the impact of a bullet. The $\frac{3}{8}$ in uniform Perspex rod spalled at a number of sections along the length when struck by a $\frac{3}{8}$ in diameter

mild-steel bullet moving at 700 ft/s. However, when grooves were introduced, fracture took place at all discontinuities. The fractures were mainly of cup and cone type. Difficulties were encountered in accurately positioning the rod so that collinear impact is secured. Fracture in such cases occurred at more sections and a greater number of smaller bars were produced than in the case of explosive loading.

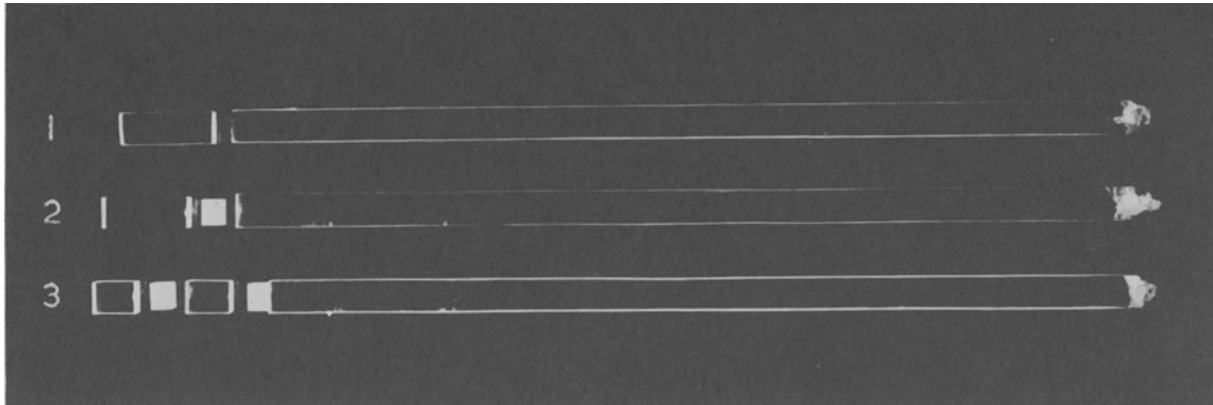


Fig. 2 Fracture $\frac{3}{8} \times \frac{3}{8}$ in section, 12.0 in long Perspex bars with peripheral grooves subjected to explosive pressure at one end.

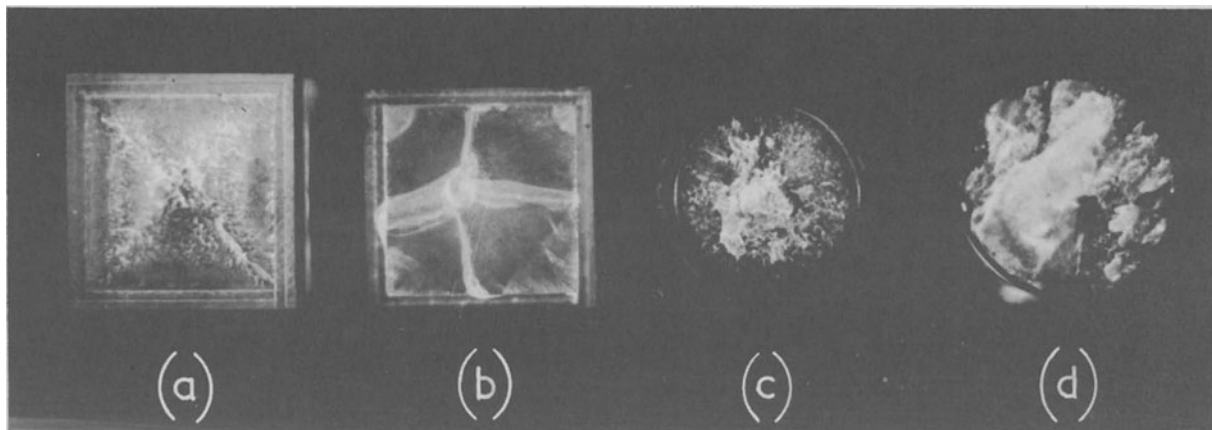


Fig. 3 Fracture patterns at sections of discontinuity. In (a) and (b) explosive loading of rectangular perspex bars with peripheral grooves, (c) impact loading of circular bars with peripheral grooves and (d) explosive loading of uniform circular bars with peripheral compression at a section along the length.

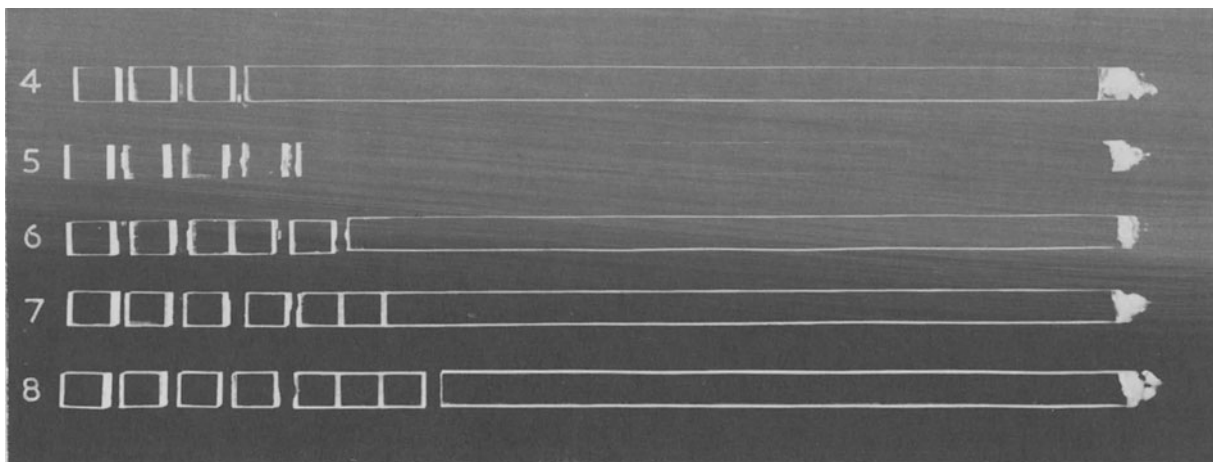


Fig. 4 Stress wave fracturing of rectangular Perspex bars with grooves on two parallel sides.

ANALYSIS

A comprehensive analysis of any of the situations described above is rather difficult. However, a rudimentary analysis based on the one-dimensional wave theory is now presented to assist in the understanding of stress-wave transmission in bars of uniform section but containing discontinuities. It is hoped that further extensions of the simplified analysis may assist in the design of proper facilities to readily control the process.

Elementary analysis of elastic stress wave in a long uniform rod

Fig. 5 shows a uniform isotropic rod transmitting a stress pulse along its length. Let u denote the displacement undergone by a plane AB in the rod which is originally distance x from O, the left-hand end of the bar which is the origin in the rod.

Then $[u + (\partial u/\partial x)\delta x]$ is the displacement of a plane A'B' which is parallel to AB but initially distant $(x + \delta x)$ from O in the unstrained state. A disturbing force applied uniformly at time $t = 0$, over the plane $x = 0$, will cause an elastic stress σ to be propagated and to be effective over typical plane AB at time t . It will be assumed that the stress is related to strain through Hooke's law and that displacements are small and elastic.

An accurate analytical treatment of such a situation would be cumbersome and it is necessary to make simplifying assumptions. It will be assumed that the effect of transverse strain and transverse inertia on the longitudinal equilibrium of the bar are negligibly small. The gravitational and all dissipative (e.g. damping) forces are taken to be negligible. Furthermore, the diameter of the rod is assumed to be much smaller than the pulse length of the applied force.

The net force on element ABB'A' causes it to accelerate so that the equation of motion for an element of rod of cross-sectional area A_0 is

$$\frac{\partial \sigma}{\partial x} = \rho_0 \frac{\partial^2 u}{\partial t^2} \quad (1)$$

where ρ_0 is the density of the material in the unstressed condition. The strain in an element of length δx is $\partial u/\partial x$ and thus

$$\sigma = E \frac{\partial u}{\partial x} \quad (2)$$

where E is the Young's modulus. Combination of equations (1) and (2) yields

$$\frac{\partial^2 u}{\partial t^2} = C_0^2 \frac{\partial^2 u}{\partial x^2} \quad (3)$$

where $C_0 = \sqrt{E/\rho_0}$ (4)

Equation (3) is a wave equation whose general solution is of the form

$$u = f(x - C_0 t) + F(x + C_0 t) \quad (5)$$

in which C_0 represents the speed of propagation. The

wave $f(x - C_0 t)$ is a forward travelling wave whilst $F(x + C_0 t)$ is a backward moving wave of different shape and size. The speed of movement of a particle in the bar is $\partial u/\partial t$, and denoting this by V we have

$$\sigma = E \frac{\partial u}{\partial x} = \frac{E}{C_0} \frac{\partial u}{\partial t} = \frac{E}{C_0} V \quad (6)$$

or substituting for E we obtain

$$\sigma = \rho_0 C_0 V \quad (7)$$

The quantity $\rho_0 C_0$ is often referred to as the mechanical impedance of the bar.

A stress pulse of a certain shape when imposed on one end of the bar will travel towards the other end with a constant speed C_0 . As long as no change in cross-section or in the material or stress system on the bar occurs, the stress pulse may be assumed to remain undistorted.

Reflection and superposition of stress waves

Equation (3) is linear and solutions to it may be superimposed, i.e. when more than one stress wave travels through the bar the net stress on, or the speed of particles in, a given plane are easily obtained by adding together the separate effects of the operative waves at that plane.

It is worth noting that (i) in a tensile-stress pulse the direction of propagation and the direction of particle movement are opposite, whilst (ii) in a compressive pulse the direction of propagation and the direction of particle movement are the same.

When a stress pulse meets a change in cross-section or in the material of the bar, reflection and transmission will take place at the boundary. For a free-ended bar the stress at the free end should remain zero for all time. This requirement when imposed on the stress wave as it arrives at the free surface necessitates a reflection of the wave with a negative stress travelling in an opposite direction to the incident wave. Similarly, in a fixed ended bar the particle displacement at that end remains zero all the time. This would necessitate a reflection of the wave without change in shape or intensity. Of course, when the incident and reflected waves can no longer be superimposed on each other at any section, they continue to be propagated without alteration in shape.

Spalling of a free-ended bar due to reflection of a compressive stress wave from a free boundary

Stress waves of various shapes occur in practice but the most common shape is an exponentially decaying stress pulse with a sharp front, as shown in Fig. 6a. This usually arises in an elastic material after attack by an explosive or the impact of a rigid mass on the surface. A typical exponential stress pulse is of the form

$$\sigma = \sigma_0 e^{-C_0 t/\lambda} \quad (8)$$

where σ_0 is the initial stress and λ/C_0 is the time constant.

On application of this stress to one end* of a freely supported bar, it travels towards the other end where it will be reflected, as shown in Fig. 6b. The compressive stress is reflected as a tensile stress and, at an intermediate interval when the reflected wavefront arrives at D, the total stress at the bar is the resultant of both the incident and reflected waves, as shown in Fig. 6c. The incident part of the pulse continues to travel towards the free end and the reflected part of the pulse continues to travel away from the free end until the pulse is wholly reflected as a tensile pulse as shown in Fig. 6d.

A material which possesses high compressive strength can deliver high compressive stress waves. On reflection, however, the large tensile stress front could well exceed the on-coming incident compressive stress by an amount larger than the tensile strength of the material of the bar. When such a situation develops at a section D, distant δ from the free end, fracture 'spalling' takes place and portion DF flies off carrying with it a momentum which is determined by the shape of the trapped part of the stress pulse. For spalling to develop in a bar of material which has a tensile strength S , therefore, we must have

$$S = \sigma_o - \sigma_o e^{-C_o t_1 / \lambda} \quad (9)$$

where t_1 is the time which the wavefront σ_o takes to traverse the length DF and back again to location D. In terms of distance along the bar $t_1 = 2\delta / C_o$ and equation (9) reduces to

$$S = \sigma_o (1 - e^{-2\delta / \lambda}) \quad (10)$$

or

$$\delta = \lambda \ln \frac{1}{(1 - S/\sigma_o)^{1/2}} \quad (11)$$

The new fracture surface will act as a second free boundary which causes the oncoming incident compressive stress in the bar to be reflected; and in a similar way further spalls may be engendered. It is thus easy to see how successive fractures or spalls may be created. It can be shown that the N th spall length is $\lambda \ln [1/(1 - NS/\sigma_o)^{1/2}]$ provided $S < \sigma_o/N$.

The momentum I_1 carried away by the first spall is found from

$$\begin{aligned} I_1 &= \int_0^{2\delta/C_o} A_o \sigma dt \\ &= \frac{A_o \sigma_o}{C_o} (1 - e^{-2\delta/C_o}) \end{aligned} \quad (12)$$

Measurements of the momentum of each spall can be used to deduce the shape of the applied pulse. The approximate shape of the pulse can also be obtained from a knowledge of the tensile strength of the bar and the length of each spall in a multiple spalling operation.

Spalling of a free-ended bar struck by a rigid mass

The situation envisaged is that in which a rigid striker of mass M impinges with a speed V_o on the end of a long bar which is freely supported. The equation of motion for M is

$$M \frac{dV}{dt} = -A_o \sigma \quad (13)$$

where σ is the stress intensity at the interface between the bar and mass M at time t , V is the speed of the interface, A_o is the cross-sectional area of the bar and ρ_o its density.

From equations (7) and (13) we obtain

$$M \frac{dV}{V} = -\rho_o C_o A_o dt$$

Integrating and noting that $V = V_o$ at $t = 0$, we obtain

$$V = V_o e^{-\rho_o A_o C_o t / M} = V_o e^{-m C_o t / ML} \quad (14)$$

where m and L represent the mass and length of the bar respectively.

Alternatively using equation (7), the stress at the interface is

$$\sigma = \sigma_o e^{-m C_o t / ML} \quad (15)$$

This is of the same form as equation (8) with the time constant $\lambda = ML/m$. This stress pulse travels along the bar until it is reflected at the free end. When the conditions of equations (9) or (10) are fulfilled, spalling takes place.

Spalling due to explosive and other pressure pulses

An explosion at one end of a bar generates a stress wave well described by equation (8). For simplicity it is sometimes approximated to a straight line of negative gradient given by C_o/λ . However, equations (8) to (12) are evidently valid and spalling is effected whenever the conditions of equation (9) are satisfied.

Other pressure pulses may also cause fracture at the free end of the bar. A single sinusoidal pressure pulse, for example, may produce a fracture at distance δ from the free end where,

$$\delta = \frac{T C_o}{4\pi} \sin^{-1} \left(\frac{S}{P_o} \right) \quad (16)$$

when the input pulse is of the form

$$P_o \sin \left(\frac{2\pi t}{T} \right) \left[1(t) - 1\left(t - \frac{T}{2}\right) \right]$$

and $1(t)$ is the Heavyside unit step function.

Propagation of stress waves in a bar of restricted lateral expansion

We consider a long bar which has its lateral dimensions completely restrained. The stresses due to the restraints in the lateral directions y and z will affect the strains in the axial direction, x , and the elasticity equations are

$$e_x = \frac{1}{E} (\sigma_x - \nu \sigma_y - \nu \sigma_z) \quad (17)$$

*Strictly, on loading, the stress distribution is three-dimensional in the first diameter of the bar.

$$e_y = \frac{1}{E} (\sigma_y - \nu\sigma_z - \nu\sigma_x) \quad (18)$$

$$e_z = \frac{1}{E} (\sigma_z - \nu\sigma_y - \nu\sigma_x) \quad (19)$$

For $e_y = e_z = 0$ we find

$$e_x = \frac{(1 + \nu)(1 - 2\nu)}{(1 - \nu)} \cdot \frac{\sigma_x}{E} \quad (20)$$

or using Lamé's constants λ and μ

$$\sigma_x = (\lambda + 2\mu) e_x \quad (21)$$

$$\text{where } \lambda = \frac{E}{(1 + \nu)(1 - 2\nu)}$$

$$\text{and } \mu = \frac{E}{2(1 + \nu)}$$

Differentiation of equation (21) with respect to x and combination with equation (1) yields

$$\frac{\partial^2 u}{\partial t^2} = C_l^2 \frac{\partial^2 u}{\partial x^2} \quad (22)$$

where the speed of longitudinal wave propagation is

$$C_l = \left(\frac{\lambda + 2\mu}{\rho_o} \right)^{1/2} \quad (23)$$

Propagation of stress waves along a bar with part of its length restricted in lateral expansion

The situation considered is shown in Fig. 7a in which an incident compressive stress wave of intensity σ_I is travelling through bar OABC. The region AB is under radial external pressure which is large enough to constrain any lateral expansion in that region. The wave speed in bars OA and BC is C_o and in AB is C_l .

On entering AA' the incident stress wave σ_I must be reflected and transmitted to allow for the sudden change in condition of stress at the discontinuity. For equilibrium of axial forces at section AA'

$$A_1 (\sigma_I + \sigma_{R1}) = A_2 \sigma_{T1} \quad (24)$$

where A_1 and A_2 are the cross-sectional areas of the free and restrained parts respectively, σ_{R1} is the intensity of the reflected stress wave and σ_{T1} of the transmitted stress wave.

The velocity of the particles at section AA' is V_{T1} where

$$V_I - V_{R1} = V_{T1} \quad (25)$$

and V_I and V_{R1} are the velocities of particles in bar OA due to σ_I and σ_{R1} respectively. Substitution of

$$\sigma_I = \rho_o C_o V_I, \quad \sigma_{R1} = \rho_o C_o V_{R1}$$

and

$$\sigma_{T1} = \rho_o C_l V_{T1}$$

into equation (25) and solving for σ_{T1} and σ_{R1} from equation (24) and (25) give for $A_1 = A_2$,

$$\sigma_{T1} = \frac{2C_l}{C_l + C_o} \sigma_I \quad (26)$$

and

$$\sigma_{R1} = \frac{C_l - C_o}{C_l + C_o} \sigma_I \quad (27)$$

The transmitted stress σ_{T1} will now be propagated through region AB until it arrives at section BB' where again it will undergo transmission into BC to be of intensity σ_{T2} and reflection back to AA' at σ_{R2} . Repeat of equation (24) and (25) for section BB' gives

$$\sigma_{T2} = \frac{2C_o}{C_l + C_o} \sigma_{T1} = \frac{4C_l C_o}{(C_l + C_o)^2} \sigma_I \quad (28)$$

and

$$\sigma_{R2} = \frac{C_o - C_l}{C_l + C_o} \sigma_{T1} = \frac{-2C_l(C_l - C_o)}{(C_l + C_o)^2} \sigma_I \quad (29)$$

where the negative sign identifies σ_{R2} as tensile.

The behaviour of the stress wave in the bar after the second transmission depends on the lengths of AB, BC and the pulse length of the stress wave. For simplicity we now consider the case when the length of AB, l , is larger than the length of BC and the pulse length. Hence, σ_{T2} will travel towards the free end of the bar CC' where it will be reflected as $\sigma_{T3} = -\sigma_{T2}$. The reflected stress σ_{T3} travels towards BB' and on encountering region AB a stress σ_{T4} will be transmitted through BB', and a stress σ_{R4} will be reflected back towards end C. The values of these stresses are

$$\sigma_{T4} = \frac{2C_l}{C_l + C_o} \sigma_{T3} = \frac{-8C_l^2 C_o}{(C_l + C_o)^3} \sigma_I \quad (30)$$

and

$$\sigma_{R4} = \frac{C_l - C_o}{C_l + C_o} \sigma_{T3} = \frac{-4C_l C_o (C_l - C_o)}{(C_l + C_o)^3} \sigma_I \quad (31)$$

Now the total stress σ' at a section just inside region AB behind BB' at the instant σ_{T4} enters BB' is given by the sum of σ_{T4} and that of the on-coming stress σ_{T1} and σ_{R2} which are now twice the length of BC behind σ_{T4} . For an exponential pulse of a shape described by equation (9) we have

$$\begin{aligned} \sigma' = & \frac{-8C_l^2 C_o}{(C_l + C_o)^3} \sigma_o + \frac{2C_l}{C_l + C_o} \sigma_o e^{-2\delta/\lambda} \\ & - \frac{2C_l(C_l - C_o)}{(C_l + C_o)^2} \sigma_o e^{-2\delta/\lambda} \end{aligned} \quad (32)$$

or

$$\sigma' = \frac{-8C_l^2 C_o}{(C_l + C_o)^3} \left[1 - \frac{1}{2} \left(1 + \frac{C_o}{C_l} \right) e^{-2\delta/\lambda} \right] \sigma_o \quad (33)$$

where δ is the length of BC.

On the other hand, the total stress σ'' at the same instant just outside the restrained region next to BB' is given by the sum of stresses σ_{T3} , σ_{R4} and the oncoming stress σ_{T2} which lags at distance $2\delta/C_o$ behind σ_{T3} . Hence

$$\begin{aligned} \sigma'' = & \frac{-4C_l C_o}{(C_l + C_o)^2} \sigma_o - \frac{4C_l C_o (C_l - C_o)}{(C_l + C_o)^3} \sigma_o \\ & + \frac{4C_l C_o}{(C_l + C_o)^2} \sigma_o e^{-2\delta/\lambda} \end{aligned}$$

or

$$\sigma'' = \frac{-8C_l^2 C_o}{(C_l + C_o)^3} \sigma_o \left[1 - \frac{1}{2} \left(1 + \frac{C_o}{C_l} \right) e^{-2\delta/\lambda} \right] \quad (34)$$

which is the same as σ' and would be expected because $A_1 = A_2$.

If fracture is to take place at BB' at the instant of arrival of σ_{T3} at BB' , the condition

$$S = \frac{8 C_l^2 C_o}{(C_l + C_o)^3} \sigma_o \left[1 - \frac{1}{2} \left(1 + \frac{C_o}{C_l} \right) e^{-2\delta/\lambda} \right] \quad (35)$$

must be satisfied, where S is the critical tensile fracture stress. However, if $l \ll \delta$ a complicated situation would arise due to the multi-reflections of stresses in the region AB. In such a situation, before σ_{T2} reaches the free end C and is reflected back to BB' , other stresses will have been transmitted through BC which originally arose from multiple reflections and transmission of σ_{R2} at boundaries BB' and AA' . A series of small amplitude stresses, all compressive for $C_l > C_o$, will be propagated through BC behind σ_{T2} . The time lag of each of these is $2l/C_l$; that is, the time for each σ_R to traverse twice across AB.

It is particularly interesting to note that because C_l is slightly larger than C_o , the factor $8C_l^2 C_o / (C_l + C_o)^3$ in equation (35) is larger than unity. For $\nu = \frac{1}{3}$ the factor is approximately 1.3. Hence, introduction of a radial compression at a section along the bar assists fracture at that section.

Stress wave transmission through stepped bars

The introduction of a groove in a bar reduces the cross-sectional area of the bar so that an incident stress wave will be reflected and transmitted at the section of discontinuity. Notwithstanding the dispersive nature of the longitudinal stress wave we assume that simple plane-wave theory still applies.

We consider an incident elastic wave of compressive stress of intensity σ_I moving to the right, see Fig. 7b, through the bar of cross-sectional area A_1 . This is partly reflected and partly transmitted at the surface of the discontinuity AA' . The stress wave transmitted into region AB of intensity σ_{T1} and that which is reflected back through bar AO, σ_{R1} may be found in a similar manner as through equations (24) and (25). Solutions of equations (24) and (25), after appreciating that $\sigma_I = \rho_o C_o V_I$, $\sigma_{R1} = \rho_o C_o V_{R1}$ and $\sigma_{T1} = \rho_o C_o V_{T1}$, yield

$$\sigma_{R1} = \frac{A_2 - A_1}{A_2 + A_1} \sigma_I$$

and

$$\sigma_{T1} = \frac{2A_1}{A_2 + A_1} \sigma_I$$

or putting $A_1/A_2 = n$,

$$\sigma_{R1} = \frac{1-n}{1+n} \sigma_I \quad (36)$$

and

$$\sigma_{T1} = \frac{2n}{1+n} \sigma_I \quad (37)$$

It is clear from equation (36) that for $n > 1$, σ_{R1} is negative, indicating a tensile wave. This is consistent with the statement made concerning reflection of a stress wave at a free surface. For a free surface we have $n \rightarrow \infty$ and hence $\sigma_{R1} \rightarrow -\sigma_I$, and for a rigid end we have $n \rightarrow 0$ and $\sigma_{R1} \rightarrow \sigma_I$.

In a similar manner to the partially restrained bar the stress wave behaviour after the second transmission is governed by the relative lengths of AB, BC and the pulse length. However, we now consider a stepped bar with a neck of length, l , which is smaller than BC. Measure time t from the instant at which σ_I enters into AA' and consider that σ_I is of exponential form given by equation (8). The situation at $t = 0$ is shown in Fig. 8a and at $t = l/C_o$ is shown in Fig. 8b. The value of n is assumed large enough not to cause a gross increase in σ_{R1} to effect fracture along OA.

We concentrate on the progress of σ_I as it propagates through the stepped bar. After passing into the end portion of bar BC, through the second change in area BB' , σ_{T1} will be transmitted and reflected as σ_{T2} and σ_{R2} respectively, as shown in Fig. 8c. We have

$$\sigma_{T2} = \frac{2}{1+n} \sigma_{T1} = \frac{2}{1+n} \cdot \frac{2n}{1+n} \sigma_I \quad (38)$$

and

$$\sigma_{R2} = \frac{(n-1)}{(n+1)} \sigma_{T1} = \frac{2n}{(n+1)} \cdot \frac{(n-1)}{(n+1)} \sigma_I \quad (39)$$

At $t = 2l/C_o$, σ_{R2} arrives at section AA' and the wavefront of σ_{T2} penetrates a distance l into bar BC as shown in Fig. 8d. After passing into the end portion of bar OA, through the first change in area AA' , σ_{R2} will be transmitted and reflected as σ_{T3} and σ_{R3} respectively. The situation at $t = 5l/2C_o$ is shown in Fig. 8e. We have

$$\begin{aligned} \sigma_{T3} &= \frac{2}{1+n} \sigma_{R2} \\ &= \frac{2}{1+n} \cdot \frac{(n-1)}{(n+1)} \cdot \frac{2n}{1+n} \sigma_I \quad (40) \end{aligned}$$

and

$$\begin{aligned} \sigma_{R3} &= \left(\frac{n-1}{n+1} \right) \sigma_{R2} \\ &= \left(\frac{n-1}{n+1} \right) \cdot \left(\frac{n-1}{n+1} \right) \cdot \frac{2n}{1+n} \sigma_I \quad (41) \end{aligned}$$

At $t = 3l/C_o$, σ_{R3} arrives at section BB' and the wavefront of σ_{T2} is at distance $2l$ from BB' into bar BC and the wavefront of σ_{T3} penetrates a distance l into bar OA. The reflected stress σ_{R3} is compressive and it adds to the stress originally available from the tail of σ_{T1} . On the other hand, the transmitted compressive stress σ_{T3} is superimposed on the tail of σ_I

which is compressive and on the tail of σ_{R1} in OA which is tensile.

After passing into the end portion of bar BC, through BB', σ_{R3} will be transmitted and reflected as σ_{T4} and σ_{R4} respectively. The situation at $t = 4l/C_0$ is shown in Fig. 8f. We have

$$\begin{aligned} \sigma_{T4} &= \frac{2}{(1+n)} \sigma_{R3} \\ &= \frac{2}{(1+n)} \left(\frac{n-1}{n+1} \right)^2 \frac{2n}{(n+1)} \sigma_1 \end{aligned} \quad (42)$$

and

$$\begin{aligned} \sigma_{R4} &= \left(\frac{n-1}{n+1} \right) \sigma_{R3} \\ &= \left(\frac{n-1}{n+1} \right)^3 \cdot \frac{2n}{(n+1)} \sigma_1 \end{aligned} \quad (43)$$

As time passes, the stress in the neck AB will undergo multiple reflections and transmissions at the discontinuities until no further stress remains in the neck. The situation is such that the stress wave in bar BC will be comprised of a number of superimposed transmitted compressive pulses, the wavefronts of which are at constant intervals of $2l$ behind the wavefront of σ_{T2} , as shown in Fig. 8g. Similarly a series of reflected stress pulses will be travelling in bar OA towards O. The only tensile stress in OA will be due to σ_{R1} and the rest are compressive. The function of the neck, therefore, seems to be to reduce the effective decay of the incident stress pulse.

The total stress transmitted in BC can be described as

$$\begin{aligned} \sigma_T &= \sigma_{T2} + \sigma_{T4} \mathbf{1} \left(t - \frac{2l}{C_0} \right) + \\ &+ \sigma_{T6} \mathbf{1} \left(t - \frac{4l}{C_0} \right) + \dots \end{aligned} \quad (44)$$

Substituting for σ_{T2} , σ_{T4} and σ_{T6} ...etc. and noting that σ_1 is exponential, viz. equation (8), we obtain

$$\begin{aligned} \sigma_T &= \frac{4n}{(n+1)^2} \sigma_0 e^{-C_0 t/\lambda} \left\{ 1 + e^{2l/\lambda} \left(\frac{n-1}{n+1} \right)^2 \mathbf{1} \left(t - \frac{2l}{C_0} \right) \right. \\ &+ e^{4l/\lambda} \left(\frac{n-1}{n+1} \right)^4 \left(t - \frac{4l}{C_0} \right) + e^{6l/\lambda} \left(\frac{n-1}{n+1} \right)^6 \mathbf{1} \left(t - \frac{6l}{C_0} \right) \\ &\left. \dots + e^{\frac{2(N-1)l}{\lambda}} \left(\frac{n-1}{n+1} \right)^{2(N-1)} \mathbf{1} \left[t - \frac{2(N-1)l}{C_0} \right] \right\} \end{aligned} \quad (45)$$

The value of the interger N is decided by the time at which σ_T is evaluated. However, as $l \rightarrow 0$, $N \rightarrow \infty$, and equation (45) gives the propagation in a uniform bar.

$$\begin{aligned} \sigma_T \Big|_{l \rightarrow 0} &= \frac{4n}{(n+1)^2} \sigma_0 e^{-C_0 t/\lambda} \left[\frac{1}{1 - \left(\frac{n-1}{n+1} \right)^2} \right] \\ &= \sigma_0 e^{-C_0 t/\lambda} \end{aligned} \quad (46)$$

The train of transmitted pulse in BC will be reflected at the free surface CC' and become σ'_T (tensile). This stress wave travels towards BB' and superimposes itself on the tail of σ_T which is still

moving on. If at a section along BC the reflected tensile stress exceeds the on-coming compressive tail by an amount just greater than the tensile strength of the bar, fracture takes place at that section. However, due to the neck, the oncoming compressive tail stress magnitude is higher at a section in BC than it would be if the neck were absent. Therefore, spall length tends, in the case of a stepped bar, to be larger. If on the other hand the stress was not large enough to produce fracture along BC, the reflected tensile stress σ'_T would penetrate into the neck BC through BB' and, in a similar manner to that which was undergone by the original stress σ_1 , would be transmitted and reflected as σ'_{T1} and σ'_{R1} respectively. The value of σ'_{T1} is higher than σ'_T , so that when it is large enough, fracture will be promoted at section BB'. Using these same arguments the total stress at section AA' at the moment σ'_{T1} penetrates into bar OA is higher than σ'_{T1} and the possibility of fracture taking place at section AA' is even greater.

For similar reasons the introduction of more necks in the bar assists fracture at the necks. Analysis of stress transmission in a bar with more than one neck is rather complicated. It is even more tedious to include secondary stress release waves when fracture occurs at a section of discontinuity.

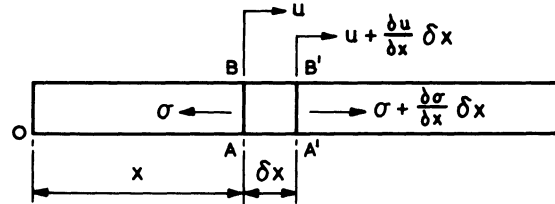


Fig. 5 Diagram of element in bar carrying a stress wave.

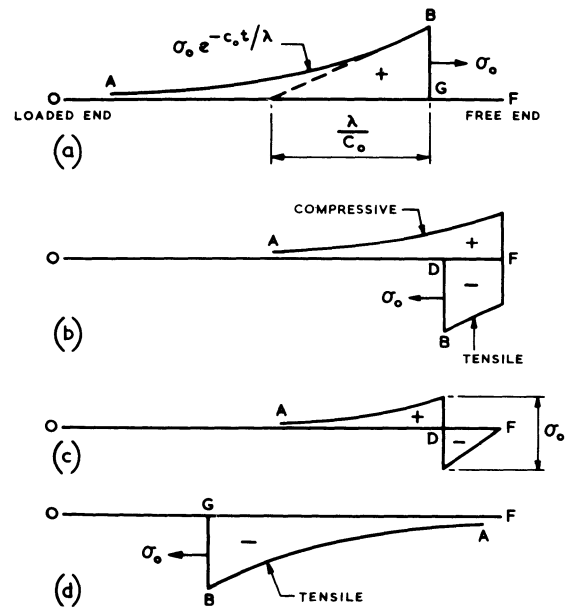


Fig. 6 Transmission and reflection at a boundary of an exponential stress pulse (a) before reaching the free end, (b) reflection of a portion of the pulse at the free end, (c) resultant stress state at the bar at the instant the wavefront arrives at section D, (d) the stress pulse completely reflected as a tensile wave travelling towards the loaded end.

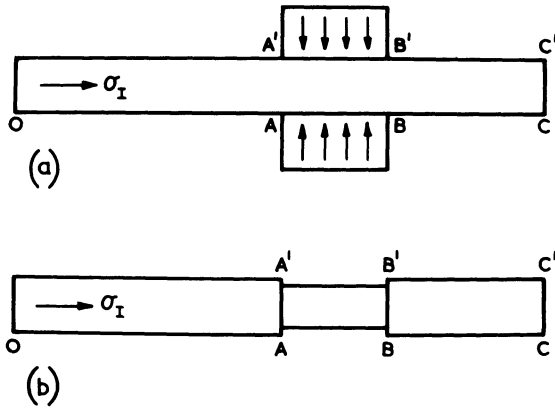


Fig. 7 Line diagrams of a bar subjected to an incident stress wave of intensity σ_I . (a) the bar has a region AB near the free end subjected to peripheral compression. (b) the bar has a rectangular groove at region AB.

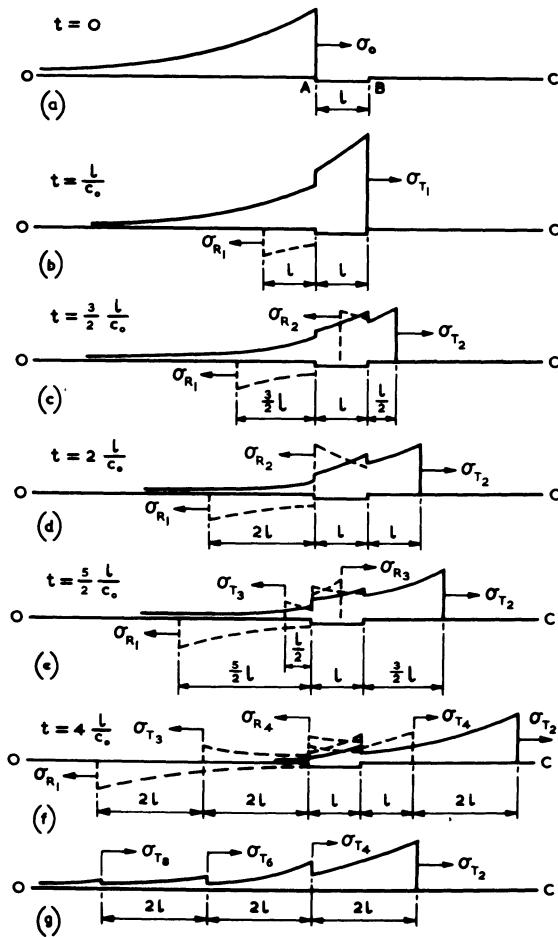


Fig. 8 Transmission and reflection of an incident exponential stress pulse along a bar having a groove, AB, of length l .

CONCLUSIONS

A technique has thus been developed for producing fracture at a number of sections along a bar. The force producing the tearing-off effect is a short duration compressive stress pulse of high magnitude applied at one end. The pulse is produced from the impact of a fast bullet or the pressure of contact explosives. The passage of the stress wave is

obstructed by the introduction of a discontinuity at a region near the free end of the bar. The compressive stress wave propagates along the bar, through the discontinuity, towards the free end where it will be reflected as a tensile stress wave travelling back towards the discontinuity. On arrival at the discontinuity the tensile stress is amplified and fracture is promoted. The discontinuity was produced by means of cutting shallow grooves on the face of the bar or by applying a lateral compressive pressure at a portion of the bar near the free end. The technique was used to cut Perspex round and rectangular section bars.

An exploratory set of tests were performed on bars with peripheral grooves and with grooves on only two sides of the bar. Cutting was achieved in bars with rectangular, square and V-shaped grooves. The effect of depth and width of the grooves seems to be an important factor. An approximate analysis using a one-dimensional theory of the process was performed and this enabled the sections at which fracture was most likely to occur to be located. A rudimentary approach was made to investigate the behaviour of an incident compressive stress wave when transmitted and reflected at regions of discontinuity.

Further investigations on the effect of stress pulse shape, geometry of grooves, distance between discontinuities, intensity of local radial force at a section to enhance fracture, material properties of the bar and geometry of the specimen on the fracture behaviour will be worthwhile and may lead to the design of controlled equipment which could produce fracture in a variety of bars of different materials and shapes.

The ideas presented may be useful in the field of fracture and necking in general and in situations where a solid is subjected to an impulsive load, or a precompressed material suddenly subjected to local release of load.

REFERENCES

1. HOPKINSON, J., Original Papers Vol. II, Cambridge University Press, pp. 316-320, 1901.
2. HOPKINSON, B., Scientific Papers, Cambridge University Press, pp. 423-474 1921.
3. LANDON, J. W., and QUINNEY, H., 'Experiments with the Hopkinson Pressure Bar', *Proc. Roy. Soc.*, 103A, p. 622, 1923.
4. THOMAS, W. N., 'The Effects of Impulsive Forces on Materials and Structures', *The Civil Engineer at War*, *Proc. Inst. Civil. Engrs.*, 3, 1948.
5. WESSMAN, H. E., and ROSE, W. A., 'Aerial Bombardment Protection', John Wiley, 1962.
6. BARON, M. L., and CHECH, R., 'Elastic Raleigh Wave Motion due to Nuclear Blasts', *Proc. ASCE*, EMI, Eng. Mech. Div., p. 57, February, 1963.
7. RINEHART, J. S., 'The Role of Stress Waves in the Communion of Brittle Rocklike Materials', *Int. Symposium of Stress Waves Propagation in Materials*, Ed. N. Davids, Interscience Publishers, 1968.
8. MYKANEN, J. P., et al., 'A New Method for Explosive Strengthening of Metals with Applic-

- ation to Produce Type Parts', Proc. 2nd. Int. Conf. of Centre for High Energy Rate Forming, Estes Park, Colorado, Vol. 1, June 13–27th 1969.
9. MIKLOWITZ, 'Elastic Waves Created During Tensile Fracture', *Trans. ASME. Jnl. of Appl. Mech.*, p. 122, March, 1953.
 10. DAVIES, R. M., 'A Critical Study of the Hopkinson Pressure Bar', *Trans. Roy. Soc. (London) Series A*, **240**, p. 375 1948.
 11. RINEHART, J. S., 'Some Quantitative Data Bearing on the Scabbing of Metals under Explosive Attack', *J. Appl. Phys.*, **22**, No. 5 p. 555–560.
 12. RINEHART, J. S., and PEARSON, J., 'Explosive Working of Metals', Pergamon Press, p. 47, 1963.
 13. RINEHART, J. S., and PEARSON, J., 'Behaviour of Metals Under Impulsive Loading', Dover Publications, 1965.
 14. KOLSKY, H., 'Fracture Produced by Stress Waves', *Fracture*, Ed: Averbach, B.L. etc., MIT Press, 1959.
 15. KOLSKY, H., 'Stress Waves in Solids', Dover Publications, 1963.
 16. JOHNSON, W., 'Impact Strength of Materials' (in press), Edward Arnold.

DISCUSSION

Query from D. Harrison

It is necessary to mark the bar at the position of fracture?

Reply

It is necessary, but an alternative is to grip the bar at the point of fracture.

Query from R. A. Pruemmer, Frannhofer, Germany

It is a well-known fact that the yield strength and fracture strength of materials increase with strain rate. In the case of loading by means of explosives, the loading speed is very high. Therefore, instead of the static fracture strength(s), the proper dynamic

fracture strength should be used in your deduction formulae. Is it possible to estimate the length of the fractured pieces in the case of a cylinder loaded by an impulse from one end, taking into account the strain rate effect?

Reply

The loading rate is probably much lower than it seems and we have no way of knowing the steepness of the head of the pulse. The strain rate associated with the decay of the pulse is about 10/s. If the intensity of the input pulse is known, the fracture stress is calculable from a knowledge of the speed at which fragments are flung off (see Rinehart & Pearson's book¹³).

Query from S. Shima

In order to control the length of chopped parts, is it necessary either to have grooves or to grip the bar at certain intervals? It seems to me that, in a bar with discontinuities at certain intervals, the tensile stress wave is lowered, rather than kept high enough to cause fracture, which can be a limit for the application of this technique.

Reply

It is necessary to put in grooves in order to pre-determine the length of bar that will be chopped off. The theory in the paper shows how the discontinuities affect a pulse, and the relation of the brittle fracture stress to the amplitude of the input pulse.

Query from G. E. Wright, Enfield College of Technology

Is there any change in mechanical properties of the fractured bars.

Reply

None that I know of.

EXPANDING SHEET FORMING METHOD FOR AUTOMOBILE BUMPERS

by

K. KOSHINO*

SUMMARY

'The expanding sheet forming method' for automobile bumpers, which have conventionally been manufactured by drawing or rolling methods, has been developed. The drawing method is very versatile for bumpers of different shapes and sizes, but the material loss is considerable. On the other hand, the adaptability of the rolling method is limited. In this expanding method, the sequence of operations is as follows. First, both ends of a sheet strip which are initially bent are gripped by jaws mounted on the sliding punches; second, the punches stretch the sheet to form corners and the channel shape; finally, the dies whose moving direction is inclined finish the corner shape by engaging the punches. This expanding method can be performed by a special die set combined with an hydraulic unit mounted on the conventional single-action press. The saving of material is as much as 20% compared with the conventional drawing method. Also, the surface thus formed is free of scratches, reducing the amount of subsequent polishing. Furthermore, it has been demonstrated in the course of plotting the deformation path that the expanding method allows greater deformation than the conventional drawing method and permits the application of low-grade materials.

INTRODUCTION

The expanding sheet forming method has been developed as an efficient method for forming steel automobile bumpers of relatively complicated shape. Conventionally, bumpers have been formed by the drawing method, by which many other car body parts are manufactured. Recently, some other forming methods have been developed and adopted for forming bumpers, but their application to various shapes is limited.

The problem in forming bumpers is usually the occurrence of fractures or wrinkles at corners with a small radius of curvature. The thickness of the steel sheet for automobile bumpers is commonly 1.2–3 mm or 5 mm, and the material is mild steel, though aluminium or stainless steel sheets are sometimes used. This paper is concerned with the process and forming techniques in the expanding sheet forming method, and discusses its merits.

THE CHARACTERISTICS OF THE EXPANDING SHEET FORMING METHOD

The main characteristic of this method is the stretching of the sheet longitudinally by sliding punches. This method has various superior characteristics over three well-known methods, that is, (a) drawing method, (b) roll forming method, and (c) bending type forming method, which have recently been

adopted to form bumpers. The following discusses the merits and disadvantages of these conventional forming methods, and the characteristics of the expanding sheet forming method.

Drawing method

This method has usually been employed to form panels of automobile body parts such as bumpers, roofs, doors, and so on. Forming by this method is shown in Fig. 1a. The steel sheet held with the blank holder is drawn in with the punch. The shape of the blank holder, the forming direction and the shape of bumpers must be considered if fractures and wrinkles at the corner are to be avoided. The formability in this method has been considerably improved owing to the recently developed blank holding device using an hydraulic system.

It is an advantage of this method that it can be widely used for forming complicated-shape parts. On the other hand, difficulties of this method are that excessive material is required for blank holding, and that many subsequent finishing processes are necessary to remove scratches and die marks made on the drawn parts.

Roll forming method

In this method, the blank which has initially been bent into a trough shape is rolled and squeezed on the die by the forming rollers, as shown in Fig. 1b. After

*Department of Process Development, Toyota Motor Co., Ltd.

that, the only process required is piercing (Fig. 1).

A merit of this method lies in the saving of material compared with the drawing method, because it saves the material for blank holding. The shape and size of the blank are nearly equal to those of the finished parts expanded on a plane. On the other hand, a drawback of this method is that the configuration at every cross-section of the bumper should be constant. This is because every part of the bumper is successively formed from one end to the other by the same forming rollers, though the depth of cross-section is not necessarily constant. This method is put into practice with a special roll forming machine.

Bending type forming method

This method has recently been developed and put into practice.⁴ The sequence of operations and forming mechanism is similar to those in the above-mentioned roll forming method. The blank, which has initially been formed into a trough shape, is bent successively from the centre toward both ends of the bumper with moving dies similar to those of the tangent bender, and finally expanded several percent longitudinally by the punches, as shown in Fig. 1c. This method affords similar saving in material and less limitation to the shape of parts compared with the roll forming method, because every part of the bumper is formed with a corresponding part of the die.

Expanding sheet forming method

This method is superior to the drawing method in the saving of material and in reducing scratches: it is also superior to both the roll forming method and the bending type forming method in forming corners of smaller radius of curvature and more complicated cross-sectional shapes.

The sequence of operations is as follows (Fig. 2). First, both ends of a sheet are initially bent and the sheet is put into the expanding die set in which two sliding punches move horizontally. Both ends of the sheet are gripped by jaws mounted on the sliding punches are engaged in forming. Just prior to the end of the longitudinal stretching, the dies move in directions which are inclined to those of sliding punches and engage in forming to finish the shape, and at this instant the supporting punch and the subsidiary die also engage in forming.

EXPANDING SHEET FORMING DIE SET

The expanding sheet forming method is characterized by the expanding motion of sliding punches and the inclined motion of dies. The expanding motion is obtained by changing the vertical motion of the main slide into horizontal motion using a cam mechanism. The expanding stroke is determined so as to stretch the sheet as much as 10–15% over the total length when calculated at the top of the cross-section of a bumper. This percentage is varied according to the dimensions and configurations of the bumpers. Each punch and die moves horizontally and vertically, respectively, and as a result the moving direction of dies is inclined to that of the sliding punches. The angle of inclination should be varied according to the

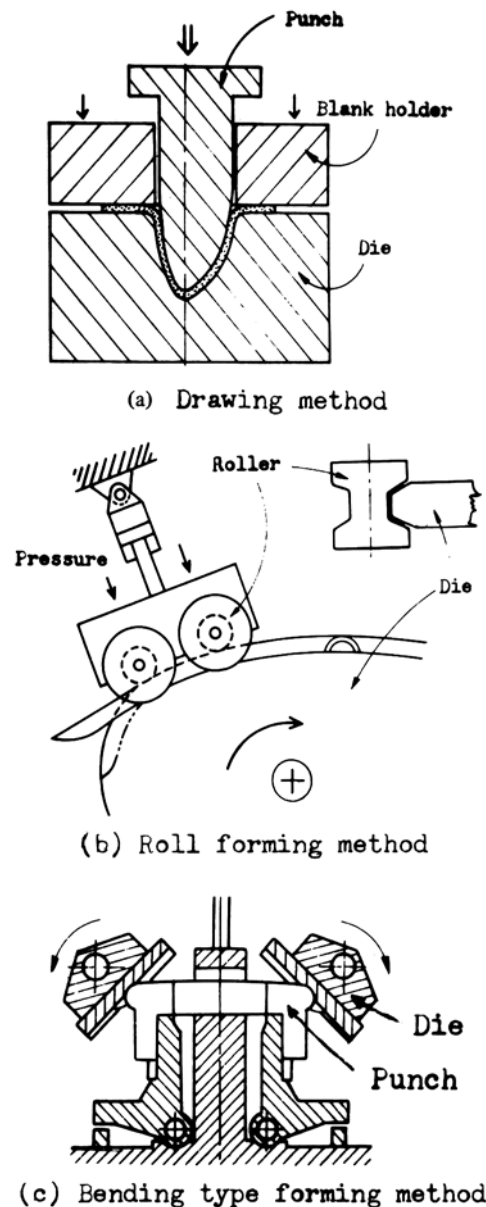


Fig. 1 Conventional methods

radius of the corners, and usually ranges between 45° and 60° . The aim of such forming is to distribute the shrinkage of the sheet and keep the rubbing direction of the sheet and the die edge natural to avoid wrinkles and scratches. A special hydraulic mechanism which is synchronized with a rapid ram motion is combined with this die set. The gripping and releasing of the sheet, lifting the supporting punch and pressing the blank at the end of stroke are all hydraulically operated procedures. The hydraulic energy is supplied by the ram motion. The response of an electric control circuit is not sufficiently fast for this mechanism, so hydraulically operated valves are used to obtain the rapid forming cycle. The timing of operations in this mechanism is as follows. Gripping jaws are operated just before the expanding motion of the sliding punches and continue gripping until the punches begin to return. The supporting punch is raised by low oil pressure simultaneously with the expanding motion of sliding punches and the oil pressure is increased when the punch makes

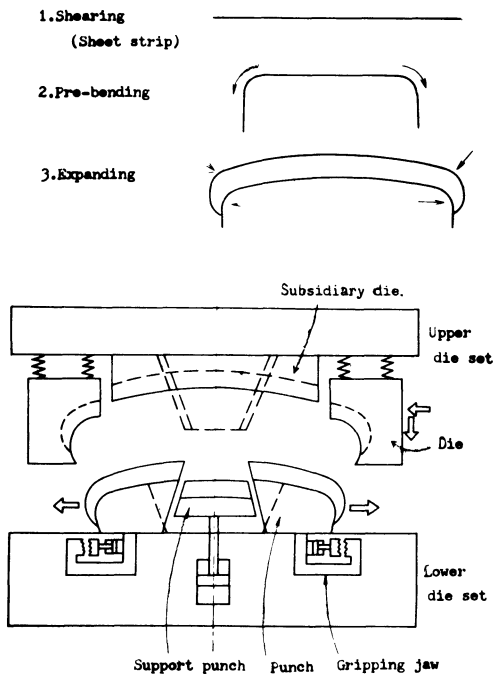


Fig. 2 Expanding methods

contact with the subsidiary die. Thereafter the supporting punch is lowered with the aid of sliding punches which return inwards while the oil pressure is decreased. The operation of each part of this mechanism is exactly timed in connection with the ram motion, and therefore either a mechanical or a hydraulic press may be used.

FORMABILITY IN THE EXPANDING SHEET FORMING METHOD

The deformation mode of material

One of the difficulties in forming bumpers is in forming the corners. The deformation mode in these corners when formed by the expanding sheet forming method was investigated. Squares scribed with longitudinal and lateral lines on the sheet were observed after forming, and the deformation pattern was obtained as shown in Fig. 3. The point at which lateral lines near the corner intersect lies at a distance 1.6 times the radius of curvature of the outer configuration of the product, and the neutral line in this bent area lies near the inner edge. The lateral deformation was small. Further, this deformation pattern scarcely varied in the forming of different bumpers. Such a deformation mode is not usually observed in the drawing method. The deformation at the corners gradually decreased with distance from the position of potential fracture, that is, the position at which deformation was closest to the deformation limit. The pattern of deformation distribution was similar to that in the drawing method. On the other hand, the deformation in the central straight portion was more than 10%, which is considerably larger than the deformation in drawing.

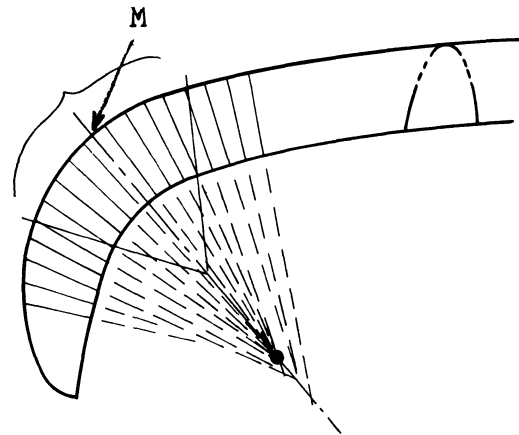


Fig. 3 Deformation pattern

The local deformation

It is important to consider the local deformations in the area near the point M, as shown in Fig. 3, where the fracture occurs. The scribed circle test, as shown in Fig. 4, was performed to clarify the effect of the



Fig. 4 Distortion of scribed circles

deformation path on the fracture. The longitudinal and lateral deformations in the area near the point M were measured at several intermediate and final stages of forming. All these materials were cold-rolled steel sheets of commercial quality and 2.0 mm thickness. The dimensions of the samples were as follows:

Sample A (drawing and expanding): 1415 mm width, 67 mm height, 49 mm depth, 106 mm corner radius

Sample B (drawing): 1415 mm width, 65 mm height, 58 mm depth, 78 mm corner radius

Sample C (drawing): 1485 mm width, 66 mm height, 67 mm depth, 94 mm corner radius.

The results are shown in Fig. 5; the results in drawing the same bumpers, and the deformation limits (initiation of necking) in various deformation paths are shown. Observing the distortion of the scribed circle at each stage, the following facts were revealed.

First path: In the first path, that is, the deformation path to the first bending point, the sheet is stretched a few per cent biaxially, both in the drawing and expanding methods.

Second path: Deformation in the second path, beyond the first bending point just mentioned,

was observed as uniaxial elongation due to longitudinal stretching. Thereafter the longitudinal elongation is permitted near 60% without fracture, approximately 15% greater than in the drawing method. The larger permissible elongation is a basic advantage in stretch-forming of channel-like parts. On the other hand, the shrinkage at the inner edge of the corner amounted to 10–20%. It is obvious from recent researches that the deformation limit of material varies according to the deformation history. This fact is also obvious in the expanding method.

Dimensions of adaptable bumpers.

From the above mentioned results, it can be predicted whether a given bumper can be formed by this method by simple geometrical consideration of the drawing in full scale of the given part. The procedure is as follows.

(i) The fan shape OAB is drawn, where \overline{OA} and \overline{OB} are the radii of curvature of the outer shape of the corner.

(ii) A point N is set on the line bisecting the angle BOA, where $\overline{MN} = 1.6 \overline{MO}$.

(iii) The circular arc CD, of which N is the centre, is drawn so as to pass through the point Q, 10 mm from the inner edge of a bumper. The distance of 10 mm is based on the assumption that the die edge passes this point.

(iv) $\widehat{AB} \leq 1.6 \widehat{CD}$ (1)

If condition 1 is satisfied for a given bumper, the expanding method is adaptable to form it.

Condition 1 was introduced as follows. By comparing the length of the arc AB with CD, the deformation on the line AB or CD can be calculated. The mean limits of elongation and shrinkage over the arcs AB and CD, respectively, were determined as follows. The shrinkage at the corner was determined not to exceed 10%, though the maximum shrinkage was measured as 20% by experiment. The maximum elongation in the position of potential fracture should be between 45% and 55%, because fracture might occur at a value over 55% and the maximum elongation under 45% is supposed too small. The mean elongation over the arc AB was determined not to exceed 45%. Using these values, the relation between the lengths of the arcs AB and CD for the adaptable bumper is given by

$$\frac{\widehat{AB}}{1.45} \leq \frac{\widehat{CD}}{0.9} \quad \text{-----} \quad (2)$$

From condition 2, condition 1 is again obtained. Comparing the calculated elongation with the actual one obtained by the scribed circle test, the deviation was less than a few per cent, and so the above-mentioned estimation of deformation proved to be accurate.

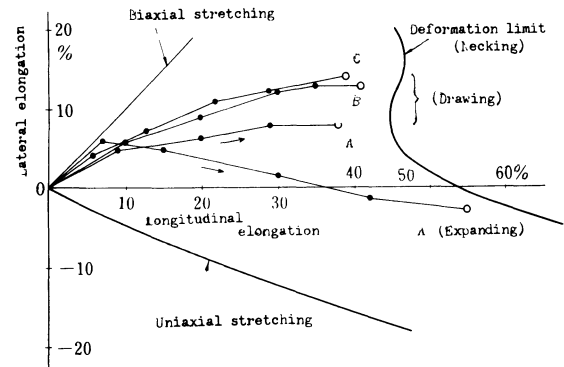


Fig. 5 Deformation paths

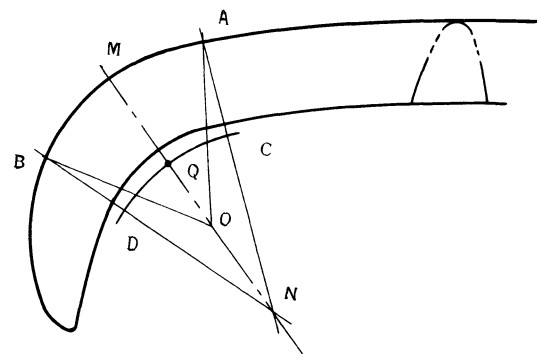


Fig. 6 Procedure for prediction of adaptability

EXAMPLE OF PRACTICAL APPLICATION

One practical example is introduced here. The expanding die set is shown in Fig. 7. The formed sample is shown in Fig. 8, where drawn samples of a similar shape are also shown. A saving in material of approximately 20% was achieved by adopting the expanding method instead of the drawing method. The size of the material used in the former and the later methods was 1630 × 180 × 1.6 mm and 1730 × 220 × 1.6 mm, respectively. Furthermore, the subsequent polishing operation has been reduced because there are fewer scratches on the surface of the bumper.

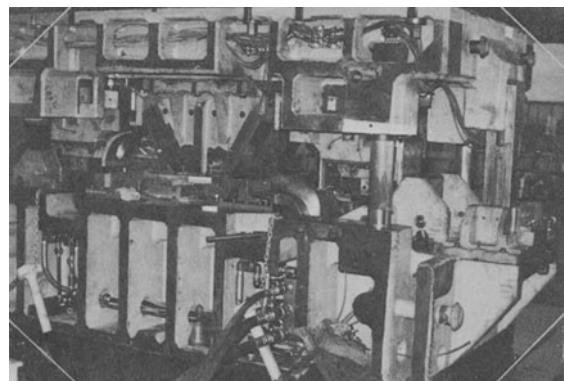


Fig. 7 Expanding die set

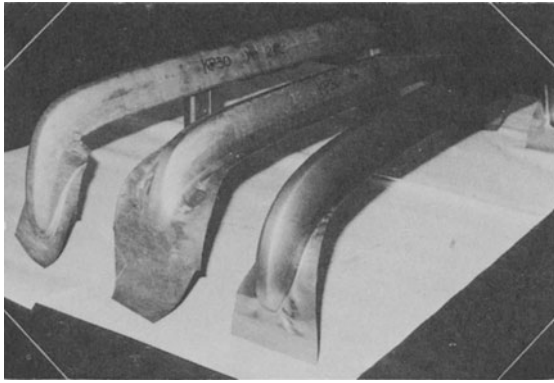


Fig. 8 The formed sample 2nd drawing (left), 1st drawing (centre), expanding (right)

CONCLUSION

The expanding sheet forming method has been developed and put into practice. The expanding die set operated in the conventional single-action press was adopted. This die set is composed of sliding punches, the dies, the subsidiary punch and die, and an hydraulic mechanism.

The procedure for judging the adaptability of the expanding sheet forming method for a given bumper has been obtained by the investigation of the deformation mode, the deformation path and the deformation limit.

The advantages of this method have been confirmed as:

1. saving material,
2. capable of using materials of low grades,
3. reducing scratches during forming.

REFERENCES

1. KOBAYASHI, T., MURATA, K., MORIMOTO, T., ISHIGAKI, H., ABE, T., and MIO, R., Pre-print of 19th Japan National Congress of Plastic working, (1968-11), 289, (in Japanese).
2. KEELER, S. P., *Machinery*, (1968-5), 92

3. NAGASHIMA, S., and NAKASHIMA, H., *Science of Machine*, 21 (1967) 12, 1637, (in Japanese).
4. Japanese Patent, No.S45-27318 (1970).
5. NAKASHIMA, H., and KIKUMA, T., Pre-print of 19th Japan National Congress of Plastic working, (1968-11), 277, (in Japanese).
6. KIKUMA, T., and NAKASHIMA, H., Pre-print of 19th Japan National Congress of Plastic working, (1968-11), 281, (in Japanese).
7. KOBAYASHI, T., MURATA, K., ISHIGAKI, H., and ABE, T., *J. Japan Soc. of Tech. of Plasticity*, 11 (1970-7) 14, 495, (in Japanese).
8. KOBAYASHI, T., Pre-print of Symposium in Autumn of Japan Institute of Metals, (1970-10), (in Japanese).
9. KEELER, S. P., *Sheet Metal Ind.*, 42 (1965), 683.
10. KOBAYASHI, T., HIDA, K., and SATO, K., *J. Japan Soc. of Technology of Plasticity*, 11 (1970-2) 109, 91 (in Japanese).
11. HIDA, K., Pre-print of Open Meeting organized by Society of Sheet Metal Forming, (1968-11), 49, (in Japanese).

DISCUSSION

Query from G. E. Wright, Enfield College of Technology

This technique provides cost savings in manufacture. Does it provide changes in structure, bearing in mind that the bumper bar is not for decorative purposes only.

There is a current emphasis on safety and a demand by insurance companies for design providing less-costly repairs.

Reply

The deformation mode in this expanding method is basically not different from that in the conventional drawing method, and the structure is not changed in forming.

It has been confirmed that the strength of the parts formed in this expanding method is equivalent to drawn parts, in testing the actual formed samples.

THE DESIGN OF A PRESS FOR USE IN THE HYDROSTATIC EXTRUSION PROCESS

by

R. W. THATCHER and J. A. PENNELL*

Presented by D. HARRISON*

SUMMARY

This is a report of the design of a compact, heavy-duty press. The main feature of the design is that the profile of the press frame is chosen to minimise the inward movement of the press columns under load so that the columns can be used as slides without the loss of strict guidance of the moving platen.

INTRODUCTION

During the development programme of equipment for hydrostatic extrusion there was found to be a need for a heavy-duty, compact press. This is a report of a design study, carried out by Vickers Ltd, into the type of press frame which has been referred to in the literature as a laminated 'picture-frame' design. Attention was thus confined to the type of frame illustrated in Fig. 1, which is built up from a number of essentially rectangular plates, through which there extends an approximately rectangular opening, which is the working space of the press. The frame illustrated has four laminations but their number and thickness is arbitrary and would depend on the particular application, the available fabrication facilities and other factors connected with the distribution of the load between the laminations.

In the Vickers laminated press frame, the main feature of the design is that the columns are used as slides and the deflection of each column is controlled to minimise their inward movement under load. It is then possible to operate the press with only a small initial clearance between the moving platen and the slides and to maintain precise guidance over the whole stroke of the press. This design retains all the strength and rigidity advantages of conventional presses but has a much lighter, and therefore more economical, structure. No additional guidance frames are required and the metal in all parts of the press is utilised efficiently.

This report is primarily concerned with the design of a horizontal 1,200 ton press with a working space of about 10 ft. Although four plates are to be used in the design, a consideration of the material specification which would give a satisfactory strength and fatigue life is not presented.

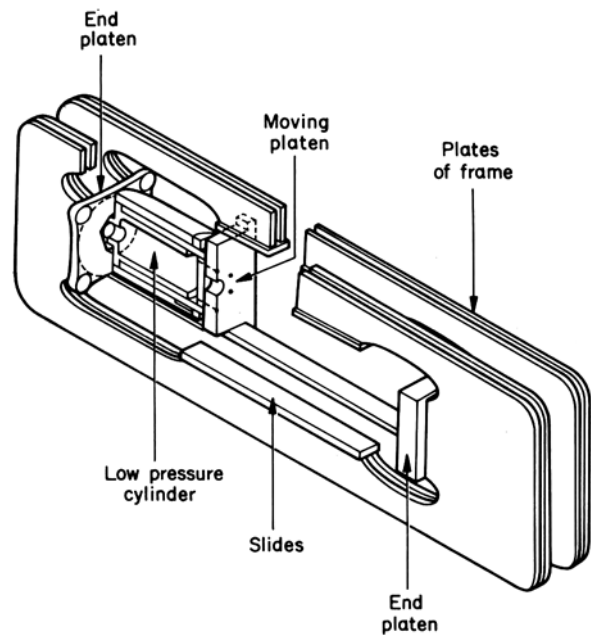


Fig. 1

GENERAL FEATURES

In the design considered, the laminations of the frame are connected together by relatively thick platens, one at each end of the working space; these distribute the load evenly over the laminations and provide a mounting for the dies, the press cylinder and other pieces of press equipment. The laminations are also connected by thinner platens attached to the inner surface of the columns, which form the slide surface for the moving platen of the press and the extrusion container. To increase the stiffness of the frame in a

*Vickers Limited, Newcastle-on-Tyne

direction normal to the laminations the assembly is 'boxed in' by thin platens around the outside of the press.

To prevent undesirable bending stresses arising in the very highly loaded, brittle, extrusion ram which is mounted on the moving platen (Fig. 2) it is essential to guide the moving parts of the press very accurately. In particular, the position of the ram and the extrusion container must be controlled so that they remain coaxial to within a few thousandths of an inch during the whole extrusion cycle. It is also important that the moving platen be firmly constrained against tilting as well as against transverse movement, as such constraints give support should eccentric loading arise, possibly during a tool failure or if the press were used for other applications (for example, cold forging).

In the design illustrated in Figs. 1 and 2, the moving platen is accurately guided along three slide surfaces: two of these, preventing transverse and vertical movement of the platen, are integral parts of the laminated press columns, as already described. The third slide is formed by a heavy cylindrical spigot mounted on the fixed platen inside the low pressure cylinder where it engages a bush pressed into the rear of the moving platen. The axial distance between this rear guide and the slide on the moving platen is sufficiently great to ensure adequate resistance to tilting of the platen and a solid support for eccentric loads. As both the spigot and the bush housing are subjected to the hydraulic pressure, there is no relative movement radially between the sliding surfaces under varying pressures in the press cylinder, that is, at different press loads. The other sliding surfaces, however, present more of a design problem in this respect because of the inward movement of the columns under load. If binding of the sliding surfaces is to be avoided it is normally necessary to work with large initial clearances, making really accurate guidance of the platen impossible. Attempts to overcome this difficulty in the past have led to the provision of auxiliary guidance frames. The cost of the extra material involved in order to have an effective guidance system makes this approach unattractive. Other solutions include using a roller guide which resists inward movement or using internally guided die sets, which eliminate the need for an accurately guided ram. The latter solution inevitably increases the tooling costs but it is the only reliable procedure on poorly guided presses, for roller guides can have certain limitations in rigidity and maximum load carrying capability which could make this method unsuitable for larger presses. In the design described here the inward deflection of the columns is controlled so that slides can be attached to them without loss in the accurate guidance of the moving platen.

THEORETICAL ANALYSIS OF THE FRAME USING THE EQUIVALENT BEAM THEORY

The controlled deflection of the slides is achieved by cutting the plates, from which the laminated frame is constructed, to a profile such that the tensile load is applied eccentrically to the columns. This eccentric

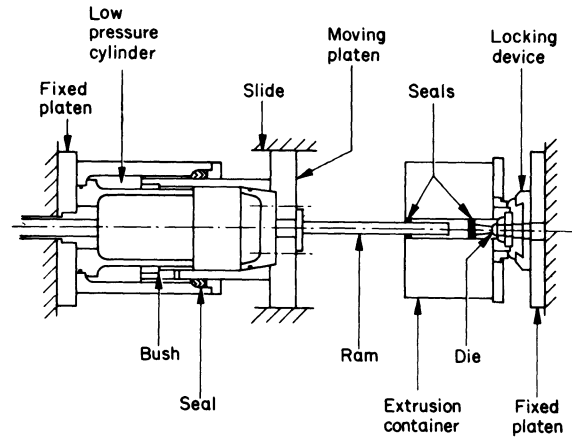


Fig. 2

load will itself cause the columns to bend and, by careful selection of the plate profile, it is possible to arrange that this deflection exactly cancels out that previously mentioned arising from the load on the end-platens. However, no satisfactory profile has been found so far to realise this ideal state and a compromise solution, minimising the total deflection along the slide, has been obtained.

Essentially, the problem was to define the profile of the plate, illustrated in Fig. 3, along the broken lines in order to minimise the deflections along $C_1 D_1$ and $C_2 D_2$ for a constant load applied uniformly along $A_1 B_1$ and $A_2 B_2$. The X -axis was an axis of symmetry and this property was used in the analysis. The obvious choice of beams, shown in Fig. 4, was not suitable to solve the problem because beams (4) and (5) have unsatisfactory length/depth ratios. To overcome this difficulty a model was built to scale and the values of the deflections and rotations at the points X_1 and X_2 , namely δ_1 , δ_2 , θ_1 and θ_2 respectively, were measured under load on $A_1 B_1$ and $A_2 B_2$. It was found that these values were approximately independent of small changes in the geometry of beams (1), (2) and (3) and therefore the analysis was carried out on these three beams with the prescribed deflections and rotations.

The overall length $L = L_1 + L_2 + L_3$ was held constant, as were the moments of inertia of each of the beams. The variable parameters were taken to be Z_1 and Z_2 , which are, respectively, the heights of the neutral axis of (1) and of (2) above the neutral axis of (3), and α_1 and α_2 . Although the positions of X_1 and X_2 were allowed to move in the Y direction, we assumed that the prescribed deflections and rotations were approximately independent of their position; this is justified because beams (4) and (5) are relatively massive compared with the small changes permitted for X_1 and X_2 . For this reason certain constraints were applied to the four variable parameters. Further constraints were applied to Z_1 and Z_2 so that any possible stress concentration caused by a change in beam cross-section at the weld joining the slide to beam (3) was avoided at C and at D.

The deflections were calculated at twenty-four equally spaced points along the neutral axis of beam (3) and the sum of squares of these deflections was minimised with respect to the four parameters Z_1 ,

Z_2 , α_1 , and α_2 . This is a constrained minimisation and the technique due to Box¹ was used to find the optimum values of these parameters. This produced an initial design and the next stage was to eradicate any unnecessary stress concentrations at points where two beams are connected.

THE DETAILED PROFILE USING PHOTO-ELASTIC MODELS

In the general design of the previous section the most likely points at which there might be a stress concentration were in the neighbourhood of a change in cross-section of the columns. A series of experiments was undertaken on photo-elastic models so that the details of the profile in such critical regions could be designed. Although these tests were not fully comprehensive, sufficient information was obtained to produce the detailed design without causing any large stress concentrations.

The highest tensile stresses were observed at S_1 and S_2 (Fig. 4) so that the design of the profile in the neighbourhood of these two points was of particular importance. Two radii were used, as illustrated in Fig. 5, in an attempt to reduce the high level of stress at these points. From the series of photo-elastic tests we found that by having a ratio of $R_1 : R_2$ of about 1:2 there was a reasonably small level of stress, as small as

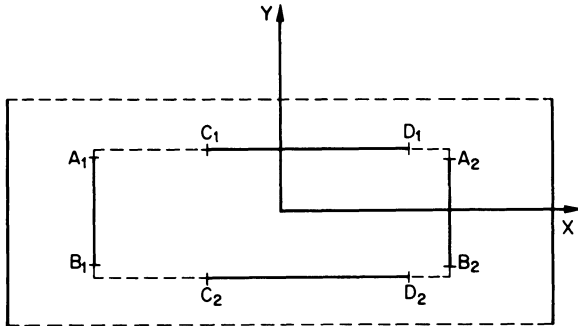
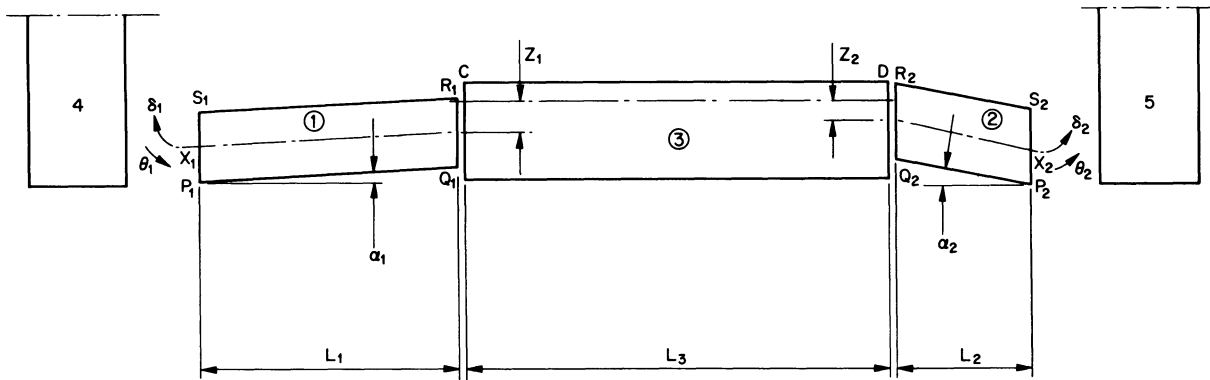


Fig. 3



----- are the beams neutral axes: that of ③ is corrected to account for the slide

Fig. 4

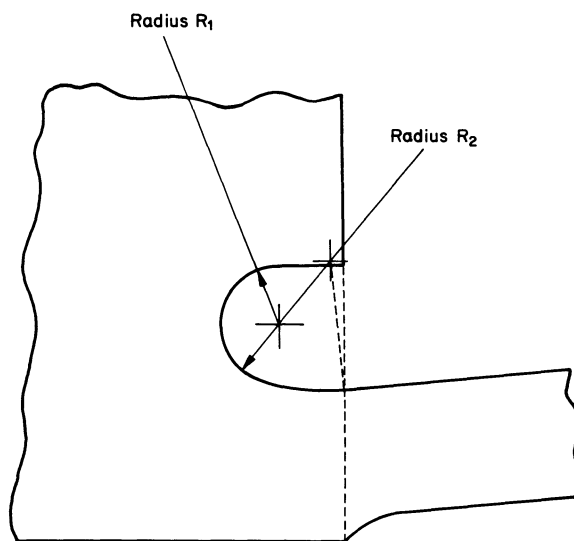


Fig. 5

could be expected from the theoretical stress calculation using the beam theory. At all other less critical points, convenient radii were chosen and the stress levels checked using a photo-elastic model.

FURTHER VERIFICATION OF THE DESIGN

Two further verifications of the design were carried out. Firstly, the frame was analysed using a numerical model set up by the finite element method (see, for example, Zienkiewicz² for a description of the technique). It was assumed that the frame behaved as a problem in plane stress. The most simple triangular element definition was adopted, in which the stress state is constant and the displacements are linear functions of the coordinates. As a general rule using this method, the finer the mesh used, the more accurate the answer obtained; that is, the more triangles used in regions of large stress gradients, the more accurate the result. One of the easiest ways to assess the accuracy achieved for a given problem is to solve it on two different grids and compare the answers. If the two results are similar it is reasonable to assume that a good numerical model has been obtained on the finer mesh. This method was used with the two grids illustrated in Fig. 6 and as both the deflections along the slide and the maximum stress levels only changed by a small amount (except in the region of S_1 at which in grid 2 a much finer mesh had been chosen) no further grid refinement was considered necessary. The slide deflections from grid 2 are shown in Fig. 7 and the stresses, together with those from grid 1, in Table 1.

Secondly, a model was constructed to scale and the deflections along the slide measured. There was considerable difficulty in accurately reading the slide deflections, but in Fig. 7 they are shown to agree very

closely with the finite element method results and fairly closely with the beam theory results. Strain gauges were also placed on the model in the regions where the maximum stress were expected. The strains measured are unlikely to be as high as those obtained in practice because of the uncertainty in selecting the actual position of peak stress.

Table 1. Stresses in tons in⁻². Comparison of stresses predicted by the different methods used

Stresses at the points:—	S_1	Q_1	S_2	Q_2
Beam theory	16.1	11.5	18.6	14.3
Photo-elastic method	17.2	12.3	20.3	10.7
Measured (scale model)	20.5	9.3	22.7	9.4
Grid 1	15.1	6.8	20.3	6.7
Grid 2	20.9	7.1	21.4	7.1

There was difficulty in making a really accurate assessment by the photo-elastic method because of the small size of the models but the stress intensity of the radii could be assessed by the bunching effect of the bands there. The stresses determined by beam theory were found to be less accurate than those determined by other methods.

Using the finite element method we found that an outward thrust of 2 tons at mid-stroke and 5 tons at the beginning of the stroke on the slide would bring its deflection to zero at full load of the press. Even if very small initial clearances are allowed, therefore, there will only be a slight tendency to bind which would be most severe at the beginning of the stroke. This compares with approximately 20 tons outward thrust if no special profile of the plates had been used.

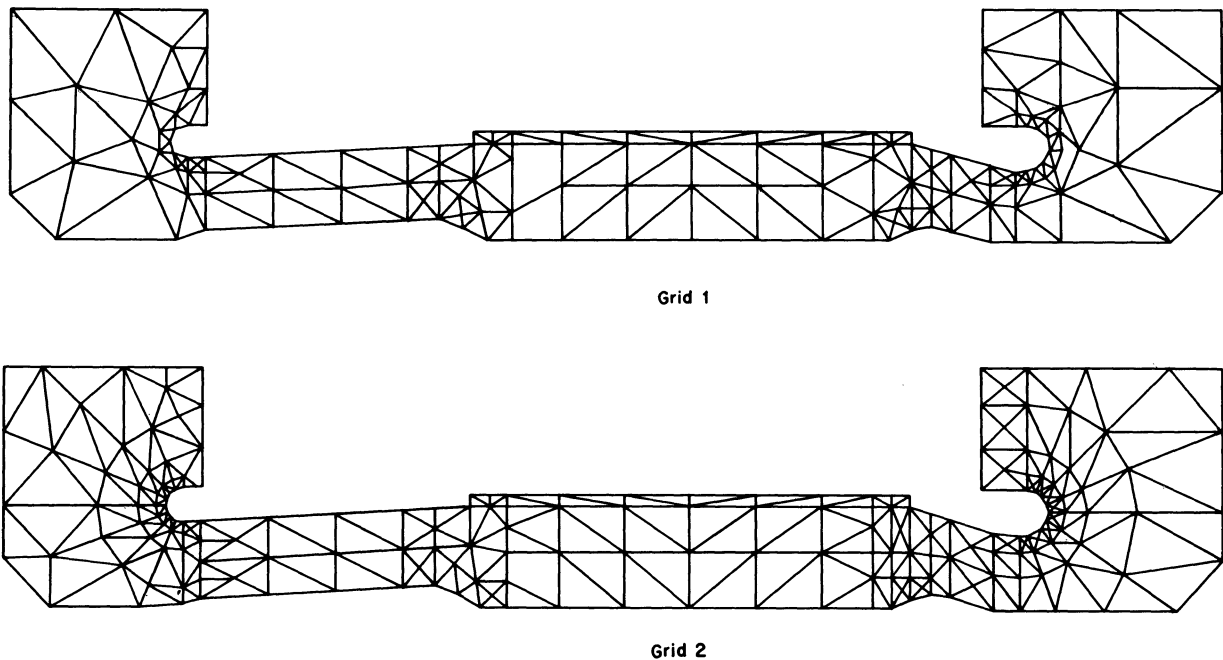


Fig. 6

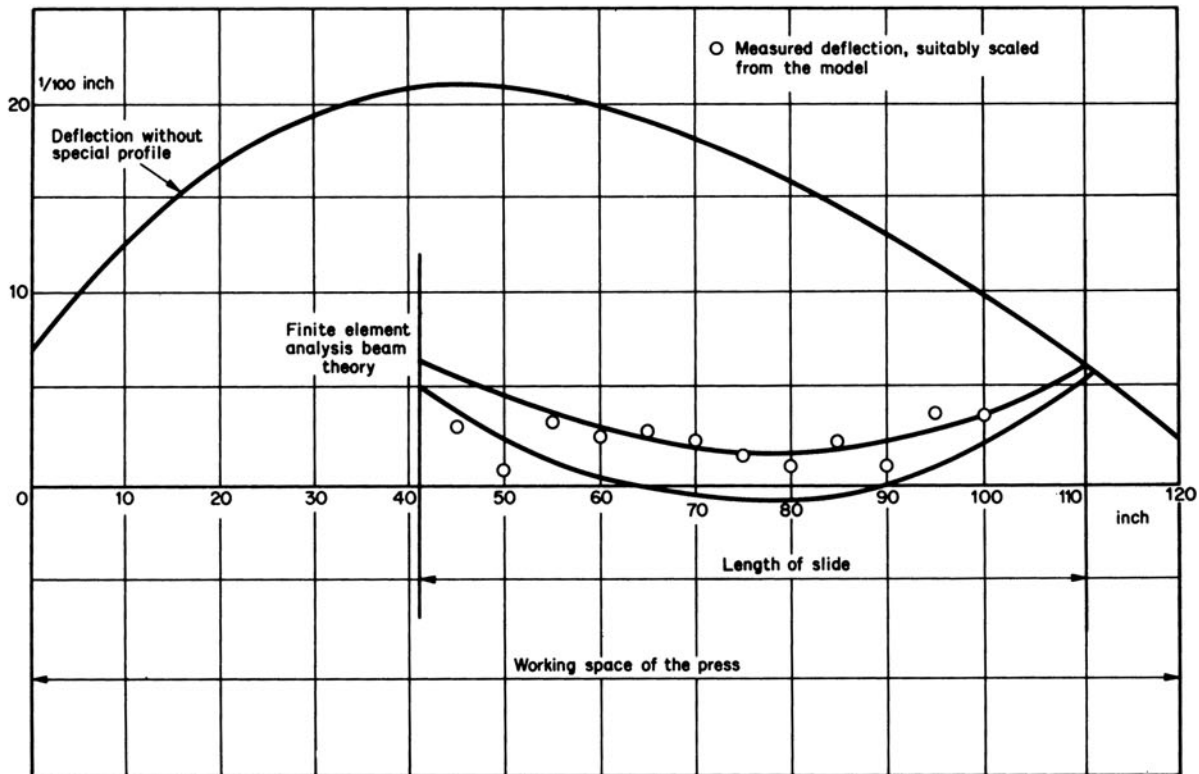


Fig. 7

CONCLUDING REMARKS

The 1,200 ton experimental press is now under construction at Vickers Ltd, built to the above design. After further results have been obtained using this press concerning peak stresses, slide deflection and frictional forces on the moving platen resulting from the bending of the slides, it will be possible to assess whether further work on reducing the slide deflections is necessary. If this does not become a necessity the results obtained so far suggest that the use of the finite element method would provide a more flexible procedure and at the same time provide results more accurate than those of the beam theory, although the success achieved with this latter approach is surprising.

ACKNOWLEDGMENTS

The authors wish to thank Messrs S. Turnbull, V. Riley and D. McLaughlin for making significant contributions to the design of the press.

REFERENCES

1. BOX, M. J., 'A new method of constructed optimisation', *Comp. Jor.*, 8, No 1, 42.52, 1965.
2. ZIENKIEWICZ, O. C., 'The finite element method in structural and continuum mechanics', McGraw-Hill, New York, (1967).
3. British Patent Application 34475/67.

DISCUSSION

Query from B. Fogg

Early in your presentation you mentioned that the Vickers picture-frame press could be used satisfactorily for cold forging as well as hydrostatic extrusion.

Whilst one is inclined to think of cold forging in terms of axially-symmetric operations, future developments will obviously include the forging of non-symmetrical components. Do the authors feel that too much emphasis has been placed on tests with axial loading, with the result that lateral stiffness has been neglected?

Reply (from D. Harrison)

The press was specifically designed for use with a small bed and large load. However, eccentric loading has been considered and tests will be carried out to determine the effect of eccentric loading on the peak stresses and deflections.

It is usual practice, however, to design tooling so that eccentric loading is kept to a minimum. This applies to any design of press.

Query from C. F. Noble, UMIST

I am concerned that you have expressed your own concern about fatigue of the area surrounding the special cut-out areas in the corners of your picture-frame design. For so-called 'autofrettage' your doubling of normal hydraulic pressure will have to cause plastic deformation in the corner areas. In other words, your design is based on a max. working load = $\frac{1}{2}$ X yield load basis. Is not $\frac{1}{2}$ a rather unusually high factor for use in industrial machines?

Further, have you considered the use of shot peening to improve fatigue life aspects, perhaps in addition to the polishing you mention?

Reply (from D. Harrison)

The plastic deformation will only take place at the areas if peak stresses occur at the stress concentration around the cut-outs. After autofrettage, a compressive stress is set up in these areas which should improve the fatigue life of the press.

Regarding a factor of safety of 2 being unusually low for industrial machines: with improved methods of stress analysis (e.g. finite element) and material control, it should be possible to work with a much lower factor of safety in the future.

We realise the benefits of inducing a surface compressive stress by shot peening, but due to the inaccessibility of the cut-outs this technique was not considered suitable.

Query from J. B. White, South Australian Institute of Technology.

One company at least is marketing a hydrostatic extrusion press with a wire-wound frame. Could the authors comment on the technical and economic merits of this in relation to their proposal?

Reply (from D. Harrison)

It is difficult to compare the economics of the picture-frame press and wire-wound presses. The picture-frame press is still in the prototype stage, so an actual firm price for a production machine has not been established. However, the wire-wound press is much more expensive than the conventional press, so we would expect the picture-frame type to be much cheaper.

The main technical merit of the Vickers picture-frame press is that there is little or no non-axial deflection, which means that accurate alignment of the ram and pressure vessel can be maintained. The wire-wound press, however, still deflects inwards, which means that additional methods of alignment of the tools are required.

DIE PERFORMANCE IN HIGH-ENERGY RATE FORGING

by

A. THOMAS and K. DENHAM*

INTRODUCTION

Attempts have been made to establish the economics of high-energy rate forging (HERF) by a synthesis of costs^{1,2}. The conclusion reached in these exercises can be no more than tentative until more experience is gained with HERF machines. But one fact emerges quite clearly; that is, that die life will be crucial in determining the overall economics of HERF.

Bakhtar¹ has stated that more than 80% of dies on a conventional plant have lives exceeding 4000 components. In general, the die life reported for HERF machines has rarely exceeded 2000 forgings. A number of investigators³⁻⁵ have discussed the die problems associated with high-energy rate forging and various explanations have been offered for this low life.

The picture is far from clear, however, as the figures quoted often refer to complex shapes or forgings made from difficult alloys. Furthermore, the use of different die materials and hardnesses in different forging machines makes comparison of die life difficult.

Although HERF has been proved successful as a process for producing forgings which cannot be made on a conventional plant, such applications are limited and if HERF machines are to be used widely they must be proved to be economic in producing conventional forgings.

This report describes a comparison of the performance of identical dies used to produce forgings on conventional plant and a HERF machine. Laboratory work was also undertaken to study the effect of HERF on abrasive wear in standardized forging conditions.

EXPERIMENTAL WORK

Works trials

The three forgings chosen for comparative die performance studies are shown in Fig. 1 and production details are given in Table 1. All dies were made from BS 224 No. 5 Die Steel, hardened and tempered to B range (363–383 HB), the cavities being sunk by turning or milling.

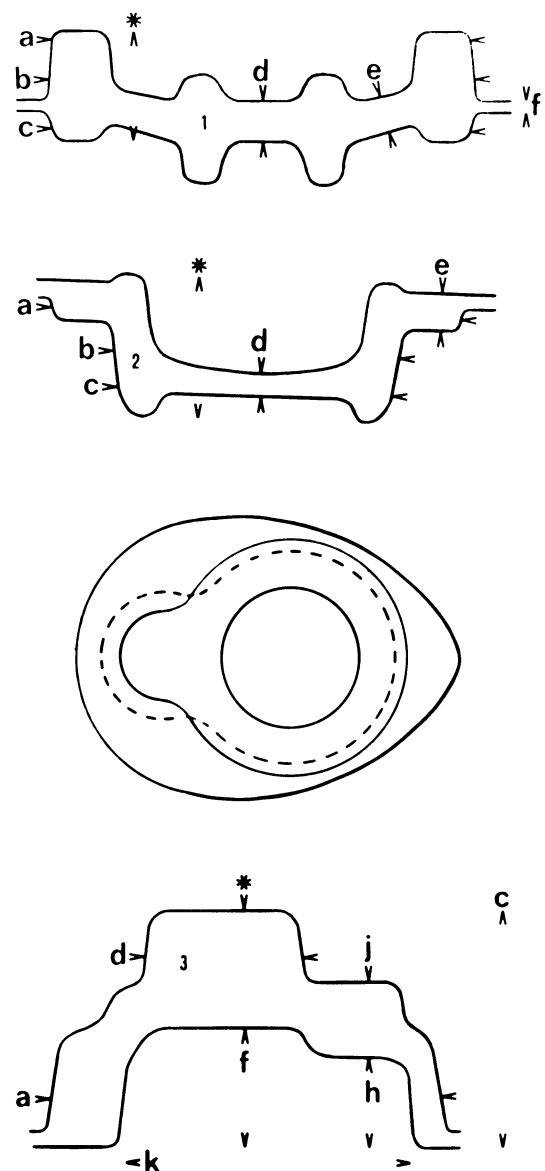


Fig. 1 Forgings chosen for comparative die wear trials. Letters indicate those dimensions on which replica measurements were made. Asterisks indicate 'non-variable' dimensions.

*Drop Forging Research Association, Sheffield.

Table 1. Forging production details

	Conventional plant	HERF machine
Component	Gear blank	Gear blank
Material	En 352	En 352
Stock size	2 in × 2 in × 4 $\frac{7}{16}$ in	2 in × 2 in × 4 $\frac{7}{16}$ in
Forging temperature	1300° C	1300° C
Heating medium	Gas	Gas
Pre-forming details	Cornered and cheesed to 5 in diameter × 1 $\frac{1}{8}$ in	Cornered and cheesed on 200 tonf press
Forging equipment	4 tonf drop hammer	USI 2000 C HERF machine of 150 000 ft lbf capacity
Forging details	Made in single die impression using 2 $\frac{1}{2}$ blows	Made in single die impression using one blow
Lubricant	Dry sawdust	None
Component	Flanged component	Flanged component
Material	En 3A	En 3A
Stock size	2 in × 2 in × 2 $\frac{3}{4}$ in	2 in × 2 in × 2 $\frac{3}{4}$ in
Forging temperature	1200° C	1200° C
Heating medium	Gas	Gas
Pre-forming details	Upset	Upset on 200 tonf press
Forging equipment	1000 tonf press	As in previous example
Forging details	One impression, single blow	One impression, single blow
Lubricant	Oil	
Production rate	250–300/h	
Component	Gear case end	Gear case end
Material	En 3A	En 3A
Stock size	2 in square bar (off-the-bar forging).	2 $\frac{1}{4}$ in × 2 $\frac{1}{4}$ in × 3 $\frac{1}{16}$ in
Forging temperature	1150–1200° C	1150–1200° C
Heating medium	Oil	Gas
Pre-forming details	Bar necked on 10 cwt stamp to bive billet length of 3 $\frac{7}{8}$ in	Forged to 2 in square on 200 tonf press for scale removal
Forging equipment	35 cwt drop hammer	As in previous example
Forging details	Forged off-the-bar in single impression using 5–6 blows	Single impression, one blow

Measurement of die deterioration

Replicas of the die cavity were taken before forging and after every fifty or one-hundred forgings; they were obtained by forging annealed aluminium into the cavities.

The following measurements were made on the replicas or dies.

(a) **Rectilinear measurements:** Using purpose built jigs the dimensions shown in Fig. 1 were measured. These dimensions were chosen after a preliminary examination of worn dies and represented those areas

where wear and deformation of the dies appeared greatest. Because of differences in die closure during forging of the replicas it was necessary to correct all measurements by reference to a 'standard measurement' taken at a position where no abrasive wear or distortion occurred.

This reference position was selected at a point where the original machining marks persisted in the die. The smallest measurement at this position was used as a datum to which all other measurements were corrected. The 'non-variable' dimensions selected are shown in Fig. 1.

(b) **Surface roughness measurements:** These were made in an attempt to obtain the rate at which abrasion of the die cavity occurred. Such measurements were useful in deciding whether dimensional changes were caused by deformation or abrasion.

(c) **Profile measurements:** Diametral or principal-axis sections were cut from replicas and the contours of enlarged projections traced to study detailed changes in die shapes. Fig. 2 shows the regions in which the shape changes were studied.

(d) **Visual examination and hardness measurements:** All dies were examined visually after use and hardness measurements were made at selected points.

Laboratory tests

Wear Tests: Laboratory wear tests were made on dies in a 20 tonf capacity C frame press and a modified 'Petro-Forge' machine.

Details of the DFRA wear test have been given elsewhere³. Briefly, the test consists of hot upsetting 2000 slugs of 1/2 in diameter x 3/4 in long to discs 0.2 in thick between flat test dies. The amount of metal worn from the dies is determined and used as an index of abrasive wear.

Table 2 shows the materials used for dies and for the forging stock.

Table 2. Stock and die materials

	Composition							
	C	Si	Mu	Ni	Cr	Mo	V	W
Die material								
No. 5 Die steel	0.6	0.3	0.6	1.5	0.6	0.25	—	—
En 40 C	0.4	0.3	0.6	0.4	3.0	1.0	0.2	—
5% Cr steel	0.3	1.0	0.6	—	5.0	2.0	0.25	1.0
12% Cr steel	0.1	0.3	0.7	2.4	12.0	1.8	0.35	—
Stock material								
Mild steel	0.2	—	0.8	—	—	—	—	—
En 24	0.4	0.3	0.6	1.5	1.0	0.3	—	—
En 57	0.2	0.6	0.8	2.0	18.0	—	—	—

Temperature and hardness measurements on dies:

Temperatures in the test dies during forging were measured using the thermocouple arrangement shown in Fig. 3, which also shows typical time-temperature traces measured in test dies. Although this arrangement obviously does not measure the true surface temperature it is a valid method of studying comparative die temperatures on both forging machines.

Hardness measurements were made at the centre of selected test dies before and after forging.

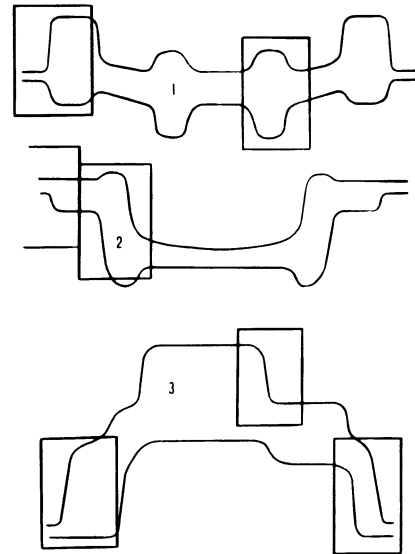


Fig. 2 Regions in test dies where enlarged replica profiles were studied.

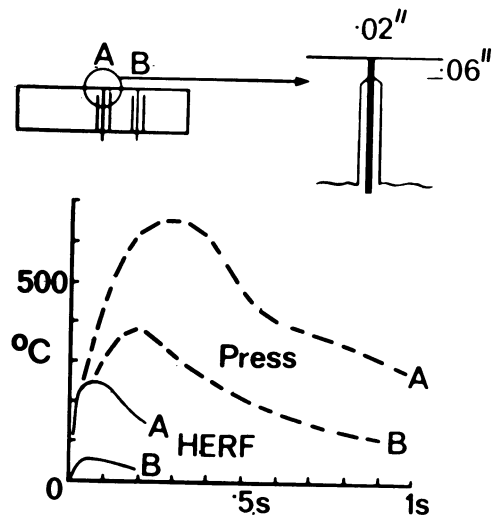


Fig. 3 Thermocouple arrangement in laboratory test dies and time-temperature traces.

RESULTS

Works investigations

Dimensional changes in dies: Fig. 4 shows a plot of one of the linear dimensions measured as a function of the number of forgings made. The line through the points is a regression line, the gradient (*m*) of which indicates how rapidly the dimension changes during forging. Such regression lines were determined for dimensions in all die cavities and Table 3 shows the mean value of *m* obtained, together with its standard deviation (*σ*). Also shown are the ratios of the values of *m* for the HERF dies and dies used on the conventional plant.

Table 3. Shapes of regression lines

	Conventional plant		HERF machine		m_H/m_C
	m_C 0.001 in/forging	σ	m_H 0.001 in/forging	σ	
1 Gear blank location					
a Flange diameter, top	0.014	0.008	0.020	0.008	1.43
b Flange diameter, centre	0.016	0.007	0.048	0.013	3.00
c Flange diameter, bottom	0.008	0.004	0.011	0.003	1.38
d Centre thickness	0.0006	0.001	0.002	0.006	3.33
e Web thickness	0.008	0.001	0.008	0.004	1.00
f Flash thickness	0.003	0.007	0.008	0.014	2.67
2 Flanged component location					
a Flange diameter, top	0.008	0.025	0.027	0.017	3.38
b Flange diameter, centre	0.017	0.021	0.040	0.011	2.35
c Flange diameter, bottom	0.011	0.019	0.027	0.014	2.45
d Centre thickness	0.001	0.009	0.016	0.007	16.00
e Flange thickness	0.008	0.012	0.017	0.006	2.12
3 Gear case end location					
a Overall length	0.039	0.015	0.056	—	1.44
b Overall width	0.039	0.016	0.110	—	2.82
c Overall height	0.018	0.025	-0.009	—	0.50
d Bass diameter, longitudinal	0.026	0.015	-0.005	—	0.19
e Bass diameter, transverse	0.033	0.018	0.085	—	2.58
f Large hole depth	0.019	0.006	-0.002	—	0.11
g Large hole diameter	-0.016	0.012	-0.006	—	4.12
h Small hole depth	0.014	0.003	-0.190	—	13.57
i Small hole diameter	-0.006	0.010	-0.078	—	13.00
j Small boss thickness	-0.001	0.007	0.150	—	-150.00
k Hole length	-0.003	0.010	0.068	—	-22.67

Although the ratio m_H/m_C in Table 3 indicates the relative die wear rates in conventional and HERF machines, the absolute values of m must also be considered when deciding whether wear is significantly different.

For the gear blank and flanged component, wear on both forging machines was of the same order of magnitude. A statistically significant difference in wear rate for these two forgings was only found on the centre flange diameter of the gear blank. In both those forgings, the profile measurements indicated a greater wear in the HERF dies at the entrance radius to the flash land. In all other places, wear on the HERF dies was not appreciably greater than on dies used in conventional plant. In the case of the HERF dies for the gear case end, however, much greater wear and deformation were indicated, both visually and by dimensional measurements.

On the hammer dies, all surfaces except the shoulder and boss on the top die and the hole base on the bottom die showed light abrasive wear. The die peg suffered heat checking with some cracks opening up to 1/32 in wide but being quite shallow. Considerable abrasive wear had occurred at position B on the flash land (Fig. 5). The peg on the HERF machine die showed no heat checking, but a combination of

mushrooming of the shoulder and heavy abrasion at C had produced a negative draft on the face of the peg. Heavy abrasion had occurred at D, but the flash land was not significantly worn.

The visual evidence thus supports the data in Table 3 which show that dimensional changes were much greater in the HERF dies than in the hammer dies. The magnitude of the dimensional changes in the HERF dies strongly suggests that deformation rather than abrasion was the principal cause (for example, small boss thickness and small hole depth).

Cracking of dies: It was possible from the aluminium replicas to detect the onset of cracking in dies. Table 4 shows the number of forgings produced in each die before cracking.

Laboratory wear tests

The results of the laboratory wear tests are shown in Fig. 6 & Fig. 7 shows the hardness changes which occurred during testing.

Table 4. Forgings produced before cracking

Component	Conventional plant			HERF machine		
	Top die	Bottom die	Total forgings	Top die	Bottom die	Total forgings
Gear blank	400	1200	1900	500	1000	1750
	500	1400	1900	200	700	950
	<u>400</u>	<u>1000</u>	<u>1700</u>	<u>300</u>	<u>500</u>	<u>1450</u>
Mean	433	1200	1833	333	733	1383
Standard deviation	58	200	116	153	252	404
Flanged component		100	800		200	700
		300	1000		100	960
		700	1200		100	1000
		100	600			
		100	500			
		—	1200			
		—	800			
		300	1600			
		100	600			
		<u>400</u>	<u>600</u>			
Mean		263	890		133	887
Standard deviation		213	354		58	163
Gear case end			2900			500
			1200			
			1400			
			<u>1900</u>			
Mean			1850			500

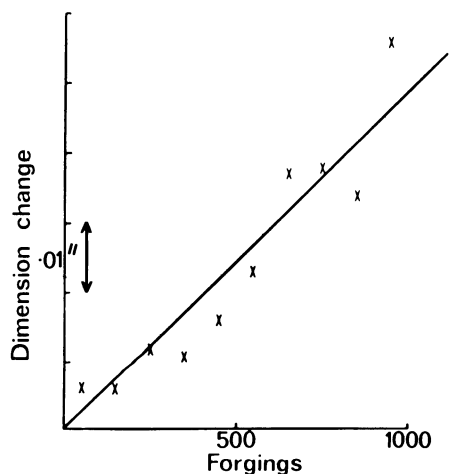


Fig. 4 Typical regression line relating dimensional change to number of forgings produced.

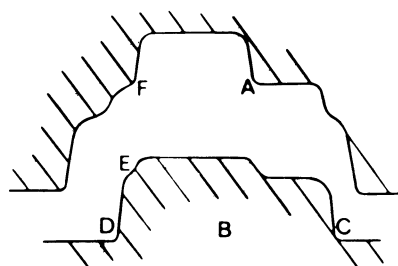


Fig. 5 Locations in gear case and dies.

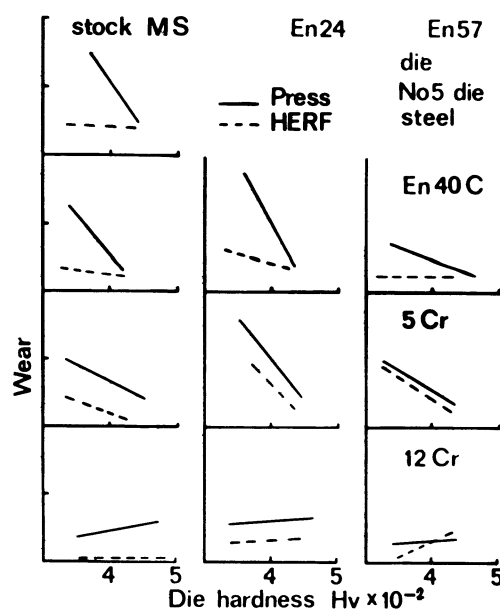


Fig. 6 Laboratory wear test results.

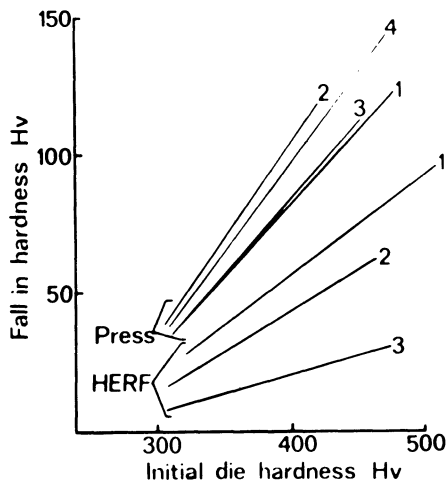


Fig. 7 Hardness changes in laboratory test dies.

DISCUSSION OF RESULTS

The results of the laboratory tests will be discussed first because they are interpreted more readily than those from the works trials.

Fig. 6 shows that wear on the 'Petro-Forge' machine dies was less than that on the press dies, whatever the combination of forging stock and die. The temperature traces in Fig. 3 indicate that the stock die contact time on the 'Petro-Forge' machine was about 0.05 s, compared with about 0.3 s on the press. This lower contact time led to less softening of the 'Petro-Forge' dies (Fig. 7) and consequently less abrasive wear. The importance of contact time on die wear has been confirmed by Ali⁴. Thus, the laboratory tests suggest that die wear on any piece of forging equipment will be related, amongst other things, to the dwell time after the forging blow has been struck. In interpreting the results of the works trials, deformation and cracking of dies must be considered as well as abrasive wear.

In the gear blank forging, those parts of the die subject to abrasive wear (*b*, *d* and *f* in Table 3) had wear rates about three times greater on the HERF machine than on the hammer. But on this particular forging the increased wear rate did not reduce the die life of the HERF machine dies unduly because cracking, rather than abrasive wear, terminated the life of the dies on both forging machines. Cracking of the HERF machine dies occurred earlier than the hammer dies and led to the 22% reduction in die life observed.

In the flanged component dies the areas most subject to abrasive wear (*a* and *d* in Table 3) also showed greater dimensional changes in the HERF dies than in the press dies. The ratio of the wear rates for the centre thickness (position *d*) was so high (16.00) that it is unlikely that wear was solely responsible for the difference observed on the two machines. It is most probable that the peg on the HERF machine dies suffered plastic deformation as well as abrasive wear. At position *a* near the flash land, the wear rate on the HERF machine was about three times that on the press; however, in this component die life on both forging machines was again determined by

cracking of the dies and was very short. In the gear case end forging, both deformation and wear were much greater on the HERF machine than on the hammer.

The magnitudes of the values m_H/m_C in Table 3 suggest that deformation was chiefly responsible for the dimensional changes in the HERF machine dies. It is probably significant that a relatively small hammer (35 cwt) was used as the conventional plant. (With such a small hammer delivering a large number of low energy blows the chance of overloading the dies is minimized).

From these results, therefore, for this forging the excess energy available in the HERF machine led to overstressing of the dies causing excessive deformation. Because of the excessive deformation on the HERF machine dies it is not possible to derive much information about the relative wear rates on the two forging machines. For this forging the die life on the HERF machine was less than one-third of that on the hammer.

Although the number of forgings considered in this investigation was limited, it is possible to draw the following tentative conclusions regarding die performance on HERF machines and a conventional plant.

(1) Abrasive wear is greater on HERF machine dies than on hammer or press dies. (This investigation suggests a wear rate three times greater on the HERF machine).

It must be remembered, however, that in all the cases considered a single die impression was used on the conventional plant. In the more general case of hammer dies in which multiple impressions are used, the wear of HERF machine dies will probably be greater than three times that in the final impression on a hammer. In such cases in which wear terminates die life, the life of HERF machine dies would be expected to be much less than that of hammer dies.

(2) Cracking occurs earlier on HERF machine dies than on hammer or press dies.

This suggests that the excess energy over that required to complete the forging is less easily controlled on HERF machines than on other plant. Because presses are constant stroke machines, no excess energy should be developed providing the dies are correctly set. On hammers the excess energy is minimized by the use of multiple blows of relatively low energy.

Excess energy differences are more likely to be minimized when HERF machines are being compared with large hammers than with small hammers, which suggests that die life will be reduced more for forgings made on small hammers than on large hammers.

(3) The above remarks regarding the effect of excess energy on cracking apply equally to its effect on deformation.

This conclusion is supported by the large reduction in die life on the HERF machine for the gear case end forging. It may be concluded that where die life is determined by abrasive wear, the life of HERF machine dies will be only one-third, or less, of that for hammers and presses. In those cases in

which die lives on hammers or presses are low because of the early incidence of cracking, the die life of HERF machine dies will not be so greatly reduced, as was the case for the flanged component. The results of this investigation suggest that in most cases die life on present HERF machines will be considerably less than on a conventional plant.

Aspects of design which seem to need attention in HERF machines are:

- (1) the long dwell time at the completion of the forging blow;
- (2) the ability to obtain closely repeatable energy delivery from one blow to the next and a method of easily and accurately setting the blow energy.

ACKNOWLEDGEMENT

The work described was carried out under Ministry of Technology contract number KJ/4M/33/CB78A.

REFERENCES

1. BAKHTAR, F., *The Engineer*, 7th March, 1969.
2. High-Rate Forging, A Study of Costs, DFRA Report, RC/67/66.
3. BRAMLEY, A. N., *Intern. J. M.T.D.R.*, 7, pp. 351–367.
4. CRAWLEY, J. and WILLS, G., 7th Intern. MTDR Conf., Birmingham (1966).
5. ALI, S. M. J., *et al.*, 11th Intern. MTDR Conf., (1970).
6. THOMAS, A., ISI Publication, p. 125.

DISCUSSION

Query from D. Harrison

We found at Vickers that the heat input to the dies came mainly from the contact of the billet with the die and the length of time required to eject the component from the die.

Reply

Temperature measurements made at DFRA have shown that heat transfer from a forging to a die is only appreciable when the forging load is applied, *unless* the forging sticks in the die. In this case high rates of heat transfer are maintained after the load is removed.

Query from M. Maj, McPherson's Ltd, Australia

Comment concerning value of the experiment in the case of identical die design and die materials for both conventional and HERF

- (1) Greater radial velocities, to the point of dynamic effects.
- (2) Shockwave creation in the parts of tooling and component. Both these call for different design and material of the die assembly.

Perhaps an ideal die for HERF should be also considered, if the results are to give some fair comparison.

Reply

Whilst appreciating the questioner's point, I would still maintain that only by standardising the die material in the tests could the effect of high rate forging be investigated.

Once the differences in performance are understood, one is in a much better position to consider the design and die material changes likely to combat the specific forms of failure that occur in high rate forging.

Query from B. W. Rooks, University of Birmingham

The influence of the forging machine characteristics on die wear.

This paper is particularly significant in that it is the first publication to compare directly the performance of dies on a HERF machine with that on conventional plant. In some respects the results on abrasive die wear are contradictory in that wear of the HERF machine's dies is greater than those of the conventional plant in the works trials, but the reverse occurs in the laboratory trials. Whilst there may be several reasons for this, the main reason would seem to be the fact that the Petro-Forge machine on which the laboratory tests were conducted has a different characteristic to the pneumatic-mechanical HERF machine on which the work trials were conducted.

The rate of heat transfer from a hot billet to the dies of a forging machine are dependent on the rate of billet deformation and the time of contact¹. Fig. 1 shows the cumulative heat transferred for three types of forging machine. The pneumatic-mechanical HERF machines generally have an extended contact (dwell) time, during which the dies are held under a pressure which may be several tons. Consequently, as can be seen in Fig. 1. the total heat input to the dies is greater than that of a hammer although still less than that of a crank press. On the other hand, Petro-Forge HERF machine has no significant after-forge contact time and its characteristic is very similar to that of a hammer, except that the shorter forging time results in less heat being transferred.

However, it is the temperature of the die surface that is important to the abrasive wear process. In this respect the high-speed process is at some disadvantage due to frictional heating effects. Fig. 2. shows the surface temperatures attained on a hydraulic press (slow speed) and on a Petro-Forge (high speed), starting with dies initially at room temperature².

At constant rates of striking a higher bulk temperature would be attained on the press than on the Petro-Forge, thus reducing the differential between the two surface temperatures illustrated in Fig. 2. Therefore, it would seem probable that the surface temperature attained with pneumatic-mechanical HERF machines will be greater than a hammer and no less than a crank press. On the other hand a short dwell time HERF machine such as the Petro-Forge will have lower surface temperatures and so abrasive wear will be less. It has been found that artificially extending the after-forge contact time of a Petro-Forge to 0.25s results in increased die wear, as illustrated in Fig. 3¹.

References

7. Rooks, B. W. & Tobias, S. A. *Shorter Dwell Times Reduce Die Wear in High Speed Hot Forging*. Proc. 3rd. Int. Conf. Cen. High Energy Rate Forming, Vail, Colorado. July, 1971.
8. Kellow, M. A., Bramley, A. N. & Bannister, F. K. *The Measurement of Temperatures in Forging Dies*. *Int. J. Mach. Tool Des. Res.* Vol 9. Pergamon Press, 1969.

Reply

I think perhaps the diagram (Fig. 2(a)) which Dr. Rooks showed in his query is unduly pessimistic with

regard to the effect of frictional heating in high rate forging.

The curves shown were measured during the upsetting of a cylinder to a high reduction, which involved a great deal of sliding and thus a lot of frictional heating.

In an actual die cavity, the shape of the die will often reduce the amount of sliding that can occur at any given point, since the vertical die walls restrict lateral metal flow.

THE PRODUCTION OF TENSILE TEST SPECIMENS BY AN ECONOMICAL BLANKING PROCESS AND ITS FEASIBILITY FOR PRACTICAL APPLICATION

by

TAKEO NAKAGAWA* YUKIO FURUKAWA† and KIYOTA YOSHIDA‡

SUMMARY

The standard practice for the measurement of mechanical properties of steel sheet uses a tensile test specimen produced by machining, which involves high production costs and appreciable time. To avoid this expensive process, an economical blanking process is proposed for producing the test specimens. Detailed experimental investigations carried out on their mechanical properties are reported here and comparison is made with machined specimens.

INTRODUCTION

Of the different materials used in industry, sheet material is generally consumed in the largest quantities. The tensile test is frequently adopted by industry to assess the quality of sheet material, and, in carrying out this test, the standard method and specimen recommended by ISO or JIS (Japan Industrial Standard) or some other National Standard, is generally used.

The tensile test is always carried out by the manufacturer of sheet, on each production batch, and the user selects the material on the basis of that tensile test value.

As such, the tensile test has been considered the most reliable test in material testing and almost all materials are now tested by this method. In some cases, the same material is tested twice, first at the place of production and then by the user. Furthermore, in special cases, the tensile test pieces are sampled from three directions, that is, longitudinal, transverse and diagonal to the rolling direction. Thus in all, a large number of tensile test specimens are required.

As far as the manufacture of the specimen is concerned, it is very important to maintain the uniformity and quality of surface finish of its parallel edges, otherwise there will be deviation from the usual necking and fracture point. With bad surface quality, fracture occurs with the crack starting from the edge, whereas non-uniformity causes the necking and the crack to start away from the centre of the specimen. These deviations cause errors in the values obtained

by the tensile test.

In view of this, it is standard practice to prepare the tensile test specimens by machining, and heavy milling is not normally permissible. This involves high production costs and appreciable time. To decrease the cost of specimen production, a blanking tool of slightly greater size can be used to preform the specimen, the gauge section then being machined to the desired size and shape.

Although this production method is important and requires investigation, there is so far no report dealing with any improvement to make it more economical. We outline here an economical process that eliminates the present expensive machining operation and describes in detail experiments carried out comparing the mechanical properties with those of machined specimens.

PRODUCTION PROCESS FOR TENSILE TEST SPECIMEN

The tensile test specimen standardized by JIS was used in this experiment, using the slightly modified form shown in Fig. 1a. Initial tests with a tool which reproduced the standard machined form (Fig. 6) resulted in the blanking tool cracking at its sharp corners. The modified form produces radii at the ends of specimens, which do not affect the tensile characteristics.

The tensile test specimens are produced by the following five methods, the merits of each being assessed from the mechanical test results.

*Institute of Industrial Science, University of Tokyo, Japan.

†Kawasaki Steel Co. Ltd., Chiba, Japan.

‡Institute of Physical and Chemical Research, Saitama, Japan.

1. Machining;
2. Blanking;
3. Blanking and filing;
4. Cut-off punching;
5. Cut-off punching and filing.

Machined specimens are prepared by shearing the sheet to a rectangular shape and then milling, to give the desired straight parallel sides and radiused ends, according to the standard. This is the most frequent method of producing tensile test specimens.

Cut-off punching¹

This is a new shearing method similar to shaving, whereby a specially designed single stroke cut-off punching tool is used (see Fig. 1b). The tool construction is as follows.

The lower part of the tool consists of a punch, stripper plate and polyurethane rubber pad for stripping, and the upper part has a primary blanking die, final blanking die (cut-off punching die) and knockout punch. The edge shavings are removed by compressed air after the specimen is knocked out. The primary blanking die plate has adequate chamfer at its back for the free development of the shavings, as shown in the enlarged detail of Fig. 1b.

It should be noted that this blanking tool is designed for material of 3.2 mm thickness, the cut-off width being 0.28 mm and the clearances 0.36 mm in the primary blanking and 0.08 mm in the final cut-off punching die. This is determined on the basis of previous research² on the influence of cut-off width as shown in Fig. 2.

Blanking process

For blanking 3.2 mm hot rolled steel sheet, the cut-off punching die is not used. The clearance is 0.36 mm, corresponding to about 11% of the thickness. For 0.8 mm cold rolled steel sheet, the primary blanking die is omitted and the cut-off punching die used, with 0.08 mm clearance, corresponding to 10% of the thickness.

Filing

This is a simple operation which can easily be applied after blanking to obtain a good surface finish. The sheared parallel edges are filed by a commercial machine using an endless belt. It should be noted that the amount of material removed is only 0.04 mm per side and generally it is found to take about 10–15 s per specimen. In mass production it can be done by batch filing.

MATERIAL SPECIFICATIONS

The material used for the experiments included ten types of 0.8 mm cold rolled steel and four types of 3.2 mm hot rolled steel, which are widely used in most industries. Hot rolled steel sheets of 1.6 mm, 2.3 mm and 4.5 mm thickness are also used for investigating the influence of thickness on the tool designed for 3.2 mm thickness.

EXPERIMENTAL RESULTS

Our experiments compared the properties of specimens produced by the different methods with machined specimens.

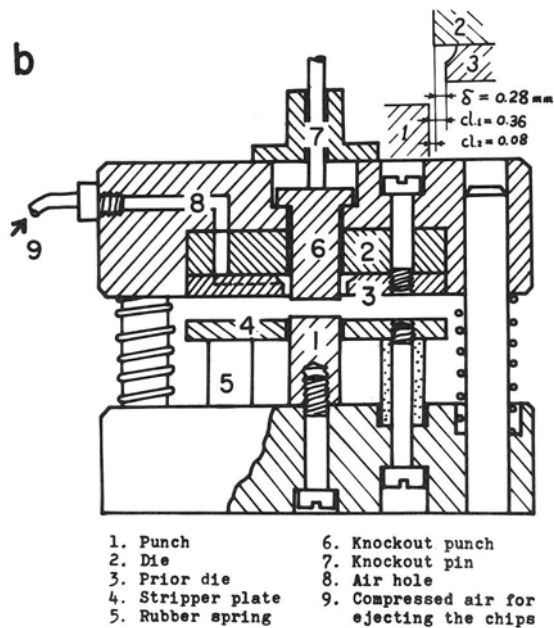
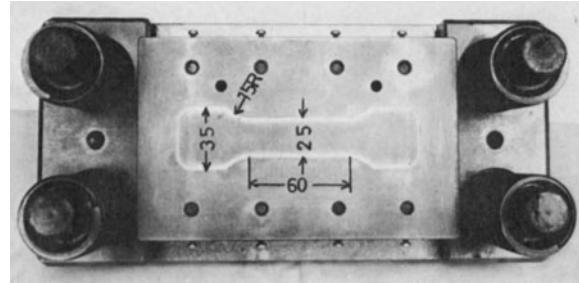


Fig. 1 Blanking and cut-off punching tool to produce tensile test specimens.

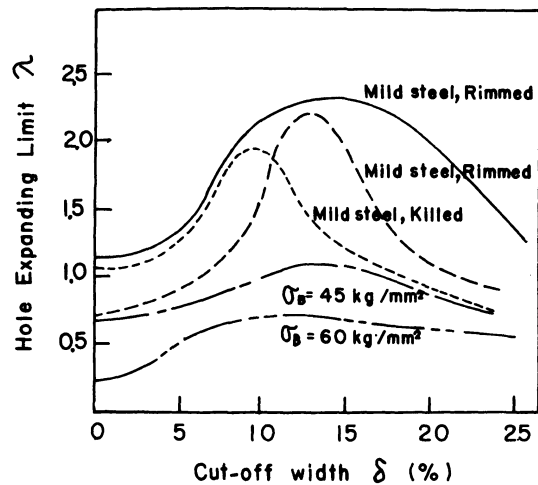


Fig. 2 Influence of cut-off width δ on the hole expanding limit when cut-off punching is introduced to burring operation.

Cold rolled steel sheet

Two comparisons are made;

- (i) blanked specimen with machined specimen; and
- (ii) blanked and filed specimen with machined specimen.

Blanked Specimen

Fig. 3 (a)–(e) show a comparison of several mechanical properties such as;

- (a) upper yield point;
- (b) ultimate tensile strength;
- (c) total elongation in 50 mm gauge length;
- (d) *n* value; and
- (e) *r* value.

obtained from tensile tests on the blanked and the machined specimens;

(a) Upper yield point.

Fig. 3a shows the yield strength comparison between the blanked and the machined specimens. The yield strength for the blanked specimen is found to be slightly higher than the normal machined value, the increase being only about 0.4 kg/mm², which corresponds to about 2% of the yield stress. This increase is very small and can be neglected, as such small differences normally occur even in machined specimens in ordinary tests. The increase in yield strength is attributed chiefly to the work-hardening zone developed on the sheared parallel sides during blanking. If it is assumed that the work-hardened region has a yield strength of 40 kg/mm² and the non work-hardened central region 20 kg/mm², for a specimen with a width of 25 mm and a thickness of 0.8 mm, the increase of 0.4 kg/mm² would correspond to work-hardening to a depth equal to one quarter of the specimen thickness.

(b) Ultimate tensile strength.

In Fig. 3b, which compares the tensile strengths of machined specimens with blanked specimens, there is clearly very little difference, probably as a result of the same tensile strength existing in the work-hardened sheared edge and in the central part.

(c) Elongation.

It is evident from Fig. 3c that the total elongation obtained from the blanked specimens is less than from the machined specimens. In particular, rimmed steel has appreciably less percentage elongation, the decrease varying from 2% to 10%. This decrease is observed to be maximal for specimens prepared across the direction of rolling and minimal for the longitudinal direction. The results almost correspond to those from hole expanding tests for punched and machined holes, which we investigated previously, and the phenomena are similar. The grain size of rimmed steel is small, with low ductility of the matrix and a large grain boundary area with appreciable impurities included; furthermore, the *r* value of rimmed steel is small. These factors yield a high sensitivity to crack formation and propagation in the work-hardened zone at the sheared edge.

From this, it seems that blanked specimens can be used with appropriate corrections, except for rimmed steel, which unfortunately is consumed in large quantities.

(d) *n* value.

The *n* value (coefficient of work-hardening) obtained from blanked specimens is similar to that for machined specimens, as shown in Fig. 3d. The values are calculated from the stress and strain relationship at the points of 10% and 20% elongation, and the results show that the deviations in the stress–strain curve between the blanked and the machined specimens are very small, over this range of elongation.

(e) *r* value.

The *r* value (Fig. 3e) is found to be slightly decreased for the blanked specimens, as a result of the restriction of width contraction caused by the work-hardening along the sheared edge. There is, however, some scatter in the results, even for the machined specimens. The deviation obtained in this experiment can be considered negligibly small.

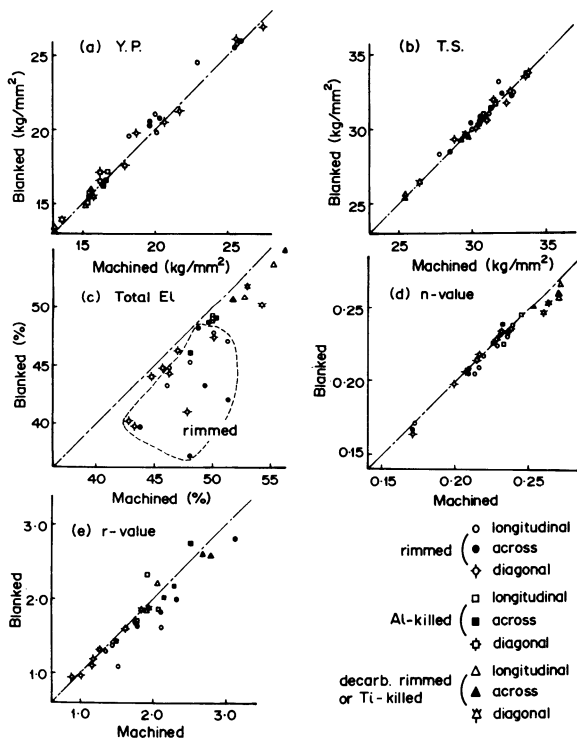


Fig. 3 Comparison of various tensile test characteristics for blanked and machined specimens in 0.8 mm cold rolled steel sheet.

Blanked and filed specimen

A filing operation is applied to the blanked specimen to improve the results. Comparing this with a machined specimen we found that the upper yield point and tensile strength values are very similar. Elongation values (Fig. 4) are much improved, compared with the blanked condition shown in Fig. 3c, and the method seems to produce a satisfactory specimen. It takes only about 10 to 15 s to file one specimen, because the amount of material to be removed is small (in the region of 0.03–0.04 mm per side).

This effect of removing a small quantity of metal by filing is very interesting, in that it produces a recovery of the elongation to that of a machined specimen. The filing operation evidently eliminates the micro-cracks in the work-hardened zone.

Hot rolled steel sheet

In this case, the machining cost is generally higher than for cold rolled sheet, because of its greater thickness, and it is necessary first to determine an economical production method for the tensile specimens.

Accordingly specimens produced by four different methods (blanking, blanking and filing, cut-off punching, cut-off punching and filing) were used in the experiments, and the results compared with those of machined specimens. Also, the effect of using the same cut-off punching tool on different material thicknesses is studied.

Blanked

The results of tensile tests on blanked specimens are shown in Fig. 5 (a-c). The yield point is increased slightly, the deviation being about 2 kg/mm², which is more than that for the cold rolled sheet. The principal reason for this is the thickness of the test specimen, which is four times that of the cold rolled sheet, giving a wider work-hardening zone.

The tensile strength values show negligible divergence, being similar to cold rolled sheet. Therefore, the tensile strength value seems to be independent of thickness. As regards percentage elongation, a decrease of about 2% to 8% is observed and therefore this method cannot be recommended for elongation measurement.

Blanked and filed

Filing the parallel sheared edges of the specimen after blanking does not appreciably improve the upper yield point, as shown in Fig. 5a. This is chiefly because the amount removed by filing is small (within 0.04 mm) and considerable work hardening remains. Elongation (Fig. 5c) is considerably improved, as with the cold rolled sheet.

Cut-off punched

The test results are also shown in Fig. 5. Compared with the blanked specimen, the yield point is similar and the elongation improved, but not as much as for the blanked and filed specimen. Fig. 6 shows the fracture appearances of the tensile test specimens. For the cut-off punched specimen, necking and failure start at the centre, resembling the behaviour of a machined test specimen, although the crack starts from the edge of the blanked specimen.

Cut-off punched and filed

This method should give the best results. There is very close agreement in the values obtained for elongation, as shown in Fig. 7c, but the yield point is not very much improved. We propose here that this method can be adopted in place of machining.

Cut-off punched and filed specimens of various thicknesses

In the cut-off punching process there should be suitable optimum clearance and cut-off width for each thickness. But, tooling costs become high if different cut-off punching tools are used and, therefore, it is desirable to use the same tool for different thicknesses. Fig. 8 (a)-(c) show the results from cut-off punched and filed specimens of thicknesses ranging

from 1.6 mm to 4.5 mm, produced by tooling designed for 3.2 mm thickness. These results suggest that the same cut-off punching tool can be used satisfactorily for thinner sheets of 1.6 mm and 2.3 mm, but for the thicker sheet (4.5 mm), the yield point and tensile strength values increase considerably. This is because the removal of material in the work-hardening zone by cut-off punching and filing is constant and independent of thickness, although the width of the work-hardening zone actually developed in shearing is proportional to thickness.

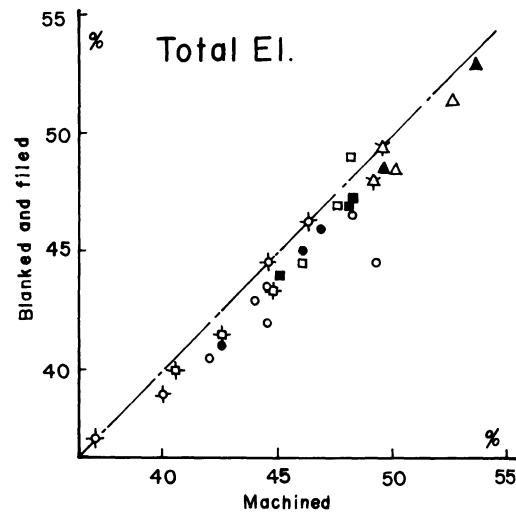


Fig. 4 Comparing blanked and filed and machined specimens of 0.8 mm cold rolled steel sheet, in terms of elongation. (Notation of the experimental points plotted is the same as in Fig. 3).

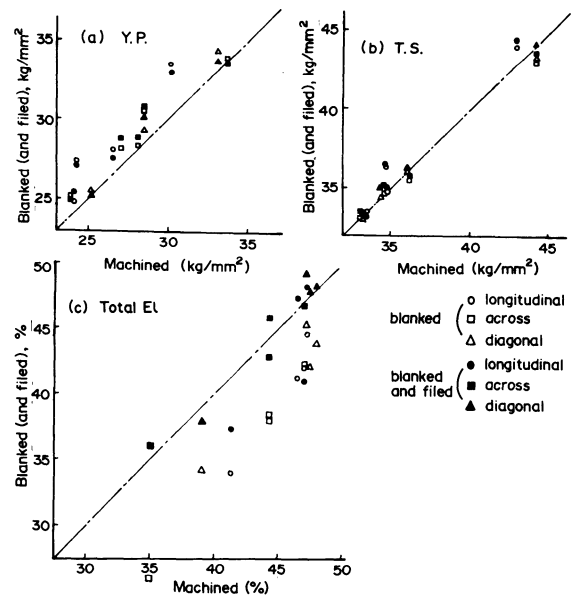


Fig. 5 Comparison of tensile properties of 3.2 mm hot rolled steel sheet prepared by blanking, filing and machining.

PRACTICAL APPLICATIONS OF BLANKED SPECIMEN

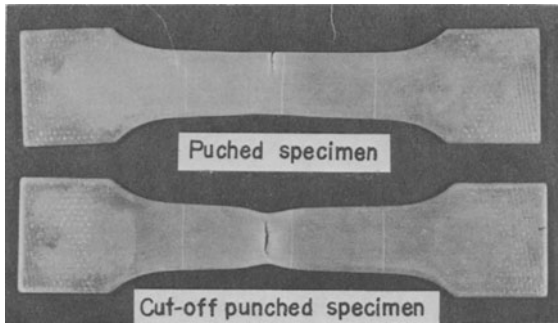


Fig. 6 Fracture appearance of 3.2 mm thick hot rolled steel specimens made by blanking and cut-off punching.

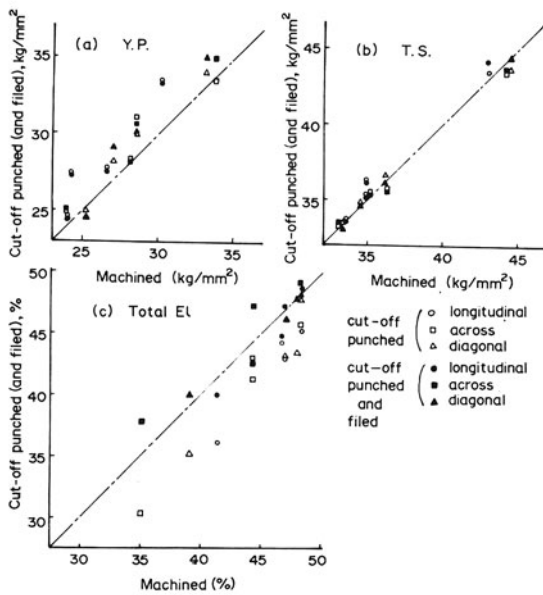


Fig. 7 Comparing tensile properties of 3.2 mm hot rolled steel specimens prepared by cut-off punching and filing and machining.

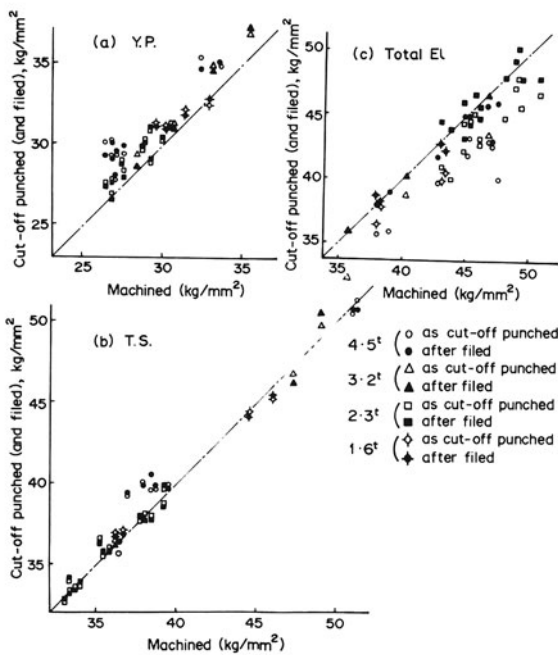


Fig. 8 Comparing tensile properties of cut-off punched and filed and machined specimens of hot rolled steel sheet in various thicknesses.

Practical feasibility of blanking process

From the above experiments, the following conclusions can be drawn.

1. For blanked specimens, the yield point increases a little, the increase becoming greater with increase of thickness. It cannot be eliminated by cut-off punching and filing. For the smaller thickness, however, the increase of yield point is very small and can be considered to be negligible in practice.
2. The increase in tensile strength is so small as to be negligible in all specimens except the thickest (4.5 mm) and accordingly the measurement can be used in practice without any correction.
3. Elongation decreases considerably for blanked specimens. It can be improved by cut-off punching and filing.
4. The extent of the work hardening zone developed in the shearing operation is proportional to the thickness of the sheet. Because the width of the tensile test specimen is fixed in accordance with the standard, the proportion affected by strain hardening increases with thickness. Therefore, the thinner the sheet the smaller the work-hardening effect in shearing.
5. Because the work-hardening zone developed in thin cold rolled sheets (for example 0.8 mm) is very small, blanked and filed specimens can be recommended for practical use.
6. For hot rolled sheets, up to 3.2 mm thick, cut-off punched and filed specimens can be recommended for practical use.
7. The same cut-off punching tool can be used satisfactorily for materials of smaller thicknesses.
8. For thicknesses of 4.5 mm and more, this process would be difficult to apply practically.

To sum up, the blanked test specimen is generally feasible in practice, except for the thicker materials.

Merit of economy in steel-making plant

There are two principal economic attractions for the introduction of blanked specimens for tensile tests. First, it reduces the cost of production by eliminating the machining process, and secondly, the blanking method is very simple and rapid, as shown in Table 1, and the result of the test can be obtained very rapidly. The advantages and merits of the application of this process in a steel plant are as follows.

At present it takes about 2½ days on average from the time of sampling out from the sheet to the time of data punching, and during this period the finished product must wait in the storage and packing yard for the test certificate. This long delay is caused by the batch system of shearing the rectangular blanks and milling. In the system proposed here, the test specimens can be produced individually when required and the time to obtain the result is reduced to 1 day, as illustrated in the flow diagram of Table 2. Decreasing the waiting time in the storage yards means quick production and despatch of the final product. Also, considerable expenditure can be saved by decreasing the handling work in the storage yard.

When the tensile test is conducted immediately

and the result is not satisfactory it can be repeated if necessary. On the basis of this test, the correct grade of steel can be assessed quickly and, in case any change is necessary in the grade of steel, it too can be achieved quickly by passing the proper instructions to the production group. Thus, the desired quality of steel, or a suitable outlet for the current product, can be determined rapidly when the tensile test results are quickly available.

ACKNOWLEDGEMENTS

We thank Mr H. Kawase of Nisshin Steel Co. for his invaluable advice, and also Mr A. Namikawa of M/S

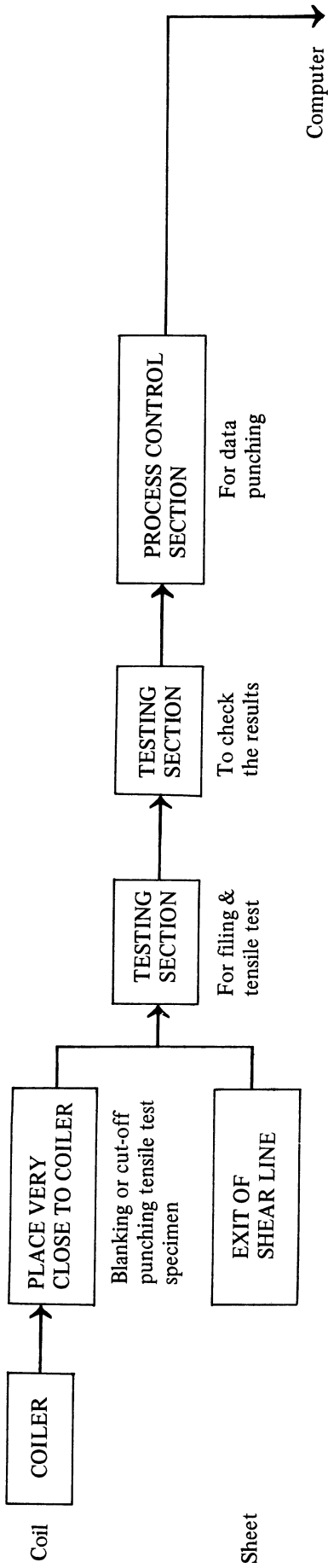
Fujitsu Ltd for his assistance in tool making. We also thank Mr V. Nagaraju of the Mechanical Engineering Research and Development Organization, India, for his kind assistance in writing the manuscript.

REFERENCES

1. NAKAGAWA, T., and YOSHIDA, K., *J. Japan Soc. of Tech. of Plasticity*, **10**, 665 (1969).
2. NAKAGAWA, T., and YOSHIDA, K., Int. Conf. on Sci. and Tech. of Iron and Steel, Tokyo, 5-1-3 (1970).
3. NAKAGAWA, T., TAKITA, M., and YOSHIDA, K., *J. Japan Soc. of Tech. of Plasticity*, **11**, 142 (1970).

Table 1. Comparison of production process of tensile test specimen

	Present Method (MACHINING)	Proposed Method (BLANKING)
Sampling from the sheet to be tested	<ol style="list-style-type: none"> (1) Development Marking on the standard size metal sheet suitably to obtain rectangular shaped blanks that envelopes the standard test piece. (2) Rough Shearing with margin allowance. (3) Precision Shearing to get the correct rectangular shape as per marking. (4) Marking of reference code number such as coil No, batch No. etc on the developed metal sheet. 	<ol style="list-style-type: none"> (1) Direct Blanking or cut-off punching from the original standard sheet or roughly sheared sheet. (2) Marking of reference code number, such as coil No, batch No. and so on.
Milling of parallel edges	<ol style="list-style-type: none"> (1) Rough Milling the sides of the clamping ends (2) Rough Milling the parallel edges and radius-curves (3) Finish Milling parallel edges and radius-curves. This operation is necessary for each side and can be done in batch system. 	Filing by endless abrasive belt for about 15 s for one specimen
Preparation for tensile test	<ol style="list-style-type: none"> (1) Identification Marking of the specimen (2) Measurement of thickness and width and calculation of cross sectional area. (3) Marking of gauge length. 	<ol style="list-style-type: none"> (1) Measurement of thickness only (measurement of coil width can be neglected) (2) Marking of gauge length.



Present flow diagram for H. R. sheet.

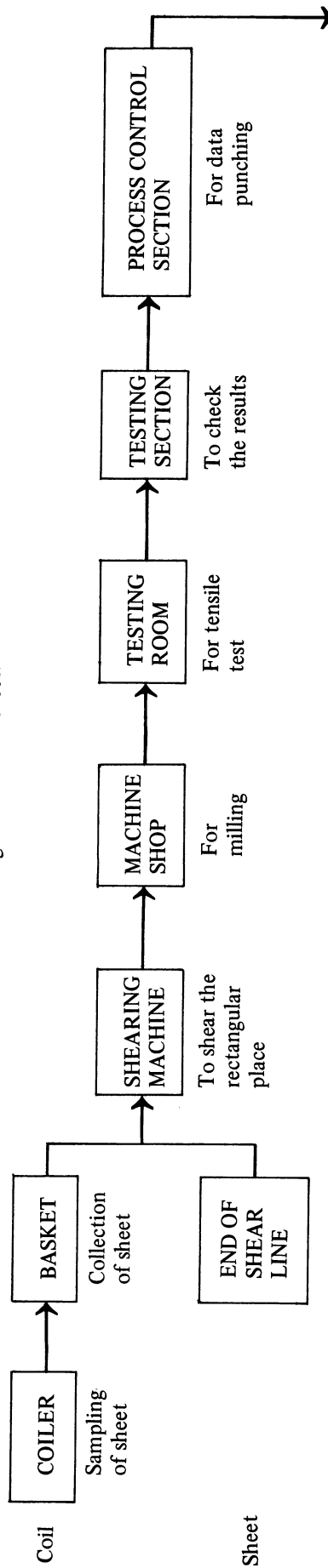


Table 2. Flow diagrams as adopted in a steel plant

DISCUSSION

Query from B. Larson, Technical University of Denmark

How many specimens can be made with the same tools without scatter in the tensiles?

I am thinking especially of R and N values which mean a great deal in sheet metalforming. Have you made investigations in that direction?

Reply

We have no experience about the life of this blanking tool, because the method had not been used practically. But, judging from our knowledge of tool life, the difference between this tool and an ordinary blanking tool is considered to be small. It is estimated that about 100 000 specimens can be blanked in 0.8 mm cold rolled mild steel sheet, and about 10 000 specimens can be cut-off punched in hot rolled mild steel sheet without any regrinding of the tool.

Query from Dr. Rolf Pruemmer, Germany

The paper presented describes an adequate method for fabricating tensile specimens of rolled steel.

I want to comment that the differences in yield strength and elongation observed with differently fabricated specimens are not only due to different amounts of work-hardening of the machined surface layers. There is also the introduction of residual stresses into the surfaces considered. Although the prestressed region is small, the mechanical properties of the bulk specimen are influenced. The amount and sign (compressive or tensile) of the residual stresses can be measured.

Reply

We did not measure the residual stress in the sheared zone, but it is considered that the residual stress has little influence on tensile test values as compared with other factors such as work-hardening, roughness and microcrack.

Of course, there is some possibility of the residual stress influencing the upper yield stress.

BENDING OF THIN-WALLED TUBES BY COMBINED EXTERNAL MECHANICAL FORCES AND INTERNAL FLUID PRESSURE

by

C. BOYD* and F. W. TRAVIS†

SUMMARY

Results of tests are described on the 'Z' bending of thin-walled tubes in brass and stainless steel using a special purpose machine which employs combined mechanical forces and internal fluid pressure. The two right-angled bends produced by the 'Z' bending operation are of fairly small radius of curvature (1.5 times tube o.d.) and of closely held circular cross-section. It is demonstrated how the provision of a controlled internal fluid pressure can eliminate wrinkles and buckles in the tube walls and suppress a tendency to the development of an oval cross-section. Photographs and a line diagram of the forming machine are presented, along with photographs of typical formed tubes.

INTRODUCTION

An increasing amount of development work in recent years has been directed to the use of a quasi-static fluid pressure in the forming and testing of metals; the pressure may be the sole forming agent or, as in the presently reported work, used in conjunction with mechanically applied forces. In most cases the pressure level employed is low—less than 10×10^3 lbf/in²—so that the resulting advantages arise primarily from the flexibility of loading thus afforded rather than an increase in ductility, which as shown by von Karman¹, Maier², Bridgeman^{3,4}, Pugh⁵ and others, requires, in general, pressures an order of magnitude greater.

A patent application⁶ in 1951 relates to the bending of brass tubes for musical instruments by a novel use of mechanical forces and subsequent fluid pressure. The tube is first compressed normally to its axis, using a shaped press tool, so that it collapses to develop a 'U'-shaped cross-section. The collapsed tube is then formed, with the convex side of the cross-section inwards, around a shaped mandrel. After insertion into a split die, the tube is hydraulically pressurised to restore its circular cross-section. This and similar techniques are described in reference 7, whilst improvements in the technique are described in reference 8. A further example of mechanical bending of a tube, and subsequent pressurisation within a split die, is in the forming of domestic sink water spouts described in reference 9.

A paper¹⁰ published in 1967 discusses the application of secondary or 'compensating' stresses during a metal working operation, to suppress tendencies to

rupture, and thus enable the realization of greater strains. In particular, a process for the bending of tubes is described in which the tubes are first filled with a fluid medium and then sealed at their ends with plugs, so that during the application of mechanical forces to the tube an internal pressure may develop to hold the tube against the forming dies and suppress buckling. Simultaneously with the bending operation, tube material is fed axially into the dies by means of hydraulic rams to provide compensating compressive stresses to offset the tensile bending stresses; and hence reduce the thinning of the tube walls. The process is described in more depth in reference 11.

A similar technique is used in the forming of a tee piece from a straight tube^{12,13}. The tube is placed within a split die, the latter having a radial opening into a branch cavity along part of its length. The tube is sealed at its ends by hydraulically operated plungers; a hole down the centre of the plungers allows oil to be introduced into the tube, and the tube is thereby pressurised independently of the forward motion of the plungers. By careful regulation of the internal pressure in relation to the axial in-feed of tube material under the advance of the plungers, it is possible to produce a branch of substantial length; too high a rate of advance of the plungers results in wrinkling and pushing of the formed tube from off its cavity walls, whilst too slow a rate of advance results in the branch being formed, essentially, by local swelling of the unsupported area only, with excessive thinning and premature rupture.

The presently reported investigation was initiated to examine the bending of tubes under combined

*Now with Munroe and Miller Ltd., Pipework Engineers, Edinburgh.

†Production Engineering Department, University of Strathclyde, Glasgow.

mechanical forces and internal fluid pressure, along the general lines of the work described in references 10 and 11, but for bends of larger curvature. Independent control of the internal pressure on the tube is also incorporated in the forming machine.

EQUIPMENT, MATERIALS, PROCEDURE

Forming machine

A photograph of the forming machine is presented as Fig. 1, and a drawing as Fig. 2. The main structural requirements of the forming machine were that it should

(i) provide powered motion in two directions, that is, for die closing and for axial in-feed of tube material,

(ii) provide and retain an independently controlled fluid pressure within the forming tube,

(iii) be of sufficient stiffness to avoid separation of the dies during the forming operation.

The die halves, item 2—shown vertically separated in Fig. 3—are bolted to sliding blocks, item 1, which run on lubricated brass pads set within the sliding block guides, item 9. Lateral, or die closing displacement, is achieved by the operation of rams item 15. Holes are drilled in the sliding blocks to accommodate the tube—as shown in Fig. 3—and axial in-feed of tube material is achieved by the operation of rams item 14. The carriage, item 7, holding the lower die half, is raised up to the die spacer, item 17, by operation of ram item 16, and locked in position by the insertion of four pegs through holes to engage in corresponding holes in the columns, item 8.

All controls and indicating gauges for the forming tool are mounted on the console shown in Fig. 1, which also houses the hydraulic pump, relief valve, electric motor and oil reservoir. Initially, hydraulic rams were connected so that one control valve regulated the flow to the two die closing rams, and a second regulated the flow to the two tube axial in-feed rams, but minor differences in friction led to unsymmetrical displacements. Separate control valves were fitted, therefore, to each of the five rams, and pointers were fitted on the machine to indicate the stroke position of each of the four main rams, symmetrical displacement being obtained by minor manual adjustment.

For full details of the design, manufacture and operation of the forming tool, the reader is referred to reference 14; the more relevant details, however, are provided below.

Die specification: To provide two 90° bends, with ½ in connecting plane length, in the form of a Z bend. The die cavity is of 3½ in diameter circular cross-section, and the mean radius of the bends is equal to 1.5 times the o.d. of the finished tube.

Die closing rams: 4 in diameter, 10 in stroke.

Tube axial in-feed rams: 6 in diameter, 10 in stroke.

Carriage raising ram: 2 in diameter, 10 in stroke.
Maximum pump pressure: 3 500 lbf/in² (for rams).

Tube internal pressure: Provided by means of a high-pressure intensifier operating from a compressed air line. Hydraulic pressures available of up to 10–15 × 10³ lbf/in² (but with reducing flow rate as pressure is increased).

Materials

The majority of tests were carried out using A.S.321 Austenitic stainless-steel solid drawn tube in the annealed condition, of 2½ in nominal bore; schedule 5's wall thickness (0.083 in), and 17 in length, as sawn. A small number of initial tests were carried out on tubing as above, but of 3 in nominal bore, schedule 10's wall thickness (0.120 in). Further tests were carried out using brass tubes ('Yorkalbro') of 76.1 mm o.d. and 2 mm wall thickness.

Procedure

The basic elements of the forming sequence of the tool are illustrated in Fig. 4: 'A' the carriage is in the lowered position and the tube inserted; 'B' the carriage is raised and locked into position; 'C' the die halves are closed by operation of the die closing rams, simultaneously with the operation of the tube axial in-feed rams and/or provision of a controlled internal pressure; 'D' the die halves are opened, the carriage lowered, and the formed tube removed.

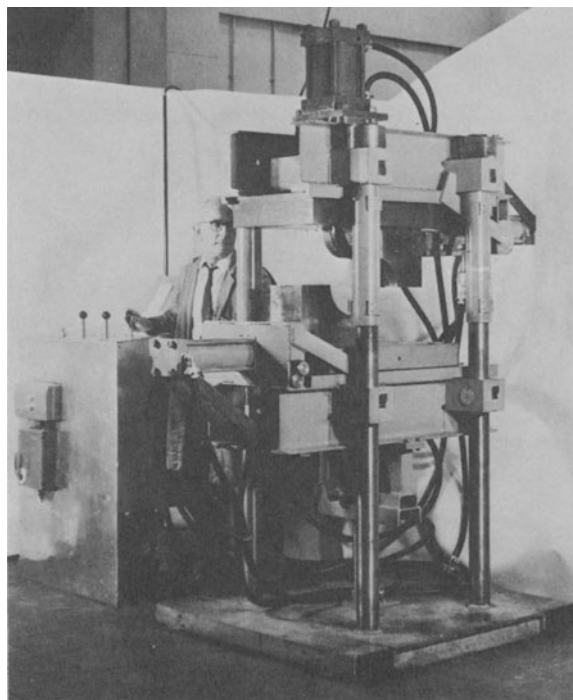


Fig. 1 Photograph of forming machine.

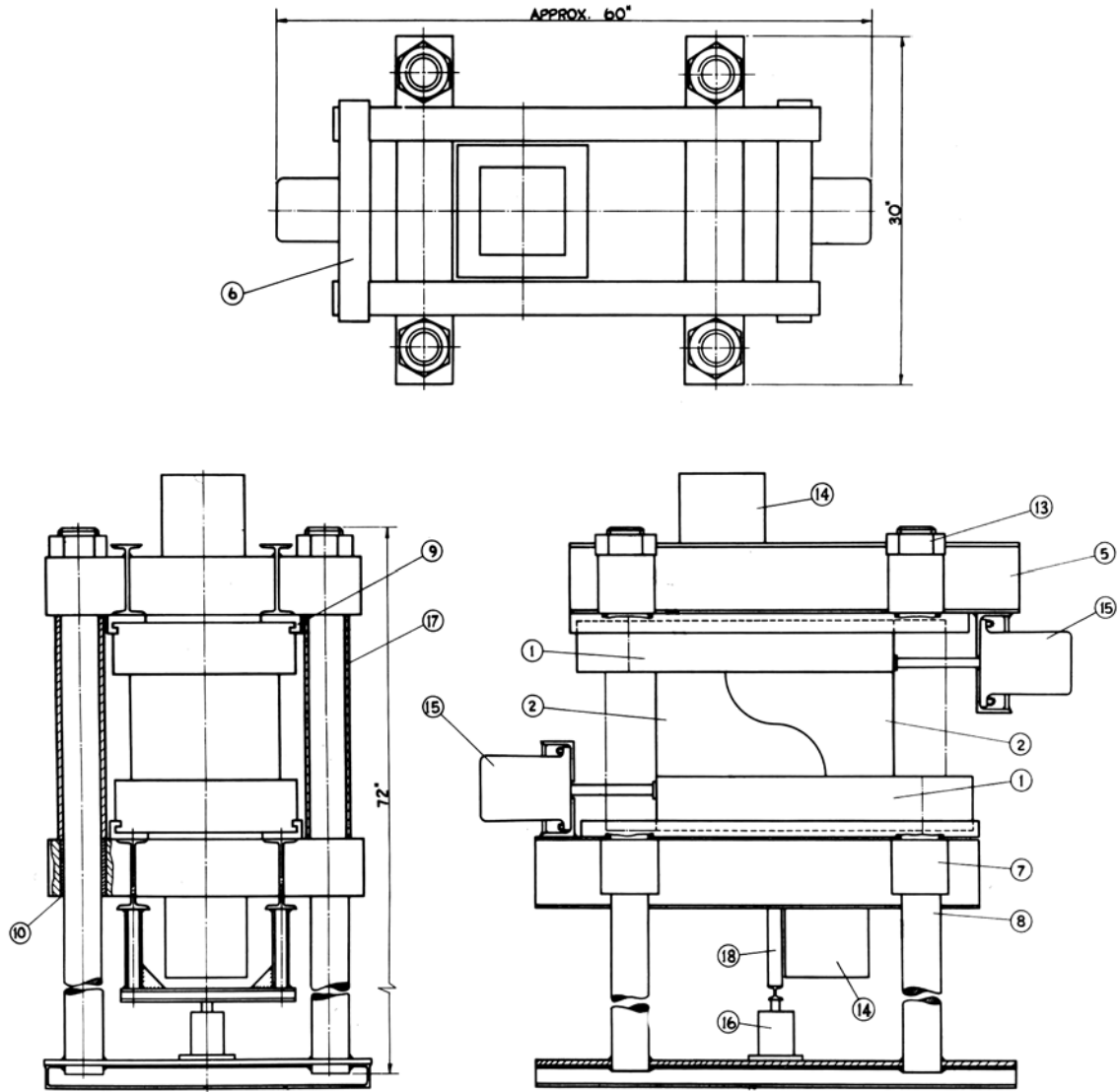


Fig. 2 Drawing of forming tool. Numbered items are as follows: 1, sliding block; 2, die half; 5, main frame; 6, mount for die closing ram; 7, carriage; 8, column; 9, sliding block guide; 10, sleeve; 13, die vertical separation nut; 14, tube axial in-feed ram; 15, die closing ram; 16, ram for raising carriage; 17, die vertical separation spacer; 18, frame for raising carriage.

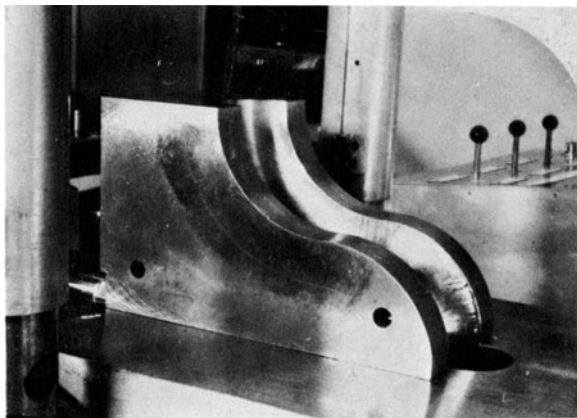


Fig. 3 Lower die half and sliding block.

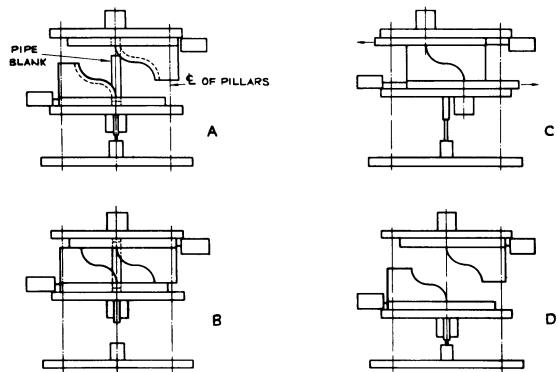


Fig. 4 Sequence of operations of forming tool.

RESULTS AND DISCUSSION

Initial tests

In these tests, 3 in nominal bore, 0.120 in wall thickness tubes were used; the latter were filled with water and fitted flush at their ends with rubber plugs prior to insertion into the forming machine. There was no provision for independent control of fluid pressure, and plane end-caps fitted to the tube axial in-feed rams served to retain the plugs and apply an axial load to the tube ends.

The pressure of the oil supplied to the tube axial in-feed rams was held constant during the tests, rising in intervals of 200 lbf/in² from 400 lbf/in² to 1200 lbf/in², so as to fully explore the effects of axial in-feed of tube material. In all cases—as shown for a pressure of 600 lbf/in² in Fig. 5—the tube was badly buckled, and what was more important, the development of ovality in the (laterally unrestrained) tube caused its central regions to extend beyond the die cavity and become trapped between the mating faces of the die halves. It was decided at this stage to carry out all further tests using tubes of smaller bore, so that the die halves could be closed without impediment; an increase of internal pressure would then expand the tube to assume the full contours of the die.

Tests using 2½ in nominal bore tubes

To accommodate the smaller diameter tubes, sleeves were fitted to the holes in the sliding blocks; a 5° semi-angle taper in the bore of the sleeve effected the transition from the approximately 2.7 in o.d. of the tubes to the 3.5 in diameter of the die cavity. A modification was made at this point to the rubber sealing plugs; the latter were of slightly smaller diameter than the tube and had a ¼ in diameter axial hole. Steel plates of the same diameter as the plugs were fitted to both sides of the plugs and held together by an Allen screw and nut. After free insertion of the plugs, the latter were expanded to grip the bore of the tube tightly by drawing together the steel plates with the Allen screw, and at the same time, the steel plates provided against extrusion of the plug material under the internal pressures developed.

In these tests also, the pressure of the oil supplied to the tube axial in-feed rams was held constant, rising in intervals of 200 lbf/in², from 400 lbf/in² to 1000 lbf/in² (at which point the tube commenced to yield before operation of the die closing rams). In all cases, the die halves closed without entrapping the tube. Irrespective of the level of the pressure of the axial in-feed rams, the tubes had a similar appearance; severe buckles had occurred to accommodate the geometric restraint imposed by the closing die halves, whilst the central length of the tubes remained straight, as shown in Fig. 6. It was concluded that specimens were commencing to bend around the die contours during the early stages of the operation but that, at some point, collapse occurred; using a tube of appreciably smaller diameter than that of the die cavity, there is initially very little confinement by the die to enable the development of sufficient internal pressure to resist buckling. If a higher axial in-feed ram pressure were used, so as to develop higher internal pressure, the correspondingly higher axial

load imposed on the tube ends would serve to promote buckling. For the particular die geometry of the presently reported investigation, it appeared necessary, therefore, to be able to develop the tube internal pressure independently.

Tests with independent internal pressure

To enable the tube to be internally pressurized independently of the forward motion of the axial in-feed rams, modifications were made to the top sealing plug, as shown (brought forward from beneath the ram) in Fig. 7. Oil is introduced into the tube from the hydraulic pipe on the left, through a hole in the ram extension and a brazed-on pipe passing through the sealing plug. Air is bled from the tube in a similar manner, to escape via the hydraulic pipe on the right, through the stop valve shown. The tube is thus placed—with the lower sealing plug fitted—in the lower die, the carriage is raised and locked, and the top sealing plug introduced by advance of the top ram. Filling and bleeding of the tube is then carried out under the control of the stop valve.

For a number of tests, carried out at different internal pressures, attempts were made to pull out the buckles by arresting the tube ends after predetermined displacements. It was found that whilst this had the desired result of removing buckles, the presence of an axial tensile stress—along with the tensile bending stresses induced by the closing of the dies and the tensile stresses due to the internal pressure—resulted in premature rupture of the tube walls in the outer curved region, either during closing of the die, or during subsequent attempts to expand the tube to fill the die. This is not surprising, and the avoidance of such failure is the reason for the introduction of the concept of 'compensating' compressive stress in the work of reference 10.

Whilst considerable effort had been made to produce tubes free from buckles upon closing of the dies, it was then considered whether this was, in fact, of great importance. It might be possible, as in the work of references 6–8, to consider only the achievement of the overall form in the initial operation, relying on subsequent internal pressurization to remove any wrinkles or buckles. Tests were carried out therefore, with the internal pressure maintained at 3000 lbf/in², and without pressure or restraint applied to the tube ends; it was found, however, that at this level of internal pressure, the die closing rams were of insufficient capacity to close the die and the tube axial in-feed rams were then advanced until this was effected. The tubes were buckled, and of similar general appearance to those of Fig. 6.

Having annealed the tubes, the final pressurization was then carried out using a high-pressure intensifier. As the rubber of the sealing plugs started to extrude during this operation, the plugs were discarded and brass caps were brazed onto the tube ends (for other than research investigations, however, one of the simpler and quicker sealing methods reported elsewhere^{5,12,13} would be required). It was found that full form was realized at approximately 5000 lbf/in², and the maximum pressure applied was approximately 7000 lbf/in². A selection of formed tubes is presented in Fig. 8.

Wall thickness variations

From measurement of the formed specimens Fig. 8, the average thickness over the inside of the bend is 0.074 in, and the average thickness over the outside of the bend is 0.046 in, representing decreases of 11% and 45%, respectively, based on the 0.083 in wall thickness of the 2½ in o.d. stock material used. Inherent in the present process, however, is an expansion of the tube from its initial o.d. of approximately 2.7 in diameter to the 3.5 in diameter of the die cavity, so that based on an equivalent (i.e. assuming no length strain) wall thickness at 3.5 in o.d. of 0.064 in, these figures represent an increase of 16% and a decrease of 29%, respectively.

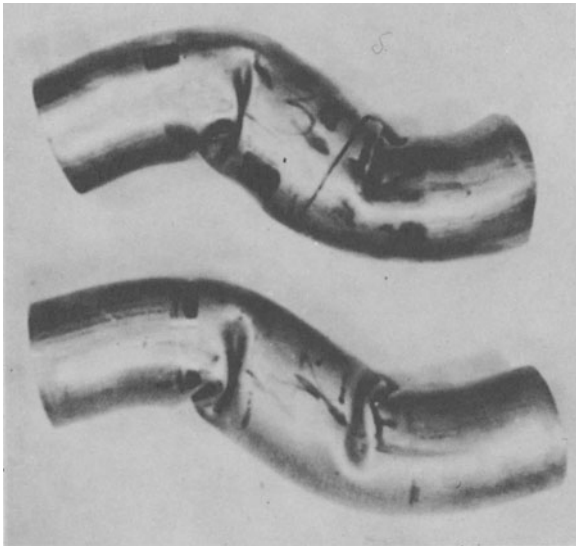


Fig. 5 Results of initial tests using stainless-steel tubes of 3 in nominal bore.

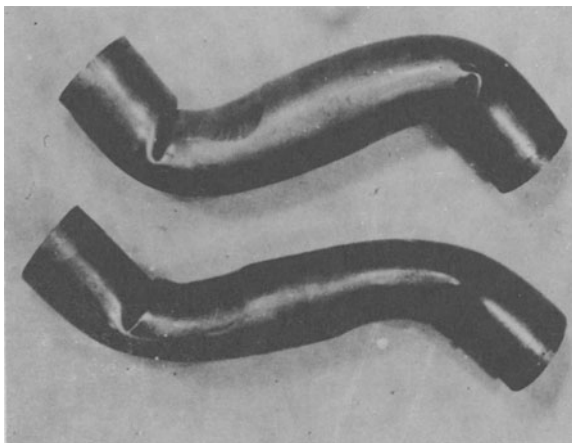


Fig. 6 Results of tests using stainless-steel tubes of 2½ in nominal bore.

Tests using brass tubes

Brass tubes were fitted with end caps, as above, and formed at an internal pressure of 1500 lbf/in², without pressure or restraint applied at the tube ends. On removal from the die, the tubes were found to be without buckles or wrinkles but not of full form and of oval cross-section at the bends. After annealing they were replaced in the die and pressurized to 3000 lbf/in² to achieve full form. After axial sectioning across a diameter, wall thickness measurements were recorded, as presented in Table 1.

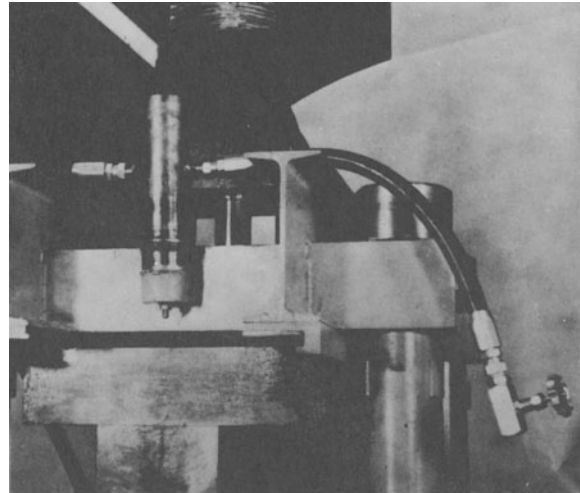


Fig. 7 Modification made to the top sealing plug to allow independent control of the tube internal pressure.

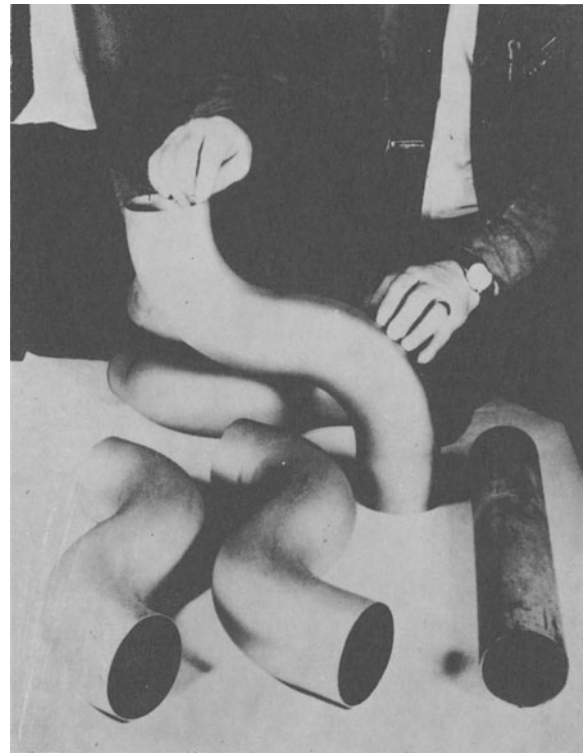


Fig. 8 Results of tests using stainless-steel tubes of 2½ in nominal bore, with independent control of the tube internal pressure.

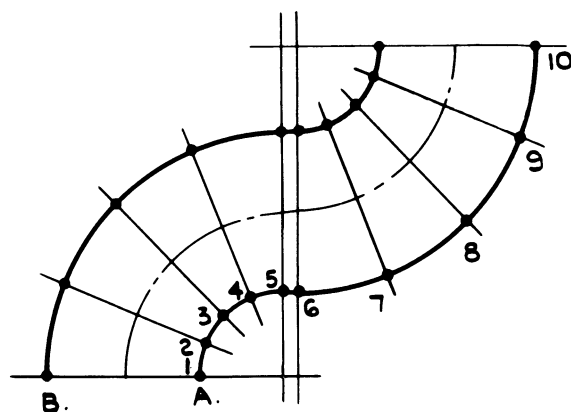


Table 1. Wall thickness of brass tubes (in)

Position	Specimen 1		Specimen 2		Specimen 3		Specimen 4	
	A	B	A	B	A	B	A	B
1	0.072	0.063	0.077	0.059	0.076	0.062	0.083	0.054
2	0.072	0.059	0.079	0.056	0.080	0.059	0.085	0.049
3	0.070	0.060	0.077	0.056	0.080	0.058	0.085	0.049
4	0.072	0.064	0.076	0.059	0.078	0.059	0.086	0.050
5	0.068	0.079	0.068	0.069	0.069	0.064	0.087	0.062
6	0.065	0.079	0.061	0.075	0.062	0.077	0.072	0.068
7	0.065	0.080	0.056	0.079	0.055	0.084	0.063	0.074
8	0.050	0.085	0.054	0.077	0.053	0.079	0.062	0.076
9	0.050	0.082	0.055	0.078	0.053	0.081	0.061	0.077
10	0.052	0.080	0.058	0.077	0.058	0.081	0.065	0.076

Based on an equivalent wall thickness at 3.5 in o.d. of 0.063 in, the average increase in wall thickness is 28% and the average decrease is 12.8%.

CONCLUSION

As may be seen from Fig. 8, and Table 1, the presently reported operation will produce smooth uniform bends of closely held circular cross-section and of tolerable variation in wall thickness; should a minimum wall thickness be specified, this can be achieved simply by use of a thicker stock tube.

It is reported in reference 10, that in the conventional method of producing bends using some kind of mandrel, a bending radius of 1.5 times the tube diameter may be obtained—only under favourable conditions—to produce a formed tube with a wall thickness reduction of about 25%. On this basis, the thickness variations of the brass bends produced by the presently reported operation compare favourably, and it is hoped that further exploration of the major experimental parameters will yield further improvement. It is felt that the main reason for the somewhat greater wall thickness variation of the stainless-steel tubes was that the die closing rams were of insufficient capacity to close the dies when using higher internal pressures, and modifications to the forming machine are in hand to provide greater die closing force.

ACKNOWLEDGEMENTS

The authors wish to acknowledge the financial assistance of Munroe and Miller Ltd., and Ford Motor Co.

Thanks are due to Mr Colin Bryden for help with the experimental work, and Professor D. S. Ross for the provision of research facilities.

REFERENCES

1. von KARMAN, T., V.D.I., Forschungsheft 118, Berlin (1912).
2. MAIER, A., 'Einfluss des Spannungszustandes auf das Formänderungsvermögen der metallischen Werkstoffe', Berlin (1935).
3. BRIDGEMAN, P. W., 'Studies in large plastic flow and fracture', McGraw-Hill, New York (1952).
4. BRIDGEMAN, P. W., 'The Physics of high pressure', G. Bell and Sons, London (1949).
5. PUGH, H. L. D., 'Recent developments in cold-forming', *Bulleid Memorial Lectures, IIIB* (1965).
6. British Patent no. 701, 112.
7. Anon, 'Hydraulic forming techniques applied to the manufacture of musical instruments', *Machinery*, 82 1089 (1953).
8. British Patent no. 808, 809.
9. Anon, 'Hydraulic forming excels for tubing', *Product Engineering*, p. 75, August 15 (1966).
10. REMMERSWAAL, J. L., and VERKAJK, A., 'Use of compensating forces and stresses in difficult metalforming operations', *Proc. Int. Conf. on Manufacturing Technology*, Ann Arbor, Michigan, September (1967).

11. British patent no. 1,029,892.
12. OGURA, T., and UEDA, T., 'Liquid bulge forming', *Metalworking Production*, p. 73, April 24 (1968).
13. OGURA, T., 'Liquid bulge forming', *Proc. 1st. Int. P.D.M.T. Conf.*, Glasgow, September (1969).
14. BOYD, C., 'The design and development of a tube bending machine employing fluid pressure and mechanical forces', M.Sc. Dissertation, University of Strathclyde, 1970.

DISCUSSION

Query from G. R. King

Dr. Travis was asked whether internal pressure was necessary during the time the dies were being closed, or whether this was used just to remove wrinkles etc.

Reply

Internal pressure was found to be necessary during the time the dies were being closed, in order to restrain the tube-ends within their seatings, and to allow the tube to strain to accommodate the greater developed length of the die cavity. In the absence of internal pressure, one end of the tube would merely pull into the die cavity to suffer excessive wrinkling and distortion. By using much longer lengths of straight tubing initially, it could still have been possible, after closing the dies, to insert end fittings and subsequently pressurise the tube, but it is the opinion of the authors that the greater length of tubing required would render this uneconomic, and that complete removal of wrinkles may not be possible under these conditions. It was also found, as reported in the paper, that a high internal pressure during closing of the dies secured a more favourable thickness-strain distribution in the former bend, and it is in this direction that further work is planned.

MACHINE TOOL FEED DRIVES AND GUIDEWAYS

SPECIAL DESIGN FEATURES OF NC CONTOURING MACHINES

by

DIPL.-ENG. GERD ENGEL.*

INTRODUCTION

Ever since numerical control systems were first applied to machine tools, increasing efforts have been made to improve feed drives. In the early stages, designers were satisfied with changing feed drive transmissions from manual lever control to remote control by incorporating electromagnetic clutches. It sufficed to provide a suitable position measuring unit for each feed axis, this unit feeding back the instantaneous tool or workpiece position.

In systems of this type, an electric cut-out arrangement which became active during targetting into a position, controlled the electromagnetic clutches in such a way that speeds changed from rapid traverse to intermediate, then to creep feed and subsequently came to a stop. Depending on the size of the masses to be moved and the response period required by clutches and contactors, this positioning cycle required 3–10 s or more, a rather important time factor. Another disadvantage lies in the fact that conventional positioning transmissions, involving clutches and a multiplicity of gears, are not free from backlash, nor is such backlash constant, which is why each position could only be approached from one direction.

As long as no tool is working while positioning is in progress, the only decisive factors are positioning accuracy and positioning time. Efforts were therefore made to reduce the inertia masses in gear transmission, to develop more accurate leadscrews—such as recirculating ball screws—and to improve anti-friction slide-ways properties. In parallel with these efforts, faster feed motors with higher output were also developed.

THE CONTROLLED FEED DRIVE

Latterly there has been an increasing demand for machine tools capable of controlling tool movements while cutting is in progress. These machines have straight-cut or continuous-path (contouring) controls.

Typical workpieces for which the machining demands such equipment are, for example, propellers and turbine blades, casting moulds and forging dies, complicated aircraft and rocketry components which have to be machined from the solid, but also simple workpieces with recesses, annular surfaces and bores, which, for time saving reasons, are milled with cylindrical milling cutters.

The feed drives of machines with straight-cut or continuous-path controls of this type have to fulfil quite different and much higher requirements than the feed drives of machines with mere positioning controls. The first demand is the direct result of the problems involved. Since multi-dimensional contours have to be machined, the tool has to describe 3-dimensional curves while maintaining a constant feed rate, and the geometrical situation is such that the components of velocity undergo continuous change along each feed axis. For this reason, every axis must have its own independent feed drive and a common distributor transmission is no longer suitable.

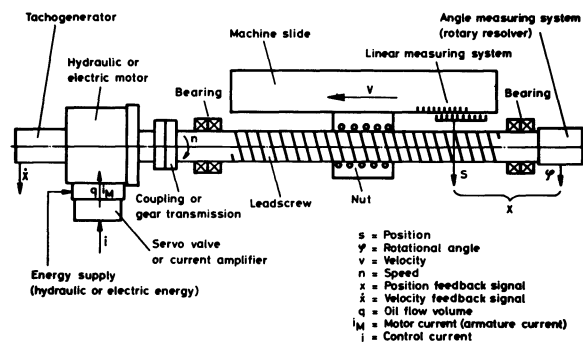


Fig. 1 Simplified model of a servo-feed drive system (Scharmann & Co., Rheydt).

An independent feed drive—shown diagrammatically in Fig. 1—consists of a number of machine elements in which energy and information flow takes place. The main constituent of such a drive is the motor. To make this motor produce a defined movement, a control signal is required which generally takes the form of a control current, i .

*Scharmann & Co., Rheydt, W. Germany.

This current is too low for the feed drive and must therefore be amplified with the aid of an energy converter (hydraulic or electric). In the case of hydraulic drive, the control current i is converted into a high-energy oil flow q with the aid of a servo valve or, in the case of an electric drive, the control current is converted to armature current i_M with the aid of a current amplifier. The armature current is proportional to motor speed. Interposing a gear train or a clutch, this motor speed produces the leadscrew speed, n . The leadscrew speed together with the leadscrew nut produces the slide speed (velocity), v . Thus v is also proportional to control current i . The position, s , of the slide can be fed back to the control system either directly with the aid of a linear measuring system or indirectly by measuring the leadscrew rotation angle, φ , with a rotary resolver (position feedback), x . A tachogenerator measures the velocity through the motor speed. This is fed back to the control system, too (velocity feedback), \dot{x} .

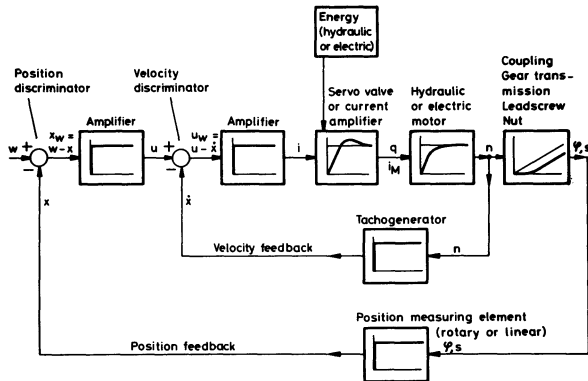


Fig. 2 Block diagram of a servo-feed drive with position and velocity feedback. (Scharmann & Co., Rheydt).

Fig. 2 shows this feed drive in the form of a block diagram. It will be seen that the control circuit is closed not only by position measuring but also by a velocity feedback. In actual fact, it is the velocity which is the main controlling factor in straight-cut or continuous-path feed drive systems. To ensure that the tool can rapidly compensate sequence errors, the control system must receive not only information concerning position but also any timed position changes—that is to say machine slide speed—and this is achieved with the aid of a tachogenerator flange mounted to the motor. Even the path control signal received from the tape determining workpiece contour is converted through an amplifier into a velocity command u which, in turn, controls the motor after further amplification.

Design requirements

A standard of the requirements which the design of a controlled feed drive must meet is given by its response behaviour to a step velocity command, Δv , fed in by the control. A good feed drive should follow this velocity step with very little time delay, T , as otherwise sequence errors will become excessive and the control loop unstable. How the actual response behaviour may appear in practice is shown in Fig. 3.

Five main properties affect the velocity response behaviour of a feed drive.

1. *Backlash.* This causes a direct time delay T_1 . It must be eliminated from a control loop.
2. *Elasticity of all machine elements.* This causes the storing of elastic deformation energy in the feed system over a certain time, T_2 , until movement starts up gradually. After initial acceleration, the stored energy is released, and overshoot occurs. This is undesirable in a control loop.

Properties of feed drive	Rigid $c = \infty$ Backlash-free $T_1 = 0$	Rigid $c = \infty$ Backlash $T_1 = \text{const.}$	Resilient $c = \text{const.}$ Backlash-free $T_1 = 0$	Resilient $c = \text{const.}$ Backlash $T_1 = \text{const.}$
Mass $m = \text{const.}$ Infin. acceler. $a = \infty$ Frictionless $\mu = 0$ Undamped $k = 0$				
Mass $m = \text{const.}$ Acceler. $a = \text{const.}$ Frictionless $\mu = 0$ Undamped $k = 0$				
Mass $m = \text{const.}$ Acceler. $a = \text{const.}$ Friction $\mu = \text{const.}$ Undamped $k = 0$				
Mass $m = \text{const.}$ Acceler. $a = \text{const.}$ Friction $\mu = \text{const.}$ Damping $k = \text{const.}$				

Fig. 3 Response behaviour of a feed drive following a theoretical velocity step. Messrs. Scharmann & Co., Rheydt.

3. *Finite acceleration.* To effect a velocity change without any time delay whatsoever would call for infinitely high acceleration. In practice this is not possible. An acceleration time constant T will therefore occur, and this must be kept to a minimum by choosing the strongest possible drive.

4. *Friction.* Friction reduces the available motor torque and therefore creates a reduction in acceleration and an increase in the acceleration time constant by an amount T_3 . Obviously, friction losses must be kept as low as possible.

5. *Damping.* Damping rounds off the curves and also reduces overshoot depending on size. A certain degree of damping is therefore desirable, but excessive damping will increase delay periods.

The subsequent paragraphs describe how the requirements outlined in the theoretical considerations presented so far can be converted into design practice:

- high stiffness of transmission elements and elimination of all play to keep the reversal span (backlash) to a minimum,
- low friction between all contributing machine elements especially between screws and nuts, as well as slideways, so that the reversal span remains small and available motor torque can be better exploited,
- adequate damping to reduce vibrations and avoid overshoot when sudden velocity changes occur,
- low inertia masses to improve velocity and acceleration behaviour.

RESILIENCE IN FEED DRIVES

Owing to the atomic structure of all materials, every machine element is elastic. A standard of the elasticity in machine elements is given by the resilience, $1/c$, as a reciprocal value of stiffness, c . In general, the stiffness formulae of all machine elements result from the relationships existing between force, and tensile or bending deflections based on the formula $c = F/x$. Basically, stiffness is proportional to the modulus of elasticity. As far as the designer is concerned, this means that highly stressed machine components should be made from material having an appropriately high modulus of elasticity. It should be borne in mind, for example, that the modulus of elasticity of cast iron is only $\frac{1}{3}$ and the modulus of compression of oil is only $1/150$ of the modulus of elasticity of steel. Cast-iron components and hydraulic piston drives should therefore be avoided in feed drives with travels greater than 400–600 mm. The cross-sectional area or the moment of inertia and length l are further factors influencing stiffness. This means that large cross-sections and short lengths should be given preference. Unsupported long shafts should be avoided when subjected to bending stresses, because stiffness decreases relative to length following the cube law.

Apart from tension, compression and bending, torsion is a further elasticity manifestation. Motors especially have a definite torsional stiffness. In hydraulic motors this depends on the modulus of compression and the oil volume contained in the motor,

while in electric motors it depends on electromagnetic factors such as inductance and magnetizing force. Many machine elements preclude the calculation of stiffness and resilience with conventional calculation methods or make such calculation very laborious. This applies particularly to the expansion of bearing bores in housings, elastic deformation of rough support surfaces or deformations occurring on screw fastenings.

Trial-based empirical equations can be established for the elongation of chains, resilience of bearing elements and gear teeth because all these components follow a certain system. The static and dynamic behaviour of columns, cross beams, beds and table assemblies can now be calculated with the aid of computers by feeding in the relevant coordinates and material data.

Screw fastenings in feed drives

A fastening device often used in machine building, but little known in terms of elasticity, is the screw. The stiffness c_s of screws and bolts can readily be calculated. Even the shoulder of the flange between screw head and abutment surface is elastic. As an approximation, such a flange could be considered as a bush with a stiffness c_B . Screw and bush are two superimposed springs whose total resilience adds up as $1/c = 1/c_s + 1/c_B$. The overall stiffness of this screw fastening is therefore smaller than the stiffness of the screw itself.

Till now it was generally sufficient to calculate a screw fastening in terms of tensile strength alone. However, if elasticity is calculated, it can readily be shown that thin screws have great disadvantages. Since with a constant modulus of elasticity, rigidity increases with screw cross-section, elongation reduces with the square of screw diameter. In addition, the screw length can also seriously reduce rigidity. It is therefore advisable, wherever possible, to use screws which are no longer than three to four times the screw diameter.

An example will illustrate how screw fastenings can be optimized. A flange bush sustaining the entire thrust of a feed leadscrew was hitherto secured to the machine bed with four screws M8 × 80 mm. Using this arrangement the available stiffness is 33 kp/μm. Without modifying the diameter of the flange, eight screws M12 × 35 mm could be accommodated. This increased the rigidity approximately by a factor of ten to 357 kp/μm. The gain in rigidity was achieved by the following modifications:

- increasing the screw diameter,
- shortening the screws,
- increasing the number of screws.

Where flange connections in feed drives are concerned, the direction of force application requires special attention. Flanges should on principle be so arranged that it is not the screws—whose tensile stiffness is not very high—which carry the load but the flange shoulders which are virtually rigid. Where the direction of force application changes, the flange connection should be so arranged that, regardless of the force application direction, the same number of screw fastenings is subjected to tensile stress.

Stiffness, efficiency and bearings for feed leadscrews

Since every material is elastic, all machine elements which are parts of a feed drive contribute towards deflections. Measurement taken on a leadscrew with a thrust bearing at one end show that the leadscrew sustains maximum deflection with almost 60% of total deflection, followed by the bearing block with almost 20% and the thrust bearing with approximately 16%. The deflection of the leadscrew nut is relatively low at approximately 8%. Clearly, stiffness improvements should therefore be applied in particular to leadscrew, bearing block and thrust bearing. The rigidity of the bearing block can be vastly increased by suitable ribbing of surrounding components in the load direction.

On numerically controlled machine tools, the feed leadscrews and nut should be not only rigid and free from friction, but also be made to a high degree of pitch accuracy, so that positions can be targetted and continuous-path curves followed without friction-caused overshoot errors. Conventional screw drives such as Acme screws are unsuitable for this purpose. Friction is too high and efficiency too low. This applies in particular to small helix angles. Leadscrews used in feed drives generally have a helix angle of 3–4°, with an efficiency around 20–30%, which is inadequate for numerically controlled machines. Rolling friction screw drives such as recirculating ball screws have, on the other hand, proved their worth for controlled movements, even with very low helix angles. Screws of this type have efficiencies above 90%, high pitch accuracy and allow the use of backlash-free nuts. Owing to rolling friction there is virtually no wear, and recirculating ball screws can therefore often be used as measuring screws as well. The stiffness of a leadscrew of fixed length can only be increased by increasing its diameter. However, there are limits to this approach because the moment of inertia increases at the fourth power of the diameter.

A further possibility of increasing system rigidity presents itself by supporting the feed leadscrew in thrust bearings at both ends (Fig. 4). With a thrust bearing at one end only, total leadscrew stiffness decreases as the distance x between nut and thrust bearing increases. If the screw runs in bearings at both ends, the maximum distance of the nut relative to

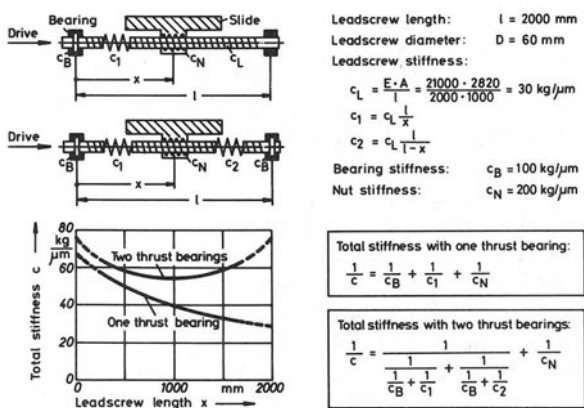


Fig. 4 Total stiffness of feed drives (Technical University, Aachen, Machine Tool Institute).

each thrust bearing is only half as long, and the two bearings together will in any event produce greater stiffness than only one bearing.

The thrust bearings themselves play quite an important part in the stiffness provided by a lead-screw system. Conventional radial bearings have low axial stiffness. Angular-contact ball bearings improve the situation, while pure thrust bearings increase stiffness to a maximum. In comparison to ball bearings, stiffness can be greatly increased by incorporating roller bearings. This is because, while ball bearings provide only a point contact between balls and races, roller bearings have linear contact and therefore tend to deform less. In addition, roller bearings can sustain greater loads and can therefore be preloaded more heavily. They are therefore still more rigid than thrust ball bearings.

The surrounding parts supporting a bearing assembly also influence the overall resilience of feed leadscrew bearing systems. Conventional bearing arrangements always employ a multiplicity of bearing rings, spacer rings and shoulder bushes, so that the number of contact surfaces is very high. However, every contact surface represents a resilience factor on account of its surface roughness, which reduces the load-carrying factor. This resilience is greater, the rougher the surface finish of the face in question, and obviously increases with the number of faces involved. For this reason, the number of spacer and other rings should be kept as low as possible and all contact surfaces should have the maximum load-carrying face area by finishing through face grinding. Spacer rings and bushes for thrust bearings should not be too narrow as they will otherwise deflect in the same way as a Belleville washer spring, which will again increase resilience. A relationship between ring width and thickness of 1:1 will generally suffice.

Preloading of machine elements

Preloaded machine elements not only achieve backlash elimination but also increase rigidity. Preloaded ball bearings, leadscrew nuts and roller slideways elements are well known, but hydrostatic slideways can also be preloaded by employing a hydrostatic retaining gib. Every preloaded machine element has a

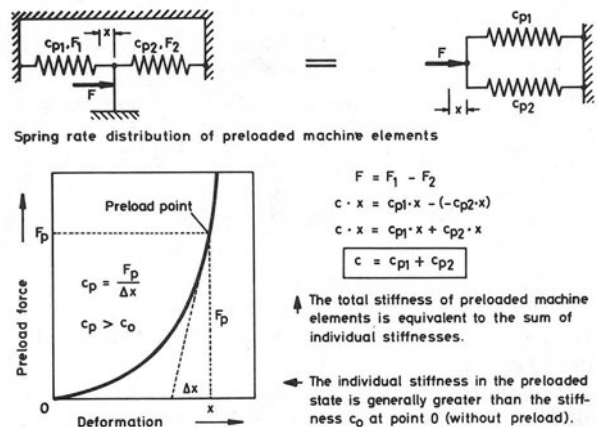


Fig. 5 Stiffness of preloaded machine elements (Scharmann & Co., Rheydt).

definite stiffness of its own. Fig. 5 thus shows two mutually preloaded elements with rigidities c_{p1} and c_{p2} and preloaded distances x_1 and x_2 . This is equivalent to the arrangement of two springs as shown in the illustration on the left-hand side of Fig. 5. As the springs are arranged in parallel, it can be said that in the case of preloaded elements the total stiffness is equivalent to the sum of individual stiffnesses. A further rigidity gain lies in the fact that almost all preloaded elements have a progressive spring rate, so that preloading by an amount x will in itself produce a greater rigidity than is possible without preload.

Friction and damping

Apart from high rigidity, numerically controlled machine tools require a high degree of accuracy. In particular, the reversal span when changing direction of feed must be kept small. This reversal span depends—apart from elasticity—directly on the friction in the feed transmission elements, especially that existing in guideways. Friction must also be kept down to avoid power losses.

With regard to rotary drive components, the advantages of low-friction recirculating ball screws as compared with Acme leadscrews have already been mentioned. Gears, frequently still used in feed drives with electric d.c. servo motors, must be under backlash-free preload and will therefore have greater friction right from the start. Such friction must be kept to the absolute minimum by precision machining of the gear flanks (lowest acceptable quality grade 5) and by running gears in over an adequate period. Longitudinal guideways represent a special friction problem. Plain slideways, as predominantly used hitherto, will still have excessively high friction even when lubricated with high-quality alloy mineral oils and will therefore cause excessive reversal spans.

Highly undesirable stick-slip manifestations are a further disadvantage. This is particularly undesirable when starting up and when using low feed rates, because friction fluctuates continuously between two different coefficients thereby generating severe vibrations. Low-friction guides, free from stick-slip, can in accordance with present experience only be achieved in two ways by:

1. roller guides,
2. hydrostatic slideways.

Roller guides have the advantage that they can conveniently be fitted to existing machines, often without extensive design modifications. A disadvantage of this arrangement lies in the fact that, despite the high stiffness of the rolling elements, the overall stiffness of the guide is not very great because stresses cannot be distributed as uniformly as in the case of plain slideways and because the surrounding parts of the guide elements are often much too weak. A further disadvantage is the low damping capacity of roller guides. Chatter vibrations, such as can arise in any metal-cutting operation, destroy the advantages of roller guides unless facilities are created which remove such vibrations through appropriate damping. This is why a compromise must often be accepted between the low friction of roller guides and the high damping capacity of plain slideways. An obvious solution suggests itself in retaining the plain slideways and

merely cancelling stress concentrations at certain points (for example as caused by the table assembly weight) by roller elements with adjustable force setting.

Hydrostatic slideways offer special advantages. The sliding surfaces are separated from each other by a thin film of oil and are therefore entirely free from metallic contact, ensuring absolute freedom from wear while friction is virtually equal to zero at all normal feed rates. Damping properties are exemplary and the stiffness of the oil film can—subject to taking appropriate measures—be made greater than the rigidity of surrounding component parts.

Unfortunately it is not easy to collect oil flowing out of hydrostatic bearings in a satisfactory manner and to return such oil free from dust and coolant contamination. For this reason, existing machines having plain slideways cannot readily be rearranged to provide hydrostatic slideways. Where new designs are involved, a hydrostatic slideway system presents no particular problems in terms of either design effort or expenditure.

The influence of inertia masses

The velocity and acceleration behaviour of a feed drive are decisively influenced by the mass of the moving machine components. Inertia forces manifest themselves more on rotational components than on masses moved in translatory directions (e.g. slide and workpiece), and it is therefore a design function to reduce rotary inertia to the absolute minimum. Based on the formula for flywheel inertia

$$WR^2 = \frac{\pi}{32} \times \gamma \times b \times d^4$$

two possibilities offer themselves to the designer:

1. choice of a lighter material (lower specific gravity γ) as far as material strength considerations permit;
2. avoidance of large outside diameters d at the expense of width b , because d is raised to the power of four in the equation, while b is merely a linear factor.

The first possibility is usually exploited by using belt pulleys made of aluminium alloys. The second possibility can be realized by gear wheels used in feed transmissions. With constant torque, the product $b \times d$ must be constant for strength reasons. If, for example, diameter d is halved, it will be necessary to double the width b , and the inertia will drop to an eighth.

The distribution of flywheel inertias and masses of feed drives varies widely depending on the type of drive chosen. Fig. 6 shows two completed feed drive designs: in the one case with an electric servo motor and in the other with a hydraulic servo motor, and these clearly indicate the difference in flywheel inertia distribution as reduced to the motor shafts. Since an electric motor delivers its output predominantly at high speeds and low torques, a gear reduction is necessary—in this case with ratio $i = 8.7$. Since, on the other hand, flywheel inertia towards the motor decreases with the square of the transmission ratio, the mass of the slide including the table load mani-

feats itself as flywheel inertia with only 3.4%, and as far as the leadscrew shaft is concerned with only 14.1% (Table 1). On account of the large inertia masses of the gears, the gear transmission contributes almost 30%. In total, there is between the inherent flywheel inertia of the motor and the flywheel inertia of the feed assembly a ratio of approximately 0.8 which can be considered as an optimum in control response for a d.c. drive.

Table 1

The following inertia masses reduced to the motor shafts, WR^2 , were calculated for the longitudinal feed drive, $z = 800$ mm, of a continuous-path control machine (Scharmann Type FB 75 NCC).			
	WR^2	kp cm ²	%
Electric d.c. drive	Table assembly + load	1.2	3.4
	Leadscrew	5.0	14.1
	Gear transmission	10.1	28.4
	External WR^2	16.3	45.9
	Motor WR^2	19.3	54.1
	Sum	35.6	100.0
External WR^2 /Motor $WR^2 = 0.85$			
Hydraulic drive	Table assembly + load	93.8	29.0
	Leadscrew	200.5	62.1
	Coupling	27.0	8.4
	External WR^2	321.3	99.5
	Motor WR^2	1.7	0.5
	Sum	323.0	100.0
External WR^2 /Motor $WR^2 = 192$			

The hydraulic drive is characterized by high torques at low speeds and can therefore be connected to the leadscrew shaft with a ratio of 1:1 using a coupling. Since the square of the transmission ratios does not manifest itself here, the table assembly together with its load contributes to the overall flywheel inertia to an extent of almost 30% while the leadscrew shaft contributes even more than 60%. The coupling at 8.4% can be almost ignored and the motor flywheel inertia of 0.5% has hardly any effect. The distribution is therefore quite different in the case of a hydraulic drive, and load differences in the table assembly greatly influence the situation. This is why hydraulic drives are frequently connected to the leadscrew system with a reduction ratio of 1.5–2.0. The examples described here indicate that the layout of the drive motors does not depend on the magnitude of static feed forces and gearbox efficiency—as would be the case in conventional feed drives—but exclusively on the size of the inertia masses to be moved.

Completed design examples

The manner in which the more important design requirements—freedom from backlash and bearing rigidity were catered for in the feed drives of a horizontal boring and milling machine with

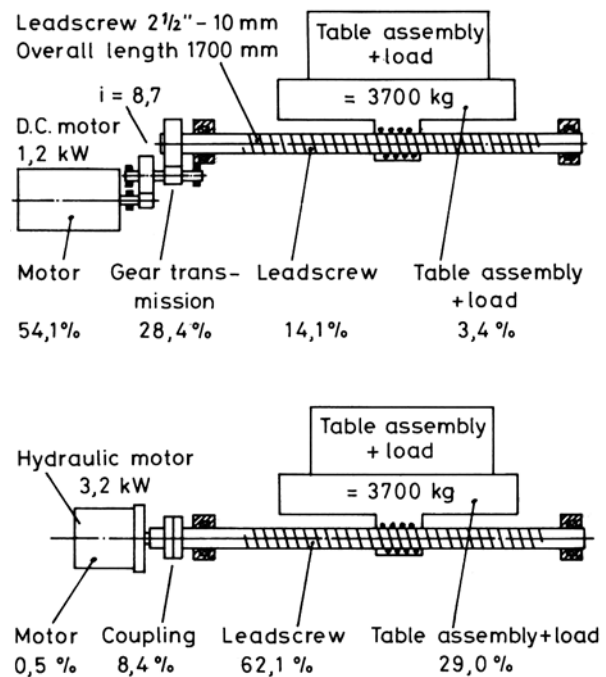


Fig. 6 Distribution of inertia masses in electric d.c. and hydraulic feed drives (Scharmann & Co.).

continuous-path control is indicated in Fig. 7, representing an electric d.c. servo drive, and Fig. 8, representing a hydraulic servo drive. The gear reduction between d.c. motor and feed screw must be entirely free from backlash and this applies in particular to mating gears, shaft bearings and connections between shaft and hub components. The shafts should preferably run in precision angular-contact ball bearings with mutual thrust preload through Belleville washer springs. Backlash in gear transmissions can be eliminated by using two drive gears with an identical number of teeth for each stage, these being offset relative to each other and secured in position when in the play-free state. Gears require increased accuracy (quality grade 5), and must be run-in adequately prior to starting up the machine. If necessary, the gears are readjusted several times during the running-in period because friction particles rub off initially; that is to say, readjustments are made until the tooth flanks are completely smooth. Connections between shafts and gears which are entirely play-free are assured by employing taper seats.

The thrust bearings used are roller cages. To increase rigidity, the races normally used in conjunction with such roller bearings are eliminated and replaced by thicker rings which cannot deflect like Belleville washers. The number of axial contact surfaces is reduced to a minimum which again benefits increased rigidity. All running and contact surfaces are surface hardened and precision surface ground. The other end of the leadscrew (not shown in the illustration) has the identical bearing arrangement, that is, the leadscrew has thrust bearings at both ends.

Fig. 8 shows a feed assembly driven by a hydraulic servo motor. The reduction transmission is eliminated in this case and replaced by a positive drive coupling. A number of hydraulic motors are very sensitive against axial and radial motor shaft

loads. Axial stresses can arise, for example, by thermal expansion of the screw coupled to the motor shaft, while radial forces are created by shaft displacement between leadscrew and motor. There is therefore a need for a coupling which can transmit the motor torque free from backlash but which nevertheless compensates for any axial or radial displacement. These conditions are met in an almost ideal manner by a cross-tenon coupling. As this coupling is well matched, it offers the additional advantage of low overall dimensions and thus low inertia.

The coupling consists of three components, and drive is transmitted by radial slots and tenons accurately ground to play-free state. The centre section has radial slots offset through 90° so that radial compensation is at all times possible in the event of shaft displacement. Cord seals keep the coupling components on a clearance spacing of approximately 0.1 mm in the axial direction. Any thermal induced axial movements are then taken up by the elasticity of these seals. The seals also prevent physical contact between the coupling components. The right-hand half of the coupling is permanently connected to the feed leadscrew by a taper seat. This arrangement ensures torque transmission entirely free from backlash. Similarly, the left-hand clutch half is pressed onto the parallel shaft of the motor using a tapered ring. A normal sliding fit with key would not be sufficient to ensure the necessary backlash elimination, as there would also then be the danger that any sudden torque changes could shear the key.

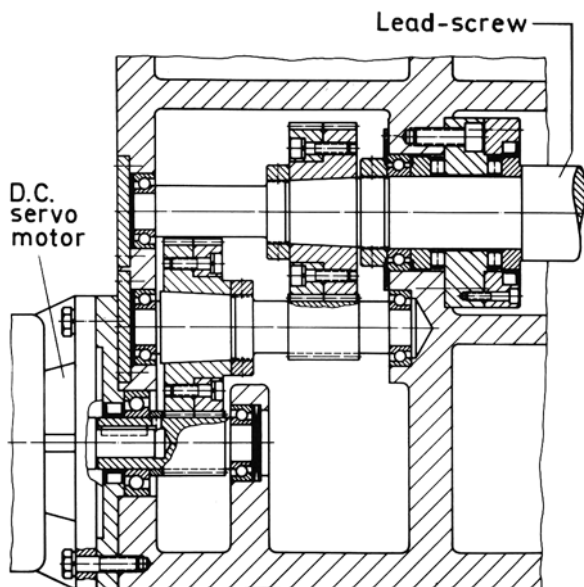


Fig. 7 Electric d.c. servo drive (Scharmann & Co.)

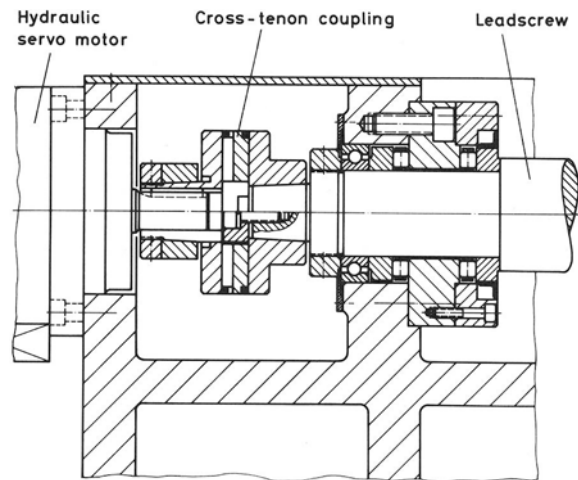


Fig. 8 Hydraulic servo drive (Scharmann & Co.)

SUMMARY AND CONCLUSIONS

This paper gives the theoretical aspects of problems arising in controlled feed drives for NC machine tools, drawing from these theoretical considerations the necessary results for practical applications.

The paper explains how rigid leadscrew systems, low-friction slideways, as well as transmissions free from play and featuring low inertia, should best be designed to achieve optimal accuracy and performance. The example quoted shows how all these requirements were met in relation to horizontal boring and milling machines with continuous-path control.

DISCUSSION

Query from A. J. Bartley, University of Newcastle

It is stated that the only satisfactory guides are either roller guides or hydrostatic slideways. Yesterday, in a paper at session 2A, it was reported that satisfactory low friction conditions and freedom from stick-slip had been achieved by using conventional slideways with PTFE inserts. I wonder whether PTFE has been tried by the author and if so what was his experience?

Reply

PTFE is a good compromise between friction and damping conditions of plain slideways and anti-friction properties of roller or hydrostatic guides, which is in many cases sufficient even for contouring machines. Up to now, there were real difficulties with the adhesive bonding of PTFE plates on cast iron components, in order to get a permanent connection. This problem has been solved, however, in a splendid way, as indicated in paper 808 'The Modula Range of NC Machine tools'. The chapter 'Slide-ways' in that paper answers this query.

Query from P. Muth

It was said that the rigidity can be increased by three methods:

- increasing the screw diameter,
- shortening the screws,
- increasing the number of screws.

An example is given in the paper, whereby all three modifications were done at the same time. This is not always possible.

Can Mr. Engel give some details according to his experience as to which one of the three methods will give the best result, and perhaps a certain percentage in increasing the rigidity by only one out of the three modifications.

Reply

If you take the screw as a bolt, you have the equation

$$C = \frac{F}{\Delta L} = n \times \frac{EA}{L} = \frac{\pi E}{4} \frac{nD^2}{L} = \text{constant} \times \frac{nD^2}{L}$$

- C stiffness of all screws
- n number of screws
- E modulus of elasticity
- F force
- ΔL elongation of the screws
- L effective screw length
- A effective cross-sectional area of one screw
- D diameter of the screw.

In this equation one can see that, taking a bigger screw diameter D will achieve the best gain in stiffness. In nearly all cases, it is possible to increase the number of screws. The possibility of shortening the screw length L is less likely. Generally the gain in stiffness by shortening the screws is not very high.

Query from Ir. Wasiuktiewicz, DIXI II, Switzerland

In order to obtain the greatest possible stiffness of the feed-drive transmission, the common practice consists of using preloaded nuts and thrust bearings on both sides of the lead screw.

The boring and milling machines have normally a large range of the feeds (2×1000 mm/min) and allow a rapid traverse at 2–10 m/min. Normally, the thrust bearings and leadscrew are chosen for the

extreme cutting conditions with the greatest work-piece to be moved. It leads to assumption of lower values for the leadscrew revolutions per minute (16–100 rev/min) and the considerable thrust forces to be transmitted (2000–4000 lb) to choose the lead-screw. The common practice is to choose as a preload value $\frac{1}{2}$ the maximum transmitted force. It happens very seldom that the machine would be used at the maximum disposable power. Nevertheless, the balls in the nut are affected by the preload (500–2000 lb) during every moment of the screw rotation.

In automatically-operated machines (NC) where every cycle begins with the rapid traverse and when the time of positioning is considerably in the overall cycle time, the screw will drive with a high number of revolutions (500–1000 rev/min) with the balls submitted to the high pressure due to their preload. It leads to the considerable rise in the temperature (20–30° over the ambient temperature) and to an important decrease in the service life at the leadscrew. It was the reason why some machine tool builders were forced to decrease by 2 to 3 times the value of the initial preload, affecting at the same time the stiffness of this element. This temperature rise can also cause some problems with the service life of the thrust bearings, when screws are fixed axially on both ends (thermal expansion 11×10^{-3} m/m 1°C) and influence the precision of the measuring device fixed on the lead screw end.

Reply

I have had experience with rising temperature only in one case, which was during a test-run of a 3-axes machine where no cutting tool was working, but table, saddle and headstock were running with rapid traverse during about 80% of the whole time of 15 min. Under normal working conditions, the average number of revolutions is low enough for there to be no considerable rise in temperature. Furthermore there is a good temperature distribution resulting from the very large surface areas of the machine tool parts. At least, length deformations of the ballscrew can generally be absorbed by the elasticity of the screw itself.

In cases where the accuracy of indirect measuring elements is disturbed by temperature deformations, machine tool users should take a direct measuring system where these deformations are eliminated.

A METHOD OF CALCULATION FOR TWO-WAY FLOW-CONTROL VALVES DEPENDING ON IMPOSED DYNAMIC PERFORMANCE

by

Dr. eng. I. MAZILU

SUMMARY

The aim of this study is to draw up a calculation method in order to design the two-way flow-control valves, and to permit the determination of the constructive parameters, which depend on the working range and the required performance. The determination of how the constructive dimensions of the control valve influence its dynamic performance was carried out on experimental models in the laboratory. The time constants were optimized by models on an analogue computer.

INTRODUCTION

When working in the dynamic regime of a hydraulic drive system there exists a complex process of the mutual influence of dynamic, mechanical and hydraulic effects. The aim of this investigation of the dynamic phenomena generated by different factors in hydraulic drive systems is to establish the variation laws of the basic hydraulic parameters (the pressure and the flow rate), as well as the mechanical parameters of the components of velocity, displacement, acceleration, force, and so on, looking for ways to attenuate the negative influences of these phenomena on the productivity and the efficiency of the machine.

Because of the large number of parameters which mutually interact in the transient regime, only approximate methods were established for the dynamics of the hydrostatic drive equipment. Because of this, the analysis adopted for this work consisted of combining theoretical calculations with the experimental determinations and the analogue computer model data, this being the best method of obtaining results which were confirmed in practice.

This work analyses one of the feed control variants for machine tools with hydraulic drive systems, more specifically those which operate by means of a two-way flow-control valve, mounted on the oil outlet line of the hydraulic motor (Fig. 1).

The instantaneous value of the controlled pressure before the flow-control valve is dependent on the dynamic characteristics of the reducing valve. It would be ideal if the controlled pressure were constant, and thus unaffected by the pressure variations in the hydraulic motor. In fact, the reducing valve, because of the inertial and friction forces, fails

to change its position in the time necessary to stop the sudden pressure variations in the hydraulic motor. Because of this, during the transitional period from the rapid displacement to the working feed, or during the variations of the cutting forces, the controlled pressure, p_r , will follow the pressure variations in the hydraulic motor with a phase lag and an amplitude ratio depending on the dynamic characteristics of the valve.

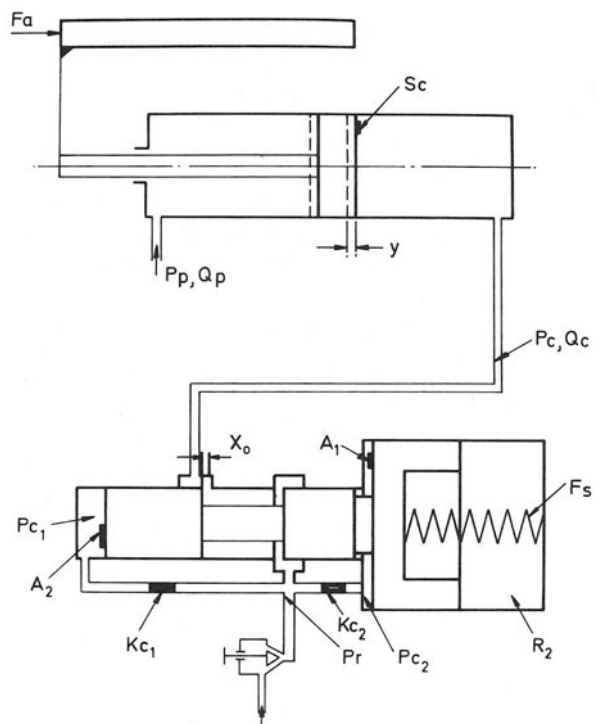


Fig. 1

CONTROL VALVE BEHAVIOUR ANALYSIS IN STEADY-STATE.

In the steady-state, the spool balance equation is

$$F_{so} + (K_r + K_H)x = p_r \cdot A \quad (1)$$

from which results the dependence of the controlled pressure p_r on the valve opening, x , which in turn is determined by the working pressure, p , in the hydraulic motor.

It follows that in the working conditions of the control valve over the whole working pressure range of the machine, the controlled feed varies according to the opening of the flow-control valve, and does not remain constant.

The deviations from the required feed are conditioned by the spring characteristics, K_r , the hydrodynamic force coefficient, K_H , and the opening variation, x , depending on the working pressure which results from the known relationship

$$Q = C_d K_s x \sqrt{\frac{2(p - p_r)}{\rho}} \quad (2)$$

K_s was noted and the valve control section gradient was considered to be proportional to the opening, x . Writing down the expression for the opening x , for the limits of the working range $[p - p_r]_{\min}^{\max}$ and expressing the controlled pressure variation depending on the nominal controlled pressure, p_r

$$p_r \max - p_r \min = \epsilon p_r \quad (3)$$

yields the expression for the steady-state error

$$\epsilon = \frac{\sqrt{\rho} K_r (1 + \frac{1}{\psi}) Q}{\sqrt{2} C_d \cdot A \cdot p_r \cdot K_s} \left[\frac{1}{\sqrt{(p - p_r)_{\min}}} - \frac{1}{\sqrt{(p - p_r)_{\max}}} \right] \quad (4)$$

The value of ψ was noted and the ratio between the spring characteristic K_r and the hydrodynamic force coefficient providing the steady-state stability.

As a result of the analysis of expression (4) the steady-state accuracy is determined by the spring characteristic K_r , the controlling surface gradient K_s and the surface size, A , on which the controlled pressure acts.

But, from this condition for achieving a steady-state accuracy, the three parameters are not single valued. This can be achieved by a requirement connected with the oil filtration accuracy, from which it is clear that the minimum controlling section opening, x_{\min} , must be unconditionally larger than the maximum size of the particles admitted through the filter, from which one obtains the relationship

$$K_s \leq \frac{Q_{\min}}{x_{\min} C_d \sqrt{\frac{2(p - p_r)_{\max}}{\rho}}} \quad (5)$$

The same considerations connected with oil filtration accuracy must be taken into account when the minimum valve opening A_{dr} is chosen. Usually, the control valve opening is rectangular, with one variable side. The width of this slit is limited for technological

reasons to values usually larger than filtration accuracy, thus limiting the admissible size of the variable side. In this way, starting from the real technological possibilities and filtration accuracy, the minimum flow-control valve opening can be established, and depending on this, the controlled pressure value can be calculated

$$p_r = \frac{Q_{\min}^2 \cdot \rho}{2 C_{dr}^2 \cdot A_{dr}^2 \min} + p_o \quad (6)$$

In order to avoid the instability region in the neighbourhood of the shutting position, the sum of the spring force variation and of the hydrodynamic force in connexion with the opening should always remain positive¹

$$\frac{dF_r}{dx} + \frac{dF_H}{dx} > 0 \quad (7)$$

From this condition the spring characteristic value can be established as

$$K_r = 2 \psi C_d \cdot K_s \cdot D_p \max \quad (7)$$

where ψ is the ratio of the spring force increase to the hydrodynamic force increase, which is assumed to be larger than 1.

From this, the surface A , on which the controlled pressure acts, can be calculated from relation (4), for the imposed steady-state accuracy.

Control valve behaviour analysis in the dynamic regime

Control valve dynamic analysis (Fig. 1) was effected by the use of the small disturbances method applied to the system; that is, the system was considered to be linear with constant coefficients.

After the application of the second of Newton's laws, and the continuity equations written after Laplace transformations, the following expressions were obtained

$$K_q (1 + T_2 s) X(s) + K_p (1 + T_1 s) P(s) = (K_p + K_d) (1 + T_3 s) P_r(s) \quad (8)$$

$$F_s - A \left(\frac{1}{1 + T_1 s} \right) P_r(s) - \frac{A^2}{K_t} \left(\frac{s}{1 + T_1 s} \right) X(s) = K_e \left(\frac{s^2}{\omega_n^2} + \frac{2\zeta s}{\omega_n} + 1 \right) X(s) \quad (9)$$

where

$$K_q = \frac{\partial Q}{\partial x}$$

$$T_1, T_2, T_3$$

$$K_p = \frac{\partial Q}{\partial P_r}$$

$$P_r(s)$$

The flow control valve amplification coefficient, $\text{cm}^2 \text{s}^{-1}$.

Time constants.

Flow-pressure characteristic coefficient of the valve, $\text{cm}^3 \text{s}^{-1} / \text{kgf cm}^{-2}$.

Laplace transform of controlled pressure increase.

- $F(s)$ Laplace transform of spring force increase.
- $X(s)$ Laplace transform of valve opening increase.
- $A = A_1 + A_2$ The surface on which the feedback pressure acts, cm^2 .
- $K_t = K_{ct} + K_{c2}$ Summary coefficient of flow-pressure characteristic of the vent on the feedback path, $\text{cm}^3 \text{ s}^{-1} / \text{kgf cm}^{-2}$.
- s Laplace operator.
- $K_e = K_H + K_r$ Equivalent spring stiffness.
- $\omega_n = \sqrt{\frac{K_e}{m}}$ Natural frequency.
- $\zeta = \frac{h_e}{2\sqrt{mk_e}}$ Damping ratio, where h_e is the viscous friction coefficient.

On the basis of equations (8) and (9) the block diagram of the system was drawn (Fig. 2).

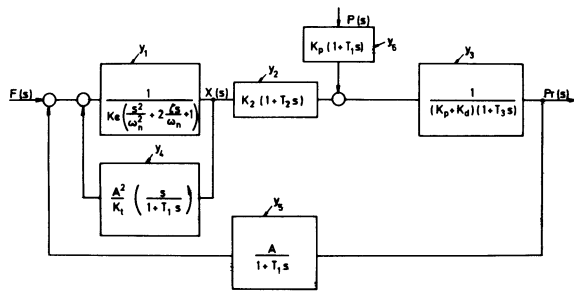


Fig. 2

$$P_r(s) = \frac{K_q (1 + T_2 s) F(s) + K_p (1 + T_1 s) \left[K_e \left(\frac{s^2}{\omega_n^2} + \frac{2\zeta s}{\omega_n} + 1 \right) + \frac{A^2}{K_t} \frac{s}{1 + T_1 s} \right] P(s)}{(K_p + K_d) (1 + T_3 s) \left[K_e \left(\frac{s^2}{\omega_n^2} + \frac{2\zeta s}{\omega_n} + 1 \right) + \frac{A^2}{K_t} \left(\frac{s}{1 + T_1 s} \right) + \frac{A}{1 + T_1 s} K_q (1 + T_2 s) \right]} \quad (10)$$

Using the method of superposition and the algebra for block diagrams from automatic control theory, the transfer function of the system was obtained.

Study of the transfer function indicated that the characteristic equation is of the fourth order with comparatively complicated form parameters, the values of which were unknown. Because of this an analytic solution was considered to be impossible in practice. Therefore, the following method of analysis was used. This consisted of the following.

- The determination of variation limits for constructive parameters of flow-control valve.
- Experimental determination of parameters influencing the response time at a step signal and of maximum transient deviation.
- Stability analysis of flow-control valve for variable ranges of the time constants.
- The optimization of constructive parameters of a control valve by an analogue computer model.

EXPERIMENTAL RESULTS

In order to make evident the influence of each constructive parameter on the dynamic performance of flow-control valves, a test stand for experimental

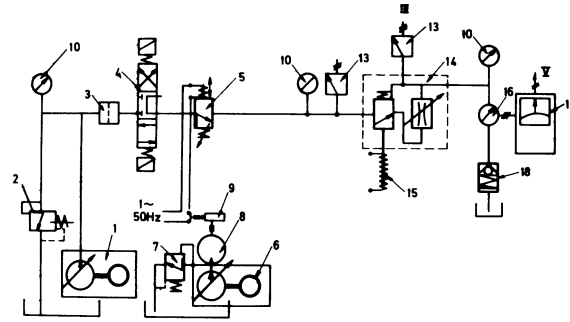


Fig. 3

models (Fig. 3) was conceived, by which controlled pressure variations were recorded for different magnitudes of the supply pressure, flow rate and constructive parameters of the flow-control valve.

The experimental models have been built up in two variants: with a cylindrical spool (Fig. 4), and with a differential spool (Fig. 5), and have been constructed with parameters which differ as follows:

- the area of the surface S on which the controlled pressure acts, $A = 1.75-5 \text{ cm}^2$;
- the gradient of the controlled pressure section $K_s = 0.06-7.85 \text{ cm}^2 \text{ cm}^{-1}$;
- the spring characteristic coefficient $K_r = 5-35 \text{ kgf cm}^{-1}$;
- the feedback flow characteristic $K_t = 0.05-40 \text{ cm}^3 \text{ s}^{-1} / \text{kgf cm}^{-2}$;
- the mass of the spool and of the spring $m = 0.045 \times 10^{-3} - 1.4 \times 10^{-3} \text{ kgfs}^2 \text{ cm}^{-1}$

The oil viscosity variation was obtained by changing the hydraulic medium temperature, within a controlled range of $\nu = 0.02-0.85 \text{ cm}^2 \text{ s}^{-1}$.

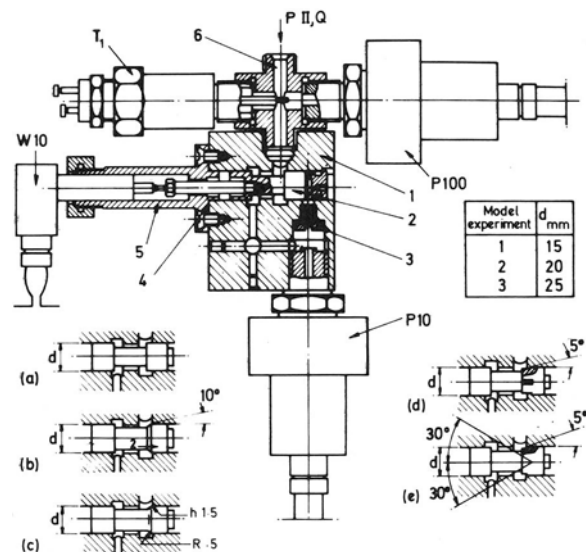


Fig. 4

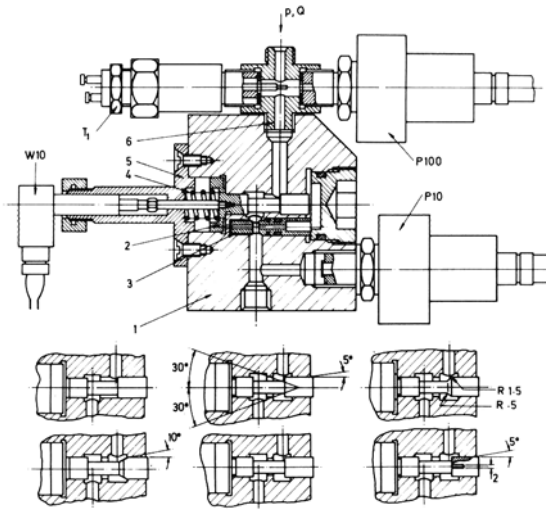


Fig. 5

Carrying out the whole range of tests according to the combination of these parameters, made it possible to draw certain conclusions which restricted the possible ranges for the constructive parameters.

In this way the influence of the flow—pressure characteristic, K_r , has been ascertained as has the vent on the feedback line on the dynamic characteristics of the system (Fig. 6).

The flow control valve behaves in a satisfactory manner only for a restricted range of values of K_r . The magnitude of this range depends on the values of the other constructive parameters (m, s, K_r, K_s) of the flow-control valve. The value of K_r from which undamped vibrations occur depends on the natural frequency of the elastic system formed by the spool and the spring.

From analysis of all data, part of which is concentrated in Fig. 6, it follows that satisfactory dynamic performances are obtained for a limited range of the values of K_r , that is

$$K_r = 0.2 - 0.55 \text{ cm}^3 \text{ s}^{-1} / \text{kgf cm}^{-2}.$$

The optimum values of the flow-control valve dynamic characteristics are obtained within this range of values of K_r provided that the other constructive parameters are adequately selected. Also I observed experimentally that the optimum value of the controlled section gradient, K_s , was different, depending on the other constructive parameters.

The control valve presents instability difficulties however, for large values of surface gradient, the small values of which give a small response time (Fig. 7—I), the increase of peak value for small values of K_s being within acceptable limits (Fig. 7—II). The upper limit of K_s has to be adequate for the avoidance of control valve obstructions caused by oil contamination.

Experimentally it has been found that for small flow rates, at the maximum pressure drop (at minimum opening), a large control section gradient leads to control valve obstruction in the steady-state when the opening is smaller than, or equal to, the size of the maximum impurities admitted by the filter. Because of this, low frequency pulsations of the con-

trolled pressure occur, however as a result of control valve opening variations. There is a self-cleaning action, which was pointed out by the experimental recordings.

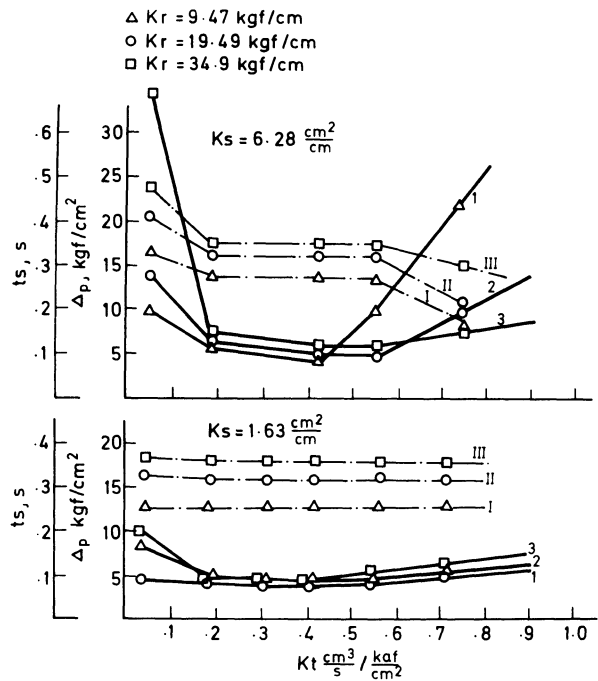


Fig. 6

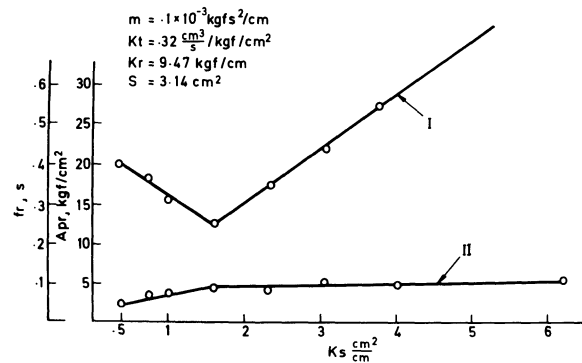


Fig. 7

From examination of the results obtained it follows that the different mode of behaviour of the same control valve is a result of the spring characteristic changing. But the share of this influence varies in different control valves, in accordance with the values of the other constructive parameters. It follows that a certain control valve achieves the highest dynamic performance for a certain value of the spring characteristic.

Experimental determination of variation ranges for constructive parameters allowed theoretical analysis of the system stability. From stability conditions the range of variation of the time constants were established, which restricted the values of the constructive parameters for which the system is stable.

Stability analysis of the flow-control valve

In order to reduce the calculation difficulties, the inner loop was analysed separately (Fig. 2), and an equivalent transfer function found.

The transfer function of the open inner loop was written in polar form

$$GH_{(U)} = \frac{K U \angle 90^\circ}{\sqrt{(T_1 U)^2 + 1} \angle \arctg T_1 U \times \sqrt{(1-U^2)^2 + (2\zeta U)^2} \angle \arctg \frac{2\zeta U}{1-U^2}} \quad (11)$$

where

$K = \frac{A^2 \omega_n}{K_e K_t}$ is the inner open loop amplification constant;

$U = \omega/\omega_n$ normalized pulsation;

$T_1' = T_1 \omega_n$, the time constant; and

$\angle \phi$ the argument or the phase angle.

In order to see how the time constant influenced the dynamic performance of the system, the attenuation-pulsation characteristic of the factors of expression (11) were traced for different ranges of T_1 , on which basis, using Black's abacus, the maximum values of the amplification constant for which the system is stable were determined. For these values of the amplification constant, the polar diagram with M contours was constructed, on which the attenuation-pulsation characteristic for the open loop were traced for extreme values of the time constant T_1 and the damping coefficient.

From the intersection of the curves obtained with the circles of the polar diagram² the attenuation-pulsation characteristics of the inner loop with unitary feedback were constructed. These curves allowed analysis by the substitution of the inner loop transfer function by the following function

$$Y_e = \frac{\frac{K_t}{A^2} + (1 + T_1 s)}{\frac{T_1''^2}{\omega_n^2} s^2 + \frac{2\zeta' T_1''}{\omega_n} s + 1} \quad (12)$$

where T_1 is the opposite of the breaking frequency of the attenuation-pulsation characteristic for the adopted amplification coefficient, K .

This substitution of the inner loop with an equivalent transfer function allowed the application without any difficulty of Nyquist's stability criterion, resulting in the variation ranges of the time constants for which the system is stable.

The constructive parameters optimization of the control valve by modelling on an analogue computer

The block diagram of the system (Fig. 2) served as a basis for establishing the modelling scheme on the computer (Fig. 8). The determination of the coefficient values was done on the basis of the

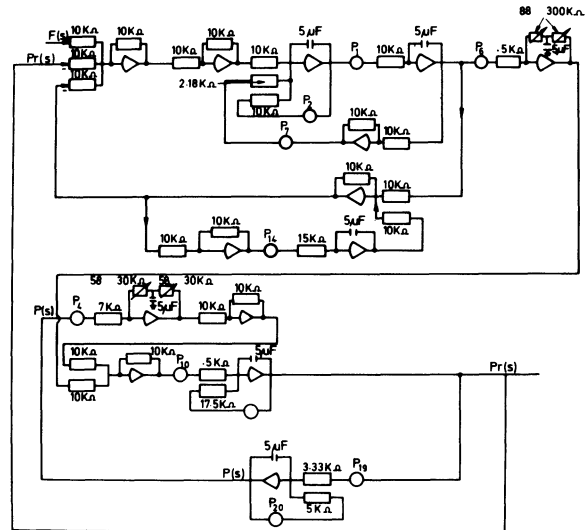


Fig. 8

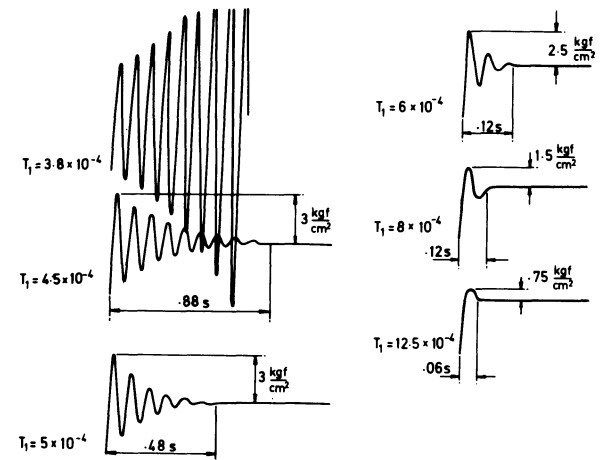


Fig. 9

Fig. 10

calculations, experimental determinations and frequency analysis effected. Thus, the physical variables of the control valve were replaced by potentiometers, which handled easily allowing a large number of tests to be made in a comparatively short time.

The system response for a step input signal was recorded in accordance with different values of the time constants T_1, T_2, T_3 included within the range

of values resulting from preliminary calculations. In Fig. 9 is shown the influence of the time constant T_1 on the response time.

The influence of the constructive parameters which do not determine the time constants was also observed with the help of analogue model. The behaviour of the analogue model reproduced accurately the experimental results which had been obtained on physical models. Using the constructive data from the study of a determined case, a flow-control valve was constructed and tested on a stand. The response time to a step input signal (Fig. 10) did not exceed the value of 0.08s imposed by the problem, and the controlled pressure was not influenced in practice by the supply pressure fluctuations, even for low frequencies (1 Hz).

REFERENCES

1. BLACKBURN, I. F., 'Mécanismes et servomécismes a fluide sous pression,' Paris, Dunod (1966).
2. SAVANT, I. C., 'Calculul sistemelor automate Bucuresti,' Ed. Technica (1967).
3. MOC. Y., 'The analysis and design of hydraulic pressure reducing valves,' *Trans. ASME B* 89, No. 2 (1967).
4. MAZILU I., 'Contributions to the study of transient phenomena in hydrostatic circuits of machine tools,' Doctorate thesis Polytechnical Institute, Bucharest (1971).

THE CHOICE OF BALLSLIDEWAYS FOR MACHINE TOOLS

by

J. DE FRAINE*

SUMMARY

Ballslideways are used in machine tools for their specific properties: very low friction and high precision.

In the design of the machine, the slideway must be chosen as a function of the load to be supported and the maximum tolerated elastic deformation. This load and deformation are mostly eccentric on the slideway and slideway manufacturers only indicate the values of the central load capacity and stiffness. This report discusses a practical method for the determination of a slideway as a function of the eccentric load and stiffness.

Nomenclature

K, A, a	constants
C_n	nominal load-capacity
n	number of balls under load
L	length of the slideway
B	distance between two rows of balls
Z	vertical deformation
Z_1, Z_2, Z_3, Z_4	vertical deformations of the points 1, 2, 3 and 4 (see Fig. 3)
Z_F	vertical deformation under the load F_z
Z_o	vertical deformation under a central load
F	force, load
F_B	maximum load per ball
F_c	equivalent central load
F_z	vertical eccentric load
F_{14}, x_{14}, F_{23} and x_{14}	load and eccentricity of the load on the rows 14 and 23 (see Fig. 3)
S_z	vertical stiffness under eccentric load
S_n	central stiffness
x, y	eccentricity of the load F_z (see Fig. 3)
S_c	equivalent central stiffness

INTRODUCTION

In modern machine tools ballslideways are used for their specific properties. The very low friction (less than 1% of the load) and the neglectable stick-slip permits a very high positioning accuracy and a small and cheap driving mechanism. Typical applications are numerical control machine tools with a ballscrew as positioning element. Even heavy cross-tables up to 400 X 500 mm in size can be positioned by hand, if mounted on ballslideways. The precision is very high,

maximum deviation of the moving table from an ideal straight line not exceeding 5 μm for 1000 mm travel. The use of ballslideways simplifies the design and manufacture of the machine. Fig. 1 shows a table with ballslideways and with classical slideways; when ballslideways are used only six surfaces have to be machined instead of twelve surfaces with classical slideways.

The classical slideways must be lubricated and a gap for the oil film is necessary, but ballslideways work without any lubrication and without play.

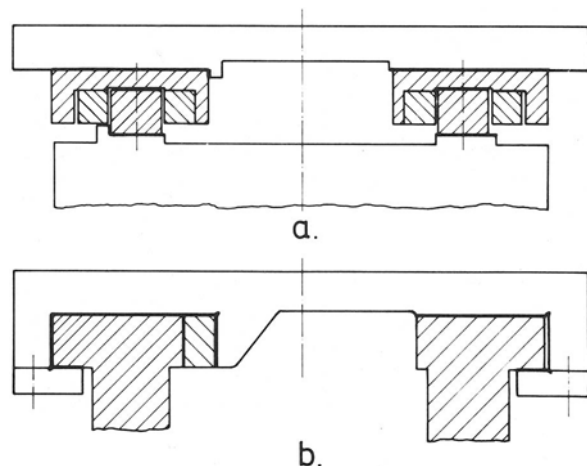


Fig. 1

*Dexter Continental, Brussels, Belgium and formerly at University of Louvain.

LOAD-CAPACITY AND STIFFNESS

When the load on the slideway increases, its lifetime will reduce and damage may even occur under heavy load. The load-capacity is the central load that a slideway can carry during a reasonable lifetime. This load-capacity is dependent on the geometry of the contact between the balls and the trackways, the materials used and their hardness, the number of balls under load and the manufacturing accuracy.

The life of identical ballslideways loaded and mounted in the same conditions varies widely. Variations of from 1 to 25 and more are very usual. This means that the nominal load-capacity indicated by the manufacturers is not a precise characteristic.

The indicated values are determined by experience and practice only. The stiffness of a ballslideway is much better known. It has been proved that the mean deformations in the slideway are the deformations of the contacts of the rolling elements and the trackways^{1,2}. Hertz developed a method for computing contact deformations and contact stresses. The deformation of a point contact is given by the formula

$$Z = KF^{2/3} \quad (1)$$

The stiffness of a ballslideway computed from the contact deformations has been found to be consistent with the experimentally-measured stiffness. The difference between theory and practice never exceeded 10% (see refs. 1 and 3).

Design of a machine with ballslideways.

First, the load on the slideway must be evaluated, the load consisting of the weight of the machine components or workpieces and the cutting forces. On the other hand, the elastic deformation produced by the cutting force may not exceed a maximum value which is a function of the expected accuracy of the workpieces to be produced on the machine.

In practice the cutting force and the weight are mostly eccentric loads on the slideways and the deformation in the cutting process is also eccentric.

But the nominal load-capacity C_n indicated by the manufacturers is the value of the maximum applicable load when this load is perfectly central on the slideway, so that each ball under load carries the same load, called the maximum load per ball (F_B).

Thus
$$C_n = n F_B \quad (2)$$

n is the number of balls under load. The stiffness given by the manufacturers is the value when all the balls have the same deformation (this is for a perfect central load). This value is called the 'central stiffness' (S_n).

The designer has determined the values of the eccentric load and eccentric stiffness necessary for the quality of his machine, but the manufacturer only indicate the nominal load capacity, C_n , and the central stiffness (value only valid for central load) in their catalogues. The designer of the machine cannot use the values of the manufacturer directly.

Equivalent central load and equivalent central stiffness

In an eccentric loaded slideway, some balls will be loaded more than others. The load on the most loaded ball must be less than or equal to the maximum load per ball, F_B .

Instead of considering the slideway with the eccentric load, the same slideway may be supposed to be loaded with a central load. The value of this load is chosen so that the load on each ball is equal to the load on the most loaded ball in the eccentric loaded slideway.

This central load is called the equivalent central load, F_c , and this load must be compared with the nominal load-capacity, C_n . If

- $F_c = C_n$ the slideway can support the eccentric load but is working at maximum capacity
- $F_c < C_n$ the slideway can support the eccentric load without working at maximum capacity
- $F_c > C_n$ the slideway cannot support the eccentric load.

Thus the condition to be fulfilled is

$$F_c \leq C_n \quad (3)$$

In the same way the equivalent stiffness (S_e) can be determined. This equivalent stiffness is the central stiffness necessary to assure a stiffness under eccentric load equal to the given stiffness (S_z). The equivalent stiffness must be less than or equal to the central stiffness of the slideway, thus

$$S_e \leq S_n \quad (4)$$

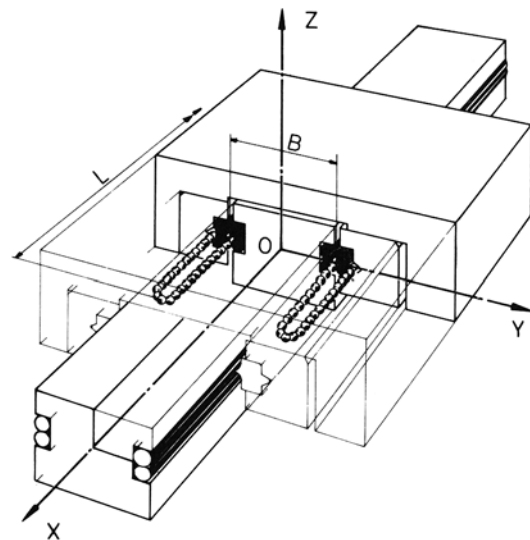


Fig. 2

Load-capacity and stiffness as a function of the eccentricity of the load

The slideway is considered to be a rigid plate, supported by two rows of elastic springs (balls). The equation of the load deformation curve of each spring is

$$F = A Z^a \quad (A, a \text{ constants}) \quad (5)$$

On the slideway a coordinate system is defined as in Fig. 2 and the following definitions apply:

Origin, centre of the rectangle formed by the rows of the balls under load; x -axis, parallel to the rows of the balls; y -axis, perpendicular to the rows of the balls in the plane of the rows; z -axis, perpendicular to the plane of the rows; L , length of the rows; and B , distance between the rows.

Fig. 3 shows the rows of elastic springs loaded with an excentric load F_z .

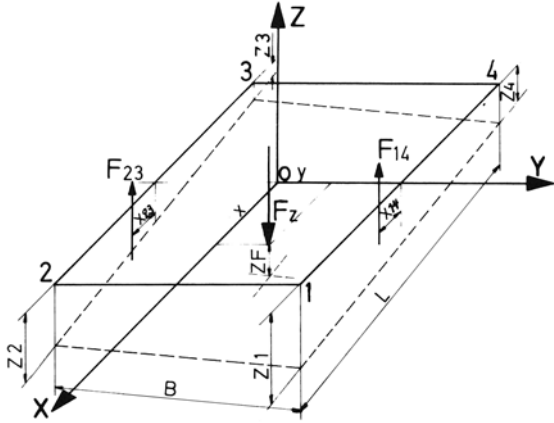


Fig. 3

The total load on the row 14 is

$$F_{14} = \frac{n}{2} \frac{A}{(a+1)} Z_1^a \cdot \frac{\left[1 - \left(\frac{Z_4}{Z_1}\right)^{a+1}\right]}{\left(1 - \frac{Z_4}{Z_1}\right)} \quad (6)$$

where $\frac{n}{2}$ is the number of balls in each row, and Z_4 , Z_1 are the deformations of the extreme points of the rows.

The eccentricity of that load is

$$\frac{x_{14}}{L} = \frac{\left(\frac{1}{2} - \frac{1}{a+2}\right) \left[1 - \frac{Z_4}{Z_1} \left(\frac{Z_4}{Z_1}\right)^{a+1}\right] - \frac{1}{2} \left[\frac{Z_4}{Z_1} - \left(\frac{Z_4}{Z_1}\right)^{a+1}\right]}{\left(1 - \frac{Z_4}{Z_1}\right) \left[1 - \left(\frac{Z_4}{Z_1}\right)^{a+1}\right]} \quad (7)$$

Formulas (6) and (7) can be written in a symbolic form

$$F_{14} = f_1 \left(Z_1, \frac{Z_4}{Z_1}\right) \quad (8)$$

and

$$\frac{x_{14}}{L} = f_z \left(\frac{Z_4}{Z_1}\right) \quad (9)$$

In the same way, the load on the second row can be computed as

$$F_{23} = f_1 \left(Z_2, \frac{Z_3}{Z_2}\right) \quad \text{and} \quad (10)$$

$$\frac{x_{23}}{L} = f_2 \frac{Z_3}{Z_2} \quad (11)$$

The point 1 is the most loaded and the equivalent central force on the slideway is

$$F_c = A n Z_1^a \quad (12)$$

Dividing formulas (8) and (10) by (12) gives

$$\frac{F_{14}}{F_c} = \frac{1}{2(a+1)} \frac{\left[1 - \left(\frac{Z_4}{Z_1}\right)^{a+1}\right]}{\left[1 - \left(\frac{Z_4}{Z_1}\right)\right]} \quad (13)$$

and

$$\frac{F_{23}}{F_c} = \frac{1}{2(a+1)} \left(\frac{Z_2}{Z_1}\right)^a \frac{\left[1 - \left(\frac{Z_3}{Z_2}\right)^{a+1}\right]}{\left[1 - \left(\frac{Z_3}{Z_2}\right)\right]} \quad (14)$$

These internal forces in the slideway must be in equilibrium with the external load, F_z . The conditions for equilibrium can be written as

$$\frac{F_z}{F_c} = \frac{F_{14}}{F_c} + \frac{F_{23}}{F_c}, \quad (15)$$

$$\frac{F_z}{F_c} \frac{y}{B} = \frac{1}{2} \frac{F_{14}}{F_c} - \frac{1}{2} \frac{F_{23}}{F_c} \quad \text{and} \quad (16)$$

$$\frac{F_z}{F_c} \frac{x}{L} = \frac{F_{14}}{F_c} \frac{x_{14}}{L} + \frac{F_{23}}{F_c} \frac{x_{23}}{L} \quad (17)$$

The four points 1, 2, 3 and 4 stay in a plane after the deformation; that is

$$Z_1 + Z_3 = Z_2 + Z_4 \quad (18)$$

The equivalent central load, F_c , was calculated as follows.

Values of the ratio $\left(\frac{Z_4}{Z_1}\right)$ and of the ratio $\left(\frac{Z_3}{Z_2}\right)$ were chosen by means of formula (18), and the ratio $\left(\frac{Z_2}{Z_1}\right)$ was computed. The values $\left(\frac{F_{14}}{F_c}\right)$, $\left(\frac{F_{23}}{F_c}\right)$, $\left(\frac{x_{14}}{L}\right)$ and $\left(\frac{x_{23}}{L}\right)$ were calculated with formulas (6), (7), (10) and (11) and finally (15), (16) and (17) gave the values $\frac{F_z}{F_c}$, $\frac{y}{B}$ and $\frac{x}{L}$. This means that the equivalent central load F_c is proportional to the excentric load F_z and a function of the eccentricity of the load, as

$$F_c = F_z f \left(\frac{x}{L}, \frac{y}{B}\right) \quad (19)$$

For a linear load-deformation curve ($a = 1$) the equivalent load can be written in explicit form as

$$F_c = F_z \left(1 + 6 \frac{x}{L} + 2 \frac{y}{B}\right) \quad (20)$$

This formula is more practical than (17). The function $f \left(\frac{x}{L}, \frac{y}{B}\right)$ had to be computed point by point, and because of the complexity of this work it was done with a digital computer. In practice, formula (20) should be used for determining the equivalent central load. Even for point contact deformations ($a = 1.5$) the exact values of F_c computed by formula (19) are

very close to the values given by the more practical formula (20).

A point contact deformation corresponds to the unrealistic case of a slideway without any pre-load. In practice slideways are pre-loaded and the deformation becomes almost proportional to the load ($a = 1$).

To compute the equivalent central stiffness, the value of the deformation under the load has to be determined geometrically, and this deformation can be written as a function of the deformation of the extreme points 1, 2, 3 and 4 of the slideway as

$$Z_F = \frac{(Z_1 + Z_2)}{2} + \frac{x}{L} \left(\frac{Z_1 + Z_2}{2} - \frac{Z_3 + Z_4}{2} \right) + \frac{y}{B} \left(\frac{Z_1 + Z_4}{2} - \frac{Z_2 + Z_3}{2} \right) \quad (21)$$

In symbolic form the ratio Z_F/Z_1 is given by

$$\frac{Z_F}{Z_1} = f_3 \left(\frac{Z_2}{Z_1}, \frac{Z_3}{Z_1}, \frac{Z_4}{Z_1}, \frac{x}{L}, \frac{y}{B} \right) \quad (22)$$

To compute Z_F the same method as for the equivalent central load may be used. From one value of the ratio (Z_4/Z_1) and the ratio (Z_3/Z_2) the values of (x/L), (y/B), (Z_2/Z_1), (Z_3/Z_1), (Z_F/Z_1) are computed. The deformation is a function of the eccentricity and the deformation of the most loaded ball, Z_1

$$Z_F = Z_1 f_4 \left(\frac{x}{L}, \frac{y}{B} \right) \quad (23)$$

If the load F_z were central, the central deformation is

$$Z_o = \left(\frac{F}{n A} \right)^{1/a} \quad (24)$$

The deformation of the most loaded ball is

$$Z_1 = \left(\frac{F_c}{n A} \right)^{1/a} \quad (25)$$

So formula (23) can be expressed as

$$\frac{Z_F}{Z_o} = \left(\frac{F_c}{F} \right)^{1/a} f_4 \left(\frac{x}{L}, \frac{y}{B} \right) = f_5 \left(\frac{x}{L}, \frac{y}{B} \right) \quad (26)$$

The deformation under an eccentric load is proportional to the deformation if that load were central and also a function of the eccentricity of the load.

The stiffness under load and the equivalent central stiffness are proportional to the inverse of the deformations, and formula (26) gives the relationships of the stiffness under load and the equivalent central stiffness.

$$S_c = S_z f_5 \left(\frac{x}{L}, \frac{y}{B} \right) \quad (27)$$

For a linear force-deformation curve ($a = 1$) the

equivalent stiffness can be written as

$$S_c = S_z \left[1 + 12 \left(\frac{x}{L} \right)^2 + 4 \left(\frac{y}{B} \right)^2 \right] \quad (28)$$

For the same reasons as those explained above the explicit formula (28) is more correct than the implicit form.

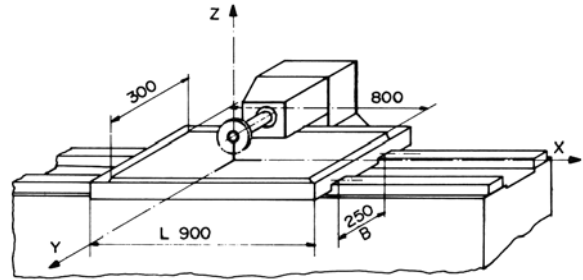


Fig. 4

Example

The method will be illustrated by the calculation of the table of a milling machine, (Fig. 4).

The useful surface of the table is 800×300 mm, the maximum vertical cutting force is estimated as 500 kg and the weight of the workpiece as 200 kg.

The maximum allowable elastic deformation, for a cutting force of 500 kg, is $10 \mu\text{m}$. The load and stiffness are most critical when the machine is working at the maximum eccentricity of the table, this being equal to half the travel.

The length L and the distance B between the slideways are 900 mm and 250 mm, respectively.

The total load on the slideway is

$$200 + 500 = 700 \text{ kg}$$

The equivalent central load can be determined easily with formula (20), thus

$$F_c = 700 \left(1 + 6 \frac{400}{900} + 2 \frac{150}{250} \right)$$

$$F_c = 3400 \text{ kg}$$

The necessary stiffness for the cutting force is equal to

$$\left[\frac{500 \text{ kg}}{10 \mu\text{m}} = 50 \text{ kg } \mu\text{m}^{-1} \right]$$

The equivalent central stiffness is calculated from

$$S_c = 50 \left[1 + 12 \left(\frac{400}{900} \right)^2 + 4 \left(\frac{150}{250} \right)^2 \right]$$

$$S_c = 242 \text{ kg } \mu\text{m}^{-1}$$

That is, the nominal load-capacity and the central stiffness of the slideway to be mounted in the machine must be at least 3,400 kg and $242 \text{ kg } \mu\text{m}^{-1}$ respectively.

DISCUSSION AND GENERALISATION

In practice seldom will a slideway be found with a nominal load-capacity and central stiffness close to the equivalent values which have been determined for the design of the machine.

The chosen slideway may be working almost at its load-capacity and have a stiffness better than that necessary for the precision of the machine, or the reverse may occur (a slideway that is stiff enough but that can carry more load than is provided).

To increase the load-capacity and the stiffness, the number of the balls or the size of the slideway has to be increased. Unfortunately this cannot be done without increasing the price of the slideway. The design will be economical when the equivalent central load and equivalent stiffness are close to the central values indicated by the manufacturers. The method of calculation proposed here can be applied to other types of slideways or structures where a load must be supported by two rows, composed of an elastic medium (for example in hydrostatic or aerostatic slideways).

The method showed that the load-capacity decreased very quickly with the eccentricity of the load, and the decrease in the stiffness is not so critical.

For example consider an eccentricity $x/L, y/B$ equal to 0.1. The load capacity is about 55% of the central load, and the stiffness is still 86% of the central stiffness.

Even for small eccentricities of the load the equivalent values for load-capacity and stiffness must be calculated.

REFERENCES

1. LEVINA, 'Selection and design parameters and calculation of anti-friction slideways', Handbook ENIMS, Moscow (1961).
2. HERTZ, 'Über die Berührung fester elastische Körper', Gesammelte Werke Band I, Leipzig (1895).
3. DE FRAINE, 'Optimalisatie van het concept en het gebruik van kogelgeleidingen uitgaande van de vervormingsanalyse', Thesis Louvain, (1968).

DISCUSSION*Query from J. Pic, Prague*

I have a point on the influence of rigidity of rolling elements.

The computation method holds only if the rigidity of both bodies is very high. If not, then the difference in rolling member loadings may be in error by several hundred percent. A rolling guideway of a plain grinding machine was calculated, and differences of 300% were found with the deformation of bodies taken into account.

Reply

In our slideway the stiffness of the mounting forces is sufficient to have the loads proposed. The compliance of the contact ball-trackway is much greater than the compliance of the other elements of the slideway.

By the application of rollers instead of balls the compliance of the contact roller-trackway is not greater than the compliance of the other bodies. I think that the difference of 300% you mention is very possible in that case.

THE IMPROVEMENT OF THE ACCURACY OF ELECTROHYDRAULIC CYLINDER DRIVES FOR NC MACHINE TOOLS BY THE USE OF ACTIVE FEEDBACK COMPENSATION

by

A. DE PENNINGTON* D. W. MARSLAND+ and R. BELL[†]

SUMMARY

An example of the use of transient acceleration feedback is described. The use of two load masses allows the effectiveness of the technique to be studied at a low (38 Hz) and a high (88 Hz) drive natural frequency. The control system response is evaluated, for input signals, by step and frequency response tests; the output stiffness is assessed by single-tooth milling loads and impact loads. A considerable enhancement of static and dynamic accuracy is demonstrated.

Nomenclature:

- C , the linearised viscous friction coefficient;
 K_a the gain constant of the acceleration sensor;
 K_p the position loop gain constant ($= K_1 K_2$);
 K_1 the forward sequence gain constant before the minor loop summing point of the position loop;
 K_2 the forward sequence gain constant of the minor loop;
 k_l the linearised crossport leakage coefficient;
 k_p the linearised pressure droop;
 T_D the minor loop transient network time constant;
 T_M the servo-valve torque-motor time constant;
 V_e the position-error voltage;
 ω_l the angular natural frequency of the hydro-mechanical load;
 ω_v the angular natural frequency of the servo-valve;
 ζ_l the hydromechanical load damping factor;
 ζ_v the servo-valve damping factor.

INTRODUCTION

The specification of the controlled axes of a numerically controlled machine tool includes references to both the static and dynamic accuracy of the control systems. The formulation of this data varies considerably as many variations in required performance can be observed in the currently available range of numerically controlled machine tools. In many cases the specification of drive performance is directly linked to the specific requirements of a customer. There are discernible trends towards the use of more general test procedures that use either a set of

standard workpiece tests, typified by those incorporated in the 'National Aerospace Standards'¹, or use statistical estimates of machine accuracy, such as those put forward by the 'National Machine Tool Builders Association'².

The statement of machine accuracy applies constraints to the gain constants and bandwidth of the control systems. The choice of drive that will satisfy these values is dictated both by the search for the most economic class of drive and by the stroke and inertia, or mass, of the controlled member. The electrohydraulic cylinder drive has the immediate attraction of providing the most simple and the most economic solution where it can be applied, but its area of application is limited by a number of design problems³. However it is widely used in small vertical milling machines and lathes.

The aim of this paper is to illustrate the improved potential of the cylinder drive if acceleration feedback techniques are employed^{3,4} instead of the ill-considered crossport leakage damping. An experimental drive has been chosen for study that can be operated with a drive natural frequency of either 88 Hz or 38 Hz. The level of performance that can be obtained without any compensation is shown to be unacceptably low. The addition of an acceleration transducer to provide a minor loop compensation technique is then studied.

The major emphasis here is on the interaction between the position-loop gain constant and the load dynamics. A number of issues, such as additional series compensation and limit cycle stability, have not been included, but a case study is available elsewhere³.

*Philips, Eindhoven, Netherlands.

+Kingston Polytechnic.

†Machine Tool Engineering Division, UMIST.

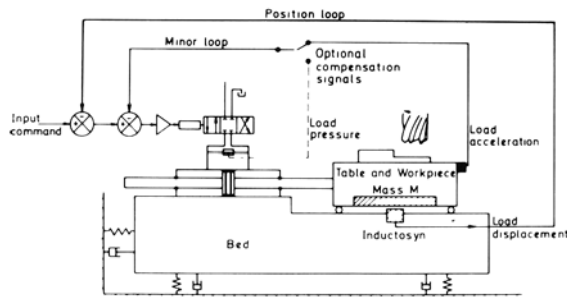


Fig. 1 Schematic view of a cylinder feed drive.

THE LINEARISED DYNAMICS OF AN ELECTROHYDRAULIC CYLINDER DRIVE

It was found that the performance of the drives we studied could be adequately covered by a linear analysis. The modelling of the electrohydraulic cylinder drive is thus confined to the construction of the transfer functions of the electrohydraulic servo-valve, and the loaded cylinder. The servo-valve can be effectively represented by the product of a lag for the torque motor coil and a quadratic lag for the hydro-mechanical section of the valve⁴. A single quadratic lag defines the dynamics of the load because there was no significant interaction between the drive and machine tool structure.

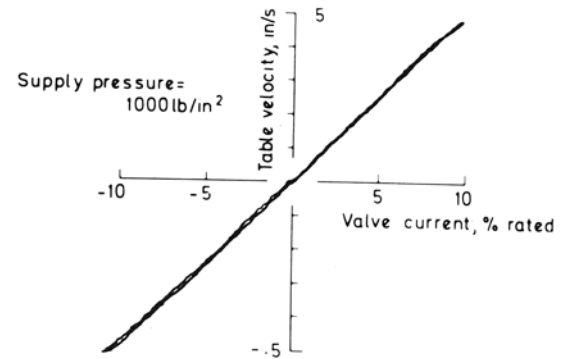
A schematic diagram of the drive is given in Fig. 1. The position loop contains no compensation facility other than gain adjustment. The minor loop is shown to be effective using either an acceleration signal or a differential (load) pressure signal (evidence to support this point is available⁴). The details of the transient network have not been included, but a full treatment of the use of this additional variable has been published^{4,6,7}.

The open loop transfer function of the control system is of the form^{3,4}

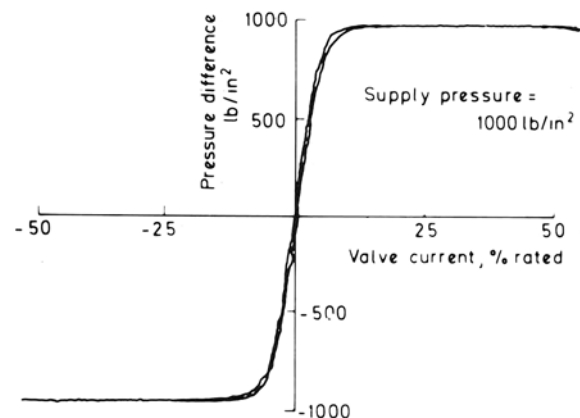
$$y/V_e = K_1 K_2 \div s \left(1 + sT_M \right) \left(\frac{s^2}{\omega_v^2} + \frac{2\xi_v s}{\omega_v} + 1 \right) \left(\frac{s^2}{\omega_l^2} + \frac{2\xi_l s}{\omega_l} + 1 \right) \quad (1)$$

The limit of performance, judged on linear system considerations, are the natural frequency of the load, ω_l and the damping factor of the load, ξ_l . It has been shown that the load damping is inadmissibly low and that it cannot be increased by hydromechanical design without some linked deterioration in drive performance^{3,5}. The constraint imposed by the magnitude of the drive natural frequency, ω_l , is removed if it is shown that an economic cylinder design can be used to achieve the required natural frequency. There is, currently, considerable uncertainty on what minimum value is necessary; it is important to note that the figures that are quoted for the required natural frequency of a leadscrew or rack drive need not be relevant as the control system structure, and design, differ considerably for rectilinear and rotary drives.

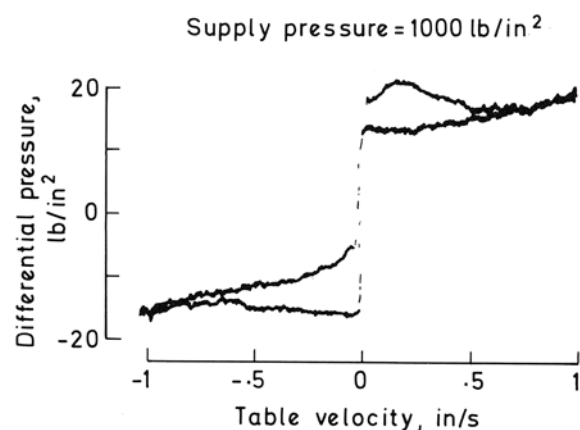
It has been shown^{6,7} that active compensation derived from an accelerometer or a differential load pressure sensor can be used to introduce adequate levels of load damping over a wide range of possible control systems. Two variants in this compensation have been proposed⁷ which, subject to the relative magnitudes of the servo-valve coil time constant, T_M , and the natural drive frequency, ω_l , satisfy all configurations that will be encountered in NC machine tool design. It has been found that if the product $\omega_l T_M$ is less than 0.5, negative acceleration feedback is effective. Thus, the compensation signal takes the



(a) The unloaded velocity-drive signal characteristic



(b) The zero-flow pressure gain characteristic.



(c) The differential pressure-table velocity characteristic.

Fig. 2 The steady-state characteristics of the drive.

form $K_a S^2 y$ and the closed loop transfer function quoted opposite in equation (1) becomes

$$y/V_e = K_1 K_2 \div s \left[\left(1 + sT_M \right) \left(\frac{s^2}{\omega_v^2} + \frac{2\xi_v s}{\omega_v} + 1 \right) \right. \\ \left. \left(\frac{s^2}{\omega_l^2} + \frac{2\xi_l s}{\omega_l} + 1 \right) + s K_a K_2 \right] \quad (2)$$

If the product $\omega_l T_M$ is greater than 0.5, the simple expedient of the use of an additional transient network⁶ in the acceleration feedback path is most effective. The feedback compensation signal is then of the form $\frac{K_a T_D S^3 y}{(1 + S T_D)}$ and the compensated

open loop position transfer function

$$y/V_e = K_1 K_2 (1 + sT_D) \div s \left[\left(1 + sT_D \right) \left(1 + sT_M \right) \left(\frac{s^2}{\omega_v^2} + \frac{2\xi_v s}{\omega_v} + 1 \right) \right. \\ \left. \left(\frac{s^2}{\omega_l^2} + \frac{2\xi_l s}{\omega_l} + 1 \right) + s K_a K_2 T_D \right] \quad (3)$$

The relative merits of negative acceleration feedback and negative transient acceleration feedback have been analysed in depth⁴ and the above statement is only intended to serve as a guide to the system design, rather than as a definitive statement. The examples quoted here use negative transient acceleration feedback. A detailed study of a system with negative acceleration feedback has been presented³.

The experimental work discussed below illustrates the improvement in drive dynamics that can be obtained by the proper implementation of equation (3). The use of series compensation to increase further the accuracy of this class of drive has not been included, as a number of other parameters have then to be considered³.

The experimental drive

The test rig used was a small vertical milling machine, considerably modified to make it suitable for this study. The drive consists of a high quality, equal-area cylinder with an effective area of 3.5 in² and a stroke of 9 in, which controls a mass of 270 lbs guided by a 'Tychoway' roller slide system. This configuration has a natural drive frequency of 88 Hz. The addition of a lead weight, which increases the load mass to 1,800 lbs, allows a drive natural frequency of 38 Hz to be realised.

The two stage, four way, electrohydraulic flow control valve has an unloaded flow rated at 5 g min⁻¹ at 3,000 lbs in⁻². The natural frequency ($\omega_l/2\pi$) of this valve is 260 Hz and the damping factor (ξ_l) is 0.75. The load velocity/drive signal shown in Fig. 2a gives a measure of the servo-valve flow characteristic. The zero velocity, load pressure/drive signal characteristic shown in Fig. 2b and the load pressure/load velocity characteristic in Fig. 2c describe the threshold characteristics of the servo-valve and cylinder. The seal friction is lower than usual in servo cylinders.

The instrumentation used included a piezo electric accelerometer, two strain gauge/diaphragm pressure transducers to develop a load pressure signal, a permanent magnet type rectilinear velocity transducer and a triple scale 'Inductosyn' to provide the position feedback signal.

A single tooth cutter was used to provide the most difficult dynamic cutting conditions, but the milling machine spindle and its drive were not adequate for exhaustive cutting tests. However, these limited cutting facilities provide the scope for a meaningful estimation of the output stiffness of the drive.

The inherent dynamic responses of the two drive configurations are shown in Fig. 3. In both cases the hydromechanical load resonance is lightly damped. The 38 Hz system has a more complex response than

the 88 Hz system, as the 1,800 lb. load mass induces a number of interacting structural resonances.

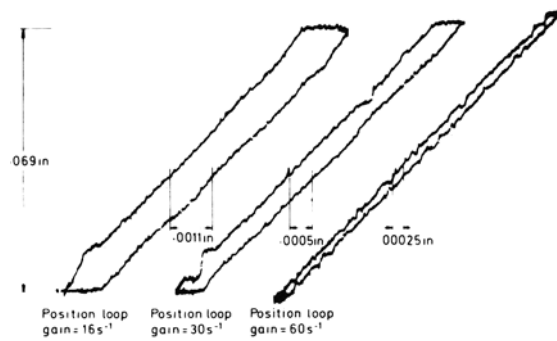


Fig. 3 The influence of position loop gain on the hysteresis of the uncompensated drive (load mass 270 lbs, natural frequency 88 Hz)

The performance of the uncompensated systems

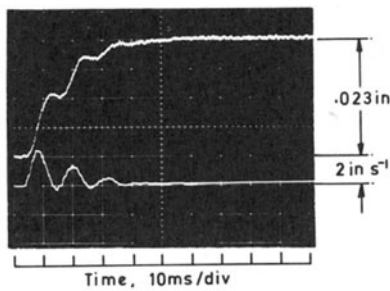
The static and dynamic capability of the uncompensated drives is to be taken as a basis for the estimation of the value of active compensation. The static performance is estimated by plotting the output displacement against the input command voltage when this signal is a low frequency triangular wave. The dynamic performance of the drive is displayed in the form of step responses and frequency responses.

The interaction between the inherent threshold dead zone of the actuator and the position loop gain is shown, for the 88 Hz system, in Fig. 4. The need for a position loop gain constant of at least 50 s⁻¹ would seem necessary from the inspection of these test results if good threshold accuracy is to be attained. The presence of greater load friction would, of course, call for a greater position loop gain constant. A dead zone of less than 10⁻⁴ in is thus possible if the control system will tolerate the required level of position loop gain constant.

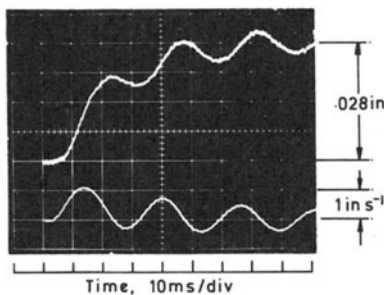
The last point is emphasized when the transient responses depicted in Figs. 5a and b are studied. The transient response of the uncompensated system is, in both cases, seen to be unacceptable. It is usual to specify a zero overshoot, fast response performance, with effective stability margins. The system transient responses fall well short of these requirements.

At this point neither of these control systems, without further development, could be used on a machine tool. The next system design would be to incorporate crossport leakage. The leakage restrictor would then be adjusted until the most effective level of performance was achieved. The uncompensated drive is again taken as the basis for the evaluation of the actively compensated drive. The omission of the leakage damped condition serves to emphasize our critical view of the technique for all but the least demanding specifications.

In both cases the poor dynamic response can properly be attributed to the low level of damping in this class of drive. The first step in any design which leads to an adequate specification, is to overcome the deficiency in damping at the load.



(a) load mass 270 lbs, natural frequency 88Hz
position loop gain constant 60 s^{-1}



(b) load mass 1800 lbs, natural frequency 38Hz
position loop gain constant 34 s^{-1}

Fig. 4 The transient response of the uncompensated systems.

Load damping

There are a number of sources of damping for this class of drive. These include the load pressure droop constant of the servo-valve (k_p), the leakage across the load ports (k_l) and the viscous damping at the load (C). In our study, the load is supported on anti-friction guideways and the effective viscous damping caused by the friction developed by the pre-loaded bearings, is the only term available. In general, it has

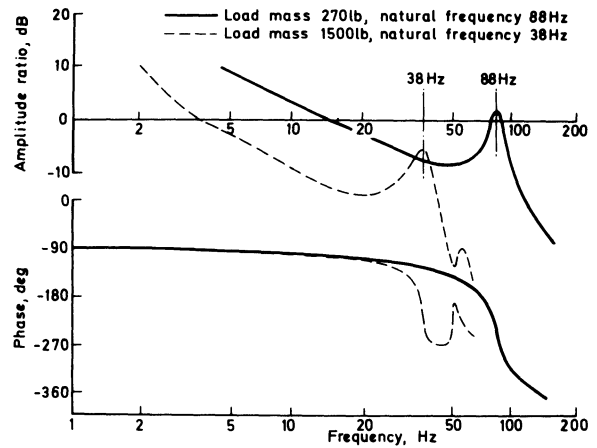
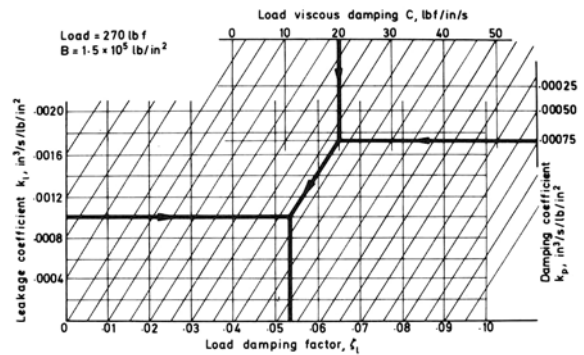


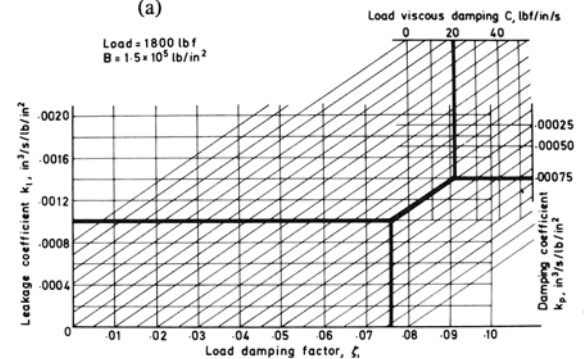
Fig. 5 The open loop frequency response characteristics of the uncompensated systems.

been found^{8,9} that all classes of guideway provide very little effective viscous damping, away from the threshold velocity region.

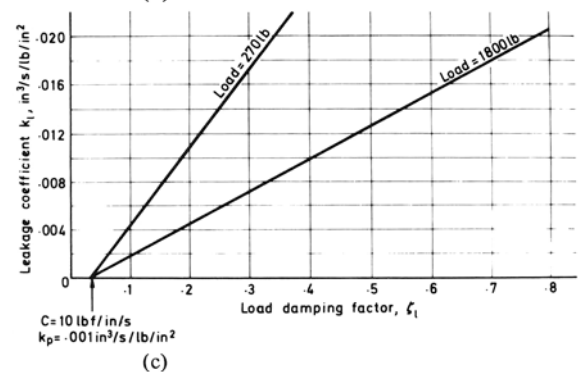
The contribution of the three components of system damping to the load damping factor is shown in Fig. 6. Fig. 6a and b illustrate the influence of a



(a)



(b)



(c)

Fig. 6 The damping of the experimental drives.

range of crossport leakage and assumed load viscous friction values. These constructions are not fully developed nomograms and it is not possible to extrapolate between parameter values with accuracy. The inherent damping in the drives as determined from Figs. 6a and b, is too low for adequate damping, that is for a level that would permit a competent position loop to be established.

At this point in the consideration of system design, a number of compensation techniques can be considered⁵; the usual procedure is to apply crossport leakage damping. The value of leakage coefficient (k_l) required in both cases can be determined from Fig. 6c. The load damping required will be in the range $\zeta_l = 0.3 \rightarrow 0.6$; for this level of damping the amount of leakage required will severely impair the performance of the actuator. The loss of speed range and the enhancement of the drive dead zone with this class of damping have been shown^{3,5} to be most undesirable.

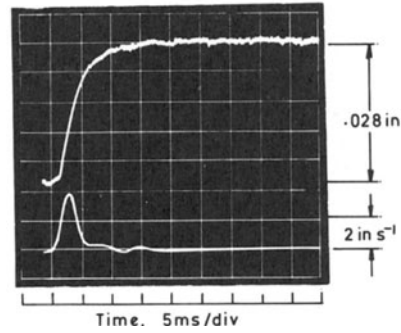
We now examine the use of an active compensation technique. The use of a minor loop compensation technique does not, in contrast to the use of crossport leakage, undermine the steady state characteristics of the actuator. In some cases, an effective hydromechanical compensation technique can be used¹⁰.

The performance of the drives with active compensation

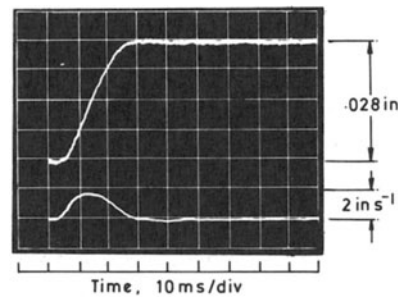
An examination of the transfer functions quoted in equations (2) and (3) reinforced by the experimental data plotted in Fig. 5, shows that the negative transient acceleration feedback was the more appropriate technique. The design procedure consists, therefore, of obtaining the balance between the position loop gain constant (K_p), the transient acceleration loop gain constant ($K_2 K_a T_D$) and the transient network time constant. The analysis was carried out on a digital computer in root locus format. The design criterion chosen was the zero overshoot condition which adequately meets the majority of machine tool specifications. No constraint was placed on the frequency response of the system, although it will be demonstrated that this class of system displays a relatively wide bandwidth.

The resultant design data and tests shown in Figs. 7 and 8 do not incorporate maximum damping of the minor loop, that is the effective load damping with the use of negative transient acceleration feedback is adjusted to a level at which the best position loop response is attained. The final choice of position loop gain constants 60 s^{-1} for the 38 Hz system and 117 s^{-1} for the 88 Hz system, are attained with the complete satisfaction of the transient response requirements. Comparison of the test responses shown in Figs. 4 and 7 emphasizes the marked difference between the uncompensated and the compensated systems.

The gain constant required in the minor loop can be competently achieved by the use of economically priced transducers and although this design procedure is more involved than current practice it is thought to offer a significant improvement in drive performance.



(a) load mass 270 lbs, natural frequency 88 Hz
position loop gain constant 117 s^{-1}
acceleration loop gain constant 8×10^{-6}
transient network time constant 6 ms



(b) load mass 1800 lbs, natural frequency 38 Hz
position loop gain constant 60 s^{-1}
transient network time constant 20 ms
minor loop gain constant 4×10^{-5}

Fig. 7 The transient response of the position control systems with transient acceleration minor loop compensation.

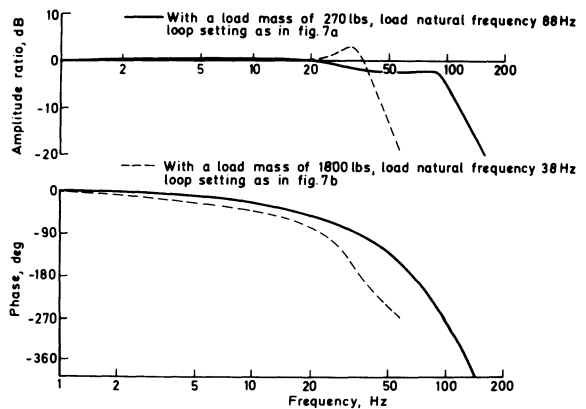


Fig. 8 The closed loop frequency response characteristics of the compensated drives.

The effect of piston position was not significant in these tests. It is possible that in some cases the shift in natural drive frequency may invalidate the use of this technique. If, however, the cylinder drive is designed as part of a control system from the start, the stroke problem can be eliminated.

The influence of load disturbances (cutting forces) on this class of control system is of considerable significance. A number of tests were carried out in order to assess, qualitatively, the output stiffness of the two drive conditions. The set of test results (Fig. 9) form a cross section of the observations.

The performance of the 88 Hz system is shown both for impact loading and single tooth milling. These load disturbances are extremely stringent tests of the output stiffness of the control system. The position loop gain constant was set at 117 s^{-1} , the transient network time constant was 6 ms and the minor loop gain constant was 8×10^{-6} . The impact tests (Figs. 9a and b) show that the compensated system is extremely effective in counteracting the initial deflection caused by the impact load. The uncompensated system has the lightly damped response that is to be expected from reduced stability margins. The position loop gain constant had to be reduced to 30 s^{-1} so that the cutting tests shown in Figs. 9c and d could be effectively compared.

The 38 Hz system response to a cutting test is illustrated in Figs. 9e and f, which show both displacement and velocity waveforms. The position loop gain constant (K_p) was 50 s^{-1} , the minor loop gain constant was 4×10^{-5} and the transient time constant, T_D , was 20 ms. The maximum deflection was approximately 10^{-3} in. The velocity trace (Fig. 9c) is the more relevant test of damping and shows that the 88 Hz system under these conditions gives a first class dynamic response to both input signals and output load disturbances.

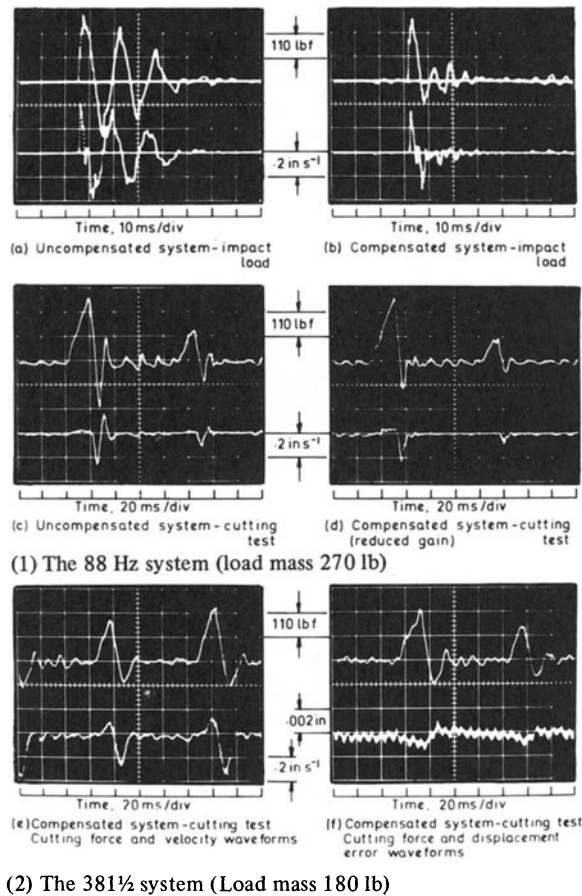


Fig. 9 Examples of the influence of load disturbances on the performance of the control systems.

CONCLUSIONS

The value of negative transient acceleration feedback has been demonstrated on two drive configura-

tions on a scale which makes the results immediately relevant to machine tool design. It has been possible to provide a completely effective control of load damping. The final static performance of each drive configuration was good with very wide position loop bandwidth and with a zero overshoot position response.

The use of accelerometers or differential pressure sensors is considered to be economically justified because cylinder drive designs incorporating these techniques are capable of performance beyond that normally considered feasible. The additional expense incurred in the use of the transducers is small compared with the cost of the rotary drive that might have to be used if the fully developed cylinder drive design were not used.

ACKNOWLEDGMENTS

The authors wish to thank Professor F. Koenigsberger for his permission to carry out this work in his Laboratories, and acknowledge the support of the Science Research Council, both for the experimental facilities and for computer facilities made available to the Institute.

REFERENCES

1. ANON., 'National Aerospace Standards 912, 913, 948, 960, 977, 978 and 979', Aerospace Industries Association of America, Washington D.C., U.S.A.
2. ANON., 'Definition and Evaluation of Accuracy and Repeatability for Numerically Controlled Machine Tools', National Machine Tool Builders Association, Washington D.C., U.S.A., 1968.
3. BELL, R., 'The Performance of Electrohydraulic Cylinder Drives for Numerically Controlled Machine Tools', Ph.D. Thesis, UMIST, 1970.
4. DE PENNINGTON, A., 'The Dynamics of Electrohydraulic Cylinder Drives', Ph.D. Thesis, UMIST, 1971.
5. BELL, R., 'The Use of Cylinder Drives on N.C. Machine Tools—A Re-Evaluation', to be published in J.M.T.D.R., 1971.
6. BELL, R., and DE PENNINGTON, A., 'The Design of Active Damping for Electrohydraulic Cylinder Feed Drives', Proc. 9th M.T.D.R. Conf., Birmingham, 1968, 1309.
7. BELL, R., and DE PENNINGTON, A., 'Active Compensation of Lightly Damped Electrohydraulic Cylinder Drives Using Derivative Signals', Proc. Inst. Mech. Engrs., 1969–70, 184, 83.
8. BELL, R., and BURDEKIN, M., 'The Frictional Damping of Plain Slideways for Small Fluctuations of the Velocity of Sliding', Proc. 8th M.T.D.R. Conf., Manchester, 1967.
9. POLACEK, M., and VAVRA, V., 'The Influence of Different Types of Guideways on the Static and Dynamic Behaviour of Feed Drives', Proc. 8th M.T.D.R. Conf., Manchester, 1967, 1127.
10. GALE, P. and BELL, R., 'An Economic Technique for the Improvement of the Stability of Hydraulic Cylinder Drives'. Paper to be given at the 12th M.T.D.R. Conf., Manchester, 1971.

DISCUSSION*Query from A. Laika, T. U., Munchen*

With rotary feed drives, velocity feedback is used. These drives are usually better damped than cylinder drives. Can one say, in general that velocity feedback is good with better damped drives, and acceleration feedback with poor damped drives?

Reply

The needs of rotary and rectilinear (i.e. cylinder) drives are very different. The rotary drive is inherently better damped and the velocity feedback is applied to provide a very linear response of motor velocity to drive signal. This result is achieved by the reduction in bandwidth of the minor loop. In the limit, with a high-gain minor loop ($\cong 350$ V/V) the

'soft servo' design, as advocated by International General Electric Ltd., is obtained. A critical part of the design is devoted to the production of high natural frequencies for the actuator and the load.

In the case of the cylinder drive, there is a rather different control problem. The dynamic limitation caused by the natural frequency of the cylinder and mass is dominant. The inherent load damping is also a problem; typical damping factor values are in the range of 0.03→0.08.

The use of leakage damping is of limited value and the use of velocity feedback is unacceptable if one attempts to achieve a good design, i.e. minimum power rating and minimum natural frequency. The application of active damping makes it possible to obtain the best level of performance both in respect to dynamic accuracy and to resolution.

AN ECONOMIC TECHNIQUE FOR THE IMPROVEMENT OF THE STABILITY OF HYDRAULIC CYLINDER DRIVES

by

P. GALE* & R. BELL†

SUMMARY

The design of hydraulic cylinder drives is discussed and particular attention is paid to the problems caused by the low inherent damping in this class of drive. The introduction of a hydromechanical network to improve drive damping is critically assessed both by analysis and experiment.

INTRODUCTION

The hydraulic ram provides the simplest and cheapest form of actuator where only a comparatively short stroke is required. This limitation on length of stroke is a consequence of the compressibility of the oil column within the actuator. In many designs the level of drive damping also imposes severe constraints on performance. The major source of damping in this class of drive is slideway friction which can be introduced by the use of plain slideways. However, the damping produced at plain slideways is a function of table velocity and design parameters. It is also necessary that the open loop drive is free of stick slip.

A major requirement on feed drives for machine tool applications is static accuracy. The elimination of non-linear slideway friction by the use of roller bearings increases accuracy. However, the use of anti-friction slideways results in reduced damping at the load in the threshold region, with a consequent limitation on the closed loop performance of the drive. In the presence of low load damping, series compensation techniques to modify the error signal are severely restricted unless the natural frequency of the drive is very high. In particular, the use of anti-resonant circuits such as the 'bridged tee' have been suggested by Shumsheruddin¹. Unfortunately, it has been shown by Belletruti and Maltaez² that the tuning of such networks is critical and maladjustment can cause a severe degradation in performance.

Most practical methods of compensating ram drives employ the use of techniques that increase the load damping. The introduction of a viscous damper at the load is unacceptable since it impairs the steady-state performance of the system. The use of viscous leakage across the ram to introduce further damping has been advocated in the past by Harpur³ and is widely used. This technique is cheap and easy to apply and can often provide an adequate solution

in those drives where maximum performance is not required. However, it has limitations, that is, it dissipates energy, reduces the maximum steady-state velocity and stiffness to external load disturbance and enhances threshold non-linearities.

An effective solution that is not subject to these drawbacks is provided by the feedback to the servovalve of an electrical signal proportional to load acceleration⁴⁻⁸. This technique, versatile though it is, is relatively expensive. Similar results can be obtained by feeding back to the servovalve an electrical signal proportional to load pressure. This method has the merit of lower cost than acceleration feedback but problems can arise in its application if high values of seal friction are present.

In this paper the use of hydromechanical transient flow networks is proposed as a cheap and effective alternative to acceleration feedback. The use of these techniques, which have been employed for sometime in flight control systems, appear to offer an economic solution to a number of machine tool drive design problems. Their value will now be assessed analytically and the significance of the analysis will be illustrated by the study of the performance of an experimental system.

METHODS OF INCREASING THE DAMPING AT THE LOAD

One of the earliest methods of increasing damping to be investigated was that of viscous leakage of fluid across the ram³. This method does not consume a great deal of extra fluid, but it is not generally appreciated that leakage leads to a decreased maximum feed rate, enhanced valve dead-band about null and a reduction in drive stiffness.

An increase in the servovalve underlap has also been shown to increase the load damping³. However, in this case the extra flow required to produce

*Cincinnati Milacron Ltd., Birmingham.

†Machine Tool Engineering Division, UMIST.

adequate damping makes the use of extra pump capacity mandatory. Investigations have been made into the use of minor loop feedback to increase damping. In particular negative velocity feedback is the most obvious form of minor loop. However, it has been shown by Bell and de Pennington^{4,5} that velocity feedback can have a de-stabilizing influence on cylinder drives with small load damping.

An alternative form of minor loop is produced by feeding back an electrical signal proportional to load acceleration or transient load acceleration. This method has been thoroughly investigated by means of root loci and analogue computer modelling^{4,5} so that criteria are laid down for the selection of the type of feedback and the value of the minor loop gain to ensure adequate damping.

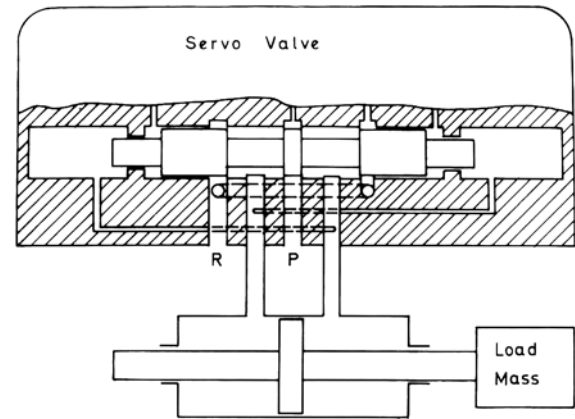
The voltage proportional to load acceleration is provided by a piezoelectric accelerometer. Without additional signal amplification, the accelerometer signal produced at low natural frequencies is inadequate. Also, where severe load disturbances are present, difficulties are experienced with saturation of the accelerometer charge amplifier. However, the use of f.e.t. input stages would appear to alleviate this problem.

An alternative form of signal, similar to the acceleration feedback signal, is provided by a pressure transducer arranged to measure the load pressure at the servovalve ports^{6,7}. This is easier to implement than acceleration feedback since the dynamic characteristics of pressure transducers are better than accelerometers. When using pressure as an alternative to acceleration signals in a closed-loop positioning system, position errors can arise due to the pressure required to overcome seal friction when the ram moves at constant velocity. The solution to this problem is to employ a high-pass filter in the feedback loop to de-couple the pressure signal.

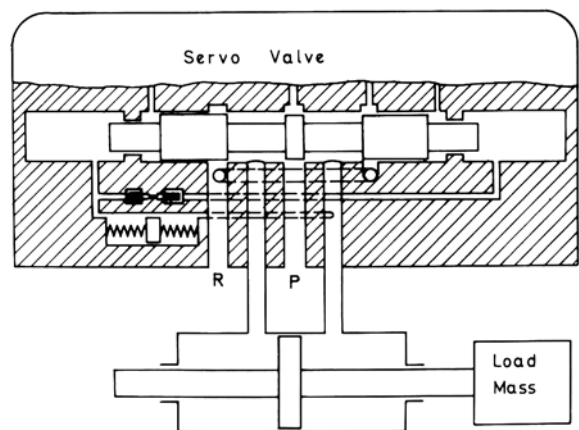
In many cases it is not possible to employ active compensation. It is desirable to seek alternatives to the use of crossport viscous leakages. A number of possible forms of hydromechanical compensation are illustrated in Fig. 1. The first two, load pressure feedback, Fig. 1a and dynamic pressure feedback are built into the servovalve. Transient flow networks can also be employed and two possible forms are illustrated in Figs 1c and 1d.

The use of load pressure feedback⁷ is somewhat infrequent as it de-rates the steady-state flow-load pressure of the servovalve characteristics. The dynamic pressure feedback technique^{9,10} is an elegant design solution, but the cost of tuning the network to the load can prove to be uneconomical. It has been used in aerospace applications; the industrial applications are very limited due to the relatively high cost of small batches of servovalves tuned to particular load conditions.

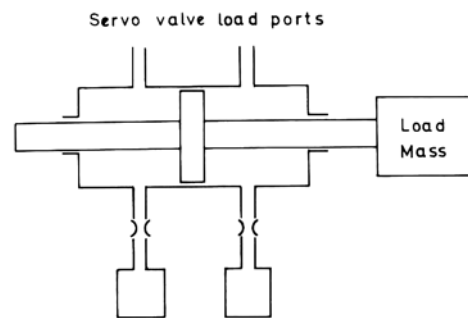
The transient flow networks are relatively inexpensive to construct and adjust. It was considered to be worth while to assess their usefulness in the machine tool field. One prime area of interest is in the design of NC machine tool feed drives, but there are many sequence controlled drives which might be improved by the successful application of these techniques.



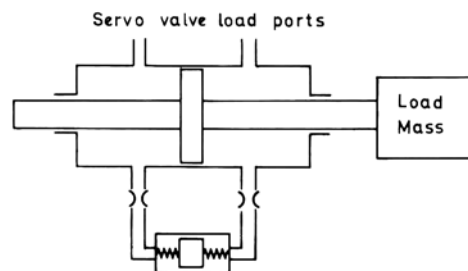
(a) Load pressure feedback



(b) Dynamic load pressure feedback



(c) Transient stabiliser tanks



(d) Crossport transient flow network.

Fig. 1 Some hydromechanical techniques to increase load damping.

Mathematical model for the drive

An electrohydraulic cylinder drive can adequately be modelled by a fifth-order transfer function⁸ of the form

$$y/V_e = K_p \div s \left(1 + sT_m \right) \left(\frac{s^2}{\omega_v^2} + \frac{2\xi_v s}{\omega_v} + 1 \right) \left(\frac{s^2}{\omega_l^2} + \frac{2\xi_l s}{\omega_l} + 1 \right) \quad (1)$$

This transfer function is developed in Appendix II.

The electrohydraulic servovalve is a complex element to model; it has been shown by Morse⁹ that a lag, T_m , for the servovalve torque motor coil and a quadratic lag (natural frequency ω_v , damping factor ξ_v) form an adequate model. The load formed by the cylinder and mass is represented by a quadratic lag (natural frequency ω_l and damping factor ξ_l).

The torque motor time constant is sometimes significant, subject to drive circuit design, but is often a second-order influence. The natural frequency of the servovalve is invariably in excess of 100 Hz. (There are some slow response valves available but they are not yet in general use). The servovalve damping factor is made high (of the order of 0.7), thus the servovalve exerts a secondary influence.

The controllability of the hydraulic cylinder is adversely influenced by its inherently low damping; this point is demonstrated in Fig. 2. The root pattern shown in Fig. 2a is a representative example. In a closed-loop position control application, the load pole damping will be the factor that restricts the scope of the designer. In an open loop drive, the absence of an adequately high damping factor will leave the system more prone to relaxation oscillations (stick-slip), due to a non-linear seal friction term, than would have been the case with a high viscous damping term.

The effect of adding a transient flow stabilizer network is to modify the load dynamics but to leave the electrohydraulic valve transfer function unchanged. The revised transfer function, which is derived in Appendix II is of the form

$$\frac{y}{V_e} = K_p (1 + sT) \div s \left[\frac{s^3 T}{\omega_l^2} + s^2 \left(\frac{1}{\omega_l^2} + \frac{2\xi_l T}{\omega_n} + \frac{RTM}{A^2} \right) + s \left(T + \frac{2\xi_l}{\omega_l} + \frac{RTC}{A^2} \right) + 1 \right] \quad (2)$$

The above transfer function contains a cubic term which replaces the load quadratic term in the transfer function for the uncompensated system [equation (1)]; the load dynamics will in general be represented by a modified quadratic term and an additional lag. The presence of the zero due to the transient stabilizer network is also significant. The effective application of the transient stabilizer network will result in a pole configuration of the form shown in Fig. 2b. This pole pattern includes a suitably transposed load pole location and the additional pole and zero due to the application of the network.

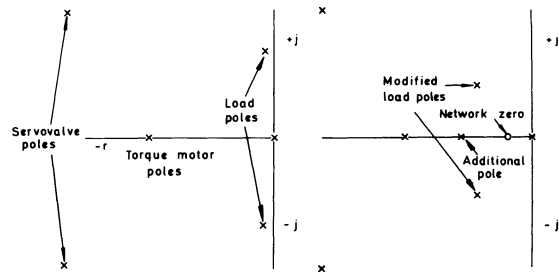


Fig. 2 Influence of the transient flow network on the linearized system dynamics:

- (a) uncompensated system;
- (b) system with transient flow network.

Example of the selection of design parameters for a transient stabiliser network

The analysis of the compensated cylinder drive which has been discussed above, and which is developed in Appendix II, specifies two design parameters, the network time constant, T , and the orifice conductance, R . The transfer function which relates the transient stabiliser flow, q_n , to the load pressure, P_l , is

$$\frac{q_n}{P_l} = R \cdot \frac{sT}{1 + sT} \quad (3)$$

where
$$T = \frac{A_p^2}{KR} \quad (4)$$

(For derivation see Appendix III.)

The modified, or compensated, system transfer function, equation (2), is an involved expression and its significance will now be assessed with the aid of an example. The system chosen for the experiments had a natural frequency of 30 Hz. The transient response for the linear model of this drive is shown in Fig. 6, that is, the case where $T = 0$.

The influence of the network on the dynamics of the drive can be demonstrated by the use of a diagram that contains the loci of the roots of the cubic term contained in the denominator of equation (2). These roots consist of the modified load poles and the additional pole due to the presence of the network. The diagram which shows the loci of the roots for the experimental system is plotted in Fig. 3. The loci are generated for a number of values of the time constant T in the range 0.2–0.01 s. The variable along the loci is the orifice conductance R .

For values of T less than 0.03 s, damping is added by the network, but since the loci curve back towards the real axis the value of R is critical and the drive natural frequency is reduced. Four distinct types of pole/zero configurations are possible as R is varied, if T is greater than 0.03 s. These are shown in Fig. 5 together with the computed transient responses for $T = 0.1$ s. The best compromise between adequate damping and speed of response is offered by the configuration where $R = 0.05$. The expanded section of Fig. 3 for the values given above, $R = 0.05$, $T = 0.1$, is shown in Fig. 4.

The study of the interaction between the choice of the variables T and R is further aided by the assessment of the transient responses of the linear model for the system with $R = 0.05$ in⁵/lbf s and T variable (Fig. 6), also with $T = 0.1$ s and R variable (Fig. 7).

These responses demonstrate that the choice of values and T and R given above provide the best transient response; the overshoot is zero and the response time is not seriously increased.

The transient responses of the linear model with a closed position loop emphasise the potential of the technique. The traces displayed in Fig. 8 reveal that an acceptable transient response with the network is achieved with the position loop constant set at 50 s^{-1} . The limitations of the uncompensated system are underlined by the trace for this condition.

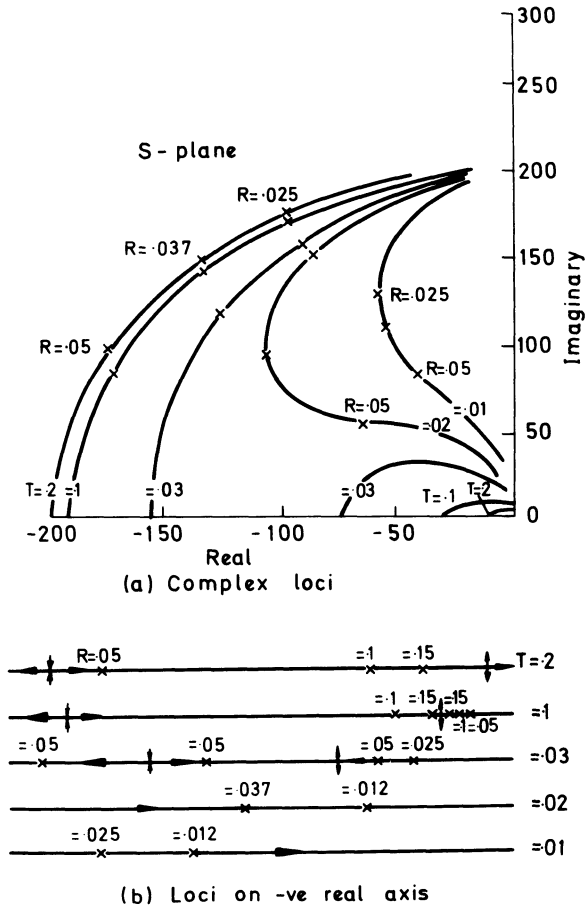


Fig. 3 Locus of the roots for the cylinder drive with hydromechanical network $\omega_n = 30 \text{ Hz}$.

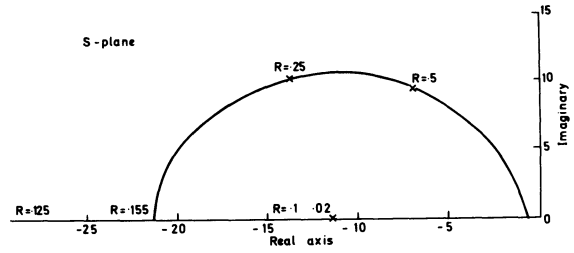


Fig. 4 Expanded section of the roots when $T = 0.1 \text{ s}$ in the range $R = 0.125 - 5.0 \text{ in}^5 / \text{lbf s}$

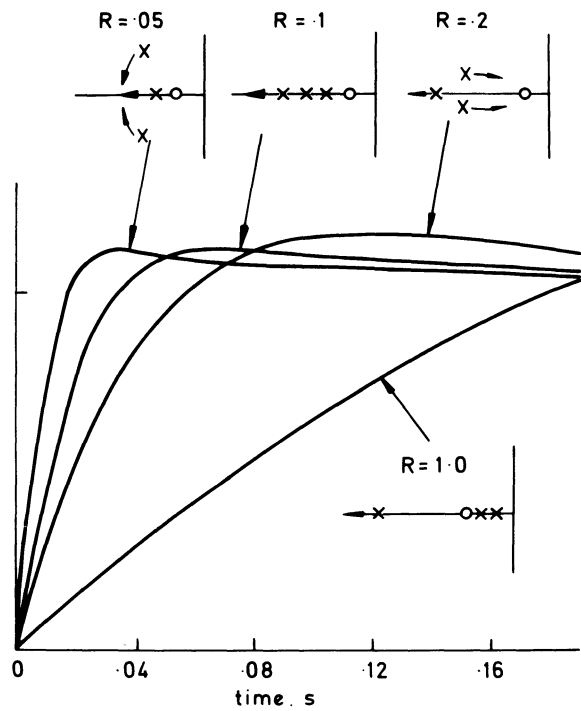


Fig. 5 Relative root positions for different values of R and the corresponding step response $T = 1 \text{ s}$.

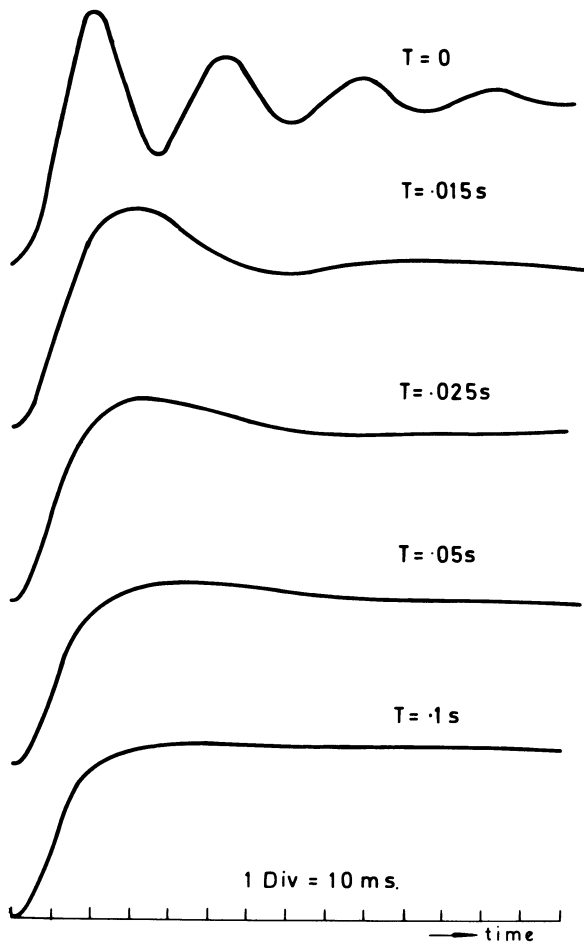


Fig. 6 Influence of the network time contact T on the transient response of the linear model ($R = 0.05 \text{ in}^5/\text{lbf s}$).

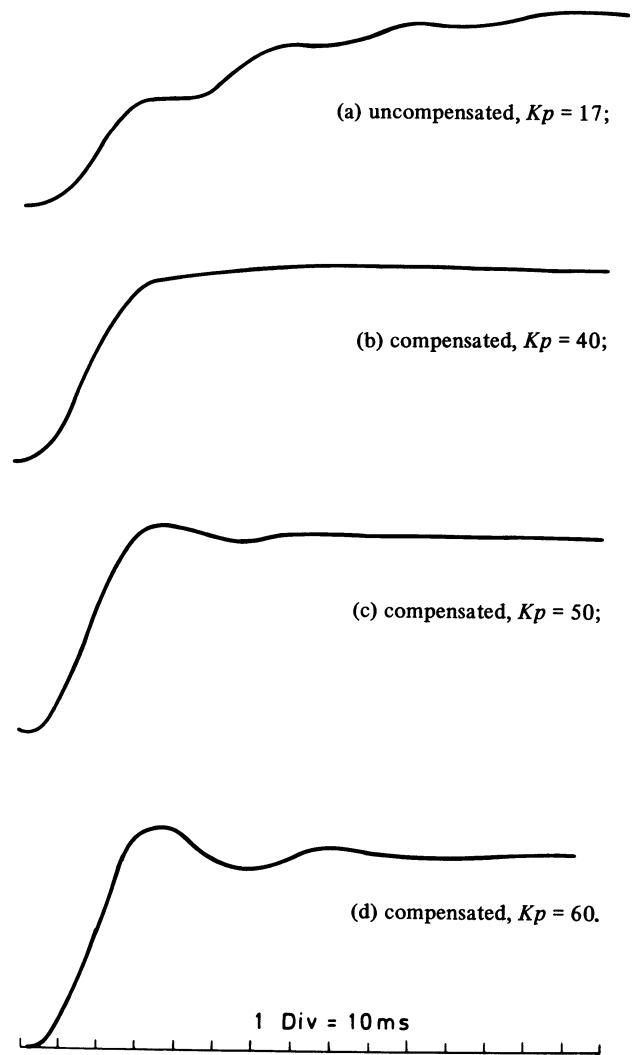


Fig. 8 Transient response of the linear model with a position feed back loop:

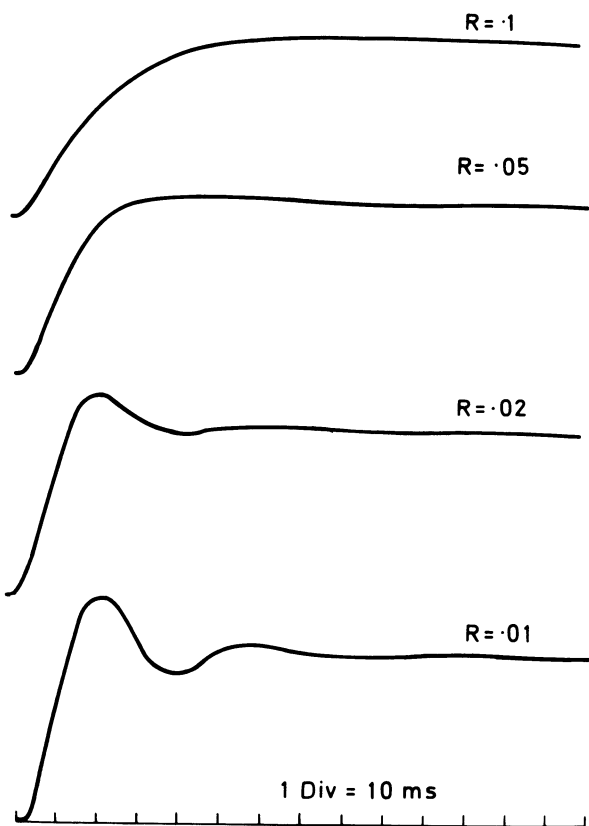


Fig. 7 Influence of orifice resistance R on the transient response of the linear model ($T = 0.1 \text{ s}$).

Design of the transient stabiliser network

Computer-aided studies have shown that a value of $T = 0.1 \text{ s}$ and a value of R in the region of 0.05 give adequate performance for the network. For the first design it was felt desirable to add greater damping than used in the model, so a value of R of 0.1 was used. Thus the transfer function of the required network is from equation A.3.9

$$\frac{q_n}{P_i} = 0.1 \left(\frac{s \times 0.1}{1 + s \times 0.1} \right) \quad (5)$$

Equation 5 was derived for a spring loaded piston in series with a single restrictor and this presupposes no restriction whatsoever on one side of the network. This is clearly an impossible condition and so the restriction required was divided between the two

sides of the spring loaded piston. A similar derivation to the single restrictor case yields the expression

$$\frac{q_n}{P_1} = \frac{R}{2} \cdot \frac{sT}{1 + sT}, \text{ where } T = \frac{2A_p^2}{RK} \quad (6)$$

comparing this with equation (5) we have

$$\frac{R}{2} = 0.1$$

that is, R for each restrictor is $0.2 \text{ in}^5/\text{lbf s}$. If a compact design is to be achieved the piston diameter must be small. Hence A_p was made equal to one square inch.

We can now calculate the spring stiffness required from equation (6)

$$K = \frac{2 \times 1^2}{0.2 \times 0.1} = 100 \text{ lbf in}^{-1}$$

The nearest commercially available spring had a stiffness of 105 lbf/in .

Much published work is available on the theoretical expression for flow in various types of restrictor but there is a lack of suitable experimental data. Thus values of R were determined experimentally for plate and capillary-type restrictors by measuring the oil flow through the restrictor for different values of pressure drop across it. During these tests it was noted that the flow/pressure relationship for plate orifices was highly non-linear and thus equation (4) was not strictly satisfied. In contrast the flow/pressure relationship for a capillary restrictor was linear over the anticipated pressure range and so this type of restrictor was retained. The mechanical layout of the network including the method used to seal the endcaps is shown in Fig. 9.

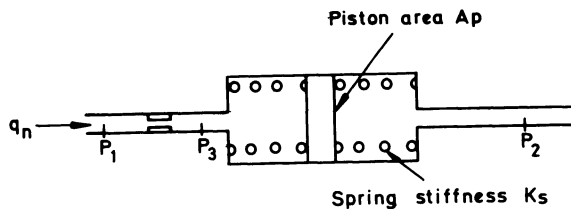


Fig. 9 Assembly of hydromechanical network piston unit

THE EVALUATION OF THE EFFECTIVENESS OF THE NETWORK DESIGN

The experimental drive was tested, open loop, by frequency response testing, transient response testing and by examination of the steady-state characteristics. The frequency response tests (see Fig. 10) show that the compensated system is adequately damped. It was not possible to test below 20% of the rated value drive signal. The transient responses quoted in Fig. 11, at 40% of rated value drive signal, demonstrate the effective action of the damper. The compensated velocity response does not fit very closely to the predicted form (see Fig. 5) but the end result is

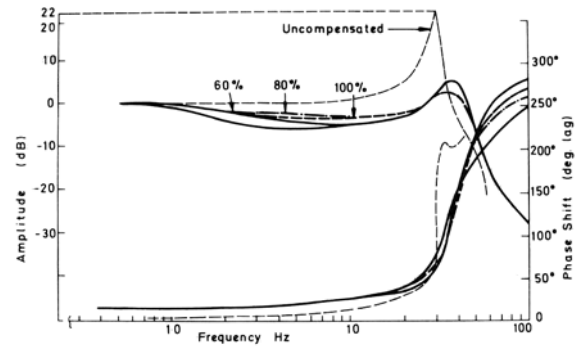


Fig. 10 The open loop frequency (velocity/drive signal) response with hydromechanical network

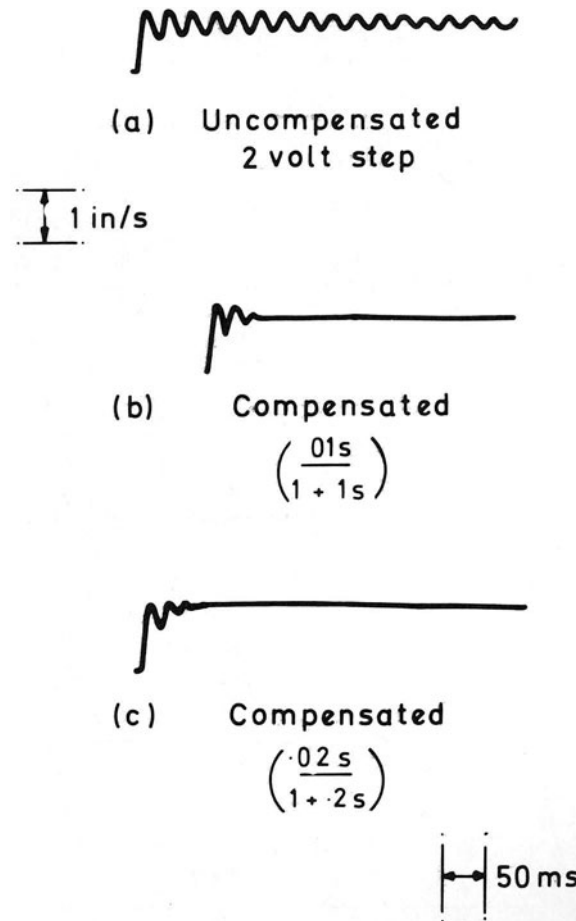


Fig. 11 The transient response of the experimental system

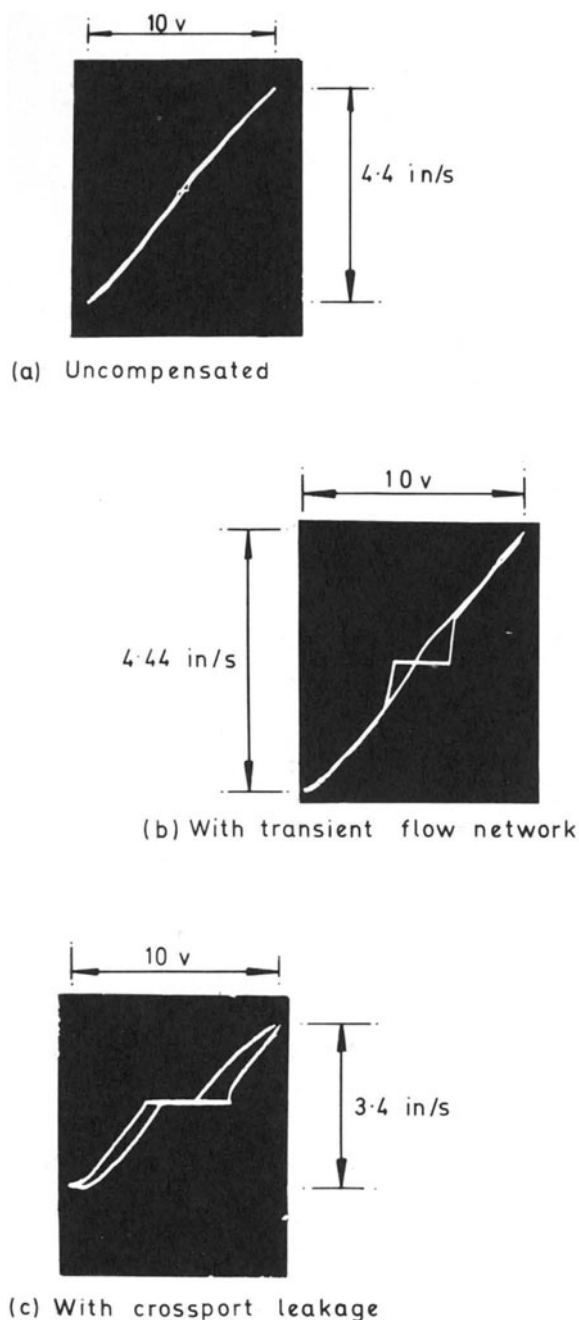


Fig. 12 Steady-state velocity/drive signal characteristics for the experimental drive.

such that the linear analysis can be used as adequate design guide.

The limitation of the technique is critically exposed in Fig. 12. The steady-state output velocity/value drive signal characteristics are given for the uncompensated system, the system with the transient flow stabilizer and the system with a crossport leakage compensator. The use of the transient stabilizer network generates less dead zone than that with crossport leakage and does reduce the speed range. A

case has been made for its use where crossport leakage is currently employed. It should be noted that active compensation techniques do not introduce any reduction to the steady-state performance of this class of drive.

CONCLUSIONS

The advantages and disadvantages of the use of transient flow stabilizer networks have been demonstrated. This type of compensation technique provides a simple, economic source of load damping. The limitation on the use of the networks is the enhancement of the dead zone that they introduce. Their use eliminates the disadvantages of power loss and the reduction in speed range which are introduced by the use of crossport leakage.

This class of compensation device will have limited application in high performance drives where the active techniques⁶ are to be preferred. They can be used to advantage on sequence controlled systems to eliminate stick slip.

The analysis of this class of system poses certain problems. The use of a simple linearized model gives a design guide, but it would be desirable to obtain a more accurate analytical model of the compensated drive.

ACKNOWLEDGMENTS

The authors wish to thank Professor F. Koenigsberger for his permission to carry out this work in his laboratories, and to Cincinnati Milacron Ltd. for their active interest and support. This research forms part of a programme of research sponsored by the Science Research Council and their support is gratefully acknowledged.

APPENDIX I

Nomenclature

A	Effective area of actuator cylinder, in^2
A_p	Area of network piston, in^2
B	Bulk modulus of the fluid, lbf/in^2
C	Load viscous friction, $\text{lbf}/\text{in per s}$
C_1	Valve leakage coefficient, $(\text{in}^3/\text{sec})/\text{lbf}/\text{in}^2$
F_{ext}	External force on the load, lbf
K_e	Torque motor and amplifier gain, A/V
K_p	Position loop gain constant
K_s	Network spring stiffness, lbf/in
K_f	Valve opening gain, in/A
K_{q1}	Valve static flow gain, $(\text{in}^3/\text{s}) \text{ per in}$
K_v	Valve pressure droop, $(\text{in}^3/\text{s})/\text{lbf per in}^2$
K_2	$K_v + C_1$, in^5/lbf
K_3	$V/2B$, $\text{in}^5/\text{lbf s}$
L	Actuator stroke, in
M	Load mass
P_1	Pressure on one side of network, lbf/in^2

P_2	Pressure on other side of network, lbf/in ²
P_o	Pressure immediately following the restrictor
P_1	Load pressure ($P_1 - P_2$), lbf/in ²
P_1	Small perturbation of load pressure, lbf/in ²
q_a	Linearized actuator flow, in ³ /s
q_c	Linearized flow due to compressibility, in ³ /s
q_l	Linearized leakage flow, in ³ /s
q_n	Linearized network flow, in ³ /s
q_v	Linearized valve flow, in ³ /s
R	Orifice conductance, in ⁵ /lbf s
s	Laplace operator, s ⁻¹
T	Network time constant, s
T_m	Torque motor time constant, s
T_{av}	Servo valve equivalent first-order lag time constant, s
V	Half the total trapped volume, in ³
$V_e(s)$	Drive signal, V
ω_1	Load natural frequency, rad/s
ω_v	Servo valve natural frequency, rad/s
x	Valve spool displacement, in
x_p	Network piston displacement, in
y	Actuator displacement
ζ_1	Damping ratio of load quadratic
ζ_v	Damping ratio of valve quadratic

Linearizing for small perturbations of x , Q_v and P_1 about some operating point on the pressure/flow characteristics

$$q_v = \frac{Q_v}{P_1} P_1 \quad (\text{A.2.4})$$

$$\text{Let } K_q = \frac{Q_v}{x} P_1 = 0 = \frac{\text{flow}}{\text{spool displacement}} = \text{static flow gain}$$

$$K_v = \frac{Q_v}{P_1} X \text{ const.} = \frac{\text{change inflow}}{\text{change in load pressure}} = \text{pressure droop factor}$$

$$\text{Therefore} \quad q_v = K_q x - K_v P_1 \quad (\text{A.2.5})$$

$$\text{now} \quad q_v = q_l + q_c + q_a \quad (\text{A.2.6})$$

APPENDIX II

Equations for a Cylinder Drive

The relationship between the valve spool displacement and the error signal requires the specification of a torque motor lag and a valve quadratic lag hence

$$\frac{x(s)}{V_e(s)} = K_e K_t / (1 + sT_m) \left(\frac{s^2}{\omega_v^2} + \frac{2\zeta_v s}{\omega_v} + 1 \right) \left(\frac{s^2}{\omega_1^2} + \frac{2\zeta_1 s}{\omega_1} + 1 \right) \quad (\text{A.2.1})$$

For a typical two-stage valve, the torque motor break frequency ($1/T_m$) is 100 rad/s, ζ_v is 0.7 and ω_v is relatively insignificant having a value of 1000 rad/s. Bearing this in mind it is possible to specify an equivalent first-order lag time constant T_{av} to approximate to equation (A.2.1) at least below 50 Hz, which is the upper limit on bandwidth of most electrohydraulic drives for machine tool applications; that is

$$\frac{x(s)}{V_e(s)} = \frac{K_e K_t}{1 + sT_{av}} \quad (\text{A.2.2})$$

Next the linear equations describing the valve controlled ram will be derived. The use of a linear approach leads to the neglect of Coulomb friction at the slideway and piston seals and servo valve nonlinearities. For a load on anti-friction slideways, and with well-designed ram seals, the Coulomb friction forces are negligible except at very low valve openings or low velocities⁵. Neglect of the servo valve nonlinearities that is when operating in the threshold or saturation regions, the load pressure effects does not induce large errors.

$$\text{Valve flow} \quad Q_v = f(x, P_1) \quad (\text{A.2.3})$$

where q_l = leakage flow
 q_c = flow due to compressibility of oil
 q_a = actuator flow
 $q_l = C_1 P_1$ (A.2.7)
 and

where C_1 is the slope of the servo valve pressure/leakage flow curve.

External leakage, across the piston for example, will be neglected in this analysis

$$\text{also} \quad q_a = Ay \quad (\text{A.2.8})$$

and assuming small perturbations of the piston about mid stroke

$$q_c = \frac{V}{2\beta} \cdot \dot{P}_1 \quad (\text{A.2.9})$$

Where V is half the total trapped volume including piping. Hence from equation (A.2.5) to (A.2.9)

$$K_q x - K_v P_1 = C_1 P_1 + \frac{V}{2\beta} \dot{P}_1 + Ay \quad (\text{A.2.10})$$

or taking Laplace transforms with zero initial conditions

$$K_{qx} - K_v P_1 = C_1 P_1 + \frac{V}{2\beta} s P_1 = Asy \quad (\text{A.2.11})$$

The force on the actuator due to hydraulic pressure is $P_1 A$ and this must be balanced by the forces due to the load and the external forces. Hence, neglecting coulomb friction

$$P_1 A = Ms^2 y + Csy = F_{ext} \quad (\text{A.2.12})$$

Equations (A.2.11) and (A.2.12) are all that are required to construct the transfer function for the valve controlled ram. This is shown in equation (A.2.1).

Manipulation of equations (A.2.11) and (A.2.12) yields the expression

$$\frac{y}{x} = \frac{K_q/A}{s \left(\frac{s^2}{\omega_l^2} + \frac{2\zeta_l s}{\omega_l} + 1 \right)} \quad (\text{A.2.13})$$

Where ω_l = load natural frequency

$$= \left(\frac{2B}{VM} [A^2 + C(C_1 + K_v)] \right)^{1/2} \quad (\text{A.2.14})$$

and ζ_l = load damping ratio

$$= \frac{(K_v + C_1)M + \frac{VC}{2B}}{2 \left(\frac{VM}{2B} [(C_1 + K_v)C + A^2] \right)^{1/2}} \quad (\text{A.2.15})$$

Equations for system with hydromechanical network

The effect of the network is to add a further term to the flow equation viz the network flow q_n so that

$$q_v = q_a + q_c + q_l + q_n \quad (\text{A.2.16})$$

$$\text{now } q_n = R \left(\frac{sT}{1 + sT} \right) P_l \text{ from equation (A.3.9)}$$

(For the development of this transfer function see Appendix III.) Using the expression for q_v , q_a , q_c and q_l previously derived and putting

$$K_2 = K_v + C_1 \text{ and } K_3 = \frac{V}{2B} \text{ we have}$$

$$K_q x = A s y + K_2 P_l + K_3 s P_l + R \frac{sT}{1 + sT} P_l$$

and substituting the load equation this becomes

$$\begin{aligned} K_q x/A &= s y [A^2 + K_2 C + s^2 K_3 M + s K_2 M + K_3 C \\ &+ \frac{R s T}{1 + s T} \cdot (M s + C)] \\ &= \frac{s y}{1 + s T} \left(\frac{s^2}{\omega_l^2} + \frac{2\zeta_l s}{\omega_l} + 1 \right) (1 + s T) \\ &+ R T s \frac{(M s + C)}{(A^2 + K_2 C)} \end{aligned} \quad (\text{A.2.18})$$

in practice $A^2 \gg K_2 C$ and so when re-arranged we have

$$\begin{aligned} \frac{y}{x} &= s \left[\frac{s^3 T}{\omega_l^2} + s^2 \left(\frac{1}{\omega_l^2} + \frac{2\zeta_l T}{\omega_l} + \frac{R T M}{A^2} \right) \right. \\ &\left. + s \left(T + \frac{2\zeta_l}{\omega_l} + \frac{R T C}{A^2} \right) + 1 \right] \end{aligned} \quad (\text{A.2.19})$$

APPENDIX III

Analysis of a transient flow network

The benefits of a fluid leakage path across the ram to increase load damping have already been enumerated. The addition of a high-pass filter to prevent leakage in the steady state eliminates the penalties of reduced drive stiffness and steady-state velocity. The transfer function of such a device would be

$$\frac{q_n}{P_l} = \frac{R s T}{1 + s T} \quad (\text{A.3.1})$$

A number of physical arrangements give this form of transfer function, but in this paper the arrangement shown schematically in Fig. 13 will be investigated.

For turbulent flow through the orifice

$$q_n \propto (P_1 - P_0)^{1/2} \quad (\text{A.3.2})$$

Linearizing this expression for small perturbations of q_n , P_1 and P_2

$$q_n \propto (P_1 - P_0) \quad (\text{A.3.3})$$

i.e.,

$$q_n = R (P_1 - P_0) \quad (\text{A.3.4})$$

where R is the conductance of the orifice which, since it is defined by equation (A.3.4), has the dimensions in⁵/lbf s. Strictly speaking it may not be constant but the implications of this will be discussed later.

Neglecting compressibility, the flow caused by movement of the piston is

$$q_n = A_p x_p s \quad (\text{A.3.5})$$

The force equation for the piston is given by

$$P_0 A_p = P_2 A_p + M s^2 x_p + B s x_p + K x_p \quad (\text{A.3.6})$$

from (A.3.4) and (A.3.5)

$$A_p s x = R (P_1 - P_0)$$

substituting for P_0 in (A.3.6)

$$(P_1 - P_2) A_p = M s^2 x_p + B s x_p + \frac{A_p^2 s x_p}{R} + K x_p$$

and noting that from (A.3.5)

$$x_p = \frac{q_n}{A_p s}$$

we have

$$(P_1 - P_2) A_p = q_n \left(\frac{Ms}{A_p} + \frac{B}{A_p} + \frac{A_p^2}{A_p K} + \frac{K}{sA} \right)$$

Writing $P_1 - P_2 = P_1$ and re-arranging, the transfer function for the network becomes

$$\frac{q_n}{P_1} = \frac{RA_p^2 s / KR}{(Ms^2 / K + Bs / K + A_p^2 s / KR + 1)} \quad (\text{A.3.8})$$

Equation (A.3.8) expresses the transfer function in its most complete form. However, the mass of the piston M and the piston viscous friction coefficient B will be small, and hence

$$\frac{q_n}{P_1} = R \frac{A_p^2 s / KR}{1 + A_p^2 s / KR}$$

i.e.,
$$\frac{q_n}{P_1} = R \frac{Ts}{1 + Ts} \text{ where } T = \frac{A_p^2}{KR} \quad (\text{A.3.9})$$

REFERENCES

1. SHUMSHERUDDIN, A. A., 'Shaping the Response of an Electrohydraulic Machine Tool Servomechanism,' 7th M.T.D.R. Conference, 1966.
2. BELLETRUTI, J., and MALTAEZ, L. P. Z., Internal UMIST report.
3. HARPUR, N. F., 'Some Design Considerations of Hydraulic Servo of the Jack Type,' *Inst. Mech. Engrs*, Conference on Hydraulic Servomechanisms, 1953.
4. BELL, R., and DE PENNINGTON, A., 'The Design of Active Damping for Electrohydraulic Cylinder Feed Drives,' 9th M.T.D.R. Conference, 1968.
5. BELL, R., and DE PENNINGTON, A., 'Active Compensation of Highly Damped Electrohydraulic Cylinder Drive using Derivative Signals,' *Proc. Inst. Mech. Engrs*, London, 1969-70, Vol. 182, Part 1, No. 4.
6. DE PENNINGTON, A., MARSLAND, D. W., and BELL, R., 'The Improvement of the Accuracy of Electrohydraulic Cylinder Drives for N.C. Machine Tools by the Use of Active Feedback Compensation', Paper to be given at 12th M.T.D.R. Manchester, 1971.
7. DE PENNINGTON, A., 'The Dynamics of Electrohydraulic Cylinder Drives', Ph.D. Thesis, UMIST, 1971.
8. WELCH, T. R., 'The Use of Derivative Feedback in High Performance Hydraulic Servomechanisms,' *Trans. A.S.M.E. Journ. Eng. for Industry*, Feb., 1962.
9. MORSE, A. C., 'Electrohydraulic Servomechanisms,' McGraw-Hill, 1963.
10. ANON., 'Dynamic Pressure Feedback', *Aircraft Engineering*, June, 1960.

THE SPECIFICATION AND PERFORMANCE OF ELECTROHYDRAULIC MOTOR DRIVES FOR NUMERICALLY CONTROLLED MACHINE TOOLS

by

S. K. CESSFORD* and R. BELL+

SUMMARY

The design of hydraulic motor drives is developed from the basis of linear analysis. The modifications introduced by drive package non-linearities are illustrated with experimental data. The design of control systems that employ electrohydraulic drive packages is both discussed and illustrated with an example.

Nomenclature

B	Fluid effective bulk modulus
C_M	Motor viscous torque loss
D	Motor displacement per revolution
G_V	Gain constant of the electrohydraulic servo-valve
J_M	Motor inertia
J_L	Load inertia
k_l	Internal motor leakage
k_p	Valve pressure droop
k_v	Valve unloaded flow gain
p_l	Load pressure
p_s	Supply pressure
V	Half the motor package trapped volume
V_e	Error signal
ζ_{ml}	Damping factor of the loaded drive package
θ_m	Angular displacement of the motor
ω_{ml}	Angular natural frequency of the loaded drive package

INTRODUCTION

There have been a number of significant developments in the range of actuators that are available for the machine tool designer. Some years ago the situation was more simple, if somewhat restricted; d.c. drives or clutch controlled gearboxes were used for many applications and electrohydraulic drives were used for the more demanding specifications. The current status of actuator development is such that the designer can select d.c. motors, electrohydraulic motors or stepping motors for a very wide range of designs.

In many cases there is no single best choice of actuator; it is often necessary to establish the technical and economic merits of a particular device and

the customer reaction to its use. The object of this paper is to quicken the designer's appreciation of the various facets of electrohydraulic drive performance that must be considered when a drive package is selected. Earlier publications have provided similar studies on d.c. motors¹ and stepping motors².

The design of electrohydraulic drives can be greatly aided by the careful use of linearized design; a definitive treatment of this topic has been published by Merritt³. The influence of threshold performance and large-signal behaviour has also to be considered if an effective design is to be produced. A number of research projects have been carried out on low-speed motors, which form the majority of the hydraulic motors that are in use, to establish the magnitude and influence of their non-linearities.

The low-speed behaviour of low-speed hydraulic motors has been extensively studied by Friedrich⁴ and Cessford⁵. The dynamic performance of this range of devices has been studied by Cessford⁵ and Luck⁶. In addition, a number of papers have been written on particular drive packages. The paper by Clarke⁷ is a good example of this type of publication.

In the context of this paper a hydraulic motor is considered to be a low-speed device if its maximum rated speed is below 2000 r.p.m. A limited number of high-speed motors have been employed and some data are available on their performance⁸.

The selection of an adequate drive package must also be matched by the competent design of the control system. The design procedure of one major systems manufacturer has been published^{9,10}; this procedure employs a velocity feedback loop from the motor, with a relatively high loop gain constant. This design concept, which is often termed a 'soft servo' design, is now widely used.

*Herbert-BSA Ltd., Coventry.

+Machine Tool Engineering Division, UMIST.

A discussion of the specification and design of electrohydraulic drives contains a number of inter-related factors. In this paper, the design is discussed first in terms of linearized analysis. The influence of drive non-linearities is then systematically considered. The discussion of motor characteristics carries with it the inference that all these terms could form, to advantage, part of the motor manufacturer's specification. In this context, it is important to note the widely varying quality of documentation provided by manufacturers. In some cases adequate data are made available and further information can be obtained. On the other hand, some devices are supported by such sparse data that they do not merit serious consideration.

THE LINEARIZED ANALYSIS OF ELECTROHYDRAULIC DRIVE PERFORMANCE

The performance of an electrohydraulic drive can be adequately assessed, to a first approximation, by the use of a linear model. It is considered essential to carry out the linear analysis and the assessment of the non-linear characteristics in parallel for the production of a competent drive design.

The linear analysis of this class of drive^{3,6} leads to the development of the following expressions for the performance of a loaded system

$$\begin{aligned} \frac{\text{motor velocity}}{\text{drive signal}} &= \frac{s\theta_m(s)}{V_e} \\ &= \frac{G_v(s) K/\omega_{me}}{s/\omega_{me} \left(\frac{s^2}{\omega_{me}^2} + \frac{2\xi_{me}s}{\omega_{me}} + 1 \right)} \quad (1) \end{aligned}$$

and

$$K = \left(\frac{k_v}{\frac{C_M}{D}(k_1 + k_p) + D} \right) \quad (2)$$

$$\omega_{me}^2 = \left\{ \left[\frac{C_M}{D}(k_1 + k_p) + D \right] \left[\frac{2BD}{J_M + J_L V} \right] \right\} \quad (3)$$

and

$$2\xi_{me} = \left\{ \frac{(J_M + J_L)(k_1 + k_p) + \frac{VC_M}{2BD}}{\left[\frac{C_M}{D}(k_1 + k_p) + D \right]} \right\} \omega_{me} \quad (4)$$

The above expressions enable adequate estimates to be made for the natural frequency and damping factor of the loaded motor. The reference to the loaded motor infers that attention must be drawn to the influence of the total inertia (load + motor), and to the trapped volume of the package, rather than just that of the hydraulic motor.

The motor displacement is the most significant parameter, ideally the expressions for motor speed and motor torque are

$$\text{motor speed} = \frac{k_v G_v}{D} \cdot V_e \quad (5)$$

$$\text{motor torque} = P_l \cdot D \quad (6)$$

It could be concluded directly from these expressions [equations (5) and (6)] that a certain size of hydraulic motor and a particular supply pressure can be chosen to meet a particular specification. However, the influence of the motor displacement, motor trapped volume and motor inertia must now be assessed to establish the significance of these parameters. The natural frequency of the loaded drive is inversely proportional to the terms $[(J_M + J_L) \cdot V]^{\frac{1}{2}}$. This parameter is often taken as a first estimate of the suitability of a particular drive design for numerical control and minimum values for the natural frequency of the loaded drive have been proposed^{7,8}. The influence of the trapped volume of the package is more significant than is the motor inertia. In general, the choice of gearbox design factors and the other principal mechanical design parameters for a low-speed hydraulic motor drive will have established the load inertia to be controlled by the motor. The relative magnitudes of the moment of inertia of a number of competing designs, for a given nominal displacement, will be of secondary significance unless a wide range of magnitudes is observed.

The trapped volume of the package will not be substantially greater than the motor trapped volume in proprietary equipment. It is most important to appreciate the harmful influence of a badly designed manifold. The existence of excessive trapped volume will undermine drive performance; the design of crossover relief valves also requires skilled effort and, on occasion, it is possible to generate undesirable noise levels from a poorly designed relief valve configuration.

The roles of motor leakage (k_e) and viscous torque loss (C_M) have to be considered. The motor leakage term is a difficult parameter to isolate; its influence is particularly significant about valve null. The viscous torque loss term is a less significant term; the balance of terms in equation (4) is such that influence of the extreme values of C_M found in commercially available motors is far less marked than the values of k_1 that are found. In practice, the influence of motor displacement and the total inertia at the motor shaft have a more dominant role in the determination of motor damping than the motor leakage and motor viscous loss terms. One important point that emerges from the consideration of equation (4) is that the level of crossport leakage required across the motor to increase motor damping is less, pro rata, than the level required in any equivalent hydraulic cylinder drive. The deterioration in steady-state characteristics caused by this technique, is less marked than is found in the cylinder drive and, therefore, the technique is of practical merit.

The calculation of the natural frequency of the motor, ω_{lm} , is sometimes made difficult by the absence of data on the drive package trapped volume ($2V$). This might appear to be an insignificant point, but in the case of a 1 in³ motor, the additional trapped volume both in the motor and the manifold

can be of the same order as the motor displacement. The other term that is difficult to define accurately is the bulk modulus of the hydraulic fluid⁸. The value of the bulk modulus for hydraulic system fluids, under controlled standards laboratory conditions, is 0.25×10^6 lbf/in². The hydraulic fluid in a motor is liable to contain a certain level of entrained air due, in some cases, to the existence of recesses that encourage the formation of small air pockets. The motor components are also elastic and not ideal rigid elements. The combined effect of these factors plus other dynamic factors make any calculations based on the use of the laboratory value of bulk modulus too optimistic. Calculations on the dynamic response of currently available devices suggest that it is better to employ a pessimistic value of the effective bulk modulus (= say 0.1×10^6 lbf/in²) if reliable design calculations are to be obtained.

Attention must now be drawn to the problems presented by the use of simplified formulae for the determination of the system natural frequencies. The discussion of dynamic performance has been based on the equations (1)–(4) which describe the performance of an hydraulic motor with an inertia load. The feed drive configuration shown in Fig. 1 is a more complex mechanical system. The lumped model shown in Fig. 1b is an approximate model for the feed drive. The determination of the system dynamic response depends on the control system configuration to be employed on the drive. The transfer functions relating the motor angular displacement or the load rectilinear displacement differ considerably⁵. It is more effective to employ a program for the evaluation of drive natural frequencies than to calculate the two natural frequencies that arise from the consideration of the hydraulic motor loaded with all the drive inertia assumed lumped at the shaft and the natural frequency of the axial mode of vibration of the leadscrew assembly. In some cases these two terms are calculated without any consideration of the interaction between them. The potential errors involved in over-simplified calculations are further emphasized by the influence of the velocity feedback loop around the motor. This technique,

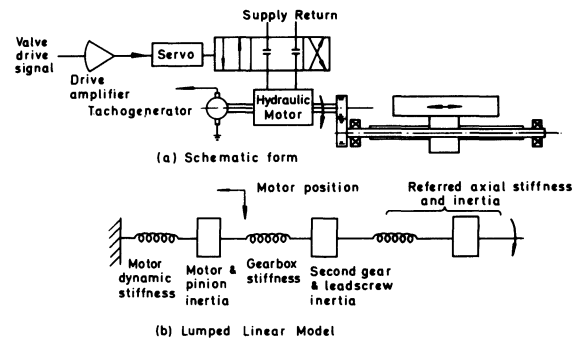


Fig.1. Machine tool feed drive with an electrohydraulic drive package.

subject to detailed design, exerts a considerable influence on the dynamic response of the motor. These points are equally applicable to the design of electric drives.

The design variables that can be employed to achieve a desired natural frequency are motor displacement and servovalve rating and supply pressure (it is assumed the transmission design has been optimized). The need to increase motor displacement in order to increase the loaded natural frequency ω_{ml} of the motor causes a considerable increase in power supply rating if the other linked areas of the drive specification are to be unimpaired. The data presented in Table 1 for a number of commercially available motors show that the range of motor displacement values available is in distinct steps. Any initiative to call for an increase in motor displacement on the basis of control-system requirements should be accompanied by adequate evidence in support of the control-system design criteria that make the change necessary.

Two possible figures of merit for a drive package emerge from the above discussion; that is, the ratio of trapped volume/displacement and the ratio of motor inertia/displacement. In general, the former is considered to be the more valuable guide to the potential dynamic capability of the actuator.

Table 1. Principal parameters of some low-speed hydraulic motors

Type	Manufacturer	Displacement (in ³)	Torque per 1000 lbf in ² (lbf in)	Maximum speed (r.p.m.)	Maximum pressure (lbf in ²)	Inertia displacement (lb in s ² in ³)	Trapped volume displacement
TRV10	Servotel	1	160	2000	2000	0.77	1.5
TRV22	Servotel	2.2	350	1500	2000	1.0	1.2
TRV50	Servotel	5	800	1500	2000	1.2	1.2
TRV76	Servotel	7.6	1200	1200	2000	1.3	1.3
25	Dowty	2.5	400	1500	2000	4.0	1.1
50	Dowty	5.0	800	1500	2000	3.1	1.1
70	Dowty	7.0	1100	1500	2000	2.4	1.1
Numadyne *	Ratier Forest	2.4	480	2000	2000	0.4	0.7
Numadyne *	Ratier Forest	4.8	760	2000	2000	0.25	0.4

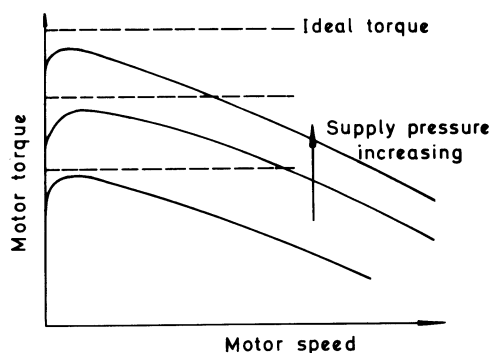
* Multi-lobe designs.

HYDRAULIC MOTOR CHARACTERISTICS AND THEIR INFLUENCE ON SYSTEM PERFORMANCE

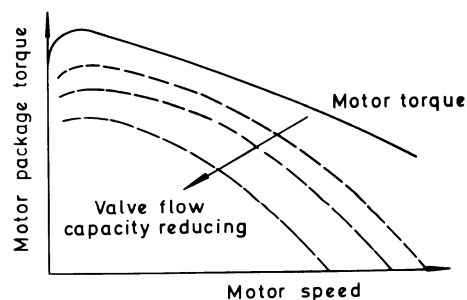
It is now necessary to follow the points developed in the consideration of the linear model with a discussion of those practical characteristics which further influence drive performance. These characteristics include the servovalve flow characteristic, the motor threshold velocity characteristics, the low-speed load pressure/velocity characteristics, the zero flow pressure gain or locked rotor characteristics and the dynamic characteristics of hydraulic motors.

Motor torque speed characteristics

The motor torque/speed characteristic is influenced by the choice of motor, the choice of servovalve and the supply pressure which is employed in a particular design. These points are illustrated in Fig. 2. Here the



(i) The influence of supply pressure on motor torque



(ii) The Influence of Valve Capacity on the torque speed characteristic of a motor package

Fig.2. Hydraulic motor torque speed characteristics.

influence of supply pressure is shown to have a proportional influence on the ideal stall torque that is developed. The influence of the motor characteristics is such that the torque available at the motor never equals the ideal stall value. In general, detailed information is not available on this type of characteristic. The full implications of the low-speed torque loss will be discussed later. The high-speed torque loss is due to a combination of motor viscous loss and the pressure drop of the servovalve flow characteristic. This point is emphasized in Fig. 2(ii). Here the influence of the choice of available flow rating is shown to

have an important effect both on the maximum speed which is attainable and on the shape of the drive package torque speed characteristic. The choice of servo valve rating and supply pressure are, therefore, seen to be critically important parameters, second only to the choice of motor displacement which, as has been shown above, is a major influence on the dynamic response of the drive.

The low-speed of threshold torque loss can best be considered by the assessment of the load pressure/velocity characteristics of hydraulic motors about valve null. Two representative traces are shown in Fig. 3. The difference in break-away pressure required between these two motors is seen to be most marked. The motor which displays the minimum breakaway pressure and has the higher viscous loss coefficient is the better choice for a control-system application. It must be remembered that very often an NC drive specification contains a direct reference to the ratio of breakaway to running torque. When this aspect of drive performance is considered, the unloaded motor load pressure/speed characteristics and the equivalent load pressure/speed characteristics of the transmission due to preload, and slideway friction, can be summed. The choice of any motor with a large ratio of breakaway to running torque is, therefore, inappropriate. The characteristics of rotating and rolvane motors are considerably better in this respect than the characteristics displayed by piston motors. In some cases, the characteristic of a piston-type motor can be improved by the presence of additional leakage but only to the detriment of other important characteristics. In those cases where the breakaway torque is considerably larger than the running torque a speed can be specified below which speeds cannot be maintained, that is, the motor has a dead band which is further aggravated by the presence of load torque from the transmission.

Either of the characteristics of the type shown in Fig. 3 can be caused to deteriorate by poor alignment. This is a problem which is common to all high-performance servo motors; in general, all high-performance motors rely on the maintenance of tight operational clearances, and the presence of axial or radial loads beyond the manufacturer's specifications will result in a marked reduction in performance.

Motor velocity characteristics

The unloaded motor velocity/drive signal characteristics are substantially linear as shown for a typical case in Fig. 4. The influence of servovalve hysteresis is evident, but the performance of a typical motor with a velocity compensation loop around it is such that the compensated motor velocity/drive signal characteristic can, subject to tachogenerator characteristics, be considered to be adequately linear.

The other aspect of the motor velocity characteristics that is to be considered carefully is the pulsation characteristic which is of considerable importance at low speeds. These pulsations, a typical example of which is shown in Fig. 5, are found to remain unchanged over a wide range of motor speeds. They are only important, however, at minimum feed speeds. Their amplitude can be reduced by the presence of a high-gain velocity loop around the motor. In Fig. 5, the influence of loop gain is demonstrated. In general, however, the nature of the compensation

used in this loop is also significant in this respect as it tends to minimize the frequency spectrum over which the compensation is effective. The influence of the velocity feedback loop is seen to have two functions: first it linearises the steady-state motor speed/drive signal characteristic, and secondly it improves the performance of the motor at low speeds. There is an intermediate range of speeds where these pulsations may have a critical effect on drive performance because, as speed increases, the pulsation frequency increases and, therefore, above the certain intermediate speed band the effect of the feedback loop is nullified.

Load pressure characteristic at zero velocity

The 'stiffness' of a hydraulic drive can be deduced in a comparative sense by studying the load pressure/drive signal characteristics of a drive package with the rotor of the motor locked mechanically. Ideally this characteristic should be a straight-line rectangular form where a line-on-line valve with an ideal motor would display an infinitely steep load pressure gain characteristic at null.

The influence of valve tolerances and motor leakage is such that these characteristics depart from the ideal form and display either a reduced slope with narrow hysteresis (i.e., leakage dominant) or a hysteresis form with steep slope (i.e., valve hysteresis dominant). Examples of these characteristics are shown in Fig. 6. This characteristic, whilst not one which is directly applicable to system calculations, serves as a valuable guide to the assessment of drive performance.

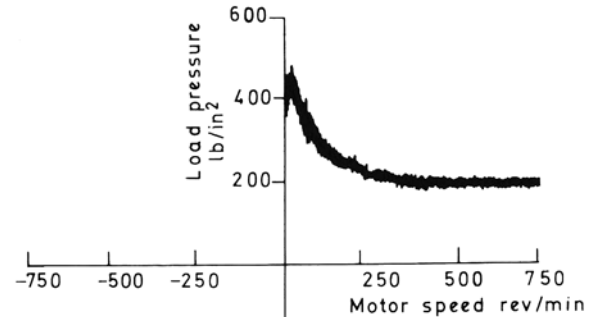
Dynamic characteristics of hydraulic motors

The results presented in this section are again restricted to the characteristics of low-speed motors. Further similar information on the performance of a high-speed package is given by Bell and Cowan⁸. The frequency response and dynamic response characteristics have to be considered.

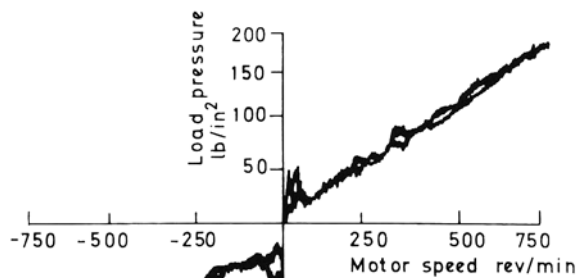
The frequency response of hydraulic drive packages is of prime importance as these characteristics are taken as a direct aid to system design. A number of factors have to be considered, the influence of two of which are shown in Fig. 7 and 8. The influence of load inertia on the performance of a drive package is shown in Fig. 7. Here the motor is tested with inertia loads of 0, X 1, X 2, X 5 and X 10 the motor inertia. The change in the characteristics follows an expected pattern, the natural frequency of the drive is progressively reduced and the system damping is increased. The results do not follow closely the trends expected of a linear system, but the relevance of the predictions made earlier from the linear analysis is established.

The other aspect of motor performance, represented in Fig. 8, is the influence of drive signal amplitude on the frequency response of a package. The influence of increased command signal amplitude induced a reduction in system gain and points to the problems posed when large-signal dynamic response or dynamic response about a large valve opening is to be considered. The general point that is to be made here is that the system dynamic response for either of

these cases is considerably diminished and, therefore, the normally linearized analysis should be used with caution.



(b) For an axial ball motor
(1 in³ displacement)



(a) For a rotvane motor
(2.2 in³ displacement)

Fig.3. Load pressure-speed characteristics of low-speed motors.

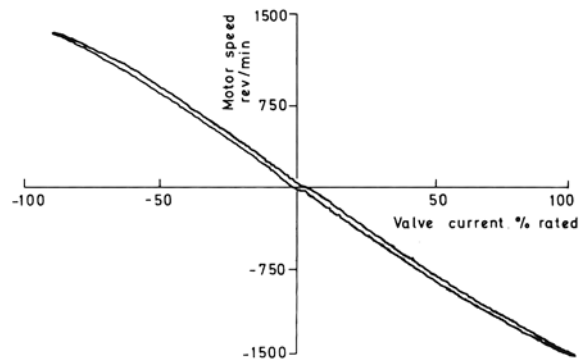


Fig.4. Unloaded motor velocity/servo valve drive signal characteristics for a rotating vane motor.

The transient response of a loaded hydraulic drive is dictated primarily by the influence of load pressure transients induced by the level of command signal changes and the degree of inertia loading at the motor. The transient response information presented in Figs 9 and 10 shows, respectively, the influence of command signal amplitude when reversing the motion from a given speed to a similar speed in the opposite sense, and the influence of the level of operating speed and the deceleration characteristics of a motor when it is commanded to return to zero speed. Considerable variation in dynamic response is observed and specialist advice would be considered essential if the ultimate in dynamic response is required from a particular package as, in the limit, system response is somewhat difficult to define from normal design data. Further data are available in the literature on dynamic response of drive packages and particular attention is drawn to theses by Cessford⁵ and Luck⁶.

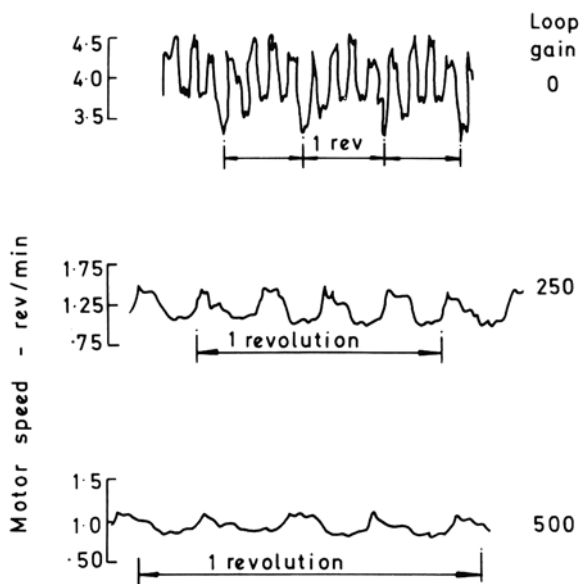


Fig.5. Influence of the velocity loop gain on the low-speed velocity pulsations of a loaded hydraulic motor.

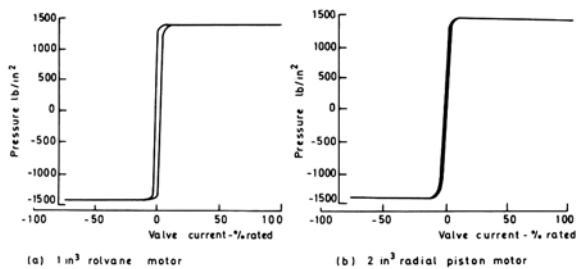


Fig.6. Locked rotor characteristics for hydraulic motors.

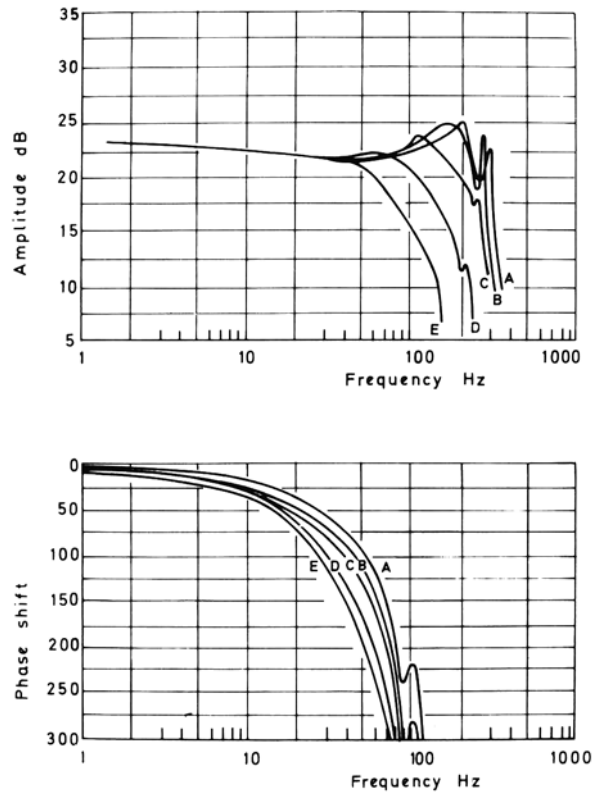


Fig.7. Influence of load inertia on the frequency response of a 2.2 in³ Rolvane motor package.

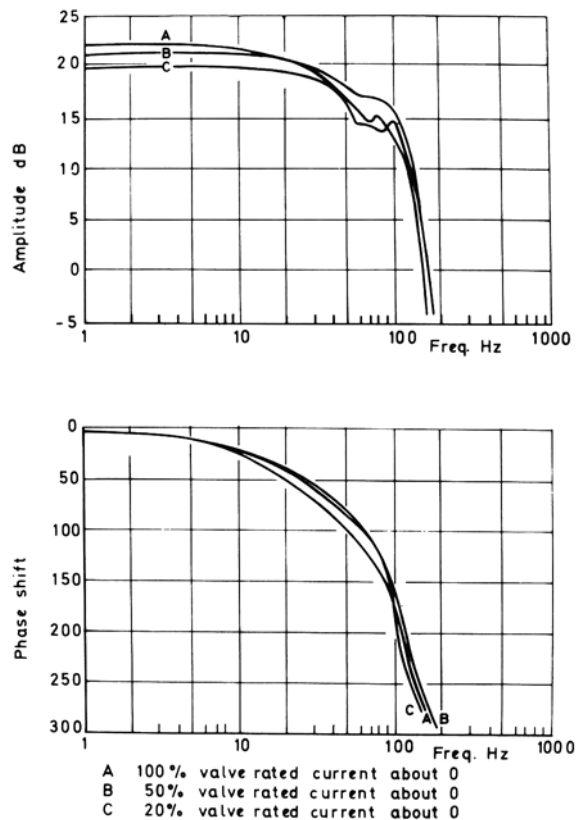


Fig.8. Input signal amplitude on the frequency response of an unloaded 2 in³ rotating van motor package.

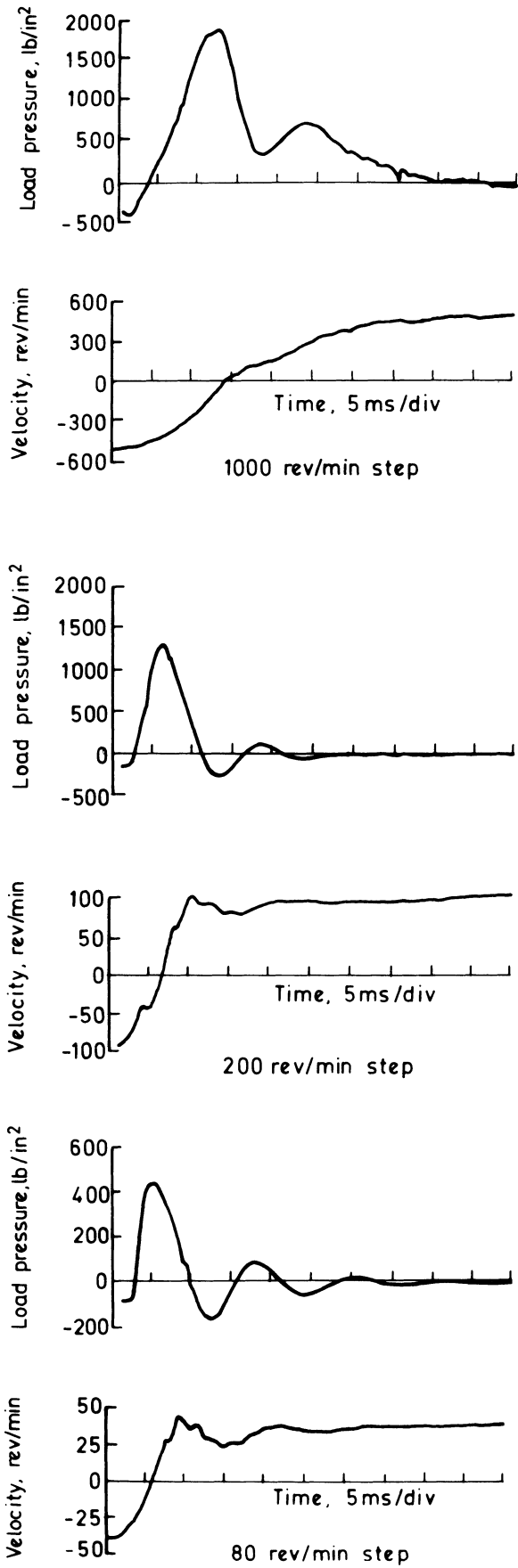


Fig.9. Influence of command signal on the transient response of a 2.2 in³ Rolvane motor with a load inertia equal to the motor inertia.

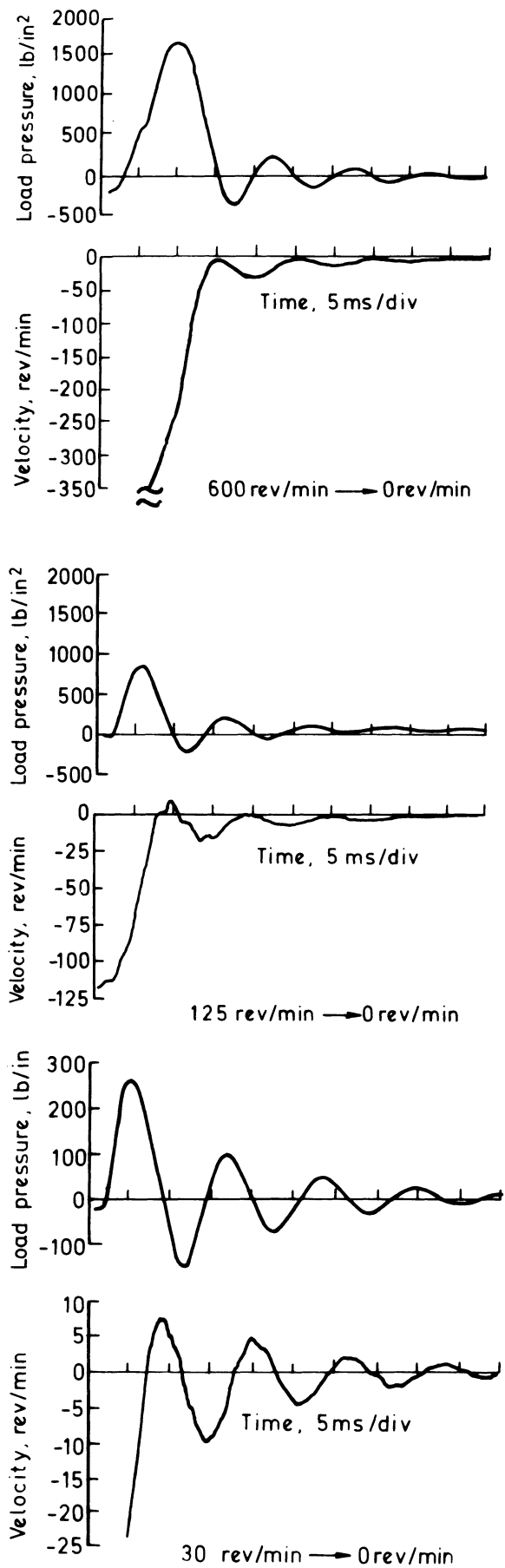


Fig.10. Load pressure and velocity responses for the deceleration of a 2.2 in³ Rolvane motor with load inertia equal to motor inertia.

THE INFLUENCE OF CONTROL SYSTEM DESIGN ON PACKAGE PERFORMANCE

The interaction between the aims of the control-system manufacturer and the problems of the machine tool designer have been referred to earlier in the discussion of the linearized analysis. The problem of choosing the required motor displacement, commensurate with the attainment of certain minimum natural frequencies, imposes constraints on the selection of motors. This procedure will depend on the particular control-system manufacturer and on his control-system design criteria. The most widely referred to design procedures are those advocated by Bakel⁹ and Dutcher¹⁰. This design procedure they advocate consists primarily of meeting a particular minimum natural frequency required ($\omega_{m1}/2\pi = 50$ Hz for a continuous path application) and for the use of a high-gain velocity feedback compensation loop. The form of this compensation loop is shown in Fig. 11.

The compensation transfer function shown in this diagram is necessary as the feedback loop would be unstable at the values of gain required without the presence of this class of network. Centre values of 350 V/V are specified and the result of this compensation technique is the production of a very linear, wide speed range drive package. Both of these end-products are extremely valuable; the price paid for these characteristics is illustrated in Fig. 12 where the frequency response of a drive package, subjected to this design procedure, is shown. The system response displays a reduction in bandwidth. This point, however, is readily offset by the system software design, as a predictable velocity lag will be encountered. A further advantage in this procedure is that it does not allow the system to display high acceleration capability; that is, acceleration levels beyond the requirements of metal cutting performance, so that the possibility of major damage to the transmission, during a fault condition due to excessive acceleration loading, is removed. This class of control-system compensation calls for a relatively low position loop gain, and very high system resolution is obtained at zero speed due to the fact that the position loop gain, at zero velocity, is the product of the position loop gain and the forward sequence gain of the velocity loop. This performance is achieved by setting a relatively high value of minimum drive natural frequency, which in some cases is very readily achieved, but in others may provide the machine tool designer with some design problems.

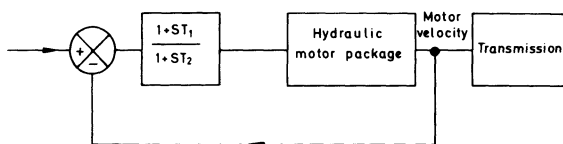


Fig. 11. Schematic form of the velocity loop.

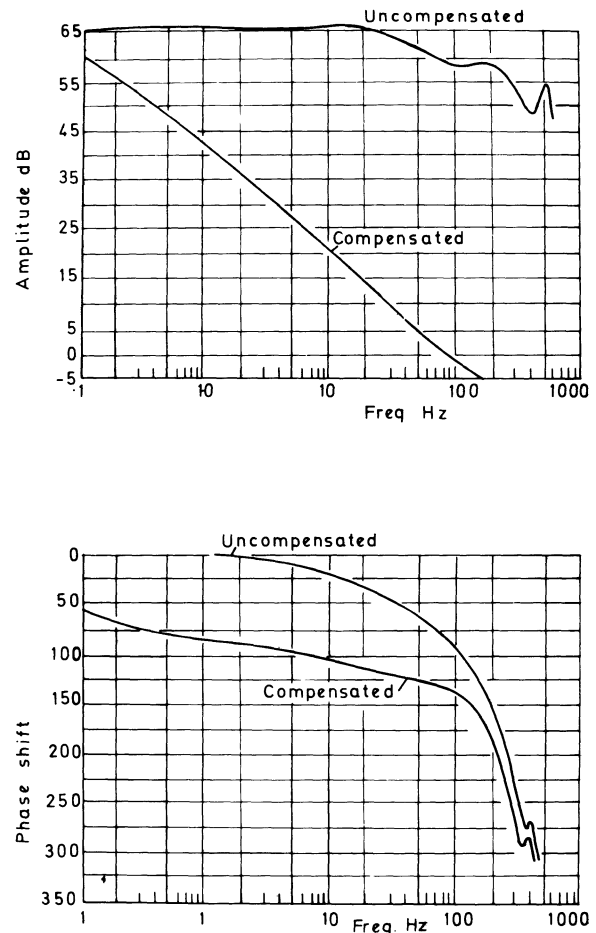


Fig. 12 The Frequency Responses of an Uncompensated and Compensated Hydraulic Drive.

CONCLUSIONS

The high performance capability of electro-hydraulic drives has been demonstrated and thus particular characteristics which merit attention, when the specification of a motor is being formulated, have been discussed. It is considered desirable that many more motor manufacturers should attempt to include reference to these characteristics in their data or in their back-up service. In general, good electro-hydraulic drive packages can be expected to produce an operating speed range, with appropriate control system design, of up to 20 000:1.

The dynamic response that is developed by a well-designed package is better than that which can be achieved by the equivalent electric drive. In the limit, the electric drive can, with careful attention to drive amplifier design, be made to approach the limit of performance of a hydraulic motor. However, on this point it should be noted that this limit is very often beyond many of the requirements of the machine tool designer.

The main advantage of the hydraulic drive package lies in its duty cycle capabilities. The thermal ratings imposed on a given d.c. motor package have no equivalent in the hydraulic package. It would seem, therefore, that when the relative merits of

electric and hydraulic drives are considered they would break down to a consideration of the good dynamic response and good duty cycle performance of the hydraulic drive offset against the often subjective reaction of a user to system contamination with, in the case of electric drives, a simpler, quieter, mechanical arrangement of adequate dynamic performance of sometimes suspect thermal ratings. Very often the choice of one drive or the other will be decided by subjective reaction rather than on technical performance.

Acknowledgments

The authors wish to thank Professor F. Koenigsberger for his help in the establishment of the programme of research. The financial help and technical involvement of Alfred Herbert Ltd. played a substantial role in the work. The financial support of the Science Research Council is gratefully acknowledged.

REFERENCES

1. KHONG, H. P., and BELL, R., 'D.C. Motor Feed Drives for Numerically Controlled Machine Tools,' Paper presented at the 11th M.T.D.R. Conf., Birmingham, 1970.
2. BELL, R., LOWTH, A. C., and SHELLEY, R. B., 'The Application of Stepping Motors to Machine Tools,' Machinery Publishing Co. Ltd., 1970.
3. MERRITT, H. E., 'Hydraulic Control Systems,' John Wiley & Sons Inc., 1966.
4. FRIEDRICH, G., 'Eigenschaften elektrohydraulischer Vorschubantriebe in Bereich Kleiner Drehzahlen', Dr. Ing. Diss. T. H. Aachen, July, 1965.
5. CESSFORD, S. K., 'An Investigation into the Design of Electrohydraulic Feed Drives', Ph.D. Thesis, UMIST, 1969.
6. LUCK, J., 'Einflussgrößen auf das Zeitverhalten elektrohydraulischer Vorschubantriebe', Dr. Ing. Diss. T. H. Aachen, 1968.
7. CLARKE, D. C., 'Selection & Performance Criteria for Electrohydraulic Servo Drives', Moog Technical Bulletin, No. 122, 1969.
8. BELL, R., and COWAN, P., 'The Performance of a "High Speed" Servomotor'.
9. BAKEL, J. F., 'Hydraulic Servo Drives for Mark Century Controls', General Electric publication SCW-1395A.
10. DUTCHER, J. L., 'Servos and Machine Design for Numerical Control', General Electric publication GET-3210.

GRINDING AND ELECTRO CHEMICAL MACHINING

OBJECTIVE METHOD FOR DETERMINING GRINDING WHEEL LIFE

by

F. SZEKERES*

SUMMARY

A new objective measuring method has been worked out in GTI which is suitable for measuring grinding wheel life. The method is based on the measurement of vibration. The frequency of vibrations that occur in grinding and that are characteristic of the grinding process was determined. Vibration amplitude-time functions contain two inflection points, the second of which indicates the end of wheel life. The correctness of the method is proved through comparison with conventional grinding parameters.

INTRODUCTION

During grinding process studies accomplished in GTI Grinding Technology Research Laboratory, experiments were made in order to work out a new and distinct measuring method for wheel life. The lifetime of a grinding wheel means that time which elapses under grinding between two dressings. For measuring the lifetime wheels which were self-sharpening only to a small extent were chosen. In practice, by measuring conventionally the quantities described below, we can conclude that towards the end of wheel life the following occur.

(1) The cutting ability of a grinding wheel deteriorates with grinding time, therefore consumed power varies while chip removal decreases or remains the same.

(2) The surface roughness and waviness of the workpiece deteriorate to such an extent that the workpiece does not meet the requirements.

(3) After grinding, visible burn marks appear on the workpiece.

(4) Using a microscope the size of plane surface which can be worn on wheel grains in grinding may be determined.

We have only considered the most frequently used quantities which determine wheel life. It is obvious from the above points that the aforementioned parameters that are characteristic of grinding can be measured only with high scatter, and wheel life determinations from them must be expressed statistically. For this reason only we searched for an unconventional exact method of measuring wheel life that had good reproducibility; this paper is aimed at presenting this method.

THE NOISE PHENOMENON ACCOMPANYING END OF WHEEL LIFE AND ITS MEASUREMENTS

An experienced skilled man recognizes on the basis of the noise if a grinding wheel is worn or not. At the end of grinding wheel life, noise pressure level and frequency content of radiated air noise changes. In grinding experiments with cross feed we tried to define the wheel lifetime by this noise phenomenon. Measurements were made with the help of a tape-recorder, as is shown in Fig. 1. Noise records were then subjected to a frequency analysis in the laboratory. After a long examination it was stated that, as the measuring area (machine shop) was acoustically undefined, i.e. for the purpose of microphone measurement, it is impossible to define the grinding wheel life. Our measurements were affected adversely by noise from other parts of the machine.

According to our investigations noise components of the grinding wheel had a great effect on the resultant noise spectrum, so its reliable evaluation in practice incurs very great difficulty.

When measuring with a microphone proved to be unsatisfactory, we changed to measuring the impact noise, i.e. vibration parameters.

As a measuring position the tailstock centre was chosen and the block diagram of the measurement is shown in Fig. 2. Vibrations were measured in two directions as follows:

(1) radial direction—the direction of the grinding compressive force (hereafter referred to as the horizontal direction), and

(2) tangential direction—the direction of the principal grinding force.

*Gepipari Technologiai Intezet, Budapest

The choice of direction of vibration measurement was considered preferable, as displacements in the radial direction were generated by the time change of compressive grinding force, while displacements in the tangential direction were generated by the time change of the principal grinding force.

By this arrangement it is expected that vibration amplitude variation against time will be characteristic of grinding tool wear.

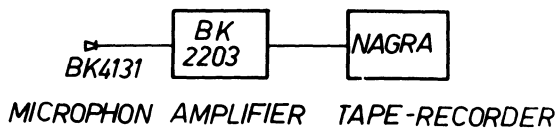
The following technological data were used in the experiments.

Depth of cut:	0.02 mm/stroke
Cross feed rate:	1 m/min
Workpiece:	31.5 rev/min
Workpiece material:	GO-3 rolling bearing steel hardened to 50 HRC approx
Workpiece diameter:	60-70 mm
Workpiece length:	450 mm
In our measurements:	60 dB = 1000 cm/s ² vibration acceleration

The vibration amplitude-time function is compared with the time change of surface roughness and machined metal volume. On the basis of this the following points are established.

- (1) The vibration amplitude, which is measurable in grinding, increases with time.
- (2) The frequency characteristic of the process falls in tertiary band of 500 Hz.
- (3) From our experiences, the life defined by the subjective method (by ear) shows good agreement with that determined from vibration amplitude-time functions.

SOUND RECORDING



SOUND ANALYZIS

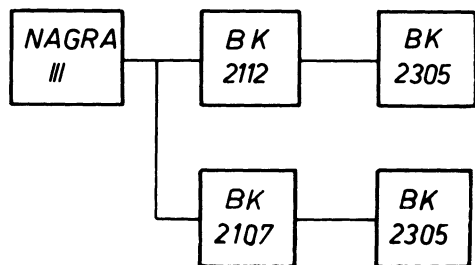


Fig. 1 Block diagram of the sound level measurements.

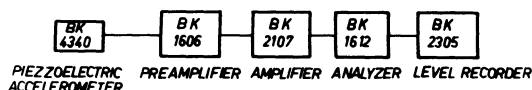


Fig. 2 Block diagram of the vibration measurements.

FREQUENCY CHARACTERISTIC OF GRINDING

Process: The cross-feed grinding method as a process is quite complicated, and because, additionally, of the scatter experienced in measurement, the in-feed grinding method was chosen for further experiments.

Determination of self-oscillation number of the work-piece-machine-tool system

For our experiments, the examinations performed by B. Bartalucci and his co-workers served as a start. Because an electrodynamic vibration table was not available, oscillations on the grinding machine were generated by striking, as is schematically shown in Fig. 3. Oscillations generated by striking were detected by an accelerometer and displayed on a cathode-ray oscilloscope screen. The vibration pattern displayed on the screen was photographed with an oscillo-record camera. Self-oscillation numbers were examined in terms of radial force, as in in-feed external cylindrical grinding different radial grinding forces belong to different in-feed rates. Considering the problem it is obvious that, in the case of greater radial force, prestress in the system establishes an effect in the oscillating system making it seem more rigid.

For a more rigid system, however, it is expected that self-oscillation numbers increase. Self-oscillation numbers measurements accomplished are drawn in Fig. 4. From this figure it is quite clearly seen that self-oscillation measurement made with striking is not a precise method; that is why minimum and maximum frequencies were revealed. From this figure it can definitely be stated that with the known machine (with a stationary machine) a self-oscillation numbers versus radial force vary from between 500 to 1300 Hz.

In Fig. 5 the measured results of B. Bartalucci and his co-workers are compared with the measured self-oscillation numbers made in our Institute. It is seen quite well that the measurements made by B. Bartalucci are in reasonable agreement with our results. The difference between the self-oscillation numbers measured on stationary machines can be explained by the different rigidity conditions of the grinding machines used by different workers.

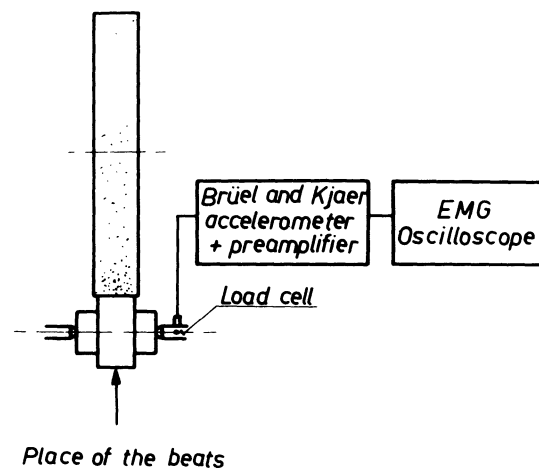


Fig. 3 Block diagram of the self-oscillation measurement.

As is shown by these studies, it is extremely interesting that the grinding machine as a dynamic system should be stable only with a radial force of defined magnitude.

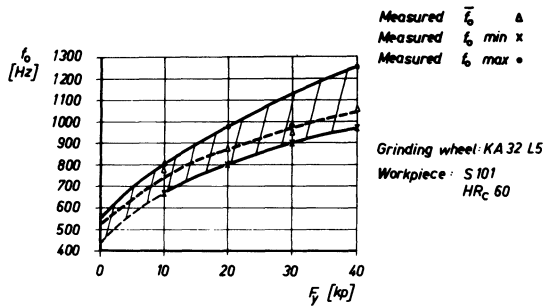


Fig. 4 Self-oscillation of the grinding machine as a function of the radial force.

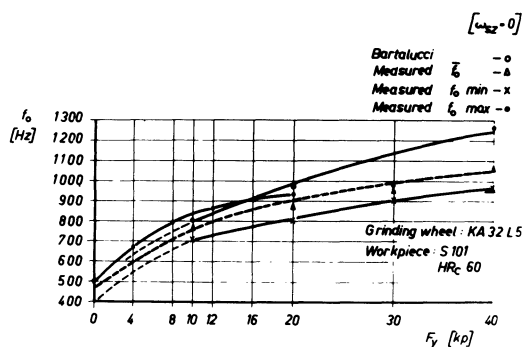


Fig. 5 The comparison of the self-oscillation measurements on two grinding machines.

VIBRATION AMPLITUDE–TIME FUNCTIONS CHARACTERISTIC OF THE GRINDING PROCESS

It is well known that, in grinding, the workpiece and the grinding wheel tend to wear in the form of a polygon. As a consequence, the grinding wheel oscillates the workpiece by striking it. In agreement with our measurements, the maximum amplitude of generated vibrations is in the range of 500–1300 Hz.

By reason of previous discussion it can be ascertained that the frequency characteristic of the grinding process in external cylindrical in-feed grinding is only the self-oscillation number that is characteristic of the instantaneous dynamics of the system and which is generated by the grinding wheel wearing to a polygon.

Discussion of vibration amplitude–time function

In Fig. 6 vibration amplitude–time functions for three different in-feed rates are presented. After examining these functions they can be divided into three sections.

First section: linkage formation lasts until the first inflection point.

Second section: time interval suitable for grinding lasts until the second inflection point.

Third section: grinding wheel is not suitable for grinding; the section starts after the second inflection point.

In our experiments it was ascertained that the previously discussed noise phenomenon accompanying grinding wheel wear begins at the second inflection point.

Accordingly wheel lifetime is defined by examining the second inflection of the vibration amplitude–time function. Wheel lifetime is considered to be the time that had elapsed from start of grinding to the second inflection point.

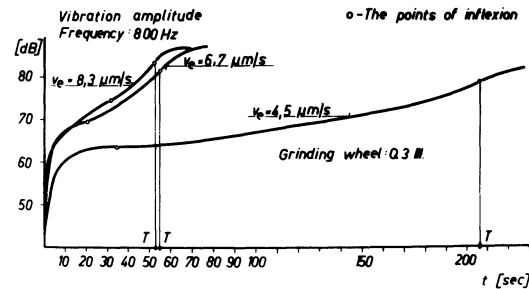


Fig. 6 The vibration amplitude–time functions.

Reproducibility of the functions characteristic of the grinding process

By further experiments we wanted to prove that time functions that were characteristic of the measured grinding wheel life, and of the process, had not been obtained accidentally but that they were reproducible with the same technological data. In a 24-times iteration the following technological data was used.

- Grinding wheel speed: 32 m/s
- Work speed: 90 rev/min
- In-feed rate: 10 microm/s
- Grinding wheel: experimental perite band grain: 50 kA
- Work material: AISI E52100 steel hardened to 52 HRc

With mathematical–statistical methods data was processed by means of an electronic computer. The individual measured magnitudes of vibration amplitudes were arranged in time sequence and they were examined by two trails to show how the values in every square second match at a probability level. According to evaluation data of the 24-times iteration match on a 95% probability level.

For reproducibility, measurements were made also on a machine with statically double rigidity. In our examinations from those measurements made on the second machine quite similar vibration amplitude–time functions were obtained with the exception that, with the statically more rigid machine, characteristic frequency was about 1250 Hz. Measured results tended to be in agreement with practice.

In the present state of development of the measuring method it has to be applied to a particular machine; through having an adequate amount of data, by means of further experiments, it becomes possible to generalize the method concerned.

Mathematical form of vibration amplitude–time function

With the help of an electronic computer it has been defined that vibration amplitude–time function was approximated best by a polynomial of the fourth

degree. Mathematical analysis showed that the coefficient of the members of the zero, first and second degree is of considerable magnitude compared with other coefficients. If, however, coefficients of members of the third and fourth degree are neglected, the curve does not contain the required inflection points. Physical meanings of the coefficients could not be defined within a short time.

This work is being continued.

By means of the empirical process function the differential equation describing the phenomenon can easily be written down. The differential equation will be a complete differential equation of the fourth degree. For the present only, it is ascertained that in external cylindrical in-feed grinding according to our experiments higher accelerations occur, the study of which is the subject of further research continuing at the present.

CORRECTNESS OF THE NEW OBJECTIVE WHEEL LIFE MEASURING METHOD

In order to prove the ability of our developed measuring method to define the end of wheel life the following conventional technological parameters are simultaneously examined:

- v_e ($\mu\text{m/s}$) in-feed rate
- T (sec) wheel lifetime
- V_t (mm^3) machined metal volume in the lifetime
- R_a (μm) surface roughness
- P_y (kP) normal radial grinding force
- Z' ($\text{mm}^3/\text{mm s}$) normal grinding performance

In Fig. 7 the results of experiments made with a type A60 $\frac{3}{4}$ K5-V10W grinding wheel of the British Carborundum Company are presented. From this figure the following statements can be made.

- (1) Wheel lifetime decreases with in-feed rate increase.
- (2) Machined metal volume increases with in-feed rate increase.
- (3) Radial force uniformly increases with in-feed rate increase.
- (4) Surface roughness deteriorates with in-feed rate increase.
- (5) Z' increases with in-feed rate increase.

From the above it is evident that wheel lifetime, in respect to the particular technological parameters, behaves as we expected.

The correctness of our measurements is also proved by the performed dressing experiment. Experiments were made with the single-crystal diamond dresser for the planning of dressing technology. Surface roughness and wheel lifetime were chosen as output parameters. As is expected from theory, experiments showed that by means of dressing, either optimal surface roughness or optimal wheel lifetime can be obtained. The two optima in Fig. 8 do not coincide, i.e. with the same cross feed rate, in order to obtain optima, different depths of cuts have to be applied in dressing.

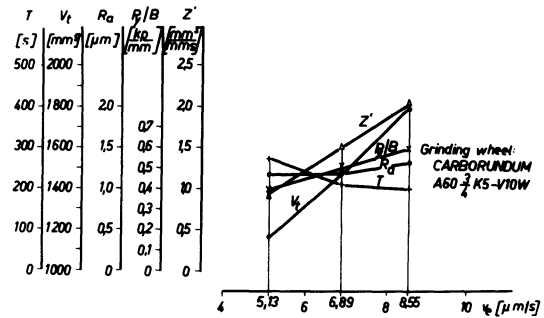


Fig. 7 Comparison diagram of the grinding parameters

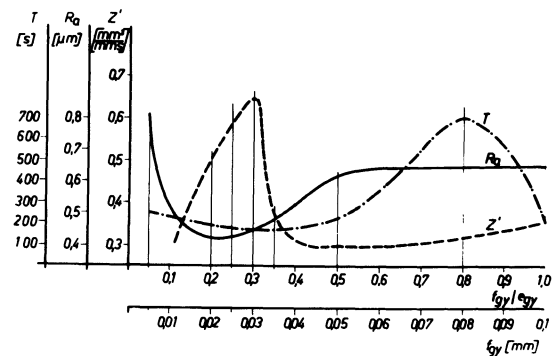


Fig. 8 Comparison of several grinding parameters as functions of the dressing technology of the grinding wheel.

CONCLUSIONS

In our opinion the wheel lifetime measuring method developed in our Institute may be of twofold importance.

In practice, we want to design a device for a high-duty grinding machine which will dress the grinding wheel after wheel lifetime has elapsed. In technological planning for choice of a grinding wheel under laboratory conditions, objective assessment of wheel lifetime is considered important.

In theory, as in this case, the vibration amplitude-time function defined by measurement is a characteristic function of in-feed grinding process; it can be of great help in more accurate knowledge of the grinding process.

ACKNOWLEDGMENTS

Acknowledgments are due to the staff of GTI Grinding Technology Research Laboratory whose enthusiastic work was of great help to this study. Computer programme and method suitable for programming was worked out by Mrs E. Kovács

REFERENCES

1. HORNING, A., *MTDR Conf.*, Manchester (1969).
2. SCHWARTZ, K. E., *Diamond Rev.*, **19**, 214 (1959).
3. BRUCKNER, K., *Industrie-Anzeiger*, No. 26, May (1969).

4. TSUWA, J. *Eng. Ind.*, (*Trans. ASME, Ser. B*), November (1964).
5. G-PAHLITZSCH and KUNTZE, E. O., *CIRP Berichte*, 2, 126–135, December (1961).
6. TOBIAS, S. A., *Schwingungen an Werkzeugmaschinen* Carl Hanser, Verlag (1961).
7. YOSHIKA, H., *CIRP*, 347–54, May (1967).
8. BARTALUCCI, B., LISINI, G. G., and VERARDI, M., *CIRP Ann.*, 16, 387–97 (1968).
9. SNOEYS, R., and BROWN, D., *ASTME*, Paper MR68–102.
10. CUNTZE, O., and PAHLITZSCH, G., *Gen. Assembly CIRP*, Liege, August (1965).
11. SZEKERES, F., *Gep*, 12, No. 7, July (1970).

ON THE ROUNDING-UP PROCESS IN HIGH-PRODUCTION INTERNAL GRINDING MACHINES BY DIGITAL COMPUTER SIMULATION

by

R. S. HAHN and R. P. LINDSAY*

SUMMARY

High-production internal grinding machines are required to grind workpieces, which have an initial runout and stock allowance, in very fast grinding cycles. The runout must be corrected before the stock allowance is used up. As the internal grinding wheel strikes the running-out workpiece, high local instantaneous force intensities on the wheel may develop and may cause the wheel to break down, resulting in a loss of straightness of the finished ground workpiece. By representing the grinding process mathematically, as well as the dynamic characteristics of the grinding machine, a computer program has been developed which traces the rounding-up process, revolution by revolution, and permits the selection of the optimum machine settings so as to grind with the shortest possible cycle without damage of the wheel and without incomplete rounding up of the workpiece.

INTRODUCTION

In order to produce the volume of manufactured items required to clothe, feed and satisfy the needs of the expanding populations of the world it is necessary to produce such items as ball and roller bearings, automotive universal joint cups, automotive hydraulic valve lifters as well as other parts in high production quantities. In producing these items in the quantities required the repetitive grinding cycle time becomes very important. For example, the shortening of an 11 s internal grinding cycle, precision grinding the bores of automotive hydraulic valve lifters, by one second can result in a cost saving of over \$1 000 000 per year for one producer of these parts. Consequently great efforts are made to shorten cycle times. However, as one increases the speed of grinding cycles, various things happen to cause a loss in quality. Wheel breakdown may cause a loss in shape or profile, workpiece size and taper fluctuations due to variable stock and variable deflections may occur, thermal damage may occur and a loss of concentricity of I.D. to O.D. may occur. In view of the above the problem is to adjust the various grinding machine parameters in such a way as to produce the shortest cycle time consistent with the desired level of quality.

Most workpieces come to the final grinding operation with varying stock allowance and varying degrees of runout, i.e. the stock allowance on a bore may not be concentric with a previously finish ground O.D. The grinding machine must then round up and

develop concentricity as well as grind the part to size. This rounding-up process involves the dynamic characteristics of the grinding machine as well as the characteristics of the grinding process.

THE ROUNDING-UP PROCESS

In a typical grinding cycle the grinding wheel approaches the 'black' workpiece at some velocity. The first contact with the workpiece is usually made at the high spot on the work. During the first few revolutions of the workpiece the wheel-work contact is intermittent as shown in Fig. 1 for the internal grinding of an inner ball bearing ring. As the high spot engages the grinding wheel, the wheel spindle deflects both laterally and angularly. This tends to concentrate the grinding force on the inner edge of the grinding wheel. Under certain conditions excessively high local force intensities (normal force per unit width of contact) can occur on the wheel. If the local force intensity exceeds the 'breakdown force intensity' extremely rapid wheel wear rates occur and the profile of the wheel will be destroyed. The 'breakdown force intensity' is shown in Fig. 2 as the abscissa where the wheel wear curve abruptly turns upward. Extensive testing of grinding wheels has

*Cincinnati Milacron, Heald Division, Worcester, Massachusetts, U.S.A.

shown that the 'breakdown force intensity (F_n)_{BD}' may be calculated by

$$(F_n)_{BD} = C (\text{vol})^{0.55} D_e^{1/4} \quad (1)$$

where vol = volume of bond in wheel

$$D_e = \frac{D_w D_s}{D_w \pm D_s} = \text{equivalent diameter}$$

C = constant depending on material ground and grain type

The volume of bond in the wheel is given by¹

$$\text{vol} = 1.33H + 2.2S - 8.0$$

where $H = 0, 1, 2, 3, \dots, 8$ for wheels of hardness

$H I J K \dots P$

S = structure number

In the early stages of rounding up, the instantaneous width of cut w varies as shown in Fig. 1 as the zone ABD. The instantaneous grinding force at the high spot, F_G , lies at the position x from the right-hand edge of the work. The instantaneous wheel depth of cut $h(x)$ is also shown in Fig. 1. The force required to produce the cut EFGH can be found as follows.

Consider Fig. 3 where a rotating wheel is pressed against a rotating workpiece. Both bodies mutually machine each other. The 'machining law' of each body depends on the induced interface force intensity. Extensive experimental tests² have shown that, for easy-to-grind materials, the volumetric stock removal rate from the workpiece, Z_w , is proportional to the interface force F_n , thus

$$Z_w \equiv v_w w h = \Lambda_w F_n \quad (2)$$

where Λ_w metal removal parameter (volume removed per unit time per unit force)

h = wheel depth of cut

v_w = work surface speed

From Eq. (2) the local force intensity can be written as

$$f(x) \equiv \frac{F_n}{W} = \frac{v_w}{\Lambda_w} h(x) \quad (3)$$

Using this equation the force required to produce the cut shown as EFGH in Fig. 1 is

$$F_G = \int_0^w f(x) dx = \frac{v_w}{\Lambda_w} \int_0^w h(x) dx \quad (4)$$

Since the shape of the cut depends on the lateral and angular wheel position as well as the surface generated in the previous work revolution, it is convenient to use a digital computer and to keep track of these quantities for each revolution. In this way a digital computer program has been written for IBM 360 which calculates force balances, cross slide movements, peak force intensities, runout, width of cut, accumulated wheel wear and stock removal.

After some grinding time the contact between wheel and workpiece ceases to be intermittent and becomes continuous. Here rounding up continues owing to the differential flexing of the spindle. The

still eccentrically running workpiece 'drives' the wheel vibrationally with a quasi-sinusoidal motion

$$\xi = \xi_0 + a \sin 2\pi n_w t \quad (5)$$

This forced motion of the wheel causes the cross slide M through the action of the flexible spindle K to execute a quasi-periodic motion $\zeta(t)$. The difference between the forced motion $\xi(t)$ and the slide motion $\zeta(t)$ is the spindle or system deflection. The instantaneous grinding force in turn produces an instantaneous wheel depth of cut which causes further rounding up. The motion of the controlled force cross slide is given by

$$\frac{d^2 \zeta}{dt^2} + \frac{c}{m} \frac{d\zeta}{dt} + \frac{K}{m} \zeta = \frac{F_A}{m} + \frac{K}{m} \xi \quad (6)$$

Using these equations the rounding up decrement Δ has been found³ to be

$$\Delta = \left[\left(1 - \frac{\Lambda_w K}{v_w W} \right)^2 + \frac{\Lambda_w K}{v_w W} \left\{ 1 + \left(1 - \frac{\Lambda_w K}{v_w W} \right) (1 - 2\nu^2) \right\} \right]^{1/2} \frac{1}{(1 - \nu^2)^2 + \nu^2 \left(2 \frac{C}{C^2} \right)^2}$$

where $\nu = 2\pi n_w / \left(\frac{K}{m} \right)^{1/2}$

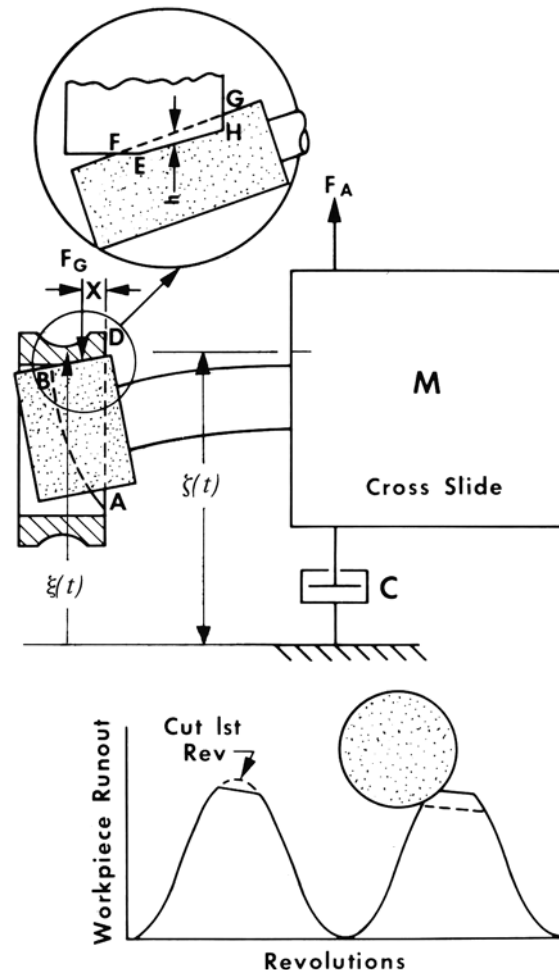


Fig. 1 Illustration showing the intermittent rounding-up phase in controlled force internal grinding.

This equation permits the computer program to calculate the continuous contact rounding-up decrement and to calculate the time required to reduce the runout to any specified level. Using Eq. (4) the computer program calculates the stock removed from the high spot each revolution during the intermittent phase of round up.

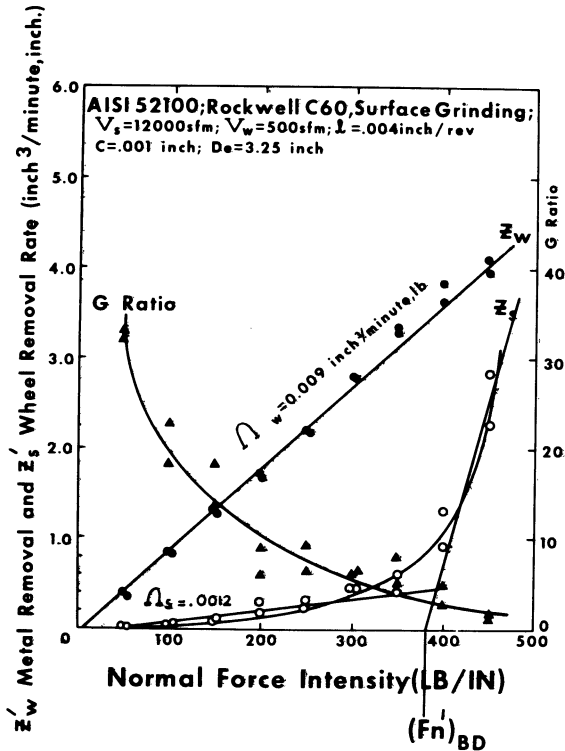


Fig. 2 Chart showing the metal removal and wheel wear characteristics of a grinding wheel including the metal removal parameter Λ_w , the wheel wear parameter Λ_s , and the wheel breakdown force intensity $(F_n)_{BD}$.

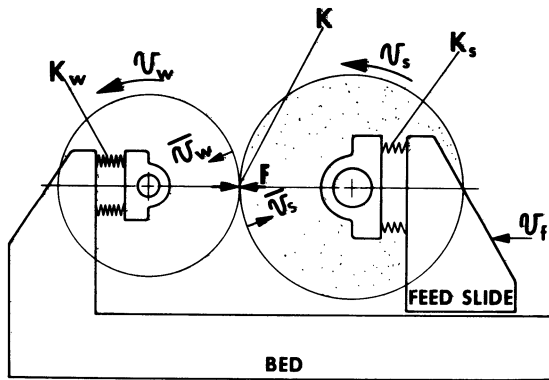


Fig. 3 Illustration defining the rate of stock removal and rate of wheel wear in the mutual 'machining' of wheel and work.

DIGITAL ROUNDING-UP COMPUTER PROGRAM

This program requires as input the 'metal removal parameter' Λ_w . This is the rate of stock removal per unit normal wheel-work interface force and is the slope of the plunge grinding velocity curve in Fig. 2.

Also required are four elastic constants associated with the lateral and angular deflection of the wheel relative to the workpiece. These are the lateral system compliance and the rate it changes with the distance x along the grinding wheel and the angular compliance and its rate of change with respect to x . Other input variables are the initial runout, the desired grinding force, cross slide mass and dashpot strength, wheel speed, work speed, wheel diameter and work diameter.

The computed results are the workpiece runout for each work revolution, the width of wheel work contact, the peak grinding force, the peak force intensity (force per unit width of contact), the accumulated wheel wear, and the required approach force to prevent excessive wheel breakdown.

In order to evaluate the accuracy of the computer program a number of tests were made on a controlled force internal production grinding machine grinding the bore of a tapered roller bearing cup. A work riding displacement transducer was arranged to read the instantaneous runout of the workpiece. Another displacement transducer was arranged to read the cross slide motion. A force transducer built into the wheelhead was arranged to read the instantaneous normal grinding force. A typical recording of these three quantities is shown in Fig. 4. The initial runout of 0.008 in (peak to valley) is shown, being reduced in about 5.5 s where the intermittent contact ceases and continuous contact starts. The peak grinding forces (top trace Fig. 4) are seen to increase to a maximum of about 300 lbf in about one second and then to fall gradually and to approach 100 lbf, the steady-state grinding force.

Since the runout on the n th revolution, $\rho(n)$, during the continuous contact phase is given by

$$\rho(n) = \rho_0(\Delta)^n \tag{8}$$

where ρ_0 is the initial runout at the beginning of continuous contact, it is convenient to plot the runout on semi-log paper as shown in Fig. 5. The upper solid curve gives the calculated runout for both the intermittent contact region and the continuous contact region. The dashed curve gives the experimental values. It will be seen that a true rounding-up decrement does not apply to the intermittent phase. The rounding-up action accelerates as the roundness improves and both computed and experimental curves curve downwards. Once continuous contact is achieved a true decrement results and a straight line relationship occurs. Initial values of the intermittent decrement are shown as well as values for the continuous decrement.

The peak grinding forces on the high spot are also shown in Fig. 5. It will be seen that the calculated values (solid curve) reach their maximum slightly before the experimentally measured values (dashed curve), although the magnitude of both values are in fair agreement. In this case the forces reach nearly three times the steady-state force.

A number of tests have been made similar to those shown in Fig. 5 and the results comparing calculated values with experimental are summarized in Table 1.

Table 1
Experimental and computed results

N_w	F_A	Revs of intermittent contact		Peak force		Initial intermittent decrement		Continuous decrement	
		Calc.	Expt.	Calc.	Expt.	Calc.	Expt.	Calc.	Expt.
760	150	70	90	353	330	0.9833	0.9868	0.9708	0.9861
480	150	30	34	189	300	0.9806	0.9800	0.9800	0.9305
760	100	126	95	276	260	0.9873	0.9901	0.9785	0.9694
480	100	62	65	307	300	0.9738	0.9805	0.9790	0.9340

Fixed data

Workpiece:	No. 3920 taper roller bearing cup
Operation:	Grind tapered bore (approx 4-7/16 O.D. X 4 I.D. X 7/8 wide)
Wheel:	A801L6 3¼ X 1 1/8 X 7/8
Wheel speed:	8500 ft/min
Work speed:	$N_w = 480$ rev/min and 760 rev/min
Coolant:	Cimperial 20 20:1
Feed force:	$F_a = 100$ and 150 lbf
Metal removal parameter:	66×10^{-6} in ³ /s lbf
Cross slide weight:	850 lbf
Dashpot strength:	11 000 lbf s/in
Wheel cross compliance coefficient:	2.8×10^{-6} in/lbf in
Compliance at inboard end of wheel:	3.7×10^{-6} in/lbf
Angular compliance cross coefficient:	0.7×10^{-6} rad/lbf in
Angular compliance of wheel:	0.9×10^{-6} rad/lbf
Dressing lead:	0.004 in/rev
Diamond depth of dress:	0.0005 in

From this table it will be seen that the computer program does simulate the rounding-up process to a reasonable degree.

The program has been used as an aid in establishing efficient production internal grinding cycles for universal joint cups, water pump bearings,

and other ball or roller bearings. The problem of optimum machine setting can be appreciated by considering the joint distribution of stock allowance and runout. The data points in Fig. 6 show the stock and runout distribution for a typical roller bearing cup. The diagonal lines show the computed stock allowance required to correct the runout at different grinding forces. As the grinding force is increased the stock allowance tends to be used up before the runout is corrected. This sets a limit on the permissible grinding force which will successfully round up a part with small stock and large runout. For the case shown in Fig. 6 a grinding force of about 90 lbf will successfully round up all parts since all data points lie above this line. Forces greater than 90 lbf will not round up the excessively running out workpieces.

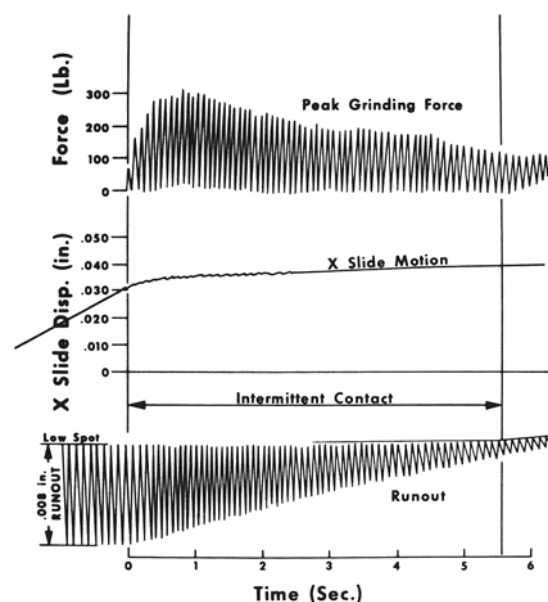


Fig. 4 The rounding up in grinding the tapered roller track of No. 3920 tapered roller bearing cups. The lower trace gives the instantaneous runout, shows the period of intermittent contact and the beginning of continuous contact at 5.6 s. The middle trace shows the cross slide advance. The top trace gives the instantaneous force pulses occurring on the grinding wheel, the steady-state force being 100 lbf.

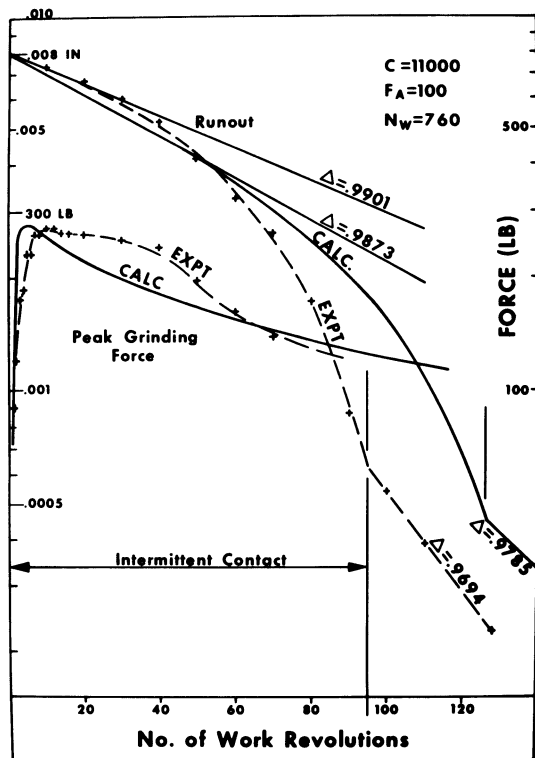


Fig. 5 Instantaneous runout and instantaneous grinding force versus number of work revolutions for the internal grinding of No. 3920 taper roller bearing cups (4.4375 in O.D.). Comparison of computed values with experimentally measured values.

CONCLUSION

The grinding process can be described mathematically through the use of the metal removal parameter Λ_w , the wheel wear parameter Λ_s and the breakdown force intensity $(F_n')_{BD}$.

The rounding-up process can be simulated on digital computers using grinding process equations and the equation of motion and deflection of the grinding machine.

The selection of machine parameters to give efficient grinding cycles which reduce grinding costs can be more readily achieved using the rounding-up program described above.

The effect of changes in work speed, system rigidity, dashpot strength, metal removal parameter and other variables on the rounding up of controlled force internal grinding machines can be investigated with the aid of the computer program described. In this way machine settings of force, dashpot strength, and work-speed can be selected which avoid excessive force intensities and wheel breakdown yet provide fast grinding cycles.

REFERENCES

- LINDSAY, R. P., 'On the metal removal and wheel removal parameters, surface finish, geometry and thermal damage in precision grinding', Doctorate Thesis, Worcester Polytechnic Institute (1971).
- LINDSAY, R.P., and HAHN, R.S., 'On the basic relationships between grinding para-

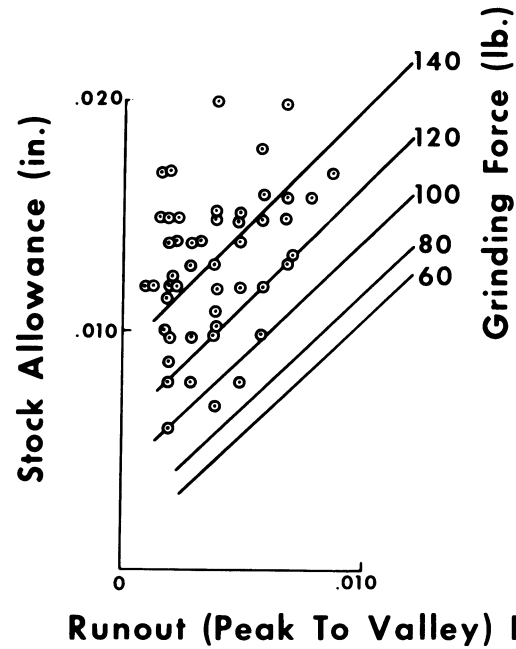


Fig. 6 Joint distribution of stock allowance and run-out. The inclined lines give the stock required to true up the runout at various grinding forces.

Workpiece: Tapered roller bearing cup LM48210

Wheel speed: 12 500 ft/min

Bore diameter: 2.227 in (average)

Wheel diameter: 1.75 in

Width of work: 0.500 in

Wheel cross compliance coefficient: 2.4×10^{-6} in/lbf in

Compliance at inboard end of wheel: 3.6×10^{-6} in/lbf

Angular compliance cross coefficient: 4.8×10^{-6} rad/lbf in

Angular compliance of wheel: 2.0×10^{-6} rad/lbf

Dashpot: 11000 lbf s/in

Weight of X slide: 850 lbf

Approach force 100 lbf

Work speed: 760 rev/min

Dressing lead: 0.001 in/rev

Compensation for wheel wear: 0.0003 on diameter

Wheel: A80M6

Coolant: soluble oil emulsion

meters', *Ann. CIRP*, 18, Pergamon Press Oxford, (1970).

- HAHN, R. S., 'Controlled force grinding—a new technique for precision internal grinding', *J. Eng. Ind. Trans. ASME, Ser. B*, 68, pp. 287–293 (1964).

DISCUSSION

Query from W. B. Rowe

At Manchester, a number of digital simulations were made of the rounding process in centreless grinding. These simulations did not involve dynamics, since it was found that static compliance and the grinding force coefficient were sufficient to give excellent correlation at sub-resonant conditions. On a controlled feed-rate grinder the significant first resonance should be well above the frequencies corresponding to a basic workpiece eccentricity. The conclusion must then be reached that the rounding-up process will be directly related to the ratio of the machine stiffness to the grinding force coefficient as described in⁴.

Reference

4. Proceedings of Conference on Specification and Tests of Metal Cutting Machine Tools held at UMIST (published 1970/1971).

In controlled force grinding, a similar condition to high stiffness may be achieved by the introduction of phase shift through the application of damping cylinders. However, one might then suspect that at certain parts of the operating frequency range, the dynamic stiffnesses will be low. Would the authors like to comment on this aspect?

Reply

The authors would like to thank Mr. Rowe for his comments regarding rounding up on centreless and feed rate grinders.

On internal controlled force grinders, the rounding up behaviour depends on the mass, natural frequency, damping, work speed and the metal removal parameter. If one chooses to operate with low damping and low workspeeds, the system is unstable and will cause the runout to increase. If one chooses to operate with low damping, but with the workspeed exceeding the system natural frequency, the oscillatory motion of the cross slide will be out of phase with the runout and a rapid rounding up action will occur. However, since it is not always convenient in practice to run the work at high speeds, controlled force grinders are usually operated with considerable dashpot strength. This removes the instability and permits rounding up at all but the lowest work speed. For further details, see³ of the paper.

GEOMETRICAL CONFIGURATIONS FOR STABILITY IN THE CENTRELESS GRINDING PROCESS

by

D. L. RICHARDS, W. B. ROWE* and F. KOENIGSBERGER**

SUMMARY

Geometric stability charts for the centreless grinding process have been developed and the results of extensive experimentation have proved their usefulness. Recommendations are given for optimum geometrical configurations and favourable grinding practice. The paper is a report on part of a research program supported by the Science Research Council.

INTRODUCTION

There are obvious causes of pronounced workpiece roundness errors arising in the centreless grinding process as a consequence of the geometrical configuration¹. This configuration is determined by the diameters of the grinding wheel, control wheel and workpiece, the angle of inclination of the workblade and their relative disposition which is caused by the variation in height of workpiece centre to a horizontal line joining grinding wheel and control wheel centres.

However, from the published reports by Rowe¹⁻³, Gurney⁴, Yonetsu⁵, Furukawa⁶, Richards¹, it is apparent that this geometric problem is essentially a question of stability and is encountered under normal dynamic operating conditions.

Therefore, after the basic geometrical relationships of the process have been defined¹ it is possible to use the Nyquist criterion to show the theoretical instabilities caused by adverse configurations.

The centreless grinding arrangement is shown diagrammatically in Fig. 1 where the workpiece is simultaneously in contact with the workblade, control wheel and grinding wheel. In order to produce stock removal, the case considered here is that where the workblade arrangement is attached to the control wheel carriage.

A computer program has been developed and used to investigate a large range of geometrical configurations and these have been compared with experimental results. The effects of machine tool resonances and variations in workpiece speed on these results are discussed. They yield a much better overall understanding of the problem of geometrical instability which will prove beneficial to practical users.

As a result it is now considered feasible to present and make use of geometrical stability charts which are comparatively simple to compute.

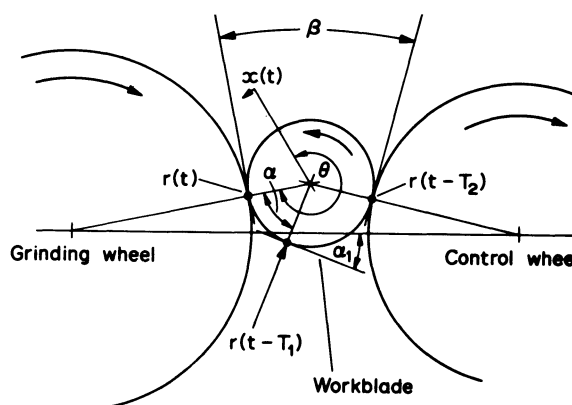


Fig. 1 Basic geometrical configuration.

MATHEMATICAL BASIS

The basic assumptions concerning the geometrical process are the same as those adopted by other researchers, which have been presented previously¹.

The basic equations which are taken to represent the process are as follows.

$$R(\theta) = X(\theta) - K_1 \cdot r(\theta - \alpha) + K_2 \cdot r(\theta - \pi + \beta)$$

or, as a function of time, the equation of constraint is

$$-x(t) = r(t) - K_1 \cdot r(t - T_1) + K_2 \cdot r(t - T_2)$$

where $x(t)$ = the magnitude of the feed movement of the grinding wheel normal to the workpiece at time t

*Department of Production Engineering, Lanchester Polytechnic, Coventry

**University of Manchester Institute of Science and Technology

$r(t)$ = reduction in radius from the workpiece reference circle determined by time t

$r(t - T_1)$ = the error on the workpiece at the workblade contact

$r(t - T_2)$ = the error at the control wheel contact
 T_1 = the time for the workpiece to revolve through an angle α

T_2 = the time for the workpiece to revolve through an angle $\pi - \beta$

The error at the grinding point at $t - T_1$ will have just reached the workblade at time t , and similarly the error ground at the time $t - T_2$ will have reached the control wheel at time t .

$$K_1 = \sin \beta / \sin(\alpha + \beta)$$

$$K_2 = \sin \alpha / \sin(\alpha + \beta)$$

K_1 and K_2 are depth of cut factors for workblade and control wheel positions respectively.

These equations may be represented in transfer function form, in the Laplace domain, as follows.

Closed-loop transfer function:

$$\frac{\Theta_o}{\Theta_i} = \frac{1}{1 - K_1 e^{-sT_1} + K_2 e^{-sT_2}}$$

Open-loop transfer function:

$$\frac{\Theta_o}{\Theta_i} = K_2 e^{-sT_2} - K_1 e^{-sT_1}$$

The method found most convenient for investigating the stability of the system represented by the closed loop transfer function is based on the Nyquist criterion. This involves the examination or measurement of the open-loop frequency response to determine whether or not it is safe to close the feedback loop, i.e. to determine the systems' absolute stability. The harmonic response to a sinusoidal input may be obtained by substituting $s = j\omega$ in the open-loop transfer function. Separating the components of

the response in phase with the input (real terms) and the components in the quadrature (imaginary terms) defined as $A-1$ and $-B$ respectively¹ the following equations are obtained

$$\text{Re}(\theta_o) = K_2 \cos \omega T_2 - K_1 \cos \omega T_1 = A - 1$$

$$\text{Im}(\theta_o) = K_1 \sin \omega T_1 - K_2 \sin \omega T_2 = -B$$

A computer program has been developed and the results obtained for these response co-ordinates covering a number of geometrical configurations for up to 50 waves on the workpiece were studied.

Figs. 2 and 3 illustrate a method of representing these results in the form of geometric stability charts. Since the parameters A and B are approximately sinusoidal functions with unit amplitude, it is only necessary to plot the values of A corresponding with the number of waves on the workpiece. Instabilities are indicated whenever A becomes negative, and the maximum negative values of A may be taken as measures of theoretical geometric instability¹.

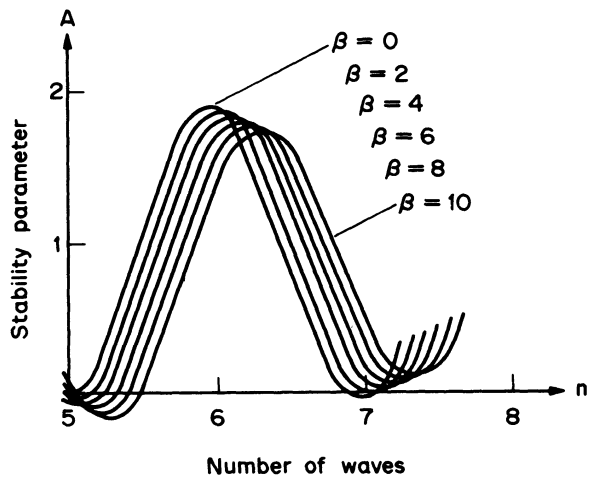


Fig. 2 Part of stability charts for various β values and blade angle $\alpha_1 = 20^\circ$.

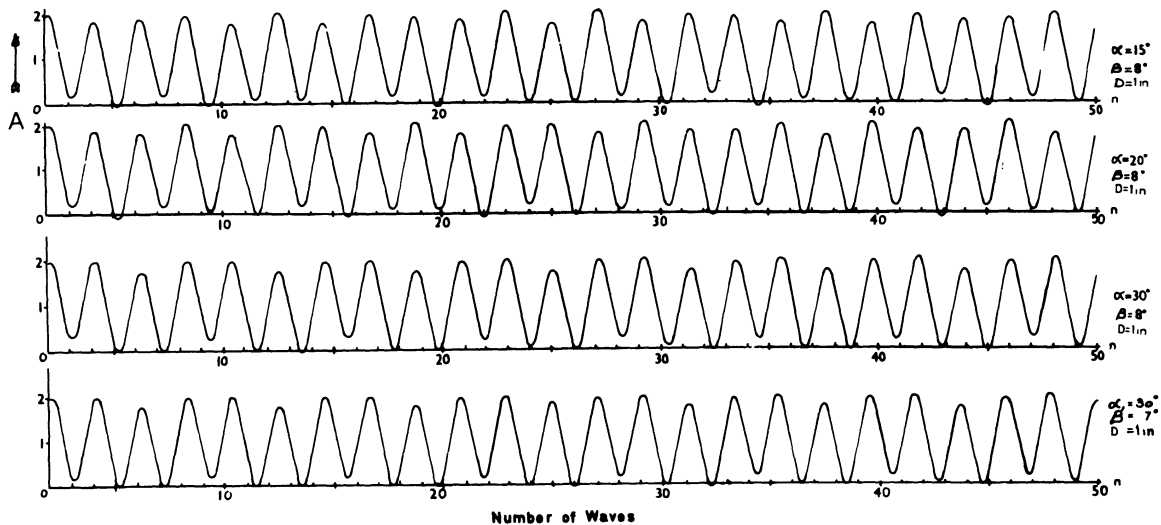


Fig. 3 Stability charts

THEORETICAL RESULTS

Fig. 2 shows a limited portion of a stability chart and illustrates how the geometric stability changes with the included tangents angle β for various orders of lobing which may occur on the workpiece. This agrees with the conclusion made by Yonetsu⁵ in that (i) the lobed shapes related to odd harmonics of order below the 11th, i.e. 3, 5, ..., etc., are more effectively removed with a large included tangent angle β , (ii) the lobed shapes related to even harmonics of order below the 10th, i.e. 2, 4, ..., etc., are more effectively removed with a small angle β .

Fig. 3 shows a selection of stability charts for various configurations and extended to cover up to 50 waves on the workpiece. The areas of potential instabilities to be avoided are indicated by the troughs on the stability charts. Because of the mildness of the instabilities it is found that in most cases these are serious only when there is a coincidence between an integer number of waves and a maximum negative value of A . A coincidence of this nature must, therefore, be avoided by selecting a more favourable geometric configuration. If there is coincidence of a positive trough on the stability chart and an integer number of workpiece waves, roundness errors of a significant level should not arise. However, in practice if the frequency corresponding to the root is close to a resonant frequency of the machine the workpiece lobes may be pronounced. This condition does not always arise but in the event may be corrected by a change in the workpiece speed as later shown in the experimental results.

Although the workpiece diameter is a parameter which determines the geometrical configuration, it has been found from the theoretical results that variations have little significance in the system. If charts as illustrated in Fig. 3 are compared, it is found that the most favourable configuration of the range so far tested is obtained when the included tangents angle β is 7° and the workblade angle α_1 is 30° .

EXPERIMENTAL CONDITIONS

Grinding machine: Wickman Scrivener No. 0 model
Grinding wheel: 5A 46/54-K5-V50 initially 11.6 in
X 3 in X 4 in bore

Control wheel: A80-R-R initially 6.7 in X 3 in X 3
in bore

Workblade angles: 0° to 45° in steps of 5°

Specimen: 0.5 in diameter X 2 in, 1.0 in diameter X 2
in, hard and soft steel

Control wheel speeds: 23, 30 and 39 rev/min,
inclination $\frac{1}{4}^\circ$

Grinding wheel speed: 1750 rev/min

Coolant: Fletcher Miller 'Cleardge' water soluble oil
1:40

Wheel dressing procedure:

1.5 in/min traverse

1 pass with 0.001 in depth of cut, return pass
0.001 in depth

1 pass no cut, return pass 0.0005 in cut

1 pass no cut, return no cut

Stock removal: 0.010 in on diameter

Spark-out time: 7 s.

Vibrations were kept to a minimum by adjustment of belts, balancing of pulleys and wheels, etc.

Infeed was continuous and controlled by a hydraulic infeed mechanism incorporating a plate cam.

Workblades: 10 workblades were carefully prepared with angles α_1 from 0° to 45° in increments of 5° . The maximum departures from the nominal angle were well within 10 minutes of arc and were checked by angle slips and Angle Dekkor.

Specimens: Both hardened and soft specimens were carefully prepared on a plain cylindrical grinding machine to within 30×10^{-6} in M.Z.C. roundness error, 7×10^{-6} in c.l.a. surface texture and 0.0002 in diameter. These parameters were checked respectively by a Talyrond, Talysurf and an electrical comparator.

GRINDING PREPARATION

Before each experimentation the grinding and control wheels were dressed by positioning the diamond horizontally opposite the point of contact with the workpiece after a 'warming-up' period of approximately 1 hour. The wheels were measured and the corresponding height of workpiece centre to grinding and control wheel centres for the appropriate included tangent angle β was calculated. The work blade setting was made using a slip gauge and a 0.0001 in dial indicator from a datum face. All height settings were within 0.002 in. In order to standardise the pre-grinding conditions of the wheels four components were ground before the actual tests were started.

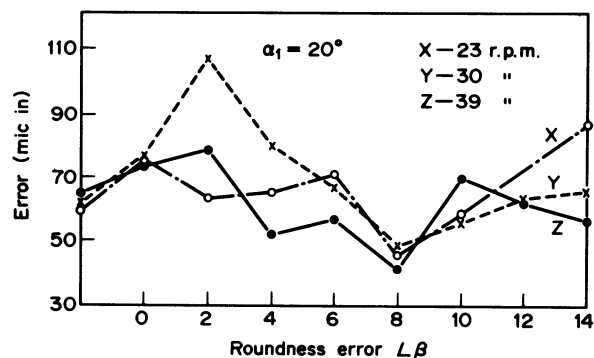


Fig. 4 Experimental roundness errors, various β values, blade angle $\alpha_1 = 20^\circ$.

EXPERIMENTAL RESULTS

Test A—Included tangent angle β and workspeed n_w
Fig. 4 shows graphically the resulting roundness errors for different values of the included tangent angle β and control wheel speeds. The blade angle was 20° . Ten specimens were ground at each test and their averages plotted. At each subsequent test, i.e. change in β angle, the initial conditions were the same as in previous tests. The lowest average departure from roundness is shown at $\beta = 8^\circ$ and 75% of the tests indicated the most favourable control wheel speed to be 30 rev/min. This is a particularly

interesting result since on the corresponding stability chart this condition is geometrically unstable for 22.0 waves and this shape has often been detected in practice. Some grinding shapes are illustrated on Fig. 5. However, the instability is obviously very mild. At a workpiece rotational speed of 3.73 rev/s and for the given experimental conditions a shape with 22 waves corresponds quite closely with the principal machine resonance at 82 c/s. In this case the resonance does not appear to make the instability severe.

When the workspeed is increased to 4.85 rev/s it is found that approximately 16 waves result, Fig. 5. This illustrates an example of dynamic chatter, at a frequency of close to 77.6 c/s. This value is below the resonant frequency of 82 c/s and confirms the prediction of Gurney⁴ that subresonant chatter is possible. The number of waves corresponding exactly with the resonant frequency would be $82/4.85 = 16.9$ waves.

The chatter at 16 waves under the joint influence of the resonance and the trough at 15.6 waves is of the mild type where waves build up gradually around the workpiece periphery and are approximately in phase with earlier waves. The chatter does not occur at 17 waves, which is close to a peak on the stability chart, and indicates incompatibility between such a shape and the grinding configuration.

It is helpful to distinguish dynamic chatter from geometric instability since in the first case improvement involves a change of workspeed or a reduction in grinding forces whereas in the second these actions may worsen the situation and may preferably require a change of geometrical configuration.

Test B—Workblade angles

As the results in Fig. 4 showed preference towards $\beta = 6^\circ - 8^\circ$, these values were used in turn with workblades of varying workblade angle α_1 from 0° to 45° in steps of 5° . Here again the same initial conditions were maintained with a control wheel speed of 30 rev/min corresponding to a workpiece speed of 3.73 rev/s.

Fig. 6 shows graphically the results of departure from roundness for various workblade angles when $\beta = 6^\circ, 7^\circ$ and 8° . The complete range of roundness errors is within approximately 55×10^{-6} in for over 200 specimens. The best results were obtained with β

$= 7^\circ$ and 8° and workblade angles 15° and 35° .

From the average trends of roundness errors for $\beta = 6^\circ, 7^\circ$ and 8° for varying workblade angles it appears that the lowest roundness errors occur when $\beta = 7^\circ$ followed by $\beta = 8^\circ$ then $\beta = 6^\circ$. The errors also decrease as the workblade angle α_1 is increased up to the point where severe instability may occur.

After the completion of the tests on workblade angles their effect on the width and depths of crater wear on the workblade was checked with the aid of a Talysurf.

As Fig. 7 shows wear is greater with increasing workblade angle. This is indicative of increased forces on the blade. There seems to be little advantage in using a workblade with an angle α_1 greater than 30° . In fact when using workblades with angles 35° and 40° there was a tendency to chatter and work bounce, to an extent that made it necessary to terminate the test as the condition became dangerous.

With a geometrical configuration of $\alpha_1 = 15^\circ$ and $\beta = 8^\circ$ the stability charts indicate that the system is geometrically stable for 22 waves, see Fig. 3. However, with a workspeed of 3.73 rev/s governed by a control wheel speed of 30 rev/min instability was apparent as shown by the typical trace in Fig. 8 indicating 22 waves. This condition was improved by changing the workpiece speed at 29 rev/min.

It is interesting to note that at the instability condition for 22 waves the process is geometrically stable but becomes dynamically unstable, a fact due to the resonance at approximately 82 c/s. This is an example of dynamic chatter, which may be contrasted with the previous example, Fig. 5, for $\alpha_1 = 20^\circ, \beta = 8^\circ, n_w = 3.73$ rev/s which was geometrically unstable. In the latter case the resonance in close proximity did in fact reduce instability rather than increasing it. In view of the improvement in the rounding action with large blade angles, on the one hand, and the tendency towards higher blade forces, increased wear and chatter at blade angles above 35° on the other, it is suggested that in experiments over the range so far considered the optimum lies with $\beta = 7^\circ$ and $\alpha_1 = 30^\circ$. A typical workpiece shape is illustrated in Fig. 8. This demonstrates the order of accuracy achievable with a small centreless grinder which, under experimental conditions, amounted to an average roundness error of 21×10^{-6} in.

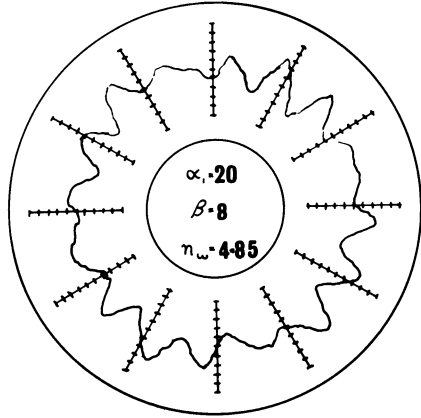
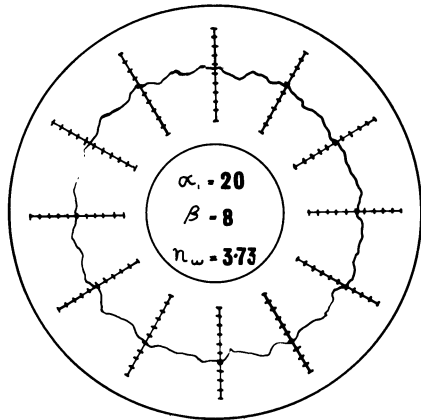
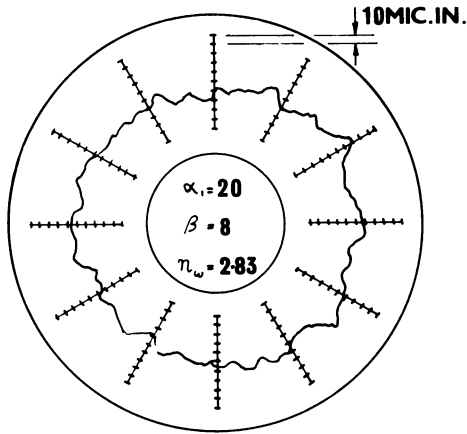


Fig. 5 Measured workpiece shapes for blade angle $\alpha_1 = 20^\circ$, $\beta = 8^\circ$.

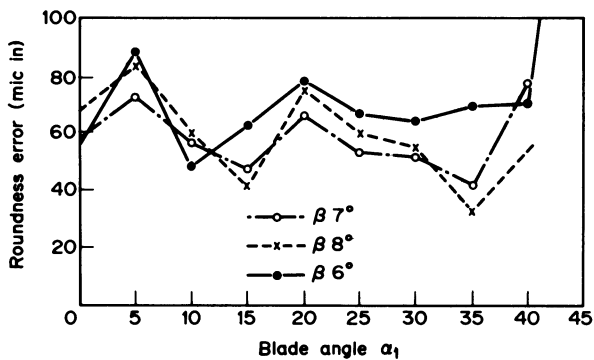


Fig. 6 Experimental roundness errors, various blade angles.

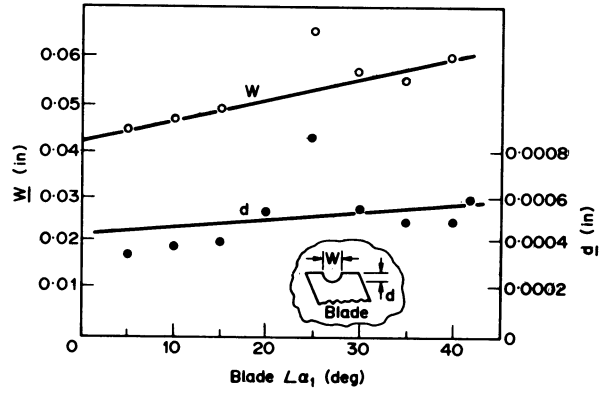


Fig. 7 Measurements of workblade wear, various blade angles.

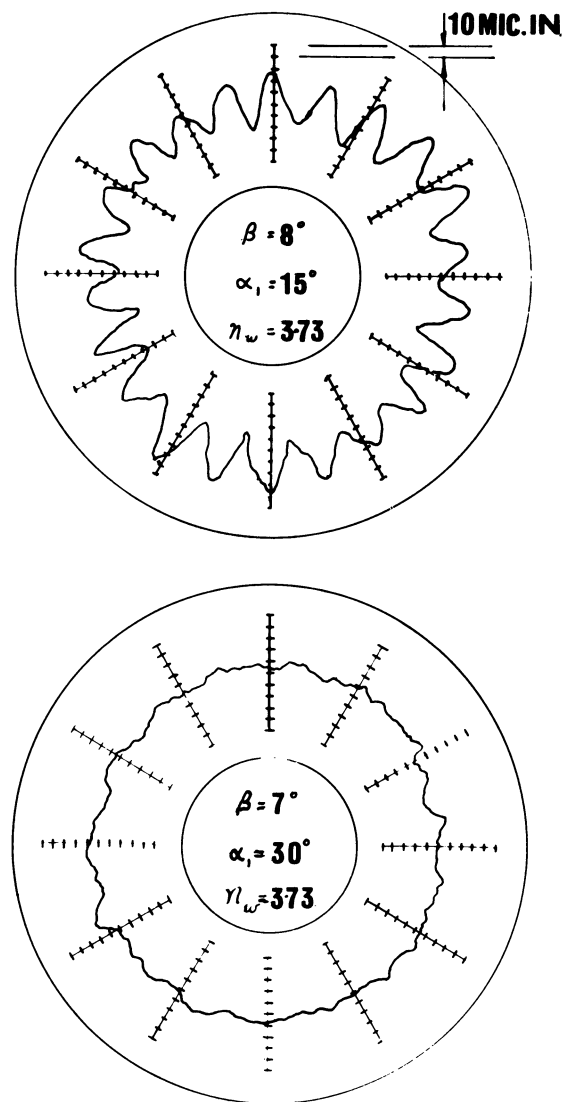


Fig. 8 Measured workpiece shapes.

CONCLUSIONS

(1) It is important to give adequate consideration to theoretical geometric stability to avoid highly unstable operating conditions. Stability charts are easy to compute and provide information which

facilitates the interpretation of the grinding results. In particular it is possible to distinguish between geometric instability and dynamic chatter.

(2) Geometric configurations which give rise to large negative values of the parameter A with an integer number of waves n should be avoided.

(3) Resonant frequencies of the machine should be as high as possible so as to minimize the tendency towards large amplitude waviness.

(4) Close proximity between a resonant frequency and a geometrical instability does not necessarily constitute an unfavourable condition.

ACKNOWLEDGMENTS

Acknowledgments are due to the Science Research Council for their financial support, and to Mr R. L. Aston, Head of Department of Production Engineering, Lanchester Polytechnic, Coventry, for the use of the facilities in the department.

Personal thanks are due to Mr K. H. Wright, Lanchester Polytechnic, who was of considerable assistance in the preparation and performance of tests.

REFERENCES

1. ROWE, W. B., and RICHARDS, D. L., 'Geometric stability charts for the centreless grinding process', to be published.
2. ROWE W. B., and KOENIGSBERGER, F., 'The work-regenerative effect in centreless grinding', *Intern. J. Mach. Tool. Design Res.*, **4**, 175-87 (1965).
3. ROWE, W. B., BARASH, M. M. and KOENIGSBERGER, F., 'Some roundness characteristics of centreless grinding', *Intern. J. Mach. Tool Design Res.*, **5**, 203-15 (1965).
4. GURNEY, J. P., 'An analysis of centreless grinding', *J. Eng. Ind. (Trans. ASME Ser. B.)*, Paper no. 63-WA-26, **87**, 163-74, May (1964).
5. YONETSU, S., 'Forming mechanism of cylindrical work in centreless grinding', *Proc. Fujihara Mem. Fac. Eng. KEIO Univ.*, **12**, No. 47, 27-45 (1959).
6. FURUKAWA, Y., MIYUSHITA, M., and SHIOZAKI, S., 'Vibration analysis and work-rounding mechanism', *Proc. 11th Intern. Mach. Tool Design Res. Conf.* (1971).
7. DALL, A. H., 'Rounding effect in centreless grinding', *Mech. Eng.*, **58**, 325, April (1946).

DISCUSSION

Query from C. F. Noble, UMIST

It appears to me that, whilst problems of feeding components into the gap might arise, considerable geometrical advantage would result if the angle β were made negative. Theoretical curves Fig. 2 are limited to positive values, as are the potential results in Fig. 4. Please comment.

Reply

Small negative values of β are not favourable for rounding-up odd order waviness on a workpiece. This configuration is sometimes employed for long slender

bars in order to maintain straightness. The authors would agree that there may be a possibility of improvement in the process by application of geometrical configurations outside the present operating range. More investigations are required to analyse all alternatives, but, as Mr. Noble has realised, this does present other problems of locating and controlling the workpiece.

Query from P. F. Jones, P. A. Management Consultants Ltd.

Would the authors please say:

- (a) How long on average it takes to solve roundness problems occurring in industry.
- (b) How many successful examples of roundness improvement, using the authors' technique in industry, have been recorded.

Reply

The authors can only report reliably from their own experience of problem-solving in industry. It is almost always possible to improve the grinding technique by taking logical account of the geometrical effect. There is, however, a reservation which must be made concerning the many other associated machine and process effects which may be involved in the total problem. It is usually necessary to make a number of improvements to the whole technique of operation, since the total result is primarily a consequence of complete interactions between forced vibrations and geometrical effects⁸.

Reference

8. ROWE, W. B., 'Factors affecting the achievement of roundness by centreless grinding', *Machinery and Production Engineering*, 984-8, Nov. 3 (1965).

Query from H. Sato, University of Tokyo, Japan.

I would like to raise a question on Fig. 3. Is any non-linearity, to limit the amplitude of the oscillations, taken into account? In other words is it because of a small margin of instability that the amplitudes seem to keep constant during their duration.

Reply

It is true that there are non-linearities in the grinding process but these are not taken into account in the technique described. The complete simulation of the process is so expensive, in terms of effort and time, that it would have no practical value of general interest to industry. However, it is surprising how good correlation between theory and experiment can be at sub-resonant frequencies, without taking non-linearities into account other than

- (a) Loss of contact between wheel and workpiece at large amplitudes.
- (b) Variation of the finite width of the line of contact between workpiece and grinding wheel.

The technique of digital simulation in the centreless grinding process has been described in³.

ELECTRON BEAM, THE MULTI-ROLE TOOL FOR MODERN FABRICATION

by

K. H. VON GROTE and A. H. MELEKA*

SUMMARY

Use of the electron beam for welding is well established, but other applications for it have developed more slowly. To-day, however, it is becoming an important tool for machining, engraving and heat treating of materials.

It is the high intensity of the beam that permits precision machining of metals, ceramics and plastics. The mechanism of this is explained in this paper, especially the formation of vapour capillaries that allow deep penetration of the beam into the material, and the different effects of single and multi-pulsing of the beam. In drilling, molten material is driven from the hole by expanding vapours, but in engraving and cutting direct sublimation of material occurs. The machining effect varies greatly with the selection of the electron beam parameters.

The beam itself is the cutting tool and because it has low inertia its rapid movements can be controlled readily. It exerts little mechanical force on the workpiece and at present beam positional control is within 0.01 mm. Beam movements are so rapid that they must be automatically rather than manually controlled. Hence, machines use numerically controlled work manipulators and the beam is electronically coordinated with the work movement. Thus errors, because of lag in mechanical movements, are avoided. Engravings or patterns of holes can be machined according to programmed information. The process offers many special capabilities but if the value of these is to be realised the component designer must be fully aware of them.

The paper describes and illustrates the application of the electron beam to numerically controlled microwelding, hole perforation, drilling, cutting and engraving.

INTRODUCTION

Electron beam not limited to welding

Electron beam (EB) welding can now be considered as an established technology, that is, a conventional technology; but other technologies have been developed using the electron beam as a cutting tool. However, progress in these fields has been slower than in the better known electron beam welding process.

In the paper I will describe some electron beam techniques that are especially suitable for precision machining. They are called electron beam machining (EBM). This technique, recently introduced, comprises microjoining as well as material removal as in EB perforation, drilling, cutting and engraving. There are other applications for the electron beam that are being developed; for example, heat treatment of metals (hardening, melting refinement) or paint curing which is based on the electron beam induced polymerization.

It will be helpful to discuss first the principles of using the electron beam as a tool. The electron beam machining equipment is a precision machine tool. The beam itself is the cutting tool; it is a tool with special

individual characteristics. The beam consists of very light, but high velocity, particles carrying momentum and energy. A special advantage is that the beam can be generated by simple means, that is by a thermionic axially-symmetric triode valve. Also, it can be shaped easily by electric or magnetic fields, permitting fast and accurate space-time control.

The electron beam has little mechanical effect on the workpiece. It acts as a pure energy beam, thus transfers little mechanical momentum and hence applies negligible forces to the workpiece. Because of this the electron beam is called a thermal tool. The electron beam is generated and operates in vacuum of about 10^{-4} mm Hg. Thus, vacuum pumping systems are required for the electron beam gun and the work chamber.

To place EBM in perspective as a precision machining process, it is useful to consider the accuracies to which some geometries can be produced. For example, in producing a beam spot of 0.025–1 mm diameter, the relative position of the beam impact, with respect to the workpiece, can be held within the small tolerance of 0.01 mm. This is, of course, not the ultimate limit of accuracy but the practical limit-

*Steigerwald Strahltechnik GmbH, Munich, Germany.

ations of EBM equipment that is currently available and already in production use. Development work is aimed at reducing these dimensions to permit machining in the micron (0.001 mm) range.

Details of specific or general electron beam machines will not be discussed in the paper. Its main purpose is to show some basic characteristics of applications suitable for electron beam machining. In this sense, the electron beam as a tool affects a *workpiece* to produce a permanent change in it, but the beam does not act as a probe to measure or display properties of a *testpiece*. The beam, a radiation of accelerated charged particles, can affect a workpiece in very different ways. The technician must control the beam's special characteristics so that it performs as a tool. The electron beam machine is not just a mechanical system, it must also control the properties of the beam to enhance its function as a cutting tool. This EBM system includes sophisticated numerical control; also components can be exchanged so that the machine accommodates the full range of EB machining applications.

CHARACTERISTICS OF ELECTRON BEAM MACHINING AND ITS APPLICATIONS AS A THERMAL TOOL

Basic features of the thermal tool

Electron beam precision machining mainly depends on the very high current density within the beam. At impact, the kinetic energy of the accelerated electrons immediately changes to thermal energy that heats the material. Consequently, the effect of this treatment depends on features of the beam and also physical properties of the affected material. The intense local heating of the target produces different phenomena depending on the properties of the material.

Usually, because the beam has a high power density, the different properties of the materials have little effect. Each shows the same fundamental characteristics during the impact with the electron beam. This is true especially for metallic materials and ceramics and also for some plastics. In this paper we will deal mainly with metallic materials.

Significantly different results can be obtained by controlling the power density distribution, the size of the impact spot, and the time duration that the beam affects the workpiece. In the case of electron beam welding, material is melted and allowed to cool rapidly. In this case every surface element in the weld is affected by the beam for a relatively long time, 10–100 ms for a spot diameter of about 0.1 mm. Hence, the thermal energy is conducted from the point of beam impact to the surrounding material, thus causing an expansion of the molten pool and producing the characteristic weld seam. For so-called 'deep welding', the formation of vapour capillaries that deeply penetrate the workpiece, is important. The beam produces a plasma whose vapour pressure holds the capillaries open; along these capillaries the electron beam energy reaches far into the workpiece. We can figuratively regard it as a linear heat source

being drawn across the workpiece. This is sometimes referred to as 'dagger' penetration. Because electron beam welding is a well-known technique, we do not want to go into more detail but one aspect is important. A channel opens before the beam and closes as it passes. Alternatively, it can be described as a hole that moves along the workpiece together with the electron beam. Molten material surrounds the beam.

The effect is different with very short electron beam pulses. Because the formation of vapour capillaries is immediate, the electron beam melts a cylindrical area of the workpiece. As a result of the high power density within the beam the vapour pressure in the vapour capillaries increases so rapidly that material is ejected in sudden bursts. The shape of the ejected material, termed 'spatters', shows that the major part of it is molten. Only a small percentage is heated to vaporisation temperature. Thus, because the beam is pulsed material is ejected so that a hole is formed.

After this, that is 'shooting' the hole, the beam is switched off immediately. The beam duration (pulse width) is normally of 5–500 μ s, but in some cases up to 5 ms depending on material thickness and hole diameter. Within this short period at high power density, heat dissipation is very localised; the basic material is practically unheated, certainly less than required for it to reach a transition temperature. Using this single pulse drilling (in mass production called EB perforation), a very thin layer is produced at the hole surface. This is material expelled from the hole when molten and then solidified again, (recast layer). The parent material (matrix) in the immediate vicinity of drilling is exposed only to a very rapid temperature cycle with low peak temperature.

Here we have described the first material removing or detaching electron beam process. EB drilling, machining or milling, as it is called, is the opposite of EB joining, that is EB welding.

Single pulse drilling or EB perforation is limited at the moment to round holes of cylindrical or tapered shapes. Sometimes, trumpet shapes are obtained. The larger diameter of a hole is at the beam entry to the workpiece.

In addition to single pulse drilling there is another technique called multipulse drilling. Holes or slots of various sizes and shapes are milled, cut or machined by repeated beam pulses and by maintaining the same spot position for every pulse. Control of beam deflection and triggering the beam pulse is programmed. Hole shapes can be produced repetitively to close tolerances by suitable processing. The power density for multipulse machining is one order of magnitude greater than for single pulse drilling.

The technique used for engraving and cutting thin films is basically different from EB drilling. By using a beam of high power density, but of short duration, direct sublimation of the material occurs. The material is evaporated directly from its solid state without passing through the fluid phase. The power density in relation to the affected volume of material is important and hence, the acceleration voltage of the electrons is reduced to 10–40 kV. The short duration of the beam avoids melting of material by heat dissipation.

Materials

What type of material can be machined by the electron beam? As already discussed, metals are readily machined. Not only electric conductors can be electron beam machined, however: it is also possible to treat insulating or semi-conducting materials. Ceramics, glass, silicon, and even plastics have been electron beam drilled.

While the basic principles of processing, as described, are the same for all materials the exact effect of the beam depends on the material properties. Clearly the thermal properties of the material are important; equally important are mechanical, crystallographic, and metallurgical properties. Thus, to optimise an electron beam machining process both the beam working parameters and workpiece characteristics must be considered. They must be made mutually compatible.

Control of the electron beam

The electron beam consists of a radiation of high velocity lightweight particles; it is this that permits its precise and fast control. The power distribution and path described by the beam spot are simple to control. The electrons have speeds of 1/3 that of light at about 150 kV accelerating voltage. Therefore, the electron beam follows changes of electric and magnetic fields practically free from lag.

Thus, we have an inertialess tool that can be favourably controlled free from lag. Since the machining speeds are very high because of the high power density in the beam, it is impractical to control manually. Neither optimised values of machining parameters nor repeatability are possible with manual control. Only precise control of electron beam processing will reveal all its possibilities and advantages. This idea, although new, has been used in applying electronic control to EB machining and EB welding machines. These have been fitted with NC systems controlling the speed and position of the work table.

During recent years, the Steigerwald group in Munich succeeded in using a programmed computer to numerically control electron beam equipment. To do this it was necessary to find a suitably fast computer and also to develop and construct an interface linking the computer to the control components of the equipment. Both the beam parameters and the movement of the workpiece are controlled directly by the computer. What is new about the NC organisation of these computer-controlled machine tools is that the workpiece motion and the beam are simultaneously controlled. In this way, any momentary deviation of the worktable speed and position (lag error) can be corrected immediately by the timing of the beam impulse. The relative position of the beam spot relative to the workpiece is kept within small tolerances. A linear incremental encoder enables the NC system to compare by a feedback the actual and nominal position of the worktable. Also accuracy is not influenced by tool forces as previously discussed. The numerically controlled Steigerwald EBM equipment, as shown in Fig. 1, comprises not only the control of the relative position between workpiece and beam, but also other working parameters are controlled, using additional computer channels,

according to preselected workpiece positions. In particular the beam current and focusing are controlled by the computer, as shown in Fig. 2. A fast computer must be used to control these many functions of electron beam machining simultaneously and with adequate speed. At present, we are using a computer with 1.5 μ s cycle time that controls the complete equipment via 256 external addresses. We carry out continuous or even dotted treatment while the workpiece is either stationary or moving. This NC system is used for electron beam welding equipment as well as for EBM equipment. Every welding curve or hole array can be programmed.

APPLICATION EXAMPLES

The following are examples of the electron beam precision machining methods we have described that demonstrate their industrial use. The power density and duration of the beam for different applications are shown graphically in Fig. 3.

Micro electron beam welding with numerical control

To stabilise a satellite in its orbit small thrust nozzles are needed that control by pulsed propulsion. On the basic part of these jet-propulsions units a number of fine welds have to be performed on areas of limited access. These workpieces are very expensive because of the pre-processing prior to welding. For this reason, a reliable production electron beam machine was needed, but designed with flexibility to accommodate different applications and to permit quick changes of working parameters to achieve the repeatability and tolerance standards developed for each application. Such a performance guarantee could be achieved only with numerically controlled equipment. A particular advantage of this equipment is that because the worktable and beam are automatically controlled many seams can be welded in succession without taking the workpiece out of the chamber.

Formerly it was necessary to fit the workpiece to a rotating fixture and make adjustments for every single circular weld. Now, circular welding can be carried out on different areas of the workpiece with different diameters and welding data as a continuous process. In this way it was possible to rationalise small batch production of different very valuable workpieces. This approach also had the advantage that the production work paid the running costs of our machine, while more time was available for other development work.

Electron beam perforation

As a first example of the material removing electron beam processes we would like to discuss electron beam perforation. Short beam pulses can be triggered in a rapid sequence by the computer. The computer receives incremental position signals from the measuring system of a continuously moving table or manipulator. Every time a programmed position is reached by the workpiece, a beam pulse is immediately triggered and a hole drilled at that position. This can be performed at extremely high speed so that, depending on individual aspects of the fabrication, up

to 3,000 holes per second can be 'shot' at precise locations. Screen printing cylinders, their designs formed by a pattern of electron beam drilled small holes, are shown in Fig. 4. Blind holes may be produced that are precisely controlled in size and depth; thus, it is possible to electro-engage intaglio cylinders using the electron beam. There are other application examples in jet engine engineering; these will be considered separately.

Electron beam perforation is applied not only where other processes fail but also where it is economically superior to the conventional processing methods. This applies for example, in the perforation of large drying drums for the paper producing industry, or large centrifuges for the sugar industry. Electron beam perforation produces 'semi-products' that were unknown until now, for example, perforated sheets of tungsten, tantalum and lead. Electron beam perforation, precisely controlled as it is, can be used to mark tapes for permanently recording information. A micro section of tapered electron beam perforated holes is shown in Fig. 5.

Electron beam drilling and cutting

Semi-products that can be made by the multipulse technique are gas burner nozzles. These have very fine holes, slots, or crosses that are needed to burn natural gas, which is replacing manufactured gas supplies. Stoves using gas with higher calorific power, must have new burners with very narrow gas passages. Automatic control, speed and quality in making the nozzles are of vital importance. Another example of applied multipulse drilling is the production of very deep, small diameter holes in materials that cannot be machined mechanically. Micrographs of multipulse electron beam drilled holes are shown in Fig. 6.

In a large number of applications, EBM (electron beam machining) is superior to the ECM (electrochemical machining) and the EDM (electrodischarge machining) because of its much higher working speed and high flexibility.

Electron beam engraving

Engraving is an EBM application that has recently become of interest. In this paper we are concerned mainly with engraving fine traces in vapour-deposited metal layers, or in strips of printed conductors and resistors. The field of application lies in the 'thin-film' and 'thick-film' techniques of the electronic industry for producing integrated or hybrid circuits. Programmed, the electron beam can engrave a complex pattern in an extremely short time. It is possible to engrave either by scanning, or by following each line. In this way, circuits can be mass produced, individual circuits can be made, or already existing circuits with passive elements can be calibrated. Examples of engraving are shown in Fig. 7.

A very sophisticated application is the filamentation of superconductor tapes. Superconductor coils are made from tapes that have a tin superconducting layer around the normal conducting core. Since second order superconductor coils are not intrinsically stable, their current carrying capacity is limited. To increase the possible magnetic field strength, the superconducting layer is separated in filaments that are formed by EB engraving or remelting.

ELECTRON BEAM: ADEQUATE DESIGN

The main concern of the application engineer is to receive pertinent enquiries and obtain viable applications for new innovations. Usually he is doomed, if the innovation is sought only as a substitute for conventional methods, to provide better results at lower costs.

The full advantage of a new technology (we should consider EBM as such a new technology) cannot be achieved if the production engineer alone asks for the electron beam. The designer also must have a clear understanding and vision for the possibilities of this uncommon tool. Both designer and production engineer must think about production methods and consequently must be well-informed about 'electron beaming'. They must be competent to judge the possibilities and evaluate the electron beam for their own use. In this context the following should be considered:

- Improved product performance.
- Reduced fabrication cost.
- Reduced material.
- Lighter component.
- Improved design.
- New products.

Each of these factors may open a new market. There are examples where several factors were combined to greater advantage.

Example 1. The designer relies on EB welding. He avoids riveted joints and saves weight. He asks for HSS steel welded to a tough steel tape and gets a cheaper, more reliable saw tape.

He designs a complex component in nimonic as a welded structure and saves time and costs of machining.

He knows that three or more welds underneath can be replaced by an EB weld and so designs a closed structure with inside reinforcement.

Example 2. The designer is convinced of EB perforation. He knows that a high hole density can be perforated into a 2 mm-thick sheet of refractory metal oblique to the surface and so improves the performance of a cooling system. At the same time he learns that the cooling component can be simplified so that it can be drawn, shaped and welded instead of cast and machined. Thus, he is able to save costs and time, achieving equal or advanced performance.

He is committed to make a diaphragm with high porosity in material resistant to both acids and bases. He chooses perforated tantalum and obtains the additional advantage that the electrolytic cell can be designed narrower.

It is impossible to give a complete list of examples for EBM. The people who are developing and constructing EB machines cannot envisage all possible applications. Consequently, it is the purpose of this paper to give a general impression of what can be done with the electron beam as a manufacturing tool. The electron beam is a multi-role tool for welding, perforating, drilling, cutting and engraving.

SUMMARY

The electron beam is a multi-role thermal tool. It can be used for electron beam welding (EBW) and electron beam machining (EBM) comprising perforation, drilling, cutting and engraving. Additionally, the electron beam is applied to the heat treatment of materials, to radiation-induced polymerisation of monomer paints, and to electro-resistant methods. EBM machine tools with numerical control (NC) are available. Their NC organisation enables a fast computer to control both the workpiece motion and the EB parameters in mutual correlation. This EB machine tool is flexible, but guarantees precise repeatability provided the workpiece has constant features. Consequently, this universal type of EBM

machine can be used favourably for research and development work as well as for small-batch production. The EB processing competes with or substitutes conventional methods such as TIG welding, ECM, EDM, mechanical machining, and so on. Its advantage is speed, accuracy, flexibility and reproducibility.

In many cases the electron beam is the only (or at least the best) tool technically capable of a production task. In other cases it is economically superior. This is true especially when the component design demands the special capability of the electron beam process.

With the aid of the electron beam, semi-products can be manufactured, such as bimetal and trimetal strips, and perforated sheets in exotic materials; and strips with narrow slots.

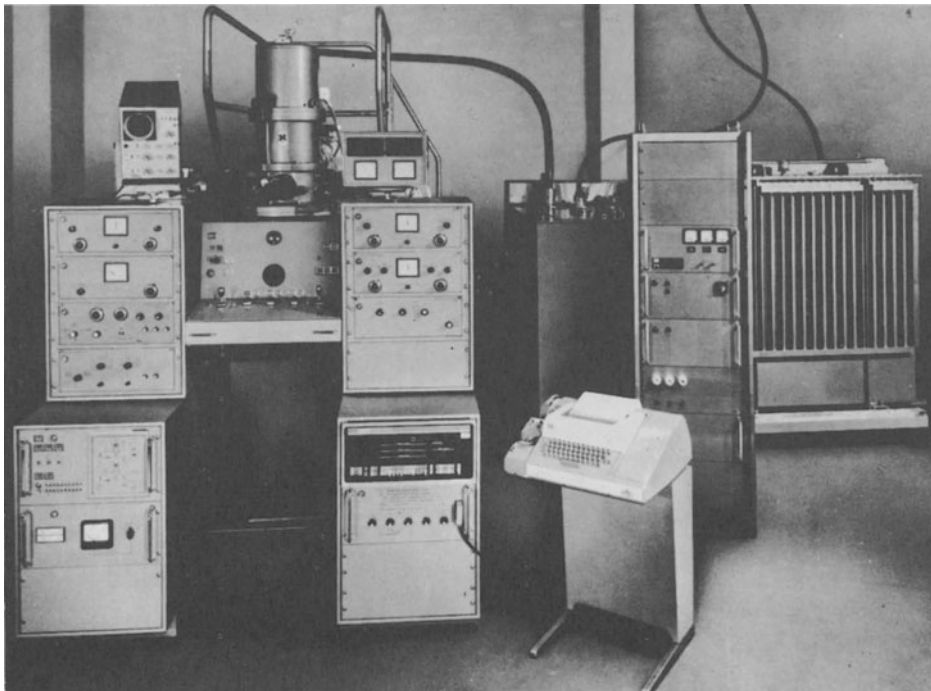


Fig.1 EBM 10/4 equipment for precise electron beam machining (EBM) with numerical control. Components from right to left: high voltage tank, high voltage control, auxiliary voltage tank (bias and filament heating), teletype and computer with interface, EB gun, control desk and rack in front of the chamber.

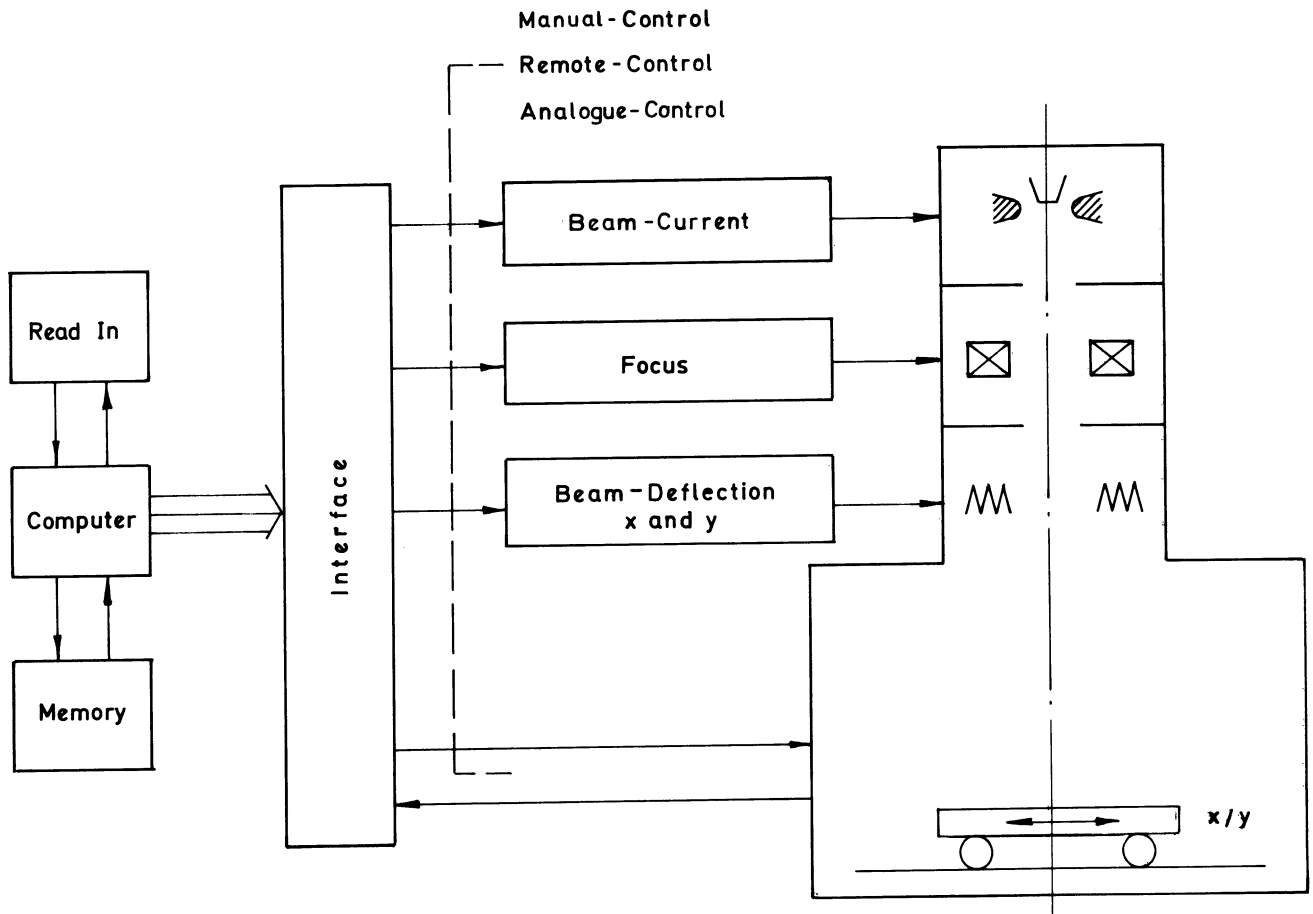


Fig. 2 Block schematic diagram of the organisation of a NC-system for EB machine tools.

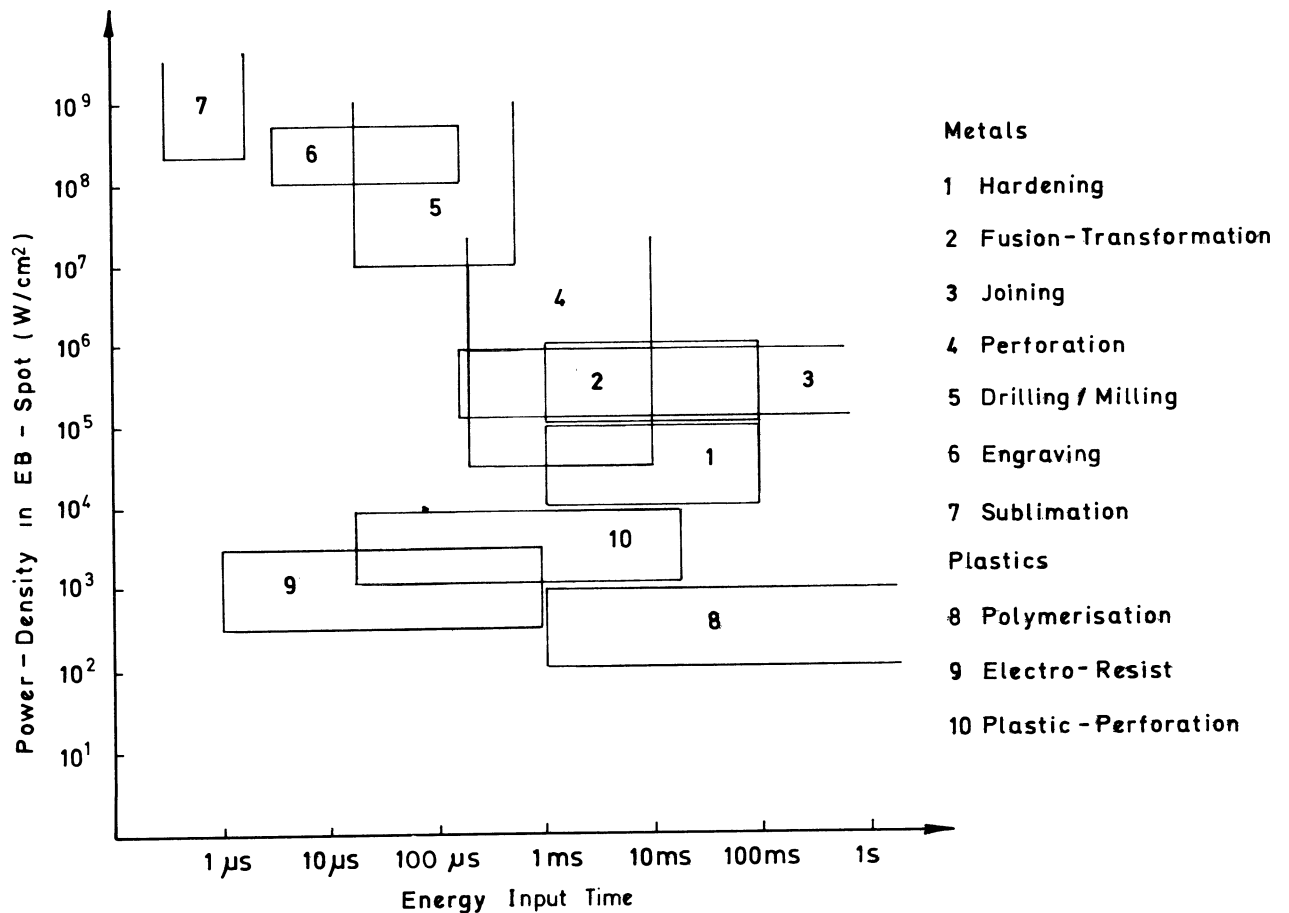


Fig. 3 Graph showing various kinds of EB applications with respect to power density of 'the spot' and effective period.

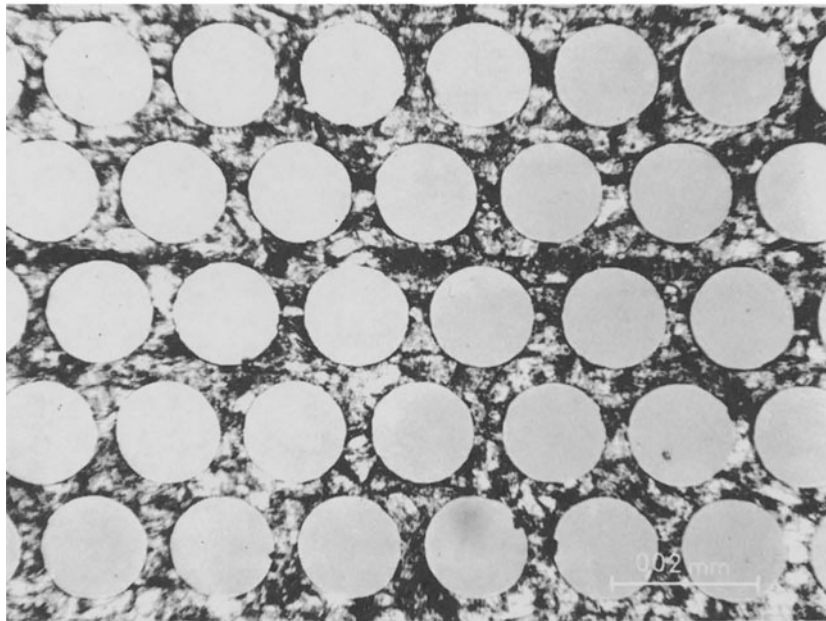
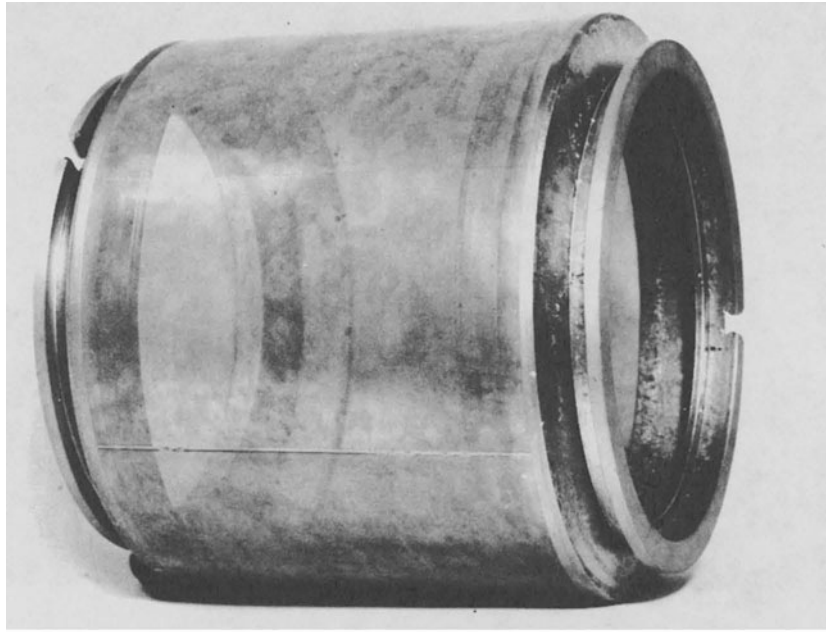


Fig. 4 Cylinder for screen printing made out of EB-perforated stainless steel sheets
 (a) Testpiece of an EB-perforated screen printing cylinder. It was made out of stainless steel sheets 0.1 mm thick welded together by EB. One of these welds has been perforated afterwards.
 (b) Section of an EB-perforated stainless steel sheet

thickness	0.080 mm
hole diameter	0.130 mm
spacing	0.170 mm
grating	150 mesh
transparency	50%
drilling time	20 μ s/hole

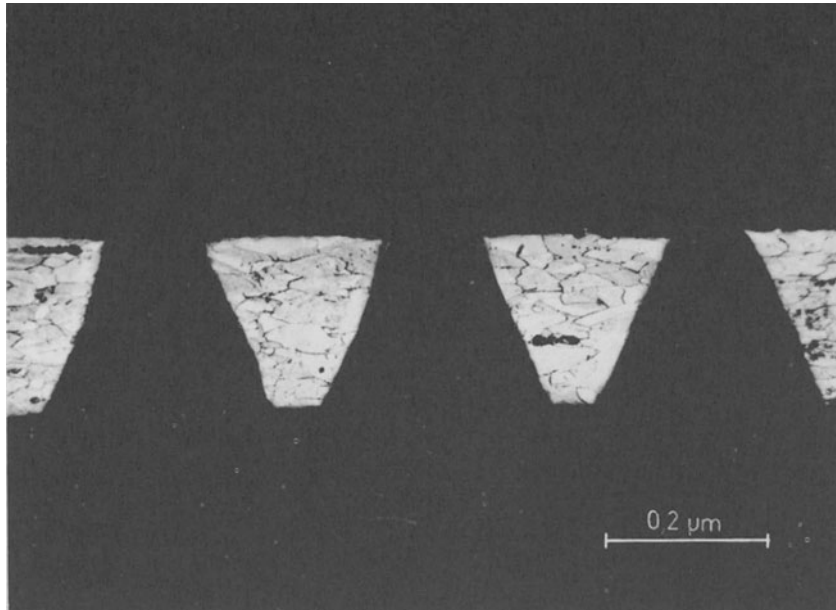


Fig. 5 Grinding micrograph of a cross-section with EB-perforated tapered holes.
Material is Nimonic 90, 0.2 mm thick
hole diameters: max. 280 μm
 min. 110 μm
drilling time: 30 μs/hole

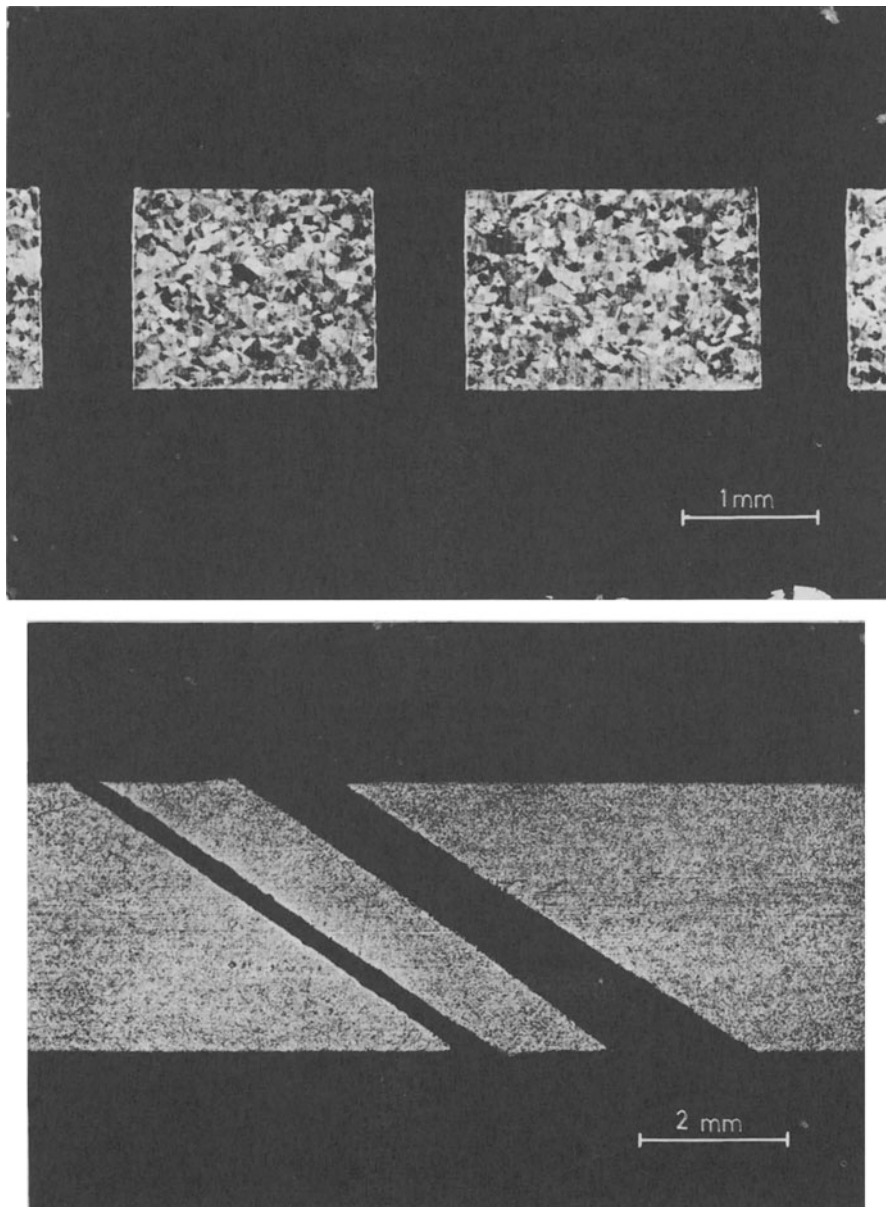
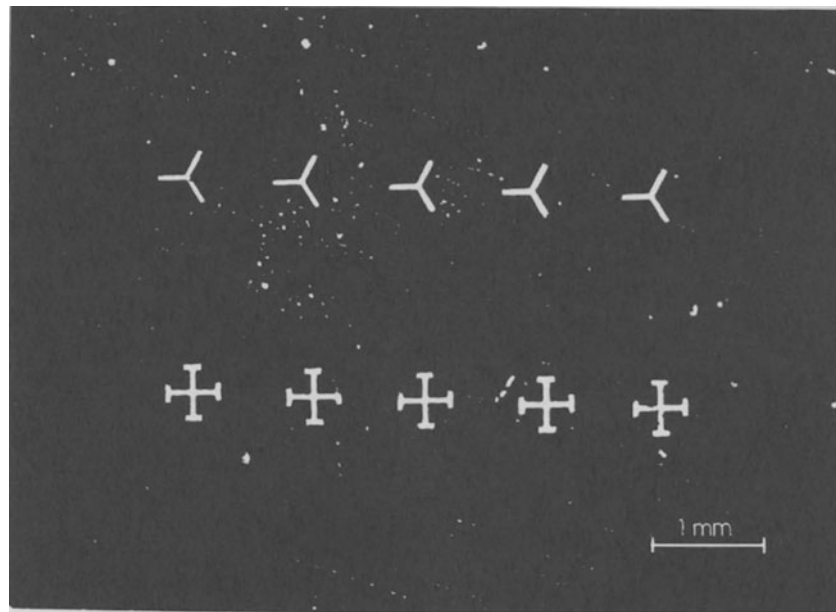


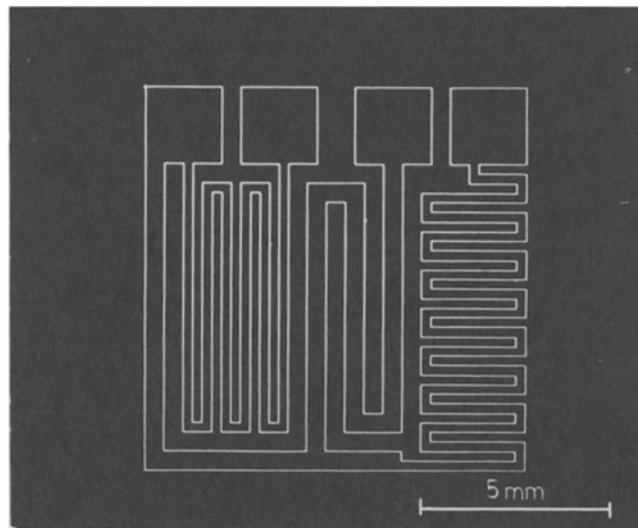
Fig. 6 EB-drilled holes

Grinding micrographs of cross-sections with EB-drilled holes. EB drilling was performed by multipulse and controlled EB deflection

- (a) Inconel 600 sheet, 1.5 mm thick, every hole pierced in 5 s. A thin recast layer covers the matrix which shows no heat induced alterations.
- (b) Nimonic sheet, 3.3 mm thick, with oblique holes (35° to the surface), one being pierced by some pulses without deflection, and the other drilled with circular deflection. Drilling time: 1.5 and 5 s. The edges of the orifice are very sharp.



a.



b.

Fig. 7 EB Cutting and engraving

(a) Micrograph of EB-cut crosses in 0.1 mm thick stainless steel.

(b) Micrograph of EB-engraved contours.

Pattern of a microcircuit with resistors. Vapour-deposited copper 1200 Angström thick on a quartz substrate. The contours were 'written' by the EB probe with a speed of 1 m/s. Positioning and EB deflection were controlled by a computer.

DISCUSSION

Query from C. F. Noble, UMIST

Do the Steigerwald Co. believe that the direct coupling between computer and electron beam machine has advantages in extending the general use of the process, or will applications be restricted to the specialised industries who, for purely technical reasons, rather than economical ones, must make use of its features.

Reply

We have already found that driving an electron beam machine by computer improves the usefulness of the equipment in general and our present range of

machines includes computer control as a standard option.

The three main advantages are:—

- (a) The computer smooths-out workpiece movement irregularities, giving much improved accuracy without unduly increasing the machine cost.
- (b) The need for computer skill is avoided and highly reproducible results guaranteed.
- (c) The need for complex tooling is removed and substituted for by a programmed tape. The designer can therefore change his requirements without thereby causing a delay to production while new tools are made. At the same time the cost of the new tools is avoided by the considerable lower cost of a modified programme tape.

Query from M. Rogers, British Aircraft Corporation, Stevenage.

- (1) What is the maximum thickness of material that has been drilled by this method so far, and the minimum and maximum diameter of holes obtained?
- (2) I assume that for blind drilling the intensity of the beam, and the number of pulses applied, govern the depth of the hole. Therefore, will any variation in homogeneity of a particular material affect the accuracy and repeatability of the operation?

Reply

- (1) Two kinds of EB-drilling have to be distinguished: multi-pulse drilling with controlled EB-deflection and single-pulse drilling (EB-perforation technique).
- (a) Multi-pulse drilling
 maximum depth: 15 mm
 ratio of depth/diameter up to 30:1

- | | |
|--|----------|
| minimum diameter (thin sheets) | 0.025 mm |
| maximum diameter (sheet of 2 mm thickness) | 2 mm |
- (b) Single-pulse drilling
 maximum depth: 6 mm
 ratio of depth/diameter up to 10:1
 minimum diameter (obtainable at ratio 1:1) 0.025 mm
 maximum diameter 1 mm

These figures refer to EB-milling of metal sheets. They may be applied to plastics as well, with some restrictions.

- (2) The EB-drilling is a material-removing EB treatment. It is a thermodynamic process depending both on the EB parameters and the thermal properties of the material. Thus, variation in homogeneity of a particular material may affect the repeatability of EB-engraving blind holes. Generally, blind holes are made by one single-pulse. The depth of the blind holes is governed by the energy density within the EB impact spot and the pulse width.

HYDRAULIC APPROACH TO ELECTROLYTE FLOW IN ELECTROCHEMICAL MACHINING

by

S. ITO and K. SEIMIYA*

SUMMARY

The inception of cavitation at a singular point where flow direction abruptly changes in parallel flow and the influence of concentration boundary layers on flow rate are analysed by hydraulic method and experimentally examined. The main results are as follows.

1. The local pressure head losses play an important role in turbulent flow on the inception of cavitation. The pressure head losses due to presence of cavitation bubbles are derived.

2. The recovery of flow rate and the change of skin friction coefficient after interruption of machining current depend on IC/Q , where I is machining current (A), C volumic evolution rate of hydrogen gas ($\text{cm}^3/^\circ\text{C}$), and Q volumic flow rate of electrolyte (cm^3/s).

INTRODUCTION

There are many theoretical and experimental researches on the electrolyte flow between electrodes and the gap thickness in electrochemical machining^{1, 2}. Inception of cavitation in a radial flow from a round or slit nozzle has been observed³.

Even in a parallel flow, cavitation is expected to occur at a singular point where flow direction abruptly changes. On the other hand, electrolytic products yielded during ECM such as metallic ions, oxides and hydroxides on the anode and hydrogen bubbles on the cathode form concentration boundary layers as they are carried away by the electrolyte flow. The boundary layers influence flow rate resulting in change of gap thickness.

In this report parallel flow leading to the inception of cavitation is theoretically and experimentally analysed, and the influence of concentration boundary layers on electrolyte flow rate is also investigated by hydraulic method.

HYDRAULIC ANALYSIS

Notation

$P(\lambda)$	pressure head loss due to friction (kg/cm^2)
$P(\xi)$	local pressure head loss due to abrupt change in sectional area of flow passage at the inlet or outlet (kg/cm^2)
$P(\zeta)$	local pressure head loss due to change of flow direction (kg/cm^2)
P	static pressure (kg/cm^2)
$P(d)$	dynamic pressure (kg/cm^2)
b	gap width (5 mm)

g	acceleration of gravity ($= 980 \text{ cm}/\text{s}^2$)
h	gap thickness (mm)
l	gap length (mm)
m	hydraulic mean depth (mm) $[= b \cdot h/2(b+h)]$
w	mean velocity across the section (cm/s)
ξ, ζ	loss coefficient
κ	a constant depending on shape and size of flow passage
λ	skin friction coefficient
ρ	density of electrolyte ($= 1.07 \text{ g}/\text{cm}^3$)
θ	angle of change in flow direction

Subscripts

i, o values at inlet and outlet, respectively
 $1, 2, 3, 4$ values at AB, BC, CD, and DE, respectively
 B, C, D values at B, C, and D, respectively
 I, II , values before and after stopping both current and feed, respectively

Hydraulic losses

Let us consider the configuration of the equilibrium gap as shown in Fig. 1a. The wedge of the tool is a right angle and 2.25 mm high.

The assumptions are as follows.

1. Local pressure head losses occur at the limited places near the changing points of shape and size of flow passage.

2. Electrode gap thickness is kept constant on a part of the tool surface, AB, etc.

3. The influence of hydrogen bubbles produced by electrolysis is negligible.

4. Hydraulic laws derived for large scale flow passage remain in this case.

*Government Mechanical Lab., Japan.

Hydraulic losses are given by the following equations

$$P(\lambda) = \frac{10^{-3} \cdot \rho}{2g} \sum_{j=1}^4 \frac{l_j \cdot \lambda_j w_j^2}{4m_j} \quad (1)$$

$$P(\xi) = P(\xi)_i + P(\xi)_o = \frac{10^{-3} \cdot \rho}{2g} (\xi_i w_i^2 + \xi_o w_o^2) \quad (2)$$

$$\begin{aligned} P(\zeta) &= P(\zeta)_B + P(\zeta)_C + P(\zeta)_D \\ &= \frac{10^{-3} \cdot \rho}{2g} (\zeta_B w_B^2 + \zeta_C w_C^2 + \zeta_D w_D^2) \end{aligned} \quad (3)$$

ζ is given as follows

$$\zeta = \kappa \sin^2 \frac{\theta}{4} \quad (4)$$

In the presence of cavitation, there is a relationship between supplied pressure head ΔP and pressure head losses as

$$\Delta P = P_i - P_o = P(\lambda) + P(\xi) + P(\zeta) + P(\text{cav}) \quad (5)$$

where $P(\text{cav})$ is pressure head losses due to presence of cavitation bubbles. $P(\text{cav})$ is supposed to represent intensity of cavitation.

Static pressure at the top of wedge-shaped tool, P_c , is calculated by the following equations

$$\begin{aligned} P_c &= P_i - P(\xi)_i - P(\lambda)_1 - P(\zeta)_B - P(\lambda)_2 \\ &\quad - P(\zeta)_C - P(d)_c \end{aligned} \quad (6)$$

$$P(d)_c = \frac{10^{-3} \cdot \rho \cdot w_c^2}{2g} \quad (7)$$

Cavitation parameter K_c is defined as

$$K_c = \frac{P_c - P_v}{P(d)_c} \quad (8)$$

where P_v is saturated vapour pressure (kg/cm^2). Cavitation parameter K_c , for the critical condition of back pressure in the inception of cavitation, is called the incipient-cavitation parameter.

Increase in skin friction coefficient

Equation to give total head losses ΔP in Fig. 1b is

$$\Delta P = P_i - P_o = \frac{10^{-3} \cdot \rho \cdot w^2}{2g} \left(\frac{\lambda}{4m} + \xi_i + \xi_o \right) \quad (9)$$

Then, the increase of skin friction coefficient $\Delta \lambda$ is calculated as

$$\Delta \lambda = \lambda_I - \lambda_{II} = \frac{4m}{l} \frac{2g}{10^{-3} \cdot \rho} \left(\frac{\Delta P_I}{w_I^2} - \frac{\Delta P_{II}}{w_{II}^2} \right) \quad (10)$$

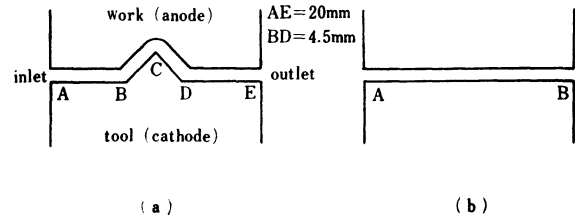


Fig. 1 Configuration of the equilibrium electrode gap during ECM.

INCEPTION OF CAVITATION

Experimental method

Fig. 2 shows a schematic diagram of experimental apparatus. An ECM cell was so designed that the electrode gap was photographed through a transparent acrylic acid resin plate as shown in Fig. 3. A wedge-shaped tool electrode of right angle as shown in Fig. 1a was used. The workpiece was pure iron bar with a cross section of 5×20 mm. The electrolyte was 10 wt% sodium chloride solution. Experiments were performed under the conditions of supply voltage 15 V, tool feed rate 1.1 mm/min and electrolyte supply pressure (inlet pressure) $16 \text{ kg}/\text{cm}^2$. Back pressure was varied from 1 to $12 \text{ kg}/\text{cm}^2$. Therefore the electrolyte flow was turbulent ($Re = 8 \sim 20 \times 10^3$). The pressures and temperatures at the inlet and outlet were measured with Bourdon's tube type pressure gauges and thermister thermometers, respectively. The electrode gap was photographed during ECM to clarify the inception of cavitation. The electrode gap thickness was measured on the photograph with a comparator.

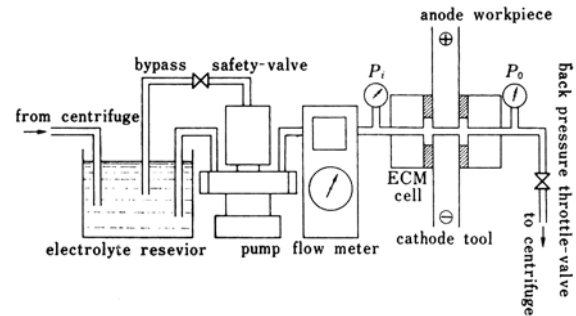


Fig. 2 Schematic diagram of experimental apparatus.

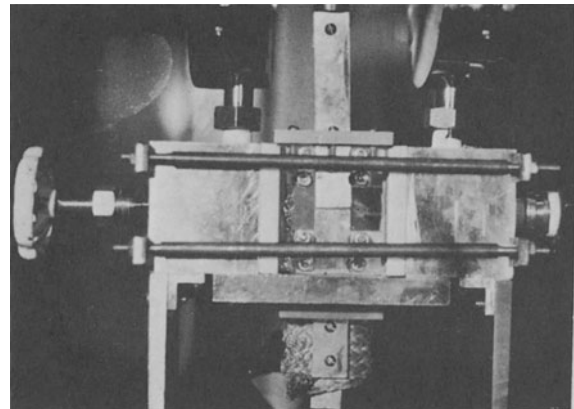


Fig. 3 Photograph of ECM cell.

Results: pressure head losses

Table 1 shows the calculated values $P(\lambda)$, $P(\xi)$, $P(\zeta)$ for $\lambda = 0.05$, $\xi_i = 0.3$, $\xi_o = 1.0$, $\kappa = 9.5$. Then $P(\text{cav})$ is derived from the following equation:

$$P(\text{cav}) = \Delta P - P(\lambda) - P(\xi) - P(\zeta)$$

The value of $P(\text{cav})$ decreases with increase in the back pressure as shown in Table 1. On the other hand, it is confirmed from the experimental results described in the following section that the cavitation area is reduced by increasing the back pressure. So $P(\text{cav})$ is concluded to be important in the evaluation of cavitation. Comparing the value $P(\lambda)$ with those of $P(\xi)$ and $P(\zeta)$, we can conclude that the local pressure head losses play an important role in ECM under the turbulent flow condition.

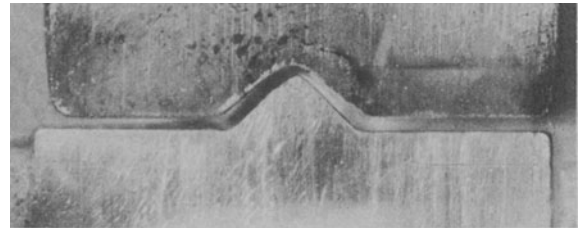


Fig. 4 Equilibrium electrode gap in which cavitation occurred.

Table 1. Pressure head losses (kg/cm^2)

No.	P_0 (kg/cm^2)	$P(\lambda)$	$P(\xi)$	$P(\zeta)$		$P(\text{cav})$
				$P(\zeta)_C$	$P(\zeta)_B + P(\zeta)_D$	
(1)	1	3.2	2.6	3.2	0.9	5.2
(2)	3	3.0	2.7	3.3	0.9	3.2
(3)	4	2.6	2.8	3.3	0.9	2.4
(4)	6	3.0	2.9	3.0	1.4	0.6
(5)	12	1.1	1.1	1.4	0.4	0

Incipient-cavitation parameter Table 2 shows the calculated values of cavitation parameter. The incipient-cavitation parameter for this case is estimated as approximately 3 from the observation of the photographs.

Table 2. Estimation of cavitation parameter

No.	P_0 (kg/cm^2)	$P(d)_C$ (kg/cm^2)	P_C (kg/cm^2)	K_C
(1)	1	4.1	6.1	1.7
(2)	3	4.1	5.9	1.7
(3)	4	4.2	5.9	1.7
(4)	6	3.8	6.7	2.0
(5)	12	1.7	11.7	7.4

Effect of back pressure Fig. 4 shows a photograph of the equilibrium electrode gap, in which cavitation occurs at the top of the wedge-shaped tool. Cavitation bubbles form a white layer in the photograph. The cavitation area corresponds to the terrace on the machined surface. It is confirmed from the observation of these photographs that the cavitation area becomes reduced with increasing back pressure. The critical value of the back pressure at which cavitation vanished was approximately $8 \text{ kg}/\text{cm}^2$.

CONCENTRATION BOUNDARY LAYERS**Experimental method**

Both the experimental apparatus and ECM cell were the same as those shown in Fig. 2. The electrode tool and workpiece shown in Fig. 1b were used.

The theoretical equilibrium gap h_t is derived from the following equation

$$h_t = 2.21 \cdot \chi \cdot (E - E_o) / 10\nu$$

where χ = specific conductivity of electrolyte ($\Omega^{-1} \text{ cm}^{-1}$)

E = gap voltage (V)

E_o = overvoltage (V)

ν = tool feed rate (mm/min)

The gap voltage was so selected by using the equation that h_t became an expected value for $E_o = 1.2 \text{ V}$.

Result and discussion

When the working current and the tool feed are simultaneously stopped during ECM by the same electric signal, the concentration boundary layers of the ECM products suddenly disappear within a few milliseconds. Then the electrolyte flow rate gradually increases until it reaches a new equilibrium. If the assumptions are allowed that the disappearance of the concentration boundary layers is regarded as a kind of a step input and that the characteristics of the electrolyte flow system is linear, the flow rate increase ΔQ is described as follows

$$\Delta Q(t) = A \left\{ 1 - \exp(-t/T) \right\}$$

where t = time variable

T = time constant of the flow system

A = a constant

Fig. 5 shows a typical example of the flow rate recorded with a self-recording flow meter. Flow rate recovery ratio ϵ is defined as

$$\epsilon = (Q_{II} - (Q_{II} - Q_I))$$

where Q_I and Q_{II} are flow rates before and after stopping both current and feed, respectively. The flow rate recovery ratio represents the degree of influence of ECM products on the electrolyte flow rate.

Fig. 6 shows the relation between flow rate recovery ratio and machining time τ , when the latter was varied from 15 seconds to 16 minutes for a fixed equilibrium gap $h_t = 0.3 \text{ mm}$. As shown in this figure the influence of ECM products on flow rate increases with machining time.

In the next experiment, h_t was varied at a constant machining time of 3 minutes. The results are shown in Fig. 7 indicating the relation between ϵ and IC/Q , where I is machining current in amperes, C is volumic evolution rate of hydrogen gas ($= 0.116 \text{ cm}^3 \text{ }^\circ\text{C}$). The dimensionless parameter IC/Q represents the mean concentration of ECM products contained in the electrolyte. The experimental result shows a significant relation between ϵ and IC/Q .

Figs. 8 and 9 show the calculated values of $\Delta\lambda$ from the same experimental data as used to obtain Figs. 6 and 7. A linear relationship between $\Delta\lambda$ and IC/Q is apparently recognized from the result shown in Fig. 9.

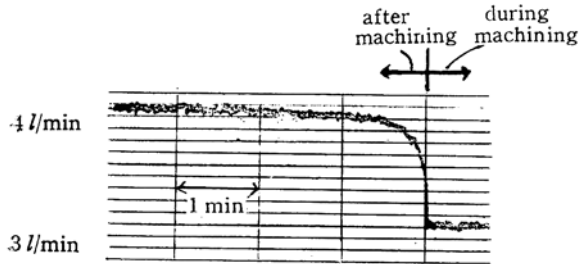


Fig. 5 Electrolyte flow rate recorded by selfrecording flow meter.

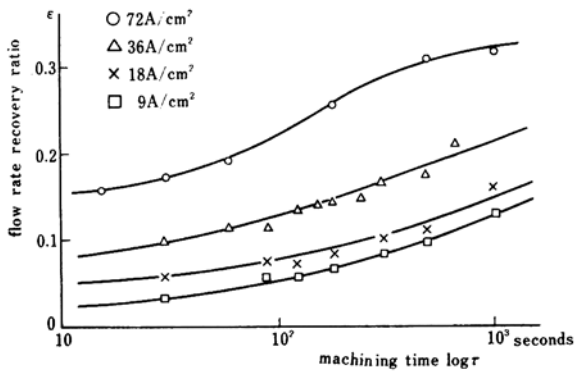


Fig. 6 Dependence of ϵ on machining time.

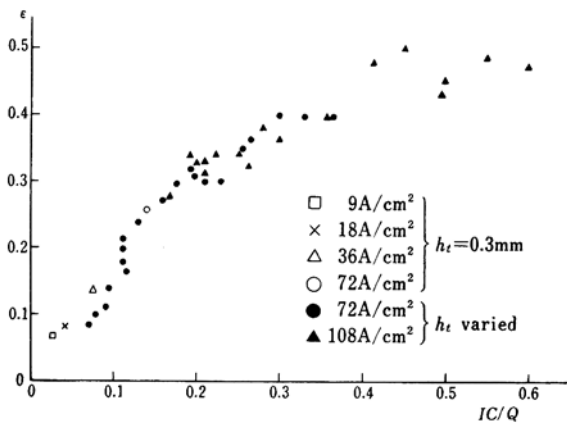


Fig. 7 Relation between ϵ and IC/Q .

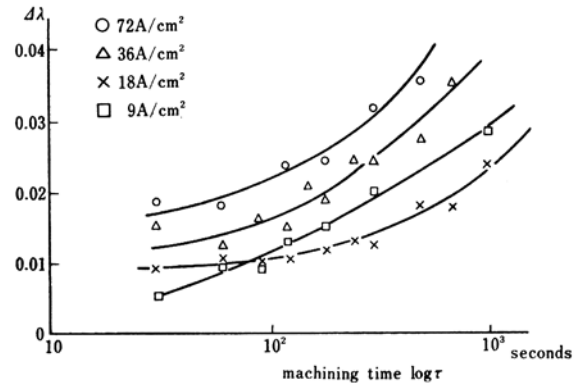


Fig. 8 Dependence of $\Delta\lambda$ on machining time.

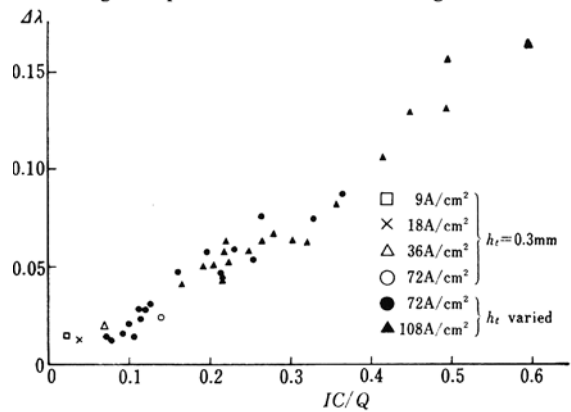


Fig. 9 Relation between $\Delta\lambda$ and IC/Q .

CONCLUSION

Parallel flow leading to the inception of cavitation is theoretically and experimentally analysed, and the influence of concentration boundary layers on electrolyte flow rate is also investigated by an hydraulic method. The main results are as follows.

(1) The local pressure head losses play an important role in turbulent flow on the inception of cavitation because $P(\text{cav})$ depends on them. The calculated value $P(\text{cav})$ represents the intensity of cavitation. The incipient-cavitation parameter in this case is estimated to be approximately 3.

(2) The influence of the concentration boundary layers of ECM products on electrolyte flow rate increases with the machining time because the skin friction coefficient of flow passage increases with the machining time. There is a close relationship between flow recovery ratio and dimensionless parameter IC/Q . Also a linear relationship exists between $\Delta\lambda$ and IC/Q .

REFERENCES

1. HOPENFELT, J., and COLE, R. R., 'Prediction of the one-dimensional equilibrium cutting gap in electrochemical machining', *J. Eng. Ind. (Trans. ASME, Ser. B)*, Paper No. 68, WA/Prod-16 (1968).
2. THORPE, J. F., and ZELKLE, R. D., 'Analytic determination of the equilibrium electrode gap in electrochemical machining', *Intern. J. Mach. Tool Design Res.*, 9, 131 (1969).
3. CHIKAMORI, K., and ITO, S., 'Flow of electrolyte in electrochemical die-sinking', *Bull. Japan Soc. Precision Eng.*, 2-4, 318 (1968).

DISCUSSION

Query from M. M. Sfantsikopoulos, UMIST

Was the centrifuge system used in the experimental set-up effective for the electrolyte cleaning? What are its specifications?

Reply

Yes it was. It was a so-called super-centrifuge, whose speed was 12 000 rpm.

VERTICAL SPINDLE ELECTROCHEMICAL SURFACE GRINDING

by

M. M. SFANTSIKOPOULOS and C. F. NOBLE*

SUMMARY

A short introduction to the operating features of vertical spindle electrochemical grinding is followed by analysis of process electromechanics on the basis of simple dynamic behaviour. Experimental results from grinding tungsten carbide with an 'Abwood' machine are illustrated and discussed in comparison with predicted performance. Side effects which have been observed during research and industrial use are summarized.

NOTATION

b	radial width of wheel rim
C	electrochemical constant = $\frac{k \cdot (V - \Delta V) \cdot \epsilon}{\sigma \cdot F}$
D	wheel diameter
e	grit protrusion height
f_1	set depth of cut or up-feed relative to grit surface
f_{1a}	actual depth of cut
f_2	table feed rate
f_{20}	critical table feed rate
F	Faraday
I	d.c. current
k	conductivity of electrolyte
l	component length (table feed direction)
t	time
L	grinding path length
R_v	material removal rate
V	applied potential
ΔV	sum of electrode potentials plus overvoltages
w	component width (transverse to table feed direction)
x_e	leading equilibrium gap
y	gap distance, wheel bond/workpiece surface
β	dimensionless factor
ϵ	chemical equivalent of workpiece
σ	workpiece density

INTRODUCTION

Since the first electrochemical grinding machines appeared nearly two decades ago, the principal field for their application has been grinding of tungsten carbide. Nevertheless, on the shop floor, electrolytic problems with this material still persist owing mainly to limited research and development. Consequently it

was chosen for study in conjunction with the comparatively new electrochemical grinding configuration upon which the paper is based: that of using the face of the grinding cup-wheel with a vertical spindle and controlled linear table traverse (EVSSG-TT).

Under normal working conditions variables such as type of electrolyte and grinding wheel, workpiece material, size and shape are given for a particular application. The process characteristics are then dependent on applied d.c. voltage, depth of cut and up-feed, table traverse feed, electrolyte flow rate and distribution. With regard to depth of cut, two principles have to be considered which directly affect the process.

With a large depth of cut the process is limited by the leading gap between wheel and workpiece as illustrated in Fig. 1a. This gap is given by the relationship

$$x_e = \frac{C}{f_2} = \beta \cdot e \quad (1)$$

If table feed rate is advanced so that $\beta < 1$ then some degree of mechanical assistance is assured but, if advanced too far, excessive mechanical action and wheel wear will result and x_e may become small enough to cause sparking and arcing resulting in permanent damage to workpiece and wheel. In consequence only quite low feed rates can be used and this allows time for adverse side effects, e.g. overcut, grooving, edge erosion, staining, which will often necessitate a purely mechanical after-grinding operation.

With shallow depth of cut or up-feed, of the order of grit protrusion height as illustrated in Fig. 1b, the limiting feed rate is far less severe and a more flexible process is provided. The discussion and experimental

*Machine Tool Division, Mechanical Engineering Department, UMIST

results reported hereafter are concerned with this type of grinding¹.

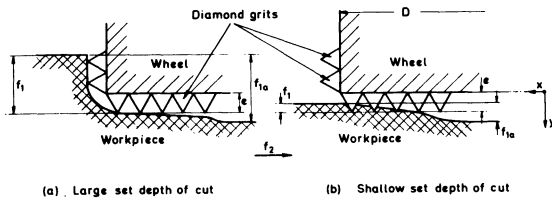


Fig. 1 EVSSG-TT techniques: (a) large set depth of cut; (b) shallow set depth of cut.

PROCESS ELECTROMECHANICS

Depth of cut

The principal features of the vertical spindle surface grinding machine are illustrated in Fig. 1b. Because of electrochemical action the actual depth of cut obtained after the first table stroke f_{1a} will, in general, be greater than the set depth f_1 (although the real f_1 may be less than apparently set because of machine tool flexibility). Considering only ideal electrochemical removal and the fundamental ECM-differential equation² (i.e. $dy/dt = C/y$ when no-vertival feed exists), then an elementary area of workpiece corresponding to a grinding path length L (i.e. grinding time $t = L/f_2$) will be machined to a depth given by

$$f_{1a} = f_1 + \left\{ 2 Ct + (e - f_1)^2 \right\}^{1/2} - e \quad (2a)$$

However, the machining time t varies with component width w as given by

$$t = \frac{1}{f_2} \left[\text{Re} (D^2 - w^2)^{1/2} - \text{Re} \left\{ (D - 2b)^2 - w^2 \right\}^{1/2} \right] \quad (2b)$$

This is illustrated in Fig. 2, exaggerated for the case of width equal to wheel diameter, where the two extremes are coincident with the inside diameter path AB and the central path CD + EF. The respective actual depths of cut correspond to

$$f_{1a, \max} = f_1 + \left[\frac{4C}{f_2} \left\{ b(D-b) \right\}^{1/2} + (e - f_1)^2 \right]^{1/2} - e \quad (3)$$

and

$$f_{1a, c/l} = f_1 + \left\{ \frac{4Cb}{f_2} + (e - f_1)^2 \right\}^{1/2} - e \quad (4)$$

There is a 'critical feed' above which an actual depth of cut equal to set depth of cut is assured, i.e. when $f_{1a} = f_1$ owing to increasing mechanical compensation. From Eqs. (3) and (4) respectively

$$f_{20, \max} \geq \frac{4C \left\{ b(D-b) \right\}^{1/2}}{f_1 (2e - f_1)} \quad (5)$$

and

$$f_{20, c/l} \geq \frac{4Cb}{f_1 (2e - f_1)} \quad (6)$$

For a typical grinding wheel diameter of 8 in with 1 in rim width the ratio between these values is

$$\frac{f_{20, \max}}{f_{20, c/l}} = \left(\frac{D}{b} - 1 \right)^{1/2} = \sqrt{7} \approx 2.65$$

Thus, unless Eq. (5) can be satisfied, transverse flatness cannot be obtained and, following an up-feed cycle at each end of the table traverse, the initial set depth will have transverse variation. Note that, in fact, although a wide component presents an extreme case, the characteristics are further complicated by electrolyte flow and wheel conditions which may counteract or aggravate the situation.

Material removal rate

Considering a typical grinding configuration with the workpiece width smaller than the 'non-conducting' wheel diameter $D - 2b$, it is easy to see that during one table stroke two current waves are developed coincident with the rim on the two halves of the wheel (Fig. 3).

Assuming workpiece feed axis to be that of the central grinding path and workpiece width sufficiently small so that differences in path length can be neglected, then the first d.c. current wave can be evaluated using Eq. (2)

$$I(t) = (V - \Delta V) \cdot k \cdot \int_0^t \frac{w \cdot f_2 \cdot dt}{\left\{ 2 Ct + (e - f_1)^2 \right\}^{1/2}}$$

$$= \frac{w \cdot \sigma \cdot F \cdot f_2}{\epsilon} \times$$

$$\left\{ \left(2C \left[t - \left(\text{Re} \left\{ t - \frac{b}{f_2} \right\}^{1/2} \right)^2 \right] + (e - f_1)^2 \right)^{1/2} \right. \right.$$

$$\left. - \left[2C \left(\text{Re} \left\{ t - \frac{1}{f_2} \right\}^{1/2} \right)^2 + (e - f_1)^2 \right]^{1/2} \right\} \quad (7)$$

The second wave was shown experimentally to be of negligible magnitude compared with the first owing to the considerable increase in electrochemical gap. Material removal, therefore, takes place mainly during the first wave* and, if a mechanical contribution is ignored, rate of removal is given theoretically by

$$R_v(t) = \frac{\epsilon}{\sigma \cdot F} \cdot I(t) \tag{8}$$

which, for $t \leq 1/f_2$, is simplified to

$$R_v(t) = w \cdot f_2 \cdot f_{1a}(t) \tag{9}$$

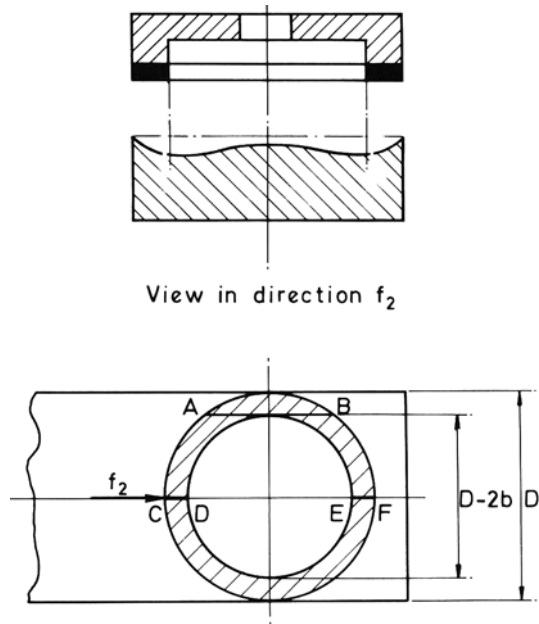


Fig. 2 Grinding path effect.

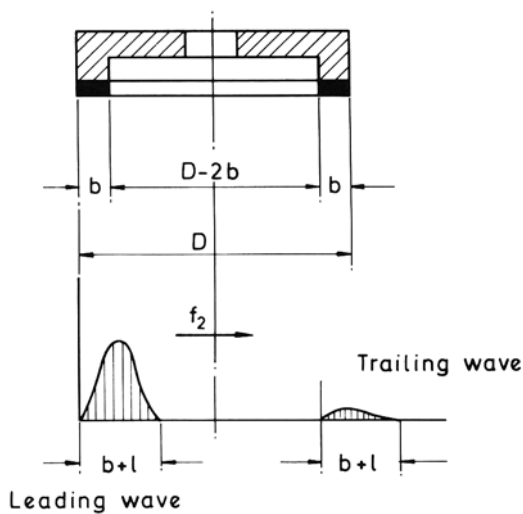


Fig. 3 Leading and trailing current waveforms.

*With EVSSG-TT the operative proportion of each table stroke is in general smaller than with other ECG methods. In the present case the proportion is approximately 1:9 and must be taken into account when making comparative assessments.

EXPERIMENTAL INVESTIGATIONS

Tungsten carbide inserts ISO grade K20, $3/4 \times 3/4 \times 3/16$ in³ were ground on an Abwood vertical spindle electrochemical surface grinding machine tool, model SG4HE, using 7.5% NaNO₂ + 2.5% NaNO₃ aqueous solution electrolyte and a metal bonded diamond cup-wheel (grit size 120, concentration 50, 8 in diameter by 1 in rim) revolving at 3000 rev/min.

Current waves developed during machining are compared in Fig. 4 with those calculated from Eq. (7). The general shape is in agreement but the power source used did not provide automatic voltage control and to make comparison more realistic the experimental curve in Fig. 4 has been corrected, i.e. $\Delta V_R = 0$. Many reasons may be attributed to the deviation from ideal conditions which still remain, e.g. electrode potential variation, electrolyte supply conditions in the gap, mechanical response of the

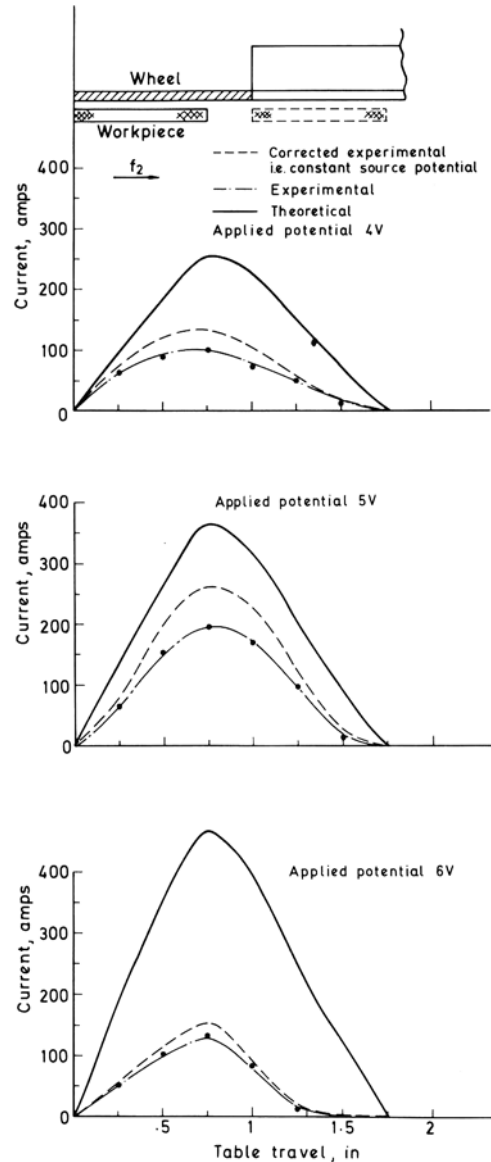


Fig. 4 Experimental, corrected and theoretical leading current waveforms at 0.0005 in. Set depth of cut and 5 ft/min table feed rate for 4, 5 and 6 volts applied potential

machine tool structure, sparking and arcing, surface resistive film on wheel, incorrect chemical equivalent value used in calculations.

In Fig. 5 the experimental volume removal rate (weight converted) versus table feed rate for different applied voltages and set depth of cut is compared with equivalent Faraday values $(\epsilon/t.F.\sigma)\int_0^t I dt$ as calculated from the observed current waveforms. Whilst the Faraday values may include a small error from use of an incorrect value for chemical equivalent and presuppose a constant 100% current efficiency, this would not affect the trends exhibited and, as expected, the curves illustrate an increasing proportion of mechanical removal as feed rate is increased. At 6 volts the difference between the two sets of curves is larger than at 4 and 5 volts over the whole table feed range but especially at the deeper set depths of cut. It is to be noted that this is brought about by twofold phenomena; a drop in Faradaic removal and a small but noticeable increase in total removal. The former must be due to adverse predominance of gas production over possible beneficial temperature rise, but to explain increased total removal several possibilities are offered: (a) increased proportion of mechanical removal—but this could not account for the total removal being greater than that for lower voltages, (b) sparking and/or arcing—this could cause additional removal directly or indirectly with (c) preferential electrochemical attack of some constituent elements thereby allowing others to be swept away by mechanical or hydrodynamic means.

The most disturbing feature in Fig. 5 is the peculiar shape of the curves at low feed rates. Another example of this is illustrated in Fig. 6, where the experimental final depths f_{1a} are compared as a mean of direct measurements and weight converted values and theoretical ratios based on purely electrochemical removal operating at a system efficiency of 37%. (This is an average for correction of the electrochemical constant C and takes account of observed changes in source potential, Faraday efficiency, machine tool response, electrolyte supply, wheel action.) Reasonably close agreement between actual and theoretical values can be seen at critical feed rates, i.e. where $f_{1a}/f_1 = 1$. Above these rates, mechanical removal is observed but because of machine deflection it is insufficient to maintain the ratio at unity.

Below critical feed rates, removal is considerably lower than electrochemically predicted and this drop is either because the workpiece surface requires coincident mechanical action to remove a passivating layer (especially important for straight WC-CO tungsten carbide grades), or because electrolyte distribution in the gap is crucial. The role of the elastic deflection of the machine tool structure should also be considered in this aspect. Unfortunately, electrolyte distribution depends on many parameters, including the supply arrangements, the grinding wheel specification and speed, voltage, depth of cut, table feed and relative workpiece position. A study of these effects is to be made but for the present it appears that, to assure dimensional control and satisfactory grinding quality, feed rates should be set to theoretically critical rates at the optimum voltage (in this case

at about 5 volts). This is especially important for repeated passes because it is the only way in which each pass can behave in like manner to its predecessor.

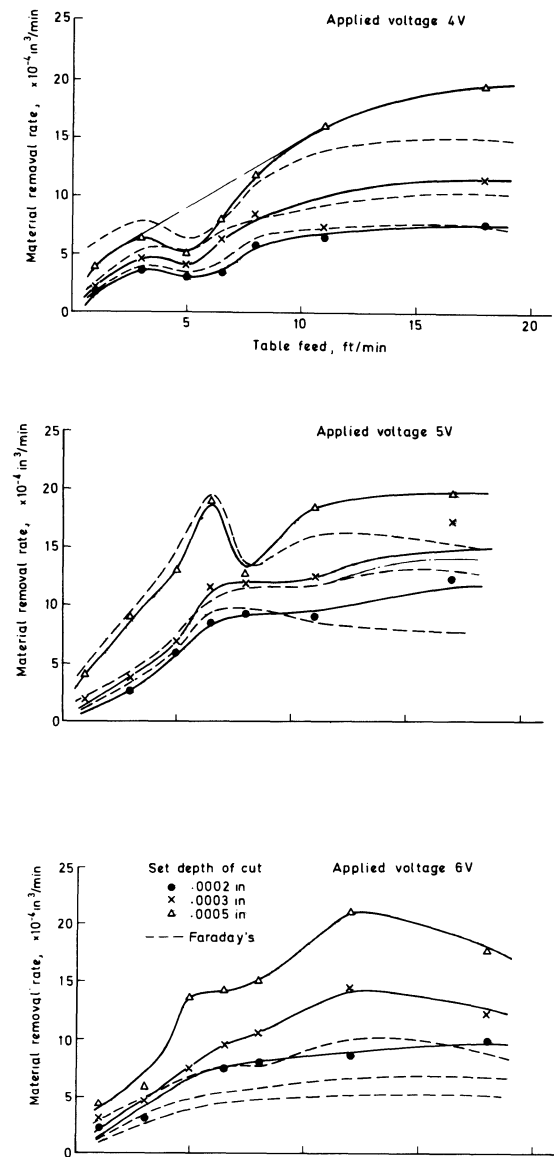


Fig. 5 Measured and equivalent Faraday removal rates versus table feed rate at three set depths of cut for 4, 5 and 6 volts applied potential.

GRINDING QUALITY/SIDE EFFECTS

Surface finish could easily be produced within acceptable limits of 6–16 μin CLA, variation depending on applied voltage, set depth of cut and table feed. However, three major disadvantageous side-effects were observed and are discussed below.

1. **Central grooving** This was noticeable on almost all specimens and is attributed to superior electrolyte retention in that area and the resulting higher electric field strength. Depth of curvature was of the order of 100...50 μin , being reduced with increasing table feed and reducing depth of cut. More severe

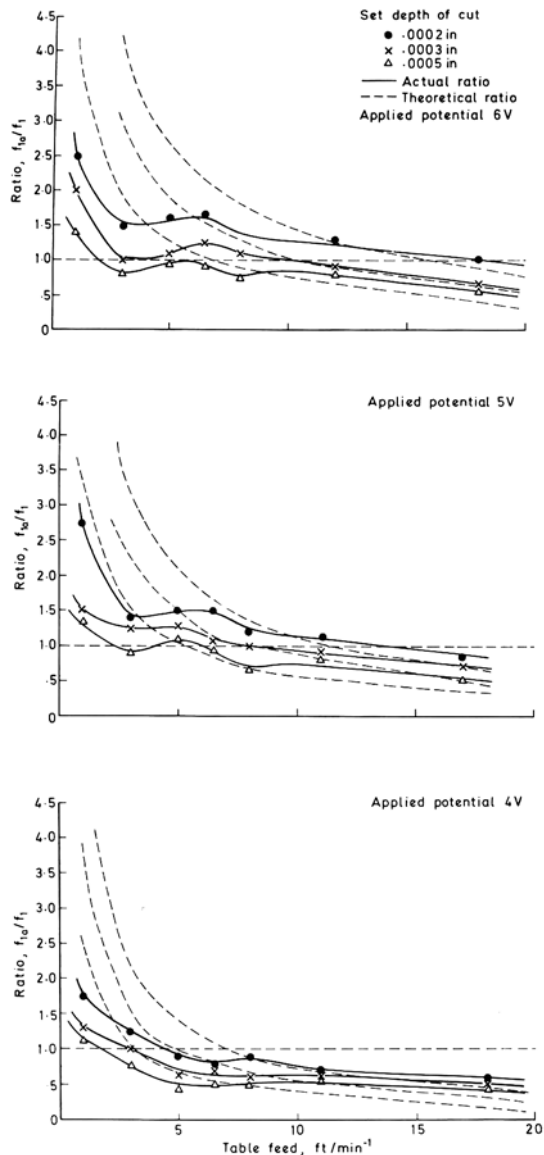


Fig. 6 Actual/set depth of cut ratio versus table feed rate at three set depths of cut for 4, 5 and 6 volts applied potential.

grooving, of several thousandths of an inch depth, has been reported³ for electrochemical peripheral surface grinding but the same reasons are given for the phenomenon. In the present case, however, it is to be noted that it more than compensates for positive curvature from width effect previously discussed theoretically and presents a serious case for investigations now proceeding into electrolyte flow conditions.

2. Edge erosion and staining Edge erosion, Fig. 7, already well known from numerous electrochemical face grinding research sources, was likewise found to lie between 40 and 200 μm . The actual size within this range was not only dependent on the set grinding conditions but also on component orientation in relation to direction of wheel rotation. Staining was always evident near the edges of the component on the four unmachined side faces (Fig. 7). It was light grey in colour and was sometimes followed by a black zone. This observation repeats industrial experience and is presumably due to stray current attack and/or adherence of electrolytic precipitates. Like edge ero-

sion it was found to be influenced by component orientation but electrolyte flow conditions and rate proved critical for its size and shape. For the depth of cut range used up to 0.005 in, stain depth measured from 0.003 to 0.005 in, as voltage increased, but, being a time-dependent phenomenon, increase in table feed rate acted favourably in reducing it. Commercial interests are reluctant to accept its appearance although no really scientific disadvantages have been presented to date. Edge erosion and staining present a second case for further examination of electrolyte flow conditions and also perhaps for a study of electrolyte type. However, in considering this last point, very serious regard must be paid to the requirements for a general purpose electrolyte which must not corrode the machine tool.

3. Resistive layer on wheel As grinding progressed a layer formed on the surface of the wheel and produced severe distortion of the current wave, Fig. 8. To maintain a 'clean' wheel is of the utmost importance if process control is to be obtained. However, the only method which the present authors found satisfactory was to use the rather severe (silicon carbide) centrifugally loaded roller dressing technique. This aspect is serious and one which could easily be ignored in industry to the detriment of process efficiency. It is, therefore, an important aspect for further research, particularly for grinding large surface areas when the deleterious effect is likely to become noticeable during a single pass.

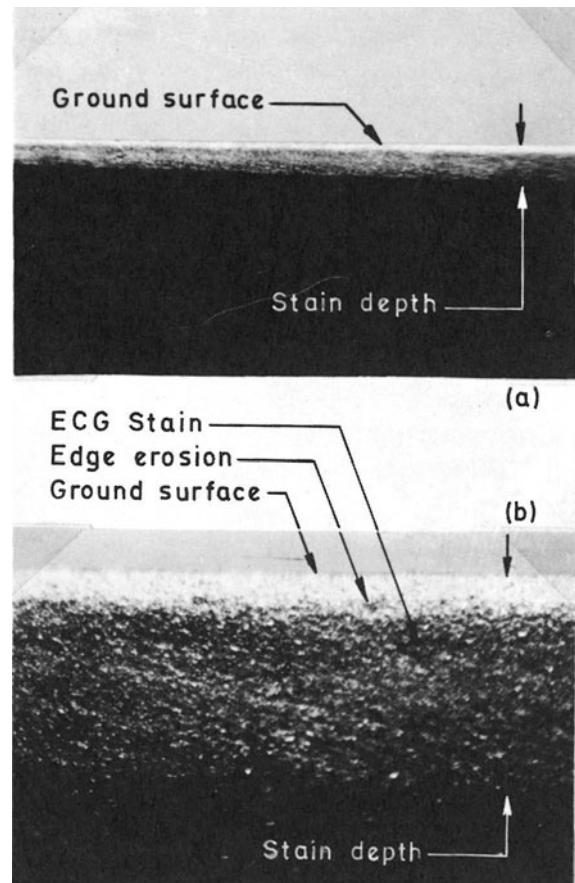


Fig. 7 Edge erosion and staining: (a) magnification 31X; (b) magnification 175X.

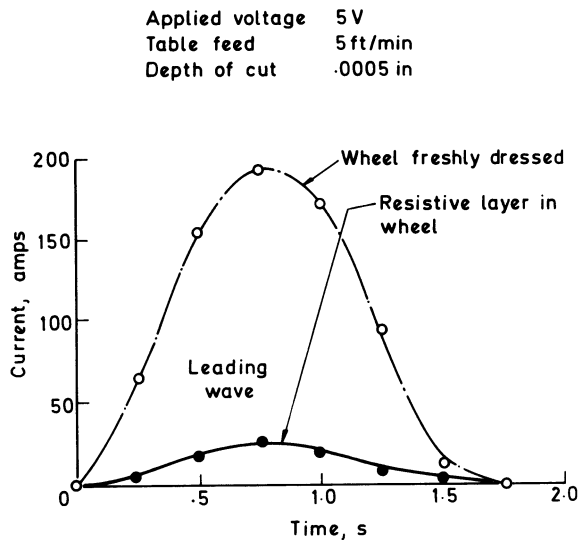


Fig. 8 Effect of resistive layer on wheel.

ACKNOWLEDGMENTS

The authors are pleased to record thanks to Abwood Machine Tools Ltd. and particularly Mr A. Peck, Mr R. Chapman and Mr H. C. Brimson for lending an electrochemical vertical spindle surface grinding machine for the research which forms the subject of this paper. Grateful thanks are also due to Hoy Carbides Ltd., especially Mr G. C. Thomsen, for provision of the tungsten carbide workpieces. UMIST is acknowledged for permitting the experimental work to be carried out in the Royce Laboratory and Professor F. Koenigsberger is thanked for his encouraging interest and support. The National Technical University of Athens is also acknowledged for the S. Niarchos Scholarship awarded to the first named author.

REFERENCES

1. SFANTSIKOPOULOS, M. M., 'Electrochemical vertical spindle surface grinding', *M.Sc. Thesis*, UMIST (1971).
2. TIPTON, H., 'The dynamics of electrochemical machining', 5th Intern. M.T.D.R. Conf., University of Birmingham (1964).
3. GEDDAM, A., 'A study of peripheral electrochemical grinding with some wheel variables', *M.Sc. Thesis*, UMIST (1969).

DISCUSSION

Query from A. Geddam

- (1) For each working traverse there are two current waves (leading and trailing). Was the trailing current wave taken into account while calculating the ratio f_{1a}/f_1 theoretically?
- (2) Fig. 8 shows the effect of the resistive layer formed on the wheel. Is this layer formation peculiar to the type of work material used, viz carbides, or is it a general phenomenon for any type of work material?

Reply

- (1) Equation (4) considers both leading and trailing waves for the theoretical determination of actual depth to set depth ratio. However, as stated in the text, the trailing wave is of negligible magnitude and only the leading wave was used for converting current to theoretical removal rate (Faraday in Fig. 5).
- (2) The resistive layer formed on the grinding wheel bond has been observed mainly while grinding tungsten carbide. It could probably be avoided by selecting another electrolyte solution, but in doing so it would be important to avoid corrosion of machine tool elements. The present solution has admirable anti-corrosive properties and we hope to solve the problem without drastic changes in chemistry.

Query from G. I. E. Wright

Although the machine had a vertical slide, were the diamonds fulfilling the normal function of providing the correct electrochemical stand-off distance?

Were experiments carried out with the wheel set at a distance independent of the diamonds?

Reply

As there is no vertical feed, but only a longitudinal table feed, electrochemical gap simply varies from the initially set $e-f$, according to the law described, theoretically, by equation (2a).

Experiments with $f = 0$ were carried out in this case: due to oxide layer formation on the workpiece surface and the lack of any mechanical action, the current density developed was quite low. In fact, no current waves were observed.

EFFECT OF SURFACE FINISH PRODUCED DURING ECM UPON THE FATIGUE LIFE OF NIMONIC 80A

by

J. M. EVANS, P. J. BODEN and A. A. BAKER*

SUMMARY

An assessment of the effect of surface finish produced during electrochemical machining upon fatigue life of Nimonic 80A has been made. Surfaces exhibiting pitting and intergranular attack showed slightly worse fatigue properties than brightened and polished surfaces but any reduction due to surface finish defects was small in comparison with that due to removal of compressive stress.

INTRODUCTION

Assessment of the influence of ECM upon metal fatigue is complicated by the presence of several surface characteristics which operate simultaneously and produce contrary effects. Dissolution removes the layer of residual stress induced into the surface of the metal by mechanical machining. When this stress is compressive, a reduction in fatigue life of the metal is produced. However, improvements in fatigue resistance due to ECM have been reported for notch sensitive materials¹⁻³ where removal of hairline cracks, notches and sub-surface defects abates possible stress raisers.

Previous research has investigated the effect of removal of compressive stress and the application of processes such as shot peening for restoring the stress after ECM^{4,5}. The quality of the surface finishes produced in ECM has been regarded only as of secondary importance. Steer *et al.*⁶ found fatigue cracks emanating from pits in an electropolished surface but it was argued⁷ that these pits only represented a small reduction compared to that produced by removal of residual stress. It has been shown⁸ that at low current densities surfaces are pitted and undergo intergranular attack. The importance ECM process of hole sinking leads to the final surface of the generated walls being pitted through such a low current density effect. Therefore, grain boundary grooving and pitting might influence metal fatigue to a greater extent than had been previously considered. Also Hempel⁹ has shown that beneficial compressive stresses induced by mechanical machining could be removed by heat treatment and fatigue lives comparable with those produced by

electropolishing were obtained. It was thus anticipated that, if an electrochemically machined component was operated at elevated temperatures in service, residual stress could be removed and the importance of any surface defects which remained after blasting operations would be magnified.

The following investigation has studied the effects of ECM surface finish upon fatigue characteristics of Nimonic 80A.

EXPERIMENTAL PROCEDURE

The shape and dimensions of the Nimonic 80A fatigue specimen are shown in Fig. 1. Specimens were prepared from forged bar by surface grinding to a thickness of approximately 1.5 mm and hand polished to 1 micron finish. Electrochemical machining was carried out in the cell described elsewhere⁸.

The specimen was mounted upon a copper anode; the sides of the specimen together with the exposed areas of the anode base were coated with an insulating paint. The same depth of metal (0.1 mm) was removed from the gauge length of each specimen, power being supplied to the cell by a Chemical Electronics 100 A potentiostat. Machining was carried out on one face only since it was assumed from the outset that the mechanically machined face would possess better fatigue resistance and would thus impose no limitation upon the electrochemically machined side.

The surface finishes studied and conditions of preparation are listed in Table 1.

*Department of Metallurgy, The University Nottingham.

Table 1. Conditions used in preparation of ECM Surfaces

Type of finish	Current density (A/mm ²)	Flow rate (m/s)	Gap width (mm)	Electrolyte
anodically brightened	3×10^{-2}	30.5	0.25	15% NaCl
brightened surface with grain boundary delineation	9.3×10^{-3}	30.5	0.25	15% NaCl
surface with hemispherical pits	1.6×10^{-3}	5.2	0.25	15% NaCl
surface with intergranular attack	3.1×10^{-4}	30.5	0.25	15% NaCl

Specimens were also subjected to conditions similar to those found in the stray current regions using electrolytes with different cutting properties. Sodium chlorate and sodium chloride (+ sodium carbonate) were the electrolytes selected with good

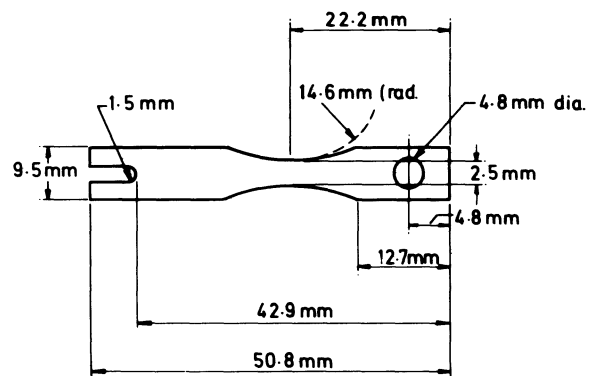
cutting properties and sodium chloride an electrolyte typical of poor cutting properties. The shape of the pits produced is shown in Fig. 2 and the conditions of preparation listed in Table 2.

Table 2. Conditions necessary to simulate stray current pitting

Electrolyte	Current density (A/mm ²)	Flow rate (m/s)	Cap width (mm)
15% NaCl	4.42×10^{-4}	30.5	0.25
15% NaCl + 2.5% Na ₂ CO ₃	3.54×10^{-4}	30.5	0.25
40% NaClO ₃	3.10×10^{-4}	30.5	0.25

Some specimens were heat treated at 950°C in air, for 1 hour, and cooled in air. Metallographic examination of sections through the specimens showed some grain boundary oxidation had occurred as expected for these alloys.

Measurement of residual stress in the specimen before and after ECM was carried out by X-ray diffraction using the two-exposure technique¹⁰. Fatigue testing was carried out in reverse bending under conditions of constant bending moment. The machine, Fig. 3, has been described more fully elsewhere¹¹. Testing was carried out in the stress range ± 247 to ± 433 MN/m².

**Fig. 1 Fatigue test specimen**

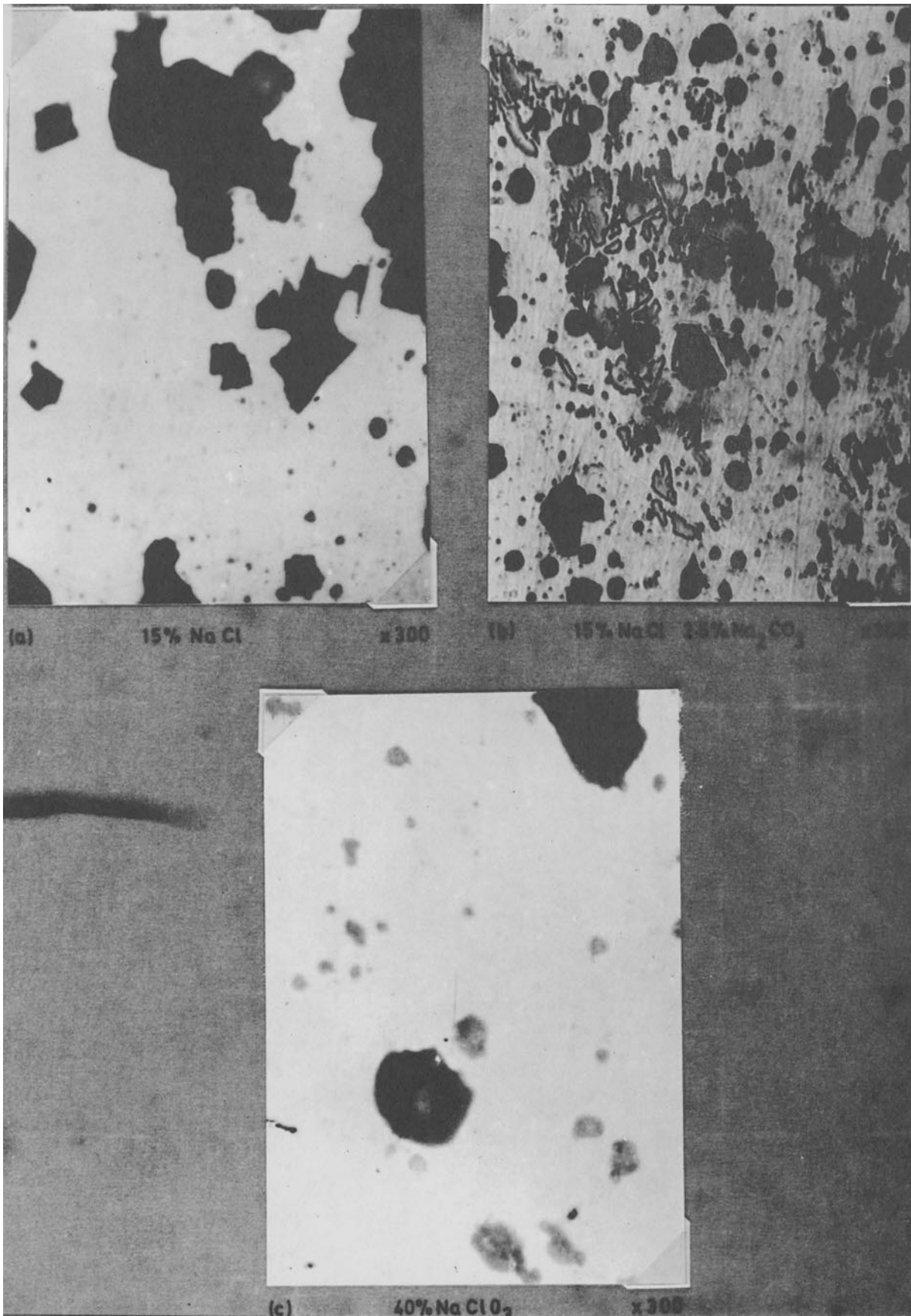


Fig. 2 Examples of stray pitting

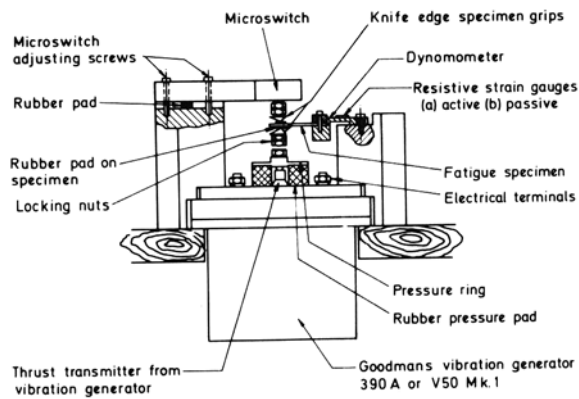


Fig. 3 Reversed bending fatigue machine (schematic)

RESULTS AND DISCUSSION

The effect of surface finish upon the fatigue life of Nimonic 80A is shown in Fig. 4. A comparison has been drawn in Table 3 of this reduction produced by different surface finishes at a stress level of $\pm 386 \text{ MN/m}^2$.

Table 3. Comparison of fatigue lives produced by different surfaces at a stress of $+ 386 \text{ MN/m}^2$

Surface finish	Fatigue life (cycles)
mechanically polished	1.68×10^6
electrochemically polished	4.9×10^5
etched	4.4×10^5
intergranular attack	4.25×10^5
hemispherical pits	3.3×10^5

The effect of deliberate introduction of surface irregularities by ECM was not as severe as had previously been anticipated. The previous findings of electropolishing upon fatigue appear to hold for electrochemically machined surfaces even though dissolution under dynamic conditions of electrolyte flow gives rise to more severe surface defects. Micro-examination of the brightened surfaces revealed fatigue cracks emanating from bright hemispherical pits. (See Fig. 5a). Examination of surface exhibiting grain boundary delineation showed that crack propagation was in the main transgranular (Fig. 5b). Again cracks were seen to originate from bright pits.

Intergranular attack did not cause a marked reduction in fatigue life. Using a carbon replica technique the depth of attack was measured as 10^{-2} – 10^{-3} mm. The results indicated that these relatively deep grooves were no more detrimental to metal fatigue than pits of smaller dimensions, i.e. 10^{-4} – 10^{-3} mm. A comparison of micrographs taken of the hemispherically pitted surface is shown in Fig. 5c–d, although these pits when viewed normally were hemispherical in nature, taper-sectioning demonstrated them to be angular at the base.

pressive stresses were operative to a depth of approximately 0.20 mm. (See Fig. 6.) Even though inaccuracies could have occurred with this method,

these results were in good agreement with fatigue measurements conducted at a constant stress level of $\pm 386 \text{ MN/m}^2$ on specimens with various depths of metal removed. It was shown that the fatigue life became constant after a depth of 0.20 mm metal had been removed (Fig. 7).

The effect of pit shape is shown in Fig. 8. Specimens machined in sodium chloride/carbonate and sodium chlorate electrolytes which promoted pits of the hemispherical variety produced almost identical fatigue values that were only marginally better than surfaces formed in pure sodium chloride electrolyte.

The results of tests conducted on specimens heat treated after ECM and mechanical machining are given in Fig. 9. Whereas there was little difference between fatigue values of electromachined specimens before and after heat treatment, the mechanically finished material after heat treatment was reduced to the same level as the electrochemically machined material. Stress measurements confirmed that heat treatment had effected a removal of compressive stress. The degree of scatter obtained with the heat-treated samples made it impossible to distinguish which electromachined finish would optimize fatigue resistance at elevated temperature.

In addition, heat treatment gave rise to internal grain boundary oxidation which may have masked surface defects arising from ECM.

It was apparent from the above investigation that removal of compressive stress was the prime motivator in reducing fatigue life of electrochemically machined material. Although cracks were seen to originate from pits, certain surface finishes did produce marginally better fatigue resistance. However, the improvement in fatigue life could only be regarded as of secondary importance. Studies to determine the effect of pit distribution were carried out using the photoelasticity technique. These suggested that, although the stress concentration factor at single point defects are high and could have a deleterious effect upon fatigue, stress concentrations around any single notch in a series of notches is considerably reduced. This reduction can be attributed to the interaction of neighbouring stress fields. Although these results should be treated with a certain degree of caution, they did suggest a trend which correlated with the results obtained, i.e. a surface containing single point defects may be more susceptible to fatigue failure than one containing a network of intergranular attack.

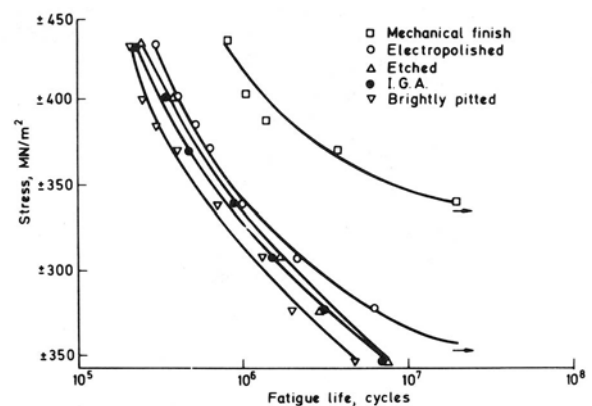


Fig. 4 Effect of surface finish upon fatigue life

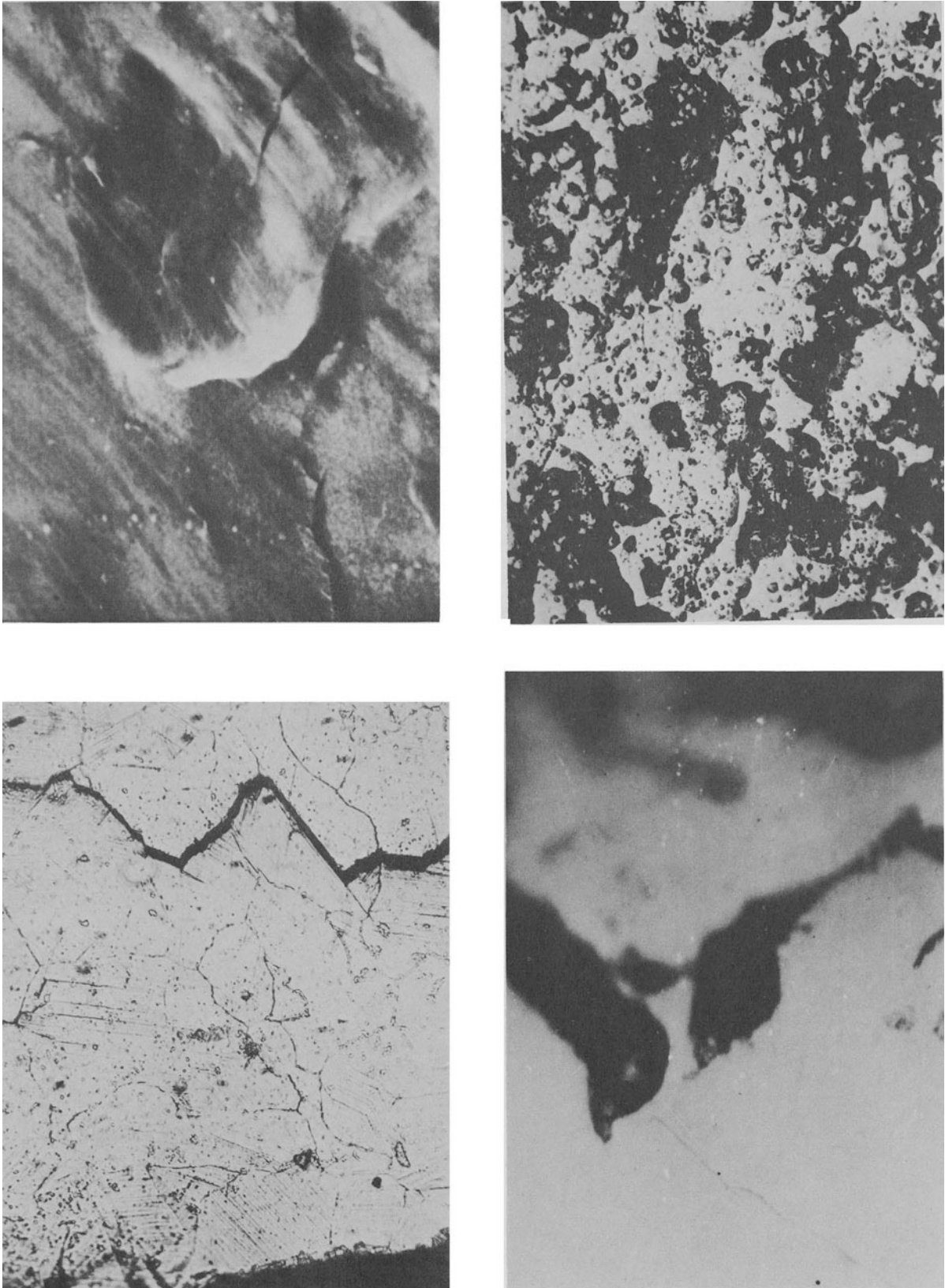


Fig. 5 (a) Fatigue crack propagating from a pit on a bright surface (mag. $\times 32,000$); (b) transangular propagation of fatigue crack on an etched surface (mag. $\times 300$); (c) hemispherically pitted surface (mag. $\times 300$); (d) taper section showing crack propagating from a pit (mag. $\times 600$).

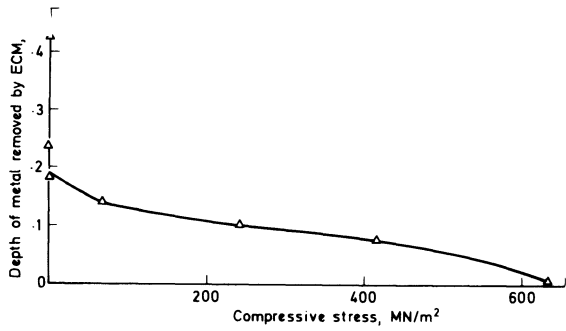


Fig. 6 Effect of depth of metal removed upon surface compressive stress.

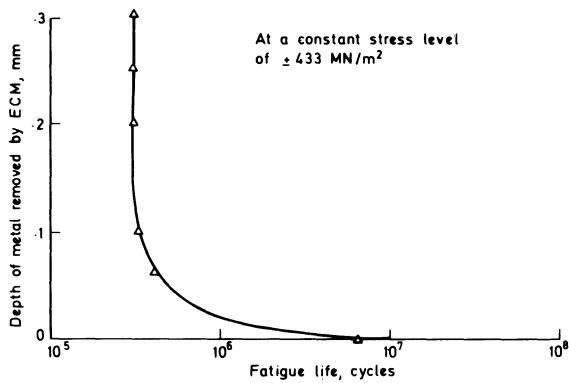


Fig. 7 Effect of metal removed upon fatigue life

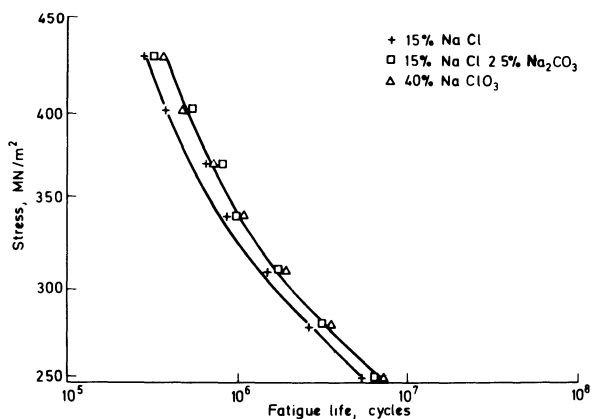


Fig. 8 Fatigue life in stray current region

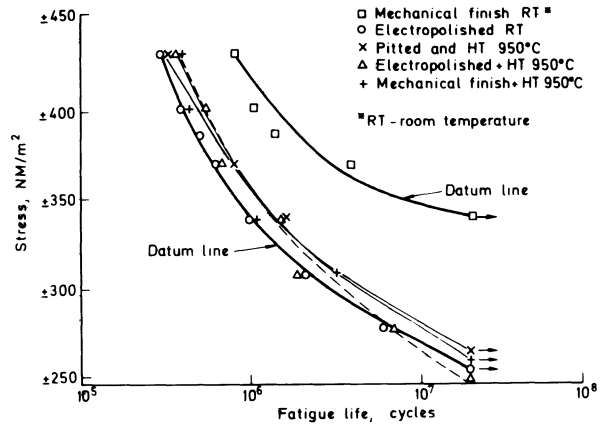


Fig. 9 Effect of heat treatment upon fatigue life

CONCLUSIONS

1. Stress in the surface outweighs minor defects in surface topography in determining the fatigue life of electrochemically machined components.
2. Anodically brightened finishes produce only a marginal better fatigue properties than do pitted surfaces.
3. Heat treatment after machining removes the residual stresses and reduces metal fatigue to the level found with electrochemical machining.

ACKNOWLEDGMENTS

The authors would like to thank the Ministry of Technology for a grant to support one of us (JME) and Rolls-Royce, (Derby) Ltd, for supplying material and equipment.

REFERENCES

1. WARD, W. V., JACOBSON, L. M., and MATTHEWS, C. O., *Trans. Am. Soc. Metals*, 54, 84 (1961).
2. SINCLAIR, C. M., CORTEN, H. T., and DOLAN, T. J., *J. Eng. Ind. (Trans. ASME, Ser. B)*, 79, 89 (1957).
3. MONDON, R., *Metal Progr.*, 83, 95 (1963).
4. ZIMMEL, L. J., *Natl. Aeronaut. Space Eng. Meeting, Los Angeles, California* (1964).
5. ROWDEN, G., *Metallurgia*, 77, 189 (1968).
6. STEER, A. T., WILSON, J. K., and WRIGHT, O., *Aircraft Prod.*, 15, 242 (1953).
7. MONDON, R., and ZENTLER GORDON, H. E., *Trans. Inst. Met. Finishing*, 31, 52 (1954).
8. EVANS, J. M., BODEN, P. J., Paper presented at *October Meeting of the Electrochemical Society, Atlantic City, October 4th-9th* (1970).
9. HEMPEL, M., *Archiv. Eisenhüttenw.*, 425 (1951).
10. BARRATT, C. S., *Structure of Metals*, McGraw-Hill, New York (1952).
11. BAKER, A. A., *Ph.D. Thesis*, University of Nottingham (1967).

DISCUSSION

Query from A. G. Hague, Trent Polytechnic, Nottingham

Figs. 4 and 9 are of a similar form, each having the same axes. Presumably Fig. 4 represents the conditions when the materials were held at room temperature and this is intended to show the effect of surface finish upon fatigue life. Fig. 9, however, claims to show the effects of heat treatment upon fatigue life. Can Fig. 9 really reveal effects of heat treatment without having first been separated from surface finish. It would seem that in Fig. 9 an extra variable, namely heat treatment has been superimposed on the types of surface finish. Perhaps had the two graphs themselves been superimposed and made into one, the effect of heat treatment for each type of surface would have been clearly seen when compared with the fatigue lives obtained on the surface finishes at room temperature.

Reply

It has been shown that the dominant factor in determining reduction of metal fatigue on electrochemical machining is the removal of compressive stress from the surface layers of the metal. Secondary reductions may be experienced with pitted surfaces or those containing intergranular attack.

Materials such as the Nimonics are used extensively in the high temperature stages of the jet-engine. The necessity for some treatment, such as shot-blasting, to restore the fatigue life of an electrochemically machined component to the level of that of mechanical machining is continually being emphasised. This investigation has shown that stress relaxation at high temperature can negate beneficial effects due to compressive stresses induced by mechanical machining at room temperature. Fig. 9 shows little difference between a mechanically machined and an electrochemically machined specimen after heat treatment at 950°C. The relevant fatigue curves produced at room temperature have been superimposed onto Fig. 9 as data lines.

MACHINE TOOL TESTING

A STUDY OF IDENTIFICATION OF DYNAMIC CHARACTERISTICS OF MACHINE TOOLS BY MEANS OF MICRO TREMOR

by

H. SATO and T. AKUTSU*

SUMMARY

This paper is a study on the identification of the dynamic characteristics of a machine tool structure such as natural frequency, approximate normal mode and damping ratio, applying the method of cross-spectrum analysis to micro tremors which are observed on the structure usually even under driving conditions without cutting. The results are compared with those by sinusoidal and random excitation.

INTRODUCTION

The vibration observed on machine tools should be avoided by change of the operation condition or suppressed by elaborate design as much as possible, whether it is self-excited vibration or forced vibration. It causes a decrease of productivity, the deterioration of work precision and surface finish. A number of researchers are working on improving the dynamic characteristics of machine tools; however, it does not seem that they have been successful enough to predict them in the process of the design. So it is still important to measure them on existing machines^{1,2}.

The dynamic characteristics of machine tools are generally observed by such methods as (1) frequency response method, (2) impulse response method, and (3) random excitation method. These all use some exciting force from the outside of the machine.

In spite of tremendous efforts for improving the dynamic characteristics of machine tools, there still usually remains a vibration with a small amplitude, micro tremor, which is caused by gear trains, driving belt and other internal moving parts of the machine even under driving conditions without cutting^{3,4}. This paper is a study into the identification of the dynamic characteristics such as natural frequency, normal mode and damping ratio, by making use of the tremor without giving any particular exciting force from outside the machine. Usually the tremor can be felt by hand. The method of cross-spectrum analysis is applied. A lathe is used for the analysis⁵⁻⁷.

GENERAL IDEA OF IDENTIFICATION BY MICRO TREMOR

It is found that the machine tool structure is usually excited with a small amplitude. This is caused by the

moving parts of the machine such as motors, belts, gear trains, work-spindle system and the cutting operation itself. This will be called micro tremor or tremor in the following. This paper is especially concerned with the tremor caused during non-cutting. These sources of excitation have periodic frequency components and some frequency components of broad bandwidth as well. It goes without saying that the tremor should be kept as small as possible from the viewpoint of machine performance.

The vibration waveforms which are observed at various points on a machine tend to be random. Thus the method of random vibration analysis such as power spectrum and cross-spectrum analysis is applicable to the identification of the vibration system. The tremor is the response of the machine to such exciting force as the above-mentioned, which contains information of the dynamic characteristics. These can be partly extracted by making observations of waveforms of the tremor measured at various points. However, the analysis in the frequency domain after Fourier transformation gives us more precise knowledge about the structural dynamic characteristics.

At first the analysis as for natural frequency is considered. Generally the damping ratio of a machine tool structure is not so large and the dominant frequency components corresponding to the natural frequencies appear in the tremor excited by the sources of excitation aforementioned. If the frequency characteristic of the exciting force is pure white noise, the natural frequency component can be read from the frequencies at which the power spectrum shows maxima. However, all the frequency components do not correspond to natural frequencies, and some dominant frequency components of the source of excitation may appear, too. The rotational

*Institute of Industrial Science, University of Tokyo

speed of the motor and spindle system and the gear tooth engagement frequencies can correspond to the frequency.

Particular parts of the structure such as panels may resonate by picking up the frequency components out of the source of excitation. This may work as the excitation to other parts of the machine.

The rotational speed of motor and spindle system and impulsive frequency decided by engaging gears can be identified, taking the operating conditions and the number of gear teeth into consideration. The part resonance can be measured by ordinary instrumentation. Thus the natural frequency can be distinguished from the frequency components of rather dominant periodic excitation.

Secondly the normal mode analysis is presented. The normal mode shape at each natural frequency can be obtained when the amplitude ratio and the phase relation of various points relative to a datum are measured. These relations between any two points are computed; applying the method of cross-spectrum analysis for the tremors observed at two points at the same time. The measuring point which is considered closer than others to the excitation source is taken as the input to the system. The transfer function between the two points is computed by the analysis. This is expressed in terms of gain and phase characteristics versus frequency. Thus it gives amplitude ratio and phase relation of any point, relative to a datum point at every natural frequency. Knowing such relations at several important points, it is possible to draw the approximate normal mode.

Finally the analysis as for damping ratio is mentioned. There are several fundamental methods to obtain the damping ratio of a structure. The simplest one it is to hit a structure and observe its 'impulse response'. The damping ratio is evaluated by the shape of damped waveform. However, sometimes it happens that the impulse response contains several natural frequencies. In such a case it is difficult to discern the damping ratio directly for each excited natural frequency. Treatment in the frequency domain is generally helpful for this analysis also.

Assuming that the system is simulated by a single-degree-of-freedom system for each mode, the shape of the power spectrum of the tremor is supposed to give the damping ratio. However, the shape of the power spectrum is easily affected by the frequency components of the input and also by the numerical computation process such as data length, sampling period and lag window or spectral window. The correction to these should be taken into consideration when using this method.

A different method which utilizes the shape of the phase characteristic is proposed here. There are those normal mode shapes for which adjacent points move in antiphase thus implying that a mode exists in between those for high natural frequencies. If the phase relation is obtained between these points, it shows a phase reversal around a natural frequency. The slope of the phase change is steep for small damping ratio and becomes gentle as it increases. This suggests that the phase relation of the transfer function can be made use of for identifying the damping ratio of higher natural frequencies. When the charac-

teristic around a natural frequency is simulated by a one-degree-of-freedom system, the theoretical transfer function of displacement response to exciting displacement $H(s)$ can be represented as

$$H(s) = \frac{2\zeta \omega s + \omega^2}{s^2 + 2\zeta \omega s + \omega^2} \quad (1)$$

where s = the Laplace operator

ω = natural circular frequency

ζ = damping ratio, given so that the theoretical phase relation may coincide with the measured one in the sense of least square of the error.

EXPERIMENTAL PROCEDURE

A 4 shaku (about 4 feet) lathe is used for the experiment. The reason that the lathe is adopted is that the shape of the machine is rather simple and fundamental from the structural viewpoint, and the effects of the structural vibration and the cutting process are easily understood in terms of relative displacement between work and tool. The measuring points of the tremor are on gearbox P1 which is considered closest to the source of excitation, on bearing box of the spindle P2, on tool post P3 and on tail stock P4 as shown in Fig. 1. As the datum points for obtaining the normal modes, P1 and P2 are adopted. For model shape measurements a strain gauge type accelerometer is used.

The tremor during driving without cutting is measured under various driving condition such as the maximum spindle speed 940 rev/min and several other low speeds, and disengaged condition of the gear coupling to the spindle. This changes the frequency components of the excitation source, so that these are distinguished from the natural frequency.

On the other hand, in order to compare the results of the analysis by the tremor with the true dynamic characteristics the usual frequency response method is carried out, also. An electro-hydraulic exciter is used, and the natural frequencies and the normal modes are identified. In addition to this, the excitation using a random waveform generated by thermal shot noise has also been performed. The vibration response to this random input is analysed by means of the cross-spectrum method, and the natural frequencies and the normal modes are confirmed.

The tremor or the vibration observed at P1, P2, P3 and P4 are recorded on a 4-channel data recorder. Thus they are transformed to digitized data on paper tape or IBM card through a high-speed A-D converter, the maximum sample speed of which is 6000/s. These form the input to a digital computer, and power spectrum, cross-spectrum and transfer function are obtained by performing the numerical computation. The natural frequency is obtained and the normal mode shape is drawn according to these results. Estimation of the coherency is taken into consideration as an index of reliability of the transfer function through the analysis.

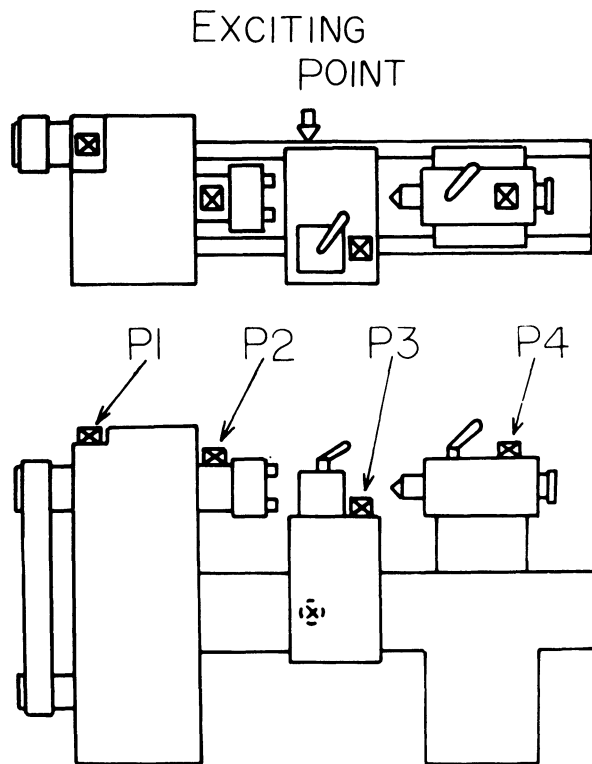


Fig. 1 General scheme of measuring points

RESULTS OF THE EXPERIMENT AND THE ANALYSIS

Observation of the micro tremor

Fig. 2 shows an example of the waveform of the acceleration measured at the points aforementioned. The spindle speed is set to 940 rev/min. The waveforms in Fig. 2 are measured by an accelerometer with a natural frequency of 80 Hz and the maximum measurable acceleration is $2.0g$. They are also processed through a low-pass filter, the break frequency of which is 70 Hz, to discover the behaviour of low-frequency components especially. These are reproduced by using a digital plotter, then the amplitude is normalized. In addition to this instrumentation an accelerometer of 300 Hz and $10.0g$ is used for measurement of higher-frequency components.

The observation of these waveforms reveals the common frequency components at all measuring points and for each frequency component the specific phase relation between two points is found. In Fig. 2 two frequency components, about 50 and 80 Hz, are conspicuous. For the former the phase relation between P1, P2, P3 and P4 are the same. However, for the latter P1 and P2 have the same phase, and P3 and P4 have reverse phase. Thus the approximate mode shape of the machine can be obtained by the synthetic observation of the tremor in the time domain. If these are transformed into the frequency domain, more details become evident.

Power spectrum and transfer function by the tremor
Fig. 3 and Fig. 4 show the power spectrum. The former is computed from records of Fig. 1 and the

latter is obtained by using the tremor including higher-frequency components. Fig. 5 provides the transfer function P3/P2. The expression for the transfer function P3/P2 means the transfer function regarding P3 and P2 as input and output to the system to be identified respectively.

The numerical computation is made by sampling period $T = 2.0 \times 10^{-3}$ s, number of data $n = 1000$, length of correlogram $h = 100$, resolution of frequency $1/2hT = 2.5$ Hz and data length $nT = 2.0$ s for Fig. 3 and $T = 5.0 \times 10^{-4}$ s, $n = 1000$, $h = 100$, $1/2hT = 10.0$ Hz and $nT = 0.5$ s for Fig. 4.

Natural frequency

Table 1a shows the frequencies where the power spectra in Fig. 3 and Fig. 4 exhibit maxima. In Table 1b the natural frequencies obtained by a frequency response method are indicated. As for the latter the excitation is performed up to 530 Hz.

(a) Analysis of the tremor (Hz)	(b) Sinusoidal excitation (Hz)
15.0 (2.5)	
25.0 (2.5)	
47.5 (2.5)	47.5
80 (10)	80
150 (10)	160
220 (10)	210
260 (10)	250, 280
310 (10)	
380–410 (10)	400
460–480 (10)	450
530 (10)	530

Frequencies of 15.0, 25.0 and 31.0 Hz correspond to the rotational speed of the spindle and the motor, and the frequency of engaging gears in unit time. These are not easily found by the direct observation of waveforms, but the expression in the frequency domain makes it possible to detect the components. The measured rotational speed of the spindle (940 rev/min) is equal to 15.7 Hz. The 24.7 Hz component is similarly identified from the motor speed. The gear coupling has the possibility to excite 125 and 313 Hz at the speed taking note of the number of gear teeth. By placing a directional microphone close to the engaging gears it was possible to assure the existence of 320 Hz. As the resolution of the computation is 20 Hz, the judgment above mentioned is given. Now it can be said that the frequency components shown in Table 1a agree well with those in Table 1b except for the frequency of excitation.

Normal modes

Normal modes defined in terms of the amplitude ratio among P1, P2, P3 and P4 are given in Fig. 6. Those based on the tremor are arranged in Fig. 6c. Fig 6a and b display the results by sinusoidal and the

random excitation. The table tells us not only the difference of the results, but also the features of the methods themselves. The results in Fig. 6c show marked disagreement with those in Fig. 6a and b from the viewpoint of mode shape coincidence. However, it is interesting to find that principal modes can be identified by analysing the tremor and without using particular external excitation.

In the case of the random excitation the data processing is the same as that used for the tremor. The necessary time for the experiment involving the excitation of the machine is usually very small in comparison with that for the sinusoidal excitation. The difference caused between the results of the random excitation and the micro tremor depends on the frequency characteristic of the input. If this is white, the analytically assumed response characteristics are well satisfied and the analysis does not introduce error, and the results ought to coincide with those by the sinusoidal excitation. Fig. 6c suggests that the characteristic of the input which caused the tremor is far from that of white noise. This naturally disturbs the transfer function and leads to difficulty in defining the normal modes.

It is difficult to measure the characteristic of the actual excitation. It is attempted to acquire frequency component of the excitation by means of the sound radiated. A directional microphone is put as close as possible to each moving part of the

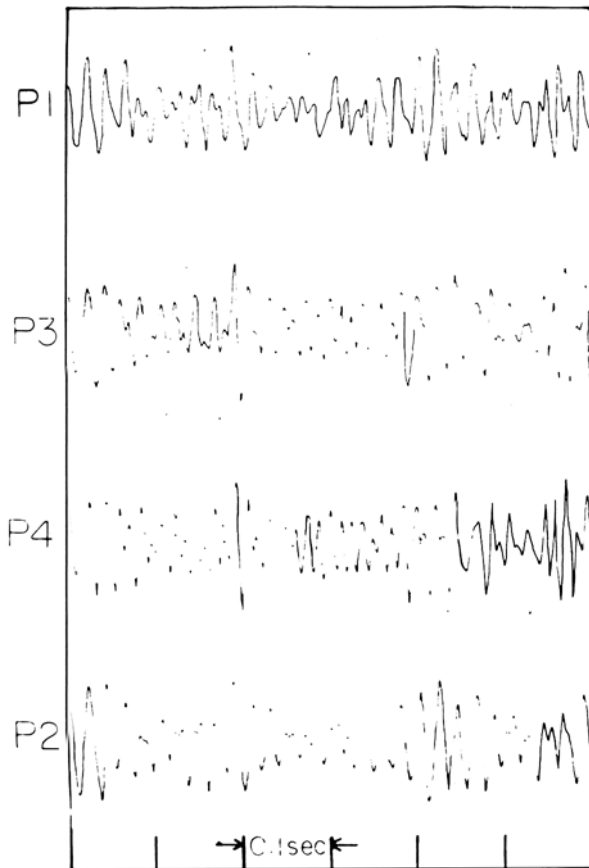


Fig. 2 Example of waveforms

machine and the power spectrum analysis is carried out for it. The frequency components which have peak power may disturb the original transfer function and as a result the computed transfer function becomes distorted. As to the extent of the distortion the coherency is referred to. The frequency components vary according to the driving condition. This explains coincidence of the modes which are dissimilar in Fig. 6a and c.

It is evident from the figure that it is difficult to identify the normal mode for higher natural frequency by making use of the tremor. But for lower natural frequencies the method is effective. In addition the tremor exists even during machining, and it may therefore be possible to relate this to machining precision and perhaps specify an index for dynamic performance of the machine.

Fig. 5 compares the transfer function P3/P2 by random excitation with that by the micro tremor. The numerical computation for the former is carried out using the same parameters as for tremor, $T = 5.0 \times 10^{-4}$ s, $n = 1000$, $h = 100$, $1/2hT = 10.0$ Hz and $nT = 0.5$ s. It is most remarkable that the coherency is higher for the former than for the latter. This is similarly true for the case of P2/P1 and P4/P2. The reason why the coherency is so high for the random excitation is that the machine is excited at a point and the excitation has a power spectrum close to the theoretical one, that is band-limited white. On the other hand the source of the excitation for the tremor is rather distributed in addition to the existence of frequency components with dominant power.

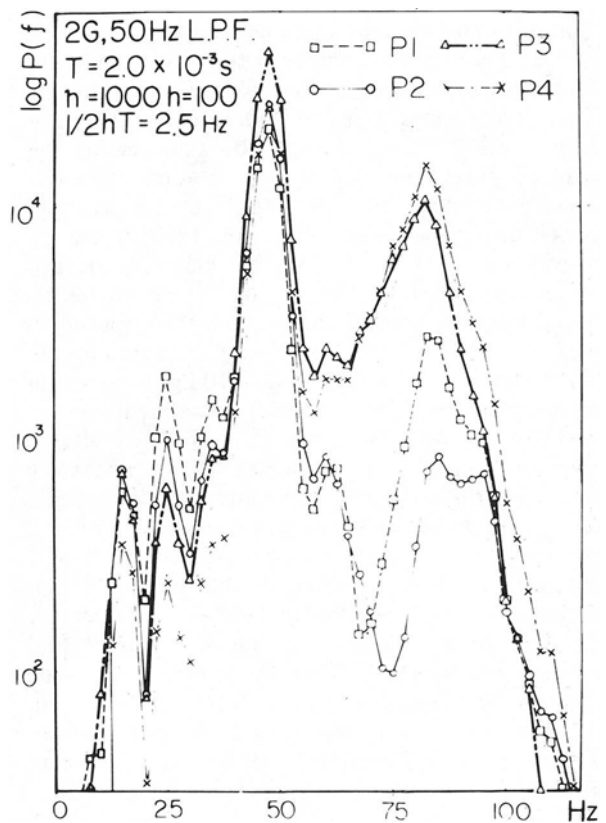


Fig. 3 Power spectra of the tremor in low-frequency range

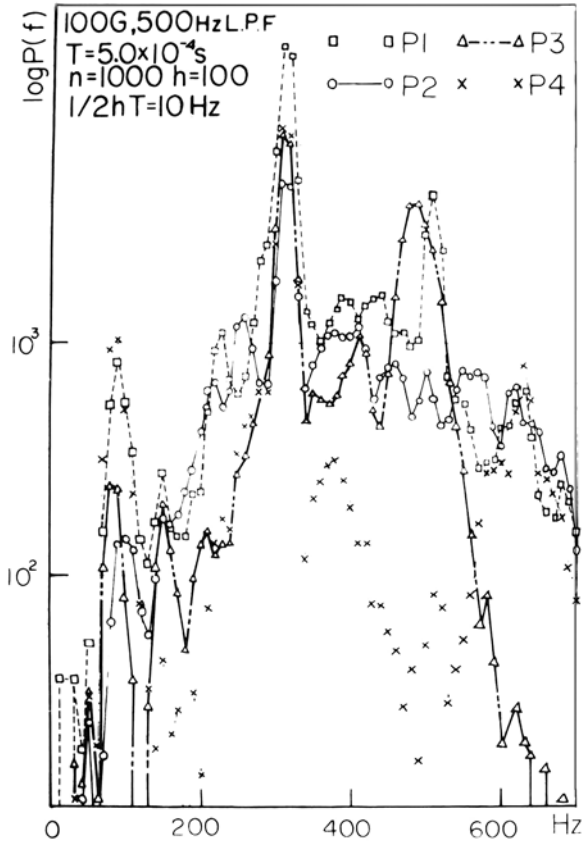


Fig. 4 Power spectra of the tremor up to high frequency

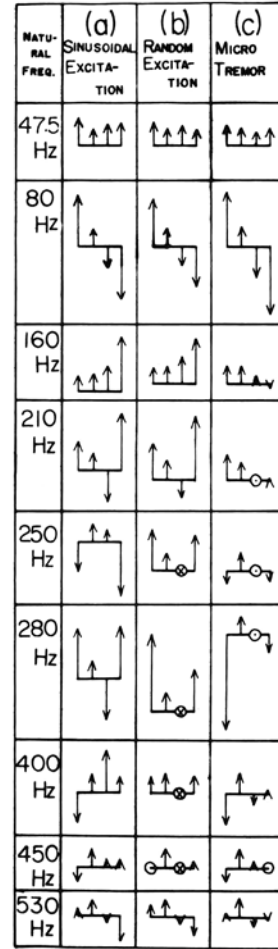


Fig. 6 Comparison of normal mode

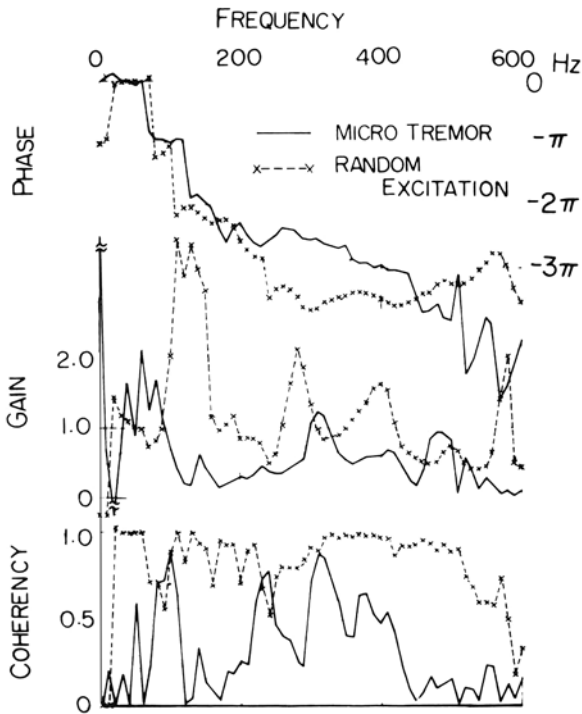


Fig. 5 Comparison of transfer function by the tremor with that by the response to random excitation

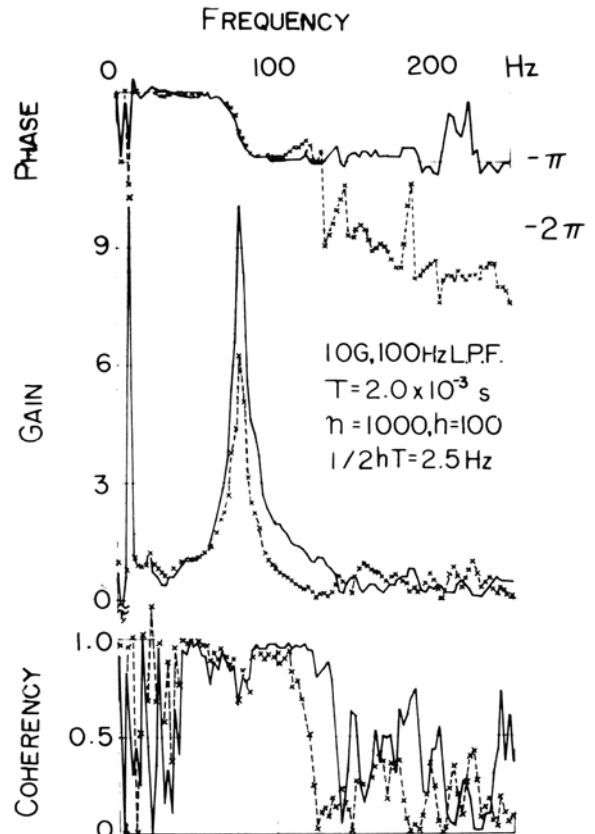


Fig. 7 Transfer function obtained for low-frequency range

Damping ratio

Fig. 7 shows the transfer function P4/P2 and P3/P2. The behaviour in the lower frequency range is seen in detail. The computation is made for $T = 2.0 \times 10^{-3}$ s, $n = 1000$, $h = 100$, $1/2hT = 2.5$ Hz and $nT = 2.0$ s. The phase relation reverses at about 80 Hz. The coherency at 80 Hz in Fig. 7 is higher than others, so the estimation can be reliable.

Assuming a one-degree-of-freedom system in the neighbourhood of the natural frequency (80 Hz), the damping ratio is obtained so as to fit the phase characteristic of the transfer function (Eq. (1)) to the phase relation of Fig. 7 in the sense of the least square of the error. The result is given as $\zeta = 0.023$. For the higher-order natural frequencies at which phase reversal occurs the same analysis can be applied.

CONCLUSIONS

It is shown for a lathe that the natural frequencies, the principal normal mode and the damping ratio can be obtained by means of the micro tremor, applying cross-spectrum analysis. The sinusoidal and the random excitation is made at the same time. This shows that, when appropriate random excitation is adopted, the normal modes can be identified at higher-order natural frequencies than when tremor is utilized. However, the advantage of the tremor method is that the machine is exposed to conditions which also occur during normal operation. Although the tremor may affect the machining precision and the surface finish, quantitative estimation will be left for the future.

ACKNOWLEDGMENTS

The authors express their gratitude to Professors N. Takenaka, A. Watari, S. Fujii and H. Shibata at University of Tokyo, and Dr H. Akaike in the Institute of Statistics of Ministry of Education for their fruitful discussions. They also owe much to Messrs K. Suzuki and M. Komazaki for carrying out the experiment. This research is partly supported by the Ministry of Education.

REFERENCES

1. HONDA, K. and YASUI, T., 'Fundamental study on dynamic stiffness of machine tool', *J. JSME*, 67-546 (1964-7) (in Japanese).
2. TOBIAS, S. A., *Machine-Tool Vibration*, Blackie, (1965).
3. SATO, H., 'Measurement of dynamic characteristics of machine tool by micro tremor', *Preprint of JSME*, 151 (1966-4) (in Japanese).
4. SATO, H. and COOK, N. H., 'An experimental study of machine tool vibration on surface finish', *Material Proc. Lab., Dept. of Mech. Eng., MIT*, (1966-7).
5. KWIATKOWSKI, A. W. and BENNETT, F. E., 'Application of random force excitation to the determination of receptances of machine tool structures', *Proc. 6th MTDR* (1965-9).
6. PEKLENIK, J., and KWIATKOWSKI, A. W., 'New concepts in investigating the manufacturing system by means of random process analysis', *Proc. 7th MTDR* (1966-9).

7. AKAIKE, H., 'Statistical measurement of frequency response function', *Ann. Inst. Stat. Math.*, Ministry of Education, Suppl. 3 (1964).

APPENDIX: GENERAL IDEA OF CROSS-SPECTRUM ANALYSIS

This is a method to predict the transfer function of a system using random analysis. This has been developed in the fields of statistical analysis.

It is assumed that $y(t)$ is the output of a system with transfer function $H(f)$, the input of which is $x(t)$, and noise $n(t)$ independent of $x(t)$ disturbs the system at the same time. Since $x(t)$ and $y(t)$ can be measured and $n(t)$ cannot be discerned, for the identification $x(t)$ and $y(t)$ only are used.

Autocorrelation functions of $x(t)$ and $y(t)$ are $R_x(\tau)$ and $R_y(\tau)$, and cross-correlation function $R_{xy}(\tau)$ are respectively computed as

$$R_x(\tau) = \lim_{T \rightarrow \infty} \frac{1}{2T} \int_{-T}^T x(t) x(t + \tau) dt \quad (2)$$

$$R_y(\tau) = \lim_{T \rightarrow \infty} \frac{1}{2T} \int_{-T}^T y(t) y(t + \tau) dt \quad (3)$$

$$R_{xy}(\tau) = \lim_{T \rightarrow \infty} \frac{1}{2T} \int_{-T}^T x(t) y(t + \tau) dt \quad (4)$$

A correlation function is sometimes called a correlogram in the case of a numerical computation. Power spectra of $x(t)$ and $y(t)$, i.e. $P_x(f)$ and $P_y(f)$, and the cross-spectrum $P_{xy}(f)$ are given by Fourier transform of (2), (3) and (4)

$$P_x(f) = \lim_{T \rightarrow \infty} \frac{1}{2T} \int_{-T}^T R_x(\tau) \exp(-2\pi jf\tau) d\tau \quad (5)$$

$$P_y(f) = \lim_{T \rightarrow \infty} \frac{1}{2T} \int_{-T}^T R_y(\tau) \exp(-2\pi jf\tau) d\tau \quad (6)$$

$$P_{xy}(f) = \lim_{T \rightarrow \infty} \frac{1}{2T} \int_{-T}^T R_{xy}(\tau) \exp(-2\pi jf\tau) d\tau \quad (7)$$

There are important relations between these power spectra and the power spectrum of noise $P_n(f)$ as follows

$$P_{xy}(f) = H(f) P_x(f) \quad (8)$$

$$P_y(f) = |H(f)|^2 P_x(f) + P_n(f) \quad (9)$$

From (8) $H(f)$ can be given as

$$H(f) = P_{xy}(f) / P_x(f) \quad (10)$$

On the other hand (8) and (9) give

$$\gamma^2(f) = \frac{|P_{xy}(f) / P_x(f)|}{P_y(f) / P_x(f)} = \frac{1}{1 + P_n(f) / P_x(f)} \leq 1 \quad (11)$$

where $\gamma(f)$ is called coherency. If $P_n(f) = 0$, that is, there is no noise to $H(f)$, $\gamma^2(f) = 1$. As the noise component to the system increases, $\gamma^2(f)$ becomes smaller than 1.0. Then the coherency gives an index of reliability of the computed transfer function.

DISCUSSION

Query from Dr. N. H. Hanna (Birmingham University)

There are a number of points in this paper that I am not clear about and I would be grateful if the authors could clarify:

1. Two accelerometers of natural frequencies 80 and 300 Hz were used in measuring tremor components in the frequency ranges of 0–100 Hz and 0–700 Hz respectively. Obviously, this will result in a distorted power spectrum which will be dominated by peaks corresponding to the natural frequencies of the accelerometers, as appears from Fig. 3 and 4. On the other hand, 50 and 500 Hz low-pass filters, presumably the purpose of which was to remove all (or most of) the frequency components above 50 and 500 Hz respectively, are reported to have been employed (see Figs. 3 and 4). However, power spectrum computations were carried out for frequencies above those mentioned which, apart from the error introduced, is very confusing.
2. Forces generated by the rotation of the gears, spindle and the driving motor have components of random nature not only in magnitude and phase but also in direction and perhaps their points of application. Therefore, the use of the function $P3/P2$ as a transfer function is misleading because, theoretically speaking, it will be a random function, that is, it will vary each time measurement is taken and the authors have not provided any experimental results to prove otherwise. It also follows that the comparison between the transfer function obtained by applying an external force in a fixed direction and at a single point, and that obtained by tremor analysis, as proposed by the authors, is not valid due to the fact that the former will be constant and the latter will not.
3. The physical meaning of the coefficient ζ defined by the authors as damping ratio, is not very clear.

Replies

1. The accelerometer used for the measurement was a strain gauge type pick-up. The characteristic around the natural frequency is damped sufficiently and the peak at the natural frequency cannot be seen through the calibration.

The frequency characteristic beyond the natural frequency decreases according to the characteristic of single-degree-of-freedom system. Then the sensitivity of the accelerometer is still large enough, even if the measurement is made above the natural frequency, provided the range is close to it. As the object of computing the power spectrum is to know the existence of the approximate natural frequency observed in micro tremor, the distortion of the power spectrum mentioned in the contribution is not serious, if the aforementioned situation is taken into consideration.

Even if the filter is used, the situation close to the break point frequency does not change from that mentioned above. The frequency components

above 50 and 500 Hz are not all removed by the low-pass filter used in this paper. However, it is effective to remove the higher frequency components in comparison with the natural frequency of the accelerometer, and the sensitivity around the natural frequency remains high enough to make the peak at about 80 Hz in Fig. 3. The distortion is not serious again. The peculiarities in the low frequency range are made clear.

2. As the characteristic of the excitation force is random, the dynamic behaviour of the machine structure can be excited. If the exciting force is sinusoidal, the machine is only excited by the frequency. If it is pure random with white power spectrum, as stated in the theory, all natural frequencies are supposed to appear. Even though the excitation force has a random nature in direction and the points application, it is advantageous in exciting the dynamic characteristic of the machine structure. However, it cannot be naturally expected that the characteristic of the tremor corresponds to that of theory, so that we have to pay attention to coherency which gives a measure of reliability for the practical computation of the transfer function.

In the practical computation of the power spectrum and transfer function the length of data is limited, and consequently the length of correlogram is also limited. According to the theory which was developed as for the power spectrum by R. B. Blackman and J. W. Tukey (R. B. Blackman and J. W. Tukey: *The Measurement of Power Spectra*, Dover, 1958) and was extended as for the transfer function by H. Akaike⁷, the lag window which limits the length of correlogram can be transformed to the spectral window which smooths the power spectrum and realises an estimated power spectrum for the theoretical one in the sense of a statistical mean. This is also applicable to the estimate of the transfer function. The theory is based on the stationarity of the phenomenon. It can be said that the assumption is reasonable for the case of the micro tremor. So it is not necessary to evaluate $P3/P2$ for each different time duration and the results described in the paper are valid. However, from an experimental viewpoint, the computation was performed several times and almost the same results obtained.

These justify the noise characteristic and can be dealt with, being satisfactorily stationary random. As mentioned above the dynamic characteristic itself is proper for each machine tool structure system. The natural frequencies which are covered by the input frequency components are excited and the effect of difference of the input nature is measured by the coherency. Then the comparison denoted by the contributor is valid. A new approach, to find out the dynamic characteristic by making use of the tremor, should be justified by comparing with the results by other methods. Fig. 6 shows this. It also describes the characteristic of each testing method for identification of the modes.

3. There are several methods to estimate the damping ratio of a machine tool structure. The method mentioned in the paper proposes a new approach to estimate the damping ratio for higher modes of the natural frequency.

It has been made obvious that the dynamic characteristic of machine tools can be represented by a one-degree-of-freedom system around the natural frequencies. However, the shape around the natural frequency of the power spectrum and the gain of the transfer function cannot be applicable for the estimation of damping, because it varies according to the analytical conditions such as data length, sampling period and length of correlogram. On the other hand, the phase characteristic is stable and is not easily affected by these and the estimated result well represents the damping ratio of the natural frequency.

Query from G. Werntie

You must change for your test various driving conditions to have different frequency components of the excitation source.

If the machine has different dynamic characteristics at different driving conditions, do you think that you will get the correct results?

Reply

Of course we have to change driving conditions, and the figures shown in the paper are examples.

I do not think that the dynamic characteristics of machine tools themselves change for different driving conditions. The shape of the power spectrum might change slightly for different driving conditions. However, this is caused by the change of exciting forces related with the different driving conditions, not by that of the different dynamic characteristics. In the case of lathes, the change of the position of the tailstock affects the dynamic characteristics of machine tools shape for a higher order of the natural frequencies.

ESTABLISHING STANDARD CUTTING CONDITIONS FOR PERFORMANCE TESTING OF UNIVERSAL METAL CUTTING MACHINE TOOLS

by

M. BURDEKIN, A. COWLEY and J. TLUSTY*

SUMMARY

The paper discusses the basis for formulating standardised conditions for practical cutting tests to reveal the chatter performance of machine tools. The conditions proposed would also be applicable to vibration testing and analysis.

The proposed conditions have been derived by due consideration to machine utilization, workpiece statistics and tool life. Examples relating to centre lathes and horizontal milling and boring machines are presented.

The paper is based upon work conducted during an investigation sponsored by the Department of Trade and Industry of the Ministry of Aviation Supply.

NOTATION

a	depth of cut
A_1	full power test
A_2	limit power test
A	position of face mill relative to workpiece
b_t	chip width per tooth in face milling
b	total chip width
b_{lim}	limit chip width at threshold of chatter
B	width of cut in slab and face milling
'B'	limit chip width test
D_{max}	maximum swing over bed
D_c	diameter of cutter
d_s	diameter of spindle
d_w	diameter of workpiece
h	undeformed chip thickness
L_{max}	maximum length of workpiece which will clamp between headstock and tailstock
L	length of test workpiece
n	cutter rotational speed
P_s	mean specific cutting pressure
Q	metal removal rate
s	feed
S	feed/min
S_t	feed/tooth = S/n
T	tool life
V	cutting speed
V_B	flank wear
V_{30}	cutting speed for a tool life of 30 minutes (based on flank wear criterion)
Z	number of teeth in cutter
Z_c	number of teeth cutting simultaneously
ϕ	engagement angle
ϕ_1	angle of first contact
\mathcal{H}	cutting edge angle (approach angle)
\mathcal{H}_f	facet edge angle
\mathcal{H}_n	secondary edge angle

INTRODUCTION

The cutting performance of a machine tool can be assessed from the results of actual cutting tests (direct tests) or by inference from the results of vibration measurements (indirect tests) on the machine tool structure. Both approaches have their special merits which have been summarised¹. However, irrespective of whether one chooses the indirect type of test (exciter test) to the direct (cutting test), the results have to be interpreted in terms of some accepted standard test conditions, otherwise an assessment of the performance of one machine or the relative performances of similar machines cannot be made. The reason for this is that all cutting conditions influence chatter and unless one has precise knowledge of the inter-relationship between factors such as workpiece material and size, tool geometry, cutting speed, feed and overhang, etc., comparisons of machines would be impossible. It would be extremely helpful, therefore, from the viewpoints of both users and manufacturers, if some standard conditions could be adopted for testing purposes on different sizes and types of universal machines. Such an approach would assist in specifying performance and reduce the cost of testing.

In the following sections, the main factors which influence the performance of the machine, as shown in Fig. 1, are considered and cutting conditions and standard cases are formulated for basic machine tool types.

POWER UTILIZATION OF BASIC PROCESSES

In metal removal processes, the power utilization of the machine is related to the metal removal rate, and for roughing operations this is some measure of the

*University of Manchester Institute of Science and Technology

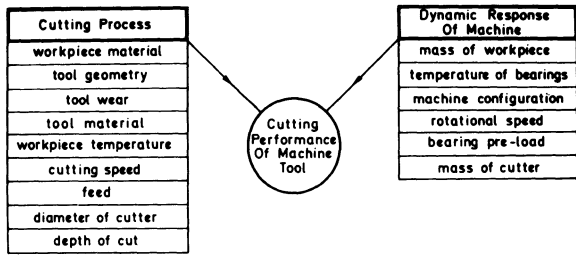


Fig. 1 Factors to be considered when specifying standard cutting conditions and test procedure

potential productivity. From this aspect therefore let us consider the basic processes of turning, boring, face milling and slab milling as shown in Fig. 2.

Thus for turning

$$Q \text{ (cm}^3\text{/min)} = V.a.s = V.b.h \quad (1)$$

where V = cutting speed (m/mm)
 a, b, h and s have units of mm
 The power dissipated is given by

$$\frac{V.b.h.P_s}{60} \text{ watts} \quad (2)$$

where P_s = mean specific cutting pressure (N/mm²)
 For face and slab milling

$$Q \text{ (cm}^3\text{/min)} = \frac{V.Z.S_t.a.B}{\pi D_c} \quad (3)$$

$$\text{Power} = \frac{V.Z.S_t.a.B.P_s}{\pi D_c \cdot 60} \text{ watts} \quad (4)$$

From the above relationships it is apparent that the metal removal rate generally depends upon three main factors; cutting speed, feed and depth of cut. These relationships also suggest that, since the metal removal rate is related to power, then the installed power of the machine is a measure of the possible metal removal rate. However, this may not necessarily apply in practice since for a given speed and feed, the depth of cut can be limited by the onset of chatter.

The limit depth of cut not only depends upon the dynamic characteristics of the structure but also upon the values of the cutting speed and feed² as shown in Fig. 3. In general within the range of cutting speeds associated with cemented carbide (c.c.) tools, the limit of stability is increased for increase in both speed and feed. Consequently, the metal removal rate as based upon the products $V.b.h$ and $V.a.s$ (Eq. [1]) does not yield an optimum condition other than that cutting speed and feed should be a maximum. However, there are practical limitations imposed on the choice of cutting speed and feed since these are dominant factors governing tool life (T). For example, the tool life equation quoted by Opitz³ for C.45 material was of the form

$$T.V^{2.56} (s.H)^{0.8} = \text{const.}$$

Since a tool life criterion is the basic parameter used in practice for selecting cutting speed and feed, then we are proposing that the cutting conditions associated with power utilization or metal removal rates should be related to tool life considerations.

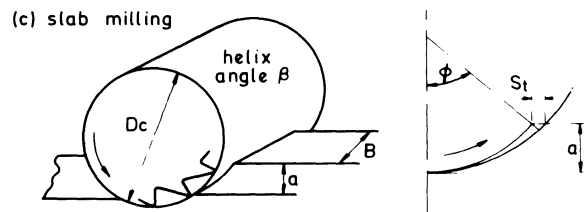
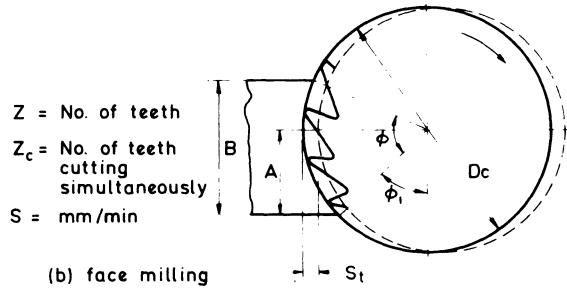
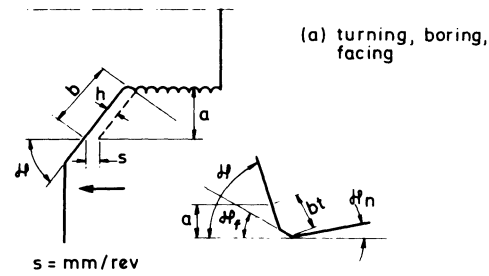


Fig. 2 Basic machining processes

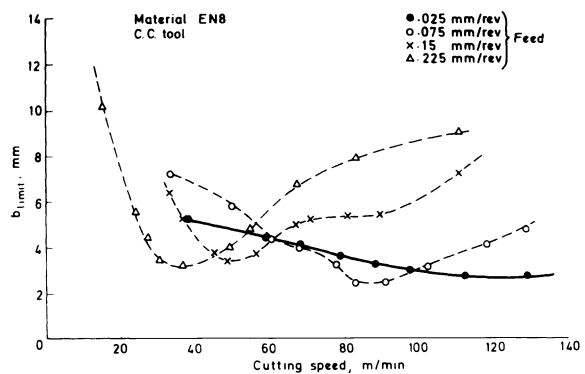


Fig. 3 Influence of feed and speed on the limit width of cut

GENERAL PERFORMANCE CRITERIA

In general it is logical for the installed power of a machine to be related to its size because the amount of metal to be removed is greater on larger workpieces. On the other hand machine stiffnesses are greater thereby allowing greater chip widths to be taken without chatter. The cutting tools are also larger and will therefore withstand greater forces.

Machines of the same nominal size can and often are also equipped with different powers and therefore classifications such as light type, heavy duty, etc., should reflect some differences in machine designs. It is therefore desirable to specify a machine's performance in more quantitative terms and consequently it is proposed that the installed power should indicate the machine's possible metal removal capabilities. However, it is obvious that this basic requirement cannot apply to all machining configurations since a

machine's chatter stability will vary, not only with speed and feed, but also with the orientation of the machining process with respect to the vibratory system. The size, mass and overhang of the workpiece can also play a significant part on the resulting stability. The combination of each of these conditions will be referred to as a *case*. Formulation of the basic cases to which full power utilization should be possible and other cases where only part of the nominal power can be utilised is based upon accumulated experience⁴ and statistical data on the most frequent sizes of workpieces as given by PERA^{5,6} and MTIRA⁷.

In addition to the above two categories, there are cases which are so difficult from the chatter aspect that the power utilization is very small and loses all significance. Examples of such operations are (a) plunge turning with form tools, (b) slab milling with form cutters or set of cutters, and (c) boring with extended boring spindle.

For these cases it is more meaningful to express the limiting conditions in terms of the limit width of cut b_{lim} . This parameter is directly related to the dynamic compliance of the machine and is predominantly governed by structural design.

Summarising the above, it is therefore proposed that performance should be based upon three criteria as follows.

- (1) Full power (A_1 test).
- (2) Limit power (A_2 test).
- (3) Limit chip width (B test).

SELECTION OF THE GENERAL TEST CONDITIONS

Workpiece material

The properties of the workpiece material obviously affects the results of the cutting tests and therefore require to be closely specified and controlled. For all cutting tests it is proposed that a low carbon steel in the normalized condition should be used, having a chemical composition equivalent to EN8, BSS970, 1955. The chemical composition and physical properties of this material are as follows

0.35/0.45 C; 0.05/0.35 Si; 0.6/1.0 Mn; 0.06 S(max);
0.06 P(max)
Ultimate tensile strength 55 kg/mm².

The reasons for choosing this material can be justified as follows.

1. Carbon steel is the material which is most frequently used on lathes. According to the survey carried out by PERA⁵ 39% of all turned components are made from carbon steel. Similar results were obtained by an M.T.I.R.A. Survey⁷. For boring machines, it was shown^{6,7} that cast iron is the most frequently used material (30–50%) and that carbon steel was the second most frequently used material (18–26%).

2. It is the lowest grade of carbon steel for which the quality is rather closely controlled.

3. Its chatter susceptibility is greater than for other commonly used materials such as cast iron and

stainless steel. From the data given by Sarwar² it was shown that cast iron and stainless steel are approximately twice as stable as low carbon steel.

4. Low carbon steel of similar specification to EN8 has been used for many years by both the 'Ma' and 'C' groups of CIRP and there is therefore data available on its machinability.

Even if one uses the material to the above specification, it is possible that the chatter characteristics could vary from different batches of nominally the same material. Consequently, in order to account for possible differences in the test material, a sample should be machined on a structure of well-defined dynamic characteristics such as the CIRP Cutting Stand¹.

Tool material and geometry

For power utilization of the machine, cemented carbide (c.c.) tools must be used in preference to HSS since they allow higher speeds and feeds to be used. The recommended grade of c.c. for roughing of steel⁸ is ISO P.30.

The choice of the tool geometry influences the magnitude of the tool life, the cutting coefficient and the directional orientation of the process. The range of standard tools available is also an important factor since this influences the choice of a suitable geometry.

From tool life considerations, the work of CIRP³ has shown that when machining low-medium carbon steel with c.c. tools, then the optimum tool life occurs with a positive rake angle γ of 6°.

Larger positive rake angles would of course give smaller cutting coefficients and generally larger limit widths of cut, but from practical considerations, large positive rake angles are not recommended on c.c. tools.

It has also been shown³ that a reduction in approach angle \mathcal{H} from 90° to 45° improved the tool life. In addition to the tool life consideration the approach angle is also one of the most important factors which affects the limit width of cut and hence the power utilization on single point tool operations. The reason for this is that it changes the direction of the cutting process with respect to the main modes of vibration of the machine and is one of the most important practical aspects governing the chatter process.

For turning operations, the modes are predominantly in the plane perpendicular to the spindle axis and thus, if we machine with a 90° approach angle, the cutting process will be very stable since both the normal to the cut surface and the direction of the resultant incremental force P would be perpendicular to the main mode plane. By introducing an approach angle less than 90°, then there is a component of P and Y in the mode plane and the process will be less stable. In practice an approach angle of 70° would be used, but for test purposes we are specifying 45° in order to exaggerate the chatter limitation. In addition to increasing the sensitivity of the test, a lower tool wear results which contributes to the regularity of the results.

For boring operations, the approach angle also influences the orientation of the cutting process with

respect to the mode direction. In these operations, the boring bar or spindle is usually responsible for chatter and such cases are usually much more compliant than the machine structure. Therefore, we do not have to exaggerate the chatter limitation in these tests and consequently a 70° approach angle is specified.

There is a further orientation to be considered when analysing the boring spindle on some horizontal boring machines. The spindles on these machines usually have two diametrically opposite axial keyways and the position of the tool with respect to the keyways is important since this can influence the magnitude of the limit depth of cut. An example from an actual cutting test is given in Fig. 4. These large variations in the limit depth of cut with angular position of the tool occur because of the possible cancellation of the response of two distinct modes of vibration which are caused by the influence of the keyways. Theoretical details of this mechanism are given in Chapter 4 of the book by Koenigs Berger and Tlustý⁴. In practice, the designer of the standard tooling for this machine can take advantage of this coupling phenomenon by ensuring that the boring tool holder is located at the optimum radial position.

Cutting tests are most efficiently carried out by using c.c. throwaway type inserts in a standard tool holder. With this type of insert, it is necessary to specify the size of the tool nose radius and indeed this is important in practice from the tool life aspect. However, from the stability aspect, more reliable results can be obtained when the limited width of cut is large compared with the nose radius and for this reason, the recommended radius is limited to 0.8 mm.

Tool wear is a practical aspect which influences the magnitude of the limit conditions. In general, sharp tools are more susceptible to chatter than 'dull' tools as can be seen from the curve of limit width against cutting time as shown in Fig. 5. In order to obtain repeatable results it is therefore necessary to change the cutting edge frequently, and to remove the initial sharpness of the tool by machining a small portion of the surface prior to each test.

Cemented carbide inserts are also recommended for face milling cutters in order to utilize the power of the machine. These inserts should be in P.30 grade c.c. with a main cutting edge angle \mathcal{H} of 75° and facet length of 1 mm. The rake angles should be generally positive with a negative primary land on the cut out edge.

The rake angles of HSS tools should be in the order of 15° positive. This value of positive rake is necessary in order to produce a reasonable cut surface at the lower cutting speeds which are generally associated with built-up edge conditions.

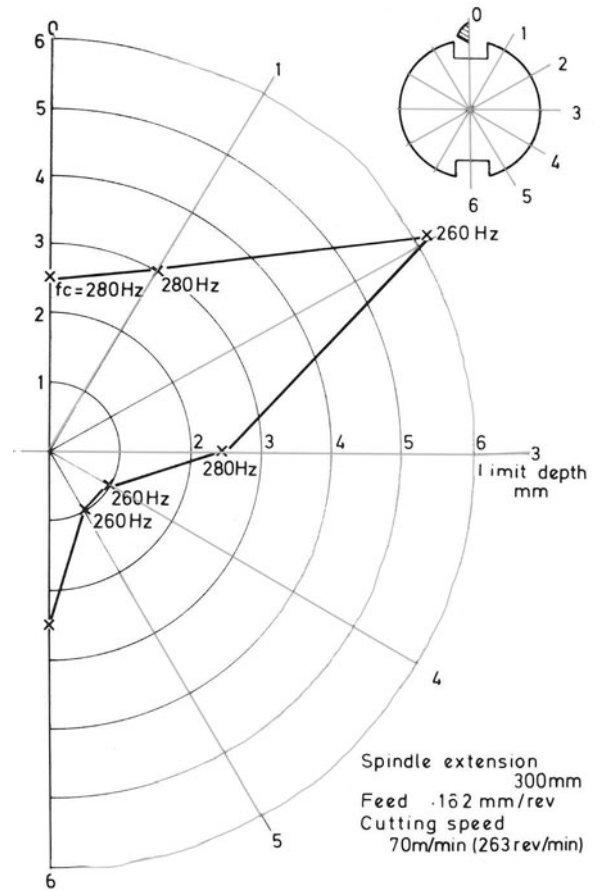


Fig. 4 Influence of tool orientation on stability in boring

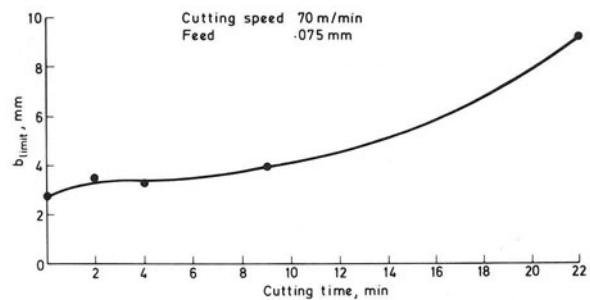


Fig. 5 Influence of cutting time on the limit width of cut

Cutting speeds and feeds

Turning

It has been shown above that for tests A_1 and A_2 , the selection of speed and feed should be based upon a tool life criterion. However, there are three variables in the tool life relationship and two of these unknowns must be specified before the magnitude of the third variable can be established. The first of these variables is the acceptable life of the tool and in practice this is based upon an economic relationship between tool and machine costs and can vary between about 10 and 60 minutes. For the A_1 and A_2 tests we are proposing that these should be based upon a tool life criterion of 30 minutes. It should also be stressed, however, that, owing to the exponent in the tool life relationship, then the difference in cutting speed for a tool life of 10 and 30 mins is only of the order of 50%. It is also logical that for turning the magnitude of the feed should be related to the size of the machine. For centre lathes the feed is specified as 1/1000 of the maximum diameter over the bed and this corresponds with the feeds used in practice as based upon a survey by MTIRA⁷. Having specified the tool life and feed, it is now possible to determine the corresponding cutting speed from the tool life relationship. This relationship is shown in Fig. 6, for the specified workpiece and tool material, and is based on VDI¹⁰ and CIRP tool life data.

For the 'B' tests both c.c. and HSS tools are specified for centre lathes. In this test we are not interested in the power utilization, but on the maximum width of the cut, particularly in plunge cut operations. The cutting conditions for these tests are different in the respect of both feed and cutting speed. For c.c. tools we are specifying feeds of 0.1 and 0.2 mm at a cutting speed of 100 m/min. This choice is based upon two considerations: (a) with higher speeds or feeds, the cutting test is difficult to carry out, owing to the change in the cutting speed especially for plunge cutting; (b) Fig. 3 and Sarwar² show that for feeds in the speed region of 100 m/min reducing feed also reduces stability—it is, therefore, necessary to carry out the 'B' test at small feeds in order to represent the dwell conditions at the finish of a plunge cut operation.

For machining with HSS tools, the recommended speed and feed is 30 m/min and 0.1 mm respectively.

Face Milling

The size of the teeth on face mills is usually independent of the diameter of the cutter, and consequently the cutting conditions should be based upon the loading on the teeth. Therefore for all c.c. face mills the proposed nominal speed and feed are 150 m/min and 0.25 mm/tooth respectively and such values have been based upon the VDI data¹¹. Owing to the geometrical conditions which are imposed on the chatter conditions when milling with a multi-tooth cutter, the lobing phenomenon can occur. Thus, in practice, the stability of the machine could vary considerably, depending upon where the lobes coincide with the nominal speed of the cutter. Hence, when carrying out the A_1 and A_2 tests on a particular configuration at the nominal cutting speed, and the specified power

cannot be achieved, then the speed should be adjusted to the next higher and lower speed of the machine in order to take account of the possible lobing effect. A practical example of the effect of changing in the cutting speed and orientation on the limit conditions for milling on a horizontal milling and boring machine is shown in Fig. 7.

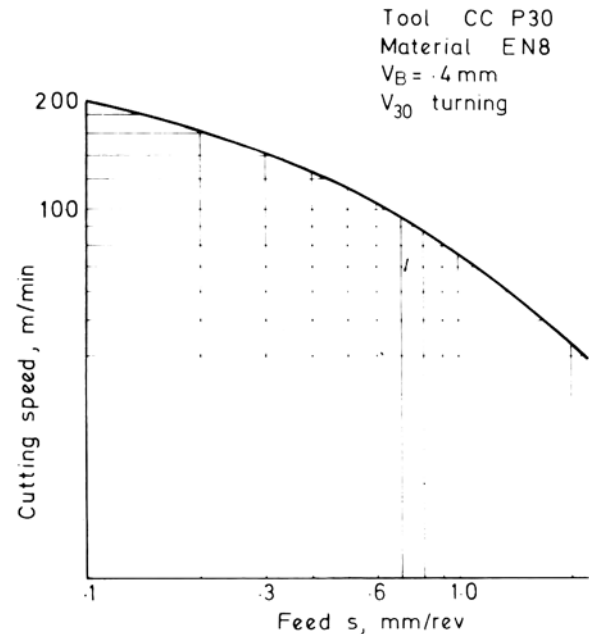


Fig. 6 Relationship between cutting speed and feed for a tool life of 30 min

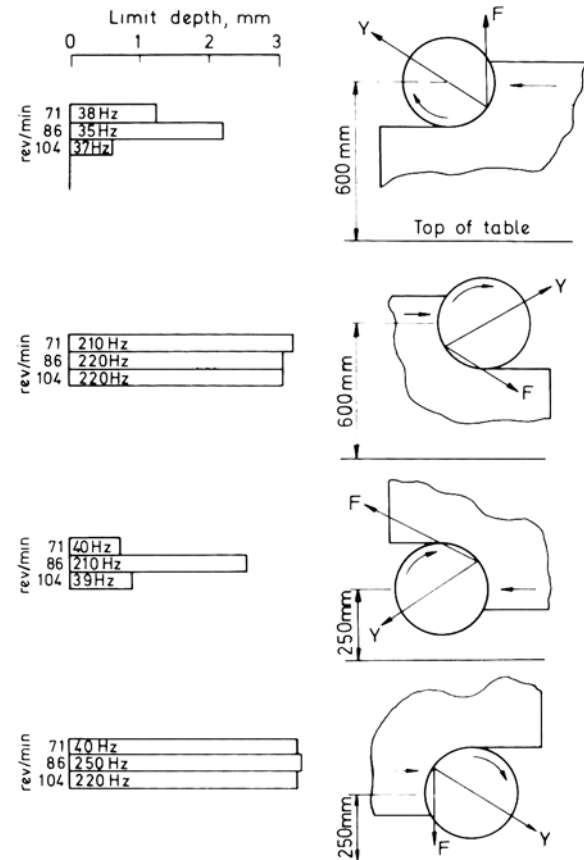


Fig. 7 Example of the influence of orientation and cutting speed on the limit depth of cut and chatter frequency for face milling

EXAMPLES OF RECOMMENDED CASES

Centre lathe

The mass of the workpiece is important on centre lathes since this forms an important part of the vibratory system; the spindle, the clamping of the workpiece, and the workpiece overhang are the most important springs in the system. It is, therefore, important to select the size of the test workpiece with due consideration to these factors.

The two basic clamping configurations are given with the workpiece held in overhang in the chuck and with longer work pieces held in the chuck and centre.

There are five proposed test set-ups for the cutting tests and these are outlined below.

1. Full power tests (A_1). The workpiece is held in the chuck and centre, and the test is carried out at the chuck and tailstock ends of the workpiece. The size of the workpiece is such that its diameter is 0.2 to 0.25 of the maximum swing over the bed and represents a workpiece which is slightly above the average size that would be machined. The length of the workpiece is 0.7 of the maximum length between chuck and tailstock but this is restricted to 6 times the workpiece diameter for long beds in order to eliminate the problems associated with slender workpieces.

2. Full power test (A_1), but with the workpiece clamped in the chuck only and with an average overhang. The workpiece diameter (d_w) is specified as 0.3 to 0.4 of the maximum swing over the bed (D_{max}) and an overhang of 0.15 to 0.17 of D_{max} .

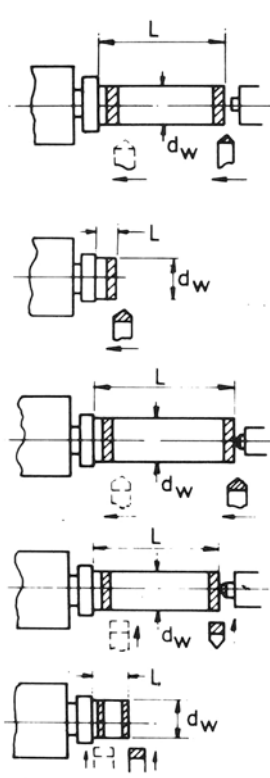
3. The limited power test (A_2). With this test a

heavy workpiece is held in the chuck and centre. The diameter d_w is specified as $0.3D_{max}$ and length 0.8 to $0.9L_{max}$ or less than $6d_w$. The test is carried out at both the tailstock and headstock end of the workpiece, and, owing to its large mass, we do not expect to use the full power of the machine and require the limiting power P_{lim} of 0.7 of the maximum power. The specified feed of $0.001D_{max}$ is the usual feed for heavier roughing operations for middle-size lathes with an average installed power. However, in high-power types of lathes greater feeds are usual in the order of $0.002D_{max}$. Therefore, if with the basic recommended feed the required power is not reached without chatter, the limit widths of cut for $S = 0.001D_{max}$ are recorded and the test is repeated with $S = 0.002D_{max}$, where finally the (A_1 or A_2) criterion is applied.

4. The limit width of chip tests ('B'). The fourth test is a plunge cut operation with an approach angle of $\mathcal{H} = 0$, and here the criterion is the limit width of cut (b_{lim}). The workpiece set-up is the same as test (1) and the test is carried out at the headstock and tailstock and with both c.c. and HSS tools.

5. This is also a 'B' test with the workpiece held in the chuck only with an overhang of $L = 0.2D_{max}$ and a diameter $d_w = 0.2D_{max}$. The test is carried out with both c.c. and HSS tools at the headstock and tailstock end of the test piece.

The smallest value of b_{lim} for the 'B' tests proposed in tests (4) and (5) above can be used to classify the chatter performance of the machine. There are four classes proposed and the specified values are based upon previous experience⁴⁹. The



Test	Cutting Conditions						Acceptable Values			
	s (mm)	V	d_w	\mathcal{H}	L	Tool	P_{max}	P_{lim}	Class	b_{lim}
A1	$\frac{D_{max}}{1000}$	V_{30}	.2 $\frac{D_{max}}{D_{max}}$ to .25	45°	.7 $\frac{L_{max}}{6d_w}$	C.C.	✓	—	—	—
A1	$\frac{D_{max}}{1000}$	V_{30}	.3 $\frac{D_{max}}{D_{max}}$ to .4	45°	.15 $\frac{D_{max}}{D_{max}}$ to .17	C.C.	✓	—	—	—
A2	$\frac{D_{max}}{1000}$	V_{30}	.3 $\frac{D_{max}}{D_{max}}$	45°	.8 $\frac{L_{max}}{L_{max}}$ to .9 $L_{max} < 6d_w$	C.C.	—	$\geq P_{max}$	—	—
B	.1 .2	100 20 m/min m/min	.2 $\frac{D_{max}}{D_{max}}$ to .25	0°	.7 $L_{max} < 6d_w$	C.C. H.S.S.	—	—	0 A B C	$>.03 D_{max}$ $>.02 D_{max}$ $>.01 D_{max}$ $<.01 D_{max}$
B	.1 .2	100 20 m/min m/min	.2 $\frac{D_{max}}{D_{max}}$	0°	.3 $\frac{D_{max}}{D_{max}}$	C.C. H.S.S.	—	—	0 A B C	$>.03 D_{max}$ $>.02 D_{max}$ $>.01 D_{max}$ $<.01 D_{max}$

Fig. 8 Proposed basic test cases for centre lathe

classes are specified for both HSS and c.c. cutting conditions and are summarized along with the above tests in Fig. 8.

Using the reasoning outlined above the basic cases for other types of lathes have been evaluated¹.

Horizontal boring machine

The tests on this machine include face milling with the cutter mounted directly onto the spindle sleeve and also onto the boring spindle. End milling and also boring with the boring spindle are also included.

When the face mill is mounted in the most rigid configuration, i.e. clamped directly onto the spindle flange, then stability generally depends upon the directional orientation and the height of the cutter above the top surface of the table. Full power utilization is required with the spindle up to a height of 0.6 of H_{max} . Since 'frame' milling is often used in practice, all the basic orientation shown in (a) to (f) of Fig. 9a must be considered and also the possibility of improving the stability by changes in speed if the specified power cannot be achieved. If then full power is only satisfied for some orientations, then the depth of cut A_{lim} should be recorded for the others.

The limit power test (A_2) is specified when the cutter is at the top of the column, i.e. where the machine is in the most compliant configuration. For this case we should expect the utilizable power to be greater than 0.75 of the nominal power.

The size of the cutters for all the milling operations are given in Fig. 9b and have been specified on the basis of the spindle diameter and the availability of standard cutters.

Other face milling tests are carried out with a smaller face mill mounted onto the boring spindle. With a spindle extension of twice the diameter of the spindle, power utilization of at least 0.5 of the nominal power is required.

For end milling operations, a 'B' test is specified with the cutter size given in the table.

The boring test (type B) is made with the tool mounted to the boring spindle. With this operation as was shown in Fig. 4 the limit depth of cut will depend upon the angular location of the cutter with respect to the key ways in the spindle. It is left to the manufacturer of the machine to locate the tool at the optimum position with respect to the key ways. The limit conditions are, of course, also a function of the spindle extension and two extensions are specified; one with thy extension of $3d_s$ and the other $5d_s$. Limit conditions are not classified but for the larger extension a minimum of 2 mm is required.

PRACTICAL PROCEDURE

The following notes may assist those who are attempting to carry out performance tests for the first time.

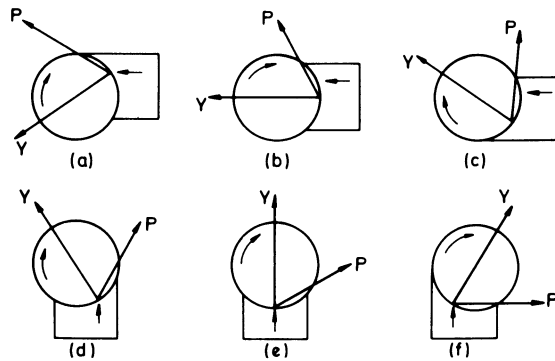
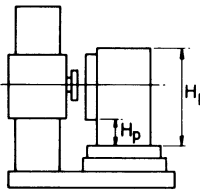
Workpiece material and tools

On most occasions, the time allocated for the availability of the machine for performance tests will be limited, and therefore valuable time can be saved if all the possible preparations are made before the tests.

**Face Milling
Selection of cutter**

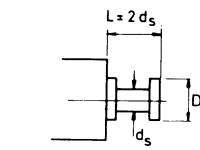
Boring Spindle Diameter	Cutter Diameter	Remarks
63mm 70,75mm 90,100 mm	200mm 250mm 315 mm	Cutter clamped directly to spindle sleeve flange or via standard adaptor to faceplate

	H_h	H_p	V	S_c mm	Remarks
A1	.6 H_{max}	.3 H_{max}	150 m/min	.25	P_{max} for Orientations (a) (b) (c) (d) (e) (f)
A2	H_{max} minus D_c	.6 H_{max}	150 m/min	.25	$P_{lim} \geq .75P_{max}$ for Orientations (a) (b) (c) (d) (e) (f)

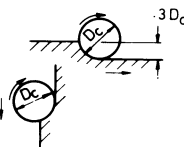


(a)

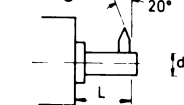
Boring Spindle Diameter	Cutter Diameter	Remarks
63mm 70,75 mm 90,100 mm	100 160 160	Extension of boring spindle = $2d_s$



End Milling



Boring



α (°)	H_h	H_p	V	S_t	Remarks
	H_{max} D_c		150 m/min	.25	$P_{lim} \geq .5 P_{max}$ in Orientations (a) (b) (c) (d) (e) (f)
			20 m/min	.1	Cutter Size d_s d_c flutes 63 25 4 70,75 40 6 90,100 50 8

Test	L	S	V	Tool	Remarks
B	$3d_s$.1	100 m/min	c c	
B	$5d_s$.	.	.	$b_{lim} \geq 2mm$

(b)

Fig. 9 (a), Proposed basic cases for horizontal boring and (b), milling machine

The workpiece sizes should be chosen in accordance with the recommended proportions and material purchased if necessary. Time can also be saved by pre-centring and facing the test pieces for lathes, etc., and mounting on the fixture in the case of boring and milling machines.

For milling and boring machines, a great saving in material cost can be made by having the workpiece specimens in the form of plates, which can be mounted on box type columns or stools. If, however, a stiff angle plate is available then this could be used with caution.

Tools and cutters should be selected in accordance with the specifications. It is advisable to have a spare set of c.c. tips available for face milling cutters in case of accidents. Face milling cutters should be mounted directly onto the flange of the milling spindle or in the case of some horizontal boring machines, onto the standard adaptor which is supplied by the manufacturer.

Cutting conditions

Select the cutting speeds and feeds in accordance with the recommendation. For the A_1 and A_2 tests on lathes, the feed should be chosen as a function of the size of the machine, and the corresponding cutting speed determined from the tool life curve (Fig. 6). Calculate the corresponding spindle speed to give this cutting speed. For milling cutters, calculate the spindle speed corresponding to the specified cutting speed.

Idle run test

Before we can establish the usable power of a machine, it is necessary to determine the power losses in the drive. This is measured by connecting a wattmeter into the power supply of the motor and obtain the power dissipation at each spindle speed.

Cutting tests

Before any tests are made the machine should be 'warmed up' by rotating the spindle in the middle speed range for approximately 15 min. This enables more repeatable results to be obtained, since experience has shown that the damping of the spindle system changes with the temperature of the bearings.

For the three types of test (A_1 , A_2 and B) the general procedure is similar for both face milling and turning operations. Here the width of cut is increased in increments until the nominal power of the machine is reached in the case of the A_1 test or that the usable power is limited by chatter for the A_2 test. The smallest practical increment in the width of cut is about 0.1 mm, but larger increments in the order of 0.5 mm can be used to establish the approximate magnitude of the limiting conditions, after which the test can be repeated in this region by using increments of 0.1 mm. Once chatter has occurred the surface is undulated and this should be cleaned off before other tests are repeated. At the limit conditions, both the width of cut and power should be

noted in the case of the A_1 and A_2 tests, and the width of cut for the B test.

Detecting chatter conditions

For face milling and turning operations with c.c. tools, there is usually no doubt when the system becomes unstable. It is, however, useful to record the amplitude and frequency of chatter by means of an absolute vibration pickup and a U.V. recorder. The actual amplitude recorded will, of course, depend upon the position of the pickup on the structure, but there will be a marked increase in the amplitude at the onset of chatter. It is also useful to measure the chatter frequency as a means of establishing which mode of the structure is responsible for chatter.

CONCLUSIONS

The work has outlined the important factors which should be considered when specifying performance tests. The advantages of interpreting the results under generally accepted conditions is stressed and in this respect general performance criteria and cases have been proposed. Other examples of specific machine types are given in by UMIST¹.

The proposals are directly applicable to assessment by cutting tests. However, many of the cases are also relevant to exciter tests but for quantitative interpretation of such results reliable data on cutting coefficients are necessary.

REFERENCES

1. *Specifications and Tests of Metal Cutting Machine Tools*, Machine Tool Engineering Division, UMIST.
2. SARWAR, M., 'Determination of the cutting conditions for cutting tests of stability against chatter', *M.Sc. Dissertation*, UMIST, January (1970).
3. OPITZ, H., 'Cutting tests with cemented carbide tools', *Rep. 3.3 CIRP-OECD/Group 'C'*, technical university Aachen, (1964); 'Behaviour of cemented carbides', *Rep. C6, CIRP-OECD/Group 'C'*, Technical University Aachen (1966).
4. TLUSTY, J. and POLACEK, M., 'Experiences with analysing stability of machine tools against chatter', *Proc. 9th MTDR. Conf., Birmingham* (1968).
5. PERA, *Survey of Turning Requirements in Industry*.
6. PERA, *Survey of Machining Requirements in Industry*.
7. MTIRA, 'The utilization of machine tools', *Res. Rep.*, No. 23 (1968).
8. *Choosing the Right Carbide*. Sandvik Coromant.
9. KOENIGSBERGER, F. and TLUSTY, J., *Machine Tool Structures*, Pergamon Press, Oxford (1970).
10. 'Cutting data for turning in non-interrupted dry cutting', *VDI Recommendation 3206*, June (1965).
11. 'Cutting data for face milling of steel with carbide tools', *VDI Recommendation 3205*, May (1960).

DISCUSSION*Query from Dr. Ing. M. A. El Hakim, Magdeburg*

The behaviour of the limiting width of cut with the tool wear obtained in Fig. 5 in this paper can be almost due to the orientation of the dynamic forces (especially those components at the tool-flank with respect to the direction of the maximum compliance of the system). Such a direction is different for each system and, therefore, the shown curve cannot be taken as a general behaviour. In many other cases, results were obtained showing a beginning stabilising effect of the wear followed by an unstabilising effect with still increasing wear, resulting in a peak by a relatively small value of wear land¹².

12. Salje, E. Self-excited vibrations of systems with two degrees of freedom *Trans. A.S.M.E.*, 78 (1956), 737–748, series B.

Reply

With reference to Dr. El Hakim's contribution concerning the influence of wear on stability. We agree that one of the reasons for this increase is the change in the direction of the incremental cutting force with respect to the modes of the dynamic system and, therefore, the effect of wear can differ for each dynamic system. However, the result shown in Fig. 5 was obtained on a simple model structure where the mode direction was approximately halfway between the incremental force direction and the normal to the cut surface. Consequently, this mode configuration was relatively insensitive to changes in the cutting force direction.

The main reason for the change in stability with wear is probably due to increased damping in the cutting process, with the increase in flank wear.

Query from J. Peters

I am sorry that I do not share the point of view of my good friends who are proposing cutting tests. Indeed, customers want cutting tests, but we are fooling them by giving them what they want. By doing so it is like giving a box of matches to a three-year-old child. In Fig. 5 you show that there does not exist such a thing as 'chatter susceptibility coefficient'. Consequently, the result of a cutting test does not give a unique definition of the quality of the machine tool as the customer would desire. The limiting depth of cut depends on speed, feed and cutting conditions. Even the minimum of the curves vary between machine tools. It may well happen, therefore, that by standardising cutting conditions you are at a minimum for one machine, and a bit shifted with respect to the minimum of another machine, and you would falsely conclude that the second one is better.

Quite a bit of work has been based on the article S. A. Tobias and Das published in 1967. We can now measure accurately the dynamic cutting force components and predict within a few % accuracy of the chatter limit: I refer to work done at VUOSO, Eindhoven, Aachen and Leuven. All these experiments precisely explain why cutting tests are not

reliable and indeed let us not forget that the U.S. Air Force launched the famous project seven years ago, precisely because of the lack of reliability of cutting tests. I feel we are now precisely ten years backwards. The problem is not to standardise cutting tests, but to make people who use them, because they are easy, aware of their limitations and very restricted validity.

Reply

Professor Peters states that the information obtained from cutting tests is limited. It is true that one cannot extrapolate the results to other cutting conditions such as different workpiece materials, tool materials, tool geometry, feeds, speeds, etc. However, we have paid due attention to these factors when formulating the test conditions and consequently most practical conditions have been covered by the minimum number of tests. Let us not overlook the fact that a cutting test also checks that the drive and clutches will transmit the nominal power. Such elements would not, of course, be considered by excitation measurements.

Because the paper is mainly concerned with cutting test procedures, it does not mean that we are against making excitation tests. We have performed many such tests for machine tool manufacturers. These are particularly useful if one is trying to locate the weakness in the structural design, and for these cases an exciter test is much more informative than cutting tests.

In principle, the results of excitation tests (receptances) can, of course, be interpreted for any cutting condition and orientation of the cutting process. However, predictions of such an analysis are not realistic at the present moment because of two main difficulties:

- Receptances which are truly representative of the structural conditions when machining, cannot easily be determined, that is, when the guideways are sliding. The work carried out at Aachen has shown that this factor can have a tremendous influence on the resulting receptances.
- Very little usable data has been published on the dynamic cutting force components, even though papers on this topic were published 10 years ago.

We are also involved in both these aspects at UMIST and consider it will be several years before they are sufficiently perfected to be accepted by the industry. In the meantime, cutting tests at standardised conditions will serve users needs.

Query from Martin D. Thomas

In your recommendation for a criterion for testing boring machines, you have apparently assumed that, provided two boring bars have the same length-to-diameter ratio, they have the same performance. In recent work at Birmingham University, a $2\frac{1}{2}$ in. dia. bar and a $1\frac{7}{8}$ in. dia. bar were used in cutting tests with a length-to-diameter ratio of 6. The stability boundary was found to be significantly different in these two cases, even taking tool orientation into consideration.

This is to be expected, as the stiffnesses of the bars will be constant if $p^3/d^4 = \text{const.}$, and the damping obeys a similarly complex relation.

Reply

We do not assume that boring spindles of the same length-to-diameter ratio will have the same chatter performance. In general, one would expect that for a given length-to-diameter ratio, the spindle with the largest diameter would perform best. In practice, one would only be comparing boring machines of similar spindle diameter. Also, in practice, the spindle bearings and drive keyways play an important part in the overall performance.

THE DEVELOPMENT OF A DYNAMIC PERFORMANCE TEST FOR LATHES

by

B. J. STONE*

SUMMARY

A cutting test procedure for comparing the chatter performance of lathes is described in outline, together with a summary of the results of the cutting tests conducted to establish the procedure. Information on the repeatability of single tests is presented, together with results showing the variations between nominally identical machines. The use of cutting tests as the basis for customer contracts is also discussed briefly.

INTRODUCTION

There is, throughout the world, steadily increasing pressure for more comprehensive testing of products offered for sale. This applies equally to machine tools and purchasers are beginning to require more quantitative information about the machine tools they buy. The properties of machine tools which may be required to be tested are many and various and the majority have been recently considered in some detail¹ in a report which considers the technical background to such tests and in many cases suggests methods of testing. Some of the quantities involved are, in principle at least, relatively simple to measure and the results are readily interpreted but in other cases it is much more difficult to specify the quantity to be measured and to devise meaningful ways of making the measurement. One of the latter, which happens to be of considerable importance, is the dynamic performance of machine tools.

The dynamic performance of a machine tool is fundamental to its chief function which is to produce a workpiece of a particular geometric form with an acceptable surface finish at as high a rate of production as is economically possible. Any limitation in dynamic performance may be manifested as a violent vibration termed chatter, which increases tool wear and power consumption, results in poor surface finish and hence limits production rates. A simple and reliable method of measuring liability to chatter would, therefore, be extremely useful to both manufacturers and users of machine tools. With the aid of such a method the dynamic performance or the ability of a machine tool to remove metal without chatter could be ascertained by any potential customer and ought to be taken into account together with cost, delivery, capacity, etc., when comparing several competitive machines.

This paper is concerned with the development of a comparative method of dynamic performance testing² for lathes. The essential problem is that of maintaining adequate control over the large number of variables that can affect the dynamic performance and lathes were chosen for the initial tests as single-point cutting is the simplest cutting operation and thus the number of variables was kept to a minimum. Even so, during the course of the work more than 650 cutting tests were conducted on 16 different machines of four different makes. Lathes are also the most commonly used machine tool.

Although the test procedure developed relates only to lathes, tests may obviously be formulated in a similar manner for other types of machine.

TEST PROCEDURE

Ideally a dynamic performance test should give information about the behaviour of the machine tool in all possible configurations and in all possible cutting operations. With the present state of knowledge, however, no simple test will give this information and a realistic objective is the development of a simple test procedure which can be applied to obtain reliable information about a machine in specified circumstances.

Two major decisions, which are interrelated, are required regarding the form of test. These are whether the test should be comparative or should give an absolute rating, e.g. coefficient of merit³ and also whether a cutting test should be used or an exciter test simulating the cutting forces³. The latter alternative arises because the liability to chatter increases with increase in the width of cut normal to the feed direction, and hence the width of cut at which chatter starts is a useful measure of the chatter performance of a machine in any given situation. This

*MTIRA Macclesfield

limiting width (b_{lim} , see Fig. 1) can be directly related to a particular characteristic of the response of the machine to an oscillating force, viz. the so-called operative chatter receptance³ and to the forces involved in cutting the particular workpiece material which require a knowledge of the dynamic cutting force coefficient^{1,4}. There are, therefore, two possible forms of test procedure involving either a cutting test to determine the limiting width or an 'exciter' test to determine the relevant dynamic characteristic. The arguments for and against each form of test are discussed briefly below together with those for comparative or absolute tests.

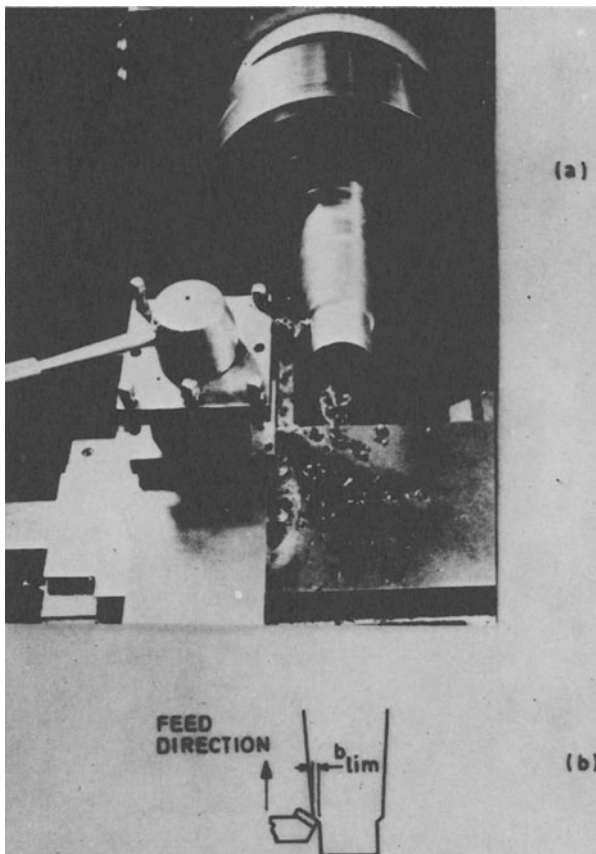


Fig. 1 Cutting test on tapered workpiece and definition of limiting width

Cutting tests or exciter tests

The main advantages normally claimed for exciter tests are the following.

(i) The variables associated with the cutting process are eliminated and the machine alone is tested so that the reliability of the result is greater.

(ii) There is no need for consumables such as workpieces and cutting tools so that, once the appropriate vibration test equipment has been purchased, no additional expenditure is involved for tests.

(iii) It is possible to test machines in various configurations and to compute the dynamic stiffness for any particular cutting direction³.

(iv) By using suitable force and displacement transducers a measure of dynamic stiffness is

obtained in the required units and thus an absolute comparison of machines is possible.

(v) The chatter performance of machines varies with rotational speed and shows the well known lobing effect^{3,5}. Thus, if cutting tests are conducted at certain speeds, a resulting false measure of performance may be obtained. The results of exciter tests have the advantage that they may be used to calculate the positions of lobes and establish minimum performance levels.

(vi) The information derived from exciter tests (e.g. natural frequencies, stiffness values) is very useful for development work, particularly when obtained in conjunction with information about the pattern of vibration in different modes—'mode plots'.

Similarly the arguments in favour of cutting tests and against exciter tests may be listed as follows.

(i) Considerable expertise is required for the interpretation of the results of exciter tests whereas the result of a cutting test, viz. a limiting width of cut, is readily understood and appreciated by users of machine tools, who are likely to view with suspicion figures which they can neither understand nor check.

(ii) The cost of cutting tests involves the expense of workpieces but this must be set against the initial cost of instrumentation required for exciter tests and the higher degree of skill required to conduct exciter tests.

(iii) In cutting tests the forces are automatically of the correct magnitude and in the correct direction, both of which may be varying in time whereas for exciter tests it is necessary to make assumptions about the levels of steady and alternating forces and, in general, both are applied in the same assumed direction which does not vary with time, i.e. there are certain factors and effects which it is impossible for the exciter test to simulate.

(iv) Cutting tests involve all the actual motions of the moving parts under both torsional and linear loading whereas exciter tests are always limited in that movement normal to the spindle axis is not possible, and movement parallel to the spindle axis is not too easy to arrange.

Thus the only major limitations of cutting tests when compared with exciter tests are those associated with the lobing effect and the reliability of measurements. The lobing effect is not very serious on lathes as the ratio of chatter frequency to rotational speed is generally such that machining takes place in a region in which the lobes overlap so that the variation of chatter performance with rotational speed is minimized. The apparently greater reliability of the results of exciter tests is not a valid reason for preferring exciter tests to cutting tests as the only method of assessing the validity of exciter tests for predicting chatter performance, i.e. of calibrating the test procedure, is to conduct a cutting test and compare the predicted results with the measured results³. It follows that it is not possible to establish the accuracy of exciter tests to any greater degree than the accuracy of a cutting test. A cutting test was therefore chosen as the better form of test at the present time and, in order to minimize the effect of variables that are difficult to control, such as the machinability of materials, or about which insuf-

ficient information is available, such as the effects of the direction of cutting forces and the frequency of vibration on the dynamic cutting force coefficient, it was decided to develop a comparative test procedure. By a comparative test is meant one which can be used to compare the performance of two or more machine tools but which does not yield an absolute rating for either. However, if, at some future time, the machinability of materials becomes more uniform it should be possible to use the test procedure as the basis for an absolute cutting test.

Test specification

The full test specification² will now be summarized and the major controls explained. Whenever possible the choice of conditions is left to the individual user of the test procedure so that he can compare two or more machines under the conditions in which he would normally operate them. If, however, the user has no particular conditions in mind, those recommended below should be used.

The objective of each test is to obtain a measure of the chatter performance of the machine under typical working conditions with as high a degree of reproducibility as possible. If chatter does not occur under the working conditions chosen, no attempt has been made to introduce artificial conditions which would tend to induce chatter but would not be encountered in practice. The degree of control specified on the different variables is imposed to aid the repeatability of results.

The test involves machining with a continuously increasing width of cut and when chatter commences the cut is stopped and the limiting width of cut measured. It is recommended that, in order to ensure the maximum reproducibility of results, a tapered workpiece should be used whenever possible. The machining operation then involves removing the tapered portion so that, as machining proceeds, the width of cut continually increases—see Fig. 1a and 1b. When the removal of a taper is not possible, e.g. in a diameter-reduction operation, arrangements are made for increasing the width of cut in discrete steps until chatter occurs¹.

The major features of the test specification are the following.

1. Condition of machine: mounting, locking of joints, warm-up time, ambient temperature.
2. Workpiece: material, initial preparation, shape, mounting.
3. Cutting tool: geometry, material, chipbreakers, tool shank, centre height.
4. Cutting configuration: horizontal lathes, vertical lathes, approach angle.
5. Cutting conditions: speed, feed, lubricant, preliminary cut.
6. Test procedure: range of speeds, feeds, maximum power, taper rests, determination of onset of chatter, maximum use of one cutting edge.
7. Interpretation of results.
8. Tests as the basis of purchaser specifications and tests.

The majority of the controls are based on current practice and knowledge and, therefore, only those

controls which are likely to be unexpected will be commented on here.

Warm-up time

It is known⁶ that the dynamic characteristics of machine tools vary for up to two hours after starting to run. However, to specify a control in terms of time is unrealistic in so far that to conduct successive tests would require, for exact control, the machine being allowed to cool to ambient temperature and then again run for the specified time. An alternative measure of warm-up time was required and the surface temperature of the housing of the front headstock bearing was found to be suitable. Fig. 2 shows

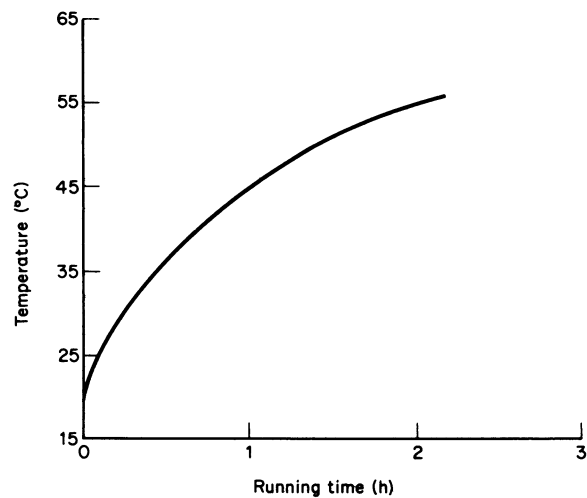


Fig. 2 Temperature rise characteristic of the housing of the front headstock bearing

the variation of this temperature with running time for a particular lathe which was run at approximately two-thirds maximum speed. The recommended test temperature has been specified as the value achieved after one hour when run at this speed. From the experience gained as a result of the cutting tests which are described in the next section, the tolerance on this temperature is $\pm 2^\circ\text{C}$ for the duration of the tests.

Workpiece material

All workpieces for use in any one set of comparative tests *must* be manufactured from the same bar. When a large number of workpieces is required then second bars from the same melt should be used. The cutting tests conducted to investigate the effect of workpiece material indicated that the above control resulted in very small variations.

Workpiece size

Workpieces of the same size are used on the machines being compared even if the machines are not of the same swing diameter. The workpiece geometry is defined relative to the smallest of the machines being considered.

Cutting tool

Throw-away carbide tips are recommended, preferably from one pack as this tends to maintain the

cutting-edge geometry at an acceptable level of consistency. For the tests involving workpieces with tapers a new tip edge should be used for each test as the state of wear is inherently controlled by the cutting operation. For operations such as facing, which require successive cuts of increasing width, the cutting edge must be 'run in'. In practice this is best achieved by conducting a 'dummy' test and then accepting up to the next three test results before using a new tip edge.

Maximum power

It is possible that for the speed and feed ranges recommended a power limitation will occur before chatter arises. The procedure that should then be adopted is to note the width of cut, to reduce the feed and to continue the test until chatter starts or another power limitation is met. In the latter eventuality the above procedure is repeated until either chatter occurs or the maximum width defined by the workpiece or cutting edge is reached. The power-limit widths are as significant when purchasing a machine as the chatter-limit widths as both impose a restraint on production.

Overhang

The width of cut at which chatter commences has been found to be particularly sensitive to the distance of the cutting position from the chuck. As the relation between this overhang and the limiting chatter width is significantly different for different makes of lathe some indication of the variation is required. This is most easily achieved on the tapered workpieces by conducting tests at different points along the taper, either on the same workpiece if possible or by using two workpieces. An example is given in the next section.

Detection of chatter

When using tapered workpieces rapid detection of the onset of chatter is essential as any delay will result in an increase in width of cut, although the rate of increase for the recommended workpieces is not great. An investigation was conducted during the project² into the possible use of a chatter detector which operated from a signal derived from the amplitude of vibration, e.g. using an accelerometer. Thus a preliminary test was conducted and when chatter arose the amplitude was recorded and stored. Subsequently the chatter detector was set to indicate when the amplitude of vibration during cutting had reached some chosen percentage of the stored value. This detector was found to be useful only when the onset of chatter was not clear. However, in the majority of cases on lathes it is possible to rely on the human ear, observation of the chip and examination of the cut surface for the detection of the onset of chatter.

For tests involving successive cuts of increasing width the width of cut is constant but rapid detection of the onset of chatter is still necessary, particularly when a small workpiece is being used for facing tests, as otherwise the diameter is reduced to such an extent that the surface speed is excessively reduced. Also the workpiece may become heated with adverse effects on the variability of results.

Workpiece temperature

The effect of workpiece temperature was investigated during the course of the project and the tests in question are described in the next section. As a result of these tests it was found that significant variations in the limiting width occur for not unusual rises in mean workpiece temperature. (This refers to the temperature away from the cutting edge.) As a result care has to be taken with tools involving successive cuts of increasing width as the workpiece may be unduly heated. This limitation does not arise when tapered workpieces are used, provided the initial temperature is controlled, as the temperature rise is inherently controlled and may be related to the width of cut.

The remaining sections of the test procedure on which comment is required concern the interpretation of the results and the use of the tests as the basis of purchaser specification and tests. These two topics will be discussed after the next section which describes some typical test results and the methods of analysis.

CUTTING TEST RESULTS

As previously indicated, more than 650 tests were conducted during the project and a representative sample will be given to illustrate the scope of the work and the statistical techniques used. It is not possible in a short paper such as this to describe in detail the statistical techniques used but these may be found in statistical text books⁷⁻⁹. However, certain terminology is required and this will be defined with reference to the cutting tests described.

The first example has been chosen simply to define some statistical terms and involves the workpiece shown in Fig. 3. This is the specified size for the smallest parallel-turning workpieces for lathes with a swing diameter of 17.5 in. Sixty test results were obtained under controlled conditions; viz. speed 495 rev/min, feed 0.005 in/rev, ambient temperature $22^{\circ}\text{C} \pm 2$, temperature of the headstock front bearing $45^{\circ}\text{C} \pm 2$, workpieces from two bars from the same melt, new carbide edge for each test, constant tool overhang and controlled initial workpiece temperature. The results are presented in Fig. 4 as a distribution curve of frequency of results against limiting width. To these results has been fitted a 'normal' distribution curve which shows that a normal distribution adequately describes the results. From this distribution curve the variance of the results (σ_0^2)—the mean square deviation from the mean—may be obtained as a measure of the spread of the results, the 95% confidence limits being approximately $\pm 2\sigma_0$. In this case these limits are $\pm 7.6\%$ of the mean and indicate the range of limiting widths in which 95 out of 100 (or 19 out of 20) results can be expected to lie. Similarly 99% confidence limits are defined as approximately $\pm 2.6\sigma_0$.

One of the main objectives was to determine, for a wide range of workpiece sizes and shapes and different makes of machines, the 95% confidence limits of test results obtained under the conditions of the specified test procedure. The effect of a large number of variables on the results was also determined so that appropriate controls could be placed

Table 1. Results and analysis of variance for tests to determine the effects of bearing temperature, workpiece temperature and speed on the limiting width of cut (all results in inches)

Speed (rev/min)	Bearing temperature 30°C		Bearing temperature 40°C	
	Workpiece temperature 30°C	Workpiece temperature 60°C	Workpiece temperature 30°C	Workpiece temperature 60°C
495	0.460	0.345	0.375	0.290
666	0.410	0.335	0.385	0.245
890	0.315	0.245	0.265	0.235

Source of variance	Sums of squares	Degrees of freedom	Mean squares	Components of variance
bearing temperature	8.2687×10^{-3}	1	8.2687×10^{-3}	$\sigma_o^2 + 3\sigma^2_{BW} + 2\sigma^2_{BS} + 6\sigma^2_B$
workpiece temperature	2.2102×10^{-2}	1	2.2102×10^{-2}	$\sigma_o^2 + 3\sigma^2_{BW} + 2\sigma^2_{WS} + 6\sigma^2_W$
speed	2.3029×10^{-2}	2	1.1515×10^{-2}	$\sigma_o^2 + 2\sigma^2_{BS} + 2\sigma^2_{WS} + 4\sigma^2_S$
bearing temperature x workpiece temperature	2.1099×10^{-6}	1	2.1099×10^{-6}	$\sigma_o^2 + 3\sigma^2_{BW}$
bearing temperature x speed	8.3752×10^{-4}	2	4.1876×10^{-4}	$\sigma_o^2 + 2\sigma^2_{BS}$
workpiece temperature x speed	1.9542×10^{-3}	2	9.7709×10^{-4}	$\sigma_o^2 + 2\sigma^2_{WS}$
residual	1.6791×10^{-3}	2	8.3957×10^{-4}	σ_o^2
Total	5.7873×10^{-2}	11		

on the variables to enable the 95% confidence limits to be kept within reasonable bounds.

As an example of the method used the tests conducted to determine the effects of bearing temperature, workpiece temperature and speed and any possible interactions between them will be described. A factorial design of experiment was used which requires all possible combinations of the variables to be tested. As two bearing temperatures, 30°C and 40°C, two workpiece temperatures, 30°C and 60°C, and three speeds, 495, 666 and 890 rev/min, were investigated, this required a total of $2 \times 2 \times 3$, i.e. 12 tests. All other possible variables were kept within prescribed limits for all the tests. The results obtained are shown in Table 1 which includes an analysis of variance.

The analysis of variance is a mathematical procedure⁷⁻⁹ which enables estimates of the different variances to be obtained.

The problem is to sort out from the test results

how much of the variability is due to random effects and how much can be attributed to systematic effects of bearing temperature, workpiece temperature and speed and to their possible interactions. This is done by combining the individual test results in a predetermined way. Calculations are made on the sums of squares of the results and are laid out in Table 1. Each mean square value obtained represents a sum of components of variance as listed in the last column and the residual variance σ_o^2 (the variance of single results due to random effects) appears in every entry.

By comparing the variance obtained from the various interactions (e.g. bearing temperature X workpiece temperature — $\sigma_o^2 + 3\sigma^2_{BW}$) with the residual variance σ_o^2 the significance of the particular interaction can be determined. If σ_o^2 is greater than $(\sigma_o^2 + 3\sigma^2_{BW})$, as in Table 1, then it is unlikely that any effect due to simultaneous changes in bearing and workpiece temperatures exists. Statistically the effect of a variable or combination of variables is

given a significance level which is determined from the ratios of the variances. A 5% significance level means that only in one test in twenty would the effect not be observed. A 5% significance level is the generally accepted deciding value and tables are available⁹ of variance ratios required for the effects to be significant at this level.

For the example given in Table 1 none of the interactions was significant at the 5% level. In this case the calculations were then repeated ignoring these interactions. The associated estimates of variance then all reduce to σ_0^2 allowing a more accurate value of the residual variance of 6.39×10^{-4} to be obtained. However, the three main effects are all more than 5% significant compared with the residual and the magnitude of the effects may be determined by calculating the mean of the results obtained at each value of the variable. Thus the results at a workpiece temperature of 30°C have a mean of 0.368 in and those at 60°C have a mean of 0.283 in. Thus a 23% reduction in width occurs for a 30°C rise in workpiece temperature. Similarly for the bearing temperature of 30°C the mean result is 0.352 in and for 40°C it is 0.299 in. Thus a 15% reduction in width occurs for a 10°C rise in bearing temperature.

In this way it is possible to specify tolerances within which the variables must be held during a test to ensure a reasonable repeatability on a single result. Tests involving those variables considered likely to be significant were conducted in two large factorial experiments using a facing operation on a small workpiece. The first experiment involved the following.

1. Material—bars from two distinct melts.
2. Make of machine—two different types.
3. Speed—two values.
4. Feed—two values.
5. Bearing temperature—two values.
6. Ambient temperature—two values.
7. Operator—two operators.

This experiment thus involved 2^7 , i.e. 128 experiments involving all possible combinations of the above. The second experiment involved the following.

1. Material—bars from two distinct melts.
2. Make of machine—two different types.
3. Tool overhang—two values.
4. Tool centre height—three values.
5. Tool clamping torque—two values.
6. Workpiece clamping torque—two values.

This experiment involved 3×2^5 , i.e. 96 experiments. Two different machines were used in each factorial experiment to reduce the possibility of overlooking effects which might be significant on only a few machines. As a result of these experiments controls were placed on the variables which it was anticipated would ensure that any cutting test result would have a repeatability of $\pm 10\%$ at the 95% confidence level,

i.e. that the result would be within 10% of the correct value in 19 out of every 20 tests.

As only small workpieces for facing had been tested in depth in the initial tests, it was thought desirable to conduct tests with a large range of workpiece sizes and cutting operations with the controls specified in order to assess the repeatability of results under a wide range of conditions. These experiments were also designed on a factorial basis so that tests were conducted at various speeds and feeds and the variability in result thus obtained was therefore of wider application than it would have been for one speed and feed. The major conclusion from the results obtained was that, when the limiting width was less than 0.35 in, the tolerance on results was greater than $\pm 10\%$; for the workpieces and operations tested the limits were found to be, at the 95% confidence level, ± 0.035 in or $\pm 10\%$; whichever is the greater.

Thus it is possible, with a cutting test, to compare lathes to a known accuracy. However, as it is anticipated that such a test procedure will be used to compare competitive makes of machine it was considered necessary to investigate the likely variations between nominally identical machines. In this way some indication would be obtained of the expected performance of subsequent machines as compared with that of the particular machine used for the comparative tests.

These further tests involved all the workpieces and operations previously investigated and batches of five machines from each of two makers of horizontal lathes were tested together with a batch of three vertical lathes. In order to illustrate the method the tests involving the workpiece shown in Fig. 3 on one manufacturer's machines will be described.

As the overhang from the chuck when chatter commences had been found to be significant tests were conducted at two values of overhang by finishing the workpieces to two different sizes. Also three speeds were investigated as recommended in the test procedure. Thus $5 \times 2 \times 3$, i.e. 30, tests were conducted and the results are recorded in Table 2, together with the analysis of variance. The residual variance (σ_0^2) was estimated from the results of previous tests. The machine effect (σ_1^2) may be calculated as shown and indicates a variation of $\pm 13.2\%$ at the 95% confidence level, i.e. 19 out of 20 machines would give results within $\pm 13.2\%$ of the mean of all 20. The mean of the results obtained for each combination of workpiece and operation on each of the five machines from one manufacturer is shown as a bar chart in Fig. 5. The variabilities of the machines made by the other two manufacturers were found in a similar way; a variation of $\pm 30\%$ at the 95% confidence level includes the majority of the results.

Table 2. Analysis of variance of turning test results on small workpieces—Manufacturer X (all results in inches)

Overhang	Speed (rev/min)	MACHINE					
		A	B	C	D	E	
H1	278	0.196	0.202	0.191	0.195	0.186	mean of all results = 0.195 in
	370	0.174	0.173	0.172	0.195	0.175	
	495	0.160	0.227	0.171	0.208	0.155	
H2	278	0.231	0.218	0.198	0.241	0.186	
	370	0.161	0.214	0.185	0.185	0.186	
	495	0.180	0.250	0.193	0.244	0.237	

Source of variance	Sums of squares	Degrees of freedom	Mean squares
machine	5.4241 . 10 ⁻³	4	1.3560 . 10 ⁻³
overhang	3.6080 . 10 ⁻³	1	3.6080 . 10 ⁻³
speed	3.0854 . 10 ⁻³	2	1.5427 . 10 ⁻³
machine x overhang	3.5216 . 10 ⁻⁴	4	8.8040 . 10 ⁻⁵
machine x speed	3.6233 . 10 ⁻³	8	4.5291 . 10 ⁻⁴
overhang x speed	9.9888 . 10 ⁻⁴	2	4.9944 . 10 ⁻⁴
machine x overhang x speed	2.7004 . 10 ⁻³	8	3.3756 . 10 ⁻⁴
residual			3.19 . 10 ⁻⁴

None of the interactions are significant; however, the machine, overhang and speed effects are significant. The machine effect is given by

$$\sigma_o^2 + 6\sigma_1^2 = 0.001356$$

but $\sigma_o^2 = 0.000319$

Therefore $\sigma_1^2 = \frac{0.001037}{6} = 0.000173$

$$\sigma_1 = 0.0131 \text{ in}$$

Thus 95% confidence limits = ± 0.0257 in

$$= \pm \frac{0.0257}{0.195} \cdot 100\%$$

$$= 13.2\%$$

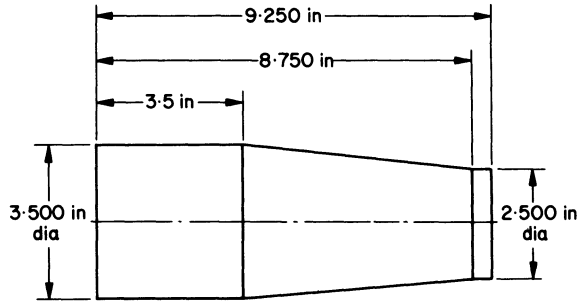


Fig. 3 Dimensions of tapered workpiece for parallel turning test on a lathe of 17.5 in swing diameter

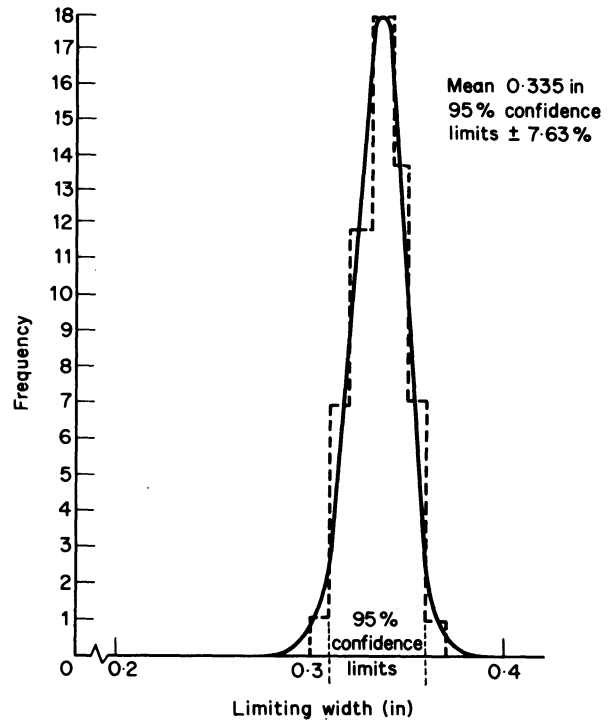


Fig. 4 Distribution curve of repeat test results

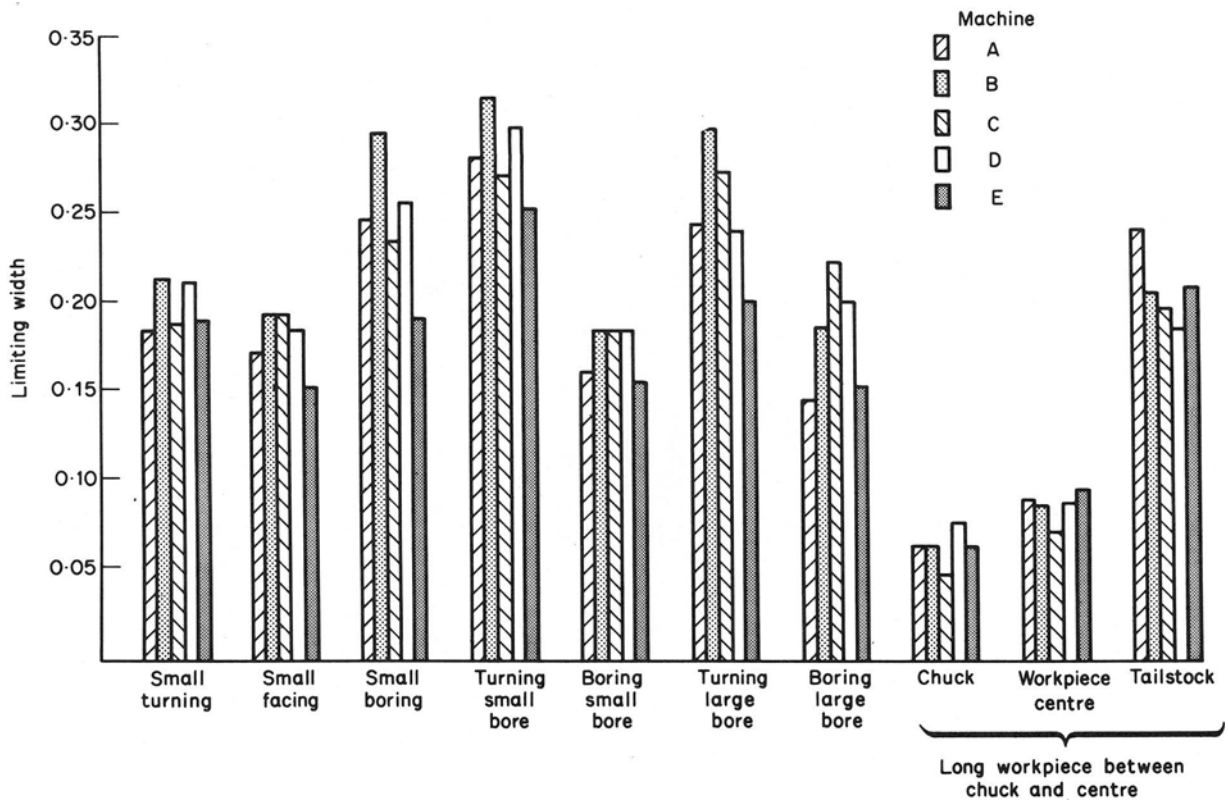


Fig. 5 The variation in performance of five nominally identical horizontal lathes for different workpieces and machining operations

INTERPRETATION OF RESULTS

When machines are being compared as individual machines then the results obtained are subject, at the 95% confidence level, to a tolerance of ± 0.035 in or $\pm 10\%$ whichever is the greater. Thus for one machine to be significantly better than another the difference should, in general, be greater than twice this tolerance. If this is not the case then it is likely that the chatter performance will not be sufficiently different to affect, for example, a purchasing decision. However, if the two machines (of the same model) were at different stages of development and it was necessary to determine which machine had the better performance than two options are available. It is necessary either to conduct repeat tests, when the repeatability limits are divided by $n^{1/2}$, where n is the number of repeats or to accept a reduced confidence level and a consequent reduction in repeatability limits².

If a machine is being tested as a sample machine with a view to purchasing several machines of the same make then the performance of the average machine of one make should be compared with that of the others. The result of one test on one machine is subject to the variability of the test (say $\pm E\%$) and to the variability of machines (say $\pm T\%$). The result will be within $\pm (E^2 + T^2)^{1/2}$ of that of the average machine at the 95% confidence level. If these limits are too large when comparing makes, then a reduced confidence level may be accepted² with a corresponding reduction in E and T or repeat tests on several sample machines may be conducted. The tolerance then reduces to

$$\pm \left(\frac{T^2}{n_T} + \frac{E^2}{n_T n_E} \right)^{1/2}$$

where n_T = the number of machines tested
 n_E = the number of tests on each machine

This tolerance applies to the mean of the results obtained.

TESTS AS THE BASIS OF PURCHASE SPECIFICATIONS

The previous section dealt with the interpretation of the results obtained in a comparative test of two different machines, whether as individual machines or representatives of their particular makes. In the latter case, when one make has been chosen in preference to others on the basis of the tests conducted the customer is likely to require some guarantee that the machines supplied will have some agreed percentage of the performance of the machine(s) tested.

As it is only the lower limit which is required only this will be determined relative to the mean of the results obtained, x . The minimum performance of the average machine at the 95% confidence level would be

$$\left\{ 100 - \left(\frac{T^2}{n_T} + \frac{E^2}{n_T n_E} \right)^{1/2} \right\} \frac{x}{100}$$

The performance of any subsequent machine may be $(T^2 + E^2/n_E)^{1/2}$ less than this, where n_E in this case is the number of tests conducted on the machine supplied. This lower level of performance should be equalled or exceeded by at least 19 out of 20 machines. However, it should be noted that one out of twenty machines may not attain this performance. If this is unacceptable, then an increased confidence level may be required but this increases the tolerances and reduces the minimum performance value.

Some simple calculations for $T = 30\%$ and $E = 10\%$ will soon show that, unless an excessive number of tests is to be conducted, the acceptance level will have to be considerably less than the mean of the tests results.

CONCLUSIONS

The work described in this paper indicates the amount of testing required to establish any cutting test procedure and shows that repeatability limits must be determined with a known confidence level for the results to have any significance. As a result of the tolerances determined for lathes it is possible by conducting repeat tests to obtain a very accurate measure of performance. Such a technique would seem admirably suited to the calibration of vibration testing methods for evaluating performance so that they might be given repeatability limits.

Finally, the repeatability limits obtained may strictly be applied only to the machines tested and the relevant materials, speeds and feeds used. However, it is anticipated that these limits will be found to be of wider application but the only sure method of verification is to determine such limits for other machines and materials.

ACKNOWLEDGMENTS

The author would like to thank the Director and Council of the Machine Tool Industry Research Association for permission to publish this paper. The work described was conducted on behalf of the Department of Trade and Industry (formerly the Ministry of Technology) by the Machine Tool Industry Research Association. The members of staff principally involved were H. Tipton, H. D. Beeson, A. C. Sen and B. J. Stone.

REFERENCES

1. 'Specifications and tests of metal cutting machine tools', *UMIST rep. Min. Technol. Proc. Conf. UMIST*, February (1970).
2. 'Dynamic performance tests for lathes', *MTIRA rep. Min. Technol. Contract No. KJ/4M/150/CB 78 A*, March (1971).
3. SADEK, M. M. and KNIGHT, W. A., 'The assessment of the chatter resistance of machine tools', *The Effects and Control of Vibration in Machinery, I. Mech. E.*, February (1970).
4. PETERS J. and VANHERCK, P., 'Machine tool stability tests and the incremental stiffness', *Rep. Gen. Assembly CIRP*, September (1968).

5. ANDREW, C., 'Chatter in horizontal milling', *Proc. I. Mech. E.*, **179**, 28 (1965).
6. CHOWDHURY, I., SADEK, M. M. and TOBIAS, S. A., 'Determination of the dynamic characteristics of machine tool structures', *MTDR Conf., Birmingham* (1968).
7. LOWE, C. W., *Industrial Statistics*, Business Books Ltd. (1968).
8. HOEL, P. G., *Introduction to Mathematical Statistics*, Wiley, New York (1966).
9. BROWNLEE, K. A., *Industrial Experimentation*, H.M.S.O., London (1947).

DISCUSSION

Query from Dr -Ing. M. A. El Hakim, Faculty of Engineering, Ainshams U/V, Cairo

The represented testing procedures in this paper are well prepared and supplied with the necessary precautions. However, the following remarks should be taken into consideration:

- (1) One should ensure that the workpiece vibrations, although being the same for all tested machines, are kept to the lowest possible limits, in order to guarantee that the measured results are only due to the behaviour of the machine tool system. This implies the specification of a sufficiently large workpiece diameter-to-length ratio.
- (2) As mentioned by the author of the paper, the limiting width of cut is sensitive to the changes in the distance from the chuck. The workpiece in Fig. 3 indicates that such changes are likely to occur and hence different limiting widths of cut are obtained.
- (3) With the tapered test specimens proposed, the development of wear during the test, especially at relatively higher values of the cutting speed, and because of the excessive workpiece length of cut, can lead to errors in the limiting width of cut.
- (4) Taking a proportion of the measured chatter

amplitude as a criterion for the onset of chatter can yield serious deviations in the limiting width of cut. The reason is that the amplitude of the self-excited vibrations is not only a function of the magnitude of the negative damping, but also the *non-linear damping* of the system. It is also independent of the initial amplitude of vibration, so that there does not exist a constant relationship of any form between the threshold of stability and the amplitude of chatter.

Reply

Dr Hakim confirms, in his points 1. and 2., factors which are covered in the paper and more particularly in the D.T.I. report of which the paper was a summary.

However, concerning point 3., for the materials tested the wear obtained was not a significant factor and the length of cut could hardly be described as excessive. If higher speeds are required to be tested, which result in excessive wear with the length of cut prescribed, it would appear most unlikely that such speeds would be acceptable in practice.

Finally, concerning point 4., the measurement of vibration amplitudes to determine the limit of stability is used only when such limits are indistinct. Thus, the limit of stability is ill-defined and some such method is essential. However, during the course of the tests conducted for the paper, the limit of stability was very clearly defined, and measurement of the amplitude of vibration was not necessary.

A NEW HYDRAULIC VIBRATOR

by

J. I. ROBERTS, R. LAWThER and G. PENDLEBURY

SUMMARY

A simple new hydraulic vibrator which does not have the disadvantages of conventional vibrators has been developed by MTIRA. The vibrator is extremely small and can usually be positioned between the cutting tool and the workpiece so as to give realistic simulation of cutting forces. It is intended for excitation by a conventional electrodynamic vibrator and permits a large steady force (preload) and small sinusoidal forces to be applied simultaneously at the most suitable point of a machine tool structure to enable the dynamic behaviour of the structure to be studied under conditions representative of those obtained in practice. An inexpensive electrical control system which maintains the amplitude of the oscillating force constant as the frequency of vibration is varied is also described.

INTRODUCTION

The vibration testing of machine tools may have as its objective either the improvement of existing machines and/or the absolute assessment of the dynamic performance of a machine¹. For the latter purpose an exact simulation of the cutting forces is required together with measurement of the amplitude and phase of the deflections in the relevant directions; furthermore, the tests should be conducted with the machine, tool and workpiece in their normal operating conditions. When, however, the objective is the improvement of a machine or trouble-shooting, then the requirements are usually not so exacting and certain approximations in the simulation may be permissible. In both cases a vibrator of some kind is necessary to simulate the cutting forces and in considering the most suitable vibrator for use in the vibration testing of machine tools it is necessary to examine the requirements of vibrators for the above-mentioned objectives.

The more stringent requirements of the exact simulation will be considered initially. These may be listed as follows.

1. Both the steady and oscillating forces must be represented exactly in both direction and magnitude, due consideration being given to the fact that the directions and magnitudes may vary with time.

2. The oscillating force should be sinusoidal at small amplitudes even when a large preload is applied. This simulates conditions at the chatter boundary¹ when the forces are such that chatter vibrations are about to ensue.

3. It should be possible to meet conditions 1 and 2 over the whole of the frequency range of interest—normally 5–500 Hz.

4. All machine movements associated with the cutting operation to be simulated should take place during the excitation, e.g. spindle rotations, table traverse, etc.

5. The vibrator should be positioned between the tool and the workpiece without disturbing the machining configuration.

6. The mass of the vibrator should be as small as possible so as not to affect the response of the machine system.

At present not enough is known about cutting forces to allow for their exact simulation although the orders of magnitude and general directions are known. Even if full information were available, however, it is difficult to imagine that any vibrator could reproduce exactly the variations in magnitude and direction that are found in practice so that from this point of view no vibrator is ideal.

Of the three types of vibrator available, viz. electrodynamic, hydraulic (using an electrohydraulic servo-valve) and electromagnetic—each has various limitations. The electrodynamic vibrator, although the most widely used type, meets few of the conditions listed above. It is large in size and mass, is difficult to use with a preload and machine movement during testing, e.g. spindle rotation, is not possible without introducing bearings and hence extra flexibility into the machine under test. The hydraulic vibrator^{2,3} has limitations because of its size and mass and also the force waveform is non-sinusoidal at low force levels and at low frequencies. Hydraulic vibrators tend to be complex and expensive and machine movement during testing is again not possible without introducing further flexibilities. The main advantage of the electromagnetic vibrator^{1,4} is that rotation and linear movement parallel with the rotational axis are

possible during testing but it is large in size and mass and usually cannot be used with the normal tooling in place.

The vibrator described in this paper has little mass, is extremely small and its only limitation is that machine movement during testing is not possible. It is therefore as suitable, if not better, for absolute performance assessment than the vibrators noted above. However, its main advantage is claimed for use in tests carried out in the development or study of machines and tooling when its small size often makes it the only available method of exciting the structure at the correct place between tool and workpiece. For this purpose the fact that relative movement of the machine and workpiece is not allowed is a minor restriction and all other requirements are met. One further point which should be stressed is that, since the vibrator is designed to be held in place merely by sandwiching it between the cutting tool and the workpiece, no modification of the cutting tool is necessary and setting up is much easier than with conventional vibrators. The vibrator has been successfully used in the investigation and solution of many chatter problems involving tooling and workpieces which would have been extremely difficult to solve in any other way.

GENERAL PRINCIPLE

The basic principle of the MTIRA vibrator is conveniently explained with reference to Fig. 1 which shows a simplified layout. Essentially it consists of two similar cylinders each having a thin diaphragm at one end with a connecting pin attached to the centre of the diaphragm. These cylinders are connected by a pipe, the pipe and cylinders being filled with oil or other fluid. The diaphragm of one of the cylinders (the transmitter) is coupled to an electrodynamic vibrator which applies a sinusoidal force to the diaphragm and thus causes a corresponding oscillation in the fluid pressure. This results in an oscillating force being applied via the diaphragm of the other (vibrator) unit to the machine under test. A pressure gauge and hydraulic jack are connected to the pipe connecting the two cylinders and a steady force can be superimposed on the alternating force applied to the machine by increasing the pressure in the fluid.

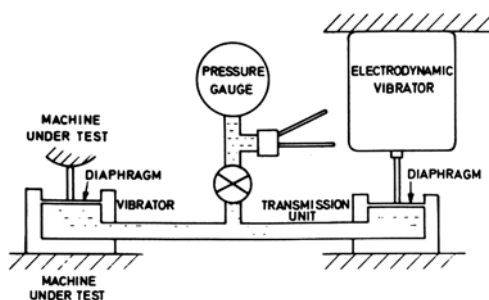


Fig. 1 Diagram showing the principle of operation of the MTIRA vibrator.

DETAILED DESCRIPTION

Detailed drawings of typical units which could be used as transmitter or vibrator units are shown in Fig. 2. The diaphragm of the unit shown in Fig. 2a is made from spring steel of thickness 0.015 in and is located on a Dowty seal or 'O' ring in the cylinder and held in place by a threaded ring. The load transmitting pin is screwed to the centre of the diaphragm and sealed with a small 'O' ring.

The chamber behind the diaphragm need be of only moderate size and the supply pipe, $\frac{1}{4}$ in diameter nylon tube, is brought in through the cylinder wall by a screwed union. As the vibrators were designed for use with Kistler load washers, to measure the oscillating force applied to the machine tool a boss is machined on the base of the vibrator in order to locate the load washer.

The units can be of almost any size. The original tests were made on units with external diameters of $1\frac{1}{2}$ in and $\frac{3}{4}$ in, with lengths of 1 in and $\frac{1}{2}$ in respectively, excluding the boss and the pin extension, and when these were found to operate satisfactorily attention was given to designing even smaller models. The smallest made up to the present time is of the form shown in Fig. 2b—a photograph of this vibrator together with the smallest available Kistler load washer is shown in Fig. 3. The vibrator is $\frac{1}{2}$ in diameter and $\frac{5}{32}$ in long, excluding the boss and pin, the diaphragm is made from spring steel of 0.005 in thickness and $\frac{1}{8}$ in diameter nylon connecting tube is used. In view of the small size the Dowty seal is omitted and the diaphragm is glued in place and retained by rolling over part of the cylinder walls. The vibrator is then a throwaway-type unit as it is more expensive to repair than to manufacture another.

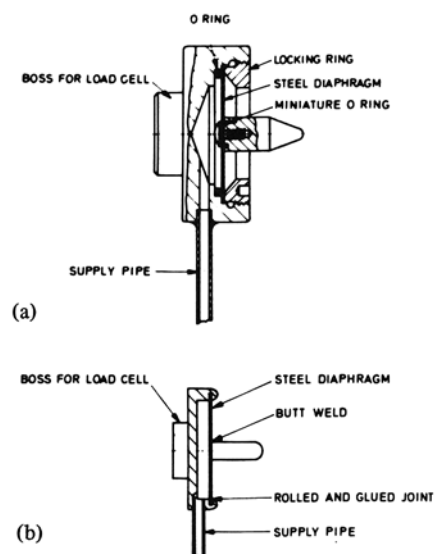


Fig. 2 Typical designs of vibrator and transmitter units: (a) large dismantlable unit; (b) small disposable unit.

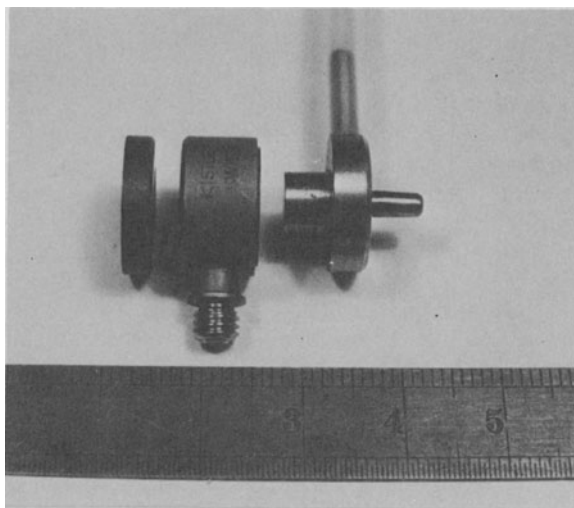


Fig. 3 A small vibrator unit ($\frac{1}{2}$ in diameter) with Kistler load washer.

CHARACTERISTICS

The characteristics of the MTIRA vibrator vary with the sizes of the diaphragms of the transmission unit and the vibrator. They are also affected by the length, size and type of connecting pipe. As it is not possible to present here the characteristics of all possible combinations of these variables, the properties of a typical combination which has been found to give acceptable results will be described and an indication given of the effect of varying some of the variables.

The vibrator system in question consisted of identical transmission and vibrator units of the type shown in Fig. 2a, each of which was $1\frac{1}{2}$ in external diameter and contained a diaphragm of 0.015 in thickness supported on a Dowty seal at a diameter of $1\frac{1}{16}$ in. The connecting pipe was 3 feet of $\frac{1}{4}$ in diameter nylon tube. The electrodynamic vibrator used to supply the oscillating force was a Goodmans V50 supplied from a power amplifier fed by a sweep oscillator, a Kistler load cell being used to measure the force applied to the transmission unit. For the tests the vibrator unit was mechanically clamped in a stiff frame as described below and a Kistler load cell was used to measure the force supplied by the vibrator.

The force supplied by the vibrator and the force applied to the transmission unit are shown in Fig. 4 as functions of frequency. These characteristics were obtained with fixed settings of both the sweep oscillator and the power amplifier. A preload of 100 lbf was applied, half of which was obtained by increasing the pressure in the oil to 300 lbf/in^2 and the other half by compressing the vibrator by means of the mechanical clamp. (If all the preload is developed by a steady pressure in the oil, then the diaphragms of both the transmitter and vibrator units will be deflected from their central positions and their linear deflection range will be reduced. When the load on the vibrator is a machine tool some of the preload can be developed by moving the machine members so as to compress the vibrator. If half the preload is developed in this way and the remaining half by increasing the hydraulic pressure, then the diaphragm of the vibrator

will be restored to a central position, allowing the maximum linear range for vibrations). Over the frequency range tested — 5–700 Hz — the force supplied varies considerably as a result of the method of excitation but, except at the upper and lower limits of the range tested, there was little loss of force between transmitter and vibrator. However, as the relation between the force supplied and the force applied is reasonably linear — see Fig. 5 — the force supplied may be increased by increasing the force applied to the transmission unit. Thus a force-control unit may be used to maintain the force supplied by the vibrator constant as the exciting frequency is varied and typical results obtained using the control system described in the next section are shown in Fig. 6. It can be seen that over the frequency range 5–400 Hz, i.e. the range normally of interest for tests on machine tools, the force supplied by the vibrator is maintained within $\pm 5\%$ of a mean value.

With the system described it was found possible to obtain a sinusoidal force output at a frequency of 0.2 Hz, albeit with a considerable reduction in force amplitude.

Similar characteristics are obtained if the vibrator unit is replaced by a smaller one, but there is a reduction in the amplitude of the alternating force output because of the reduction in area of the diaphragm. This reduction in force transfer can be avoided by using a smaller transmitter unit. With the smaller vibrator units the range of linear displacement will, of course, be reduced.

Because of the small areas of the diaphragms the amplitude of the deflection of the structure under test has to be limited if non-linear effects are to be avoided. However, with the system described above a peak-to-peak amplitude of 0.007 in at 100 Hz is possible before non-linear effects are observed and this amplitude is more than adequate for most machine tool tests, many of which are carried out at peak-to-peak amplitudes of less than 0.001 in. It is, of course, standard practice to observe both displacement and force signals on a double-beam oscilloscope so that any gross non-linear behaviour is easily detected.

When testing a machine structure the amplitude will tend to be large at the natural resonant frequencies of the structure, but it can be controlled by using the setting-up procedure for the force-control system described in the next section. Alternatively, by using the displacement signal as the control signal the dis-

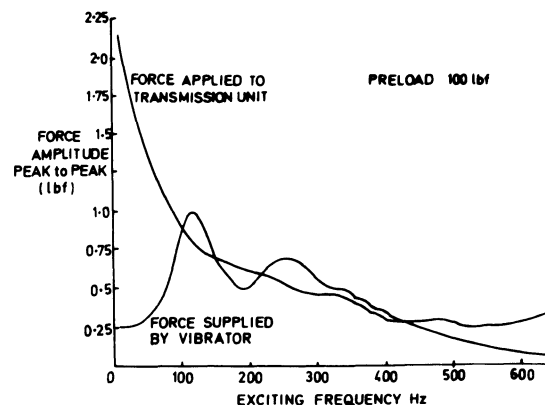


Fig. 4 Forces applied to transmitter and developed by the vibrator in a test rig.

placement can be maintained at a constant value within the range of vibrator. The changes in mechanical impedance with frequency would be obtained from measurements of the force developed. This would give a direct measure of the mechanical impedance of the system rather than the commonly measured receptance.

Various types of connecting pipe, e.g. rubber hose and copper pipe, have been tested but, compared with the nylon pipe, these give excessive force reduction at low frequencies and more and larger resonance peaks in the force output.

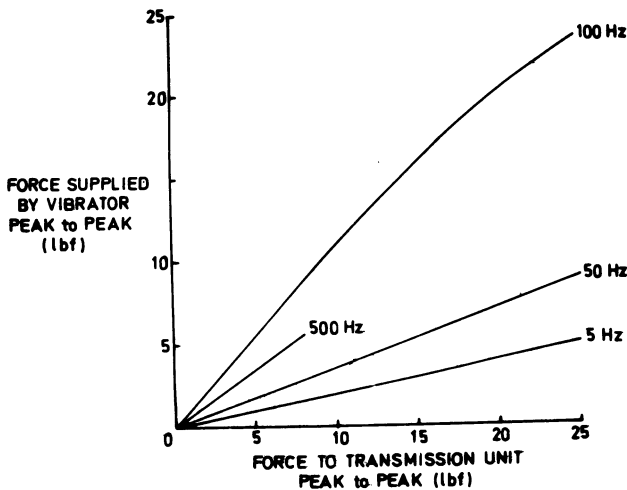


Fig. 5 Force transmission characteristics at various frequencies.

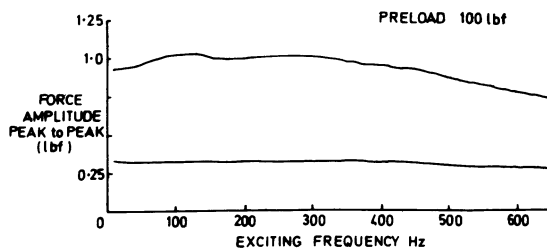


Fig. 6 The force developed by the vibrator with the force-control unit in operation.

FORCE-CONTROL SYSTEM

The need for some method of force control has been outlined above. Various phase differences between the forcing signal applied to the electrodynamic vibrator and the force signal generated by the force transducer dictate the use of a d.c. method of force control in which the force signal is rectified and if the level differs from a preset value the rectified voltage is used to vary the gain of an amplifier between the oscillator and the electrodynamic vibrator.

A block diagram of the complete system developed at MTIRA is shown in Fig. 7 and the circuit diagram of the force-control system appears as Fig. 8. Any convenient force-measuring instrumentation may be used; the system adopted uses a Kistler piezo-electric crystal and a charge amplifier. The

control system uses four 709 operational amplifiers; the first acts as a pre-amplifier with a voltage gain of 10, the following pair being connected as a full-wave rectifier with a voltage gain of about 20. A variable-gain amplifier, consisting of the fourth 709 and a field-effect transistor TRI can have a voltage gain between 10^3 and 10^{-1} depending on the magnitude of the rectified force signal.

Resistor RVI allows the amplitude of the force signal fed into the control circuit to be varied. Blocking capacitors CI prevent any d.c. signal from the charge amplifier from entering the control circuit and the value of CI in conjunction with resistor RI defines the lower frequency-response limit of the input amplifier, A, the gain of which is given by the ratio of R3 to R1. Amplifier B acts as a half-wave, unity-gain rectifier whose output is either zero or a positive half sine wave. If the ratio of resistor R9 to R12 is two, then the sinusoidal input via R9 and the half-wave inverted input via R12 combine and produce a negative-going full-wave rectified signal at the output of amplifier C. A + 10 volt d.c. offset is introduced at the output of C by connecting resistor R13 to the -15 volt rail. This offset is introduced to 'back off' the steady force signal and thus permit the change in force amplitude to control the gain of amplifier D. When setting up the system there is no force signal to cancel the offset voltage and so diode D6 is used to prevent forward biasing of the field-effect transistor.

A simple low-pass filter, R19-C9, is required between the rectifier output and the gate of the field-effect transistor to keep the ripple at the gate at a low level. If this is not done, the ripple voltage may be sufficient to modulate the source-drain resistance of the field-effect transistor and cause signal distortion in the output from amplifier D. When D6 is reverse biased for any reason any charge in C9 is able to leak away through resistors R18 and R19.

The source-drain resistance of a field-effect transistor can be altered by varying the voltage on its gate terminal and this is used as the controlling element in the system. Measurements on a Ferranti ZTX 370 field-effect transistor gave a resistance variation from

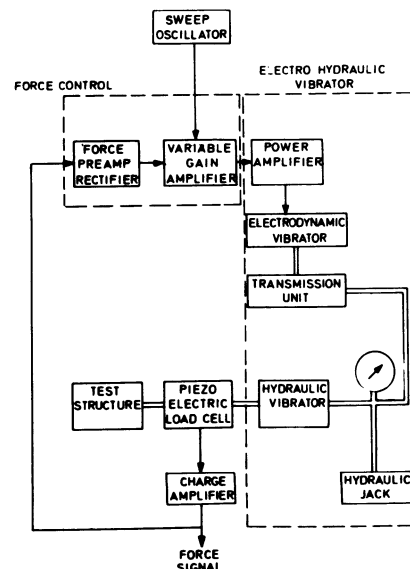


Fig. 7 Block diagram of force-control system.

less than 100 ohm to several megohms for a gate voltage change from 0 V to -7 V. Used as shown, it was possible to vary the gain of amplifier D from less than unity up to around 10^3 .

Amplifier D receives a constant-amplitude voltage signal from a variable-frequency oscillator and provides the power amplifier with sufficient signal to maintain the force output from the charge amplifier constant. Any increase or decrease in force signal is amplified, rectified and, by means of the field-effect

transistor and amplifier D, controls the drive to the electrodynamic vibrator to oppose the change.

A moving-coil meter is used to monitor the output signal level from amplifier D. This is an aid during the initial setting-up procedure and also provides a crude indication of the force variations during testing.

Other components shown on the diagram are used for biasing and stabilising the 709 amplifiers and follow standard practice.

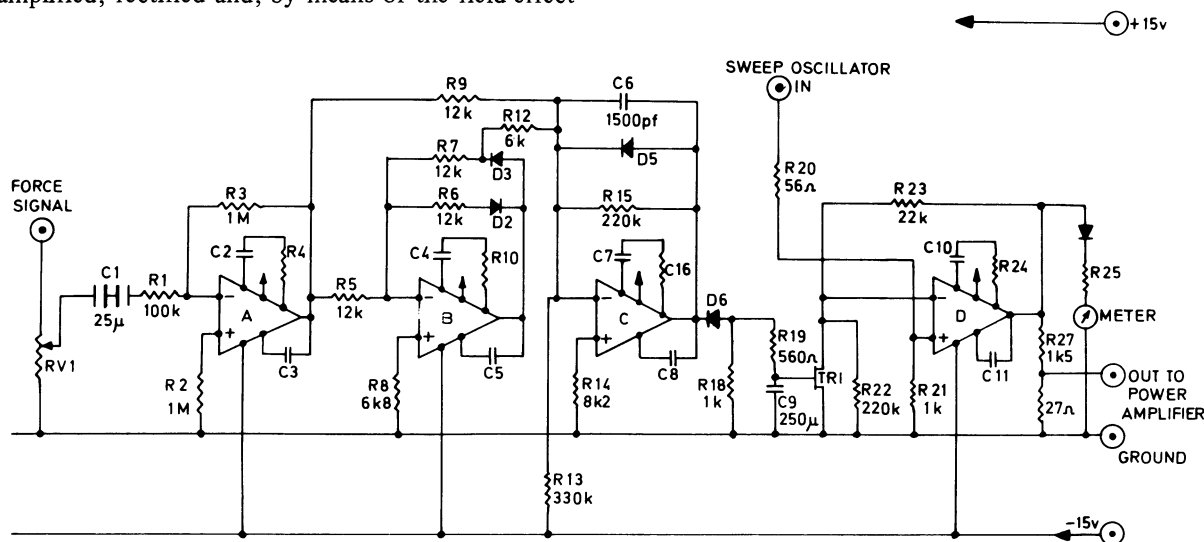


Fig. 8 Circuit diagram of force-control system.

SETTING-UP PROCEDURE

An initial test of the system to be investigated is made without the force control operating to find the frequency at which minimum force occurs. This will usually be at a resonance of the system. With *RV1* turned down to remove the force signal from the input, thereby allowing amplifier D to have maximum gain, the amplitude of the oscillator signal is increased until the meter reading reaches a mark on the scale which indicates that the amplifier output is almost at saturation. The gain of the power amplifier is now increased until it too is almost in saturation. In the working condition the driving signals will now be incapable of causing electronic saturation. With the oscillator set at the frequency for minimum force, the force-signal input to amplifier A is increased slowly by adjusting *RV1* until the output meter indicates a small reduction in reading. In this condition the smallest force signal that will be encountered is just balancing the reference value determined by the d.c. offset in amplifier C and is therefore controlling the gain of amplifier D which is still near the point of maximum gain. The system is now ready for use. Any required adjustment in the force applied to the structure under test can be made by increasing the gain of the charge amplifier and/or increasing the setting of *RV1*.

Fig. 4 and 6 show the applied force as a function of frequency with and without force control. The frequency response of the electronic control is flat between 1 Hz and 10 kHz but the fall off in response of the hydraulic system limits the useful maximum

response to about 1 kHz. In order to overcome the reference d.c. offset and control satisfactorily the force signal at the slider of *RV1* must be at least 50 mV r.m.s. If this input is too low, the control system will not operate correctly.

CONCLUSIONS

The vibrator and control system described are both simple and inexpensive systems which greatly extend the usefulness of commonly used vibrator systems. Thus small oscillating forces superimposed upon large preloads may be applied to structures and because the vibrator can be mounted merely by sandwiching it between, say, tool and workpiece structural modifications are eliminated and set-up times reduced. The MTIRA vibrator overcomes most of the limitations of conventional vibrators and is expected to prove of great value in all types of vibration testing. The vibrators described have already proved their worth in practical machine tool trouble-shooting, particularly when the problem is associated with workpiece or tooling.

The MTIRA vibrator and the control system are the subject of patent applications and arrangements are being made for their manufacture and sale.

ACKNOWLEDGEMENTS

The authors wish to thank the Director and Council of the Machine Tool Industry Research Association for permission to publish this paper and Messrs H. C.

Beeson, T. Brigg and Dr B. J. Stone for their advice and help during the development and testing of the vibrators and control circuits.

REFERENCES

1. CHOWDHURY, I., SADEK, M. M. and TOBIAS, S. A., 'Determination of the dynamic characteristics of machine tool structures', *Proc. Inst. Mech. E.*, **184**, Part I (1969-70).
2. OPITZ, H., KALKERT, W. and REHLING, E., 'Design and application of electro-hydraulic exciters for the investigation of large machine tools', *Proc. 5th MTDR Conf., Birmingham* (1964).
3. SMITH, J. D., 'Machine tool vibrator design', *The Engineer*, Nov. 10 (1967).
4. KWIAKOWSKI, A. W., 'A magnetic vibrator for determination of machine tool dynamic characteristics', *Proc. 9th MTDR Conf., Birmingham* (1968).

INSPECTION AND ACCEPTANCE TESTS FOR NC MACHINE TOOLS

by

K. JUSTEL*

INTRODUCTION

The increase in sales of NC machine tools has made it necessary to reshape the existing specifications of acceptance for these machines. Previously in Germany the Schlesinger acceptance, which involved only the static behaviour of the machine, was the standard for all machines. Even today conventional machines are inspected with regard to the Schlesinger acceptance, normally guaranteeing half tolerances.

Since the conventional machine has been more and more replaced by NC machines, the automatic control of the machine positions, without the influence of manual intervention, required the extension of existing standard tests and also the creation of new specifications considering the static and dynamic behaviour of the machine, and the acceptance by test workpieces. Also the functional control became more complicated as a result of the automatic operation under tape control.

The US standards in this field, such as NASA originate from the aircraft industry and consider especially the requirements of machining aluminium, etc., on contouring machines. For Germany therefore it was found necessary to establish new recommendations, which have already been published or are still under treatment in the German VDI (Association of German Engineers).

One of the most important recommendations, which has been in use now for about 3 years, is the VDI 3254 'NC machine tools, positioning accuracy, definitions and static characteristics'. This standard defines the move into position tolerance (deviation of position and range of positioning variation) along the controlled axis of the unloaded machine.

The latest and improved recommendations, which include also the range of reversal or backlash, were published in the spring of 1971.

Two groups of errors are differentiated:

1. Systematic errors or deviations. These errors are reproducible and have a clear value and sign at each point in the machining range. Systematic errors are inaccuracies of transducer scales, geometric deviations of machine slides, backlash in gears and spindles, etc.

2. Statistical errors or deviations are not reproducible and change value and sign at the same measuring point on repeated measurements. The range of statistical errors can be measured and is defined as 'standard deviation'.

STATIC BEHAVIOUR WITH BACKLASH

Along and parallel to each axis and at a location representing the average working range, a number of measuring points (normally five points are recommended) at a distance of about 50 mm are positioned from both sides in order to calculate the range of deviation from the desired value (Fig. 1).

The definitions in this figure are

T_{EU}	absolute accuracy
$6\sigma + \bar{U}$	R_{PU} range of deviation of position including backlash
\bar{U}	average backlash
\bar{A}_u	average deviation of position
s	average standard deviation
X_i	arithmetic average of average values X_i from both positioning directions
X_i	different values of measurement at point X

In contrast with the ISO standard, here, over the whole range of one axis, a constant average backlash \bar{A}_u and a constant average standard deviation $\bar{s} = (s\uparrow + s\downarrow)/2$ is calculated. The arrows symbolize the direction of positioning. This method seems to be accurate enough to represent the static behaviour of the machine and minimizes the expenditure of inspection and acceptance. If only five random tests at each axis point are made, the following correction factors are valid for the calculation of the standard deviation.

N	2	3	4	5	6	7	8
d_2	1 128	1 693	2 059	2 326	2 534	2 704	2 847

*Scharmann, GmbH, West Germany

The factor d_2 is the denominator in the respective formula for s .

Fig. 2 shows the Gauss distribution for one measuring point.

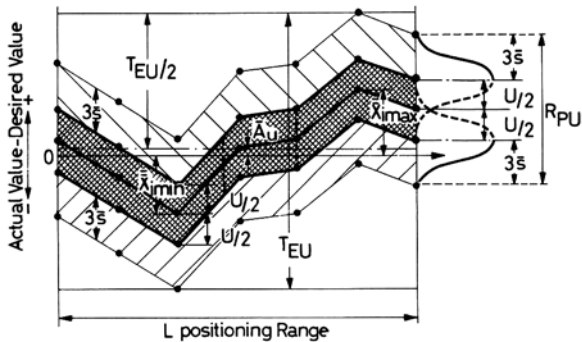


Fig. 1 Static deviations with backlash

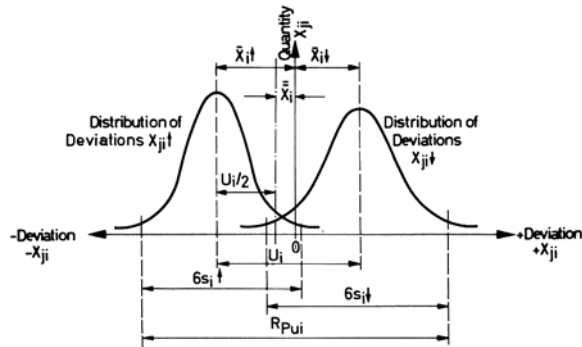


Fig. 2 Example of distribution of deviations X_{ji} at one test point i including backlash.

STATIC BEHAVIOUR WITHOUT BACKLASH

In the case of a point-to-point or straight-cut control, or especially in order to bore holes with close centre distance tolerances, it is necessary to position each point from one direction in order to eliminate any backlash in the mechanical system.

Here the diagram in Fig. 3 shows the position tolerance curve and definitions in this case. All formulas defining the absolute accuracy and average standard deviation are the same except the inclusion of average backlash.

Fig. 4 shows the Gauss distribution at one measuring point in this case.

TOLERANCE PATTERN FOR ANY DESIRED LENGTH OF AXIS MOTION

The absolute accuracy cannot be defined over an infinite length of table or headstock motion, because close tolerances are mostly within distances of a maximum of about 1000 mm. This is the reason why the permissible deviations are referred to a variable basic length of about 1000 mm with and without backlash. The pattern in Fig. 5 therefore allows

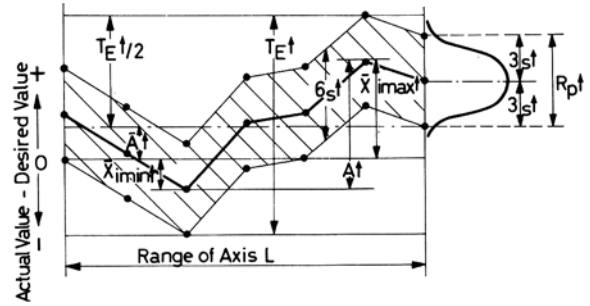


Fig. 3 Static deviations without backlash (positioning from one direction)

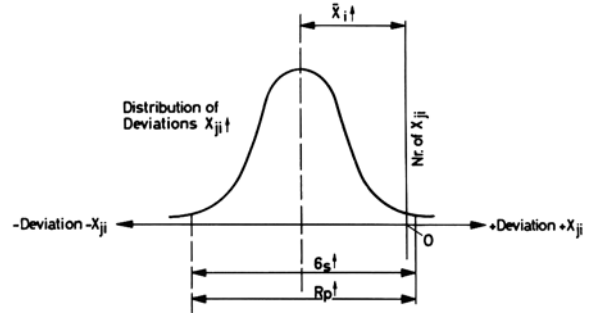


Fig. 4 Distribution of deviations X_{ji} at one test point i without backlash (positioning from one direction)

beyond this basis length a linear opening of the pattern. The tangent $(\Delta T_{Ezui}/2)/\Delta L$ of this cone is not bound by specifications and can be defined by the machine tool builder or by the special needs of the customer. Within the range of one axis, this pattern can be moved in a horizontal and vertical direction (Fig. 6). All deviations from the desired value over the whole range of the machine are guaranteed to be within the borders of this pattern.

Inspection of NC machines with test workpieces

In order to include machining errors and dynamic response into the test value, a recommendation for inspection of NC machines with test workpieces is in preparation. This test recommendation includes test workpieces for drilling, turning and contouring machines.

Normally the test workpiece is one of the actual workpieces provided for the customer's production, so that at the moment there is no urgent need for special test workpieces involving additional costs. In special cases, and for fulfilling respective contracts with the customer, the NASA standards are used.

The German VDI will in the future, in order to correspond with the ISO standard, also extend this existing recommendation to the more complex and time-consuming method of ISO, but only when the majority of our customers are convinced that it is necessary. This recommendation includes all necessary information with negligible inaccuracy for testing NC machine tools.

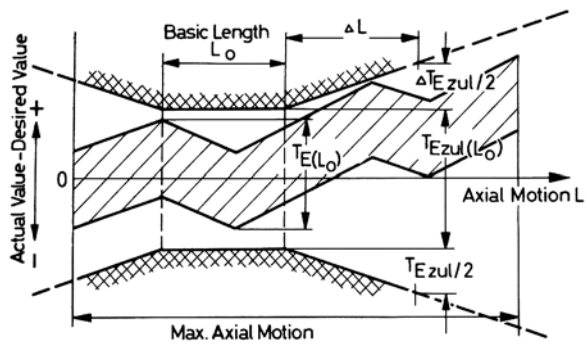


Fig. 5 Pattern for the tolerance band

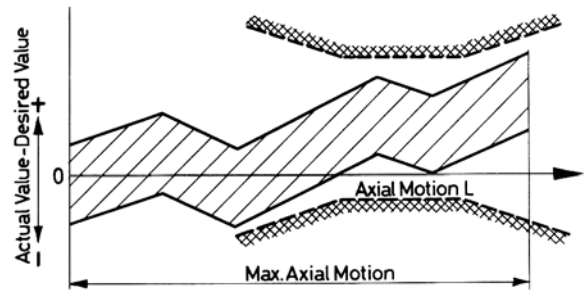


Fig. 6 Parallel moved pattern

POSITIONING ACCURACY OF NUMERICALLY CONTROLLED MACHINE TOOLS

by

C. P. HEMINGRAY, A. COWLEY and M. BURDEKIN

SUMMARY

This paper discusses the practical implications of existing formalized recommendations for the evaluation of positioning accuracy of numerically controlled machine tools. The appraisal of the recommendations is based upon the results of a testing programme sponsored by the Department of Trade and Industry of the Ministry of Aviation Supply and supported by Staveley Industries Limited.

The merits and deficiencies of the existing recommendations are discussed on a statistical basis using results obtained from practical tests. A new recommendation for the specification of positioning accuracy is proposed which is based upon a sound statistical and practical evaluation of the results obtained from the testing programme.

INTRODUCTION

This paper confines itself to those elements of machine tool inaccuracies which have their origin in the control system (as modified by the machine). The resultant errors will form only a part of the errors in workpieces produced by the machine, any measurements taken referring only to the line, along which they were determined and the machine/environment state during the course of the test. Geometrical errors, thermal effects, and the influence of workpiece weight are all measurable machine properties that will contribute to workpiece errors as well as to any measurements taken, as will tooling, clamping and cutting force deflections among many others. Hence we cannot assume that any set of positioning errors as evaluated will give a complete picture of likely workpiece accuracy.

No methods of performing the proposed tests are described: some of the results given were in fact determined with a line standard, and others using a laser interferometer. If care is taken, the measuring errors with either of these systems should not be expected to exceed $\pm 1 \mu\text{m}$ (0.000 04 in) over lengths up to one meter (39 in).

The results quoted here are illustrations taken from the results of a recent testing program, during which the positioning accuracy of several totally different numerically controlled machine tools was examined. This process showed up several aspects of positioning accuracy which do not appear to be covered in the various published recommendations and it is on these aspects that this paper will concentrate.

EXISTING SPECIFICATIONS

Two major specifications for evaluating the positioning accuracy of numerically controlled machine tools have been issued, by Verein Deutscher Ingenieure (VDI) in Germany¹ and the National Machine Tool Builders Association (NMTBA) in America². The NMTBA document has been increasingly used in America and Europe by machine tool builders³, and the VDI method has found growing acceptance in Germany. Reference is made to positioning accuracy by MTTA, MTIRA and BEAMA⁵.

NMTBA specification

The definition of accuracy proposed by NMTBA is: 'Numerical control system accuracy at a point is defined as being the sum of the signed value of the difference between the mean and the target at any point plus the value of the dispersion at that same point which gives the largest absolute sum.'

To establish this value, a series of random positions are programmed, and the position attained determined, for a certain number of repeats at each position. The mean at each position is determined and compared with the target, the errors being plotted as shown on Fig. 1. The theoretically perfect target is defined to be half-way between the extreme values of error, the dispersion at each point having been determined using the standard statistical formula

$$\text{dispersion} = 3\sigma = 3 \left\{ \frac{\sum (X - \bar{X})^2}{N - 1} \right\}^{1/2}$$

where X = data value

\bar{x} = mean of values

N = number of values

σ = standard deviation

The accuracy is then evaluated as shown.

Two values of accuracy as proposed, one (A_b) for bi-directional approaches and one (A_u) for uni-directional motion, with associated values of dispersion evaluated in identical ways ($3\sigma_b$ and $3\sigma_u$). Lost motion at a point is defined in terms of the difference between the right and left approach means at any given point. We are informed that about 99.74% of probable values are covered by such a deviation in both directions from the mean, and for two standard deviations the figure is 95.44%, 'somewhat smaller probabilities resulting if the distribution is not normal'.

The main points to note are as follows.

The dispersion is evaluated for each point, from the sum of the squares of the difference between each trial and the mean at the position.

It appears that random selection of points is advised.

Direction of approach is included in the definition. If no direction of motion is defined, it is assumed that uni-directional positioning is to be used.

VDI recommendation

The VDI approach can be explained with reference to Fig. 2. As before, a series of random positions is selected, and positioned to a number of times. (Neither a number of positions nor a number of repeats is recommended in the document, but the illustrative example has fourteen points each positioned to five times.) The mean position attained at each point is determined and compared with the commanded position and the errors plotted as shown, thus giving 'mean position deviation' similar to the theoretically perfect target of the NMTBA specification. Position scatter width R_p , being twice the dispersion, is evaluated from the mean of the range of extreme values at each target position. The standard deviation of each point can be determined by dividing the range by a factor depending on the number of samples.

$$\sigma_i = \frac{R_i}{d}$$

where σ_i = standard deviation of sample

R_i = range of sample

d = correction factor

and $R_p = 6\sigma_{\text{mean}}$

From⁴ the correction factor (where N is the number of points in the sample) is

N	2	3	4	5	6	7	8	10	12
d	1.13	1.69	2.06	2.33	2.53	2.70	2.84	3.08	3.26

It is stated in the specification that: 'It (position scatter width) can be assumed with adequate certainty to be constant over the whole measuring length.' Also, no reference is made to the direction of motion and its effect on position scatter width (or dispersion). However, it is stated that the following parameters of the test must always be specified: slide-way length, approach feed rate, load on machine, ambient conditions, the number of measuring points and random samples, and the duration of the test.

Comparison

It is apparent that the 'accuracy' as defined by NMTBA is a half of the 'positioning tolerance' as defined by VDI. Both specifications, despite their different methods of evaluation, say that 99.73% of all results should fall within \pm three standard deviations of the mean at any position. But, whereas NMTBA strongly imply that the 'dispersion' can be expected to vary along an axis, VDI say not. The other main difference of significance, apart from the list of parameters VDI require, is that NMTBA have a bias towards defining accuracy in terms of a uni-directional approach, whereas VDI do not refer to the matter at all.

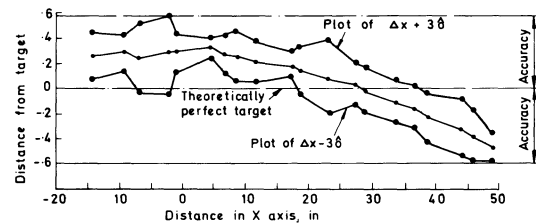
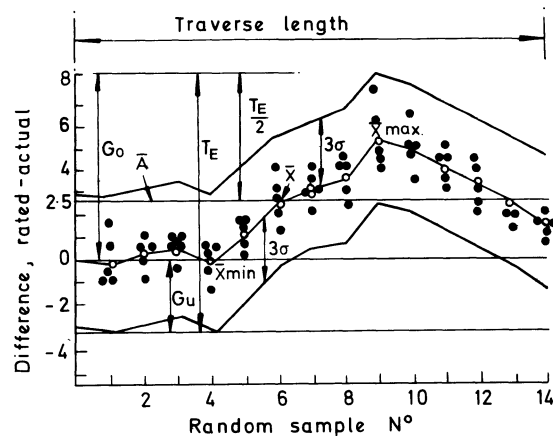


Fig. 1 NMTBA accuracy check



$$\text{Mean position deviation } \bar{A} = \frac{\bar{X}_{\text{max}} + \bar{X}_{\text{min}}}{2} = \frac{5.3 - 0.2 \mu\text{m}}{2} = 2.55 \mu\text{m}$$

$$\text{Tolerance limits } G_{o,u} = \bar{A} \pm \frac{(\bar{X}_{\text{max}} - \bar{X}_{\text{min}}) + 3\sigma}{2} = [2.55 \pm 5.648] \mu\text{m}$$

$$\text{Positioning tolerance } T_E = \bar{X}_{\text{max}} - \bar{X}_{\text{min}} + 6\sigma = 11.3 \mu\text{m}$$

$$\text{Positioning scatter width } R_p = 6\sigma = 5.8 \mu\text{m}$$

Fig. 2 VDI accuracy check

EVALUATION OF SYSTEMATIC ERRORS

Both major standards, and as far as is known most Western users of the standards, evaluate both repeatability and systematic error by positioning a certain number of times (typically 5–13) to a certain number of points (typically 6–15) distributed along the axis being investigated. Typically any set of errors observed is made up to two components: ‘cyclic error’ and ‘progressive error’, ignoring the effect of errors due to repeatability and time. ‘Cyclic error’ can be considered as any error component which repeats itself at least once along an axis of the machine tool, and ‘progressive error’ as non-cyclic error. Especially with machines which position off the lead-screw, cyclic error can be a large proportion of the total errors. To take an extreme (but not totally unrealistic) example: assume a system with a 50 μm cyclic error with pitch of 100 mm as the only error component, and a total distance of travel of 600 mm. It can be seen easily (Fig. 3) that, if 7 points equally spaced are chosen, no error will be revealed, but, if 6 are chosen, the pattern will look like a regular systematic error. Now normally accuracy is especially critical over short distances: thus cyclic error is a more serious form of error than progressive error. Taking an actual set of results, in Fig. 4 the two types of error are illustrated. It can be seen that in distances up to about 100 mm the short-term cyclic errors, repeating every 6.28 mm (0.25 in), will predominate. It would have been very difficult to discern this cyclic error if a set of purely random points had been chosen. The easiest way of differentiating between the two types of error is to perform two tests on each axis. The first is designed to determine dispersion and progressive error over the whole stroke, and uses a certain number of points (10–20 would normally be quite adequate) at a pitch designed to be a factor of the period of any suspected cyclic error. The second uses a much smaller travel (25 mm is normally adequate) the interval chosen being around 0.5 mm.

A proposal, issued by VUOSO in Prague, recommends that in order to reveal periodic as well as cumulative error the measuring increments should be related to the measured range as follows.

Measuring range	Increment size
0–0.2 mm	0.01 mm
0–2 mm	0.1 mm
0–20 mm	1.0 mm
0–200 mm	10 mm
whole stroke	100 mm

It is not to be expected that more than two range tests will normally be required, however.

It is required to establish cyclic and progressive errors as a consequence of the relationship between tolerances and workpiece dimensions. In general, the smaller the dimension, the smaller the allowed tolerance. This is based on the requirements of the ISO system of limits and fits, as in BS 4500 (1969). Thus, cyclic error can predominate in classifying a machine into an accuracy group, even if it is only a half of the

observed progressive error. Thus the axis quoted conforms with regard to progressive error to IT 7 easily, but the cyclic error is worse than that allowed for on IT 9 tolerance classification.

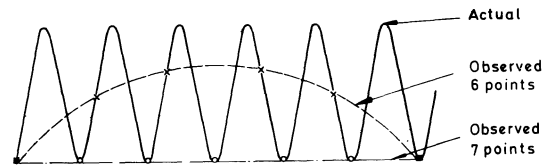


Fig. 3 Effect of step size on observed errors

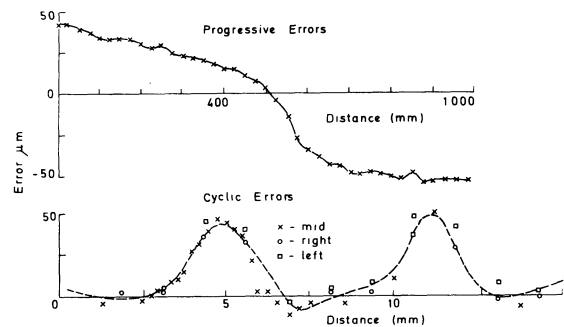


Fig. 4 Errors over whole stroke and over 15 mm

EVALUATION OF SCATTER

Significance of difference in dispersion

The NMTBA document defines dispersion at each point, whereas the VDI document evaluates the same parameter as a mean of that at all the positions. In carrying out tests on machines, dispersion has been observed to vary, but not greatly. Fig. 5 shows results from one axis of an actual machine, with both the VDI values and the NMTBA values of dispersion included. It is questionable whether or not the dispersion variation could have occurred solely because only a few samples were taken. Applying standard statistical tests (e.g. Dixon and Massey⁴), it is possible to estimate the likelihood of any given variation arising, as a function of the observed dispersions and the number of samples. Applying the tests shows that there is more than one chance in 20 of the largest of the observed variations in dispersions, as shown in Fig. 5, occurring. As 13 points were chosen, one can conclude that the VDI method of giving one value of dispersion (position scatter width) appears, on the basis of the results quoted, to be perfectly adequate for this axis of this machine.

To date, for a number of totally different machines types and control systems tested, no significant variation in dispersion has been observed. One can tentatively conclude that a single value of dispersion is perfectly adequate. This confirms the VDI recommendation in this respect.

Lost motion

The VDI document ignores the effects of lost motion, and the NMTBA version assumes that one can treat a

machine that has considerable lost motion by exactly the same statistical techniques as those used for a machine with no lost motion. However, if one performs tests on a machine which has a fairly large dead zone, and plots the results in the form of a histogram, as has been done in Fig. 6, it is apparent that the standard techniques are not really adequate. It is fairly easy to demonstrate that there is a unique relationship between the bi-directional standard deviation (which is $\frac{1}{3}$ of dispersion as previously defined), the uni-directional deviation, and the lost motion, as given by

$$\sigma_b^2 = \sigma_u^2 + \frac{1}{4} L^2$$

where σ_b = bi-directional standard deviation

σ_u = uni-directional standard deviation

L = lost motion

This formula has been confirmed (within normal error limits) in the cases where L is sufficiently large compared with σ_u to render the comparison valid.

With this formula, it is possible to evaluate the actual dispersion, as a function of σ_b , to include '95%' or '99.7%' of all results as a function of the ratio of lost motion to uni-directional standard deviation L/σ_u . The results are shown plotted on Fig. 7, and it can be seen that if L/σ_u is greater than about 4, conventional theory over estimates the likely dispersion by 50% or more. The results shown on Fig. 6 confirm this to some extent, as 4% of the results fall outside the 95% limits as modified, but none outside the un-modified limits (although 5% of the results would be expected to do so).

It is clear that, if the lost motion is large, bi-directional repeatability as conventionally evaluated is unnecessarily pessimistic: the information needed is lost motion and uni-directional repeatability, which is sufficient to evaluate all the required information. Both parameters are required, as it is obviously undesirable to specify that only uni-directional position is to be allowed on any machine. Thus the actual limits for bi-directional dispersion should in all cases be given (if necessary, as derived from Fig. 7), together with the uni-directional dispersion if the machine has a large lost motion.

In cases where the lost motion is less than about twice the uni-directional standard deviation, one can usually ignore the corrections proposed here and evaluate bi-directional dispersion from all the results.

To put forward specific recommendations, if lost motion is greater than 50% of the dispersion, evaluated according to the VDI method, the method as outlined below should be used. If less, the VDI method is adequate. The method proposed is the following.

1. evaluate mean lost motion.
2. evaluate the mean uni-directional dispersion, for both directions of motion, and then take the average of the two values: divide by 3 to obtain uni-directional standard deviation σ_u .
3. determine the ratio L/σ_u .
4. from Fig. 7, determine the appropriate correction factor, c , for the given ratio.
5. then bi-directional dispersion = $3 \times c \times \sigma_u$.

Precision of results

As previously stated, this paper does not attempt to discuss the methods of position measurement, the accuracy of which must be evaluated. But, given a certain known level of errors in measurement, there are two sources of error. The first error, as might be expected, arises from the errors in the checking method. This error should only affect the deviation obtained, as the calibration of the master should be known, so systematic error should be eliminated (not forgetting temperature effects). However, the measurements will have some dispersion due to the checking errors, as well as the inherent level of the dispersion of the machine. These combine according to the formula

$$\sigma_u^2 = \sigma_m^2 + \sigma_e^2$$

where σ_u = (1/3 dispersion) = measured standard deviation

σ_m = (1/3 dispersion) = actual standard deviation of machine

σ_e = (1/3 dispersion) = standard deviation of checking system

Thus if

$$3\sigma_e = 1 \mu\text{m} \quad (\text{typical})$$

$$3\sigma_u = 5 \mu\text{m} \quad (\text{typical})$$

$$3\sigma_m = 4.9 \mu\text{m} \quad \text{not } 4, \text{ as might be expected}$$

The second error arises from the very fact that only a fairly small number of samples is taken. This effect has already been seen to some extent in discussing how much variation in dispersion is needed before it can be said that the variation is unlikely to arise by chance. In addition, any individual mean can only be said to lie within limits given by the mean

$$\pm \frac{2\sigma}{\sqrt{N}}$$

where σ = standard deviation of results for positioning method chosen

N = number of samples at each point

Strictly, this only gives the 95% level, i.e. there is one chance in 20 that the mean will fall outside these limits, but this error width is normally considered adequate.

Thus, with 5 samples and a dispersion of 5 μm , any mean can be relied on to $\pm 1.5 \mu\text{m}$, and with 7, to $\pm 1.25 \mu\text{m}$.

The dispersion, as evaluated by the NMTBA techniques, can be said to lie within $\pm 2\sigma/(2N)^{1/2}$ (again, to 95% level).

The errors involved using the VDI method for dispersion are less straightforward to determine, but can *roughly* be said to be $\pm 2\sigma/N^{1/2}$, i.e. 40% greater than using the NMTBA method, over the range of samples size of 5–8. Thus, the VDI example, using 5 attempts at 14 points, gives 3σ (i.e. dispersion) to

about $\pm 25\%$: if each sample of the NMTBA example is evaluated using their method, and the mean dispersion taken, this can be relied on to $\pm 12\%$. It is interesting to note that both NMTBA and VDI say that 99.73% (i.e. quoting to 1 part in 10 000) of all points lies within quoted limits. In fact, all that can strictly be said is that the value of dispersion quoted should be accurate to $\pm 12\% - \pm 25\%$, and hence it is almost certain that only a very small minority of points (less than 3%) will fall outside the quoted limits.

It is a personal opinion that the VDI method of evaluating dispersion is so much easier as to render its use in practice desirable over the NMTBA method, despite the small sacrifice in precision.

Effect of drift

It has been observed on more than one machine that over the course of the positioning test, the whole set of results drift over the half an hour or so it takes to conduct the test. The cause of this has not always been clear, although it has on occasion been traceable to lack of balance in the null-circuit in the machine control system. But, whatever the cause, the main effect has been to increase the observed dispersion. A typical drift over half an hour is shown on Fig. 8 which is based upon the same set of results as Fig. 5. The results were corrected for drift, and the dispersion excluding the drift is also shown on Fig. 5. The effect can be seen: repeatability is increased from $4.8 \mu\text{m}$ (0.0002 in) to $15 \mu\text{m}$ (0.0006 in) if drift is included.

Drift is easy to evaluate, if a little tedious. The procedure which has been used is to establish first the mean for each position. Then the average difference of the set of results taken initially from the means is determined, and similarly for each set of results. (This ignores, of course, any drift during one traverse of the axis, but this can usually be done.) The drift is then plotted, and a mean drift established, enabling the results to be corrected for drift, as was done for the example quoted. This drift is not to be confused with errors caused by thermal expansion, in which the progressive error will change but not, normally, the dispersion. Such thermal expansion has not been observed to occur in this series of tests, but it is known that some machines with hydraulic feed drives which position off the lead-screw are prone to such errors.

If, as is usually the case, the drift observed is a short-term effect, it is recommended that the dispersion be evaluated after correction for drift, but that a statement of the amount of drift be included. However, if (as has been observed), the drift is continuous, the dispersion should be given as a function of time. To enable any drift to be observed, it is also advised that no test during which it is established should last less than half an hour: hence, if the drift is established from the test for dispersion, the test should take at least half an hour.

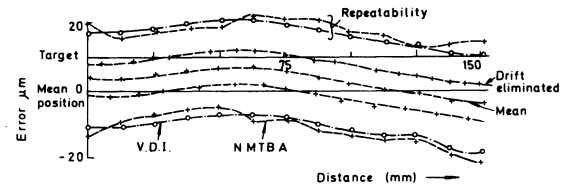


Fig. 5 Example of repeatability evaluation

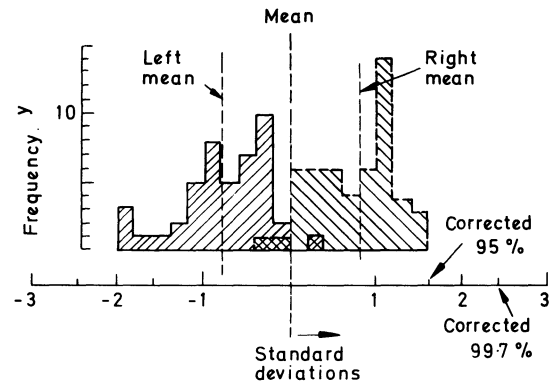


Fig. 6 Histogram of 102 trails at a point

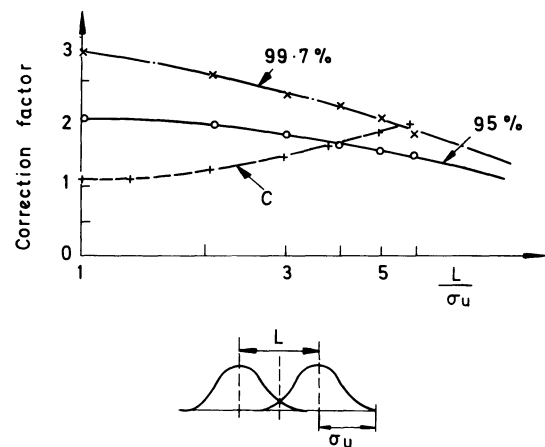


Fig. 7 Correction factors for lost motion

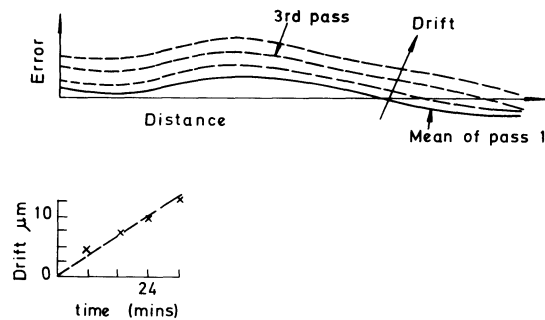


Fig. 8 Diagram of drift

CONCLUSIONS

It has been shown that neither of the two current specifications will give an adequate picture of all errors likely to be encountered in practice. The effects of lost motion, cyclic error, and drift have all been observed to affect the positioning accuracy of machines, but are all dealt with inadequately, if at all, in the specifications. It has also been shown that the precision that can be expected is nowhere near as great as might be assumed from a cursory reading of either document. It is therefore recommended as follows.

1. For any machine tool axis being considered, the following should be determined: progressive error, cyclic error (including period), lost motion, drift (if present), thermal expansion (if present), and uni-directional dispersion. Bi-directional dispersion should be established from the lost motion and uni-directional dispersion as described in Section 4.2, if the lost motion is sufficiently large.

2. Dispersion is to be evaluated following the methods proposed by VDI, for the whole axis.

3. A minimum of 100 positions should be used to evaluate the uni-directional dispersion, lost motion and progressive errors in each axis, preferably made up to 5 complete cycles (i.e. both ways) to a minimum of 10 points. Uni-directional dispersion shall be determined for both directions of motion together with the mean lost motion.

4. The position increment for the dispersion test shall be chosen to be a whole number of pitches of any likely cycle error. The cyclic error shall be evalu-

ated over a suitable fraction of the machine travel, 25 mm being suggested.

5. Most of the parameters as recommended by VDI should be recorded for each test, i.e. slideway length, approach feed rate (if relevant), ambient conditions, the number of measuring points and random samples, and the duration of the test. It is also recommended that the position of the line along which accuracy is determined be recorded, relative to the co-ordinate axes of the machine tool.

REFERENCES

1. Verein Deutscher Ingenieure (VDI), 3524 *Genauigkeitsangaben bei numerisch gesteuerten Werkzeugmaschinen (Begriffe und Kenngrößen)*, April (1965). (*Statement of Accuracy of numerically controlled Machine Tools, Terms and Characteristics*, Transl. UMIST (1970)).
2. National Machine Tool Builders Association, *Definition and Evaluation of accuracy and Repeatability for Numerically Controlled Machine Tools*, June (1968).
3. MARKLEW, J. J., 'Qualification of the terms "accuracy" and "repeatability" for NC positioning', *Machinery and Prod. Eng.* 869, 3rd June (1970).
4. DIXON and MASSEY, *Introduction to Statistical Analysis*, 3rd edn. McGraw-Hill, New York (1969).
5. MTTA, MTIRA and BEAMA (joint publication), *Maintenance and Field-testing of Numerically Controlled Machine Tools*.

MACHINE TOOL TESTING— A PRACTICAL APPROACH

by

J. W. ANDERSON*

SUMMARY

As NC machines find increasing use in the metal working industries, manufacturers are faced with demands for greater accuracy and improved reliability. In meeting these requirements, the machine tool test specification must keep pace with the demand. Whilst extensive testing at the prototype stage, i.e. design and development testing, is justified, it is certainly uneconomic to continue this into the production stage. It is equally essential, however, from the customer's point of view, that a realistic program of production testing be fulfilled. Limitations of time and economic considerations make it essential that the test program be rapidly executed yet comprehensive. This paper gives an account of how one machine tool manufacturer has met and overcome the problem.

INTRODUCTION

NC machine tools are becoming more and more acceptable to the user as a means of achieving economic production of small to medium batches.

While he surveys the field to find a machine to meet his production requirements, the potential customer must compare each machine with its competitors—this he does by reference to a technical sales specification. Later, however, when the enquiry becomes an order, his interest centres on the machine's performance in relation to the sales specification. Thus, the manufacturer has to provide evidence of his machine's capabilities by means of its conformance to a test specification.

The development of a test specification for a typical standard NC machine tool is the subject of this paper. The machine chosen to illustrate the point is a numerically controlled horizontal boring and milling machine, one of a range of machines designed and manufactured by Giddings and Lewis-Fraser Ltd. at the factory in Arbroath, Scotland. (see Fig. 1.)

A typical sales specification might read as follows.

Spindle diameter:	5 in
Table size	60 in X 96 in
Table travel (<i>X</i> axis):	96 in
Headstock travel (<i>Y</i> axis):	60 in
Spindle travel (<i>Z</i> axis):	36 in
Saddle travel (<i>W</i> axis):	48 in
HP at spindle:	25
HP at feed drives:	10

All 4 axes (*X*, *Y*, *Z* and *W*) under point-to-point numerical control.

Much has been written, in recent times, on the subject of machine tool testing, some of the most recent work on the subject being published by the machine tool Engineering Division of UMIST in the proceedings of the conference *Specifications and Tests of Metal Cutting Machine Tools*, February 1970. Other National Bodies such as NASA (USA) have adopted practical test specifications to meet their own specific requirements—in this case the aerospace industry.

The approach to testing described in this paper is simple and practical, making maximum use of modern measuring equipment and techniques. As such, it is by no means claimed as unique. Such methods are finding increasing use throughout the machine tool industries of the world. The intention here, is to illustrate how, using such techniques and equipment, test time may be kept to a minimum whilst guaranteeing the user value for money and a reliable product.

Tests performed on machine tools fall into three main categories.

1. Design or development tests.
2. Production tests.
3. User tests.

Design or development tests fall outside the scope of this paper. They are usually extensive and exhaustive, aimed at proving the design specification. From the results of these tests the technical specification is drafted.

User tests are commonly simplified or scaled-down versions of **production tests**, aimed at providing a ready means of *USER* assessment as to how the machine is maintaining its manufactured accuracy. Both have the common aim of proving the technical

*Division of Giddings and Lewis Incorporated, Fond du Lac, Wisconsin, USA

specification. The paper concentrates on the development of production tests procedures.

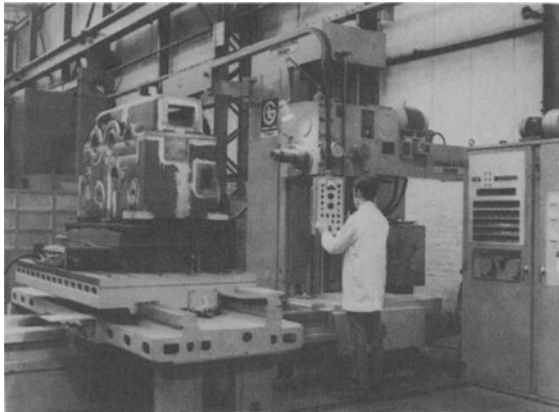


Fig. 1

PRODUCTION TESTS

These are composed of the following.

1. In-process inspection—during the manufacturing cycle of machine units and the complete machine.
2. Final alignment inspection—after assembly is completed.
3. Operational quality evaluation of the finished product, prior to shipment.

In-process inspection—machine units

Most manufacturers treat these tests as a matter of routine. Demands for greater accuracies, however, dictate that the techniques employed require frequent revision. Following the accepted metrology 'rule of ten', the instrument used in a check must be a factor of 10 better than the part being checked—for example, where measurements are to be better than 0.0001 in. the measuring instrument requires a resolution of 0.00001 in.

Such accuracies can only be achieved using electronic gauging or air gauging—both systems are currently in use in the above checks. Once the practice of using electronic gauging is established, it is a short step from the conventional 'indicating' instruments like the 'Mitronic' micro-comparator (Fig. 2—seen here checking spindle runout) to the 'recording' type such as the Sheffield 'Accutron' (Fig. 3).

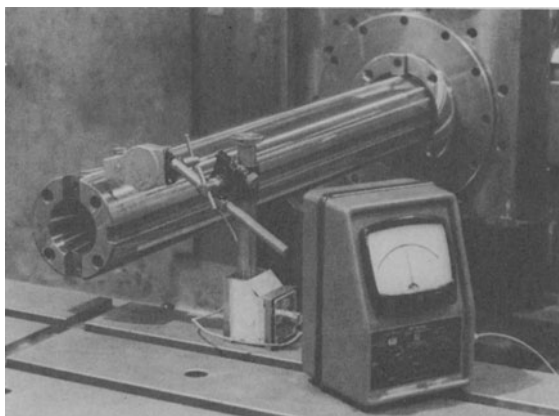


Fig. 2

Similar techniques are available—and in current use—for measurements of spindle sleeve bearing preload. Where previously rotational *torque* was used as a criterion, it is now possible to relate preload to the *axial deflection* under a given *load*—a plot of load/deflection for push-pull conditions on the spindle sleeve indicating the preload state. Measurement of deflection is by electronic indicator and load is determined by an electronic load-cell (Fig. 4).

In-process inspection—final assembly

A similar series of tests is carried out during assembly of the machine. In the main, these can be classed as 'alignment' checks—flatness, straightness, parallelism, squareness of one major element to another—as the assembly progresses.

In carrying out these 'in-process' checks, maximum use is again made of electronic instrumentation for indicating flatness, straightness, squareness and level—instruments such as the 'Talyvel' electronic level (Fig. 5), and the autocollimator and reference optical polygon (Fig. 6). The former has a resolution of 0.000005 in. per in. compared with the more conventional 'block level' which is typically 0.0005 in. in 10 in., and the latter indicates angular misalignments down to 1s. of arc.

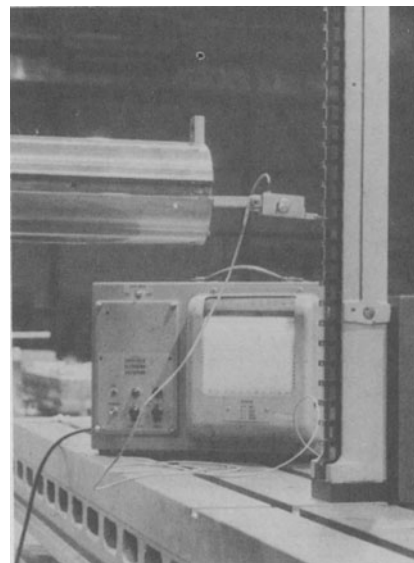


Fig. 3

Final alignment inspection

The well-known Schlesinger alignment specifications are the 'reference manual' for all alignment checks. Since their introduction some 40 years ago, tolerances have, however, been tightened up considerably, to meet the requirements of modern practice. It is not uncommon nowadays to meet alignment tolerances of 0.0001 in. per ft. which, on a machine of the size under consideration, gives ample proof of the need for sophisticated inspection techniques—and indeed, equally precise production aids! Figure 6 illustrates a typical alignment check being performed—in this case, the squareness of a table cross-slot to the tee-slot. Fig. 7 gives a graphical representation of another typical Schlesinger alignment check.

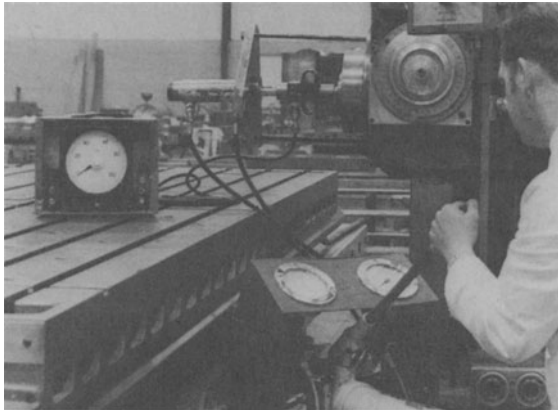


Fig. 4

Up to this stage, inspection has been carried out by an experienced shop-floor inspector, whose product knowledge and training enables continuous quality monitoring to take place as an integral part of the production cycle—prevention rather than cure! Until recent times, little has been done beyond this stage, to evaluate the performance of the machine under service conditions—apart from the occasional ‘cutting test’ prior to shipment. For a modern high-quality machine, the test program has hardly begun! The completed machine now passes to a specialist group, for *operational quality evaluation*—the vital stage before being passed to the customer.

Operational quality evaluation (OQE)

OQE is a check on *function*—for conformance to the design specification. From a knowledge of the design requirements and a study of the machine operating modes, it is possible to draft a test specification which will ensure that the original design requirements are fulfilled on the production models. OQE is carried out by a skilled ‘team’ of mechanical and electronic technicians, using techniques and equipment chosen for ease and speed of operation and accuracy of determination.

Tests fall naturally into four categories.

1. Electronic OQE.
2. Mechanical OQE.
3. Positioning accuracy and repeatability checks.
4. Reliability checks.



Fig. 5

1. Electronic OQE

The first part of the process has already taken place, at the time the NC system was assembled as a unit. Before ‘marriage’ to the machine, an extensive series of simulation tests has been performed, lasting some 100 hours. The electronic checkout described takes place *after* ‘marriage’ to the machine.

Operating in planned sequence, control elements now work under load and perform many operating cycles in a short time interval where previously each may have operated only a few times under no-load conditions. Premature component failures are as a result precipitated and indeed can be considered as desirable *now*, rather than later! In general, electronic components are extremely reliable, and any impending failures will usually occur during the first 200 hours of operation—thereafter, failure rates are greatly reduced, and after 1000 hours, are of very small proportions.

A test manual giving precise test instructions is used in conjunction with a check-list by the technician, throughout the test programme. Failure of any test results in immediate correction before proceeding.

‘Power circuits and interlocks’ OQE. This involves checks on voltage levels, fuses, overloads, motor rotations and associated circuitry: pressure and float-switch set-up: operation of relays, solenoids, switches, brakes, clutches, limits-of-travel switch set up: feed and speed range operation: hydraulic, lubrication and oil-cooling system operation.

Functional OQE. A series of tests on ‘systems’, and their function. Each axis of the machine under numerical control is checked individually and in combination with other axes where appropriate. Digital and analogue systems are set and checked, followed by ‘dial-in’ modes of operation and finally ‘tape checks’. This latter series comprises all feed and speed selections, fixed cycles—positioning and machining variations—depth and cutter compensations and a variety of miscellaneous functions.

An illustration of the extent of these tests can be given by examining the checkout of the *slowdown computer*. The electronic circuit controls the slow-down pattern of the feed drive, during a positioning cycle. The feedback system compares actual position data with preset switch-point data to initiate slow-down as data parity is achieved for each switch-point. The feed-rates selected by the computer are compared with manually-selected feed-rates by means of a tape/bypass switch. The physical slow-down is influenced by delays in relays, solenoid-operated hydraulic valves, and planetary brake response, and this is examined in greater detail later under *Planetary drives*.

‘Tape’ checks use individual tape modules for each machine control feature. When joined together, they form a complete test-tape which is passed to the user as a maintenance and training aid—together with the program printout, a step-by-step checkout procedure for the complete range of machine control features is immediately available, ‘tailor-made’ for the user’s own machine.

2. Mechanical OQE

The use of specialized items of equipment makes this a simple, routine task. The machine functions under review are controlled by a combination of hydraulic brakes, clutches, solenoid-operated valves, etc., the correct inter-action of which determine 'satisfactory' machine operation.

Hydraulic systems. Of major concern in any hydraulic system is the extent of undetected leakage. Where 'rotating joints' supply clutches and brakes, radial (running) clearances must be carefully controlled to avoid excessive leakage. Internal leakage in solenoid valves and clutch/brake actuators, etc., may not be immediately obvious, and a ready means of determining the extent of such leakage is required.

The test illustrated (Fig. 8) is a short-cut method of making this evaluation. A planned combination of feed/speed/direction of motion/auxiliary functions allows the influence of each hydraulic component in the system to be assessed. The equipment consists of an accurate means of measuring the quantity of oil passing through the system in a given time—leakage will reduce the measured quantity.

Oil-cooling system. Accurate machine alignments are of little consequence if heat generated in the working parts of the machine is not controlled. *Lubri-cool* is an oil-circulating system with heat exchanger, which gives automatic control of oil temperature within approximately $\pm 2^\circ\text{F}$ about ambient. Independent circulating systems control oil flow to the headstock and transmission (base), either through or bypassing the heat exchanger.

Temperature settings are monitored over a period of time, and the on/off characteristics of the system studied, for speeds and feeds through the operating range, up to the maximum. Initial settings are by accurate electronic thermometer, final operation checks by thermocouple and ultra-violet recorder.

Planetary drives. The correct operation of the planetary (epicyclic) gear system depends on selecting a combination of hydraulic brakes. A u.v. recorder with input from a tachogenerator coupled to an external rotating member (Fig. 9) plots the planetary drive response during feed-rate changes (notably these in the slow-down pattern of a NC positioning cycle).

These plots are compared with 'typical' results obtained during prototype testing. Response of each machine axis separately, or any combination of axes can be checked by this means.

Power absorption. The power required to move each machine axis in forward and reverse directions, is measured by wattmeter, at selected feed rates up to the maximum (fast traverse rate).

In assessing the power absorption of the spindle bearings and drive planetary throughout the speed range, the final spindle drive is disconnected mechanically. This allows the power absorbed by the spindle bearings to be separated from that absorbed by gearing.

Headstock 'tilt'. A critical area on any horizontal borer is the motion of the headstock on the column. Insufficient clearance between headstock and column may give rise to physical damage to one or both sliding surfaces or result in NC positioning errors. Excessive clearance will cause misalignment of the spindle,

particularly where large extensions are used. The influence of the hydraulic clamps between headstock and column is equally critical.

A simple means of checking these effects is illustrated in Fig. 10. This shows a 'Talyvel' electronic level being used to measure variations of head inclination as it positions up or down the column, and the influence of the power clamps, at prescribed positions near the limits of travel.

Vibration levels. Portable vibration-measuring equipment gives a quick and accurate means of testing the out-of-balance condition of rotating parts, and their influence on vital areas like the spindle (Fig. 11).

Noise levels. Noise level checks at strategic positions around the machine are made using portable equipment. Fig. 12 illustrates a typical acceptability curve for the machine in question.

Machining criteria. Cutting tests are the most common means of evaluating a machine tool's capabilities. When these are coupled with power checks, a realistic assessment of the effectiveness of drive clutches, clamps, brakes, etc., while *under power*, can be made. Typical cutting tests include (a) milling—maximum metal removal rates—full rated horsepower of the drive motor (check horizontal and vertical 'lap', flatness, finish); (b) drilling—spade drilling operations—maximum spindle thrust; (c) boring—balanced-cut conditions—'Davis' block tooling—saddle feed (check hole size, finish).

3. Positioning accuracy and repeatability checks

'Control accuracy'. Tests are designed to check out the resolution of the *fine* systems of measurement—either inductosyn scales or resolvers. A test-tape with programmed increments as indicated below commands each axis in turn. Actual position is then compared with command position, and plotted to give a permanent record.

Axes using Inductosyn feedback—
increments of 0.001 inch to 0.015 inch,
increments of 0.005 inch to 0.100 inch.

The check is over 1 inductosyn 'pitch'.

Axes using resolver feedback—
increments of 0.005 inch to 0.100 inch,
increments of 0.025 inch to 0.375 inch
or 0.625 inch.

The check is over 1 complete screw pitch.

An optical line standard is used to evaluate each axis, although the advent of the laser interferometer has both simplified and speeded up this operation.

'Accuracy' and 'repeatability'. Tests are carried out with the machine 'free' (no constraint) and in a no-load condition. Test equipment requires a high degree of precision. This is commonly a Line Standard such as the *Starret-Webber* lug-bar, in conjunction with an electronic 'indicating' or 'recording' system. The lug-bar is composed of a series of 'steps' at 1 inch or 25 mm intervals, having a total span of 38 inches or 950 mm—accuracy of step spacing 0.000 002 inch cumulative. Fig. 3 illustrates the check on headstock (Y) axis.

A test tape commands the axis to position to each of 6 data points within a 36 inch span, from alternate

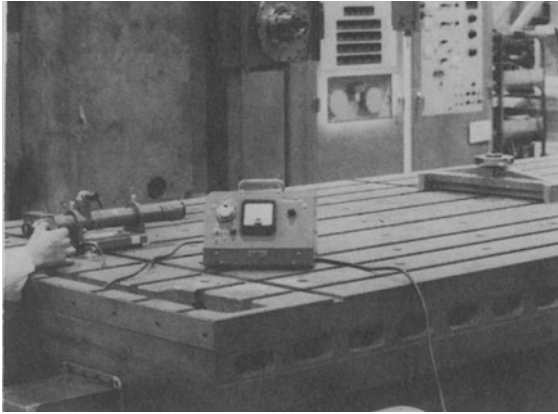


Fig. 6

directions, reversal taking place outside the extreme data points. A total of 13 round-trips is made. Using the recorded data, a statistical analysis is performed to give the accuracy and repeatability for each axis, to 3-sigma limits. Appendix 1 gives a brief account of the interpretation to be put on the results. Although 13 round-trips are made, the final 7 only are used in the analysis. This makes allowance for temperature effects (particularly in Resolver feedback systems) by giving an initial warm-up period for the axis to stabilise.

Laser techniques. The most recent innovation in carrying out these checks is to use a *laser interferometer* as the 'reference', in place of a line-standard.

Advantages claimed are as follows.

(i) Data points can now include all programmable digits, where previously whole numbers only were possible, e.g. 1.1213, 5.9439, 9.5601, 16.3727, 29.0005, 33.4583 inches. Reversal points at 0.0000 and 37.7500 inches.

(ii) No re-zeroing. The lug-bar must be repositioned several times in order to set-up the 10-inch long Inductosyn scale spars on a 'long' axis. The laser interferometer has a usable travel of up to 1800 inches.

(iii) Only the test axis is moved—all other axes remain clamped. With the lug-bar, a second axis at right-angles to the test axis is programmed, to bring the indicator stylus into contact with the lug-bar.

(iv) Inherent accuracy—the Perkin-Elmer Laser-gage accuracy is ± 1 part per million + 1 count, at distances up to 1800 inches. This means, effectively, that over a distance of 100 inches, the measuring accuracy is 0.0001 inch.

(v) Time-savings. A typical time for 1 axis, including set-up is $1-1\frac{1}{2}$ hours, compared with 4-6 hours for the lug-bar.

(vi) Automatic compensation for environmental temperature, part temperature and barometric pressure. Relative humidity is manually compensated by digit switches. Readings are automatically 'corrected' to standard measuring temperature of 20°C (68°F).

(vii) Automatic print-out of results—no manual recording or manipulation.

Typical laser-gauge set-ups are illustrated in Figs. 13 and 14.

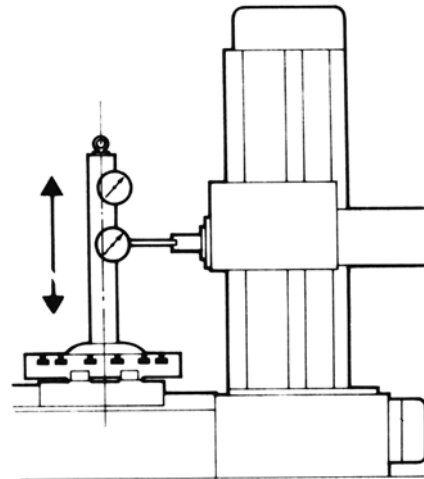


Fig. 7

4. Reliability checks

The machine is now cycled continuously for a period of 16 hours, broken down into four 4-hour periods. The test tape is from a quality assurance cycling program which subjects the machine to conditions of service far in excess of normal production operations. During the entire period, records are maintained of hydraulic/lubrication pressures and oil/atmospheric temperatures.

During the first two 4-hour periods any faults which occur—mechanical or electronic—are noted, and if the machine cycle can be continued without adverse effects, the entire 4-hour period is run. Any fault which necessitates immediate correction results in the re-run of that period.

During period 3, only 1 fault however insignificant is allowed, and if this can be by-passed without adverse effects this is permissible. The final 4-hour period must run completely free of faults—if a fault does occur, the test procedure reverts to period 3 and recommences from that point onwards. The successful completion of periods 3 and 4 terminates the test.

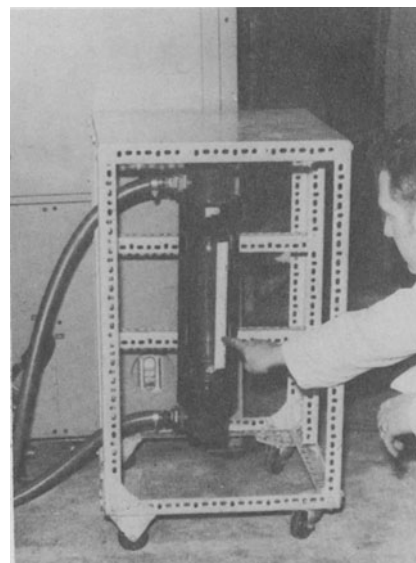


Fig. 8

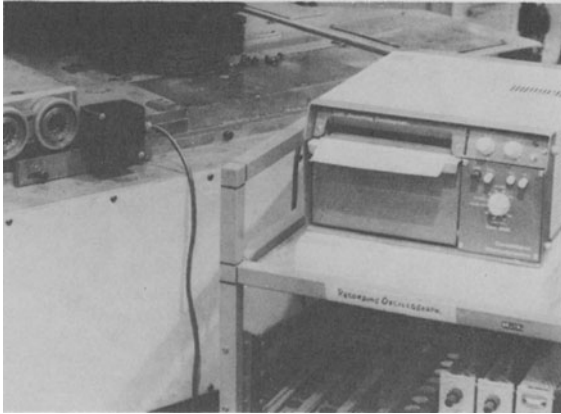


Fig. 9

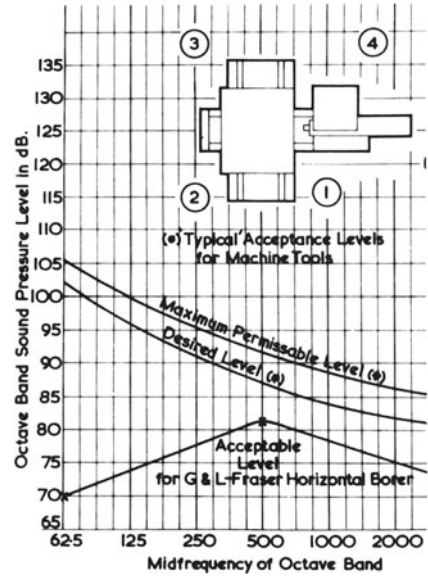


Fig. 12

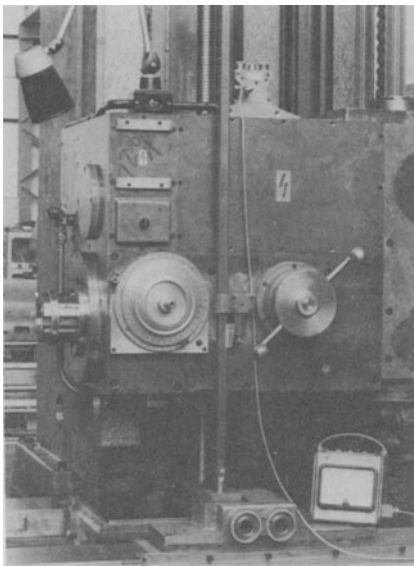


Fig. 10

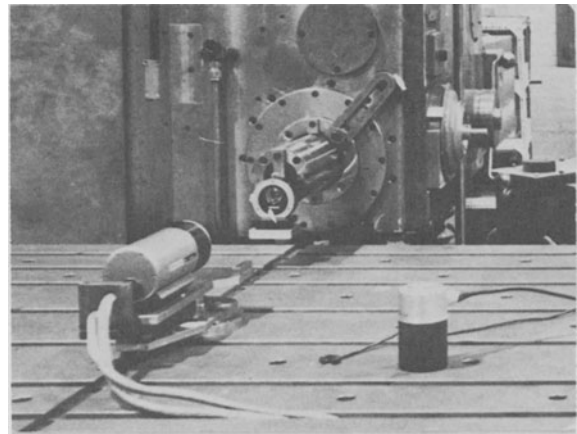


Fig. 13

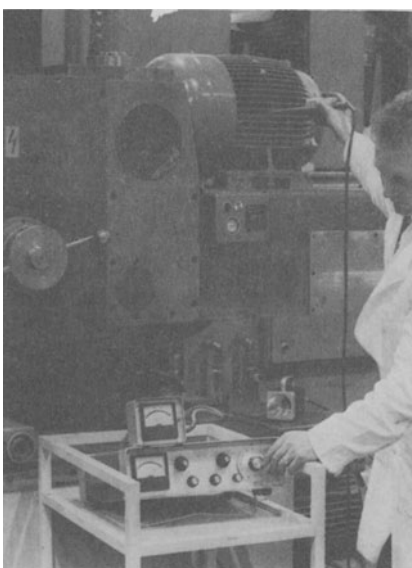


Fig. 11

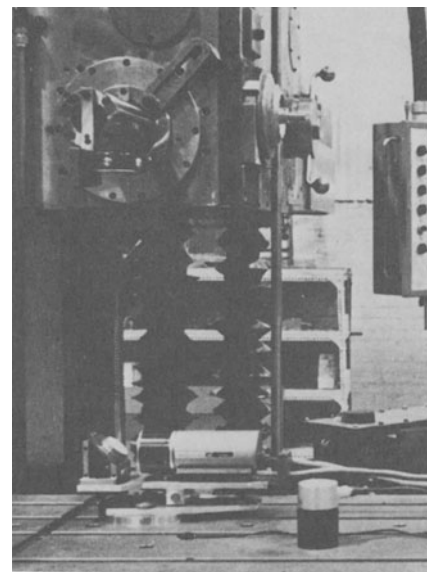


Fig. 14

APPENDIX I

NC ACCURACY AND REPEATABILITY TO '3-SIGMA' LIMITS AND INTERPRETATION OF THE RESULTS

The Company has adopted the NMTBA (National Machine Tool Builders Association) June 1968 *Recommendations for the Definition and Evaluation of 'Accuracy' and 'Repeatability'*. These provide precise definitions for the terms commonly used to describe the performance of a machine tool under numerical control.

'Accuracy' is defined as 'the sum of the signed value of the difference between the mean and the target at any point plus the value of dispersion at that same point'.

'Repeatability' is defined as 'the expected dispersion on each side of the mean, resulting from a series of trials when approaching any given point under the same conditons'.

Machine accuracies are normally quoted as 'plus and minus' values. Since the zero or starting point can lie anywhere within the total accuracy spread, it is considered necessary to reposition the theoretically perfect target to establish a reference zero at the mean of the extreme accuracy points. This follows the workshop analogy of repositioning the workpiece or fixture reference point to minimize dimensional variations within the work zone.

The use of 3-sigma limits or 3 standard deviations in determining accuracy or repeatability is an accepted statistical procedure. 3-sigma limits give 99.74% probability of all positioning attempts at a target point falling inside the specified limits. 3-sigma limits, by derivation, are automatically quoted as 'plus and minus' values.

Again, quoting NMTBA

$$\text{'mean' } x = \frac{\sum X}{N}$$

where x = data value

$\sum X$ = sum of all data values

N = number of data values = 7 unless otherwise specified

$$\text{'repeatability' } S = \left(\frac{\sum (X-x)^2}{N} \right)^{1/2}$$

and

$$\text{3-sigma 'repeatability' } 3\sigma = 3 S \left(\frac{N}{N-1} \right)^{1/2}$$

where S = standard deviation of sample without regard to sample size

Fig. 15 shows a typical spread of test results for 6 data points, for both approach directions. Unless otherwise required or specified, *unidirectional* approach is to be assumed (NMTBA), the larger of the two unidirectional values found for any given point or series of points being taken as representative of the machines' capabilities. Note the repositioned target, displaced from the original target, to coincide with the average of the excursion limits shown by the 'full' lines. The 'dotted' line is the mean excursion for each of the chosen data points. When 3-sigma 'repeatability' limits are superimposed on the mean line, for each data point, the 'full' lines giving maximum and minimum excursions are obtained. 3-sigma 'accuracy' is then quoted as plus and minus half of the excursion limits enclosed by the 'full-line' envelope, as illustrated in Fig. 15.

Similar treatment of all 12 data points, taken together, would result in the *bi-directional* values being obtained. A computer program utilizing data printed-out by the laser-gauge is commonly used in the evaluation.

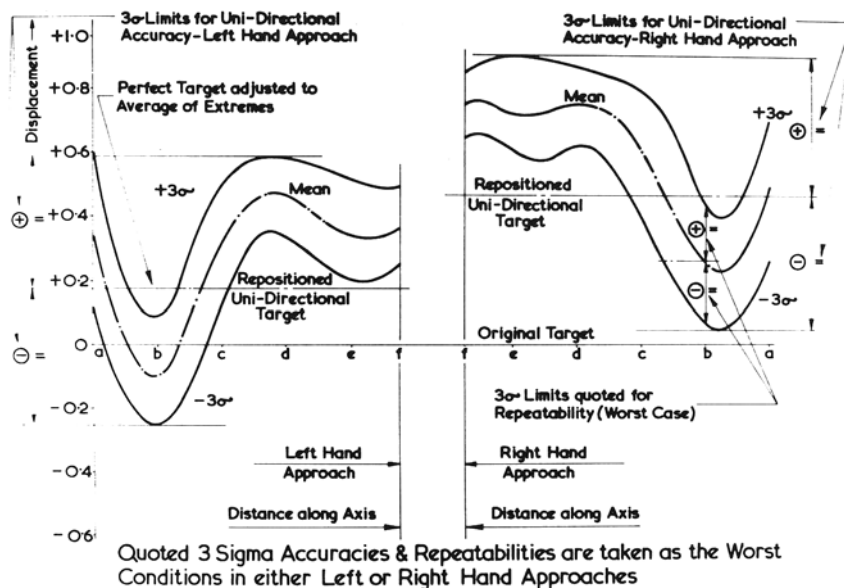


Fig. 15

TECHNIQUES FOR TESTING ACCURACY OF NC MACHINE TOOLS

by

J. TLUSTY*

SUMMARY

In dealing with the problem of defining and testing the accuracy of NC machine tools we are looking for such a concept of test where accuracy in the whole working zone of the machine would be established and the procedure is practical enough so as to enable us to include the effect of thermal, weight and clamping deformations in the test cycle.

The paper describes how a system of tolerances expressing the accuracy of NC machines, and of measurements checking it has been derived and, in some instances, practically applied and verified. This system may be called 'the linear system of accuracy of NC machine tools' because the word linear appears in describing the various features of the system; measurements are made along selected *lines* in the working zone of the machine, only *linear* (translative) and no angular deviations connected with the motions of the bodies of the machine are measured, tolerances are expressed as *linear* functions of distances of points in the working zone (although any other type of function may as well be chosen). We speak of a *system* because rules for tolerances and rules for selecting necessary measurements are stated which may be non-ambiguously applied to all types of NC machine tools. For a particular type of machine one particular number of measurements along one particular set of lines result from this system. This signifies that the system may be used as a basis for standardisation.

INTRODUCTION

The method of tape programmed semi-automatic 'master part trace test' is suitable for our purpose. It is a non-machining technique in which the workpiece is represented by the 'master piece' and the tool by a corresponding displacement transducer. Such instrumentation is usually used as it permits the signals of the transducer to be recorded, and the record to be subsequently analysed. In principle, the commonly used measurements of 'straightness of motion' (see Fig. 1(a)) in which a gauge slides on a straight edge in such a way that for example the straight edge is an element of a 'master part'; and of 'positioning accuracy' (shown diagrammatically in Fig. 1(b)), are elements of the 'master part trace test'. In Fig. 1(b) the 'positioning accuracy' measurement is shown in the three possible practical materialisations: (1) using a reading head (simple optical or photoelectric and a master scale); (2) a mirror and a laser interferometer; (3) a contact type displacement gauge and a 'step-bar'. In these instances the positioning measurement relates to the master part trace test in such a way that the elements of the master part are represented, respectively, by (1) the scale, (2) the laser beam, (3) the step-bar. It should be realized that these are fundamental measurements of displacement

(errors of positions) relative between the tool represented by the transducer and mirror, respectively being attached in the instance of Fig. 1 to the spindle and the workpiece represented by the various elements which are attached in this instance to the table of a machine. As previously stated these measurements were 'elements' of the whole test and, as shown in Figure 1, each of the measurements was carried out along one line only in the possible working zone of the machine.

The measurements assembled in Fig. 1 are the three basic elementary 'linear' measurements, i.e. measurements of translative errors caused by the motion of a body. Apart from these the motion of a body is also always accompanied by errors in the form of angular motions which will be mentioned later, but not eventually included in our 'linear' system of measurements.

Let us, at this stage, determine the denotation of the three linear errors. Assume a denotation of co-ordinate axes, for the particular machine tool type, as shown in Fig. 1(a). In this instance, we are dealing with errors related to the motion of the table, i.e. the co-ordinate motion X . If this motion was ideally accurate the two gauges in Fig. 1(a) and any of the gauges in Fig. 1(b), would give a constant signal. For the cases of Fig. 1(b) this means: (1) the head always

*McMaster University, Hamilton, Ontario, Canada

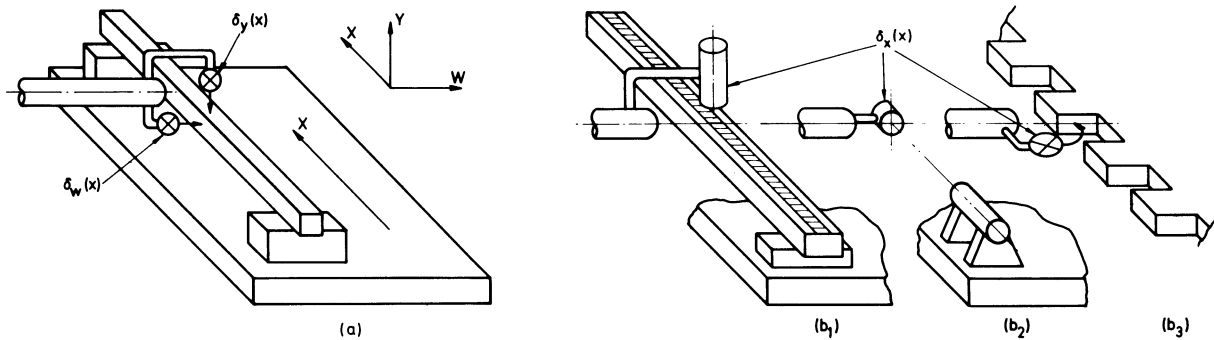


Fig. 1

reads exactly on each line of the master scale; (2) the readings of the counter connected to the laser interferometer are always identical with the position commands of the tape; (3) the gauge gives the same signal on every step of an exact step-bar. The variations of the signals of the gauges represent errors of the motion to be found along the one direct line of the workpiece parallel to X in which the straight-edge or scale or laser beam or step-bar, respectively, are situated. These errors will be denoted by the letter δ and an index determining the direction of the error. In brackets following the letter δ the letter will be given denoting the co-ordinate motion of which the errors concerned are functions. Thus:

$\delta_y(x)$ is the error of straightness of X motion as measured in Y direction and of its parallelism to table surface (or of its squareness to Y motion)

$\delta_w(x)$ is the error of straightness of X motion as measured in W direction (and of its squareness to W motion)

$\delta_x(x)$ is the error of positioning in X ,

all of them reflected to the particular line in the working zone. The above formulations relating to parallelism, or squareness of a motion to a part of the machine or to another motion, would need additional explanation which is not considered necessary within the frame of the present paper.

In practical terms, apart from the theoretical basis for the system presented above, the paper deals with how to determine the minimum necessary number of measurements, how to determine the situation of the lines along which the measurements have to be made, and consequently, how to design the master workpiece and how to write the program for the test cycle of motions, and furthermore how to evaluate the results of the measurements. At this stage, it is appropriate to say that the method of evaluation of accuracy of NC machine tools, as proposed here, and as based on some practical experience, does not envisage the use of a digital computer (but for an auxiliary part, that of statistical evaluation of each positioning measurement separately). An analogue way of using a graphical template applied to the graphs of element measurements is preferred because it is quick, simple and very informative.

There are a number of reasons for avoiding the use of a machining test: (a) it is more expensive and time consuming, especially as for statistical reasons, several (e.g. five) test workpieces have to be made and subsequently measured, which again may be a difficult

problem; (b) the effects of tool wear and workpiece distortions cannot be separated from those of the machine inaccuracy. If the non-cutting test is arranged so as to give results for the whole working zone, including thermal, weight and clamping effects, it is undoubtedly preferable.

THE TOLERANCE LAWS

Often, unfortunately, methods for testing are proposed and discussed without having clearly determined the definition of what is to be tested. We do not want to commit such a mistake, and therefore do not start discussing the accuracy test unless we have established the definition of accuracy of an NC machine tool and formulated corresponding tolerance rules to be satisfied by the results of the test.

We are omitting to consider 'dynamic errors' occurring in the servomechanisms controlling the coordinate motions, such as those caused by different velocity errors (different gain) in the individual axes and by overshoots and undercuts. Additional checks on these errors can rather easily be formulated.

The accuracy of an NC machine tool is best expressed by a comprehensive evaluation of errors of positions of points in the working zone of the machine. For the purpose of establishing this type of approach to the problem, let us start with a technical comment concerning coordinate systems. In all practical applications it is necessary to realise that we have to deal with three coordinate systems:

- (1) The system of coordinate motions of the bodies of the machines; i.e. the system in which the machine motions are controlled. Let us denote the coordinates in this system by indices 1.
- (2) The system of coordinates of the points belonging to the workpiece, i.e. the coordinate system of the working zone WZ. These coordinates will have indices 2.
- (3) The coordinate system of tool positions with respect to the tool carrier, denoted by indices 3.

For illustration see Fig. 2. In the diagram (a) one coordinate direction on a horizontal machine is dealt with, the one parallel with the spindle axis. There are two machine motions in this direction: table motion W , and spindle retracting Z (maximum extension Z_0 being considered as its origin). In the spindle, tools of various lengths can be changed. Considering the spindle end as the origin for the tool system, the tool point is determined by the coordinate Z_3 . In the set-up shown, the coordinate of the point in the working

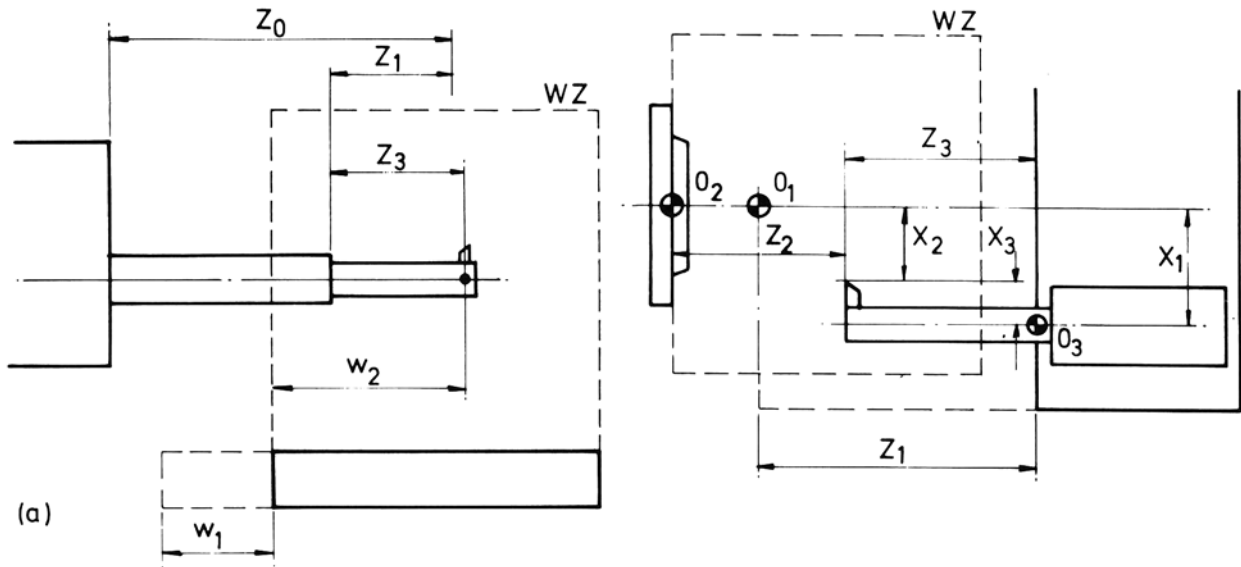


Fig. 2

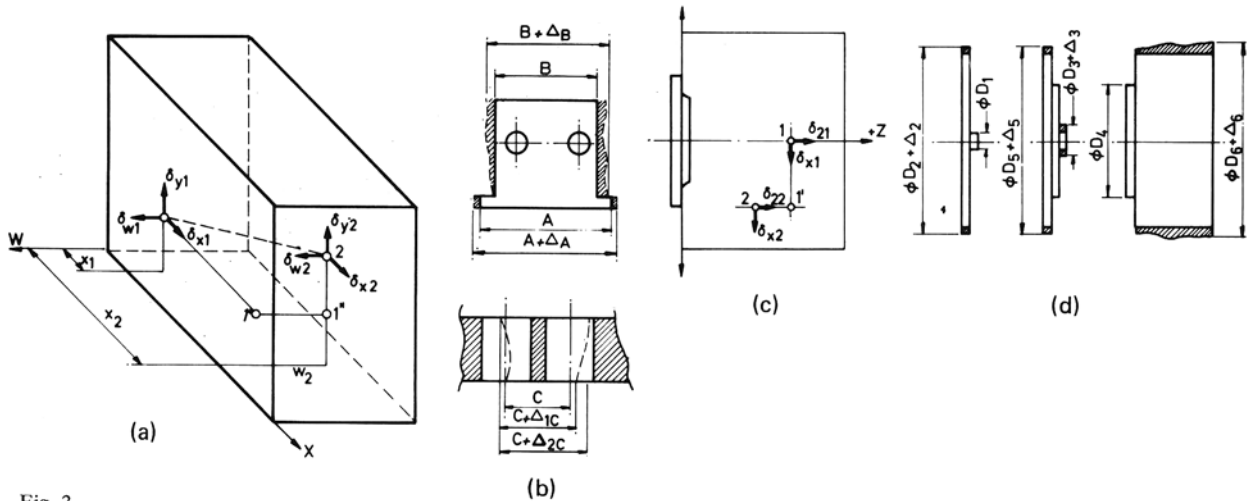


Fig. 3

zone which is being machined is w_2 , with the table edge as the origin of the coordinate system 2. A corresponding equation of transformation between coordinates w_1, w_2, z_2 may be written.

Case (b) depicts these coordinate systems on a chucking lathe. The motion of the slide is related to the origin O_1 , by coordinates x_1, z_1 of the point O_3 belonging to the slide. The point O_3 is chosen as the origin of coordinates x_3, z_3 determining the position of the tool point with respect to the slide. The tool point coincides with the point of the workpiece being machined, and belonging to the coordinate system of the WZ with the origin O_2 fixed on the spindle. The coordinates of the point of tool-workpiece contact in this system are x_2, z_2 . Again corresponding transformation equations between x_1, x_2, x_3 and z_1, z_2, z_3 respectively, could be written.

Your attention will now be concentrated on the system 2 only—of the points in the working zone of the machine. In Fig. 3 the working zones of machines (a) with non-rotating workpiece (three-dimensional WZ) and (b) with rotation workpiece (two-dimensional WZ), are diagrammatically shown.

In Fig. 3(a), a point 1 is shown with coordinates x_1, y_1, w_1 , in the chosen system of work zone (workpiece) coordinates. For simplicity, the previously mentioned index 2 for coordinates of work zone is omitted here. Because of errors connected with the coordinate movements of the machine, the position of the point 1 is not exact and it differs from the ideal position by errors $\delta_{x1}, \delta_{y1}, \delta_{w1}$, measured in the three directions of coordinates. The position of another point numbered 2, has errors $\delta_{x2}, \delta_{y2}, \delta_{w2}$.

The absolute errors of the positions of any point of the work zone by themselves are of no practical significance. The accuracy of the workpiece relates to dimensions and these are determined by the relative distances of pairs of points. Usually, dimensions are determined separately in the three basic directions, and tolerances for errors of dimensions increase with increasing dimensions.

The two sketches in Fig. 3(b) illustrate a special point: generally, it is to be accepted that the tolerance of a certain dimension measured in one direction, e.g. horizontally in our diagram, will also increase with the dimension of the measured surface

in the other direction, e.g. the vertical one in our diagram. For the dimension A , the actual surfaces being such as shown by broken lines and by the dashings, the error of the dimension is Δ_A . The surfaces determined by the dimension B (which is practically equal to A) are longer in the vertical direction. Therefore an error Δ_B greater than Δ_A is assumed. The distance of the axes of two holes should ideally be C . The actual form and location of the axes may be such as shown by the broken lines. For very short holes an error Δ_{1C} and for deep holes a greater error Δ_{2C} are found respectively.

The following initial rules for the accuracy of positions of workzone points may be assumed:

- (R1) Tolerances are to be stated for relative errors of positions of pairs of points.
- (R2) The relative errors will be considered separately in each coordinate. Thus, the relative errors are simply differences of absolute errors

$$\begin{aligned} \delta_{x1,2} &= \delta_{x1} - \delta_{x2} \\ \delta_{y1,2} &= \delta_{y1} - \delta_{y2} \\ \delta_{w1,2} &= \delta_{w1} - \delta_{w2} \end{aligned}$$

- (R3) The permissible relative errors (tolerances) increase with the distance of the two points concerned.
- (R4) The distance of two points will be considered separately in each of the coordinates. Thus, e.g. in our diagram Fig. 3(a), the direct distance of the points 1 and 2 as shown by the broken line is of no concern for the tolerances. The distances apply, as they are covered by the machine movements $1-1'$, $1'-1''$, $1''-2$, when moving from point 1 to point 2.
- (R5) Each of the relative tolerances mentioned in (R2) depend on all the three component distances mentioned in (R4). This rule may be explained, e.g. by considering the relative error $\delta_{x1,2}$ in the direction X . By moving $1-1'$, the positioning error $\delta_x(x)$ along this distance applies. By moving $1'-1''$, the error $\delta_x(w)$ of straightness of motion W in the direction of X applies. By moving $1''-2$, the error $\delta_x(y)$ of the straightness of motion Y in the direction X applies.

In Fig. 3(c), a diagram analogous to that of 3(a) is given relating to the two-dimensional WZ of, e.g. a lathe. Usually, a diameter is understood as an absolute dimension. Actually, however, it is measured again as a dimension between two points on the circumference of the workpiece and, fundamentally, it results from a radial displacement of the tool. Such a displacement is again measured as the distance of two points. Machining a diameter passing through points $1', 2$ may signify moving from the point 1 to point $1'$ in the setting motion and from point $1'$ to 2 in the machining motion.

The rules (R1) to (R5) of the previous case apply here as well. In the diagram (d) of Fig. 3 illustrations are given of two aspects of these rules.

Firstly, the relationship between tolerance and diameter size is discussed. With manually operated machines it may well be assumed that the tolerance

increases with diameter size, being very small for very small diameters. This is so because the error is determined solely by the error of measuring the diameter before final cut and the measuring gauge error is supposed to increase with the size measured. This is illustrated by comparing the small diameter D_1 without any error with the great diameter D_2 with error Δ_2 . In an NC machine this case applies if the tool position is corrected on spindle axis and, consequently, every diameter other than zero is obtained by displacing in the X coordinate from point $x_1 = 0$ to a point $x_2 = D_2/2$. It may, however, also be that the tool position is corrected in respect to a diameter $D_4 = 0$. Neglecting, for simplicity, the error of the correction, the diameter D_4 will be machined without error while both the greater diameter D_5 and the smaller diameter D_3 will have errors Δ_5 and Δ_3 respectively. These errors will increase with the differences $(D_5 - D_4)$ and $(D_4 - D_3)$ respectively.

Secondly, it is shown that the error of a diameter depends not only on the size of the diameter (dimension in X) but also on the length of that diameter (dimension in Z). All the previous diameters were drawn as very thin discs with virtually no dimension in Z . The diameter D_6 is shown rather long. Correspondingly, the error Δ_6 is assumed to be greater than the error Δ_5 of the diameter $D_5 = D_6$.

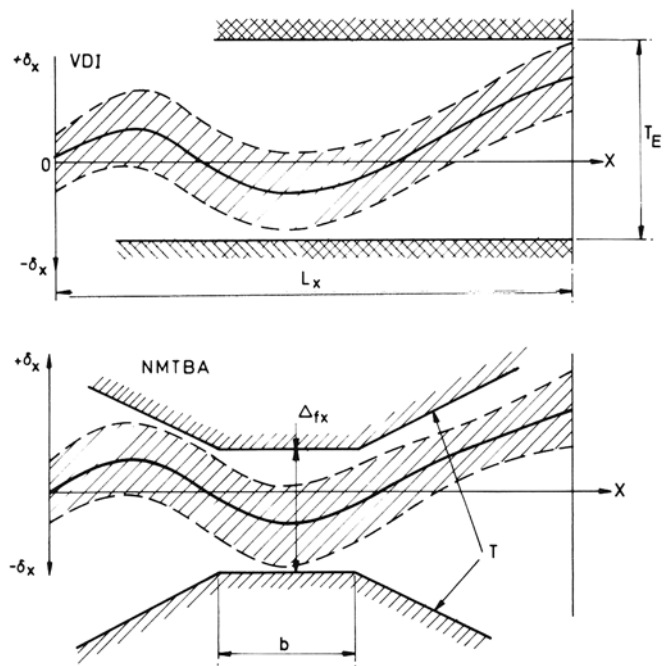


Fig. 4

Now, it is necessary to formulate the assumed rules in a more precise way. Firstly, the relationship between error and distance has to be determined. Two different formulae have been proposed for positioning accuracy, one by the German VDI 3254 and the other one by the American NMTBA. These are illustrated in Fig. 4. The diagram shown is a typical example of the result of a measurement of positioning accuracy along a direct line, say $\delta_x(x)$. The error δ_x as function of distance travelled shows a systematic trend (full line) and a scatter (broken

lines). In this way a field of errors δ_x is obtained as shown by the dashed area. The mean δ_x is deliberately chosen as zero for $x = 0$. However, the zero line for δ_x may be shifted upwards or downwards meaning that it is only the difference of the errors of two points which matters.

It may also be said that the error δ_x has a certain range (span) for every value of the coordinate x . This range may be caused not only by scatter but also by thermal deformations.

The requirement expressed in the VDI 3254 is that the difference between maximum and minimum values of δ_x along the whole travel L_x must not exceed the required tolerance, T_E . In this way, however, an error equal to T_E may be generated over any small distance of travel.

The NMTBA expresses the requirement by using a template T which permits a certain fundamental value Δ_{fx} of the error over a basic distance b . For distances greater than b the permissible error increases in proportion to the excess of distance beyond b . The template is applied to the graph of the error in such a way that the whole figure of the error field must always be fully enclosed in the template while the template is shifted in the direction of the x axis and it is at the same time freely moveable as a whole in the direction of the δ_x axis. This expresses the relativity of the error.

Having to choose between the VDI approach and that of NMTBA we do not accept either and propose a third formula which is closer to the NMTBA in that it permits an increase of error with distance. However, it will contain the VDI formula as a special case.

Let us, first, see the ISO formula for tolerances of workpiece dimensions. In Fig. 5 the values of tolerances δ in the IT5 class are plotted in relation to the dimension D . It is seen that the relationship (curve a) is non-linear and that for the dimension approaching zero the tolerance approaches a certain minimum value. The formula for all other IT classes is the same but for the scale of δ and with the exception of the three finest classes ITO1, ITO, IT1, where the relationship is linear, again with a certain value of tolerance for zero dimension.

Our proposal is to linearise the ISO curve. For middle size machines the linearisation can be such that the linearised formula gives identical values of δ with the original one for $D = 63$ mm and $D = 420$ mm. The linearised relationship is shown by the direct line b and it is for IT5.

$$\delta = 10 \mu\text{m} + 40 \mu\text{m}/1000 \text{ mm}$$

For small machines the curve a could be replaced by a different direct line approximating it in the low range of dimensions.

Accepting this type of relationship also for tolerances of positioning accuracy a template as shown in Fig. 5(b) is obtained. It is similar to the template of NMTBA but for not having any basic distance over which the fundamental error Δ_f would extend, i.e. $b = 0$ (see Fig. 4). Expressing the graphical template by a corresponding formula we have

$$|\delta_{x_2} - \delta_{x_1}| \leq A + K |x_2 - x_1| \quad (1)$$

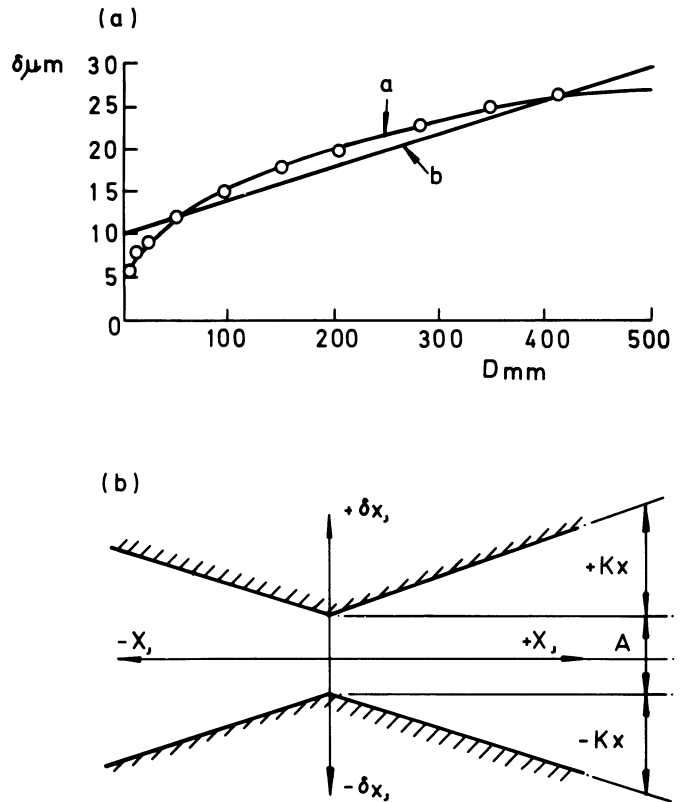


Fig. 5

which says that the error of the distance $(x_2 - x_1)$ between any two points 1 and 2 being on one line parallel with the axis X (see Fig. 3(a), for points 1 and 1') which is obtained as the difference $(x_2 - x_1)$ of the absolute errors in the direction X of the positions of the two points is composed of a constant A and a term proportional by K to the distance of the two points. Whether the resulting error is positive or negative (the distance is greater or smaller) is irrelevant as well as whether the distance is travelled in the $+X$ or $-X$ directions. This is expressed graphically by the symmetry of the template around both the δ_x and x axes and, in Eq. (1), by using absolute values of the differences on both sides of the equation.

Till now, tolerancing of positioning errors has been discussed. However, obviously, the same type of formula may be used for the errors of straightness and directions of motions. It is well imaginable that e.g. in the measurements shown in Fig. 1(a) when these are made in both directions of motion and, possibly also with stoppings and clampings, the signal of the gauges will show a certain basic span independent of distance of travel and that in addition the signal will change in direct proportion with distance travelled as a result of non-parallelity of the motion with table surface. The constants A and K in the formula may be chosen differently for every different type of error. If appropriate, the choice of $K = 0$ may be made which makes the formula equal to the VDI one.

The above errors have been considered when moving in one coordinate direction only. If moving, e.g. from point 1 to point 2 of Fig. 3(a), the previously assumed rule which has been discussed in relation to diagrams 3(b) and 3(c) applies, and each

of the errors is not only dependent on one coordinate movement only as in formula (1).

Thus, eventually, the general set of formulae is obtained for the tolerances for errors of positions of points in the working zone

$$|\delta_{x_2} - \delta_{x_1}| \leq A_{xx} + K_{xx}|x_2 - x_1| + A_{xy} + K_{xy}|y_2 - y_1| + A_{xz} + K_{xz}|z_2 - z_1| \quad (2)$$

$$|\delta_{y_2} - \delta_{y_1}| \leq A_{yx} + K_{yx}|x_2 - x_1| + A_{yy} + K_{yy}|y_2 - y_1| + A_{yz} + K_{yz}|z_2 - z_1| \quad (3)$$

$$|\delta_{z_2} - \delta_{z_1}| \leq A_{zx} + K_{zx}|x_2 - x_1| + A_{zy} + K_{zy}|y_2 - y_1| + A_{zz} + K_{zz}|z_2 - z_1| \quad (4)$$

if the three coordinates are x, y, z and where x_1, y_1, z_1 and x_2, y_2, z_2 are the coordinates of any pair of points in the working zone respectively.

The individual constants A and K may have different values. However, it is recommended that the pair of A and K be chosen as the same multiples or fractions by powers of 2 of the linearised IT5 values.

For a two-dimensional case an illustration of the significance of the formulae may be given in a form analogous to that in which the tolerance formula is graphically expressed by the template in Fig. 5(b). In Fig. 6 a two-dimensional template is shown as applied to a graphical representation of the δ_x error as function of displacements in two directions X and Y . The template consists of two surfaces, one of them composed of four planes marked by points 1, 2, 3, ... 9 and the other one symmetric to it with respect to the X, Y plane. The minimum distance between the two parts of the template is denoted $2a$. The sections of the template by planes passing through the point 9 and perpendicular to X and Y respectively, are the single dimensional templates $\delta_x(y)$ (4, 9, 8) and $\delta_x(x)$ (2, 9, 6) of the type shown in Fig. 5(b). The template of Fig. 6 could be applied to a topographical type of diagram $\delta_x(x, y)$ in such a way that the diagram should always be fully enclosed between the two surfaces of the template while moving the template all over the X, Y plane and leaving it free to move in the δ_x axis. This illustration has not a practical significance and it is given here in order to give a better idea of the significance of the formulae (2), (3), (4) which cannot, however, be graphically expressed in the full three-dimensional form.

The formulae (2), (3), (4) are devised as the simplest linear form of tolerances. Generally, any other form could be used for the relative errors $(\delta_{x_2} - \delta_{x_1}), (\delta_{y_2} - \delta_{y_1}), (\delta_{z_2} - \delta_{z_1})$ as functions of the distances $(x_2 - x_1), (y_2 - y_1), (z_2 - z_1)$. As long as the individual terms of the functions remain such that they each include only one of the $(x_2 - x_1), (y_2 - y_1), (z_2 - z_1)$ variables, the procedures of testing and evaluating the accuracy would remain the same as those presented in the following and using the formulae (2), (3), (4).

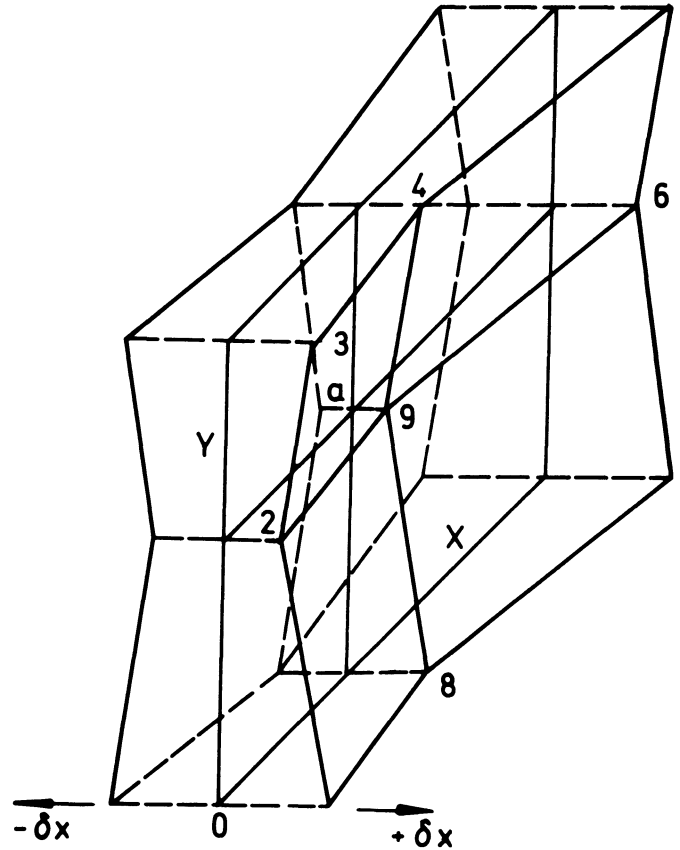


Fig. 6

Having decided on the tolerances of the positions of points in the working zone of the machine, and these representing the accuracy of a workpiece which would be machined without any tool wear and without any distortion by heat or cutting forces, the tolerances for the accuracy of machine motions are simply found by correlating the motions of the machine with the positions of points in the WZ.

In this way, it can be required that the three component errors

$$\delta_i(j), \text{ where } i = x, y, z.$$

satisfy the formulae (2), (3), (4) for all the three directions $j = x, y, z$, measured along any direct line in the working zone of the machine for all possible correlations of the (x_1, y_1, z_1) and the (x_2, y_2, z_2) systems of coordinates.

By measuring along direct lines which are each of them parallel with some of the coordinate axes, each of the equations (2), (3), (4) is split into three separate conditions. For eq. (2) it will be

$$(2,1): \quad |\delta_{x_2}(x) - \delta_{x_1}(x)| \leq A_{xx} + K_{xx}|x_2 - x_1| - \text{positioning accuracy of motion X}$$

$$(2,2): \quad |\delta_{x_2}(y) - \delta_{x_1}(y)| \leq A_{xy} + K_{xy}|y_2 - y_1| - \text{straightness of motion Y measured in direction X}$$

$$(2,3): \quad |\delta_{x_2}(z) - \delta_{x_1}(z)| \leq A_{xz} + K_{xz}|z_2 - z_1| - \text{straightness of motion Z measured in direction X}$$

It is, of course, unrealistic to make an infinite number of measurements along an infinite number of lines in the WZ. The minimum necessary number of measurements will be determined in the following paragraphs.

It may also be required that the stated accuracy of motions be achieved within a range of thermal states of the machine, in extremes of weight loading of the machine, with or without the use of the clampings of the machine elements.

EFFECT OF ANGULAR MOTIONS. RULES FOR LINEAR MEASUREMENTS

It has been mentioned above that apart from the three linear (translative) errors, shown in Fig. 1 and measured along one direct line in the working zone, there are further types of angular motions by which the motion of a body differs from an ideal linear translative motion.

Considering the motion X of the table of a boring and milling machine, see Fig. 7, the three angular deviations as functions of the coordinate x will be denoted by the letter and by an index determining the coordinate axis around which the angular motion takes place. Or else, the names pitch, roll and yaw can be used, analogous to the motions of ships:

- $\epsilon_x(x)$ – roll
- $\epsilon_y(x)$ – yaw
- $\epsilon_w(x)$ – pitch

The three linear errors $\delta_x(x)$, $\delta_y(x)$, $\delta_w(x)$ as measured in the point a connected to the spindle and along a particular line parallel to the motion X , e.g. the line passing through points a and d , include in themselves the combined effect of translative deviations of the motion of the table and of its angular deviations as reflected to the line a, b .

If the linear errors $\delta_x(x)$, $\delta_y(x)$, $\delta_w(x)$ are measured in points b and c , i.e. along the lines passing through these points which are offset with respect to the line passing through point a by O_y and O_w respectively, the results of these measurements will generally differ from that of the measurement in a . The difference is caused by the effect of the angular motions. Only in the special case when the motion X of the table was purely translative i.e. the angular variations $\xi_x(x)$, $\xi_y(x)$, $\xi_w(x)$ were zero the results of measurements of $\delta_x(x)$, $\delta_y(x)$, $\delta_w(x)$ would be identical for all positions of the point of measurement.

The offsets O_y and O_w are the usual ones encountered in this type of machine tool. In Fig. 7 also the offset O_x is shown, which however, applies only in the special cases of twin-spindle machines. In such a case the measurement of linear errors made with the gauge attached to point a of the first spindle applies for machining with tools attached to this spindle only while the results for point d of the second spindle differ by the effect of the angular motions expressed through the offset O_x .

Often, test specifications for accuracy of machine tools are made in such a way that in order to specify non-ambiguously the accuracy of the motion of such a body as is the table in Fig. 7 the measurement of

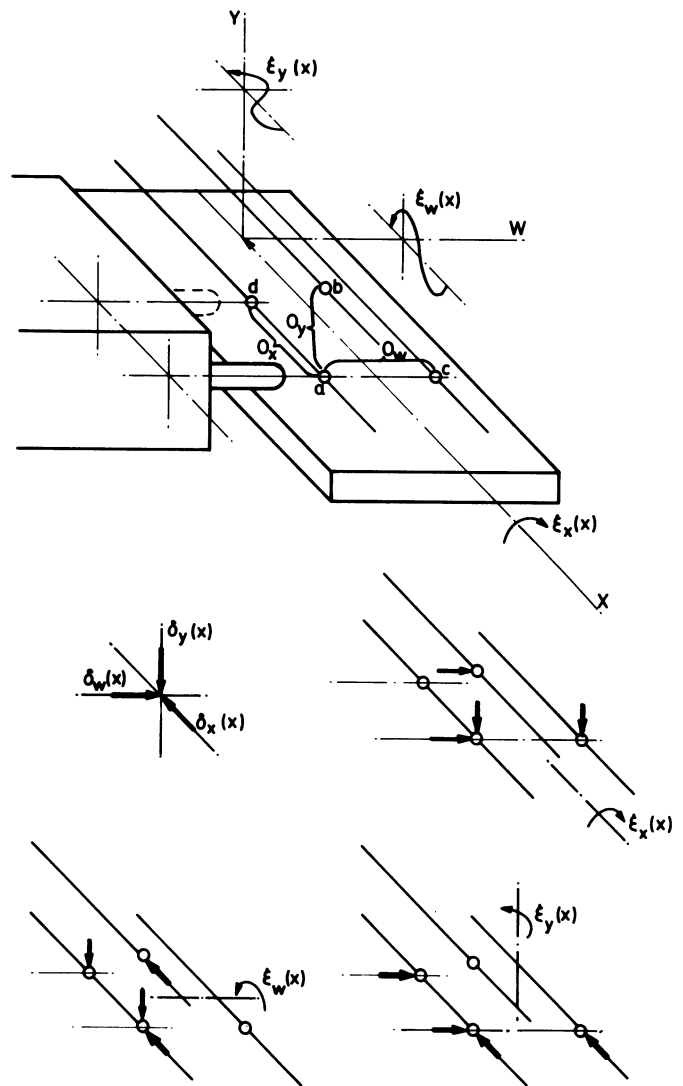


Fig. 7

the linear deviations $\delta_x(x)$, $\delta_y(x)$, $\delta_w(x)$ along a selected line in the WZ is prescribed as well as measurements of the angular motions $\xi_x(x)$, $\xi_y(x)$, $\xi_w(x)$.

We do not use this method in our system, for two reasons. The first one is that some of the angular motion measurements are difficult. Although the pitch and the yaw can be easily measured using an autocollimator, it is a difficult technique to incorporate into the 'masterpiece'. The measurement of roll is possible with the use of two electronic levels in differential connection, provided that it is the roll around one of the horizontal axes.

Roll around a vertical axis is measured with great difficulties. The second reason is that there is no direct criterion for determining the tolerances for the angular motions as their effect is additional to the effect of the translative deviations and both should be limited together. Therefore, we do not directly measure the angular deviations at all and check only their effect in an implicit way by making an increased number of measurements of the linear deviations δ_x , δ_y , δ_w .

The effects of the individual angular deviations are included by measuring linear deviations in pairs as it is shown in the lower part of Fig. 7, for deviations connected with the motion X of the table of the boring and milling machine. The illustrations are given using arrows as symbols for the three types of measurements

$\delta_x(x)$ — positioning accuracy
 $\delta_y(x)$ — straightness and direction in Y
 $\delta_w(x)$ — straightness and direction in W

to be carried out with techniques shown in Fig. 1.

It is seen that the following angular deviations affect the following linear (translative) deviations through the following offsets

Angular deviation affects linear deviation through offset

$\epsilon_x(x)$	$\delta_y(x)$	O_w
	$\delta_w(x)$	O_y
$\epsilon_y(x)$	$\delta_x(x)$	O_w
	$\delta_w(x)$	O_x
$\epsilon_w(x)$	$\delta_x(x)$	O_y
	$\delta_y(x)$	O_x

For single spindle machines, the two effects caused by the offset O_x do not apply. In a similar manner the effects of angular deviations could be derived also for the other coordinate motions of the machine (those of the slide, of the headstock, of the spindle).

It is necessary to determine, in each case, which are the applicable offsets and which are the linear measurements affected through them. In determining the applicable offsets it should be kept in mind that an *offset is a variation of the position of the point of machining (of the position of the measuring gauge) with respect to the moving body concerned (Rule A)*. The significance of this rule will be explained later by examples.

The most important aspect of our technique is the following statement: *If the particular pair of measurements of linear deviations are made at extreme offsets, they represent two extreme values of the particular deviations, (Rule B)*. Results of measurements along lines situated between the lines of extreme offsets are enclosed by the results obtained at extreme offsets and they could be evaluated by linear interpolation between the extreme values.

Consequently, *if the required tolerances are satisfied by results measured at extreme offsets they are satisfied automatically also for results measured along all lines between the two extreme offsets (Rule C)*.

For illustration, let us consider Fig. 7. The error $\delta_w(x)$, straightness of motion X measured in the direction W , is influenced by the angular deviations $\epsilon_x(x)$ combined with the offset O_y . Therefore, two measurements of $\delta_w(x)$ are necessary (for a single spindle machine). These measurements will be made in points a and b with a gauge reading in the direction

W on straight-edges which are parallel with the motion X . Let us situate these two straight-edges and, consequently also the points a and b so that point a is practically on the table and point b at maximum height possible over table. The two functions $\delta_w(x)$ measured at points a and b respectively will be the extremes for $\delta_w(x)$. If they satisfy the tolerance according to Eq. (4) (taking into account the first term only on the right side of the equation), then $\delta_w(x)$ satisfies this tolerance for motions in the whole working zone.

As another example let us consider the error $\delta_x(x)$ of positioning in the direction X . As shown in Fig. 7 this error is influenced by the combination of the angular deviations $\epsilon_w(x)$ with offset O_y as well as by the combination of the angular deviations $\epsilon_y(x)$ with offset O_w . Consequently, positioning measurement must be made along lines passing through points a , b , c , provided that these are situated in the corners of the working zone box, i.e. O_w equals the width of the table and O_y equals the Y travel of the headstock. However, still another measurement is necessary, such that both offsets O_w and O_y combine simultaneously at extreme values, i.e. along a line above c in the height of b . If the results of these four measurements satisfy the tolerance requirement

$$|\delta_{x2} - \delta_{x1}| \leq A_{xx} + K_{xx} |x_2 - x_1|$$

then this tolerance is satisfied in the whole working zone of the machine.

In the illustrated way the minimum necessary number of measurements of linear deviations and their locations in the working zone of the machine can be derived for any machine tool type. Having determined these measurements a corresponding master workpiece can be designed.

For evaluation of the accuracy test of a machine, each set of results is checked against a tolerance formula of the type explained by Eq's. (2.1), (2.2), (2.3) and by analogous equations obtained by decomposing Eq's. (3) and (4). These checks are most easily made by expressing the result of each measurement graphically and applying a template representing the corresponding tolerance formula as has been explained in connection with Fig. 5.

As yet, the effect of angular deviations of the motion of a body on linear measurements made during the motion of that body only has been discussed. However, angular motions produced during the motion of a body A may also affect the linear errors measured during the motion of another body B in those cases where the body B is carried on top of the body A . We shall not analyse this aspect in detail here. It should only be stated that this aspect does not influence the choice of the minimum necessary measurements which, when selected as described in the preceding are always more than sufficient to supply data also for this particular aspect. It is only in the evaluation of the results of the measurements where this particular aspect imposes constraints additional to those expressed by the tolerance equations (2), (3), (4). This point will best be explained on the basis of an example in the following paragraph.

DETERMINING THE MINIMUM NUMBER OF LINEAR MEASUREMENTS. DESIGN OF THE MASTER WORKPIECE. THE TEST CYCLE

By applying Rules A, B, C derived in the preceding paragraph on the individual machine tool types the minimum number of linear measurements and their locations may be determined. Let us illustrate the procedure by giving two examples, one for a machine tool with a three-dimensional working zone and the other one for a machine tool with a two-dimensional working zone.

Following the explanations given in Fig. 7, the minimum necessary linear measurements for a table type horizontal boring machine are diagrammatically shown in Fig. 8. The working motions of the machine are X, Y, W . The motion of the spindle Z is not considered a working one but only a setting one. Therefore, no linear error measurements will be made connected with this motion which will be considered only in determining extreme offsets.

straightness errors in direction $Y, \delta_y(x)$, along lines A and B
 straightness errors in direction $W, \delta_w(x)$, along lines A and C

For measurements to be made during the motion W of the slide, see diagram (c). Remembering Rule A, that offsets are determined with respect to the moving body concerned, we find that the tool position varies with respect to the slide in the central Y, W plane only. Thus, there are only two extreme positions of lines parallel with motion W , those denoted E and F . The length of these lines is a sum of the travel W_x and of the variation in tool length z_3 , assuming that travel Z_1 is equal to W_1 . The variation in tool length determines also the possible offset O_w . According to Rules B and C and to geometric considerations, the maximum offset O_y given by the distance of the lines E and F combined with the roll $\epsilon_w(w)$ influences the measurement $\delta_x(w)$ and combined with the pitch $\epsilon_x(w)$ it influences the measurement $\delta_w(w)$. The roll has no effect on $\delta_y(w)$ because there exists no offset O_x . However, the offset O_w influences both $\delta_y(w)$ and $\delta_x(w)$ by the effect of the pitch and the yaw respectively. Consequently, the following measurements are necessary:

positioning accuracy $\delta_w(w)$, along lines E, F
 straightness errors in direction $Y, \delta_y(w)$, along line E in two points distant by O_w
 straightness errors in direction $X, \delta_x(w)$, along line E in two points distant by O_w

For measurements to be made during the motion X , see diagram (d). The only possible offset of the tool with respect to the headstock, which is the moving body concerned, is the one created by extending the spindle (coordinate z_1) and by varying the length of the tool (coordinate z_3 , see Fig. 2(a)). Thus, we have the lines G and H located at extreme offsets. The following measurements are necessary:

positioning accuracy $\delta_y(y)$, along lines G and H
 straightness errors in direction $X, \delta_x(y)$, along lines G and H
 straightness errors in direction $W, \delta_w(y)$, along line G .

A 'master workpiece' could now be designed which would consist of straight edges and step-bars (or scales) assembled together in such a way as to make possible all the measurements. Also, a corresponding gauging head should be prepared. There are several possible solutions not to be discussed here.

The evaluation of the test consisting of the mentioned measurements is first of all based on checking the results of every one of the measurements separately against the corresponding tolerance formula. We shall say a little more about this in the following paragraph. Here, let us just explain the point of the effect of angular motions of a body on linear measurements made during the motion of another body. This effect may only concern measurements of 'straightness and direction'. In the case of the machine of Fig. 8 it affects the measurements of $\delta_x(y)$ and $\delta_w(y)$ because these are made on straight edges fixed to the table. Therefore, the vertical position of these straight edges is influenced by the

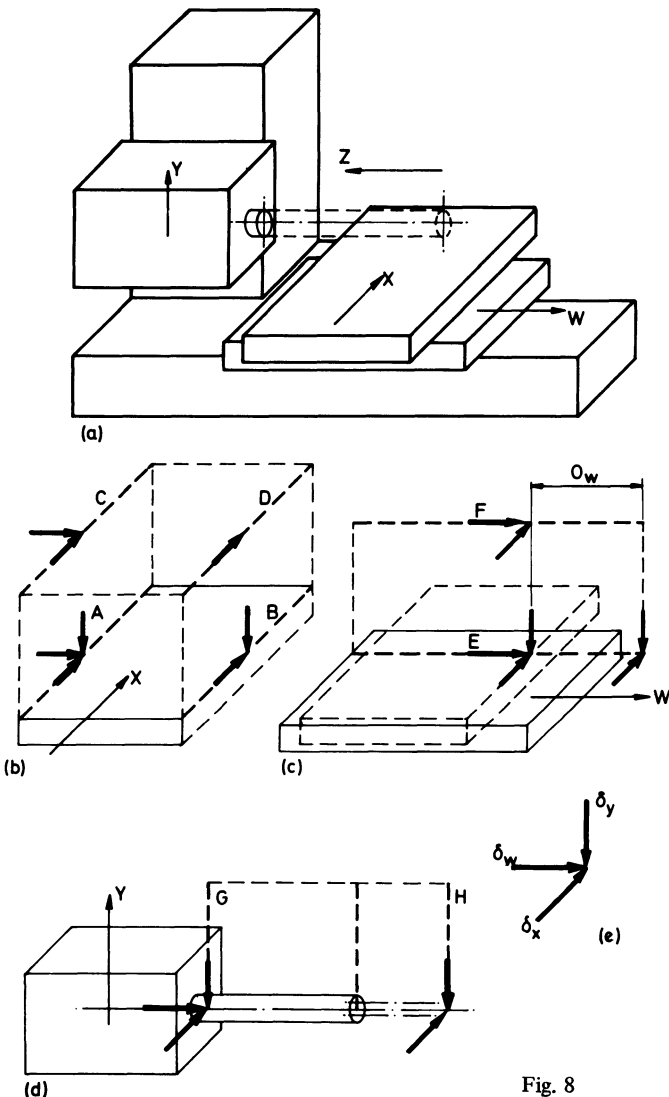


Fig. 8

The measurements to be made during the motion X of the table are based on explanations given in Fig. 7 and they are shown in Fig. 8(b). They are:

positioning accuracy $\delta_x(x)$, along lines A, B, C, D

deviations $\epsilon_w(w)$ and $\epsilon_x(w)$ respectively from horizontally of the slide which carries the table. These deviations directly affect the 'direction' of measurements $\delta_x(y)$ and $\delta_w(y)$. Therefore, a separate restriction must be imposed on $\epsilon_w(w)$ and $\epsilon_x(w)$ which as yet has not been contained in the tolerance 'template' applied to the results of the individual linear measurements. Such a restriction is best expressed by an additional constraint on results of measurements $\delta_x(w)$ and $\delta_w(w)$. This additional constraint should limit the difference between results of these two measurements as obtained along the lines of E and F respectively.

Our second case, the two-dimensional one, is that of a chucking lathe, shown in Fig. 9. There are two coordinate motions X and Z, two types of linear deviations connected with each of these motions: $\delta_x(x)$, $\delta_z(x)$, $\delta_x(z)$, $\delta_z(z)$ and just a single type of angular deviation ϵ_y , connected with each of these motions: $\epsilon_y(x)$, $\epsilon_y(z)$. The axis Y is assumed perpendicular to both X and Z. It could be easily shown that the two other angular deviations do not apply here.

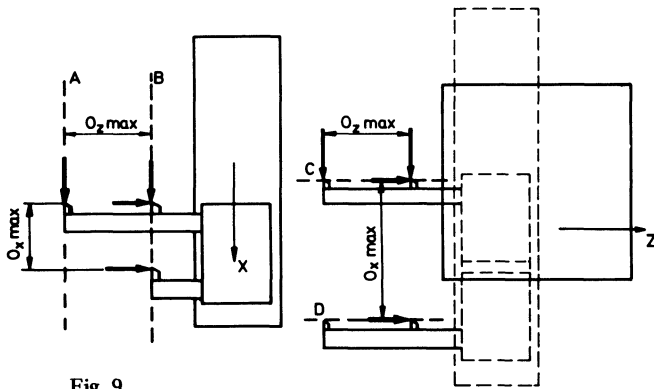
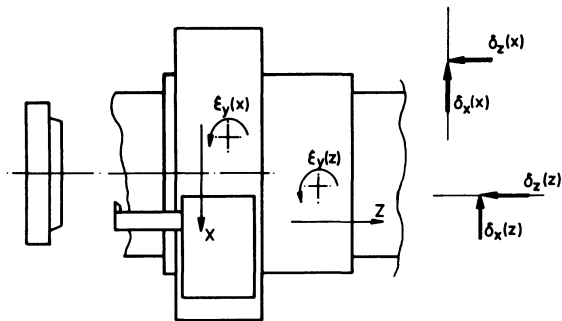


Fig. 9

In the lower part of the figure the applicable offsets are shown as well as the necessary linear measurements. For the motion X, of the cross-slide, the possible offsets are determined by the extreme possible positions of the tool with respect to the tool holder fixed to the slide. They are denoted O_{xmax} and O_{zmax} and they indicate the positions of lines A and B (relative positions with respect to the cross-slide) and the positions of gauges in which the measurements have to be made. They are

positioning accuracy in X, $\delta_x(x)$, along lines A and B

straightness errors in direction Z, $\delta_z(x)$, along line B at two points distant by O_{xmax}

For the motion Z of the longitudinal slide, the extreme offsets in the Z direction are the same ones as for X and they are given by the shortest and the longest tool holders respectively. The extreme positions of the tool in the X direction, related to the longitudinal slide are those of machining the smallest and the greatest diameters as it is indicated by the offset O_{xmax} which differs from that belonging to the motion X. The following measurements are necessary

positioning accuracy in Z, $\delta_z(z)$, along lines C and D

straightness errors in direction X $\delta_x(z)$, along one of the two lines, at two points distant by O_{zmax}

Let us illustrate this case by the description of the design of the master workpiece as it has been developed, with the author's cooperation, at the machine tool company HEID in Austria. Their lathe was one with two turret heads. The various possible locations of tools in each of the turret heads are shown in Fig. 10. It is seen that $O_{zmax} = 300$ mm. The O_{xmax} offset is rather small and it is of no significance because the actual O_{xmax} offset is determined by the distance of the tools in the two turret heads. Correspondingly, the test was made with measuring heads L1, K1, L2, K2, attached to holders shown in Fig. 11. The O_z offset between the heads L1, L2 and K1, K2 is 300 mm. The O_x offsets correspond to the actual possible tool positions. Each of the measuring heads had three gauging contacts denoted α , β , γ , all of them actuating one inductive type displacement transducer. The three contacts make it possible that the head traces the various templates representing the master workpiece. The drawing in Fig. 11 gives the coordinates in the X_3, Z_3 system of the contacts. These are used in writing the program for the measuring cycle.

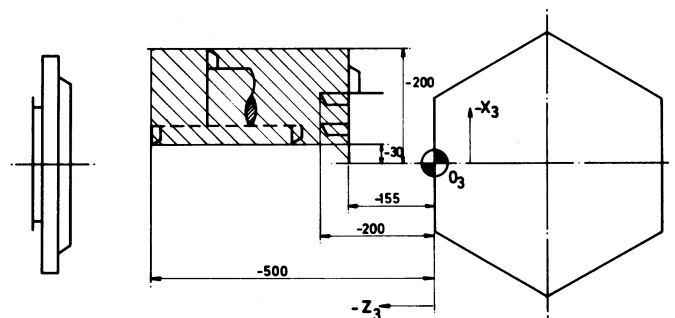


Fig. 10

In Fig. 12 the master workpiece design is diagrammatically shown. The master piece is shown in four positions, A to D. It is an assembly of templates fixed to one baseplate which is attached to the spindle flange. As shown in the diagram A, in one plane passing the spindle axis, there is the X straightness template in one line with the X positioning template (step bar). In the spindle axis a cylindrical mandrel is fixed which is used for Z straightness measurements. In the position B which is obtained by rotating the spindle one half revolution the X straightness and the X positioning templates have changed places enabling

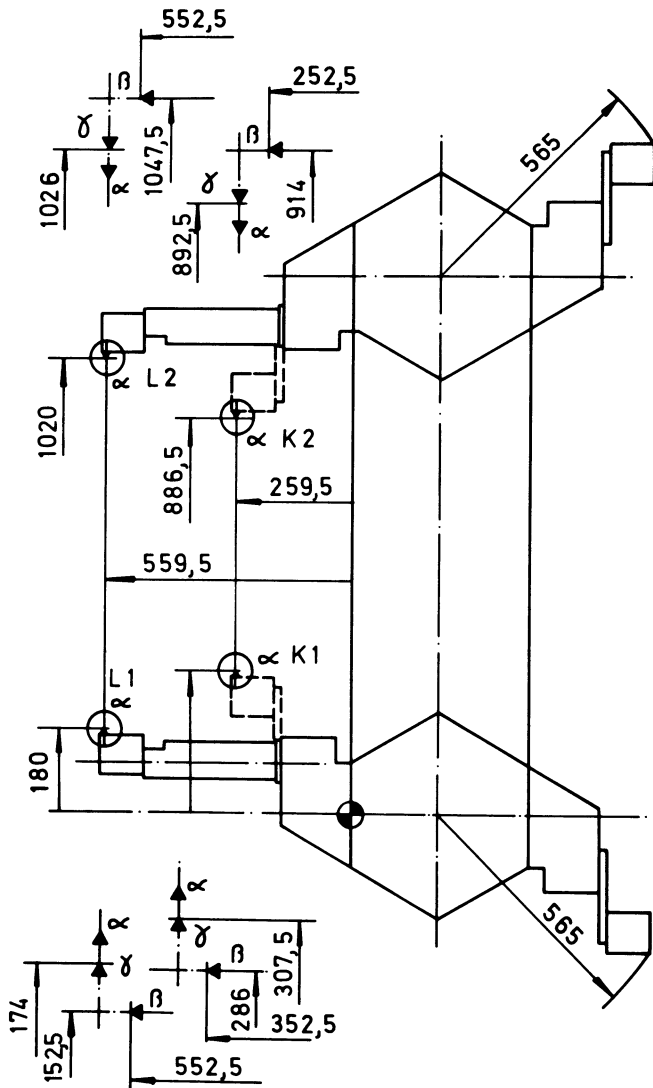


Fig. 11

the measurements with heads attached to the other turrets. The O_x offset for Z positioning measurements is obtained here not on lines passing through zero and maximum diameters (lines C and D of Fig. 9) but in lines displaced on both sides of the spindle axis on maximum diameter. This is so because machining is also carried out behind and in front of spindle axis using the two available turret heads. Therefore, the Z positioning template which is situated in a plane passing through the spindle axis at 90° to the plane of templates shown in positions A and B can be brought once in front of the spindle axis, position C , and the second time behind it, position D . In this way a rather simple design of the master piece enables all the necessary measurements as it is used in four different positions around the spindle axis. The number of the necessary measurements is slightly higher than shown in Fig. 9, for several reasons. The first one is that some additional measurements are necessary because of the two tool heads. The second one is that Z straightness measurements must be repeated at two 180° distant positions of the mandrel, in order to eliminate the possible non-parallelity of the mandrel with spindle axis. The third one is that because of practical aspects of the design of the master piece the Z positioning template is

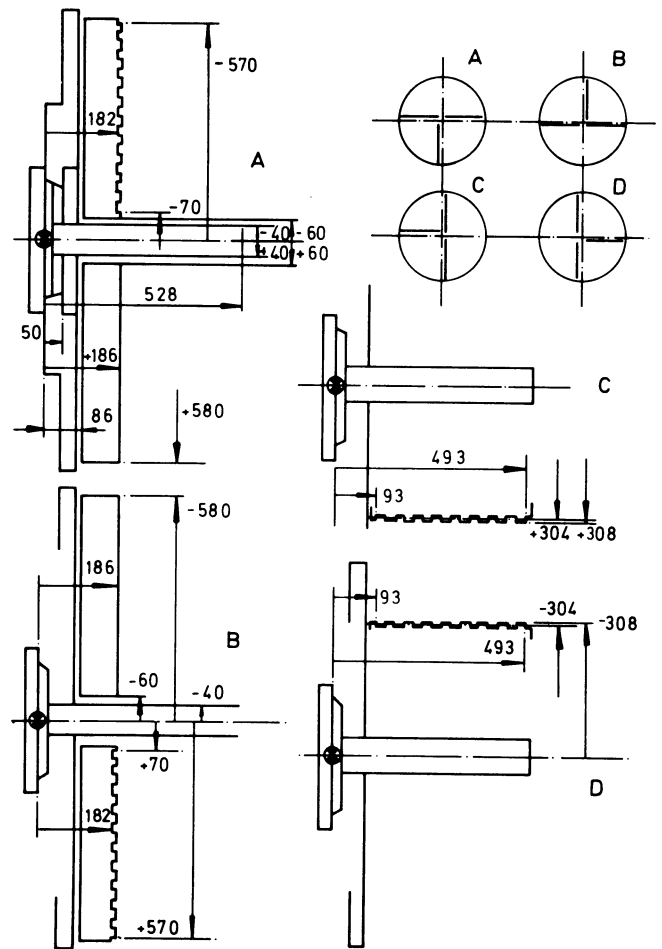


Fig. 12

shorter than the useful Z travel and must, therefore, be read in two steps, with the short gauge holder and with the long one. The possible non-squareness of the X straight edge template to the spindle axis is eliminated by the possibility of adjustment of the position of this template while a 180° swivel check is made.

The test cycle in which all the necessary measurements are automatically carried out while the machine is controlled by a test punched tape, is diagrammatically shown in Fig. 13. The whole cycle consists of 14 measurements. The type of each measurement is noted in the diagrams by determining the deviation measured, e.g. $\delta_x(x)$, the turret head concerned, where $T1$ denotes the front head and $T2$ the rear head, and the type of measuring head holder, where LH and SH stand for long and short holders respectively. The positions A to D of the master piece are also given in the diagram. All straightness measurements are made once in both the plus and minus directions. All positioning measurements are made with five repetitions of approach to every step in one direction and with five approaches to three selected steps in the other direction. In this way a statistical evaluation is possible and dead zone is determined. The whole test cycle took about 80 minutes and all results were recorded for subsequent evaluation.

EVALUATION OF RESULTS

In the preceding paragraph it has been shown how to determine the minimum necessary number of linear measurements so as to obtain the basic set of measurements which can in a fully comprehensive way express the effect of errors connected with the individual coordinate motions on the accuracy of relative tool-workpiece motions in the whole working zone of the machine. It has been shown that this basic set of measurements can have the form of a semi-automatic measuring cycle in which gauge heads representing tools trace a master workpiece representing a universal set of machining operations.

The evaluation of the basic set of measurements is rather simple. First, all of them are expressed graphically. For measurements of 'straightness and direction' the result is usually obtained directly in the required graphical form as a continuous record of the signal of the tracing head, preferably recorded in such a way that the direction of the recording paper is reversed when the direction of the measured motion is reversed. The measurements of 'positioning accuracy' have to be statistically processed first. After that, they are again expressed in a graphical form such as in Fig. 4.

Subsequently, each of the graphs is checked separately using the corresponding graphical template as it has been described in the preceding, in connection with Figs. 4 and 5. The individual parts of the tolerance conditions (2), (3), (4): they have the form shown in Fig. 5(b) which in every case is determined by the values of the constants A and K . For a particular machine tool model, particular values of constants A and K apply, to be given in the specification of the model. The correlation is such that for all $\delta_x(x)$ measurements the constants A_{xx} and K_{xx} apply, for $\delta_x(y)$ the constants A_{xy} and K_{xy} , etc., for $\delta_y(x)$ the constants A_{yx} and K_{yx} , for $\delta_w(x)$ the constants A_{wx} and K_{wx} , etc. The requirement is that all of the measurements satisfy the tolerance conditions. If they do, it is proof that in the conditions in which the test cycle has been carried out the accuracy of the machine is such as required.

Because the semi-automatic test technique is rather quick it is possible to require the test to be

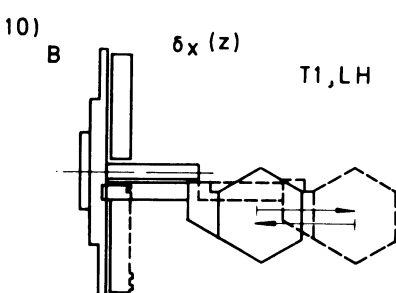
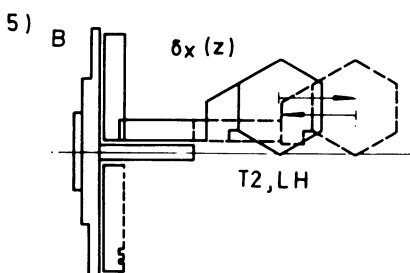
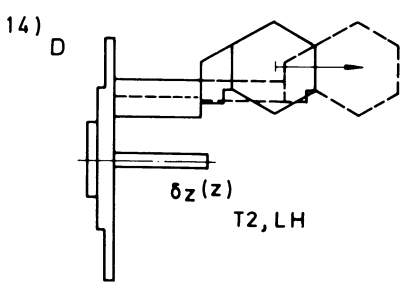
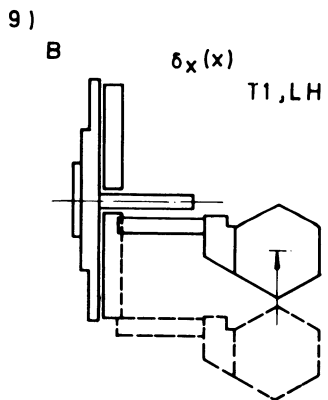
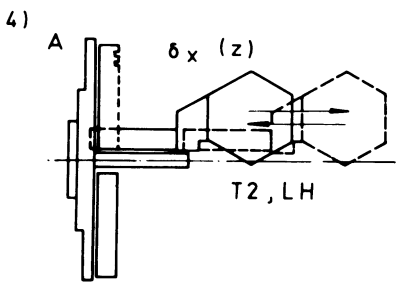
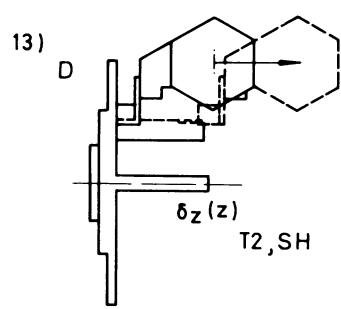
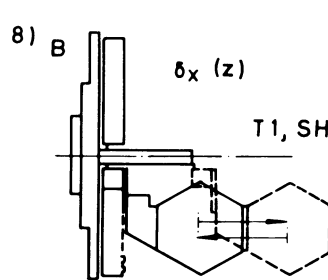
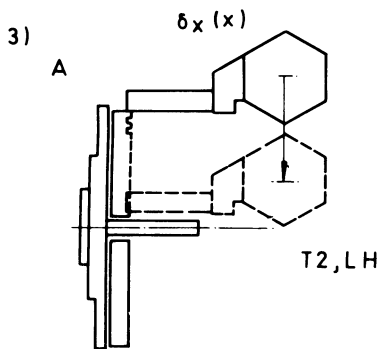
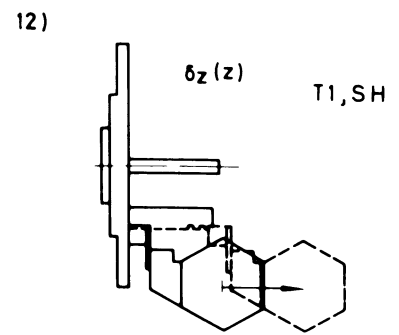
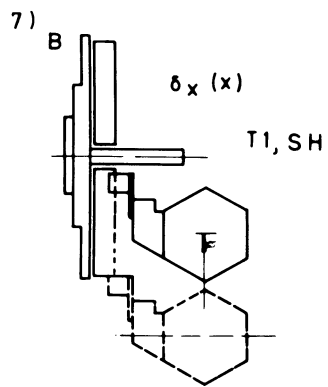
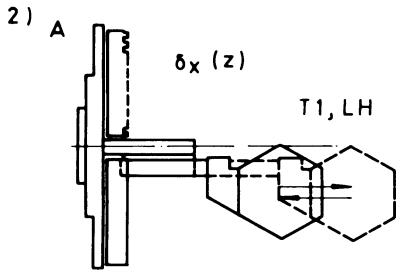
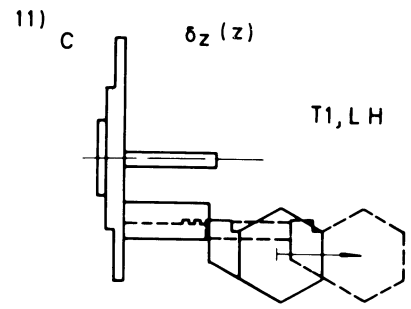
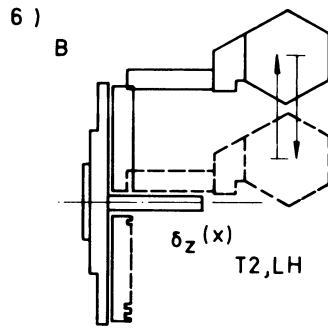
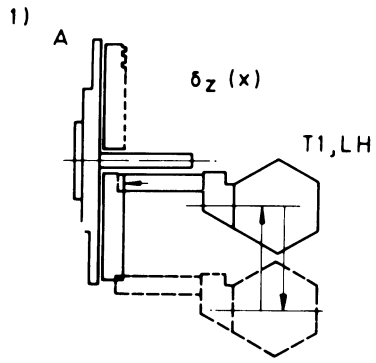
repeated at various conditions. For example, it may be required for a horizontal boring and milling machine that the test be made with satisfactory results both for a non-loaded table and for a table loaded with a specified maximum weight of workpiece.

The most common requirement is that the machine should give the required accuracy in a range of thermal states. The corresponding test is such that the above mentioned basic cycle is repeated through the desired thermal cycle of idle motions of the machine. In all particular cases it has been usually found that, considering the peculiarities of the thermal deformations of the machine, only certain parts of the basic measurements cycle have to be repeated through the thermal cycle of the machine. This, usually, leads to considerable simplifications of the procedure. For a horizontal table type boring and milling machine it may be acceptable that all pertinent heat sources act on the column and headstock group of the machine. In such a case the measurements connected with the Y motion only have to be repeated, see Fig. 8(d).

It is, however, important to realise that the repeated measurements of a particular item of the set of measurements must not be evaluated separately. All of the results, of a particular type of repeated measurement represent a 'range' of the errors. They have to be plotted together, allowing for some corrections corresponding to the usual manual corrective interventions into the machining cycle, and they all together have to enter into one tolerance template.

ACKNOWLEDGEMENT

The author expresses his thanks to Mr M. Schobel, managing director and chairman of HEID machine tool company for his understanding and support during the development of the semi-automatic testing technique for the company's NC lathes and for his permission to publish the data shown in Figs. 10, 11, 12, 13. He is also very grateful to Mr Wagner, Mr Smetana and Mr G. Sollnar of HEID company for their very active cooperation in this particular development work.



METAL PROCESSING

METALLURGICAL AND RESIDUAL STRESS INVESTIGATIONS OF EXPLOSIVELY WELDED SPECIMENS

by

R. PRÜMMER*

INTRODUCTION

Explosive welding is a method which has already gained many applications such as the cladding of pressure vessels, heat exchanger tubes and chemical reactor tubes. The main advantage of this method is that metals can be welded which cannot be bonded by fusion welding, either because of too great differences in their melting points or because of the creation of intermetallics in the bond zone. Explosive cladding can also be achieved within great areas, up to 5 m X 2 m; theoretically unlimited, if there were no environmental limitations due to noise. Because of this, most of the experiments are performed in quarries. In recent years much work has been performed in cladding different materials and different shapes¹⁻⁵, and the mechanism of welding was also extensively investigated^{1-4, 6, 7}. Much work is concerned with the joint efficiency and the strengths achieved. Since the material is subjected to changes due to shockwaves, such as intense plastic deformation, phase changes, and large mechanical twinning^{2,4,8,9} near the bond zone, examinations of the bonding strength are of interest. The strength is also affected by the presence of residual stresses. These can give rise to fractures or can lead to stress corrosion near the bond zone without any external applied load. It therefore seems worth investigating the stress state of an explosively welded specimen. As steep stress gradients are to be expected near the bond zone, the strain determination has to be performed within small areas. The X-ray method seems to be the most appropriate one in this case. A weld between an aluminium alloy and a mild steel is investigated.

THE WELDING PROCESS

The possibility of explosive welding metals was discovered accidentally during explosive forming experiments of metal sheets, when the sheets happened to be bonded to the die¹⁰. At present 'explosive welding' has gone into fabrication. Several companies supply explosion clad plate products. A quite common arrangement of explosive welding is

shown in Fig. 1. A flyer plate is inclined at a small angle α against the base plate. The upper side of the flyer plate contains an explosive layer which is detonated by the detonator. Fig. 2 shows the situation a few microseconds after ignition. Owing to the high detonation pressure (of the order of 10^{10} N/m², dependent on kind of explosive), the flyer plate is accelerated instantaneously and hits the base plate at an inclination angle β , the collision angle. At the collision point K a high stagnation pressure and shear stress is created, which causes the material to flow. A jet is formed which removes thin surface layers from both the flyer and base plate. Thus, 'clean' surfaces are impacted and a metallic bond is achieved. There are several problems, such as choosing the right inclination angle α , and more especially the right kind and amount of explosive.

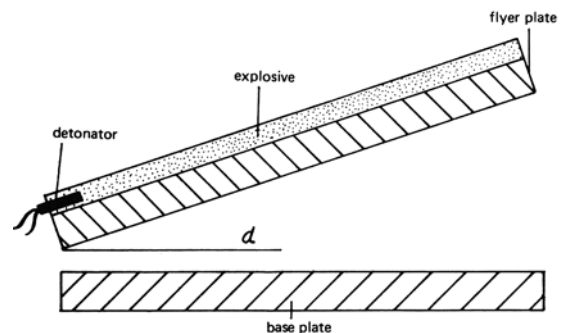


Fig. 1

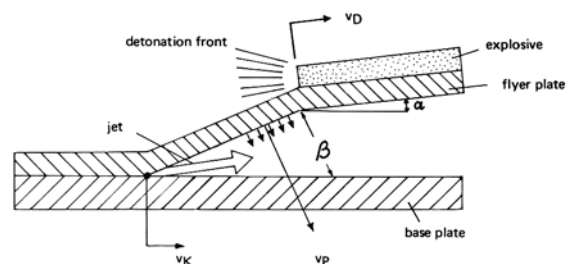


Fig. 2

*Arbeitsgruppe für Hochenergie-Bearbeitung, 7341 Amstetten, Germany.

The flyer plate is accelerated by the explosive to the velocity v_p . The collision point K travels with the velocity v_K . The following relations exist, as can be seen from Fig. 2

$$\frac{v_p}{v_D} = \sin(\beta - \alpha)$$

where v_D = velocity of detonation front, and

$$v_K = \frac{v_p}{\sin \beta}$$

In order to obtain an explosive weld, the plate's velocity v_p should exceed a minimal value. This requires either a large amount of explosive or a relatively small amount of an explosive with a high detonation velocity. In an arrangement of the plates with zero inclination ($\alpha = 0^\circ$), the detonation velocity should not be greater than 100–120% of the bulk sound velocity³ of either one of the two metals to be explosively bonded.

The weld to be examined consisted of an unalloyed steel St 37, 5 mm thick, and an aluminium alloy AlZnMg 1.25 mm thick. The steel plate was chosen as the flyer plate, as being the more ductile plate. The detonation velocity of the explosive was $v_D = 3900$ m/s. The ratio of mass of explosive to mass of flyer plate was 0.44, the inclination angle was $50'$. The velocity of the collision point was measured to be $v_K = 3680$ m/s, the collision angle was $\beta = 7^\circ$ and the plate's velocity was $v_p = 445$ m/s.

METALLURGICAL INVESTIGATIONS

From the centre of the 500×130 mm clad plate, a block of $50 \times 30 \times 30$ mm was cut with one of the removed surfaces parallel to the direction of collision (Fig. 3). After mechanically polishing this surface, the 'work-hardened' surface layers were removed electrolytically. This is important because of the X-ray residual stress measurements, as the surface layer concerned is very thin.

The microhardness $HV_{0.3}$ measured at the cut out area is shown in Fig. 4, plotted against distance from the interphase. An increase in hardness is observed in both materials after shock loading. There seems to exist a minimal hardness both in aluminium and in steel at a distance of about 0.5 mm from the interphase, whereas immediately next to the interphase an increase is observed. The increase is due to the formation of intermediate phases near the weld zone. Fig. 5 shows the bond zone in 100-fold magnification. Near the wavy interphase in iron, severe deformation has occurred. At greater distances from the interphase in iron, mechanical twin-formation is observed. Such twinning is only observed in low-temperature or high-strain-rate deformation.

Microradiographic investigations

To dig deeper, microradiographic investigations were performed as shown in Fig. 6. The upper part is the iron concentration near the bead, the lower part, the electron absorption picture. The iron concentration picture shows that there is no homogeneous distribution of iron in the intermediate phase. The phase is not in equilibrium due to the fact that during explosive cladding there is no, or only little, diffusion.

Therefore, stresses of great magnitude cause the intermediate phase to fracture. The fractures are revealed in the electron absorption picture.

Residual stress investigation

The stresses which lead to fractures in the bond zone of the explosively welded aluminium–steel sample are expected to be active within small areas. The requirements for stress measurement therefore are

1. nondestructive measurement,
2. within small areas.

In this case, the X-ray method is the most capable. The measurements are performed nondestructively within a very small area of 0.3 mm diameter. A primary X-ray beam is incident obliquely on the specimen's surface and is reflected at lattice planes of the crystallites of the polycrystalline specimen, Fig. 7. The basic equation is Bragg's law

$$2D \sin \vartheta = \lambda \quad (1)$$

where D is the lattice spacing, ϑ the Bragg angle, and λ the X-ray wavelength. When D is altered, owing to residual stresses, a change in diffraction angle ϑ is observed. The way the measurements are performed is demonstrated schematically in Fig. 8. The incident X-ray beam P is reflected at lattice planes and is recorded on an X-ray film. At the same time the interference line of a thin layer of a proper reference powder is recorded. The distance between both lines, Δ_1 and Δ_2 , is a measure of the strain in the directions

$$\psi_1 = \psi_0 - \eta \quad (2)$$

and

$$\psi_2 = \psi_0 + \eta$$

with $\eta = 90^\circ - \vartheta$ and ψ_0 the incident angle with respect to the normal of the specimen's surface. The strain in directions ψ_1 and ψ_2 is given by

$$\epsilon_{\psi_1} = c(\Delta_1 - \Delta_0) \quad (3)$$

and

$$\epsilon_{\psi_2} = c(\Delta_2 - \Delta_0)$$

where c is a constant¹¹, and Δ_0 is the distance between the interference line of the reference powder and the specimen. When the exposures are taken in a plane given by the normal and the direction of the stress σ_1 , and assuming a plane stress state with the principal stresses σ_1 and σ_2 to be active in the surface, the lattice strain is given, by linear theory of elasticity, as

$$\epsilon_{\psi} = \frac{\nu + 1}{E} \sigma_1 \sin^2 \psi - \frac{\nu}{E} (\sigma_1 + \sigma_2) \quad (4)$$

where E is Young's modulus and ν Poisson's ratio. When several ϵ_{ψ} values are determined in different ψ -directions and plotted against $\sin^2 \psi$, a linear relationship is obtained (Fig. 9). The slope gives the stress

$$\sigma_1 = \frac{\partial \epsilon_{\psi}}{\partial \sin^2 \psi} \cdot \frac{E}{\nu + 1} \quad (5)$$

The intersection $\epsilon_{\psi=0}$ with the ordinate gives the sum of the principal stresses

$$\sigma_1 + \sigma_2 = -\frac{E}{\nu} \cdot \epsilon_\psi = 0 \quad (6)$$

Measurements were performed on the sample (Fig. 3) in order to investigate the stresses σ_1 and σ_2 as a function of distance from the interphase of the explosively welded specimen. The radiation used was Co-K α . The (420)-lattice planes of aluminium, and the (310)-lattice planes of ferrite were measured. By this method, no corrections due to possible alternations of the elastic properties^{12,13} of the material are necessary. Back reflection exposures obtained at a point 1 mm away from the interphase in steel and Al-alloy are shown in Fig. 10. The outer doublet is the reference powder's, the inner doublet the specimen's interference. The broadening of the interference line of Al indicates a work hardening which has occurred in the Al-alloy during shock loading.

Typical lattice strain distributions obtained in steel near the interphase are demonstrated in Fig. 11. The slopes define a stress in the longitudinal direction (parallel to the interphase) of $\sigma_1 = -20 \text{ kg/mm}^2$, and in transverse direction (perpendicular to the interphase) of $\sigma_2 = -9 \text{ kg/mm}^2$. In good agreement with the single determinations, the sum of the principal stresses obtained from the intersection with the ordinate is $\sigma_1 + \sigma_2 = -29 \text{ kg/mm}^2$.

In Figs. 12 and 13 the plot of the stress σ_1 acting parallel and the stress σ_2 acting perpendicular to the interphase is given as a function of distance from the interphase. The stresses near the interphase are compressive.

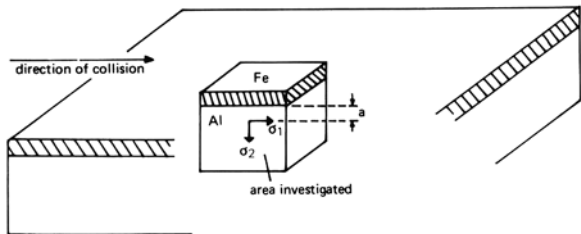


Fig. 3

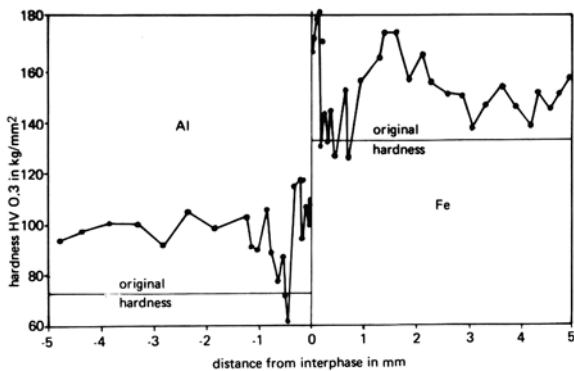


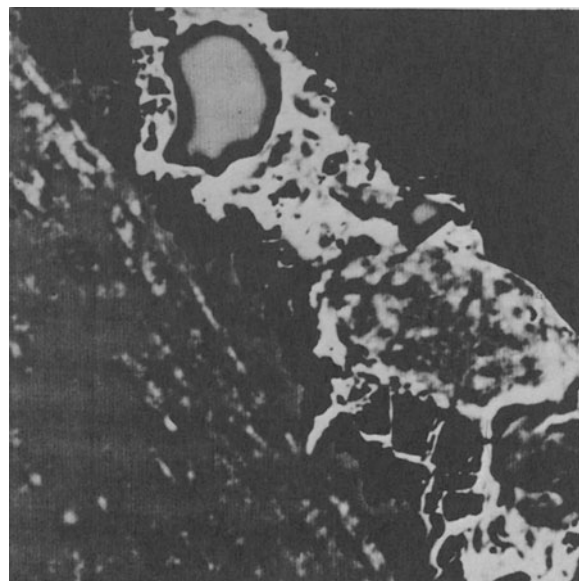
Fig. 4



Fig. 5 Bond zone of the explosive steel-aluminium alloy-clad, 100 x.



a) Fe-concentration picture.



b) Electron absorption picture.

Fig. 6 Microradiographic investigation of the weld, 600 x.

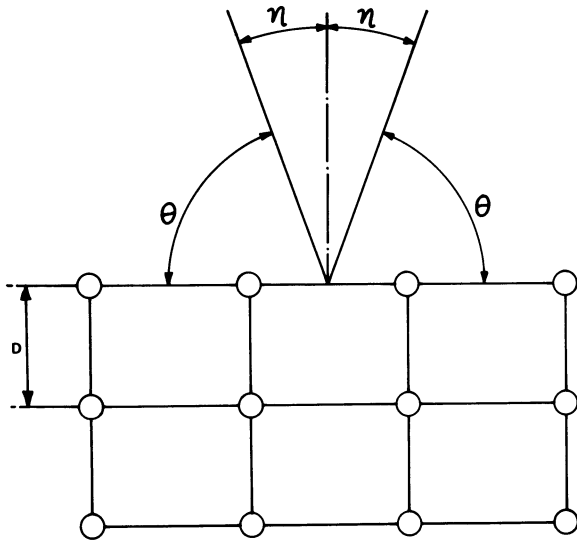
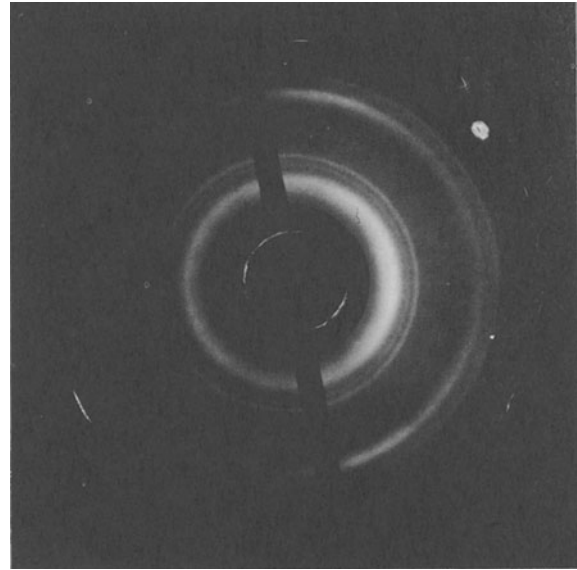


Fig. 7



a) Al-alloy, (420) plane

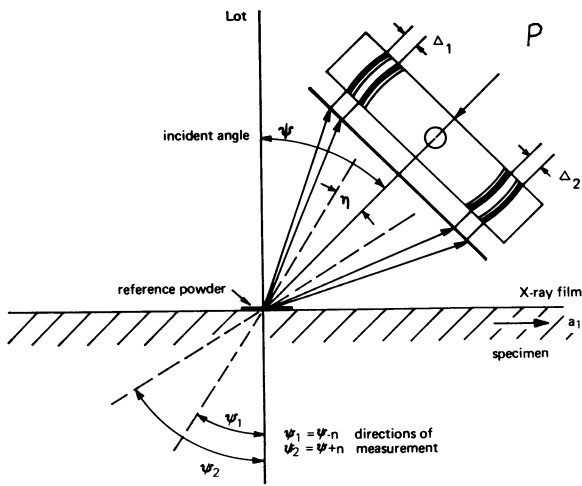
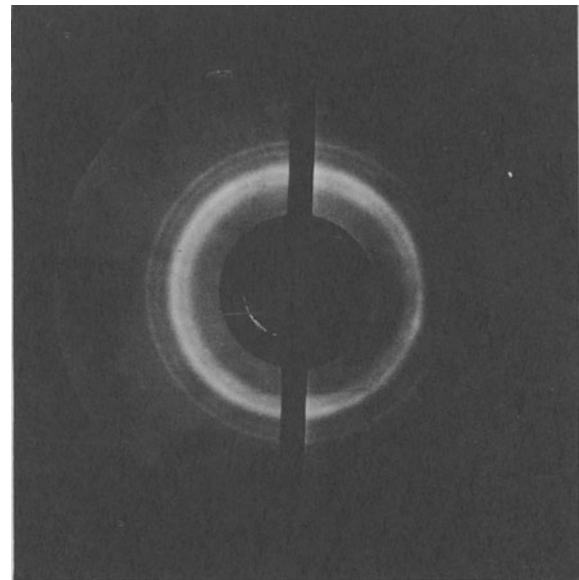


Fig. 8



b) Steel, (310) ferrite plane

Fig. 10 Typical back reflection patterns for X-ray stress measurement, Cobalt-K α -radiation.

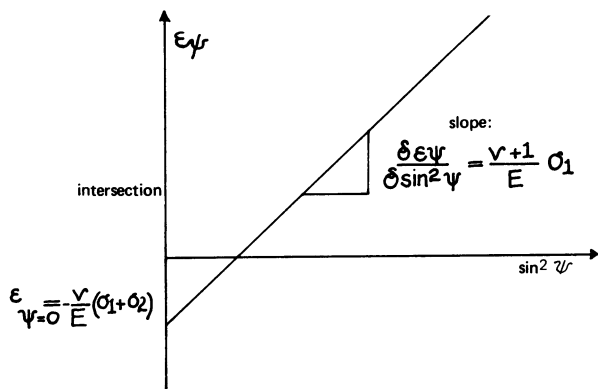


Fig. 9

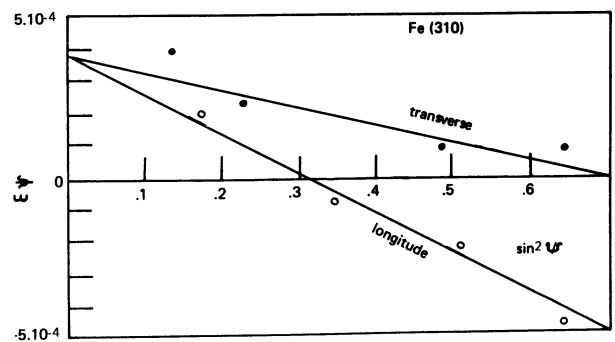


Fig. 11

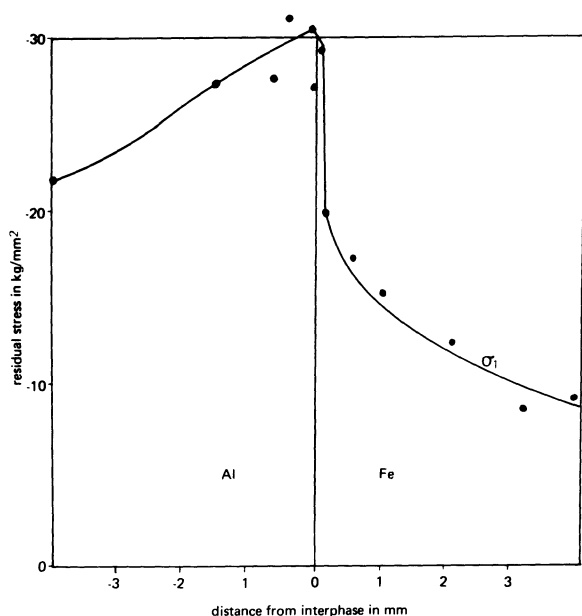


Fig. 12

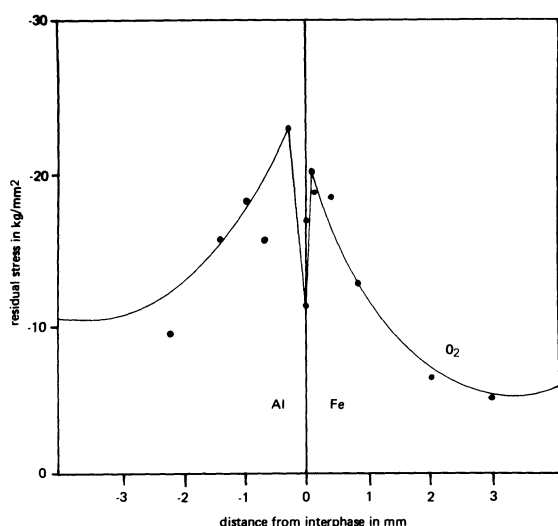


Fig. 13

DISCUSSION OF RESULTS

The most surprising fact is the magnitude of residual stresses observed near the interphase of explosively welded aluminium-steel. These are in the order of the yield strength of the materials. There is no doubt that strength is influenced by these stresses. In fact the strength of the clad product was low.

The longitudinal stress σ_1 shows a discontinuity at the interphase, the transverse does not. This agrees with the requirement of compatibility. The jump of the longitudinal stresses at the interphase should be in the ratio of Young's modulus for the two materials. For steel and aluminium this is 1:3. The observed ratio is 1:2. The deviation can be explained by the method of measurement. Due to a steep stress

gradient near the interphase, the irradiated area, 0.5 mm in diameter, is still too great for resolution.

Usually in fusion welding tensile stresses are expected in the bead of the weld. This is confirmed experimentally when the heat input during welding is constant with respect to the specimen's thickness^{13,15}. The fact that compressive stresses are observed in the explosive weld shows that quite different processes are acting, although there exists evidence for molten zones in the interphase and a jet of liquid metal. The very high pressure during impact and the reflected tensile shock waves are the main parameters determining the residual stress state.

Therefore, further experiments taking account of collision-point velocity and the plate's velocity during explosive welding on the residual stress state, and herewith on the strength of the clad product, have to be performed.

REFERENCES

- CROSSLAND, B., and WILLIAMS, J. D., 'Explosive Welding', *Metallurgical Reviews*, **15** (1970), p. 79.
- CROSSLAND, B., and BAHRANI, A. S., 'A Review of Explosive Welding Research', Int. Conf. Center for High Energy Forming, Denver, Colorado 1967.
- HOLTZMANN, A. H., and COWAN, G. R., 'Bonding of Metals with Explosives', Welding Research Council, **104** (1965), p. 1.
- KELLER, K., 'Beiträge zum Explosivplattieren', *Z. Metallkunde*, **59** (1968).
- KLEIN, W., 'Verbundmechanismus beim Explosionsschweißen', *Schweißen und Schmieden*, **19** (1967) p. 1.
- COWAN, G. R., and HOLTZMANN, A. H., 'Flow Configurations in Colliding Plates: Explosive Bonding', *J. Appl. Phys.*, **34** (1963), p. 928.
- HUNT, J. N., 'Wave Formation in Explosive Welding', *Phil. Mag.*, **17** (1968) p. 669.
- BURKHARDT, A., HORNBOGEN, E., and KELLER, K., 'Übergang zu turbulentem Fließen in Kristallen', *Z. Metallkunde*, **58** (1967), p. 410.
- VERBRAAK, C. A., *C.I.R.P. Annalen*, **11**, No. 3 (1962/63).
- FAIRLIE, J., 'Explosive welding and forming open another door for industry', *Weld. Engineer*, **44** (1959), p. 61.
- MACHERAUCH, E., and MULLER, P., 'Das $\text{Sin}^2\psi$ Verfahren der röntgenographischen Spannungsmessung', *Z. angew. Physik*, **13** (1961), p. 305.
- PRÜMMER, R., and MACHERAUCH, E., 'Recent Developments in X-Ray Stress Analysis', III. Int. Conf. Exp. Stress Anal., 1966 Berlin, *VDI-Berichte*, **102** 1966, p. 48.
- PRÜMMER, R., 'Basic Principles and Applications of X-Ray Analysis of Residual Stresses', *Kerntechnik*, **13** (1971), p. 68.
- TALL, L., 'Residual Stresses in Welded Plates—A Theoretical Study', *Welding Journal*, **43**, Res. Suppl. (1964), 10–s.
- PRÜMMER, R., 'Residual Stresses due to Electron Beam Butt Welding of a 0.32% Plain Carbon Steel', *J. Soc. Mat. Sci., Japan*, **17** (1967), p. 1066; *DVS-Berichte*, **5** (1969), Strahltechnik III, p. 63.

DISCUSSION

Query from Prof. Loewy, Technical Institute, Haifa

How is the bondage influenced by contamination by oxides or oily layers?

Could these layers be pressed out in spite of the high speed of welding?

Or, should the platen be mechanically or chemically cleaned (sand blasted)?

Reply

This question is very important for the practical application of the explosive welding process. At first, one would guess that very clean surfaces are necessary during collision, but there exists experimental and theoretical evidence for the formation of a jet of liquid metal. This jet is ejected from the surfaces involved in collision, so that oxides and oily layers are swept away and a metal-to-metal bond can be achieved. However, as the mass of the jet is proportional to the masses of the colliding plates, problems could arise if these plates were very thin. The jet could then be too weak to produce this surface cleaning process. Therefore, in order to be sure, the surfaces in our research are cleaned by grinding.

Query from S. Shina

(1) Regarding Figs. 12 and 13, I wonder why integrations of each residual stress tend to zero.

(2) If at the outer surfaces residual stresses are tensile, it seems to me more important to examine the tensile residual stresses, rather than compressive ones, so far as the fracture of sheet metals is concerned.

Reply

(1) In this investigation the most important region was the one near the interphase, as the most severe metallurgical changes occur there. Of course, due to the requirement of balance of forces, tensile stresses should occur at a greater distance from the interphase.

(2) This is right, as tensile stresses have a bad influence on fatigue behaviour, whereas compressive stresses improve fatigue behaviour, when materials of similar microstructure are considered.

FORMING FORCE REQUIRED FOR TUBE-FORMING

by

Y. TOZAWA* and K. KAWADA†

SUMMARY

In the tube-forming process chosen as the subject of this study, a U-formed blank is formed into the tube by a semi-cylindrical punch and die without mandrel. The deformation process of each portion of the U-formed blank and the shape of formed tube are investigated experimentally, and the diameter of U-forming punch, to minimize the deviation of the shape of formed tube from a circle, is found. The deviation from a circle decreases with an increase of the applied force, and the suitable force for tube-forming with close tolerances is obtained theoretically after consideration of the deformation process. The force required for tube-forming without regard to tolerances is lower than this.

INTRODUCTION

There are various processes in the forming of cylindrical parts from sheet metal, and also various types of operations and tools used in the press-forming process. The tube-forming process discussed in this paper is that of a flat blank which is first bent into a U-shape by cylindrical punch; the U-formed blank is then formed into circular shape by a semi-cylindrical punch and die without mandrel. This process is widely used in the forming of small diameter rings and even in the forming of large ones for pipes.

The expression for estimating the force required for U-bending has already been presented by the authors¹ and is comparatively small. However, there are very few reports on the force required for tube-forming, which is comparatively large. In this paper, the force required for tube-forming with close tolerance is examined experimentally and theoretically.

EXPERIMENTAL

A testing machine was used for forming in the experiment. Under the condition of air bending, flat blanks were first bent into a 180° U-shape by cylindrical punches having diameters, d , of 22, 28, 33 and 38 mm, and the U-formed blank was formed to the tube without mandrel by a semi-cylindrical punch and die having a diameter, D , of 40 mm.

Before forming, points were marked on the side of the blank. Several photographs were taken during forming, as shown in Fig. 1. The curvature of each portion of the blank was measured from the shape of

blank recorded photographically at each stage. The process of deformation of each portion was revealed by the result.

Fig. 2 shows the distribution of curvature at several stages during forming. Each portion of the blank is at first bent into a large curvature; a certain portion is then partly unbent into a curvature smaller than that of the tool and finally formed in the shape of the tool. Thus, the process of deformation in each portion of blank varies considerably with the diameter of the U-forming punch, the diameter of which consequently also affects the shape of formed tube.

The diameters of formed tubes were measured as a , b , and c as in Fig. 3, in addition to the measurement of the gap z in the touching part. Fig. 4 shows the effect of the diameter of the U-forming punch on the shape of formed tube. If the diameter of U-forming punch d is small, the diameter of tube a is greater than b ($a > b$), and in the case of large d , a is less than b ($a < b$) in addition to causing the gap z in the touching part, and if that is suitable, a becomes equal to b ($a = b$). These relations are affected by the applied force in tube-forming as shown in Fig. 4.

When the blank is formed, the U-forming punch being of suitable diameter, the greater the force of tube-forming becomes, the closer to a circle the shape of tube becomes. Fig. 5 shows one example of the changes of tube diameters a , b and c with the applied force. If the applied force is small, a and c are greater than the tool diameter, and in contrast to this, b is less than the tool diameter. The difference in the values of a and c is caused by the existence of straight

*Department of Iron and Steel Engineering, Nagoya University, Nagoya 464, Japan.

†Department of Mechanical Engineering, Chiba University, Chiba 280, Japan.

parts near the touching part. When a certain force is applied in tube-forming, c becomes nearly equal to a , namely, the straight parts disappear. Therefore such a force is considered to be the force required for tube-forming without regard to tolerances. And the difference between a , or c , and b decreases with an increase of the applied force and the shape of formed tube is nearly circular.

The change in the shape of tube by increasing the forming force is found directly from the profiles as shown in Fig. 6. In (i) of the figure, straight parts near the touching part are visible; in (ii) the straight part disappears, but the diameter in the vertical direction, through the touching part, is longer than that in the horizontal direction; (iii) is nearly circular. These profiles correspond to (i), (ii) and (iii) in Fig. 5, respectively.

Finally, the force suitable for forming the close tolerance tube is found experimentally according to the measured values of the diameters of the formed tube. The results are shown in Table 1.

Table 1 Forming stress required for tube-forming

Material	t mm	F kg/mm ²	n	σ_{me} kg/mm ²	
				Experimental	Calculated
C-steel A	0.8	50.0	0.20	26	23.3
" B	0.8	82.0	0.22	44	43.6
" B	1.2	82.0	0.22	46	47.5
" C	0.8	96.0	0.21	56	52.9
Aluminium	0.8	19.1	0.04	18	19.0
Copper	0.8	32.7	0.04	33	32.3

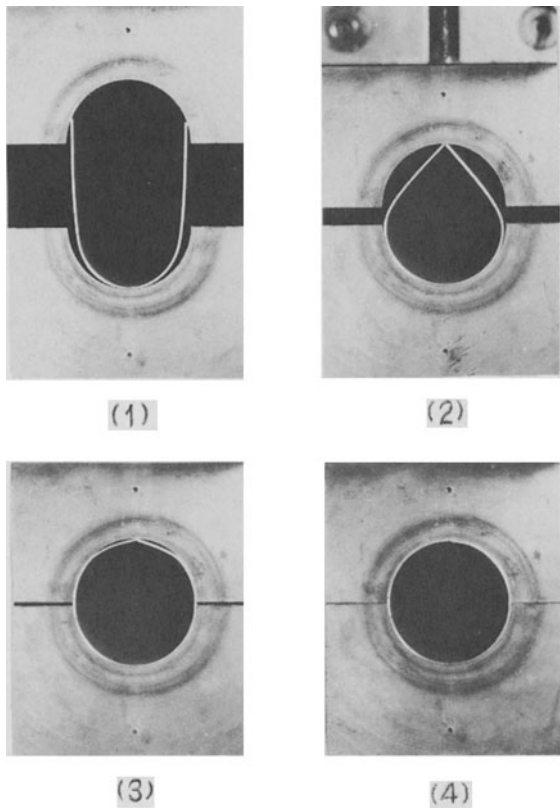


Fig. 1 Shapes of the blank during tube-forming: (1) initial stage; (2) and (3) under forming; (4) final stage.

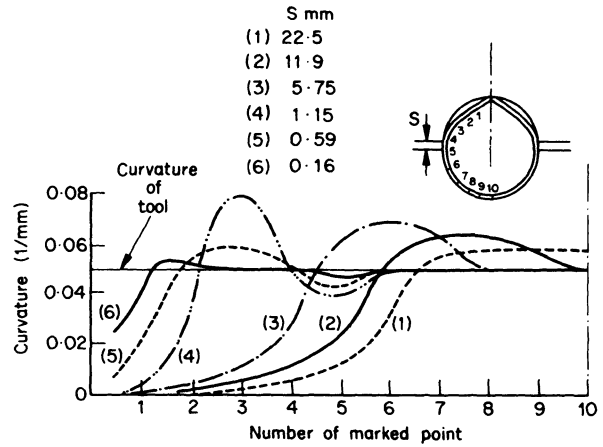


Fig. 2 Distribution of the curvature during forming.

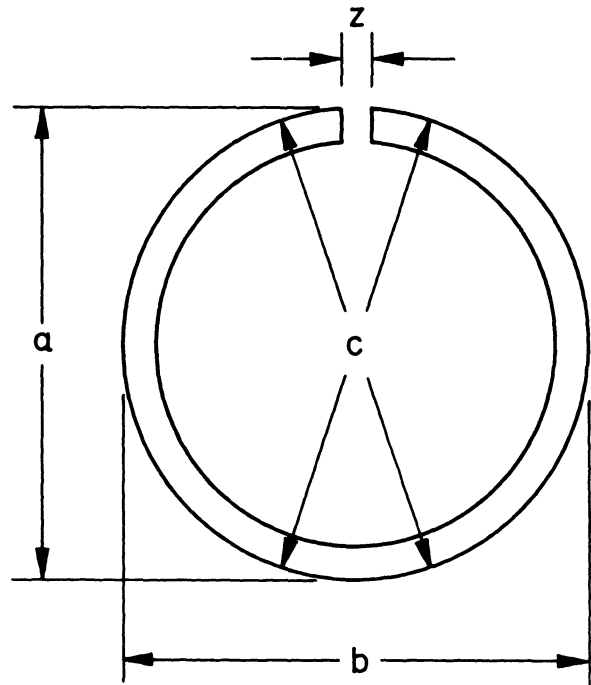


Fig. 3 Measurement of the diameters of the formed tube and gap in the touching part.

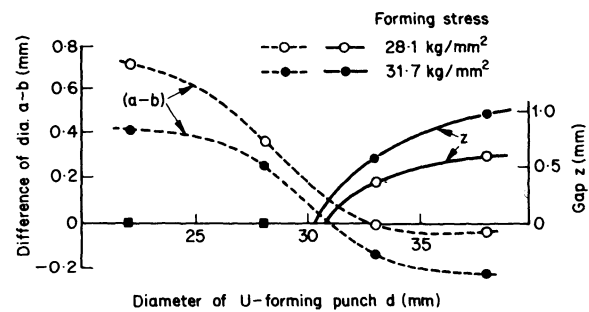


Fig. 4 Effect of the U-forming punch on the shape of the formed tube.

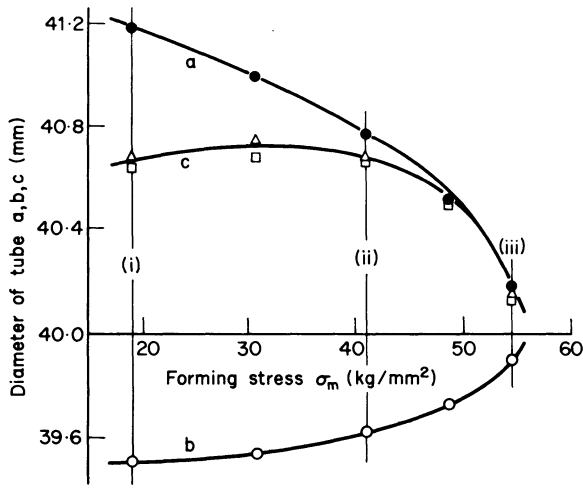


Fig. 5 Changes of diameters with applied force.

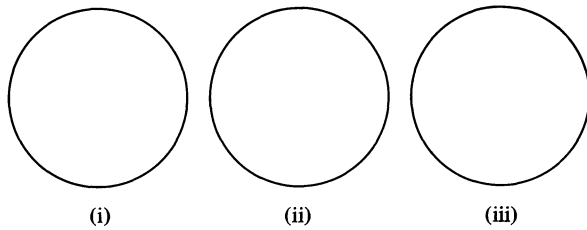


Fig. 6 Profiles of the formed tube.

THEORETICAL STUDY FOR FORCE REQUIRED

The analysis has been made by one of the authors² for the case in which a sheet is bent and then stretched in the circumferential direction of the bend. As a result of the analysis, the magnitude of suitable stretching stress for reducing the amount of springback has been expressed by the following formula

$$\sigma_{me} = \frac{F}{1+n} \left(\frac{2}{\sqrt{3}} \right)^{1+n} \kappa^n \quad (1)$$

where F and n are arbitrary constants when the stress-strain curve obtained by tensile test is represented by

$$\sigma = F \epsilon^n$$

and κ is the relative curvature defined by

$$\kappa = \frac{t}{2\rho}$$

where t is the thickness of sheet and ρ is the radius of curvature of the central plane of the bent sheet. Even in the case of compression after bending, which has been examined by the same person³, when the mean compressive stress is taken in place of the stretching stress, one attains the same result as in equation (1).

If a flat blank is bent monotonically from zero curvature to κ , when the compressive stress applied to the bent sheet attains σ_{me} , calculated from

equation (1), the springback becomes very small and thereafter shows the least change. However in the case of tube-forming, a blank is compressed after bending and unbending as mentioned above, so the deformation process of the blank should be taken into consideration in order to apply equation (1).

In unbending, a material deforms in the opposite direction to that of pre-straining, and the behaviour of the deformation in the opposite direction in the material may be different from the initial behaviour because of the workhardening and the Bauschinger effect. These phenomena are examined in the following experiments.

Specimens were bent through an angle θ_0 over the tools of different radii R and, after unloading, the springback angle $\Delta\theta_0$ was measured. Subsequently, the bent specimens were unbent, and the springback angle $\Delta\theta_1$ was measured after unloading. On the other hand, when a specimen is bent monotonically to relative curvature κ , the change of relative curvature by springback is calculated by the following formula

$$\Delta\kappa = \frac{3F}{E(2+n)} \left(\frac{2}{\sqrt{3}} \right)^{n-1} \kappa^n \quad (2)$$

In order to apply equation (2) to the calculation of the springback of the unbent specimen, the effective relative curvature κ_a , which is to be taken in place of κ , was examined under two assumptions. They are that (a) the material has no Bauschinger effect and workhardens with the increase of the sum of strain increment taken along the strain path, and (b) the material workhardens with increase of the subsequent strain without regard to the pre-strain. These assumed behaviours are plotted as a stress-strain curve in Fig. 7. If a specimen is bent to relative curvature κ_0 and unbent to zero, the effective relative curvature $\kappa_a = 2\kappa_0$ in case (a), and $\kappa_a = \kappa_0$ in case (b). In the case of the unbent specimen, when κ_a is taken in place of κ , the change of relative curvature $\Delta\kappa_a$ can be calculated according to equation (2). In Fig. 7, the results of calculation together with those of experiment are shown. It is clear from the figure that the experimental values $\Delta\theta_1/\theta_0$ are greater than $\Delta\theta_0/\theta_0$, and are also closer to the calculated curve of (a) than that of (b).

The deformation behaviour of the pre-strained material is examined by yet another experiment. Specimens were bent over the tools and after unbending were stretched; the springback angle $\Delta\theta_1$ was then measured. The relation between the stretching stress σ_m and $\Delta\theta_1$ is shown in Fig. 8. In the figure the values of σ_{me} calculated from equation (1), where κ_a is taken in place of κ , are also indicated on the abscissa, in which (a) and (b) represent the assumptions used which correspond to those mentioned, and (1) to (4) represent the diameters of the tools. From the figure it is found that the calculated values of σ_{me} under assumption (a) are in better agreement than those in the experiment. Based on the results obtained in the way described, the relative curvature summed up along the process of deformation is used for the effective relative curvature κ_a .

In tube-forming, the process of deformation differs in each portion of the blank as shown in Fig. 2

and therefore κ_a also varies. However, only the maximum value of κ_a becomes a reference standard in deciding on the force required for the reduction of springback for all parts of the blank. The maximum value of κ_a varies with the diameter of the U-forming punch, but if it is assumed that during forming any portion of the blank is bent to double the curvature of tube to be formed, one may obtain $\kappa_a = 3t/(D-t)$. Therefore, by substituting into equation (1),

$$\sigma_{me} = \frac{F}{1+n} \left(\frac{2}{\sqrt{3}} \right)^{1+n} \left(\frac{3t}{D-t} \right)^n \quad (3)$$

and the forming force required for tube-forming is

$$P_e = 2lt \frac{F}{1+n} \left(\frac{2}{\sqrt{3}} \right)^{1+n} \left(\frac{3t}{D-t} \right)^n \quad (4)$$

where l is the length of the tube.

The values of σ_{me} calculated from equation (3) together with that obtained by experiment are shown in Table 1. From the results it may be concluded that the suitable force for tube-forming with close tolerances can be calculated from equation (4).

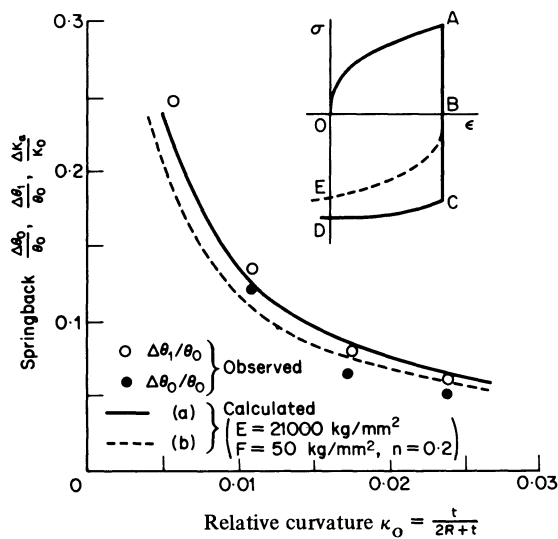


Fig. 7 Springback after bending and unbending.

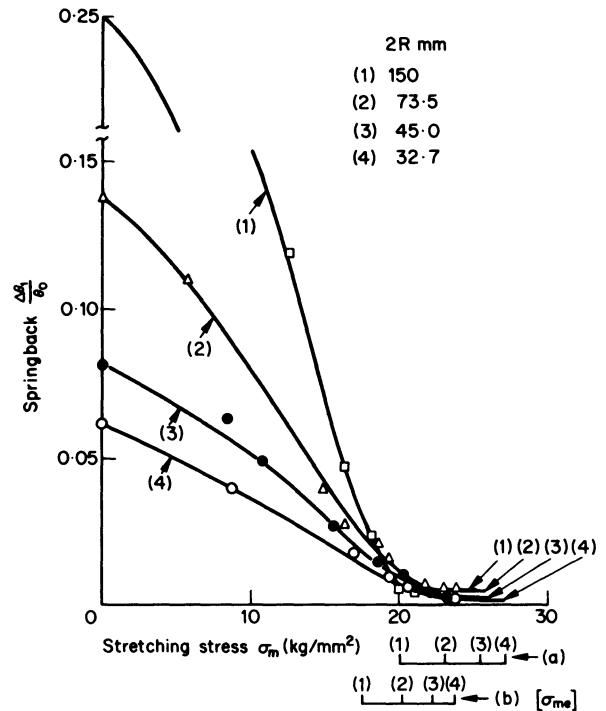


Fig. 8 Suitable stretching stress for reducing the springback.

CONCLUSION

In the forming process in which a U-formed blank is formed into a tube by semi-cylindrical punch and die without mandrel, the force required for tube-forming without regard to tolerance is comparatively small. In order to get a tube with close tolerance, the U-formed blank should be formed by an optimum diameter punch and a fairly large force needs to be applied for tube-forming. The suitable force for tube-forming with close tolerances can be calculated from the formula presented in this paper.

REFERENCES

1. BABA, A., TOZAWA, Y., and KAWADA, K., Research Reports of Faculty of Engineering Chiba University, 13 (1962), 23, p. 33, p. 39.
2. TOZAWA, Y., Proc. of 7th Japan National Congress for Applied Mechanics, 1957, p. 49.
3. TOZAWA, Y., Research Reports of Faculty of Engineering Chiba University, 14 (1963) 26, p. 1.

A STUDY OF THE STRAIN HISTORIES AND DRAWING-IN IN A PRESSED STEEL SHELL

by

R. A. ETHERIDGE* and F. J. MORBEY†

SUMMARY

The control of metal flow in sheet metal forming is generally aimed at avoiding strain concentrations leading to fracture and those compressive strains which lead to puckering. Flow can be controlled by different means, such as draw beads, shape and size of blank, holes, shape of die, and so on. In practice, the details of the flow are usually unknown to the engineer; he sees only the final result, and that only in terms of the presence or absence of puckers.

For sheet metal to be deformed into a particular shape, it must have formability, but the determination of this quality is not an easy task. A particular metal may form excellently for one pressing, and fail when used for another of a different shape. The pressing considered in this investigation had proved difficult to produce, due to fracture at a critical section and the presence of excessive puckering. The history of the strains occurring in the critical section was obtained from measurements of deformed grids on progressively formed shells and the data recorded in triangular co-ordinates, thus enabling strain histories and the mode of deformation of particular elements to be observed.

Measurement of drawing-in were made from tracings of the periphery of the formed pressings and plotted against the punch penetration, so that the rate and amount of drawing-in during forming could be shown. The influence of drawing-in is discussed. Finally deformation rotation of the elements was observed from the deformed grid, and its influence on the results discussed.

INTRODUCTION

Pressed components may be produced in several different ways and in an almost infinite range of forms, varying from simple axisymmetric shells to those of intricate and asymmetric form. Most pressed shells used in the construction of motor vehicle bodies are of the latter type and consequently it is difficult to predict the behaviour of any given pressing from available test data or procedures. In fact it is perfectly possible to have a situation whereby a particular material will form readily for one pressing and yet fail when used for one of a different shape, even though the forming quality suggested by sheet metal tests was good (there are twenty such tests listed by Shawki¹).

A further problem is created by the type of process used, owing to the fact that in indentation processes (that is, pure stretch forming) the mechanical properties of the material are critical to the stability of the process, whereas in a drawing operation the control of drawing-in is the factor that most predominantly governs pressing quality. Consequently, the

type of process, material choice and blank geometry are usually based on experience and the particular solution is based on arbitrary judgements. There is little recourse to experimental technique, and if a pressing fails to draw, or tears, the blank shape or control parameters are changed according to empirical rules based on the previous experience of the tool designer. It is also perfectly possible for a component to fail under production conditions even though the same pressing was capable of being drawn in the try-out shop. In these circumstances it is usual to further modify the process empirically to suit the production machine.

It is advantageous, therefore, to have a knowledge of the strain distribution over the surface of a production pressing drawn under known conditions, so that the possibility of fracture can be minimized or eliminated. Some work has already been carried out on such analysis by Keeler² and Goodwin³ and the former carried out laboratory tests on pressings under controlled conditions and compared the results with those for production automotive pressings in order to construct a formability curve. He claimed that the

*Lecturer in the Department of Production Engineering, University of Aston in Birmingham.

†Production Engineer, Pressed Steel-Fisher Division, British Leyland Motor Corporation.

strains measured from the surface of production pressings could be directly related to the controlled experimental results and conclusions drawn about how near to fracture were such production shells.

This paper is concerned with a pressing which was difficult to draw and was near to the fracture limit at a critical section of the component. The experiments described were carried out on the production press and the surface strains measured from a grid etched in the surface. The methods of analysis differed from those developed by Keeler.

STATEMENT OF THE PROBLEM

The pressing used for the investigation is shown in Fig. 1 and is readily seen to be asymmetric with

complex geometry. Wrinkling due to convergent drawing-in is also present. The original tooling layout for the pressing called for a blank of trapezoidal form using an extra deep drawing quality steel C.R.2 (see Appendix). This blank form failed to draw and the resulting failure at the critical section can be seen in Fig. 2.

A change in material to a stabilized extra deep drawing quality steel C.R.1 (Appendix 1) also produced tearing at the critical section and a successful pressing was not obtained until large cut-outs were made in the blank, near to the critical sections. The modified area can be seen on the drawn shell, (Fig. 1). It was decided at this stage to investigate the strain distribution in the critical zone and to determine the extent and effect of the drawing-in.

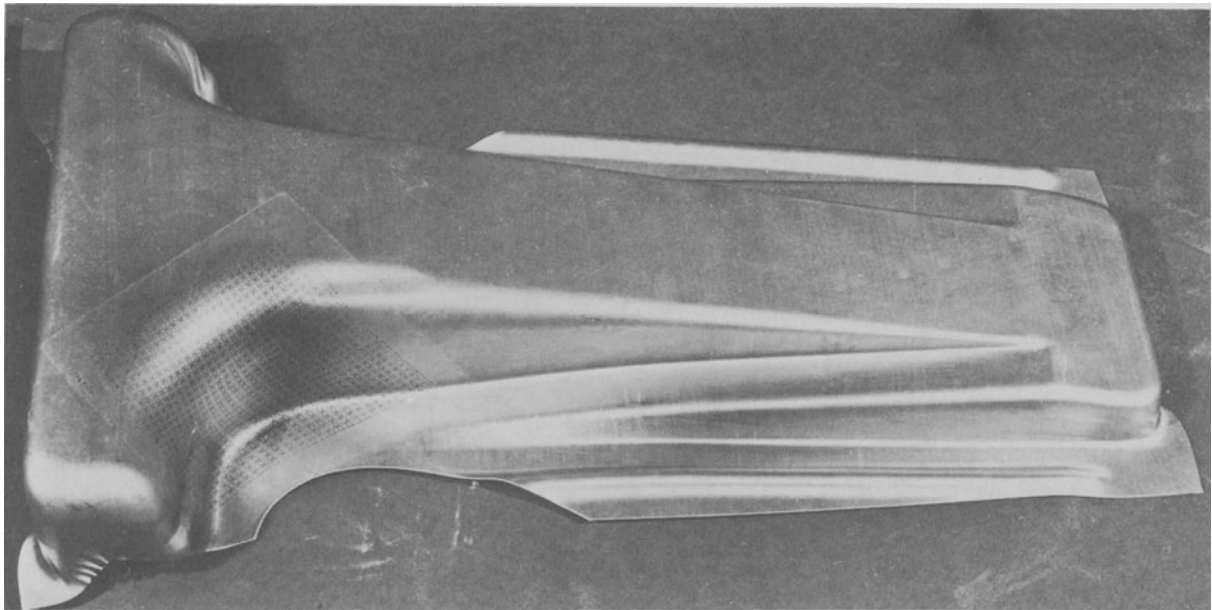


Fig. 1 Photograph of shell.

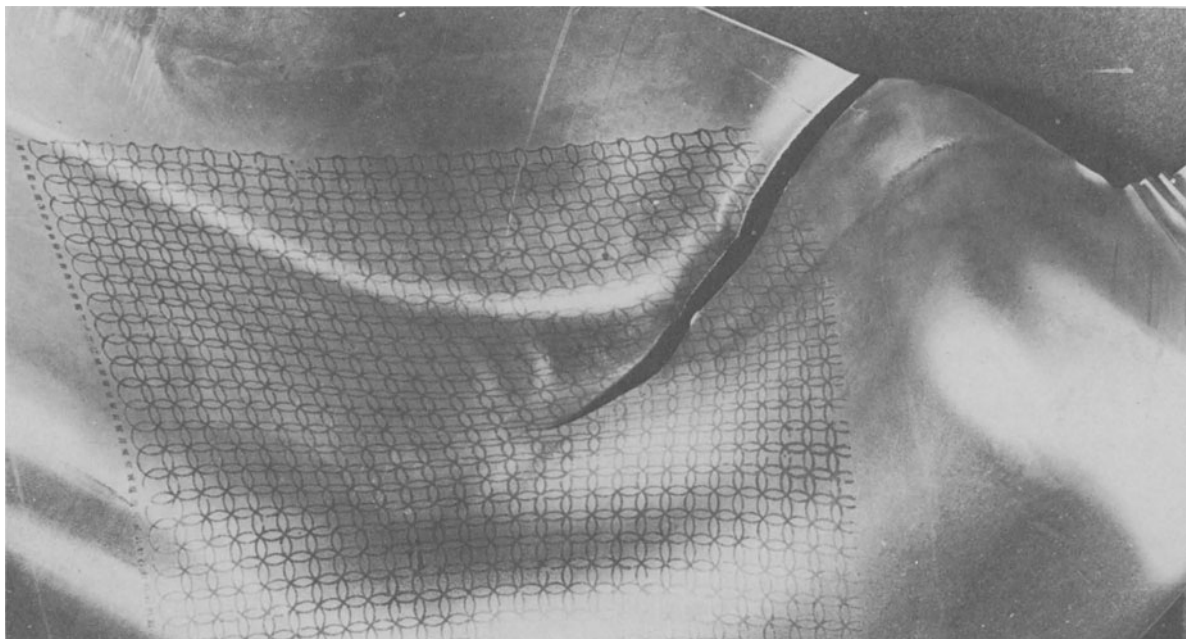


Fig. 2 Photograph of split shell.

EXPERIMENTAL TECHNIQUES

The experimental procedures used fall into four main areas:

- (a) preparation of the blanks,
- (b) forming,
- (c) strain measurement,
- (d) measurement of drawing-in.

(a) Preparation of the blanks

Blanks of stabilized extra deep drawing quality steel were drawn from normal production stock and cleaned well using 'Genklene'. Twenty-two blanks were prepared altogether, thirteen of which had cut-outs near to the critical area and nine had no cut-outs. In order to examine the surface strains, a grid of intersecting circles (Fig. 3) was etched onto each specimen in the critical area. The choice of grid was largely dictated by availability and although a discussion of the advantages of various grid patterns is outside the scope of this paper, it would have been more advantageous in this case to have used a square grid of chequer-board pattern. However, the circular grid made measurement of the principal strains easy, since these were obtained by measuring the major and minor axes of the resulting ellipse after straining (Fig. 3). Measuring the co-ordinates of the parallelograms formed by the intersections of this grid for the investigation of rotation was infinitely more tedious.

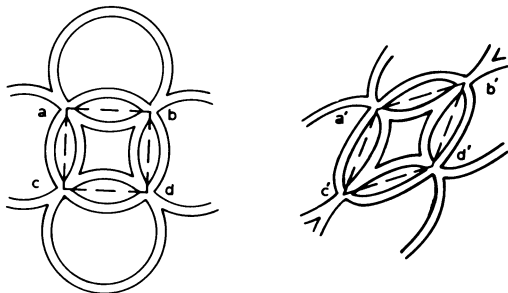


Fig. 3 Undeformed and deformed grid patterns.

The electrolytic technique used has been previously described by Bowers and Brookes⁴ and Pearce and Drinkwater⁵, but it is briefly described again. The blanks were marked with location lines in order that the stencil could be placed in exactly the same orientation on each blank and the surface sprayed with Electrolyte K.130. The marking unit, comprising stencil, absorbent pad and stainless steel electrode was then placed over the area in the correct relationship and a low a.c. voltage applied to the electrode for about four seconds. The stencil was made from an insulating material and treated so that current could only flow where required, and consequently on the positive half-cycle ferrous ions would leave the metal surface and react with the electrolyte. New ions thus formed would be deposited on the surface during the negative cycle and thus produce a black mark on the metal in those areas in contact with the treated sections of the stencil. After removal of the electrode and stencil the work area covered by the grid was treated with a neutralizing agent (Neutralite N.4) and then lightly sprayed with oil to prevent rusting.

(b) Forming

The shells were formed in stages in order to investigate the strain history from the flat sheet to a fully formed shell. A clearing DF.2475-84 double-action hydraulic press with air cushions was used for the tests, and punch penetrations at each stage are shown in Table 1. These were obtained by retracting the ram of the production press to set positions and then allowing it to move through its entire stroke at normal speed, since it was impossible to operate on full stroke and stop the press at given intervals. Seven stages were obtained by this method; from a shallow partial form up to a fully formed shell. No lubricants were used throughout the forming operation.

Table 1

Ref.	No. of pressings	Punch penetration (in)
Blank with cut-outs		
A1	3	0.47
A2	1	0.77
A3	1	1.62
A4	3	1.99
A5	1	2.33
A6	1	2.75
A7 (fully formed)	3	3.40
Blank with no cut-outs		
B1	3	0.47
B4	3	1.99
B7 (fully formed)	3	3.40

(c) Strain measurement

The steep gradients and rapidly changing curvatures in the critical section ruled out conventional strain measuring techniques using microscopes, due to problems of orientating the optical axis normal to the particular planes considered. It was necessary, therefore, to consider alternative methods, of which the replica technique described here was the most successful.

The section of grid to be examined was deposited with a thin carbon film by means of a candle flame and the surplus lightly dusted off with a cotton wool swab, thus leaving a light trace attached to the etched surface of the grid. A piece of 'Sellotape' was then firmly pressed onto the area under examination, care being taken to minimize stretching of the tape. The tape was then removed, thus retaining an image of the grid on the adhesive face; the image was preserved by pressing the tape firmly onto a piece of stiff paper.

In order to check the accuracy and repeatability of measurement, an undeformed grid was traced off by the method described and measurements of the replica compared with the actual grid on the flat blank. It was found that, for the circle size of 0.236 in used in the investigation, a change in length of 0.002 in was present owing to stretching of the tape, giving rise to an error of +1.0% in the natural strain.

Measurements from the 'replicas' were made on a 'Nikon' Model 5A profile projector using a 10 X magnification. Two methods of determination were used: (a) direct measurement of the magnified image using a precision scale; (b) the micrometer scales on the instrument. Repeated readings by the two methods showed an error in measurement of less than 0.002 in, that is, less than 1.0% natural strain. At small strain values it was necessary to use reference circles to determine the major and minor axes of the deformed grid circles.

When measuring the change of shape of the square (described by the points $a b d c$ in Fig. 3) into the parallelogram $a' b' d' c'$, it was found extremely tedious to determine the points of intersection for deformed circles representing the largest strains, again indicating the usefulness of using a square chequer-board for examining rotation effects. Repeated checks were made of these measurements so that accuracy should be of the best possible order.

(d) Measurement of drawing-in

For the pressing considered, the mode of drawing-in was complicated due to the fact that at one end the geometry was shallow and at the other end relatively deep; two draw beads had also been included as an additional control device. It is clear from examining Figs 1 and 2 that little or no drawing-in occurred at some sections, whilst massive divergent drawing-in occurred adjacent to the critical section in order that necking should be avoided. The other feature of this shell was the presence of convergent drawing-in leading to wrinkling in the deepest sections.

In order to measure the drawing-in, a special fixture was made so that the series of incremental pressings could be located relative to a drawing board and paper; a tracing of the outside shape at each penetration was then obtained. The tracings were superimposed one on top of the other to show the progress and rate of drawing-in.

Owing to the fact that the rate of drawing-in varied around the pressing it was necessary to divide the perimeter into a series of zones for the purpose of analysis. These can be seen in Fig. 4 and are further referred to in Fig. 8.

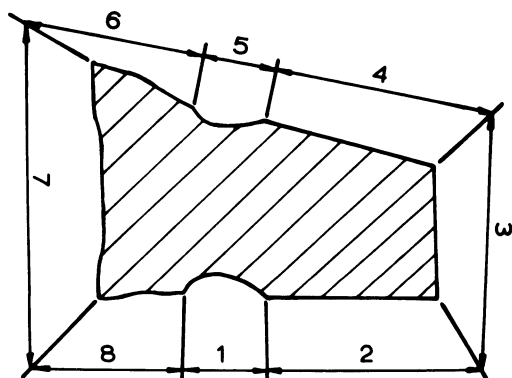


Fig. 4 Allocation of zones for drawing-in.

ANALYSIS OF RESULTS

The results will be discussed under the following headings:

- (a) strains,
- (b) deformation rotation,
- (c) drawing-in.

(a) Analysis of strain distribution

Although the pressings were drawn on a production press with less control than the authors would have preferred, the repeatability of measurements from pressings for the same drawing stage was nevertheless good. It was found convenient to plot the strains in triangular co-ordinates as proposed by Hsü⁶ because the three principal strains can easily be represented in the same plane by this method, and the strain history and strain rate of an element can also be interpreted directly.

Strain measurements were made along the line and normal to the line of the critical section for unsplit specimens, thus determining the critical strains in the region of failure. An estimate of the strain distribution in the area of the split was also made by measuring the strains for a series of elements parallel and adjacent to the split. Strain measurements perpendicular to the split were also made.

The resulting strain histories for elements along the critical section for unsplit specimens are drawn in triangular co-ordinates in Fig. 5 and the reference numbers (AQ 39, etc.) are the grid locations for the element concerned. The full circles show the strains adjacent to the split, measured on the shell drawn from blanks with no cut-out and, therefore, represent an estimate of the fracture strain. The strain path for the element sustaining the greatest strain (AQ 39) lies along a line of characteristic index $\eta = 8$, a line of pure tension, where $\epsilon_2 = \epsilon_t$ (ϵ_t is the through thickness strain). The strain paths for the other elements lie above and below this line and approach characteristic indices of $\eta = 7$ and $\eta = 9$ which are lines of pure shear. (The reader should consult reference 6 for a more-detailed treatment and interpretation of their meaning).

The full lines in Fig. 5 are the strain paths for each element and the dotted lines are the loci of states of strain for the various elements at a constant punch

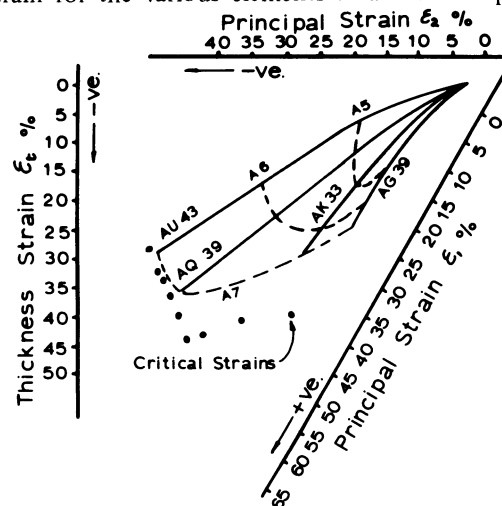


Fig. 5 Strain paths along critical section.

penetration. Clearly the change in intervals between these lines along a given strain path is a measure of the strain rate for the element concerned. Examination of Fig. 5 shows that the strain rate for elements AU 43 and AQ 39 was virtually constant, whilst the strain rate for elements AK 33 and AG 29 decreased for increasing penetration.

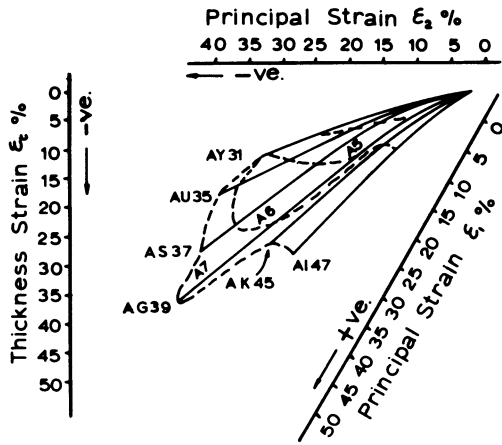


Fig. 6 Strain paths normal to critical section.

Fig. 6 shows the strain histories for elements normal to the critical section (that is, passing across the line where necking is likely to occur and result in failure). The development of the neck can be clearly seen, owing to the fact that any strain path indicates progressive thinning. Element AQ 39 is obviously deforming at a nearly uniform strain rate, whilst adjacent elements show decreasing strain rate; an indication of localized thinning leading ultimately to necking and failure.

The estimated fracture strains obtained from the split pressing show that even for the pressing with cut-outs the maximum finite strains are dangerously near to the critical values. Obviously, better control of drawing-in would give a more uniform distribution of strain and thus give a less localized thinning of the material. More uniform distribution of the strains would permit greater punch penetrations before failure occurs and, in the case of this pressing, probably the use of a cheaper work material and less control over the other factors such as die wear and lubrication.

The most important aspect of these results is the effect of strain history on final strain distribution and the finite strain at the end of forming. Neither Keeler nor Goodwin considered the effects of strain path or strain history in the construction of their formability charts, but simply used the final strain. The results of this investigation show that the strain path has a critical effect on the final strain and that the final strains in given pressings might well vary owing to the control of the process being inadequate. Obviously, pressings which might be critical according to final strain might well be non-critical if the strain history could be better controlled, as was the case here considered.

Finally, observation of the estimated fracture strains (full circles in Fig. 5) do not show a continuous envelope and consequently led the authors to believe that the strain paths might not be coaxial and that deformation rotation of the elements was present. This is examined in the next section.

(b) Deformation rotation

In order to test whether deformation rotation was present it was necessary to measure the deformation of an initially square element into a parallelogram and at the same time devise some mathematical test to determine rotation from the geometry of the deformed element.

Hsu⁷ has shown that when deforming a square containing an inscribed circle into a parallelogram containing an ellipse, a parameter ϕ will remain constant for coaxial strains but not for non-coaxial strains, that is, ϕ will vary if deformation rotation has occurred. ϕ is defined as the orientation angle to the original Cartesian framework of the deformed ellipse major axis. A variation in the parameter ϕ was observed and Table 2 shows the results obtained.

Table 2

Stage of pressing	Grid ref.	AU 43	AQ 39	AK 31
A7		28°29'	32°15'	35°45'
A6		24°32'	24°45'	34°53'
A5		21°15'	21°41'	28°49'
A4		—	21°23'	22°52'
Total rotation		7°14'	10°52'	12°53'

Great difficulty was experienced in obtaining these results due to the grid used and the measurements were repeated several times for the purpose of accuracy.

The presence of rotation in this pressing can only contribute to failure because energy has to be imparted to the element to produce this effect. In fact for such rotation to occur shearing must take place, which could be brought about by differential drawing-in, a situation inherent in a pressing of this complexity. It is not unlikely, therefore, that such rotations will occur in other production pressings and would obviously be a contributing factor to failure during drawing.

(c) Drawing-in

Owing to the marked degree of asymmetry exhibited by the component it proved necessary to divide the periphery of the drawn shell into zones (Fig. 4). For the blank with cut-outs it was observed that the rate of drawing-in at zones 2, 3 and 4 was very small for small punch penetrations, whilst in zones 1, 5, 6, 7 and 8 a high rate of drawing-in occurred for the same penetrations. This can be seen in Fig. 7. As the shell was reaching full form it can be seen that the rate of draw-in increases in all zones, and in zones 3 and 7 the metal has totally run into the pressing with resultant earing in these vertical sections.

The results for the blank form that produced a split specimen are shown in Fig. 8. It is readily seen that the rate of drawing rapidly increases in all zones at all punch penetrations. This would obviously be expected since the critical section requires extra metal fed in at a high rate, but a restriction is offered by the straight sides of the blank adjacent to the critical section. Since the metal can only move in normal to the periphery at zones 1 and 5 for this blank shape, adjacent sections must move in also. This restriction would obviously be the major contributory factor leading to necking and failure, since it prevents metal moving into the divergent zone of the critical section at a rate which leads to uniform strain distribution.

Wrinkling occurred in specimens drawn from both blank forms and is seen prominently in zone 6. This is owing to the fact that more metal flows into zone 6 at a given punch penetration than flows into zone 5, due to the axial offset of the form at this section.

The important points which emerge from the examination of drawing-in are

1. that the rate of drawing-in and its control have a predominant effect on the strain distribution, and consequently on the fracture strain;
2. differential drawing-in, such as experienced in this shell, leads to rotation of the elements and thus contributes to failure;
3. asymmetry leads to uncontrolled drawing-in which gives rise to compressive stresses in convergent regions and, hence, wrinkling which in itself is a failure mechanism in many pressings;
4. control of drawing-in is virtually impossible if two adjacent sections require massively different rates of drawing-in.

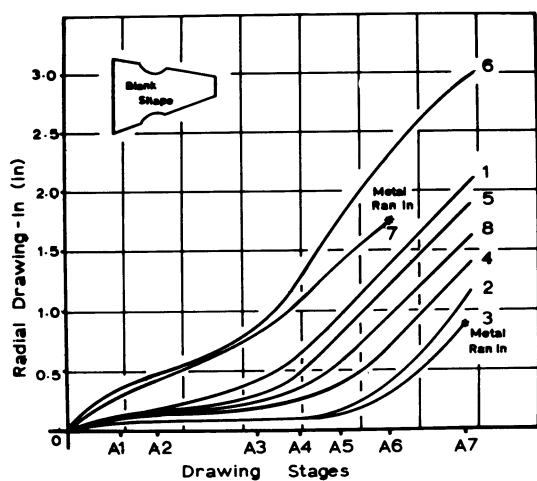


Fig. 7 Drawing-in against punch penetration for unsplit shell.

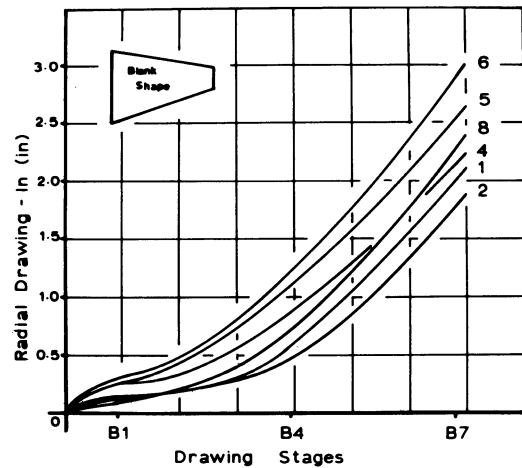


Fig. 8 Drawing-in against punch penetration for split shell.

DISCUSSION

It is a fact that theoretical understanding of press work has lagged behind the practical applications and that successful pressings are produced in spite of the minimal knowledge of the control parameters. This investigation has shown that some quantitative measure of the 'condition' of a pressing can be achieved through measurement of the strains and drawing-in and that such knowledge could be used to produce better components with a more uniform strain distribution.

It is apparent that the most important feature of a drawing operation is control of the drawing-in; namely, that the amount, distribution and timing should be known for every pressing. Quantitative data on the 'condition' of a pressing has far reaching implications, the least of which would be to replace opinion by documented records of the effects of lubrication, blank size and blank material. Production pressings could also be monitored so that changes in the process would be determined and any necessary action taken. Material cost is obviously a major consideration and if a better knowledge of the strain distribution were available, a cheaper material could be used even in cases such as the shell considered here.

It is usually argued that if a pressing forms without failure, it is satisfactory, but the evidence produced by this experiment shows that some pressings may well be so near to failure that small changes in the process could well lead to fracture; or in the worst case failure in service. A knowledge, therefore, of the critical strain levels can not only save in material costs, but also avoid costly production breakdowns.

ACKNOWLEDGEMENTS

The authors would like to thank the British Leyland Motor Corporation for the use of their extensive facilities during the period of the project; further for their permission to publish the results of this investigation.

They also acknowledge the many discussions with Professor T. C. Hsü (Professor of Applied Mechanics in the Department of Production Engineering, Univer-

sity of Aston in Birmingham) about theoretical considerations and also his help with the experimental design.

REFERENCES

1. SHAWKI, G. S. A., 'Assessing the Deep Drawing Qualities of Sheet', *Sheet Metal Industries*, 1965, **42**, p. 363.
2. KEELER, S. P., 'Determination of Forming Limits in Automotive Stampings', *Sheet Metal Industries*, 1965, **42**, p. 683.
3. GOODWIN, G. M., 'Application of Strain Analysis to Sheet Metal Forming Problems in the Press shop', *S.A.E.*, January 1968, Paper 680093.
4. BOWERS, I, and BROOKES, I., 'The Electrochemical Marking of Strain Grids', Research & Development Dept. Pressed Steel Fisher Ltd., Technical Note No. 64, 1968.
5. PEARCE, R, and DRINKWATER, I. C., 'Some Aspects of Electrochemical Marking', *Sheet Metal Industries*, 1968, **45**, p. 751.
6. HSÜ, T. C., 'The Characteristics of Coaxial and Non-coaxial Strain Paths', *J. Strain Analysis*, 1966, **1** (3), p. 216.
7. HSÜ T. C., Private communication.

APPENDIX

Material specifications

E.N. Spec	Quality	% C Max	% Mn Max	% S Max	% P Max	Code
E.N.2A/1	{ Stabilized E.D.D.Q. }	0.075	0.450	0.030	0.025	C.R.1
E.N.2A/1		0.080	0.450	0.035	0.030	C.R.2

Material test record (thickness 0.033 in)

Yield Point lb/in ²	U.T.S. lb/in ²	Elong %	R Value	Erichson Value	Rockwell 'B' Scale
29 300	47 000	44	1.90	11.0	48

THE QUANTITATIVE EFFECT OF TOOL GEOMETRY AND STRAIN-HARDENING ON THE CRITICAL PUNCH FORCE IN CUP DRAWING

by

J. A. G. KALS*

SUMMARY

A relation between tensile curves and critical punch force in the deep drawing of cylindrical products is developed. Both the work hardening effect and the geometry of the drawing punch are taken into account. A reasonable correspondence between the analytical results and the experimental data can be established. Finally, the practical significance of the mathematical model is shown by giving a criterion for the minimum corner radius of the punch. Moreover, the usefulness of the model is confirmed on the basis of some observations on deep drawability and geometric similarity in formability tests.

INTRODUCTION

Deep drawability can be influenced radically by many factors which may constitute the difference between the successful production of a stamping and breakage during pressworking operations. Many individual drawing steps may be required to produce a stamping. In order to reduce the number of drawing operations, the drawing ratio, defined between the blank diameter and the average cup diameter, has to be chosen as high as possible. The limit of deformation is reached when the load, required to deform the flange, becomes greater than the load-carrying capacity of the cup wall.

The required punch load depends on a large number of drawing conditions, such as forming properties of the sheet material, sheet thickness, drawing ratio, blank diameter, die-profile radius, hold-down pressure and friction conditions. On the other hand, the critical punch load is influenced by the punch profile radius, the punch diameter and by lubrication, sheet thickness and material properties as well. Changes of lubricant and material characteristics caused by speed fluctuations are other factors that may influence formability. The actual value of the limiting drawing ratio is fixed by all these coinciding forming conditions.

In this paper a theory is described which enables a calculation of the critical punch load and of a favourable dimension of the corner radius of the punch. In order to limit the complexity of the mathematical problem to a minimum, a number of validity restrictions have to be made with respect to the following theory:

- (i) it is assumed that deformation speed effects can be neglected;
- (ii) the working sheet materials are homogeneous, plastic-rigid and isotropic;
- (iii) friction effects can be neglected;
- (iv) comparatively thin sheet material only is considered, so that bending effects do not have to be taken into account;
- (v) a relatively small punch-edge radius in relation to the punch diameter.

The direct practical significance of this theory may be based on the fact that special literature of objective information concerning the selection of a useful punch-profile radius in relation to formability limits is lacking.

ANALYSIS

The current stress and strain state in the critical cross-section

In radial drawing of the flange region the material is being upset in a tangential direction. This results in an increasing sheet thickness and a hardening of the material. These effects are stronger as a volume element is moved further into the direction of the die cavity. So the increase in sheet thickness is restricted to the outer flange areas. Contrary to this, and especially under critical drawing conditions, the inner flange area is stretched very considerably during the initial increase of the punch force. This holds particularly for the material originally over the die wall. Therefore, the failure will be located exclusively in the stretched area near the

bottom of the cup wall. The exact location of the failure, caused by exceeding the stability limit in stretching, depends on the material and the forming conditions, particularly on friction.

As a preliminary to the analysis of the stretching limit, the failure location is assumed to be exactly on the borderline between the cup wall and the rounded edge of the punch. With favourable friction conditions, and a relatively large edge radius being exceeded, the fore-going will be a fair approximation of reality (see Fig. 1). A laborious procedure can be avoided by representing the rounded cup area as a part of a torus.

Let σ_ϕ and σ_t be the average axial and circumferential stress components in the critical cross-section and p the local normal pressure between the punch and the cup wall. The equation of equilibrium is

$$\frac{p}{s} = \frac{\sigma_\phi}{\rho_{st}} \left(1 + \frac{s}{2r_{st}}\right) + \frac{\sigma_t}{r_{st}} \left(1 + \frac{s}{2\rho_{st}}\right) \quad (1)$$

where

- s = the momentary cup wall thickness
- r_{st} = the punch radius
- ρ_{st} = the punch profile radius

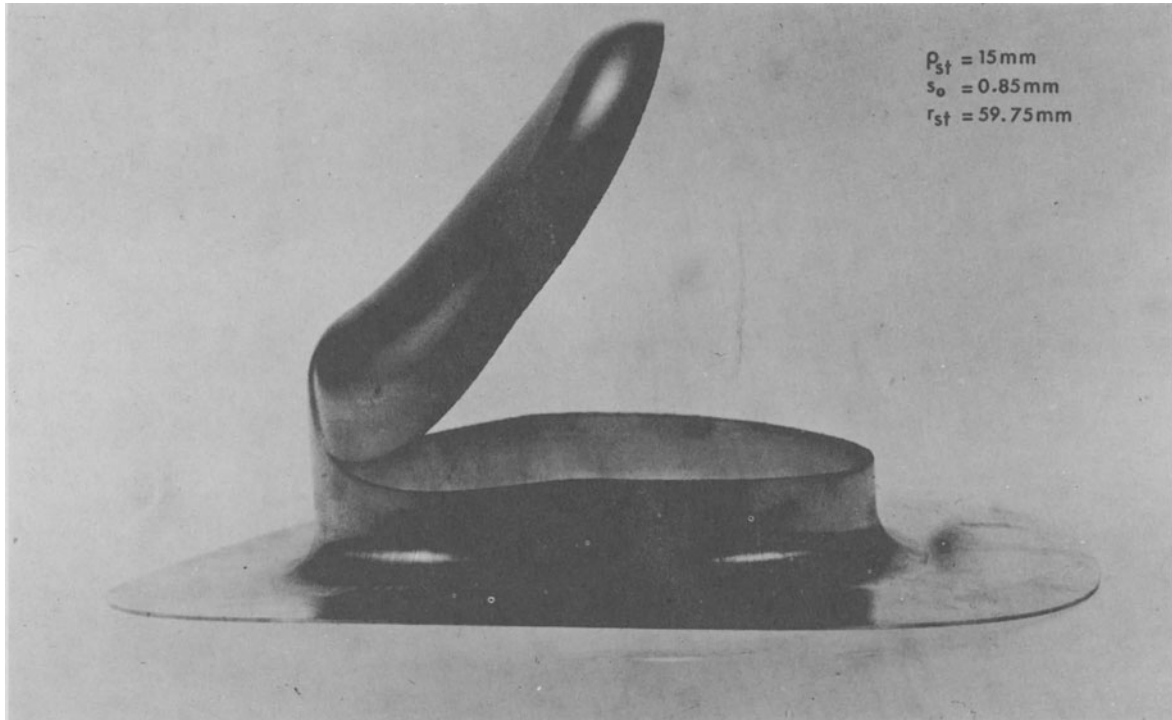


Fig. 1 Failure usually occurs in the rounded edge, close to the cylindrical wall area.

According to the simplifying assumptions, failure takes place in a symmetry plane of the torus as shown in Fig. 2.

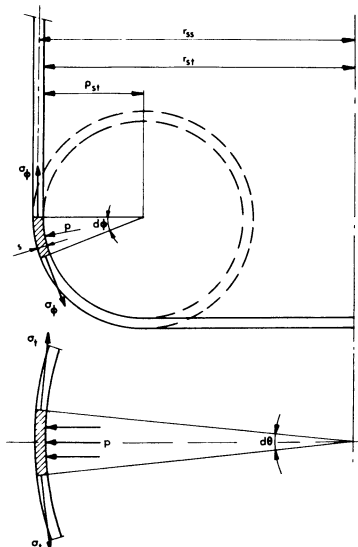


Fig. 2 Schematic stress state in the critical cross-section of the cup wall.

An immediate simplification of equation (1) can be achieved by using the restriction $s \ll \rho_{st}$. In this case, case, equation (1) reduces to

$$\frac{p}{s} \approx \frac{\sigma_\phi}{\rho_{st}} + \frac{\sigma_t}{r_{st}} \quad (2)$$

In the first instance the normal stress component σ_n depends on the inner wall pressure p . Thus far ($0 \leq i \leq 1$)

$$\begin{aligned} \sigma_n &= -ip \\ &\approx -is \left(\frac{\sigma_\phi}{\rho_{st}} + \frac{\sigma_t}{r_{st}} \right) \end{aligned} \quad (3)$$

The axial stretching of the cup wall during the initial increase of the punch load is compensated exclusively by a reduction in wall thickness, as the punch effectively precludes straining in the circumferential direction. The decrease of the average cup radius r_{ss} by the reduction in thickness may be neglected when $s \ll r_{st}$. As a consequence

$$d\delta_t = 0 \quad (4)$$

Let $d\delta_t$, $d\delta_\phi$ and $d\delta_n$ be the principal components of an increment of strain. Since there is no change in volume the following relation exists

$$d\delta_t + d\delta_\phi + d\delta_n = 0 \tag{5}$$

Hence

$$d\delta_\phi = -d\delta_n \tag{6}$$

The Lévy–von Mises equations may be expressed for the normal and the axial direction, respectively:

$$d\delta_n = d\lambda \left(\sigma_n - \frac{\sigma_t + \sigma_\phi}{2} \right) \tag{7}$$

$$d\delta_\phi = d\lambda \left(\sigma_\phi - \frac{\sigma_n + \sigma_t}{2} \right)$$

where $d\lambda$ is a scalar factor of proportionality. If this is combined with the straight strain-path as expressed in equation (6), we obtain the following necessary condition for the stress state:

$$\sigma_n = 2\sigma_t - \sigma_\phi \tag{8}$$

Now, the average normal stress σ_n can be eliminated from equation (3). Thus

$$\sigma_t \approx j\sigma_\phi \tag{9}$$

where

$$j = \frac{r_{st}}{\rho_{st}} \cdot \frac{\rho_{st} - is}{2r_{st} + is} \tag{10}$$

Finally, equations (8) and (9) may be combined to give

$$\sigma_n \approx (2j - 1) \sigma_\phi \tag{11}$$

It seems fair to regard the equations (9) and (10) as a reasonably good first approximation of the complete current stress state in the critical cross-section.

For applications requiring a high accuracy, it will eventually be necessary to exclude the simplifications from the theoretical framework. At present, however, a practical approximation is wanted. So, for the time being additional mathematical complexity does not seem to be worth while.

The current load of the cup wall

Von Mises suggested that yielding occurs when the second stress-tensor invariant reaches a critical value $\bar{\sigma}$. In connection with our problem this criterion may be written in terms of the principal components of the stress state. Thus

$$2\bar{\sigma}^2 = (\sigma_t - \sigma_\phi)^2 + (\sigma_\phi - \sigma_n)^2 + (\sigma_n - \sigma_t)^2 \tag{12}$$

where $\bar{\sigma}$, the effective stress, is a parameter depending on the amount of strain. The concept of a yield criterion is not restricted merely to loading directly from the annealed state, as is sometimes thought. In combination with equation (12), we have from (9) and (11)

$$\bar{\sigma} \approx \sqrt{3} (1 - j) \sigma_\phi \quad (0 < j < 1) \tag{13}$$

In order to include the strain hardening effect in the theoretical model, $\bar{\sigma}$ has to be related to a certain measure of the total plastic deformation. A quantity

$d\bar{\delta}$, known as the generalized or effective plastic strain increment, is defined in terms of the principal strain increments by the equation

$$d\bar{\delta} = \left[\frac{2}{3} (d\bar{\delta}_1^2 + d\delta_2^2 + d\delta_3^2) \right]^{1/2} \tag{14}$$

Apart from the numerical factor, $d\bar{\delta}$ is the same invariant function of the plastic strain increment tensor, as $\bar{\sigma}$ is of the components of the deviatoric stress tensor. The use of the previous equations (4) and (6), and integration of (14), result in

$$\bar{\delta} = \int d\bar{\delta} = \frac{2\delta_\phi}{\sqrt{3}} \tag{15}$$

This integration is the simplest and most natural way to satisfy the obvious requirement that the measure of total distortion must involve the summation of some continually positive quantity over the whole strain path. In this case integration is very simple because the components of any strain increment bear constant ratio to one another. Besides, it is worth noting that this strain model has the additional advantage that the general requirement of minimum dissipation of specific strain energy is satisfied automatically.

Turning now to the strain hardening relation between $\bar{\sigma}$ and $\bar{\delta}$; it is assumed that the following generalized form of an early empirical power law, due to Nadai, fits well to many sheet materials

$$\bar{\sigma} = C (\bar{\delta} + \bar{\delta}_0)^n \tag{16}$$

where C (characteristic stress) and n (strain hardening exponent) are material constants. The quantity $\bar{\delta}_0$ may be considered to include the strain history. Extending Nadai's equation in $\bar{\delta}_0$, results in C and n are essentially independent of strain history. According to the results taken from many tensile tests on different sheet materials, the introduction of $\bar{\delta}_0$ has the additional advantage of considerably higher accuracy in approximating real stress–strain curves of materials with an unknown strain history. Typical examples are given in Figs 3 and 4.

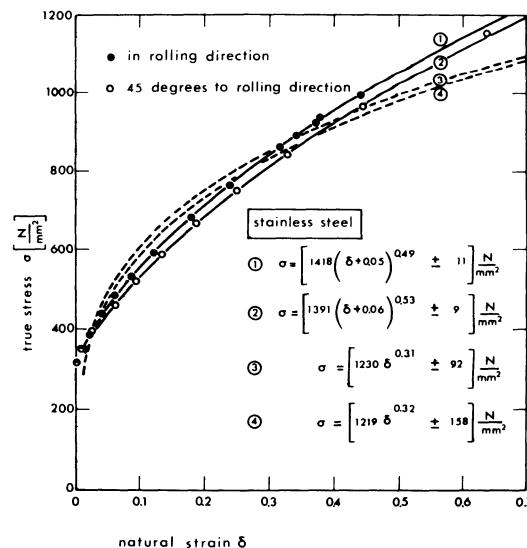


Fig. 3 The usual form of Nadai's equation in comparison with the generalized one and the results of tensile tests.

From equations (13) and (15), the actual form of (16) becomes

$$\sigma_\phi \approx \frac{C}{(1-j)\sqrt{3}} \left(\frac{2}{\sqrt{3}} \delta_\phi + \bar{\delta}_o \right) \quad (17)$$

Substitution of σ_ϕ in the general expression for the cup wall load (Fig. 2) gives

$$F = 2\pi s \left(r_{st} + \frac{s}{2} \right) \sigma_\phi = 2\pi s r_{ss} \sigma_\phi \quad (18)$$

which results in

$$F \approx \frac{2\pi}{\sqrt{3}} \cdot \frac{C s r_{ss}}{1-j} \left(\frac{2}{\sqrt{3}} \delta_\phi + \bar{\delta}_o \right)^n \quad (19)$$

According to the general definition of a logarithmic strain, we can write

$$s = s_o \exp(\delta_n) \quad (20)$$

where s_o is the initial sheet thickness. Combining equations (6) and (20), we find

$$s = s_o \exp(-\delta_\phi) \quad (21)$$

The required relation between the load F and the axial strain δ_ϕ is obtained by substituting this formula in equation (19)

$$F \approx \frac{2\pi}{\sqrt{3}} \cdot \frac{C r_{ss} s_o}{1-j} \left[\exp(-\delta_\phi) \right] \times \left(\frac{2}{\sqrt{3}} \delta_\phi + \bar{\delta}_o \right)^n \quad (22)$$

Finally it is to be noted that the present expression for the axial load on the critical cross-section of the cup wall is applicable for calculating also the punch force, with the limitation that friction forces can be neglected. This simplification has previously been assumed.

The critical punch load

The elongation of the partially formed cup wall is accompanied by a reduction in thickness; that is, a decrease in the cross-sectional area A , and thereby a strengthening by strain hardening. Initially the strain hardening effect dominates in view of the stretching force

$$\frac{dF}{d\delta_\phi} = \frac{d}{d\delta_\phi} (\sigma_\phi A) = \sigma_\phi \frac{dA}{d\delta_\phi} + A \frac{d\sigma_\phi}{d\delta_\phi} > 0 \quad (23)$$

Therefore, the cup wall can now support the larger deep-drawing load, so flange forming can continue. With only a few exceptions, the strain hardening effect $d\sigma_\phi/d\delta_\phi$ decreases with increasing strain level (Figs 3 and 4). In the continuation of the deep-drawing process, an ultimate strength of the cup wall will be reached when both the strain hardening and the stretching term in equation (23) cancel each other and we have

$$\frac{dF}{d\delta_\phi} = 0 \quad (24)$$

When the chosen drawing ratio implies a further increase of the drawing force to be necessary for continuous deformation of the flange region, this

load can no longer be transmitted through the lower cup wall. Finally, the load carrying capacity of this structurally weak link in the system appears to decrease with the punch going on continuously. The stamping then starts releasing elastically, with the exception of the lower region of the cup wall, and this plastic region shrinks into a circumferential constriction.

If the stability limit is once exceeded, plastic straining continues only in the necked part of the cup wall, and consequently no further straining will take place in the remaining part. Thus, equation (24) is the limiting condition of forming and, in general, it seriously reduces the achievable amount of overall deformation in those processes where stretching occurs. It is therefore the deep drawability limit.

For our purposes it may be sufficient to consider r_{ss} and j as being constant in differentiating equation (22), otherwise no explicit solution for the critical amount $\delta_{\phi k}$ of the axial component of strain can be obtained. Then, introducing the criterion of necking by differentiating (22) and setting it to zero, we may write

$$\delta_{\phi k} \approx n - \frac{\sqrt{3}}{2} \bar{\delta}_o \quad (25)$$

as a good approximation. The material with the higher n -value is characterized by a steeper stress-strain curve (Figs 3 and 4). The critical strain value at maximum punch load is larger for higher n -values. Generally the n -value primarily influences stretchability. The most important effect of a high n -value is to improve the uniformity of the strain distribution in the presence of a stress gradient, and necking happens to be a strong non-uniformity of the strain distribution. According to equation (25) and to practical experience, pre-straining diminishes formability.

Inserting this strain ceiling, in combination with equations (10) and (21), in the expression of the cup wall load, (22), we obtain

$$F_k \approx \frac{2\pi}{\sqrt{3}} C r_{ss} s_o \rho_{st} \left(\frac{2n}{\epsilon\sqrt{3}} \right)^n \times \frac{2 r_{st} e^n + i s_o \exp \left[\frac{(\sqrt{3}/2) \bar{\delta}_o}{\epsilon} \right]}{\rho_{st} r_{st} \exp \left[n - (\sqrt{3}/2) \bar{\delta}_o \right] + i s_o (r_{st} + \rho_{st})} \quad (26)$$

The last term in the numerator may be neglected according to the previous assumption for relatively thin sheet materials. Furthermore, this equation may be simplified, by the introduction of dimensionless quantities, to

$$F_k^* \approx i \frac{(4\pi/\sqrt{3}) (2n/\sqrt{3})^n}{\left[(1/\rho_{st}^*) + (1/r_{st}^*) \right] + \exp \left[n - (\sqrt{3}/2) \bar{\delta}_o \right]} \quad (27)$$

where

$$F_k^* = \frac{F_k}{C r_{ss} s_o}; \quad \rho_{st}^* = \frac{\rho_{st}}{s_o}; \quad r_{st}^* = \frac{r_{st}}{s_o} \quad (28)$$

and where r_{ss} is the average local cup radius at maximum wall load [equations (20) and (25)]

$$r_{ss} = r_{st} + \frac{s}{2} = r_{st} + \frac{s_0}{2} \exp\left(\frac{\sqrt{3}}{2} \bar{\delta}_0 - n\right) \quad (29)$$

A problem still to be solved concerns the numerical value of the stress parameter i [equation (3)]. The normal stress distribution may be approximately linear, so the value of i that we are looking for seems to be 0.5. Nevertheless it is better to choose the maximum value $i = 1$, for it is evident that instability must be initiated at the punch side of the cup wall, according to the assumption of uniformly distributed axial and tangential stresses. If a constant value $i = 1$ is combined with equation (27), the following expression is finally obtained

$$F_k^* \approx \frac{4\pi}{\sqrt{3}} \left[\frac{2n}{\sqrt{3}}\right]^n \left[\frac{1}{\rho_{st}^*} + \frac{1}{r_{st}^*} + \exp\left(n - \frac{\sqrt{3}}{2} \bar{\delta}_0\right) \right]^{-1} \quad (30)$$

A representation of this relation is given in Fig. 5.

Theoretical results

Of course, the present solution is only a simplification of a more complex process, but this first step may shed some light on the mechanism of failure in deep drawing. Equation (30), as shown in Fig. 5, permits some interesting conclusions:

(i) Obviously, the load-carrying capacity of the cup wall vanishes very rapidly with decreasing edge radius below a definable limit of ρ_{st}^* . Practically, this effect implies the punch cutting into the cup wall. According to Oehler and Kaiser¹ the minimum value of the edge radius should preferably be chosen to equal five times the initial sheet thickness. A value $\rho_{st}^* = 15-25$ is judged as being still more recommendable. These empirical data support our foregoing theory clearly. Nevertheless, experimental investigations are necessary in order to compare the theoretical results with reality more systematically.

(ii) Strain hardening only slightly effects a change of the critical ρ_{st}^* -value.

(iii) The effects of ρ_{st}^* and r_{st}^* on the critical punch force are identical. To consider this fact may be useful in detecting failures of small stampings.

(iv) A noteworthy phenomenon being observed is that the critical punch force is smaller for larger n -values, due to larger stretchability, until instability occurs. The corresponding curves appear to pass through a minimum value at about $n = 0.8$. It can be shown (see p. 10) that the maximum punch load necessary to deform the flange region also decreases with increasing n -values. The corresponding curves $F_{max}(n)$ appear to decline steeper than $F_k(n)$. So, ultimately, the limiting drawing ratio shows a slightly progressive increase with increasing n -values.

(v) The opposite influence of the 'strain-history' parameter $\bar{\delta}_0$ [equation (25)] is shown in Fig. 6.

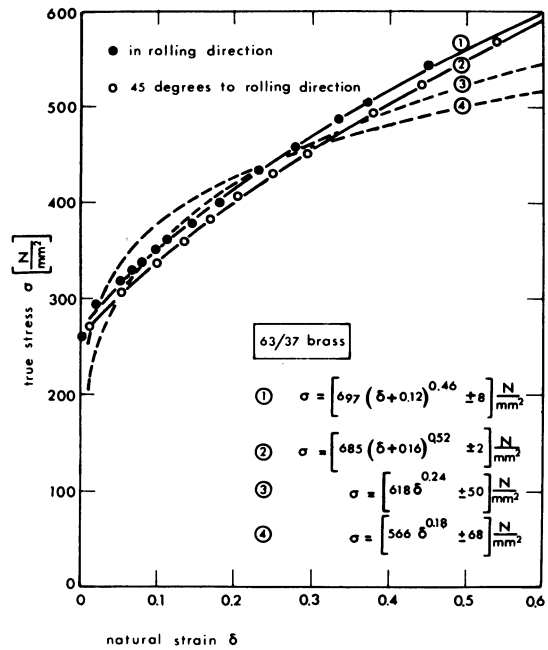


Fig. 4 The usual form of Nadai's equation in comparison with the generalized one and the results of tensile tests.

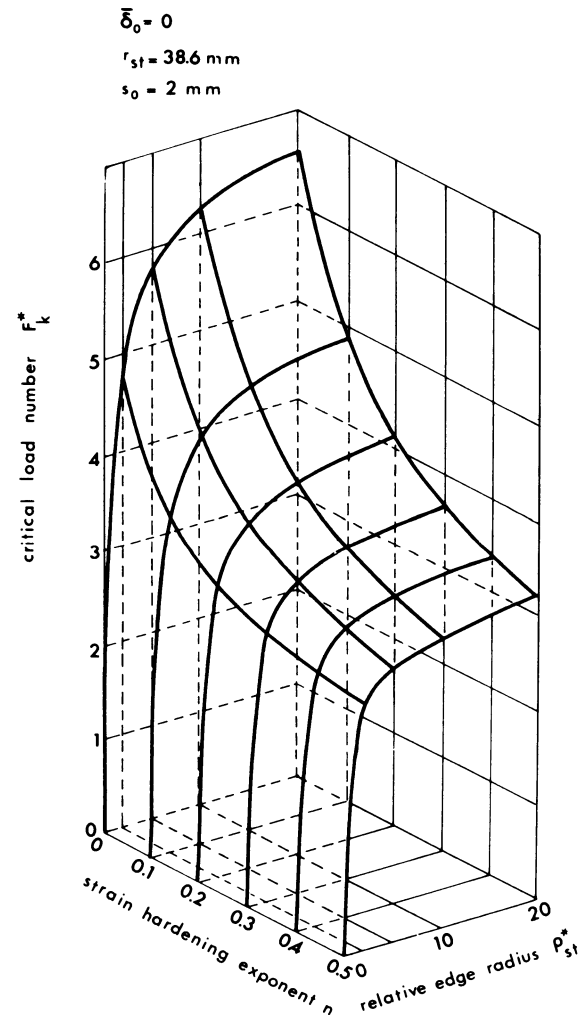


Fig. 5 Theoretical curves according to equation (30) for $\bar{\delta}_0 = 0$, $r_{st} = 38.6$ mm, $s_0 = 2$ mm.

Finally a restriction has to be made with regard to the practical validity of equation (30). At very low values of the punch-edge radius in relation to sheet thickness, that is, where the edge is cutting into the wall, the validity of the presupposed deformation model may become doubtful. So Fig. 5 has to be understood merely as a representation of the mathematical relation in this region. According to the previous assumption of relatively small values of the edge radius, the validity of the theoretical equation has to be restricted in this respect too. It has been observed that the instability region is moving towards the punch centre at increasing edge radius.

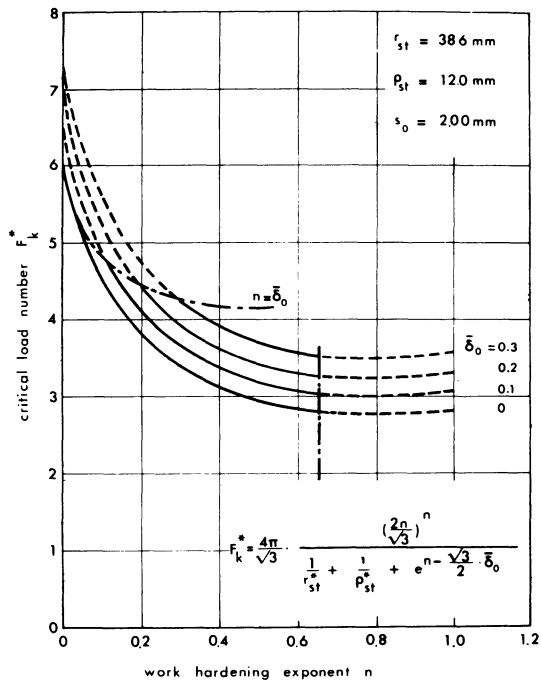


Fig. 6 Theoretical relation between critical load number, strain-hardening exponent and strain-history parameter.

EXPERIMENTAL RESULTS

In order to obtain the material data, tensile tests were carried out intermittently at a mechanical tensile test machine. The local plastic strains could therefore be measured separately by measuring the cross-sectional area of the test specimen after discharging the material every now and then. The material constants have been computed according to the least-squares criterion. A number of ten sheet materials ($s_0 \approx 2$ mm) was selected on the basis of small earing in deep drawing. Nevertheless, this planar anisotropy effect increases slightly in the direction of increasing test numbers (Table 1). Tensile tests were carried out at 0° , as well as 45° , to the rolling direction. The results are given in Table 1.

Table 1. Results of tensile tests and deep-drawing tests (sheet materials as received).

Nr	sheet material	in rolling direction				45 degrees to rolling direction				F_{kw} [kN]
		s_0 [mm]	C [$\frac{N}{mm^2}$]	n [-]	$\bar{\delta}_0$ [-]	s_0 [mm]	C [$\frac{N}{mm^2}$]	n [-]	$\bar{\delta}_0$ [-]	
1	72/28 brass	1.97	791	0.56	0.04	1.92	786	0.57	0.04	179
2	stainless steel	2.09	1418	0.49	0.05	2.06	1391	0.53	0.06	358
3	stainless steel	2.01	1512	0.57	0.06	2.01	1460	0.61	0.08	343
4	63/37 brass	1.96	719	0.37	0.08	1.99	687	0.35	0.08	191
5	63/37 brass	1.93	697	0.46	0.12	1.93	685	0.52	0.16	181
6	alum (Si)	1.90	437	0.28	0.02	1.91	433	0.27	0.02	116
7	alum (99.5%)	1.96	140	0.33	0.01	1.95	138	0.39	0.03	34
8	nickel	2.06	1166	0.46	0.01	2.03	1104	0.44	0.01	255
9	copper	1.95	408	0.27	0.16	1.94	421	0.45	0.29	135
10	steel (Cu)	1.98	895	0.27	0.02	1.95	904	0.30	0.04	270

The best fitting stress-strain curves on the basis of the original Nadai equation (without strain history parameter) can be reconstructed with the values in Table 2.

Table 2. Experimental results according to the engineering form of the Nadai equation and measured values of the plastic anisotropy parameter

Nr	sheet material	in rolling direction		45 degrees to rolling direction		plastic anisotropy parameter	
		C [$\frac{N}{mm^2}$]	n [-]	C [$\frac{N}{mm^2}$]	n [-]	R_0 [-]	R_{45} [-]
1	72/28 brass	754	0.45	724	0.42	0.96	0.99
2	stainless steel	1230	0.31	1219	0.32	0.96	0.98
3	stainless steel	1346	0.37	1387	0.40	0.92	0.96
4	63/37 brass	553	0.13	583	0.16	0.77	0.88
5	63/37 brass	566	0.18	618	0.24	0.89	0.90
6	alum (Si)	410	0.22	408	0.22	0.45	0.52
7	alum (99.5%)	137	0.30	133	0.31	0.68	0.67
8	nickel	1132	0.43	1069	0.40	0.81	0.88
9	copper	335	0.06	339	0.06	0.68	0.78
10	steel (Cu)	778	0.17	714	0.14	0.79	0.88

The deep-drawing tests were carried out on a hydraulic press with low punch velocities and a rather arbitrarily chosen tool geometry with $r_{st} = 38.6$ mm and $\rho_{st} = 12.0$ mm. It is a well-known fact that the load carrying capacity of the cup wall decreases slightly as the drawing ratio further exceeds the limiting value. This is due to the introduction of local instability before the forming of the bottom rounding has been completed. In this case necking occurs nearer to the flat bottom and also the critical cross-section is not perpendicular to the moving direction of the punch. Therefore, the critical drawing load has to be measured exactly at the limiting drawing ratio. In order to obtain these values of F_k , both the maximum drawing force F_{max} and the critical punch load F_k have been measured as a function of the drawing ratio. The required value of F_k can be taken as the intersection of both of these curves. The results are given in the last column of Table 1. Fig. 7 shows a satisfying correspondence between the calculated values F_k and the experimental values F_{kw} of the critical punch force.

According to equation (28) the characteristic stress C holds a rather dominant position with relation to the absolute value of the critical punch load. By eliminating this quantity, the effect of strain hardening can be made clear. Therefore in Fig. 8 the theoretical and experimental values of the dimensionless critical load number are compared. A stronger scattering can be observed in this representation. Nevertheless, the theoretical effect of strain hardening may be considered to be verified as well. It is probable that the divergence may be partly attributable to plastic anisotropy, especially in the case of the points plotted for materials 8, 9 and 10 in Table 2. In order to compare experimental and theoretical results (Fig. 6) with respect to the hardening effect on the critical load number as well, equation (30) has been evaluated according to the standard Nadai equation ($\bar{\delta}_0 = 0$) using the values in Table 2. Fig. 9 shows the results.

Every deep-drawing experiment so far mentioned has been carried out with a constant punch geometry. In order to verify the theoretical effect of the punch-edge radius (Fig. 5) separately, an additional series of experiments had to be carried out. The experimental results and the corresponding theoretical curves according to equations (27) or (30) are shown in Fig. 10. Equations (27) and (28) have been evaluated with the following data from tensile tests

rolling direction	$C = 798 \text{ N/mm}^2$
	$n = 0.54$
	$\bar{\delta}_0 = 0.06$
45° to rolling direction	$C = 760 \text{ N/mm}^2$
	$n = 0.57$
	$\bar{\delta}_0 = 0.08$

From Fig. 10 it is again found that equation (30) is a satisfactory approximation of reality. These experiments have been repeated for the larger relative sheet thickness s_0/r_{st} as practised in the former series of experiments. The results are given in Fig. 11. From this graph, in comparison with Fig. 10, it appears that

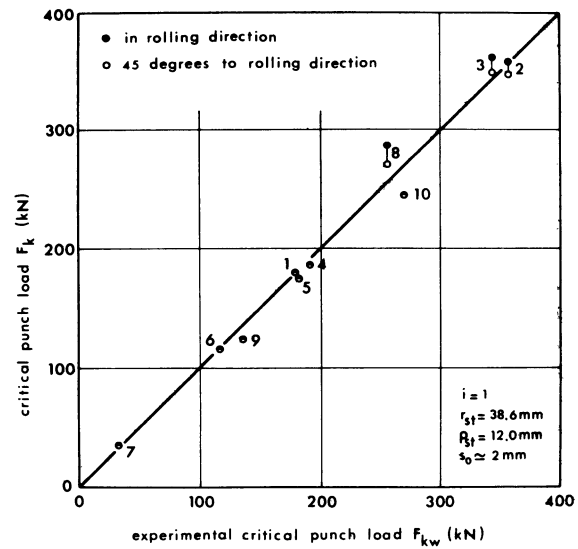


Fig. 7 Theoretical versus experimental values of the critical punch load.

the validity restriction to comparatively thin sheet materials (see p. 2) may not be overlooked. In addition, it is worth noting that the divergence of the plotted points in both the figures equals approximately the initial sheet thickness.

Even though some other variables to some extent exercise control over the deep-drawing process, equation (30) seems to give a true picture of the main conditions effecting the load-carrying capacity of the cup wall. Of course this study was only a first attempt to analyse the deep-drawing process and greater accuracy could probably be achieved with the aid of numerical calculation procedures. Many useful purposes, however, do not appear to be served by the application of rigour in an analysis for the sake of exactness.

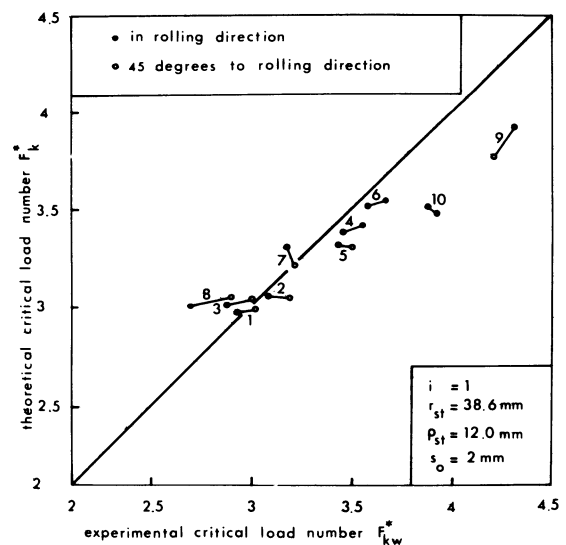


Fig. 8 Theoretical versus experimental values of the critical-load number.

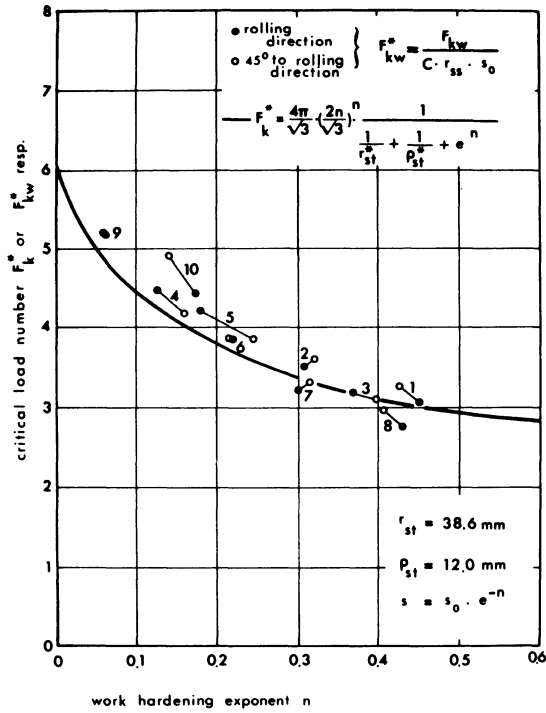


Fig. 9 Experimental results verifying the approximate validity of equation (30) with respect to the work-hardening effect (numerical data from Table 2).

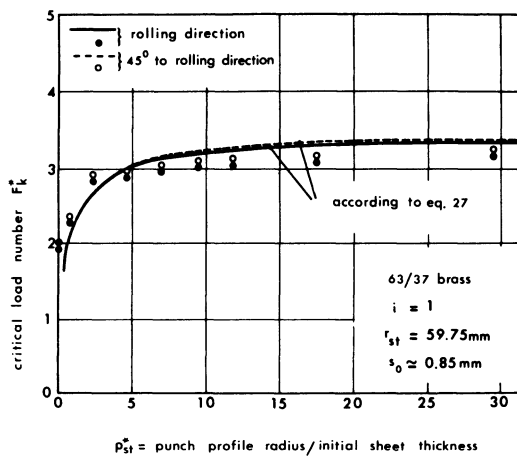


Fig. 10 Experimental and theoretical relationship between the critical-load number and the punch-edge radius for a relatively thin sheet material.

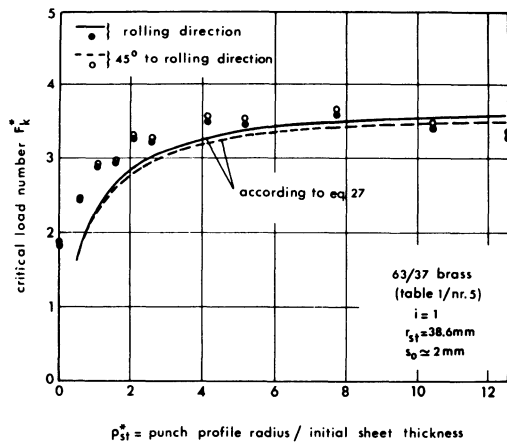


Fig. 11 Experimental and theoretical relation of the critical-load number and the punch-edge radius for a larger relative sheet thickness.

APPLICATIONS

Finally, some significant engineering aspects of the foregoing theoretical failure model will be elucidated briefly. In trying out stamping tools, it is often necessary to change to a more formable material, to modify the die design and even to change the stamping design in order to form a new product successfully. This takes time and money, and illustrates the need for a better understanding of sheet-metal formability and for objective formability testing methods. Of course, formability alone is not the sole criterion which has to be taken into consideration when sheet metal, tool geometry and production conditions have to be selected; but it is an inevitable one.

Punch geometry and formability

It is convenient to introduce a parameter

$$\eta = F_k^*/(F_k^*)_{\max} \tag{31}$$

defining a practical, useful value of F_k^* in proportion to an imaginary maximum value

$$(F_k^*)_{\max} =$$

$$\frac{4\pi}{\sqrt{3}} \left(\frac{2n}{\sqrt{3}} \right)^n \left\{ \frac{1}{r_{st}^*} + \exp \left[n - (\sqrt{3}/2) \bar{\delta}_0 \right] \right\}^{-1} \tag{32}$$

which results from equation (30) for $\rho_{st}^* \rightarrow \infty$. Substitution of (30) and (32) in (31), results in

$$\rho_{st}^* = \frac{\eta}{1-\eta} \left\{ \frac{1}{r_{st}^*} + \exp \left[n - (\sqrt{3}/2) \bar{\delta}_0 \right] \right\}^{-1} \tag{33}$$

This expression enables the evaluation of a favourable punch edge rounding as a function of the initial sheet thickness, the strain hardening exponent, the punch diameter and the chosen η -value. In the case represented in Fig. 10, for example, the following values are obtained from equation (33)

η	ρ_{st}^*
0.75	5
0.86	10
0.90	15

Another more complex criterion might be defined in terms of a steepness limit as

$$\partial F_k^*/\partial \rho_{st}^* \leq q \tag{34}$$

In general, the admissible slope tangent q has to be selected depending on the maximum drawing force in proportion to the critical punch load. Though this criterion would be a better one it is not going to be developed here. At present the experimental data appear to be too slight to make the additional mathematical complexity worth while.

As indicated in the introduction, the present study is part of a study directed to a theoretical analysis of some factors influencing deep drawability. In deep drawing, the overall deformation limit—limiting drawing ratio β_0 —can be defined as the ratio of the maximum blank diameter, that can be drawn into a cup

without failure, to the average diameter of the cup wall. This limit of deformation is reached when the load F_{\max} , required to deform the flange, becomes equal to the load carrying capacity F_k of the cup wall. A noteworthy aspect of taking F_{\max} into account is that the die-edge radius ρ_{zr} has an effect on it that is opposite to the effect of the punch-edge radius on the critical punch load. Experimental values illustrating this are shown in Fig. 12. Several experimental curves are shown in Fig. 13 for different drawing ratios β_o . The corresponding measured F_k -values are also plotted. In the particular case of equal values of ρ_{st} and ρ_{zr} being selected—as often happens in practice—the limiting drawing ratios are fixed in dependence on the tool geometry by the intersections of the F_{\max} curves and the F_k curves. Experimental and theoretical research in this field is going on in order to find a useful expression for F_{\max} and, finally, for the limiting drawing ratio as a function of tool geometry and strain hardening behaviour of sheet metals. Finally, looking at Fig. 13, the observation can be made that the limiting drawing ratio has a practical maximum with respect to optimization of tool geometry.

Strain hardening and formability

It has been pointed out already in the theoretical results that the required drawing force F_{\max} decreases slightly more than its critical value with increasing n -value. This results in larger values of the limiting drawing ratio as the strain hardening exponent becomes larger. This proposition still has to be made acceptable in order to give an outlook on the importance of the n -value as a basic material quantity affecting deep drawability. Let σ_ϕ and σ_t be the radial and circumferential stress components in the flange at radius r . With the restriction that friction effects and the blank holder pressure may be disregarded, the equation of equilibrium is

$$\frac{d}{dr} (\sigma_\phi s r) = \sigma_t s \tag{35}$$

where s is the local thickness of the blank. From many experiments, the strain state in the annulus appeared not to be a plane one, as is sometimes thought. The sheet thickness was found to be independent of r as a reasonably good first approximation. This leads to

$$\frac{d\sigma_\phi}{dr} = \frac{\sigma_t - \sigma_\phi}{r} \tag{36}$$

The relation between the radial stress component σ_ϕ and the circumferential one σ_t , if r_a = external blank radius is given by

$$\sigma_t = \sigma_\phi \frac{r^2 + r_a^2}{r^2 - r_a^2} \tag{37}$$

as can be shown² with the aid of the Lévy–von Mises equations. Substitution in the equation of equilibrium, followed by integration, leads to

$$\sigma_\phi = k \left(\frac{r_a^2}{r^2} - 1 \right) \tag{38}$$

where k is the integration constant.

The analytical expression for k can be obtained by using the boundary condition of a uniaxial peripheral stress state. Hence, with the tensile stress-strain relation (16), we may write

$$(\sigma_t)_{r=r_a} = -(\bar{\sigma})_{r=r_a} = -C \left(\ln \frac{r_{ao}}{r_a} + \bar{\delta}_o \right)^n \tag{39}$$

where r_{ao} is the initial radius of the blank and r_a the external radius at a certain moment. Substitution of equation (38) in (37), followed by combination with equation (39), gives

$$k = \frac{C}{2} \left(\ln \frac{r_{ao}}{r_a} + \bar{\delta}_o \right)^n \tag{40}$$

and

$$\sigma_\phi = \frac{C}{2} \left(\frac{r_a^2}{r^2} - 1 \right) \left(\ln \frac{r_{ao}}{r_a} + \bar{\delta}_o \right)^n \tag{41}$$

To investigate the influence of work-hardening on the drawing force we must find the sheet thickness. With the restriction of s being independent of r , and further of a uniaxial peripheral stress state in combination with the condition of constant volume and the Lévy–von Mises equations, the current flange thickness appears to be

$$s = s_o \sqrt{\frac{r_{ao}}{r_a}} \tag{42}$$

Since we are interested in the work-hardening effect only, within the scope of this paper, the effect of the punch edge and the—for the rest important—local friction may be represented in a greatly simplified way. Let r_s be the average radius of the drawing clearance. Then, the equation for the current drawing force is

$$F \approx 2\pi r_s e^{\mu\pi/2} s(\sigma_\phi)_{r=r_s} \tag{43}$$

where μ is the friction coefficient. Substitution of equations (41) and (42) gives

$$F \approx \pi s_o r_s C \left(\frac{r_{ao}}{r_a} \right)^{1/2} \left(\ln \frac{r_{ao}}{r_a} + \bar{\delta}_o \right)^n \left(\frac{r_a^2}{r_s^2} - 1 \right) \tag{44}$$

or

$$F^* \approx C \left(\frac{r_{ao}}{r_a} \right)^{1/2} \left(\ln \frac{r_{ao}}{r_a} + \bar{\delta}_o \right)^n \left(\frac{r_a^2}{r_s^2} - 1 \right) \tag{45}$$

where

$$F^* = F / (s_o r_s C) \tag{46}$$

The punch force reaches its maximum value for $r_a = r_{ak}$. Then, with

$$\left. \begin{aligned} \beta_o &= r_{ao}/r_s \text{ ('drawing ratio')} \\ \beta_k &= r_{ak}/r_s \end{aligned} \right\} \tag{47}$$

we obtain

$$F^*_{\max} \approx \pi e^{\mu\pi/2} \left(\frac{\beta_o}{\beta_k} \right)^{1/2} \times \left(\ln \frac{\beta_o}{\beta_k} + \bar{\delta}_o \right)^n (\beta_k^2 - 1) \tag{48}$$

where β_k can be calculated with

$$\beta_o = \beta_k \exp\left(2n \frac{\beta_k^2 - 1}{3\beta_k^2 + 1}\right) \quad (49)$$

This expression has been obtained by differentiating equation (45) with respect to r_a , followed by equating to zero.

Now, the nature of the work-hardening effect on deep drawability can be studied by evaluating the general condition $F_{\max}^* = F_k^*$ with the aid of equations (30) and (48). The theoretical values—represented by the curves in Fig. 14—are obtained with a digital computer, omitting the geometrical terms in equation (30) and for $\delta_o = 0$. Thus, both calculated force numbers F_{\max}^* and F_k^* may be considered maximum values with respect to tool geometry. The substantial correctness of the theoretical tendency of the work-hardening effect may be demonstrated by the experimental work of Arbel³. His results (Table 3) are also shown in Fig. 14.

In order to eliminate friction effects, these tests were carried out without a blank-holder. It was therefore essential to use a sheet thick enough to prevent folding. Contrary to the original values, the limiting drawing ratios have been recalculated according to the following relation [see equation (29)]

$$\beta_o \max = \frac{r_{ao}}{r_{ss}} = r_{ao} / (r_{st} + \frac{s_o}{2e^n}) \quad (50)$$

Table 3. Experimental data of Arbel³ showing the limiting drawing ratio $\beta_o \max$ as a function of the work-hardening exponent n ($r_{st} = 1.1$ in; $s_o = 0.125$ in).

material	$(2r_{ao})_{\max}$ [in.]	n	$2r_{ss}$ [in.]	$\beta_o \max$
65/35 brass	2.625	0.54	1.173	2.24
18/8 stainless steel	2.625	0.52	1.174	2.24
copper	2.553	0.34	1.189	2.15
alum	2.450	0.28	1.195	2.05
alum	2.420	0.25	1.197	2.02
hard brass	1.850	0.07	1.217	1.52

The last metal in Table 3 had a very marked directionality and was tested to assess the results obtained with a metal of low formability. From the form of the dotted line (Fig. 14) Arbel³ concluded that little progress, from the deep-drawing point of view, can be expected from new alloys of a high work-hardening exponent. Though an approximation, our foregoing theory brings to light the fact that too much importance has presumably been attached to the last metal. In that case Arbel's conclusion should have to be reversed to the opposite sense. Recent studies in superplasticity⁴ support our conclusion. Research

activities are going on in order to analyse the additional effects of friction, anisotropy and the drawing edge on formability.

Simulative testing methods

There exist three main methods for determining the forming characteristics of sheet metal.

(i) Testing the fundamental plastic properties of the sheet metal—the use of the determined quantities has been demonstrated in this study.

(ii) Comparative testing on the basis of arbitrarily chosen formability parameters—the use of the resulting values should be restricted to make sure that properties do not vary from coil to coil, etc.

(iii) Testing by simulating forming operations—even in the case of carefully controlled geometric similarity there is the problem of the scale factors. Whether or not a small diameter punch—the Swift flat-bottom cup test for example—can truly represent a punch used to draw a geometrically similar cup 10 or 20 times larger in diameter is questionable.

Complete similarity exists when the limiting drawing ratio obtained from a scale test equals the value observed in production conditions. A free choice of the material characteristics and the initial sheet thickness can be overlooked for practical reasons; also a controlled change in friction conditions. Thus, the rules of similarity can be obeyed only by adjusting the testing tool geometry. Hence, if equation (30) holds—and under the simplifying restriction that the load numbers F_k^* and F_{\max}^* under testing conditions must be equal to the values under production conditions—one of the rules of geometrical similarity can be formulated from (30) as

$$\frac{1}{\rho_{st}^*} + \frac{1}{r_{st}^*} = \frac{1}{c} = \text{constant} \quad (51)$$

Solutions are shown in Fig. 15 for different c -values. Owing to the diminishing steepness of the part of the curves of practical interest, it is clear that it will be impossible to realize the right geometrical scale conditions in most of the cases. It must be noted that common testing conditions are expressed at the bottom left-hand side of the graph.

It appears that no matter how much any simulative test is perfected, no single deep-drawing test is presumably sufficient to evaluate formability in an accurate way. Similar findings have been expressed by Shawki⁵ on the basis of many attempts to correlate results from different tests. Nevertheless, it is evident that there is a real need to be able to predict or evaluate the formability of sheet metal in combination with tool geometry and working conditions. For the time being a careful theoretical analysis of deep drawing on the basis of fundamental plastic properties seems to be the only way.

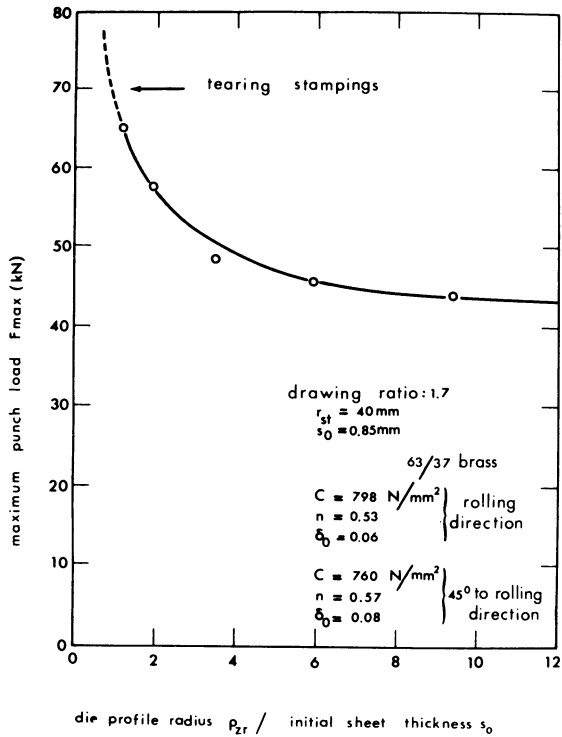


Fig. 12 Experimental values of the necessary drawing force as a function of the relative die-edge radius.

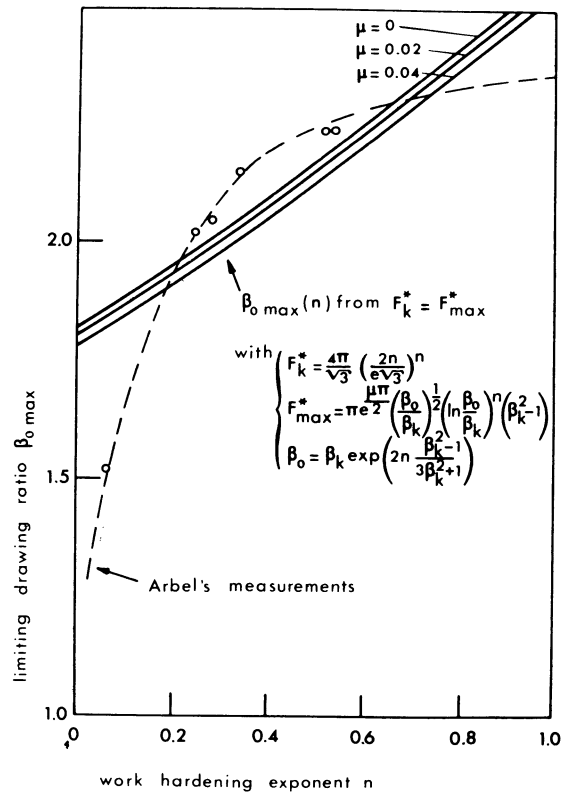


Fig. 14 Theoretical work-hardening effect on the limiting drawing ratio compared with experimental data of Arbel³.

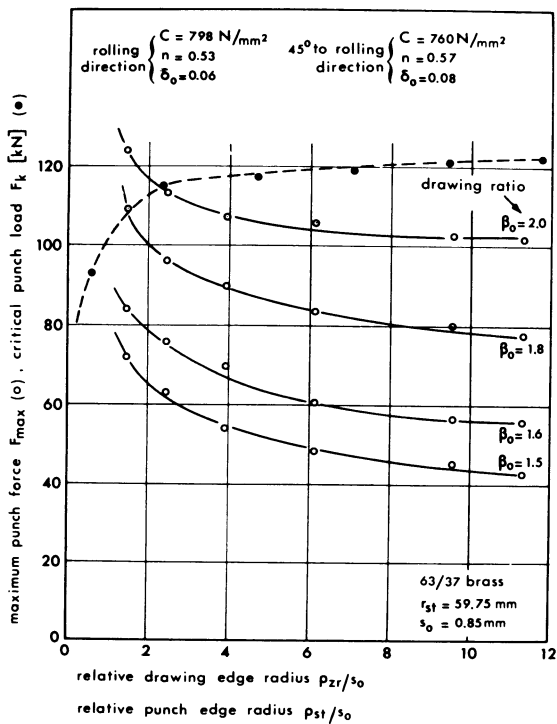


Fig. 13 Experimental curves representing the required drawing force F_{max} as a function of the relative die-edge radius ρ_{2r}^* for different values of the drawing ratio β_0 and the critical-punch load F_k as a function of the relative punch-edge radius ρ_{st}^* .

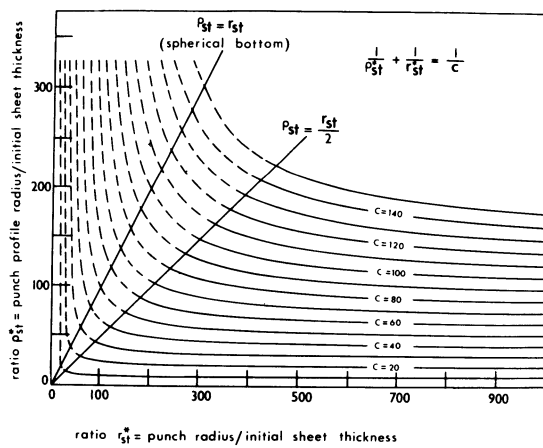


Fig. 15 Curves representing the theoretical condition for geometrical similarity in scale testing.

REFERENCES

1. OEHLER, G. W., and KAISER, K., 'Schnitt-, Stanz- und Ziehwerkzeuge', Springer-Verlag (1957), p. 292.
2. KALS, J. A. G., 'Dieptrekken', Eindhoven University Press (1969), p. 4.15.
3. ARBEL, C., 'The Relation between Tensile Tests and the Deep Drawing Properties of Metals', *Sheet Metal Industries*, 27 (1950), pp. 921-926.
4. SCHRODER, G., and WINTER, K., 'Superplastische Werkstoffe—ein Ueberblick', *Industrie-Anzeiger*, 92, nr. 20 (1970), pp. 425-430.
5. SHAWKI, G. S. A., 'Assessing Deep Drawing Qualities of Sheet'; Part 1: 'Stretch-Forming and Wedge-Drawing Tests', *Sheet Metal Ind.*, 42 (1965) pp. 363-368; Part 2: 'Deep Drawing Tests', *Sheet Metal Ind.*, 42 (1965), pp. 41-424; Part 3: 'Combined Simulative Tests', *Sheet Metal Ind.*, 42 (1965) pp. 525-532.

ADDITIONAL REFERENCES

1. SIEBEL, E., *Steel*, 94 (1934), p. 37.
2. SACHS, G., *Proc. Inst. Automobile Eng.*, 29 (1934), p. 588.
3. CHUNG, S. Y., and SWIFT, H. W., *Proc. Inst. Mech. Engrs.*, 165 (1951), p. 211.

DETERMINATION OF TOOL-LIFE EQUATIONS BY STEP TURNING TEST

by

T. S. KIANG and G. BARROW*

SUMMARY

Conventional tool-life tests involve large consumption of work material and testing time. They are also restricted to a large extent to machines with continuously variable spindle speed drive. The method described here approximates the variable machining-rate test by a number of small constant-speed steps. The tool-life equations thus obtained agree well with those established by conventional tests. The test can be conducted on any normal machine-shop lathe and the savings of material and time over conventional tests are significant.

INTRODUCTION

The conventional laboratory method of tool-life testing, first studied by Taylor¹ in 1907, usually consists of machining with a cutting tool, either until complete failure occurs or to a predetermined amount of flank wear, measured by a microscope. In either case, the test demands a great deal of time and material, and thus involves considerable cost in order to obtain a relatively small amount of tool-life data. It is obvious, therefore, that methods for the rapid evaluation of tool life, using a small amount of material and at less cost, are desirable.

Many rapid and approximate test methods have been evolved and investigated by various workers, a number of which have been described and discussed by Kiang². However, because of various practical limitations and associated shortcomings, these methods are still not widely accepted as standard testing methods.

Of these methods, the facing test has been most extensively studied³⁻⁷. It involves an operation in which the linear increase in cutting speed with time is observed. Sun⁸ showed that the adjustment to the equilibrium conditions (for example temperature, force, and so on) during facing cuts should be quite rapid. In the facing test, the cutting speed, instead of being changed to another steady value (as in the conventional test), is varied gradually but continuously. It can be expected that, however rapid the response of the various cutting characteristics to the changes in cutting conditions, there could be a persistent gap between the changes and responses. Thus, the actual cutting conditions may not correspond to the steady-state conditions. Furthermore, the facing test also

suffers from the inherent disadvantage that the cut is taken towards the periphery, from a point near the centre of the bar and it is in this region where the largest probability of material variation would be expected from a metallurgical point of view. These are the main reasons that the facing test does not produce accurate tool-life data.

Heginbotham and Pandey^{9,10} have studied two other variable machining tests—taper turning and variable-speed turning—with a view to eliminating the effect of material variations in the radial direction of the test bar. Using these methods, the time taken in a test when operating between two particular cutting speed limits can be controlled effectively. However, it is still not known when the rate of increase in cutting speed in a taper-turning or variable-speed turning test will produce inaccurate results because of temperature lag or lead.

It seems that the variable machining operation can be represented by a large number of small constant-speed steps in order to eliminate the temperature lagging effect on the total performance of the tool and thus the accurate determination of tool-life equations. The cutting time is extended sufficiently to allow steady-state conditions to be established during each step. The method has been studied¹¹ using only two cutting steps. It is proposed that the number of steps should be increased, the validity and practical application of which is studied in this work.

ANALYSIS

To facilitate the analysis of the test, the concept of 'degree of wear, G ' is introduced, expressing the ratio of the tool wear (at a given moment of time) to the

*Machine Tool Engineering Division, UMIST

accepted wear criterion; that is, at the initial moment of cutting $G = 0$ (for a new sharp tool), and $G = 1$ when the permissible amount of tool wear is reached.

The tool-life criterion chosen for the present work was 0.015 in mean flank wear, and therefore

$$G = \frac{\text{amount of mean flank wear reached in time } t}{0.015}$$

The Taylor tool-life equation states that

$$VT^n = C \quad (1)$$

and this may be re-written as

$$T = \left(\frac{C}{V}\right)^{1/n} \quad (2)$$

Then the amount of tool life consumed, per unit time, at a particular speed would be

$$\frac{1}{T} = \left(\frac{C}{V}\right)^{1/n} \quad (3)$$

In the variable rate test, the cutting speed is a continuous function of time. Thus the fraction of tool life reached at V_1 after a time interval t_1 would be

$$\int_0^{t_1} \left(\frac{V_1}{C}\right)^{1/n} dt = \left(\frac{V_1}{C}\right)^{1/n} t_1$$

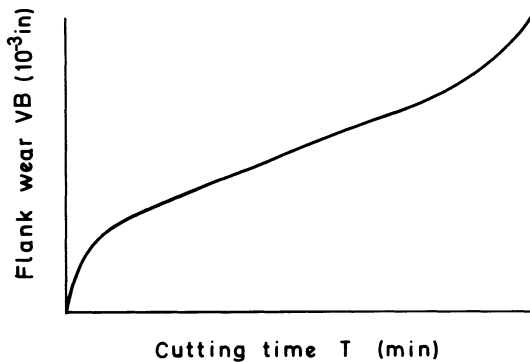


Fig. 1 A typical flank wear-cutting time curve

Now, assuming that the flank wear/cutting time curve follows a linear relationship (a typical curve of which is shown in Fig. 1) when the test is performed in a step manner the time periods have a discrete character; thus, tool life is determined by direct summation of the individual tool-life values reached during each step of constant-speed turning. Therefore, when the tool fails

$$\sum_{i=1}^m \left(\frac{V_i}{C}\right)^{1/n} t_i = 1$$

If the fraction of tool life is reached after m steps, then

$$\sum_{i=1}^m \left(\frac{V_i}{C}\right)^{1/n} t_i = G \quad (4)$$

$$\text{or } \sum_{i=1}^m \frac{t_i}{T(V_i)} = G \quad (5)$$

because T is a function of V .

If two tests are conducted, a set of simultaneous equations will result

$$\sum_{i=1}^{m_1} \left(\frac{V_i}{C}\right)^{1/n} t_i = G \quad (6)$$

$$\text{and } \sum_{i=1}^{m_2} \left(\frac{V_i}{C}\right)^{1/n} t'_i = G' \quad (7)$$

After expansion, these may be written as

$$\left(\frac{V_1}{C}\right)^{1/n} t_1 + \left(\frac{V_2}{C}\right)^{1/n} t_2 + \dots + \left(\frac{V_{m_1}}{C}\right)^{1/n} t_{m_1} = G \quad (8)$$

$$\left(\frac{V'_1}{C}\right)^{1/n} t'_1 + \left(\frac{V'_2}{C}\right)^{1/n} t'_2 + \dots + \left(\frac{V'_{m_2}}{C}\right)^{1/n} t'_{m_2} = G' \quad (9)$$

If the cutting conditions are so chosen that

$$t_1 = t_2 = t_3 = \dots = t_{m_1} = t$$

$$\text{and } t'_1 = t'_2 = t'_3 = \dots = t'_{m_2} = t'$$

$$\text{and } m_1 = m_2 = m$$

$$V_1 = V, V_2 = aV, V_3 = a^2V, \dots, V_m = a^{m-1}V$$

$$\text{and } V'_1 = V^1, V'_2 = bV^1, V'_3 = b^2V^1, \dots, V'_m = b^{m-1}V^1$$

$$\text{for } 0 < a < 1, \quad \text{and} \quad 0 < b < 1$$

Equations (8) and (9) become

$$\left(\frac{1}{C}\right)^{1/n} t V^{1/n} [1 + a^{1/n} + (a^{1/n})^2 + (a^{1/n})^3 + \dots + (a^{1/n})^{m-1}] = G \quad (10)$$

$$\text{and } \left(\frac{1}{C}\right)^{1/n} t' V'^{1/n} [1 + b^{1/n} + (b^{1/n})^2 + (b^{1/n})^3 + \dots + (b^{1/n})^{m-1}] = G'$$

Dividing equation (10) by equation (11)

$$\left(\frac{t}{t'}\right) \frac{V^{1/n}}{V'} \frac{\sum_{i=0}^{m-1} (a^{1/n})^i}{m-1} = \frac{G}{G'} \quad (12)$$

Assuming that the $\log T - \log V$ of the Taylor equation is a straight line, and making $b = a$, n can be found from equation (12), as

$$n = \log\left(\frac{V}{V'}\right) / \log\left(\frac{Gt'}{G't}\right) \quad (13)$$

The value of C can then be calculated from equation (10) or equation (11).

PRESENT INVESTIGATION

All the tests were conducted on a Swift testing lathe, the spindle speed and sliding feed of which was infinitely variable between 104–5000 r.p.m. and 0.0002–0.048 in/rev., respectively.

Two workpiece materials were used for the tests—En 8 and En 26 according to BS 970:1955. Two grades of Kenna-metal carbide inserts—K11 and K3H were used for the respective work materials.

The test pieces were 6 in diameter, 2 ft long bars in the ‘as received’ condition. The cutting conditions chosen were: feed = 0.008 in/rev., and depth of cut = 0.080 in. The cutting speeds were selected in the range 500–900 ft/min⁻¹.

RESULTS AND DISCUSSION

Initially the tests were performed using new sharp tools. It was found that the results (Tables 1 and 2) were not satisfactory. The values of n and C were somewhat higher than those found from conventional tests.

Table 1.

Work/Tool pair	Speed-range	Pre-worn	G	t
En8/K11	570–700	—	0.473	2
	489–600	—	0.46	2.5
	728–900	0.009 0.0096	0.36 0.42	1.5
	570–700	0.0095 0.0078	0.286 0.286	2
En26/K3H	489–600	—	0.42 (average of 2 min)	1
	406–500	—	0.466 (average of 3 min)	1.5
	489–600	0.0078 0.0082	0.267 0.24	1
	406–500	0.0084 0.0087	0.213 0.233	1.5

Table 2

Work/Tool pair	Step turning test			Conventional test
		New sharp tools	Pre-worn tools	
En8/K11	n	0.611	0.554	0.58
	C	4085	4400	4000
En26/K3H	n	0.645	0.345	0.352
	C	2718	1526	1250

In view of this discrepancy it was necessary to check the validity of the analysis by means of the available data. Using the results from the conventional tests, the following calculations were made.

The analysis shows that the fraction of tool life reached after m steps is expressed by equation (5)

$$G = \sum_{i=1}^m \frac{t_i}{T(V_i)}$$

Now, taking En 8/K 11 as a test sample, the theoretical tool life reached after five steps should be (from Fig. 2):

$$G = \frac{2}{34.7} + \frac{2}{32} + \frac{2}{29} + \frac{2}{26.5} + \frac{2}{24.1} = 0.348$$

However, the actual tool life consumed was

$$G = \frac{0.0062}{0.015} = 0.473$$

Similarly $GT' = 0.332$

$$\text{and } G' = 0.46$$

Using G and GT the values of n and C were found to be 0.557 and 4406 respectively, which were in good agreement with those obtained from the conventional test and indicated that the analysis was correct.

The values of G , which are higher than the theoretical values, are thought to be attributable to the first phase of flank wear/cutting time characteristics (that is the initial rapid wear period) (Fig. 1). The cutting speeds used in the tests were well above 500 ft/min⁻¹, therefore b.u.e. would not affect the results. In the conventional tests, this rapid wear period occurs at all speeds and the cutting time is usually extended sufficiently so that the final results are hardly affected. In the step turning test, it has been assumed that the relationship between flank wear and cutting time is linear. However, example (4) does not take this initial rapid wear into account. Therefore, the actual tool wear (G) will inevitably be higher than the theoretical values. Thus an error is introduced when subsequently computing n and C . This phenomenon was also observed by Heginbotham and Pandey⁹. When pre-worn tools were used, this rapid wear phase could be entirely eliminated. The flank wear would proceed in the 'as worn' conditions and assume a linear relation with time. Furthermore, it is well known that the variations in the results of tool-life tests are usually great. Therefore, repeat tests at each speed range are necessary and the average values of G must be used.

As the tests were not orthogonal it was necessary to put the artificial wear land on the tool flank face as well as on the nose radius. This is a difficult operation and it was decided to produce it by actually

cutting the workpiece with the tool at high speed and low feed. Using this method, a wear land of 0.009 in could generally be obtained within 7 min of cutting and the amount of material consumed was very limited. To obtain a more natural wear land, the tools were run-in for about 30 s at the first speed of the range of speeds tested. The final pre-worn wear land was then measured.

The relationship between flank wear and cutting time was essentially linear beyond 0.007 in flank wear for all speeds. However, in order that the final wear criterion (0.015 in mean flank wear) was not exceeded at the end of a test, and to reduce the effect of possible measuring errors on the results, the pre-worn wear lands were selected between 0.007 and 0.010 in.

Tests results using pre-worn tools are shown in Tables 1 and 2, and Figs. 2 and 3, and it is clear that they correlate very well with those of the conventional tests. There is less than 5% difference in the values of n for the respective work/tool pair. The effect of temperature lag seems to have been removed. The actual responses of the temperature

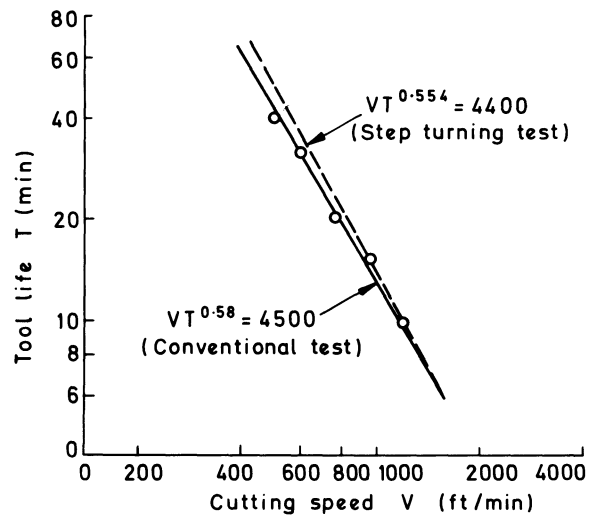


Fig. 2 Tool life-cutting speed relationship (En 8/K11, $s=0.008$ in/rev, $a=0.080$ in)

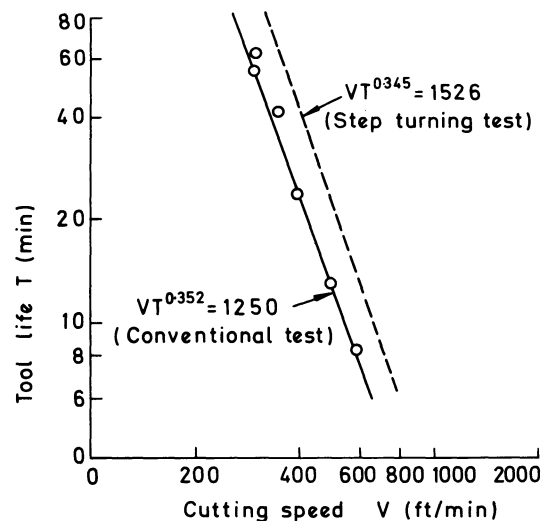


Fig. 3 Tool life-cutting speed relationship (En 26/K3H, $s=0.008$ in/rev, $a=0.080$ in)

Table 3

Test method	Material		Testing time (min)	No. of test tools
	Work/tool pair	consumption (in ³)		
Step turning	En8/K11	214	143	4
	En26/K3H	126	137	4
Conventional	En8/K11	670	392	5
	En26/K3H	565	660	6

and force were not measured for each change of speed. However, the temperature tests indicated that the response was very rapid indeed. Therefore, when the cutting intervals t were chosen between 1 and 2.5 min, steady-state conditions were used for most of the time interval.

As one set of tests could be completed within one or two passes along the test bar, the material variation could hardly affect the results. Depending on circumstances, this effect may to some extent be even less than in the conventional test. It is thus clear that step turning is a valid approximation to, and possibly a replacement for, the conventional test. However, there is a limitation to the applicability of the test, in that it can only be applied to work/tool pairs which have a linear relationship between $\log T$ and $\log V$ as this is the basic assumption made in the analysis.

Repeatability is a problem facing all forms of tool-life tests, variations of up to 200% having been observed in some cases. Initial tests using step turning indicated that this was so. Results from a single set of tests are neither accurate nor reliable; at least one repeat test is necessary to obtain an average value of G for subsequent calculations. As the demand for testing time and material is small (Table 3) when using step turning tests, repeat tests can be done without involving too much cost.

Reasonable values of a and t for the tests were chosen arbitrarily, and seemed to be satisfactory. To approximate the facing test, the number of steps used should be large; twenty or thirty steps can be used with a cutting time of, say, 20 s for each step, which is sufficiently long to allow the steady-state conditions to be established. If this is done, the effect on tool life for engaging and disengaging the tool, some 20 or 30 times within 10 min of cutting, will become rather considerable, as suggested by Barrow and Spencer¹². It seemed therefore, that $m = 5$ was a reasonable choice, which has been justified by demonstration.

Conventional tests are restricted to a certain extent to machines with continuously adjustable spindle speeds and this limits the possibility of establishing tool-life equations to metal cutting laboratories which have lathes with a special drive for stepless control of spindle speeds.

In this investigation the cutting conditions have been chosen so that equations (8) and (9) can be solved without the aid of a calculating machine. A lathe with infinitely variable spindle speeds was used for the tests, and it was then a relatively simple matter to select a convenient value of speed ratio a

to cover a reasonable speed range within which b.u.e. was unlikely to be formed. In an ordinary machine shop in which this type of special lathe is not available, tests can be carried out on a lathe which has spindle speeds arranged in a fixed ratio. In this case, the length of the bar should be sufficiently long that one test can be completed within one pass along the bar. If this is not possible, equations (8) and (9) have to be solved as they are.

CONCLUSIONS

From this series of tests on both En 8 and En 26, using carbide tips, it has been demonstrated that the step turning test has several advantages over conventional tests and other quick testing methods:

- (a) Information regarding the tool life and machinability of various materials can be obtained within a very short period of time. The savings over the conventional test vary between 200–400%.
- (b) Consumption of test material is low, being about 25–30% of that required in conventional tests.
- (c) With a sufficient number of repeat runs (at least one repeat) test results are comparable with those obtained by conventional tests.
- (d) The method is simple and can be performed equally well on any conventional machine shop lathe with little extra effort in mathematical calculations.

To obtain reliable test results all test tools should be pre-worn and the cutting intervals should be so chosen that the flank wear/cutting time characteristics operate in the linear region for all cutting speeds.

Tests using new sharp tools produce values of n and C which are too high and cannot be relied on, which is attributed to the initial rapid wear during the first step turning.

Although the advantages of using the step turning test are apparent, considerable experimental care is required in order to obtain accurate results. Moreover, good results cannot be expected on all tool and workpiece combinations. With these points in mind we recommend the use of step turning tests only in cases in which conventional tests are impossible and by personnel with experience of machinability testing.

REFERENCES

1. TAYLOR, F. W., 'On the Art of Metal Cutting,' *Trans. A.S.M.E.*, **28** (1970), p. 31.
2. KIANG, T. S., M.Sc. Dissertation, Victoria University of Manchester (1970).
3. KRAUS, C. E., and WEDDELL, R. R., 'Determination of Tool Life Cutting Relationship by Facing Cuts,' *Trans. A.S.M.E.*, **59** (1937), p. 885.
4. LORENZ, G., 'Determination of Tool Life Exponent from Quick Facing Tests,' *C.I.R.P. Annals*, **XII** (1963), p. 217.
5. KARDOX, A., 'Comparative Analysis of Some Rapid Tool Life Determination Methods,' *Acta Technicon Hung.*, **46** (1964), p. 95.
6. BROWN, R. H., and TAO, H. S., 'Machinability Testing for the Production Workshop,' Factory and Plant (Australia) (1965), p. 38.
7. RADHA KRISHNA, M. A., and ARORA, R. P., 'Comparison of Methods of Machinability Rating,' *Inst. Engrs. (India)-J.*, **48**, No 9, Part ME5 (1968), p. 523.
8. SUN, E. Y. C., Ph.D. Thesis, Victoria University of Manchester (1955).
9. HEGINBOTHAM, W. B., and PANDEY, P. C., 'Taper Turning Tests Produce Reliable Tool-Wear Equations,' *Advances in M.T.D.R.* (1966), p. 515.
10. HEGINBOTHAM, W. B., and PANDEY, P. C., 'A Variable Rate Machining Test for Tool Life Evaluation,' *Advances in M.T.D.R.*, **163** (1967).
11. PODURAEV, V. N., and YAROSLAVTSEV, V. M., 'Tool Life in Interrupted Cutting,' *Russian Machines and Tooling*, **XV**, No. 10 (1968), p. 37.
12. BARROW, G., and SPENCER, R. M., 'Some Factors Influencing the Reliability of Tool Life Tests,' *C.I.R.P. Annals*, **XVIII** (1970), p. 199.

DISCUSSION*Query from A. H. Redford, USALF*

There would appear to be two features of the step turning test which raise doubts about its usefulness. Firstly, if as appears to be the case, there is to be an international standard on machinability tests with standard tool failure criteria, the results of any tests where the wear is less than that recommended cannot establish, beyond doubt, that the tool would not have reached the tertiary wear stage before the completion of a standard long-term test.

Secondly, it is inevitable that, as the change in tool wear to be measured decreases, any errors in measurement of the wear become more significant. It would be of interest to know what the authors consider to be the minimum amount of wear which could be measured for the results to be significant.

Reply

Dr. Redford has raised two important points regarding the step turning test. With reference to the first point, it is possible with experience to know which combinations of tool and workpiece materials will give wear lands of the value proposed in the standard

test (i.e. 0.015 in. or 0.4 mm). However, in general it is preferable to run the test in such a way that 0.015 in. mean flank wear has been reached at the end of the test. If this is done with the highest speed as the last step, it is reasonable to assume that 0.015 in. mean flank wear would be reached over the range of speeds tested.

If the final wear on the tool at the end of the test is 0.015 in. and a sharp tool was used, the measuring accuracy is the same as that used in the conventional test. However, if preworn tools are used, it is essential to have the preworn land of a reasonable size (say 0.007 in.) so that both this value and the amount worn in the test of approximately 0.008 in. can be measured with a reasonable degree of accuracy.

Query from J. B. White, South Australian Institute of Technology

This contribution is perhaps equally relevant to the paper 'Tool Life Equations and Machining Economics' by G. Barrow.

Some researchers use with enthusiasm the facing test, coupled with a statistical analysis of the results, as a quick and allegedly-reliable means of predicting both the tool-life component n and the cutting speed for a 60 min. tool-life '1/60'. Would the author please elaborate on the merits that he considers the step turning test may have over the facing test?

From analyses I have made of a few sets of facing test data with approximately 35 tests per specimen at varying speeds, the safe V_{60} have been approximately only 50% of the mean V_{60} . By 'safe V_{60} ' I define the speed which would give not more than 2½ % (nominally) failures if used in real operation. The mean V_{60} is obtained from a regression analysis of the 35 sets of data and must lead to 50% premature failure in real operations.

I would appreciate the authors' comments on my view that 'any test data and analysis thereof which does not yield the lower safe limits of n or V_{60} cannot be of any significant value to an engineer or technician planning real processes'.

Reply

We have run comparative tests of the facing and step turning methods and found that far less material and time (in some cases only 25%) is used in the step turning test for the same degree of confidence. In addition to this, the facing test is not really suitable for small diameter barstock.

The authors do not agree with Mr. White that any test which does not yield the lower safe limits of n or V_{60} values is of no practical use, since the mean values obtained in a laboratory test can be (and have been) successfully modified for use under practical conditions. Whilst in certain cases statistical techniques can be advantageous, it should be remembered that when using a regression analysis for tool-life studies, it is usual to make the dubious assumption that the $\log T - \log V$ plot is a straight line. Several workers in the past have done this and have in our opinion produced V_{60} values of less significance than by a graphical technique. This last comment does not

apply to the step turning test, since we have assumed a linear Taylor plot and recommended its use only where linear Taylor plots are likely to occur.

Query from G. E. Wright

$VT^n = C$ is only true for a given feed, depth of cut, coolant and constant tool geometry, tool material and workpiece material.

In both the taper turning and step turning techniques, the depth of cut is varying constantly and intermittently respectively. For this case the equation should be changed to $VT^n d^m = C_1$ for each depth of cut. Could the author comment on how this has been overcome?

Reply

It is possible that Mr. Wright was misled by some of the slides shown during the presentation of the paper, which do not appear in the published paper. Neither in the case of the taper turning nor step turning test does the depth of cut vary. In view of this the test has to be repeated for various depths of cut etc. and it is better to use the concept of 'equivalent chip thickness' (b_e) and obtain an equation of the form $VT b_e = C$ from a short series of tests.

THE EFFECT OF COMPONENT TOLERANCE ON OPTIMUM MACHINING CONDITIONS

by

J. R. CROOKALL* and R. C. MALTBY*

SUMMARY

The economics of cutting is influenced both by resetting and replacing of tooling, on the grounds of dimensional drift and unserviceability, respectively. Finer tolerances cause a reduction in optimum speeds and feeds, and machining cost and time rise sharply for tolerances below about 0.002 in. The analysis constitutes a fairly general case; omission of the tolerance aspect results in a special case applicable primarily to roughing operations. The effect of relating tolerance to surface finish requirements is also examined.

INTRODUCTION

In a previous paper¹ the 'performance envelope' concept, representing the permissible and desirable regions of machining, was developed. This involved an analysis of both the time and cost of machining, which indicated the 'desirable' regions of operation, according to several criteria. The various constraints on the operating range were examined, such as power, surface roughness, and workpiece deflection. Also, cutting failure modes such as cratering and deformation were considered, as well as the flank-wear mode on which the analysis was based. The present paper examines further the 'economic' aspect with regard to the component tolerance on the dimension being machined, which is of course set by the designer.

Much has been said in a general way about the cost of quality, but this is notoriously hard to quantify. Many believe that the cost C rises exponentially as tolerance δ becomes increasingly fine, according to a function of the form

$$C = \alpha \delta^{-\beta} + \phi \quad (1)$$

where α , ϕ and β are constants. But such general statements must have doubtful applicability in particular circumstances, if they do not take account of the *reasons* for possible cost increases. These might include the necessity for a slower operation, the use of more expensive tooling, or production method itself (for example, grinding instead of conventional cutting), or the necessity for more frequent re-setting attention to compensate for dimensional drift due to wear.

In fact, only if the tool can be permitted to deteriorate to its maximum wear criterion without violating the dimensional tolerance required of the component, will tolerance not affect the optimum conditions of machining. Normally, the dimensional drift which accompanies wear of the tool in use will necessitate resetting of the tool, perhaps several times, before it is deemed to have failed for the purpose of cutting, and therefore needs replacing or regrinding. The exception to this situation is when separate roughing and finishing tools are used, and this is obviously a useful expedient in some instances. However, this paper concerns those cases in which the same tool is used for both roughing and finishing, or a single pass only is taken.

Considerations of optimal machining conditions naturally bring about the high wear rates associated with rapid stock removal, and hence the frequency of attention required for re-setting will obviously become increasingly significant (irrespective of the permitted maximum wear) as component tolerances are decreased.

TIME AND COST EQUATIONS

The economics equation for a production process contains three general terms which are functionally distinct. One expresses the time or cost consumed in setting up and loading the machine, another involves the active (actual cutting) time, and a third term involves the reconstitution of the machine between active periods as a direct result of its use; the latter is in effect a 'rate penalty' term. The first term is independent of the conditions of operation of the

*Imperial College of Science and Technology, London

process itself, and is eliminated on differentiation of, say, the cost equation, to evaluate the minimum-cost operating conditions. The second term decreases as the rate-determining parameters of the process rise, and the last term increases with increasing rate of operation. It is the balance of the opposing factors of the second and third terms which determines the optimum operating conditions. The derivation of time and cost equations for turning, which includes the effect of component tolerance, involves the incorporation in the rate-penalty term of the re-setting aspect occasioned by any given tolerance. The general considerations are otherwise similar to those of the earlier paper¹.

Production time per piece

The time per piece for set-up and loading, t_n , and for turning diameter D over length L , can be expressed as

$$t_n + \frac{\pi DL}{sv} \quad (2)$$

where s and v are respectively the feed and speed of turning. The depth of cut is presumed equal to the depth of the layer to be removed (that is, for single pass). The remaining task is to determine the tool reconstitution time per piece, and this must introduce the frequency with which it is necessary to either reset or change the tool, and hence the tool life and wear rate.

It is necessary to use a generalized tool-life equation, and as previously¹, two alternatives may be considered. Thus a tool-life relationship in which speed, feed and depth of cut, and possibly tool geometrical variables, are separate terms, or a relationship involving the 'equivalent chip thickness' as a simplifying expedient must be used. The two tool-life expressions are

$$v(TQ)^n s^m a^p k^\mu = V \quad (3)$$

$$v(TQ)^n (Gs)^m = \lambda \quad (4)$$

where $G_s = b_e$, the equivalent chip thickness, and

$$G \approx a \left[\frac{a - r(1 - \sin s_c) + r}{\cos s_c} + r(\pi/2 - s_c) \right]$$

The intention here is to adopt the somewhat simpler form of equation (4), for reasons discussed earlier^{1,2}, and associated mainly with the considerable reduction in cost and material in evaluating tool life, using equivalent chip thickness as a parameter.

Fig. 1a represents a typical flank-wear curve at constant speed (that is, the development of the flank wear land ' F ' shown in Fig. 1b). It is normal practice to confine the practical use of a tool to the almost linear 'secondary' region of the curve, as in the 'tertiary' region the wear rate is accelerating, and there is an increasing probability of catastrophic failure. Brewer³ investigated premature failures, and found that their likelihood of occurrence was dependent to the power 2.78 on the permitted flank wear. The wear-time curve is approximated by the linear relationship

$$F = F_f + kt$$

where k is the wear rate dF/dt , and representation of wear behaviour must be within the limit of linearity at F_{fo} . The tool life for any particular value of flank wear F may be obtained using the interpolation fraction

$$Q = \frac{F_{fo} - F_f}{F - F_f}$$

from the generalized expression for tool life

$$T = \frac{1}{Q} \left(\frac{\lambda}{(Gs)^m v} \right)^{1/n} \quad (5)$$

For a component diametral tolerance δ , the tool must be reset when the development of flank wear (Fig. 1b) reaches a value

$$F^* = \frac{\delta}{2} \cot \gamma \quad (6)$$

(neglecting the effect of rake angle). Hence when the permissible flank wear before the tool is *changed* for the general case, is F , the number of resets during the life of a tool is equal to

$$\frac{F - F_f}{F^*} = \frac{2(F - F_f)}{\delta \cot \gamma} = \frac{2(F_{fo} - F_f)}{\delta Q \cot \gamma} \quad (7)$$

This, in effect, represents a 'reset interpolation fraction' Q^* , and the machining time between resets is thus

$$T^* = \frac{\delta \cot \gamma}{2Q(F - F_f)} \left(\frac{\lambda}{(Gs)^m v} \right)^{1/n} \quad (8)$$

The number of resets per piece is represented by the time to turn length L divided by the time between resets, and the product of this and the tool-resetting time t_s gives the tool-resetting time per piece as

$$\frac{2\pi DL t_s (F_{fo} - F_f)}{\delta \cot \gamma} \frac{v^{1/n-1} s^{m/n-1} G^{m/n}}{\lambda^{1/n}} \quad (9)$$

Obviously, the number of resets during the life of the tool must in practice be an integer. This may be derived from equations (5) and (8) as T/T^* , and it is evident that this is the same as equation (7).

Considerations of tool *changing* frequency are similar. Hence the number of tool changes per piece times the tool-changing time t_w gives the tool-changing time per piece, which becomes

$$\pi DL Q t_w \frac{v^{1/n-1} s^{m/n-1} G^{m/n}}{\lambda^{1/n}} \quad (10)$$

Thus the total time per piece to machine a component is the sum of equations (1), (9) and (10), giving

$$T_p = t_n + \pi DL \left[\frac{1}{sv} + \frac{v^{1/n-1} s^{m/n-1} G^{m/n} Q}{\lambda^{1/n}} \right] \times \left(\frac{2t_s(F-F_f)}{\delta \cot \gamma} + t_w \right) \quad (11)$$

Minimum production time per piece

In the usual way, differentiation of equation (11) with respect to each of the metal-removal parameters v and s in turn, will yield the minimum production time per piece. Thus, with respect to speed

$$\frac{\partial T}{\partial v^p} = 0 = \pi DL \left[-\frac{1}{sv^2} + \frac{v^{1/n-2} s^{m/n-1} G^{m/n} Q}{\lambda^{1/n}} \right] \times \left(\frac{1}{n} - 1 \right) \left(\frac{2t_s(F-F_f)}{\delta \cot \gamma} + t_w \right)$$

giving

$$v_{to} = \frac{\lambda}{(Gs)^m} \left[Q \left(\frac{1}{n} - 1 \right) \left(\frac{2t_s(F-F_f)}{\delta \cot \gamma} + t_w \right) \right]^{-n} \quad (12)$$

and with respect to feed

$$\frac{\partial T_p}{\partial s} = 0 = \pi DL \left[-\frac{1}{s^2 v} + \frac{v^{1/n-1} s^{m/n-2} G^{m/n} Q}{\lambda^{1/n}} \right] \times \left(\frac{m}{n} - 1 \right) \left(\frac{2t_s(F-F_f)}{\delta \cot \gamma} + t_w \right)$$

hence

$$s_{to} = \frac{1}{G} \left(\frac{\lambda}{v} \right)^{1/m} \left[Q \left(\frac{m}{n} - 1 \right) \left(\frac{2t_s(F-F_f)}{\delta \cot \gamma} + t_w \right) \right]^{-n/m} \quad (13)$$

There is therefore no absolute minimum time per piece in terms of both speed and feed; thus for constant s there is a speed for minimum time and vice versa. Lowest overall time for the single-pass case* is achieved by using the highest practical feed, and the associated v_{to} . The subject of constraints has been treated more fully in an earlier paper¹.

Production cost per piece

If production costs are regarded as cost-weighted times, the establishment of the equation for total cost of machining, already given that for production time, is relatively straightforward. However, aspects such as tool depreciation cost, which have no counterpart in the time equation, are additional. It is partly for this reason that the optimum operating conditions when evaluated on a cost basis almost inevitably differ from those derived from the time analysis. Hence minimum

*However it has been demonstrated elsewhere⁴ that, although this holds for a single pass, under certain conditions, lowest overall cycle time is obtained when more than one pass is taken.

cost and minimum-time operation cannot be achieved simultaneously.

Proceeding in a similar manner, the cost of set-up and loading time, and of machining time, can be obtained from equation (2) by a cost 'weighting' R_1 , which represents the total overhead, machine-hour rate, and direct labour costs (but excluding tooling costs) per unit time, giving

$$R_1 (t_n + \frac{\pi DL}{sv}) \quad (14)$$

The cost of the time required to reset, and to change the tool, can also be obtained as products of R_1 and the resetting time per piece and the tool-changing time per piece, from equations (9) and (10), respectively. Hence cost of resetting time and tool-changing time is

$$\pi DL R_1 \frac{v^{1/n-1} s^{m/n-1} G^{m/n} Q}{\lambda^{1/n}} \times \left(\frac{2t_s(F-F_f)}{\delta \cot \gamma} + t_w \right) \quad (15)$$

However, the additional factor of the cost of providing the cutting edge itself must now be considered.

The two types of cutting tool used in practice are the indexable insert type and the integral type, and reconstitution is of course different for each. Thus, whilst a tool change with the indexable or 'throw-away' type simply involves turning the insert to a fresh cutting edge, the integral type must be removed completely for regrinding. The cost of regrinding can be considered as the sum of costs which are independent of the amount to be ground away, expressed as R_2 money units per regrind, and costs involved in reconstituting the tool point. The latter consists in grinding back the flank face of the tool by an amount $F \sin \gamma$ (see Fig. 1b), plus an additional safety margin q to remove any possibly damaged material near the tool edge. If R_3 is the cost of grinding unit depth of clearance face (hence the total cost for the cutter-grinding operation is involved, in a manner analogous to that being considered here), the cost of a regrind is equal to

$$R_2 + R_3 (q + F \sin \gamma)$$

The regrinding cost per piece involves the frequency of the necessity for tool changing [compare with equation (10)], and becomes

$$\pi DL Q \frac{v^{1/n-1} s^{m/n-1} G^{m/n}}{\lambda^{1/n}} \times \left[R_2 + R_3 (q + F \sin \gamma) \right] \quad (16)$$

In the case of throwaway tips, $R_2 = R_3 = 0$, and hence this whole expression becomes zero.

Tool depreciation at each reconstitution will depend, in the case of regrindable tools, on the fraction of available material (and hence total available life) which is to be ground away, or for indexable inserts upon the number of available cutting edges. For regrinding, if the total removable stock is U , the possible number of regrinds will be $U/(q + F \sin \gamma)$. Thus for a tool costing W money units, the depreciation cost per cutting edge is

$$\frac{W}{e + U/(q + F \sin \gamma)}$$

For integral tools $e = 1$. For indexable inserts, e is set equal to the number of cutting edges available (typically 3, 4, 6 or 8), and $U = 0$. Hence the general expression for depreciation cost per piece is

$$\pi DL Q \frac{v^{1/n-1} s^{m/n-1} G^{m/n}}{\lambda^{1/n}} \left[\frac{W}{e + U/(q + F \sin \gamma)} \right] \quad (17)$$

The total cost per piece of machining is the sum of equations (14), (15), (16) and (17), giving

$$C = R_1 t_n + \pi DL \left[\frac{R_1}{sv} + \frac{v^{1/n-1} s^{m/n-1} G^{m/n} Q}{\lambda^{1/n}} \right. \\ \left. \times \left\{ R_1 \left[\frac{2t_s(F - F_f)}{\delta \cot \gamma} + t_w \right] + R_2 \right. \right. \\ \left. \left. + R_3 \left(q + F \sin \gamma \right) + \frac{W}{e + U/(q + F \sin \gamma)} \right\} \right] \quad (18)$$

It should perhaps be repeated at this stage that equations (11) and (18) have been derived assuming the tool-life equation (4) involving equivalent thickness as a parameter. The equivalent equations for time and cost of machining in terms of the alternative equation (3) are obtained simply by substituting the term $a^{p/n} k^{u/n}$ for the term $G^{m/n}$ in equations (11) and (18).

Minimum cost per piece

Differentiating equation (18) with respect to cutting speed yields

$$\frac{\partial C}{\partial v} = 0 = \pi DL \left[-\frac{1}{sv^2} + \frac{Q v^{1/n-2} s^{m/n-1} G^{m/n} \left(\frac{1}{n} - 1 \right) S}{\lambda^{1/n}} \right]$$

where

$$S = R_1 \left(\frac{2t_s(F - F_f)}{\delta \cot \gamma} + t_w \right) + R_2 \\ + R_3 (q + F \sin \gamma) + \frac{W}{e + U/(q + F \sin \gamma)}$$

Thus the cutting speed for minimum cost is

$$v_{co} = \frac{\lambda}{(Gs)^m} \left[\frac{R_1}{QS} \left(\frac{n}{1-n} \right) \right]^n \quad (19)$$

and similarly the feed for minimum cost is

$$s_{co} = \frac{1}{G} \left(\frac{\lambda}{v} \right)^{1/m} \left[\frac{R_1}{QS} \left(\frac{n}{m-n} \right) \right]^{n/m} \quad (20)$$

Thus no absolute minimum cost per piece exists, the situation being analogous to that for production time, considered previously.

Cost and time relationships

The relationship between cutting speeds for minimum cost and minimum time can be obtained from equations (12) and (19). Setting

$$Y = \frac{2t_s(F - F_f)}{\delta \cot \gamma} + t_w$$

representing the combined time for tool resetting and tool changing, and

$$Z = R_2 + R_3 (q + F \sin \gamma) + \frac{W}{e + U/(q + F \sin \gamma)}$$

representing the combined replacement costs of the cutting edge itself at each replacement

$$\frac{S}{R_1 Y} = 1 + \frac{Z}{R_1 Y} \quad (21)$$

as $S = R_1 Y + Z$. Thus the minimum-time cutting speed will always exceed the minimum-cost speed by the additional factor $Z/R_1 Y$, representing the balance of costs of the tool itself per cutting edge and that of the tool-changing time. The implications are that tooling which is itself expensive (for example, a milling cutter), or inexpensive tools which can be rapidly changed (for example, throwaway inserts) will cause greater separation of the respective minima in terms of cost and time.

It can be shown that the optimum machining conditions, whether in terms of cost or time, occur at constant values of tool life. The constant tool life for minimum cost is different from that for minimum time, and this underlies the separation of machining conditions for these two criteria. From equation (5), the tool life T_{co} corresponding to v_{co} is

$$T_{co} = \frac{1}{Q} \left[\frac{\lambda}{(Gs)^m v_{co}} \right]^{1/n} \quad (22)$$

Substituting the right-hand side of equation (19) into equation (22), the tool life for minimum cost is obtained

$$T_{co} = \frac{s}{R_1} \left(\frac{1}{n} - 1 \right) \quad (23)$$

Similarly, from equations (5) and (12), the tool life for minimum time is

$$T_{to} = Y \left(\frac{1}{n} - 1 \right) \quad (24)$$

Thus tool life at minimum time depends only on the combined tool resetting and changing factor Y , and

the speed index n of the tool-life relationship, and is thus constant for a given tool/work situation. In fact the effect of optimization is to select the cutting variables in a way which makes the tool life equal to the value pre-determined by equation (23) or (24). The tool life for minimum cost, T_{co} , will only equal T_{to} in the unusual case when

$$Y = \frac{s}{R_1}$$

i.e. when the replacement tooling is of zero cost.

The effect of component tolerance

Consider the 'open tolerance' case, that is when

$$\frac{2t_s (F - F_f) = 0}{\delta \cot \gamma}$$

This now represents the 'normal' case when the effect of tolerance is not considered. The effect of component tolerance can be related to this 'open tolerance' case as a ratio. Denoting the 'open tolerance' value of a parameter* by a prime, the ratio of minimum-cost cutting speed for a tolerated cut to that without tolerance, can be shown to be

$$\frac{v_{co}}{v_{co}'} = \left(\frac{S'}{S}\right)^n \tag{25}$$

which is

$$\frac{v_{co}}{v_{co}'} = \frac{R_1 t_w + Z}{R_1 \left[t_w + \frac{2t_s (F - F_f)}{\delta \cot \lambda} \right] + Z} \tag{26}$$

In terms of the speed for minimum time, it can be seen that

$$\frac{v_{to}}{v_{to}'} = \left(\frac{Y'}{Y}\right)^n = \left(\frac{t_w}{Y}\right)^n$$

which is

$$\frac{v_{to}}{v_{to}'} = \left[\frac{t_w}{t_w + \frac{2t_s (F - F_f)}{\delta \cot \gamma}} \right]^n \tag{27}$$

Thus the relative effect of tolerance upon the optimum cutting speeds in terms of either cost or time increases as the tolerance itself is made finer with respect to the permissible flank wear†, and also as the resetting time increases.

*'Open tolerance' in this context implies $\delta \geq 2F \tan \gamma$, and not $\delta = \infty$.

†Note that the 'permissible flank wear' which is implied in this analysis is that which occurs at the constant wear rate $dF/dt=k$, namely $(F-F_f)$. In the use of this analysis in practice, particularly if relatively fine tolerances are involved, the fairly standard practice of using tools with slightly radiussed cutting edges should be adopted, allowing wear due to cutting to begin in the region of F_f . In any case this would be wise practice, to avoid the rapid 'primary' stage of wear, in which the dimension cut would be changing quite rapidly relative to the tolerance required. The alternative might be to take a 'running-in' cut. This aspect becomes less significant as δ/F_f increases.

Similarly for optimum feeds

$$\frac{s_{co}}{s_{co}'} = \left(\frac{S'}{S}\right)^{n/m} \tag{28}$$

$$\frac{s_{to}}{s_{to}'} = \left(\frac{Y'}{Y}\right)^{n/m} \tag{29}$$

and for optimum tool lives

$$\frac{T_{co}}{T_{co}'} = \frac{S}{S'} \tag{30}$$

$$\frac{T_{to}}{T_{to}'} = \frac{Y}{Y'} \tag{31}$$

Evidently the optimum tool lives increase as the tolerance becomes finer, and this has a reciprocal effect upon the cutting parameters speed and feed. The inevitable effect upon production cost and time is detrimental. This relative increase in production cost and time can be judged from equations (18) and (11), but the resulting expressions remain unwieldy. The effect can best be demonstrated by an examination of computed values.

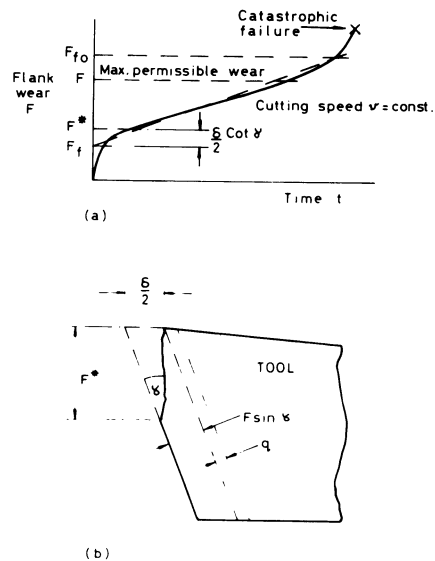


Fig. 1 The effect of component tolerance upon optimum machining conditions.

COMPUTED RESULTS

A computer program was used to evaluate the effect on machining XC45 steel with a P.30 carbide tool, for varying speeds and component tolerances. The program output includes cost and time per inch turned, tool life, tool resetting cost, velocity at minimum cost, velocity at minimum time and power consumption.

However, two alternative circumstances are likely to obtain in the finish-machining region:

- (a) that the tolerance criterion is independent of surface roughness, in which case the latter is simply maintained within a given maximum value;
- (b) that tolerance and surface roughness criteria are related, thus better surface finishes are associated with finer tolerances.

These two circumstances will be investigated separately.

The effect of tolerance for constant surface roughness

The general effect of tolerance on optimum cutting speeds and tool lives is shown in Fig. 2. The stepwise appearance of the curves represents the increasing number of resets required (which can only be integer quantities) as the tolerance becomes finer. It should be noted that as the tolerance tends towards zero, the velocities at minimum cost and time also tend to zero, and tool life tends to infinity, as does the cost and time of machining. The values of v_{co} and v_{to} vary according to the component tolerance, and the 'normal' optimum conditions are true only for roughing operations where no tool resetting is required. In practice however, where a single cut must confer the correct dimension within tolerance, different optimum conditions must ensue according to the tolerance required. This can be seen also from equations (26) and (27) for the economic cutting speeds, and equations (30) and (31) for the economic tool lives.

Machining times (and also costs) are presented as time (or cost) per piece per unit turned length circumferentially (i.e. for the case when $\pi DL=1.0$). The relationship of machining time with speed and tolerance is plotted bi-logarithmically in Fig. 3a. The 'open tolerance' case is here represented by the curve $\delta \geq 0.0045$ in (that is, $\delta \geq 2F \tan \gamma$), which gives the cutting speed at minimum time as 755 ft/min. At this speed the time per unit length is 0.025 min/in. However at the fine tolerance of 0.0005 in the time per unit length at the same speed would be 0.054 min/in, that is, a time estimate would be in error by a factor of two. Machining to this tolerance it may be seen that the cutting speed should be 480 ft/min, and the time per unit length would then be 0.04 min/in, this reduction in cutting speed paradoxically reducing the time to machine a unit length by a factor of 1.35 times from the normal 'optimum'. The reason for this is more apparent from Fig. 3b, in which the same data are cross-plotted as lines of constant cutting speed. These lines tend to cross over between regions of coarse and fine tolerance (see for example lines of 400 and 1000 ft/min). Under open-tolerance conditions ($\delta \geq 0.0045$ in) machining time decreases rapidly with cutting speed at first, but reaches a turning point and then begins to rise (as in Fig. 3a);

by definition of 'open tolerance' conditions there is no resetting, hence this behaviour is due to the increasing incidence of regrinding at higher speeds. At fine tolerances (say $\delta = 0.001$ in) it may take longer to machine a given length at a high speed (for example, 1000 ft/min compared with 400 ft/min) due to the fact that as wear rate rises rapidly with speed, more resets per unit turned length may be required at the higher speed. As the tolerance becomes finer, this effect is more pronounced, and the cutting speed at minimum time falls.

The relationships for machining costs are similar to those for time. Machining cost per unit turned length circumferentially (that is $\pi DL=1.0$) is plotted bilogarithmically in Fig. 4 against cutting speed. At 472 ft/min and a tolerance of 0.0045 in, the cost is 0.40 pence per inch; however if the tolerance is reduced to 0.0005 in, the cost at the same speed would be 0.50 pence per inch, an increase of 25% on that which would be estimated if the effect of tolerance was ignored. In fact at the finer tolerance the cutting speed should be 404 ft/min, and the associated cost would then be 0.48 pence per inch.

These results have been evaluated for a feed of 0.006 in/rev, which is intended to represent an average finishing condition. At higher feeds the effect of tolerance becomes increasingly more pronounced, through its effect upon the rate of tool wear. It should be stressed that the 'open tolerance' condition represents the boundary only of a zone in which the conditions for machining in practice are expected to lie—that is, in which a finite tolerance must be applied.

The effect of tolerance for variable surface roughness

It would be reasonable to assume that over a range of required tolerances the appropriate surface roughness would also vary. This would be achieved in machining by a variation of feed, since this exerts a strong influence upon roughness (second power law). Whilst there is no generally accepted relationship between tolerance and surface roughness requirements (the two aspects being functionally distinct, although there is some interaction), it is obvious and logical that fine tolerances, whether for clearance, transition, or interference fits, presuppose a good surface finish, and vice versa.

A relationship of tolerance δ with roughness h of the basic form

$$\delta = K h^p \quad (32)$$

where K and p are constants, will be assumed here, which is based on some evidence of Boltz⁵. A sufficiently reliable relationship over the range of possibilities for finish turning can be obtained by setting $K = 77.0 \times 10^{-6}$, $p = 1.0$, and where δ and h are in inches and micro-inches C.L.A., respectively.

An expression for the 'ideal' C.L.A. roughness height has been derived by Brewer⁶, namely

$$h = \frac{10^6}{18\sqrt{3}} \cdot \frac{s^2}{r} \quad (33)$$

where s is the feed in inches per rev, and r is the tool nose radius. Actual surface roughness can be related

to the 'ideal' value, based on the feed mark geometry, by a factor u which is to a first approximation constant for machining outside the built-up edge region¹. Combining equations (32) and (33) and inserting the values mentioned, yields

$$\delta = \frac{10^6}{18\sqrt{3}} \cdot \frac{Ks^2}{r} (1 + u) \tag{34}$$

or

$$\frac{\delta}{s^2} = \psi \tag{35}$$

where $\psi = 72.0$, and is sensibly constant for a given cutting situation. Using this relationship, the feed per revolution is reduced as the square root of the tolerance, over the range of finish machining, thus maintaining the relationship between tolerance and surface finish represented by equation (32). This can be seen from Fig. 5a, which also shows the effect of tolerance on conditions at minimum machining time, namely time, cost, and cutting speed. As before, the stepwise appearance is due to the number of re-sets required, and it is evident that cost and time rise at an ever-increasing rate with decreasing tolerance. However compared with the earlier results for constant feed (Fig. 2), although the optimum cutting speed in Fig. 5 undergoes fluctuations, the general decreasing trend is absent. This is due to opposing trends; hence as decreasing the feed raises the cutting speed (other factors constant), the effect of the resetting term arising from the tolerance (see Fig. 2) is the reverse, and hence the combined effect on speed in this case is not very great. Nevertheless the overall effect of tolerance on time and cost* of machining is fairly considerable, due both to the direct effect of decreasing feed, and to that of increased resetting.

A point of comparison† with the constant-feed case is obtained by reading values of parameters for a feed of 0.006 in/rev. Using this point as a basis, it can be seen that by reducing the tolerance from 0.0027 in to 0.0005 in results in an increase in machining time by a factor 1.33 for a constant surface finish, and by 2.50 for the variable finish case. A similar condition exists for the condition of minimum cost (Fig. 5b), from which it is evident that the increase in cost for the same values of tolerance are 1.14 and 2.02 for fixed and variable finish, respectively. The velocity at minimum cost shows a slight rise as tolerance decreases.

It is interesting and noteworthy that, in this case, no dramatic changes in machining conditions result from a substantial decrease in tolerance, (apart from the steady fall in feed, which in any case was an assumed condition). And yet the time and cost of machining according to any criterion increases considerably as the tolerance, over the range achievable in conventional machining, becomes small. It is considered that the un-dramatic change in machining conditions may frequently give the superficial and false impression that the effect of tolerance on productivity is relatively inoffensive. In fact, Fig. 5 suggests that an approximately exponential relationship between cost and tolerance of the form of equation (1) does hold: the value of the index β in this case is about -0.4.

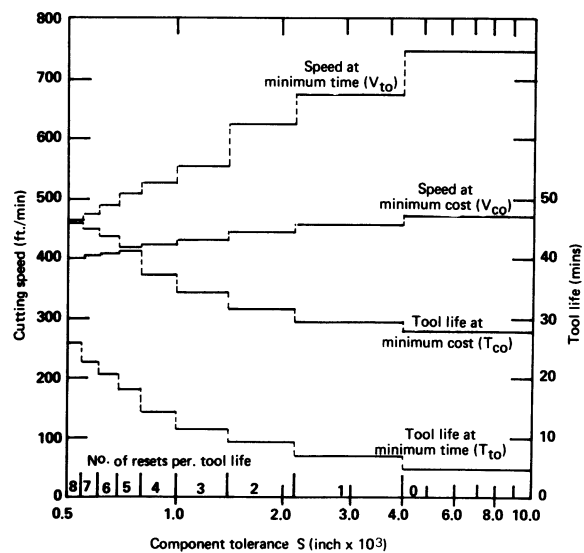
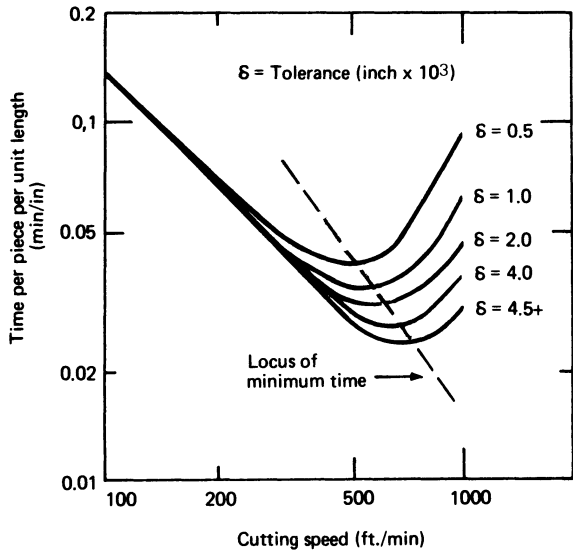


Fig. 2 Effect of component tolerance on optimum cutting speeds and tool life.

*As discussed in an earlier paper¹, cost at minimum time and time at minimum cost are of interest as they define the extent of the increase in cost and time above their respective minima which can be tolerated. Extension of this gave rise to the concept of the 'economic envelope of operation' developed in that paper.

† By interpolation.



(a)

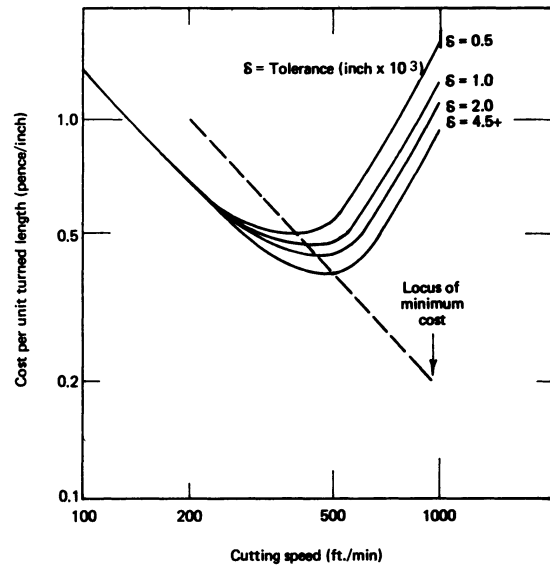
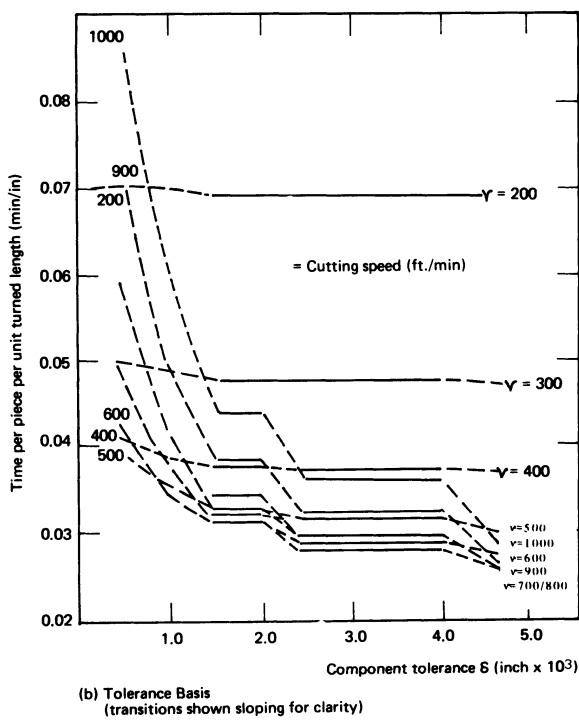
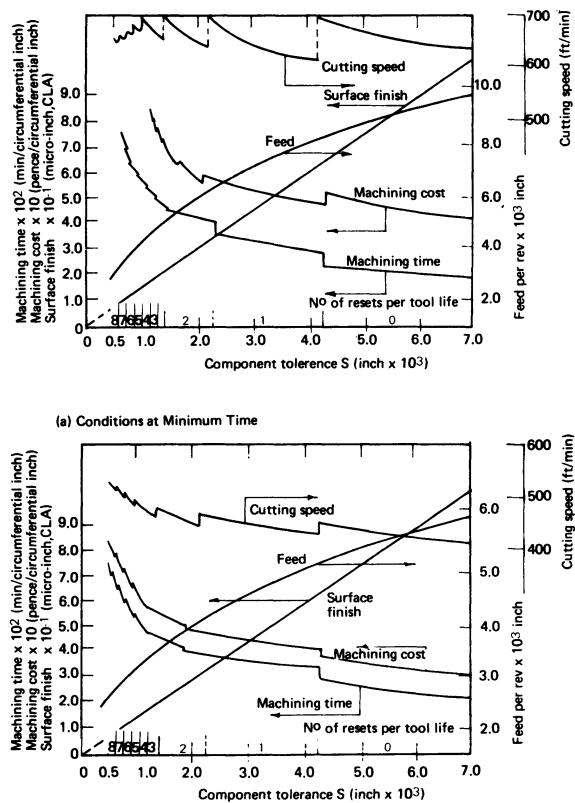


Fig. 4 Relationship of machining cost with cutting speed and component tolerance.



(b)

Fig. 3 Relationship of machining time with cutting speed and component tolerance: (a) cutting speed basis; (b) tolerance basis.



(b) Conditions at Minimum Cost

Fig. 5 Cost, time, and machining conditions for variable-feed case: (a) conditions at minimum time; (b) conditions at minimum cost.

CONCLUSIONS

1. Machining cost and time under optimum conditions are significantly affected by component tolerance. Inclusion of the tolerance effect enables representation of the general machining requirements and conditions to be achieved for the single-cut case: its exclusion renders the analysis suitable only for roughing cuts.

2. The effect of tolerance depends upon whether a constant surface finish, or a given relationship between tolerance and surface finish, is deemed to hold. In the former case, optimum cutting speed decreases as tolerance becomes finer. For the latter, however, the effect upon speed is somewhat uncertain, though not marked, and feed decreases monotonically. The overall effect is thus an ever-increasing machining cost and time, for this more realistic case, having a reasonable resemblance to an exponential relationship.

3. The consideration of the effect of tolerance may serve to assist in defining more precisely the limitations of conventional machining for finishing, whether these are economic or technological. Thus, in addition to the increasing cost with decreasing tolerance—and hence the probable greater economy of an alternative operation such as grinding—the necessary decreasing feed or speed, or both, may, with some materials, cause a transition into the built-up edge region of machining, and hence a more severe limitation on what can actually be achieved.

REFERENCES

1. CROOKALL, J. R., 'The performance-envelope concept in the economics of machining', *Int. J. Mach. Tool Des. and Res.*, **9**, Sept. 1969, pp. 261–278.
2. CROOKALL, J. R., Contribution to discussion, O.E.C.D. Seminar on Metal Cutting, Paris, Sept., 1966, pp. 201–203.
3. BREWER, R. C., 'On the economics of the basic turning operation', *Trans. A.S.M.E.*, **80**, 1958, pp. 1479–1489.
4. CROOKALL, J. R., and Venkataramani, N., 'Computer optimisation of multipass turning', *Proc. Int. Conf. on Prod. Eng. Res.*, Birmingham, 6–10 April, 1970, published in *Int. J. Prod. Eng. Res.* **9**, No. 2, 1971, pp. 247–260.
5. BOLTZ, R. W., 'Designing for Production', Part 5, No. 1 of 'Metals Engineering Design', A.S.M.E. Handbook, McGraw-Hill, 1953, pp. 277–283.
6. BREWER, R.C., C.I.R.P. Ann XIV, **11**, 1966.

DISCUSSION

Query from Dr. G. Barrow, UMIST

The author has shown that cost is increased by resetting the tool. Would it not be more economical to use a lower flank wear criterion and index the tool?

Reply

As we understand Dr. Barrow's question, he would be correct if the indexing time was shorter than the resetting time, and the accuracy of re-location of the tool tips was satisfactory.

Query from A. G. Hague, Trent Polytechnic, Nottingham

I often wonder whether metal cutting engineers place too much reliance on the traditional flank wear measurement (Fig. 1). Such a measurement is, after all, a single dimensional quantity which is taken to represent 'wear' which, by its very nature, must be three-dimensional. Even if we can accept this factor, anyone who has tried to measure 'flank wear' knows how indeterminate this dimension can be, by smearing from the B.U.E. and also from the oxide films which develop on the flank face. Again, the wear-band on the flank does not always obligingly remain uniform and the experimenter is then faced with the dilemma of where along the flank wear length is the measurement taken.

The Taylor equation, which is essentially empirical and invariably hides much scatter in the results, also derives from this single dimensional feature which we call 'wear'. In fact since the theory contained in this paper does itself derive from the Taylor equation, then it becomes even more emphasised how important it is to get the tool-life criterion correct in the first instance.

Reply

We agree with Mr. Hague that flank wear is only one criterion of the deterioration of a cutting tool, and that this point is widely neglected. In¹ of our paper, some attempt was made to accommodate other modes of tool failure such as cratering and deformation in the form of constraints, and some discussion of this point was made in our paper. The advantage of the flank-wear criterion is that it is *relatively* easy to measure and varies virtually continuously with cutting time, which is important in setting-up an economic model of the process. (See also reply to Dr. Stevenson).

Query from A. H. Redford, USALF

The authors' work on the effect of component tolerance on the economics of the machining process is not relevant to most practical turning operations. If, for example, a 0.015 in. flank wear land is considered as the criterion for tool failure and it is assumed that wear on the minor cutting edge clearance face is of the same order (in general this will be less). The increase in diameter of the component from cutting with a new tool to the end of the useful life of the tool would be approximately 0.0015 in. It is considered that the tolerance band in most practical operations would be greater than this.

The equation relating tolerance to surface finish would appear to be in error. In the few cases where a change in diameter of greater than 0.0015 in. could

not be tolerated, surface finishes better than 20 micro-in. would be compatible with the tolerance and it would not generally be practicable to achieve this by turning. Further, for super-fine turning operations, the simple relationship relating surface finish to the geometry of the process would not even be approximately true.

Reply

We agree with Mr. Redford in principle that the tolerances on many components are greater than the 0.0015 in. he quotes; nevertheless critical dimensions frequently exist, and must of course be allowed for. Taking his value, even for tolerances greater than about 0.0015 in., Fig. 5 shows that the effect of tolerance upon cost or time is by a factor of some 50% or more relative to the 'open tolerance' case. Although not marked, this in our view is not negligible. For finer tolerances than this, significant increases in cost and time are evident. Taking these two points together, it would seem that the point of sensible limitation technologically in conventional machining practice also demarks the region of reasonably economic operation predicted by the theory. This measure of agreement between the theory of machining economics and general practice is perhaps a satisfying confirmation of the former, and *ipso facto* its relevance to the latter.

Mr. Redford has tried to read too much into certain aspects of the analysis. Contrary to his suggestion, there is no error in the derivation from the quoted reference. However, on points of detail, firstly the important aspect (to which reference is made in the paper) is that there is of course no rigorous relationship between tolerance and surface finish requirements on components. A broad relationship with an expectedly wide scatter band exists according to Boltz, and we have used the mean of this band. Secondly, tolerance is normally related to component diameter or size, although this specific aspect was neglected. However, over a diameter range of 0.5 to 4.0 in., BS 1916: 1953 Part 2 gives a tolerance range 'which can be *reasonably* expected

under *average* conditions' (our italics) as 0.001 to 0.0023 in. for centre-lathe, and 0.00065 to 0.0015 in. for high-quality turning. We took this into account in quoting our ranges. Finally, in relating flank wear on major and minor cutting edges, we obtained advice on the *reasonableness* of this assumption from the research group on finish turning at Delft University. Although we are inclined to agree that undue extrapolation of our results into the super-fine turning region must be regarded with caution, the general principles that the paper seeks to enunciate are valid.

Query from Dr. M. G. Stevenson, University of N.S.W.

The tolerance variation described is one due to systematic tool wear. Random variability for a constant tool profile may also make up a substantial proportion of the process variability. The random variance would be made up, amongst other things of tool and work deflections and heating. These effects could be expected to increase with increasing feed. Hence, there is another reason to decrease feed with decreasing tolerances, and the machining costs could rise even more rapidly with decreasing tolerance, than shown in Fig. 5.

Reply

The statistical variability of wear is another important aspect, which is mentioned by Dr. Stevenson (and also by Mr. Hague), and one which we are currently examining. Dr. Stevenson has made an important point concerning work and tool deflection, which obviously affects the accuracy of a part. These can be treated systematically also as constraints on the use of high feeds particularly; in this region larger separating forces occur between the tool and the work. Although not considered in the present paper, the deflection constraint has been included in other work to which reference is made.

Temperature effects are considerably more difficult to ascertain. Determination of the effective temperature distribution below the instantaneous cut surface would appear to be a very complex problem.

THERMOELECTRIC CHARACTERISTICS OF CARBIDES

by

C. BUS, N. A. L. TOUWEN, P. C. VEENSTRA, A. C. H. VAN DER WOLF*

SUMMARY

Thermoelectric characteristics from 0° C to 1000° C are determined for several grades of carbide versus Pt. The characteristic of Pt versus C45N-steel is also obtained. From these, the thermoelectric characteristics of the carbides versus C45N-steel can be derived. The calibrations are carried out in a radiation furnace set-up, and the specimen consists of a bar of square cross-section 12.5 mm² and approximately 300 mm in length.

INTRODUCTION

The aim of this investigation is to obtain numerical data for the relationship between thermoelectromotive forces and temperatures for several grades of carbide and workpiece material (C45N). For reasons of proper calibration, every experiment was carried out versus platinum (Pt). This metal has many advantages, such as:

- high melting point,
- great stability as far as corrosion is concerned,
- no transformation points.

TEST METHOD & MATERIALS

The calibration set-up consists of a radiation furnace and a cooling device, as can be seen in Fig. 1. One end of the test bar is placed in the furnace, the other end in the cooling device. Both ends of the bar are connected with a platinum wire. The temperatures of the hot and cold junctions are measured by Cr/Al thermocouples and are put on paper-tape by means of a datalogger. At the same time the e.m.f. voltage between the hot and the cold junctions of the calibration bar is put on this tape.

A good contact at the junctions is assured by the weight of the furnace. The hot end of the calibration bar is protected against corrosion by means of an inert gas, and the cooling device is operated by water and keeps the cold junctions at approximately 13° C.

As mentioned before, the tests are carried out for several grades of carbides and the workpiece material C45N. The carbides used are Sandvik grades S1, S2, S4, S6, HO5, H1p, H10, H13, H20 and FO2.

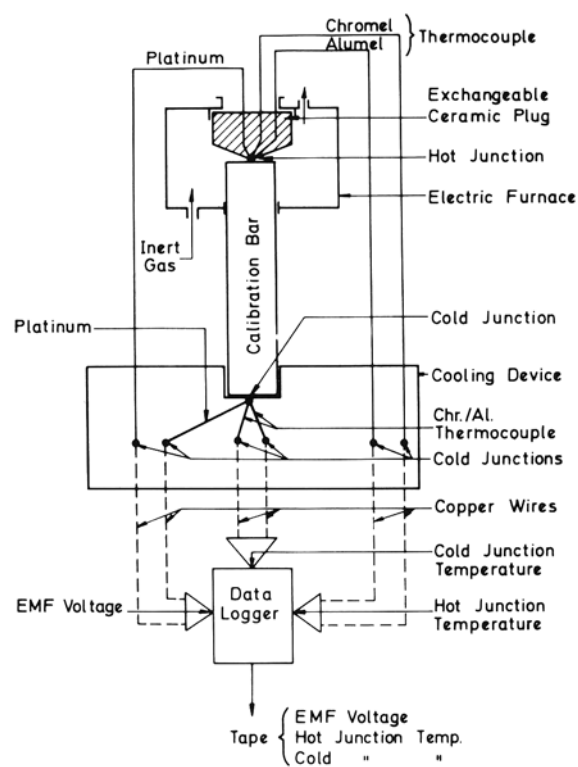


Fig. 1 Calibration set-up.

NUMERICAL ELABORATION (see Fig. 2)

Starting data: A paper-tape with in preset-time on two channels datalogged non-scaled measured values of the hot junction temperature (e.m.f. voltage of the Cr/Al thermocouple) and the e.m.f. voltage

*Eindhoven, University of Technology, the Netherlands

between the hot and the cold junction of the calibration bar involved (= difference voltage). For a qualitative control and a counting of the couples of the measurements the tape is read through (program A-327-14a). Next, the measurements are mutually adjusted in order to eliminate the influence of the preset-time-interval (the difference voltage belonging to the hot junction is found as the arithmetic mean of the preceding and next measurement) and to introduce the scaling (program A-3948-5). At the same time the adjusted measurements are represented on paper-tape in two ways:

1. all measurements at the hot junction with matched difference voltages, and
2. equidistant chosen hot junction values with matched difference voltages (interpolated).

With the aid of series 1 a graph is made: the Cr/Al thermoelectric voltage of the hot junction along the horizontal axis and, the difference voltage of the calibration bar involved along the vertical axis (A-3943-11). In order to get the final data of the calibration curve, the following two corrections are necessary. First, a correction for the increasing temperature of the cold junction of the calibration bar during the experiment must be made. Secondly, a correction for the translation of the coordinates to a common starting point (in accordance with the zero-point of the Celsius scale) must also be made.

With the help of well-known data on the Cr/Al thermocouple, the graph already made with tape 1, and the measured temperatures of the cold junction, the corrections mentioned above are carried out on the adjusted measurements of tape 2 (program A-4571-3). Furthermore, in this program the voltage of the hot junction in millivolts Cr/Al is converted into degrees Celsius. With a regression-program (A-2080-6), the polynomial coefficients of the calibration curve are calculated, used model:

$$\text{calibration bar voltage versus Pt} = aT + bT^2 + cT^3 \quad (1)$$

For plotting the graph of the calibration curve corresponding to the calculated formula (with program A-3943-11), the coordinates are first made with a sub-program (A-1908-3). Given the choice, it is also possible to plot the underlying measurements (tape 2) in the same graph. In Fig. 3. the calibration curve with the measurements of the carbide grade S2 versus Pt is given.

RESULTS

The results of all measurements are listed in Table 1. In this table the coefficients a , b , and c are given for the carbides mentioned and the workpiece material C45N. Moreover, the 2σ -value (σ = standard deviation) of every coefficient as calculated by the regression-program is given.

In general, the shape of the calibration curves are parabolic. It is possible to obtain the e.m.f. relationship between one of these carbides and C45N-steel. Therefore, the e.m.f. of S2 versus C45N is

$$\text{e.m.f. } \frac{S2}{C45} = \text{e.m.f. } \frac{Pt}{C45} - \text{e.m.f. } \frac{S2}{Pt}$$

In numerical values (see Fig. 4)

$$\text{E.M.F. } \frac{Pt}{C45} = +(0.129 \times 10^{-1})T - (0.644 \times 10^{-5})T^2 + (0.549 \times 10^{-8})T^3$$

$$\text{E.M.F. } \frac{S2}{Pt} = -(0.949 \times 10^{-2})T - (0.34 \times 10^{-6})T^2 + (0.497 \times 10^{-8})T^3$$

$$\text{E.M.F. } \frac{S2}{C45} = +(0.224 \times 10^{-1})T - (0.610 \times 10^{-5})T^2 + (0.052 \times 10^{-8})T^3$$

The carbide grade FO2 and the C45N-steel have a positive e.m.f. against Pt; this can be seen from the coefficient a in Table 1. The heating-process calibrations are less stable and they do not reproduce so well, as far as the materials with a negative e.m.f. are concerned.

The data of Table 1 are obtained from three or more well reproducible calibrations of the cooling-

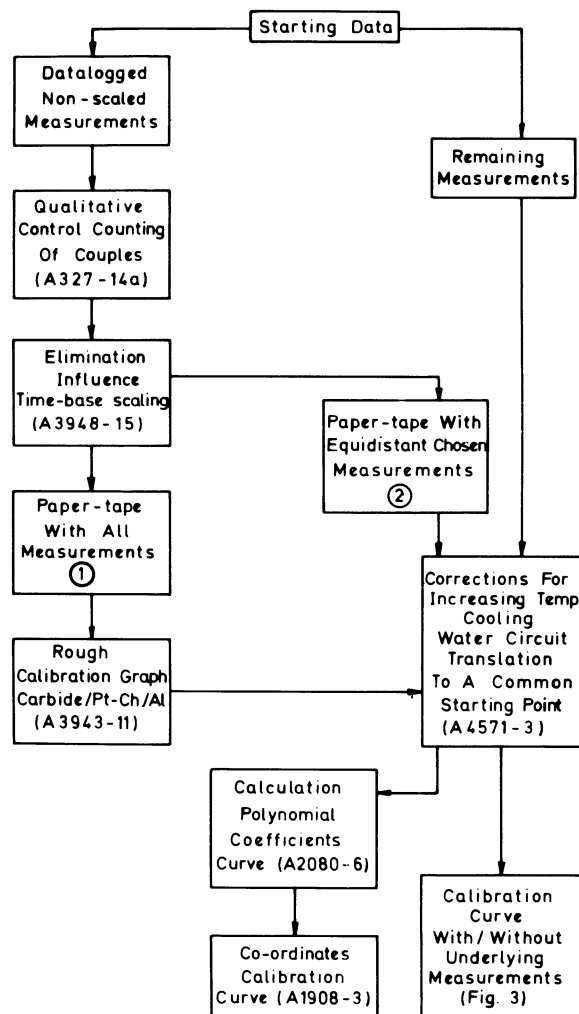


Fig. 2 Flow-chart of the numerical elaboration.

Table 1. Coefficients of equation 1 for several grades of carbide and steel C45N.

Materials versus	E.M.F. coefficients with 2σ -values						
	Pt	a	2σ	b	2σ	c	2σ
carbide grade S1		-0.349×10^{-2}	0.3×10^{-4}	-0.198×10^{-5}	0.8×10^{-7}	$+0.479 \times 10^{-8}$	0.6×10^{-10}
carbide grade S2		-0.949×10^{-2}	0.4×10^{-4}	-0.343×10^{-6}	0.100×10^{-6}	$+0.497 \times 10^{-8}$	0.7×10^{-10}
carbide grade S4		-0.729×10^{-2}	0.4×10^{-4}	$+0.746 \times 10^{-6}$	0.111×10^{-6}	$+0.387 \times 10^{-8}$	0.8×10^{-10}
carbide grade S6		-0.1015×10^{-1}	0.5×10^{-4}	-0.426×10^{-5}	0.15×10^{-6}	$+0.830 \times 10^{-8}$	0.11×10^{-9}
carbide grade H05		-0.1090×10^{-1}	0.9×10^{-4}	$+0.807 \times 10^{-6}$	0.260×10^{-6}	$+0.475 \times 10^{-8}$	0.19×10^{-9}
carbide grade HIP		-0.866×10^{-2}	0.5×10^{-4}	$+0.164 \times 10^{-5}$	0.16×10^{-6}	$+0.374 \times 10^{-8}$	0.11×10^{-9}
carbide grade H10		-0.914×10^{-2}	0.8×10^{-4}	-0.569×10^{-5}	0.23×10^{-6}	$+0.865 \times 10^{-8}$	0.19×10^{-9}
carbide grade H13		-0.841×10^{-2}	0.7×10^{-4}	$+0.571 \times 10^{-7}$	0.22×10^{-6}	$+0.493 \times 10^{-8}$	0.16×10^{-9}
carbide grade H20		-0.997×10^{-2}	0.10×10^{-3}	-0.496×10^{-5}	0.30×10^{-6}	$+0.849 \times 10^{-8}$	0.22×10^{-9}
carbide grade F02		$+0.430 \times 10^{-2}$	0.5×10^{-4}	$+0.454 \times 10^{-5}$	0.16×10^{-6}	-0.106×10^{-8}	0.12×10^{-9}
steel C45N		$+0.129 \times 10^{-1}$	0.1×10^{-3}	-0.644×10^{-5}	0.42×10^{-6}	$+0.549 \times 10^{-8}$	0.30×10^{-9}

process. As already mentioned the calibration curves of the materials having a negative e.m.f. are parabolic. The formula

$$\text{E.M.F.} = aT + bT^2 + cT^3$$

describes a curve through all the measuring points of the calibration series with very good technical accuracy (see Fig. 3).

The C45/Pt calibration has a loop in the upper range of the curve. This loop is caused by the $A_{1,2,3}$ transformation energy. The A_c transformations absorb energy. During the A_r transformations the absorbed energy is released. If no transformation should occur, the calibration curve should be in the middle of the loop just mentioned, because the absorbed energy and the released energy are of equal quantity (see Fig. 5). The coefficients of the calibration curve are determined to the average value of the A_c and A_r curve.

At present, research is going on in the laboratory into the backgrounds of being less stable of the carbide calibration curves in the heating-process.

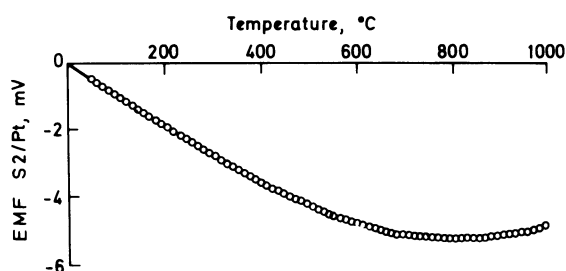


Fig. 3 E.M.F. S2/Pt as a function of the temperature ($^{\circ}\text{C}$).

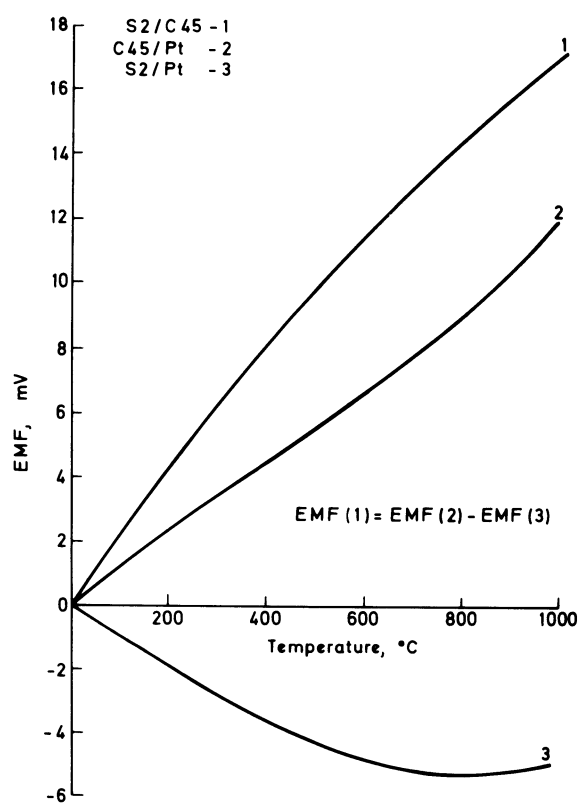


Fig. 4 E.M.F. S2/C45, E.M.F. C45/Pt and E.M.F. S2/Pt as a function of the temperature.

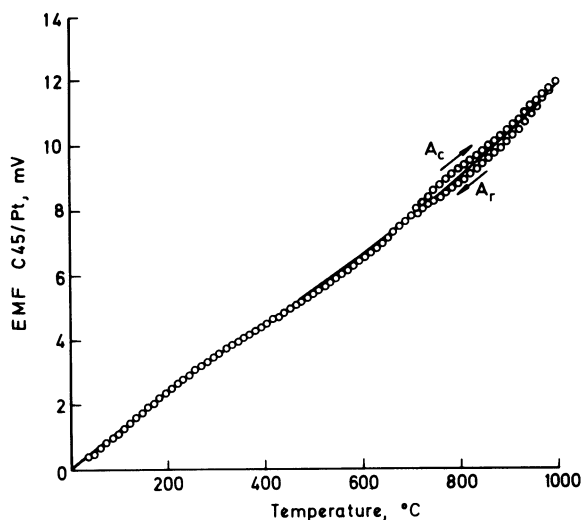


Fig. 5 E.M.F. C45/Pt as a function of the temperature. The curve through the plotted loop determines the average value of the A_c and A_r energy.

REFERENCES

1. VEENSTRA, P. C., BUS, Chr., and ZWEEKHORST, E. T. W., Preliminary report on the measurement of cutting tool temperature (WT-0072), on behalf of CIRP-conference, Cincinnati 1963. Also published in Dutch in 'Metaalbewerking', 29 (1964) 16, pp. 1-5.

DISCUSSION

Query from A. G. Hague, Trent Polytechnic, Nottingham.

I cannot see how these results can have any bearing towards predicting temperature at the tool/workpiece interface for, in the set-up of Fig. 1., neither the chemically-clean surface nor the extremely high inter-face pressure encountered in actual cutting operations have been taken into account.

Reply

The calibration bar, the platinum wire and the thermocouple Cr/Al are in the hot junction welded together by the first heating up to about 1200°C, so there is a clean chemical contact. Afterwards, several calibration runs were made.

The contact in the hot junction of our setup has the same character as in the actual cutting operations. The thermoelectric characteristics of thermocouples are independent of inter-face pressure.

CARBIDE SIZE AND DISTRIBUTION AND THEIR EFFECT ON THE PERFORMANCE OF HIGH-SPEED-STEEL TOOLS

by

IVO KVASNICKA*

SUMMARY

Heat treatment of tools, composition and structure of high-speed-steel are important metallurgical factors influencing the performance of cutting tools. The effect of chemical composition and heat treatment on the cutting performance is now known, but the effect of structure on the behaviour of high-speed-steel tools during machining is not sufficiently known at present.

This study is an attempt to explain the influence of the size of carbides and their distribution in the steel matrix on the tool life of high-speed-steel tools. The study evaluates three different structures of commercial high-speed-steel 18-4-1 type (AISI type T1) bar stocks of 50 mm (2 in.) diameter. The size of carbides and their distribution were determined quantitatively on a Quantimet instrument and qualitatively on a metallographic microscope. Grain size, heat treated hardness and distortion were determined before the evaluation of tool life. Tool life has been estimated for turning and face milling.

The performed tests show that the carbide size distribution is the most important factor to influence the character of steel and tool life. Coarse carbide particles in matrix unfavourably influence mainly the grain size, toughness and increase variation in tool life. The influence of distribution of carbides proved to be less important than their sizes when tested.

INTRODUCTION

The industrial production of high-speed-steel bar stock comprises a set of operations which more or less influence heat treatment, mechanical and technological properties of the cutting tool. The steel producer and consumer are interested in methods of evaluating the quality of the produced bars and so avoid the production of imperfect tools. Checking the quality of steel is rather problematical due to available measuring methods, to lack of possibility in statistical control and insufficient knowledge of the effect that important factors have on the life of high-speed-steel tools.

One of the important determinants of quality of high-speed-steel bars is the size of carbides and their distribution in the matrix. We can generally say that optimal structures should have fine carbides uniformly distributed throughout the steel matrix. However, this ideal structure cannot be reached by commercial technique in bars larger than 40 mm (1.5 in.) diameter. Therefore it is necessary that the steel producer and the customer must know whether the effect of carbide size is more important than the effect of their distribution and what quality is still permissible for a good tool.

The Department of Tool Materials in the National

Research Institute for Materials in Prague has been working on the solution of these problems, in which high-speed-steel of the 18-4-1 type (AISI type T1) has been used. This steel, because of its chemical composition, contains a large quantity of eutecticum and coarse eutectic carbides.

EVALUATED STRUCTURES

The aim of this work was to evaluate the influence of three selected structures differing in size of carbides and the manner in which the carbides were distributed on the cutting properties of high-speed-steel tools. Bars 50 mm (2 in.) diameter were produced from three heats A, B and C by different techniques of casting and hot working. The chemical composition of the heats and reduction in cross sectional areas of the bars are shown in Table 1.

TABLE 1 Analysis and reduction (%)

Heat	C	Cr	W	Mo	V	Reduction
A	0.74	4.26	17.20	0.12	1.21	60
B	0.75	4.11	17.90	0.08	1.16	40
C	0.75	4.14	17.65	0.10	1.05	120

*Department of Tool Materials, National Research Institute for Materials, Opletalova 25, Prague 1, Czechoslovakia.

The microstructure (of the three bars) in the annealed condition was determined in four cross sectional areas cut 250 mm (10 in.) apart. Four specimens of 2.5 sq. cm in area, which were taken from places situated $\frac{1}{4}$ of the diameter under the surface, were tested. The area of the microsections was parallel or perpendicular to the direction of forging. Frequency distributions of carbide size were determined quantitatively on a Quantimet instrument and the distribution of carbides in the microstructure were examined qualitatively under a metallographic microscope. The etchant $\text{KMnO}_4 + \text{NaOH} + \text{H}_2\text{O}$ was used under temperatures of 90°C (200°F) to etch the microsections for the Quantimet. The microsections for the metallographic microscope were etched with Nital.

Figs. 1 to 3 show typical examples of the microstructures of the three heats. The experimental results gained with the QTM instrument are shown graphically in Fig. 4. The microstructure of heat A (Fig. 1), which is usual in high-speed-steel bars of larger dimensions contains a large amount of fine carbides less than 3 microns in size (Fig. 4). The carbides are formed into bands. The microstructure of heat B contains an increased quantity of medium carbides of 3 to 6 microns in size which are distributed uniformly or in thin bands. The microstructure of heat C (Fig. 3) has a high quantity of medium carbides and an increased number of coarse carbides of 12 to 15 microns in size and contains heavily banded carbide regions.

The specimens for experimental work on heat treatment and single point tools for turning and face milling were taken from the bars in the same way as the specimens for the QTM instrument, i.e. from places situated $\frac{1}{4}$ of the diameter under the surface.

BEHAVIOUR OF STRUCTURES DURING HEAT TREATMENT

A large amount of experimental work has been done on the influence of carbide size and distribution on the heat treatment of tested cutting tools made from the heats. Some of the interesting results obtained at the laboratory are summarised below.

Austenite grain size

Austenite grain size is the significant factor influencing such properties of high-speed-steel as red hardness and toughness. The check test of grain size gives us a view of the quality of high-speed-steel bars and accurate knowledge of the actual tool temperature in the furnace during hardening.

Influence of hardening temperature on the austenite grain size of 20 mm ($\frac{3}{4}$ in.) cube specimens was measured. Hardening temperature as an independent variable was chosen in a desirable range of $1240\text{--}1320^\circ\text{C}$ ($2265\text{--}2405^\circ\text{F}$) which is recommended for this type of steel. Holding time in the salt bath was three minutes and then the specimens were quenched in oil. Obtained grains were examined on the metallographic microscope by the intercept Snyder-Graff method.

Fig. 5 illustrates the correlation between austenite grain size and hardening temperature for the speci-

mens of the three heats. The microstructure of specimen of heat C containing a large number of coarse carbides measurably affected the rapidity of grain growth at the tested temperatures. Fine grains (in size higher than 12) were not reached even at low hardening temperature and the microstructure had an appearance of overheated steel at 1300°C (2370°F). This behaviour is caused by a smaller number of the fine carbide particles influencing the rate of grain growth. Heat A with a large amount of fine carbides retained much finer grains than heats B or C and overheating began at a higher hardening temperature of 1320°C (2405°F). Austenite grain size of the microstructure of heat B was between heats A and C values.

Heat treated hardness

Specimens of the same 20 mm ($\frac{3}{4}$ in.) cube size were tempered three times after quenching (see Table 2). In order to obtain the complete transformation of the retained austenite, soaking time during tempering was 45 min. Hardness in the hardened and tempered condition was measured on a Rockwell instrument and microstructures were determined on the metallographic microscope. Rockwell hardness increases with the more uniform distribution of carbide particles and is not dependent on the size of carbides. On the other hand, the variation in microhardness increases with a growing amount of coarse carbides in the microstructure. The matrix of tempered martensite corresponds to the austenite grain size. Coarse-grained steel contributes to the coarse crystal of tempered martensite and fine-grained steel has the opposite behaviour.

TABLE 2 Heat treatment conditions and hardness

Heat	Hardening Temp.	Time	Tempering	Hardness (Rockwell C)
A	1260°C	3 min	$3 \times 570^\circ\text{C}$ ($3 \times 1060^\circ\text{F}$)	65.5
B	(2300°F)			66.5
C				65.0
A	1280°C	3 min	$3 \times 570^\circ\text{C}$ ($3 \times 1060^\circ\text{F}$)	65.5
B	(2335°F)			66.5
C				65.0
A	1300°C	3 min	$3 \times 580^\circ\text{C}$ ($3 \times 1080^\circ\text{F}$)	66.0
B	(2370°F)			67.0
C				65.5

Distortion during heat treatment

Specimens used were $30 \times 30 \times 10$ mm ($1\frac{1}{4} \times 1\frac{1}{4} \times \frac{3}{8}$ in.) in size with a hole 15 mm ($\frac{1}{2}$ in.) diameter, the axis of which was perpendicular to the direction of forging of the bars. The specimens were quenched in oil from 1280°C (2335°F) and tempered three times at 570°C (1060°F) for 45 min. Dimensional changes after quenching and each tempering were determined by a micrometer parallel and perpendicular to the direction of forging. Circularity of the ground hole was estimated on a Talyrond instrument.

Fig. 6 shows the variation ranges in dimensional changes. The specimens of heats A and B have similar dimensional changes but the specimens of heat C deformed longitudinally much more than transversely. The main reason for this anisotropy can be

attributed to the reduction of coefficient of thermal expansion by the heavily banded carbide regions and to orientation of the grains in the direction of hot working. Dimensional changes between different conditions of the specimen are affected by the amount of retained austenite.

Circularity of the ground hole of all specimens changed after heat treatment to ovality, with the longer axis parallel to the direction of hot working.

TOOL LIFE TESTING

An investigation has been conducted to compare cutting performance, in terms of tool life, of the single point tools made from the evaluated structures. Cutting performance depends on a combination of properties, of which three have a predominant significance: red hardness, wear resistance and toughness. As coarse carbides disproportionately distributed in the matrix make difficulties connected with tool failure due to decrease in toughness, the evaluation of tool life performance by turning a difficult-to-machine alloy and face milling was carried out. Due to the wide extent of testing, the paper describes only some of the results showing the correlation of tool life and carbides in the structure.

Turning experiments

The experiments were carried out on the lathe with a variable-speed drive. Tool tips $10 \times 20 \times 30$ mm ($3/8 \times 3/4 \times 1\frac{1}{4}$ in.) in size with the main edge parallel or perpendicular to the direction of hot working were used.

The tips of the three structures were quenched in oil from 1280°C (2335°F) and tempered three times at 570°C (1060°F) for 45 min. The hardness after tempering was 65 to 66.5 Rockwell C (see Table 2). The following tool geometry for the tip held in a toolholder was chosen: Normal rake $\gamma = 10^\circ$, normal clearance $\alpha = 8^\circ$, cutting edge inclination $\lambda = 0^\circ$, cutting edge angle $\mathcal{H} = 75^\circ$ and 0.4 mm (0.016 in.) nose radius. Grinding of the tip was made according to the ISO/TC 29/WG 22 draft proposal 'Tool life testing with single point turning tools'.

The test material was a high-strength austenitic alloy with the following chemical composition and data: 0.46% C, 5.46% Mn, 3.63% Cr, 1.07% Ni and $\sigma_B = 114$ to 130 kp/mm². This material does not form a steady built-up edge near the nose of the tool and mechanical stresses the cutting edge.

The tool life for each tool material was determined for several different cutting speeds in accordance with Taylor's formula expressing the relation of cutting speed and tool life between grindings.

The cutting test was performed dry at 1.5 mm (0.06 in.) depth and 0.125 mm (0.005 in.) feed with cutting speeds of 5, 6, 7 and 8 m/min (15, 18, 21 and 24 ft/min). The tool life of the tip was characterised by the absolute cutting time required to produce a flank wear land of 0.3 mm (0.012 in.). Flank wear land dimensions were measured and the condition of working edge was checked on a shop microscope of 15 times magnification.

Fig. 7 illustrates the correlation of tool life and cutting speed for the three evaluated structures deter-

mined from the experimental tests. Values of V_{45} (the cutting speed in m/min for a 45 min tool life) and exponent n , that were obtained by application of the least square analysis, are presented in Table 3.

TABLE 3

Heat	Direction of cutting edge	V_{45} (m/min)	Exponent n	Cutting edge condition
A	parallel	5.1	0.27	good
	perpendicular	5.2	0.26	good
B	parallel	4.4	0.48	microbreaking
	perpendicular	4.9	0.34	microchipping
C	parallel	3.3	0.55	microbreaking
	perpendicular	4.2	0.43	microchipping

The tips with the structure of heat A have the greatest values of V_{45} and the longest tool life. The cutting edge conditions after cutting were good. The values of V_{45} for the heat C are 35% or 20% lower than those for heat A. The cutting edges of the tips of heats B and C parallel to the direction of forging were damaged by microbreaking, the cutting edges situated in the perpendicular direction were damaged by microchipping.

Milling experiments

Milling experiments employed an A5V type vertical milling machine. A face milling head of 160 mm ($6\frac{1}{4}$ in.) diameter with three mechanically held insert cutters was used. The insert cutters were set-up in such a way that their cutting edges were not influenced by each other.

The insert cutter of 16 mm ($5/8$ in.) square and 100 mm (4 in.) length had its axis parallel to the direction of forging. The cutters of the three evaluated structures were quenched in oil from 1260°C (2300°F) and tempered three times at 570°C (1060°F) for 45 min. The hardness after tempering was 65 to 66.5 Rockwell C (see Table 2). The tool geometry was as follows: normal rake $\gamma = 15^\circ$, normal clearance $\alpha = 8^\circ$, cutting edge inclination $\gamma = -5^\circ$, cutting edge angle $\mathcal{H} = 75^\circ$ and 1.0 mm (0.04 in.) nose radius.

The material for the milling experiments was a constructional steel bar of 100 mm (4 in.) square and 1000 mm (3 ft.) long. The nominal chemical composition and the actual strength of the material were as follows: 0.56% C, 0.65% Mn, 0.27% Si and $\sigma_B = 65$ to 75 kp/mm².

The experimental conditions were constant: i.e. cutting speed 14 m/min (42 ft./min), feed 0.8 mm/tooth (0.032 in./tooth), depth of cut 1.5 mm (1/16 in.), dry.

Tool life was determined in each test on the basis of the wear curve. The flank wear land of the insert cutters was photographed during cutting. Then the width of the wear was measured from the photos and plotted against the cutting time. The criterion for the end of tool life was the flank wear land of 0.4 mm (0.016 in.). The condition of the cutting edge after machining was observed on the shop microscope of 15 times magnification.

Correlation between tool wear and cutting time

for the four insert cutters from each heat is shown in Fig. 8. The results of the tool life measurements, the arithmetic mean and their deviations are summarised in Table 4.

TABLE 4

Heat	Tool life (min)	Mean	Deviation
A	40; 39; 42; 23	36	± 24%
B	33; 12; 48; 4 *)	31	± 56%
C	36; 13; 25; 15	21	± 48%

* Value was eliminated from the set.

The difference in the average tool life between the tools from heats A and B is very small. But mean tool lives alone do not indicate conclusively that these heats differ in machining behaviour. We must bear in mind that tool life will be shorter than mean in 50% of the cases. The estimate is safe only in the case when tool life is determined from the low limit of the correlation. Regression analysis shows that the variation in tool life of heat A is smaller than that of heat B, and therefore, the structure of heat A is more useful especially in automation. The significant difference is between the average tool life and its variation of the insert cutters of heats A and C. The results indicate a correlation existing between the sizes of carbide and cutting properties. It may be explained by the effect that coarse carbides have on the decrease in toughness connected with chipping or breaking of working edge during cutting.

CONCLUSIONS

1. The experimental results demonstrate that a correlation exists between carbide size distribution and cutting properties of high-speed-steel tools especially during interrupted machining.
2. Grain coarsening of high-speed-steel, which occurs when carbides in the structure are large (approximately higher than 8 to 10 microns in

size), indicate the decrease in toughness and the lower resistance to interrupted cutting in milling or shaping operations.

3. The coarse carbides placed in the cutting edge decrease the ability of the tool to withstand impact without chipping or damage and increase the variation in tool life.
4. Machining of the difficult-to-machine materials requires a high-speed-steel tool without the coarse carbides in the structure even when turning.
5. It has been found that the distribution of carbide particles has a much lower influence on tool life and cutting properties than the absolute size of the particles.
6. Since an increase in tool size results in greater carbide size variation, a suitable type of high-speed-steel containing a lower quantity of eutecticum (e.g. AISI type M2) must be selected for a large tool.

REFERENCES

1. KVASNICKA, I. and VESELY, V., 'Vliv velikosti a rozlozeni karbidu na vlastnosti a rezivost rychlorezne oceli', Research Report, National Research Institute for Materials, 1970.
2. PAYSON, P., 'The Metallurgy of Tool Steels', New York, 1962.
3. HARVEY, R. F., 'Pin Point Carbides Can Greatly Improve High-Speed-Steel', *Cutting Tool Engineer*, March, 1968
4. RODIC, A. and J., 'Uticaj velicine karbida na osnovne karakteristike brzoreznih celika', *Zastita Materijala*, XIII, 1965.
5. EUGENE, F., 'Contribution a l'etude de l'homogeneite des outils en acier rapide', C.I.R.P. Annalen, XII, 3, 1966.
6. ISO/TC 29/WG 22, 'Tool Life Testing with Single Point Turning Tools', Second Draft Proposal, 1970.



Fig. 1 Microstructure in annealed condition of specimens taken from the bar stock of heat A. Magnification 500 ×.

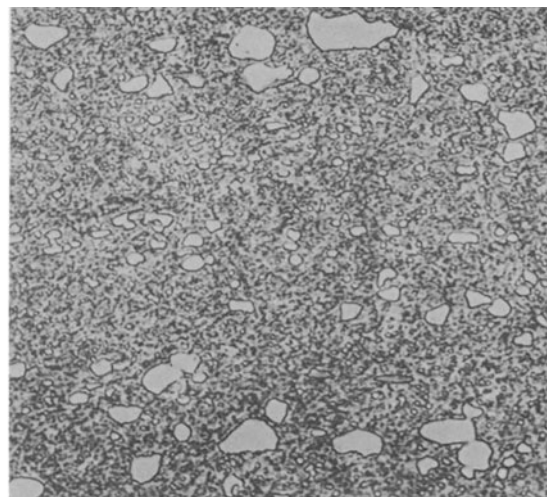


Fig. 2 Microstructure in annealed condition of specimens taken from the bar stock of heat B. Magnification 500 ×.

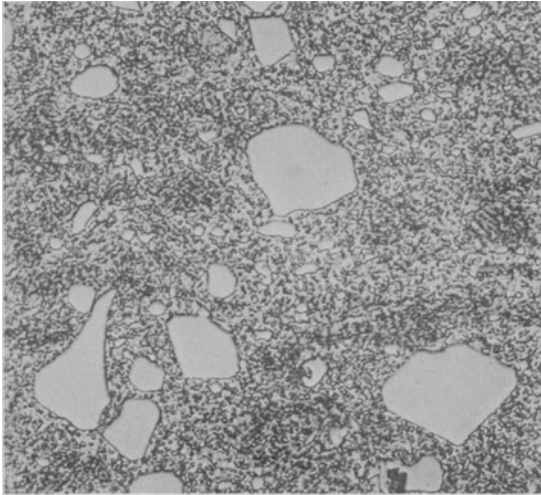


Fig. 3 Microstructure in annealed condition of specimens taken from the bar stock of heat C. Magnification 500 X.

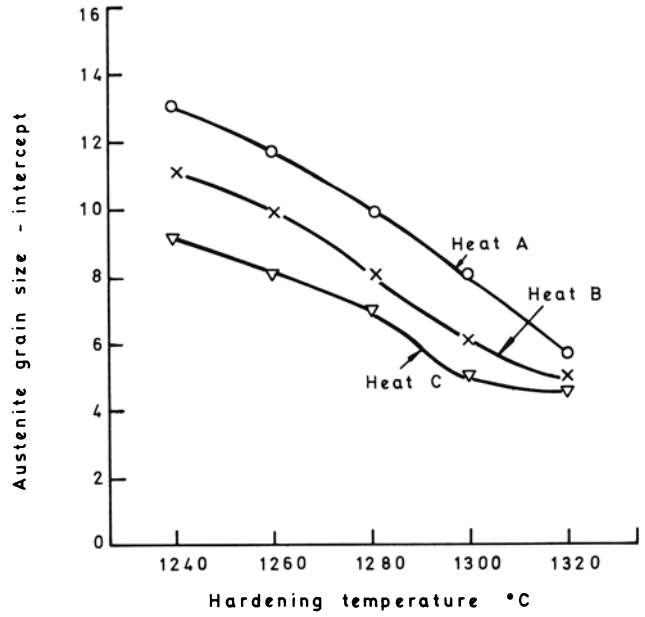


Fig. 5 Correlation between austenite grain size and hardening temperature of 20 mm (3/4 in.) cube specimens.

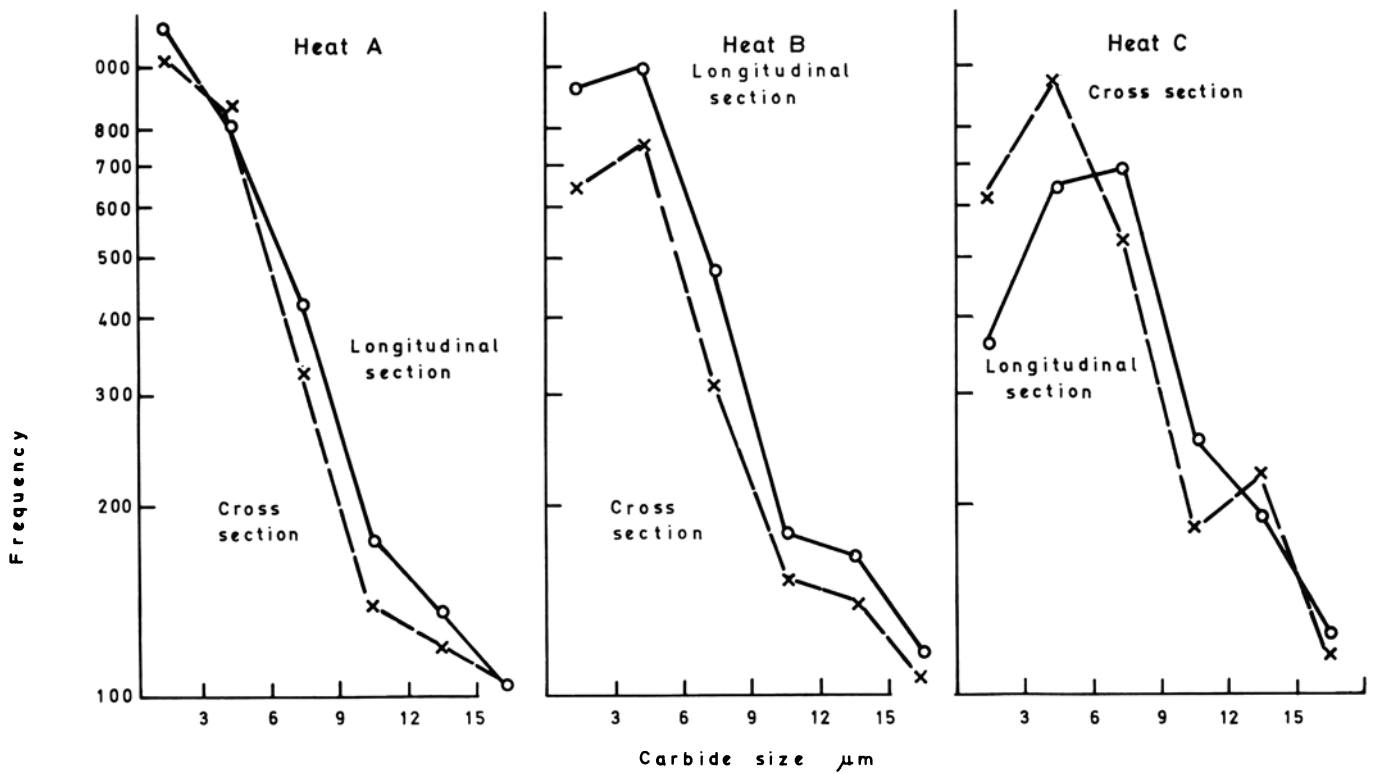


Fig. 4 Frequency distributions of carbide size for specimens of heats A, B and C.

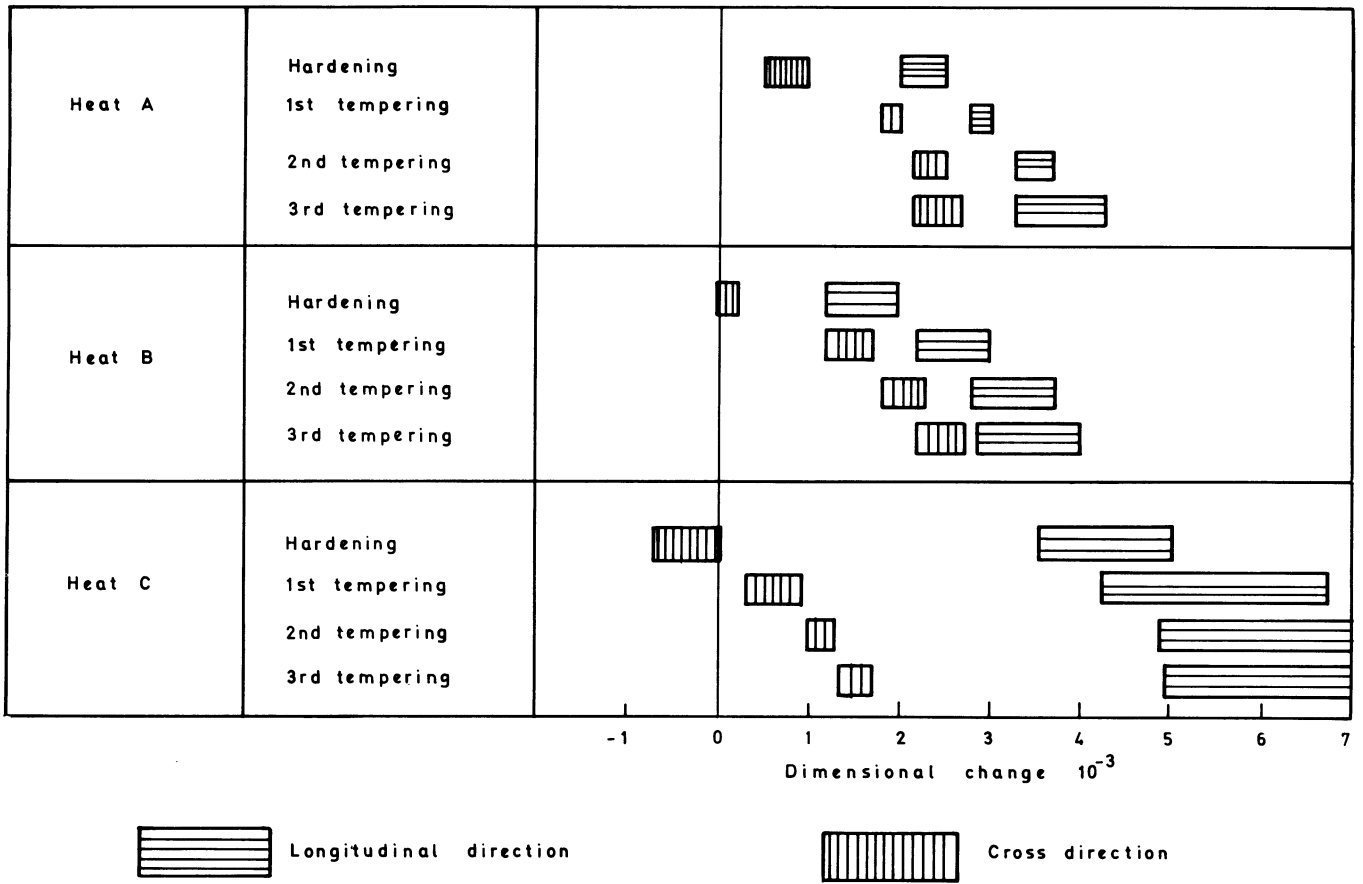
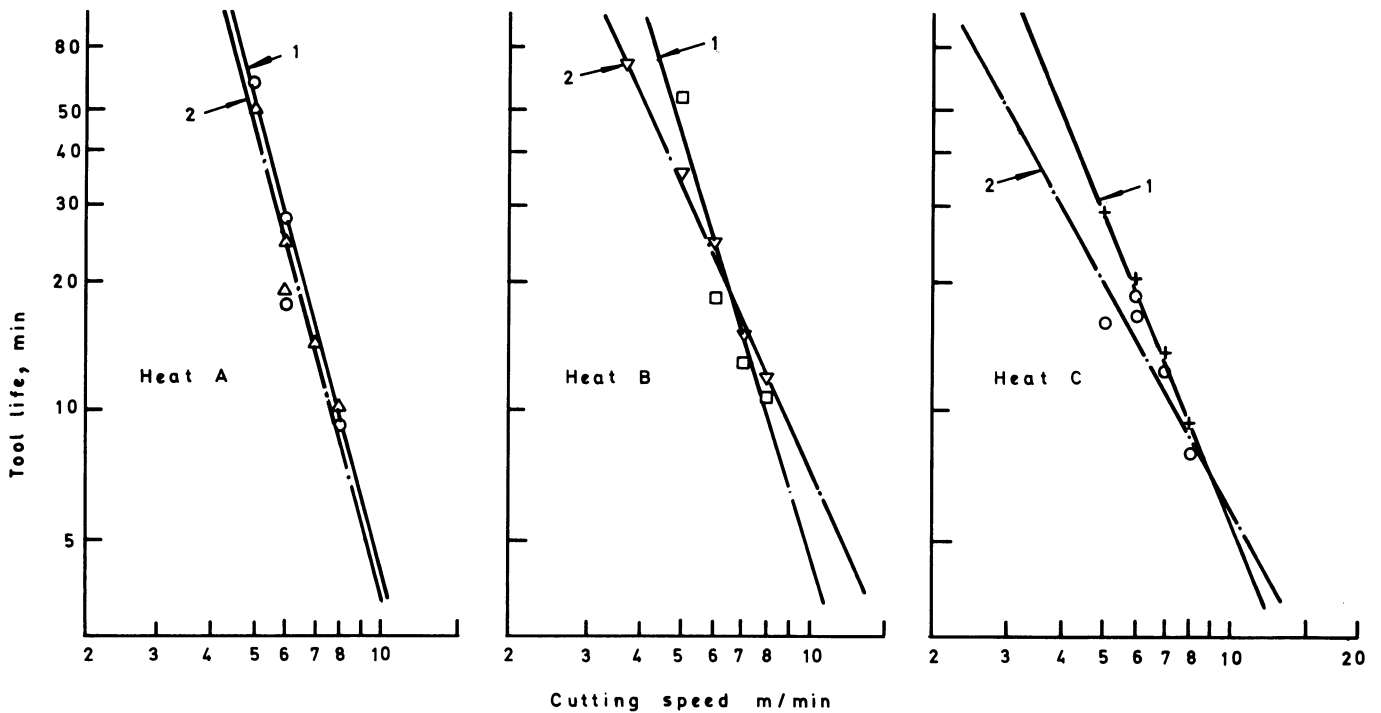


Fig. 6 Dimensional changes in the evaluated heat treating specimens.



- 1 Cutting edge parallel to the direction of forging
- 2 Cutting edge perpendicular to the direction of forging

Fig. 7 Correlation of tool life and cutting speed for single point turning tools made from heats A, B and C.

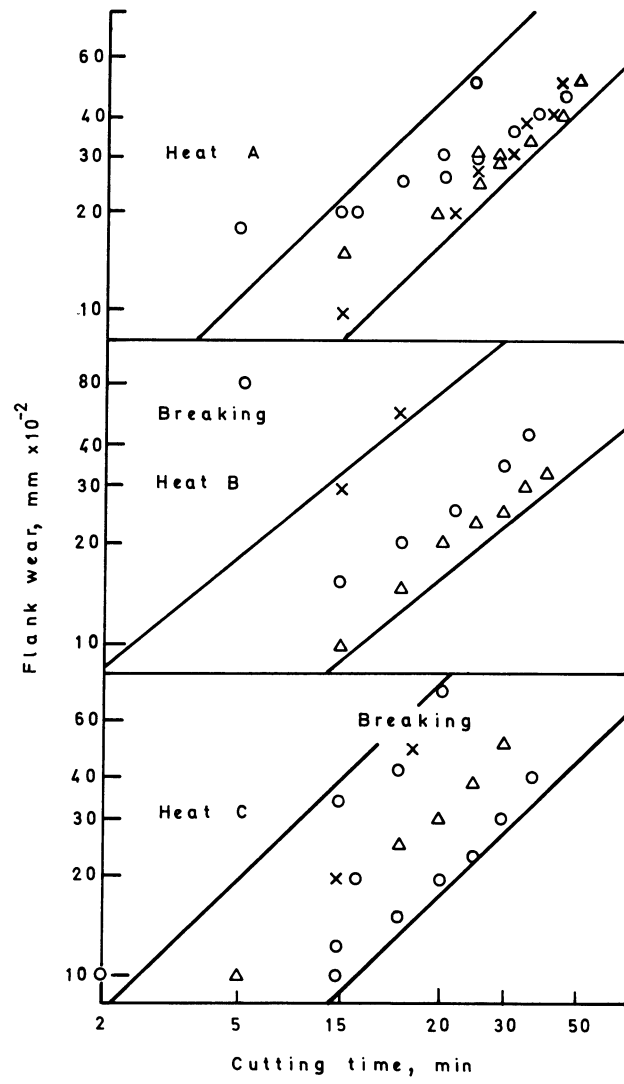


Fig. 8 Correlation between tool wear and cutting time for insert milling cutters made from heats A, B and C.

DIGITAL COMPUTER AIDED DESIGN AND CONTROL

THE PROGRAMMED APPROACH IN CONTROL SYSTEMS

by

R. DOANE* and D. HOLLAND†

SUMMARY

The basic principles that separate the programmed approach from more traditional direct approaches are discussed and examples given. The programmed approach is shown first in its application to sequential control of mechanical systems, and then briefly in its application to numerical controls. Finally, the limitations of the programmed approach are considered, and non-programmed alternatives briefly discussed.

DESCRIPTION OF PROGRAMMING

Programming and its expression in software or firmware are distinct from more direct (hardware) techniques in the way system behaviour is defined. Table 1 shows what these differences are for electronic controls. In essence, the programmed approach to electronic controls divides the problem of system

TABLE 1 Comparison of the characteristics of programmed and direct approach to control system design

Direct approach	Programmed approach
Electronic circuits and their 'hardwired' interconnections define all parameters of system behaviour.	Electronic circuits and their 'hardwired' interconnections define a class of possible system behaviour patterns. The programme defines the specific details of system behaviour.
The details of how the system is intended to behave are 'remembered' by the circuitry and wiring.	The details of how the system is intended to behave are stored on punched paper tapes, magnetic tapes in magnetic cores etc. (software) or in woven wire memories, diode arrays etc. (firmware).

design into two parts: electronic hardware to define a class of available system characteristics and a programme or programmes to specify the details within that class.

There are many well-known mechanical devices that have used the programmed approach successfully. The music box, for example, is capable of a class of system characteristics called 'playing a tune'. The particular tune played depends on a mechanical memory comprising a drum or disc with pegs or tabs arranged to programme the sequence of musical notes making up the particular tune to be played.

This drum or disc memory holding the musical programme would be called firmware in today's terminology, because the programme can be altered only with a physical change. Many music boxes, however, play more than one tune and some elaborate ones are designed for easy replacement of one whole programme by another.

The 'player piano' or 'pianola' is another programmed musical device, but it uses software instead of firmware. The perforated paper strips that control the tune-playing behaviour of the pianola are more easily interchanged than are music-box programmes. Ease of programme change is characteristic of systems programmed in software.

Advantages of the programmed approach

One can think of many other programmed devices in common use long before the advent of reliable solid-state electronics: everything from tumbler and combination locks to Jacquard weaving looms and automatic screw machines. Whenever the programmed approach has been applied, it has allowed several helpful changes in both design and use of the system (see Table 2). The separating of details relating to the specific applications away from general system design problems makes both parts of the job more manageable. One of the most important consequences for the use of electronic controls is the possibility of having the controls built by people who have only a general idea of the use to which the systems will be put, while the programmes are prepared by people who need to know little about

*Digital Equipment Corporation, Maynard, U.S.A.

†Digital Equipment Company Limited, Reading, England.

controls but who understand the application intimately. The total manpower made available by this division is potentially much greater than the number of people who can be expected to learn both sides of the control system problem.

TABLE 2 Advantages of programmed approach

Direct approach	Programmed approach
Details of system function must be considered together with other problems, such as physical arrangement and interconnections.	Outlines of system capabilities must be considered together with other problems such as physical arrangement and interconnections.
	Details of system function may be considered at a different time, in a different place, by different people who need not be burdened with questions of physical arrangement, interconnections etc.
If malfunctions occur, diagnosis requires a complete knowledge of the system.	If malfunctions occur after a period of successful operation, the programme is known to be good. Diagnostic aids built into the programme may be used to isolate the fault. Sometimes a diagnostic programme can be used in place of the entire working programme for self-checking. A complete detailed knowledge of the system may not be required.
Changes in system function require rethinking the system design and rebuilding the physical system; sometimes the entire system can be replaced easier than the existing system could be salvaged.	Errors in the programme can be searched out in a methodical way before the programme is installed in the system. Changes can be made by preparing a modified programme, without the need to worry about wide-ranging consequences. Redesign or reassignment of the equipment obsolesces only the programme.

THE PROGRAMMED APPROACH IN SEQUENTIAL CONTROL

The first class of problems discussed require the sequencing of a mechanism or process through a series of discrete steps. In a sense, the music box referred to previously is an example of a programmed controller, but with a significant exception: the music box is run by a timer. For maximum productivity industrial processes are self-timed wherever possible. That is, a feedback sensor tells the control when the goal of each step has been reached, and the next step is initiated immediately. Such controllers employ timers only when specific steps have goals for which no adequate completion sensor is available.

Until recently machine tools were almost invariably controlled by panels of relays designed by the direct approach. Relays are used because of their low cost and the ease with which they interface with limit switches and so forth. However, the increasing costs of design, manufacture and maintenance of these systems together with the increasing complexity of the machines being controlled has led many users and builders of machine tools to consider the alternative.

Fig. 1 shows the first known application of the programmed approach for sequential control. This PDP-14 programmable controller replaced a relay controller in May of 1969 to control a Reichaur grinder at the General Motors HydraMatic Plant, near Detroit, Michigan. Since then hundreds of such controllers have been installed on a wide variety of machines and mechanical systems. The largest single category of applications has been for the control of 'transfer' machines, which are highly integrated manufacturing systems used in the automotive industry and others for high volume automatic production.

PDP-14 and PDP-14/L programmable controllers are also used in such diverse applications as conveyor switching, control of automated parking garages, and auxiliary function control on large numerically controlled machines.

Fig. 2 shows the main components of a PDP 14/L programmable controller. The programme is built into a wire braid (in the sub-system labelled 'Memory'). The wire braid technique, an outgrowth of the technology used to operate critical systems aboard the Apollo missions, offers maximum security in the control of equipment that could be dangerous. There is no way that the programme can be lost or altered short of physically changing the arrangement of wires in the braid. This firmware concept accounts in large measure for the speed with which the PDP-14 series of controllers has been accepted. (The controller is described in rather more detail in Appendix 1).

A key part of the PDP-14 concept is the provision of software aids for the preparation and pre-testing of programmes, before they are implemented in a wire braid. The PDP-8/E computer system shown in Fig. 3 can be used with a programme called BOOL-14 to create a description of the wire braid from statements that specify the interrelations that are desired between stimuli to the controlled device (motor starters, solenoid valves etc.) and responses (limit

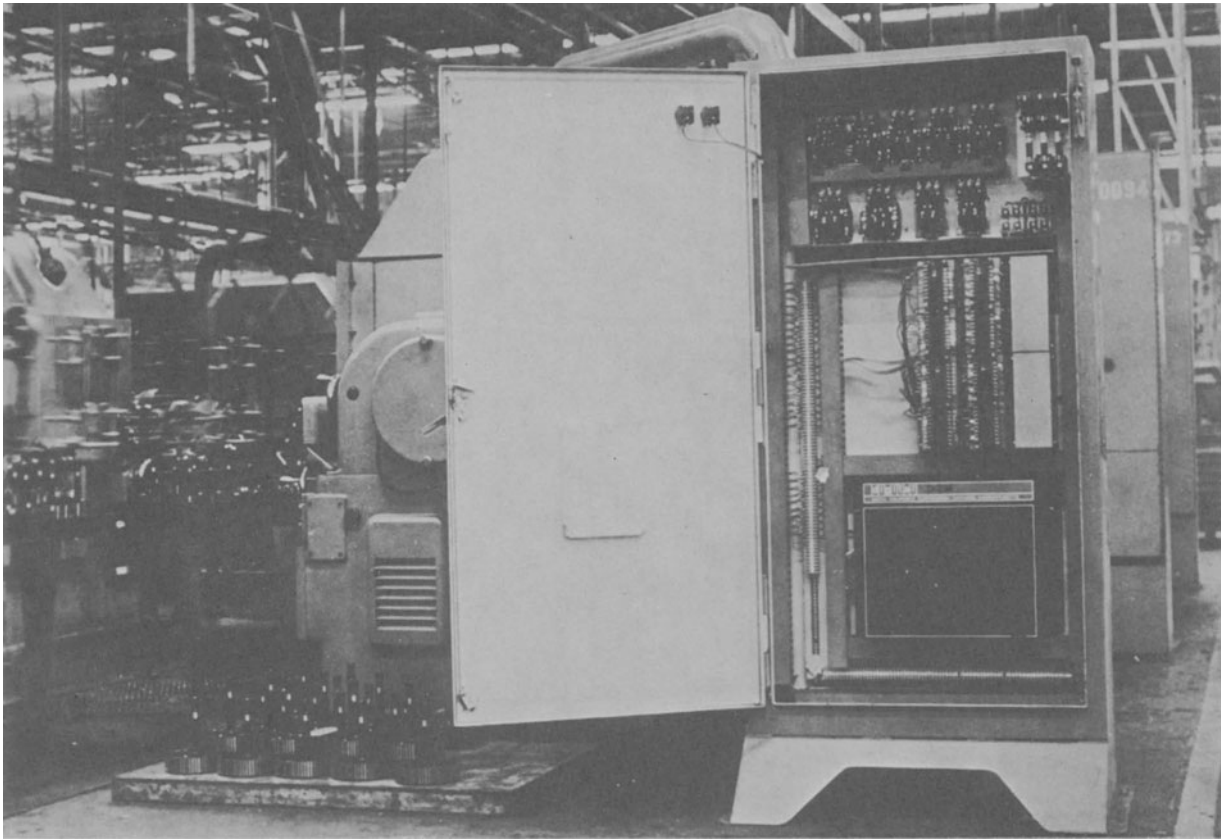


Fig. 1 PDP-14 installation controlling grinder at General Motors Hydra-Matic plant.

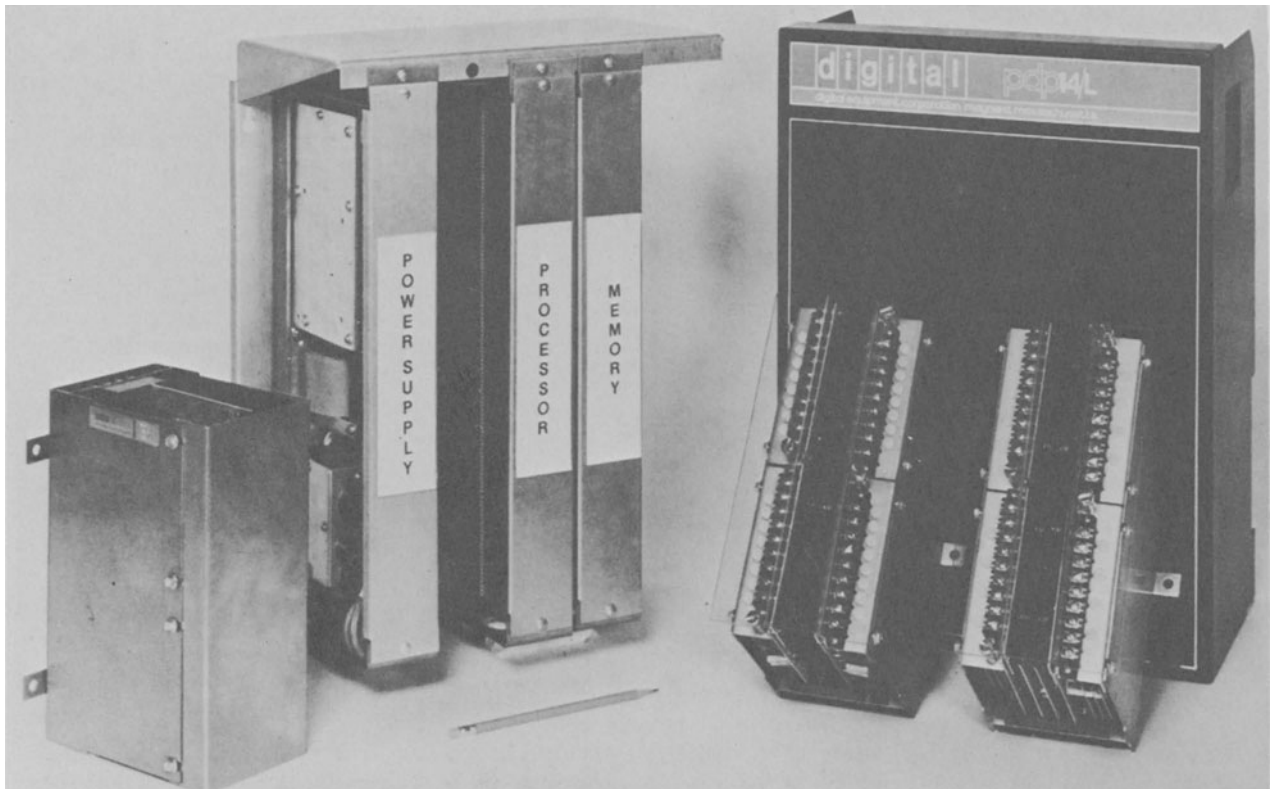


Fig. 2 Main components of PDP-14/L programmable controller.



Fig. 3 PDP-8/E computer system.

switches and the like). After preliminary checking and modifications have been made, the same PDP-8/E can be used to actually run the system, using the output of BOOL-14 with another programme called SIM-14, to allow the PDP-8/E to simulate the functions of the wire braid temporarily.

The most recent development of the PDP-14 concept is the introduction of MAP-14 (machine analogue package) which provides a sophisticated maintenance tool for those users who have a number of important machine tools controlled by PDP-14 systems. MAP-14 enables the user to make a record of the functioning of a machine tool at the time of acceptance and to use the record to point out differences later, when the machine is malfunctioning. This technique is invaluable for finding the 'operationally random' or intermittent fault.

One major manufacturer of transfer machines reported that his machines used to spend about half their time in assembly and mechanical test, and the other half being checked as operating systems while the controls were being tested and revised. In his first PDP-14 experience, the system test phase required less than 2 days due to the pre-testing and easy revision made possible by BOOL-14 and SIM-14. His shops are, therefore, able to build and ship twice as much equipment as before, with no increase in floor-space. Also, his customers are better served by the increased reliability and ease of updating they get with the PDP-14, and this machinery builder has saved the price of a new factory.

PROGRAMMABLE CONTROLLER INSTALLATIONS

There are now a number of PDP-14 installations in Europe. The first in the U.K. was on a transfer machine supplied by Snyder Limited to the South Wales plant of Girling Limited. The machine has been in production for some six months, during which

time the PDP-14 controller has been faultless.

In this application, the PDP-14 resulted in direct savings in the cost of steelwork. Due to space limitations at the user's plant a conventional relay panel would need to have been mounted on a special overhead gantry. Because of the relative compactness of the PDP-14 control system it was possible to mount the controls on the same level as the machine. This installation has demonstrated the merits of the programmed approach in general and PDP-14 read-only memory and software systems in particular. Because of the use of BOOL-14 and SIM-14 no significant changes in PDP-14 read-only memory were required after installation. Minor changes that subsequently proved necessary were easily performed by the user's engineering staff.

Fiat, in Italy uses programmable controllers on machine tools producing engine and gearbox parts. A total of five PDP-14 systems are used on a transfer machine supplied by Lassalle-Chimat for the production of FIAT 127 gearbox cases. Three of the controllers are used for direct control of one part of the machine, while two are used to monitor conventional controls in another part of the machine. This dual approach is intended to provide valuable information on the economics of programmable controllers and computer monitoring systems.

A second transfer machine manufactured by Fiat themselves using two PDP-14 controllers has been in production since February 1971 machining engine components. Downtime on the machine due to the controllers is said to be zero.

THE PROGRAMMED APPROACH IN NUMERICAL CONTROL

Numerical control differs from sequential control because not just the sequence of events, but their timing and geometry are established by the control system. Numerical controls are the earliest form in

which the programmed approach to control systems gained widespread acceptance in electronic form.

Since numerical control is itself an expression of the programmed approach to control systems, it might be thought that the ultimate has been reached. However, there are two ways in which further progress has been made.

(1) The first is in the preparation of the NC part programme. Just as *BOOL-14* and *SIM-14* are tremendously helpful in preparing and debugging a programme to be used in a *PDP-14*, similar software aids are available for preparing the programmes that are needed to run a numerically controlled machine tool. The same *PDP-8/E* system shown in Fig. 3, for example, can run *QUICKPOINT-8* for preparing point-to-point tapes for drilling, simple milling and punching on a variety of NC machines. With about 30 different post processors already available, and well over 100 installations, *QUICKPOINT* is saving an average of 50% of the labour that used to be spent in preparing NC tapes manually. The *PDP-8/E* can also

be expanded to run *UNIAPT*, allowing it to prepare NC tapes for large, multiaxis work. For turning, a programme called *EasyProg* has been developed in Germany by a lathe manufacturer, to use the same *PDP-8/E* processor. With these and other software aids, preparing part programmes can be greatly simplified.

(2) The second development concerns the use of software to interpret NC part programmes and to supply extended capabilities such as machine-side editing of part programmes and the reporting of exceptional circumstances affecting productivity to supervisors and management. Fig. 4 shows a system of this type called *Mini DNC*. It simultaneously runs two independent machine tools, interpreting their separate part programmes, and at the same time can be used for the preparation of simple part programmes to be run later. The system allows programmed speeds and feeds to be optimized from the control panel at the machine, and prints the circumstances for the supervisor if production is



Fig. 4 Mini DNC system.

interrupted. The Mini DNC design is oriented to the same smaller NC machines for which QUICKPOINT was developed, and has the same PDP-8 processor built in. Larger DNC systems have been built around the same processor and also around the PDP-11. The use of software to interpret software, as in these systems, is a new and growing dimension of the programmed approach to control systems.

Limitations of the programmed approach

It would hardly be fair to finish a discussion of these developments without paying some attention to their limitations. There are two significant boundaries to the usefulness of the programmed approach in control systems, both based on economics.

(1) The first is that a control system needs a certain size to support the specialisation of functions inherent in the programmed approach. Below that size, which for a programmed controller like the PDP-14/L might be close to 100 relays at current European wage rates, economic justification must be based on indirect factors. Such factors might be: improved reliability, the need for added system features such as on-line monitoring, or the time and floor space savings referred to earlier. As wage rates rise and new products are introduced, the crossover point will continue to move towards this class of system.

(2) The second boundary concerns flexibility. If one wishes to build 100 or 1000 systems all alike, and all having a single, never-changing task, the flexibility of the programmed approach does not pay-off so well. This can be especially true if a wide variety of specialised unique circuit functions are needed in an otherwise small system. For such cases there are two types of equipment available: the highly-developed logic modules using both integrated and discrete component circuitry available from a number of suppliers, and the new PDP-16 processor recently introduced by DIGITAL using the proprietary 'Chartware' concept for simple tailoring of complex but single-function systems.

The future of the programmed approach

The technology for a programmed approach to many controls problems has been available for almost a decade, and the last few years have seen a remarkable increase in the variety and number of operating installations. Henceforth, the rate at which the benefits of this approach become realised will depend mostly on the rate at which potential beneficiaries learn about it.

As a way of encouraging this learning process DIGITAL has established training centres in Reading and elsewhere in Europe and publishes a variety of free tutorial material as well. Much of this effort is admittedly product oriented, but a number of educators have found some of the published materials to be worth using as texts in class, and the training courses have been praised by many who found them helpful in understanding the overall possibilities as well as the specific details.

The programmed approach to control systems is ready to go to work almost anywhere in industry, and the development of programming aids is making some

applications merely routine. A knowledge of this approach should be one of the resources that every builder and user of control systems has ready at hand.

APPENDIX 1

DESCRIPTION OF EQUIPMENT MANUFACTURED BY DIGITAL

PDP-14 system components

The PDP-14 control system is a unified assembly of three basic units:

- Input interface boxes (I-boxes)
- The PDP-14 programmed control unit
- Output interface boxes (O-boxes)

All system inputs and outputs are designed for 110–125 VAC, 50/60 Hz single-phase, compatible with the present industry standard (see Fig. 5).

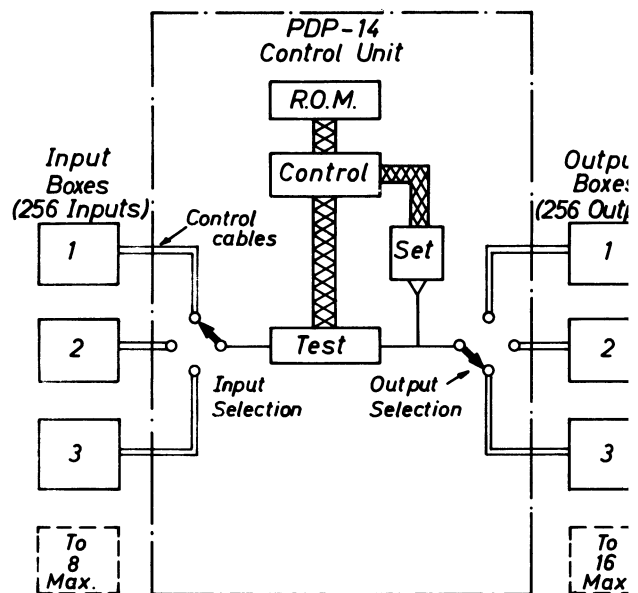


Fig. 5 PDP-14 system diagram.

(a) Input boxes

The I-boxes are signal-conditioning devices; they accept 120 VAC inputs from two-state sensing devices such as limit switches, pushbuttons, proximity switches, pressure switches and photocells. These inputs are converted into signals which are proper for our solid-state equipment. They then pass along control cables to the PDP-14 control unit. Each I-box contains 32 inputs. A maximum of eight I-boxes, providing a total of 256 inputs, is permitted in one PDP-14 system.

Input boxes may be substituted for output boxes to expand the input capabilities (in increments of 32) to a maximum of 512 inputs.

(b) PDP-14 control unit

The control contains a wire matrix or 'braid' which is the memory of the entire unit. It is called a 'read-only' memory (ROM) because it cannot be altered electrically (that is written on). The ROM is actually a list of permanently-wired electrical instruc-

tions which are 'read' by the control to determine its operation.

The control operates in a way analogous to scanning a relay ladder diagram rung-by-rung. Each rung of the ladder represents a specific group of sensed input conditions which must be satisfied to cause a change in the condition of an output. The ROM contains instructions in small groups, each corresponding to a single rung in the ladder. The ROM directs the control to select each input specified in a group and test whether it is on or off (this is the action performed by the 'Test' unit shown). Finally, the specified output is selected and set on or off, based on the test results (this is the function of the 'Set' blocks). The control now continues to the next group of inputs and outputs and repeats the process. This action proceeds one instruction at a time, but so fast that all inputs are checked and outputs properly changed in thousandths of a second; in fact, usually faster than one or two hundred relays could respond.

(c) Output boxes

Control signals sent from the control are accepted by the O-boxes to activate selected 120 VAC outputs. Each output is a triac, the solid-state equivalent of a remotely-controlled switch. Once set on, each output remains on and supplies power until it is set off by a new control signal.

Output boxes have an additional system function: they can be interrogated by the control unit to determine whether their outputs are on or off. In this mode, they can be considered as control inputs.

Each output of an output box can be connected to its own source voltage and to loads, such as solenoids, motor contactors, small motors, lamps and signalling devices.

Each output box contains 16 outputs. A total of 16 O-boxes providing 256 outputs may be incorporated in one PDP-14 systems.

Read-only memory

The heart of the control operation is the read-only memory (ROM). The ROM contains all the instructions which allow the control to sample specific groups of inputs and then select a specified output and turn it on or off. The ROM is provided in one to four separate plug-in sections, each of which has over 1 000 locations in which control instructions are stored. The number of sections required is determined by the size of the control 'problem'—the number of inputs and outputs, and the number of control decisions that must be made.

The ROM is an actual physical matrix or 'braid' of solid wires permanently-embedded in a potting compound and surrounded by electronic sampling circuits (96 transformer cores) in a sandwich packaging. The arrangement of the braid wires is determined in a series of computer-aided steps, which result in a punched paper tape. This tape is used to operate an automatic wire placing machine or 'loom' which forms a wire braid. This braid, returned to be installed in the control unit, represents the specific solution to the individual control problem. Whenever this element is changed, the PDP-14 system behaves as though it were rewired, allowing you complete

flexibility in changing machine operations and retrofit.

In operation the ROM acts like a series of wires strung through and around small current transformers. Each wire represents eight individual control instructions, which are read by sending a current pulse through it. The readout is in groups of eight instructions. The single desired instruction is selected from these eight. Only the transformers with wires running through their cores will be energised. The pattern of energised transformers is then read as an electronic instruction code. The code is the 12-bit binary instructions which are understood by the PDP-14 control unit (see Fig. 6).

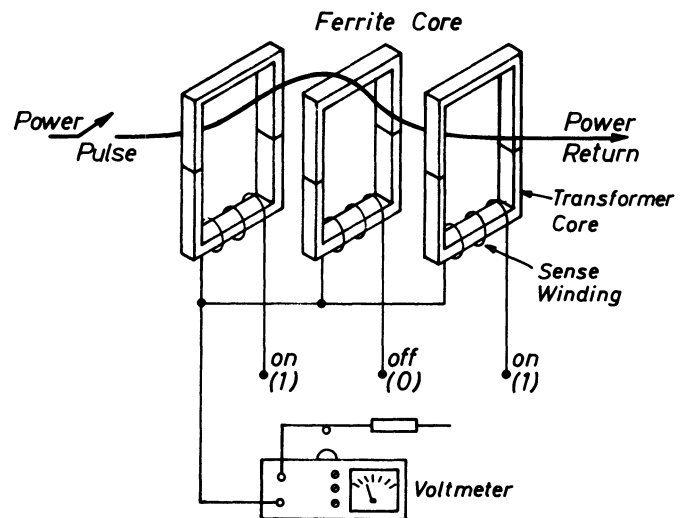


Fig. 6 Schematic of three PDP-14 ROM transformer cores.

It is possible to change as many as 20 wires (about 15%) of the ROM by cutting out wires and manually replacing them with new ones.

Accessories

In addition to normal outputs, the PDP-14 system may be equipped with solid state timers, retentive memories, and storage outputs. The timers and retentive memories are provided in an accessories box (A-box). The storage outputs are provided in a storage module consisting of 16 storage outputs.

The solid state timers may be adjusted to provide timing functions from fractions of a second to thirty seconds. The retentive memories are mercury-wetted relays which provide 1-bit of storage information after a power failure. The storage outputs provide temporary storage of intermediate processing, results and status information and are sometimes used for communication between the PDP-14 and the monitoring computer.

Also supplied as an accessory is an auxiliary power supply which is required for large PDP-14 systems.

Programming the PDP-14

Programming in the PDP-14 system is simply the procedure used to generate the read-only memory (ROM) to control a process or machine. PDP-14 programming does not require previous computer

experience but it does require experience in machine control.

PDP-14 programmes provide relationships between inputs (limit switches, pushbuttons, selector switches etc.) and outputs (solenoids, motor contractors, indicator lights etc.). These relationships or control functions, may be expressed as Boolean equations which, when solved for particular input values, specify the state (ON or OFF) of an output.

Machine inputs and outputs must be assigned to the PDP-14 input (I) and output (O) boxes before a PDP-14 control programme can be written.

These assignments permit the PDP-14 instructions to test the state of specific inputs and outputs. Once these assignments are made, the inputs and outputs are referred to by unique numbers preceded by an X for an input or a Y for an output. For programming purposes, these X and Y numbers represent specific input and output devices.

Boolean representation of machine control

Programming a PDP-14 requires familiarity with simple Boolean representations of control functions. These representations consist of 'operators' and 'variables'. The variables of PDP-14 control equations are inputs (X's) and outputs (Y's). The variables have two 'states' namely, ON and OFF. The operators in these equations are (AND) + (OR) and / (NOT). Parentheses may be used within equations to group variables.

For example the equation:

$$Y_{10} = X_{23} + X_{21} * Y_7$$

is read 'output 10 is set ON when input 23 is ON, or when both output 7 and input 21 are ON'. This equation instructs the PDP-14 to test input 23; if it is ON set output 10 ON. If input 23 is OFF test output 7 and input 21; if they are both ON, set output 10 ON. If neither set of conditions is satisfied set output 10 OFF.

The above equation could be represented by the ladder diagram shown in Fig. 7.

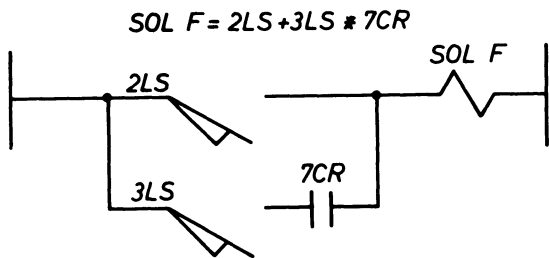


Fig. 7 Where SOL F corresponds to Y10; 2LS corresponds to X23; 7CR corresponds to Y7; and 3LS corresponds to X21.

A set of control functions similar to the preceding example comprise a PDP-14 programme. A series of equations corresponding to these functions and written in terms of X's and Y's are then translated into the PDP-14 machine code programme using BOOL-14.

BOOL-14

Is a translator programme for control equations. It operates a PDP-8 family computer and translates the equations into the PDP-14 machine code instructions needed to solve these equations. The machine code instructions will later be woven to form the ROM for the PDP-14. Before this happens, however, the programme should be rigorously tested and debugged. This is done with SIM-14. The translation for two equations is:-

$$Y_{10} = X_{23} + X_{21} * Y_7$$

0000	2423	TXN	023
0001	5407	JFN	007
0002	2021	TXF	021
0003	1007	TYF	007
0004	5007	JFF	007
0005	3010	SYF	010
0006	0344	SKP	
0007	3410	SYN	010

$$Y_{17} = X_2 + X_{51} + X_3 * Y_7 + X_4 * Y_{21}$$

0010	2402	TXN	002
0011	2451	TXN	051
0012	5423	JFN	023
0013	2003	TXF	003
0014	1007	TYF	007
0015	5023	JFF	023
0016	2004	TXF	004
0017	1021	TYF	021
0020	5023	JFF	023
0021	3017	SYF	017
0022	0344	SKP	
0023	3417	SYN	017

The resultant PDP-14 programme is a 'closed-loop' of disjoint instruction groups. Each group of instructions solves an equation for one output, setting it on or off. For example, if a machine control requires twenty outputs, there are twenty equations and instruction groups in the control programme. The last instruction group is terminated with a 'jump' to the first instruction group. The construction of the programme is illustrated in Fig. 8.

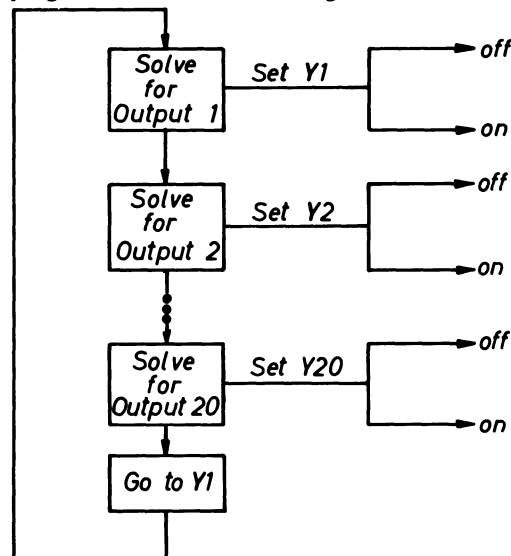


Fig. 8 Construction of the programme.

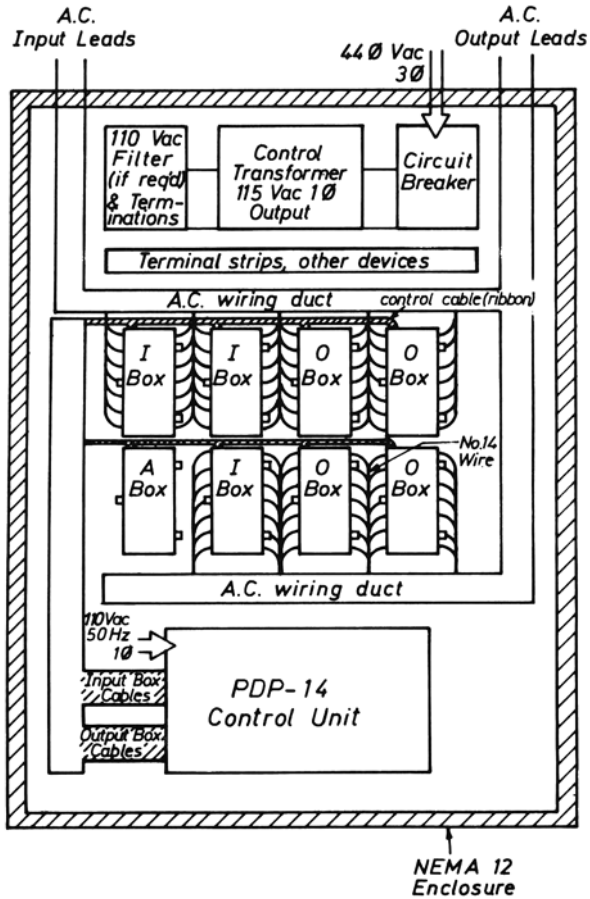


Fig. 9 PDP-14 system layout example.

SIM-14

Is a PDP-8 based programme which simulates PDP-14 operation in two modes. The user may operate in an offline or local mode to debug or modify his programme completely within the PDP-8. When relatively certain that the programme is correct, the user may switch to on-line mode where the programme is executed to control the machine's operation.

Local mode debugging offers three features for testing programmes:

- (1) The user supplies input states for a given equation and SIM-14 reports the resultant state of the output. This proceeds equation-by-equation.
- (2) The user generates a complete truth table, or binary array, which completely defines the state of an output for all possible input states. This is also done for each equation.
- (3) The user tests the complete programme using simulated execution. He tests the complete programme in sequence by specifying input states. Changing output states are reported by SIM-14. The user continues to vary input values to test all segments of the programme.

The following are sample truth tables as generated by SIM-14 for the two equations which were translated by BOOL-14.

$$Y_{10} = X_{23} + X_{21} * Y_7$$

.TA1Ø
.X23
.X21
.Y7
.SØ

A XØ23
B XØ21
C YØØ7

ABC
ØØØ = Ø
ØØ1 = Ø
Ø1Ø = Ø
Ø11 = 1
1ØØ = 1
1Ø1 = 1
11Ø = 1
111 = 1

$$Y_{17} = X_2 + X_{51} + X_3 * Y_7 + X_4 * Y_{21}$$

.TA17
.X2
.X51
.X3
.X4
.Y7
.Y21
.SØ

A XØØ2	Ø1Ø111 = 1	11Ø111 = 1
B XØ51	Ø11ØØØ = 1	111ØØØ = 1
C XØØ3	Ø11ØØ1 = 1	111ØØ1 = 1
D YØØ7	Ø11Ø1Ø = 1	111Ø1Ø = 1
E XØØ4	Ø11Ø11 = 1	111Ø11 = 1
F YØ21	Ø111ØØ = 1	1111ØØ = 1
	Ø111Ø1 = 1	1111Ø1 = 1
ABCDEF	Ø1111Ø = 1	11111Ø = 1
ØØØØØØ = Ø	Ø11111 = 1	111111 = 1
ØØØØØ1 = Ø	1ØØØØØ = 1	
ØØØØ1Ø = Ø	1ØØØØ1 = 1	
ØØØØ11 = 1	1ØØØ1Ø = 1	
ØØØ1ØØ = Ø	1ØØØ11 = 1	
ØØØ1Ø1 = Ø	1ØØ1ØØ = 1	
ØØØ11Ø = Ø	1ØØ1Ø1 = 1	
ØØØ111 = 1	1ØØ11Ø = 1	
ØØ1ØØØ = Ø	1ØØ111 = 1	
ØØ1ØØ1 = Ø	1Ø1ØØØ = 1	
ØØ1Ø1Ø = Ø	1Ø1ØØ1 = 1	
ØØ1Ø11 = 1	1Ø1Ø1Ø = 1	
ØØ11ØØ = 1	1Ø1Ø11 = 1	
ØØ11Ø1 = 1	1Ø11ØØ = 1	
ØØ111Ø = 1	1Ø11Ø1 = 1	
ØØ1111 = 1	1Ø111Ø = 1	
Ø1ØØØØ = 1	1Ø1111 = 1	
Ø1ØØØØ = 1	11ØØØØ = 1	
Ø1ØØØ1 = 1	11ØØØ1 = 1	
Ø1ØØ1Ø = 1	11ØØ1Ø = 1	
Ø1ØØ11 = 1	11ØØ11 = 1	
Ø1Ø1ØØ = 1	11Ø1ØØ = 1	
11Ø1Ø1 = 1	11Ø1Ø1 = 1	
Ø1Ø11Ø = 1	11Ø11Ø = 1	

PDP-8/E

Is the latest addition to our very successful 'family-of-8' range of computers introduced in 1965, of which over 10 000 have now been installed. The basic specifications are:-

Word size	—	12 bits
Memory cycle time	—	1.2 μ s
Memory size	—	4 096 words expandable to 32 768 words
Physical size	—	19 in. rack, 10½ in. high, 24 in. deep

The PDP-8/E features considerable advances, both in its electrical and mechanical design which enables its full memory expansion capability to be contained within the processor cabinet.

The elimination of conventional back-to-back wiring, by the use of a printed wiring system known as the OMNIBUS, has greatly enhanced reliability.

PDP-11

The PDP-11 family of computers of 1970 introduced the concept of the UNIBUS, which gives the machine very powerful real time characteristics. The basic specifications for the PDP-11/20 are:

Word size	—	16 bits
Memory cycle time	—	950 ns
Memory size	—	4 096 words expandable to 124K
Physical size	—	19 in. rack, 11 in. high

The full range of the PDP-11 family provides machines varying from low cost OEM to high powered computational machines.

PDP-16

This is the most recent development in low cost computer systems. The PDP-16 does not have a single specification since it is in fact a made-to-measure computer. The systems are made up from large function macro-modules known as RTM (register transfer modules). These modules permit systems to be built to solve specific problems. In these applications, the PDP-16 can offer higher speed or lower cost, or both. Basic specifications for PDP-16 systems:

Word size	—	any multiple of 8, 12 or 16
Memory	—	read-only or random access available in a wide variety of sizes and speeds
Instruction set	—	basic instructions include add, sub- tract, negate and several logical functions. Any instruction can be micro-programmed.

APPENDIX 2

FURTHER READING

1. 'Standard Programmable Machine Control Systems at Hydra-Matic' by William S. Stone, presented at the 34th Annual Machine Tool Electrification Forum, Pittsburgh, Pen. 26/27th May, 1970.
2. 'Computer-aided Cycle Programming of a British-built Snyder Transfer Machine' by A. W. Astrop *Machinery*, 7th October, 1970.
3. 'Direct Numerical Control' by Ian Fallows *Instrument Practice*, February, 1971.
4. 'The Register Transfer Module Design Concept' by Gordon Belland and John Grason. *Computer Design*, May, 1971

A SYSTEM FOR DIRECT NUMERICAL CONTROL OF MACHINE TOOLS

by

G. SPUR and W. WENTZ*

SUMMARY

Systems for direct numerical control (DNC) include usually a small high-speed real time electronic computer, communicating directly with the NC machines to be controlled by means of a dispatcher. The computer used in the DNC-system NC 700 has a capacity of core storage of 16 K words. Software and hardware are in modular structure to control units up to six machine tools of varied manufacture and type. All control data are located on a magnetic tape. The data output is initiated by the NC machine tools and requires an intermediate storing device, here a part of the core memory. In addition to the dispatching function, the DNC system includes programs in order to register and to work up production data. The basic DNC program is completed by a number of user programs. All part-programs are stored on a magnetic tape and so, for instance, are easy to bring up to date. In the last few months such systems have been presented in the USA, Japan and Western Europe and should be installed in such factories where many NC machine tools are to be controlled. Because of the automatic information flow and by simplifying the control units of the machine tools, DNC can be used economically.

INTRODUCTION

The use of computers is necessary in automatic systems when either the number of functions to be executed in order to control the process is large or the speed of the process itself is very fast. Conventional machine tools are difficult to be integrated into automatic production systems. Through the development of Numerical Control (NC), a suitable link has been created in order to integrate machine tools into a process control system.

A recent development in the field of automatic information flow in the factories at the single-piece and low-series production are systems for direct numerical control (DNC). They render possible the on-line connection of NC machine tools to a process computer. Thus it is possible to give the machine control data directly to the control unit and avoid the conventional paper tape. There the control data are stored on a mass storage and, when requested, are put out directly to the NC machine tools. The connection to the control unit can be behind the tape-reading device or at the corresponding registers and memories.

In the first case the original control unit is nearly completely conserved, while only the fragile paper tape reader is eliminated. Such a system is well prepared to integrate NC machines which already are used in the factories into a DNC system. Thus there is always the possibility of a quick change to the conventional tape-reader mode.

Another method of machine tool control is known as computer numerical control (CNC) and is mentioned here in order to show the difference from DNC. The main typical difference is the density of the information flow per work progress. The information flow from the paper tape to the numerical control can be regarded as quasi-static. In contrast, the subsequent transformation in the control unit by the interpolator is a dynamic proceeding. The delimitation between DNC and CNC is the intersection between quasi-static and dynamic information processing. When several axes are interpolated by a computer and at the same time the above-mentioned characteristics of DNC are realized, the delimitation between the DNC and CNC is within the software of the computer¹.

The machine control unit (MC), which only has become known in connection with DNC systems, contains characteristics of conventional or hardware NC and of CNC or software NC. There only such functions are performed which would take a computer too much computing time. The other functions will be executed by the available computer².

While the NC machines used in 'systems behind the tape-reader' (BTR) also work without a computer, machines with MCU are only functionable with a DNC device. The different types of control units, which can be linked to a DNC system, are shown in Fig. 1.

Besides the dispatching of control data DNC

*Lehrstuhl und Institut für Werkzeugmaschinen und Fertigungstechnik, Technische Universität, Berlin.

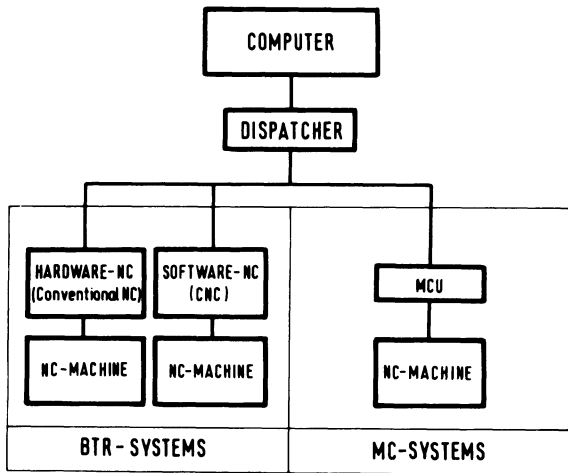


Fig. 1 Classification of DNC systems

systems mainly have administrative tasks. They reduce the considerable expenditure which can be met even in smaller factories in order to store and prepare paper tapes. Newly installed control data programs can quickly and easily be improved after a test run. The on-line connection of the machines with the computer is used in larger systems to transmit production data. These data are obtained at the machines, computed and either put out on a teletypewriter or transmitted to a superior computing system.

Producer	System	Computer	Core memory	Number of linked machines
AEG-Telefunken	NC 700	AEG 60-10	16...32 K Words	32 by a unit
Bendix	Dynapath			
Cincinnati		CIP 2100	16...56 K	64
Ex-Cell-O		Raytheon 706	16 K Words	
Farrel		Spiras 65	64 K Words	
Fujitsu	Fanuc T	Hidic 100 and Hitac 7250		10 50
	Fanuc K	Facom 250-20		7
General Electric	CommanDir	PAC 30	16...64 K Bytes	15
Kearney & Trecker	Gemini	IBM 1800 or Hewlett Packard 2114 B and 2116 B	32 K Bytes 8 K Words 32 K Words	80 37
Lodge & Shipley		PDP 8 I	4 32 K Words	
Mitsubishi Electric	Meldas	Melcolm 350/30 F	24 K Words	18
MoLins	System 24	IBM 1130	4...32 K Words	7
Monarch	CompTrol	PDP 8	4...32 K Words	6 by a unit
Oki	Computrol 45	Okitac 4500	8...64 K Words	32...128
Siemens		Siemens 301	16 K Words	15...60
Sundstrand	Omnicontrol	IBM 360/30...50	65...512 K Words	15...255
Tokyo Shibaura Electric	Toshiba 2000	Tosbac	32 K Words	20
Tridea		Honeywell H112		10
Warner & Swasey		PDP 8 I	4...32 K Words	14 Axis
Westinghouse		Univac 9200 and P 2000	8 32 K Bytes	30

Fig. 2 Performed DNC system

PERFORMED DNC SYSTEMS

In 1970 about thirty DNC systems have been presented at the machine tool exhibitions in Hannover (Germany), Chicago (USA) and Osaka (Japan). It must be mentioned that most of them were still in an early state of development (Fig. 2). Only a few have so far been industrially used. As an example the following can be mentioned: CommanDir (General Electric), Omnicontrol (Sundstrand) and Fanuc T' (Fu jitsu).

The CommanDir system of General Electric is a small central processing unit with a large drum storage capable of operating up to 15 machine tools simultaneously (Fig. 3). The heart of the processor and core memory subsystem is a general purpose minicomputer—the GE-PAC 30. Its core memory has a cycle time of one microsecond and a capacity that ranges from 16 to 64 K. The processor is provided with a telecommunication printer and a drum memory. Machining information is supplied to each numerically controlled machine by data distributor linked to the computer. An auxiliary scanner provides the interface between the computer and the operator at the machine tool. All these components reside in a central location.

At each machine tool, an operator's station provides the NC and the operator with a communication link to the computer. The major subsystems are

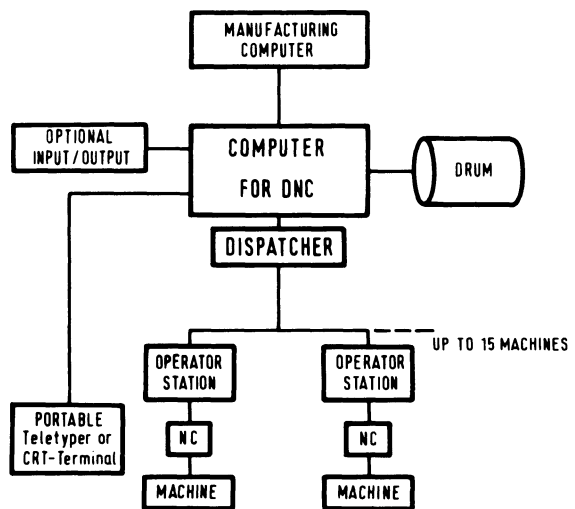


Fig. 3 System CommanDir (General Electric)

the processor and core memory drum subsystem, the telecommunication printer and paper tape reader, NC interface and communications operator's station and the software system.

The CommanDir system is designed to work in conjunction with a conventional machine tool controller at each NC machine. In operation, the machine operator selects the control data program for the part to be machined. The computer's central processor retrieves this program from the drum storage and the machine is directed from the stored program. The control system bypasses the tape reader and thereby eliminates most of the time delays inherent in the use

of taped part-programs and tape readers. Since there are used conventional numerical controllers with tape readers, the machine tools can be operated individually from their tape reader if it is desired³.

Sundstrand's Omnicontrol system was the first working DNC system in the world (Fig. 4). In 1968 it was installed in a plant of Pontiac Motor Division of General Motors Corp. to control four NC machines. This system is able to control up to 255 machines. Five components are involved in the Omnicontrol system. The general-purpose computer of the IBM 360 series compiles and stores the required data, which are stored on a disc.

The Omnicontrol master is located in the data-processing room. This unit establishes contact and directs the flow of data between the computer and the machine console unit (MCU). It contains one interpolating and buffer unit for each machine attached to it. One Omnicontrol master is capable of controlling up to 15 machines. Via a high-speed selector channel up to 17 Omnicontrol master units can be connected to an IBM 360/50 computer.

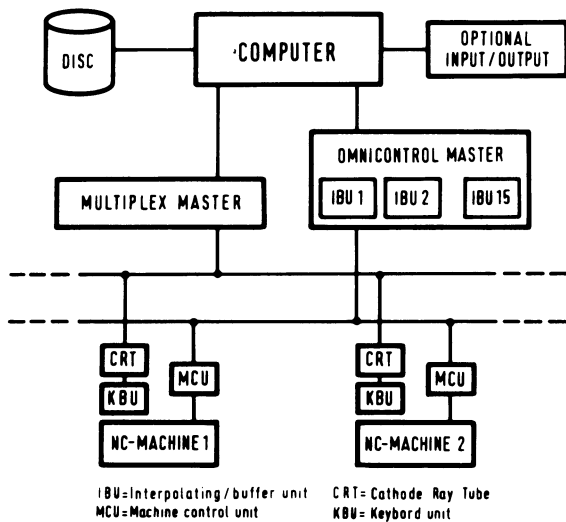


Fig. 4 System Omnicontrol (Sundstrand Corporation)

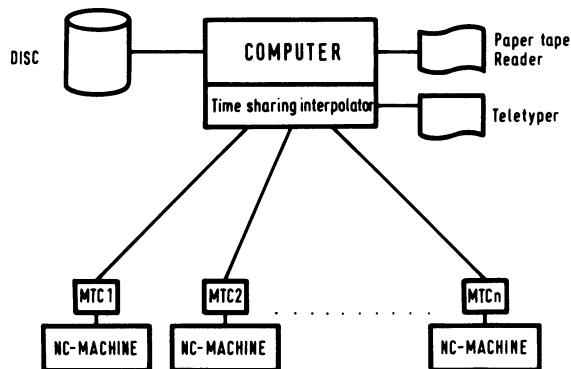


Fig. 5 System Fanuc T (Fujitsu Limited)

The cathode-ray tube master (CRTM) is also located in the data-processing room. It controls the individual cathode-ray tube units (CRT's) and relays CRT instructions to the computer. The machine console unit is located at the machine. It contains the machine logic and machine control. The function of the machine logic is to communicate with the machine tool.

The cathode-ray tube (CRT) is located at each machine for two-way communication with the computer. CRT's can be remotely located also for supervisory monitoring.

Fujitsu's Fanuc System T is able to control up to 50 machines. The functions of the system are NC machining, on-line processing of conversational FAPT, and on-line production control (Fig. 5). The control equipment consisting of the computer and the time-sharing NC (TSNC) is located in the control room. A simple machine control unit (MCU) at the machine and the TSNC are taking⁴ the place of the individual NC.

In the machining mode, first the machining data are taken out of the magnetic disc by an interruption signal from TSNC. These data are processed through the TSNC and will be given out to each MTC in form of pulse trains on a time sharing basis. Besides, auxiliary signals necessary to operate the machines are transmitted to the MTC.

In the conversational mode part-program statements can be processed by the group control equipment. During the processing of the part-program the coordinate values are printed immediately and the toolpaths are drawn. By detecting an error part-programming can be interrupted and directly corrected. The system can also perform production control. Following the input instructions to the group control equipment, it can make out the relevant operation schedule of NC machines.

SYSTEM NC 700

The DNC system NC 700, which has been developed by the Institute of Machine Tools of the Technical University of Berlin in collaboration with the AEG/TELEFUNKEN Company, will be described in the following, especially the problems of configuration and such of software and hardware. This system has been introduced to the public at the Hannover Machine Tool Fair in 1970 by Spur *et al.*⁵

The heart of the DNC system is an AEG process computer of the type 60-10. The following station—the dispatcher—is linked to the different NC machine tools by cables. The control data as well as the users' programs are stored on magnetic tape. The primary input of all programs is done by an optical paper tape reader. A teletyper serves as terminal for commands of the operator. In cases of danger and for special commands there is a second teletyper for recording. Fig. 6 shows the configuration of the system as it has been demonstrated at Hannover. Six machine tools equipped with different types of numerical control were supplied with control data by the DNC centre.

The computer has a core storage capacity of 16 K words with 12 bits each. At an instruction length of

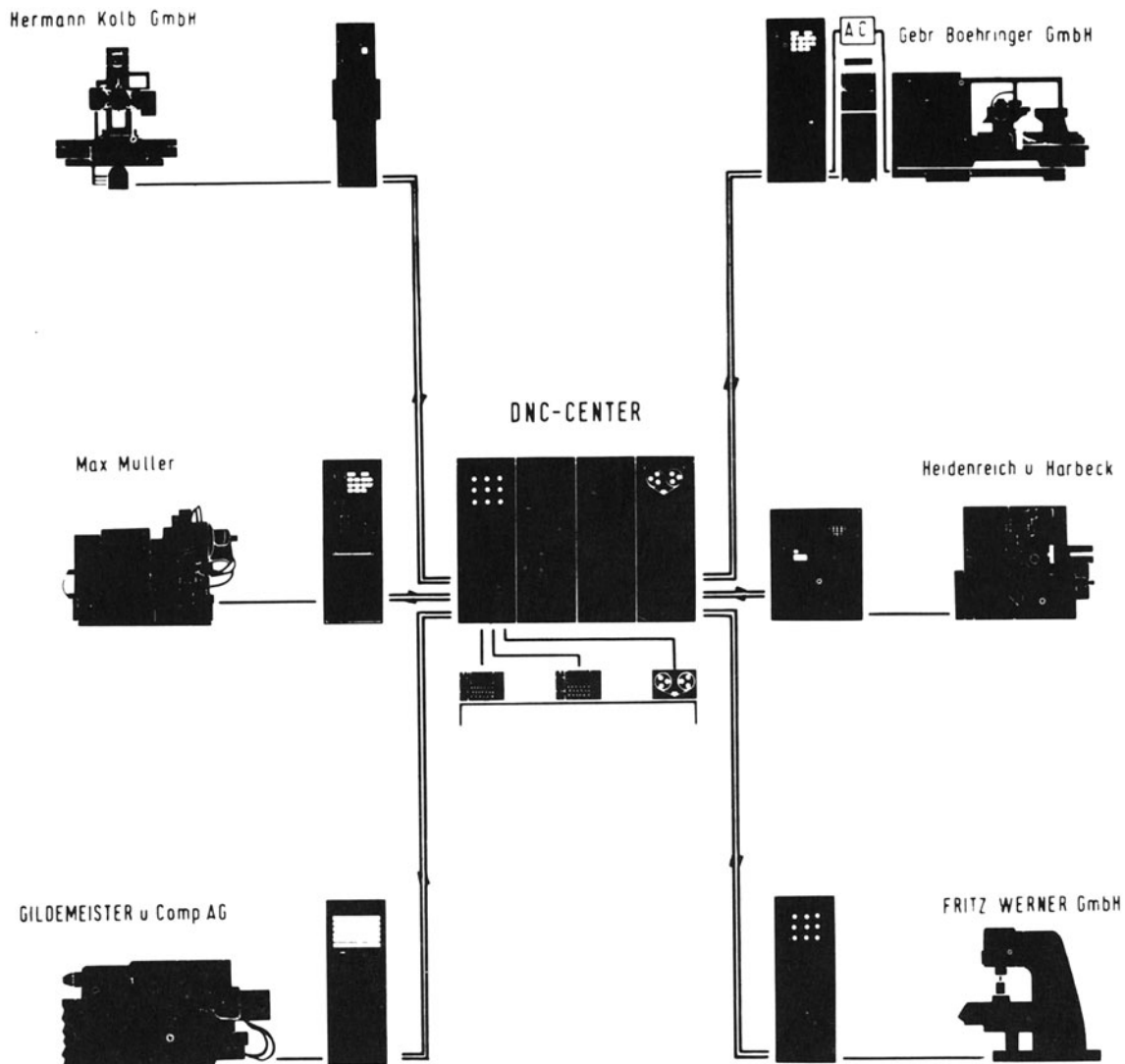


Fig. 6 System NC 700 (AEG/TELEFUNKEN)

24 bits it works with the single address mode. The cycle time of the computer is about $1.0 \mu\text{s}$. 66 hardware instructions can be used. Two data channels give the connection of the central unit with the peripheral devices. The data transfer between accumulator and peripheral units is managed by the program controlled data channel. The direct data channel serves for transport of data blocks between core storage and tape devices. The transmission of data to the tape during the main run of the program, once initiated, is done by the hardware of the computer. Thus, only the program passage time is prolonged.

The computer has an interruption system which sets priorities within four levels. The level of first priority controls core storage capacity and the supply voltage. Level two interrupts in time with the clock while level three and four provide interruption of the control board and the process devices.

The heart of the computer receives an interrupt that has been produced in the dispatcher in the third and fourth level. This dispatcher is the connection

between the central processing unit and the different DNC adapters at the numerical control of the machine tools. It has been especially developed for high-speed data transfer at DNC systems and allows the connection of groups of six machines.

The design of the software and hardware of the DNC system contains the possibility of connecting numerical controls of different types. It must be expected that the numerical control of different producers and generations differ in the conditions for read-in of control data. Older control devices mostly have a mechanical paper tape reader so that the data rate is not greater than 50 signs per second. On the other hand, there are some which are able to read in more than 1000 signs per second. Thus, two modes for the data output have been developed. At machines with a high rate of read-in, one interrupt will be answered with a whole data block, while, on such with a low rate, only one sign will follow one interrupt. There the output frequency is determined by the numerical control, that means by the speed of

forming a new interrupt. An adaption of the control data output speed to the read in speed of the numerical control is necessarily given.

For three reasons mainly the output sign by sign will be preferred for the future.

1. The connection of numerical controls with a low read-in speed will be possible.

2. Numerical control devices with a data buffer do not always read in up to the end of the block. They often stop at the word-address, which means a switching function, and then do not continue to send out interrupts. There is no longer a need for an extensive software to recognize the special stops of read-in.

3. Computer numerical control systems read in control data of the next block in a computing interval. A transfer block by block without extensive changes in the software and hardware of the CNC system would be impossible.

The control data of NC machines flow over the output register of the dispatcher as well as all data groups for the control board of the DNC adapter and such for the control of supplementary functions.

The dense data transfer between the DNC centre and the working stations requires the registration of a large number of interrupts. Therefore the dispatcher possesses a significant interrupt administration, which organizes the sequential treatment of all advices by a priority circuit.

The DNC adapter is located between the dispatcher and the linked numerical control devices. It organizes the interval distribution of information. The control data are transferred directly when they are adapted to the internal logic at the numerical control device. All other arriving information serves either for registration on the control board or for the control of supplementary devices. The DNC adapter also takes over information of the control board and the numerical control device itself and transfers them to the dispatcher.

All function programs which are necessary for the DNC system are organized by a central administration. It takes care of a due time and logical work of all instructions of the linked devices by noting the real time. The peripheral devices only process information much slower than the central processing unit provides them. Thus, there would be a long time of waiting. This time is registered by the administration and issued for the run of some other programs. So several programs are running quasi-parallel: the NC 700 works in multi-programming mode.

The special structure of the core storage of the used computer requires a program administration of its own. The core storage is divided into 16 blocks of 1 K word: only four blocks can be addressed at the same time. The blocks 0 and 1 can always be addressed and, together with two given blocks, form the available working area of four blocks. Order for programs are principally not executed directly, they are first stored on a list where they are later investigated and then worked off. If all lists are worked off, the administration program runs into a waiting loop where new orders to advices are asked for.

During the direct numerical control of the machine the computer runs in the interrupting mode so that, at the arrival of an interrupt, the program just

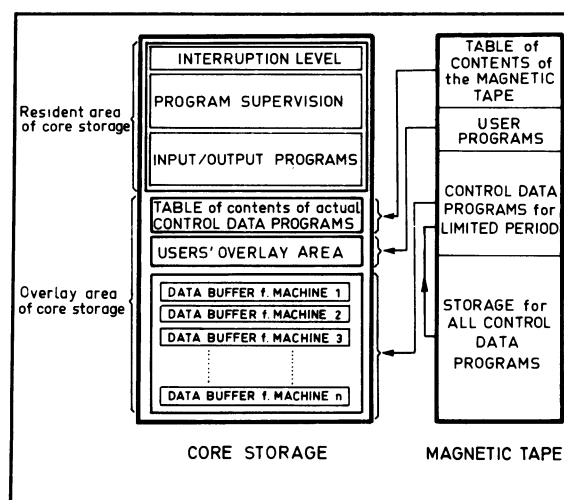


Fig. 7 Programme and data storage.

running will be interrupted and an identification of the interrupt will be possible. By the interrupt administration the single interrupts can get a different priority in order to provide the numerical control devices in time with control data. By a special program, the internal clock gives the date and time. So the real time of the devices can be surveyed and special programs can be started in defined intervals.

In order to get the DNC system working, resident and interchangeable programs, as well as control data for the NC machines, are needed (Fig. 7).

Resident programs are permanently located in the core storage of the computer and accomplish mainly administration functions and organize the output and input of data to the linked devices. For the output data to the NC machines there are two programs: one for the output block by block, the other for the output sign by sign. The interchangeable programs, mostly user programs, will be transferred over a resident distribution program from the magnetic tape into the core storage. The storage of the resident programs and data needs 6 K words. The overlay area as data buffer for the NC machines has 7 K words. As external mass storage in the system NC 700 a magnetic tape is used. Each tape will be divided into four parts. At the beginning of the tape a table of contents is located which makes it possible to find again stored programs in the shortest way. All the user programs and some system programs are stored in the second part of the tape and if needed will be transferred into the core storage. A further part of the tape is reserved for the storage of control data programs which are needed in a defined working period. The fourth part of the tape, which is the largest part, serves as storage for all control data programs. In this part up to 4000 control data programs of average length can be stored.

For the initial read-in of control data programs the ordinary paper tapes without any changes are used. From the core storage they are transferred to the magnetic tape block by block. During the read-in all control data are translated into the ISO code so that all information is written in one code.

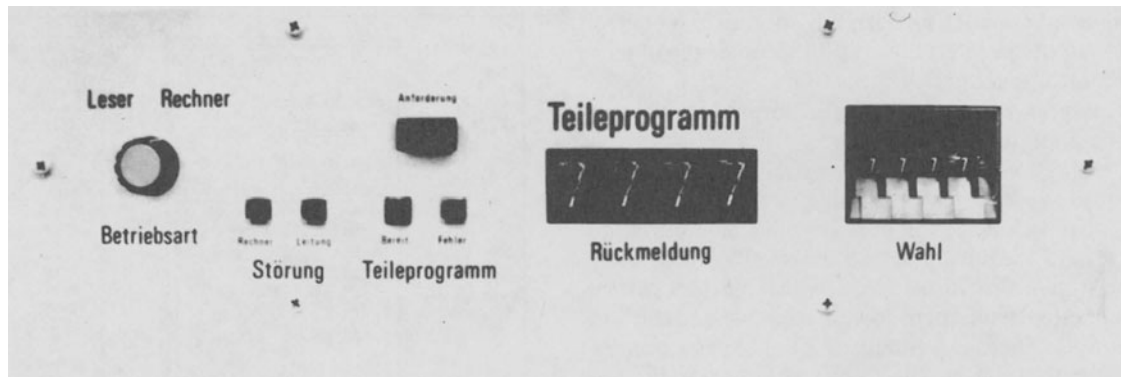


Fig. 8 DNC-adapter.

At the beginning of each planning period, which can be a day, a week and so on, the operator inserts into the computer the actual manufacturing list. These control data programs will be searched out of all stored programs and then transferred into the reserved area of the tape. To enable the operator at the machine to correspond with the computer the DNC adapter has some units for input and output of information (Fig. 8). At the selection of a control data program certain parameters are examined and if accomplished the first two blocks are transferred from the tape to the core storage. At control units with a fast read-in circuit one interrupt initiates the read-out of a whole block. Then the output time for one sign is about $150 \mu\text{s}$. On one with a low-speed read-in circuit one interrupt initiates only one sign. There the time needed is about $350 \mu\text{s}$. During the output of control data no interrupts are allowed, so the data transfer will be accomplished in a defined time. After the data transfer new interrupts are admitted. At the output the signs are retranslated into the code needed by the numerical controls. When they arrive at the DNC adapter they are examined and if necessary given out up to three times. To guarantee a data output without delay a part of the core storage is formed as alternating storage. The transfer of data from the magnetic tape to the alternating storage happens during the output from data to the NC machine tools. If a greater number of NC machines are linked to the numerical control system, a data buffer with a shorter access time is needed. This may be a magnetic disc or a drum. The information flow of the system is shown in Fig. 9.

By the combination of output data and feedback information of the machining, process manufacturing data will be found out. So, for instance, the kind and number of control data programs which are called by the NC machines are registered on a list which gives information about the machined parts. The working time of the machines and the time needed per work-piece as well as breakdowns are registered on a list.

To maintain the control data programs, user programs have been developed which render possible the correction and the extension of data programs. There are also programs which give the possibility of printing control data programs and lists which block up and reprint special programs.

The further development of the system NC 700 intends to allow for an integration into a superior manufacturing system. For that purpose the manufacturing data will be collected and serve as basis for manufacturing planning and manufacturing control.

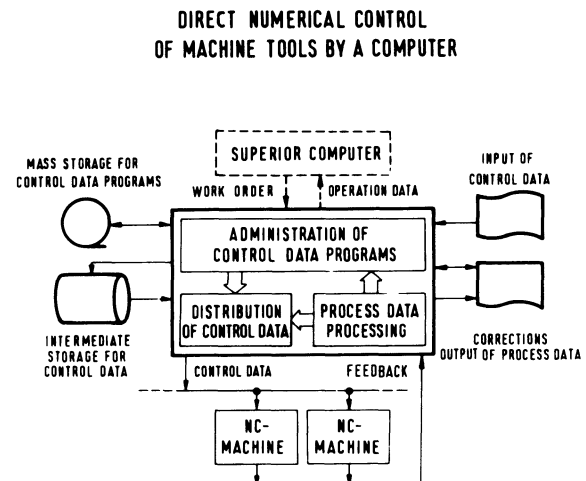


Fig. 9 Information flow within the system NC 700

AC IN CONNECTION WITH NC 700

Besides the already stated advantages, a process computer for direct numerical control of machine tools also offers the possibility of taking over control functions in adaptive systems. The installation within the hardware of these functions would not be economic. Since there is all the equipment for information exchange between computer and numerical control, there is only the necessity for an additional control unit as access to the wire link.

Deriving from the principal of the system the AC programs have a minor priority. Only such control functions are processed by the computer which when totally missing initiate a lower quality of control. A cost-optimizing AC system can be regarded as an example. To process the large number of tasks involved a digital computer is needed. Because of the high costs of that unit and in case it can only be needed for one AC system, the economy of such an optimizing control can be doubted.

At the automatic control of tool path by AC units the access to a process computer can be useful. In the case of constrain control with automatic control of tool path on turning one must deal with equally high costs for the realization of the hardware as it would amount to on a two-axis-contouring control. Therein the costs of cut division are twice as much as for feed control. This is as far as our experience is concerned.

The advantage of automatic cut division is primarily to avoid cuts into the air when dimensions of the non-machined workpiece vary strongly and secondly in the short cut of programming time. By thus lowering the main time of cutting, there can be, on the other hand, a longer idle time or even a lower efficiency during the last path. The control of depth of cut is started only when the feed as the main figure of control has passed certain limits. When during the last cut a deviation from the wanted workpiece contour occurs by means of keeping the limits of feed, a subsequent cut cannot be avoided which causes higher idle time. In those cases where several cuts are necessary to machine the wanted contour the depth of cut during the last passage is determined by chance when firmly programmed limits of feed exist. Feed cannot be extended to ever higher values as thus the surface roughness is negatively influenced, so it occurs that at low depths of cuts an optimal efficiency cannot be reached.

The disadvantages pointed out can be avoided by a high expense on programming; this may be reduced by access to a DNC computer.

In the field of cut optimization by a process computer, efforts are presently being undertaken at the Institute for Machine Tools of the Technical University, Berlin in collaboration with the companies Boehring, Goppingen, and AEG/TELEFUNKEN, Seligenstadt. As a first result, a numerically controlled lathe with an AC system on cut division and lined to a DNC system has been presented at the Hannover Fair in 1970. Fig. 10 shows the information flow of such a control system. An independent control unit at the machine takes over all functions which are permanently necessary. The control functions in the computer correct the control data program.

It can be subsequently said that by connecting DNC and AC new possibilities arise which allow economic realization for highly developed control systems.

REFERENCES

1. SPUR, G., 'Einsatz von Prozeßrechnern für DNC- und AC- Systeme', *Rep. Intern. Machine Tool Conf., Leipzig Spring Fair* (1971).
2. LÜCKE, P., 'Möglichkeiten beim Einsatz von Prozeßrechnern zur direkten numerischen Steuerung von Werkzeugmaschinen', *Dr.-Ing. Diss. TH, Aachen* (1970).
3. 'New computer numerical control system', *Machinery*, 76, No. 8, 90-91 (1970).
4. *Fujitsu Group Controls, FANUC System-T, FANUC System-K*, Fujitsu Limited Communications and Electronics, Tokyo, Japan.

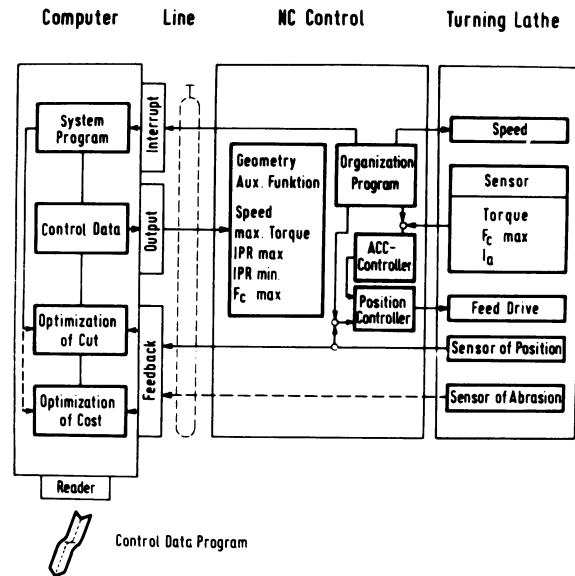


Fig. 10 Information flow for adaptive control of a turning lathe

5. SPUR, G., ADAM, W. and WENTZ, W., 'System zur direkten Steuerung von NC-Werkzeugmaschinen durch einen Prozeßrechner', *ZwF*, 66 No. 3, 115-121 (1971).

DISCUSSION

Query from S. Taylor, University of Birmingham

The extensive use of computer jargon and terminology can be confusing to many engineers. This aspect of direct numerical control is largely the province of the programmer and can often be handled in a variety of ways. Engineers who may be contemplating using DNC or the other computer techniques should not be deterred by involved problems of computer organisation, except in so far as they concern costs and economics. One of the attractions of a computer is that specialist knowledge can be incorporated in programmes and subsequently used by a non-specialist in the field.

Reply

The use of computers in manufacturing systems and machine tool design will surely increase in the future. Engineers must therefore know how to apply computers in an optimal way.

Actually, small process computers of low cost are used for manufacturing control, to collect manufacturing data, to produce special part-programmes or, as have seen during the Conference, to control machine tools directly. To profit by the whole core storage capacity and the computing speed of these small computers, the user must be acquainted with the operating conditions.

It must be said, that the training of engineers in many European countries includes instruction on computers and their operating conditions.

Query from Wasiukiewicz, Dixi II, Switzerland

There is already a great deal of work being done by the technical universities in West Germany on DNC control systems. But it is at the very beginning of the new phase in technical progress in which we have to learn to live with the electronic computers.

It is difficult to speak about a product which is involved in a constant development. It takes time to establish the correct use of this universal tool, which is the computer 'excellence'. Nevertheless, it is necessary to predict the next logical step in the development of DNC systems.

Because of its nature, the computer fulfils three principal functions, namely to collect information, compute this information and then dispatch the data at a given time to a given place.

Historically, the first attempt was made to use the computer as a coordinator of the group of machines and at the same time use the storage facilities available. Feedback information was used to control the production process. Unfortunately, this solution involved an important capital investment: the machines were equipped with the complete NC cabinets. Another possible configuration is a central

computer replacing the expensive NC of each machine. Only a small interface will be necessary to meet the individual requirements of each machine. It is quite sure that the right solution lies between these two extremities. The next very important step would be the derivation of the optimum distribution of the hardware between the central computer and the machine's own NC. Because of reliability, investment and running costs of such sophisticated equipment, there is a great deal of work to do. The present paper shows the technique of collecting the information properly and effectively.

Reply

I fully agree with you. First results in the field of CNC (computer numerical control) have been presented at this conference. Latest developments on DNC (direct numerical control) are obviously tending towards simplified machine control units (German: Rumpfsteuerung). An example has been shown at the 14th Aachener Werkzeugmaschinen-Kolloquium. Furthermore, it turns out that on-line connection of DNC-Systems with high-level production control-systems will be of increasing interest.

REPORT ON A SPECIAL DNC SYSTEM

by

G. STUTE and R. NANN*

SUMMARY

A DNC system was developed for a manufacturing system comprising about 20 NC machines. The requirements put on this system as well as its design will be described and discussed, especially the signals being transmitted between the computer and the numerical control, the electrical characteristics of the transmission lines, the organization of the computer programs and the disc storage.

INTRODUCTION

The requirements to obtain the best possible amortization of high-investment production equipment, rapid throughput of the parts and better transparency of the manufacturing data could be realized economically in the field of production through an increased rate of automation. The automation of the material and information flow is the substantial criterion for the technical solution of these tasks.

The development and introduction of the numerical control resulted in an important step forwards in the automation of the information flow. The numerical control processes automatically the technological and geometrical data input to produce output signals, which act on the control elements of the machine tool to realize the required functions.

The numerically controlled machine tool is, however, similar to an isle of automation, as long as it is not connected to an automatic information flow, i.e. as long as the data to be processed in the control is carried manually to the machine tool.

The supervision of the functional order of the NC and the monitoring of the manufacturing data remains up to now mainly a task of the operator. For a more advanced automation, it is also necessary to collect and evaluate these data automatically for management information. For this informational feedback, attention should be paid to the number of the parts and their production time, the tool application frequency and tool life, as well as to the shut-down times and their reasons.

The most powerful tool for the automation of information processing is the digital computer. The above-mentioned problems could be solved through the use of a computer to distribute the machining information to the individual NC's and to collect the manufacturing data.

DNC SYSTEMS

Under the name DNC (direct numerical control) there have been so far about 20 systems developed in USA, Japan and Europe, in which the NC's are connected to digital computers. The advantages resulting from the introduction of the DNC, and which should prove its economy, consist mainly of three factors.

1. Management information. The exact plant monitoring through the collection of all necessary data allows a more efficient planning and therefore a higher loading of the NC machines. For this purpose, the kind and frequency of the troubles, their sources as well as the shut-down times, are of interest.

2. Increase in the efficiency of the machine tools. This depends mainly upon the quick and error-free preparation of the NC programs for the machines, the removal of tape and tape reader as a source of numerous troubles and the restriction of the necessary manual manipulation, therefore minimizing the operator errors and the prevention of arbitrary interventions in the program flow, e.g. through feed-rate reduction.

3. Improved possibilities for test and correction of NC programs. This problem is of great interest when small series or single parts should be produced.

The principle set-up of such a DNC system is shown in Fig. 1. All NC programs which are required for the connected machines during the period in consideration are stored in a large-capacity storage, such as a magnetic disc or drum. The real-time computer, which manages this storage, can take over, upon command, segments of the desired NC program in its core storage. The numerical data output from the computer through a digital input/output device to the NC appears in the format dictated by the NC, i.e. most often blockwise.

The transmitter T adapts the output signals of the

*Institut für Steuerungstechnik der Werkzeugmaschinen und Fertigungseinrichtungen, University of Stuttgart, Germany

digital I/O device, regarding frequency and power, to the transmission lines characteristics. By the receiver R, the arriving signals are transformed to the internal power level of the NC. For conventional NC's, at which the input data are equivalent to those on the tape, numerical data input should be behind the tape reader (BTR). Should the NC close to the machine be specially designed for the DNC operating mode, special data conventions should be used. The transmission of the data collected at the machine to the computer takes place in a similar way.

Peripheral devices of the computer serve the operation of the DNC system and the data input/output. As most of the modern computers have connection capabilities to other computers, the DNC systems lend themselves to the incorporation in higher level information processing systems.

This generalized structure of a DNC system has been modified by some companies. Sundstrand, for example, in its Omnicontrol System, has separated the machine control into a part close to the computer, and another one, close to the machine tool. Kearney and Trecker has designed its system, Gemini, as a satellite computer system with small computers to handle the functions of data gathering, buffering and distribution to the individual machine tools. Some systems, like Gemini, as well as the system described in this paper, perform the data input/output in a program-controlled mode; other systems, like for example the DNC system of Siemens, are designed for device-controlled operation with the NC. Device-controlled means that the digital I/O device operates with the NC independent of the program control of the central processing unit. When connecting a numerical control to a computer, the functions which should be left close to the machine and those which should be transferred to the computer have to be considered in detail. Fig. 2 shows the different steps of DNC, i.e. the various positions of a separation line between the computer and the NC.

In a first step the functions of the tape reader, i.e. the numerical data input, are carried out by the computer. In this case the computer offers the data in the same format as the tape reader. The signals being supplied between the control and the computer are exactly the same as between the control and the tape reader. A second step may be that a number of operating and supervising functions, carried out by the operator in the conventional tape mode, should be transferred to the computer. These functions are, for example, 'NC cycle start', 'NC cycle stop', 'NC reset', and the monitoring of voltage and temperature. Also in this stage there will be no functions taken out of the control. When the feeding of the NC program number to the computer is done through an automatic input device, a fully automatic NC operation could be realized already at this stage.

A further DNC step is that the functions of manual input should be taken over by the computer. The most important are the mode of execution, tool offset, feed-rate over-ride, zero position and manual numerical data input. At this stage a substantial part of the control is eliminated from the hardware close to the machine. Without the computer, the control could no longer be operated.

Some problems are confronted within the last step, in which the interpolation of contours is completely or partly taken out of the control. The calculation of new position commands must be done at a high frequency and this requires much computing time. For technological reasons it is also necessary that the output of position commands should be made at a fixed frequency, otherwise the feed rate would oscillate. This demand is difficult to fulfil for time-sharing computing, with the different NC's as users. At the present state-of-the-art it is not advisable to replace the hardware interpolation completely by software. A division may be possible, according to which the computer has to make a coarse interpolation, and the NC hardware the fine one.

The characteristics of DNC systems could be summarized in the following: step of the DNC, type and number of the NC's which can be connected, volume of signal transmission, transmission frequency, the way of electrical data transmission, the possible distance between computer and NC, the I/O operation mode, computer size, programming language, type and size of the large-capacity storage,

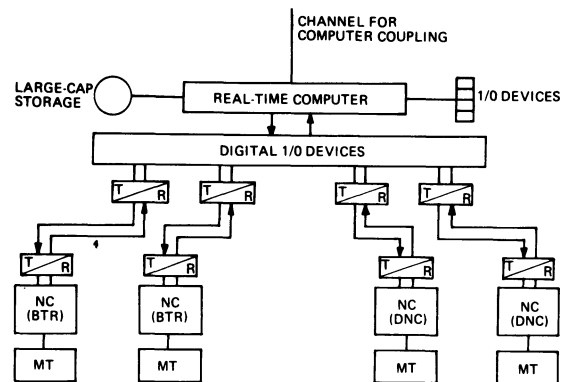


Fig. 1 Structure of a DNC system

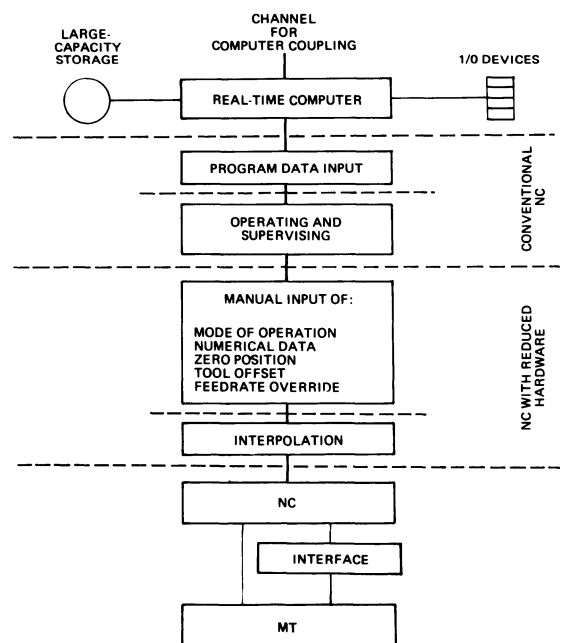


Fig. 2 Steps of DNC

its organization, the methods of operating the system and the conversation possibilities with the computer.

All these points have to be considered when designing a DNC system in order that its components be well matched to each other. Doing so makes it possible to keep the necessary investments at a level allowing an economical operation of a DNC system.

DESIGN OF THE DNC SYSTEM

It was specified that the DNC system should control a production system comprising about 20 NC machine tools, mainly boring and milling machines. For every NC machine there have to be about 30 to 50 programs, so that the organization of the large-capacity storage has to manage about 1000 NC programs.

It was also specified to realize a fully automatic trouble-free service. For operational safety as well as economical considerations, conventional NC's should be used, so that switching to the tape operation should be possible in case of trouble.

To be prepared for a future automatic workpiece loading, the connection to the program number input should be so designed that it could also accept signals coming from a conveyor control. This was important in view of testing the conditions at start and end of a program. Simple operation was desired, so as to reduce mistakes to a minimum. In the case of malfunctioning or error, sufficient conversation possibilities should be available to allow an efficient trouble-shooting. Furthermore, the recording of the production process was considered to be necessary. The whole system, comprising both hardware and software, should be so designed that it could be extended up to the maximum computer capacity—and naturally it has to work with a minimum cost-to-performance ratio.

In the discussion of Fig. 2 it was mentioned that the first two steps of DNC, i.e. computer-controlled program data input, operating and supervising, could be made without substantially changing the NC hardware. Since conventional NC's were planned in the system due to reliability and investment viewpoints, the system was laid out on this stage. The automatic program number input required a special device.

Fig. 3 shows the signals being supplied between the computer and the NC, to maintain the required mode of operation.

Firstly, the NC program required from the large-capacity storage should be given to the computer. For this purpose, a program number plug should be put into the program number input device and with the signal 'program No. input start' an interrupt in the computer is effected. Accordingly, a program is started in the computer, which reads in the number, tests and transliterates it. Then the corresponding program will be searched for in the storage. When the program is found, the computer replies to the input with the signal 'program No. correct'. With manual loading of the parts, the NC will be reset and started from the program number input device. With automatic workpiece change, on the other hand, a new program number could be input as long as the previous part is being machined. When the program

number is not correctly coded or when the NC program is not stored, the computer replies to the input with the signal 'program No. false'. The corresponding workpiece could then not be machined.

After the start, the NC requests the data blocks with the interrupt 'numerical data request'. This is similar to the signal 'tape reader on' in the tape mode. The block will be transmitted character by character on eight parallel lines, and the data input in the NC will be triggered by a timing signal. If the control recognizes a false character, e.g. in a parity check, it produces the interrupt 'data error'. The computer then resets the error and repeats the data transmission. If it is not possible to transmit the data correctly after three repetitions, the control would be stopped by the signal 'cycle stop', and the false information will be printed out on the computer typewriter. The operator could correct the false data through a conversation program, and the computer will start the NC again.

If in a continuous path control the servo error exceeds its limit, the control would stop the drives and transmit an interrupt signal to the computer. After removal of the trouble the NC will be restarted. The end of the NC program, i.e. receiving and decoding the last block, will be signalled with 'end of program'. Now the input of a new program number will be permitted by the computer.

After deciding upon signals between the computer and the NC, the data input/output mode should be discussed. The advantages of the program-controlled I/O mode are based on the flexibility and adaptability of the computer. This mode allows a free choice of the type and number of the connected NC's, output format and frequency, as well as the kind and number of the signals transmitted between the computer and the NC. It is also possible to secure the data transmission against noise through the formation of additional checking marks. Furthermore, the use of standard I/O devices is cheaper than the application of special DNC devices. The main disadvantage of the program-controlled mode is the high time loading of the computer due to the many output operations, which often need a much longer time than the core cycle. A further disadvantage is the existence of short waiting times with multiple call of the data output program, since the computer could feed only one machine at a time.

With the device-controlled mode, on the contrary, the data output device takes over the data blockwise from the core storage simultaneously with the program flow. The data is buffered in the external device and is transmitted with a fixed frequency independent of the computer program control. This results in a great relief of the computer, and several NC's could be operated simultaneously if the buffer capacity is large enough. The disadvantages of this system are the poor adaptability and the high costs of the special DNC devices.

Owing to the intensive signal exchange in this case, a single device for the program-controlled I/O has been necessary. So it was decided to limit the set-up of the system to this device. However, it has been important to make the data output as quick as possible, so as to make full use of the computer speed,

and to prevent the unallowed waiting times of the individual NC's. When choosing the computer and its devices, it has been recognized that the computer has a maximum input/output rate of 16,000 bit/s. For the system in consideration, it has been necessary to make two outputs per character; in the first output, the data lines have to be set and, in the second, the timing signal has to be sent. Therefore, the maximum output frequency of the computer was 8000 characters/s. The maximum input rate of the NC's is 10 000 characters/s. A rate of 16 000 bit/s has therefore been specified for the transmission system.

Owing to some economical factors, this transmission system was designed for d.c. Some safety measures were provided to prevent disturbances, or at least to recognize them. The lines were chosen to have a very low resistance; the voltage and current level were relatively high. For the purpose of error recognition, the signals are transmitted on two non-equivalent lines. In addition, the NC performs a vertical redundancy check on each arriving character.

The program-controlled output mode enables a further longitudinal redundancy check. This concept of a program-controlled output mode allows excellent checking possibilities in the hardware as well as in the software. The DNC system is now operating at a transmission rate of 5000 characters/s without any false character arriving at the connected NC's. Comparing this value with the 300 characters/s of a conventional tape reader it would be recognized that a great number of NC's could be fed with data, without substantial waiting times. If it is possible to make the program-controlled data transmission sufficiently quick, such that to be able to give always complete information blocks to each NC at a time, then it would be possible to connect all machines to one bus line. A further signal for selecting the NC should then be added to the operating signals shown in Fig. 3. The main advantage of this bus line is that the number of digital computer outputs is very low. Since there is only one bus line, sophisticated testing logic can be used. Regarding the high transmission power level, it is also interesting to note that the power supply unit could be kept as small as possible. The complete DNC structure decided upon is shown in Fig. 4.

The program number input signals are also transmitted through a bus line owing to their relative rarity. The program package has been so designed that one or a few functions can be done by a single program. Each program could be called by each of the connected NC's. The program package consists of 12 DNC programs and 7 service routines. The operating system of the Siemens computer 301 organizes the program flows according to their priorities. Some programs are segmented according to the required response time of their functions. It has thus been

possible to keep the core capacity occupied by the DNC system programs within 3 K words.

The organization of the NC programs and the disc storage is of a great consequence. About 1200 NC programs can be stored according to a proper administration, i.e. independently from the operating system.

Despite the relatively high access time of a disc storage, the buffer area in the core storage could be kept very small through the shifting of the called programs to preferred cylinders.

The computer system configuration comprises the central processing unit, Siemens 301, with 8 K words core capacity, each of 24 bits, a disc storage having a capacity of 1600 K words, a tape reader and a tape punch, a typewriter and control inquiry station.

Through the use of the bus line principle, the choice of the program-controlled input/output mode, the simple way of data transmission, the parallel organization of the programs, and the application-oriented administration of the disc storage, a system has been designed which permits an economic DNC operation, owing to its low investments and high reliability.

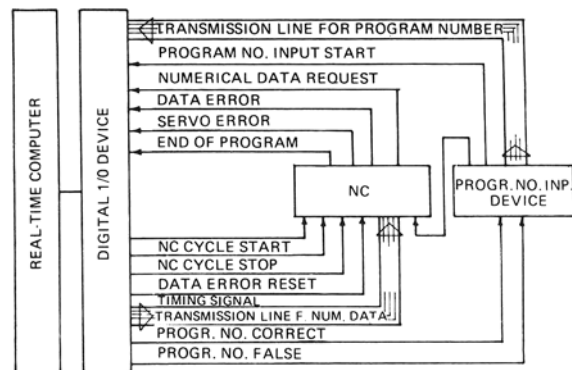


Fig. 3 Signals supplied between NC and real-time computer

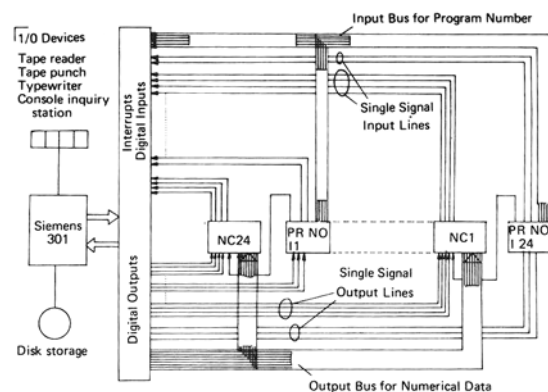


Fig. 4 DNC system structure

THE DESIGN AND DEVELOPMENT OF A NUMERICAL CONTROL SYSTEM USING A SMALL DIGITAL COMPUTER

by

C. J. CHARNLEY and V. SRINIVASAN

SUMMARY

The report outlines an investigation into the design and development of a numerical-control system using a small digital computer and electrohydraulic pulse motors to provide coordinate positioning of machine-tool slides. Problems encountered during commissioning and testing are mentioned.

INTRODUCTION

The aim of the project is to investigate the possibility of using a small computer to control the operation of a machine tool. The problem is essentially to replace

the conventional or dedicated NC system with its use of 'hard wired' techniques by a computer with its stored program or 'software' approach. It is interesting to note that computer control was envisaged in the conceptual stage of numerical control in 1949,

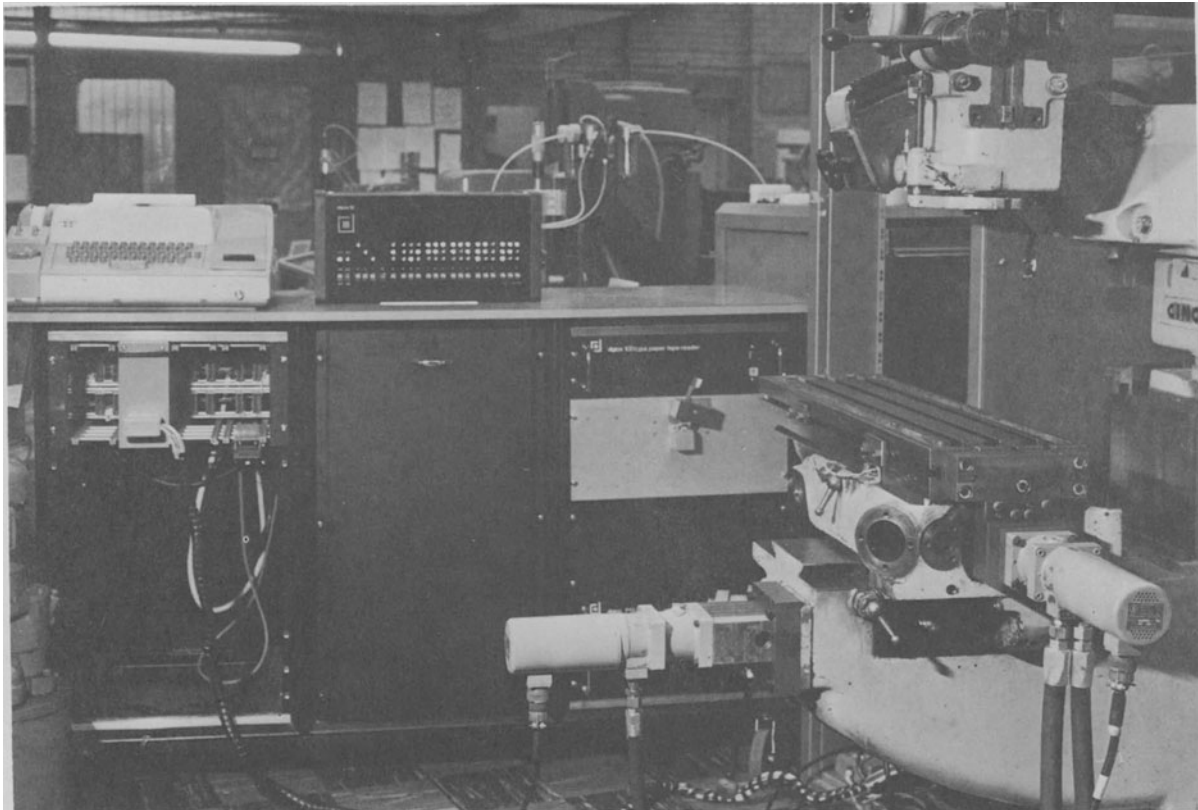


Fig. 1 General view of system, showing Digico computer (mounted on trolley with interfaces for general on-line experimentation), Cincinnati milling machine and Fugitsu electrohydraulic stepping motors.

when the Massachusetts Institute of Technology undertook a project 'to develop a system applicable to machine tools for controlling the position of shafts in accordance with the output of a computing machine'. The reasons which have ruled out this stored program approach in the past have been: (1) economic—the high cost of core memories; (2) realizable speeds of operation—access to memory stores took too long; and (3) lack of interest by computer manufacturers—partly because of the small size of the market. The position has changed recently with the introduction of microelectronic and integrated-circuit devices giving higher speeds of operation and cheaper small computers.

This report outlines the background and techniques which evolved in the design and development of a control system (Fig. 1) capable of moving a machine slide to coordinate positions, under the direct control of a small computer.

CHOICE OF APPROACH

The use of computers in a production organization is illustrated in Fig. 2 which also includes the three levels of direct numerical control (DNC) identified by Burgon¹. These three different types of DNC are identified as follows.

Level 1—machine control

The computer is only concerned with the metal cutting process in individual machine tools, leading to a replacement of the conventional hard wired logic by stored program logic for interpolation and machine functions.

Level 2—job control

The computer is still concerned with the individual machine, but the control is taken a stage further to include the loading of tool sets, part programs and workpieces.

Level 3—workshop control

The computer is used to control a group of machine tools and peripheral work transfer devices to follow a production schedule. This involves the total organization of a cell of machine tools so that the workpieces can be routed from storage areas through proper machine heads.

As well as the three levels of direct computer control listed, computers can also be used for the computation work necessary in a modern working organization, for example for preparing part programs, production schedules and production plans. Normally this work is performed separately from the real time environment using batch processing methods.

Stored programme control

The benefits claimed for DNC include: a reduction in cost and increase in reliability because of the elimination of the electro-mechanical or electro-optical tape reader and its associated punched tape; better control of operations because of the ease of communication between the computer and the operator, together with the ready availability of information for manage-

ment; versatility of performance and operation because the program can readily be suited to the individual machine with only minimal changes in hardware. Furthermore, compensation for errors in the machine can readily be incorporated together with more advanced forms of control (for example, adaptive control) as they become available.

The problems to be overcome include the increased risks and cost of failure if operations are too highly centralized, together with the considerable time and cost required for the development of suitable software. A particular problem to be resolved is how much of the control should be performed by software and how much by hardware, as all input and output information would have to be digital whereas the amplifier and position transducers might well be analogue devices.

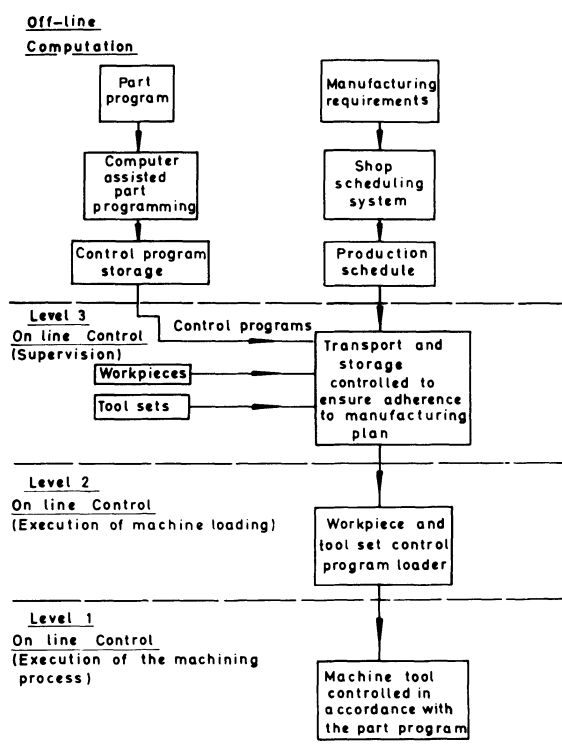


Fig. 2 Levels of control association with direct numerical control.

DEVELOPMENT OF THE CONTROL SYSTEM

In view of these considerations, it was decided to take as an initial target the development of a DNC system suitable for level 1 control which could be incorporated into higher levels at a later stage. The system (Fig. 1) would be suitable for point-to-point or linear path operations and would be based on the use of a Cincinnati milling machine, a Digico Micro 16 computer and electrohydraulic stepping motors which were available in the Department and the Cranfield Unit for Precision Engineering (CUPE). This approach would enable the ideas to be tested at the lowest possible cost and not restrict future development. We also thought that a low-cost approach, as envisaged, would more readily meet the requirements of the

general engineering industry and would contrast with the complex, high capital cost systems developed elsewhere.

To determine some of the technical factors influencing the design we referred to surveys carried out at Cranfield² and work by PERA³ in which it was shown that nearly 90% of operations were performed on workpieces smaller than 750 mm (30 in); corresponding positional accuracies were from ± 0.125 – 0.025 mm (± 0.005 – 0.001 in). On this basis it was decided to design for an accuracy of ± 0.025 mm (± 0.001 in), a rapid traverse greater than 80 mm s^{-1} (200 in min^{-1}), with acceleration and deceleration rates as high as possible to provide minimum positioning times over the generally short traverses involved.

Organization of system

It was decided to make the operation of the machine tool asynchronous, that is, not time dependent on the central processor of the computer. This would enable an interrupt operation of peripheral equipment so that the computer would not have to stop, during an input/output operation, and wait for the function to be completed. As far as possible, input/output units would operate through a standard interface in the hope that fewer technical difficulties would arise during installation and commissioning (however, there seem to be nearly as many standard interfaces as computer manufacturers).

The output from the computer would be sent to registers associated with each axis controlled and any other functions provided. After these registers have been set with command position data, the movement of the machine slides is initiated and the computer is then free to continue with important processing or to deal with other peripherals. The presence of data in the command registers can be detected and made to move the slides in the correct direction. It was envisaged that a feedback generator from the slides would cause the command register to count down as the slides moved towards their demanded position, so that the count in the registers reaches zero when the demanded position is reached. This condition can again be detected and made to generate an interrupt in the computer, so that each axis of the machine tool could be controlled asynchronously and effectively. To keep the system simple, we decided to use an open-loop configuration, which seemed to be a feasible proposition for the accuracy required, with the available pulse motors driven directly from output pulses from the computer.

The key parameters that affect the choice of a particular pulse motor, when it is considered for open-loop application, are: (a) power (or torque) output; (b) start and stop speeds; and (c) steady-state speed. The output torque determines whether the motor is capable of delivering a sufficient torque to accelerate and decelerate the table at the desired rate. The start and stop speeds affect the performance of the motor in high-speed operation; Electrohydraulic Pulse Motors (EHPM) can be operated at various speeds depending on the load on the output shaft, but usually the starting and stopping speeds are lower than the maximum steady-state speeds. The perform-

ances of EHPMS currently available have been compared by Budzilovich⁴.

Machine control logic

The basic system is shown in Fig. 3 and operates as follows. The oscillator produces a square wave train of fixed frequency pulses which is fed to a variable pulse-rate divider controlled by a fraction register; the reduced frequency output from the divider is taken through a mode selector (manual or automatic) to two registers. On automatic operation, the modified pulse train is fed to the Auto Register and Down Counter (ARDC), which is used to hold the demanded position information in the form of binary digits and is capable of being set from the computer accumulator. The input pulse train causes this register to count down to zero and, at the same time, feed pulses to the EHPM. Thus, when the ARDC reaches zero, the EHPM will have received the number of pulses equal to the value set by the computer. A zero detector stops the register counting down when all the bits are zero and then pulls down the computer interrupt line to indicate that a demanded position has been reached.

On manual operation, the modified pulse train is fed to the manual register and up/down counter which is used to count up or down depending on the direction of travel. The pulses are sent to the EHPM and to the register by depressing manual control buttons for rapid traverse or fine traverse. When the desired position is reached, the register contains the total distance moved manually. This can be input to the computer by depressing an attention input button. The information sent to the computer can be used to correct an existing program or to build up manually a new program.

In order to vary the frequency of the pulse train sent to the EHPM, an acceleration/deceleration detector is used to monitor the value of the data set in the ARDC such that, if the demanded movement is greater than a certain minimum value, the Fraction Register (FR) is made to count up to an upper value. Thus, acceleration takes place because the frequency of the pulse train to the EHPM is increased each time the FR receives a pulse; this continues until the FR reaches its highest value and the frequency of the pulse train reaches its maximum. When the demanded movement equals a certain minimum value, the acceleration/deceleration detector reverses the sequence and cause the FR to count down to its minimum value; this reduces the frequency of the pulse train to the EHPM in steps, causing it to decelerate. After the fraction register has reached its minimum value, the pulse-train frequency also assumes a constant low frequency. The EHPM is moved at this low rate until the ARDC reaches zero. In this way, two desirable functions are achieved.

1. The EHPM is fed with the number of pulses equal to the demanded movement.

2. The frequency of the pulses fed to the EHPM is maintained, so that the starting and stopping frequencies are well within its capability. Also, depending on the demanded movement, the EHPM is made to

accelerate to its maximum speed and then decelerate towards the target. Thus, the positioning time is kept to a minimum.

The functions of the device decoder and function decoder are to decode instructions from the computer and gate pulses to various parts of the system. There is usually one set of function and device decoders for each machine, whereas the units referred to previously relate to one axis of the machine.

Mode selection

For effective manual control of the machine, the following facilities have been built into a manual control panel.

1. A manual/automatic operation selection switch to indicate to the computer whether the machine is under manual or automatic control; an interrupt is generated whenever the changeover is made from manual to automatic or the converse.

2. A general re-set switch, used to set up initial conditions in the circuitry to ensure that random states are eliminated.

3. Rapid/fine traverse control switches and an associated direction control switch.

4. An attention input switch, used to indicate to the computer that data are ready to be transferred from the manual register to the accumulator.

Interface requirements and facilities

A device interface is an intermediary unit between the computer interface and the actual device logic, the function of which is to accept the data from the computer interface highways and detect any particular information relevant to itself. After detection, any data present on the computer interface are gated into the appropriate areas of the device.

The devices under control here are the two machine axes, and the transfer of data to and from the computer is accomplished by using input/output instructions, which have two parts called channel addresses and peripheral commands. The channel address denotes a code by which a particular device can be selected; as there are six bits for these the computer can handle a total of sixty-three devices. The peripheral command denotes a code by which a selected device can be made to perform specific functions. The various input/output instructions that effect the control of the two axes are the following:

1. set data into automatic register—this transfers data from the accumulator into the automatic register;

2. enable interrupt—this enables the particular axis register to interrupt the computer after the demanded movement has taken place. This instruction was included so that if the control program was too long, or when interrupts would be inconvenient, the interrupt mechanism could be turned off for a period; enabling the interrupt, thus restores the status and activates any waiting condition;

3. disable interrupt:

4. read manual register—this causes data to be read from the manual register to the computer accumulator, leaving the register clear of data from previous movements and ready for further movement;

5. clear interrupts and read status register—this re-sets the interrupt flag in the devices and also copies the contents of the status register into the accumulator. The status register provides information about the reason for the interrupt, that is, whether it was generated by manual/automatic changeover, attention input or end of movement.

Pulse motor drive circuit

To keep the cost to a minimum, it was decided to build a unit to control two motors with all the circuitry housed in the same cabinet (Figs. 4, 5 and 6). The drive unit consists of two parts: (1) a logic level stage that converts the incoming clock pulses into five pulse outputs for each of five motor coils; and (2) an amplifier stage that steps up the power output for each coil so that the motor can be driven under full load.

Software

So far, most of the effort expended has gone towards designing, assembling and testing the hardware so that equipment would be available for experimentation. But, a simple program has been developed and used to demonstrate the operation of the system under computer control. The principal program is kept in locations 1–17. The test program is loaded into core using the Octal debug routine and then entered by typing J2000 as command input. Locations 2031 and 2032 contain the data that are alternately sent to the automatic register. The program is written so that after each cycle of EHPM operation, the computer is interrupted and control transferred to the debug routine. In this way, every time the command J2000 is typed the EHPM is rotated through 4096 steps, the direction being changed each time. Used as a simple test program, this provides a method by which the accuracy and repeatability of the system can be measured over various distances, and investigations are proceeding into the development of further software.

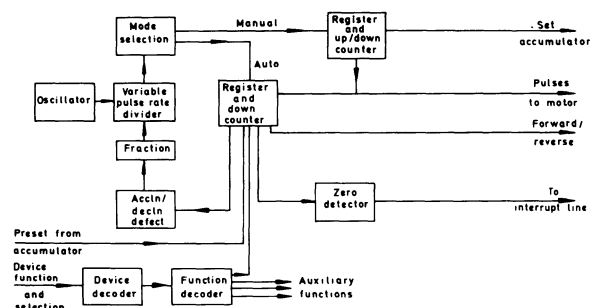


Fig. 3 Machine control system block diagram.

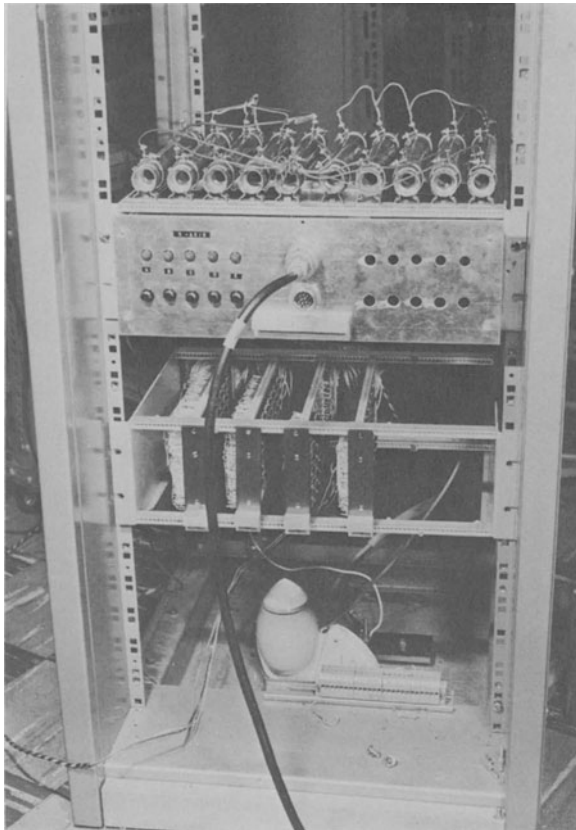


Fig. 4 Power amplifier and logic level sub-racks mounted in modular cabinet following International Standard Equipment Practice (ISEP).

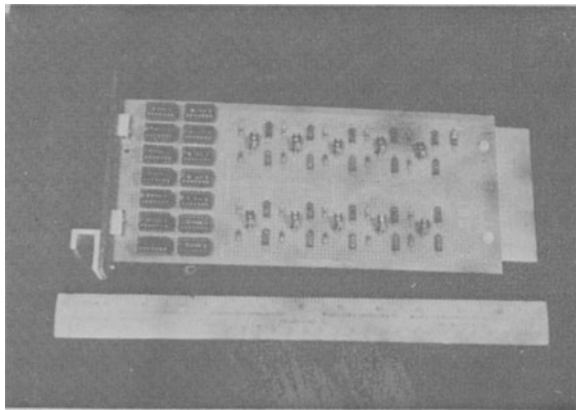


Fig. 5 Drive logic card containing EHPM drive logic and the first stage of the power amplifier.

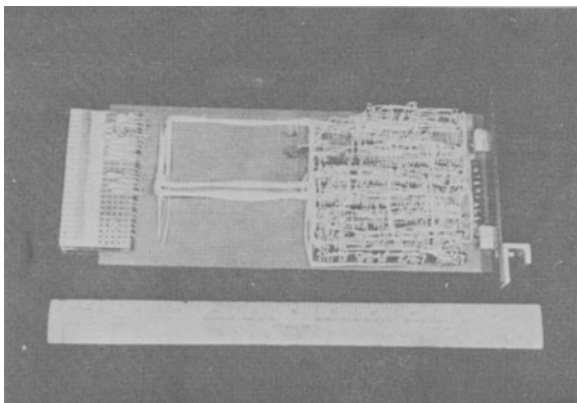


Fig. 6 Device interface card showing the labelling of each logic package and wire-wrapped connections.

DISCUSSION AND CONCLUSIONS

The system has been shown to operate successfully under both manual and automatic control, although further development is clearly necessary to improve operation and to overcome some of the problems which have arisen. For example, under manual control, inaccurate pulse counts occurred, apparently caused by random fluctuations on the switch contacts. Because of the high currents being switched in inductive conditions in the amplifier stage, interference is a problem, and for effective operation, the power amplifier must be effectively screened and isolated. Furthermore, care must be taken to reduce the effect of random noise and other external interference on the power supply to ensure reliable operation. It was also found necessary to increase the acceleration time of the EHPM to ensure satisfactory operation with a maximum operating frequency of 3 kHz, and it seems that further increases would have to be incorporated for higher operating frequencies.

As indicated previously, most of the effort expended so far has gone towards designing, assembling and testing the hardware so that equipment would be available for experimentation. More effort will now go into the development of the necessary software to test and prove the system fully and we hope to report on this when this paper is presented. In the future, the operation of the system under real-time control should be evaluated to provide information about the developments and associated costs required to make the system suitable for general industrial use. Other aspects, such as the possibility of time sharing so that several machines can be controlled from one computer, should also be investigated.

This discussion would not be complete without a consideration of the costs involved in adapting such a direct-numerical-control system for industrial use. The most expensive part of the system is the EHPM quoted at £500, which, together with the £150 cost of the control circuitry, including the power amplifier and logic elements, gives a total basic hardware cost of £650 per axis. On this basis, the system seems to compare very favourably with conventional NC systems and provides an inexpensive method of incorporating Direct Numerical Controls into conventional situations. The system could be used on a progressive retrofit basis in situations in which cost and simplicity are important and accuracy requirements are not very critical, which is the case in many general engineering situations. In conclusion, we suggest that a relatively simple low-cost system, such as that outlined here, may be the means of introducing numerical control in its latest form to a much broader range of industry.

ACKNOWLEDGMENTS

The authors acknowledge the help given by D. W. McQue of the Instrumentation Section of the Cranfield Institute of Technology and J. Dinsdale and members of the staff of the Cranfield Unit for Precision Engineering for their help and the loan of equipment.

REFERENCES

- BURGON, C. J., '*The Control of Machine Tools by Computer*' The Machine Tools Industry Research Association, Macclesfield; Conference on Adaptive Control of Machine Tools (April 1970).
- BOSHIER, G., and POWELL, E. A., Management & Technical Survey Report, 'The Design of Numerically Controlled Drilling Systems using Fluidic Elements,' Design Project 1966/7, Cranfield Institute of Technology, Cranfield.
3. PERA, '*Survey of General Machine Requirements in Industry*,' PERA Report, Melton Mowbray (1970).
 4. BUDZILOVICH, P. N., '*Use Electrohydraulic Stepping Motors for All-Digital Drives*,' *Control Engineering* (January 1970).

COMPUTER APPROACH TO DYNAMICALLY OPTIMUM DESIGN OF MACHINE TOOL STRUCTURES

by

M. YOSHIMURA and T. HOSHI*

SUMMARY

A system of computer programs is described as a tool developed for computation of structural dynamics and dynamic optimization of machine tool structures. Based on energy equations of a mechanical system at resonance, an approach to the optimum design is developed theoretically, and demonstrated by numerical results on a particular planer-type milling machine.

INTRODUCTION

Because of recent developments in computer technology, methods are available for a designer to obtain the estimated harmonic response and mode shapes of a proposed design of a machine tool structure. Dynamically optimum design, however, should be approached by revising the proposed design according to some appropriate principle which will lead to more balanced dynamic behaviour of the structure.

Introduced here is a system of computer programs developed for computing the dynamics of three-dimensional structures and a set of theories which will help a designer in approaching optimum design.

The computer program system is based on the principle of synthesis of receptance established by Bishop and Johnson¹, and it computes the harmonic response, mode shape, strain distribution and energy (kinetic, potential and dissipated energies) distributions of the composite system, from input data about the sub-systems (such as uniform beams having distributed mass, other simple configurations the dynamics of which can be readily calculated theoretically, and springs and dampers, which are combined to compose the objective system).

The optimum design theories are developed based on equilibrium principles of mechanical energy in a structure at resonance. A set of simple rules are given by the theory, and the approach is demonstrated in proposing a design change of a particular planer-type milling machine.

OUTLINE OF SYNTHESIS OF RECEPTANCE PROGRAM SYSTEM

Using the receptance notations, the relationship between exciting forces $F_1 e^{i\omega t}$, $F_2 e^{i\omega t}$, ———, $F_n e^{i\omega t}$ exerted on a member and the oscillatory displacements $X_1 e^{i\omega t}$, $X_2 e^{i\omega t}$, ———, $X_m e^{i\omega t}$ measured at the points where the forces are applied is expressed in matrix algebra as follows:

$$\begin{pmatrix} X_1 \\ X_2 \\ \vdots \\ X_m \end{pmatrix} = \begin{bmatrix} \alpha_{1,1} & \alpha_{1,2} & \dots & \alpha_{1,n} \\ \alpha_{2,1} & \alpha_{2,2} & \dots & \alpha_{2,n} \\ \vdots & \vdots & \ddots & \vdots \\ \alpha_{m,1} & \alpha_{m,2} & \dots & \alpha_{m,n} \end{bmatrix} \begin{pmatrix} F_1 \\ F_2 \\ \vdots \\ F_n \end{pmatrix} \quad (1)$$

where F_j is the amplitude of force exerted at a point A_j , X_i is the amplitude of displacement at a point A_i , and α_{ij} is the receptance between points A_i and A_j . The dynamic behaviour of all the members of a composite system is expressed in the form of equation (1).

Receptances of each sub-system member can be calculated from the vibration theory of an elastic body. Using the restraint conditions for displacements and forces at joints, receptances α_{ij} of all sub-systems are synthesized. Repeating the series of computations for many different frequencies in the frequency range of interest, the harmonic response and natural

*Department of Precision Engineering, Faculty of Engineering, Kyoto University, Sakyo-ku Kyoto, Japan 606.

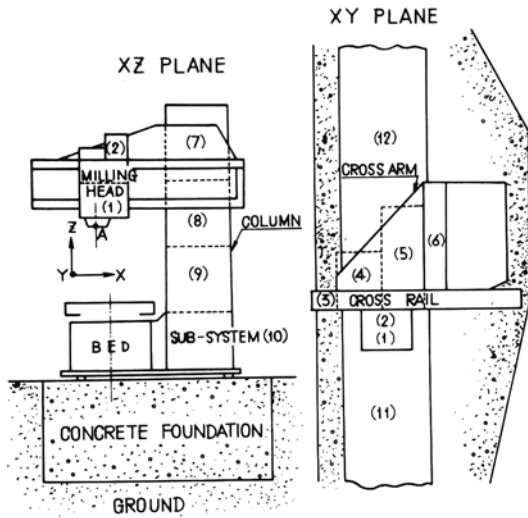


Fig. 1 Single-column planer-type milling machine analysed by the program system.

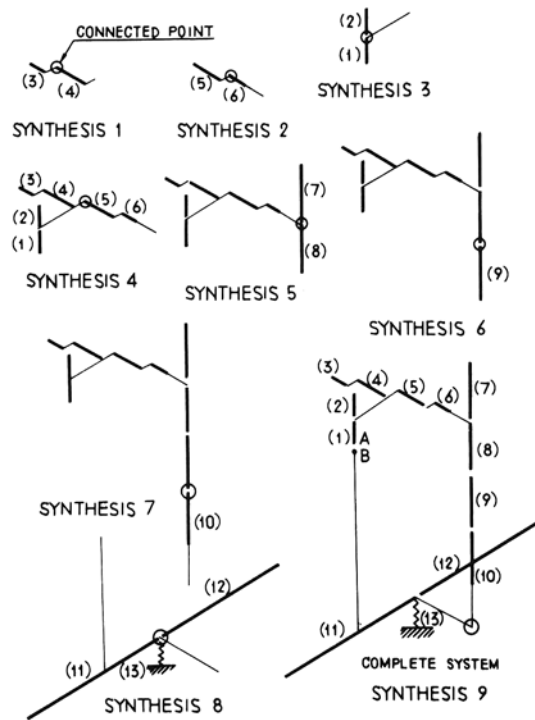


Fig. 3 Sequence of synthesis for computation of dynamic response of single-column planer-type milling machine. Fine lines indicate massless, completely rigid bars. Sub-system 13 represents a set of springs equivalent to the elastic ground.

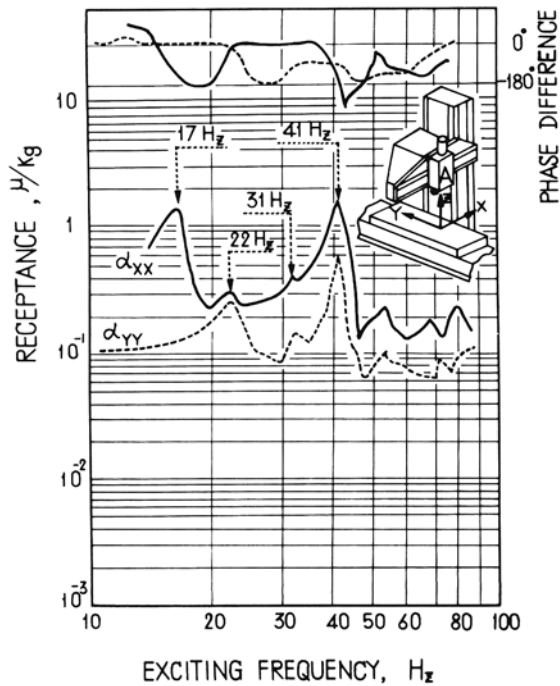


Fig. 2 Empirical harmonic response curves of receptances α_{xx} and α_{yy} at the point A of single-column planer-type milling machine.

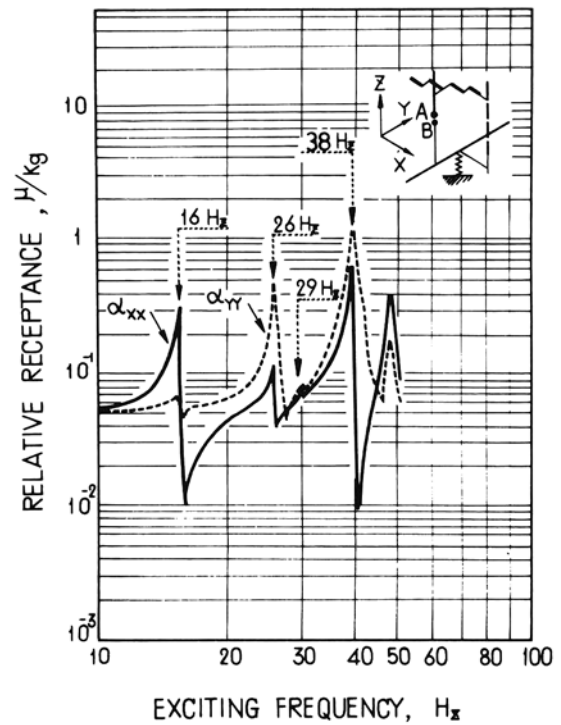


Fig. 4 Computed harmonic response of direct receptances α_{xx} and α_{yy} between points A and B in x- and y-directions respectively.

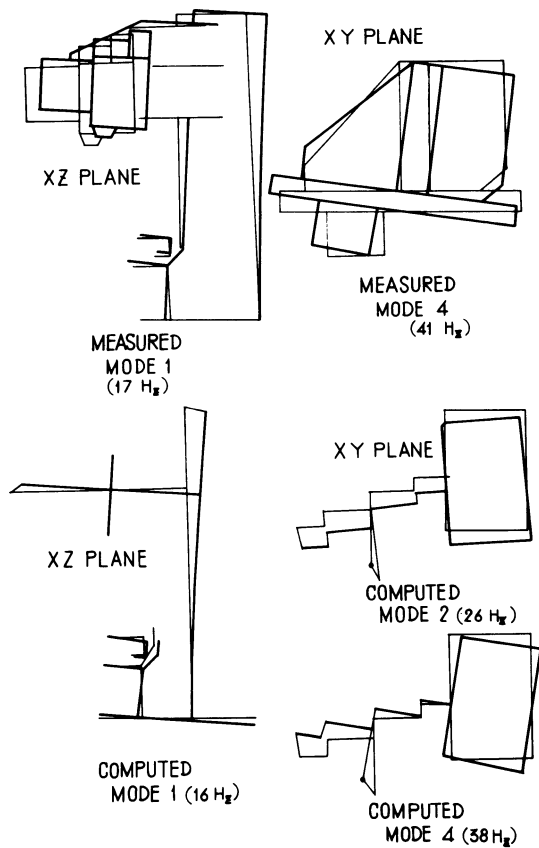


Fig. 5 Measured and computed results of mode shapes of single-column planer-type milling machine.

THEORIES OF APPROACH TO OPTIMUM DESIGN

In analysing the dynamics of a complex three-dimensional structure, it is essential to observe the whole system and analyse it macroscopically. For this purpose, the vibration system can be considered based on the balance between input, kinetic, potential and dissipated energies. These energies are distributed along the axes of members, and are calculated by integrals along the axes. Therefore, the axis through a system is in this sense, considered as the path of integration, and it is referred to as an 'integral path' in this study.

A machine structure consists of sub-systems which are connected to each other by either a single or a combination of bolted joints, welded joints, bearings, slideways and so on. By way of explanation, we assume that a system A consists of N sub-systems $B_1, B_2, \dots,$ and B_N , where each of those N sub-systems is made of uniform material and each junction (bolted joint, bearing or others) between sub-systems also forms a sub-system.

In general, a system has infinite degrees of freedom, and so an infinite number of natural frequencies. For a structure in resonance at any natural frequency, the following two relations are essential:

1. Maximum kinetic energy, T_A , of the whole system is equal to maximum potential energy, V_A , of the whole system.

2. At steady resonance, input energy per cycle, I_A , at a resonant condition is equal to the summation of dissipated energies per cycle, D_A , through the whole system.

At an m^{th} natural frequency ω_m , the N sub-systems have energy $(T_{1m}, V_{1m}, D_{1m}), (T_{2m}, V_{2m}, D_{2m}), \dots,$ and (T_{Nm}, V_{Nm}, D_{Nm}) respectively, where first subscripts 1, 2, $\dots,$ and N indicate sub-system numbers. General three-dimensional structures are subjected to combinations of bending, torsional and longitudinal vibrations. The potential and kinetic energies of the total system are respectively equal to the sum of those in all the sub-systems, and they are expressed by

$$T_{Am} = T_{1m} + T_{2m} + \dots + T_{Nm} \quad (3)$$

$$V_{Am} = V_{1m} + V_{2m} + \dots + V_{Nm} \quad (4)$$

The sum of the dissipated energy of all the sub-systems is

$$D_{Am} = D_{1m} + D_{2m} + \dots + D_{Nm} \quad (5)$$

At the m^{th} natural frequency, the relationship $T_{Am} = V_{Am} = E_{Am}$ holds, as previously stated. Assuming that the damping energy of each sub-system is proportional to its potential energy, the following equations are obtained:

$$\frac{D_{1m}}{V_{1m}} = \gamma_1, \frac{D_{2m}}{V_{2m}} = \gamma_2, \dots, \frac{D_{Nm}}{V_{Nm}} = \gamma_N \quad (6)$$

where $\gamma_1, \gamma_2, \dots, \gamma_N$ are constants which correspond to the so called 'loss-coefficients' $\eta_s = \frac{D_s}{2\pi V_s}$ and their values are inherent to the material of the sub-system and the condition of the junction. They can be considered as latent damping factors for the sub-systems and junctions.

Accepting the assumptions that the potential energy is proportional to the square of the amplitude of the displacement and D_{Am}/V_{Am} is far less than 0.5, the logarithmic decrement, δ_{Am} , at the m^{th} mode of the total system A is expressed by

$$\delta_{Am} = \frac{1}{2} \frac{D_{Am}}{V_{Am}} = \frac{1}{2} \frac{D_{Am}}{E_{Am}} \quad (7)$$

Denoting the ratio of potential energy in each sub-system to the potential energy of the total system by

$$\frac{V_{1m}}{V_{Am}} = \zeta_{1m}, \frac{V_{2m}}{V_{Am}} = \zeta_{2m}, \dots, \frac{V_{Nm}}{V_{Am}} = \zeta_{Nm} \quad (8)$$

and substituting equations (6) and (8) into equation (7), we obtain

$$\delta_{Am} = \frac{1}{2} \sum_{i=1}^N \gamma_i \zeta_{im} \quad (9)$$

This equation embraces an important principle: that is, if, for an arbitrary mode of a structure, the ratio ζ

is large at the sub-system or the junction at which the latent damping ability, γ , is large, this effectively results in a large logarithmic decrement for the mode.

Considering a machine tool structure as shown in Fig. 6, the tool-work relative displacement at the cutting point C occurs in various principal directions at different natural modes. Denoting the angle between the cutting force direction and the principal direction of the m^{th} order mode by θ_m , the angle between the normal-to-cut-surface direction and the principal direction by φ_m , the cutting force amplitude by F_e , the tool-work relative displacement in the normal-to-cut-surface direction by X_c , and the same in the principal direction by X_m , the preceding relation (2) yields an expression of the cutting point compliance at the m^{th} order mode as follows

$$\left(\frac{X_c}{F_e}\right)_m = \sin \beta \cdot \cos \theta_m \cdot \cos \varphi_m \cdot \frac{\pi \cdot X_m^2}{D_{Am}} \quad (10)$$

In this equation, β stands for the phase difference between the force, F_e , and the displacement, X_c , and D_{Am} represents the energy dissipated per cycle as a result of the relative displacement, X_m . Substituting equation (7) into equation (10), we obtain

$$\left(\frac{X_c}{F_e}\right)_m = \sin \beta \cdot \cos \theta_m \cdot \cos \varphi_m \cdot \frac{\pi \cdot f_m}{\delta_{Am}} \quad (11)$$

where

$$k_m = \frac{2E_m}{X_m^2} = \frac{1}{f_m} \quad (12)$$

E_m in the last equation stands for the maximum instantaneous value of either the potential or kinetic energy stored in the system.

k_m and f_m as defined by (12) are the modal stiffness and the modal flexibility, respectively, of the relative motion at the cutting point in the principal direction at the m^{th} order mode caused by the cutting force. If we denote the relative displacement in the cutting force direction by X_e , and that in the normal-to-cut-surface direction by X_c , equations (10) and (11) can be written as follows

$$\left(\frac{X_c}{F_e}\right)_m = \sin \beta \cdot \frac{\pi}{\overline{X_e} \cdot \overline{X_c}} \quad (13)$$

$$\left(\frac{X_c}{F_e}\right)_m = \sin \beta \cdot \frac{\pi \cdot f_m'}{\delta_{Am}} \quad (14)$$

where

$$f_m' = \frac{X_e \cdot X_c}{2E_m} = \frac{1}{k_m'} \quad (15)$$

and k_m' and f_m' as defined by equation (15) are the modal stiffness and the modal flexibility, respectively, of the relative motion at the cutting point in

the normal-to-cut-surface direction at the m^{th} order mode caused by the cutting force.

If we designate the static compliance of the relative motion in the normal-to-cut-surface direction caused by the cutting force by f_{st} , we have

$$f_{st} = \sum_{m=1}^{\infty} f_m \quad (16)$$

where f_{st} depends on the static stiffness of the so called 'main force loop' of the structure, as indicated in Fig. 6.

In order to have a minimum chance of regenerative chatter, a known criterion exists, which is, that the maximum real negative part of the compliance of the relative motion in the directional normal to cut surface caused by the cutting force must be small. This is equivalent to the compliance as formulated in equations (10), (11), (13), or (14) being small at modes of any order. According to equation (13), this requires that $D_{Am}/X_e \cdot X_c$ be large for every mode.

More practical rules are obtained by consulting equations (14) and (15): namely, for a minimum chance of regenerative chatter, the following requirements should be satisfied for every mode:

1. logarithmic decrement of the total system δ_{Am} is large, and
2. modal flexibility f_m' is small.

Referring to equation (9), the first requirement is favoured by selective allocation of greater latent damping at the parts of the structure where potential energy is distributed.

On the other hand, equation (15) shows that the modal flexibility f_m' can be calculated without knowledge of damping factors in the system. From equation (16), it is apparent that an optimum design is such that the static compliance f_{st} is small, and evenly shared by modal flexibilities in many modes.

From the theories developed in this approach to the design of a dynamically optimum structure is reduced to a set of practical procedures as follows:

(i) for every resonance mode identified, compute the distribution of kinetic and potential energy in the system, and also calculate the modal flexibility, either by equation (12) or (15),

(ii) focus on the particular mode where the modal flexibility is predominantly high, and by consulting the energy distribution at the mode, propose a design change such that energy is more evenly distributed in the system,

(iii) after repeating the second procedure a sufficient number of times, try to allocate greater latent damping at the parts of the machine at which greater potential energy is stored.

Example of a proposed redesign

Using the energy distribution data computed by the synthesis of receptance program system, we can evaluate the original design of the planer-type milling machine, and propose a revised design. Energy distribution and modal flexibility of the original design are tabulated in the left-hand side of Table 1.

It is clear that resonance at the fourth order mode is detrimental: more than half the total potential energy is stored by the torsional deformation of the column. Distribution of potential energy stored by the bending and torsional deformation at this mode is depicted in Fig. 7. It is understood that such dense energy distribution along the column results in the

Table 1 Comparison of original and revised (50% greater torsional stiffness of the column) designs of the planer-type milling machine in terms of modal flexibility and energy distribution.

Item	Original Design					Revised Design		
	Static compliance	Mode 1 16 Hz	Mode 2 26 Hz	Mode 3 29 Hz	Mode 4 38 Hz	Static compliance	Mode 4 42 Hz	
Static and modal Flexibility In μ/kg								
x-direction y-direction z-direction	4.73×10^{-2}	2.00×10^{-3}	1.06×10^{-3}	1.39×10^{-5}	9.63×10^{-3}	4.04×10^{-2}	1.06×10^{-2}	
	4.78×10^{-2}	7.87×10^{-5}	3.17×10^{-3}	1.27×10^{-4}	2.82×10^{-2}	3.58×10^{-2}	1.85×10^{-2}	
	3.35×10^{-2}	6.72×10^{-3}	2.62×10^{-4}	1.65×10^{-5}	1.31×10^{-3}	3.35×10^{-2}	3.45×10^{-3}	
Ratios of kinetic energy taken by								
	Milling head	0.119	0.0529		0.266		0.278	
	Cross arm and cross rail	0.215	0.0902		0.286		0.320	
	Column	0.451	0.137		0.0955		0.157	
Bed and concrete foundation		0.215	0.718		0.343		0.233	
	Total	1.0	1.0		1.0		1.0	
Ratios of potential energy restored in								
	Milling head							
	Cross arm and Cross rail	Bending Torsion						
	Column	Bending Torsion		0.0560		0.00617		0.00603
				0.00459		0.0375		0.00298
	Bed and concrete foundation	Bending Torsion		0.0686	0.0780	0.198		0.439
				0.000346		0.506		0.360
	Ground	Bending Torsion		0.760	0.826	0.0676		0.0905
				1.0	1.0			
Total							0.0973	
Total							1.0	

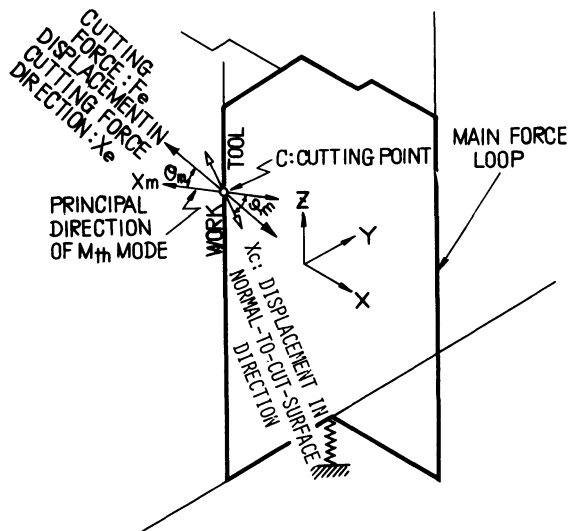


Fig. 6 Illustration of the coordinate system used in theoretical analysis.

highest modal flexibility in the y -direction. In the first and second order modes, about 80% of the potential energy is stored in the ground, which presumably has high damping ability.

Tentatively, it was proposed to increase only the torsional stiffness of the column by 50%. The right-hand column of Table 1 indicates that such a change resulted in increased natural frequency, a different share of the potential energy and decreased modal flexibility in the y -direction.

CONCLUDING REMARKS

A system of computer programs developed for the estimation of the dynamic characteristics of three-dimensional structures is described as a method to approach a dynamically optimum design of machine tool structures. Theories have been developed based on the energy principle and a set of simple principles presented for the optimum seeking process. Calculations are demonstrated on a planer-type milling machine.

Continued studies will be aimed at a computer-aided design system of machine tools, in which optimum design would be approached by a proposed flow chart, as shown in Fig. 8. After functional specifications are written, integral paths of the system should be proposed first of all. Being free from the existing designs of similar structures, various integral paths of a machine system should be compared. Using the computer technique, mode shapes, the distribution of kinetic, potential and dissipated energies and modal flexibilities at the cutting point are computed. Those results are checked against the dynamic requirements and necessary modifications are made on the integral paths, until objective functions attain satisfactory values. Then, details of each sub-system are determined, and at this stage, requirements from economic, manufacture, thermal stability, and so on should be incorporated, to ensure a successful design.

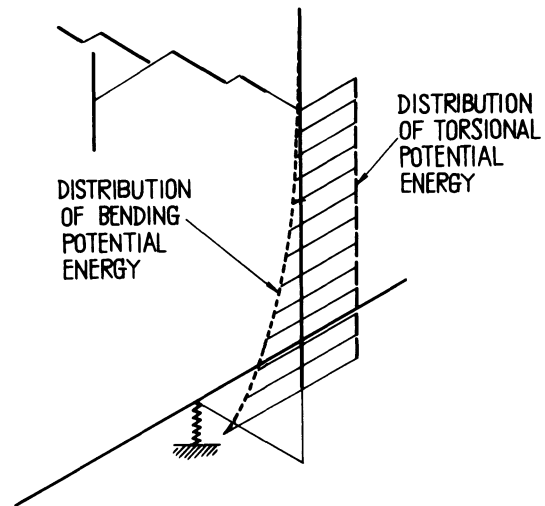


Fig. 7 Distributions of bending and torsional potential energy along the column in the fourth order mode.

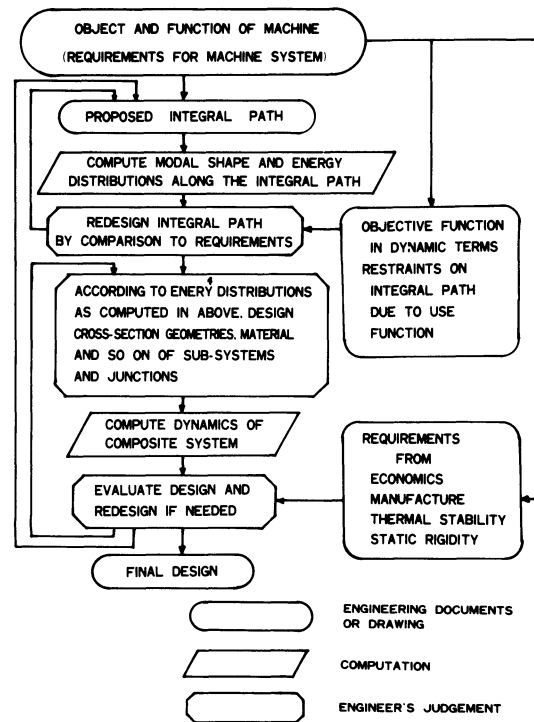


Fig. 8 Proposed flow chart for optimum design process of structures with respect to dynamic behaviour.

ACKNOWLEDGMENTS

We thank Dr Keiji Okushima, Professor at Kyoto University, for his support for this study.

REFERENCE

1. BISHOP, R. E. D., and JOHNSON, D. C., 'The mechanics of vibration,' (Cambridge University Press, 1960).

DISCUSSION*Query from C. Andrew, University of Bristol*

This is a very interesting method. However, with frequency response methods in general, there are problems of economy, because the complete calculation has to be carried out at every frequency. This is when an eigenvalue solution can show to advantage, because only a minor calculation is carried out at every frequency. We have developed a combined eigenvalue and receptance method that seeks the advantages of both techniques. The eigenvalue part has so far been calculated with a humped-parameter model. This has an advantage over uniform beam analysis if the machine tool manufacturer has not made his machine of such elements. However, if a particular element is uniform (and important) one can put in the appropriate receptances. For such an element, it is particularly advantageous to apply damping uniformly, and one should be able to predict the effects of the introduction of damping inserts.

I should be very interested to know if the authors have carried out a comparison of their method with humped-parameter methods.

Query from J. Hammill, University of Bristol

The authors refer to the natural frequencies of the system. These appear to be obtained by determining the receptances of each sub-system at a number of discrete frequencies and searching for the maximum response of the composite system. If so, does this not represent a very time-consuming procedure, which is subject to inaccuracy, in that there is no guarantee that the true resonant frequency has been obtained?

Query from S. Satyamurty, T. U. Munchen.

I wish to add to Professor Andrew's remarks. From my own work concerning the synthesis techniques using receptances, I have found that it can be very desirable to use the eigenvalue descriptions in order to obtain the maximum advantages of the synthesis technique. We have successfully obtained closed expressions for the transfer function of a composite system knowing the lumped parameter description of the sub-systems. However, when we needed to calculate the eigenvalues of the composite system, we found that the required computer capability was very large. I would like to know the experience of the author in this connection.

Query from S. Taylor, University of Birmingham.

Optimisation is based on a theory which relates damping to strain energy distribution. Hence, structural modifications are proposed according to the energy distribution.

Consequently, the improvements tabulated for the planing machine are based on improving the torsional stiffness of the column. This modification will surely improve the machine irrespective of damping considerations, so the table does not demonstrate the validity of the theory. This comment is not intended to suggest that the theory is not valid nor is it intended to derogate some interesting ideas.

General Reply

Three main points may be said to relate to the practical usefulness of the synthesis of receptance programme system introduced by the authors. From a practical point of view, it is true that this method requires considerable computer capability and substantial computer time. Presently, with the use of FACOM 230-60 processor, whose specification is as tabulated below, a three-dimensional analysis of a knee-type milling machine takes 202 sec cpu time to be carried out for only eight discrete frequencies.

The working core size required was 55 026 words (42 bits/word). By repeating several jobs as above, it was practical to identify the resonant frequencies within 1% accuracy.

FACOM 230-60 (Kyoto Univ.)

computation on	Add and Sub.	2.27 μ sec
floating point	Mult.	3.68 μ sec
number	Divide	5.12 μ sec
Core memory		
Size	42 bit (Flag 4, data 36, parity ch. 2)	
Cycle time	0.92 μ sec/double word	

On the other hand, this method is characterised by the following practical features over the lumped-parameter method:

- (1) The composite system is analyzed as if it were composed of a distributed mass. Thus, lumped-mass description is unnecessary.
- (2) The building-block principle brings about several advantages, such as the possibility of the expansion to a composite system having many members, easiness in evaluation of alternative designs of particular members, and inclusion of members whose responses are expressed by empirical transfer-function formulae.

Because the lumped-parameter, receptance, and finite element methods have their own characteristic features and drawbacks, it is desirable to make selective or combined use of various methods depending on the character of the structure to be analysed, the size and speed of the computer available, and the kind of information requested by the client.

The question by Dr. Taylor is concerned with the optimisation theory proposed by the authors. Considering the present limited knowledge on structural damping, a practical optimisation procedure is proposed which essentially consists of the following two steps:

- 1st step, optimum distribution of mass and stiffness,
- 2nd step, optimum allocation of damping.

In the present report, however, only an example of the 1st step is demonstrated and tabulated.

The authors look forward to future opportunities to report an example of the succeeding 2nd step, which should verify equation (9) of this report, and also confirm the validity of the proposed theory.

EFFICIENCY AND ACCURACY OF THE FLEXIBILITY AND STIFFNESS METHODS FOR THE CALCULATION OF BEAM-LIKE REDUNDANT STRUCTURES

by

L. VAN DEN NOORTGATE*

SUMMARY

In this report a critical study is made of the flexibility and stiffness methods for the static calculation of beam-like structures. I found that the computation speed and the accuracy of both methods are essentially determined by the number of elements in the structure and the degree of redundancy. Several computer trials have shown that the flexibility method is the most economic and the most accurate for the calculation of structures with a small degree of redundancy. The stiffness method is the most efficient for the calculation of highly redundant structures.

Practical values are given enabling one to choose the optimal computation method in each case.

INTRODUCTION

There are several methods for the calculation of the static and dynamic behaviour of beam-like structures. The most important approaches are the flexibility and the stiffness methods. Many authors^{1,2,4} mention the theoretical differences between the two methods but few practical comparisons have been made.

In this report a criterion has been proposed enabling the choice of the most efficient and the most economic method for a particular case of a static calculation. This criterion, called the degree of redundancy, is defined as the sum of the number of additional foundation joints and twice the number of closed loops, divided by the number of elements. The first section briefly reviews the fundamentals of each of the methods and both the advantages and disadvantages are discussed. Next, the computation speed of each of the corresponding computer programs will be discussed. Special attention has been paid to the accuracy of the results.

FUNDAMENTALS OF THE FLEXIBILITY AND THE STIFFNESS METHOD

A massless continuous beam, loaded only at its ends, is generally considered as the basic building element of all structures for the flexibility as well as for the stiffness method. The load-deformation relationship can easily be set up for such an element. This relationship is written as follows

In the stiffness method:

load vector = element stiffness matrix \times displacement vector;

In the flexibility method:

displacement vector = element flexibility matrix \times load vector.

The most general building element is a free-free beam (Fig. 1). The stiffness matrix of a free-free beam exists because, by displacing the ends of a free-free beam by an arbitrary value, a unique set of forces is required to keep the beam in equilibrium. This stiffness matrix, however, is singular and therefore its inverse, yielding the flexibility matrix, does not exist.

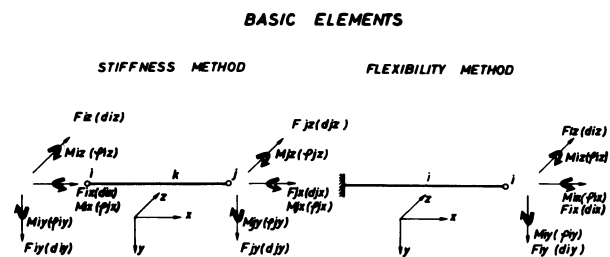


Fig. 1 Basic elements—stiffness method, flexibility method.

It is clear that a given set of forces at the ends of the free-free beam does not correspond with a unique displacement vector (rigid-body motion) because the beam is massless.

Obviously, for a given set of loads a unique deformation of the beam exists because the deformation of a beam corresponds to the relative displacement of both ends. It can also be physically represented by the displacement of one of the ends, while the other end is rigidly clamped. For this reason, the basic building element in the flexibility method is a cantilever beam (Fig. 1). This kind of building element possesses some disadvantages in the case of redundant structures as will be seen.

Element flexibility and stiffness matrices (Fig. 1)

To each element is attributed a three-dimensional right-handed coordinate system (x, y, z); the x -axis coincides with the element axis, and the y and z axes with the principal axes of the beam cross-section. In the flexibility method, the x -axis is chosen positive from the 'assumed' clamping end towards the free end. In the stiffness method, the positive direction of the x -axis is arbitrary. Conventionally, if the ends of an element are i and j and the x -axis is taken positive from i towards j , the end i is called near-end, and the end j 'far-end'.

To each free end of the elements three displacements and three rotations are attributed, totalling six degrees of freedom. The *element flexibility matrix*, S_i , of the element i is a 6×6 matrix, relating the displacements of the free end, i , of the element to the loads acting on this point as

$$D_i = S_i F_i \tag{1}$$

The *element stiffness-matrix*, K_k , of the element k with near-end i and far-end j , is a 12×12 matrix relating the loads acting on the points i and j and the displacements of these points

$$\begin{bmatrix} F_{ik} \\ F_{jk} \end{bmatrix} = \begin{pmatrix} K_k \end{pmatrix} \cdot \begin{bmatrix} D_{ik} \\ D_{jk} \end{bmatrix} \tag{2}$$

The stiffness matrix K_k can be decomposed into four 6×6 matrices. Equation (2) then becomes the following expression, which is more convenient for the further explanation

$$\begin{Bmatrix} F_{ik} \\ F_{jk} \end{Bmatrix} = \begin{bmatrix} K_{11k} & K_{12k} \\ K_{21k} & K_{22k} \end{bmatrix} \cdot \begin{Bmatrix} D_{ik} \\ D_{jk} \end{Bmatrix} \tag{3}$$

The flexibility matrix, as well as the stiffness matrix, are symmetric. The calculations of the elements of both matrices have been described in detail.^{4-6,7}

Structural flexibility and stiffness matrices

The basic building elements of the structure have to be connected properly in order to build up the complete structure; two types of conditions have to be fulfilled: compatibility and equilibrium conditions.

These conditions obviously have to be expressed in a coordinate system, common to all elements of the structure.

For this reason a structural coordinate system (X, Y, Z) has to be defined. The position of this frame of reference is arbitrary, but is usually chosen in such a way that the transformation equations of the element coordinate system to the structural coordinate system are as simple as possible.

The displacement vectors and load vectors, which are described in the element coordinate system by the equations (2) and (3), have to be transformed into the common structural coordinate system by means of a transformation matrix, T .

After this operation the assembly of the structure can be calculated.

ASSEMBLY OF THE STRUCTURE IN THE FLEXIBILITY METHOD

A structure is usually connected with the foundation at one or more points. One of the elements connected with the foundation is chosen as element (1). In the flexibility method, the basic building element is a cantilever beam. For element (1) the assumed clamping point coincides with the foundation points. The assumed clamping points of the elements which have to be connected to element (1) are coupled to the free end of element (1). The other elements are coupled in a similar way. An example of this operation is given in Fig. 2.

To the free end of an arbitrary element only clamping points of other elements can be coupled. Neither closed loops nor additional foundation joints can be made by this procedure. If the structure is redundant, further operations are obviously necessary. The importance of this particular feature will be

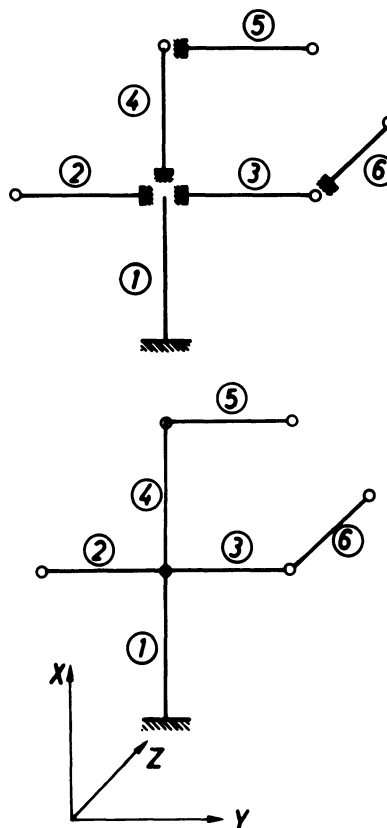


Fig. 2 Assembly of structure following the flexibility method.

discussed in more detail. Redundant structures have to be first transformed into isostatic ones by properly cutting the closed loops and by eliminating the additional foundation joints (Fig. 3).

Assembly procedure

For setting up the flexibility matrix of the complete structure the following procedure is followed.

Joint *i* of the structure can be displaced either by

(a)–The elastic deformation of the element *i* itself, caused by all the forces acting on the joints further away from the foundation and belonging to the same branch of the structure.

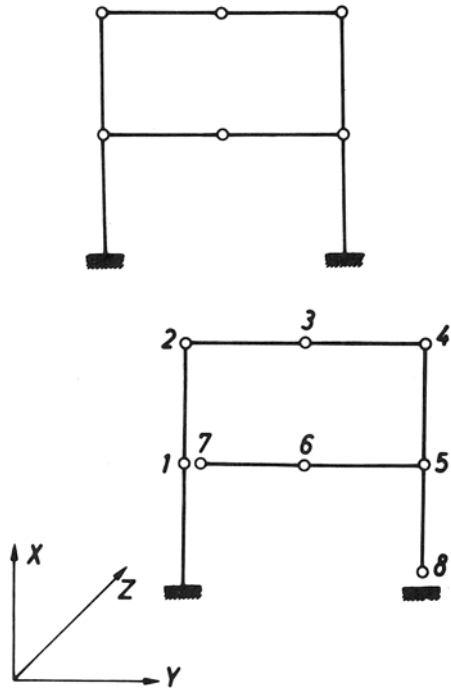


Fig. 3 Redundant structures using the flexibility method.

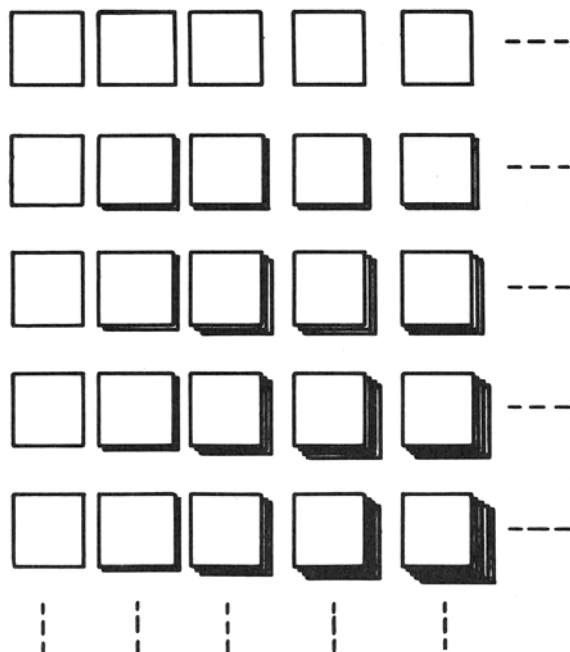


Fig. 4 Construction of the flexibility matrix for an unbranched structure.

(b)–The displacement of the assumed clamping point of the element *i*, conforming to a rigid body displacement.

Similarly, the displacement of the assumed clamping point of the element *i* is caused in turn by an elastic deformation and a rigid displacement, and so on.

The displacement of a joint corresponding to a row of the structural flexibility matrix, is composed of the sum of a large number of terms. This number increases for joints further away from the foundation. Fig. 4 illustrates the construction of the flexibility matrix of an unbranched structure. Each block corresponds to a 6 × 6 matrix.

Redundant structures

For redundant structures, two conditions have to be fulfilled.

(a) The relative displacement of the cuts must be zero.

(b) The internal redundant forces must be in equilibrium with the external forces.

These conditions determine the redundant forces as a function of the external forces. The redundant forces can then be replaced in all the equations by these functions.

Obviously, this procedure involves a large number of operations, which increase rapidly with the degree of redundancy.

Finally, the last step of the calculation of the static deformation of the structure consists of multiplying the flexibility matrix by the load vector. Several load cases can easily be considered by subsequently multiplying the flexibility matrix by the corresponding load vectors.

Conclusions

The following conclusions can be drawn.

(i) The construction of the flexibility matrix involves a large number of operations, increasing drastically with the number *n* of elements: (for an unbranched structure, the number of 6 × 6 matrices to be calculated is equal to $\sum_{i=1}^n i^2$)

(ii) The number of operations rapidly increases with the degree of redundancy.

(iii) The final step in the calculation, consisting of the multiplication of the flexibility matrix by the load vector, requires a short time compared with the setting-up time of the flexibility matrix itself.

(iv) Several load cases can easily be calculated without further difficulties.

SIMPLIFICATION OF THE FLEXIBILITY MATRIX.

The flexibility matrix of isostatic structures can be simplified considerably. It has been assumed that, in each joint and in each direction, a force and a moment can be applied. In practice, however, the number of loads really acting on the structure is usually small compared with the total possible

number of loads, which is equal to six times the number of joints.

Thus, the number of non-zero elements in the load vector is small and consequently most of the columns of the flexibility matrix would be multiplied by zero in the ultimate step of the calculation. Obviously, these columns of the matrix do not require any calculation and therefore the actual number of operations may be reduced up to one hundred times, depending essentially on the dimensions of the matrix and the number of non-zero forces.

In the case of redundant structures, it is clear that a large part of the matrix must still be calculated because the displacements of all joints, caused by the redundant forces, have to be calculated. Almost the entire flexibility matrix must be calculated for highly redundant structures.

Assembly of the structure in the stiffness method

Assembly procedures

The free-free beam being the elements of the structure can be coupled quite easily by applying the equilibrium equations. Indeed, the external forces applied to a particular joint must be in equilibrium with the sum of the internal forces in the various elements coming together in that joint. Consider element *k* with near-end *i* and far-end *j*, and let F_i and F_j be respectively the external forces in the joints *i* and *j* and F_{ik} and F_{jk} respectively the internal forces in the element *k*.

The equilibrium equations for joint *i* and *j* are:

$$F_i = F_{ik} + \text{contributions from other elements meeting at joint } i. \tag{4}$$

$$F_j = F_{jk} + \text{contributions from other elements meeting at joint } j. \tag{5}$$

Combining equations (4), (5) and (3)

$$F_i = F_{11k} D_i + K_{12k} D_j + \text{contributions from other elements} \tag{6}$$

$$F_j = K_{21k} D_i + K_{22k} D_j + \text{contributions from other elements.} \tag{7}$$

The displacements of the near-end *i* and far-end *j* of the element *k* are equal to the displacements of the joints *i* and *j* of the complete structure (compatibility condition). The presence of an element between joints *i* and *j* seemingly has the effect of transferring the four blocks of the element stiffness matrix to the structural stiffness matrix according to the following scheme:

$$\begin{matrix} & \begin{matrix} \text{column } i & \text{column } j \end{matrix} \\ \begin{matrix} \text{row } i \\ \text{row } j \end{matrix} & \left[\begin{array}{cc} \vdots & \vdots \\ \text{---} K_{11k} \text{---} & \text{---} K_{12k} \text{---} \\ \vdots & \vdots \\ \text{---} K_{21k} \text{---} & \text{---} K_{22k} \text{---} \\ \vdots & \vdots \end{array} \right] \end{matrix} \tag{8}$$

Application of this procedure to all elements in the structure produces the complete structural stiffness matrix.

Example

In order to illustrate the construction of this complete matrix by means of a particular example, a joint *j* is considered at which three elements, *k*, *l* and *m* intersect (Fig. 5). It is assumed that the *x*-axis of each element is oriented in such a way that *j* is a near-end for member *l* and a far-end for members *k* and *m*; when the structural stiffness matrix is completed, the 6 × 6 matrix, K_{jj} , of the complete matrix will be the superposition of three blocks which are part of the corresponding element stiffness matrix

$$K_{jj} = K_{11k} + K_{22l} + K_{11m} \tag{9}$$

ASSEMBLY OF THE STIFFNESS MATRIX

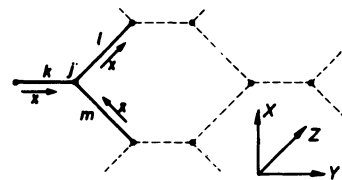


Fig. 5 Assembly of the stiffness matrix.

Because no load-displacement equation is required to formulate the equilibrium of foundation-joints, the structural matrix has no row and no column corresponding to these foundation joints; only 6 × 6 blocks corresponding to the unknown displacements should be calculated.

Furthermore, the stiffness matrix is a band-matrix, the bandwidth being determined by the largest difference between the joint numbers of the elements. This property considerably reduces required memory core in the computer.

Simplification

The evaluation of the displacement vector for a given load vector, being the last step in the calculation, generates a large number of operations. For this purpose, the modified decomposition method of Cholesky³ has been used. With this method the bandwidth of the structure matrix is conserved during the decomposition. Moreover, only the back substitution is to be repeated when more than one load vector is considered.

The following conclusions can be drawn.

(i) The number of 6 × 6 matrix blocks to be calculated for the composition of the structural stiffness matrix is small compared with the flexibility method. Indeed, only four blocks have to be calculated for each element.

(ii) The presence of foundation joints reduces the number of calculations, because for these elements, only one 6 × 6 block has to be calculated.

(iii) The structural stiffness matrix of redundant structures is obtained in the same way as for isostatic structures because the equilibrium conditions are automatically satisfied in each joint.

(iv) The stiffness matrix is a band-matrix, yielding a considerable reduction of computer memory.

(v) The evaluation of the displacement vector involves a large number of operations.

COMPUTATION TIME AND ACCURACY OF THE PROGRAMMES BASED ON THE FLEXIBILITY AND ON THE STIFFNESS METHOD

Advantages and disadvantages

The advantages and disadvantages of both methods may be summarized as follows:

(i) The construction of the complete flexibility matrix is a time-consuming operation. But, in the case of isostatic structures, the matrix can be considerably simplified.

(ii) For highly redundant structures, a large number of further operations are required when using the flexibility method.

(iii) Finally, when using the stiffness method a set of simultaneous equations has to be solved, which may also prove to be a time-consuming operation.

The net effect of these considerations of the computation time associated with the computer programs has been evaluated further.

Computation time

Comparison criteria

The parameters determining this computation time are not necessarily identical in both methods. Therefore, the basis for comparison must be found in the structure itself.

Convenient parameters for the comparison are:

the number of elements of the structure; and

the number of foundation joints and the number of closed loops.

For the flexibility method as well as for the stiffness method, the computer-time is almost a quadratic function of the number of elements.

Because of the method of construction of the complete structure stiffness matrix, the computation time associated with the stiffness method is approximately independent of the degree of redundancy of the structure. With respect to this parameter, the inverse is true for the calculation time associated with the flexibility method. For the flexibility method various computer runs have experimentally proved that the closing of an additional loop roughly requires a twofold increase of time compared with the introduction of another foundation joint.

The *degree of redundancy* can thus be defined as: $(\text{the number of additional foundation joints}) + (2 \times \text{number of closed loops}) / (\text{number of elements})$ (10).

Practical examples

The computer times corresponding to various arbitrarily chosen structures are reviewed in Fig. 6. The ordinate value is the Central Processor time* divided by the square of the number of elements. The abscissa value is the degree of redundancy defined by equation (10).

The values corresponding to the flexibility method as well as to the stiffness method show a certain amount of scatter, because the computation time is

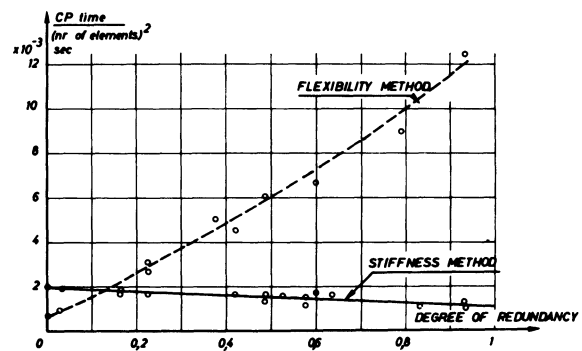


Fig. 6 Computation time with the flexibility and the stiffness methods.

assumed to be a quadratic function of the number of elements. In Fig. 6, the number of elements ranges from 8 to 115 and the number of external loads from 1 to 4. Especially with the flexibility method, the computer time also depends on the way the structure is branched. The calculation time associated with the stiffness method also depends on the bandwidth of the stiffness matrix, which may vary between wide limits. But, none of those additional factors seems to have a particularly important influence on the computer time. Moreover, the scatter is relatively small; from Fig. 6, I conclude that:

1. the computer time associated with the flexibility method increases strongly with the degree of redundancy;

2. the computer time with the stiffness method slightly decreases with the degree of redundancy. This can be explained because the number of the 6×6 blocks to be calculated by building up the structural stiffness matrix, depends only on the number of elements; however, for an increasing degree of redundancy, the total dimension of the matrix decreases and the set of simultaneous equations will be solved faster;

3. in comparison with the stiffness method, the flexibility method is three times faster for the case of isostatic structures but about ten times slower for the case of highly redundant structures. The break even point is at a degree of redundancy of about 0.15. That means that for example, for a

* The programmes were run on a CD 6600 computer.

structure with 100 members, the flexibility method is the most efficient if the number of closed loops does not exceed seven or eight or the number of foundation joints (without closed loops) does not exceed fifteen.

The computer times mentioned evidently depend also on the detailed programming. In this respect it is interesting to note that both programs are set up by the same person.

A second comparison is given by Fig. 7. This shows a truss structure, which was made isostatic by cutting all closed loops and the right foundation joint. This structure has been used to study the

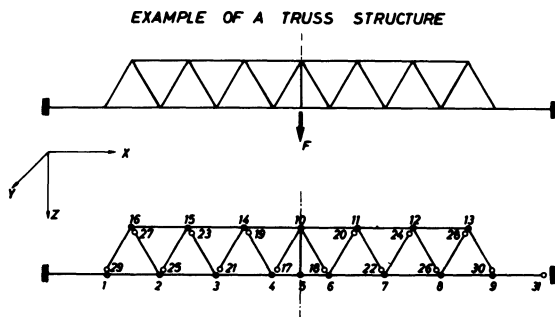


Fig. 7 Example of a truss structure.

importance of the degree of redundancy without the influence of other parameters. Subsequently, joint 31 is fixed to the foundation and the cuts (30-9, 29-1, 28-8, and so on) closed. In another step, the joints 31, 30, 29, 28, and so on were subsequently fixed to the foundation. The computation times obtained both by the flexibility method and the stiffness method are plotted against the degree of redundancy (Fig. 8).

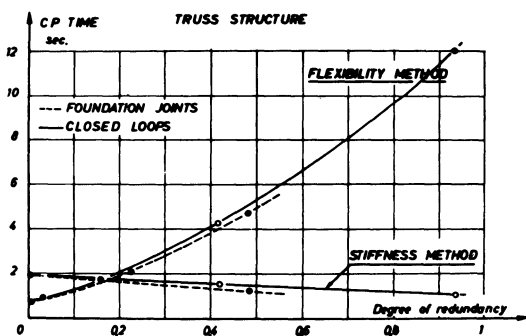


Fig. 8 Computation time with the flexibility and the stiffness methods—truss structure.

The following points can be observed.

For the flexibility method the time increase required for an additional closed loop is about 2.3 times larger than the time required for an additional foundation joint.

In the stiffness method, the time for the calculation of the completely closed structure is about 53% of that for the open structure.

The break even point for the closed loops as well as the foundation joints corresponds to a degree of redundancy of about 0.16. This value corresponds very well to the mean value 0.15, found by Fig. 6.

Conclusion

The flexibility method is obviously efficient only for the calculation of structures with a small degree of redundancy. For the calculation of highly redundant structures, however, the stiffness method is superior. In this case, the reduction of computer time may be considerably larger than the gain achieved with the flexibility method in the case of isostatic structures [ratio 12 against 3].

ACCURACY OF THE COMPUTATION

Comparison criteria

Computation errors have their origin in rounding off errors during mathematical operations. The magnitudes of the errors for both the flexibility method and the stiffness method have been evaluated in a particular case by means of the structure represented in Fig. 7. This structure is symmetric with respect to one axis coinciding with the joints 10 and 5. The load F is acting in the direction of the axis of symmetry. The deflections of the mutual symmetrically situated joints (for example, 16-13, 15-12, and so on) must be identical and the rotations of the joints 5 and 10 around the y -axis must be zero.

In order to obtain the computation error as a function of the degree of redundancy, a similar procedure to that used for the study of the computation time was followed.

To begin with, an isostatic structure (Fig. 7) was considered; but in order to regain symmetry, joint 31 was fixed to the foundation. Subsequently, the closed loops were made two by two symmetrically and, in a second step the symmetric foundation joints (30-29, 28-27, and so on) were fixed two by two.

The results of computations showed that in all cases, symmetry was conserved (6 significant figures were printed) in the flexibility method as well as in the stiffness method. In none of the cases, however, was the rotation of the joint 5 (φ_{y5}) exactly zero. The value of φ_{y5} varies between 10^{-17} and 10^{-22} . The maximum displacement, which is always obtained in joint 5, varies between 0.5×10^{-6} and 0.6×10^{-9} , and the maximum rotation around the y -axis varies between 0.15×10^{-5} and 0.7×10^{-8} .

Practical results

In Fig. 9, the value φ_{y5} is plotted on a logarithmic scale against the degree of redundancy for both the additional foundation joints and the closed loops.

In both cases, the error of the stiffness method decreases with the degree of redundancy. This can be explained by the fact that the total dimension of the stiffness matrix decreases and the solution of the equation may be more accurate. For the foundation joints, the decrease is steeper than for closed loops because the number of mathematical operations necessary for obtaining one element of the stiffness matrix is smaller and, consequently, the rounding off

errors are smaller. On the contrary, the error in the flexibility method slightly increases for an increasing degree of redundancy.

The break even point corresponds, in both cases, to a degree of redundancy of about 0.21, which corresponds well with the break-even point observed for the computation time criterion.

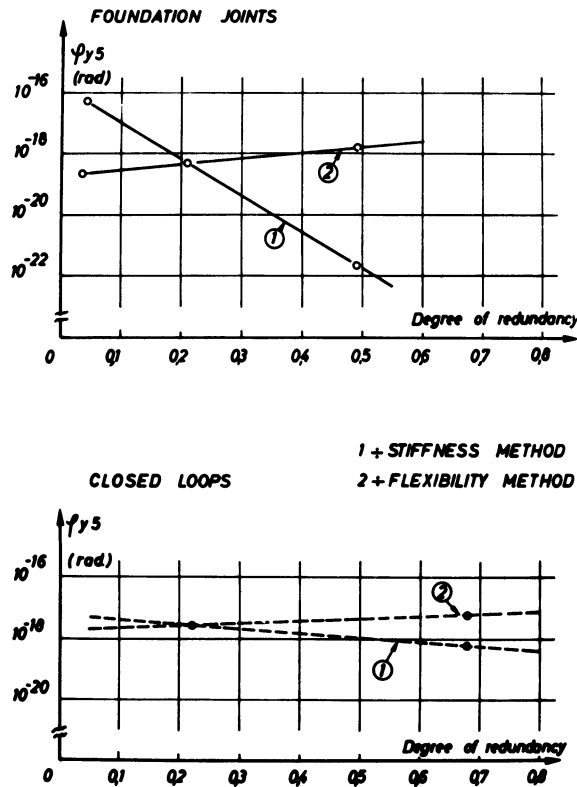


Fig. 9 Accuracy with the flexibility and the stiffness methods.

GENERAL CONCLUSIONS

Generally speaking, the flexibility method is usually superior for the static calculation of structures with a small degree of redundancy in terms of economics and accuracy. The stiffness method is seemingly the most economic and accurate method for the static calculation of highly redundant structures. I conclude that both methods are complementary.

By means of the proposed break-even points, it is possible to choose for each practical case the most efficient method. Flexibility methods should be applied if the degree of redundancy of the structures does not exceed 0.15. Stiffness methods should be preferred for higher degrees of redundancy. The flexibility method should, for example, be preferred for the calculation of radial drilling machines, horizontal milling machines, one-column presses and so on; the stiffness method should be preferred for the calculation of lathe beds, redundant truss structures, portal milling machines and so on.

REFERENCES

1. LIVESLEY, R. K., 'Matrix methods of structural analysis', (Pergamon Press, 1969).
2. HURTY, W. C., and RUBINSTEIN, M. F., 'Dynamics of structures,' (Prentice Hall, 1964).
3. ZUMUHL, R., 'Matrizen und ihre technischen Anwendungen,' (Springer-Verlag, 1964).
4. DOPPER, W., 'Ein Beitrag zur Berechnung von Maschinenelementen und Gestellbauteilen von Werkzeugmaschinen mit Digitalrechner Programmen,' (Dissertation, T. H. Aachen, 1968).
5. COWLEY, A., 'The prediction of the dynamic characteristics of machine tool structures' (Thesis, Manchester, 1968).
6. WEAVER, W., 'Computer programs for structural analysis,' (Van Nostrand Co., 1967).
7. VAN, L., den NOORTGATE, 'Calculation of static and dynamic characteristics of axial structures,' (C.R.I.F., 1970).

DISCUSSION

Query from S. Taylor, University of Birmingham.

I agree that the main disadvantages of flexibility methods are redundancy difficulties and the fully-utilised flexibility matrices. On the other hand, two advantages have not been considered.

- (1) Three deflections at any station point are adequate for most practical purposes, whereas six degrees of freedom are mandatory for stiffness methods. Slopes can be calculated from the deflections if required. This leads to a factor of roughly 4 in reduction of computing time and cost.
- (2) There is no need to have a station point between every pair of elements as is necessary in stiffness methods. Again this leads to a reduction in matrix sizes, time and cost.
- (3) In addition, the truss structure mentioned has a very narrow band-width and is particularly advantageous to the stiffness method. A representative selection of structures would give wide variation of times using stiffnesses due to the differences in band-width unless the structure were small enough or the computer large enough to handle them entirely in the core store. In particular, there is doubt when different programmes are compared, even if they are both developed by the same man.

Considering all these points, I believe that the area in which the flexibility approach is favourable is much larger than the author suggests.

Replies

- (1) Even in the flexibility method, the reduction to three degrees of freedom for each station point cannot be used throughout the programme for the following two reasons:
 - (a) A static load on a structure consists in many cases not only of forces, but also of bending and torsional moments. The corresponding rotational degrees of

freedom need to be introduced in the computation.

- (b) If the structure is redundant, the redundant forces have to be calculated for *all the six degrees of freedom*.

For high redundancies, about 95% of the computation time is due to this calculation, where no reduction is possible. Moreover, the slope of the curve of Fig. 6 corresponds to the additional time needed for the calculation of the increasing number of redundant forces with obligatory six degrees of freedom.

This results in the fact that, even if a reduction to three degrees of freedom is used where possible, the position of the break-even point will practically not be influenced.

- (2) Indeed, an advantage of the flexibility method is the possibility of not considering some of the station points. The same effect, however, may be obtained in the stiffness method, by combining it with transfer matrices. Neither of these possibilities was considered in the present programmes.

For highly redundant structures, however, in almost all station points, redundant forces are applied. Obviously, those points may not be skipped. Therefore, the computation time for a degree of redundancy of 1 will not considerably be influenced (see Fig. 6). Again, the position of the break-even point will remain practically unchanged.

- (3) The results of the truss structures were not used for setting-up the general curves of Fig. 6. As mentioned in the paper, the structures used for Fig. 6 are chosen arbitrarily with widely varying characteristics. The selection of the structures may therefore be considered as representative: all computations were done in the core store of the computer, which can handle up to 150 beam elements in the stiffness method. This number may be considered as largely sufficient for machine tool construction.

For all the mentioned reasons, the general conclusions of the paper are valid, namely the trend of the curves and the position of the break-even point. The latter is of course to be considered as an order of magnitude.

THE FINITE-ELEMENT METHOD APPLIED TO THE DEFORMATION ANALYSIS OF THIN-WALLED COLUMNS

by

S. HINDUJA and A. COWLEY*

SUMMARY

The paper presents the results obtained from computations of the deformations of thin-walled box-type column structures when subjected to both torsional and bending loads. The computed results, which correspond to various finite-element representations of the columns, are compared with experimentally derived values and with calculations based on closed form analytical expressions.

The accuracy of the computed static deformations depends on the specific nature of the finite-element model adopted. The results presented in the paper indicate the degree to which the resulting accuracy increases as the finite-element model becomes more refined. Some considerations regarding computing costs are also explained.

INTRODUCTION

Up to the present time the response of machine tool manufacturers to the computer aided design techniques, which have been developed and demonstrated over the past decade, has been somewhat limited. In the area of structural design the application of computer procedures which have appeared in the literature have been based on the analyses of simple topological models comprising concentrated masses interconnected by beam-like elastic elements. Such a simplification obviously imposes a serious constraint on the type of structure that can be analysed with acceptable accuracy. On the other hand approximating to the true structural geometry in this way yields a substantial simplification in the mathematical problems involved in determining the static and dynamic stiffness characteristics of the structure. Typical examples are described^{1,2} from which it is evident that the main limitations of the beam-like element approach are:-

(i) It is often difficult to define the equivalent beam characteristics of machine tool structural elements, particularly those of non-slender form and with internal ribbing, apertures, etc.

(ii) The stiffness characteristics of both fixed and sliding joints cannot always be defined with adequate accuracy.

(iii) The damping behaviour of structural elements and joints is not yet (claimed to be) adequately appreciated even by the more academic research workers.

The latter limitation might be considered as

belonging to a separate category since it affects only the accuracy with which dynamic behaviour may be predicted. The remaining two limitations influence the accuracy in computing both static and dynamic stiffness characteristics and this paper is concerned primarily with the first.

In order to overcome the difficulties mentioned in (i) a number of finite-element computer programmes have been developed at UMIST which, to date, permit a structure to be represented, for the purpose of computation, by an assembly of beam-like elements, rectangular and triangular plate elements and solid prismatic elements (Fig. 1). The programmes, which are restricted presently to the computation of static deformations, are currently being employed in analysing rather simple structural elements with the aim of establishing both the accuracy and cost of this technique of analysis.

The basic features of the programmes, together with the results of some preliminary applications, have been described in (3). This paper describes the results of further applications of finite-element technique.

NOTATION

a_1, a_2 , etc.	Coefficients of displacement functions
b	Mean width of column
E	Modulus of elasticity
h	Mean depth of column
L	Length of column
P	Applied loads
t	Aspect ratio h/b
u, v, w	Displacements in x, y and z directions respectively

*Department of Mechanical Engineering, UMIST, Manchester.

x	Distance from column base to cross section at which displacements are required
x_p	Distance from column base to point of application of load
δ	Wall thickness
ϵ	Aspect ratio L/h
θ_x, θ_y or θ_z	Rotation (or slope) of a point about X, Y and Z axes respectively
γ_{xy}	Shear strain at a point within a plate situated in a plane containing x and y axes
ν	Poisson's ratio
G	Modulus of rigidity
T	Torque applied

function forms the starting point in the derivation of the 'stiffness matrix' of the element which is simply a relationship between the forces and resulting displacements of the element's nodal points. In the case of thin plate elements it is necessary to prescribe displacement functions expressing the possible deformation of the plate under plane stress and when subjected to out-of-plane (bending) forces. These two considerations result respectively in the derivation of an 'in plane stiffness matrix' and a 'bending stiffness matrix' which are assumed to be independent properties.

Since the resulting accuracy of the computed deformation of a structure depends primarily on the choice of displacement functions, those which have been used in the UMIST programs will be briefly discussed.

THE FINITE-ELEMENT METHOD

The finite-element method has been applied to the analysis of a variety of mechanical structures primarily in the civil engineering and aerospace industries and the works of Clough⁴, Zienkiewicz⁵, Argyris⁶ and others have contributed notably to its growth. The method requires the structure to be subdivided into a number of basic elements, finite in dimensions and particular in shape. Typical basic elements include thin plates of triangular, rectangular, or general quadrilateral form, beams, solid prismatic elements, etc. (Fig. 1). A complete structure is built-up by the connection of such finite-elements to one another at a definite number of nodal points, those for a rectangular plate being situated at its four corners. The finite-element is constrained to deform according to a prescribed pattern which is expressed in mathematical form by a 'displacement function' expressing the displacement under load of any point within the boundaries of the element as a function of the precise position of that point. The displacement

DISPLACEMENT FUNCTIONS

The displacement functions used for the derivation of the stiffness matrices of the individual elements are enumerated below. Any of these formulations can be used simply by calling for the appropriate routine.

Routine RECT

This routine is used for the formulation of the stiffness matrix of a rectangular plate element. It consists of three alternative formulations written as sub-routines, any one of which may be adopted, depending on the requirements of the application.

RECT 1

Computes the stiffness matrix of a plate based on a simple linear four-term displacement function⁴ for the deformation of the plate in its own plane, thus:-

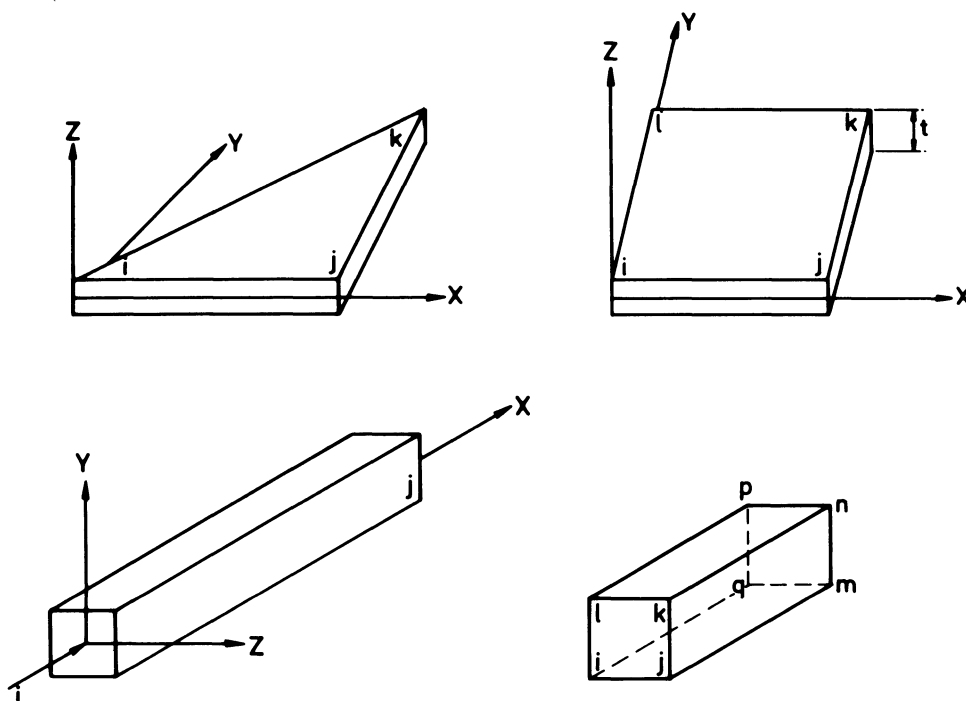


Fig. 1 Basic elements.

$$\begin{aligned} u &= a_1 + a_2x + a_3y + a_4xy \\ v &= a_5 + a_6x + a_7y + a_8xy \end{aligned} \quad (1)$$

For the out of plane (bending) properties the function (9) used is

$$\begin{aligned} w &= a_1 + a_2x + a_3y + a_4xy + a_5x^2 + a_6y^2 + a_7x^2y \\ &\quad + a_8xy^2 + a_9x^3 + a_{10}y^3 + a_{11}x^3y + a_{12}xy^3 \end{aligned} \quad (2)$$

A total for six degrees of freedom is associated with each corner node namely, three displacements (u , v and w) and three rotations (θ_x , θ_y and θ_z). The resulting stiffness matrix is an array of stiffness values relating the forces and moments at the nodes to the corresponding displacements and rotations. Thus, for the four-node rectangular element the stiffness matrix contained 24 rows and columns. It should be noted that when using the displacement functions specified above, it is not possible to derive the plate stiffness coefficients associated with a moment about the Z axis and the corresponding rotation θ_z . In this case these stiffness coefficients are taken to be zero.

RECT 2

This sub-routine performs the same functions as RECT 1, but the in-plane displacement functions adopted are modified in accordance with the proposals of Cheung⁷, who has demonstrated that for certain types of structure they yield an improvement in the accuracy in determining deformations

$$\begin{aligned} u &= a_1 + a_2x + a_3y + a_4xy + \left(\frac{\nu}{1-\nu} a_4 - a_8/2\right) y^2 \\ v &= a_5 + a_6x + a_7y + a_8xy + \left(\frac{\nu}{1-\nu} a_8 - a_4/a\right) x^2 \end{aligned} \quad (3)$$

where ν = Poisson's ratio.

RECT 3

This sub-routine is also similar to RECT 1, but the in-plane displacement function used is a linear-cubic eight-term polynomial

$$\begin{aligned} u &= a_1 + a_2x + a_3y + a_4xy + a_5xy^2 + a_6xy^3 + a_7y^2 \\ &\quad + a_8y^3 \\ v &= a_9 + a_{10}x + a_{11}y + a_{12}xy + a_{13}x^2y + a_{14}x^3y \\ &\quad + a_{15}x^2 + a_{16}x^3 \end{aligned} \quad (4)$$

If an analysis is performed taking into consideration only the in-plane properties of the element, the four degrees of freedom associated with each node are u , v , θ_z and the shear strain γ_{xy} . If, however, as is usually the case, this function is being used in conjunction with the twelve-term displacement function for the analysis of space structures, then owing to difficulties encountered during transformation, γ_{xy} is put to zero. The suppression of γ_{xy} implies that the angle included between two sides remains undistorted.

Routine tric

In this routine the stiffness matrix of a triangular plate is evaluated based on the simple 3-term in-plane displacement function, viz

$$\begin{aligned} u &= a_1 + a_2x + a_3y \\ v &= a_4 + a_5x + a_6y \end{aligned} \quad (5)$$

and the nine-term displacement function in bending (8),

$$\begin{aligned} w &= a_1 + a_2x + a_3y + a_4xy + a_5x^2 + a_6y^2 + a_7x^3 \\ &\quad + a_8y^3 + a_9xy^2 \end{aligned} \quad (6)$$

The five degrees of freedom associated with each node are u , v , w , θ_x and θ_y . Like RECT 1, θ_z is also included with the stiffness coefficients equated to zero.

Routine BE26

The stiffness matrix for the beam is derived by specifying independent displacement functions for the tensile, torsional and bending deformation shapes. The three displacement functions are

$$\begin{aligned} u &= a_1 + a_2x \\ v &= a_3 + a_4x + a_5x^2 + a_6x^3 \\ w &= a_7 + a_8x + a_9x^2 + a_{10}x^3 \\ \theta_x &= a_{11} + a_{12}x \end{aligned} \quad (7)$$

It is not necessary to specify independent displacement patterns for θ_z and θ_y because they are directly related to v and w respectively ($\theta_z = \frac{dv}{dx}$ and $\theta_y = \frac{dw}{dx}$).

Routine PR83

The displacement function used for the rectangular prism is

$$\begin{aligned} u &= a_1 + a_2x + a_3y + a_4z + a_5xy + a_6yz + a_7xz \\ &\quad + a_8xyz \end{aligned} \quad (8)$$

with similar functions for v and w . Each of the eight nodes has three degrees of freedom, namely, u , v and w .

During the analyses of the column structures, only the rectangular and triangular plate elements have been used. Analyses have been performed using three alternative formulations in the case of rectangular elements, and the results clearly indicate the influence of the prescribed displacement functions used on the resulting accuracy.

RESULTS OF COLUMN ANALYSES

The column chosen for analysis is shown in Fig. 2. The dimensions (mm) of the column shown were selected primarily because detailed experimental results were already available from Dreyer¹⁰. The column, which is shown in the figure with transverse

partitions, has in fact been analysed under the following conditions.

- (i) With no transverse partitions.
- (ii) With a uniform end cover plate.
- (iii) With five uniform transverse partitions.
- (iv) With five cored transverse partitions.

The loading employed (Fig. 2) subjects the column to both bending and torsion. The loads are applied at three positions (l_a , l_b , l_c) along the length of the column. To determine the deformation resulting from loads at each of the three positions, different finite-element meshes (Fig. 3) have been used. By examining the results obtained for the various meshes the convergence of the computed deflections to the exact value can be ascertained and related to mesh configuration.

The size of each plate has been maintained as square as possible. This has been done, when making a finer mesh, by increasing the number of divisions along the length and width of each panel simultaneously. The notation $m \times n$ denotes that there are m divisions along the length and n divisions across the width in each wall of the column.

For the last three meshes in Fig. 3, advantage is taken of the symmetrical nature of the column and only one half of the column is analysed. This is done by imposing appropriate restraints on the nodes which lie in the plane of symmetry. (The y and z coordinates of such nodes are $y = 0$ and $z = \pm \frac{1}{2}$ width of column.) The restraints to be imposed will depend on the nature of loading. The restraints, when the column is subjected to a pair of symmetrical bending

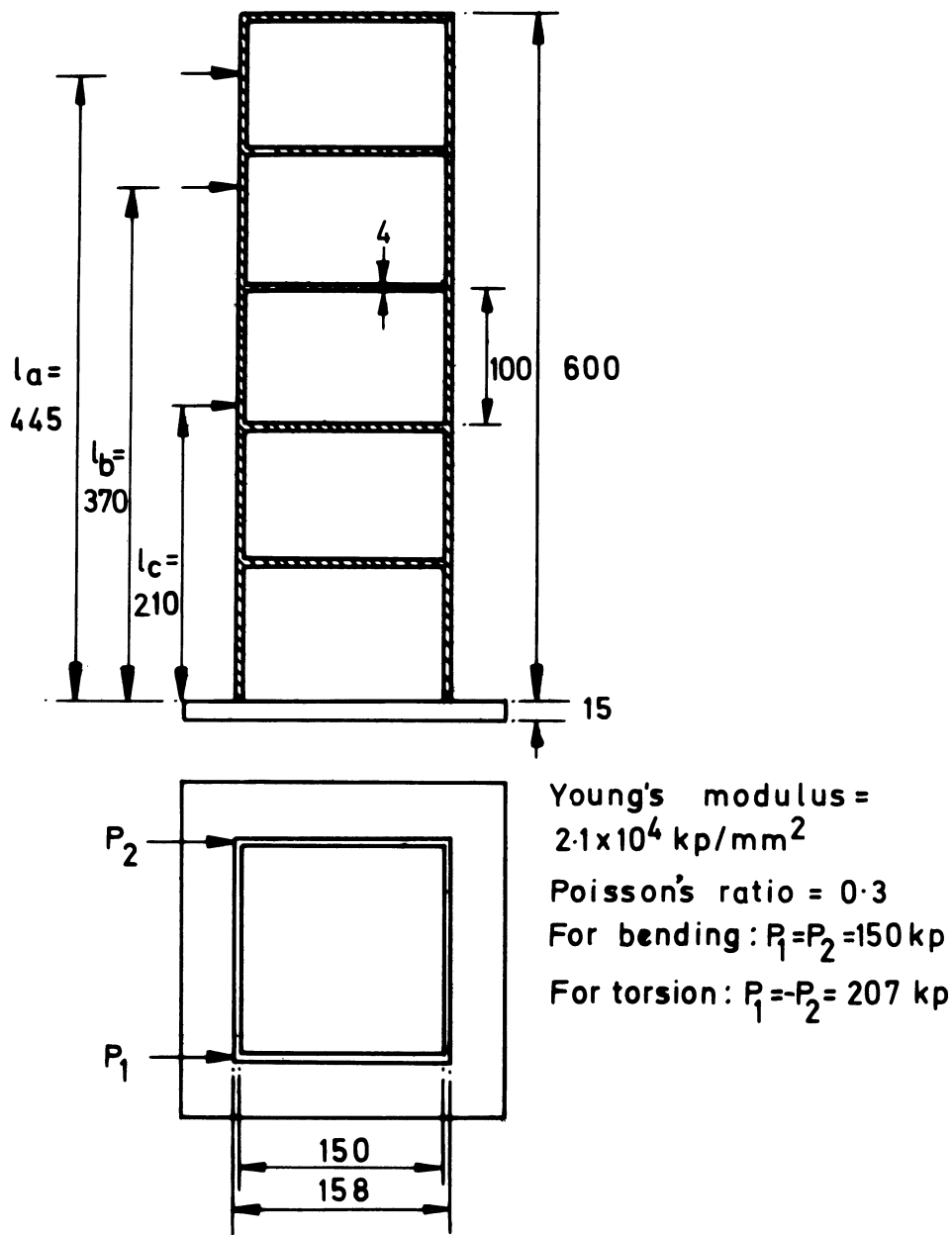


Fig. 2 Box column with horizontal partitions.

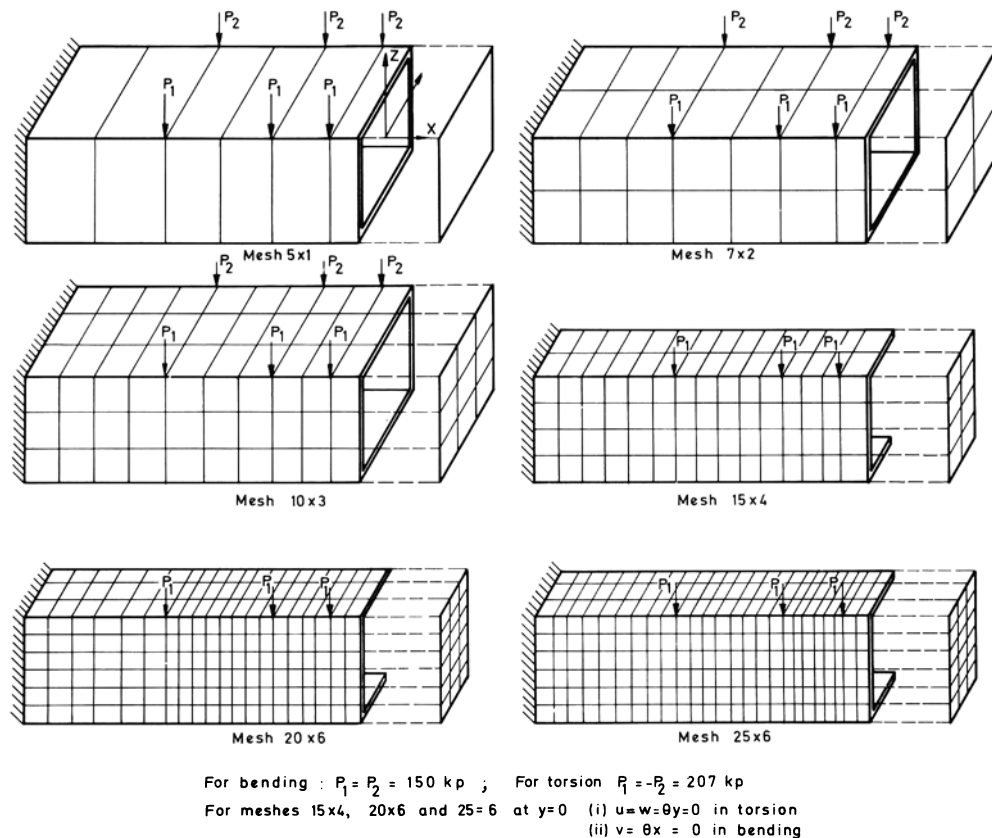


Fig. 3 Meshes used for column with/without end-plate.

loads, are $v = \theta_x = 0$ and in the case of the skew-symmetric torsional load, $u = w = \theta_y = 0$. In the case of torsion, the axial displacement u for nodes lying on the line of symmetry is zero because at these points there can be no warping.

For the column with the end-plate, it was found convenient to consider the cover plate as a separate substructure and compute its stiffness matrix in terms of the nodes which connect it to the main column.

In the last three meshes, since some of the internal nodes lie on the line of symmetry and since the restraints with bending loads are different from those with torsional loads, it is necessary to compute two different substructure stiffness matrices for the cover plate.

The introduction of horizontal partitions at regular intervals of 100 mm made it necessary to alter the lengths of the elements slightly, but the number of elements in each mesh has been retained as such. Since the horizontal partitions and the cover-plate are identical, the substructure stiffness matrix derived for the cover-plate can be used for the partitions also.

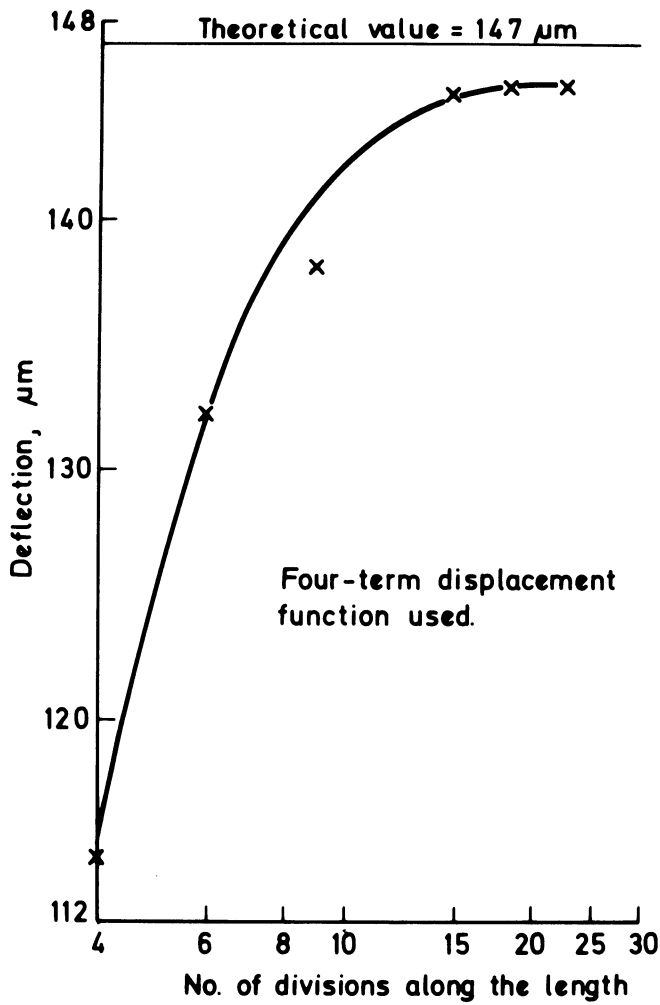
Open column in torsion

The rigidity of box-shaped columns is usually calculated taking into account only the membrane stiffness of the walls. This is often justifiable because machine tool columns are usually thin-walled and moreover, if the flexural stiffness of the walls is also taken into consideration, the theoretical analysis becomes lengthy and complicated. However, this column whose wall-thickness:width ratio is about 0.026, is

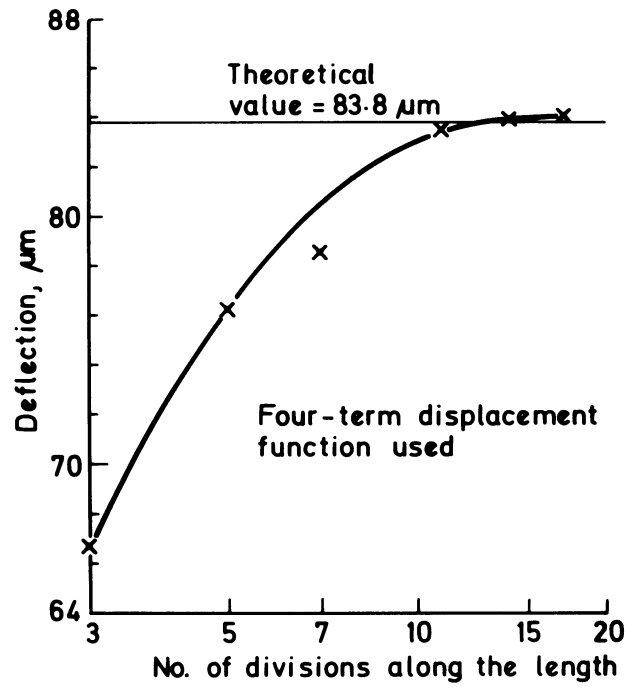
analysed both by taking into consideration and neglecting the flexural stiffness of the walls. In each case the theoretical values are calculated from the formulae given in¹¹; these formulae are reproduced in the appendix.

Fig. 4 shows the computed results obtained when the column is loaded in torsion by two skew-symmetric loads. The 'number of divisions' refers to the number of elements along the length of the column between the fixed end and the loaded plane. To obtain these results the stiffness matrix formulation using the sub-routine RECT 1 (four-term displacement function) has been adopted and only the inplane (membrane) stiffness of the walls is considered, (that is the bending stiffness of the walls is assumed to be zero). Fig. 4(a) shows the deflection (average deflection of loaded plane) resulting from a load applied near the free end of the column distant I_a from the clamped end. It is evident that, as the mesh becomes more refined, the finite-element results converge to within 1% of the theoretical result obtained using equations (3) and (4) of the appendix. Similar correlation is obtained when the load is applied at I_b with the deflection also referred to the section of I_b (Fig. 4(b)).

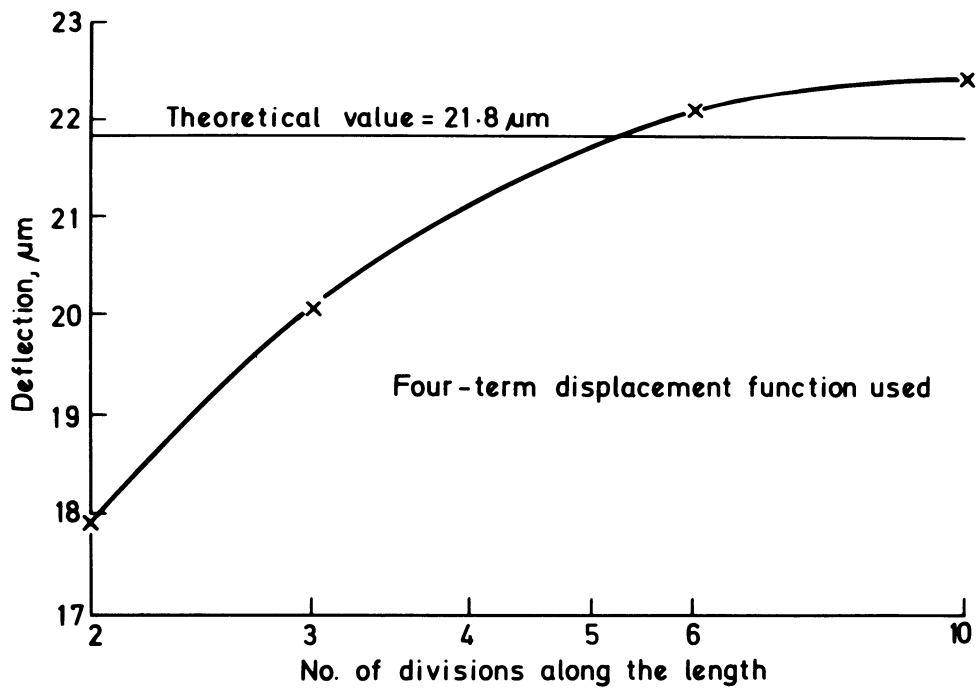
However, at I_c the finite-element solution converges to a value some 3% higher than the theoretical result. The probable reason for this discrepancy is that the formulae of the appendix cannot be applied with sufficient accuracy when the effective loaded length: width ratio of the column approaches unity and when loaded at I_c this ratio is approximately 1.3.



(a) loaded at I_a .



(b) loaded at I_b .



(c) loaded at I_c .

Fig. 4 Column loaded in torsion by two skew-symmetric loads.

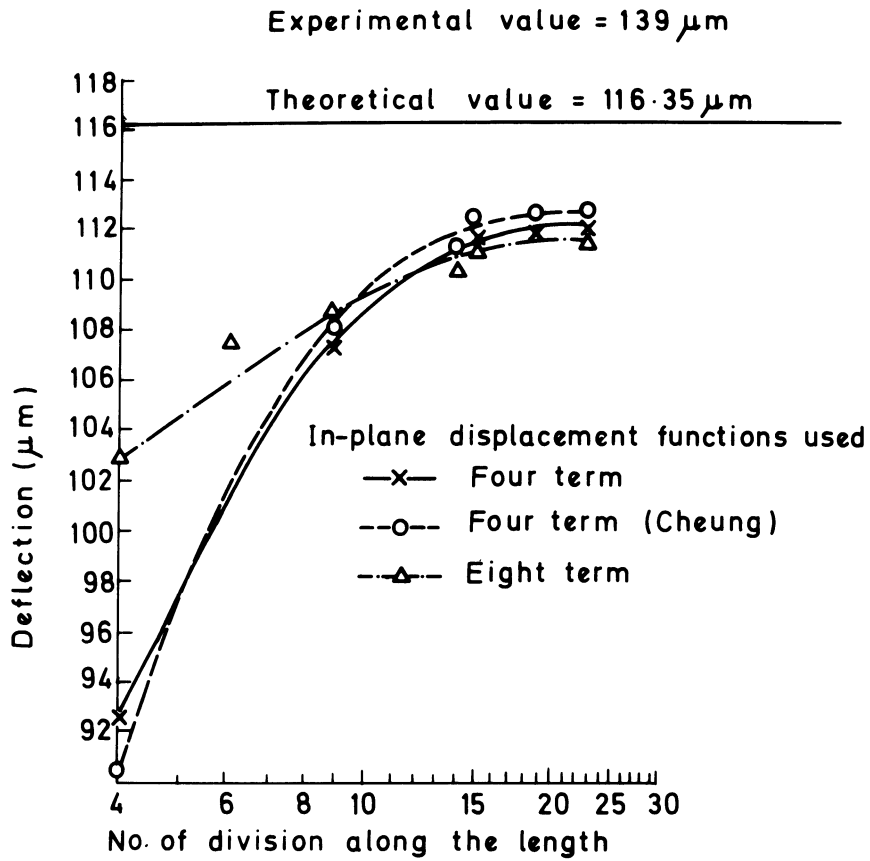


Fig. 5 (a) loaded at I_a .

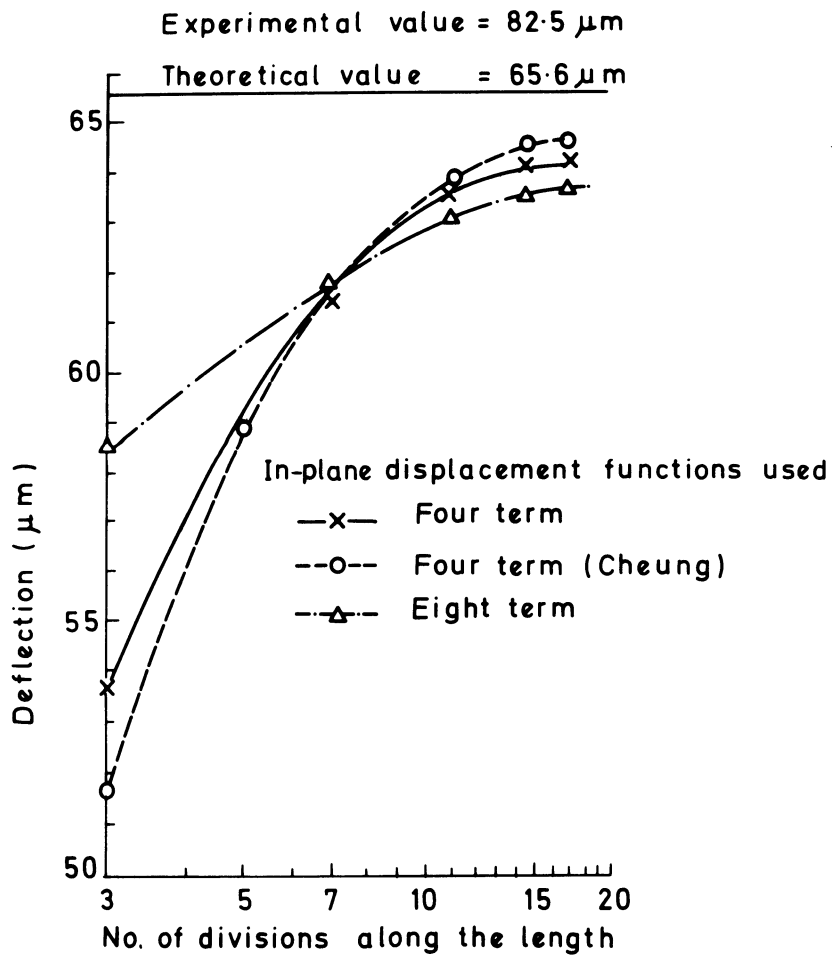


Fig. 5 (b) loaded at I_b .

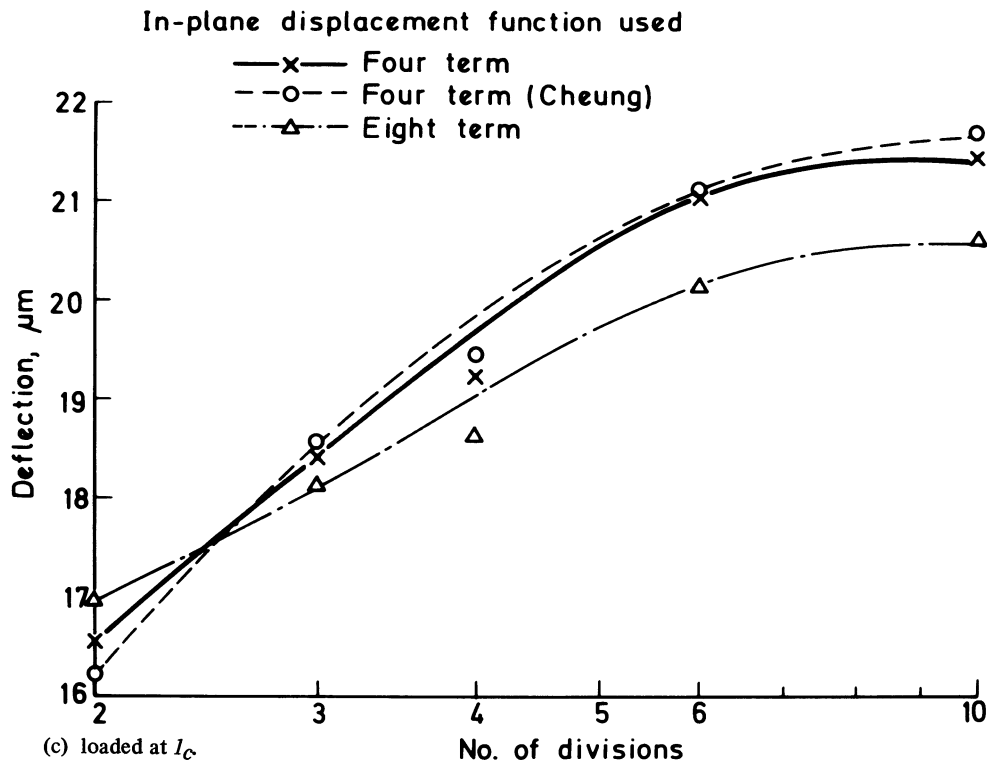


Fig. 5 Convergence of finite-element results.

The convergence of the finite-element results when taking into consideration the flexural stiffness of the column walls is shown in Figs. 5(a), (b) and (c) for the same loading cases as previously considered. The computed results corresponding to the three alternative stiffness matrices obtained using RECT 1, RECT 2 and RECT 3 are shown, together with the theoretical deflection obtained using equations (1) and (2) of the appendix and the experimental results obtained by Dreyer.

From the finite-element computations it was found that the deflections obtained for the two meshes 20×6 and 25×6 were virtually identical, which indicates that the convergence is completed and further refinement of the model would be of no benefit. The curve at I_a converges to within 3% of the analytical solution, whereas at I_b the error is much smaller. However, at I_c there is considerable disagreement between the converged value and the theoretical result. The finite-element result can be expected to be more reliable, because it can be argued that, if the solution has converged to the analytical result at I_a , it ought also to be correct at I_b and I_c .

The stiffening of the column due to the inclusion of the flexural stiffness, varies from 24% at I_a , to 14% at I_c , which is quite considerable. This is indicative of the error to be expected when a theoretical analysis

of a column based on the simpler formulae is performed.

Comparing the results obtained from the three different formulations, there is no appreciable difference between those obtained with a four-term and four-term (Cheung) in-plane displacement functions. It has been shown in an earlier analysis of a cantilever beam³ that the use of these two four-term functions yields exactly the same answer when the plate is square. For the meshes used to assess the convergence of these functions, each plate element has been maintained almost square.

The third formulation (eight-term cubic linear in-plane displacement function combined with a twelve-term bending displacement function) yields results, for coarser meshes, which are better than those obtained from the other two. This curve, which is flatter, converges ultimately to a slightly lower value of deflection. This difference can be attributed to the fact that it was necessary to impose a physical constraint when using this formulation as previously mentioned (i.e. $\gamma_{xy} = 0$). The reason for this cannot be dealt with here but it should be appreciated that any such constraint must lead to a reduction in the resulting deflection. In other words the constraint is equivalent to increasing the stiffness of the structure.

Dreyer has compared the experimental results

TABLE 1 Deflection values of open column in torsion

Loading plane	y deflection (μm)			z deflection (μm)		
	finite-element	theoretical	experimental	finite-element	theoretical	experimental
I_a	112.8	116.25	139	90.9	98.4	100
I_b	64.7	65.6	82.5	48.05	50.78	58
I_c	21.77	14.4	26.5	9.11	5.9	9.5

In-plane displacement functions used

- x— Four term
- -o- - Four term (Cheung)
- ·-△- · Eight term

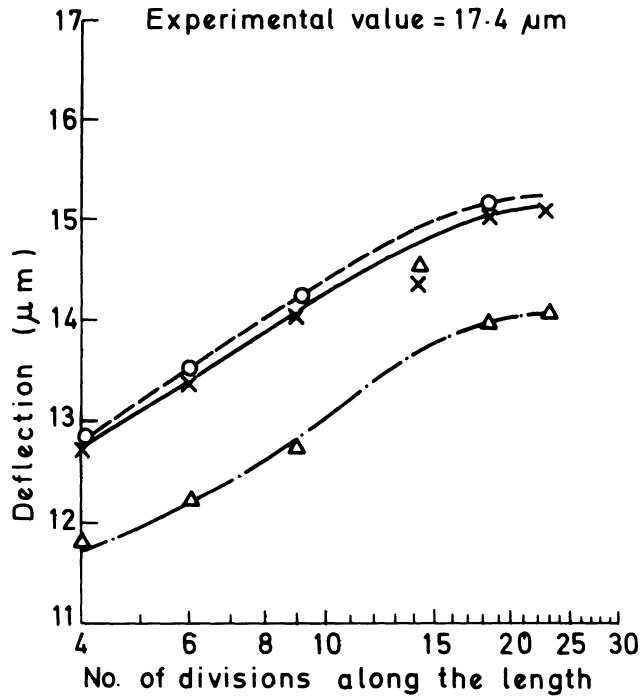


Fig. 6 (a) loaded at I_a .

In-plane displacement functions used

- x— Four term
- -o- - Four term (Cheung)
- ·-△- · Eight term

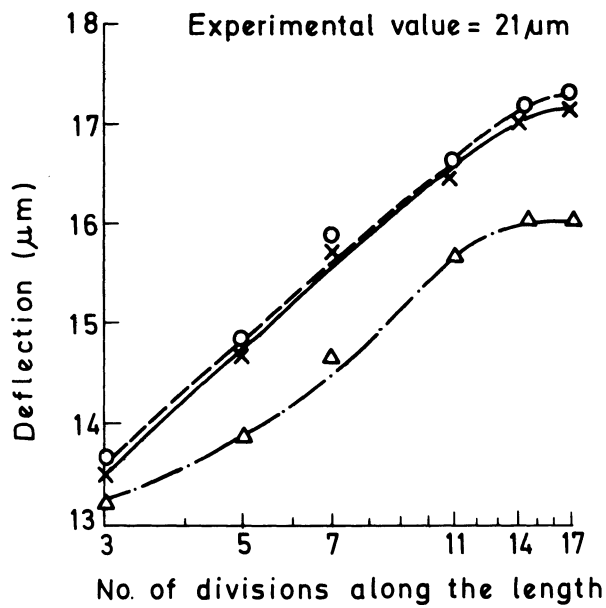


Fig. 6 (b) loaded at I_b .

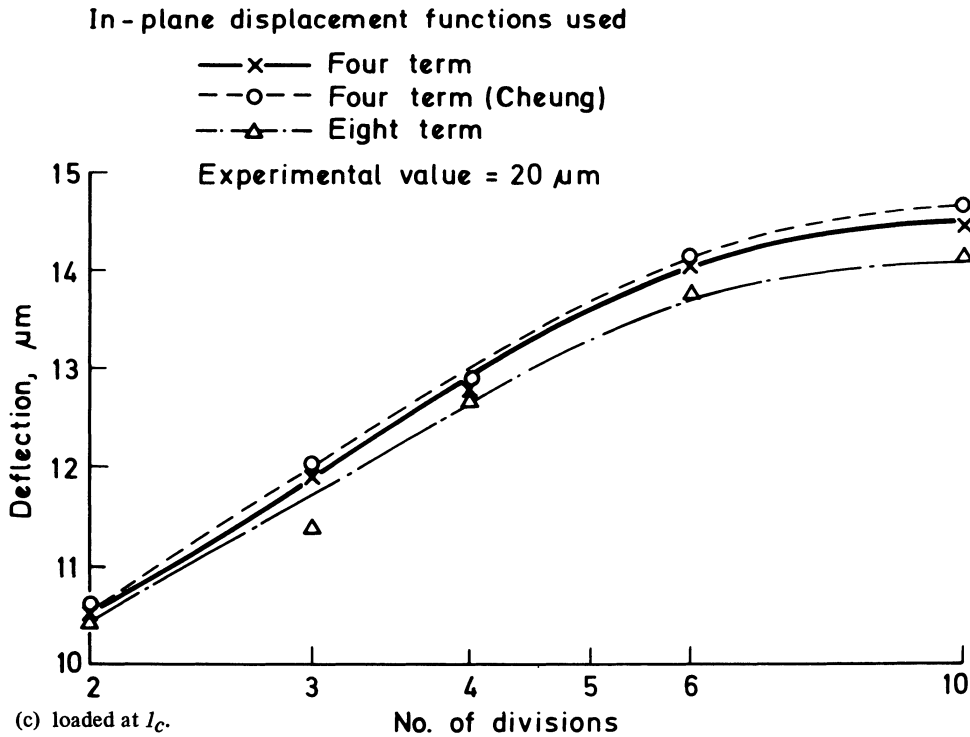


Fig. 6 Convergent curves for column with end-plate loaded in torsion.

obtained for the open-ended column with the analytical solution, which takes into account only the membrane stiffness of the walls and has reported good agreement between the experimental and analytical results. Instead, he should have compared the experimental results with the values obtained from the formula, which takes into consideration the transverse bending stiffness of the walls also. In such a case any difference between experimental findings and predicted results could only be attributed to the fixation condition at the base of the column. The theoretical analysis assumes the column to be rigidly clamped at the base, whereas in fact some flexibility will be apparent at the base joint.

The finite-element, theoretical and the experimental results are summarised in Table 1. If the finite element and the experimental results are compared, the error, due to the flexibility of the base increases, (as one would expect) from 19% at I_a to 28% at I_c .

Column with end-plate in torsion

The convergent curves for the column with an end-plate subjected to the same skew-symmetric loads at I_a , I_b , I_c are shown in Figs. 6(a), (b) and (c). The curves do not exhibit the monotonic characteristic observed in the case of the open-ended box column. This is because the displacement of the loaded plane

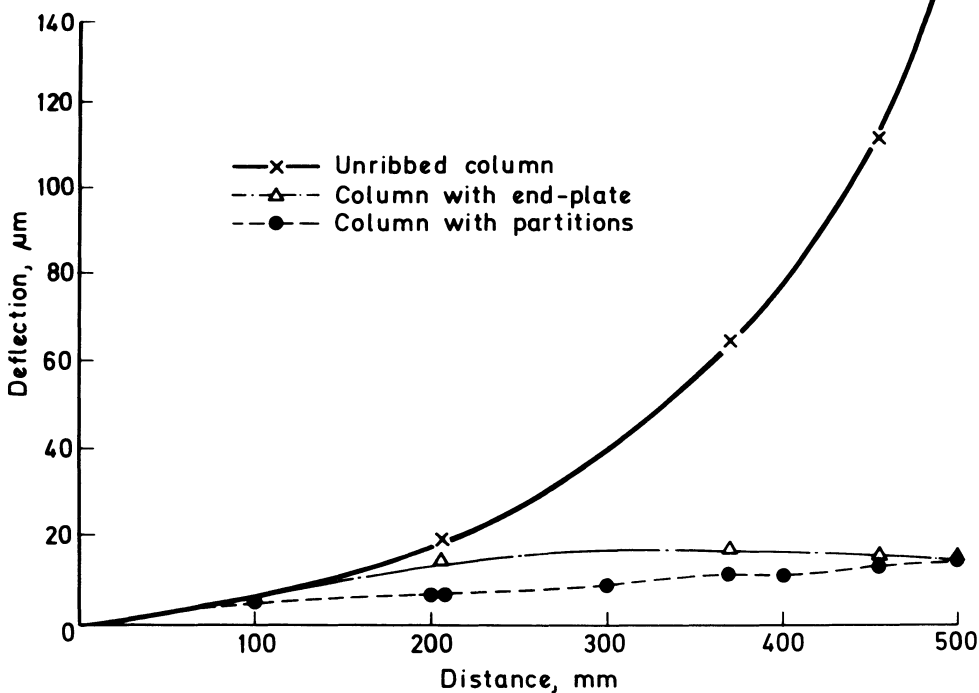


Fig. 7 Deflection characteristics of column in torsion.

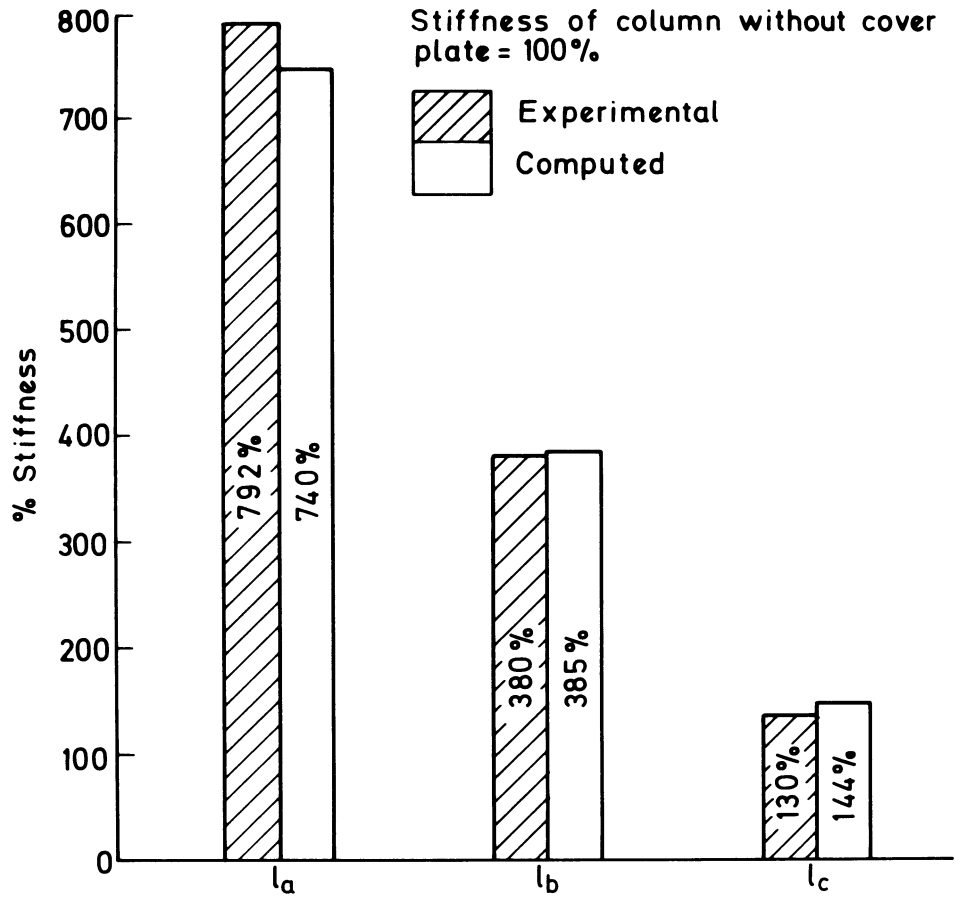


Fig. 8 Histogram: comparison of stiffness of column, with and without cover plate.

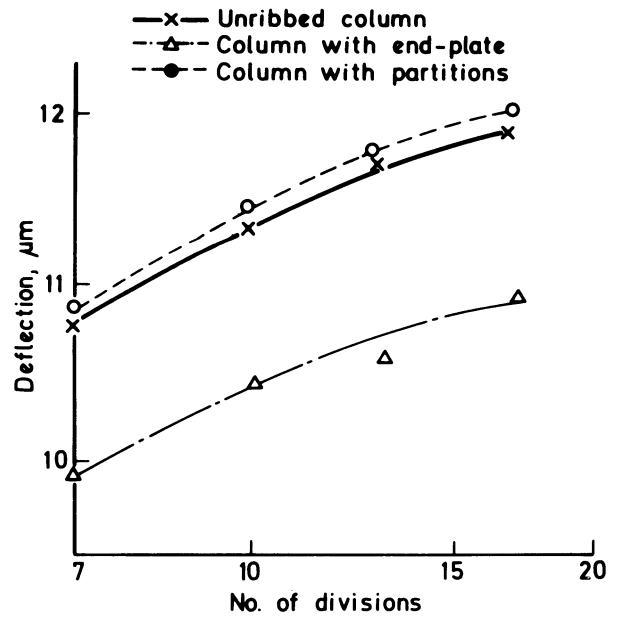
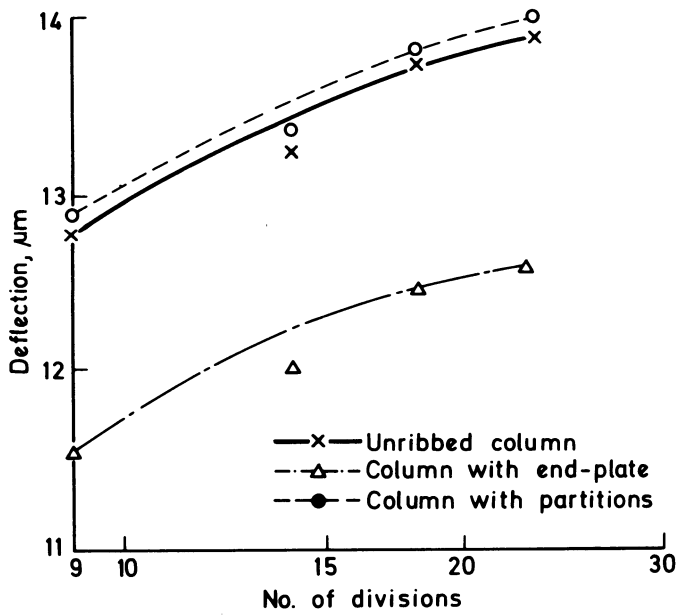


Fig. 9 (a) loaded at l_a .

(b) loaded at l_b .

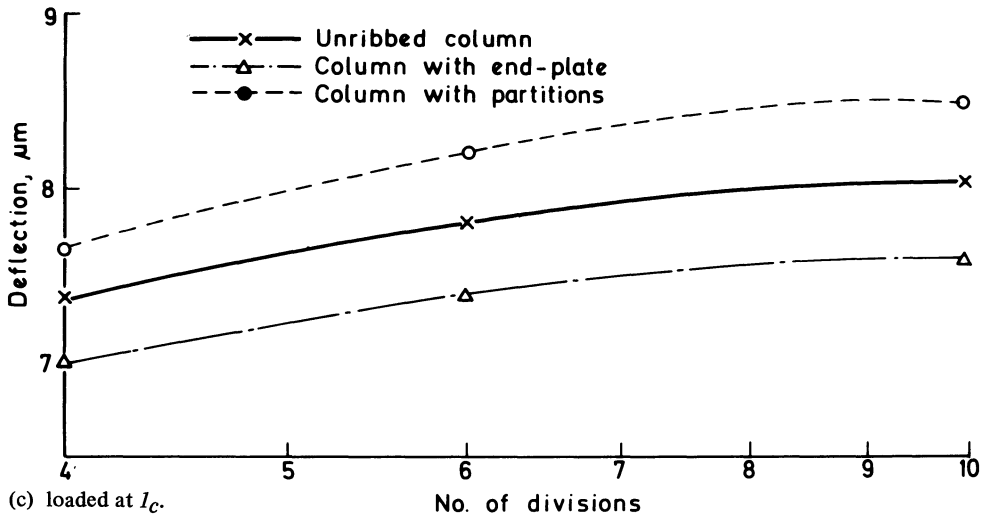


Fig. 9 Convergent curves for column with partitions loaded in torsion.

is plotted against the number of elements between the base and the loaded plane. In the case of a column with a cover plate, this can be misleading, because the mesh subdivision between the loaded plane and the cover plate also has a considerable effect on the rate of convergence.

On comparing the curves, it is noted that at l_b convergence is much slower than at l_a . This can be explained by the fact that the load-deflection curve (see Fig. 7) is approximately parabolic, with its maximum deflection at the centre.

The finite-element results in this case can be compared neither to the corresponding analytical formulae given in¹¹ (because these formulae neglect the resistance offered by the walls to bending) nor to the experimental values, due to the flexibility of the bolted flange. However, an indirect comparison with the experimental results can be made by comparing the percentage increase in stiffness at l_a , l_b and l_c due to the addition of the end-plate. This is indicated in the histogram of Fig. 8.

Column with transverse partitions in torsion

Fig. 9 shows the convergent curves obtained when the box column with horizontal partitions is loaded in torsion. When analysing the results, it was found that, as the mesh was refined, the deflection at the unloaded corners remained constant, whereas at the points of application of load it increased steadily. This is probably due to the high stress gradient at the points of load application. Since the deformation of the front panel is more important than that of the back panel, it was decided to plot in the figure the deflection at the point of application of the load rather than the average deflection of the loaded plane.

As in the case of the column with an end-plate, the finite-element results are indirectly compared with those obtained experimentally by Dreyer, by comparing the increase in stiffness caused by introducing transverse partitions (Fig. 10).

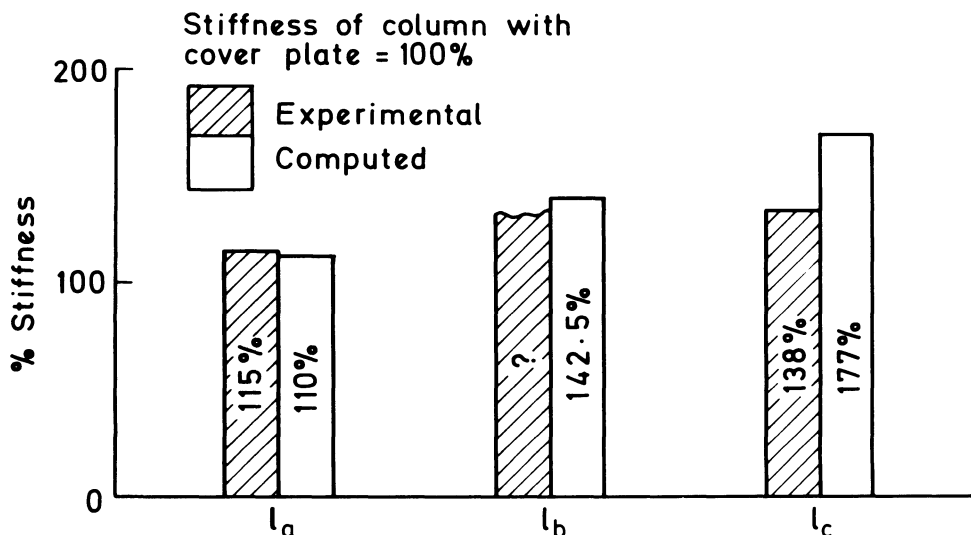


Fig. 10 Comparison of stiffness of column with cover plate and with partitions.

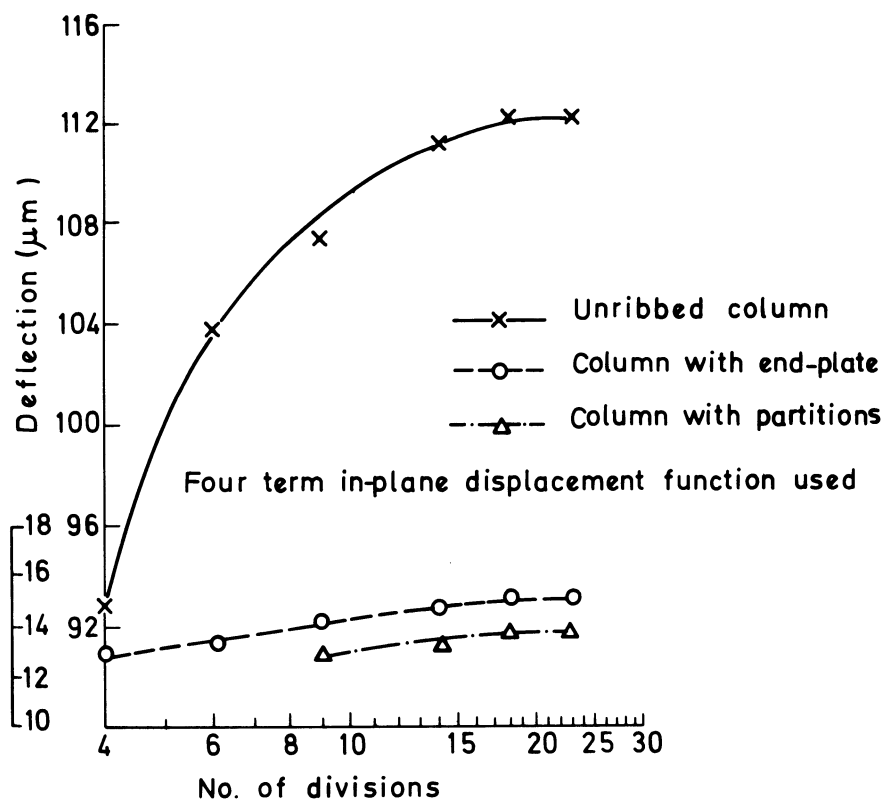


Fig. 11 (a) loaded at I_a .

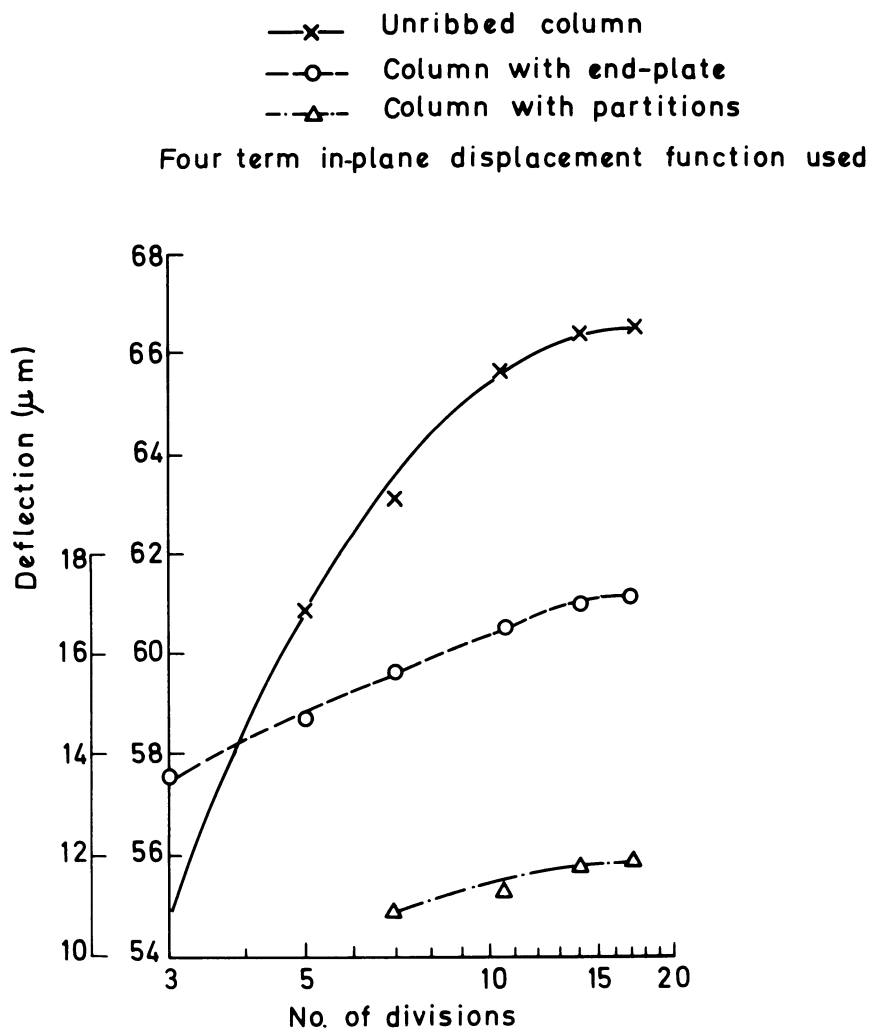


Fig. 11 (b) loaded at I_b .

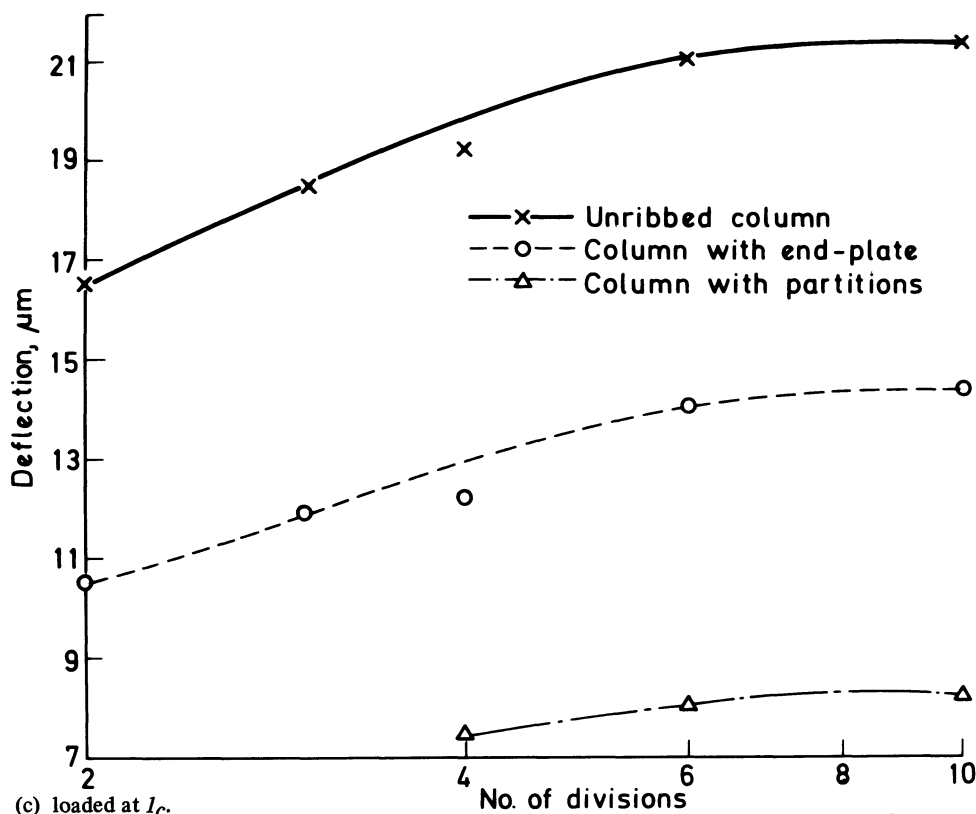


Fig. 11 Comparison of convergent curves for column loaded in torsion.

Comparison of convergent curves for unribbed columns

Figs. 11(a), (b) and (c) show the convergent curves obtained for the above-mentioned cases at I_a , I_b and I_c . Since a comparison is being made, only the results obtained from the first formulation (RECT 1) are shown. The introduction of a cover-plate makes the convergence at I_a become virtually flat, but the curve at I_c , which is farthest from the end-plate, remains virtually unaffected. With the addition of horizontal partitions, the curves I_b and I_c also become flat. It can be noted from Fig. 7 that even though the load-deflection curve in between the partitions does not vary linearly, the overall load-deflection curve can be approximated by a series of straight lines, which can be satisfied by using the four-term in-plane displacement functions.

Cross-sectional deformation

The two main components into which the total cross-sectional deformation can be split are

- (1) rotation (θ) of the cross-section due to the twisting of the column.
- (2) distortion of the cross-sectional contour, the magnitude of which is indicated by ψ . It represents the amount of distortion of the (right) angle between the walls.

Fig. 12 shows the deformation of the loaded cross-sections when the column is subjected to torsional loads. From the figure the following observations can be made.

- (1) In the case of the open box, the cross-sectional distortion (ψ) is far greater than the rotation

(θ) of the cross-section. At I_a ψ is as much as 10 times θ .

- (2) When a cover-plate is attached to the column, there is very little out-of-plane deformation, i.e. the walls remain plane. This is because the cover-plate provides the necessary transverse bending stiffness.
- (3) The introduction of an end-plate also causes the magnitude of ψ to decrease considerably. The maximum decrease occurs at I_a whereas at I_c , ψ is still greater than θ .
- (4) With transverse partitions, the greater part of the deformation is due to the rotation of the cross-section. ψ does not become zero because none of the loads (I_a , I_b , I_c) is applied in a plane containing a partition. One point to mention is that, due to the localised deformation at the junction of the front and side walls, the rotation of the front wall is greater than that of the back wall. Since the deflections at the tool point will be determined only from the deformation of the front panel, θ_1 is obtained only from the front panel. This localised deformation (the difference between the w -deflections of the loaded and unloaded corners of the cross-section, is about $4 \mu\text{m}$ corresponding to between 10% a and 50% b of the mean value of w) obviously is also present in the case of the open column, but it becomes more apparent as the overall deformation of the cross-section reduces.
- (5) The introduction of a cover-plate or transverse partitions does not alter the cross-sectional rotation θ . This constant computed value is

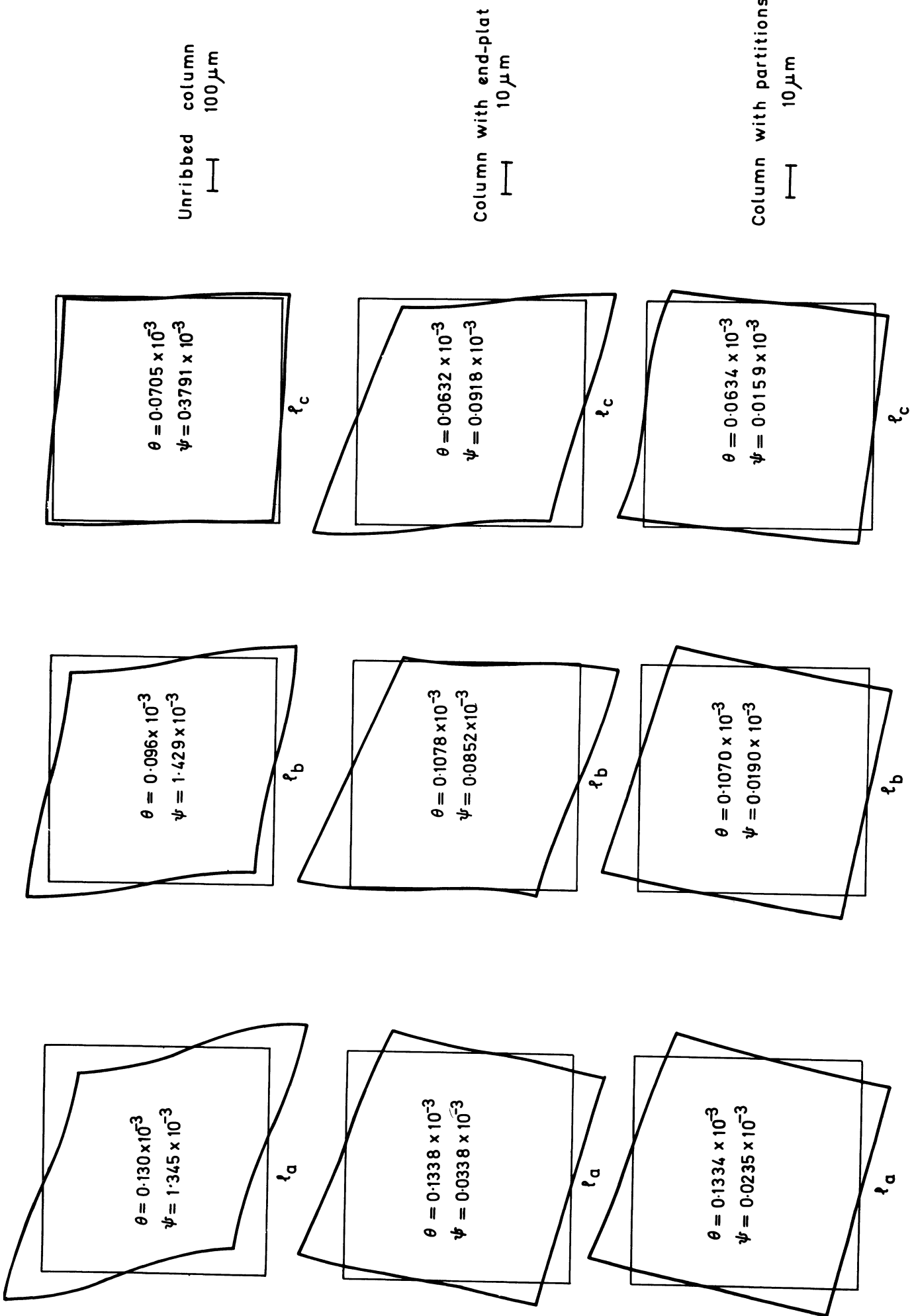
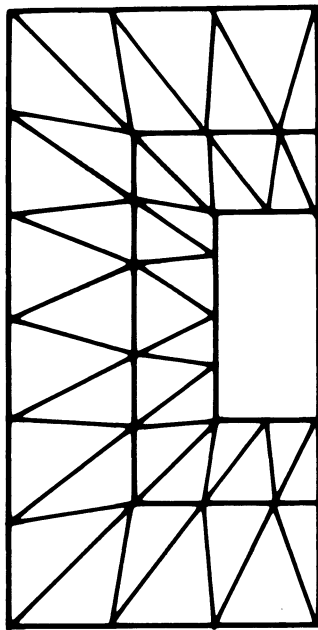
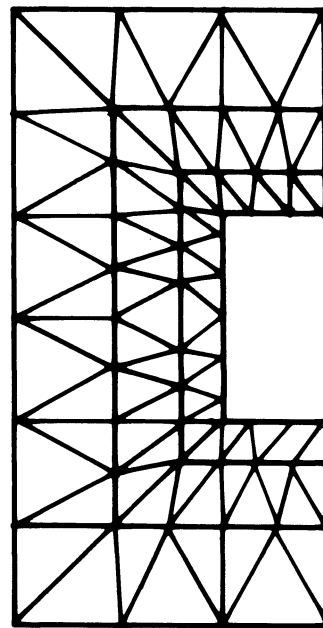


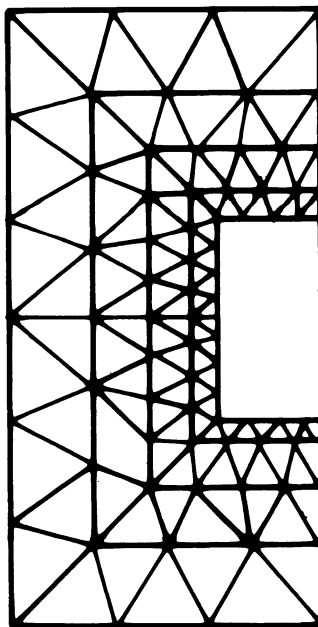
Fig. 12 Cross-sectional deformation of column in torsion.



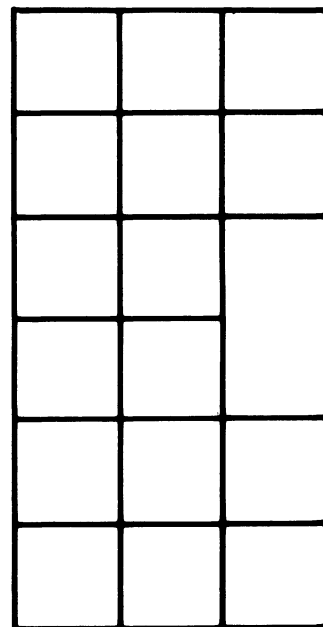
21 Nodes



46 Nodes



64 Nodes



14 Nodes

Fig. 13. Different mesh subdivisions for partition with core hole.

nearly equal to that calculated from the theory of pure torsion.

$$\theta = \frac{T(b+h)}{2G\delta b^2 h^2}$$

Column with cored transverse partitions

The transverse partitions used in practical column construction are of the cored type to facilitate manufacture and to accommodate balance weights, etc.

The effect of varying the size of the opening on the torsional stiffness of the column can be very easily studied by the finite-element method. But before this can be done, a preliminary investigation into the effect of varying the mesh subdivision in the partition on the displacements of I_a , I_b and I_c has been carried out. For this purpose the mesh employed for the main column (20 X 6) is kept constant, while the mesh in the partition whose core hole area is equal to 1/9 that of the full partition, is gradually refined. The four meshes employed for this semi-partition are shown in Fig. 13. For the purpose of comparison, the only one possible rectangular mesh has been used. Incidentally, the finest triangular mesh is roughly the maximum size of substructure that can be handled at present with the Atlas computer.

The convergent curves (Fig. 14) at I_a , I_b , I_c are seen to be very similar to each other, there being in each case a variation in computed deflection of approximately 5% with increasing refinement of the triangular mesh. A more interesting observation is that the rectangular mesh gives displacement values which are nearly equal to those obtained by the finest triangular mesh. Since the difference between the values obtained from the two fine meshes is small, it can be concluded that the curves have almost completely converged. Hence, when the size of the opening is being varied, the number of internal nodes in the mesh for the semi-partition is maintained constant at 64. This will ensure that the error in the computed deflection remains constant. The grids used for partitions having a core hole of 1/4, 9/16 and 3/4 are shown in Fig. 15. In the last case, the substantially reduced width of the partition does not

permit a graded triangular mesh around the aperture; hence a mixture of rectangles and triangles has been used. Had it been possible to use a triangular mesh, the results would not have been very different, because it was shown earlier that a coarse rectangular mesh yielded results which were nearly equal to those produced by the finest triangular mesh.

The variation in the flexibility of the column with the size of opening in the partitions is summarised by the histogram in Fig. 16. It shows that initially the percentage increase in flexibility is nearly the same at I_a , I_b and I_c , but beyond a certain value ($A/A_0 = 1/4$) the flexibility at I_a increases rapidly. From this, it can be concluded that if an opening, equal in area to 1/4 of that of the partition is provided, there is no appreciable decrease in the stiffness. On the other hand, if a shallow rib, whose depth is one-tenth the width of the column, is introduced into an open column, its stiffness is increased as much as 3 times.

Column with and without end-plate in bending

The open column has been subjected to a pair of symmetrical bending loads at I_a , I_b and I_c . The convergent curves obtained from the same meshes as previously described are shown in Fig. 17. Indicated in the figure are the experimental values from Dreyer and the values obtained from the approximate formulae given¹¹.

Comparing the computed results with each other, the first two formulations yield similar curves, whereas the third formulation, which is based on the eight-term in-plane and the twelve-term bending displacement functions, yields higher initial values.

The difference between the initial values obtained from the first or second formulation and the third formulation decreases from I_a to I_c . If the assumption is made that in this thin-walled column the membrane action plays an important role, the more rapid convergence with the third formulation can be attributed to the eight-term in-plane displacement function, which would permit the cubically-varying deflection curve to be approximated much more easily than the linear four-term function. As the loading plane is varied from I_a to I_c , the effective length of the column is reduced and with it the advantage possessed by the eight-term function over

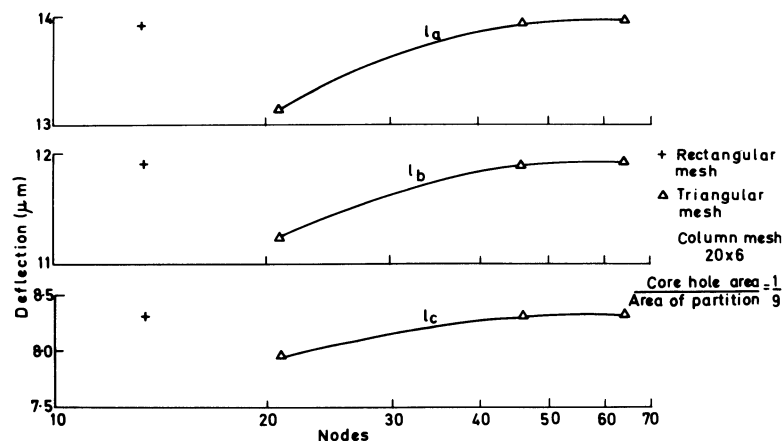


Fig. 14 Convergent curves for ribbed column with core holes loaded in torsion

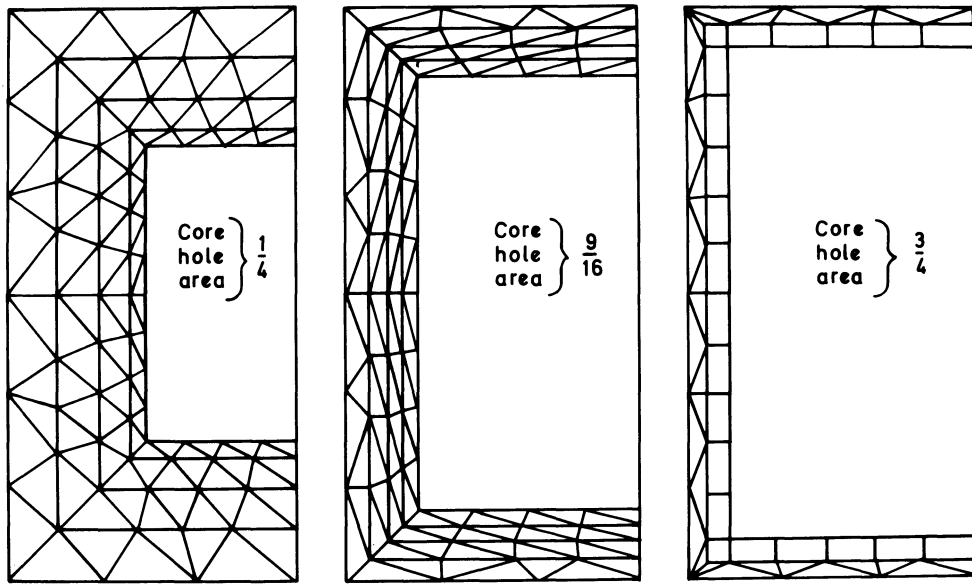


Fig. 15 Mesh subdivision of partition with varying core hole area

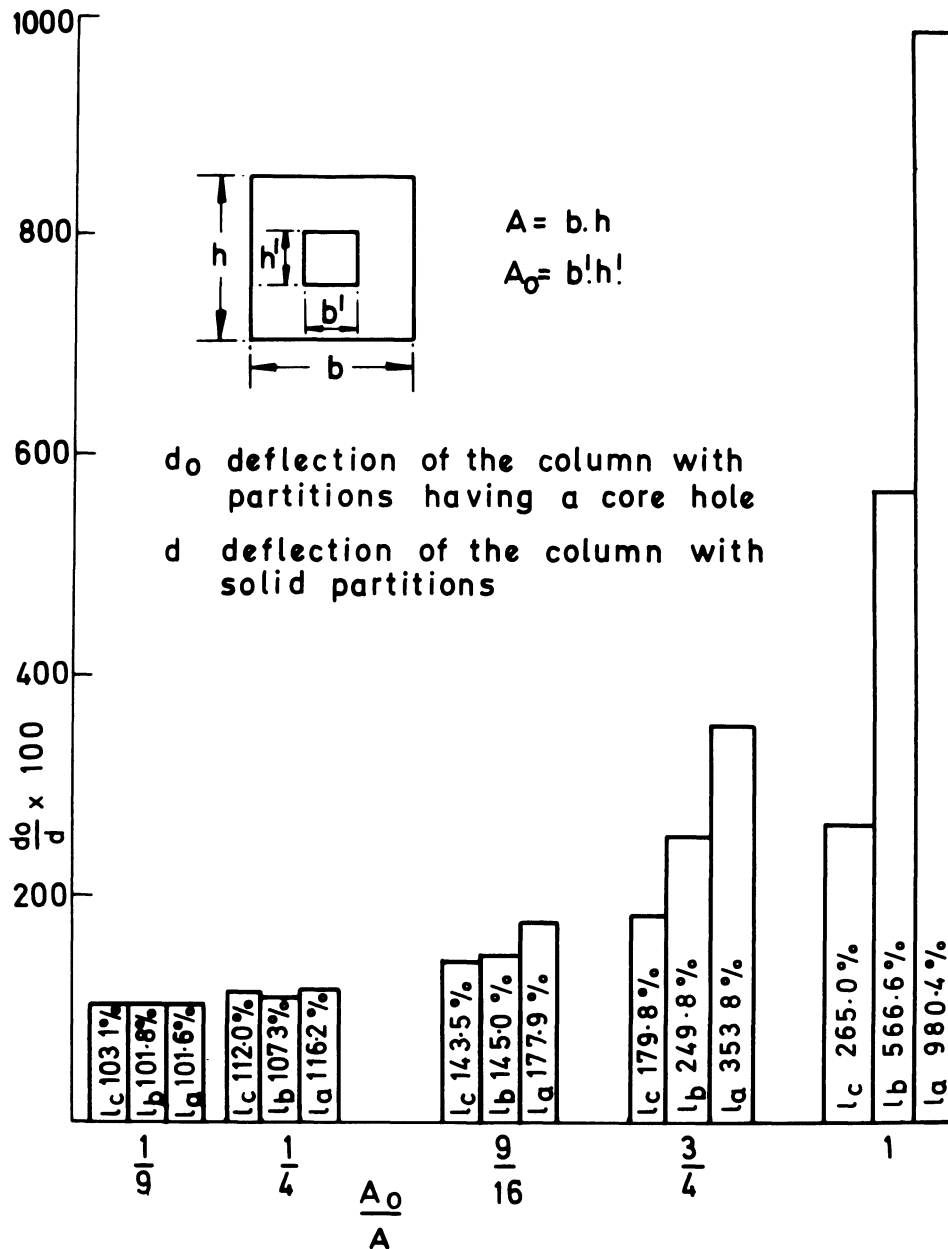


Fig. 16 Effect of varying the core hole area on the torsional stiffness of the column.

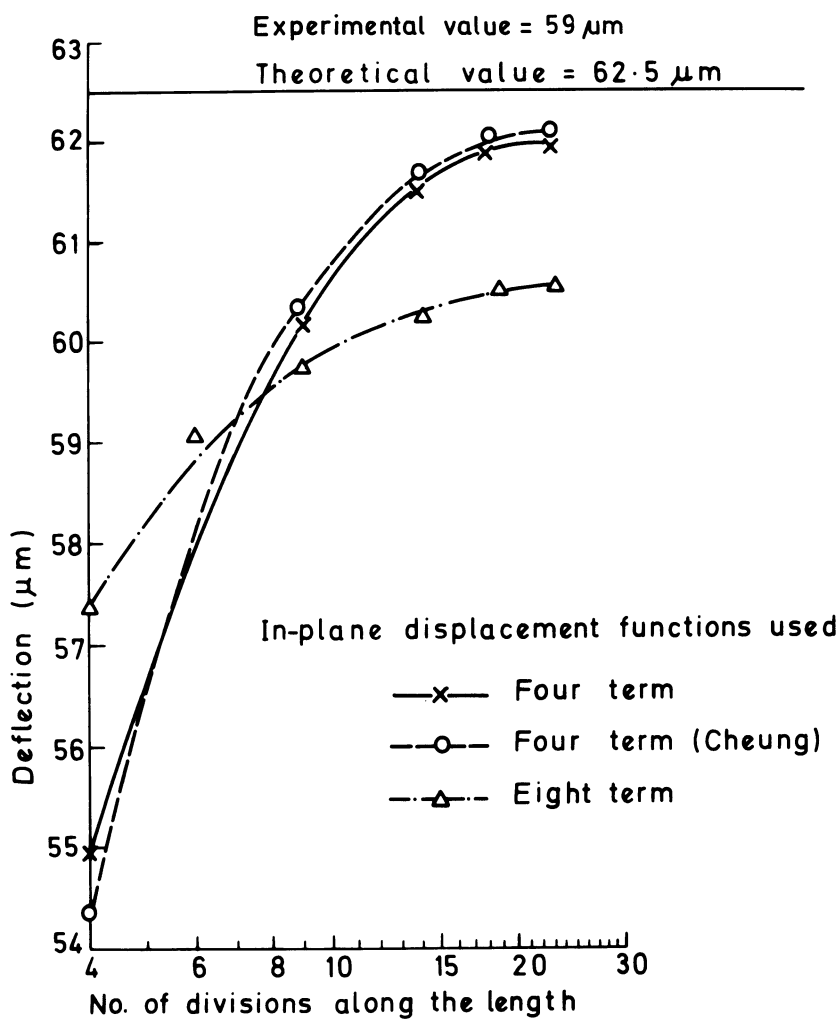


Fig. 17 (a) loaded at I_a .

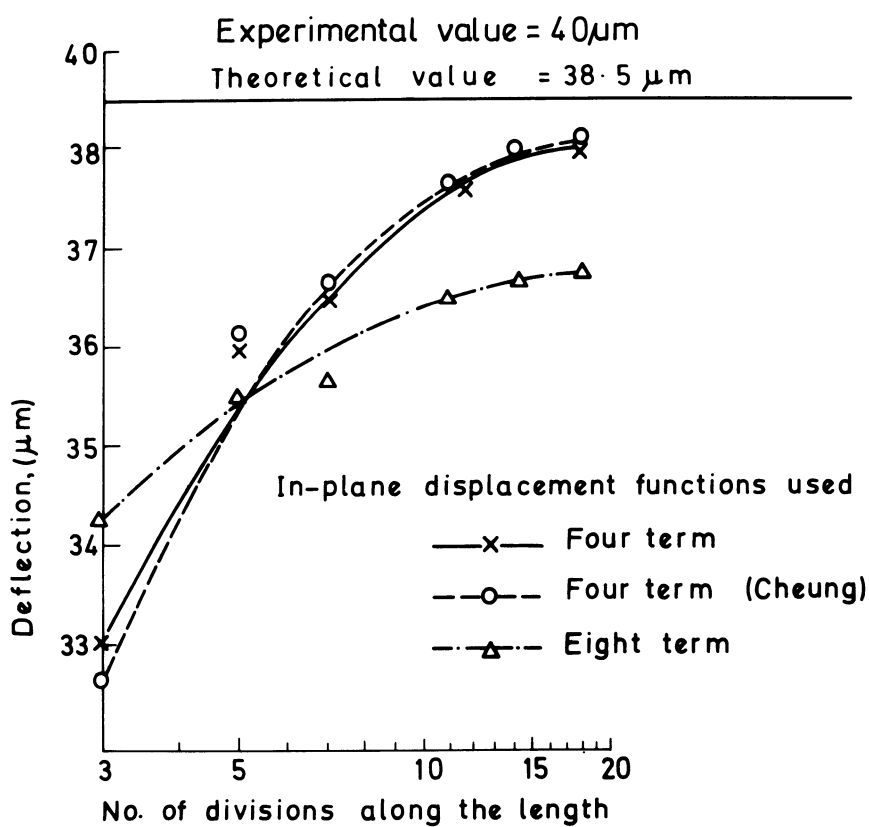


Fig. 17 (b) loaded at I_b .

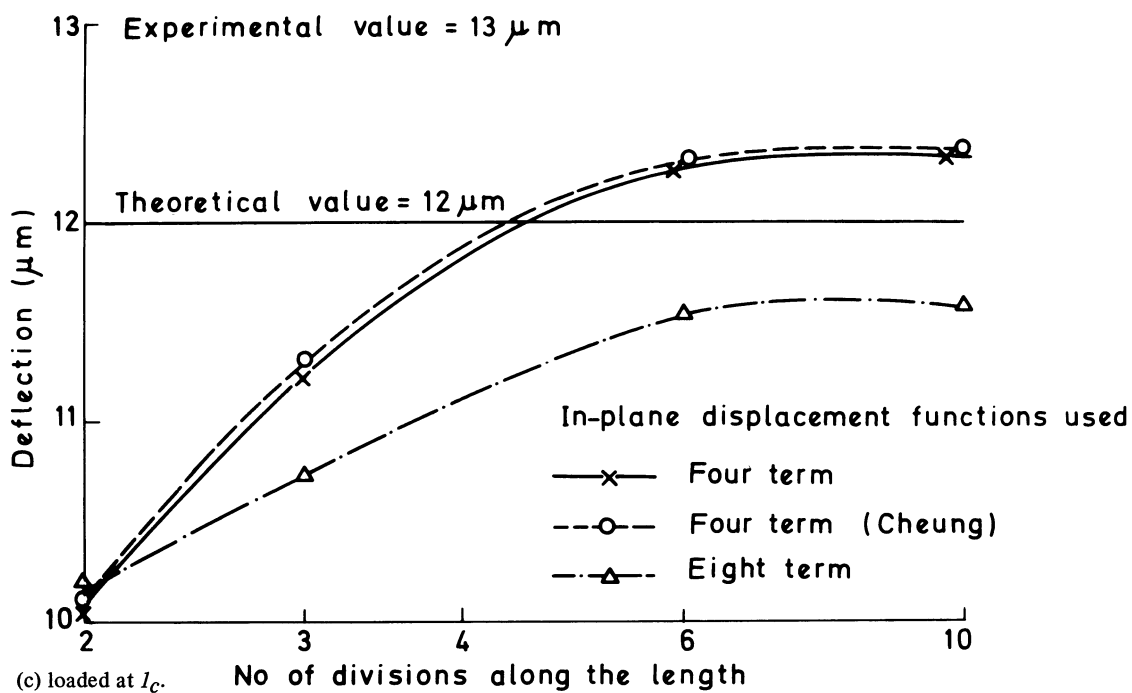


Fig. 17 Convergent curves for unribbed columns loaded in bending.

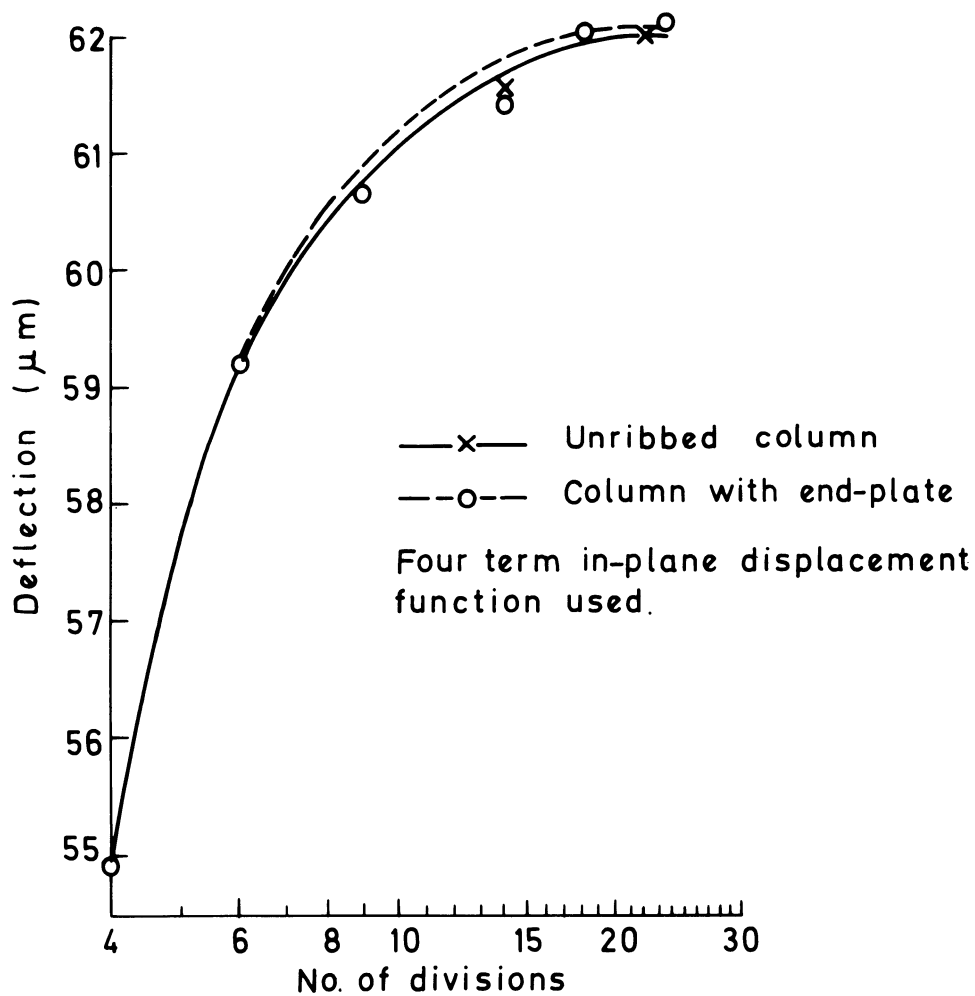


Fig. 18 Comparison of convergent curves for column loaded in bending at I_a .

the two four-term functions.

The difference between the converged values obtained from the first, second and third formulations (about $2 \mu\text{m}$) can be attributed to the constraint imposed on the shearing strain when using the third formulation as mentioned previously.

The convergent curves obtained for the column with an end-plate are shown in Fig. 18. The curves are not only similar in shape to those obtained for the open box-column, but also of the same magnitude. This confirms that the addition of an end-plate does not affect the rigidity of the column in bending. In view of this further investigations on the column, that is with transverse partitions, were not carried out.

COMPUTING COSTS

The computing cost incurred for the static analysis of a structure, excluding the cost for data preparation, can be divided into two categories:

- (a) the cost for evaluating and storing the stiffness matrices of the different elements and sub-structures:
- (b) the cost involved in assembling the individual element stiffness matrices in the final structural stiffness matrix and solving for the nodal deflections.

The cost for (a) can be minimised by subdividing the structure in such a way that it contains as many geometrically-similar elements as possible. For such similar elements only a single stiffness matrix calculation need be performed.

Therefore, having determined the total number of sets of different elements in a particular structure, the cost for (a) can be estimated with reasonable accuracy. When using the Atlas computer the cost for a rectangular element stiffness matrix evaluation is approximately 20 np. The cost for a beam element is considerably less than this whilst for the triangular plate and solid prismatic elements the cost is a little more. However, this part of the cost is usually very much smaller than that required for (b). This portion of the total cost cannot be easily predetermined since it depends upon a number of factors, the most important of which are:

(i) The nodal bandwidth which is equal to the maximum numerical difference between the numbers associated with any two adjacent nodes. It should be mentioned here that every node in the complete structure must be labelled with a different numerical value (starting with zero for a fixed node), for the purpose of identifying a particular storage area in the computer with the particular nodal deflection.

The total computer storage requirement and/or the number of transfers between working store and backing store is directly related to the nodal bandwidth. Therefore, the structural nodes should be numbered in such a way as to produce a minimum nodal bandwidth.

(ii) The number of equations to be solved. This is equal to the product of the number of structural nodes and the number of degrees of freedom

associated with each node. For the analysis of three dimensional structures it will generally be equal to six times the number of nodes.

(iii) The number of different loading cases of interest. In this case the cost is simply proportional to the number of loading cases.

As an indication of the cost of the type of analysis described here, consider the case of the unribbed column with a mesh sub-division of 20×6 . The time required to compute the eight different stiffness matrices for the rectangular elements was approximately 6 s on the Atlas computer, which corresponds to a computing cost of about £1.60. On the other hand the time required for (b) was 2.2 min, corresponding to a cost of £27.40. The structure contained 260 nodes each having six degrees of freedom, which involves the solution of 1 560 simultaneous equations, and the nodal bandwidth was 14. Table 2 gives a general breakdown of the costs of the various analyses.

TABLE 2 Computing costs

Mesh	Unribbed column (£)	Column with end-plate (£)	Column with partitions (£)
5×1	3.75	4.0	—
7×2	7.20	8.25	—
10×3	19.20	25.65	28.10
15×4	12.40	14.55	18.15
20×6	29.0	32.20	37.65
25×6	36.75	39.60	44.35

It should be appreciated that the above costs are applicable only to the Manchester Atlas computer used. The costs involved in other computers could (and probably would) be substantially different. It is likely, however, that the costs quoted are minimum values since the programmes used have been written with careful consideration of the particular features of the Atlas computer and the associated system of costing.

CONCLUSIONS

The finite-element technique is without doubt a valuable aid to the analysis and synthesis of machine tool structures and structural elements. Clearly it is technically superior to the alternative techniques of physical model analysis and vastly more versatile than the simpler beam-like element techniques. The major limitation to its everyday use is the potential computing costs, which may be excessive. To contain the cost of such analysis special skill is required in prescribing a suitable finite-element model. The required skill can only be achieved by familiarity with the application of the programmes to the particular type of structure under consideration. It is therefore unlikely that the technique will, in the immediate future, be exploited directly by the machine tool designer. However, with suitable collaboration between designer and specialist the method appears to have substantial potential.

For the type of column structure considered in the paper it is evident that both the membrane and flexural stiffnesses of the column walls should be

taken into consideration. For the evaluation of the membrane stiffness either the simple linear four-term displacement function or the four-term Chueng function can be recommended. The more complex eight-term displacement function does not exhibit any significant improvement in accuracy as was initially expected. Indeed there is a danger that with a fine mesh model this formulation can lead to an incorrect result. Although the structures analysed here are of rather simple configuration the techniques are equally suitable for more realistic machine tool columns, for which one might reasonably expect a similar degree of accuracy in the computed results.

REFERENCES

1. TAYLOR, S. and TOBIAS, S. A., 'Lumped constants method for the prediction of the vibration characteristics of machine tool structures', *Proc. 5th M.T.D.R. Conf.*, Pergamon, 1964.
2. COWLEY, A. and FAWCETT, M. A., 'Analysis of machine tool structures by computing techniques', *Proc. 8th M.T.D.R. Conf.*, Pergamon, 1967.
3. COWLEY, A. and HINDUJA, S., 'The finite-element method for machine tool structural analysis', *Annals of the C.I.R.P.*, Vol. 18, 1970.
4. TURNER, M. J., CLOUGH, R. W., MARTIN, H. C. and TOPP, L. J., 'Stiffness and deflection analysis of complex structures', *J. Aero Space Sci.*, 23, (1956).
5. ZIENKIEWICZ, O. C., 'The finite-element method in structural and continuous mechanics', McGraw Hill, 1967.
6. ARGYRIS, J. H., 'Continua and discontinua', *Proc. Conf. Matrix Methods of Structural Analysis*, Wright Patterson Air Force Base, Ohio (1965).
7. CHEUNG, Y. K., 'Finite-element methods', Ph.D. Thesis, University of Wales, Swansea (1964).
8. CLOUGH, R. W. and TOCHER, J. L., 'Finite-element stiffness matrices for analysis of plates in bending', *Proc. Conf. Matrix Methods of Structural Analysis*, Wright Patterson Air Force Base, Ohio (1965).
9. ZIENKIEWICZ, O. C. and CHEUNG, Y. K., 'The finite-element method for analysis of elastic isotropic and orthotropic slabs', *Proc. Inst. Civ. Engrs.*, 28, (1964).
10. DREYER, W. F., 'Über die steifigkeit von werkzeugmaschinenstaendern und vergleichende untersuchungen an modellen', Dissertation, T. H. Aachen, (1966).
11. KAMINSKAYA, V. V., LEVINA, Z. M. and RESHETOV, D. N., 'Bodies and body components of metal cutting'.

APPENDIX

FORMULAE FOR TORSIONAL DEFLECTIONS

The deflection at any point in a thin-walled column clamped at its base and loaded in torsion can be expressed by two orthogonal components w and v (see Fig. 3 for coordinate system). These components can be calculated from the following formulae¹¹.

$$v = \frac{-P}{E\delta} \cdot \frac{\epsilon t^2}{2} \left\{ \frac{\Delta c}{\Delta} \cdot \epsilon \cdot t \frac{x^2}{L^2} - \frac{2.5}{t^2} \cdot \frac{x}{L} + \frac{\Delta d}{\Delta} \epsilon^2 t^2 \frac{x^3}{L^3} - 0.625 \frac{x}{L} (2+t) \right\} \quad (1)$$

$$w = \frac{P}{E\delta} \cdot \frac{\epsilon t}{2} \left\{ \frac{\Delta c}{\Delta} \cdot \epsilon \cdot t \frac{x^2}{L^2} + \frac{2.5 x}{L t} + \frac{\Delta d}{\Delta} \epsilon^2 t^2 \frac{x^3}{L^3} - 0.625 \frac{x}{L} (1+t+t^2) \right\} \quad (2)$$

$$\text{where } \Delta = 4A_1A_2 - A_3^2, \Delta d = 2A_2A_5 - A_3A_4, \\ \Delta c = 2A_1A_4 - A_3A_5$$

$$A_1 = \frac{(1+t)\epsilon t^3}{48} \left\{ 12 \epsilon^2 t^2 + 1.875 (1-t)^2 + 1.5 (1+4t+t^2) + \frac{48 \epsilon^2 t^2}{(1+t)^2} \cdot \frac{\delta^2}{h^2} (0.57 \epsilon^4 t^4 + 0.52 (1+t) \times (2+t^2) + 0.13 (1-t)^2 - 0.5 \epsilon^2 t^2 (3+2t+t^2)) \right\}$$

$$A_2 = (1+t) \frac{\epsilon t^3}{12} \left\{ 1 + \frac{48 \epsilon^2 t^2}{(1+t)^2} \cdot \frac{\delta^2}{h^2} \cdot \frac{\epsilon^2 t^2}{5} \right\}$$

$$A_3 = \frac{(1+t)\epsilon t^3}{12} \left\{ 3 \cdot \epsilon \cdot t + \frac{48 \epsilon^2 t^2}{(1+t)^2} \cdot \frac{\delta^2}{h^2} \cdot \frac{\epsilon^3 t^3}{3} - 0.156 \epsilon \cdot t (3+2t+t^2) \right\}$$

$$A_4 = \epsilon^2 t^2 \left\{ \frac{x_p^2}{L^2} + 2.5 \frac{(1-t)}{(1+t)} \frac{\delta^2}{h^2} \epsilon^2 \cdot t^2 \right\}$$

$$A_5 = \epsilon t \left\{ \epsilon^2 t^2 \cdot \frac{x_p^3}{L^3} - 0.625 \frac{x_p}{L} (1+t+t^2) - 0.3125 (1-t^2) - \frac{(1-t)}{(1+t)} \epsilon^2 t^2 \frac{\delta^2}{h^2} 1.041 (3+2t+t^2) - 2 \epsilon^2 t^2 \right\}$$

If only the membrane stiffness of the walls is considered then the displacements w and v at the cross-section where the load is applied are given by

$$w = \frac{P\epsilon}{2E\delta t^2} \left\{ 4 \epsilon^2 (1+t)^2 + 3t^2 + 2t + 0.5 \right\} \quad (3)$$

$$v = -\frac{P\epsilon}{2E\delta t} \left\{ 4 \epsilon^2 (1+t)^2 + 0.5 (t^2 - t + 1) \right\} \quad (4)$$

DISCUSSION

Query from S. Taylor, University of Birmingham.

Better accuracy is obtained by finite elements if the load and displacement are at different points. This is because it avoids the effects of local loads which are less accurately represented. Consequently, a smaller number of elements will suffice in this case. With a very small number of large elements, the effect could be appreciable.

Reply

This is generally true and is borne out by the results shown in Table 3 below. It can be observed from these results that, as the mesh is refined, the deflection at the unloaded corner remains constant, whereas that at the loaded corner steadily increases. The difference between the deflections at the unloaded and the

loaded corners is due to the localised deformation occurring at the junction of the side walls and the front walls. In practice, however, the localised deformation may form an insignificant component of the total deformation because the load, which is transmitted to the column via the slideways, is spread over a sufficiently large area.

TABLE 3

Mesh	I_a		I_b	
	Loaded corner (μm)	Unloaded corner (μm)	Loaded corner (μm)	Unloaded corner (μm)
10 × 3	12.77	9.426	7.357	4.125
15 × 4	13.24	9.448	7.592	4.216
20 × 6	13.75	9.464	8.078	4.218
24 × 6	13.91	9.464	8.283	4.219

METAL CUTTING

TOOL-LIFE EQUATIONS AND MACHINING ECONOMICS

by

G. BARROW*

SUMMARY

Since F. W. Taylor first expressed the life of cutting tools in a mathematical form, several workers have proposed alternative equations. The important equations used in the past are reviewed and their validity discussed. The effects of tool-life criteria and machining conditions are considered, and the feasibility of incorporating the various equations into economic machining analyses are discussed.

INTRODUCTION

The need for accurate assessment of tool life has increased considerably in recent years with the development of numerically controlled machine tools and optimization procedures. The general trend has been the development of equations relating tool life to the machining variables involved. Although there are considerable advantages in using these equations for the prediction of tool life, there are cases in which discrete values of tool life are adequate, particularly for application in industry. When evaluating economic cutting conditions there are obvious advantages in using tool-life equations rather than discrete values.

When considering the validity of tool-life equations it should be remembered that they are all empirical in nature. In view of this it is impossible to make any firm decision that a particular equation is valid for all cutting conditions. Several of the equations discussed are applicable to a wide range of machining operations; in many cases, however, they have only been applied to turning operations. In view of this the following discussions are based on the turning operation only.

TOOL-LIFE CRITERIA

Before considering the form of tool-life equations it is essential that the end of the life of a cutting tool is specified. In view of the wide range of material combinations and cutting conditions encountered in practice, this is not an easy task.

In general, a tool may reach the end of its useful life by any of the following modes:

- (1) clearance or flank face wear,
- (2) rake face or crater wear,

- (3) plastic deformation of the cutting edge,
- (4) thermal cracking and mechanical chipping of the cutting edge.

Tool failure in the case of (3) and (4) is generally catastrophic in nature and should be avoided. It is, therefore, normal to consider tool life in terms of flank or crater wear (Fig. 1). It should be noted that in many cases, thermal deformation of a mild form does not lead to immediate tool failure, but accelerates the rate of flank wear.

Because catastrophic tool failures should be avoided, it is essential that certain limits on wear should be stipulated. The following values are recommended.

Carbide and ceramic tools

Flank wear as depicted in Fig. 1:

$$VB = 0.015 \text{ in}$$

$$VN = 0.030 \text{ in}$$

$$VB_{\max} = 0.030 \text{ in}$$

When applying these criteria it is suggested that the end of tool life be defined as when the wear reaches one of the limiting values stated.

Crater wear:

$$KT = 0.004 + 0.3 s \text{ in}$$

where s = feed in mm/rev.

High speed steel tools

$$VB_{\max} = 0.060, \text{ or complete failure.}$$

Complete failure of high-speed steel is particularly recommended for cases in which material build-up on the tool makes measurement very difficult. Although the failure of tools by crater wear does occur, experi-

*Division of Machine Tool Engineering, Department of Mechanical Engineering, UMIST.

ence has shown that, provided the correct tool material is used, failure by flank wear is usual. In view of this, tool-life equations are usually developed using a flank-wear criterion.

The quoted values of flank wear for carbide tools are by no means arbitrary. A judicious choice has to be made between values which are too high (high forces and increased chance of premature failure) and values too low (short tool lives). An indication of the problems involved can be obtained by considering Fig. 2 which shows schematically the relationship between flank wear and time. Three stages are identifiable:

- (a) an initial rapid wear rate,
- (b) an approximate constant wear rate,
- (c) another zone of rapid wear which leads to eventual failure.

It is clear from Fig. 2 that there are considerable advantages in utilizing the linear portion of the curve as much as possible. The value of flank wear reached before the second (linear) stage is reached varies considerably for different tool and workpiece combinations. There is, however, a general trend depending on the type of carbide, as shown in Fig. 2. The curves in Fig. 2 are very approximate, as the properties of the carbide within each I.S.O. group considerably affect the wearing mechanism. In some cases, VB may be as much as 0.013 in before the linear portion of the curve is reached (the shape of the linear portion approaches zero in some cases). The mean level of flank wear (VB) should, therefore, be greater than this value.

Carbide tools will often cut satisfactorily with flank wear values in excess of those which are suggested. There is, therefore, some 'safety margin' which is an

advantage when considering the intrinsic scatter in tool-life results.

Although the above values for flank wear are those generally recommended, there are cases in which lower values have to be considered in view of the following factors:

- (a) influence of tool wear on surface finish and dimensional tolerance,
- (b) with certain tool and workpiece combinations (and cutting conditions) fracture of the tool edge at certain values of flank wear,
- (c) there is also evidence¹ that with some high-strength materials, metallurgical damage of the machined surface occurs at high flank-wear values.

The choice of tool-life criterion has a considerable influence on the form of tool-life equation, as shown in Fig. 3. It is, therefore, difficult to compare tool-life data if different criteria are used to define the end of tool life.

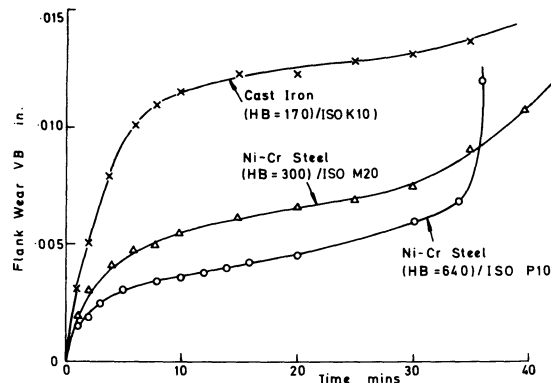


Fig. 2 Specimen flank wear-time characteristics.

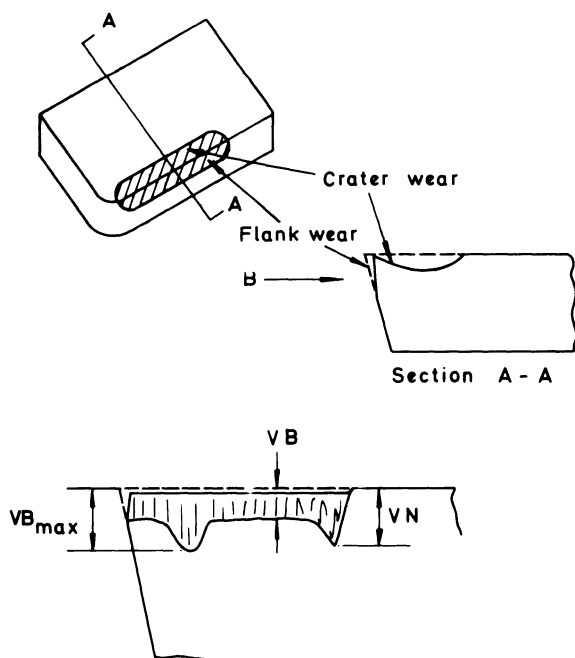


Fig. 1 General configuration of tool wear.

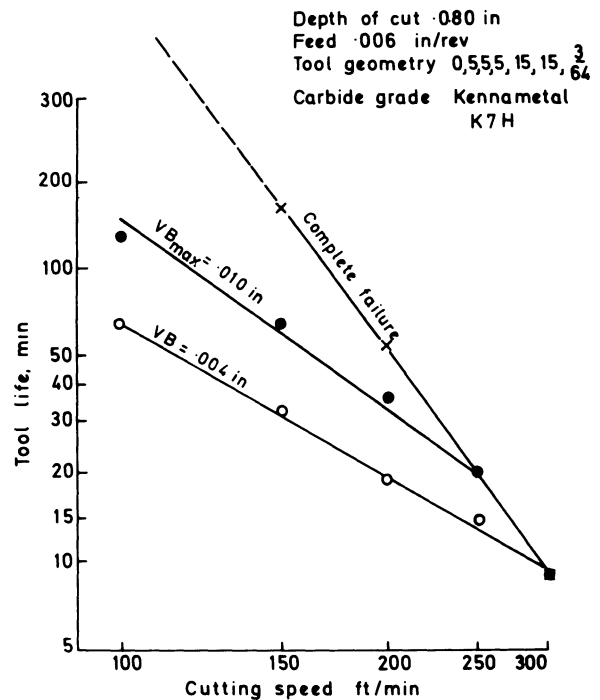


Fig. 3 Comparison of tool-life criteria for RS141 steel (U.T.S. 115 ton f/2 HB 470).

TOOL-LIFE EQUATIONS

Taylor-type equations

The best known tool-life equation is that of Taylor³

$$VT^\alpha = C \quad (1)$$

where V is the cutting speed, T the tool life, α the slope of the $\log T$ - $\log V$ plot and C the so-called Taylor constant; that is the cutting speed for a 1 min tool life.

This formula indicates a linear relationship between $\log T$ and $\log V$ (that is, α is a constant). Experience has shown that in general a curve results from a $\log T$ - $\log V$ plot and that constant α is a special case which occurs in certain conditions. Fig. 4 shows linear Taylor plots obtained at UMIST, and Figs. 5-8 show non-linear Taylor plots obtained by other workers. In Fig. 6 the curves have been plotted in accordance with the concept of equivalent chip thickness, which will be discussed in detail at a later stage. It is, however, sufficient at this stage to consider it as an equivalent feed.

Figs 4-8 and general experience of tool-life testing suggests that non-linear Taylor plots are most likely to occur in the following conditions:

- when machining high-strength, thermal-resistant materials with all types of tool materials,
- when machining in conditions which give very long tool lives,
- at high rates of metal removal,
- in finish turning conditions as indicated by Kronenberg⁷.

There are many cases in which these general rules are contradicted. But, until the mechanism of tool wear is more fully understood, it is impossible to define clearly the conditions in which a Taylor equation with constant α applies. These general rules do, however, indicate the conditions in which extreme care in determining tool life is advisable and indicate the dangers of extrapolating tool-life curves.

The Taylor equation seems to be reasonably valid when machining carbon and low alloy steels with all types of tool material in semi-roughing conditions (depth of cut 0.050-0.150 in and feeds of less than 0.020 in) when cutting with speeds to give a tool life of between 10 and 50 min. Fortunately, when using carbide throwaway tools, one is chiefly interested in tool lives of 10-50 min, because it is in this region that optimum economic conditions are approached. An exception to this is in the case of transfer lines, where it is usual to change tools at half or full shift intervals (that is, tool lives of 240 min and more). This is usually the region of maximum curvature and extrapolation of a Taylor curve into this region can give considerable errors.

Kronenberg⁸ has suggested a method of 'straightening' a curved $\log T$ - $\log V$ plot. This is achieved by adding or subtracting a constant straightening factor, K_s , to or from all values of speed and tool life, and re-plotting the results in the form

$$(V \pm K_s)T^{\alpha_1} = (C \pm K_s) \quad (2)$$

The curvature of the original data determines whether the straightening factor is added or subtracted, as indicated in Fig. 9. Kronenberg used trial and error methods to determine K_s and checked his guess by the equation

$$\alpha_1 = \frac{\log [V_2 + (K_s/V_1) + K_s]}{\log (T_1/T_2)} \quad (3)$$

Yellowley and Barrow⁹ have shown that equation (2) implies that

$$\alpha = \alpha_1 \pm \frac{K_s \alpha_1}{V} \quad (4)$$

Therefore, if the amount of non-linearity is small, K_s and α_1 can be obtained by plotting $1/V$ against α .

Equation (1) only relates cutting speed to tool life for a particular tool-workpiece combination, and does not consider other cutting variables and tool geometry. To connect tool life with several variables, Taylor derived the equation

$$VT = C_1 [1 - 8/7 (32r_e)^2] / \left\{ S^{2/5} + 5 + (2 \cdot 12/32r_e) (48a/32r_e)^{2/15} + 0 \cdot 16 (32r_e)^{1/2} + 0 \cdot 8 (32r_e) / [6 (32r_e) + 48a] \right\} \quad (5)$$

where V_T is the cutting speed for tool life T , S is the feed, a is the depth of cut, r_e is the tool nose radius, and C_1 is a constant.

Although this equation includes the important variables, feed and depth of cut, it is too complex and limited to be of any practical use. Taylor considered that feed and depth of cut could not be combined into a single variable. But, Kronenberg⁷ used the data obtained by Taylor and found that in most cases the area of cut ($S \cdot a$) could be used as a single variable. By plotting data in the form of $\log V_T$ - $\log A$, he developed the relationship

$$V_T = \frac{C_2}{(1000 A)^z} \quad (6)$$

Where C_2 is a constant, that is the cutting speed for an area of cut of 0.001 in², A is the area of cut and z the slope of the $\log V_T$ - $\log A$ plot.

Combined with Taylor's relationship $V_T \alpha = C$, equation (6) becomes

$$VT^\alpha = \frac{60^\alpha C_2}{(1000 A)^z} \quad (7)$$

A shape effect was introduced by considering the slenderness ratio $G = a/S$, so that

$$VT^\alpha = \frac{C_2 (G/5)^u 60^\alpha}{(1000 A)^z} \quad (8)$$

where u is a constant and the term $G/5$ relates G to an average value of G which Kronenberg considered to be 5.

Although equation (8) considers both feed and depth of cut, the nose radius is not taken into account. Thus, the equation omits a relatively impor-

tant variable and is felt to be inferior to equations using the concept of chip equivalent which are discussed later.

Although Taylor connected tool life with cutting speed, feed and depth of cut in separate equations he never attempted to combine them together. This is now done regularly and is known as the 'Extended Taylor Equation',

$$T = \frac{C_3}{V^{1/\alpha} S^{1/\beta} a^{1/\gamma}} \quad (9)$$

C_3 , α , β and γ being constant.

This equation is used extensively but it still omits tool geometry and assumes that the exponents α , β and γ , are constant. As in the simple Taylor equation, this is not generally so and large errors can occur. The general trend of tool life with the cutting speed, feed and depth of cut is shown schematically in Fig. 10. The amount of curvature in a particular case depends on the tool and workpiece combination and the cutting conditions.

Provided α , β and γ are reasonably constant, equation (9) is quite useful, but the evaluation of α , β , γ and C_3 is, however, quite laborious as at least three sets of tests involving fifteen tool-life values are required.

Equations based on the chip-equivalent concept

In the 1930s Woxen^{10,11} suggested that tool life could be related to cutting temperature, by evaluating a heat balance in steady-state cutting conditions. He showed that cutting temperature was a direct function of the chip equivalent, q , for a given cutting speed and tool-workpiece combination. The chip equivalent q is defined as the ratio between the length of the tool edge contacting the work (L) and the area of cut (A) as shown in Fig. 11,

$$q = L/A \text{ in}^{-1}$$

In some cases the inverse of the chip equivalent is used and is called the equivalent-chip thickness, h_e . The proposal by Woxen that temperature is a function of chip equivalent has been substantiated by several workers using tool-work thermocouple techniques.

Woxen assumed that the conditions resulting in constant temperature also resulted in a constant tool life. Using this assumption he was able to predict the shape of a $V_T - \theta$ plot, as shown in Fig. 12. The form of the plot was very similar to a $V_T - q$ plot, as indicated in Fig. 13. Using the form of Fig. 13, Woxen proposed the tool-life equation

$$V_T = G_T (q_0 + q) \quad (10)$$

He found that in general, $V_T - q$ plots were not linear and introduced the factor $(1/1+gq)$ to account for this fact and amended his equation to

$$V_T = G_T \left(\frac{q_0 + q}{1 + gq} \right) \quad (11)$$

where g is a constant.

Tool life T was introduced as a separate factor by

adding the term $(T_x/T)^\alpha$ and assuming that the Taylor equation was generally valid.

$$\therefore V = \left(\frac{T_x}{T} \right)^\alpha G_s \left(\frac{q_0 + q}{1 + gq} \right) \quad (12)$$

where T_x is a certain tool life, say 30 min, and G_s is a constant, dependent on the work and tool materials and is related to T_x .

Woxen recognized that the Taylor exponent, α , could vary and added a further term to overcome this difficulty, thus

$$V = \left[\left(\frac{T_x}{T} \right)^\alpha + g_1 T \right] G_s \left(\frac{q_0 + q}{1 + gq} \right) \quad (13)$$

where g_1 is a constant.

Although the equations developed by Woxen seem to be valid for a wide range of cutting conditions, they are rather complex and difficult to use. The complexity of the equations is chiefly because of non-linearities in the original $V_T - q$ plot, which was made in a linear manner. If $\log V_T$ is plotted against $\log q$, the resulting terms are often linear (or nearly so), thus tool life can be expressed as

$$VT = Jq^j \quad (14)$$

where J and j are constants.

Equation (14) can be expanded to include tool life as a separate term, resulting in

$$VT^\alpha = C_4 q^j \quad \text{or} \quad VT^\alpha q^\delta = C_4 \quad (15)$$

Colding¹² and Brewer and Rueda¹³ used relationships of the form of equation (15) and showed that the exponents α and δ are not necessarily constant. Extensive tool-life testing at UMIST has shown, however, that although curved plots do occur when using the chip equivalent rather than the individual variables, the amount of curvature is considerably reduced.

Using dimensional analysis, Colding proposed an equation of the form

$$K + aX + cY - Z + hXZ = 0 \quad (16)$$

or in a more general form

$$K + aX + bY^2 + cY + dY^2 + eZ^2 - Z + fXY + gYZ + hXZ = 0 \quad (17)$$

where $X = \log q$, $Y = \log V$, and $Z = \log T$, and a , b , c , d , e , f , g and h are constants.

The validity of equation (17) is shown in Fig. 14 for the turning of 0.45% carbon steel. Equations (16) and (17) are valid over a wide range of cutting conditions and can cope with tool-life curves with considerable curvature, but the evaluation of the constants to a reasonable degree of accuracy involves at least twelve tool-life points and the use of digital computation techniques.

Konig–Depiereux equation

Konig and Depiereux⁶ developed an equation which can accommodate non-linearities in the $\log T$ – $\log V$ and $\log T$ – $\log S$ plots. Typical curves of this type are shown in Fig. 7. The considerable variations in slope of the curves are shown in Fig. 8.

The slope of the $\log T$ – $\log V$ curve can be expressed as

$$K = K_V V^m \quad \text{or} \quad -K = \left(\frac{\partial \log T}{\partial \log V} \right)_S$$

and of the $\log T$ – $\log S$ curve

$$i = i_S S^n \quad \text{or} \quad -i = \left(\frac{\partial \log T}{\partial \log S} \right)_V$$

$$\therefore -K = \left(\frac{\partial \log T}{\partial T} \frac{\partial T}{\partial V} \frac{\partial V}{\partial \log V} \right)_S$$

which gives

$$\left(\frac{\partial T}{\partial V} \right)_S = -T K_V V^{m-1}$$

and

$$\left(\frac{\partial T}{\partial S} \right)_V = -T i_S S^{n-1}$$

$$\text{Now } dT = \frac{\partial T}{\partial V} dV + \frac{\partial T}{\partial S} dS$$

which leads to

$$\int \frac{dT}{T} = \int -K_V V^{m-1} dV + \int -i_S S^{n-1} dS$$

$$\therefore T = \exp \left(\frac{-K_V}{m} V^m - \frac{i_S}{n} S^n + C \right) \quad (18)$$

If the slope of the $\log T$ – $\log V$ curve is constant the equation is modified to

$$T = \exp \left(\frac{-i_S}{n} S^n + C \right) V^{-K} \quad (19)$$

Konig and Depiereux developed computational techniques to evaluate the various constants and predict the tool-life curves from only five wear tests. Fig. 7 shows how the predicted curves are consistent with the experimental points.

Discussion

The general validity and accuracy of the various tool-life equations have already been mentioned. It is, however, pertinent at this stage to consider all the equations together and to attempt certain recommendations. It has already been mentioned that the various tool-life equations are empirical. In view of this, when discussing the general validity of the

equations one has to rely very much on experience.

The criteria for acceptable equations are as follows:

- (a) produce a good 'fit' to experimental points,
- (b) cater for a wide range of cutting parameters, speed, feed, depth of cut, and so on.

In order to satisfy the second criterion the equations of interest are.

- (1) extended Taylor equation,
- (2) Kronenberg's equation,
- (3) all equations using the chip-equivalent concept,
- (4) Konig–Depiereux equation.

Of these four, the equations using the chip-equivalent concept are particularly useful because, as well as the machine variables (speed, feed and depth of cut) they also include the tool approach angle and nose radius. The Konig–Depiereux equation does not cater for depth of cut in its present form, but does take non-linearities into account.

If one considers the intrinsic scatter in tool-life results (even with closely controlled tool and workpiece materials), it is doubtful whether the more sophisticated tool-life equations (catering for non-linearities) are really necessary or indeed applicable at present, except, of course, in cutting conditions in which extreme non-linearities are expected, as previously mentioned. In other words, when evaluating the constants in equations (9) and (15), a reasonable amount of non-linearity can be accommodated when applying the necessary 'safety factor'. Although it is relatively simple to apply confidence limits to a Taylor equation, it is usually adequate to use graphical techniques as the Taylor plot cannot automatically be assumed to be linear. The same argument applies to several of the statistical techniques proposed for tool-life testing.

In many cases tool-life data are not required in the form of equations but in a tabular form. If this is the case, an ideal technique is the one produced by Yellowley and Barrow⁹, which uses the tool-life equation,

$$V T^\alpha h_e^\delta = \text{constant}$$

and recognizes the fact that α and δ may not be constant. The equation is expressed in the form of a T – V – h_e plot, as shown in Fig. 15. The technique has been reported in detail⁹ but it is relevant here to outline the plotting procedure as follows:

- (1) evaluate one V – T curve over the required practical range of conditions at average values of feed and depth of cut (constant h_e),
- (2) evaluate the tool lives corresponding to other conditions of feed and depth of cut (various values of h_e) at an average velocity.

Having established the tool-life points as indicated, it is possible to draw a straight line through the points at constant velocity and parallel lines through the other velocity points (Fig. 15). If α and δ are constant, the lines will all be parallel and spaced in accordance with a logarithmic series. In this case only five points are required in order to predict the tool life over the full working range. But, if α and δ do vary it is necessary to draw the 'best' set of parallel

lines through the data points and so average out the errors caused by non-linearities. For this, more data points are required and it is recommended that further points should be chosen where maximum curvature is to be expected, that is at low speeds and high feeds, and at high speeds and low feeds. The technique has been applied⁹ to the data of Konig and Depiereux shown in Fig. 7 using seven data points, and enabled the remaining tool lives to be predicted with considerable accuracy.

The data in Fig. 15 were obtained using several feeds and depths of cut and for two approach angles, and demonstrate the validity of using the equivalent chip thickness in tool life studies. From Fig. 15 it is possible to obtain tool-life data in a tabular form over a wide range of cutting conditions. There are several formulae for calculating the equivalent-chip thickness, depending on the type of tool and cutting conditions. Whitehead¹⁴ has developed formulae for round, square and triangular throwaway tipped tools for all the usual combinations of feed and depth of cut. In view of the complexity of these equations, the use of nomograms is recommended.

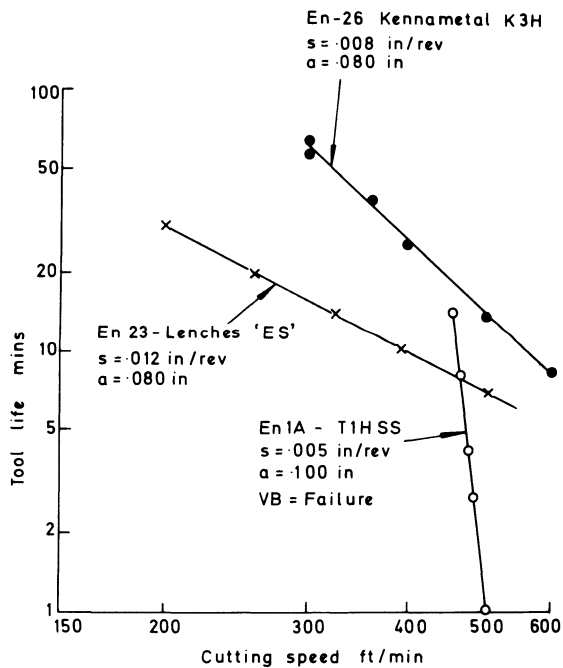
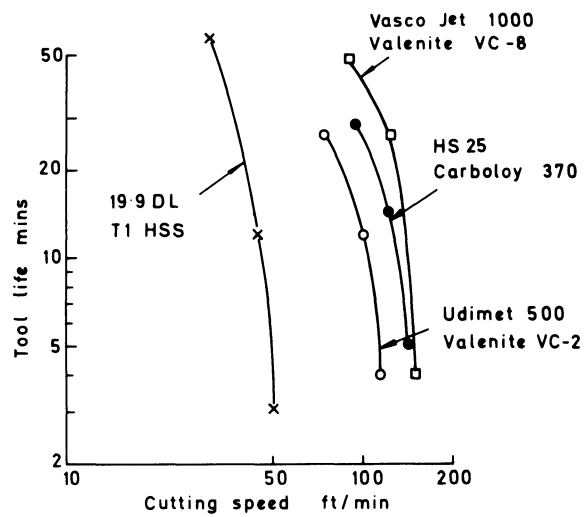


Fig. 4 Tool life curves for various tool and workpiece combinations.



Vasco Jet 1000 (Hot Work Die Steel) $s = .009$ in/rev, $a = .100$ in
 19-9 DL (Austenitic Stainless Steel) $s = .009$ in/rev, $a = .002$ in
 Udimet 500 (Nickel Base Alloy) $s = .009$ in/rev, $a = .100$ in
 HS 25 (Cobalt Base Alloy) $s = .009$ in/rev, $a = .100$ in
 Tool Life Criteria, Carbide VB = .015, HSS VB = .060

Fig. 5 Tool life curves for high strength thermal resistant materials⁴.

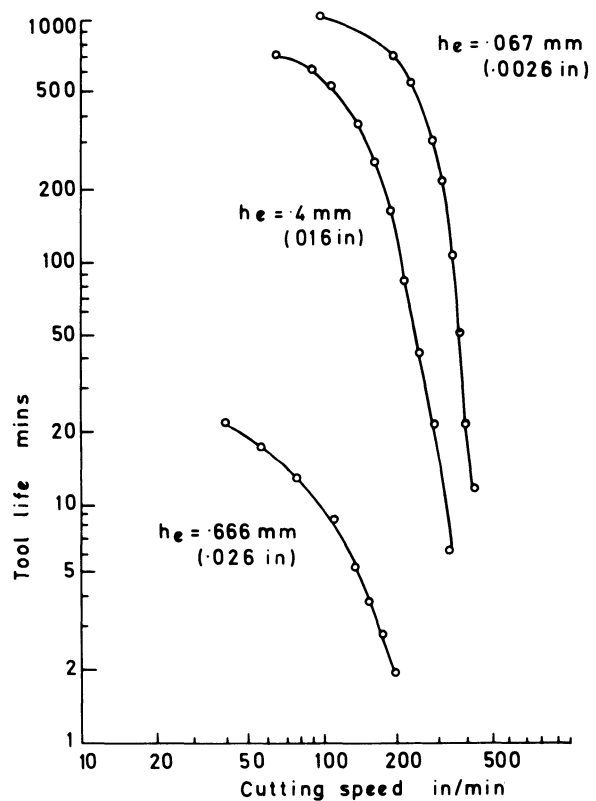


Fig. 6 Tool life curves when machining a carbon steel with carbide tools⁵.

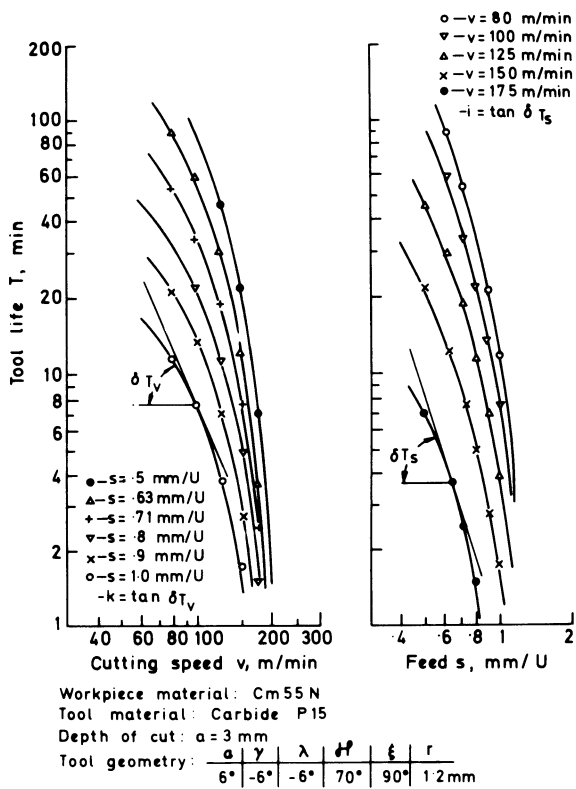


Fig. 7 Typical tool-life curves with varying slopes⁶.

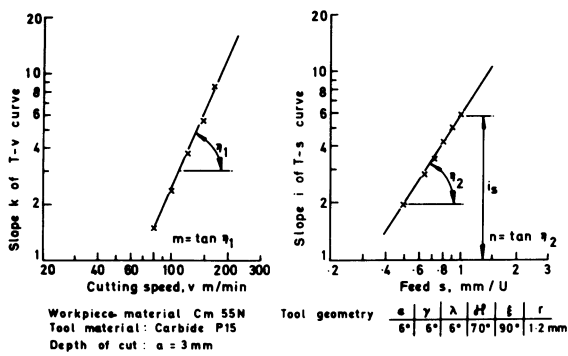


Fig. 8 Graph showing variations in the slope of the $T-V$ and $T-S$ curves⁶.

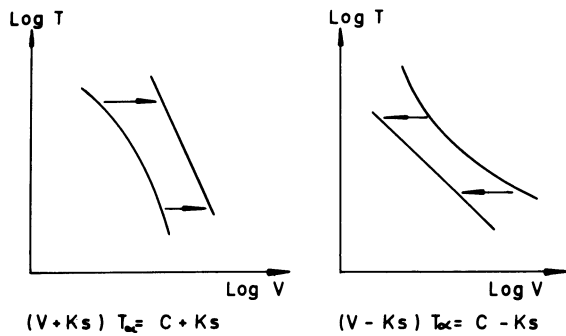


Fig. 9 Kronenberg's method of modifying a curved Taylor plot.

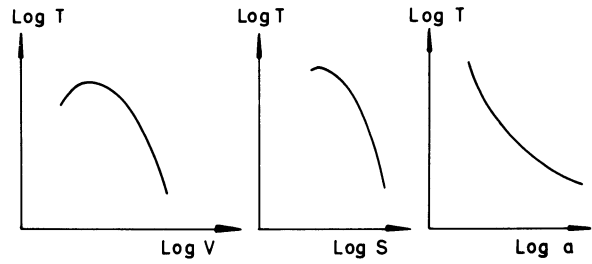


Fig. 10 General trend of tool life with speed, feed and depth of cut.

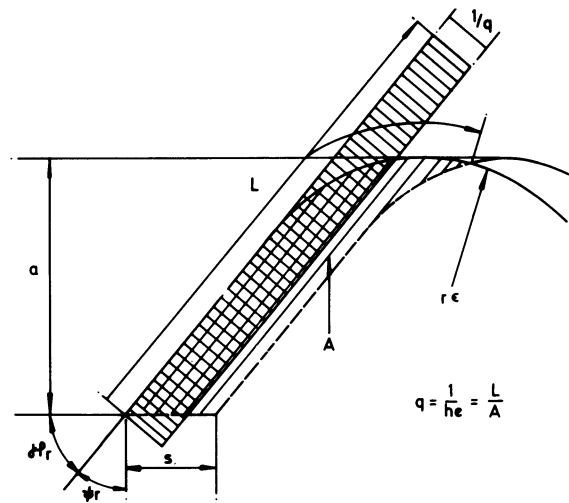


Fig. 11 Definition of chip equivalent.

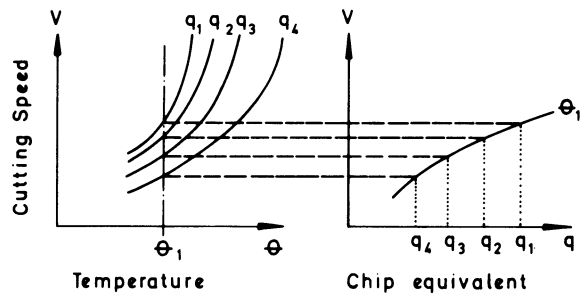


Fig. 12 Influence of chip equivalent on cutting temperature¹¹.

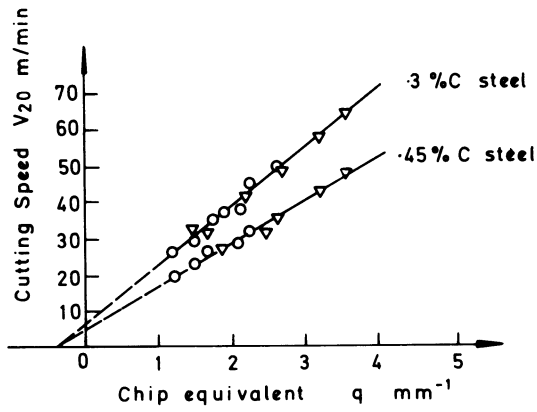


Fig. 13 Influence of chip equivalent on tool life¹¹.

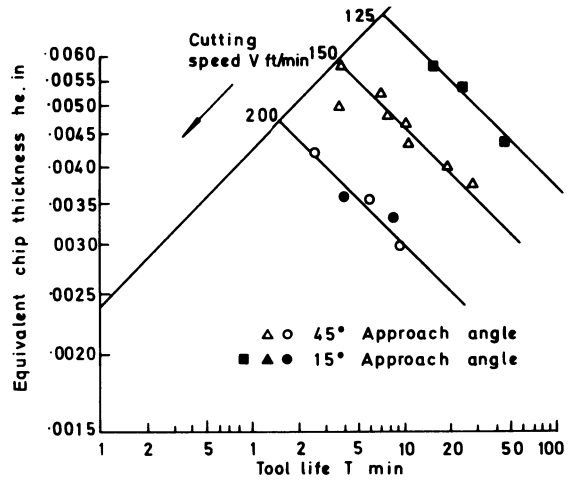


Fig. 15 T-V-he plot for En 26 steel (HB = 640)/Kennametal K5H.

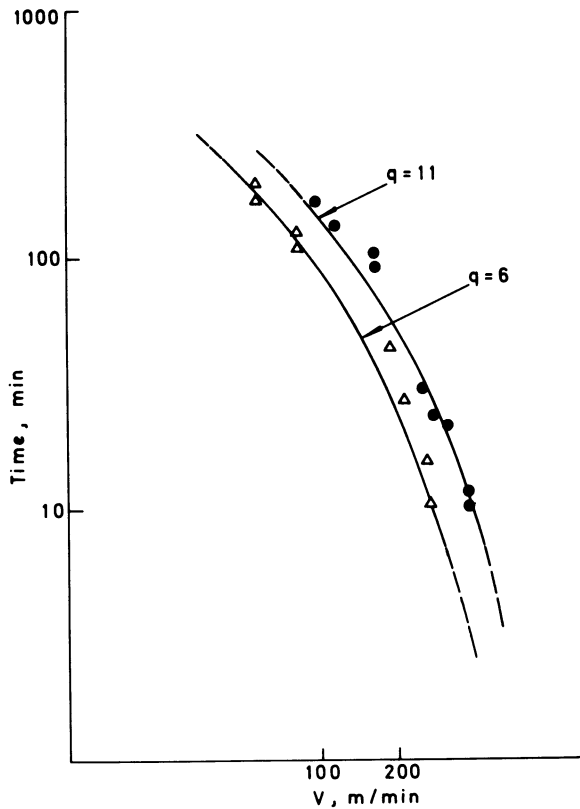


Fig. 14 Wear curves showing fit of calculated-wear curves to actual data points for carbide tool turning of 0.45% carbon steel.

MACHINING ECONOMICS

A considerable amount of work has been undertaken concerning machining economics. It is only possible here to discuss some of the available literature and emphasis will be placed on the role that tool life equations play in evaluating optimum economic cutting conditions.

The selection of economic cutting conditions is complicated to a certain extent by the large number of variables involved. True optimum conditions can rarely be achieved, because of tool and workpiece variability, inadequate machine tools and insufficient cost data, and so on. It should also be remembered that optimum conditions for one operation may not be the same for a complete manufacturing system.

Machining cost and time per component

The machining cost per component is made up of several different costs. There are several ways of expressing these, and the one shown here has been used by several workers in the past.

(a) *Non productive cost*

$$C_1 = x T_1$$

(b) *Machining cost*

$$C_2 = x T_2$$

(c) *Tool changing cost*

$$C_3 = x T_3 (T_{cut}/T)$$

(d) *Tool cost*

$$C_4 = y (T_{\text{cut}}/T)$$

where x = cost rate (labour, overheads, depreciation, and so on), T_1 = non-productive time, T_2 = machining time (feed engagement) $\approx T_{\text{cut}}$, T_3 = cutting edge change time, T_{cut} = actual cutting time, T = tool life, y = tool cost per cutting edge.

$$\begin{aligned} \therefore \text{Total cost } C_T &= C_1 + C_2 + C_3 + C_4 \\ &+ (\text{material cost, } C_5) \end{aligned} \quad (20)$$

After the material specification has been determined, the material cost can be omitted from the analysis and the total cost of 'machining' can then be written

$$C = x (T_1 + T_2 + \frac{T_2}{T}) + y \frac{T_2}{T} \quad (21)$$

The machining time per component can be written as

$$T = T_1 + T_2 + T_3 (\frac{T_2}{T}) \quad (22)$$

as $T_{\text{cut}} \approx T_2$.

The variation of cost and time per component with cutting speed is shown in Fig. 16. Similar trends exist with the other principal cutting variables, feed and depth of cut.

Economic criteria

The economic criteria normally considered are the following.

- minimum cost per component,
- maximum production rate per component,
- maximum profit rate per component.

The minimum cost per component is found by minimizing equation (21) and the maximum production rate by minimizing equation (22). For the maximum profit rate per component criterion it is essential that the income per component is known, that is:

Profit rate, $P_r =$

$$\frac{\text{Income per component } (I) - \text{Cost per component } (C)}{\text{Time per component } (T)}$$

$$\text{that is, } P_r = \frac{I - C}{T} = \frac{I - y (\frac{T_2}{T})}{T_1 + T_2 + T_3 (\frac{T_2}{T})} \quad (23)$$

and the maximum profit can be found by maximizing this equation.

Several workers have used one or all of these criteria in evaluating economic cutting conditions. It can be seen from equations (21) (22) and (23) that in order to evaluate economic cutting conditions, it is essential that information is available regarding cost, time and tool-life data. Although it is not essential that tool-life data be expressed in a mathematical form, it is certainly more convenient and most workers use some form of tool-life equation.

Restrictions on optimum cutting conditions

In most practical cases it is impossible to apply the

theoretical optimum cutting conditions because there are several constraints on the process. These have been discussed by several workers^{13,15,16} and in general the following factors have to be considered.

Machine tool maximum feed and speed restriction—

This is an obvious point but in some cases 'stepped' feeds and speeds can create similar problems.

Machine tool maximum power—Cutting power can be expressed as

$$P = \frac{K_p V S^a a^b}{\eta}$$

Where K_p , a and b are constants depending on the tool and workpiece combination, and η is the efficiency of the machine-tool drive.

Workpiece rigidity—On certain workpieces the maximum force applied may have to be restricted because of excessive deflections.

Surface finish—The theoretical peak-to-valley height of a round nosed tool is

$$h = \frac{S^2}{8 r_e}$$

When finish machining it is almost certain that the feed must be limited to achieve the required surface finish.

Cutting tool—In certain cases the cutting conditions must be limited to avoid failures of the cutting tool caused by other types of failure than those considered in evaluating the tool-life equations.

Analysis based on the Taylor or extended Taylor equations

The extended tool-life equation

$$T = \frac{C_3}{V^{1/\alpha} S^{1/\beta} a^{1/\gamma}}$$

can be modified to

$$T = \frac{A}{V^{1/\alpha} S^{1/\beta}} = \frac{B^{1/\alpha}}{V^{1/\alpha}}$$

by considering cases when depth of cut and feed and depth of cut are constant.

Using the extended Taylor equation, there are three principal variables (V , S and a) to consider. Brewer¹⁷ showed that wherever possible it is most economical to remove the required material in one pass. Although this is usually true if no constraints are imposed, it does not generally lead to the most economical conditions, as indicated by Crookall and Venkataramani¹⁸. But, the multi-pass case is extremely complex and it is doubtful at present whether the refinements obtained are justified. I am of the opinion that analyses of multi-pass cases are 'a step in the right direction', but industry can still benefit considerably by applying the much more simple single-pass case. In

view of this, the analyses considered are all based on single-pass machining.

Considering constant depth of cut and a cylindrical workpiece of length l and diameter D , equations (21) and (22) can be re-written

$$C = x T_1 + \frac{x l}{\lambda V S} + x T_3 \frac{l}{\lambda A} V^{(1/\alpha-1)} S^{(1/\beta-1)} + \frac{y l}{\lambda A} V^{(1/\alpha-1)} S^{(1/\beta-1)} \quad (24)$$

$$\text{and } T = T_1 + \frac{1}{\lambda V S} + \frac{T_3 l}{\lambda A} V^{(1/\alpha-1)} S^{(1/\beta-1)} \quad (25)$$

where $\lambda = 12/\pi D$.

The two cutting variables, V and S , are independent, so that no unique optimum occurs. As tool life is usually more sensitive to changes in velocity than feed the 'best' optimum is usually obtained by utilizing the highest possible feed. Minimum cost and maximum production rate are, therefore, obtained when $\partial C/\partial V = 0$ and $\partial T/\partial V = 0$, respectively. This gives optimum tool life for minimum cost

$$T_{v_m} = (1/\alpha - 1) \left(\frac{x T_3 + y}{x} \right) \quad (26)$$

and for maximum production rate

$$T_{v_p} = (1/\alpha - 1) T_3 \quad (27)$$

Armarego and Brown¹⁵ obtained similar expressions for the maximum profit-rate criterion and have composed the three criterion, as shown in Fig. 17, from which it is clear that it is possible to make a loss when using the minimum-cost or maximum-production-rate criterion. But, provided relatively high feeds are used, the maximum-profit-rate conditions are somewhere in between the conditions which give minimum cost and maximum production rate. Although the maximum profit rate is undoubtedly the best criterion to use, the analysis is complex and some knowledge of the selling price is required. In practice, evaluating the proportion of the selling price to allocate to each operation is a difficult, if not impossible, task. Therefore it is usual to use the minimum-cost or maximum-production-rate criteria. It is good practice to use conditions between those which give minimum cost and maximum production rate, as suggested by Hayes¹⁹.

Analyses using the chip equivalent or equivalent-chip thickness concept

Colding^{5,12}, Brewer and Rueda¹³ and Radford and Richardson¹⁰ have used the chip equivalent (or equivalent-chip) thickness concept in machining economics. Brewer and Rueda considered the equation

$$V T^\alpha h_e^\delta = \text{constant}$$

Realizing that feed was an important variable, however, (particularly for surface finish constants) they modified the tool-life equation as follows, so as to retain feed as an independent variable.

$$V T^\alpha (GS)^\delta = \text{constant}$$

where $G = h_e/S$. They also considered the optimum values of wearland to give minimum tool costs when using brazed-tipped tools, which seems to be an unnecessary sophistication. Except for these minor modifications the analysis was identical to that already discussed. Brewer, however, preferred the use of nomograms to mathematical analysis.

Colding⁵ modified equation (21) to the form

$$C = x T_2 \left(1 + \frac{t_v}{T} + \frac{T_1}{T_2} \right) \quad (28)$$

where $t_v = Tx + y/x$ and is defined as the time equivalent of tool cost and tool changing computed in terms of equivalent machining time. Equation (28) can also be written in the form

$$C = \frac{x W_c}{L} \frac{1}{PS} \left(1 + \frac{t_v}{T} + \frac{T_1}{T_2} \right) \quad (29)$$

where W_c is the volume of metal to be removed per component, that is,

$$W_c = \frac{dW}{dT} x T_2 = T_2 V S a \text{ in}^3$$

$$\text{thus } T_2 = \frac{W_c}{L x PS}$$

where $PS = V/q$ the specific productivity per unit length of cutting edge, L .

The productivity, P , is then given by

$$P = PS \times \frac{T}{T + t_v} \text{ in}^3 \text{ min}^{-1} \text{ in}^{-1}$$

Using a generalized tool-life equation of the form

$$\phi(X, Y, Z) = 0$$

where $X = \log q$, $Y = \log V$ and $Z = \log T$. Colding showed that the maximum value of P (minimum cost) occurs when

$$\frac{\partial Z}{\partial Y}_{X=X_i} = - \left(1 + \frac{e^z}{t_v} \right)$$

Economic cutting conditions can be found by digital computation or by using a simple graphical technique as shown in Fig. 18, in which productivity P is plotted against Z , with X as a parameter, using graphical tool data.

Konig–Depiereux analysis

Konig and Depiereux⁶ used a cost equation of the form

$$K = \frac{x T_2 \lambda}{la} + \frac{x}{a S V} + \frac{x T_3 + y}{a T S V} \quad (30)$$

where K is the cost per unit volume. By incorporating their tool-life equation

$$T = \exp \left(-\frac{KV}{m} V^m - \frac{i_s}{n} S^n + c \right)$$

into equation (30), and differentiating showed that the economic cutting conditions could be evaluated from the following equations

$$V^m [(K_v/n) + (K_v/m)] - \log \frac{x}{x T_3 + y} + c$$

$$= -\log (K_v V^m - 1) \quad (31)$$

and

$$S^n = [\log \frac{x}{x T_3 + y} + c - \frac{K_y}{m} V^m - \log (K_v V^m - 1)] i_s/n \quad (32)$$

Equation (31) does not contain the feeds and the economic cutting speed can be calculated uniquely, as shown in Fig. 19.

Discussion

The problems of applying a maximum-profit-rate criterion have already been discussed, together with the probability of making a loss when using the maximum-production-rate criterion. In view of this it is recommended that the minimum-cost criterion be used, realizing, of course, that this will not yield the maximum profit. In some cases (for example, sub-contract machining) the maximum profit rate can be applied successfully.

Because of the high cost of obtaining the extended-tool-life equation, analyses using the chip-equivalent concept seem to have certain advantages. If the procedure suggested by Colding is used, data are readily available for a wide range of cutting conditions and the graph can be used for several cases provided that the cost, time and tool-life data do not vary. This is also true of the Konig-Depiereux analysis. A particularly good feature of both these analyses is that they readily indicate the influence of the various practical constraints on machining costs. On the other hand, using the extended Taylor equation approach, reasonable cutting conditions can be chosen very rapidly by the use of equation (26), changes in cost rate and tool costs being catered for when required.

One of the principal features of most analyses is that it is usual to use one cost rate, x , to determine non-productive, machining and tool-changing costs. This assumes that the machine tool costs the same amount to operate whether it is cutting or not. Although this is obviously not the true situation, the use of different cost rates is difficult to apply in practice.

It should also be remembered that the tool-life data used are necessarily rather conservative. One cannot, therefore, expect the application of the various economic analyses to yield precise results. But, the analyses should at least approach optimum conditions.

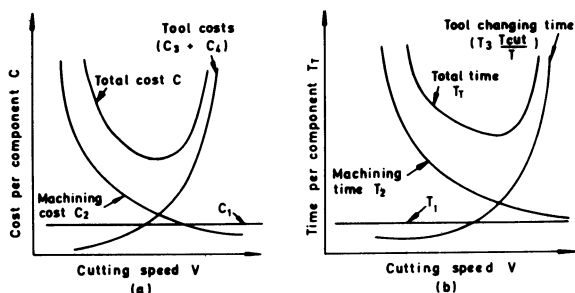


Fig. 16 Variation of cost and time per component with cutting speed.

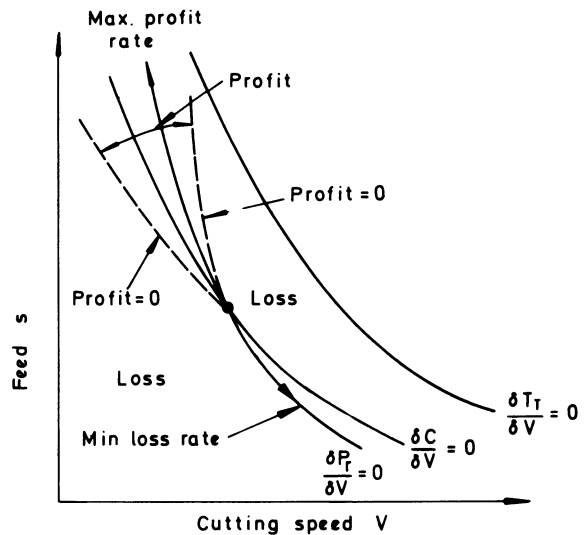


Fig. 17 Speed-feed curves for three criteria showing profit and loss regions.

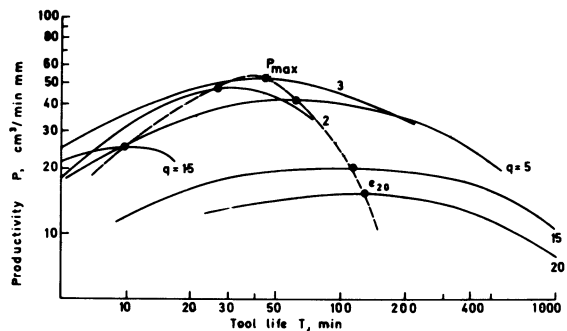


Fig. 18 Graphical procedure to determine optimum cutting conditions.

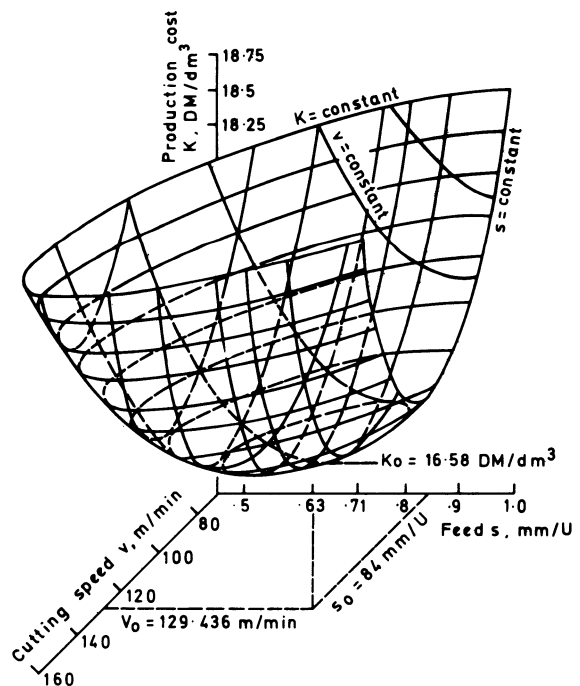


Fig. 19 Variation of cost with feed and speed.

SUMMARY OF PRINCIPAL CONCLUSIONS

Depending on the complexity tolerated, it is possible to describe empirical tool-life data in a reliable mathematical form.

The Taylor-type equations are not generally valid, and should only be used when it is known that the indices are essentially constant.

Equations using the chip equivalent or equivalent-chip thickness concept are valid and possess considerable advantages in terms of reduced experimental effort.

In view of inadequate time, cost and tool-life data, economic analyses can only yield approximate optimum conditions.

REFERENCES

1. DICKINSON, G. R., 'Experience in the Machining of Ultra High Strength Steels,' Proc. 10th Intern. MTDR Conf. (1969).
2. BARROW, G., 'The Wear of Carbide Tools During Hot Machining of Alloy Steels,' Proc. 7th Intern. MTDR Conf. (1966).
3. TAYLOR, F. W., 'On the Art of Cutting Metals,' *Trans. A.S.M.E.*, 28, (1907).
4. U.S.A.F. Report No. AD 220540, U.S. Dept. of Commerce.
5. COLDING, B. N., 'Machinability of Metals and Machining Costs,' *Intern. J. MTDR*, 1 (1961).
6. KONIG, W., and DEPIEREUX, W. R., *Industrie Anzeiger*, 91 (1969).
7. KRONENBERG, M., 'Machining Science and Application,' (Pergamon Press, 1966).
8. KRONENBERG, M., 'Replacing the Taylor Formula by a New Tool Life Equation,' *Intern J. MTDR*, 10 (1971).
9. YELLOWLEY, I., and BARROW, G., *Fertigung*, No. 1 (1971).
10. WOXEN, R., *Tekn. Tidskr. Stockholm Mekanik* 6, No. 61 (1931).
11. WOXEN, R., 'A Theory and an Equation for the Life of Lathe Tools,' *Ingeniorsvetenskapskademien Handlengor*, No. 119, (Stockholm, 1932).
12. COLDING, B. N., 'A Three Dimensional Tool Life Equation Machining Economics,' *Trans. A.S.M.E.*, 81 (1959).
13. BREWER, R. C., and RUEDA, R. A., 'A Simplified Approach to the Optimum Selection of Machining Parameters,' *Engineers Digest*, 24, No. 9 (1963).
14. WHITEHEAD, J., 'The Chip Equivalent Method of Cutting Tool Life Prediction,' M.Sc. Dissertation, University of Manchester (October, 1970).
15. ARMAREGO, E. J. A., and BROWN, R. H., 'The Machining of Metals,' (Prentice Hall, 1969).
16. CROOKALL, J. R., 'The Performance Envelope Concept in the Economics of Machining,' *Intern J. M.T.D.R.*, 9 (1969).
17. BREWER, R. C., 'On the Economics of the Basic Turning Operation,' *Trans. A.S.M.E.*, 80 (1958).
18. CROOKALL, J. R., and VENKATARAMANI, V., 'When it Pays to Machine in More than One Pass,' *Metalworking Production* (Jan, 1971).
19. HAYES, T. E., 'How to Cut with Carbides by HI-E Machining,' *American Machinist*, 99, No. 27 (1955).

DISCUSSION*Query from F. B. Hinderwell*

Since tool life prediction is said to be largely a question of curve fitting, could the author give some indication of the degree of repeatability obtained in the tests, particularly with different samples of material to the same nominal specification.

Reply

It is not easy to give a general answer regarding the repeatability of tool-life tests, since a large number of factors are involved even when machining material of the same minimal specification. One has to consider not only the workpiece material but also the tool material and, where industrial application is concerned, the variability from machine to machine.

Provided some sort of tool material control such as visual inspection for micro-chipping and correct blending of nose radii etc. is employed, it is possible to reduce the variability of the tool material to small limits. It should, however, be realised that the quality control at the basic manufacturing stage is also of importance and in my experience this control varies considerably for different manufacturers. Using 'good' tools, differences in tool-life of $\pm 100\%$ (in some cases even higher) have to be tolerated for materials supplied to normal specification standards. When one considers the more exotic materials which have tighter specifications the variability is considerably reduced.

When considering tool-life variability, it should be remembered that industry is usually concerned with metal removal rate and in view of the fact that tool-life is very dependent on cutting speed, a small reduction in cutting speed can easily accommodate the $\pm 100\%$ variability in tool-life at a given cutting speed.

Query from P. F. Jones, P. A. Management Consultants Ltd.

It is important to recognise the difficulty of applying much of the theoretical work in metal cutting economics to the practical industrial situation. In the first place single point turning of plain diameters is only a small part of machining work in industry. Secondly, the absorption costing technique implied in the general approach used is misleading as a much higher proportion of cost than that assumed is often fixed per part produced. Bearing in mind the numerous variables and practical problems in the average machine shop, the best approach to economics is to consider incremental costs before and after a change is made. Provided sensible practical criteria are applied what is required is a simple methodology not advanced theoretical conceptions.

Reply

The author would like to thank Mr Jones for his valuable comments regarding the difficulty of applying theoretical work in metal cutting to the practical industrial situation. However, whilst I appreciate Mr Jones's concern I believe that the analyses reported in the paper can assist the engineer in achieving reduction in costs, etc.

Although the work described was undertaken on single point tools it should be remembered that the basic concepts can be (and have been) applied to other operations. Whilst the method of 'incremental' costs suggested by Mr Jones is obviously a valuable tool it is surely advisable to have an indication of the consequences of a change in production rate, etc., beforehand.

Query from Prof. J. Peters

I like very much your approach using the concept of equivalent-chip thickness or chip equivalent.

A week ago at the CIRP meeting we discussed the results of our cooperative grinding work, as well as the combination of data of different authors published in literature.

Thus, the question arose: Would we use the equivalent-chip thickness or its inverse the chip equivalent? It was decided to prefer the equivalent-chip thickness because it is more directly related to feed, whereas the value of chip equivalent increases as the chip thickness decreases.

Reply

I should like to thank Professor Peters for his comments and would agree with him that it is preferable to use equivalent-chip thickness rather than chip equivalent.

SELECTION OF CUTTING SPEEDS BASED ON UNCERTAIN DATA

by

RICHARD L. KEGG*

SUMMARY

This paper considers how the sensitivity of the cost or time response to deviations in speed, from the theoretical optimum speed, decreases as the value of Taylor's exponent n increases, and evolves some clear, practical rules.

INTRODUCTION

In selecting cutting speeds for machining, it has always been taught that for each combination of machining conditions there is one unique speed that gives minimum cost. This unique speed can be calculated if the two constants of the Taylor tool-life equation:

$$v T^n = C \quad (1)$$

are known. It has also been taught that the exponent n is reasonably constant for a given cutting tool material, and that variations in workpiece machinability and machining conditions cause only the constant C to vary. Pilafidis¹ has recently shown that this is wrong. Table 1 is a summary of his analysis of 140 selected tool-life curves from published literature. The tool-life exponent is not a well-behaved constant. It now appears that two of the inputs to the machining economics equations are highly variable, uncertain quantities.

As an example of the uncertainty of n , the CIRP cooperative research² has shown that even under highly standardized, carefully monitored laboratory conditions, n can vary over a range of 3:1. The uncertainty of the tool-life equation may be further illustrated by statistical analysis of machinability data.³ contains several tool-life vs. cut speed curves consisting of more than the usual number of data points. One of these curves is replotted in Fig. 1. From this we see that a straight line fits the data very well, but that some scatter is present. Fig. 2 shows the amounts by which the data deviate from the best straight line. A statistical analysis of these data (see Appendix) tells us the following: There is a 10% probability that the actual life of any given tool will lie outside a 20:1 range around the best tool-life curve. This means that, even having carried out such thorough testing, there is a good chance that our best estimate of tool-life will be off by a large factor when applied to a single case. Since this degree of scatter was obtained in a doctoral thesis, we might expect normal data-taking to produce even wider variations.

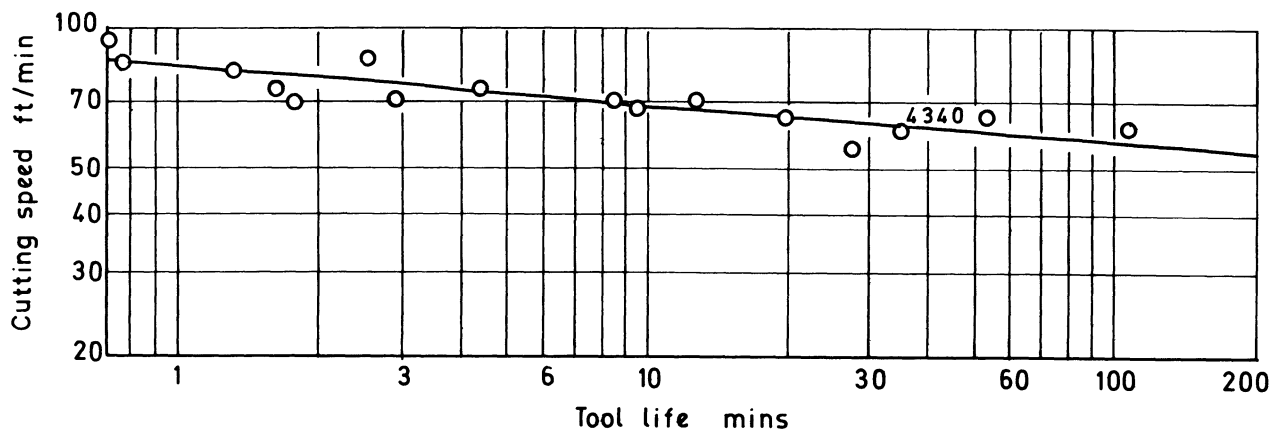


Fig. 1 Plot of tool-life against cutting speed.

*Cincinnati Milacron Inc., U.S.A.

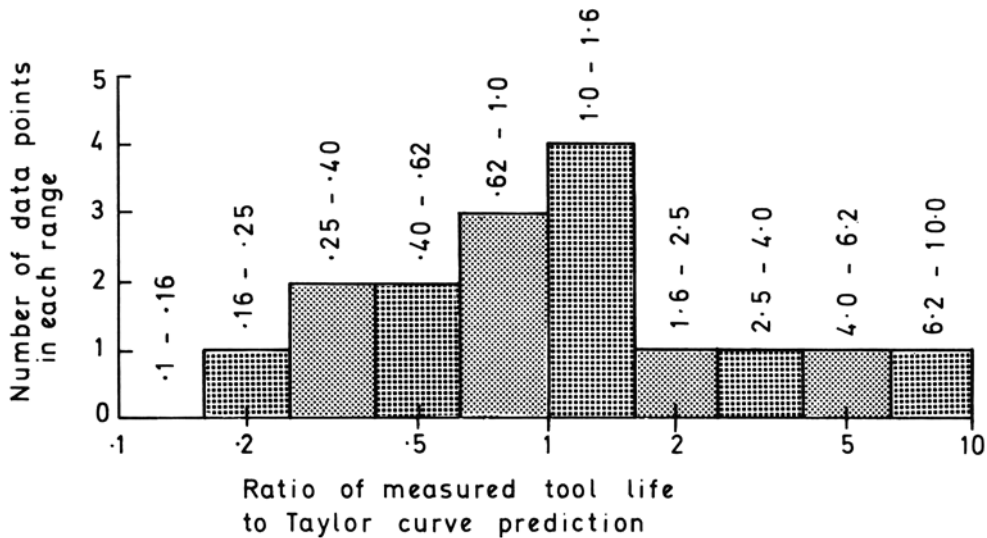


Fig. 2 Ratio of measured tool-life to Taylor curve prediction.

If tool-life data are actually as variable as these results would indicate, we should seriously question the value of minimum cost calculations. We must make it very clear that the calculation of specific optimum cutting conditions gives only a best estimate which may actually be a poor one. But even though we cannot accurately predict the optimum speed, we can make good use of economic analysis. The most useful results for those who actually select speeds in practice are the general rules-of-thumb which apply to all machining situations, regardless of specific machinability data. For example, from Gilbert's results⁴ we may derive the following rules:

1. For expensive tools, longer tool-life is more economical.
2. For difficult-to-change tools, longer tool-life is more economical.
3. For expensive machines or expensive labour, shorter tool-life is more economical.
4. For difficult-to-machine materials, longer tool-life is more economical.

These rules are useful and valid whether our data is vague or precise, repeatable or scattered. But now that we recognise that the data is very likely to be scattered and that our best estimates of cutting speed may be very far from optimum, are there any new rules we may use to minimize the results of these errors? The best answer in the literature comes from Ermer and Faria-Gonzalez⁵. After plotting and analysing normalised cost curves, they concluded that 'The sensitivity of the cost or time response to deviations in speed, from the theoretical optimum speed, decreases as the value of Taylor's exponent n increases'. The objectives of the present paper are to extend and investigate this interesting conclusion in more detail, so that some clear, practical rules can be discovered.

ANALYSIS OF CUTTING ECONOMICS

The cost of a machining operation on a single work-piece is the sum of handling costs, cost of machining time and cost of tool consumption.

$$C_c = C_m t_h + \frac{\pi d L C_m}{1000 s} \cdot v^{-1} + \frac{\pi d L (C_m t_a + C_s)}{1000 s C^{1/n}} \cdot v^{\frac{1-n}{n}} \quad (2)$$

- where C_c machining cost per part (\$)
 C_m cost of operating time (\$/min)
 t_h part handling time (min)
 d workpiece diameter (mm)
 L workpiece length (mm)
 s feed per revolution (mm)
 v cutting speed (m/min)
 t_a tool change time (min)
 C_s cost of tool consumed (\$ per change)
 T tool-life (min)
 C, n are constants from the tool-life equation

Gilbert found from equation (2) that the cutting speed which gives minimum cost is

$$v_{ec} = C \left[\frac{n}{1-n} \cdot \frac{C_m}{C_m t_a + C_s} \right]^n \quad (3)$$

Now what we want to do is to find out what happens to the machining costs as we move away from this optimum speed. Mathematically, we want to see how the function $C_c(v)$ varies around the point $C_c(v_{ec})$. To do this it is most convenient to represent the function $C_c(v)$ by its Taylor series expansion around the point $C_c(v_{ec})$.

For speeds greater than v_{ec} the cost equation may be represented as

$$C_c(v_{ec} + dv) = C_c(v_{ec}) + C'_c(v_{ec}) dv + C''_c(v_{ec}) \frac{dv^2}{2} + C'''_c(v_{ec}) \frac{dv^3}{6} + \dots \quad (4)$$

For speeds less than v_{ec} the series is

$$C_c(v_{ec} - dv) = C_c(v_{ec}) - C'_c(v_{ec}) dv + C''_c(v_{ec}) \frac{dv^2}{2} - C'''_c(v_{ec}) \frac{dv^3}{6} + \dots \quad (5)$$

Where $C_c(x)$ is the value of the cost function at $v = x$
 C'_c is the first derivative of the cost function with respect to speed
 C''_c is the second derivative of the cost function with respect to speed
 dv is the deviation from v_{ec}

There are two interesting things we can find out from these series. One is the cost penalty we must pay if we deviate from the optimum speed. This will give us some idea of when it is most important to estimate the optimum cutting speed accurately

$$\Delta C_c = C_c(v_{ec} \pm dv) - C_c(v_{ec}) \quad (6)$$

The second is the difference between the cost penalties above and below the optimum cutting speed. Since we recognize that our estimate of the optimum speed will be in error, we should like to determine whether it is better to overestimate or underestimate

$$\Delta C_c^+ - \Delta C_c^- = C_c(v_{ec} + dv) - C_c(v_{ec} - dv) \quad (7)$$

If we carry out the differentiation of the cost equation (2) and substitute into equations (4), (5) and (6), keeping only the first two non-zero terms of the series, we get

$$\Delta C_c = \frac{\pi d L C_m}{2000 s n v_{ec}} \left(\frac{dv}{v_{ec}} \right)^3 \left[\frac{v_{ec}}{dv} \pm \frac{1}{3n} \mp \frac{5}{3} \right]$$

When dv is only a few percent of v_{ec} , the other bracketed terms may be neglected

$$\Delta C_c = \frac{\pi d L C_m}{200 s n v_{ec}} \left(\frac{dv}{v_{ec}} \right)^2 \quad (8)$$

Equation (8) gives the cost penalty to be paid for non-optimum cutting speed. Clearly the penalty for larger workpieces, lighter feeds, lower speeds and high machine and labour costs. Since a low value of n generally indicates poor machinability, we can also note that this causes an increase in the cost penalty beyond that associated with lower operating speed.

We can summarise these results by saying:

- (a) It is more important to estimate speed accurately for expensive machining operations.
- (b) It is most important to estimate speed accurately when the work material has poor machinability.

The result (a) is obvious and does not require any mathematics to prove. The second conclusion seems reasonable when we consider the meaning of n . A low value of n means that tool-life changes sharply with changing cut speed. Thus, overall costs will be very sensitive to errors in speed selection for workpiece-

tool combinations which give poor machinability (low n).

Now the second thing we want to analyse is the cost difference between overestimating the optimum speed and underestimating it. Substituting the derivatives of the cost equation into equations (4), (5) and (7), discarding higher powers of very small quantities and simplifying, we obtain

$$\Delta C_c^+ - \Delta C_c^- = \frac{\pi d L C_m}{300 s n^2 v_{ec}} (1 - 5n) \left(\frac{dv}{v_{ec}} \right)^3$$

By inspection we see that this quantity is positive for n values greater than one-fifth and negative for values less than one-fifth. For smaller n , the cost penalty is greater above the economic speed than below. For larger n , the cost penalty is greater below the economic speed than above. In other words:

- (c) For difficult-to-machine materials it is better to set the cut speed too low than to set it too high.
- (d) For easy-to-machine materials it is better to set the cut speed too high than to set it too low. The dividing line is at $n = 0.2$.

Now let us see if these mathematical results are reasonable. We know that when the tool wear rate is very sensitive to speed changes (low n), the tool cost changes more rapidly with speed than the cost of time does. We also know that above the optimum speed, the tool cost is the dominant cost, while below optimum the cost of time is greatest. Therefore, for low n , the cost will change more rapidly above optimum (where the tool sensitivity to speed is fully felt) than below. Then, for materials with poor machinability (low n) it will be better to underestimate the optimum speed than to overestimate it.

CONCLUSIONS

Four rules can be used to help select cutting speeds for lowest cost, in spite of uncertain machining data:

- (1) For materials of poor machinability (n under 0.2) it is better to have the cut speed too low than too high.
- (2) For materials of good machinability (n over 0.2) it is better to have the cut speed too high than too low.
- (3) The more expensive the machining operation, the more important it is to choose cutting speed accurately.
- (4) It is most important to get the best balance between tool cost and cost-of-time when machining difficult workpiece materials.

REFERENCES

1. PILAFIDIS, E. J., 'Observations on Taylor "n" values used in metal cutting', *Annals of the CIRP*, Vol. XVIII, 1970.
2. LORENZ, G., 'The interplay between machining research and industrial experimentation', *Prod. Engr.*, Vol. 45, p. 544, 1966.
3. HENKIN, A., 'The influence of some physical properties of machinability of metals', Ph.D. Dissertation, University of Michigan, June, 1962.

4. GILBERT, W., 'Economics of machining', *Machining Theory and Practice, American Society for Metals*, pp. 465-485, 1950.
5. ERMER, D. S. and FARIA-GONZALEZ, R., 'An analytical sensitivity study of the optimum machining conditions', *ASME Paper 67-WA/PROD-20, July 1957.*

$$\sigma^2 = \left(\frac{1}{16} \cdot 13.5266\right)$$

$$\sigma = 0.92$$

From tables of the normal distribution we see that 90% of the time we can expect actual data to fall within $\pm 1.65 \sigma$ of the prediction, T_p . Therefore, 90% of the time:

$$\ln T_p - 1.65 \times 0.92 \leq \ln T_{\text{exp}} \leq \ln T_p + 1.65 \times 0.92$$

$$\ln T_p - 1.52 \leq \ln T_{\text{exp}} \leq \ln T_p + 1.52$$

$$\ln \frac{T_p}{4.58} \leq \ln T_{\text{exp}} \leq \ln (4.58 T_p)$$

$$0.219 T_p \leq T_{\text{exp}} \leq 4.58 T_p$$

APPENDIX

The data in the first four columns of Table 2 is copied from³. The remaining columns are derived to evaluate the standard deviation according to

$$\sigma^2 = \frac{1}{N} \sum \left(\ln T_{\text{exp}} + \frac{1}{n} \ln v - \frac{1}{n} \ln C \right)^2$$

From (3) we find that

$$n = 0.0782$$

$$\ln C = 4.4081$$

and calculate

$$\frac{1}{n} \ln C = 56.3695$$

Using this information to compute the last two columns of Table 2, we find

This means that ninety percent of the data can be expected to lie between one-fifth of the best Taylor curve estimate and four-and-one-half times the best estimate. The converse tells us that 10% of the time we can expect this tool life data to be scattered over a range of greater than 20:1.

Fig. 2 shows that the data is distributed fairly normally.

TABLE 1

Process	Tool material	Common cast irons and steels		Aerospace materials	
		Median "n"	Range	Median "n"	Range
Turning	HSS	0.25	0.09-0.55	0.15	0.09-0.25
	Carbide	0.45	0.10-0.80	0.20	0.15-0.25
	Ceramic	0.45	0.30-0.65	-	-
Milling	HSS	0.50	0.10-0.75	0.15	0.05-0.30
	Carbide	0.42	0.15-0.60	0.15	0.05-0.70
	Ceramic	-	-	-	-

TABLE 2

	Cutting velocity V (ft/min)	Tool-life T (min)	ln V	ln T	$x + \frac{y}{0.0782}$	z^2
					-56.3695	
			y	x	=z	
1	70.0	2.8	4.24850	1.02962	-1.01124	1.02260
2	60.0	34.0	4.09435	3.52637	- .48272	.23301
3	65.0	19.6	4.17439	2.97553	- .01303	.00016
4	70.0	1.75	4.24850	0.55962	-1.48124	2.19407
5	80.0	1.3	4.38203	0.26236	- .07096	.00503
6	75.0	1.6	4.31749	0.47000	- .68864	.47422
7	55.0	27.5	4.00734	3.31419	-1.81056	3.27812
8	85.0	0.75	4.44266	-0.28769	+ .15431	.02381
9	60.5	106.0	4.10265	4.66344	.75749	.57379
10	65.3	53.0	4.17800	3.97030	1.04069	1.08303
11	67.5	9.4	4.21213	2.24071	- .26524	.07035
12	70.5	8.3	4.25562	2.11626	.16645	.02770
13	70.5	12.4	4.25562	2.51770	.56789	.32249
14	75.0	4.3	4.31749	1.45862	.29998	.08998
15	85.0	2.5	4.44266	0.91629	1.35829	1.84495
16	95.0	0.7	4.55388	-0.35318	1.51107	2.28333

USE OF THE SCANNING ELECTRON MICROSCOPE TO STUDY THE FUNCTION OF MANGANESE SULPHIDE INCLUSIONS IN RESULPHURISED FREE-MACHINING STEELS

by

W. J. WILBER,* A. W. J. CHISHOLM† and E. J. PATTINSON†

SUMMARY

The scanning electron microscope provides the means for a new approach to the study of the mechanism by which manganese sulphide inclusions affect the machinability of free-machining steels. The use of this instrument in the experimental work described here has led to the conclusion that manganese sulphide inclusions affect the machinability of resulphurised steels chiefly by promoting the formation of a stable built-up cap on the cutting edge of the tool, which protects the cutting edge and reduces the rate of tool flank wear. A mechanism, embodying phenomena which are construed to be peculiar to the machining of resulphurised steel, is proposed here to explain how manganese sulphide inclusions promote this built-up cap formation. This function of manganese sulphide in re-sulphurised steel differs from that advanced previously, which relies on the formation of lubricating films on the tool surfaces.

INTRODUCTION

Approximately half a million tons of non-alloy free machining steels are produced annually in this country alone¹ and this figure is increasing each year. These steels represent an appreciable percentage of the total national production of bar material, and the continued improvement in machine tools and systems designed for high output rates has resulted in a considerable demand for steels of this type possessing an improved and more consistent machinability.

The free machining properties of these steels are usually obtained by the addition of either lead or sulphur to the melt during the production of the steel; of these, sulphur is used particularly extensively. Unlike lead, however, there is still controversy about the mechanism by which sulphur improves the machinability of low-carbon steels; consequently, further research in this field is of considerable interest to the steel industry in its search for better steels.

Early research on this subject^{2,3} suggested that manganese sulphide acted as an interfacial lubricant between tool and chip, but Shaw et al.⁴ considered that this explanation was inadequate, because friction tests indicated that manganese sulphide was a poor solid lubricant. Usui and Shaw⁵ suggested that the addition of sulphur to the steel reduced the flow stress of the steel at the high strain rates occurring in metal cutting. Trent⁶ proposed a mechanism by

which manganese sulphide inclusions could act as an internal lubricant within the steel as it passed through the secondary flow zone. He suggested that the inclusions become drawn out into long thin plates, which allow adjacent layers of steel to flow over each other under much reduced stresses. Trent considered, however, that manganese sulphide functioned as an internal lubricant as well as an interfacial lubricant. The influence on machinability of the frequency of manganese sulphide inclusion within the steel was clearly indicated by Richardson and Chisholm⁷, who found that an increase in the number or frequency of inclusions in ferrous materials was accompanied by a reduction in the chip-tool friction coefficient; they suggested that this was caused by the manganese sulphide acting as an extreme pressure lubricant between the chip and tool.

The recent commercial development of the scanning electron microscope^{8,9} has enabled a new approach to be made to the study of these and related problems. The principal advantage of this instrument in metal cutting research is its inherently large depth of focus and an ability to examine directly specimens up to 10 mm cube in size. In this study, the scanning electron microscope was used in a comparison of the machining characteristics of a resulphurized low-carbon steel with those of a non-resulphurised steel which otherwise had approximately the same chemical analysis. Special attention

*City of Birmingham Polytechnic, Perry Barr, Birmingham.

†Department of Mechanical Engineering, University of Salford, Salford.

was given to the examination of the flank and rake faces of the cutting tool, together with specimens of the chip underside and workpiece surfaces. It is hoped in this way to establish more clearly the mechanism by which manganese sulphide inclusions affect the machinability of free-cutting steels.

EXPERIMENTAL WORK

Work material

The resulphurized steel used in the investigation was received as standard EN1A material in the 'as rolled' condition. It contained 0.26% sulphur and was all obtained from the same heat. The non-resulphurized steel was specially prepared so that it was nominally identical to the resulphurized steel except for its manganese sulphide content. The steels were given a normalizing treatment to ensure uniformity of grain size and hardness before conducting the cutting tests.

Cutting and wear tests

The cutting tests were conducted on a high speed test lathe at a number of cutting speeds between 50 and 700 ft/min. Measurements of tool wear, cutting force and rake face contact lengths were made for both steels at each cutting speed.

One of the objects of the work was to examine the influence of manganese sulphide on built-up edge formation; cutting conditions were therefore chosen for the tests, such that a built-up edge would not normally form with non-resulphurized steels. Cemented-carbide tools containing TiC reduce the tendency towards built-up edge formation;^{10,11} consequently, a tool composition of 6% Co, 16% TiC and 73% WC was chosen for these tests. The tool tips were specially prepared from the same powder mix and were all sintered in the same area of the sintering furnace, in order to keep variations in their properties to a minimum.

In selecting the tool geometry, an unusually high tool rake of 30° was chosen in order to minimize further the formation of a built-up edge. A plan approach angle of 30° was used to help give approximately orthogonal cutting conditions while still machining a solid bar¹². The grinding and lapping of the tools was carried out in a specially designed fixture¹³.

By means of a special mirror attachment, it was possible to examine the flank face of the tool through an optical microscope without removing the tool from its holder¹³. This device also enabled a permanent photographic record of the development of the flank wear scar during the tool-wear tests to be obtained without altering the relative position of the tool and workpiece. A two-component metal cutting dynamometer, similar to that of Chisholm and McDougall¹⁴, was used to record the components of the resultant cutting force.

At the end of each cutting test, the carbide tip was removed from the tool holder, and both the flank and rake faces examined in the scanning electron microscope. The rake face contact length was determined from photomicrographs produced by this means. A specimen of the chip was also mounted so that the underside could be examined; the need to conserve

the special non-resulphurized test steel made it necessary in most cases, however, to study the transient workpiece surface produced by the tool flank by means of replicas.

DISCUSSION OF RESULTS

Wear test results

The results of the wear tests showing the effects of cutting speed on flank-wear rate and cutting forces are presented in Figs. 1a and b, respectively. These results are discussed in conjunction with the evidence provided by photomicrography and with reference to the different regions of the chip-tool workpiece system.

Flank face characteristics with non-resulphurized steel

When machining non-resulphurized steel at cutting speeds of 50 and 150 ft/min, severe chipping of the cutting edge occurred (Fig. 2a). As the cutting speed increased, this type of damage was considerably reduced; nevertheless, it persisted to a small degree, even up to the maximum cutting speed of 700 ft/min. It is considered that chipping of the cutting edge was largely caused by the brittleness of the grade of tool material used. Although this makes it generally unsuitable for the machining of non-resulphurized steel at low cutting speeds in practice, its use in these experiments was, as explained previously, to minimize the formation of a built-up edge. The chipping of the cutting edges did, however, inadvertently serve to enhance certain differences in the machinability of the non-resulphurized and resulphurized steels.

A built-up edge was not observed when cutting non-resulphurized steel throughout the entire speed range investigated. At cutting speeds of up to about 400 ft/min, many isolated particles of material were seen to adhere to the flank wear scar in an apparently random fashion (Fig. 2b). Above this speed, the material adhering to the flank wear scar was visible chiefly as a continuous layer. This layer increased in length, perpendicular to the cutting edge, as the cutting speed increased until, at 700 ft/min, almost the entire width of the wear scar was covered with a built-up layer (Fig. 2c).

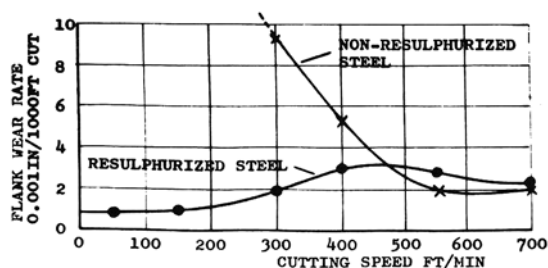
Ignoring the results of tests in which excessive damage to the cutting edge rendered the results unreliable, Fig. 1a shows that the flank-wear rate when machining non-resulphurized steel was much higher at low cutting speeds than for the resulphurized steel; the difference, however, decreased with increasing cutting speed until at 700 ft/min the values obtained were similar for both steels

Flank face characteristics with resulphurized steel

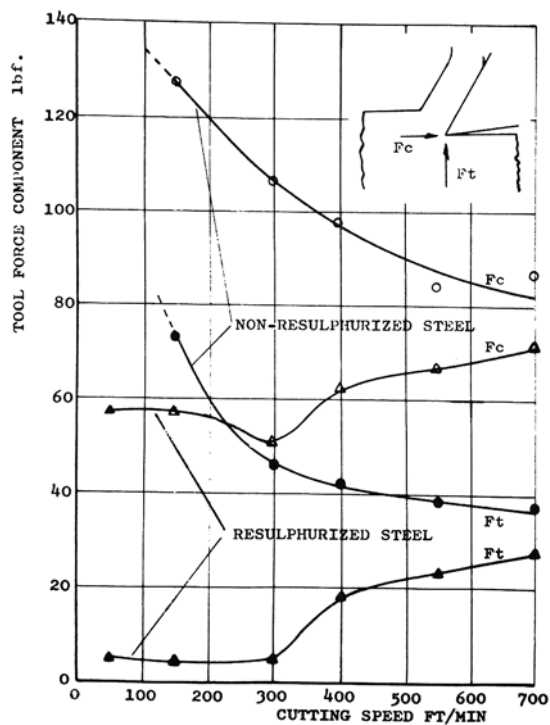
The appearance of the flank surfaces of tools used for machining resulphurized steel was in marked contrast to that of tools used on non-resulphurized steel. Although the choice of cutting conditions virtually eliminated the formation of a built-up edge with non-resulphurized steel, this aim was not achieved when machining resulphurized steel. With the latter steel, a significant build-up of material occurred on

the tool throughout the whole speed range, although its form depended on the cutting speed.

At cutting speeds between 50 and 300 ft/min, the build-up of material was in the form of a cap, restricted to the cutting edge of the tool (Fig. 3a). This view, taken normal to the flank, is typical of conditions along the cutting edges of tools used at speeds up to 300 ft/min. The height of the built-up cap is not constant along the cutting edge; similarly, the wear scar (outlined in Fig. 3a) is also irregular. The irregularity of the wear scar is more obvious in the optical micrograph of Fig. 3b, obtained in earlier experiments. Areas of the flank surface are visible which are almost completely devoid of a wear scar, but these are associated with pronounced built-up caps located on the cutting edge. It seems that these relatively unworn areas of the flank surface have been afforded almost continuous protection during machining; it is thought likely, therefore, that the built-up caps in such cases are virtually permanent in nature.



(a)



(b)

Fig. 1 Comparison of the effect of cutting speed on tool flank-wear rate and cutting forces when machining resulphurised and non-resulphurised low-carbon steels. Tool composition, 6% Co, 16% TiC, 73% WC, Tool rake 30°, tool clearance, 3°; undeformed chip thickness, 0.0055 in; Helical distance cut, 1500 ft.

At cutting speeds of more than 300 ft/min, a different form of material build-up appeared at discrete areas on the flank surface. The build-up consisted of a layer of material extending for a considerable distance perpendicular to the cutting edge (Fig. 3c). As the cutting speed was increased, this type of built-up layer became more extensive, until, at speeds of more than 550 ft/min, it covered almost the complete width of the flank. The wear scar itself also became more uniform in width at these cutting

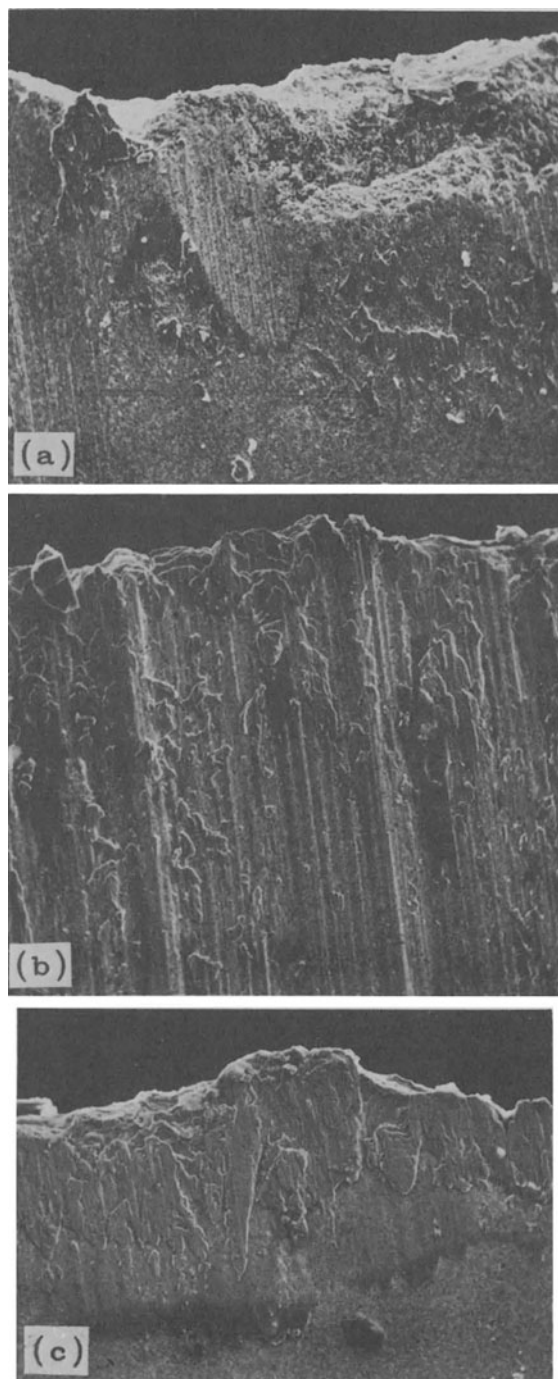


Fig. 2 Tool Flank Characteristics obtained when cutting non-resulphurized steel. Helical distance cut, 2000 ft.

- (a) (x200) Cutting speed 50 ft/min. Chipping of the cutting edge.
- (b) (x200) Cutting speed 300 ft/min. Showing the adherence to the tool flank of particles of material.
- (c) (x200) Cutting speed 700 ft/min. Typical built-up layer.

Comparison of flank wear of the two steels

It seems that the built-up cap established when machining the resulphurised material at low cutting speeds has a significant influence on the wear process on the tool flank. The rapid formation of the built-up cap when cutting this material protects the cutting edge from the chipping (Fig. 2a) which occurs when machining non-resulphurized steel at the lower cutting speeds. In Fig. 3d, the built-up cap has been carefully dislodged to reveal the cutting edge beneath, which is still relatively undamaged, even though the tool has machined a considerable quantity of material. Moreover, it was also observed that no particles had adhered to the flank surface of the tool, other than those which formed the built-up cap (see Fig. 3a). It is therefore suggested that in machining resulphurised steel, the presence of the built-up cap not only reduces the chipping of the cutting edge, but also decreases gradual wear on the flank. It is significant that at high cutting speeds, when built-up layers occur on the tool flanks with either steel, the flank wear rates were found to be approximately identical for the two steels. Thus, at these high cutting speeds, and in the conditions studied, resulphurisation seems to confer no advantage on machinability, as measured by tool flank wear rate.

The behaviour of the built-up layer and built-up cap on the tool flank when machining these two materials was also found to be reflected in the cutting force components. When machining the resulphurised steel at speeds of up to 300 ft/min, the values of the two force components, F_c and F_t , are both low compared with those obtained with the non-resulphurised steel (Fig. 1b). Both force components increased for the resulphurised steel with increasing cutting speed until, at about 700 ft/min, they had values similar to those obtained with non-resulphurised steel. The sudden increase in cutting force which occurred at about 300–400 ft/min coincides with the transition from the built-up cap formation to a built-up layer. Since throughout this range of cutting speed, the chip thickness and the rake face contact length remained substantially constant, the observed increase in the cutting force seems to be associated solely with this change on the tool flank. This also suggests that the built-up cap, when present, projects towards the workpiece and substantially reduces contact between the tool flank and the workpiece surface.

It is significant that in a detailed examination of the flank wear scar with an electron probe micro-analyser, no deposits of manganese sulphide were observed on the flank surface over the speed range in which there was a built-up cap on the cutting edge. This indicates that the reduction in wear rate at these speeds with resulphurised steel was not caused by manganese sulphide acting as an interfacial lubricant. When cutting at speeds at which a built-up layer formed on the tool flank, isolated deposits of manganese sulphide were observed in hollows in the built-up layer and in the surface discontinuities at the end of the layer furthest from the cutting edge. It is unlikely, however, that any potential of manganese sulphide to act as a lubricant influenced the wear rate at these speeds either, as the wear rates for both resulphurised and non-resulphurised steels became similar (Fig. 1a).

Workpiece surface characteristics

When machining resulphurised steel at cutting speeds at which a built-up cap was formed, the workpiece surface was characterized by the presence of many craters, with grooves emanating from them, ploughed into the surface (Fig. 4). The frequency with which these craters appeared corresponded closely to the frequency of occurrence of manganese sulphide inclusions in the steel; it was therefore thought that the craters were probably caused by the manganese sulphide inclusions. The material filling these craters was subsequently positively identified by the electron probe micro-analyser as manganese sulphide. The associated grooves were also seen to be smeared with manganese sulphide.

To study the mechanism of formation of these craters and grooves, specimens of the workpiece surface were mounted in bakelite and sectioned to show the manganese sulphide inclusions emerging onto the surface. The bakelite was then carefully removed and, utilizing the large depth of focus of the scanning electron microscope, both the sectioned surface and the workpiece surface were examined simultaneously. The typical inclusion shown in the photomicrograph (Fig. 5) has been plastically deformed in the direction of cutting. It has, however, eventually been fractured, a groove subsequently forming in the work surface. Some of these inclusions deformed less easily than others; some deformed in a brittle manner. In every case, however, a groove started from the point at which the inclusion reached the surface. This effect occurred at all cutting speeds although the built-up layer on the tool flank tended to provide a subsequent smoothing effect at higher speeds.

No evidence of similar craters or grooves could be found on the workpiece surfaces produced when machining non-resulphurised steel.

Rake face and chip underside characteristics

The scanning electron microscope was used to compare the under-surfaces of the chips produced when machining the resulphurised and non-resulphurised steels. The under-surfaces of chips of the former natural were much smoother when machined at the lower cutting speeds. This difference diminished considerably at speeds of more than 100 ft/min. The rake face contact lengths also became similar for both steels at the higher cutting speeds. Examination of the tool rake face after machining the resulphurised steel revealed several areas of manganese sulphide deposit, which were positively identified by the electron probe micro-analyser. The presence of such deposits probably contributes to the formation of the smooth chip under-surface. These deposits of manganese sulphide may or may not act as lubricant films.

In order to ascertain how manganese sulphide reaches the rake face, a series of chip cross-sections was examined in the optical microscope. We observed that at all cutting speeds, the inclusions in the secondary deformation zone were drawn out into long thin plates (Fig. 6a), although the degree to which this occurred depended on the cutting speed. At the lower speeds, the inclusions were not greatly deformed, but at more than 200 ft min⁻¹ the inclusions became progressively more drawn out. Frequently, the layer of

metal intervening between the thin inclusion plate and the tool face appeared to have fractured (Fig. 6b), allowing some slipping to occur within the inclusion plate, rather than at the chip-tool interface. In this situation, manganese sulphide could be in direct contact with the rake face, and could therefore give rise to the observed deposits. An increase in feed to 0.010 in./rev or a reduction in the rake angle to 20°

resulted in much thicker layers of manganese sulphide on the rake face (Fig. 7). Here, the deposit extends over almost the complete contact length. These observations are consistent with the idea that an increased contact pressure between chip and tool is likely to increase the deposition of manganese sulphide by pressing the drawn out inclusion (Fig. 6b) into more intimate contact with the rake face.

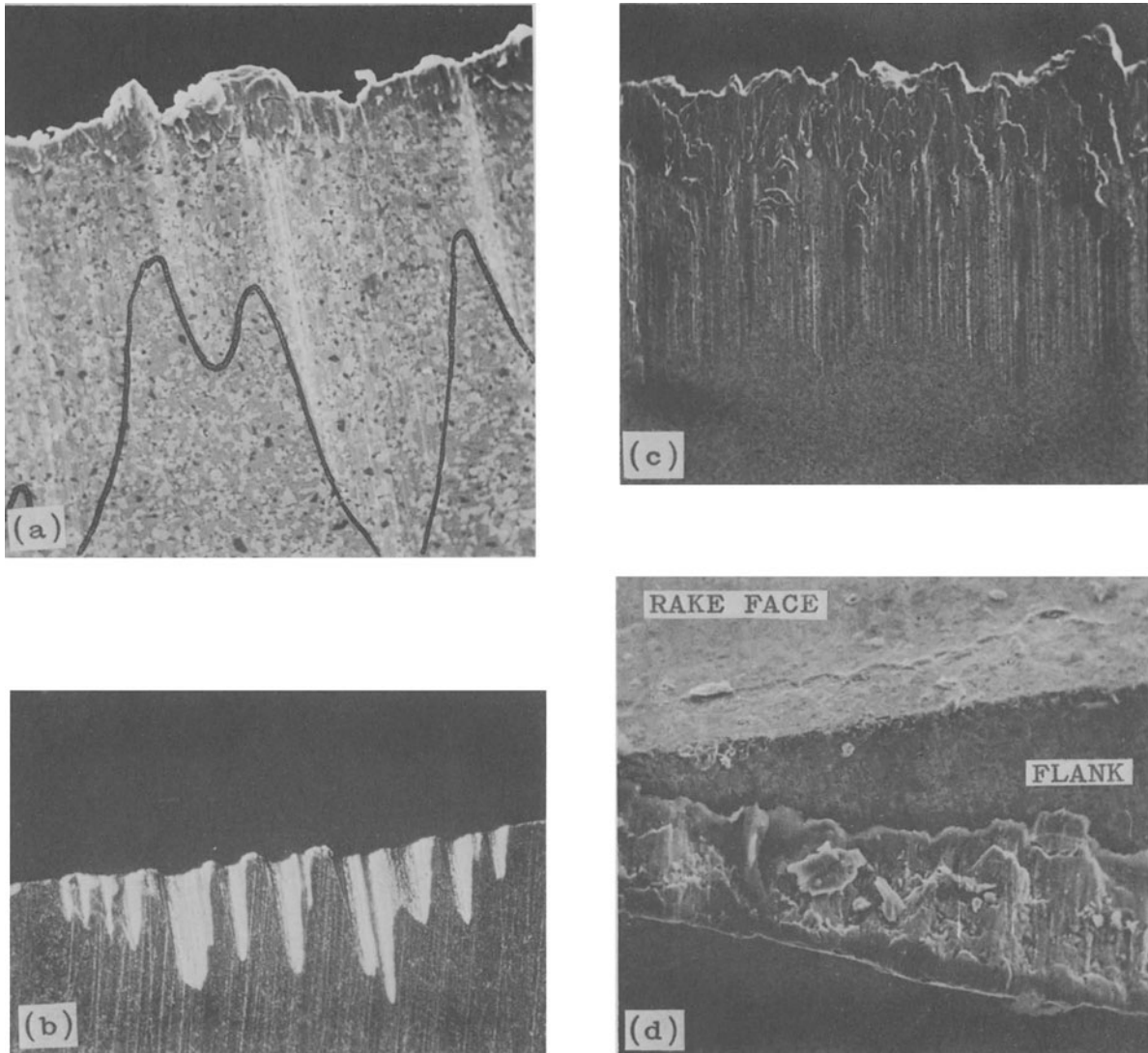


Fig. 3 Tool flank characteristics obtained when cutting resulphurised steel. Helical distance cut, 2000 ft.

(a) (x500) Cutting speed 50 ft/min. Typical built-up cap on the cutting edge of the tool with the wear scar outlined.

(b) (x25) Cutting speed 200 ft/min. Helical distance cut, 5000 ft.

Illustrating the irregular wear scar associated with built-up cap formation (optical photomicrograph).

(c) (x200) Cutting speed 400 ft/min. Built-up layer typical of those which begin to form at cutting speeds of more than 300 ft/min.

(d) (x500) Cutting speed 150 ft/min. Built-up cap dislodged from the cutting tool revealing the virtually undamaged cutting edge.

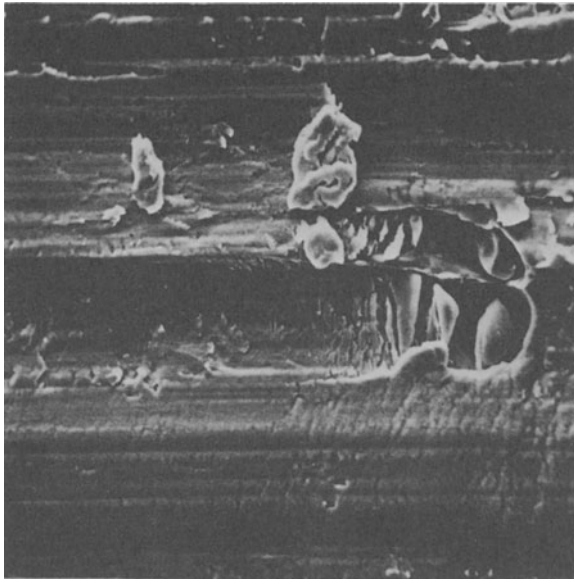


Fig. 4 (x1,000) Craters and associated grooves in the transient work surface when cutting resulphurized steel. Relative motion of the tool is from right to left.

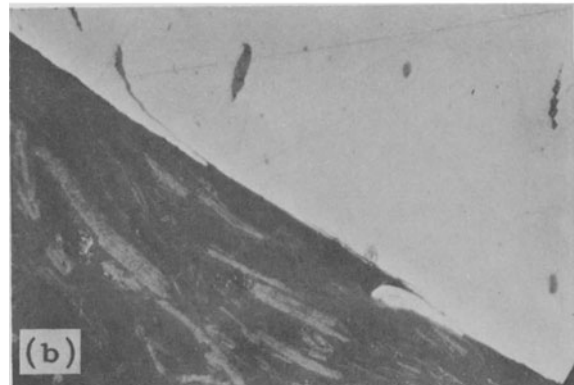
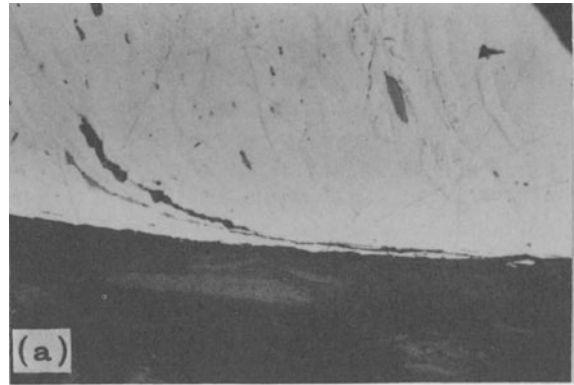


Fig. 6 Section through the undersurface of chips from resulphurized steel. Cutting speed 150 ft/min.

(a) (x600) Inclusions drawn out into long thin plates which are separated from the rake surface by a thin layer of metal.
 (b) (x600) The metal layer in this case has fractured and temporarily become attached to the tool, allowing the inclusion to come in contact with the rake surface.

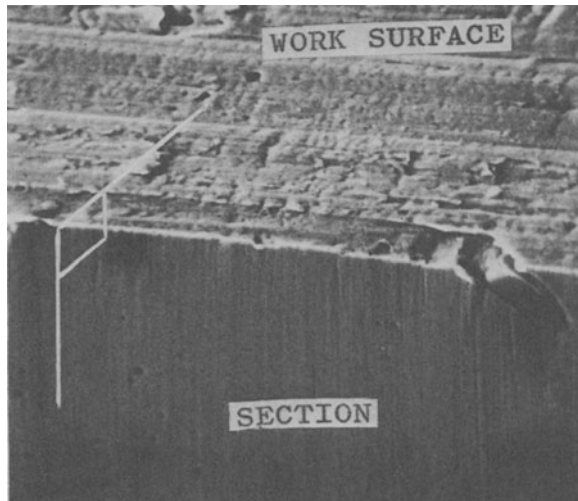


Fig. 5 (x560) Work surface and section through work surface showing groove starting from the point at which a deformed inclusion reaches the work surface. Relative motion of the tool is from right to left.

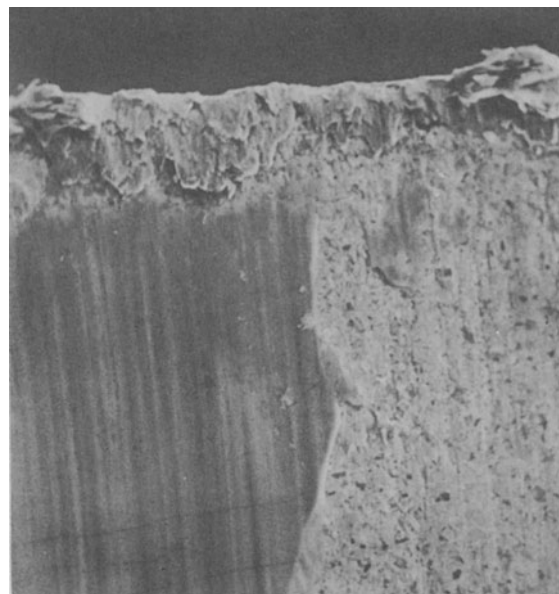


Fig. 7 (x500) Manganese sulphide deposit on the tool rake surface (the deposit has been removed towards the right). Cutting speed 400 ft/min. Undeformed chip thickness, 0.010 in/rev.

MECHANISM FOR THE PROMOTION OF BUILT-UP CAP FORMATION BY MANGANESE SULPHIDE INCLUSIONS

The most significant difference between the two steels appears to be the formation of a stable built-up cap when machining the resulphurised material. Fig. 8 illustrates a proposed mechanism for the promotion by manganese sulphide inclusions of the formation of this built-up cap structure on the tool. This mechanism offers an explanation of the various phenomena discussed which have been observed to be peculiar to the machining of resulphurised steel. Fig. 8a shows an inclusion which is in the path of the cutting edge of the tool. As it approaches the highly stressed area near the cutting edge, the inclusion is drawn out with the surrounding metal (Figs 8b and c) until only a very thin layer of metal separates it from the cutting edge. A velocity gradient will exist across the metal layer as one side will be retarded because of the friction force exerted by the tool, while the other side will move with the velocity of the drawn out inclusion. As the metal layer becomes drawn out further, it will become thinner and consequently the shear stress will increase at the interface between the layer and the inclusion. If the shear stress should exceed the shear strength of the inclusion, shear would occur at the inclusion. Fracture would eventually take place at the sides and ends of the thin metal layer as illustrated; this would leave the thin metal layer attached to the cutting edge, as shown in Fig. 8d. Successive repetitions of such a process would promote the formation of a built-up cap, each subsequent inclusion causing further thin metal layers to be deposited on the cutting edge, thus producing a built-up cap of laminar form. Eventually the cap would reach a critical size at which it would begin to break down. A state of equilibrium would occur in which the rate of breakdown balances that of build-up but, as only the outer layers have been observed to break away during cutting tests, the main body of the built-up cap is considered to be relatively stable.

Naturally, inclusions do not always approach the cutting edge as symmetrically as portrayed in Fig. 8 and many, while passing close enough to affect the formation of the built-up cap, would be carried away completely in either the chip or the workpiece. In such cases, only the relevant part of Fig. 8 would be operative. When there are no inclusions in the material, the formation of a built-up cap cannot be promoted in this way. No cap was observed when cutting non-resulphurised steel in the conditions of this test series.

CONCLUSIONS

(1) This investigation has clearly shown that, in the lower speed range of the machining conditions studied, the principal effect of adding manganese sulphide to low-carbon non-alloy steel is to cause a stable built-up cap to form on the cutting edge. Both resulphurised and non-resulphurised steel also produce built-up layers on the tool flank surfaces at

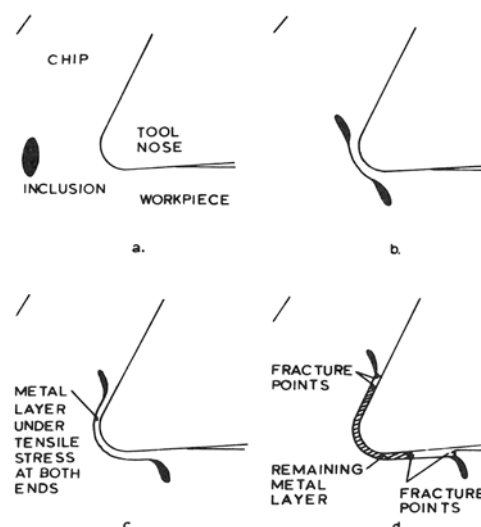


Fig. 8 The use of the scanning electron microscope to study the function of manganese sulphide inclusions in resulphurised free-machining steels.

W. J. Wilber and A. W. J. Chisholm

the higher cutting speeds studied.

(2) In the lower speed range, the resulphurised cutting forces compared with the non-resulphurised steel. At higher speeds, the differences tended to disappear and the value of adding manganese sulphide to the steel appears to be diminished.

(3) No deposits of manganese sulphide were observed on the tool flank surface when cutting at lower speeds, and only small isolated deposits were observed when cutting in the higher speed range.

(4) The evidence presented here seems to show that neither in the high nor the low cutting-speed ranges does manganese sulphide affect the flank-wear rate by acting as an interfacial lubricant.

(5) The under-surfaces of the chips produced by machining resulphurised steel were substantially smoother than those produced by machining non-resulphurised steel in the lower cutting-speed range. This was attributed to the formation of manganese sulphide films, which were identified on the tool rake face; these films do not necessarily act as a lubricant.

(6) The evidence presented suggests that these deposits of manganese sulphide are formed when the thin metal layers, which initially separate drawn out inclusions from the tool rake, are left attached to the cutting edge, allowing the inclusion material to come into intimate contact with the rake surface.

(7) Craters and associated grooves were formed on the transient workpiece surface when machining resulphurised steel as a result of the presence of manganese sulphide inclusions in the material.

(8) The reduction in tool-wear rate and cutting forces with resulphurised steel is attributed to the effect of manganese sulphide inclusions in forming a stable built-up cap, and a mechanism explaining the way in which manganese sulphide inclusions promote this formation has been proposed here.

REFERENCES

1. MOORE, C., 'The steelmakers approach to machinability,' MTDR Conf. No. 9, M.S.43 (1968).
2. MERCHANT, M. E., and ZLATIN, N., 'Basic reasons for good machinability of free machining steels,' *Trans. A.S.M.*, **41**, (1949), pp. 647-677.
3. BOULGER, F. W., LANKFORD, W. T., HARTNER, H. E., and GARVEY, T. M., 'Force relationships in machining low carbon steels,' *Trans. A.S.M.E.*, **79**, No. 5 (1957), pp. 1155-1164.
4. SHAW, M. C., USUI, E., and SMITH, P. A., 'Free machining steel: III. Cutting forces; Surface finish and chip formation,' *Trans. A.S.M.E.*, **B**, **83** (1961), pp. 181-193.
5. USUI, E., and SHAW, M. C., 'Free machining steel: IV. Tools with reduced contact length,' *Trans. A.S.M.E.*, **B**, **84** (1962), pp. 89-102.
6. TRENT, E. M., 'Metallurgical changes at the tool/work interface,' I.S.I. Special Report No. 94 (1965), pp. 77-88.
7. RICHARDSON, B. D., and CHISHOLM, A. W. J., 'A study of the effect of non-metallic inclusions on the machinability of two ferrous materials,' *Proc. Inst. Mech. Engrs.* Paper 18, (1965), pp. 129-142.
8. OATLEY, C. W., NIXON, W. C., and PEASE, R. F. W., 'Advances in electronics and electron physics,' **21** (Academic Press, New York, 1965).
9. THORNTON, P. R., 'Scanning electron microscopy,' (Chapman and Hall, 1968).
10. TRENT, E. M., 'Tool wear and machinability,' *J., Inst. Prod. Engrs.*, **38**, No. 3 (1959), pp. 105-130.
11. MARSTON, G. J., and MURRAY, J. D., 'Summary report on the machinability of low carbon free-cutting steels,' B.S.C. Internal Report, Ref. No. AM.5267/24/68/A (1968).
12. CHISHOLM, A. W. J., and McDOUGALL, D., 'Progress report on an experimental investigation into the effect of strain hardening on the mechanics of orthogonal cutting,' D.S.I.R., M.E.R.L. Plasticity Report No. 61 (1952).
13. WILBER, W. J., 'The effect of manganese sulphide inclusions on the mechanism of cutting and tool wear in the machining of low carbon steels,' PhD Thesis, University of Salford (1970).

DISCUSSION*Query from Dr G. Barrow, UMIST*

The author has assessed the performance of his cutting tools by considering wear rate and not some definite end point of tool life. This can be very misleading, since previous workers have shown that tool life is not always dependent on wear rate.

It is suggested that a protective cap is formed. Whilst this is undoubtedly true, both the forces and

contact length are reduced. In view of this the reduction in the temperature and stresses could explain the reduced wear rate.

Reply

The authors thank Dr Barrow for his comments and, in reply to his first point, acknowledge the fact that the rate of tool flank wear is not always an indication of tool life when machining certain materials. However, the results from preliminary tests carried out by the authors, together with the results from an earlier research programme⁷ indicated that, when machining resulphurised steel, the rate of tool flank wear was, in fact, indicative of total tool life and hence was an acceptable criterion for comparing the machinability of the two steels.

In considering the second point, the suggestion that the reduction in tool wear rate may be due to a reduction in the tool forces, contact length and hence temperature, is, of course, a valid one, but the results from an earlier research programme⁷ suggested that the presence of manganese sulphide inclusions in the steel resulted in temperature reductions in the region of only 100°F. It was considered that such a small reduction would not account for the substantial changes observed in tool flank wear rate.

Query from Dr M. G. Stevenson

The results are very interesting, particularly the relative absence of MnS film on the rake face. We agree with the small cap on the nose, but do not believe that this is the entire cause of the drop in forces in comparison with a plain carbon steel. Perhaps we should not yet dismiss the effect of the inclusions on shear flow stress. This effect may not exist in the primary zone, but could well exist in the secondary zone, where the deformations are far higher and cracking between inclusion/grain boundaries can occur. The resultant reduction in flow stress at the secondary zone can give the reduction in cutting forces found.

Reply

The authors appreciate the confirmation concerning the presence of the small cap on the nose of the cutting tool and agree that a reduction in the tool forces could also have been caused by the manganese sulphide inclusions causing a reduction in the shear flow stress in the secondary flow zone. Indeed, the mechanism for built-up cap formation outlined in the paper depends on preferential shear taking place within inclusions in this zone, and further work is being carried out in this field. It is, however, emphasised that the main beneficial effect of the cap is a reduction in tool flank wear rates, the reduction in tool forces being only a secondary effect.

ASSESSING MACHINABILITY FROM FUNDAMENTAL WORK MATERIAL PROPERTIES

by

W. F. HASTINGS, P. L. B. OXLEY and M. G. STEVENSON*

SUMMARY

We describe here a theory of machining which enables the stresses, forces and temperatures in machining to be predicted from fundamental work material properties and cutting conditions. We show how the predicted temperatures can be related to tool life.

INTRODUCTION

The aim of investigations into the mechanics of machining is to provide a theory which will enable parameters such as stress and temperature to be calculated from work material properties and such cutting conditions as speed and tool geometry. Such a theory would be very helpful in understanding machinability, as it would enable estimates of power consumption, and, more importantly, tool life, to be made from the calculated stresses and temperatures. The present trend to more sophisticated metal cutting machine tools, including the introduction of adaptive control, makes the need for a successful theory of machining even more pressing.

Although cutting tools (drills, reamers, milling cutters, and so on) can be very different in shape, the basic material removal process by a wedged shape cutting edge is always the same. Therefore, the basic mechanics of machining can be studied by considering cutting with a single straight cutting edge, and most researchers have done this. It is also usual to limit attention to the relatively simple case of orthogonal machining, in which the straight cutting edge is set parallel to the newly machined surface and normal to the cutting direction. If the depth of cut, t (Fig. 1), is small compared with its width then the process is approximately one of plane strain, which simplifies the plasticity theory used in the analysis. A further simplification is to consider only continuous chip formation (no cracks in the chip or built-up edge) where all parameters are constant with time. In this report only the idealized orthogonal process is considered, but it should be pointed out that a proper understanding of this will throw much light on machining in practical cutting conditions.

Investigations using cine filming techniques and quick-stop devices have shown that chip formation can be represented as shown in Fig. 1. The chip is formed by plastic deformation in a zone running

from the cutting edge to the work/chip-free surface. It leaves this zone curled, that is, there is a velocity gradient across the chip, and in order to contact the plane tool face, further plastic flow occurs in the chip adjacent to this face. The problem is to calculate the size and shape of the plastically deforming regions, the associated stresses, strains, strain-rates and temperatures, the thickness and curvature of the chip, and the length over which the chip and tool are in contact. The given conditions are the tool geometry, in this case the rake angle, α (Fig. 1), the depth of cut, t , the cutting speed and the appropriate properties of the work and tool materials. The problem as stated in this way has yet to be solved and all existing theories make some simplifying assumptions. The best known theories are based on the shear plane model of chip formation and will be briefly considered first.

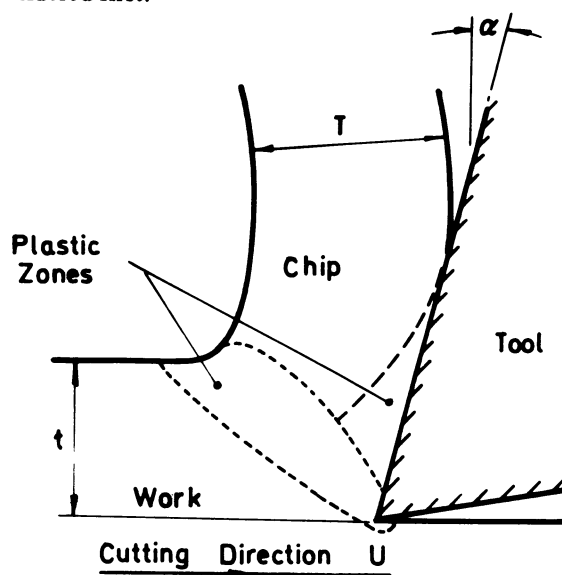


Fig. 1 Orthogonal chip formation.

*University of New South Wales, Australia

SHEAR PLANE THEORIES

In the shear plane model, the chip is assumed to be formed by shear along a straight shear plane, AB (Fig. 2); material approaches the shear plane AB with the work velocity U which is changed instantaneously at AB to the chip velocity V . There is no velocity gradient across the chip and the chip curl is neglected. The instantaneous change in velocity at AB requires a discontinuity in the tangential velocity along AB which is only permissible if the work material is assumed to be rigid-plastic and to deform with constant flow stress. This limitation therefore applies to analyses based on the shear plane model.

For a given depth of cut t (Fig. 2) and rake angle α , it is clear that the geometry of Fig. 2 cannot be completed unless either the chip thickness, T , or shear angle ϕ (the angle between the shear plane AB and the cutting direction) is known. Without a knowledge of ϕ (or T) no estimate of cutting forces and so on can be made. There have been many attempts to predict ϕ in terms of known parameters, the best known of which in the literature are those due to Ernst and Merchant^{1,2}.

The shear plane AB is a direction of maximum shear strain rate (it is infinite in this direction as a result of the velocity discontinuity) and therefore from plasticity theory it can be assumed that, for an isotropic material, AB will also be a direction of maximum shear stress. Ernst and Merchant¹ made use of this in the following way. They considered the equilibrium of the chip under the action of the force system shown in Fig. 3. The tool is assumed to be perfectly sharp and the resultant cutting force, R , is transmitted by the tool-chip interface and the shear plane AB. R can be resolved into various sets of components (Fig. 3): F and N are the frictional and normal forces at the tool-chip interface, F_S and F_N are the shear and normal forces on AB, and F_C and F_T are the cutting forces in the cutting direction and normal to this direction. Frictional conditions at the tool-chip interface are represented by a mean angle of friction, λ , with $\tan \lambda = F/N$. By means of this force diagram and the geometry of Fig. 2, the shear stress along AB was expressed in terms of cutting forces, rake angle α (Fig. 2), friction angle λ and shear angle ϕ . ϕ was then selected to make AB a direction of maximum shear stress, which gave

$$\phi = \frac{\pi}{4} + \frac{\alpha}{2} - \frac{\lambda}{2} \quad (1)$$

Merchant² later derived this same equation by selecting ϕ to make the work done in machining a minimum.

Another well-known equation was derived by Lee and Shaffer³ who by applying ideal plasticity theory (in which the flow stress is assumed constant) and making other simplifying assumptions, showed that

$$\phi = \frac{\pi}{4} + \alpha - \lambda \quad (2)$$

For a given value of $(\lambda - \alpha)$ both equations (1) and (2) give a single value of ϕ . Experimental values of ϕ ,

calculated for measured values of chip thickness T , from the equation

$$\tan \phi = \frac{t/T \cos \alpha}{1 - t/T \sin \alpha} \quad (3)$$

which is derived from the geometry of Fig. 2, and λ , calculated for measured cutting forces, from the equation

$$\tan (\lambda - \alpha) = \frac{F_T}{F_C} \quad (4)$$

are given in Fig. 4. These show that ϕ can vary over a wide range even for a constant value of $(\lambda - \alpha)$.

There have been a number of attempts to modify both equations (1) and (2) in order to obtain better agreement with experimental results, the most notable of which was by Merchant² himself. In deriving equation (1) he had assumed that the shear strength along the shear plane was independent of the normal stress on this plane. By taking the possible dependence of shear strength on normal stress into account, Merchant obtained the equation

$$2\phi = C' + \alpha - \lambda \quad (5)$$

where C' is a constant for a given material and represents the dependence of the shear strength on the normal stress. By varying C' better agreement can be obtained between theory and experiment. Unfortunately the variation of shear strength with normal stress required to satisfy cutting data is too large. Kobayashi and Thomsen⁴ introduced the concept of effectiveness, which is essentially a measure of the departure from the minimum energy solution of Merchant [equation (1)]. An effectiveness value of unity corresponds to equation (1) and smaller values of effectiveness give a lower value of ϕ for a given value of $(\lambda - \alpha)$ than equation (1). By choosing suitable values of effectiveness it is possible to satisfy any experimental value of ϕ . Although useful in collating experimental data (for example, it seems that effectiveness is constant for a given material and cutting speed) the value of the analysis is limited by the lack of any obvious fundamental relationship between effectiveness and work material properties or cutting speed.

The simplified shear angle problem has clearly not been satisfactorily solved. Indeed, it seems that the shear plane model of chip formation is too far removed from actual chip formation to allow a successful solution. Experiments show that the cutting process is very dependent on the cutting speed but, except for associated variations in friction angle λ , speed is not taken into account in shear angle solutions. If instead of basing the analysis on the shear plane model of chip formation, a finite shear zone is considered, then cutting speed can be introduced into the analysis in terms of the strain-rate in the shear zone. It is then possible to take those material properties which are strain-rate dependent into account.

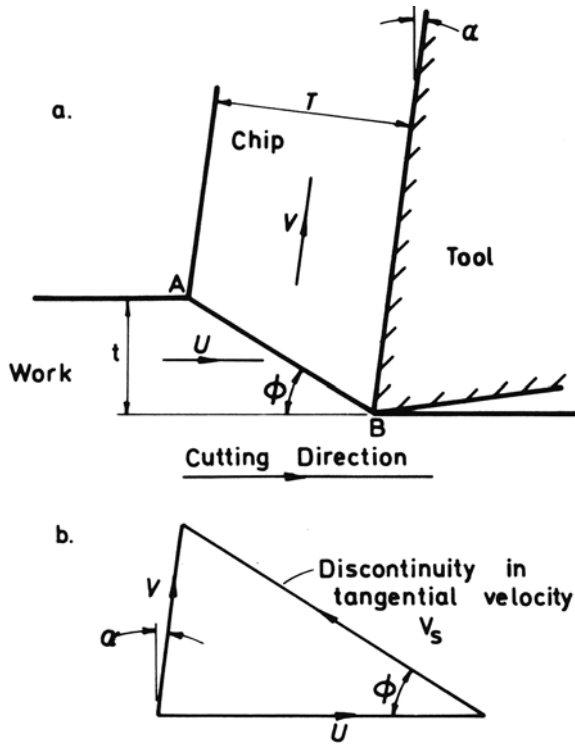


Fig. 2 Shear-plane model.
a. Cutting geometry
b. Velocity diagram

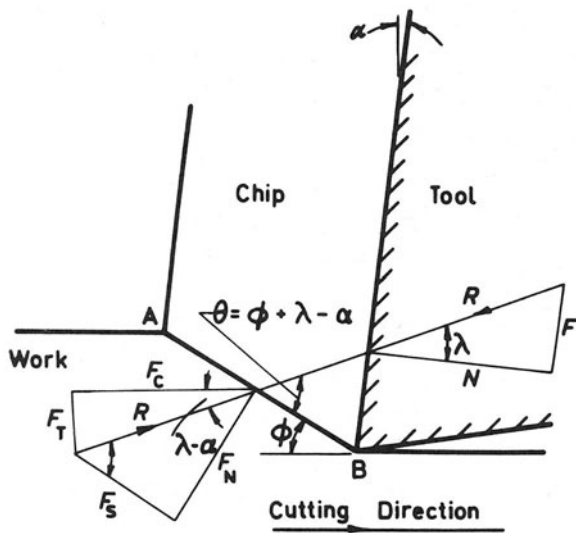


Fig. 3 Force diagram.

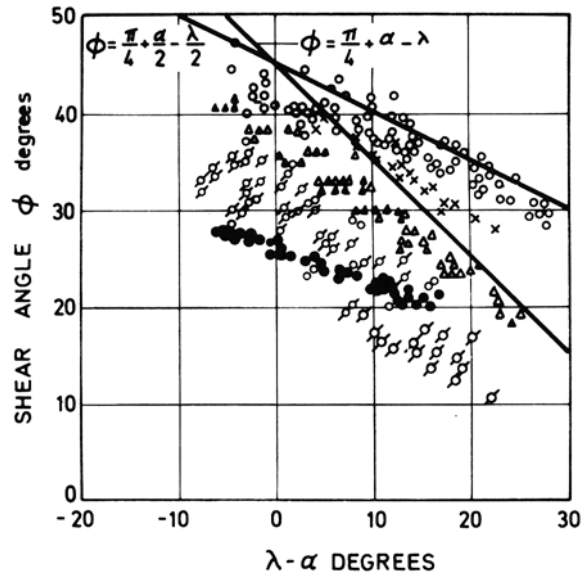


Fig. 4 Experimental shear angle and mean friction angle results.

- 2024-T4 aluminium alloy
- × 6061-T6 aluminium alloy
- △ SAE 1112 steel (as received)
- ◇ SAE 1112 steel (annealed)
- alpha brass

SHEAR-ZONE THEORY

Oxley and Welsh⁵ noted that the assumptions of the shear-plane model meant that no account could be taken of the work material's flow stress characteristics, such as strain hardening, or the influence of strain rate (cutting speed) on these characteristics. To overcome this problem, they introduced a parallel-sided shear-zone model (Fig. 5) in which the work velocity changes to the chip velocity through a finite zone CDEF with no discontinuities in velocity and a finite, calculable, strain rate within the zone. The work material is still assumed to be rigid-plastic and isotropic with CD, AB and EF the directions of maximum shear strain-rate and maximum shear stress. The overall geometry of the shear-zone model (Fig. 5) is the same as for the shear-plane model with the centre shear line AB equivalent, geometrically, to the shear plane; chip curl is again neglected. The force diagram (Fig. 3) is equally applicable to the shear-zone model.

By considering the stress distribution along AB (Fig. 5) and the direction of the resultant cutting force it can be shown⁶ that

$$\tan \theta = 1 + 2 \left(\frac{\pi}{4} - \phi \right) - \frac{k_{EF} - k_{CD}}{2 k_{AB}} \frac{l}{\Delta s_1} \quad (6)$$

where θ (Fig. 5) is the angle made by the resultant cutting force with AB; ϕ is the shear angle; k_{CD} , k_{AB} and k_{EF} are the shear flow stresses along CD, AB and EF; and l and Δs_1 are the length and width of the shear zone. From geometry

$$\theta = \phi + \lambda - \alpha \quad (7)$$

where λ is the mean angle of friction as previously defined and α is the tool rake angle. The total shear strain occurring in the shear zone is given by

$$\gamma_{EF} = \frac{\cos \alpha}{\sin \phi \cos (\phi - \alpha)} \quad (8)$$

and the mean (maximum) shear-strain rate by

$$\dot{\gamma}_{SZ} = \frac{0.2U \cos \alpha}{\Delta s_1 \cos (\phi - \alpha)} \text{ s}^{-1} \quad (9)$$

where U is the cutting speed in ft/min and Δs_1 is measured in inches.

Equations (6) to (9) are sufficient to calculate the shear angle ϕ for given values of λ , α and U if the flow stress characteristics of the work material and the width Δs_1 of the shear zone are known. Conversely, the theory can be used together with cutting data to calculate the flow stress characteristics of the work material at very high strain rates.

The qualitative success of this theory can be demonstrated by considering the experimental results in Fig. 4 and the stress/strain curves for the corresponding work materials (Fig. 6). Assuming that the stress/strain curve of a work material is approximately linear, equation (6) can be written in the form

$$\tan \theta = 1 + 2 \left(\frac{\pi}{4} - \phi \right) - \frac{m \gamma_{EF}}{2 k_{AB}} \frac{l}{\Delta s_1} \quad (10)$$

where m is the slope of the shear stress/shear strain curve. It follows from this equation that large values of m/k_{AB} yield small values of θ and therefore, from equation (7), small values of ϕ . Table 1 gives values of this parameter estimated from the stress/strain curves in Fig. 6 and it can be seen (Fig. 4) that materials with large values of m/k_{AB} do machine with small values of ϕ .

Table 1

Material	m/k_{AB}
SAE 1112 steel (as received)	0.14
2024-T4 aluminium alloy	0.10
SAE 1112 steel (annealed)	0.25
6061-T6 aluminium alloy	0.11
Alpha brass	0.42

This comparison is only qualitative because the stress/strain curves are from 'static' (low strain-rate) tests and the machining results are for very high

strain-rates and temperatures. The quantitative success of the theory in accounting for the influence of strain-rate and temperature has been described in a series of recent papers.⁶⁻¹⁰ The next section considers a re-analysis of Merchant's² results in terms of the new theory.

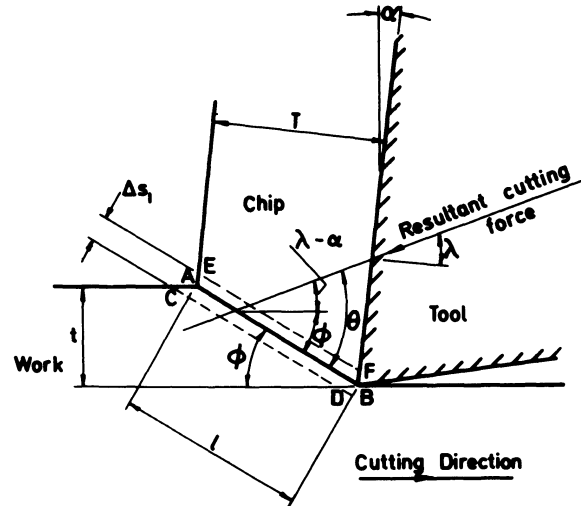


Fig. 5 Shear-zone model.

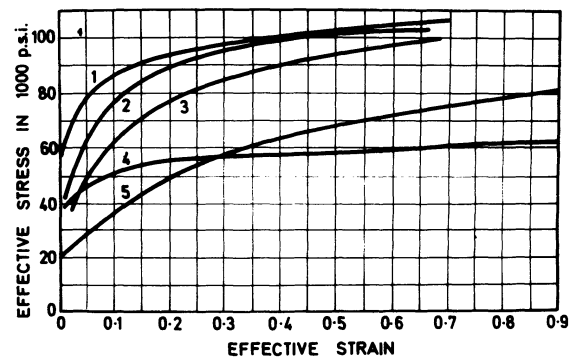


Fig. 6 Stress/strain curves for materials in Fig. 4.

- 1 SAE 1112 steel (as received)
- 2 2020-T4 aluminium alloy
- 3 SAE 1112 steel (annealed)
- 4 6061-T6 aluminium alloy
- 5 alpha brass

MODIFIED SHEAR-ZONE THEORY

Experimental measurements of strain-rate along streamlines⁹ have shown that the maximum value of maximum shear strain-rate occurs very close to the plane defined by AB (Fig. 5) with $\dot{\gamma}_{AB}$ given by

$$\dot{\gamma}_{AB} = \frac{C V_S}{l} \text{ s}^{-1} \quad (11)$$

where V_S (in. s⁻¹) is the shear velocity which is equal to the velocity discontinuity as shown in Fig. 2, l (in.) is the length of AB and C is a constant for a given material. The distributions of strain-rate also show

that approximately half the total strain in the chip has occurred at AB, with $\dot{\gamma}_{AB}$ given by

$$\dot{\gamma}_{AB} = \frac{1}{2} \frac{\cos \alpha}{\sin \phi \cos (\phi - \alpha)} \quad (12)$$

where ϕ (Fig. 5) is the shear angle and α the tool rake angle. If now the flow stress characteristics of the work material are expressed by the well-known linear log stress/log strain relationship

$$\sigma = \sigma_1 \epsilon^n \quad (13)$$

where σ_1 and n are constants defining the stress/strain curve for given strain-rates and temperatures, it can be shown¹⁰ that equation (10) reduces to

$$\tan \theta = 1 + 2 \left(\frac{\pi}{4} - \phi \right) - Cn \quad (14)$$

where C and n are the constants in equations (11) and (13) respectively. For given values of α and λ (mean friction angle), equations (7) and (14) can be used to calculate ϕ , as long as C and n are known, and the corresponding forces can be found if the shear stress along AB is known. The strain-rate results⁹ show that for a low-carbon steel, C is equal to 5.9, and in analysing Merchant's machining results which are for a steel with a somewhat higher carbon content this value will be assumed to be still applicable. A reverse analysis of Merchant's machining results in which the above theory is used to calculate σ_1 and n yields the relationships

$$\begin{aligned} \sigma_1 &= 61.31 + 21.91 \log \dot{\epsilon} \\ n &= 0.246 - 0.041 \log \dot{\epsilon} \end{aligned} \quad (15)$$

where σ_1 is in units of 1000 lb in⁻² and ϵ in units of s⁻¹. The range of $\dot{\epsilon}$ over which these equations apply is 10⁴–10⁵ s⁻¹. It should be noted that equations (15) do not include a temperature term. This means that for the conditions considered, temperature effects were negligible compared with strain-rate effects. But, had a wider range of conditions been considered which could, for example, have included pre-heating of the work, then temperature effects would have had to be included. It would have been preferable if equations (15) had been obtained other than from machining tests as their use to predict machining results would then have been more convincing. Until recently, however, independent tests, such as high speed compression and tension tests, were not possible at strain-rates equal to those in machining. Some recent results¹¹ on low-carbon steel obtained other than by machining tests are encouraging as they not only confirm the trends of equations (15) but also give good quantitative agreement with them.

For given values of α , t (depth of cut, in.), U (cutting speed, ft min⁻¹) and λ , the shear angle ϕ and corresponding cutting forces can be found as follows. A reasonable estimate is made of the value of ϕ , and V_S ($V_S = 0.2 U \cos \alpha / \cos (\phi - \alpha)$) and l ($l = t / \sin \phi$) calculated and substituted into equation (11) to give

$\dot{\gamma}_{AB}$. The corresponding value of n is then found from (15) (note $\dot{\epsilon}_{AB} = \dot{\gamma}_{AB} / \sqrt{3}$) and substituted in equation (14) to give θ which is then used in equation (7) to give λ . This process is repeated by varying ϕ until the value of λ obtained agrees with the given value. Having found ϕ , the cutting forces in the direction of cutting (F_C) and normal to this direction (F_T) are calculated from the equations

$$\begin{aligned} F_C &= \frac{t w k_{AB} \cos (\lambda - \alpha)}{\sin \phi \cos (\phi + \lambda - \alpha)} \\ F_T &= \frac{t w k_{AB} \sin (\lambda - \alpha)}{\sin \phi \cos (\phi + \lambda - \alpha)} \end{aligned} \quad (16)$$

where k_{AB} is the shear flow stress along AB and w is the width of cut. k_{AB} ($k_{AB} = \sigma_{AB} / \sqrt{3}$) is found from (13) and (15) using the appropriate value of ϵ_{AB} ($\epsilon_{AB} = \dot{\gamma}_{AB} / \sqrt{3}$) found from equation (12) with $\dot{\epsilon}_{AB}$ as before. Values of ϕ and cutting forces found in this way are within $\pm 5\%$ of Merchant's experimental values.

In practice, the mean friction angle λ cannot be taken as given information as it cannot be measured independently of machining tests and is found to vary widely with changes in cutting conditions. A more useful method in which the friction is described by the shear strength in the chip material along the tool-chip interface has recently been developed, and is briefly as follows: the magnitude and direction of the resultant force transmitted by AB are calculated for a range of values of ϕ as described above. Its position can also be calculated by taking moments of the stresses along AB about B. It is then assumed that the tool is perfectly sharp and that the tool-chip interface transmits the same resultant as AB, which is therefore known in magnitude, direction and position. If the distribution of normal stress at the tool-chip interface is assumed to be triangular, with the maximum value at the cutting edge, it is possible to calculate the length of tool-chip contact and also the mean shear stress τ_{INT} along this length. Typical values of shear stress found in this way for a range of values of ϕ are given by the full line in Fig. 7. We presume that actual values of ϕ will fall on the curve to the right of the maximum point as then any decrease in shear stress at the interface brought about by, say, lubrication, will increase ϕ as is observed in practice.

To find the actual value of ϕ , the chip strength at the interface is considered as a function of temperature and strain-rate (the influence of changes in strain being negligible in this region) with the shear flow stress k_{CHIP} for Merchant's material given by

$$k_{CHIP} = 111 - 0.144 \theta_{MOD} \quad (17)$$

where the units of k_{CHIP} are 1000 lb in⁻² and θ_{MOD} ($340 < \theta_{MOD} < 560$) is the velocity-modified temperature which is given in this case by

$$\theta_{MOD} = \theta_{INT} (1 - 0.145 \log \dot{\gamma}_{INT}) \quad (18)$$

where θ_{INT} ($^{\circ}\text{K}$) is the mean absolute temperature at the tool–chip interface and γ_{INT} (s^{-1}) is the shear strain-rate at the interface. θ_{INT} is calculated from the equation

$$\theta_{INT} = \theta_W + \theta_{SZ} + \frac{\theta_I}{2} \quad (19)$$

where θ_W is the initial work temperature, and θ_{SZ} and θ_I are the temperature increases in the shear zone and along the tool–chip interface, respectively. By considering the plastic work in the shear zone it can be shown that

$$\theta_{SZ} = \frac{(1-\beta)}{12J\rho St} \left[\frac{F_C}{w} - \frac{\tau_{INT} h \sin \phi}{\cos(\phi-\alpha)} \right] \quad (20)$$

where β is the proportion of heat conducted into the work, J is the mechanical equivalent of heat (ft lb/C h u), ρ is the density of the work material (lb in^{-3}), S is its specific heat (C h u/lb $^{\circ}\text{C}$), h is the length of tool–chip contact and all other terms are as before. β is calculated from the empirical equations

$$1 - \beta = 0.4, \text{ if } R_T \tan \phi < 0.5 \quad (21)$$

$$1 - \beta = 0.5 + \frac{0.5}{\log 40} \log (R_T \tan \phi)$$

if $0.5 < R_T \tan \phi < 40.0$ and $1 - \beta = 1.0$ if $R_T \tan \phi > 40.0$, where $R_T = 720 \rho S U t / K$ is a thermal number with K the thermal conductivity (C h u/in. h $^{\circ}\text{C}$). By considering the work done at the tool–chip interface and making some simplifying assumptions it can be shown that

$$\theta_I = \frac{1.13 \tau_{INT}}{J} \left[\frac{5 U h \sin \phi}{\rho S K \cos(\phi-\alpha)} \right]^{1/2} \quad (22)$$

In calculating temperatures the following properties are assumed; $\rho = 0.26 \text{ lb in.}^{-3}$; $S = 0.26 \text{ C h u/lb } ^{\circ}\text{C}$; $K = 2.1 \text{ C h u/in. h } ^{\circ}\text{C}$; $J = 1400 \text{ ft lb/C h u}$. The shear strain-rate at the interface is calculated from the empirical equation

$$\gamma_{INT} = \frac{10}{T} \left(\frac{12V}{60} \right) \text{ s}^{-1} \quad (23)$$

where V is the chip velocity (ft min^{-1}) and T is the chip thickness (in.). To find the solution for ϕ for given cutting conditions, equations (17)–(23) are used to calculate k_{CHIP} for the same range of values of θ as used in calculating τ_{INT} (Fig. 7). The results for k_{CHIP} found in this way are given by the broken line in Fig. 7. The solution is taken as the intersection point of the two curves, as at this point the resolved shear stress τ_{INT} is equal to the value of k_{CHIP} given by the corresponding temperature and strain-rate, the process being in equilibrium. When this intersection occurs to the left of the maximum point of the τ_{INT}

curve as in Fig. 7b, the solution is taken as the maximum point and the tool–chip interface is no longer a direction of maximum shear stress. In considering Merchant's results, only two intersections were to the left of the maximum.

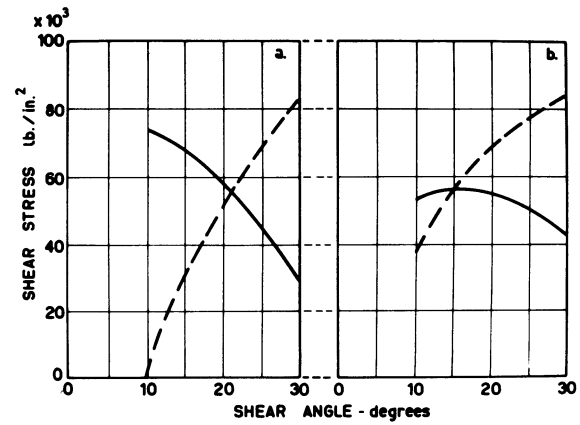


Fig. 7 Curves of τ_{INT} (full line) and k_{CHIP} (broken line) showing method of solution for ϕ .

RESULTS AND DISCUSSION OF RESULTS

Values of ϕ calculated as above for Merchant's cutting conditions are given in Fig. 8a and b together with the corresponding values of mean friction angle λ found from equation (7). Values of cutting force F_C calculated from (16) are given in Figs. 9a and b and values of cutting horse-power calculated from the equation

$$\text{H.P.} = \frac{F_C U}{33\,000} \quad (24)$$

where F_C is in lb and U in ft min^{-2} , appear in Fig. 9c.

The predicted values of ϕ , λ , F_C and cutting horse-power can be seen to be in excellent agreement with Merchant's experimental results. The theory successfully predicts that an increase in cutting speed (Fig. 8a), depth of cut (Fig. 8b) or rake angle (Figs. 8a and b), will increase ϕ and that an increase in cutting speed and depth of cut and a decrease in rake angle will decrease λ . The decrease in λ with increase in depth of cut (Fig. 8b), which is a somewhat surprising result, can be explained as follows. The increase in depth t increases the chip thickness T without seriously changing the chip velocity V , thus reducing γ_{INT} (equation 23), and also increasing θ_{INT} . Both these changes increase θ_{MOD} (18) and thus reduce k_{CHIP} (17) and with this lower frictional resistance, λ decreases. The theory also predicts that an increase in cutting speed, a decrease in depth of cut or an increase in rake angle will reduce the cutting force F_C , as shown in Figs. 9a and b, and the experimental results confirm this. The predicted decrease in horse-power with increase in rake angle (Fig. 9c) is also confirmed experimentally.

Fig. 10 gives the results of the temperature calcul-

ations and shows that both the shear zone and interface temperatures increase with an increase in cutting speed and decrease with an increase of rake angle. No experimental values of temperature are available for Merchant's tests for comparison, but the trends are similar to those obtained experimentally by others. Tool life is known from experimental studies to be very dependent on the temperature of the cutting edge. For example, the results of Takeyama and Murata¹² suggest a relationship of the form

$$L = A(\theta_T)^M \quad (25)$$

where L is the tool life (defined as the life for 0.024 in flank wear), θ_T is the average temperature of the

tool (measured by a tool-work thermojunction), and A and M are constants for a given tool material. Considering these temperature results (Fig. 10) in conjunction with equation (25) it is possible to derive an approximate relationship between tool life and cutting speed. When machining a heat resistant alloy steel with an I.S.O. P10 carbide, Takeyama and Murata's results give

$$L = 72 \theta_T^{-23} \quad (26)$$

where L is in minutes and θ_T in degrees K. Substituting the values of θ_{INT} for $\alpha = -10^\circ$ (Fig. 10) into equation (26) gives the result indicated by the full line in Fig. 11. It is interesting to note that the equation of this line is

$$U^{4.9} L = 10^{15.4} \quad (27)$$

which transforms into the usual form of the Taylor tool-life equation giving

$$UL^{0.2} = 1340 \quad (28)$$

where 1340 is the cutting speed in ft min^{-1} for a 1 min tool life. The temperature exponent in equation (26) seems to be rather large and a value of -10.0 (equivalent to a decrease in the temperature sensitivity of the tool) results in the exponent of equation (28) becoming 0.5. This range of values for the exponent (that is, 0.2–0.5) is often quoted for carbide tools.

We now have a system of equations which allow us to investigate the effects of variations in work material properties such as σ_1 and n on tool life. Allowing σ_1 to vary by $\pm 10\%$, which roughly corresponds with the 'as received' range of hardness values for a given steel, we obtain the two dotted lines in Fig. 11. Taylor¹³ in an experimental investigation of tool life found a residual variance in $\log(\text{tool life})$ of 0.0049. Assuming a reasonable number of tool-life observations (say about twenty) this residual variance can be shown to be roughly equal to a variation of ± 0.15 in $\log(\text{tool life})$ at the 95% confidence level. An examination of the plotted results in Fig. 11 shows a variation of approximately ± 0.16 in $\log(\text{tool life})$ at constant cutting speed. It therefore seems that variations in σ_1 (hardness) could be responsible for the variations in tool life observed in practice. The theory is now being used to investigate the influence on tool life of variations in other work material properties, including the thermal properties.

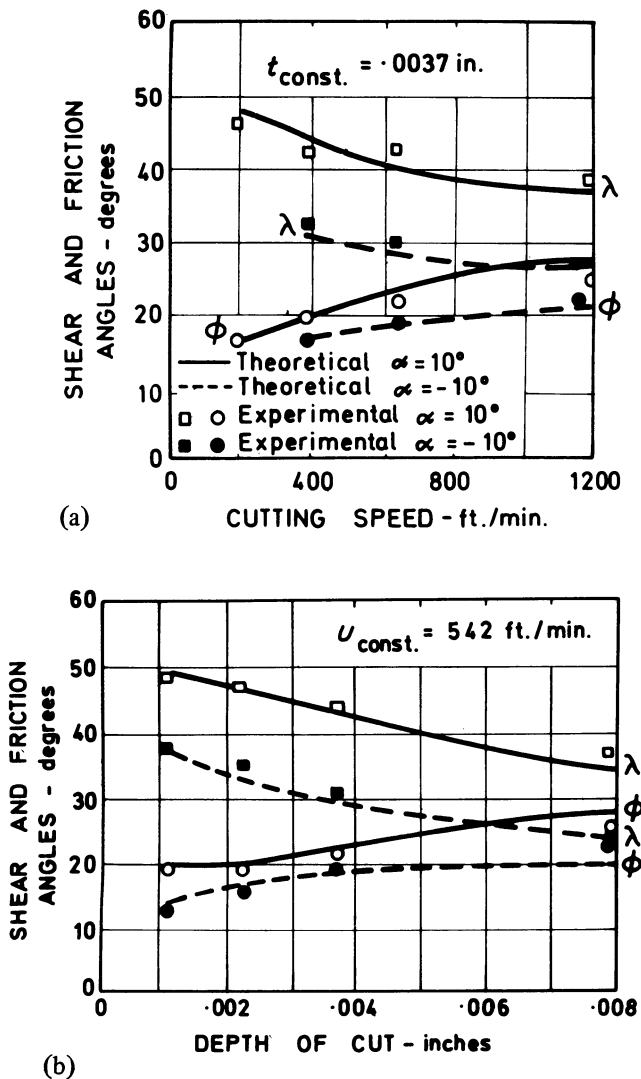
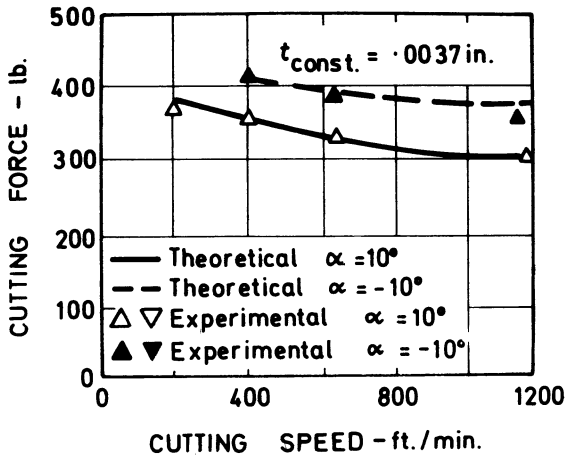
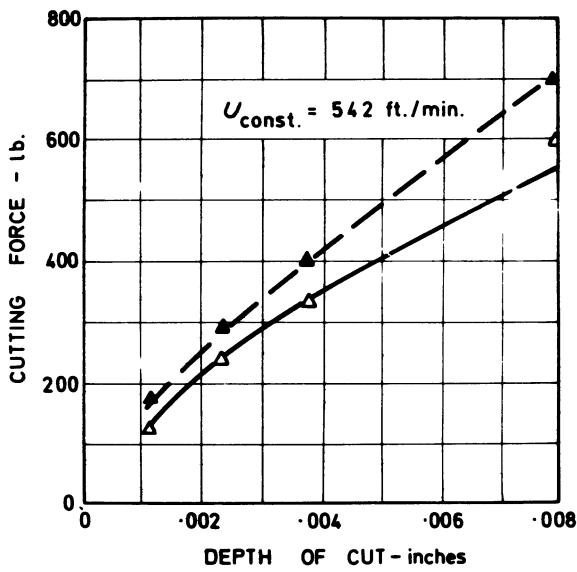


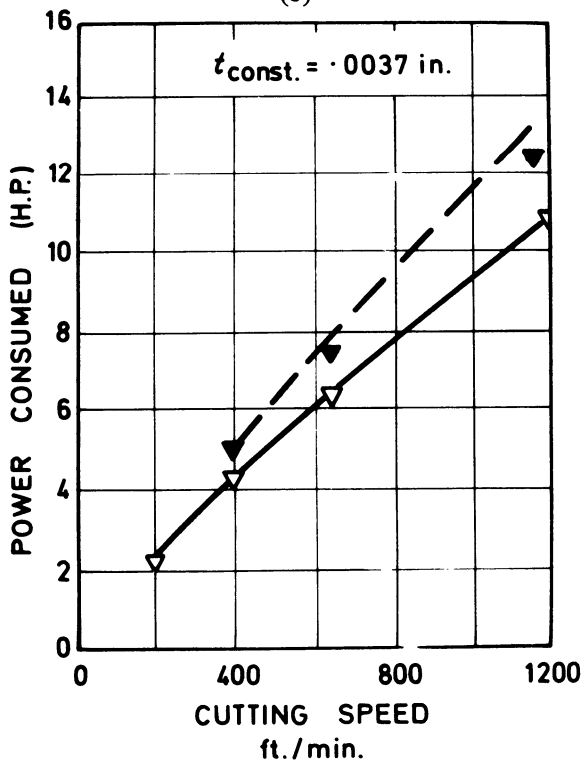
Fig. 8 Comparison of predicted and experimental shear and friction angles.



(a)



(b)



(c)

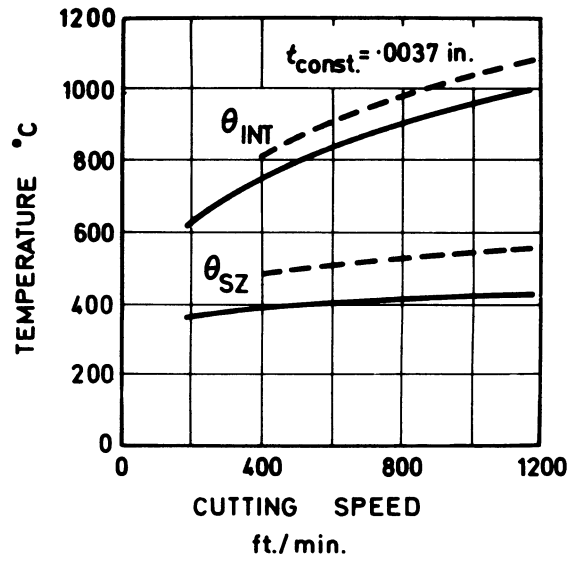


Fig. 10 Calculated shear zone and interface temperatures.

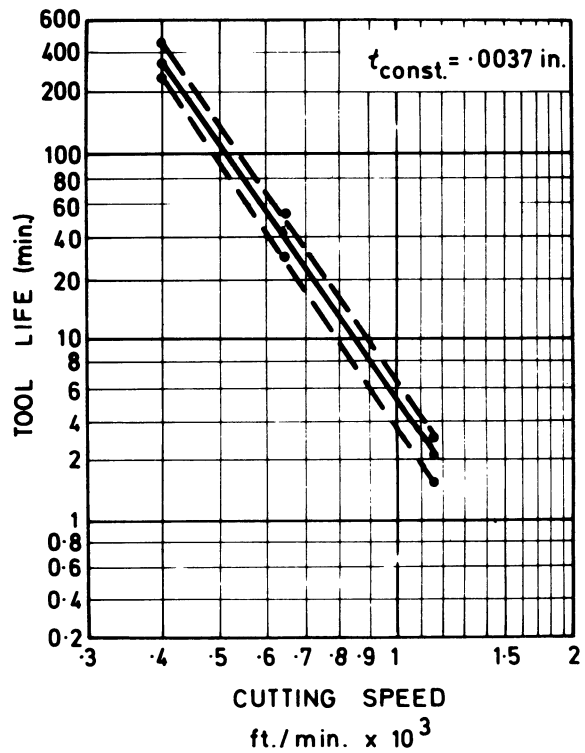


Fig. 11 Tool life/cutting speed graph.

Fig. 9 Comparisons of predicted and experimental cutting forces and power consumption.

REFERENCES

1. ERNST, H., and MERCHANT, M. E., 'Chip formation, friction and high quality machined surfaces,' *Surface Treatment of Metals*, American Society of Metals (1941), p. 229.
2. MERCHANT, M. E., 'Mechanics of metal cutting process,' *J. Appl. Phys.*, **16** (1945), p. 267.
3. LEE, F. H., and SHAFFER, B. W., 'Theory of plasticity applied to a problem of machining,' *J. Appl. Mech.*, **18**, (1951), p. 405.
4. KOBAYASHI, S., and THOMSON, E. G., 'Metal cutting analysis—II New parameters,' *Trans. ASME* (1961).
5. OXLEY, P. L. B., and WELSH, M. J. M., 'Calculating the shear angle in orthogonal metal cutting from fundamental stress/strain/strain-rate properties of the work material,' Proc., 4th Intern. MTDR Conf. (1963).
6. FENTON, R. G., and OXLEY, P. L. B., 'Mechanics of orthogonal machining: allowing for the effects of strain-rate and temperature on tool-chip friction,' *Proc. Inst. Mech. Engrs.*, **183** (1968–69), p. 417.
7. FENTON, R. G., and OXLEY, P. L. B., 'Mechanics of orthogonal machining: predicting chip geometry and cutting forces from work-material properties and cutting conditions,' *Proc. Inst. Mech. Engrs.*, **184** (1969–70), p. 927.
8. OXLEY, P. L. B., and STEVENSON, M. G., 'Measuring stress/strain properties at very high strain-rates using a machining test,' *J. Inst. Met.*, **95** (1967), p. 308.
9. STEVENSON, M. G., and OXLEY, P. L. B., 'An experimental investigation of the influence of speed and scale on the strain-rate in a zone of intense plastic deformation,' *Proc. Inst. Mech. Engrs.*, **184** (1969–70), p. 561.
10. STEVENSON, M. G., and OXLEY, P. L. B., 'An experimental investigation of the influence of strain-rate and temperature on the flow stress properties of a low carbon steel using a machining test,' *Proc. Inst. Mech. Engrs.*, **185** (1970–71), p. 741.
11. CAMPBELL, J. D., and FERGUSON, W. G., 'The temperature and strain-rate dependence of the shear strength of mild steel,' *Phil. Mag.*, **21** (1970), pp. 63–81.
12. TAKEYAMA, H., and MURATA, R., 'Basic investigation of tool wear,' *Trans. ASME* (J. Engineering for industry), **B85**, (1963), p. 33.
13. TAYLOR, J., 'Carbide cutting tool variance and breakage: unknown factors in machining economics,' Proc. 8th Intern. MTDR Conf. (1967).

THE USE OF A CUTTING FORCE SPECTRUM FOR TOOL WEAR COMPENSATION DURING TURNING

by

N. AKGERMAN and J. FRISCH*

SUMMARY

The variations of tangential cutting force during finish turning of AISI-1045 and AISI-4130 steel have been measured for depth of cut from 0.001 to 0.008 in. Changes in tool geometry, such as the reduction of rake face areas as a wear criterion, have been obtained and the consequent modifications of the depth of cut on the workpiece were related to the cutting force spectrum. This relationship between machining variables has been incorporated into a control algorithm and the flow chart suggesting numerically controlled turning with corrections for tool wear is presented here.

NOMENCLATURE

A_{ci}	Uncut chip cross-sectional area, in ² .
A_{fi}	Flank wear area, in ² .
A_w	Lost rake area, in ² .
D	Workpiece diameter, in.
E	Modulus of elasticity, lbf in ² .
F_c	Vertical cutting force, lbf.
F_h	Horizontal cutting force, lbf.
K	Constant
M	Bending moment, lbf in.
R_a	$R_m + R_s$, dimensionless
R_m	Ratio of A_{fi} / A_{ci} , dimensionless
R_s	Ratio of slopes A_{ci} and A_{fi} against d , dimensionless
W	Calibration weight, lbf.
a	Moment arm of cutting forces, in.
d	Instantaneous depth of cut, in.
d_o	Initial depth of cut, in.
Δd	Resolution of crossfeed mechanism, in.
f	Feed, in rev ⁻¹ .
I/c	Section modulus of tool bit, in ³ .
i	Subscript; $i=0$ before cutting, $i=1,2,\dots$ before i th indexing of tool.
l_{hi}	Height of flank wear area, in.
l_{si}	Length of side cutting edge, in.
s	Instantaneous projected length of side cutting edge, in.
s_i	Initial and projected length of side cutting edge, in.
ϵ	Strain, microin. in. ⁻¹
ϵ_c	Calculated strain, microin. in. ⁻¹
ϵ_m	Measured strain, microin. in. ⁻¹
θ_s	Instantaneous side cutting edge angle, degrees

θ_{si}	Side cutting edge angle, degrees
θ_e	End cutting edge angle, degrees
θ_{sc}	Side cutting edge clearance angle, degrees
θ_{ec}	End cutting edge clearance angle, degrees
θ_{br}	Back rake angle, degrees
θ_{sr}	Side rake angle, degrees
ϕ_c	Resultant clearance angle, degrees

INTRODUCTION

The recent rapid development of Direct Numerical Control (DNC) of manufacturing processes has made it possible to consider self-optimizing adaptive control as a method for on-line use of various controllers. As discussed by a number of investigators^{4,8,10,11} the principle involves the measurement of pertinent quantities such as tool forces during metal turning during the manufacturing process and using the information as an input for a control loop. Measurements of temperatures, machine frequencies, surface measurements and other parameters as well as tool forces can be incorporated into the direct computer control loop of the manufacturing process to achieve multivariable optimizing strategies for the particularly desirable characteristics of the end product.

Although decreased manufacturing costs are desirable, the implied aspects of this generality are: improved tool life, better surface finish, increased production rates and other features. As an impetus to undertaking this investigation we considered the case of metal turning when it is desirable to complete the cutting of a surface without interruption.

*Department of Mechanical Engineering, University of California, Berkeley.

This might be, for example, the case in which expensive materials under very close tolerance and surface finish specifications are being machined. Because tool wear is unavoidable and may, in fact, occur and make it impossible to otherwise complete the operation, it is desirable to monitor such wear and compensate the tool position by means of an adaptive control loop. It has been reasonably well established^{1,2,3,5,6,9} that correlations between tool wear and such cutting parameters as tool forces, temperatures, friction and so on can be established.

Realizing from the literature on metal turning the strong interdependence between a changing force spectrum and tool wear, a theoretical model is presented which relates the wear on the rake and flank faces of the tool tip to the cutting force vectors and the changing depth of cut on the work-piece. These essentially linear relationships have been experimentally verified during turning off AISI 1045 and AISI 4130 steel. By means of a microscope-camera attachment on the lathe for monitoring tool geometry changes, and an electric resistance strain-gauge dynamometer on the toolbit, the pertinent quantities of wear and force values have been determined for future duplications in DNC production conditions. We present an algorithm for incorporating the on-line force measurements into the closed loop of a computer controlled turning operation which then compensates tool wear by the tool position adjustments to effect the desired depth of cut.

THEORY

The theoretical model of wear has been developed in two sections. The first deals with the expected geometry caused by wear considering the lost rake area and decrease in uncut chip cross-section. These are areas PP'A and ABCP to ABC'P' shown in Fig. 2. The second section deals with the observed variations in vertical cutting forces F_c and their relationship to both the decrease in uncut chip cross-sectional area and the increase in flank wear land.

The uncut chip cross-sectional area constitutes one of the primary parameters relating cutting forces to wear. As shown in the rakeface geometries of Fig. 2, the area ABCP represents an uncut chip cross-sectional area before wear A_{c0} . After some wear, the depth of cut decreases from d_0 to d and ABC'P' becomes the new instantaneous uncut chip cross-section A_{ci} . This trapezoidal area is derived from the rake face geometry and cutting parameters.

From Fig. 2

$$A_c = \frac{h}{2}(s_0 + b_0)$$

$$h = f \sin \theta_{so}$$

$$s_0 = d_0 / \sin \theta_{so}$$

Transferring line CP without rotating such that point C coincides with B and using the law of sines

$$b_0 = s_0 - \frac{f \sin \theta_e}{\sin(\theta_e + \theta_{so})}$$

Substituting $s_0 = d_0 / \sin \theta_{so}$ in this equation and using the new expression for b_0 , together with $h = f \sin \theta_{so}$, results in an expanded equation for A_c , namely

$$A_c = fd_0 - \frac{f^2 \sin \theta_e \sin \theta_{so}}{2 \sin(\theta_e + \theta_{so})}$$

The general expression for instantaneous uncut chip cross-sectional area is found by replacing d_0 by d and θ_{so} by θ_s , yielding

$$A_c = fd - \frac{f^2 \sin \theta_e \sin \theta_s}{2 \sin(\theta_e + \theta_s)} \tag{1}$$

Given the initial tool geometry it can be seen that θ_s is a function of d , which can also be derived from triangle PP'A where

$$\frac{e}{\sin(\theta_{so} - \theta_s)} = \frac{s_0}{\sin \phi}$$

After substituting $s_0 = d_0 / \sin \theta_{so}$, $e = (d_0 - d) / \sin \theta_e$, $\phi = \theta_e + \theta_s$ and dividing the numerators and denominators by $\cos \theta_s$.

$$\frac{\sin \theta_e + \cos \theta_e \tan \theta_s}{\sin \theta_{so} - \cos \theta_{so} \tan \theta_s} = \frac{d_0 \sin \theta_e}{(d_0 - d) \sin \theta_{so}}$$

Rearranging this yields

$$\tan \theta_s = \frac{d \sin \theta_{so} \sin \theta_e}{d_0 \sin(\theta_{so} + \theta_e) - d \sin \theta_{so} \cos \theta_e} \tag{2}$$

After expanding the denominator of equation (1), substitution of equation (2) into (1) gives

$$A_c = d \left[f - \frac{f^2 \sin \theta_e \sin \theta_{so}}{2d_0 \sin(\theta_{so} + \theta_e)} \right] \tag{3}$$

which shows the uncut chip cross-sectional area as a linear function of the depth of cut.

The loss of rake area caused by wear, which is measured from photographs of the tool tip such as that shown in Fig. 8, is given as area PAP' in Fig. 2 and

$$A_w = \frac{1}{2} g \cdot s$$

Since $s = s_0 \cos(\theta_{so} - \theta_s) + e \cos \phi$, $g = e \sin \phi$. Substituting these terms shows that the wear area

$$A_w = \frac{1}{2} \left[\frac{d_0 - d}{\sin \theta_e} \sin(\theta_s + \theta_e) \right] \times \left[\frac{d_0}{\sin \theta_{so}} \cos(\theta_{so} - \theta_s) + \frac{(d_0 - d)}{\sin \theta_e} \cos(\theta_s + \theta_e) \right] \tag{4}$$

is a function of the depth of cut, being zero for $d = d_o$ and $\theta_s = \theta_{so}$. When d and θ_s are zero, the wear area becomes a maximum

$$(A_w)_{\max} = \frac{d_o}{2} \left(\frac{d_o}{\tan \theta_e} + \frac{d_o}{\tan \theta_{so}} \right) \quad (5)$$

Plots showing the linear relationship of A_w against d from the above equations as well as corresponding experimental points are shown in Figs. 4 and 5.

The vertical cutting force has two components, one of which is used in deforming the chip, the other existing as a friction force on the flank, which increases as the wear land on the flank increases. The latter component is assumed to be zero in a newly ground tool, so that at the beginning of a cut the vertical force goes entirely into chip formation. Correspondingly, when all possible wear has occurred, so that $A_c = 0$, the vertical force is entirely frictional. There are two first-order parameters determining F_c , A_c , and A_f the flank wear area.

The triangular flankwear area shown as AP'F in Fig. 3 can be found from the geometric relationships of the tool flank shown in that figure.

$$A_f = \frac{1}{2} l_s \times l_h \quad (6)$$

As the height of the flankwear area l_h and the length of the side cutting edge l_s change as wear proceeds, they can be expressed as functions of the depth of cut d . They are also dependent on the resultant clearance angle ϕ_c which can be measured, therefore,

$$\left. \begin{aligned} l_s &= \frac{d}{\sin \theta_s \cos \theta_{br} \cos \theta_{sr}} \\ l_h &= \left[\frac{d_o - d}{\tan \phi_c} - (d_o - d) \tan \theta_{br} \right] \cos \theta_{br} \end{aligned} \right\} \quad (7)$$

$$\tan \phi_c = \frac{k \cos \rho}{\sin (\theta_{so} + \theta_e)} \sin \theta_e + \tan \theta_{ec} \cos \theta_e \quad (8)$$

where

$$k = \left[\tan^2 \theta_{ec} + \tan^2 \theta_{sc} - 2 \tan \theta_{ec} \tan \theta_{sc} \cos (\theta_{so} + \theta_e) \right]^{1/2}$$

$$\cos \rho = \frac{\tan^2 \theta_{sc} + k^2 - \tan^2 \theta_{ec}}{2 \tan \theta_{sc} \times k}$$

The following equation is proposed as a relationship of the cutting force F_c to both A_c and A_f

$$F_c = K (R_a A_c + A_f) \quad (9)$$

where

$$\left. \begin{aligned} R_a &= R_m + R_s \\ R_m &= \frac{(A_f)_{d=0}}{(A_c)_{d=d_o}} \\ R_s &= \frac{d(A_f)/d(d)}{d(A_c)/d(d)} \end{aligned} \right\}_{d=0} \quad (10)$$

R_m constitutes the ratio of maximum areas, and R_s is the ratio of slopes when the depth of cut is considered to be zero. Given the initial tool geometry and depth of cut, R_m and R_s are determined. At the beginning of a cut $A_f = 0$, R_a and A_c are determined from the tool geometry and F_c is measured. Therefore, equation (9) can be rewritten to obtain K as

$$K = \frac{(F_c)_0}{R_a [(A_c)_{d=d_o}]} \quad (11)$$

The value of K is affected by variables such as workpiece material, cutting fluids and so on. However, as can be seen in Fig. 6, the theoretical curve starts and coincides with the initial experimental points for F_c and d . With increasing tool wear the depth of cut, d , decreases and, if a dynamometer is used to measure F_c , then by means of direct numerical control, equations (10) and (11) can be used to anticipate changes in d . Therefore, F_c can be used as feedback variable in the control algorithm.

Assuming a crossfeed resolution Δd , the tool will be indexed whenever $d_o - d \geq \Delta d$, causing an increase in A_c of $f\Delta d$. With inward movement of the tool the geometries of A_c and A_f will change, however. Instead of calculating d after each F_c measurement it will be more efficient to compute that value of F_c at which tool indexing should occur. The tool will be indexed when $F_c \leq F_{ci}$, where F_{ci} is the calculated force level at which the i th indexing takes place. A_{ci} and A_{fi} are then defined as those areas just before the i th indexing.

Derivation of the equations for $\tan \theta_{si}$, A_{ci} , A_{fi} , are not repeated for the sake of brevity, but are given for $i \geq 1$ as:

$$\tan \theta_{si} = \frac{d_o - \Delta d}{(i\Delta d / \tan \theta_e) + [d_o + (i-1)\Delta d] / \tan \theta_{so}} \quad (2a)$$

and

$$A_{ci} = (d_o - \Delta d) \times \left[f - \frac{f^2 \sin \theta_e \sin \theta_{so}}{2 [d_o + (i-1)\Delta d] \sin (\theta_e + \theta_{so})} \right] \quad (3a)$$

Immediately after the i -th indexing, the uncut chip cross-sectional area is $A_{ci} + f\Delta d$ and decreases to $A_{c,(i+1)}$ just before the next indexing.

Using $\tan \phi_c$ from Equation (8), the value of A_{fi} can be determined from

$$A_{fi} = \frac{1}{2} l_{si} + l_{hi} \quad (6a)$$

and

$$\left. \begin{aligned} l_{si} &= \frac{(d_o - \Delta d) \sin \theta_{si}}{\cos \theta_{br} \cos \theta_{sr}} \\ l_{hi} &= i \Delta d \left[\frac{1}{\tan \phi_c} - \tan \theta_{br} \right] \cos \theta_{sr} \end{aligned} \right\} \quad (7a)$$

Using the analysis given, the following control algorithm can now be outlined.

1. Read in the initial tool geometry and cutting parameters, θ_{so} , θ_e , θ_{se} , θ_{ec} , θ_{br} , θ_{sr} , d_o , Δd , and f .
2. Calculate R_a from equation (10).
3. Start cutting and measure F_c . Determine K from equation (11).
4. Set $i = 0$.
5. Set $i = i + 1$.

6. Determine A_{ci} and A_{fi} .
7. $F_{ci} = K (R_a A_{ci} + A_{fi})$.
8. Measure F_c .
9. If $F_c > F_{ci}$, go to 8. Otherwise go to 10.
10. Increment the tool inward by amount Δd .
11. Go to step 5.
12. End.

The computer will be looping between steps 8 and 9, measuring F_c and comparing it with F_{ci} . It is desirable to take, say, 500 samples in 5 s for averaging and noise filtering. The actual sample number depends on the force transducer sensitivity, equipment characteristics as well as on the desired smoothness of the signal. Another method for obtaining a smooth signal would be to compare the present F_c value with the previous value. Because an increased F_c implies an increase in d which is impossible, the computer program is instructed to set the present F_c value to the previous one. Finally, electronically filtering the signal before it is sampled by the computer would achieve the desired smoothness.

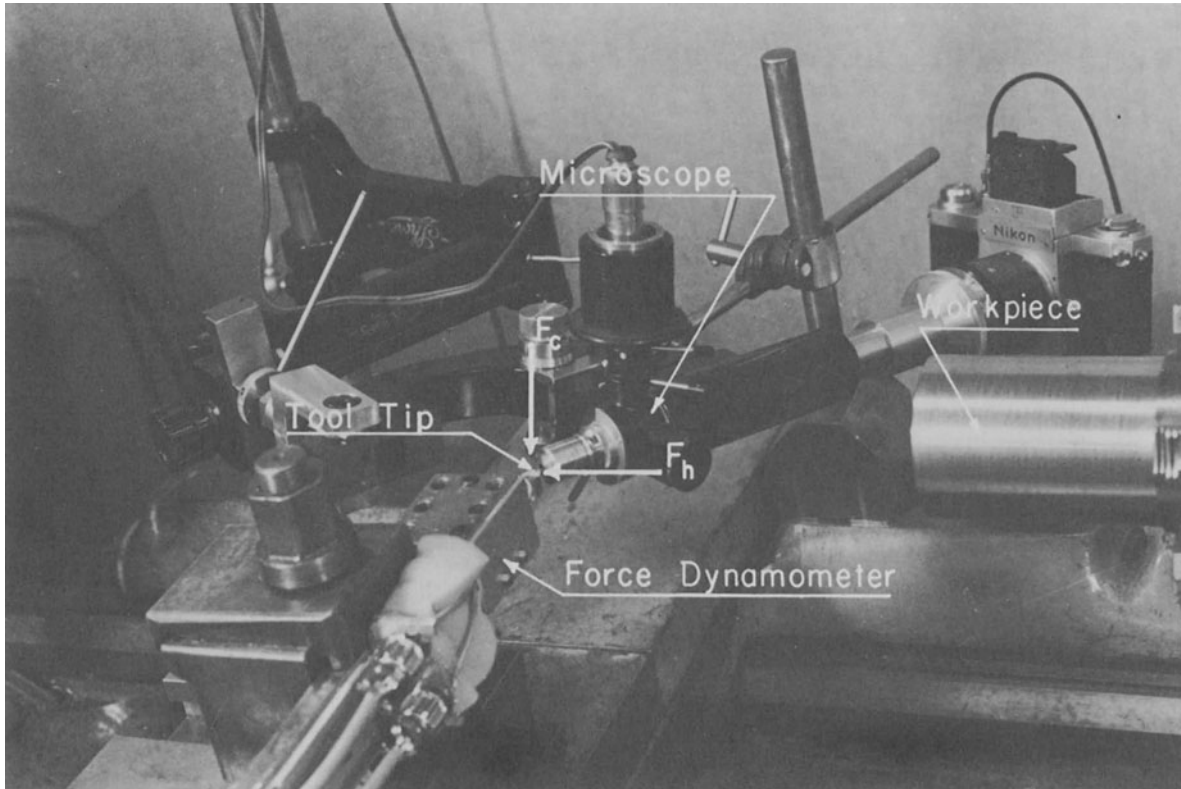
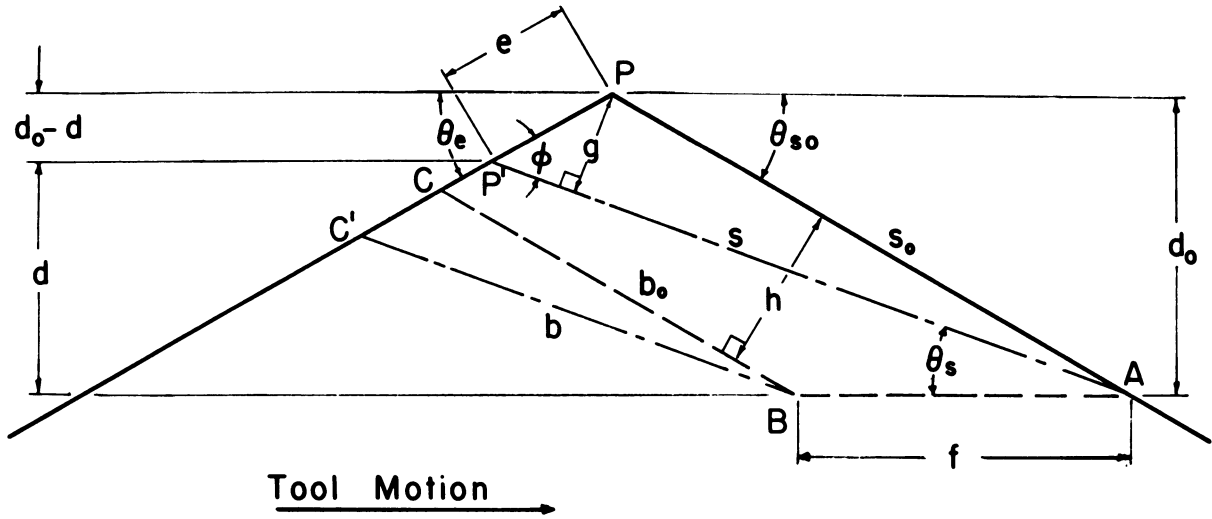


Fig. 1 Photograph showing experimental test apparatus.



Schematic Diagram of Rake Face Showing the Different Geometric Variables

Fig. 2 Schematic diagram of cutting tool rake face geometry.

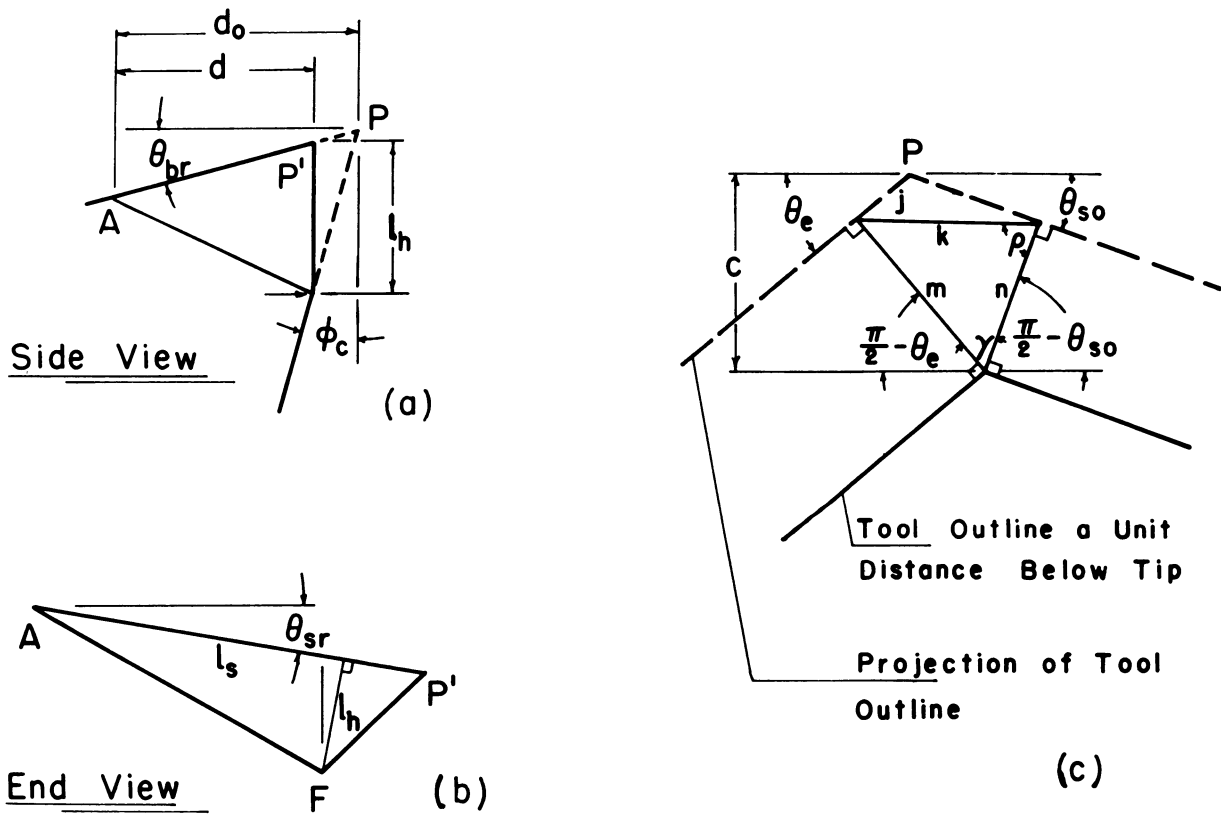


Fig. 3 Schematic diagram of cutting tool flank geometry.

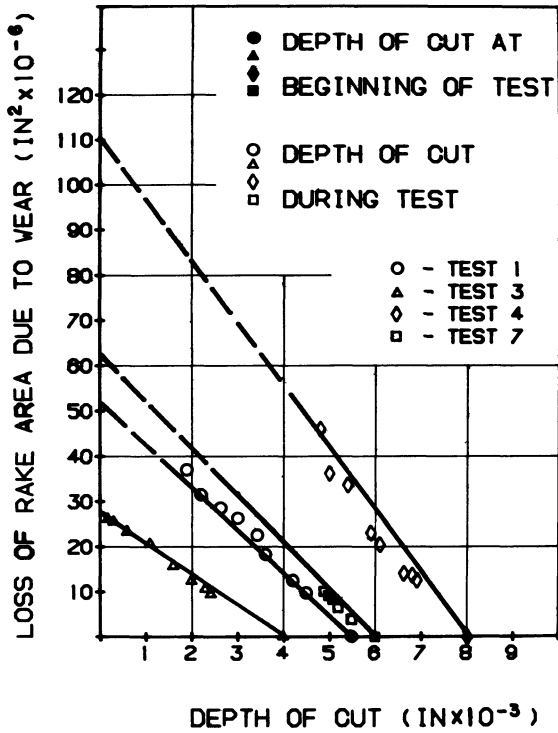


Fig. 4 Calculated and experimental tool rake area wear against depth of cut for initial cutting depths above 0.004 in.

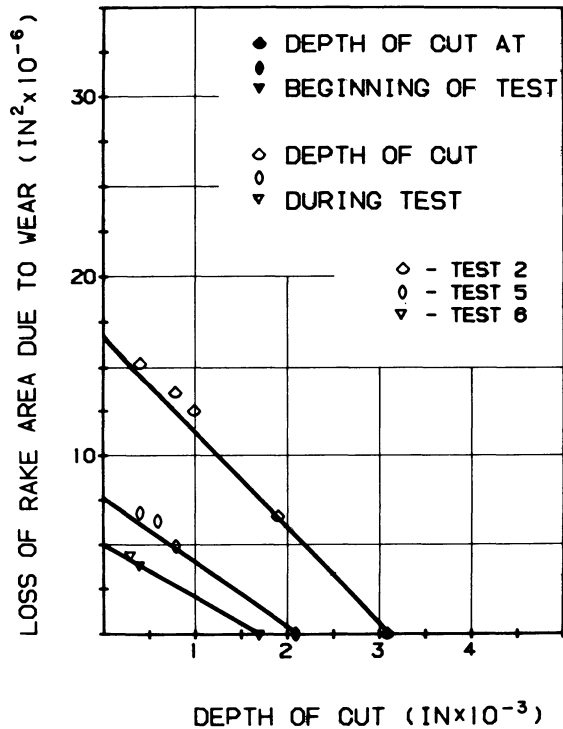


Fig. 5 Calculated and experimental tool rake wear against depth of cut for initial cutting depths below 0.004 in.

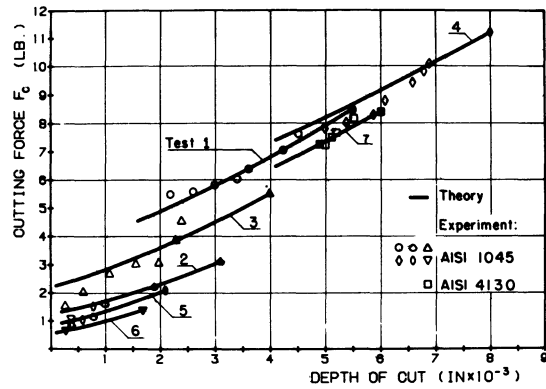


Fig. 6 Calculated and experimental cutting forces against depth of cut for AISI-1045 and AISI-4130 steel.

EXPERIMENTS

The experimental tests were conducted on a 14 X 30 in lathe with the workpiece mounted on a high-precision air bearing spindle, instead of the regular headstock. However, feed was obtained through the regular lathe drives with a carriage monitoring dial accurate to ± 0.0005 in/ft⁻¹. The workpiece materials were AISI-1045 medium carbon steel and AISI-4130 molybdenum steel, and the cutting tool was high speed steel. The cutting speed and feed were held constant at 100 f.p.m. and 0.002 in./rev, respectively. Tests were performed at different depths of cut, ranging from 0.0017-0.008 in, without cutting fluids.

The angles used in the tool geometries were: 5°, back rake; 0°, side rake; 30°, side cutting edge; 10°, side clearance; 30°, end cutting edge; and 10°, end clearance. The nose radius was considered nominally to be zero. The tool bit was instrumented with four temperature compensated electric resistance strain-gauges to make up the force dynamometer, shown in Fig. 1 which illustrates the test apparatus configuration. The two gauges on the vertical toolbit sides measured the strain caused by the horizontal force and the other pair on the top and bottom surfaces measured that caused by the vertical force during cutting. For each newly ground tool configuration, the distance from the tip to the centre of the strain-gauges was re-measured as the moment arm. As shown in Fig. 8, Vickers indentations were made on the tool rake and flank faces for the purpose of establishing a fixed coordinate system from which the losses in rake and flank areas can be measured, as wear progresses. The cutting was stopped at intervals of 1 in. along the workpiece and by means of the microscope on the three-axis support, shown in Fig. 1, the rake face and flank were photographed for evaluation later. For output of the electric resistance strain-gauges in the force dynamometer the signal was fed into two carrier amplifiers which were synchron-

ized to avoid spurious component readings. The amplifier outputs were fed into attenuators, set to obtain 2 V output at 2 cm of vertical oscilloscope beam deflection. An eight-track Sanborn 3907A magnetic tape recorder with a maximum input signal level of ± 2 V was used for recording the strain readings from the dynamometer. The two force signals were recorded in FM at $3\frac{3}{4}$ i.p.s., (maximum rise time 20 ms) and played back at 60 i.p.s., giving a 16:1 time compression.

Each experimental test was initiated by preparing the mounted workpiece with a carbide tool and checking alignment for parrallelism with the Bedways, and calibrating the tool, with its Vickers indentation coordinates, for strain-gauge signals to the recording equipment. After obtaining all the necessary measurements of tool position, workpiece diameters and so on, the cut was started with a certain initial depth of cut. As mentioned previously, the cut was interrupted to photograph the tool for wear and checking of the instrument calibrations. Data analysis of the tape-recorded signal from each test was accomplished by digitizing the analogue signal onto computer tape through an analogue to digital converter system attached to a PDP-7 computer. Sampling and evaluation of the digitized data and the conversion to force values was done by computer sub-routines which, although they have been described in detail¹²,

have been omitted here. The digitized force measurements were plotted from punched tape output on a Gerber automatic drafting machine. A typical plot of vertical and horizontal forces against cutting distance is shown in Fig. 7. The reduction in rake face and flank areas was measured with a planimeter from photographs such as the one shown in Fig. 8 and the information used to correlate the change in depth of cut to the corresponding force measurement.

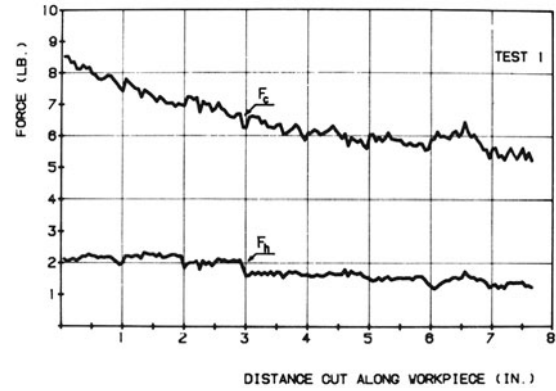


Fig. 7 Typical plot of experimental tool forces against cutting distance for AISI-1045 steel from dynamometer records.

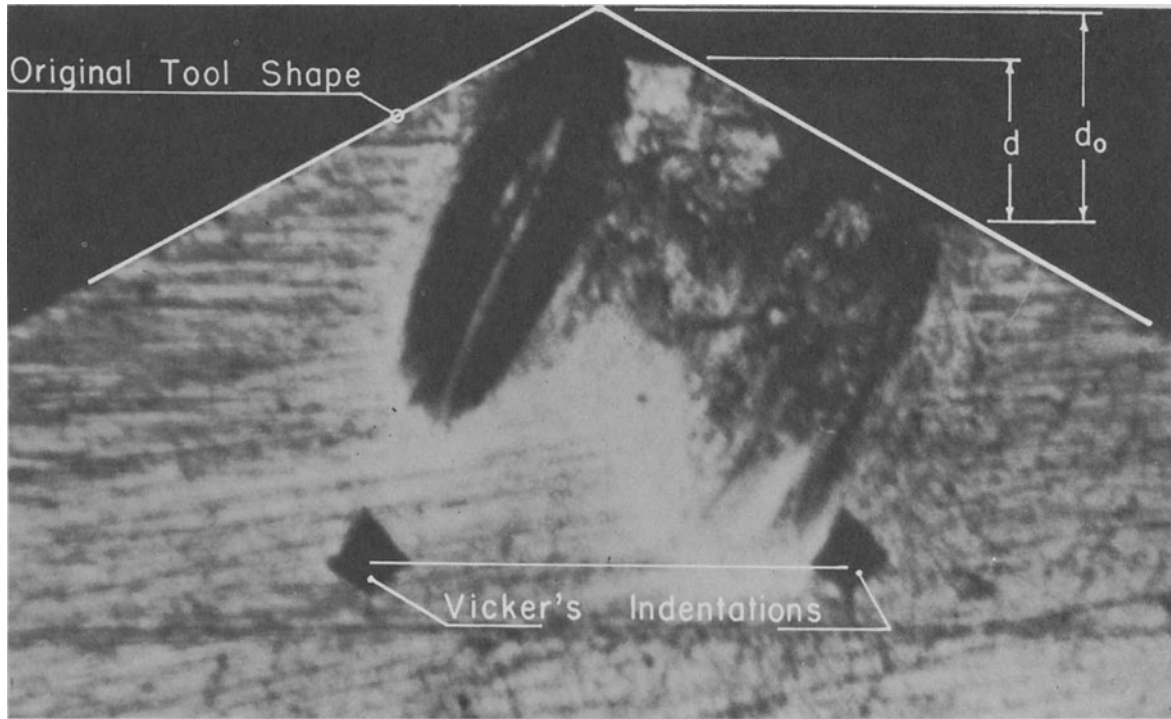


Fig. 8 Typical photograph of worn tool rake face showing Vickers reference marks and change of depth of cut.

RESULTS AND DISCUSSION

The theoretical as well as experimental results show the two distinct aspects of the study, one being the relationship of wear geometry to the instantaneous depth of cut and the other the wear geometry related to the vertical cutting force. Although the uncut chip cross-sectional area is not easily measurable, the theoretical model permits derivation of A_w , the lost rake area caused by wear. By superimposing the original tool contour on all successive photographs of the rake face, as shown in Fig. 8, the wear area can be measured to a high degree of accuracy. These measurements are listed in Table 2 for seven tests, six of which were performed on AISI-1045 and, for verification purposes, one was performed on AISI-4130. The depths of cut corresponding to these quantitative tool wear values are also shown in Table 2, and the details of pertinent test characteristics have been assembled in Table 1. The latter table also shows the amplifier sensitivities¹² necessary for quantizing the forces from strain-gauge recordings. The wear losses in rake areas from Table 2 have been plotted in Figs. 4 and 5, the solid points signifying the initial depth of cut. The proximity of test points to the theoretically calculated lines verifies the linear relationship between these two parameters. Although wear rate is a function of material properties, the wear geometry remains essentially one in which the above-mentioned linear relationship continues as wear

progresses over a considerable cutting distance for the two materials under consideration and initial depths of cut ranging approximately from 0.001 to 0.010 in.

Theoretical and experimental efforts were directed towards a correlation between the cutting forces and wear geometry as an index of the changing depth of cut when metal turning is progressing. The cutting force F_c consists of the chip deforming component and the friction component on the flank wear area, which are brought together in the area relationship shown in equation (10). This equation does not require arbitrary constants for its solution as all necessary parameters such as initial tool geometry, depth of cut and feed, are determined. The theoretical cutting forces are plotted against depth of cut, d , and the experimental values against the depths of cut from Table 2 are found to correlate with the curves passing through the initial values of d , shown as darkened points. The typical plots of experimentally determined cutting forces F_c and F_h are shown in Fig. 7. However, such a larger value of F_c makes it a more desirable parameter against which tool wear through changes in depth of cut can be anticipated. The relationships established here between continuously recorded cutting forces and measured tool wear are shown to be usable quantities for a computer algorithm by means of which direct numerical control in maintaining a prescribed depth of cut can be achieved during metal turning.

Table 1. Test data

Test No:		1	2	3	4	5	6	7
Moment arm (in)		0.9589	0.9554	0.9504	0.9450	0.9188	0.9015	0.8935
Initial depth of cut (in)		0.0055	0.0031	0.0040	0.0080	0.0021	0.0017	0.0060
Diameter of piece (in)		2.930	2.904	2.877	2.843	2.804	2.804	2.495
Distance between Vickers indentations (in)	Rake	0.01535	0.01575	0.01587	0.01587	0.01575	0.01575	0.01575
	Flank	0.00787	0.00984	0.00984	0.00984	0.00984	0.00984	0.00984
Amplifier sensitivity ($\mu\epsilon \text{ cm}^{-1}$)	F_c	50	20	20	50	10	10	50
	F_h	10	10	10	10	10	10	20
Material		AISI 1045	AISI 4130					

Cutting velocity = 100 surface ft min⁻¹. Feed = 0.002 in. rev⁻¹.

Table 2. Depth of cut and tool wear measurements from rake face photographs

Test No 1		Test No 2		Test No 3		Test No 4		Test No 5		Test No 6		Test No 7	
Depth of cut (in $\times 10^{-3}$)	Tool wear * (in ² $\times 10^{-6}$)	Depth of cut (in $\times 10^{-3}$)	Tool wear * (in ² $\times 10^{-6}$)	Depth of cut (in $\times 10^{-3}$)	Tool wear * (in ² $\times 10^{-6}$)	Depth of cut (in $\times 10^{-3}$)	Tool wear * (in ² $\times 10^{-6}$)	Depth of cut (in $\times 10^{-3}$)	Tool wear * (in ² $\times 10^{-6}$)	Depth of cut (in $\times 10^{-3}$)	Tool wear * (in ² $\times 10^{-6}$)	Depth of cut (in $\times 10^{-3}$)	Tool wear * (in ² $\times 10^{-6}$)
5.5	0.0	3.1	0.0	4.0	0.0	8.0	0.0	2.1	0.0	1.7	0.0	6.0	0.0
4.5	9.7	1.9	6.6	2.4	9.2	6.9	12.2	0.8	4.9	0.4	3.9	5.5	3.2
4.2	12.4	1.0	12.3	2.3	10.4	6.8	13.3	0.6	6.3	0.3	4.4	5.2	6.3
3.6	18.4	0.8	13.5	2.0	12.5	6.6	13.4	0.4	6.6			5.2	6.4
3.4	22.7	0.4	15.2	1.6	17.6	6.1	20.1	0.4	6.8			5.2	
3.0	26.3			1.1	20.4	5.9	23.0					5.1	8.2
2.6	28.9			0.6	23.4	5.4	33.7					5.0	8.9
2.2	31.3			0.3	25.3	5.0	36.0					4.9	9.9
1.9	37.0			0.2	26.3	4.8	46.0						

*Loss of rake area of tool caused by wear.

CONCLUSIONS

For the materials and test conditions of the experimental investigation described here, together with the theoretical analysis, the following conclusions may be drawn.

1. A linear relationship exists between the principal cutting force and the instantaneous depth of cut during turning of AISI-1045 and AISI-4130 steel in the test conditions described.

2. Tool wear, as measured by loss of rake and flank areas, is linearly related to the resulting change in depth of cut.

3. Continuous monitoring of force dynamometer recordings allows the tool position to be adjusted to maintain the desired depth of cut over the length of the turned workpiece.

4. The use of a tool force dynamometer as a monitoring device for adaptive control in direct numerical control (DNC) machining has been evaluated.

5. An algorithm to achieve prescribed dimensional requirements in DNC metal turning, when possibly excessive tool wear occurs, has been presented.

REFERENCES

- ZOREV, N., 'Metal Cutting Mechanics,' Pergamon Press (1966).
- INYONG HAM, 'Fundamentals of Toolwear', ASTM Paper No. MR pp. 68-617.
- MICHELETTI, G. F., DEFILIPPI, A., and IPPOLITO, R., 'Tool Wear and Cutting Forces in Steel Turning,' CIRC Annals, XVI, pp. 353-360.
- DEFILLIPI, A., and IPPOLITO, R., 'Adaptive Control in Turning: Cutting Forces and Tool Wear Relationship,' CIRC Annals, XVII, pp. 377-385.
- BER, A., and FRIEDMAN, M. V., 'On the Mechanism of Flank Wear in Carbide Tools,' CIRC Annals, XV, pp. 211-216.
- LOLADZE, T. N., 'Problems of Wear and Strength of Cutting Tools,' CIRC, Annual Assembly (1967).
- GROZMAN, F. K., and HEMMING, A. V., 'Problems Involved in the Development of Adaptive Techniques to Improve the Productivity of NC Lathes,' Proc. 11th Intern. MTDR Conf., Birmingham (1970).
- PORTER, B., and SUMMERS, R. D. M. J., 'The Performance of the Self Optimizing Strategies in the Adaptive Control of the Metal Cutting Process,' Intern. J. M.T.D.R., 8, (1968), pp. 217-237.
- BHATTACHARYYA, A., and HAM, I., 'Analysis of Tool Wear Part I: Theoretical Models of Flank Wear,' A.S.M.E., Paper No 68-WA/PROD-5, (1968).
- KNIGHT, W. A., SADEK, M. M., and TOBIAS, S. A., 'Automatic Determination and Digitization of Machine-Tool Frequency Response Data', Proc. 11th Intern. MTDR Conf., Birmingham (1970).
- JONA, M. G., 'Contribution to the Development of Geometrical Adaptive Control in Turning,' Proc. 11th Intern. MTDR Conf., Birmingham (1970).
- AKGERMAN, N., and FRISCH, J., 'The Use of Cutting Forces Spectra for Tool Wear Compensation,' University of California Engineering Res. Report No MD-71-1 (1971).

DISCUSSION

Query from A. H. Redford, U.S.A.L.F.

If the system is to be used for very fine finishing operations with very fine tolerances, has any work been carried out into investigating the effect of varying mechanical properties of the workpiece on the accuracy of the system.

Reply

No work has been specifically done to investigate the

effect of varying mechanical properties of the workpiece. In our experiments the workpiece material was used in the as-received condition and our observation is that a tolerance of ± 0.0005 in. can be maintained while turning a piece of about 3 in. diameter and 8 in. long. It may be possible to operate in a narrower tolerance band by employing a filtering logic, whereby signals that are very high or very low with respect to the previous signal level will be disregarded.

SYSTEM DESIGN AND IDENTIFICATION

DESIGNING IN DIGITAL SPACE

by

W. B. HEGINBOTHAM*

SUMMARY

It is shown that, by using a digital space table, a draughtsman can make use of a simplified NC machine tool positioning system, in order to cater for most dimensional problems.

INTRODUCTION

Apart from the consideration of strength, stiffness and mechanical functioning, the allocation of dimensions in engineering components is left to the individuality of the designer and draughtsman. To some extent decisions are influenced by styling and other factors such as ease of maintenance or servicing but generally however the decision to make something 25 mm thick or space screws round a 5 cm pitch circle diameter is somewhat arbitrary and there may be an almost infinite combination of dimensions all of which would produce satisfactory strength, functioning, aesthetic appeal, serviceability and reliability.

The consequence of this is that, by and large, the specifications for machine tools are influenced by the need to incorporate an enormous range of flexibility so as to cater for variability. A numerically controlled machine tool is a supreme example of automated flexibility which will cater for whims in design down to dimensional differences of something like 0.02 mm. *This is not to say that we need to produce parts to less accuracy but that the 'network' of design space is too fine. Also, the finer the network the more expensive is the means which has to be used to cater for its whims.* It would seem sensible to coarsen the design network whilst still maintaining the precision with which we can reproduce this network. Drilling holes, for instance, could be carried out by automatic, non-feedback type positioning devices which can be made much cheaper if a coarse digital network is adopted and the designer educated to use dimensions from rectangular arrays which are multiples or functions of the digital network.

An example of such a machine is shown in Fig. 1; it was developed using the efforts of three undergraduate project students, Marshall¹, Arnold² and Good³. The positioning system uses the principle

whereby double-acting air cylinders are adapted so as to generate exact lengths, e.g. 0.5 mm, 1 mm, 2 mm, 4 mm, 8 mm, ..., which can be cascaded together so as to generate any length in 0.5 mm steps up to the maximum sum of all the extended lengths of the cylinders. Such a system can be very precise and its control system relatively simple.

In this case a fluidic control system with a drum programmer was used and the layout of the system is as shown in Fig. 2. The positioning system was therefore 'open loop' but its state monitored and sequentially interlocked with the functioning of the drilling and tapping heads. The basic accuracy of the system (max cumulative error) was ± 0.002 in and the basic incremental dimension $1/32$ in. The max traverse in two directions was $7\ 31/32$ in.

Another system⁴ has been applied to a programmable assembly machine using a unique system of mechanical locks. This particular system has an accuracy of ± 0.03 mm over a travel of 250 mm for 95% confidence limits and will repeat to ± 0.02 mm at any position.

Immediately the question arises: how does one cater for dimensions which, owing to other reasons, do not turn out to be an integer function of the basic network spacing? For instance, if any gearing is involved in the design, then the space will have to provide discrete dimensions coinciding with the centre distances for running standard gears.

How, therefore, might one get over this problem when designing in a rectangular digital space network? The following elementary analysis will show that a much wider range of possibilities is feasible than one might imagine and by accepting a suitable design philosophy a wide range of conditions can be catered for. Fig. 3 illustrates the situation in a plane square digital network where the co-ordinates of any point are (mk, nk) : m and n are integers and k is the

*Production Engineering Department, The University, Nottingham.

network spacing. It is immediately obvious that with different values of prime numbers for m and n there are a large number of other networks which can be generated at other angles to the original one, the number of which is determined by the size of the network itself (Fig. 4). Considering one quadrant bounded by $OyOx$ (Fig. 3), each of which subtend Q spaces, then it can be shown that the total number of dimensions one can obtain measuring from OO throughout the whole space is given by

$$Z_T = (Q + 1)^2 - 1 \quad (1)$$

where Q is the number of integers of the basic network bounding the problem.

In this space, however, there will be duplication of dimensions in different directions, that is, when the root $(n^2 + m^2)^{1/2}$ is the same, i.e. in a direction governed by, say, when n/m is equal to 3 and when n/m is equal to $1/3$. Hence the total number of discrete dimensions in the system will be contained between the line $y = x$ and the Ox axis and this can be deduced as follows

$$Z_u = \frac{Z_T - Q}{2} + Q$$

Therefore substituting from (1) gives

$$Z_u = \frac{(Q + 1)^2 + Q - 1}{2}$$

Therefore

$$Z_u = \frac{1}{2} Q (Q + 3) \quad (2)$$

Depending on the fineness of the grid, there may be dimensions inside the number Z_u which are very

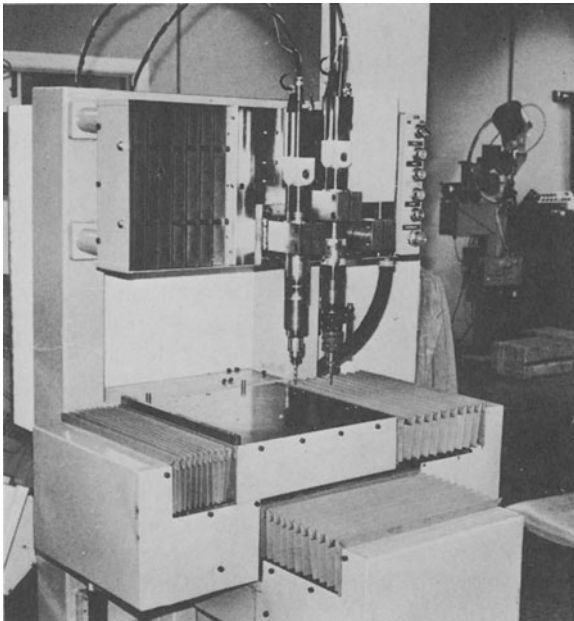


Fig. 1

nearly the same and could be used for a similar function but these numbers will occur by natural coincidences and, if the numbers are expanded to enough decimal places, then they will be slightly different. There will be other exact duplications if $(m^2 + n^2)^{1/2}$ is the same even though m and n are different, e.g. $(1^2 + 8^2)^{1/2} = (4^2 + 7^2)^{1/2}$.

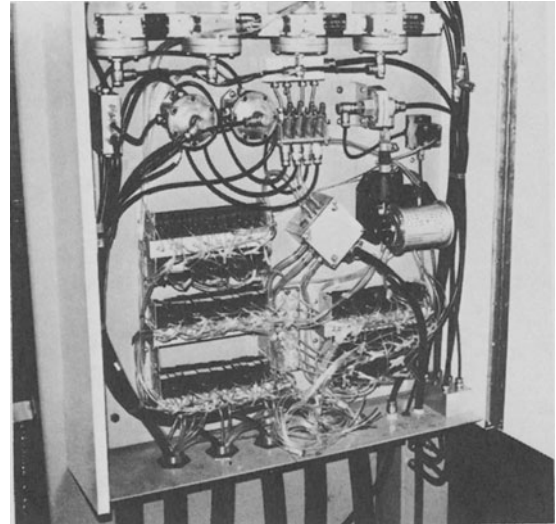


Fig. 2

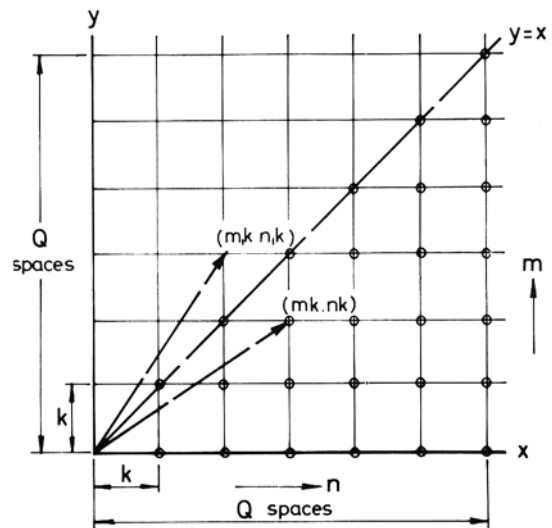


Fig. 3 Characteristics of a plane square digital network.

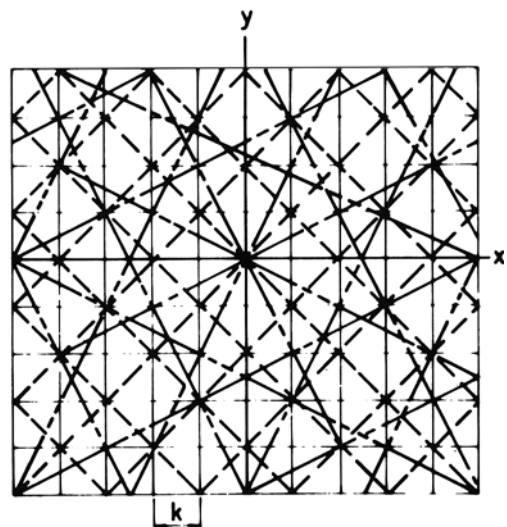


Fig. 4 Derivation of subsiding networks.

DIRECTION IN WHICH A PARTICULAR NUMBER CAN BE OBTAINED

This will clearly depend on the ratio m/n . Hence starting at the origin (Fig. 5) we can measure in two directions to give the same length

$$m < n \quad \theta_1 = \tan^{-1} \left(\frac{m}{n} \right)$$

$$m > n \quad \theta_2 = \tan^{-1} \left(\frac{m'}{n'} \right) = \tan^{-1} \left(\frac{n}{m} \right)$$

Clearly $\theta_2 = 90^\circ - \theta_1$

If we start to measure from co-ordinates $m_1 - n_1$ then the choice will be much wider (Fig. 6). There are two families of vectors mirrored about line $y = \pm x$ when $m < n$. We can measure in direction

First family $\theta_{11} = \tan^{-1} \left(\frac{m}{n} \right)$

$$\theta_{11} + 90^\circ$$

$$\theta_{11} + 180^\circ$$

$$\theta_{11} + 270^\circ = -\theta_{12}$$

$m > n$

Second family $\theta_{12} = 90^\circ - \theta_{11}$

$$\theta_{12} + 90^\circ$$

$$\theta_{12} + 180^\circ$$

$$\theta_{12} + 270^\circ = -\theta_{11}$$

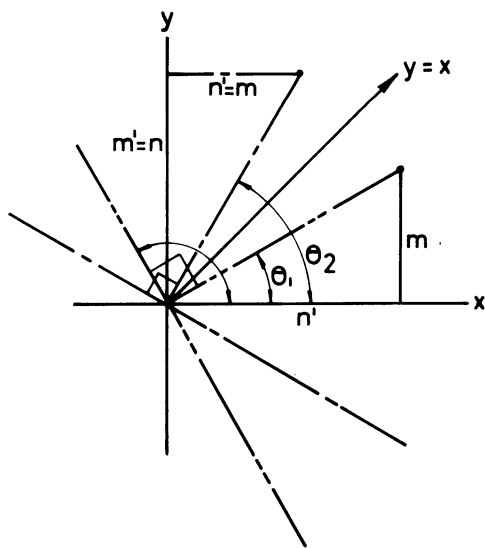


Fig. 5

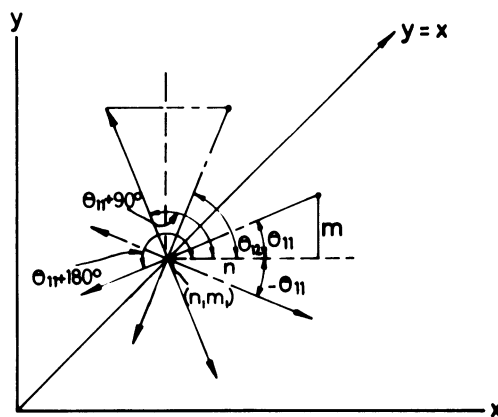


Fig. 6

TERMINOLOGY

		θ_{jj}
$i = 1$	n	$j = 1$ or 2
refers to angle		refers to 1st or 2nd family
number in system		$j = 1 \quad m < n$
		$j = 2 \quad m > n$

The number of networks available is not easily calculable but will be a function of the number of prime numbers in between 1 and Q which bound the network. However, the basic network spacing obtainable will be $(m^2 + n^2)^{1/2}$ where neither m nor n has a common factor. Therefore any length which can be obtained can be given as: $L = kI (m^2 + n^2)^{1/2}$, where k is the primary grid spacing, I is any integer and $(m^2 + n^2)^{1/2}$ is the size of the derived grid inclined at an angle $\tan^{-1} (m/n)$ to the Ox axis.

In order to simplify the problem of experimenting with different sized networks a 'unit network' table has been developed, that is, taking $k = 1$ and finding all the sizes measured from OO which can be obtained in between a line $y = x$ and the Ox axis. The number of these available is at present limited by the size of the store on the KDF9 computer in the Cripps Computing Centre, University of Nottingham, but it is possible to deal with problems where $Q = 100$. A sample section of the unit digital space chart is shown on Table 1.

It is clear that use of the 100 units of digital space need not be restricted to the space covered by the computer because we can shift our origin of co-ordinates and indeed we need to do this to set up particular dimensions for particular positions. The numbers are printed out in order of magnitude and can be used as follows.

If the dimension required is Z and k is the basic network spacing, then Z/k will give the unit number to look for in the unit digital space table. Therefore the nearest number to this is selected and then multiplied by k to give the actual dimension which can be obtained. By reading off the appropriate values of n and m on the table, the various directions in which one can obtain this dimension can be derived (Fig. 6).

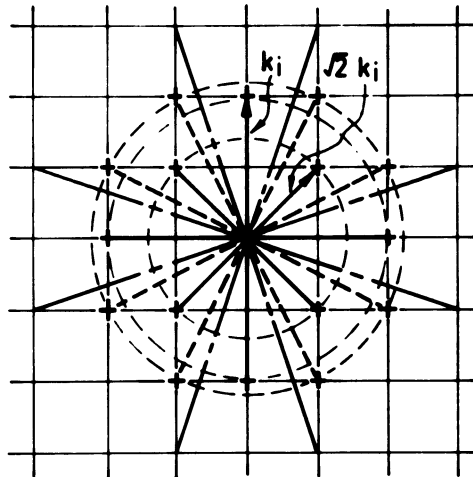


Fig. 7 Alternative arrays of hole spacings on constant pitch circle diameters.

Table 1

Range 82-0000 to 84-0000

L	I	m	n	θ (deg)	L	I	m	n	θ (deg)
82-0000	82	0	1	0-00	82-0000	2	9	40	12-68
82-0061	1	1	82	0-70	82-0244	58	1	1	45-00
82-0366	1	57	59	44-01	82-0549	1	3	82	2-10
82-0975	2	2	41	2-79	82-0975	2	23	34	34-08
82-1523	1	43	70	31-56	82-2010	1	14	81	9-81
82-2192	2	3	41	4-18	82-2192	2	27	31	41-05
82-2800	1	29	77	20-64	82-2922	2	18	37	25-94
82-3286	1	53	63	40-07	82-3468	1	34	75	24-39
82-3772	3	5	27	10-49	82-3893	2	4	41	5-57
82-4621	4	8	19	22-83	82-4621	4	13	16	39-09
82-5409	3	9	26	19-09	82-5651	1	16	81	11-17
82-6196	1	51	65	38-12	82-6378	1	30	77	21-29
82-7103	1	21	80	14-71	82-7345	37	1	2	26-57
82-7587	3	19	20	43-53	82-7647	5	7	15	25-02
82-8010	2	25	33	37-15	82-8070	1	56	61	42-55
82-8613	1	25	79	17-56	82-8734	2	6	41	8-33
82-9277	23	2	3	33-69	82-9699	2	11	40	15-38
83-0000	83	0	1	0-00	83-0060	1	31	77	21-93
83-0060	1	43	71	31-20	83-0241	1	2	83	1-38
83-0963	1	4	83	2-76	83-0963	1	53	64	39-63
83-1865	2	19	37	27-18	83-1865	2	7	41	9-69
83-2166	1	6	83	4-13	83-2166	5	9	14	32-74
83-2406	1	23	80	16-04	83-2406	1	40	73	28-72
83-2947	1	7	83	4-82	83-3547	2	21	36	30-26
83-3847	1	32	77	22-57	83-4086	1	51	66	37-69

THE GENERATION OF PITCH CIRCLE DIAMETERS FOR SPACING HOLES ROUND A FLANGE

Four hole locations are easily obtained at diameters of $2kl$ or $\sqrt{2}kl$ and this will give an even spacing of four holes in each case but with holes on the x and y axis in the former case at 45° to Ox and Oy in the latter case.

Eight hole spacings can be obtained at discrete

ratios of m/n which will result in pairs of holes mirrored about the lines $y = \pm x$. This means that for eight hole spacings round a flange we can obtain symmetrical arrays of groupings of pairs of holes about these two lines. (See Fig. 7.) It may be possible to get almost exactly equal spacings by choosing m and n correctly.

Other types of network need to be explored such as rectangular networks with k_1x and k_2y in the x and y directions respectively or equilateral triangular

networks, the latter having the advantage that, if using a set of plates pre-drilled with holes, then each hole would be in a position where its radial distance from its adjoining hole was the same. The two controlling movements would, therefore, have to be inclined at 60° and the mathematics of this type of space needs developing.

EXAMPLE

A typical but elementary design problem is that of designing a gear base and this can be dealt with as follows.

From Fig. 8, the following data is obtained

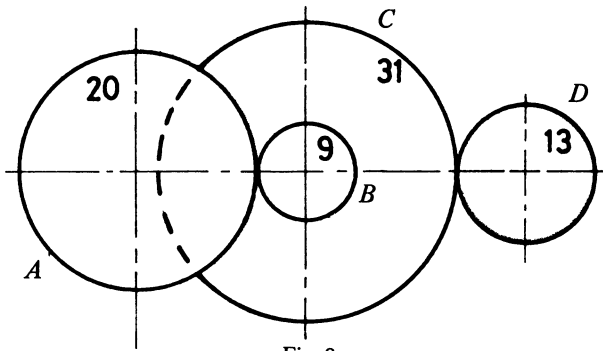


Fig. 8

Wheel	N	PCD
A	20	2.5
B	9	1.125
C	31	3.875
D	13	1.625

Centre distances

$$AB = 1.25 + 0.5625 = 1.8125$$

$$CD = 1.9375 + 0.8125 = 2.7500$$

use 0.040 in grid spacings

$$\text{Thus size in a unit network} = \frac{1.8125}{0.040}$$

$$AB = 45.3125$$

$$CD = \frac{2.75}{0.040} = \underline{68.75}$$

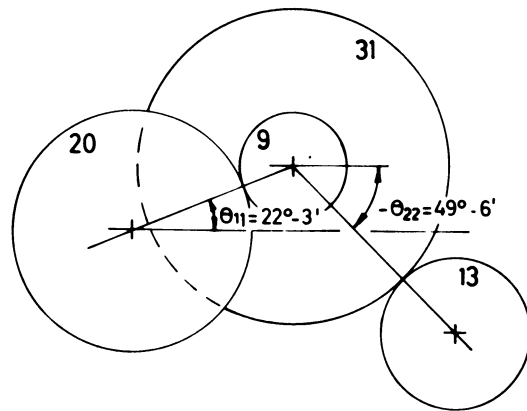


Fig. 9 Layout of gearbox

	From chart	I	m	n	True length	θ_{11}	θ_{21}	θ_{12}	θ_{22}
AB	45.31	1	17	42	1.8124	$22^\circ-3^1$			
CD	68.7677	1	45	52	2.750708		$40^\circ-54$		$49^\circ-6^1$

$$\frac{17}{42} = 0.405 \quad \theta_{11} = 22^\circ-3^1$$

$$\frac{45}{52} = 0.866 \quad \theta_{22} = 40^\circ-54^1$$

$$\tan^{-1} \theta_{22} = \tan^{-1} 52/45 = 1.155 \quad \theta_{22} = 49^\circ-6^1$$

Thus it is seen that any designer draughtsman by using the digital space table can utilize a simplified numerically controlled machine tool positioning system to cater for most dimensional problems with which he is likely to be faced.

Range 48-0000 to 50-0000

<i>L</i>	<i>I</i>	<i>m</i>	<i>n</i>	θ (deg)	<i>L</i>	<i>I</i>	<i>m</i>	<i>n</i>	θ (deg)
48-0000	48	0	1	0-00	48-0104	1	1	48	1-19
48-0416	2	1	24	2-39	48-0521	1	10	47	12-01
48-0937	3	1	16	3-58	48-1041	1	33	35	43-32
48-1664	4	1	12	4-76	48-2597	1	27	40	34-02
48-2701	1	11	47	13-17	48-3011	1	22	43	27-10
48-3735	6	1	8	7-13	48-3839	1	15	46	18-06
48-5077	1	7	48	8-30	48-5077	1	12	47	14-32
48-6621	8	1	6	9-46	48-7032	2	8	23	19-18
48-7647	1	23	43	28-14	48-7955	1	34	35	44-17
48-8365	3	11	12	42-51	48-8467	1	19	45	22-89
49-0000	49	0	1	0-00	49-0102	1	1	49	1-17
49-0408	1	17	46	20-28	49-0408	1	2	49	2-34
49-0918	1	3	49	3-50	49-1630	1	4	49	4-67
49-2443	5	4	9	23-96	49-2443	1	11	48	12-91
49-3356	1	15	47	17-70	49-3660	1	6	49	6-98
49-4065	1	29	40	35-94	49-4773	12	1	4	14-04
49-5177	2	17	18	43-36	49-5782	1	33	37	41-73
49-6488	1	23	44	27-60	49-6488	1	28	41	34-33
49-7293	1	13	48	15-15	49-7393	1	25	43	30-17
49-8197	1	9	49	10-41	49-9300	3	9	14	32-74

ACKNOWLEDGEMENTS

The author would like to thank Dr G. E. Rippon for solving the computer programming problems associated with the development of the digital space table.

Thanks are also due to the Department of Trade and Industry for their support by a research contract on programmable assembly machines which stimulated this work.

REFERENCES

- MARSHALL, D., 'Design and development of a high-speed pneumatic linear positioning device including the design of a sequential fluid logic system', *Undergraduate Project*, Department of Production Engineering and Production Management, University of Nottingham.
- ARNOLD, L. A., 'Design of a numerically controlled drilling, tapping and counter-boring machine and associated control system utilizing fluid logic units', *Undergraduate Project*, Department of Production Engineering and Production Management, University of Nottingham.
- GOOD, R. T., 'The design of a fluidic control system for a drilling machine with pneumatically positioned work-table', *Undergraduate Project*, Department of Production Engineering and Production Management, University of Nottingham.
- ASHLEY, J. R., HEGINBOTHAM, W. B., and PUGH, A., 'Developments in programmable assembly Machines', *Proc. 1st Natl. Symp. on Ind. Robots*, IIT Research Institute, Chicago.

DISCUSSION

Query from A. H. Redford, U.S.A.L.F.

Has the author carried out any work on adding a coarse pitch angular motion to the system. If so, what kind of effect does this have on the accuracy of the system.

Reply

We have not carried out any work on adding an incremental angular motion to this system. We have considered the feasibility of doing this, but any such addition would, of course, put up the cost of the system which would decrease the differential in costs between a full numerically controlled system and our present incremental set up. I therefore consider that we should concentrate on using the simplest system that can be devised to control the position of the working heads, because the basic cost of such a device is one of the main factors. The whole idea behind this paper is to show how a cheap and simple device using a 'coarse' design space can be utilised most effectively. We have, of course, considered the possibility of making an incremental angular table using the locking system that is the main feature of the positioning system described in the paper.

A COMPUTER-AIDED STUDY OF THE TEXTURE OF THE WORKING SURFACES OF GRINDING WHEELS

by

C. P. BHATEJA, A. W. J. CHISHOLM and E. J. PATTINSON*

SUMMARY

A computer-aided technique for studying the surface texture of the working surfaces of grinding wheels has been developed. This has been used to investigate the effect of wheel dressing conditions on the behaviour of the grinding wheel surface during use in grinding. It has been found that the total number of surface asperities on the working surface of a sharp wheel is virtually independent of the dressing feed, though with a degree of bunching of asperity peaks towards the outer region of the wheel surface. The degree of bunching of these asperity peaks decreases with increasing coarseness of dressing. The valleys in the surfaces, on the other hand, have a Gaussian-type frequency distribution. Significant changes in the forms of the frequency distributions of both asperity peaks and valleys on the working surface of the grinding wheel occur when the wheel becomes substantially worn. It is thought that the technique may be used in further studies of the wearing action of grinding wheels.

INTRODUCTION

The dressing of a grinding wheel has been shown to influence the geometry of the wheel surface¹ and the wheel's wear characteristics². The dressing process affects the active grit density on the wheel surface and hence the cross-sectional area and length of the grinding chips produced in grinding³, all of which are important basic parameters of the grinding process. The grinding wheel's behaviour during grinding is thus governed by the characteristics of its working surface.

The present investigation was concerned with a detailed study of the texture of the working surface of the grinding wheel, and of the effects of wheel dressing and wheel wear. Several parameters commonly used to describe the characteristics of surface texture have been used in this study of grinding wheel surface texture. These have been evaluated using digital techniques from the surface profiles obtained with the aid of a profilometer. The effects of different dressing feeds, of workpiece hardness and of wheel wear were studied in the grinding of steel on a surface grinding machine using alumina grinding wheels.

EXPERIMENTAL PROCEDURE AND TEST CONDITIONS

Dressing treatment

The grinding wheel used in the experiments was a plain cylindrical-type white alumina wheel. Dressing

was carried out by traversing a diamond tool in a path parallel to the wheel axis across the peripheral surface of the wheel. The angle between the tool axis and a radial line in the wheel at the point of contact was 10 degrees lagging with respect to the peripheral motion of the wheel. A special traversing mechanism was used to provide known uniform dressing feed rates. So that the initial condition of the grinding wheel was always constant prior to giving the wheel the selected experimental dressing treatment, a preliminary dressing was given to the wheel consisting of several passes of a diamond tool at a constant feed of 1.25×10^{-4} in/rev, but with decreasing depths of cut, as follows:

No. of passes	Depth of cut (in)
4	0.0005
20	0.00025
10	0.0001

The final dressing treatment (Table 1) was then carried out in a single pass using a special diamond tool preserved for the purpose.

Grinding experiments

The grinding operation used in the experimental work was carried out without cross feed on a conventional horizontal spindle surface grinding machine. The in-feed was established normal to the ground surface of

*University of Salford

the workpiece after each traverse of the workpiece; it was measured by means of a dial indicator micrometer. Grinding was carried out on a carbon steel, both in a hardened and in an unhardened condition. Tests were performed in each case with a coarsely dressed and a finely dressed wheel (Table 1). In all the four tests (designated as Tests 1 to 4) grinding was carried out until 1 in³ of work material per inch width of active wheel surface had been removed. The width of the workpiece was smaller than that of the grinding wheel. By interrupting the grinding operation at intervals and by using the wheel to grind a thin steel blade, and thereby to reproduce the wheel's worn stepped profile on the blade, it was possible to measure the development of radial wheel wear during each test. The height of the step on the measuring blade was determined by means of an inductive-type comparator gauge.

To explore the texture of the grinding wheel surface a profilometer was used which employed a diamond stylus capable of being traversed parallel to the wheel axis across the wheel surface. The surface profile was obtained as the output from an inductive-type transducer actuated by the stylus and using a strip chart recorder. The stylus was a 90 degree pyramid having a tip radius of 0.001 in. Several profilograms were obtained at each of a number of randomly located places around the wheel circumference, for every determination of the wheel texture. The profilograms were converted into numerical data using an electronic trace follower facility; the various surface texture parameters described in the following section were evaluated with a digital computer. The computer programs used for these determinations were written⁴ in Algol.

Table 1. Experimental conditions

<i>Grinding wheel</i>			
Specification:	WA 100 I V 7G (White alumina grit and Vitrified bond)		
Size:	8 in × $\frac{3}{4}$ in × 2 in		
<i>Workpiece material</i>			
Chemical Composition:	(%)		
	carbon 1.0 manganese 1.3 silicon 0.3		
	chromium 0.5 tungsten 0.5 vanadium 0.2		
Hardness	HV 240		
Heat treatment	Heated to 800°C, hardened by quenching in oil and tempered at 100°C		
Final hardness	HV 840		
<i>Dressing conditions</i>			
Type:	Single point diamond dressing		
Depth of cut of the dressing tool:	0.001 in		
Dressing feed	<i>Test No.</i>	<i>Dressing feed (in/rev)</i>	<i>Condition of work material</i>
	1	0.001	unhardened
	2	0.013	
	3	0.001	hardened
	4	0.013	
<i>Grinding conditions</i>			
Type:	surface		
Wheel speed:	4500 ft/min		
Workpiece speed:	60 ft/min		
Wheel depth of cut:	0.00025 in/pass		
Cross feed of the workpiece table:	None		

SURFACE TEXTURE PARAMETERS

The texture of the working surface of a grinding wheel consists of asperities having different shapes and sizes and arranged at different radial distances from the wheel axis. In a single cross section or profile of the wheel surface, each asperity appears as a pair consisting of a peak and an adjoining valley. To specify the surface texture parameters used in this study, it is necessary first to define an imaginary line called the mean line⁵. This lies in the general direction of the surface profile (i.e. in the direction of the X axis, Fig. 1) and is such that the sum of the areas enclosed between the line and the profile on each side of the mean line are equal. The distance between the highest peak and the lowest valley in the wheel surface profile, measured perpendicular to the mean line, is referred⁵ to as the maximum peak-to-valley height, H_{pv} .

The centre line average height, CLA, (Fig. 1) is defined⁵ as

$$CLA = \frac{1}{L} \int_0^L |Y - H_m| dX \quad (1)$$

The bearing area characteristic of the surface⁶ is represented by the curve obtained by plotting the ratio, for a particular height level, of the sum of the intercepts in the solid material parallel with the X-axis to the total length of the surface at the height level, against the height level concerned. An associated parameter is the degree of fullness⁷ of the surface, D_f : this is the ratio of the area between the section profile and the lowest valley level, to that of the rectangle passing through both the highest peak and the lowest valley and completely enclosing the profile.

The frequency distributions of the occurrence of peaks radially in the wheel were expressed in terms of the cumulative radial distributions of the asperity peaks above specified height levels in the wheel profile. This distribution was expressed as a percentage of the total number of peaks which occurred in the section profile under consideration. The frequency distribution was plotted against radial distance in the wheel. At the outer surface, that is at the highest peak level of the profile, the percentage of peaks by this procedure was zero (Fig. 1). The cumulative distribution

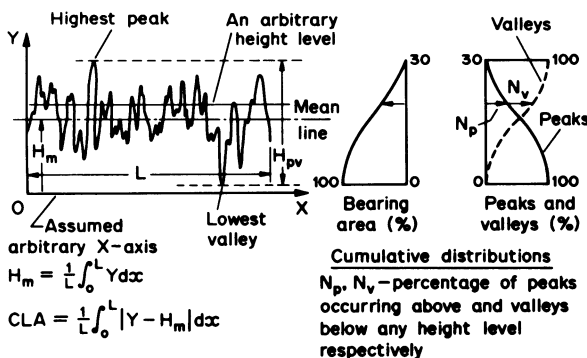


Fig. 1 Surface texture parameters

of valleys was correspondingly defined as the percentage of all valleys which occurred below a given radial height level. The percentage of valleys at the outer surface was, thus, 100.

DISCUSSION OF RESULTS

Radial wheel wear

The radial wear of the grinding wheel found in Tests 1 and 2 on the unhardened steel exhibited the three usual stages of wear, primary, secondary and tertiary (Fig. 2). However, when grinding the hardened steel (Tests 3 and 4) wheel wear was not so severe, and only the first two stages of wear were observed; the rapid increase in wear associated with tertiary wear did not occur during the duration of these particular tests. The coarse dressing feed in both cases gave generally higher amounts of radial wheel wear than the fine dressing feed.

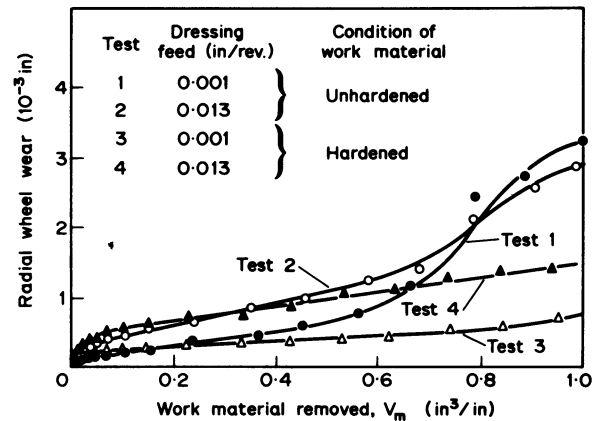


Fig. 2 Wear characteristics of the grinding wheel

The distribution of asperities

Fig. 3 shows typical cumulative radial distribution curves of asperity peaks and valleys for a sharp grinding wheel. Different symbols have been used in the figure for the results from individual profilograms. The shapes of the curves for the peaks and for the valleys are seen to be significantly different. Attempts were made to fit empirical relationships to these curves and it was found that the distribution of peaks could be fitted approximately using a polynomial relationship, while the distribution of valleys could be fitted approximately with a Gaussian relationship.

The polynomial relationship may be expressed mathematically as

$$N_p = 1 - (1 - h)^n \quad (2)$$

where N_p represents the ratio of the number of peaks occurring within a depth h below the highest peak to the total number of peaks throughout the whole of the surface profile. Mean curves were drawn from several profilograms for the distribution of peaks for sharp wheel surfaces (Fig. 4). From these, the values of the exponent n were estimated to be approximately 4.0 and 2.5 for the fine and coarse dressing feeds respectively.

The polynomial type distribution of peaks means,

Table 2. Summary of results from the analysis of the surface of the grinding wheel

Test No.	Volume of work material removed, V_m (in^3 per in)	Stage of wheel wear or condition of wheel surface	Radial wheel wear (10^{-3} in)	Degree of fullness, D_f	Maximum peak-to-valley height, H_{pv} (10^{-6} in)	Centre-line average height, CLA (10^{-6} in)	Total number of asperities per in, N
1	0.000	Primary	0.000	0.642	2210	472	192
	0.105			0.639	2701	550	194
	0.238	secondary	0.350	0.628	3337	618	182
	0.455			0.547	3680	691	177
	0.998			0.431	3949	739	167
2	0.001	primary	0.055	0.592	2805	555	194
	0.051			0.592	3144	609	192
	0.244	secondary	0.650	0.541	3650	722	171
	0.584			0.526	3908	733	169
	0.987			0.511	4193	751	163
3	0.000	sharp	0.000	0.650	2299	467	196
	0.957	worn	0.700	0.618	2839	572	164
4	0.000	sharp	0.000	0.600	2751	560	193
	0.942	worn	1.400	0.631	6476	1220	138

in effect, that the percentage of peaks occurring within the active region of the grinding wheel surface (that is the region concerned most with cutting material) is greater than that which would occur if the distribution was random, or even uniform. This bunching of asperity peaks towards the active outer region of the wheel is accentuated when a fine dressing feed has been used. Using the results of Fig. 4 and the value of H_{pv} given in Table 2, it can be estimated that, for a wheel dressed with a fine feed, approximately 35% of the total number of peaks lie within the active region with the depth of cut actually used during grinding, compared with only 15% for the coarsely dressed wheel.

The results in Table 2 show that the total number of asperities which occur on a sharp wheel surface is the same for both the fine and the coarse dressing feed. The estimated values of the corresponding *active* grit densities per square inch of wheel surface area are 12 500 and 5400 for the finely dressed and coarsely dressed wheels, respectively. An actual count using an optical microscope of the density of active grits for similar experimental conditions resulted⁴ in values of 10 500 per in^2 and 4600 per in^2 . The discrepancies in the values obtained by the two methods may have been caused by elastic deformation of both wheel and workpiece during grinding⁸. The coarse feed thus leaves fewer asperities within the active region of the sharp wheel surface. It also gives a greater maximum peak-to-valley height for the surface profile (Table 2). This indicates that the effect of dressing penetrates deeper into the surface at the coarser dressing feed. This is consistent with the hypothesis proposed by Pattinson and Chisholm² that the severity of the damage caused to the wheel surface material increased with the magnitude of the dressing

feed.

The mean bearing area curves for the sharp wheels (Fig. 5) are consistent in shape with the cumulative distribution curves described above. The fine dressing feed gave a greater bearing area at all intermediate height levels compared with the coarse dressing feed.

Effects of wheel wear

Changes in type of wheel wear which occurs as wear develops during the wheel life between dressing treatments may be expected to be reflected in the characteristics of the wheel surface; such changes may be studied using the techniques described above. The possible usefulness of these techniques for the study of the mechanism of wheel wear in grinding may thus be examined.

The primary wear stage ceases when about 0.08 in^3 of work material per inch of wheel width has been ground (Fig. 2). In this stage of wear, the shapes of the cumulative asperity distributions were found to remain virtually unchanged, as did the total number of asperities, N (Table 2). Further, only modest changes were observed in the degree of fullness, D_f , and the maximum peak-to-valley height, H_{pv} . These observations are consistent with a wear mechanism involving mainly grit fracture. Such a mechanism would tend to maintain the sharpness of the wheel surface and hence the original geometrical characteristics of the dressed wheel surface, since wear by fracture would be similar in its influence to the actual dressing process.

Comparison of Fig. 6a with Fig. 3 shows that, during the secondary stage of wheel wear, there was still no substantial change with increasing wheel wear in the character of the cumulative distribution curves for the asperity peaks or valleys; however, in the

polynomial type of curve for the distribution of asperity peaks, reductions in the values of the exponent n were found to occur for both dressing feeds. A number of other changes also occurred in the values of the parameters of the wheel surface (Table 2). The total number of asperities, N , decreased; moreover, both the maximum peak-to-valley height, H_{pv} , and the CLA height of the profile increased. The changes in the cumulative distribution of peaks along with the observed changes in N and H_{pv} mean that the number of asperities which occurred within the outer height levels of the wheel decreased with increasing wear.

These trends are thought to be consistent with a wear mechanism consisting *mainly* of gradual attrition of the asperity peaks; in this mechanism clusters of small asperity peaks would merge into one another to form large single asperities, a process which would result in the observed reduction in the number of peaks in the active cutting region of the wheel surface. However, the observed decrease in the degree of fullness, D_f , and the rise in the maximum peak-to-valley height with increasing wear (Table 2) suggest that wear or changes in the wheel during the secondary stage occurred by fracture at the lower height levels in the surface.

When the wheel wear becomes severe, as in the tertiary stage (Tests 1 and 2 in Fig. 2), the cumulative distribution curves of asperity peaks change from the polynomial type to the Gaussian type (Fig. 4). This change means that with the occurrence of severe tertiary wear the number of peaks within the active region of the grinding wheel surface is reduced considerably. A corresponding reduction in the bearing area at any level in the wheel surface profile also occurs (Fig. 5). Fig. 6 shows that the change in the cumulative distribution of the valleys in the tertiary wear stage is not nearly as great as that of the peaks. Even though the same amount of work material had been ground in the tests on hardened steel, where

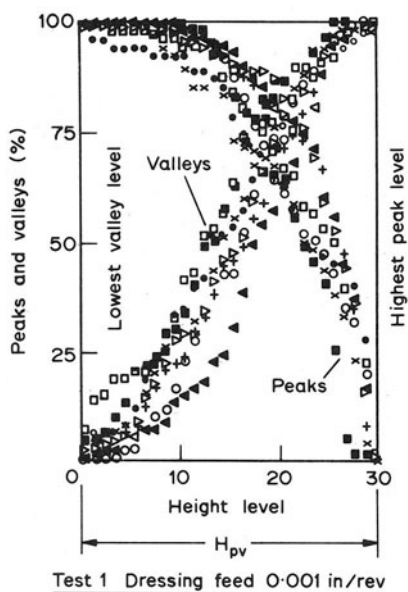


Fig. 3 Cumulative radial distributions of peaks above and valleys below any height level on the working surface of a sharp grinding wheel

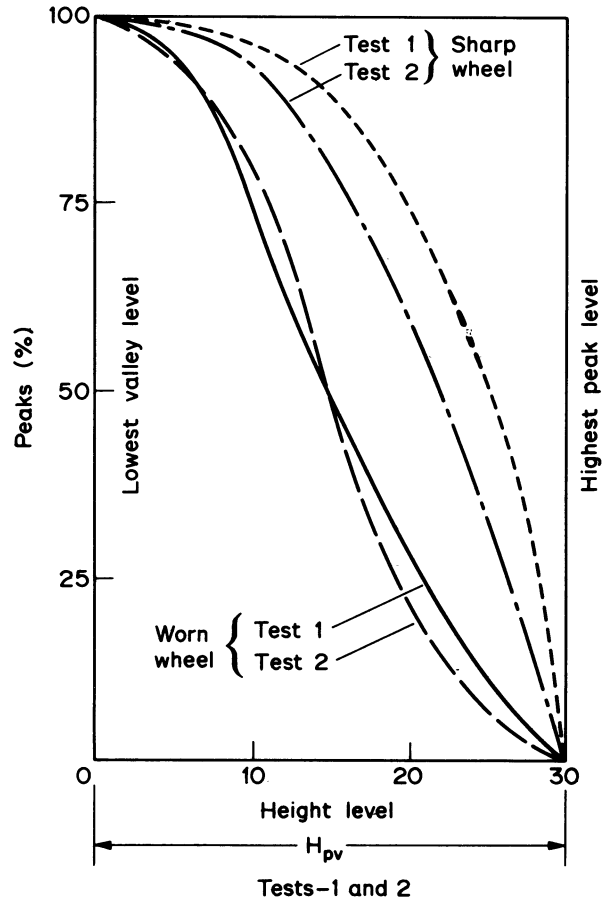


Fig. 4 Mean cumulative radial distribution curves for peaks on the grinding wheel surface

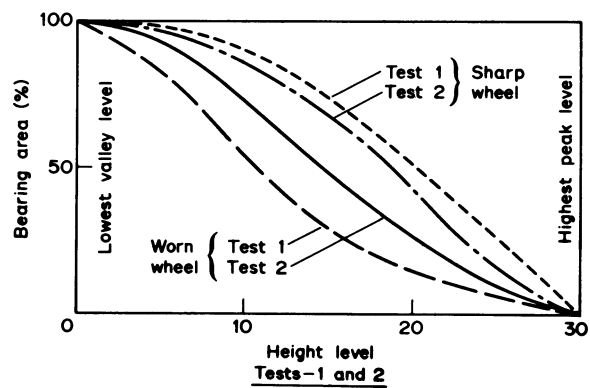


Fig. 5 Mean bearing area curves for the sharp and the worn grinding wheel

tertiary wear did not develop, it is of interest to note that no changes in the types of the cumulative distribution curves for peaks and valleys did in fact occur (Fig. 7).

A mechanism in which complete or large portions of grinding grits are removed from the bond material is illustrated diagrammatically in Fig. 8. Also shown qualitatively are the resulting changes to be expected in the cumulative distributions of peaks and valleys. Thus, this type of wear mechanism would tend to reduce significantly the bunching or concentration of asperity peaks within the active region of the wheel surface profile. Such changes do in fact occur with

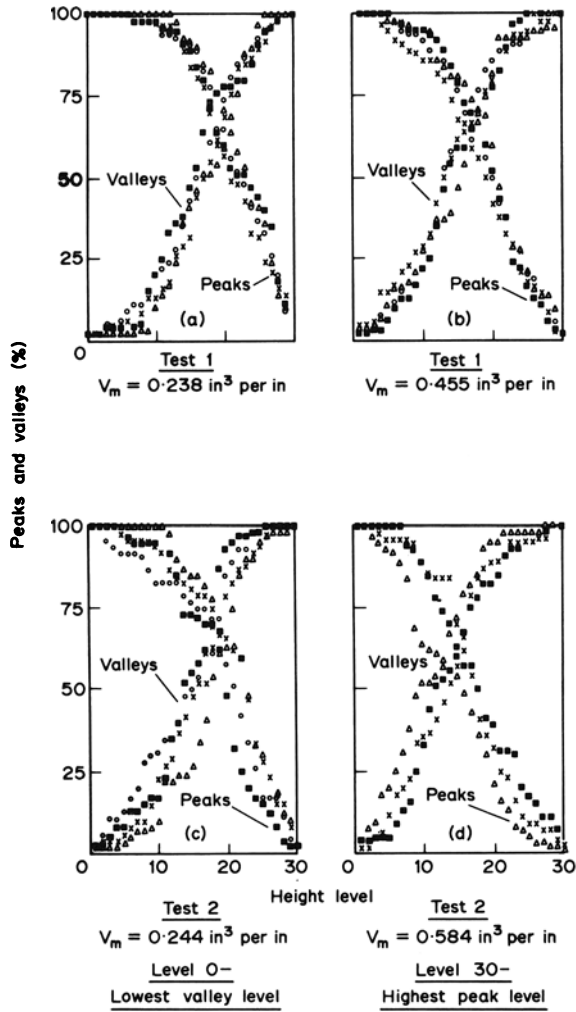


Fig. 6 Cumulative radial distributions of peaks and valleys on the grinding wheel surface before and after the onset of tertiary stage

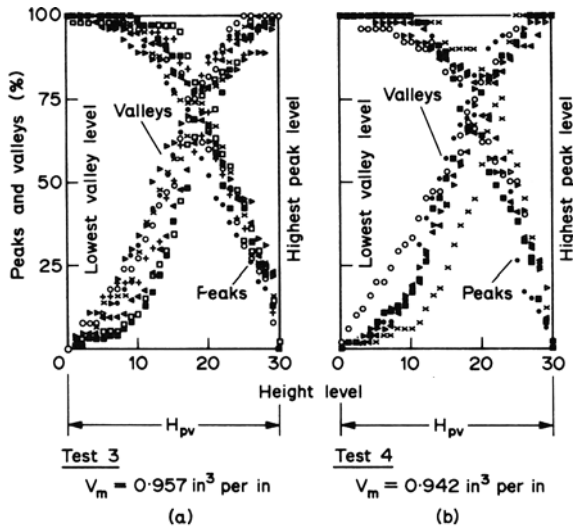


Fig. 7 Cumulative radial distributions of peaks and valleys on the worn grinding wheel surface

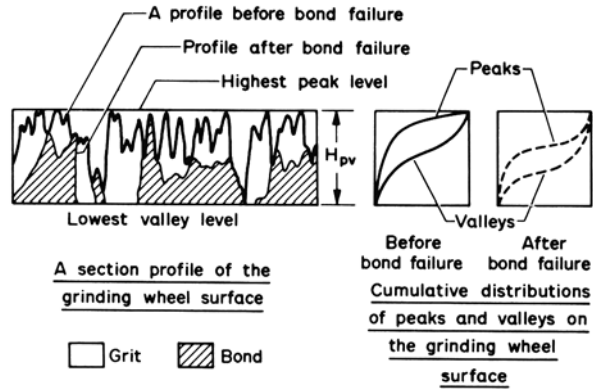


Fig. 8 Effect of bond failure on the cumulative radial distributions of asperity peaks and valleys on the grinding wheel surface

tertiary wear (Figs. 4 and 6). This mechanism of bond post rupture may also explain the large reductions observed in the bearing area (Fig. 5) and in the degree of fullness, D_f , (Table 2) of the surface, both of which would not occur if wear by attrition predominated during this stage of wheel wear. The large increase in H_{pv} (Table 2) is also consistent with bond post rupture.

It will be noted that tertiary wear which involves large amounts of radial wheel wear, caused apparently by bond post rupture in the wheel, would cause an obvious loss of wheel form.

CONCLUSION

A technique for the numerical analysis of the texture of the working surface of a grinding wheel has been developed. This method has been applied to the investigation of the effects of the wheel dressing feed on the wheel surface geometry, both for freshly dressed wheels and for wheels worn during grinding.

For a sharp or freshly dressed wheel, the curve representing the cumulative radial distribution in the wheel of the surface asperity peaks was found to be polynomial in form. The curves were shaped such that the peaks were bunched more towards the outer periphery of the wheel surface (that is towards the wheel's active region) than towards the wheel centre. This bunching of the peaks towards the wheel's active region was less pronounced with the coarser dressing feed than with the fine feed. The valleys in the surfaces, on the other hand, were randomly distributed radially, for both the coarse and the fine dressing feeds; thus the cumulative radial distribution curves for the valleys approximated to a Gaussian type. It follows that there were many more peaks than valleys in the active outer region of the wheel's surface, an effect more marked when the wheel had been dressed with the fine feed. Perhaps rather surprisingly, the total number of asperities on the sharp wheels was little affected by the magnitude of the dressing feed used.

Consistent with these surface characteristics were the further observations that the bearing area, at a given depth, and the degree of fullness were greater for the fine dressing feed; the fine feed also gave

lower values of average roughness and peak-to-valley roughness.

It was found that wheel wear only significantly affected the surface characteristics of the wheel with the onset of tertiary stage wear. With this heavy wear, which was only detected when grinding the unhardened materials, the cumulative radial distribution of asperity peaks changed from the polynomial to the Gaussian form, whilst that of the valleys changed from the Gaussian to the polynomial form. The latter displayed the greater concentration of valleys towards the wheel centre. Thus, for badly worn wheels, the excess number of peaks over the number of valleys in the active region of the wheel surface was less than for sharp wheels. Furthermore, the actual number of asperity peaks occurring within the active region of a worn wheel surface was reduced considerably. These changes could be used to indicate the onset of tertiary wear and hence the end of the useful life of a grinding wheel. One obvious effect of diamond dressing on a worn grinding wheel was therefore to produce a rearrangement of asperities on the wheel surface causing, within the active region, significant increases in both the actual number of asperity peaks and the 'excess number of peaks over valleys'.

The technique established in this work has been used to study the mechanism of wear during the primary, secondary and tertiary stages of wheel wear. The results suggest that the changes observed in the parameters used in this work to describe the wheel surface texture are consistent with the predominance of a particular mechanism of wear in each of these stages.

REFERENCES

1. PAHLITZSCH, G., and APPUN, J., 'Effect of truing conditions on circular grinding', *Ind. Diamond Rev.*, **14**, 185-9 September, 212-7, October (1954).
2. PATTINSON, E. J., and CHISHOLM, A. W. J., 'Effect of dressing techniques on grinding wheel wear', *Intern. Conf. Manuf. Tech., Michigan*, pp. 601-16 (1967).
3. BACKER, W. R., and MERCHANT, M. E., 'On the basic mechanics of the grinding process', *J. Eng. Ind. (Trans. ASME, Ser. B)*, 141-8, January (1958).
4. BHATEJA, C. P., 'The influence of dressing on the performance of grinding wheels', *Ph.D. Thesis*, University of Salford, (1970).
5. 'Centre-line-average height method for the assessment of surface texture', *British Standards Institution*, No. 1134 1961 (1961).
6. REASON, R. E., 'The measurement of surface texture', in *Workshop Technology*, Part II (Ed. H. W. Baker). 2nd edn., Cleaver Hume Press, London, pp. 417-75 (1960).
7. MILLER, L., *Engineering Dimensional Metrology*, Edward Arnold, London, p. 38 (1962).
8. HAHN, R. S., 'On the nature of the grinding process', *Proc. 3rd Intern. MTDR Conf., Birmingham*. p. 129 (1962).

DISCUSSION

Query from M. M. Sfantsikopoulos UMIST

Did the combination of grinding wheel grit size 100 with a tip radius of 0.001 in. of the diamond stylus prove satisfactory as far as repeatability of the profilograms is concerned?

Reply

The two main requirements of the stylus are sensitivity and stability, and obviously each could be improved at the cost of the other. Tests were conducted to determine an optimum geometry and material of the stylus and the 90° diamond pyramid stylus with a tip radius of 0.001 in. was found to be quite satisfactory for the grinding wheel used.

DIGITAL COMPUTATION OF SURFACE TOPOGRAPHY

by

H. KALISZER *, D. J. GRIEVE † and G. W. ROWE ‡

SUMMARY

This paper deals with the selection of equipment for digital surface topography measurements and the theoretical and practical aspects of the digital computer programming required.

Amplitude and frequency characterization of a surface by computation of digital records is discussed with reference to engineering requirements and the practical accuracy obtainable. The application of these techniques to three-dimensional surface measurements is also included.

INTRODUCTION

Modern engineering surface topography was initiated by Abbot and Firestone¹ in 1933 who first built a stylus measuring device; very little was known about the importance of surface finish at that time. Since then measuring equipment (still mainly stylus devices) has improved considerably and there has been increasing debate concerning which surface parameters are important. Unfortunately, different parameters are useful indicators for different properties so ideally several should be available. Commercial

analogue devices become more expensive as the number of parameters evaluated is increased and they are usually limited to centre-line average height (R_a) (see Fig. 1) and peak-to-valley height (R_{max}). However, digital computation is now widely available, and elaborate analytical processing is quite possible with no extra capital outlay once basic facilities are available.

This paper deals with the problems of obtaining accurate digital results by optimum use of equipment and programming techniques.

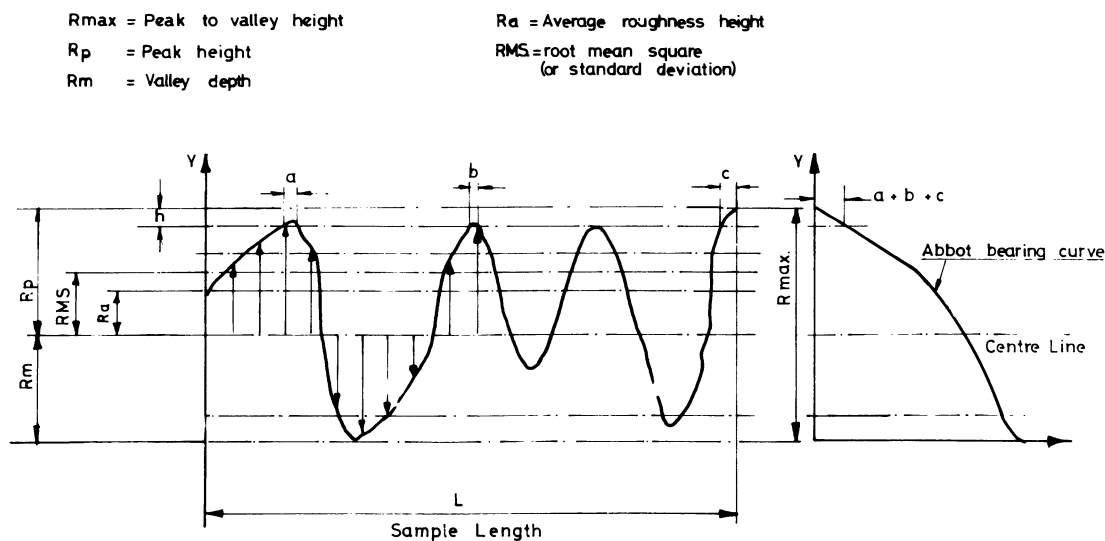


Fig. 1 Definitions of surface topography parameters.

*Department of Mechanical Engineering, University of Birmingham.

†I.M.I., Birmingham.

‡Department of Industrial Metallurgy, University of Birmingham.

SPECIFICATION OF THE PROBLEM

Recent research shows that the following parameters may be useful for certain engineering specifications. R_a (general), slope²⁻⁵ and bearing area⁶ (for joint stiffness), bearing area and peak-to-valley height (for lubrication). Slope is a frequency characteristic: the others are amplitude characteristics.

Typical modern equipment measures the average roughness height, (R_a or CLA), peak height, valley depth and peak-to-valley depth. In addition, a profilogram of the surface is also provided. For a full discussion of such devices readers are referred elsewhere^{7, 8}.

DIGITAL EQUIPMENT

Digital equipment (Fig. 2a) should be capable of providing with high accuracy all the results that the analogue devices can. Our equipment is typical and will be described in detail. Fig. 2b shows the schematic layout. Regardless of whether new equipment is to be bought, consideration must be given to minimum requirements. It is ideal to have on-line facilities available, but this is seldom possible owing to excessive tie-up of computer time; the usual mode of operation is off-line with a suitable means of data storage (punched tape in our case). The exact choice of equipment depends on available funds; Table 1 compares some of the possible devices.

Before a decision is made on the above the ordinate spacing must be chosen. This depends on the surface characteristics with which the recording speed and the stylus traversing speed must be commensurate. Commercial equipment usually provides three or four stylus traversing speeds and digital recording speeds. Table 2 shows the range of ordinate spacing available with the authors' Talysurf III and Solatron analogue-to-digital converter (A.D.C). A very large number of close ordinates is usually undesirable as

differentiation becomes less accurate and computer time is increased.

For the purpose of this paper the authors considered surfaces with roughness $R_a \geq 1\mu\text{m}$. Such surfaces can be generated by a variety of common production processes including not very fine grinding. On the basis of the above assumption an ordinate spacing of $5\mu\text{m}$ appeared to be the best compromise. Such spacing was obtained by a stylus traversing speed of $50\mu\text{m/s}$ and a recording speed of 10 ordinates/s. Since the published analysis is only intended to characterize surface microtopography all surfaces were selected with negligible waviness. For such surfaces the sample length equals the length of stylus traverse (the analysis of waviness by digital means is fully described by Whitehouse and Reason¹¹).

The sample length depends on the object to be measured, number of ordinates and ordinate spacing. Work by Sharman¹⁰ indicates that samples of at least 300–500 ordinates are required for accurate computation when considering amplitude characteristics; our work suggests 500 ordinates (for amplitude characteristics) and 1000 ordinates (for frequency characteristics). Most of our specimens were 10 mm long from each surface; samples 7.5 mm long were recorded, containing a sample size of 1500 ordinates.

The remaining problem is to finalize the choice of A.D.C. The Solatron apparatus made for the purpose incorporates a standard voltage source to shift bipolar to unipolar signals, saving the recording of one character (the + or – sign). Easy adjustments and remote start facilities are normal fitments. The Solatron has a special control unit for use with various commercial surface topography measuring devices, which eliminates the need for external amplifiers and such. The Talysurf III provides a modified and unmodified profile for digitizing purposes. Filtering, if required, is carried out by digital programming.

Table 1. Analogue-to-digital converter characteristics

Device	Maximum character recording speed/s	Comparative cost	Comparative record density	Can data be fed directly to computer?
Magnetic tape	200–800	10	1000	Yes
Punched paper tape	80–150	1	10	Yes
Punched cards	35	1	1	Yes
Teleprinter	35	1	2	No

Table 2. Ordinate spacing as a function of A.D.C. speed and stylus traversing speed

Digitizing speed (ordinate/sec)		4	10	20
Stylus speed in/s	Horizontal gearbox magnification setting	ordinate spacing (in)		
0.04	(x 5)	0.010	0.004	0.002
0.01	20	0.0025	0.001	0.0005
0.002	100	0.0005	0.0002	0.0001
0.0004	500	0.0001	0.00004	0.00002

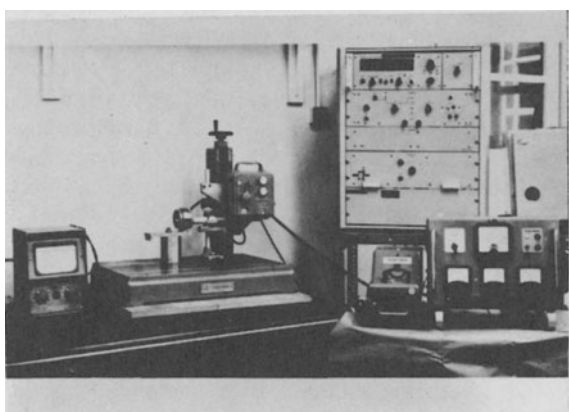


Fig. 2a. General arrangement of the computerized equipment used for surface topography measurement.

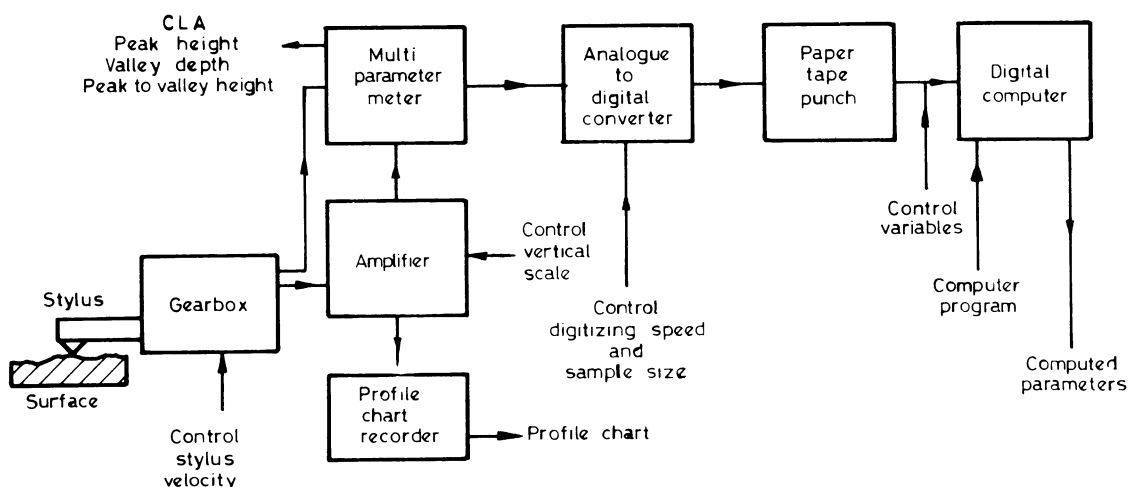


Fig. 2b Computerized surface measuring equipment (schematic).

PROGRAMMING

Parameters may be split into two categories, amplitude and frequency characteristics. As a signal is measured in the form of amplitudes, the R_a , R_{max} are relatively simple to program; however, frequency characteristics require greater care in their evaluation. Amplitude characteristics require some type of centre line or mean line to be fitted to the data before they can be evaluated. A number of standards and articles deal with this topic^{8,11}.

First a centre line is established as a reference from which an integrated average of the whole of the defined length of the profile is obtained. The centre

line has the nominal shape of the defined length and is so positioned that the sum of squares of equally spaced ordinates measured from it is a minimum. The centre line or mean line is found automatically by electrical integrating instruments built into most of the available surface measuring devices.

When examining by digital methods the microtopography of a specimen free from waviness, a straight centre line was fitted to the recorded data (see appendix). The equation which determines the location of the centre line is the following (Fig. 3):

$$\hat{y}_i = \bar{y} + b(i - \bar{i}) \tag{1}$$

Frequency characteristics

There are three principal ways of characterizing frequency:

- (i) Fourier and power spectrum analysis,
- (ii) autocorrelation functions,
- (iii) derivatives.

Fourier analysis and autocorrelation functions are powerful techniques that may be programmed without difficulty¹⁸ and a fair amount of work has been carried out^{19,20} and continues in this aspect of surface measurements. However, results are still largely theoretical, although attempts are being made to link theory with engineering properties.

Many surface properties are directly dependent on derivatives, mainly the first and second.^{2-5, 21, 22} For this reason the authors use derivatives for frequency characterization. There are a number of difficulties associated with the evaluation of derivatives whether carried out by analogue or digital computation. Using the equipment described, the ordinate values are recorded to three significant figures which represents an 'average accuracy' of one part in 500 or 0.2% which will be fairly constant, as will be the ordinate spacing. The accuracy of the difference depends on the magnitude of the difference. For normal surfaces, slopes are less than 15°, usually 1-5° and less for worn surfaces². Fig. 4

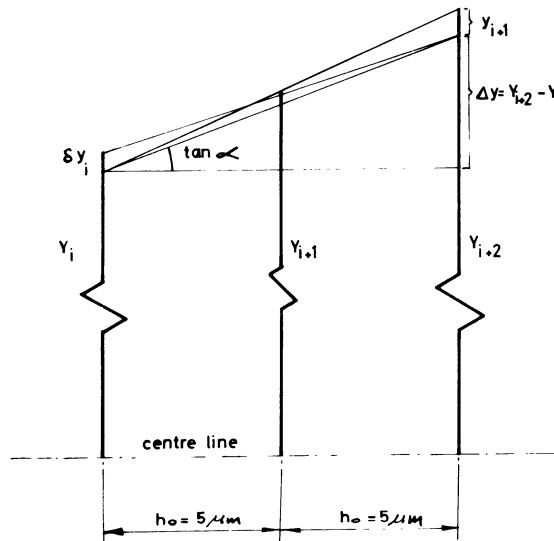


Fig. 4 Errors occurring during differentiation.

shows the errors that are typical using a simple differentiation formula, the accuracy of the derivative being one order of magnitude less than the accuracy of the original signal. The resulting derivatives will be scattered about their true values, so some means of smoothing (removing random electrical and mechanical noise) must be employed. A large number of smoothing techniques have been known for many years¹⁸ but the time required for manual computation discouraged their use until electronic digital computation facilities became available. The following paragraphs examine relevant aspects of the topic.

Kopal²³ recommends first that the sample interval (ordinate spacing) to minimize 'noise' is chosen by a method which in practice amounts to trial and error.

This is impractical in most instances as most A.D.C.s have only a limited range of speeds which, even when combined with the range of stylus traversing speeds, is unlikely to give a large well-covered range of ordinate spacings (see Table 2). The authors preferred to choose an ordinate spacing as described in the section 'Digital Equipment' and then check the accuracy when the smoothing technique has been chosen (see below).

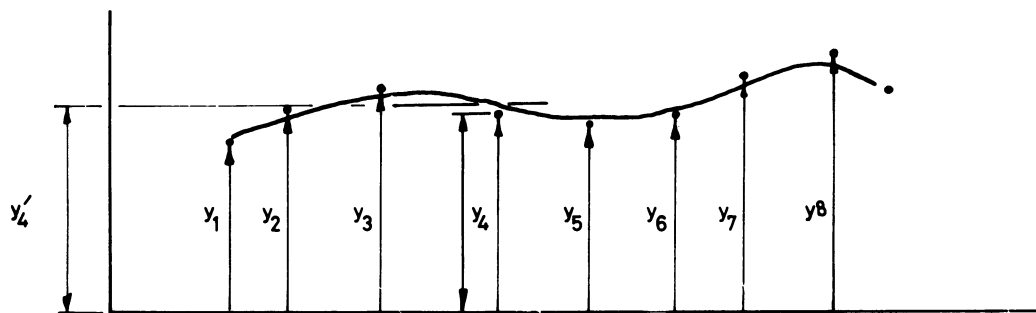
The actual form of smoothing depends on the likely noise level and usually involves fitting a second, third, fourth or even higher-order polynomial (or an approximation to one, to three or more adjacent ordinates). The smaller the order of the polynomial fitted to the number of adjacent ordinates considered, the greater will be the smoothing, as the fit will be less accurate. The choice of polynomial is largely empirical and is not significant provided the same one is used for all computations. The authors used a fourth-order polynomial fitted to seven adjacent ordinates¹⁸, the least squares fit being used. Fig. 5 shows how this is done. It should be noted that the entire polynomial is not required, only the value of the smoothed ordinate Y'_4 to replace the ordinate Y_4 . The calculation in Fig. 5 is then performed on the ordinates $Y_2 - Y_8$ giving the smoothed ordinate Y'_5 to replace the ordinate Y_5 . The calculation is applied to successive ordinates along the profile until all have been smoothed.

$$\begin{aligned} \text{Average digitizer accuracy } \delta y &\approx 0.2\% \\ \text{Average slope } \alpha &\approx 2^\circ \\ \text{Hence } \Delta y &= 2 h_0 \tan \alpha \approx 0.35 \mu \\ \text{For average value of Ra} &\approx 2.5 \mu \rightarrow \delta y = 0.005 \mu\text{m} \\ \text{Slope accuracy } \frac{\delta y}{\Delta y} &= \pm \frac{0.005}{0.35} \approx \pm 1.4\% \\ \text{Variation in slope values} &= \frac{\Delta y \pm \delta y}{2 h_0} \\ &= 0.035 \pm 1.4\% \end{aligned}$$

A series of experiments was carried out using the smoothing technique described to establish the accuracy of the method. The main test involved using the program to evaluate surface topography parameters of a standard series of data for which exact analytical solutions were known. The values of a sine series were taken from trigonometrical tables, recorded at 15° intervals (24 values per wavelength, to three significant figures). The evaluated parameters agreed closely with the theoretical values (Table 3), being more accurate than the results evaluated by the same program without smoothing. Real surfaces do not consist of a single sine series but may be approximated by a combination of different sine and cosine series (20) of different frequencies (Fourier series).

Table 3. Errors of parameters evaluated from a sine series

Parameter	Error %	Type of parameter
R_a	0.15%	Simple average
Standard deviation (σ)	0.15%	Simple average
Peak height	0.5%	Highest point (individual)
Valley depth	0.5%	Lowest point (individual)
First derivative average modulus	2%	Average of first derivative
Second derivative average modulus	3%	Average of second derivative



y'_4 is replaced by the smoothed value given by:

$$y'_4 = \frac{1}{231} [131y_4 + 75(y_3 + y_5) - 30(y_2 + y_6) + 5(y_1 + y_7)]$$

This is the least square fit polynomial

Fig. 5 Smoothing by fitting a polynomial.

The higher harmonics of such a series will not be sampled in such a satisfactory way, but these comprise a smaller part of the surface, so the overall error will not be large and will be within 10–15% for the evaluated derivatives of most real surfaces. To obtain this accuracy, the first derivatives must be smoothed in the same way before the parameters are evaluated and the second derivatives evaluated and smoothed in turn.

APPLICATION IN THREE DIMENSIONS

accurate measurements in three dimensions which is not prohibitively time consuming. A comparison of various techniques is given by Grieve²⁴. The stylus device has most often been used in the past for engineering surfaces¹⁵ and we have developed this technique and increased its scope to enable a very wide range of

The characterization of three-dimensional phenomena should enable any directionality or variation in uniformity across a measured sample to be clearly shown. In the study of surface topography the main problem has been to develop a method of making objects to be repeatedly measured at the same place with reasonable speed (using a modification of Williamson and Hunt's relocation technique²⁵). The authors record 22 000 spot heights from an area 0.25 mm by 5 mm, depending on the scale required²⁶; the data consisting of 25 close parallel profiles each containing over 900 ordinates. Amplitude characteristics are evaluated in an analogous way to that described in the earlier section, a two-dimensional array of ordinate heights being used rather than the one-dimensional array.

A directional surface is one on which machining marks in one direction predominate, for example, a

turned or shaped surface. A non-directional surface is one on which any marks are in random directions, that is, sand-blasted or spark-eroded surfaces. These directional properties may in certain instances be of interest, for example, in sliding contacts. Although it is usually possible to distinguish such surfaces without difficulty, some quantitative frequency characterization is desirable. The authors use derivatives.

When examining multiple-profile records such information is available by finding derivatives in two mutually perpendicular planes that are also perpendicular to the surface, that is, parallel to the profile direction (Fig. 6),

$$(b_4 - b_2)/2 h_o \tag{6}$$

and perpendicular to the profile direction

$$(c_3 - a_3)/2 h_p \tag{7}$$

Data smoothing in two directions is more complex than in one direction, but may be programmed with-

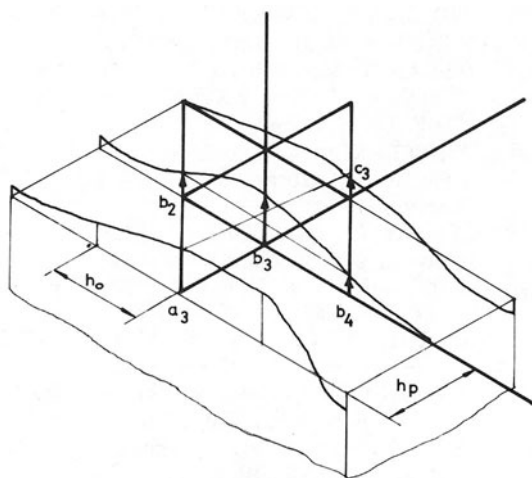


Fig. 6 Derivatives in two directions.

out difficulty, especially if a large capacity computer is available. Simple methods of smoothing are recommended; three or five adjacent ordinates in each direction should be fitted to a low-order polynomial, the geometric or arithmetic mean of the two values for the coinciding smooth ordinates being chosen as the actual smoothed ordinate.

An important advantage of surface representation in three dimensions is that true high spots of the surface may be found easily, that is, a point above its eight nearest neighbours is a true summit (Fig. 7). In a single profile, an indicated high spot may in fact only be on the side of a summit. The authors have found that there are only about half the number of true summits in a surface as there are peaks indicated in single profile analysis for random sand-blasted surfaces.

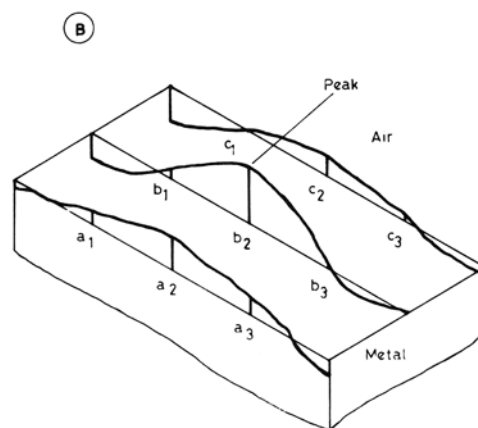
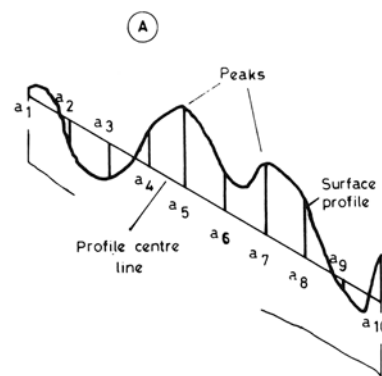


Fig. 7 Definitions of peaks and true summits.

Generally, the authors consider that single profiles give sufficient information for almost all applications when considering non-directional surfaces, and for many applications even when considering directional surfaces.

CONCLUSION

The paper describes theoretical and practical techniques for investigating amplitude and frequency characteristics of surface topography measurements by numerical methods. Although the examples considered are of surface topography, the authors' field of interest, much of the information is applicable to any type of data.

ACKNOWLEDGMENTS

The authors wish to thank Professor S. A. Tobias and Professor E. C. Rallason for providing facilities for the work, and the Science Research Council and G.K.N. Ltd. for various aspects of financial support.

APPENDIX

As can be seen from Fig. 3 the parameter a represents the intercept and parameter b the slope of the centre line. The ordinates with respect to the centre line can be determined numerically as follows:

$$y_i^* = y_i - \hat{y}_i \tag{1}$$

$$\hat{y}_i = a + bx_i \tag{2}$$

If one introduces a centroid with coordinates,

$$\bar{x} = \frac{\sum x_i}{N} \quad \text{and} \quad \bar{y} = \frac{\sum y_i}{N}$$

(where N = number of ordinates), then all calculations can be considerably simplified. In particular it can be shown that

$$y_i = \bar{y} + \frac{(x_i - \bar{x})y_i}{(x_i - \bar{x})^2} \tag{3}$$

where $a = \bar{y}$ and $b = \frac{\sum(x_i - \bar{x})y_i}{\sum(x_i - \bar{x})^2}$

For constant ordinate spacing $\Delta x = \text{constant}$

$$\begin{aligned} x_1 &= \Delta x \\ x_2 &= 2\Delta x \\ x_3 &= 3\Delta x \\ &\dots\dots\dots \\ x_i &= i\Delta x \\ \bar{x} &= \bar{i}\Delta x \end{aligned} \tag{4}$$

By considering equations 1, 2 and 4

$$y_i^* = y_i - \left[\bar{y} + \frac{(i - \bar{i})y_i}{(i - \bar{i})^2} (i - \bar{i}) \right]$$

where y_i^* = value of ordinates with respect to the centre line
 y_i = value of recorded ordinates with respect to an arbitrary datum

REFERENCES

1. ABBOT, E. J., and FIRESTONE, F. A., 'Mechanical Engineering', 55, 1933, p. 569.

2. HALLIDAY, J. S., I. Mech. E. Conf., 'Lubrication and Wear', 1957, p. 647.
 3. HALLIDAY, J. S., Proc. Inst. Mech. Engrs., London, 169, 1955, p. 277.
 4. BLOK, H., Proc. Roy. Soc., A 212, 1952, 480.
 5. ARCHARD, J. F., J. Appl. Phys., 32, 8, 1961, p. 1420.
 6. REASON, R. E., 5th M.T.D.R. Conf., Birmingham, 1964.
 7. REASON, R. E., HOPKINS, M. R., and GARROD, R. I., 'Report on the Measurement of Surface Finish by Stylus Methods', Rank Taylor, Hobson, Leicester, 1944.
 8. B. S. 1134, 1961, 'Centre-line-average height method for assessment of Surface Texture', British Standards Institute.
 9. NAKAMURA, T., Bull. Jap. Soc. Pre. Eng., 1, 4, 1966, p. 240.
 10. SHARMAN, H. B., N.E.L. Report No. 230, 1966.
 11. WHITEHOUSE, D. J., and REASON, R. E., 'Equation of the Mean Line of Surface Texture Found by Electric wave filters', Rank, Taylor, Hobson, Leicester, 1965.
 12. HOEL, P. G., 'Elementary Statistics', Wiley and Sons, London, 1963.
 13. REASON, R. E., 6th M.T.D.R. Conf., Manchester, 1965.
 14. WHITEHOUSE, D. J., 'Metrology of Surfaces', I. Mech. E. Conf., Oxford, 1968.
 15. WILLIAMSON, J. B. P., 'Metrology of Surfaces', I. Mech. E. Conf., Oxford, 1968.
 16. PESANTE, M., 12th C.I.R.P., 1962.
 17. SILIN, R. I., and FREDERICK, J. R., 16th C.I.R.P., Paris, 1966.
 18. WHITTAKER, E. T., and ROBINSON, G., 'The Calculus of Observations', Blackie and Son, London, 1924.
 19. AL-SALIHI, Ph.D. Thesis, Dept. of Mech. Eng., University of Birmingham, 1968.
 20. DUNIN-BARKOVSKY, I. V., 'Metrology of Surfaces', I. Mech. E. Conf., Oxford, 1968.
 21. CLARK, W. T., CONNOLLY, A., and HIRST, W., Brit. J. Appl. Phys., 14, 1963, p. 20.
 22. GREENWOOD, J. A., and WILLIAMSON, J. P. B., Proc. Roy. Soc., A295, 1966, p. 300.
 23. KOPAL, Z., 'Numerical Analysis', Chapman and Hall, London, 1955.
 24. GRIEVE, D. J., M.Sc. Thesis, Dept. of Mech. Eng., University of Birmingham, 1969.
 25. WILLIAMSON, J. B. P., and HUNT, R. T., J. Sci. Inst. (J. of Phys. E), Ser. II, I, 1968.
 26. KALISZER, H., GRIEVE, D. J., and ROWE, G. W., 19th C.I.R.P., Geneva, 1969.

CHOOSING MANUFACTURING RESOURCES

by

G. A. E. SEWELL*

SUMMARY

From a basis of a known work load and the known capabilities of manufacturing resources, a set-theoretic analysis leads to the identification of constraints bearing upon the process of resource selection in any given case. A suitable criterion of optimality then permits an optimal selection to be made by linear or other mathematical programming methods.

INTRODUCTION

It is the purpose of this paper to describe a method of selecting those resources best suited to undertake a given work load. Whilst in this paper attention is focused on resources such as the machinery used in the manufacturing industry, a similar approach may be used in the treatment of other resource selection problems.

The necessity of brevity prevents a complete treatment of this subject in this paper and a detailed analysis is developed in the publications quoted later¹⁻³.

DOMAINS OF CAPABILITY

The detailed analysis² of the properties of domains of capability may be illustrated by means of the familiar Venn diagram. Thus, for example, Fig. 1 represents the universe of resources (machines) which are or may be of current interest. Any particular machine will be represented by a point within the defined universe. For convenience, sub-regions may be identified which contain exclusively points relating to specific sets of machines, that is collections of machines, each of which possesses certain specified properties. Frequently any given set may be further divided into sub-sets. Thus, for example, the set M_L of all lathes may be regarded as being compounded of type A lathes and type B lathes. This union is expressed algebraically as

$$M_L = M_A \cup M_B \quad (1)$$

It is also convenient to define a universe of work as in Fig. 2. Every job of work can be represented by a

point in this universe. Sets of work having particular properties can be identified. For example, by scanning through the whole universe of work, job by job, and identifying all those jobs which could be done by a specific machine, a set of jobs is obtained which constitutes the domain of capability of that machine. If such a scanning operation is to be carried out by automatic computers, it is convenient to make use of sentential functions^{2,5} to relate the significant properties of work and machines.

The domain of capability of a particular machine is shown in Fig. 2 as domain C_m . Since the whole universe of work has been scanned, any job which could be done by this particular machine will be represented by a point within C_m . Clearly, C_m will also be the domain of capability of all the other machines whose construction and performance are identical to those of the given machine.

The work which is tendered to any particular workshop is, of course, a small part of the universe of work and is represented by the shaded region, W , in Fig. 2. It is obvious that none of this work, W , lies within C_m , so that this workshop has no use for type m machines. Type 1 machines (domain of capability C_1) can undertake part of the work of the workshop and, indeed, could undertake other work also.

Machines of type 2 are in a similar state to those of type 1. However, in the case of type 3 machines, work is available which would exercise their full capability.

If machines of types 1, 2 and 3 were the *only* ones available, then, clearly, no matter how many of such resources were chosen, much of the load on the workshop could not be executed. This illustrates that some selection problems are insoluble.

The domains of capability of type 2 and type 3

*University of Salford.

machines intersect, indicating that for some work a choice has to be made as to which type of machine shall be chosen to do it.

The work which could be done by type 2 machines is identified as the intersection, W_2 , of sets, namely

$$W_2 = W \cap C_2 \tag{2}$$

and for type 3 machines similarly

$$W_3 = W \cap C_3 \tag{3}$$

The work which could be done by either type 2 or type 3 machines is W_{23} , where

$$W_{23} = W \cap C_2 \cap C_3 \tag{4}$$

Finally, in this illustration, the work which can be done by type 2 machines *only* is

$$W_{02} = W_2 - (W_2 \cap C_3) \tag{5}$$

$$= W_2 \cap C_3' \tag{6}$$

where C_3' is the part of the universe of work lying outside C_3 .

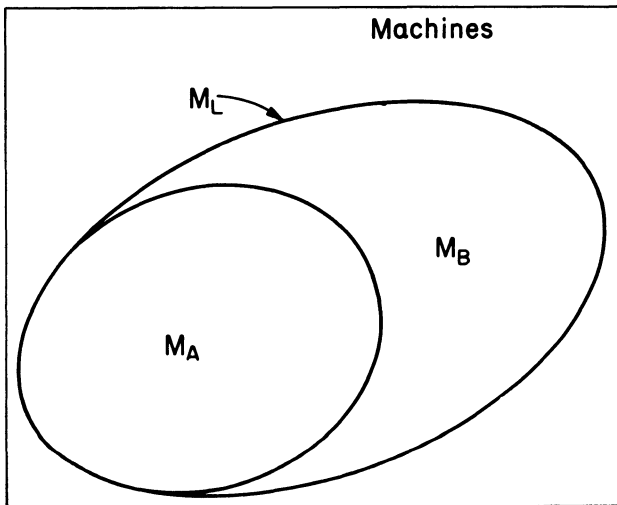


Fig. 1

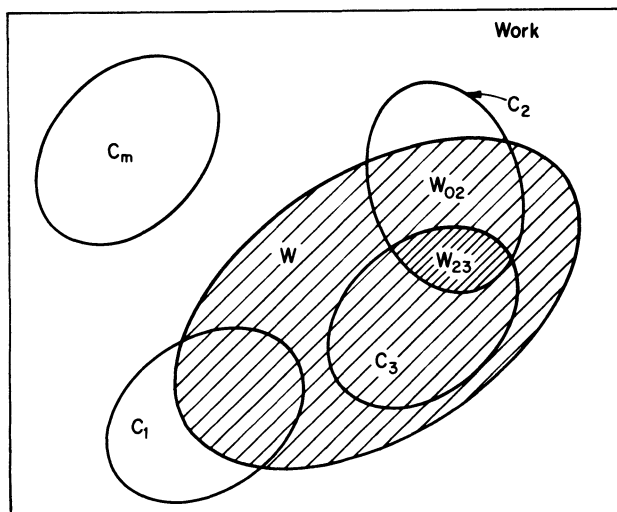


Fig. 2

CONSTRAINTS ON RESOURCE SELECTION

Following the method described by Sewell and Porter³, let it now be supposed that W is the amount of work tendered to the workshop, not in total but every month, then, clearly, it is necessary to select a sufficient number of type 2 machines to complete W_{02} in a period not longer than one month. This condition is expressed by the relationship

$$E_2 N_2 \geq L_{02} \tag{7}$$

where N_2 of type 2 machines are required, each having E_2 (hours) of productive capacity and where L_{02} (hours) is the duration of the productive phases of W_{02} . Because of the time required for setting, maintenance and so on, E_2 will be less than the working hours per month.

In reality, the work W will be subject to fluctuation and progressive change, necessitating an analysis¹ admitting statistical variation of various parameters. For the present, it is convenient to take W as an average quantity and therefore effectively constant.

Similarly, for type 3 machines, the constraint

$$E_3 N_3 \geq L_{03} \tag{8}$$

is obtained.

So far, no account has been taken of the work W_{23} , which can be done by either type 2 or type 3 machines. With respect to work W_{23} , it is *not* true to say that either one of the two types of machine is a *necessary* resource, since to each choice an alternative exists. There is, however, another set of machines able to do this work W_{23} , which does *not* permit any alternative choice, that is either W_{23} is done by machines drawn from this new set or it is not done at all. This new set is in fact the *union* of the sets of type 2 and type 3 machines, namely

$$M_2 \cup M_3 = M_u \tag{9}$$

whose domain of capability is

$$C_2 \cup C_3 = C_u \tag{10}$$

The work this new set is required to undertake is clearly

$$W \cap (C_2 \cup C_3) = W_{02} \cup W_{23} \cup W_{03} \tag{11}$$

and its capacity $(E_2 N_2 + E_3 N_3)$ is constrained by the requirement that

$$E_2 N_2 + E_3 N_3 \geq L_{02} + L_{03} + L_{23} \tag{12}$$

It is therefore required to choose N_2 and N_3 in such a way as not to violate these constraints and presumably, so that some function of N_2 and N_3 , such as operating cost or profit, is optimized.

Evidently it is the fact of the intersection of C_2

and C_3 that yields the important third constraint, since, for example, although the constraint which refers to the union ($C_1 \cup C_2$), namely

$$(E_1N_1 + E_2N_2) \geq L_1 + L_{02} \quad (13)$$

is valid, it is not of importance, being less restrictive than the associated constraint

$$E_1N_1 \geq L_1 \quad (14)$$

and

$$E_2N_2 \geq L_{02} \quad (15)$$

Normally, of course, it is necessary to consider the case of many machines having a variety of specifications and multitudinous intersections of their

SOME OTHER APPLICATIONS AND EXTENSIONS

Although it has been convenient to refer to the domains of capability of machines, it is not necessary to restrict the conception in this way. A 'machine' is in fact any system for doing work. In general therefore, a domain of capability could be that of a machine tool, a workshop, a firm, an industry or a complex of international technological functions.

In particular, by defining the domains of capability of resources within a certain workshop and those of the external world at large, it is easy to investigate the merits of sub-contracting work. In this case, a straightforward application of the above method will indicate precisely which work should be sub-contracted and which retained.

In a second application, a novel type of machine may be conceived and it may be required to know

$$\begin{array}{rcl}
 E_1N_1 & \geq & L_a \\
 E_2N_2 & \geq & L_c \\
 E_3N_3 & \geq & L_e \\
 E_4N_4 & \geq & L_g \\
 E_1N_1 + E_2N_2 & \geq & L_a + L_b + L_c \\
 E_2N_2 + E_3N_3 & \geq & L_c + L_d + L_e \\
 E_3N_3 + E_4N_4 & \geq & L_e + L_f + L_g \\
 E_1N_1 + E_2N_2 + E_3N_3 & \geq & L_a + L_b + L_c + L_d + L_e \\
 E_2N_2 + E_3N_3 + E_4N_4 & \geq & L_c + L_d + L_e + L_f + L_g \\
 E_1N_1 + E_2N_2 + E_3N_3 + E_4N_4 & \geq & L_a + L_b + L_c + L_d + L_e + L_f + L_g
 \end{array} \quad (16)$$

domains of capability. Constraints of the form just considered may be identified from the intersection of particular pairs of domains of capability and, subsequently, the machine sets of the given pair may be regarded as uniting to form a new and more comprehensive set having a correspondingly extended domain of capability. An investigation of the intersection of this new domain of capability with others leads to the identification of further important constraints. In this way, a hierarchy of progressively more comprehensive machine sets and the corresponding constraints may be identified. Ultimately, either a single class will be obtained which includes every essential machine type or several ultimate but disjoint classes will be defined. In either case, all the constraints required for the solution of the selection problem will be obtained. For example, the constraints appropriate to the system shown in Fig. 3 are as given in (16).

In practice of course, the whole process can be carried out easily by a computer programmed to execute a simple algorithm in order to identify a complete set of constraints and then to determine the required optimal solution by, for example, a well-known method of integer programming.

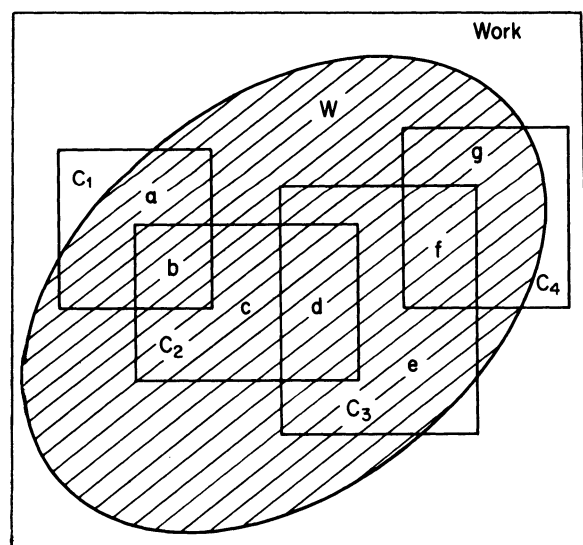


Fig. 3

whether the machine should be made and used within a given workshop or not. For example, the relative merits of owning and using lathes which are also capable of slot-milling operations may be investigated. It is relatively easy to define both the domain of capability of such a machine and the cost of making and operating any appropriate number of them. Hence the relative advantages of innovations in manufacturing system design may be assessed in relation to the advantages of already established systems.

An application or extension of the above analysis, which is to some extent still the subject of research, is that in which the calculation indicates not only which machines are required but where they should be placed in the particular workshop and by what means workpieces should be transported between them.

This type of application is particularly important when analysing the case of factories employing production lines in which some machines are necessarily markedly under-utilized. In effect, the cost of moving workpieces around the shop floor requires balancing against the cost of having little-used machines.

The method of analysis is broadly similar to that developed above and yields a similar complement of constraints. However, since the topography and potential layout of the workshop must be included in the analysis, it is convenient to stipulate that each set of machines shall consist of not more than one member. The number of elements per machine set is thus one or zero. If several machines of the same type are required, this is achieved by including multiple similar sets (each with either zero or one member).

The positioning of individual machines is constrained by geographical domains of the elements involved. Thus the geographical domains of machines and gangways may not intersect and both those domains must lie within the domain of the workshop itself.

The various possible methods of inter-machine transport, such as trucks, conveyors, cranes and porters, can be defined as machines having domains of capability. The constraints which relate to these transport devices have two particular features: (i) a very large number of constraints is obtained, even with small numbers of work stations, and (ii) the constraints include terms whose value depends upon the location of work stations and are non-linear.

At the time of writing, this general problem has been solved in simple cases only. Various ways of improving the tractability of this problem to solution are known. For example, if internal transport is provided by methods other than conveyors, the

problem can be reduced to the linear form described above.

If the inclusion of conveyors is necessary, the magnitude of the problem may be reduced by stipulating that *loop* conveyors (closed circuits) shall be the only type considered. If, by an inspired guess in a given case, it can be said that only certain of the total possible number of conveyor routes need be considered, the particular problem reduces to an easily handled size.

CONCLUSIONS

In this paper a set-theoretic approach has been used to show how the problem of the selection of resources to undertake a defined programme of work may be reduced to a form suited to solution by well-known methods of mathematical programming.

The approach described is such that the whole process of data reduction can be performed conveniently by automatic computers.

Whilst the basic method is particularly suited to the treatment of problems in which work stations are grouped according to function, other problems may also be treated and in its extended form the method will indicate the ideal location of work stations and forms of internal transport in suitably tractable cases.

Other applications of the method include the problems of sub-contracting work, the properties of machine design innovations and the allied problem of machine replacement or renovation.

The method is also applicable to general problems of resource selection: for obvious reasons it has been convenient to confine attention to the choice of manufacturing systems.

REFERENCES

1. SEWELL, G. A. E., 'The optimal selection of manufacturing resources', Ph.D. Thesis, University of Salford.
2. SEWELL, G. A. E., and PORTER, B., 'Domains of capability of manufacturing systems', *Intern. J. Systems Sci.*, 1971, 1, No. 3, 297-301.
3. SEWELL, G. A. E., and PORTER, B., 'Constraints on the synthesis of optimal manufacturing systems', *Intern. J. Systems Sci.*, 1971, 1, No 4, 355-365.
4. To be published.
5. TARSKI, A., 'Introduction to Logic', Oxford University Press, Oxford (1946).

METAL FORMING

THE ANALYSIS OF ROTARY FORGING INVESTIGATIONS AS AN AID TO DESIGN

by

E. APPLETON* and R. A. C. SLATER†

SUMMARY

The paper presents further results of the research which has been pursued by the authors into the subject of rotary forging with an experimental machine using pure lead as a model material to simulate the forging of hot steels. Solid circular cylinders of different height/diameter (H/D) ratios, and also hollow circular cylinders of constant internal/external diameter ratio ($d/D = 0.5$) but different H/D ratios, were upset slowly by rotary forging involving different magnitudes of axial force. The interrelationship between the axial force, number of revolutions of the upper rotary platen and the resulting deformation of the cylinders was investigated. This interrelationship is presented in a simple and convenient form which is intended to assist designers or users of this type of unconventional machine. Experimental results are also given for the energy required to rotary forge the solid circular cylinders.

	NOTATION		
A	a constant	$\dot{\alpha}$	angular speed of upper rotary platen about the axis of the machine
D	external diameter of solid and hollow cylindrical specimens	β	angular displacement of upper rotary platen about its geometric axis
d	internal diameter of hollow cylindrical specimens	$\dot{\beta}$	angular speed of upper rotary platen about its geometric axis
E_T	translational energy transmitted to specimen during upsetting	θ	angle of inclination of the geometric axis of the upper rotary platen to the vertical axis of the machine
E_R	rotational energy transmitted to specimen during upsetting		
$E = (E_T + E_R)$	total energy transmitted to specimen during upsetting		
F_A	axial force exerted on specimen		
H_0	initial height of cylindrical specimens		
H_1	final height of cylindrical specimens		
H	vertical height of cylindrical specimens at any instant		
n	an index		
$R = (H_0 - H_1)/H_0$	fractional reduction		
T	instantaneous torque to which specimen is subjected		
T_m	mean torque to which specimen is subjected		
α	angular displacement of upper rotary platen about the axis of the machine		

INTRODUCTION

Rotary forging is a novel metal forming process which is intended to permit smaller machines, involving lower capital cost, to be used for suitable forging applications. The rotary forging concept and the essential design features of the experimental machine used during this present study have been introduced and discussed previously^{1,2} and will, therefore, only be briefly referred to here.

In this process, the workpiece is positioned between a flat lower platen which is capable of vertical movement only and a skewed upper conical platen, of apex angle 160° , which can be rotated about the vertical axis of the machine and also about its own geometric axis. The application of a relatively

*Research Student, Department of Mechanical Engineering, University of Salford. Now, Lecturer in Mechanical Engineering, The University of Manchester Institute of Science and Technology.

†Senior Lecturer in Mechanical Engineering, Department of Mechanical Engineering, University of Salford. Now, Senior Lecturer in Manufacturing Engineering, Department of Mechanical Engineering, The City University, London.

small axial force, via the platens, initially causes the upper platen to be indented into the workpiece. This indentation produces a small plastically deforming zone below the upper rotary platen-workpiece interface and within this zone both radial and circumferential flow occurs. If the plastically deforming region is then rotated relatively through the workpiece material by rotation of the upper conical platen about the vertical axis of the machine, the workpiece is upset in a progressive manner. It has been shown¹ that the axial force required for slow rotary forging is a small fraction of that required for the conventional slow upsetting of circular cylinders having H/D ratios of less than unity. The authors² have also referred to the practical bounds which are significant in the application of the rotary forging process for the upsetting of circular cylinders using pure lead as a model material to simulate the forging of 'warm' and 'hot' steel. These bounds are associated with the formation of 'mushroom' heads during the upsetting of relatively tall billets when the magnitude of the axial force is inadequate, and also with the phenomenon of tensile instability followed by fracture at the centre of shallow billets. The investigations described in the present paper refer, principally, to conditions producing specimens which are within the previously defined acceptable bounds for satisfactory rotary forging.

The current research has been directed towards an investigation of the rotary forging process with particular reference to the interrelationship of the important forging parameters which influence the upsetting of solid and hollow circular cylinders. By expressing these relationships in a simple algebraic or graphical form, the authors intend to assist designers and users of these unconventional machines. Two particular aspects are considered which have stimulated interest during past discussions.

The economic viability of any mass production facility is highly dependent on the cycle rate of that facility. For a simple single-stage process such as hot die forging using a single blow or stroke, the process cycle may be classified into three phases. These are

- (a) the loading or charging time,
- (b) the deformation or metal working time, and
- (c) the ejection or retraction time.

The period devoted to each phase of the cycle is dependent on the particular process. However, it is obvious that in the case of rotary forging, the first and last phases in a production cycle will be limited by the auxiliary equipment and are not likely to be affected by the characteristics of the rotary forging process. It is also likely that the deformation or metal working time for rotary forging will be longer than certain metal forming techniques such as high rate forming. Thus, information relating to the metal working time is important because it is this which may commend or detract from the industrial application of the process. The investigations reported in this paper have necessarily been restricted to slow rotary forging from practical considerations of control and capacity of the experimental machine. Nevertheless, it is envisaged that the speed of rotation of the upper platen would be high for an industrial application. Having selected the speed of rotation of the upper platen, the period for the metal working

phase is then dependent on the number of revolutions required to perform the desired operation.

The first relationship discussed is that between the number of revolutions required to perform a desired deformation, in this case the required fractional reduction in height during simple upsetting, and the effect of axial force and initial specimen shape.

The second aspect discussed concerns the total energy required to effect the desired deformation. The energy required to perform an upsetting operation by rotary forging is supplied from two sources. Translational energy is supplied by the vertical motion of the lower platen and its magnitude is given as the product of the constant axial force and the reduction in specimen height. Hence, this translational energy can be expressed as

$$E_T = F_A (H_0 - H_1) \quad (1)$$

The other source of energy is the rotational energy supplied during rotation of the upper conical platen. This energy component is given as the product of the instantaneous torque and the angular displacement of the upper platen and can be expressed as

$$E_R = \sum_0^\alpha T d\alpha \quad (2)$$

Because the torque has been found to be a variable during an upsetting operation, the form of equation (2) is necessary.

The principal objectives of this paper are therefore:

- (1) to present the interrelationships which exist between the important rotary forging parameters during the slow upsetting of solid and hollow circular cylinders as an aid to design, and
- (2) to discuss aspects concerned with the energy required to effect the upsetting operation.

INSTRUMENTATION OF THE EXPERIMENTAL ROTARY FORGING MACHINE, FORGING CONDITIONS AND SPECIMEN MATERIALS

The experimental rotary forging machine employed for these investigations, illustrated in the photograph of Fig. 1, has been described in detail elsewhere^{1,2}. Only the minor modifications which were necessary to accommodate the various transducers will, therefore, be described here.

Three transducers have been fitted to the machine and by means of these it was possible to monitor (a) the torque applied to the specimen, (b) the reduction in height during an upsetting operation, and (c) the angular position of the upper conical platen at any instant during the process. The signals from the transducers were indicated with the aid of a UV recorder.

Torque transducer

A torque transducer was devised for measurement of the torque applied to the specimen by the upper rotary platen. The simplest method for indicating this torque was found to be by measuring the reaction torque at the lower platen. A diagrammatic arrangement of the lower platen-pressure spindle incorporating the torque transducer is presented in Fig. 2. The torque meter is provided at the reduced diameter

portion of the pressure spindle on which four strain gauges are bonded and connected to form a Wheatstone bridge circuit. The Wheatstone bridge circuit was used to control the balance under conditions of zero torque and the reaction torque at the lower platen produced an output signal which was amplified and displayed on a U.V. recorder. The gauge system was self-compensating for bending of the pressure spindle, temperature changes and axial load changes. The calibration of applied torque as indicated by the U.V. recorder galvanometer-spot displacement was determined by mounting the lower platen-pressure spindle assembly in a torsion testing machine and applying known magnitudes of torque. The calibration was found to be substantially linear.

Angular displacement transducer

A simple, inexpensive, angular displacement transducer, as shown in Fig. 3, was designed and manufactured to measure the angular position of the upper rotary platen at any instant.

The drive shaft from the main gear reduction unit was extended above the horizontal transmission gears

and was used to drive through a miniature gearbox producing a 9:1 gear reduction. The output from the miniature gearbox was then used, in turn, to drive a ten-turn potentiometer via a disc clutch coupling. This clutch coupling could be set to rotate the potentiometer spindle without slipping. After the travel of the potentiometer was completed the clutch would slip and thus prevent the potentiometer from over-running. The difference in voltage across one of the ends of the potentiometer and the moveable tapping was used to indicate the angular position of the upper rotary platen at any instant. Once again, the output signal was indicated by means of the U.V. recorder.

Linear displacement transducer

A resistance-type linear displacement transducer was used to measure the movement of the pressure spindle and hence the lower platen relative to the support plate of the machine. The displacement of the lower platen is equal to the reduction in height of the specimen and by this means it was possible to record the instantaneous specimen height during deformation.

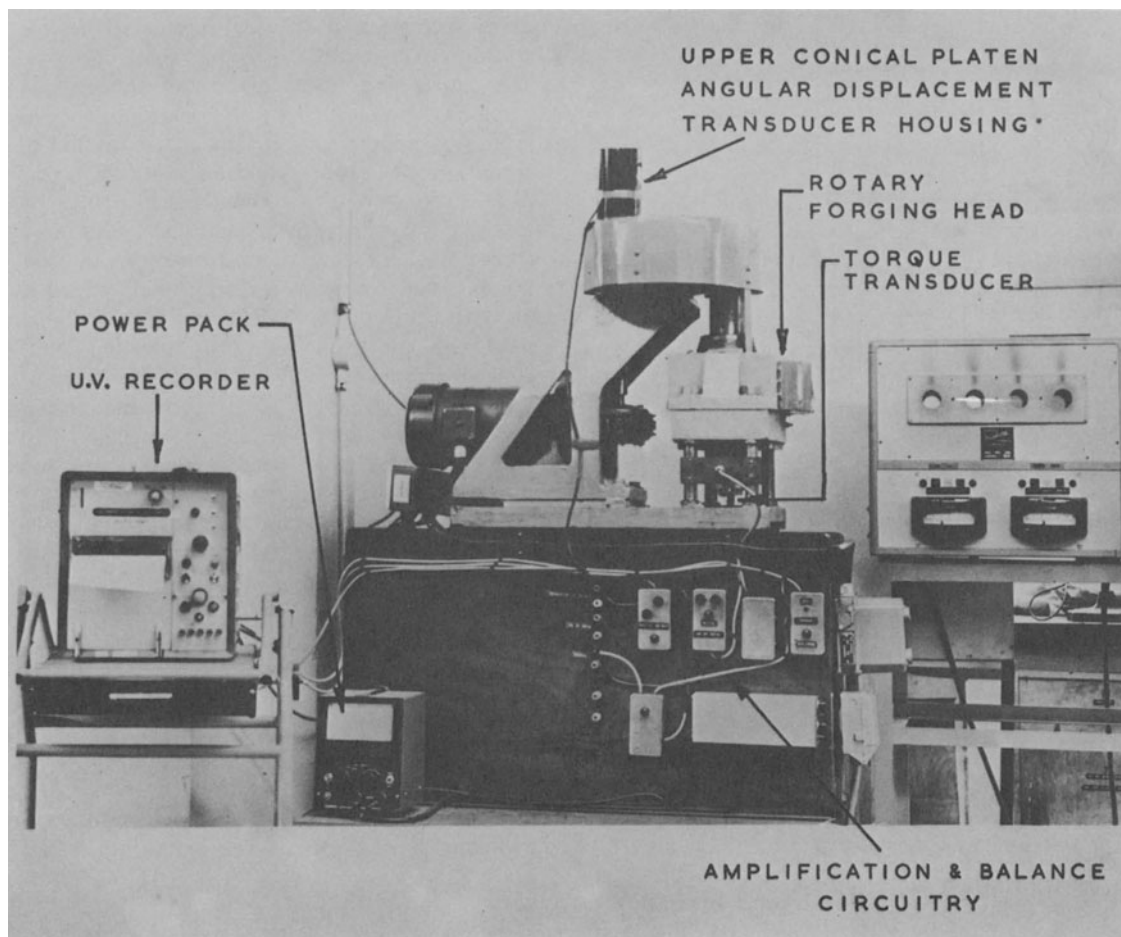


Fig. 1 Side view of the experimental rotary forging machine showing location of transducers and other instrumentation (linear displacement transducer not visible).

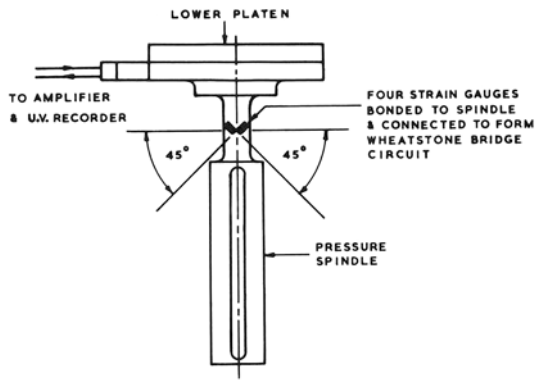


Fig. 2 Lower platen-pressure spindle assembly incorporating the torque transducer.

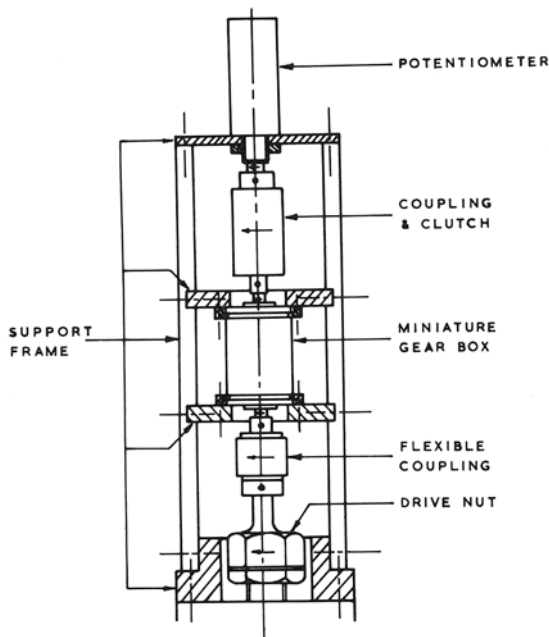


Fig. 3 Angular displacement transducer.

Forging conditions

The experimental rotary forging machine is capable of considerable variation in the forging conditions. However, for the investigations reported here, certain parameters were maintained constant. All of the experiments were performed using the minimum-speed setting for rotation of the upper conical platen ($\dot{\alpha} = 7.93$ rev/min) although the machine is capable of rotational speeds up to a maximum of 80 rev/min. The upper platen was not rotated about its geometric axis ($\beta = 0$). A further condition relating to the upper rotary platen was that the inclination of its geometric axis to the vertical axis of the machine was maintained constant at its maximum value, namely, $\theta = 10^\circ$. This angle is necessary in order to produce specimens having parallel upper and lower plane surfaces with the particular upper platen geometry that was used.

Previous investigations have shown that frictional conditions at the lower platen are important especially for upsetting using a flat lower platen. In this

case, only the frictional forces are available to maintain the specimen in an axial position during what is essentially a non-axisymmetrical process. Thus, for reasons of specimen positional stability, a rough, high-friction lower platen was used and found to be satisfactory.

Pure lead cylindrical specimens

For these experiments, pure lead specimens were machined having a nominal diameter of 1 in but with height/diameter (H/D) ratios varying between $\frac{1}{8}$ and 1. Hollow cylindrical specimens were also manufactured having a nominal external diameter of 1 in and an internal diameter of $\frac{1}{2}$ in. These specimens were of H/D ratios varying between $\frac{1}{4}$ and 1. All the specimens were initially annealed in boiling water for a period of 30 min and then allowed to cool.

EXPERIMENTAL PROCEDURE AND MEASUREMENTS

Relation between fractional reduction and number of revolutions of the upper conical platen (α) for cylindrical specimens of different initial (H/D) ratios using constant axial force

The upper and lower platens of the experimental machine were cleaned with trichloroethylene and the lever system was carefully balanced for the no-load condition. A solid cylindrical specimen of initial H/D ratio = 1 was then lightly smeared with machine oil and placed centrally under the upper conical platen. Accurate positioning of the specimen was effected by means of a template which located onto the lower platen. This platen was then raised until the specimen was just touching the upper conical platen. The U.V. recorder was then switched on and the datum positions of the traces were adjusted. The paper was then arranged to leave the recorder at a suitable speed. After a few seconds the rotary forging machine was loaded by means of the lever system, thus subjecting the specimen to the required constant axial force ($F_A = 792$ lbf). The depth of indentation of the upper platen into the specimen was proportional to the displacement of the appropriate trace at that instant. After the drive motor was started the upper conical platen was allowed to rotate for approximately twenty revolutions. The specimen was then removed and examined for defects and shape. The entire procedure was then repeated for other initial H/D ratios of $3/4$, $1/2$, $7/16$, $3/8$, $5/16$, $1/4$ and $1/8$, and again for hollow cylinders having initial H/D ratios of 1, $3/4$, $1/2$ and $1/4$.

Relation between fractional reduction and number of revolutions of the upper rotary platen (α) for cylindrical specimens subjected to different values of axial force ($H/D = 1$).

The above procedure was repeated for this phase of the investigation. However, in this case, solid and hollow cylindrical specimens having an initial H/D ratio = 1 only were used but were subjected to different magnitudes of axial force.

Relation between total deformation energy and fractional reduction during the slow rotary forging of solid cylinders with different values of axial force ($H/D = 1$).

The total energy required to effect a given fractional reduction by rotary forging was measured experimentally by summation of the rotational energy supplied to the specimen via the upper conical platen and the translational energy supplied by means of the lower platen.

The energy available from the upper conical platen was determined from the torque-angular displacement trace produced by monitoring the output signals from the torque and angular displacement transducers to the U.V. recorder during the deformation. A mean value of torque was determined for each revolution of the upper conical platen and thus the rotational energy supplied during a single revolution was equal to the product of the mean torque (T_m) and the angular displacement 2π radians. The total rotational energy was then given as the summation of such components during the whole deformation process.

Hence, rotational, energy supplied by the upper conical platen is given by

$$E_R = \Sigma_0^\alpha (T_m \cdot 2\pi) \quad (3)$$

where α is the number of complete revolutions.

The energy supplied by the lower platen was determined simply from the product of the known value of axial force (F_A) exerted on the specimen and the reduction in height of the specimen. The reduction in height was indicated by means of the third U.V. recorder trace.

RESULTS AND DISCUSSION

Relation between fractional reduction and the number of revolutions of the upper conical platen (α) for cylindrical specimens of different initial H/D ratios using constant axial force

This relationship was investigated for pure lead solid cylindrical specimens having initial H/D ratios varying between 1/8 and 1 which were upset by rotary forging maintaining various constant magnitudes of axial force (F_A). In addition, the relationship was also investigated for pure lead hollow cylinders having initial H/D ratios varying between 1/4 and 1. However, it is considered appropriate to present in Fig. 4 and Fig. 5, respectively only those relationships corresponding to a constant axial force of 792 lbf as being representative of all the results obtained during these particular investigations.

By referring to Figs 4 and 5, it is interesting to note that the relation between fractional reduction and the number of revolutions of the upper conical platen is of the form

$$R = A \alpha^n \quad (4)$$

in which A is the fractional reduction corresponding to *one* revolution of the upper conical platen and n is the constant slope of all the graphs which are plotted logarithmically.

As might be anticipated, the value of A for both the solid and hollow circular cylinders is seen to be dependent on the initial H/D ratio. However, the

value of n is independent of the initial or current H/D ratio and has the constant approximate value of 0.4.

Relation between fractional reduction and number of revolutions of the upper conical platen (α) for cylindrical specimens with different values of axial force ($H/D = 1$)

The relationships corresponding to a constant initial (H/D) ratio of unity are illustrated in Fig. 6 and Fig. 7 for the solid cylinders and hollow cylinders respectively. These are also of the same form described for the previous two cases and defined by equation (4). The value of A is now shown to be dependent on the magnitude of the axial force involved, but the index n is, once again, found to be unaffected and has the same value as for the previous cases.

During this particular investigation, the range and number of experiments employed permitted a more detailed study to be made of the character of the constant A . The manner in which A , that is, the fractional reduction produced after a single revolution of the upper conical platen, varies with the axial force is illustrated in Fig. 8.

The 'mushroom' effect which was previously noted for solid circular cylinders^{1,2} is also evident during the slow rotary forging of hollow cylinders. The hollow cylindrical specimens shown in Fig. 9 indicate that the extent of this undesirable effect is reduced as the magnitude of the axial force is increased. It will also be seen that both inward and outward flow occurs.

Relation between total deformation energy and fractional reduction during the slow rotary forging of solid cylinders with different values of axial force ($H/D = 1$)

A particular case is considered in Fig. 10 for solid pure lead cylinders having an initial H/D ratio of unity, in which the experimental relation between the total deformation energy and fractional reduction is shown for different values of axial force.

For relatively high values of axial force, that is, $F_A \geq 1300$ lbf, the experimental points are seen to approximate to a single curve, indicating that the efficiency of the process is not affected significantly by the magnitude of the axial force producing the deformation. In fact, the process, by its nature, dissipates energy from the upper conical platen to supplement that supplied by the lower platen. For example, if the axial force is reduced for a particular deformation then a consequently greater number of revolutions of the upper conical platen are required to supply the necessary total energy to effect the desired deformation. However, for low values of axial force, that is $F_A < 1300$ lbf, the relationship is seen to vary with the axial force. This can be explained in terms of the 'mushroom' effect. It follows that the formation of a 'mushroom' head on the specimen would require less energy than if the deformation were more homogeneous. Curves corresponding to values of axial force F_A of 792 lbf and 1032 lbf could be expected to deviate from the single curve as is the case shown in Fig. 10. By referring to Fig. 6 it can be seen that the transition from the deformation

displaying a 'mushroom' head characteristic to a more homogeneous final specimen shape occurs when the axial force is about 1300 lbf, thus further supporting the views expressed.

For purposes of comparison, a theoretical curve is also presented in Fig. 10 which shows the deformation energy required to effect a given fractional reduction for the conventional upsetting of a solid, pure lead cylinder, having the same initial dimensions as the test specimens. In this case, the upsetting operation is assumed to be homogeneous and the material to be rigid-perfectly plastic. From previous work² it is known that the mean quasi-static yield stress $Y = 2180 \text{ lbf/in}^2$ at the ambient temperature of 21°C and the mean engineering strain-rate of $17 \times 10^{-3} \text{ s}^{-1}$. The deformation energy (E) is then given by

$$E = VY\epsilon = VY \ln \left[\frac{1}{1-R} \right] \quad (5)$$

in which V is the volume of the cylinder, ϵ the natural compressive strain and R is the fractional reduction.

When comparing the experimental and theoretical curves it must be remembered that the energy required for homogeneous deformation during low values of fractional reduction will appear as an overestimate, since the test material is considered as

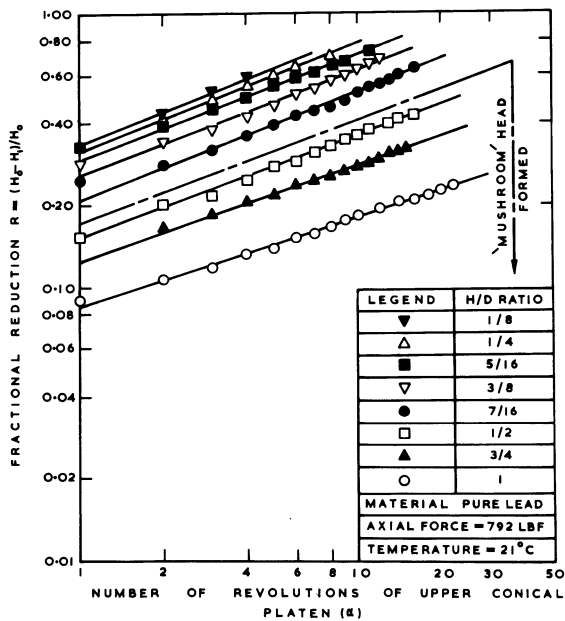
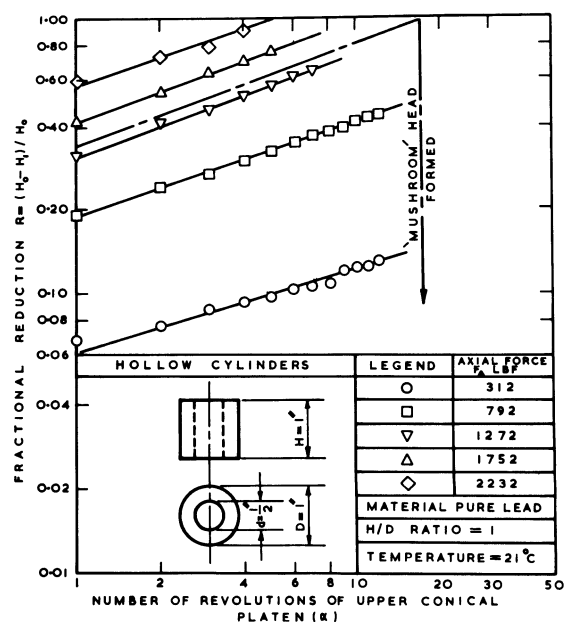
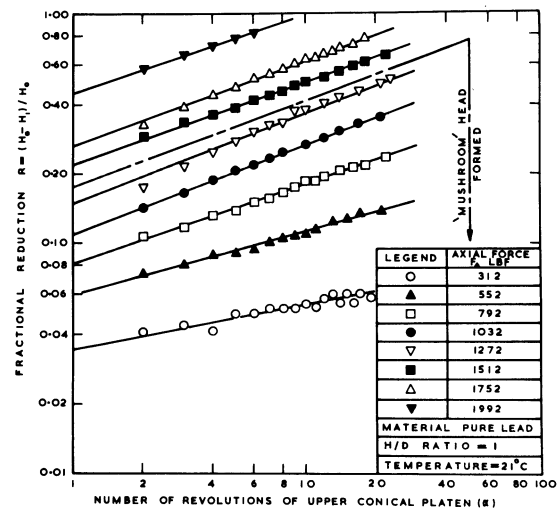
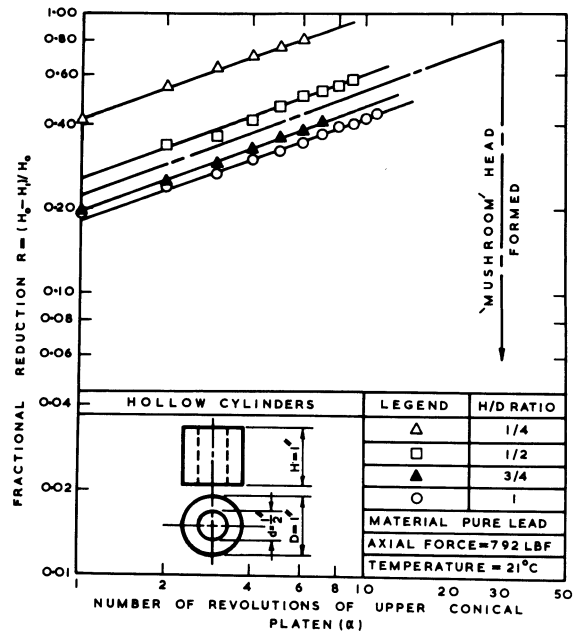


Fig. 4 (above) Relation between fractional reduction and the number of revolutions of the upper conical platen (α) for solid cylinders of different initial H/D ratios using constant axial force ($F_A = 792 \text{ lbf}$).

Fig. 5 (top right) Relation between fractional reduction and the number of revolutions of the upper conical platen (α) for hollow cylinders of different initial H/D ratios using constant axial force ($F_A = 792 \text{ lbf}$).

Fig. 6 (centre right) Relation between fractional reduction and number of revolutions of the upper conical platen (α) for solid cylinders with different values of axial force ($H/D = 1$).

Fig. 7 (bottom right) Relation between fractional reduction and number of revolutions of the upper conical platen (α) for hollow cylinders with different values of axial force ($H/D = 1$).



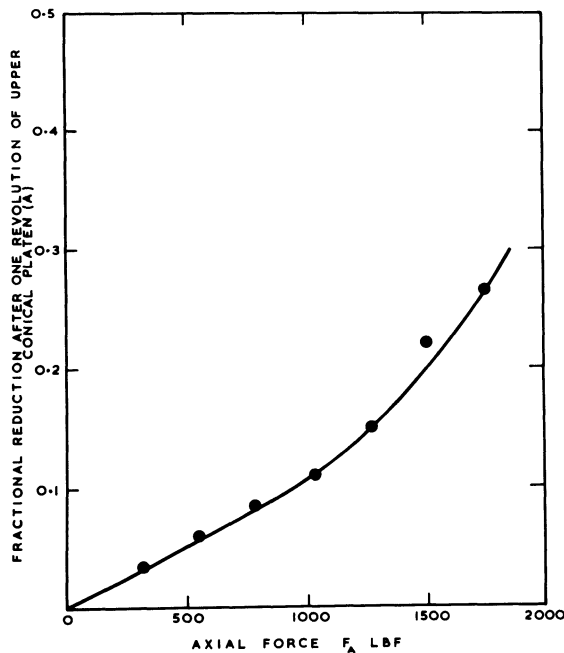


Fig. 8 Relation between constant A in equation $R = A\alpha^n$ and axial force (F_A) for solid cylinders of pure lead ($H/D = 1$).

rigid—perfectly plastic, whilst the pure lead used approximates to an elastic—perfectly plastic material having a relatively low elastic modulus. Nevertheless, Fig. 10 shows that because upsetting by the rotary forging process is inhomogeneous, the energy required to effect a given fractional reduction is not likely to be less than that for conventional upsetting.

CONCLUSIONS

1. A general expression involving experimentally determined constants describes the relationship between the fractional reduction (R) and the number of revolutions of the upper conical platen (α) for various rotary forging conditions. This expression is of the form

$$R = A \alpha^n$$

2. The value of the index $n \approx 0.4$ is the same for solid and hollow circular cylinders and is independent of the initial H/D ratio and axial force involved. The constant A , however, is dependent on both the initial H/D ratio of the cylinder and axial force employed.

3. The total energy required to effect a given fractional reduction during upsetting by rotary forging is independent of the axial force involved, provided the 'mushroom' head effect is avoided.

4. Because upsetting by the rotary forging process is inhomogeneous the energy required to effect a given fractional reduction is not likely to be less than that for conventional upsetting.

ACKNOWLEDGEMENTS

The authors express their gratitude to Professor A. W. J. Chisholm, Chairman of the Department of Mechanical Engineering, University of Salford, for his encouragement to pursue this study.

The technical assistance given by the Departmental Workshop and Laboratory staffs, particularly during the manufacture of specimens and instrumentation, is sincerely appreciated. Thanks are also due to Mr J. Howe for his assistance during the preparation of the illustrations and to Miss J. Eyre who was responsible for typing the manuscript.

Mr E. Appleton is indebted to the Science Research Council for the award of a Research Studentship which enabled him to undertake the investigations.

REFERENCES

1. SLATER, R. A. C., BAROOAH, N. K., APPLETON, E., and JOHNSON, W., 'The rotary forging concept and initial work with an experimental machine', *Proc. Inst. Mech. Engrs.*, 184, Part I, No. 32 (1969–70), p. 577.
2. SLATER, R. A. C., and APPLETON, E., 'Some experiments with model materials to simulate the rotary forging of hot steels', *Proc. 11th Int. Mach. Tool Des and Res. Conf.*, University of Birmingham, September (1970).

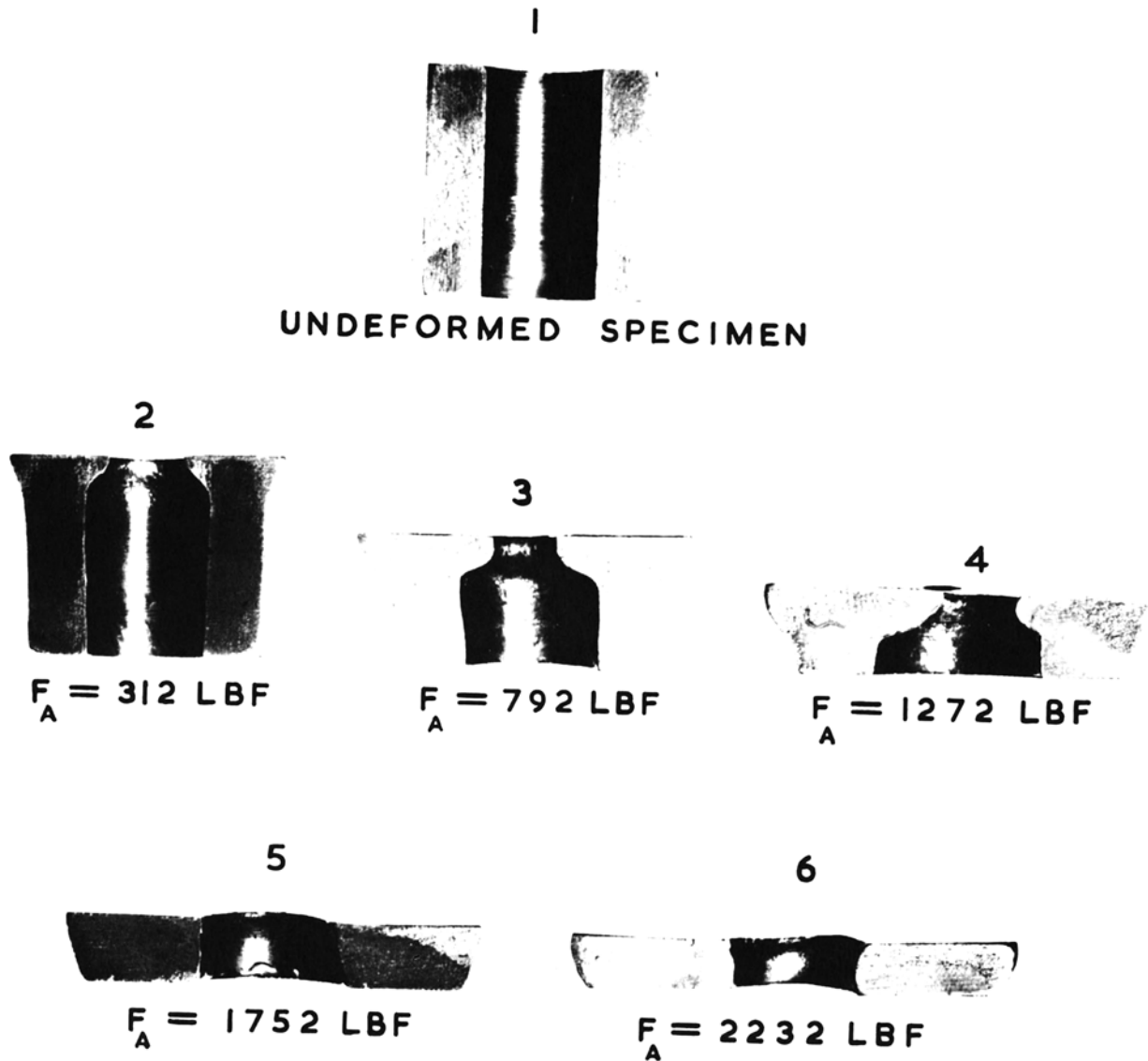


Fig. 9 Effect of axial force on the rotary forging of pure lead hollow cylinders ($H/D = 1$).

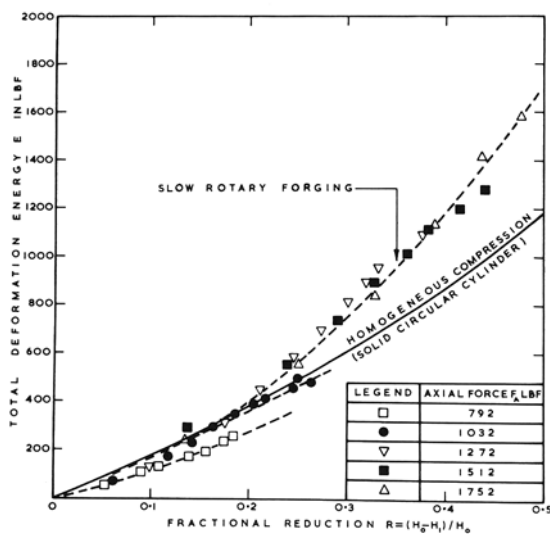


FIG. 10 RELATION BETWEEN THE TOTAL DEFORMATION ENERGY AND FRACTIONAL REDUCTION DURING THE SLOW ROTARY FORGING OF SOLID CYLINDERS USING DIFFERENT VALUES OF AXIAL FORCE ($H/D = 1$)

Fig. 10 Relation between total deformation energy and fractional reduction during the slow rotary forging of solid cylinders with different values of axial force ($H/D = 1$).

DISCUSSION

Query from C. Jubb

It is stated that 'the energy required for homogeneous deformation during low values of fractional reduction will appear as an overestimate'. The reason given is that the lead deforms elastically as well as plastically. In other words, the elastic work is ignored. Neglecting this form of work would surely lead to an underestimate rather than an overestimate of the energy requirements.

Reply

It is recognised that lead only approximates to the behaviour of an idealised rigid-perfectly plastic material and has a small component of deformation which is elastic. However, Dr Jubb's assumption that the elastic work has been ignored is not quite correct. In fact, the work associated with the elastic deformation has been determined assuming the mean uniaxial yield stress of value Y as Fig. 11 indicates.

The deformation energy/unit volume is represented by the area under the true stress-natural strain curve, i.e.

$$E/V = \int \sigma d\epsilon$$

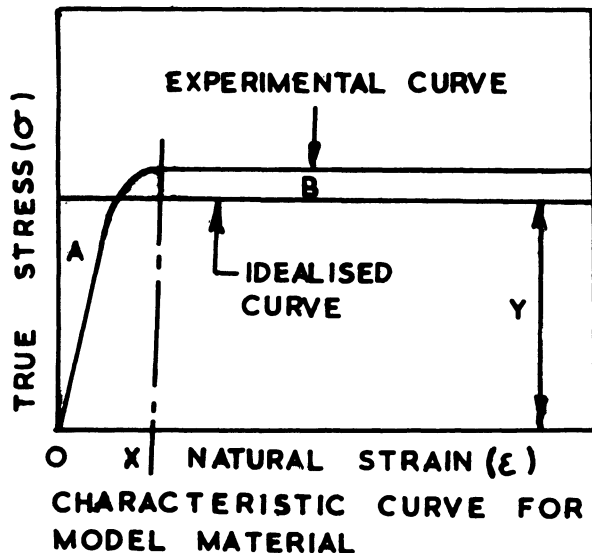
If the area A is equal to area B, then the mean yield stress is given by Y such that,

$$E/V - Y\epsilon = \int \sigma d\epsilon$$

Considering the curve up to low values of strain (O-X): the area below the experimental curve is less than that below the idealised rigid-perfectly plastic line for the same strain range, that is,

$$V \int \sigma d\epsilon < V Y \epsilon$$

The energy required for homogeneous deformation assuming a rigid-perfectly plastic material having a mean yield stress Y thus appears as an overestimate for low values of strain, compared with the case for an elastic-plastic deformation.



Query from D. B. Laycock

Is any information available as to how the final product shape is developed? That is, does the product shown in Fig. 9, associated with the highest axial force, develop via the sequence shown for the lower axial forces, so that the mushroom head is always developed, but subsequently eliminated when the higher axial forces are employed?

Reply

This and previously-published papers have dealt with the mushroom head phenomenon in terms of an undesirable final shape of an upset cylindrical product and, therefore, no description has been given of the transient formation of a mushroom head. Nevertheless, it is known that the formation of a mushroom head during the upsetting of a circular cylinder could have certain industrial applications.

It is possible, however, to present a qualitative description of the progressive formation of a mushroom head. Firstly, by employing a high axial force, the plastically deforming zone beneath the upper rotary platen will extend to the lower platen and a mushroom shaped product will not be formed. The magnitude of the axial force required to achieve this condition depends mainly on the initial H/D ratio of the specimen. If a reduced axial force is used it is possible to achieve the condition for which, initially, the plastically deforming zone does not extend to the lower platen, but after a few revolutions of the upper platen and an appropriate reduction in specimen height, the plastically deforming zone reaches the lower platen and flow in the lower portion of the specimen takes place, producing a somewhat truncated shape. The use of a considerably reduced axial force will not produce a plastically deforming zone which extends to the lower platen and the increase in the specimen diameter in the upper portion causes a further decrease in the penetration of the plastic zone as deformation proceeds. If the decrease in depth of penetration of the plastically deforming zone is greater than the reduction in specimen height, flow at the lower platen will never take place and a characteristic mushroom shape will be produced.

Query from S. Shima

I am not familiar with rotary forging. But I really do not see why you have used pure lead as specimens. If you are thinking of only hot forging for application, pure lead is a good model material. However, if you are going to apply this technique to cold forging, the linear relationship between the fractional reduction and logarithm of number of revolutions and also deformation pattern (mushroom type etc.) would be different for other workhardening material.

Reply

Although the authors are in agreement with much of this contribution there is probably some need for clarification of the relationship of this work to possible industrial application of the process.

Firstly, because of the limited capacity of the experimental rotary forging machine, it has only been possible to use model work materials. However, this limitation on the experimental programme is not overwhelming and there is still a formidable amount of research which may be carried out using model materials. It is recognised that results obtained using model materials, or indeed any model technique, must be carefully studied in order to draw conclusions that may be extended and applied to forecasts for the forging of engineering materials.

It is stated clearly at several points in the paper, including the summary, that for this particular investigation pure lead was used as a model material to simulate the forging of hot steels. The investigations up to this time have been subjected to a practical limitation of forging load. However, it should be emphasised that there are indications given in previously published work that the application of

rotary forging could be quite extensive, including the hot, warm or cold forging of plain carbon and alloy steels. Obviously in the case of the rotary forging of a workhardening material, the relationship,

$$R = A \alpha^n,$$

is not expected to be valid nor as conveniently mathematically described. However, it is possible that the relationship may be described by the equation

$$R = A \alpha^{f(R)}$$

where $f(R)$ indicates that the gradient of the logarithmic relationship is a function of the deformation.

TOOL-LIFE TEST IN CLAMP SHEARING OF STEEL BAR AND WIRE

by

T. NAKAGAWA* and K. MIYAMOTO†

SUMMARY

At present the clamp shearing method is being used almost exclusively on pure non-ferrous metals for obtaining the smooth sheared edges of the bar but it has not been adopted for steel material because of the short life of the shearing tool. Here the tool-life tests are conducted on several kinds of low-carbon steel bar and wire, using a specially designed hydraulic clamp shearing machine, and are compared with the results for copper.

INTRODUCTION

The 'clamp shearing' method is one in which the axial movement of the bar is restricted in shearing time by clamping. This shearing method has already been put to use in the precision shearing of bar and wire. However, there is a limit to the type of material sheared by this method and only non-ferrous material like pure aluminium, copper and lead has been used successfully. There is no clear prospective idea at present in the field of precision shearing of steel bar and wire, but its development is strongly desired in the billet production required for the cold forging of steel.

From some preliminary experiments and estimates, it is generally supposed that the life of shearing tools is short when used on steel. However, this paper now deals in greater detail with tool-life tests conducted on several kinds of low-carbon steel bar and wire, using a specially designed clamp shearing tool and a newly developed hydraulic clamp shearing machine.

METHOD OF TOOL LIFE TEST

Clamp shearing tool and machine

Two types of clamp shearing tool are used in this tool-life test. The first is one using a polyurethane rubber die cushion (see Fig. 1a) which can easily be attached to an ordinary mechanical press. In this case, it is inevitable that work material sticks on the side face of the moving blade: it results from the clamped state of the bar at the time of its backward stroke.

In the second type, a hydraulic clamp shearing

machine, as shown in Fig. 1b, is used to overcome this defect. It is a specially designed machine in which the clamping force is released when the moving blade reaches the bottom dead point of its stroke. The experiments are done at 30 strokes/min and the actual shearing speed is 60–80 mm/sec. Here both the shearing force and clamping force are available from the same hydraulic source. The clamping force is magnified three times by a lever action and the bar clamping is done by two clamping plates with semi-circular grooves along them. The bar is restrained from bending or jumping by the friction between both the clamping grooves, and is also restricted from any axial movement. The bar is fed continuously between rollers which are driven by an electric motor. This machine is also provided with a bar supply device, so that the bar or wire may be sheared fully and automatically.

Shearing tool

Both blades are of open type with a semicircular shape, as shown in Fig. 1c, and have been designed so that no separate knock-out device is required. In the polyurethane cushioned tool, the material of the tool is ordinary heat-treated die steel (quenched and ground), while in the other cases the cutting edge is made of cemented carbide. This cemented carbide blade is selected to be of rather soft quality to avoid any chipping, but the hardness may be as high as HRC 84.

The tool construction and tool geometry are almost the same as that described in a previously presented paper¹ but in addition a roller bearing is used here to guide the shearing blade and thus avoid scoring between the blade and stopper plate. Though

*Institute of Industrial Science, University of Tokyo, Japan

†Miyamoto Industries Ltd., Tokyo, Japan

Table 1. Bar and wire materials tested

No.	Material	Heat treatment	Mechanical properties				Tool material	Lubricant used	Number of sheared pieces produced, <i>N</i>
			Dia. of bar × length	Tensile strength (kg/mm ²)	Elongation (%) (G.L.)	Reduction of area (%)			
1	Steel 0.05% C	Hot rolled	5.5 8 mm	32.0	25.9 (100 mm)	80.5	Die steel	Bonderite and Bonder lube and machine oil	10 000
2	Steel 0.05% C	Hot rolled	10.0 10 mm	33.0	32.5 (50 mm)	81.0	Cemented carbide	Oil with MoS ₂	50 000
3	Steel 0.1% C	Hot rolled-annealed and drawn	10.0 10 mm	44.2	29.3 (35 mm)	74.7	Cemented carbide	Bonderite and Bonder lube and oil with MoS ₂	11 000
4	Steel 0.2% C	Hot rolled-annealed and drawn	10.0 10 mm	49.3	29.3 (35 mm)	76.9	Cemented carbide	Bonderite and Bonder lube and oil with MoS ₂	12 000
5	Copper (pure)	Cold drawn (full hard)	14.9 14 mm	35.1	20.7 (41 mm)	62.5	Cemented carbide	Oil with MoS ₂	30 000

zero clearance is desirable to get a good sheared surface, about 0.01 mm clearance has been adopted in actual practice to avoid scoring. The clamping force is equal to three times the shearing load.

Bar and wire material tested

The tool-life test was conducted on four types of steel and also on pure copper as detailed in Table 1. In cases 1 and 2, the material of the bar is the same as low-carbon steel but the sizes of bar differ in the ratio of 1:2, approximately. In cases 3 and 4 the bar material is annealed to increase the ductility. In case 5, copper material has been used for comparison only. In all cases, except case 1, cemented-carbide tools are used with the hydraulic clamp shearing machine.

EXPERIMENTAL RESULTS

The tool-life test was continuously conducted without any intermediate checking on the tool to avoid the change of shearing conditions.

Sheared surface

The main advantage of clamp shearing is to get a good, smooth sheared surface. Fig. 2 shows the appearance of a sheared surface obtained in the experiment. Some small hair cracks are observed in all pieces. In the case of steel of 0.05% C cracks looking like scratch cracks start appearing from 30 000 pieces onwards and these become more clear and visible thereafter. In the case of 0.1% C steel the cracks start earlier and are comparatively bigger and deeper in size than in the case of 0.05% C. In the case of 0.2% C steel the material cannot be sheared successfully as it produces deep cracks in the middle of the section due to its low ductility. Contrary to this, in the case of copper the surface is very clear and no big cracks are observed even after 30 000 shearing strokes. This is because of its high ductility.

Fig. 3 shows the typical roughness change of sheared surfaces measured with regard to a certain number of shearing strokes for 10 mm diameter steel bars of 0.05% C and also 15 mm diameter copper bar. From measurements, the following observations have been made: The surface roughness increases as the number of shearing strokes increases. This rate of increase in roughness is different for different materials; the less ductile the material, the greater is the rate of increase in roughness.

When the roughness of the remaining end of the billet was compared for the same 0.05% carbon steel after 10 000 shearing strokes, it was found that the 5.5 mm diameter steel bar had greater roughness than the 10 mm diameter bar. This increased roughness is caused by sticking on the moving quenched die steel blade.

Wear of tool

Fig. 4 shows a photograph of the blade surfaces of the shearing tool after 50 000 strokes for 0.05% C steel. The tool is observed to have carried the wear trace on its surface. Consequently some sticking of the work material in the form of molten steel is observed on the side face of the cemented-carbide tool blade and is understood to be due to a temperature rise under high axial pressure causing the sheared surface of steel bar to melt and stick to the blade. The same sticking breaks down in the subsequent shearing cycle, along with some carbide tool material, which finally results in greater surface roughness on the sheared billet (see Fig. 3).

This wear of the cemented carbide is quite high and unexpected; it may be due to the softness of cemented carbide. However, in the above experiment, the cemented-carbide tool was chosen, not on the basis of hardness, but on stiffness to avoid unnecessary chipping. Therefore it can be assumed that the cemented-carbide tool of greater hardness will have a longer life.

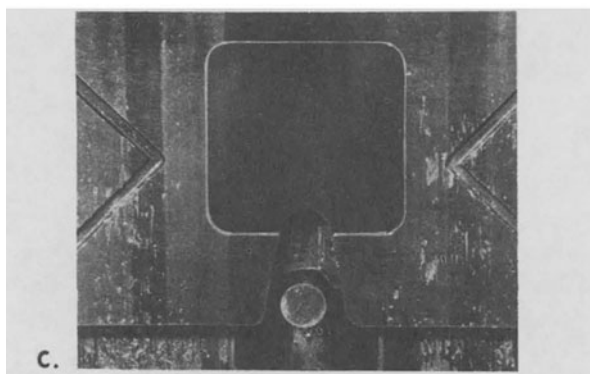
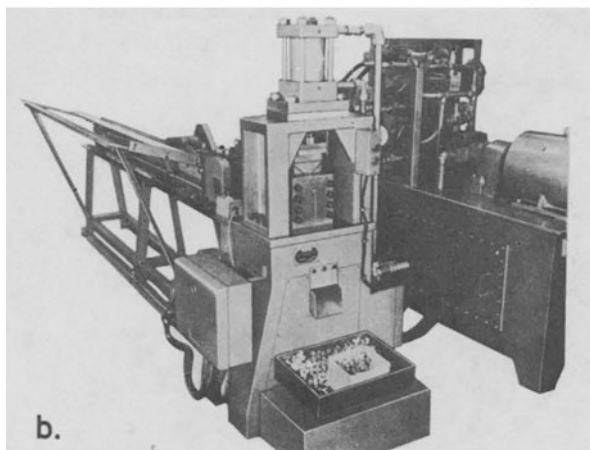
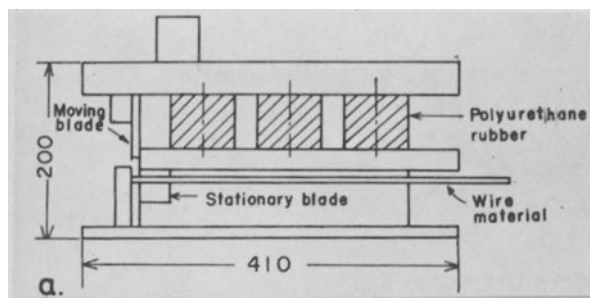


Fig. 1 (a) Clamp shearing tool using the polyurethane die cushion for 5.5 mm diameter 0.05% C steel wire.
 (b) Hydraulic clamp shearing machine for 10 mm diameter steel bar and 15 mm diameter copper.
 (c) Shearing tool blades of cemented carbide attached to the above hydraulic machine.

Fig. 5 shows the roughness profile of shearing tools used on different materials as measured along X-X. It is observed that the roughness profile obtained in the case of 0.05% C steel after 50 000 strokes is the same as that for 0.1% C steel after 11 000 strokes. This clearly indicates that the tool life for 0.05% carbon steel material is about five times that of 0.1% carbon steel; in the case of copper no wear is observed on the tool.

In the case of 5.5 mm diameter steel of 0.05% C, the moving blade is found to have some sticking on its surface, whereas the stationary blade does not have so much. This sticking occurs mainly during the backward stroke of the moving blade, damaging the remaining end of the clamped bar before the next shearing cycle occurs, thereby leaving some hatches on the sheared end.

From the above results on 10 mm diameter steel of 0.05% C, the wear of the shearing blade is found to be about 25μ after 50 000 strokes which results in an increase of clearance to 50μ . The reason for the occurrence of scratch cracks (see Fig. 2) may be due to this increase in clearance. This is further confirmed by the results of shearing tests carried out for different values of clearance using a clamp shearing mechanism.

From Fig. 6, which shows the above test results and the sheared surface obtained for different clearances, it can be seen that the sheared surface obtained for a clearance of 0.04–0.06 mm is the same as the sheared surface obtained at 50 000 strokes.

Quality of sheared billet

Fig. 7 shows the relation of number of strokes against burr height and weight of sheared billet, respectively. It can be seen that the height of burr developed is almost constant irrespective of the number of strokes. It is well known that the height of burr depends on the amount of cutting-edge radius of the tool which in turn results from the wear of the tool. It can thus be concluded that the wear of a tool increases with the number of strokes, but the amount of cutting-edge radius is almost constant with the stroke number.

It was also noted that the difference in burr height observed on the two ends of the sheared billet was not much. In any event, the burr height obtained by this clamp shearing is so small, less than 0.3 mm, that it can easily be removed in a simple barrel-finishing machine. Therefore the burr problem in clamp shearing is not a major one. From Fig. 7b it can be seen that the variation in weight is within $\pm 0.5\%$. From these results, it can be stated that a billet produced in this way is better than a saw-cut billet. As regards the perpendicularity of the sheared plane with the billet axis, it is within 1° , and the radius of steel billet corner is about 3–4% of its diameter, except in the case of copper, for which it is about 1.5%. The variation in these values is very small, even for a large number of shearing strokes.

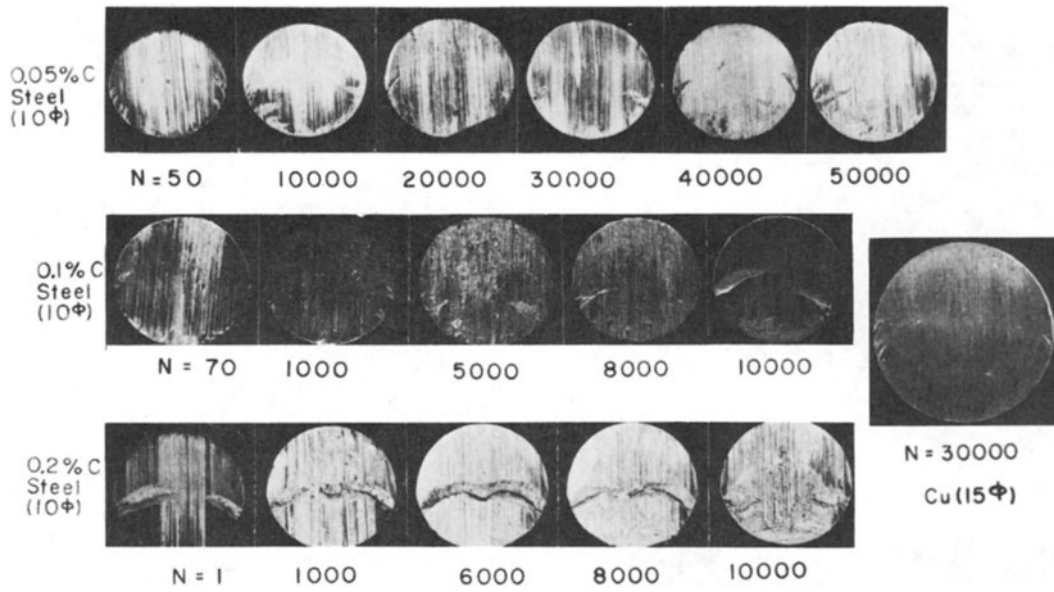


Fig. 2 Appearance of sheared surfaces of bars (the remaining end of the billet).

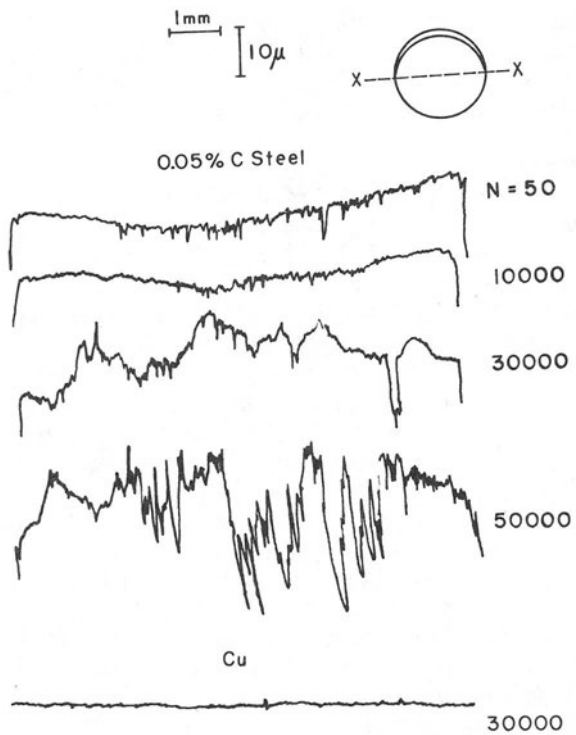
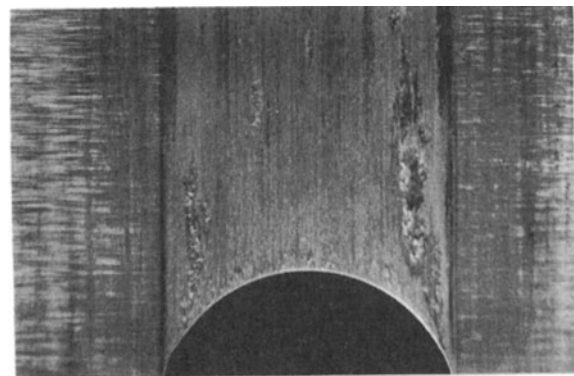
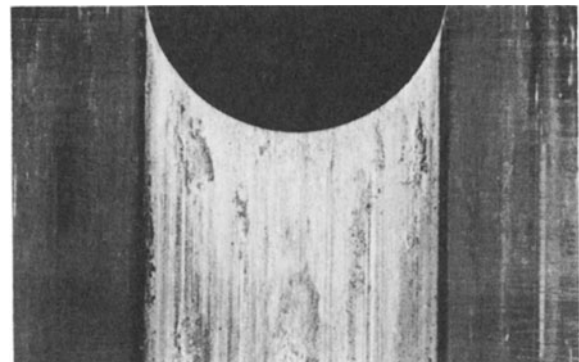


Fig. 3 (above) Surface roughness of sheared billets of 10 mm diameter 0.05% C steel (the remaining end of the billet).



Moving blade



Stationary blade

Fig. 4 (right) Appearance of shearing blades of cemented carbide after 50 000 shearing strokes of 10 mm diameter 0.05% C steel bar.

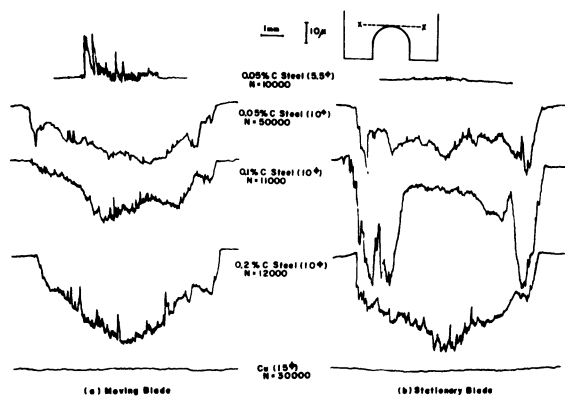


Fig. 5 Surface profiles of shearing blades measured in X-X direction after tool-life tests.

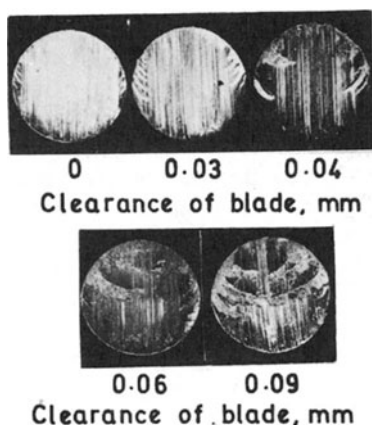


Fig. 6 Appearance of sheared surface of 10 mm diameter 0.05% C steel bar for different clearances.

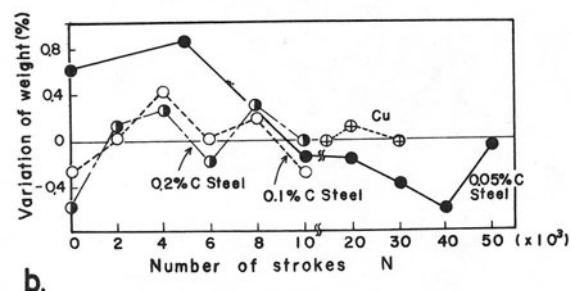
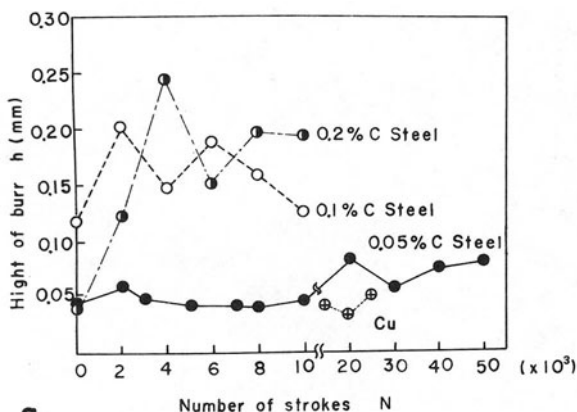


Fig. 7 Accuracy of sheared billets; (a) burr height in sheared billet, (b) variation of weight in sheared billet.

ACKNOWLEDGMENT

The authors would like to thank Mr M. Oshima of Miyamoto Industries Ltd. and Mr M. Nagase of Tokyo University for their assistance in these tool-life tests; M/S Kobe Steel Ltd. and M/S Nippon Steel Corporation for the steel bars and wire, and also Mr K. Asami of M/S Brother Industries Ltd. for his assistance in tool making. Further, they wish to thank Mr V. Nagaraju of the Mechanical Engineering and Development Organization, India, for his kind assistance in writing the manuscript.

REFERENCES

1. NAKAGAWA, T., and MAEDA, T., Preprint of 4th Int. Cold Forging Conf., Düsseldorf, 351 (1970).
2. FUKUI, S., MAEDA, T., and NAKAGAWA, T., Sci. Papers of Inst. Phy. Chem. Research, 64, 1 (1970).

DISCUSSION

Query from M. Maj, McPhersons Limited, Australia.

Possible improvements of the results. When working on the problem of cropping of steel (K1016) 0.16% C for consequent backward extrusion, similar problems of surface imperfections were observed. The cropping was done by the Hungarian type cold flow method, where axial stresses are applied, which is to some extent similar to the clamp shearing method of Professor Nakagawa. Considerable improvements were noted when:

- (a) A small land was created by grinding a relief above the cutting edge of the moving and stationary dies, as per Fig. 8, and the backing plate relief was made.
- (b) Speed variation led to considerable improvement in the face finish, that is, higher speeds produced a better finish.

The second phenomenon markedly worsened the tool-life and in consequence simple high energy rate cropping has been adopted and a special small petroforge type machine built. Could Professor Nakagawa comment on the two phenomena above?

Annealing of steel bar of 0.1% prior to cropping to increase the ductility of the material.

If one considers following with cold forging operations, such as backward extrusion, there might be a danger of undesirable workhardening affecting these operations.

This might lead to the need for a secondary annealing before the extrusion in some cases and put in doubt the whole economics of the process.

Has workhardening been observed in the 'clamp shearing' process? If so, did it affect further processing (if the slugs were used for backward extrusion)?

Reply

A similar type of relief is used in clamp shearing of non-ferrous material. In the case of steel, sticking can be avoided to some extent by the introduction of relief of blades, but it seems difficult to obtain any remarkable improvement of the tool-life.

Speed effects in clamp shearing and axial compressive shearing were observed, the same as you point out, and details are published¹. This speed effect is attributable to the temperature rise by adiabatic plastic deformation in the shearing zone.

Clamp sheared slugs have about 10–15% work-hardening layer relative to diameter. Those slugs annealed after being sheared are just equivalent to machined slugs for extrusion, and, if not annealed, they can be extruded without trouble. But the maximum force in the extrusion of a clamp sheared slug is about 10% larger than that of a machined slug. This difference is comparatively small because the sheared end surface of a slug does not suffer from much deformation in most cases of extrusion².

Query from Dr. M. K. Das and V. G. Wong, University of Birmingham.

High axial compressive stresses are generated in the clamped shearing process. Though this compressive stress is useful from a crack suppression point of view (thereby resulting in a good quality billet), sticking

friction occurs at the tool surface, as proved by the experimental results reported in the present paper. Therefore, it is essential, for the interpretation of tool-life data, to know the current axial compressive stress generated. Clearly, a material having a higher tensile strength will generate higher axial stress, and will adversely affect the tool wear, as can be seen from Fig. 5.

Other variables of interest will be the initial surface roughness of the tool blade surfaces, abrasive wear characteristics of the tool material and the sharpness of the cutting edges. It will be useful to have some of these figures, at progressive stages of the tool-life tests, along with load-penetration profiles (both axial and in the shearing directions).

Reply

The axial compressive force originated in clamp shearing has already been measured and reported: it is about half the shearing resistance¹. It is better for the tool wear to reduce this axial compressive force, but difficult to control this force in clamp shearing.

I don't think that the surface roughness of a shearing tool is an important factor in this case.

We did not measure the stroke-load curve, but this curve will be changed to some extent by the sticking and wear. This report does not deal with the analysis of tool wear, but with tool-life in a practical case.

ELASTIC STRESSES AT SEALS IN PLAIN AND NECKED OPEN-ENDED CYLINDERS UNDER INTERNAL AND EXTERNAL PRESSURES

by

B. LENGYEL and D. C. HARVEY*

SUMMARY

The finite-element method of stress analysis has been used to compute elastic stresses at the seals in plain and necked cylinders under internal and external pressures, under open-ended conditions. The analysis indicates that although tensile axial as well as hoop stresses are present at the seals, away from the seals the stress conditions are significantly more severe, so that fatigue failures due to repeated pressures would not normally be expected in the vicinity of the seals for either type of cylinder made of ductile materials. Experiments indicate the validity of this conclusion. However, additional axial compressive loading must be provided when the absence of axial tensile stresses could be important, such as in the brittle liner of an open-ended compound vessel for very high cyclic pressures.

INTRODUCTION

With the development of new manufacturing processes which employ very high fluid pressures, such as hydrostatic extrusion or the isostatic compaction of powders, a great deal of attention has been focused in recent years on various container designs suitable for high cyclic pressures. An initial study has indicated¹ that open-ended compound containers made of concentric cylinders, with a pressurized fluid layer between the component cylinders, could provide a promising solution to this design problem. Two alternative designs of this type have been put forward: two or more concentric cylinders with the interfacial supporting fluid layer between them under static pressure and, alternatively, where the supporting fluid pressure is built-up in constant proportion to the bore pressure, the 'floating liner' design².

It has been realized, furthermore, that experiments using cyclic bore pressures and static or cyclic supporting pressures on monobloc open-ended cylinders offer a convenient way of investigating the effect of the various stress components in container fatigue, and that such experiments might yield results on which the design of compound vessels for cyclic pressures could be based³. Investigations have therefore been commenced both to establish fatigue design criteria for pre-stressed compound vessels and to prove the usefulness of the fluid support principle in vessels for high cyclic pressures.

In previous experiments monobloc cylinders with closed ends have been subjected to cyclic bore pres-

ures and the results analysed with reference to the Lamé stresses in the bore^{4,5}. It was found that the bore shear-stress range primarily determined the fatigue life. Other work⁶ established that while the axial tensile stress remained the intermediate principal stress, it had no effect on the life of thick-walled cylinders subjected to repeated internal pressure.

In the present experiments, however, the tensile hoop stresses are reduced or completely suppressed in the open-ended cylinder by pre-stressing with a static outside pressure or by the application of a cyclic supporting pressure. In such conditions the stresses at pressure discontinuities, particularly possible tensile stresses in the cylinder wall introduced by the seals, might cause failure at Lamé stresses significantly less than the critical values. The same could of course apply to the liners of pre-stressed compound containers. It is therefore important to analyse the wall stresses at pressure discontinuities in compound containers as well as in the fluid supported cylinders used in the fatigue experiments. This report describes the analysis of stresses at seals in a plain and in a necked open-ended cylinder, the specimens used in fatigue tests under internal and external pressures. The geometry of the specimens is broadly similar to proven specimen designs used by Morrison et al⁴ and Austin and Crossland⁵. The general conclusions of the analysis are valid also for the liners of fluid supported compound vessels.

An analysis of the stresses in the necked static support specimen (Fig. 1a) could be achieved experimentally by strain gauge or photoelastic methods.

*Department of Mechanical Engineering, Imperial College, London

The use of strain gauges could prove difficult in the seal region in a fluid pressure environment, and problems would certainly arise if through-the-wall stresses were needed. Three dimensional photoelasticity using either the stress-freezing or sandwich technique appears to be a better experimental technique, although only very small model pressures would be needed, and under these conditions the viscoelastic behaviour of the rubber seal would not be representative. A theoretical analysis by Kudo and Matsubara⁷ revealed that stress discontinuities in cold forging dies are greatly influenced by Poisson's ratio. This would cast doubt on the validity of the stress freezing photoelastic approach in this application. However, the sandwich technique has been successfully employed to determine the stress distribution in an extrusion container during extrusion⁸.

A variety of methods are available for theoretical analysis of the discontinuity and steady stresses in a thick-walled cylinder subjected to a band of pressure. One of the most exhaustive treatments of the subject is given in the 'Thick-Walled Cylinder Handbook'⁹ where the Fourier integral method is used to calculate the stress distribution in plain semi-infinite cylinders with internal pressure, internal shear, external pressure, or external shear loading. Similar results are reproduced by Timoshenko and Goodier¹⁰ from the paper by Barton¹¹. In these analyses the pressure loading is assumed to reduce instantaneously to zero at the end of the pressure band, which probably represents a more severe situation than in practice with a rubber seal and mitre ring. The fact that analysis of semi-infinite cylinders does not take account of end effects in short cylinders is a further unrepresentative feature.

Kudo and Matsubara⁷ used the successive over-relaxation method due to Southwell to calculate the stresses induced in a cylindrical die of finite length by a band of uniform internal pressure. The analysis shows that considerable constraint is provided by the pressure-free ends of the die so that hoop stresses less than the corresponding Lamé values are present in the pressurized portion of the die. The maximum constraint is provided when the pressure-free length is greater than 0.5 to 1.0 times the bore diameter, in the case of a pressurized length equal to the bore diameter. Lamé hoop stresses are only achieved when the pressurized length is greater than three times the bore diameter for the case of $K = 5$ ($K = \text{outside diameter/bore diameter of the cylinder}$) and a pressure-free length equal to the bore diameter. Although most of the analysis assumes a rectangular or step pressure distribution, an example is given of a trapezoidal or ramp pressure distribution. This has the effect of significantly reducing the amplitude or severity of the stress discontinuities.

Thick-shell analysis has been used¹² to investigate stress distributions in a thick-walled vessel subject to equal internal and external pressure. The results of finite element analysis were also presented and provided a useful comparison. Two arrangements were considered, one an open-ended cylinder with a ram seal halfway down the bore, and the other an open-ended cylinder with a rigidly constrained end and pressure over the whole length. The analysis

shows that significant tensile longitudinal stresses are induced in the bore of the cylinder on the ram side of the seal and that the magnitude and distribution of longitudinal stress is unaffected by the nature of the pressure drop at the seal, be it a step function or ramp function over 0.2 in. The latter conclusion contradicts the findings of Kudo and Matsubara⁷ and seems intuitively unlikely. Furthermore, the finite-element-predicted longitudinal stress distribution exhibits a sharper stress discontinuity than the thick-shell analysis, although the peak values are in agreement. Tensile longitudinal stresses in the bore are also predicted near the end of the constrained cylinder. However, higher tensile stresses can be found in the same region on the outside of the component. It was agreed in the discussion on this paper that the loading case of zero internal pressure with external pressure could give rise to significant discontinuity stresses and should not be ignored.

The numerical method of boundary-point-least-squares¹⁴ was used by Simonen et al¹³ to examine discontinuity stresses in a plain cylinder of $K = 2$. No end effects were considered and a ramp function pressure drop over a length of 0.05 in was assumed. Internal and external pressure loadings were applied separately, and the conclusion in both cases was that the most severe shear stresses were to be found in the pressurized portion of the cylinder away from the discontinuity.

The examples quoted in the previous paragraphs serve to show the importance of detailed analysis of stress discontinuities at seals in high-pressure cylinders. The most significant feature of such discontinuities is the possibility of longitudinal tensile stresses. Both the longitudinal and hoop stress conditions are greatly influenced by factors such as the relative pressurized and unpressurized lengths of the cylinder, the K ratio, and the pressure drop function. A further complication not dealt with in previous analyses is the precaution usually taken with fatigue specimens of necking the cross-section in the region of intended failure. It was decided to examine the plain and necked static support specimens, $K = 1.75$,

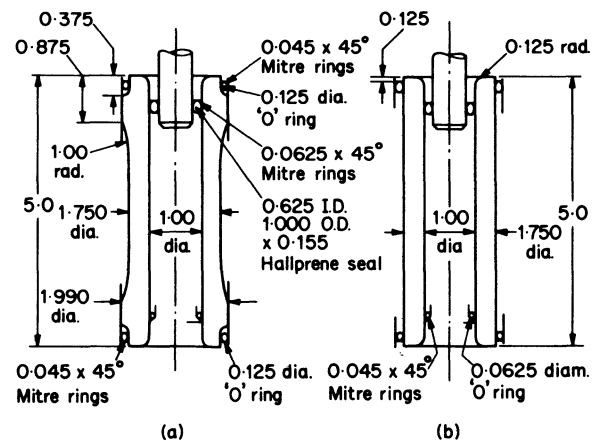


Fig. 1 Necked (a) and plain (b) cylinders of $K = 1.75$ with seals. All dimensions in inches. The position and dimensions of the seals on the plain specimen are the same as on the necked specimen.

for internal and external pressure loadings (Fig. 1). The finite-element method seemed the best choice for analysis, and a programme was already available¹⁵ for axisymmetric solids of revolution.

FINITE-ELEMENT ANALYSIS OF THE TEST SPECIMENS

The finite-element method of stress analysis is today the major computer-orientated stress-analysis technique, and is rapidly gaining acceptance as an alternative to the traditional experimental techniques. The subject is treated at length by Zienkiewicz¹⁶. The method involves the division of a structure or continuum into a number of small ('finite') elements, commonly triangular in cross-section, interconnected at their corners. These connecting points are known as nodes, and external loading is applied to the body via the nodal points. In the case of plane stress or plane strain the elements are effectively triangular laminae, and in the axisymmetric case are rings of triangular cross-section.

Two specimen geometries were analysed using an Imperial College (Mechanical Engineering Department) axisymmetric finite-element programme on the College IBM 7094 computer. The programme has the facility for elastic-plastic analysis, although only elastic analysis was performed. The necked and plain versions of the static support specimen were selected for analysis, although the information gained about stress discontinuities at seals and the specimen length required to develop Lamé stress conditions would read across to other similar geometries, such as the dynamic support specimen.

The finite-element mesh was made as fine as possible within the limitations of the programme and the available computer core store. The mesh was defined uniformly along the length of the specimen. This was considered preferable to the alternative of a coarser mesh away from stress concentrations and a finer mesh around the stress concentrations themselves, as the stress gradients are too severe in a thick-walled cylinder even in Lamé stress regions for a true representation of the total stiffness of the cylinder by a coarse mesh. The configuration used in the analysis is shown in Fig. 2, and it will be noticed that the mesh coarsens radially outwards from the bore. The radial heights of the elements were calculated to give the same hoop stress gradient radially across each element. The pitch of the elements axially is 0.1 in. Because of geometrical symmetry about the centre sections of both the necked and plain specimens, it is sufficient to consider only half the total length of each specimen, as shown in Fig. 2, which is an illustration of the final version of the input data as drawn by the Calcomp plotter.

Two loading conditions were analysed for each specimen geometry. The first condition was unit internal pressure applied uniformly to a fixed length of the bore, and then a linear decrease to zero over one element length, that is 0.1 in. The second condition was unit external pressure again decreasing linearly to zero over one element. The positions of these ramp function pressure drops correspond closely to the extreme positions of the mitre rings in the static

support rig. The internal and external mitre rings were 1/16 in and 3/64 in long, respectively. Both upper and lower external seals were 1/8 in diameter. The ram seal was 9/32 in long and the lower internal seal was 1/16 in diameter. Thus the assumption made in the finite-element analysis loading was that the pressure drop occurred mainly in the mitre ring, and that the seals themselves transmitted pressure hydrostatically for a good proportion of their length. This assumption seems reasonable, although there is no direct evidence to support it. The loading conditions are shown diagrammatically in Fig. 2.

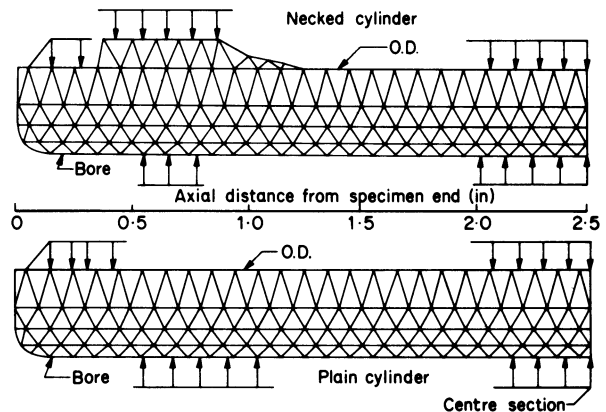


Fig. 2 Finite-element mesh and pressure loading of plain and necked cylinders.

RESULTS OF ANALYSES

The results of finite-element analyses on both the plain and necked static support specimen for internal and external pressure are summarized in Figs 3–8. The vertical axes indicate stresses in any unit per unit pressure, if both stress and pressure are expressed in the same unit. Or, in other words, the stresses are given as a multiple of the pressure loading. The plots were obtained by first plotting the element stresses for elements closest to the inside and outside surfaces, which gave the general trend of the distributions. Boundary stress conditions were then evaluated by taking radial cross-plots at appropriate intervals and extrapolating to the boundaries. The somewhat laborious procedure is achieved numerically in more sophisticated finite-element programmes. Nevertheless the cross-plots provide a useful check both on the accuracy of the finite-element results, and on the degree of guesswork involved in extrapolation. Fig. 3 shows a few hoop stress cross-plots for the plain cylinder with internal pressure. It can be seen that in the central region of the specimen the element stresses lie very close to the true Lamé stress distribution. In the seal region, however, the radial distributions are changing rapidly particularly near the bore. Extrapolation is more doubtful in this region, and if greater accuracy were required, a much finer finite-element mesh would be essential. The hoop stress cross-plots for the necked specimen with internal pressure, and the external pressure cases, exhibited similar characteristics to Fig. 3. The axial

stress cross-plots were also clearly defined except in the region very near to the seal where extrapolation was more doubtful. These local inaccuracies however are of only minor importance in the overall longitudinal stress distribution plots Figs 4–8.

Internal pressure loading

Figs 4 and 5 deal respectively with the plain and necked specimens under unit bore pressure. The concept of the necked design is of course to minimize any undesirable stress conditions in the seal region, and thereby ensure fatigue failures within the necked region only. The hoop stress distributions do show that the reduction of stress takes place more gradually over a longer distance in the necked specimen, but that this also has the effect of reducing the specimen length over which Lamé conditions apply. In the plain specimen the hoop stress distribution is within $1\frac{1}{2}\%$ of the Lamé values for a total length of $2 \times 1\frac{1}{4}$ in = $2\frac{1}{2}$ in out of the 4 in length subjected to fluid pressure. The corresponding length for the necked specimen is about 2 in. The magnitude of the bore hoop stress σ_θ discontinuity is 0.15 stress units per unit pressure, that is 15% of the bore pressure in both cases, although the discontinuity takes place at a slightly higher stress level in the plain cylinder. For pressure p and Poisson's ratio ν the discontinuity range for a step function pressure drop is $2\nu p^7$, say 0.56 units in the present case if $p = 1$. The ramp function pressure drop over 0.1 in applied in the finite-element analysis is the reason for this difference. It has been shown⁷ that a ramp function over 0.031 in causes the discontinuity range to fall to about 0.42 units. If in the same way the step function discontinuity curve were terminated at points corresponding to a ramp function over 0.1 in the discontinuity range would fall to about 0.2 units per unit pressure.

The axial stress σ_z distributions at the bores of both plain and necked cylinders are very similar, slightly lower peak stresses occurring in the necked cylinder. At the pressure-free ends of the cylinders tensile axial stresses are predicted, but only of about 0.18 units magnitude. On the other hand, the peak compressive axial stress in the pressurized region is about 0.5 units giving a total discontinuity range of 0.68 units per unit pressure. The corresponding range for a step-function pressure drop would be 1.0 unit, although this time the difference is not so directly related to the pressure-drop function. It is more likely that the proximity of the seal to the end of the cylinder has reduced the magnitude of the tensile axial stress. Larger tensile axial stresses are in fact predicted on the outside diameter of the specimen, although these would not normally be significant.

The shear stress σ_{rz} vanishes over the bore surface and thus the so called 'Bore' σ_{rz} stress distribution refers to material just below the bore surface.

External pressure loading

The stress distributions due to unit external pressure are shown in Figs 6 and 7. The necked cylinder again exhibits a more gradual decay of bore and outside diameter hoop stress (σ_θ) than the plain cylinder but,

as before, this is associated with a smaller length of the cylinder for which Lamé conditions apply. The plain cylinder hoop stress values, however, are within 1% of the Lamé values for some $2 \times 1\frac{1}{2} = 3$ in of the total 5 in length of the cylinder. As the external seal is very near to the end of the cylinder, the hoop stress discontinuity which would be expected on the outside diameter has no opportunity to develop.

Tensile axial stresses σ_z are generated at the bore in the pressurized region of peak magnitude 0.38 units per unit pressure in the plain cylinder, and 0.24 units in the necked cylinder. Corresponding compressive axial stresses can be observed on the outside diameter although the stresses in the necked cylinder are increased considerably in the large-diameter region because of the additional axial fluid pressure loading. The shear stress σ_{rz} just below the outside surface, and referred to as 'O.D.' σ_{rz} exhibits the characteristic peak in the region of the seal, and in the necked cylinder a second peak can be observed in the transition region between the radiused and parallel portions of the specimen.

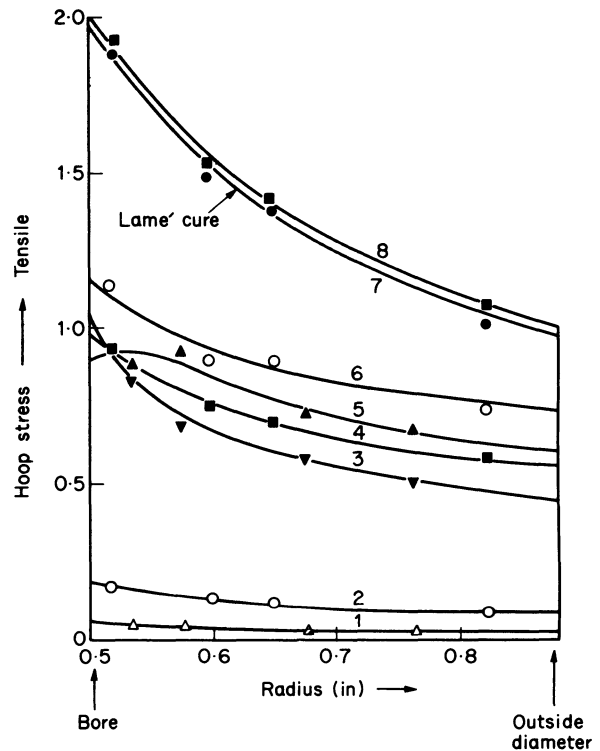


Fig. 3 Radial cross-plots of element hoop stresses. Plain cylinder with unit bore pressure. Axial coordinate of cross-plots: 1, 0.15 in; 2, 0.2 in; 3, 0.45 in; 4, 0.5 in; 5, 0.55 in; 6, 0.6 in; 7, 2.4 in; 8, 1.5 in.

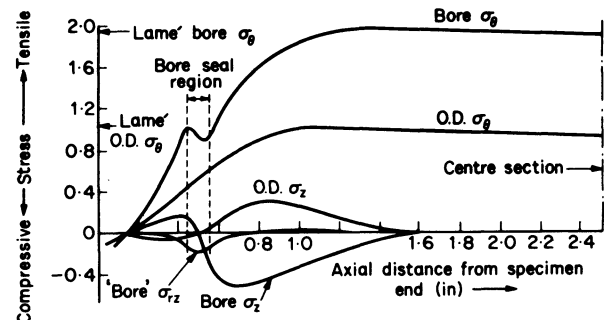


Fig. 4 Stresses at the bore and on the outside diameter (O.D.) of the plain cylinder with unit bore pressure.

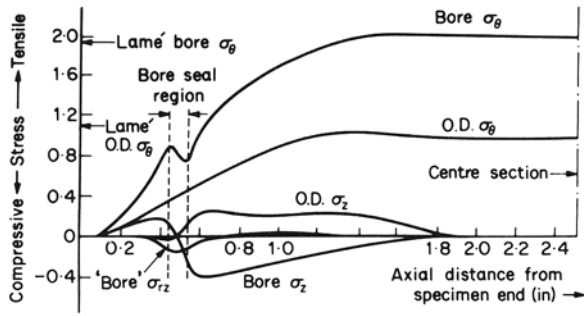


Fig. 5 Stresses at the bore and on the outside diameter (O.D.) of the necked cylinder with unit bore pressure.

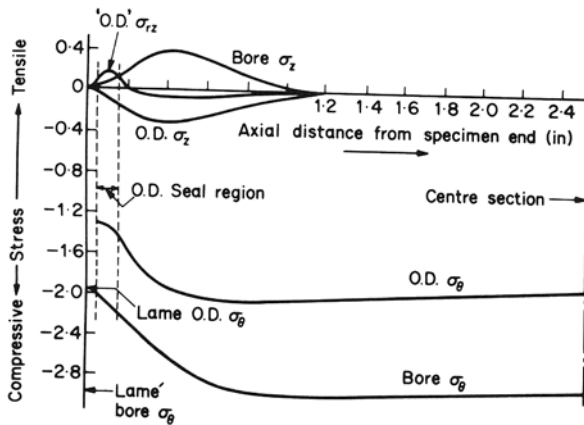


Fig. 6 Stresses at the bore and on the outside diameter (O.D.) of the plain cylinder with unit external pressure.

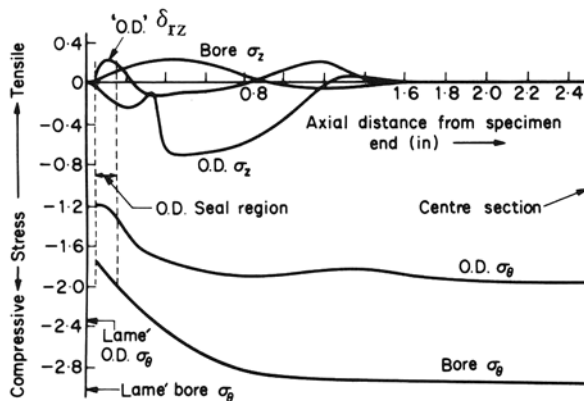


Fig. 7 Stresses at the bore and on the outside diameter (O.D.) of the necked cylinder with unit external pressure.

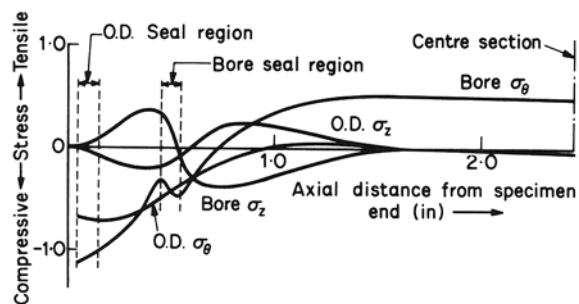


Fig. 8 Stresses at the bore and on the outside diameter (O.D.) of the plain cylinder with external pressure half the bore pressure of unity.

CONCLUSIONS

(a) The difference between the stress distributions in necked and plain cylinders is so small that there is little advantage in using a necked specimen design. In fact, apart from manufacturing simplicity, the plain cylinder is more attractive because of the greater uniformity of stress conditions in the central region of the specimen.

(b) The tensile axial stresses at the pressure-free end of the bore of a cylinder with internal pressure are considerably less than the tensile hoop stresses in the same area, therefore their effect is probably negligible in fatigue. The same argument applies to the tensile axial stresses predicted on the outside diameter in the pressurized region of the specimen. As the nominal bore hoop stress at the seal is about half of the Lamé value, fatigue failures due to repeated pressure should not occur at the seal unless fretting damage at the mitre ring becomes significant.

(c) The case of external pressure loading is applicable to the situation in a static support fatigue test when the internal pressure is reduced to zero. In this case the axial tensile stress at the bore could be important, particularly in a brittle material with low tensile strength. However, in a material such as EN25 the very large compressive hoop stresses would considerably retard (if not prevent) the development of a fatigue crack.

(d) A most important condition is when both internal and external pressure loadings are present, such as in a static support or dynamic support fatigue test. In Fig. 8 the stress distributions have been plotted from Figs 4 and 6 for the case of a plain cylinder, when the external pressure is half the internal pressure and the latter has the value of unity. It can be seen that although a tensile Lamé hoop stress of 0.48 units is present at the bore in the central region of the specimen, in the seal and pressure-free regions the bore hoop stress is entirely compressive. However, the tensile axial stress at the bore in the seal region is augmented by the external pressure loading, achieving a peak of almost 0.4 units. This would not normally be serious in fatigue for a ductile material such as EN25, owing to the small range of the axial stress and the presence of local compressive hoop stresses. If the internal and external seals were opposite one another, rather than displaced as in the present case, then the axial stresses due to internal and external pressure loading would tend to cancel out and this would help to minimize tensile axial stresses. However, the displacement of the seals is an essential design feature of the necked specimen, and it was a matter of convenience to use the same arrangement for the plain specimen. An additional axial compressive stress would need to be provided even with opposite seals, if it were important to eliminate tensile stresses altogether.

(e) These conclusions indicate that fatigue results on plain cylinders of ductile materials under cyclic pressure are representative of the effect of Lamé stresses. There is no need, therefore, for the use of necked cylinders with their more complex manufacturing and testing problems, which could become particularly troublesome in testing under simul-

taneous internal and external pressures. Experiments have proved the validity of this conclusion: fatigue failure in the vicinity of the seals has never occurred in specimens of EN25 steel. A typical fracture of these specimens is shown in Fig. 9.

(f) This analysis indicates, furthermore, that axial tensile stresses at the seals in the fluid-supported brittle liner of an open-ended compound vessel could cause fatigue failure at cycle lives less than those predicted from the Lamé stresses. Optimum designs could be developed for such cases by carefully selecting the position and configuration of the seals and by axially pre-stressing the liner.

(g) The accuracy of the analysis of stress discontinuities at the seal is dependent, not only on the fineness of the finite-element mesh, but also on the gross assumptions made about the normal and shear loadings at the seal. Knowledge of these loading conditions is needed if the design and positioning of high pressure seals is to be optimized.

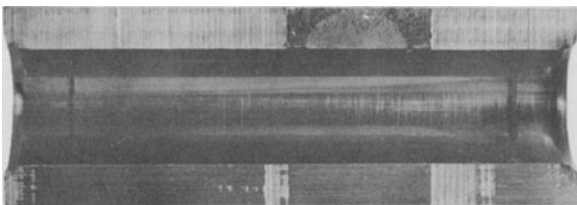


Fig. 9 Typical fatigue failure of EN25 plain cylinders.

ACKNOWLEDGMENTS

The financial assistance of the Science Research Council and Rolls-Royce Limited is gratefully acknowledged. The authors thank Dr D. J. Hayes for the use of the finite-element programme.

REFERENCES

- LENGYEL, B., BURNS, D. J., and PRASAD, L. V., 'Design of containers for a semi-continuous hydrostatic extrusion production machine', Proc. 7th Int. M.T.D.R. Conf., Pergamon Press, Oxford, 1966.
- LENGYEL, B., and ALEXANDER, J. M., 'Design of a production machine for semi-continuous hydrostatic extrusion', *Proc. Inst. Mech. Engrs.*, 1967-68, 182, Part 3C, p. 180.
- HARVEY, D. C., and LENGYEL, B., 'Pressure vessels under cyclic loading; test rig and initial results', *Advances in Machine Tool Design and Research*, 1968. Pergamon Press, Oxford.
- MORRISON, J. L. M., CROSSLAND, B., and PARRY, J. S. C., 'Strength of thick cylinders subjected to repeated internal pressure', *Proc. Inst. Mech. Engrs.*, 1960, 174, p. 95.
- AUSTIN, B. A., and CROSSLAND, B., 'Low-endurance fatigue strength of thick-walled cylinders: development of a testing machine and preliminary results', *Proc. Inst. Mech. Engrs.*, 1965-66, 180, p. 43.
- BLASS, J. J., and FINDLEY, W. N., 'The influence of the intermediate principal stress on fatigue under triaxial stress', *Materials Research and Standards*, 1967, 7, 254.
- KUDO, H., and MATSUBARA, S., 'Stress analysis in cylindrical dies of finite length subjected to a band of internal pressure', *J. Japan Soc. for Technology of Plasticity*, 1968, 9, p. 86.
- EL-BEHERY, A. M., and LAMBLE, J. H., 'Stress distribution in an extrusion container found by the sandwich technique', *Strain*, 1969, 5, p. 209.
- 'Thick-Walled Cylinder Handbook' Report No. WAL 893/172, 1954, Watertown Arsenal Laboratory.
- TIMOSHENKO, S., and GOODIER, J. N., 'Theory of Elasticity', McGraw-Hill, 1951, p. 388.
- BARTON, M. V., 'The circular cylinder with a band of uniform pressure on a finite length of the surface', *J. Applied Mechanics, Trans. A.S.M.E.*, 1941, 8, A-97.
- MOHAUPT, U. H., PICK, R. J., and BURNS D. J., 'Bending stresses in elastic thick-walled cylindrical pressure vessels', First International Conf. Pressure Vessel Technology, Delft, 1969, p. 195.
- SIMONEN, F. A., MEYER, G. E., FIORENTINO, R. J., and SABROFF, A. M., 'Design of containers for large scale hydrostatic extrusion', 25th National Conference of Fluid Power, 1969.
- HULBERT, L. E., and SIMONEN, F. A., 'On the solution of axisymmetric elastic stress problems by the boundary point least squares technique', First International Conf. Pressure Vessel Technology, Delft, 1969.
- HAYES, D. J., 'Axisymmetric finite-element stress analysis programme', Imperial College, unpublished.
- ZIENKIEWICZ, O. C., 'The finite element method in structural and continuum mechanics', McGraw-Hill, 1967.

DISCUSSION

Query from C. F. Noble, UMIST

It appears that the cylinder design you have considered in your paper is more appropriate to isostatic compacting than hydrostatic extrusion. In the former only relatively small movement of the piston will be incurred. However, in hydrostatic extrusion the movement will be considerable and since the seal is usually attached to the piston the configuration will be completely different at the end of the stroke from that shown in Fig. 1. Does your analysis err on the safe side under this condition and, if so, why?

Reply

The paper analyses stresses at seals in fatigue specimens. We agree that, in hydrostatic extrusion, conditions could be different when the seal is attached to the plunger, but this is by no means always the case. Unfortunately, no data is available in the literature regarding the relative merits of stationary and moving seals in fatigue. Work is being carried out at present at Imperial College, which should provide some guidance to designers on this particular point.

AUTHORS' AND CONTRIBUTORS' INDEX

(Authors' page numbers are in bold type)

- Akgerman, N., **517**
 Akutsu, T., **281**
 Alexander, J. M., **51**
 Al-Hassani, S. T., **129**
 Anderson, J. W., **325**
 Andrew, C., **95, 104, 446**
 Appleton, E., **557**
 Barker, A. A., **271**
 Barrow, G., **20, 379, 481, 506**
 Bartley, A. J., **185**
 Bell, R., **199, 207, 217**
 Bhateja, C. P., **535**
 Blaschke, W. S., **13**
 Boden, P. J., **271**
 Boyd, C., **169**
 Burdekin, M., **289, 319**
 Bus, C., **397**
 Cessford, S., **217**
 Charnley, C. J., **433**
 Chisholm, A. W. J., **499, 535**
 Cowley, A., **289, 319, 455**
 Crookall, J. R., **387**
 Das, M. K., **572**
 Davies, B. J., **120**
 Denham, K., **153**
 Doane, R., **411**
 El Hakim, M. A., **21, 297, 308**
 Engel, G. H., **179**
 Etheridge, R. A., **359**
 Evans, J. M., **271**
 Farnworth, G., **31**
 Farnworth, R., **69**
 Fogg, B., **151**
 De Fraine, J., **193**
 Frisch, J., **517**
 Fujimoto, C., **81**
 Furukawa, Y. F. Y., **161**
 Gale, P. C., **207**
 Gautschi, G. H., **113**
 Geddam, A., **270**
 Grieve, D. J., **543**
 Grindrod, D., **31**
 Von Grote, K. H., **247**
 Hague, A. G., **87, 277**
 Hahn, R. S., **235**
 Hammill, J., **446**
 Hanna, N. H., **287**
 Harrison, D., **139, 159**
 Harvey, D. C., **573**
 Hastings, W. F., **509**
 Hefford, H. E., **40**
 Heginbotham, W. B., **529**
 Hemingray, C. P., **319**
 Hinderwell, F. B., **492**
 Hinduja, S., **455**
 Holland, D., **411**
 Hoshi, T., **439**
 Huntley, E. J., **121**
 Ito, S., **260**
 Ito, Y., **81, 98**
 Johnson, W., **129**
 Jones, P. F., **246, 492**
 Jubb, C., **564**
 Justel, K., **315**
 Kaliszer, H., **543**
 Kals, J. A. G., **367**
 Kawada, K., **355**
 Kegg, R. L., **496**
 Kiang, T. S., **379**
 King, G. R., **175**
 Koenigsberger, F., **241**
 Kondo, K., **61**
 Koshino, K., **142**
 Kvasnicka, I., **401**
 Laika, A., **205**
 Larson, B., **168**
 Lawther, R., **309**
 Laycock, D. B., **565**
 Ledergerber, A., **7**
 Lengyel, B., **573**
 Lenz, E. L., **108**
 Levy, H., **108**
 Lindsay, A. R., **235**
 Loewy, K., **108**
 Macdonald, R. L., **25**
 Maeda, K., **61**
 Maj, M., **67, 159, 571**
 Maltby, R. C., **387**
 Marsland, D. W., **199**
 Masuko, M., **81, 98**
 Mazilu, I., **187**
 Meleka, A. H., **247**
 Miyamoto, K., **567**
 Morbey, F. J., **359**
 Morton, I. S., **40**
 Muth, P., **186**
 Nakagawa, T., **161, 567**
 Nann, R., **429**
 Noble, C. F., **151, 246, 256, 265, 565**
 Van den Noortgate, L. F., **447**
 Noppen, R., **95**
 Oxley, P. L. B., **509**
 Pattinson, J., **499, 535**
 Pendlebury, G., **309**
 Pennell, J. A., **147**
 De Pennington, A., **199**
 Peters, J., **21, 120, 297, 493**
 Pic, J., **197**
 Primmer, R., **168**
 Pruemmer, R. A., **139**
 Prummer, R., **349**
 Quinton, D. R., **51**
 Redford, A. H., **526, 534**
 Richards, D. L., **241**
 Roberts, J. I., **309**
 Rogers, M., **257**
 Rooks, B. W., **69, 159**
 Rose, R., **121**
 Rowe, G. W., **543**
 Rowe, W. B., **239, 241**
 Russell, A., **120**
 Sato, H., **246, 281**
 Satyamurty, S., **446**
 Schofield, R. E., **87, 89, 104**

AUTHORS AND CONTRIBUTORS INDEX continued

- Seimiya, K., 260
Sewell, G. A. E., 551
Sfantsikopoulos, M., 263, 265, 541
Sheen, J. S., 121
Shillam, N. F., 15
Shima, S., 139, 565
Slater, R. A. C., 557
Sparkes, C. A., 41, 48
Spur, G., 30, 421
Srinivasan, V., 433
Stevenson, M. G., 509
Stone, B. J., 299
Stute, G., 429
Szekeres, F., 229
Taylor, S., 427, 446, 453, 476
Tewari, N. K., 95
Thatcher, R. W., 147
Thomas, A., 153
Thomas, M. D., 297
Thorneycroft, M. C., 25
Thornley, R. H., 22, 89
Tlusty, J., 289, 333
Touwen, N. A. L., 397
Tozawa, Y., 355
Travis, F. W., 169
Veenstra, P. C., 397
Vickersstaff, T. J., 126
Waite, S., 67
Wasiuktiewicz, I., 186, 428
Wentz, W., 421
Werntie, G., 288
White, J. B., 152
Wilbur, J., 499
Van Der Wolf, A. C. H., 397
Wong, V. G., 572
Wright, G. I. E., 139, 270
Yoshida, K., 161
Yoshimura, M., 439

SUBJECT INDEX

Adaptive control, Session	5	measurement of damping of a bolted joint	100
direct feedback to a vertical milling machine	17	mechanism of the approach of surfaces	90
economics in turning operations	12	optimum interface pressure of a bolted joint	97
Computer-aided design		resilience of feed drives	181
finite-element method of structural calculation	455	specification and performance of electrohydraulic motor drives	217
machine-tool structures	439, 447, 455		
Computer control		Machine-tool feed drives and guideways, Session	177
design and development of a small DNC system	433	Machine-tool testing, Session	279
direct numerical control	429	determination of the minimum number of linear measurements	341
DNC system	421	dynamic performance tests for lathes	299
programmed approach in control systems	409	establishment of standard cutting conditions	289
Digital computer-aided design and control, Session	409	hydraulic vibrator	309
Electrochemical machining, Session	248	identification by micro-tremor techniques	281
electrochemical surface grinding, vertical spindle	265	inspection and acceptance tests for numerical control machine tools	315
electrolyte flow	259	linear system of accuracy of numerical control machine tools	333
electron-beam machining	247	numerical control machine evaluation	325
influence of surface finish on fatigue life of Nimonic 80A	271	positioning accuracy of numerical control machine tools	319
Grinding, Session	227	positioning accuracy repeatability tests	328
computer-aided study of surface texture	535	production tests	326
digital computer simulation of rounding-up process	235		
manufacturing resource selection	551	Metal cutting, Session	479
stability of centreless grinding process	241	cutting-force measurements	116
surface topography, digital computation of	543	cutting-force measurements with multi-component piezoelectric transducers	113
wheel-life determination	229	cutting-speed selection	495
Machine-tool element design, Session	79	effective component control of hot tool machining	387
acceleration feedback	199	electron microscope studies	499
analysis of joint deflection	91	high-speed tools influence on carbide size and distribution	401
anti-friction slideways, load capacity and stiffness of rolling ball element	194	machinability assessment	507
damping capacity of a bolted joint	102	machining economics	481
design of hydromechanical networks	211	re-sulphurised free machining steels	499
disc clutches	107	thermoelectric characteristics of carbides	397
elastic and plastic components of deflection	89	tool-life equations	481
electrohydraulic drives, active compensation	199	tool-life equations by step turning test	379
hydromechanical compensation	207	tool-wear compensation using cutting-force spectrum	517
flow control valves, two-way	187		
influence of machined lay orientations	83	Metal forming, Sessions	49, 127, 555
influence of surface roughness	84	clamp shearing	567
joints, horizontal stiffness and microsliding	81	cup drawing	367
machine-tool design, design features for NC contouring	179	elastic stresses at seals	514
		expanding sheet forming	141

SUBJECT INDEX continued

explosive welding, metallurgical and residual stress investigations	349	direct numerical control	429
hot forging	69	DNC system	421
hydrostatic extrusion	51	inspection and acceptance tests for numerical control machine tools	315
hydrostatic extrusion, design of a press	147	linear system of accuracy of numerical control machine tools	333
isocompaction tests	54	machine-tool design, design features for numerical control	
isostatic compaction	54	contouring	179
opposed die-shearing process	62	modular design	31
precision shearing	61	numerical control lathe, design	25
pressed steel shear, strain history and drawing-in	359	tool setting	26
rotary forging	557	numerical control machine evaluation	325
stress-wave fracturing	129	positioning accuracy of numerical control machine tools	319
stress-wave transmission through step bars	136	positioning accuracy repeatability tests	328
tube-forming forces	355	production tests	326
Metal processing, Session	347	programmed approach in control systems	409
Numerical control, Session	23	System identification, Session	527
acceleration feedback	199	digital studies, designing in	529
appearance considerations	121		
design and development of a small DNC system	433		